Advancing the Chemical Understanding of Hydrogen Sulfide and Related Reactive Sulfur Species with Small Molecule Tools for Delivery and Sensing

by

Kaylin G. W. Fosnacht

A dissertation accepted and approved in partial fulfillment of the

requirements for the degree of

Doctor of Philosophy

in Chemistry

Dissertation Committee:

Ramesh Jasti, Chair

Michael Pluth, Advisor

Vickie DeRose, Core Member

David Garcia, Institutional Representative

University of Oregon

Summer 2024

© 2024 Kaylin Grace Workman Fosnacht

This work is openly licensed via CC BY-NC-ND 4.0.



DISSERTATION ABSTRACT

Kaylin Grace Fosnacht

Doctor of Philosophy in Chemistry

Title: Advancing the Chemical Understanding of Hydrogen Sulfide and Related Reactive Sulfur Species with Small Molecule Tools for Delivery and Sensing

Reactive sulfur species (RSS), such as thiols, polysulfides, hydrogen sulfide (H_2S), and persulfides (RSSH), play essential roles in biological chemistry, including roles in redox homeostasis and small molecule signaling pathways. Previously known as a toxic gas, H_2S was established as a gasotransmitter in the late 1990's and is defined as a membrane permeable small molecule that is endogenously produced and involved in specific cell signaling pathways. For this reason, the association of H_2S imbalances with various diseases, such as Parkinson's disease, diabetes, and asthma, has been studied and changes in endogenous H_2S are indicated as a potential disease biomarker. More recently, the importance of persulfides and other RSS in addition to H_2S has become a major research focus due to their overlap in activity with H_2S and newly discovered importance in biological processes. In particular, recent work has further clarified that many cellular signaling processes initially attributed to H_2S are likely due to persulfides. Overall, understanding the RSS pool both fundamentally and also in biological systems is crucial. Carefully developed tools to both detect and deliver RSS are needed to further understand the rich chemistry of RSS within the body.

Within this dissertation three main aims are addressed: (1) improved H_2S sensing tools for longer duration studies, (2) donor molecules that release RSS, and (3) increasing fundamental understanding of persulfide reactivity. Chapter I is a comprehensive review of fluorescent probes of H_2S and other RSS and includes discussion of the important advantages and limitations of each probe type. Chapter II features a cell-trappable H_2S probe that provides a large, selective fluorescence turn-on to H_2S and was used to sense H_2S in live cells. Chapter III details a palette of thiol-activated H_2S donors that also produce a fluorescent response in the blue to NIR emission

wavelength range. Notably, the NIR donor was applied to live rats to image the fluorescence turn-on when subcutaneously delivered. Chapter IV describes the development of a small library of esterase-activated persulfide donors and kinetic analysis of persulfide release, donor side reactivity, and observed persulfide persistence. Chapter V is a combined computational and experimental analysis of persulfide reactivity with thiols where increasing steric bulk or electron withdrawal near the persulfide can shunt persulfide reactivity through the transpersulfidation pathway. Experimentally, we used a persulfide donor and persulfide trapping agent to monitor and measure transpersulfidation from a bulky penicillamine-based persulfide to a cysteine-based thiol, which is the first direct observation of transpersulfidation between low molecular weight species. This dissertation includes previously published co-authored material.

CURRICULUM VITAE

NAME OF AUTHOR: Kaylin G. W. Fosnacht

GRADUATE AND UNDERGRADUATE SCHOOLS ATTENDED:

University of Oregon, Eugene
Saint Martin's University

DEGREES AWARDED:

Doctor of Philosophy, Chemistry, 2024, University of Oregon
Bachelor of Science, Chemistry, 2019, Saint Martin's University

AREAS OF SPECIAL INTEREST:

Small Molecule Organic Synthesis
Chemical Tool Development
Chemical Biology of Reactive Sulfur Species

GRANTS, AWARDS, AND HONORS:

Beetham Graduate Fellowship, University of Oregon, 2023–2024
NSF GRFP Honorable Mention, University of Oregon, 2020
Chemistry Research Award, Saint Martin's University, 2017–2018
Organic Chemistry Tetrahedral Award, Saint Martin's University, 2016–2017

PUBLICATIONS:

Fosnacht, K.G.; Sharma, J.; Champagne, P.A.; Pluth, M.D. Transpersulfidation or H_2S Release? Understanding the Landscape of Persulfide Chemical Biology. *Journal of the American Chemical Society* **2024**, *Accepted*.

Fosnacht, K.G.; Dorogin, J.; Jefferis, P.M.; Hettiaratchi, M.H.; Pluth, M.D. An Expanded Palette of Fluorescent COS/H_2S-Releasing Donors for H_2S Delivery, Detection, and In Vivo Application. *Angewandte Chemie International Edition* **2024**, *63*, e202402353.

Fosnacht, K.G.; Pluth, M.D. Activity-Based Fluorescent Probes for Hydrogen Sulfide and Related Reactive Sulfur Species. *Chemical Reviews* **2024**, *124*, 4124–4257.

Fosnacht, K.G.; Hammers, M.D.; Earp, M.S.; Gilbert, A.K.; Pluth, M.D. A Cell Trappable Methyl Rhodol-Based Fluorescent Probe for Hydrogen Sulfide Detection. *Chemistry – An Asian Journal* **2022**, *17*, e202200426.

Fosnacht, K.G.; Cerda, M.M.; Mullen, E.J.; Pigg, H.C.; Pluth, M.D. Esterase-Activated Perthiocarbonate Persulfide Donors Provide Insights into Persulfide Persistence and Stability. *ACS Chemical Biology* **2022**, *17*, 331–339.

Lovell, T.C.; Fosnacht, K.G.; Colwell, C.E.; Jasti, R. Effect of Curvature and Placement of Donor and Acceptor Units in Cycloparaphenylenes: A Computational Study. *Chemical Science* **2020**, *11*, 12029–12035.

Fernandez-Delgado, O.; Castro, E.; Ganivet, C.R.; Fosnacht, K.; Liu, F.; Mates, T.; Liu, Y.; Wu, X.; Echegoyen, L. *ACS Applied Materials & Interfaces* **2019**, *11*, 34408–34415.

ACKNOWLEDGMENTS

First and foremost I would like to thank my advisor, Professor Michael Pluth, for allowing me to join his lab and spend my doctoral degree working in his lab. I am especially grateful to Mike for giving me the freedom to work on research projects I am passionate about and also helping me gain many valuable skills as an organic chemist, chemical biologist, and overall researcher. Thank you to my committee members, Professors Ramesh Jasti, Vickie DeRose, and David Garcia. Thank you to my graduate student members, Drs. Terri Lovell, Carrie Levinn, and Christie McDevitt, who initially guided me through graduate-level research. Thank you to my current lab members, Dr. Ismail, Haley Smith, Andy Davis, Keyan Li, Jasmine Collins, and Juan Hernandez and past members, Dr. Michael Wade Wolfe, Dr. Shiva Moaven, Dr. Toby Sherbow, Dr. Annie Gilbert, Dr. Turner Newton, and Dr. Matt Cerda, for the support along the way. Thank you to my undergraduate Kaitlyn Klotz for being a great mentee and willingly running many columns throughout our year together,

To my family, who have been my biggest supporters along the way, thank you to my mom Kellie, my dad Kimball, and my sister Kenna who offered me a nice haven away from the stress of school during my visits back to Washington. Thank you to all the friends I made in Eugene for being there throughout my time here and for the fun times during hikes, bar crawls, trivia, TV show nights, game nights (notably playing Dance Dance Revolution), bouldering, and more. Thank you to all my friends from Washington who were down to clown whenever I visited and who tolerated me being very bad at replying to their texts. Thank you to my biggest fan, Daniel, who has been there for the good and bad times during graduate school and who I can’t wait to experience the future with. Thank you to our cats, Rory and Arnold, who are the two cutest little beans and who supported me by laying on me as I worked on presentations, papers, and this dissertation.

Lastly, I would like to thank the University of Oregon, Beetham family, NIH (R01GM113030), and NSF (CHE-2004150) for funding.

To my family & Daniel.

TABLE OF CONTENTS

Chapter Page

I. ACTIVITY-BASED FLUORESCENT PROBES FOR HYDROGEN SULFIDE AND RELATED REACTIVE SULFUR SPECIES 33

1.1 Introduction 33

1.1.1 Background 33

1.1.2 Properties and Biological Synthesis 34

1.1.3 Roles of H_2S and RSS in Biology 36

1.1.4 Tools for Investigating Biological H_2S 37

1.1.5 Scope of the Review 39

1.2 H_2S Fluorescent Probes: Reduction of Oxidized Nitrogen Motifs 41

1.2.1 Azide Reduction 41

1.2.1.1 Direct Azide Reduction 42

1.2.1.2 Azide Reduction and Self-Immolation 60

1.2.1.3 Azide Reduction and Intramolecular Reaction 66

1.2.1.4 Azide Reduction with Dual Reactivity 70

1.2.1.5 FRET-Based Azide Reduction 73

1.2.1.6 Targeted Azide-Based Probes 78

1.2.1.7 Luminescent Azide Reduction 87

1.2.2 Nitro Reduction 90

1.2.3 Other Oxidized Nitrogen Motifs 95

1.3 H_2S Probes Based on Dichalcogenide Reduction or Exchange 98

1.3.1 Disulfide-Based H_2S Probes 98

1.3.2 Selenenyl Sulfide and Diselenide-Based H_2S Probes 106

1.3.3 Selenoxide-Based H_2S Probes 109

1.4 Electrophilic H_2S Probes 110

1.4.1 2,4-Dinitrophenyl (DNP) Cleavage 111

1.4.2 2,4-Dinitrobenzenesulfonate (DNBS) Cleavage 136

1.4.3 Nitrobenzofurazans (NBD) Cleavage 148

1.4.4 Other Electrophilic Platforms 170

1.4.4.1 Cyclizations from Aldehydes and α,β-Unsaturated Ketones 170

1.4.4.2 Addition to Aldehydes and Subsequent Ester Cleavage 173
1.4.4.3 Cyclization from Electron-Poor Styrenes 175
1.4.4.4 Addition to Benzyl Electrophiles and Subsequent Ester Cleavage 176
1.4.4.5 Acrylate Cleavage 177
1.4.4.6 Thiophene-2-carboxylic Acid Ester Cleavage 179
1.4.4.7 Cyanate Cleavage 181
1.4.4.8 Addition to Conjugated Systems and Cyclization 182
1.4.4.9 Addition to α,β-Unsaturated Ketones 186
1.4.4.10 Addition to Conjugated Indolium Motifs 188
1.4.4.11 Additional Electrophilic Approaches 195
1.5 Metal-Based H_2S Probes 208
1.5.1 Metal Precipitation 208
1.5.1.1 Cu^{2+} Precipitation 209
1.5.1.2 Zn^{2+} Precipitation 227
1.5.1.3 Cd^{2+}/Hg^{2+} Precipitation 229
1.5.1.4 Other Metals 231
1.5.2 Metal Coordination 232
1.5.2.1 Small Molecules Approach 233
1.5.2.2 Protein Approaches 236
1.6 Fluorescent Probes for Sulfane Sulfur-Containing Species 238
1.6.1 Electrophilic Probes 239
1.6.1.1 *p*-Nitrofluorobenzene Cleavage 244
1.6.1.2 2-(Benzoylthio)benzoate Cleavage 247
1.6.1.3 Other Approaches 251
1.6.2 Nucleophilic Probes 258
1.6.3 Reduction-Based Probes 262
1.7 Conclusions and Future Perspectives 263
II. A CELL TRAPPABLE METHYL RHODOL-BASED FLUORESCENT PROBE FOR HYDROGEN SULFIDE DETECTION 267
2.1 Introduction 267

2.2 Results and Discussion 269
2.2.1 Probe Design and Synthesis 269
2.2.2 Spectroscopic Properties and Selectivity 270
2.2.3 Response to H_2S and Cell Trappability in Live Cells 271
2.3 Conclusion 274
2.4 Experimental Section 274
III. AN EXPANDED PALETTE OF FLUORESCENT H_2S-RELEASING DONORS FOR H_2S DELIVERY, DETECTION, AND IN VIVO APPLICATION 280
3.1 Introduction 280
3.2 Results and Discussion 282
3.2.1 Donor Synthesis 282
3.2.2 Spectroscopic Properties and Response to Thiol Activation 283
3.2.3 Selectivity to Sulfur, Nitrogen, and Oxygen Species 286
3.2.4 Application to Live Cells 287
3.2.5 Application to Alginate Hydrogels for In Vivo Imaging 288
3.3 Conclusion 290
IV. ESTERASE-ACTIVATED PERTHIOCARBONATE PERSULFIDE DONORS PROVIDE INSIGHTS INTO PERSULFIDE PERSISTENCE AND STABILITY ... 292
4.1 Introduction 292
4.2 Results and Discussion 294
4.2.1 Donor Design and Synthesis 294
4.2.2 Persulfide Release 295
4.2.3 Persulfide Donor Side Reactivity and Byproduct Investigation 300
4.2.4 Persulfide Persistence 302
4.3 Conclusion 303
4.4 Experimental Section 304
V. TRANSPERSULFIDATION OR H_2S RELEASE? UNDERSTANDING THE LANDSCAPE OF PERSULFIDE CHEMICAL BIOLOGY 312
5.1 Introduction 312
5.2 Results and Discussion 315
5.2.1 Computational Investigation of Persulfide Reactivity with Thiols 315
5.2.1.1 Effect of Electronic Effects on Persulfide Reactivity 316

5.2.1.2 Effect of Steric Substitutions on Persulfide Reactivity..... 318
5.2.2 Experimental Transpersulfidation Observation and Measurement..... 320
5.3 Conclusion 326
VI. CONCLUDING REMARKS..... 327
APPENDICES 329
A. CHAPTER II SUPPLEMENTARY INFORMATION 329
B. CHAPTER III SUPPLEMENTARY INFORMATION 343
C. CHAPTER IV SUPPLEMENTARY INFORMATION 391
D. CHAPTER V SUPPLEMENTARY INFORMATION 414
REFERENCES CITED..... 504

LIST OF FIGURES

Figure Page

1. **Figure 1.1**. Simplified schematic of mammalian H_2S production pathways. Involved intermediates and enzymes include S-adenosyl methionine (SAM), S-adenosyl-L-homocysteine (SAH), betaine homocysteine S-methyltransferase (BHMT), methionine synthase (MTR), cystathionine γ-lyase (CSE), homo-lanthionine (HLT), α-ketobutyrate (α-KB), cystathionine β-synthase (CBS), cystathionine (Cysth), cysteine aminotransferase (CAT), D-amino acid oxidase (DAO), 3-mercaptopyruviate (3MP), and 3-mercaptopyruvate (3-MST). 36
2. **Figure 1.2**. Annual publications (blue) and citations (orange) pertaining to fluorescent probes for hydrogen sulfide. Data from Web of Science. 38
3. **Figure 1.3**. Examples of common competing analytes for H_2S including reactive sulfur species (RSS), reactive selenium species (RSeS), reactive oxygen species (ROS), and reactive nitrogen species (RNS). 39
4. **Figure 1.4**. Early examples of fluorescent H_2S probes based on azide group reduction 43
5. **Figure 1.5**. (a) Fluorescent response of 10 μM **2** treated with 100 μM H_2S at 25 °C in 20 mM pH 7.4 PIPES buffer. Cell images of HEK293T cells in (b) the absence of **2**, (c) with **2** + 250 μM H_2S, and (d) brightfield overlay with the Hoechst nuclear dye. Reproduced and modified with permission from ref 88. Copyright 2011 American Chemical Society. 44
6. **Figure 1.6**. Examples of azide-based fluorescent H_2S probes based on 1,8-naphthalimides. 45
7. **Figure 1.7**. Examples of azide-based fluorescent H_2S probes based on *bis*-naphthalimides. 47
8. **Figure 1.8**. Examples of azide-based fluorescent H_2S probes based on xanthene dyes. 48
9. **Figure 1.9**. (left) Two-dimensional slices of light sheet fluorescent microscopy (LFSM) images of larval zebrafish gavaged with 5 μM **24** + 250 μM DATS + 250 μM GSH or **24** only. (right) Fluorescence quantification of larval zebrafish gavaged with different combinations of **24**, DATS, and GSH. Reproduced with permission from ref 111. Copyright 2015 American Chemical Society. 48
10. **Figure 1.10**. Examples of azide-based fluorescent H_2S probes based on BODIPY chromophores. 50
11. **Figure 1.11**. Examples of azide-based fluorescent H_2S probes based on coumarin, naphthalene, and related chromophores. 50
12. **Figure 1.12**. Additional examples of azide-based fluorescent H_2S probes based on various fluorophores. 53

13. **Figure 1.13**. Examples of azide-based fluorescent H_2S probes based on dicyanoisophorone and related conjugated systems. 54

14. **Figure 1.14**. Examples of azide-based fluorescent H_2S probes based on phthalimides. 55

15. **Figure 1.15**. Examples of azide-based fluorescent H_2S probes based on phenanthroimidazole. 56

16. **Figure 1.16**. Examples of azide-based fluorescent H_2S probes based on benzoxazole and benzothiazole 56

17. **Figure 1.17**. Examples of azide-based fluorescent H_2S probes based on conjugated and polyaromatic chromophores. 57

18. **Figure 1.18**. Additional examples of azide-based fluorescent H_2S probes based on various chromophores. 58

19. **Figure 1.19**. Examples of sulfonyl azide-based fluorescent H_2S probes. 59

20. **Figure 1.20**. Examples of self-immolative azide-based fluorescent H_2S probes. 61

21. **Figure 1.21**. Examples of self-immolative azide-based fluorescent H_2S probes based on ESIPT chromophores. 62

22. **Figure 1.22**. Examples of self-immolative azide-based fluorescent H_2S probes based on BODIPY chromophores. 62

23. **Figure 1.23**. Examples of self-immolative azide-based fluorescent H_2S probes that function at extended wavelengths. 63

24. **Figure 1.24**. Additional examples of self-immolative azide-based fluorescent H_2S probes that also report on changes in viscosity. 64

25. **Figure 1.25**. Examples of self-immolative "analyte replacement" azide-based fluorescent H_2S probes. 65

26. **Figure 1.26**. Additional examples of self-immolative azide-based fluorescent H_2S probes with various chromophores. 66

27. **Figure 1.27**. Examples of azide-based fluorescent H_2S probes that function through subsequent intramolecular cyclization to remove a protecting group. 68

28. **Figure 1.28**. (a) Selectivity of 10 μM **122** in response to 5 mM of H_2S and different analytes. (b,c) Corresponding visible and fluorescent response, respectively, of 50 μM **122** in response to different analytes. Reproduced with permission from ref 202. Copyright 2015 Royal Society of Chemistry. 68

29. **Figure 1.29**. Additional examples of azide-based fluorescent H_2S probes that function through subsequent intramolecular cyclization. 69

30. **Figure 1.30**. Examples of azide-based fluorescent H_2S probes that contain dual reaction sites to report on multiple types of species. 71

31. **Figure 1.31**. Fluorescent responses from **137** in zebrafish pretreated with NEM followed by different combination of Cys, Hcy, GSH, and H_2S. Reproduced with permission from ref 214. Copyright 2019 Elsevier. 72

32. **Figure 1.32**. Examples of azide-based fluorescent H_2S probes that function through FRET mechanisms..... 74

33. **Figure 1.33**. Examples of azide-based fluorescent H_2S probes based on coumarin / naphthalimide FRET pairs. 74

34. **Figure 1.34**. Examples of azide-based fluorescent H_2S probes based on naphthalimide / rhodamine FRET pairs. 75

35. **Figure 1.35**. Examples of azide-based fluorescent H_2S probes based on fluorescein isothiocyanates. 76

36. **Figure 1.36**. Additional examples of azide-based fluorescent H_2S probes that function through FRET mechanisms. 77

37. **Figure 1.37**. (top) Fluorescent images of **160** incubated with increasing amounts of H_2S in HeLa cells. (bottom) Linear relationship of the measured fluorescence ratio against H_2S concentration. Reproduced with permission from ref 232. Copyright 2020 Royal Society of Chemistry. 78

38. **Figure 1.38**. Examples of azide-based fluorescent H_2S probes targeted to the lysosome. 79

39. **Figure 1.39**. Examples of azide-based fluorescent H_2S probes targeted to the mitochondria. 81

40. **Figure 1.40**. Example of using probe **171** to investigate H_2S generation in a Parkinson's disease model. (a,b) Ratiometric fluorescence response from **171** in cultured astrocytes from WT and DJ-1-KO mice. (c) Quantification of CBS mRNA. (d) CBS and DJ-1 quantification. Reproduced with permission from ref 242. Copyright 2013 American Chemical Society. 81

41. **Figure 1.41**. Examples of azide-based fluorescent H_2S probes targeted to the endoplasmic reticulum and Golgi apparatus. 83

42. **Figure 1.42**. Additional examples of azide-based fluorescent H_2S probes based with different targeting groups..... 84

43. **Figure 1.43**. Examples of cell trappable azide-based fluorescent H_2S probes..... 86

44. **Figure 1.44**. Fluorescent response of (a,e) 5 μM **2**, (b,f) 5 μM **25**, (c,g) 2.5 μM **189**, and (d,h) 2.5 μM **190** in HUVECs. Panels (a-d) show the response after incubation for 30 minutes, and panels (e-h) show the response after further incubation for 60 minutes after replacing the media showing the enhanced cellular retention of **190**. Reproduced with from ref 112. Copyright 2013 National Academy of Science. 86

45. **Figure 1.45**. Examples of azide-based luminescent H_2S probes. 88

46. **Figure 1.46**. Examples of azide-based H_2S probes based on lanthanide luminescence. 89

47. **Figure 1.47**. Examples of fluorescent H_2S probes based on nitro group reduction. 91

48. **Figure 1.48**. Selectivity of 5 μM (a) nitro-naphthalimide **206** and (b) azido-naphthalimide **4** showed the significantly reduced selectivity of the nitro functional group toward high concentrations of Cys and GSH. Reproduced with permission from ref 90. Copyright 2012 Royal Society of Chemistry. 91

49. **Figure 1.49**. Additional examples of H_2S probes based on nitro group reduction with naphthalimide chromophores. 92

50. **Figure 1.50**. Additional examples of H_2S probes based on nitro group reduction with various chromophores. 93

51. **Figure 1.51**. Examples of H_2S probes based on nitro group reduction and intramolecular cyclization. 94

52. **Figure 1.52**. Additional examples of H_2S probes based on nitro group reduction with various chromophores. 94

53. **Figure 1.53**. Additional examples of H_2S probes based on nitro group reduction with hydrophobic chromophores. 95

54. **Figure 1.54**. Examples of H_2S probes based on reduction of nitroso and N-oxide groups 96

55. **Figure 1.55**. Examples of H_2S probes based on reduction of nitroso hydroxylamines. 97

56. **Figure 1.56**. Examples of H_2S probes based on reduction of tetrazines. 97

57. **Figure 1.57**. Examples of H_2S probes based on reduction of azo compounds. 98

58. **Figure 1.58**. Early examples of disulfide-based fluorescent probes for H_2S. 99

59. **Figure 1.59**. Additional examples of fluorescent H_2S probes based on disulfide cleavage and subsequent cyclization. 100

60. **Figure 1.60**. (a) Fluorescent response of 10 μM **255** with 1) control; 2) 50 μM NaSH; 3) 200 μM Cys; 4) 200 μM GSH; 5) 200 μM Hcy; 6) 200 μM Na_2SO_3; 7) 200 μM $Na_2S_2O_3$; 8) 50 μM NaSH + 200 μM Cys; 9) 50 μM NaSH + 200 μM GSH. (b) YZ-4-074 donor used for cell studies. Fluorescent response from **255** after incubation (c) with or (d) without 100 μM YZ-4-074. Reproduced and modified from ref 304. Copyright 2014 John Wiley and Sons. 100

61. **Figure 1.61**. Additional examples of fluorescent H_2S probes based on disulfide cleavage and subsequent cyclization with naphthalimide chromophores. 101

62. **Figure 1.62**. Additional examples of fluorescent H_2S probes based on disulfide cleavage and subsequent cyclization based on hydroxyflavone and coumarin chromophores. 102

63. **Figure 1.63**. Additional examples of fluorescent H_2S probes based on disulfide cleavage and subsequent cyclization. 103

64. **Figure 1.64**. Examples of fluorescent H_2S probes based on unsymmetric disulfide cleavage and subsequent cyclization. 104

65. **Figure 1.65**. Fluorescent images and associated quantification of H_2S detection using 10 μM **276** in Raw 264.7 cells pre-treated with either 2 μM fluvastatin or fluvastatin with PAG. Reproduced with permission from ref 323. Copyright 2015 Royal Society of Chemistry 105

66. **Figure 1.66**. Examples of fluorescent H_2S probes based on symmetric disulfide cleavage and subsequent cyclization. 105

67. **Figure 1.67**. Examples of fluorescent H_2S probes based on selenenyl sulfide cleavage and subsequent cyclization. 106

68. **Figure 1.68**. Additional examples of fluorescent H_2S probes based on selenenyl sulfide cleavage and subsequent cyclization..... 107

69. **Figure 1.69**. Examples of fluorescent H_2S probes based on alkyl selenenyl sulfide cleavage and subsequent cyclization..... 108

70. **Figure 1.70**. Examples of fluorescent H_2S probes based on diselenide cleavage and subsequent cyclization. 108

71. **Figure 1.71**. Examples of fluorescent H_2S probes based on selenoxide and sulfoxide reduction..... 110

72. **Figure 1.72**. Examples of fluorescent H_2S probes based on DNP cleavage with BODIPY chromophores. 112

73. **Figure 1.73**. Examples of fluorescent H_2S probes based on DNP cleavage with naphthalimide chromophores. 113

74. **Figure 1.74**. Examples of fluorescent H_2S probes based on DNP cleavage with coumarin chromophores..... 114

75. **Figure 1.75**. Examples of fluorescent H_2S probes based on DNP cleavage with Nile red and Nile blue chromophores. 115

76. **Figure 1.76**. Examples of fluorescent H_2S probes based on DNP cleavage with red-shifted chromophores. 117

77. **Figure 1.77**. Examples of fluorescent H_2S probes based on DNP cleavage with xanthene-based chromophores. 119

78. **Figure 1.78**. Examples of fluorescent H_2S probes based on DNP cleavage with cyanine-based chromophores. 121

79. **Figure 1.79**. Fluorescence imaging of endogenous H_2S in HCT116 tumor-bearing mice through tail vein injection of **369**, including (a) time course, (b) ex vivo fluorescence imaging of isolated organs, (c) time course fluorescence quantification, and (d) organ fluorescence quantification. Reproduced and

modified with permission from ref 400. Copyright 2021 American Chemical Society..... 121

80. **Figure 1.80**. Additional examples of fluorescent H_2S probes based on DNP cleavage with extended wavelength chromophores..... 122

81. **Figure 1.81**. Examples of fluorescent H_2S probes based on DNP cleavage with targeting groups. 124

82. **Figure 1.82**. Examples of fluorescent H_2S probes based on DNP cleavage with cationic chromophores. 125

83. **Figure 1.83**. Examples of fluorescent H_2S probes based on DNP cleavage with flavone-based chromophores. 127

84. **Figure 1.84**. Additional examples of fluorescent H_2S probes based on DNP cleavage with small molecule chromophores. 128

85. **Figure 1.85**. (top) Proposed mechanistic difference for the role of an *ortho* aldehyde in H_2S-mediated DNP cleavage. Bottom panels: (a) Reaction of **412** with 10 equiv. of H_2S. (b) Reaction of **413** with 10 equiv. of H_2S. (c,d) Selectivity of **413** for H_2S over competing analytes, including blank, HS^-, F^-, Cl^-, Br^-, I^-, SCN^-, CO_3^{2-}, AcO^-, NO_3^-, NO_2^-, PO_4^{3-}, HPO_4^{2-}, $H_2PO_4^-$, $S_2O_3^{2-}$, $S_2O_7^{2-}$, SO_4^{2-}, SO_3^{2-}, HSO_3^-, HSO_4^-, CN^-, GSH, Hcy, Cys, NAC, $C_6H_5NH_2$, $C_6H_5CH_2NH_2$, $H_2NCH_2CH_2NH_2$, and $HOCH_2CH_2NH_2$. Reproduced and modified with permission from ref 438. Copyright 2014 Royal Society of Chemistry..... 129

86. **Figure 1.86**. Examples of fluorescent H_2S probes based on DNP cleavage with benzothiazole and benzoxazole chromophores..... 130

87. **Figure 1.87**. Additional examples of fluorescent H_2S probes based on DNP cleavage..... 131

88. **Figure 1.88**. Additional examples of fluorescent H_2S probes based on DNP cleavage with amine-based chromophores. 132

89. **Figure 1.89**. Examples of fluorescent H_2S probes based on DNP cleavage and subsequent intramolecular cyclization..... 133

90. **Figure 1.90**. Examples of fluorescent H_2S probes based on DNP cleavage with AIE..... 134

91. **Figure 1.91**. Examples of luminescent H_2S probes based on DNP cleavage..... 135

92. **Figure 1.92**. Examples of fluorescent H_2S probes based on cleavage of DNP thioethers adjacent to esters. 136

93. **Figure 1.93**. Examples of fluorescent H_2S probes based on DNBS cleavage with BODIPY chromophores..... 137

94. **Figure 1.94**. Examples of fluorescent H_2S probes based on DNBS cleavage with coumarin and related chromophores..... 138

95. **Figure 1.95**. Examples of fluorescent H_2S probes based on DNBS cleavage with naphthalimide chromophores. 140

96. **Figure 1.96**. Additional examples of fluorescent H_2S probes based on DNBS cleavage with benzothiazole and related chromophores. 140

97. **Figure 1.97**. Examples of fluorescent H_2S probes based on DNBS cleavage with porphyrin and related chromophores. 141

98. **Figure 1.98**. Examples of fluorescent H_2S probes based on DNBS cleavage with xanthene based chromophores. 142

99. **Figure 1.99**. Examples of fluorescent H_2S probes based on DNBS cleavage with extended wavelength chromophores. 143

100. **Figure 1.100**. Additional examples of fluorescent H_2S probes based on DNBS cleavage 145

101. **Figure 1.101**. Examples of fluorescent H_2S probes based on DNBS cleavage with triphenylamine chromophores. 146

102. **Figure 1.102**. Examples of fluorescent H_2S probes based on DNBS cleavage with organelle targeting groups. 147

103. **Figure 1.103**. Examples of fluorescent H_2S probes based on 2,4-dinitrophenyl sulfonamides cleavage. 147

104. **Figure 1.104**. (a) General reactivity of NBD electrophiles with H_2S to generate NBD-SH. (b) Evolution from initial reported reactivity to fluorogenic ether-based probes to fluorogenic piperazine based systems with improved selectivity. 149

105. **Figure 1.105**. Examples of fluorescent H_2S probes based on NBD-ether cleavage with coumarin based chromophores. 150

106. **Figure 1.106**. Examples of fluorescent H_2S probes based on NBD-ether cleavage with benzothiazole based chromophores. 150

107. **Figure 1.107**. Additional examples of fluorescent H_2S probes based on NBD-ether cleavage. 151

108. **Figure 1.108**. Examples of fluorescent H_2S probes based on NBD-ether cleavage with xanthene based chromophores. 152

109. **Figure 1.109**. (top) Response mechanism from **543** in response to Cys/Hcy and GSH/H_2S. (bottom) Fluorescent response of **543** at 643 nm and 543 nm against different analytes, with Cys, Hcy, GSH, and H_2S highlighted. Reproduced and modified with permission from ref 562. Copywrite 2019 Royal Society of Chemistry. 153

110. **Figure 1.110**. Examples of fluorescent H_2S probes based on NBD-ether cleavage with BODIPY chromophores. 154

111. **Figure 1.111**. Examples of fluorescent H_2S probes based on NBD-ether

cleavage with extended wavelength chromophores. 155

112. **Figure 1.112**. (top) General reactivity of NBD-amines with H_2S. (bottom) Second order rate constants for the reaction of H_2S with different NBD amines. 157

113. **Figure 1.113**. Examples of fluorescent H_2S probes based on NBD-amine cleavage with coumarin based chromophores. 157

114. **Figure 1.114**. Examples of fluorescent H_2S probes based on NBD-amine cleavage with naphthalimide chromophores. 159

115. **Figure 1.115**. Additional examples of fluorescent H_2S probes based on NBD-amine cleavage. 159

116. **Figure 1.116**. Additional examples of fluorescent H_2S probes based on NBD-amine cleavage with fluorescein and rhodamine based chromophores. 161

117. **Figure 1.117**. Examples of fluorescent H_2S probes based on NBD-amine cleavage with BODIPY chromophores. 162

118. **Figure 1.118**. Additional examples of fluorescent H_2S probes based on NBD-amine cleavage with extended wavelength chromophores. 163

119. **Figure 1.119**. (a) Fluorescence response from FHC, HCT116, and HT29 cells treated with **593** and H_2S inhibitor AOAA. (b) Fluorescence response from FHC, HCT116, and HT29 cells treated with **593** and siRNAs for endogenous H_2S production. (d) In vivo images of mice with itratumoral injection of **593** differences from control (C1-C3) and tumor sites (T1-T3). (d) Quantified fluorescence from each site showing higher H_2S generation in T3 (HCT116) and T2 (HT29) tumoral sites. Reproduced and modified with permission from ref 612. Copywrite 2017 Royal Society of Chemistry. 163

120. **Figure 1.120**. Examples of fluorescent H_2S probes based on NBD-amine cleavage targeted to the lysosome. 164

121. **Figure 1.121**. Examples of fluorescent H_2S probes based on NBD-amine cleavage targeted to the ER. 165

122. **Figure 1.122**. Examples of fluorescent H_2S probes based on NBD-amine cleavage targeted to the mitochondria. 166

123. **Figure 1.123**. Examples of cell trappable fluorescent H_2S probes based on NBD-amine cleavage. 167

124. **Figure 1.124**. Examples of fluorescent H_2S probes based on NBD-amine cleavage with dual reactivity sites for other analytes. 168

125. **Figure 1.125**. Examples of fluorescent H_2S probes based on NBD-amine cleavage with additional H_2S reactive groups. 169

126. **Figure 1.126**. Examples of fluorescent H_2S probes based on tandem reactivity with an aldehyde and α,β-unsaturated ketone. 172

127. **Figure 1.127**. Competing pathways for addition of H_2S to aldehyde-containing α,β-unsaturated ketone systems. Reproduced with permission from ref 653. Copyright 2015 American Chemical Society. 172

128. **Figure 1.128**. Examples of fluorescent H_2S probes based on cleavage of 2-carboxybenzaldehyde esters. 174

129. **Figure 1.129**. Examples of fluorescent H_2S probes based on addition to electron poor styrenes. 176

130. **Figure 1.130**. Examples of fluorescent H_2S probes based addition to aliphatic electrophiles 177

131. **Figure 1.131**. Examples of fluorescent H_2S probes based on acrylates cleavage..... 178

132. **Figure 1.132**. Examples of fluorescent H_2S probes based on thiophene-2-carboxylic acid ester cleavage. 180

133. **Figure 1.133**. Examples of fluorescent H_2S probes based on cyanate ester and thiocyanate cleavage. 182

134. **Figure 1.134**. Examples of fluorescent H_2S probes based addition to electron poor conjugated systems and subsequent cyclization. 183

135. **Figure 1.135**. Examples of fluorescent H_2S probes based reductive cleavage followed by thiophene formation. 185

136. **Figure 1.136**. (a) Fluorescent images captured the H_2S distribution in *C. elegans* wild type N2 treated with 200 μM of **683**. (b) Fluorescence imaging of endogenous H_2S in wild type N2, germline-deficient glp-1 and cth-1 mutants. (c) Associated fluorescence intensities across the anterior of the intestine. Reproduced with permission from ref 704. Copywrite 2018 Royal Society of Chemistry. 185

137. **Figure 1.137**. Additional example of H_2S mediated reductive cleavage followed by thiophene formation to form a fluorescent product. 186

138. **Figure 1.138**. Examples of fluorescent H_2S probes based addition across an α,β-unsaturated ketone. 187

139. **Figure 1.139**. Examples of fluorescent H_2S probes based on addition into indolium motifs conjugated to coumarin chromophores. 188

140. **Figure 1.140**. (a-c) MCF-7 cells treated with 10 μM of **696** and mitochondrial marker Deep red. (a) Pseudocolor image of 660-750 nm band excited at 488 nm, (b) image of 660-750 band exciting at 633 nm, and (c) overlay channels. (d-k) Images of MCF-7 cells monitoring dual emission mode of excitation at 488 nm. (d,f) Include incubation with 10 μM of **696**. (g-i) Include pre-incubation with 10 μM of **696** followed by 200 μM of NaSH. Panels (d,g) correspond to 500-560 nm), (e,h) correspond to 650-799 nm, and (f,i) correspond to ratiometric images. Panels (j) and (k) show temporal profiles of area of interest 'D' and other

regions, respectively. Reproduced with permission from ref 715. Copyright 2013 John Wiley and Sons. 189

141. **Figure 1.141**. Additional examples of fluorescent H_2S probes based on addition into indolium motifs conjugated to coumarin chromophores. 190

142. **Figure 1.142**. Additional examples of fluorescent H_2S probes based on addition into indolium motifs. 191

143. **Figure 1.143**. Additional examples of fluorescent H_2S probes based on addition into indolium motifs conjugated to chromophores. 192

144. **Figure 1.144**. Examples of fluorescent H_2S probes based on addition into indolium motifs with an AIE response. 192

145. **Figure 1.145**. Additional examples of fluorescent H_2S probes based on addition into indolium motifs with additional reactivity. 193

146. **Figure 1.146**. Examples of fluorescent H_2S probes based on addition into conjugated benzothiazolium motifs. 194

147. **Figure 1.147**. Examples of H_2S addition to a spiropyran based system. 195

148. **Figure 1.148**. Examples of fluorescent H_2S probes based addition to electron poor alkenes. 196

149. **Figure 1.149**. Example of an H_2S probe based on H_2S reaction with a 2,3-dicarbonitrile motif. 197

150. **Figure 1.150**. Examples of fluorescent H_2S probes based addition to an alkenes to modify hydrogen bonding. 198

151. **Figure 1.151**. Examples of fluorescent H_2S probes based addition to imines. ... 199

152. **Figure 1.152**. Examples of fluorescent H_2S probes based on ebselen derivatives. 200

153. **Figure 1.153**. Additional examples of electrophilic fluorescent H_2S probes operating by various mechanisms. 201

154. **Figure 1.154**. Additional examples of electrophilic fluorescent H_2S probes operating by various mechanisms. 202

155. **Figure 1.155**. Examples of fluorescent H_2S probes based on addition to pyrilium motifs 204

156. **Figure 1.156**. Examples of fluorescent H_2S probes based cleavage of BODIPY selenoethers. 205

157. **Figure 1.157**. Example of a fluorescent H_2S probe based on cleavage of a BODIPY thioether. 206

158. **Figure 1.158**. (top) Schematic of **780** reacting with both H_2S and NO. (bottom) Colonic smooth muscle cells treated with DEA·NONOate followed by **780** and NaSH in cycle 1. Cycle 2 included additional treatment with DEA·NONOate

and NaSH. Reproduced with permission from ref 786. Copyright 2021 John Wiley and Sons. 206

159. **Figure 1.159**. Additional examples of fluorescent H_2S probes based on addition to BODIPY electrophiles. 207

160. **Figure 1.160**. Examples of fluorescent H_2S probes based on electrophilic coumarins. 208

161. **Figure 1.161**. Examples of fluorescent H_2S probes based on Cu^{2+} precipitation from functionalized cyclen ligands. 210

162. **Figure 1.162**. (left) Response from **787** upon treatment with H_2S and GSH. (right) Fluorescent response of **787** in HeLa cells treated with exogenous H_2S. Reproduced with permission from ref 794. Copywrite 2011 American Chemical Society..... 210

163. **Figure 1.163**. Examples of fluorescent H_2S probes based on Cu^{2+} precipitation from other macrocyclic ligands. 212

164. **Figure 1.164**. Examples of fluorescent H_2S probes based on Cu^{2+} precipitation from functionalized di(picolyl)amine and related ligands. 213

165. **Figure 1.165**. Examples of fluorescent H_2S probes based on Cu^{2+} precipitation from functionalized quinoline and related pyridine ligands. 214

166. **Figure 1.166**. Examples of fluorescent H_2S probes based on Cu^{2+} precipitation Cu^{2+}-binding peptides ligated with fluorescein chromophores. Cu^{2+} ions have been omitted for clarity because local coordination environments were not identified. 215

167. **Figure 1.167**. Examples of fluorescent H_2S probes based on metal precipitation metal-binding peptides ligated with dansyl chromophores. Metal ions have been omitted for clarity because local coordination environments were not identified. 217

168. **Figure 1.168**. Examples of fluorescent H_2S probes based on Cu^{2+} precipitation with luminescent reporters. 218

169. **Figure 1.169**. Examples of fluorescent H_2S probes based on Cu^{2+} precipitation from hydrazine and hydrazide ligands tethered to xanthene-based chromophores. 220

170. **Figure 1.170**. Additional examples of fluorescent H_2S probes based on Cu^{2+} precipitation from hydrazine and hydrazide ligands containing various chromophores. 220

171. **Figure 1.171**. Examples of fluorescent H_2S probes based on Cu^{2+} precipitation from hydrazine and hydrazide ligands with a 2:1 ligand to Cu^{2+} stoichiometry..... 221

172. **Figure 1.172**. Examples of fluorescent H_2S probes based on Cu^{2+} precipitation from imine-based ligands..... 222

173. **Figure 1.173**. Examples of fluorescent H_2S probes based on Cu^{2+} precipitation benzimidazole, triazole, and benzothiazole ligands. 223

174. **Figure 1.174**. Examples of fluorescent H_2S probes based on Cu^{2+} precipitation from other nitrogen-based coordination environments. 225

175. **Figure 1.175**. Examples of fluorescent H_2S probes based on Cu^{2+} precipitation from oxygen-based ligands. 226

176. **Figure 1.176**. (top) Response of **887** upon addition of Cu^{2+} and H_2S. (bottom) Example of the fluorescent response of **887** in HeLa cells upon addition of Cu^{2+} followed by H_2S. Reproduced with permission from ref 897. Copywrite 2019 Elsevier. 227

177. **Figure 1.177**. Examples of fluorescent H_2S probes based on Zn^{2+} precipitation. 228

178. **Figure 1.178**. Examples of fluorescent H_2S probes based on Cd^{2+} precipitation. 230

179. **Figure 1.179**. (top) Ratiometric response from **899** in response to H_2S. (bottom) Change in cellular fluorescence after treatment of HeLa cells incubated with **900** with H_2S. Reproduced with permission from ref 908. Copyright 2014 John Wiley and Sons. 230

180. **Figure 1.180**. Examples of fluorescent H_2S probes based on Hg^{2+} precipitation. 231

181. **Figure 1.181**. Examples of fluorescent H_2S probes based on precipitation of other metals. 232

182. **Figure 1.182**. Examples of Zn^{2+} complexes that bind HS^- to provide a change in fluorescence response. 233

183. **Figure 1.183**. Additional examples of Zn^{2+} complexes investigated for HS^- binding to generate a fluorescence response. 234

184. **Figure 1.184**. (top) Change in fluorescent response from **915** upon addition of H_2S and acetic acid. (bottom) Fluorescent response from HepG2 cells treated with (a) no addition, (b) 120 μM of **923**, (b)120 μM of **923**-SH, and (d) 120 μM of **923** with 250 μM NaSH. Reproduced with permission from ref 928. Copyright 2020 American Chemical Society. 235

185. **Figure 1.185**. Additional examples of metal complexes used to investigate coordinative approaches for H_2S detection. 236

186. **Figure 1.186**. (a) General schematic for **936** in which a turn-on fluorescent response is generated using the change in rHbI absorbance upon H_2S binding to modulate the fluorescence of a Pacific Blue fluorophore. (b) General selectivity of **936** against competing species, and (c) demonstration of reversibility up purging with Ar. Reproduced with permission from ref 941. Copyright 2018 American Chemical Society. 237

187. **Figure 1.187**. (left) Copper site in Cu-azurin. (b) Fluorescence response of Atto 620-labelled Cu-azurin **938** after addition of 50 μM NaSH and 80 μM $K_3[Fe(CN)_6]$. Reproduced with permission from ref 943. Copyright 2019 American Chemical Society. 238

188. **Figure 1.188**. Early examples of fluorescent H_2S_n probes based on cleavage of *p*-nitrofluorobenzene esters. 240

189. **Figure 1.189**. Additional examples of fluorescent H_2S_n probes based on cleavage of *p*-nitrofluorobenzene esters. 240

190. **Figure 1.190**. Examples of fluorescent H_2S_n probes based on cleavage of *p*-nitrofluorobenzene esters with BODIPY chromophores. 241

191. **Figure 1.191**. Examples of fluorescent H_2S_n probes based on cleavage of *p*-nitrofluorobenzene esters with naphthalimide chromophores. 242

192. **Figure 1.192**. Examples of fluorescent H_2S_n probes based on cleavage of *p*-nitrofluorobenzene esters with ratiometric responses. 243

193. **Figure 1.193**. Additional examples of fluorescent H_2S_n probes based on cleavage of *p*-nitrofluorobenzene esters. 245

194. **Figure 1.194**. Examples of fluorescent H_2S_n probes based on cleavage of *p*-nitrofluorobenzene esters with extended wavelengths. 246

195. **Figure 1.195**. Examples of fluorescent H_2S_n probes based on thioesters cleavage and subsequent cyclization using xanthene based chromophores. 248

196. **Figure 1.196**. (top) General strategy for developing different fluorescent responses from both an H_2S_n and H_2S reactive site. (bottom) Blue (a-d) and green (e-h) channels of HeLa incubated with **984** followed by treatment with (a,e) vehicle; (b,f) Na_2S; (c,g) Na_2S and NaOCl; (d,h) Na_2S_2. Reproduced with permission from ref 989. Copyright 2016 John Wiley and Sons. 249

197. **Figure 1.197**. Additional examples of fluorescent H_2S_n probes based on thioesters cleavage and subsequent cyclization. 250

198. **Figure 1.198**. Additional examples of fluorescent and luminescent H_2S_n probes based on thioesters cleavage and subsequent cyclization. 251

199. **Figure 1.199**. Examples of chemically reversible probes for H_2S_n/HSSR detection based on nucleophilic addition to a fluorophore core. 252

200. **Figure 1.200**. (top) Schematic of the reactivity of **998** with per-/poly-sulfides. (middle) Ratio images at different time points of the response from A549 cells treated with **998** followed by addition cycles of BnSSH and NEM. (bottom) Quantified fluorescent response at ratio after different cycles of BnSSH and NEM addition. Reproduced with permission from ref 1001. Copyright 2018 John Wiley and Sons. 252

201. **Figure 1.201**. Examples of fluorescent H_2S_n probes based on cleavage of α,β-unsaturated esters. 254

202. **Figure 1.202**. Examples of fluorescent H_2S_n probes based on addition to electron poor vinyl coumarins and subsequent cyclization. 255

203. **Figure 1.203**. Examples of fluorescent H_2S_n probes that provide different responses for H_2S_n and GSH. 255

204. **Figure 1.204**. Examples of fluorescent H_2S_n probes based on ester cleavage. ... 256

205. **Figure 1.205**. Examples of fluorescent H_2S_n probes based on cleavage of substituted nitrobenzenesulfonyl groups 257

206. **Figure 1.206**. Examples of NBD ether probes for the discrimination of GSH, Cys/Hcy, and H_2S_n. 257

207. **Figure 1.207**. Examples of fluorescent H_2S_n probes based on nucleophilic thiol addition to sulfane sulfur species and subsequent cyclization using xanthene based chromophores 259

208. **Figure 1.208**. (top) Brightfield (A, D), fluorescence (B, E), and overlaid Images (C, F) of HeLa cells treated with **1032** and Na_2S_2. (bottom) Differences in fluorescence from normal COS-7 and CSE overexpressing cells and also normal and CARS2 KO HEK293T cells. Reproduced with permission from ref 1017. Copyright 2022 Elsevier. 260

209. **Figure 1.209**. Nucleophilic probes based on sulfane sulfur mediated spirocyclization. 260

210. **Figure 1.210**. Examples of fluorescent H_2S_n probes based on nucleophilic selenol addition to sulfane sulfur species and subsequent cyclization using xanthene based chromophores. 261

211. **Figure 1.211**. Examples of fluorescent H_2S_n probes based on nitro group reduction. 263

212. **Figure 1.212**. H_2S_n-mediated reduction of **1049**. 263

213. **Figure 2.1**. (a) Prior rhodamine-based cell-trappable H_2S probes based on azide reduction and associated fluorescent responses for H_2S (F/F_0). (b) This work reports a cell-trappable methylrhodolazide-based H_2S probe, **CT-MeRhoAz**. 268

214. **Figure 2.2**. Synthesis of **CT-MeRhoAz**. Structures are shown in the closed lactone tautomer for simplicity. 270

215. **Figure 2.3**. Fluorescence turn-on of **CT-MeRhoAz** (5 μM) in response to H_2S (250 μM NaSH, 50 equiv.) in 50 mM PIPES buffer (100 mM KCl, pH 7.4) at 37 °C. λ_{ex} = 480 nm, λ_{em} = 490–650 nm. Slit width: 0.4 mm. The experiments were performed in triplicate and results are expressed as mean ± SD (n = 3). 271

216. **Figure 2.4**. Selectivity of **CT-MeRhoAz** (5 μM) in the presence of competing analytes (250 μM, 50 equiv.) including NaSH, L-cysteine, DL-homocysteine, glutathione, $Na_2S_2O_3$, Na_2SO_3, Na_2SO_4, H_2O_2, KO_2, DEANONOate, $NaNO_2$, and 5 mM glutathione, respectively. λ_{ex} = 480 nm, λ_{em} = 490–640 nm. The

experiments were performed in triplicate and results are expressed as mean ± SD (*n* = 3). 272

217. **Figure 2.5**. Fluorescence imaging of **CT-MeRhoAz** in HeLa cells. Cells were incubated with 5 μM **CT-MeRhoAz** for 45 minutes with either (a) vehicle, (b) pre-treatment with 20 μM AOAA for 45 minutes, or (c) post-treatment with 200 μM NaSH for 45 minutes and then imaged. Barscale: 50 μm. 272

218. **Figure 2.6**. Cell trappability experiments of (a) **CT-MeRhoAz** and (b) MeRhoAz in HeLa cells. Cells were incubated with AP39 (100 nM) for 1 hour and then incubated with the probe (5 μM) for 45 minutes. Cells were washed with fresh media every 10 minutes and imaged at 5, 30, and 60 minutes. Bar scale: 50 μm. 273

219. **Figure 3.1**. (a) Selected small molecule fluorogenic COS/H_2S donors that incorporate different fluorophores and H_2S-releasing scaffolds. (b) Activation mechanism for COS/H_2S and fluorophore (FL) release from donors **1**–**5**..... 281

220. **Figure 3.2**. Synthetic pathway of fluorogenic COS/H_2S donors **1**–**5**..... 283

221. **Figure 3.3**. Fluorescence response (F/F_0) and H_2S release from COS/H_2S donors (a) **1**, (b) **2**, (c) **3**, (d) **4**, and (e) **5**. General conditions: **1**–**3** or **5** (10 μM) with Cys (100 μM) and CA (25 μg mL^{-1}) in PBS buffer (10 mM, pH 7.4) at 25 °C. Donor **4**: (50 μM) with Cys (500 μM) and CA (50 μg mL^{-1}) in PBS buffer (10 mM, pH 7.4) at 25 °C. The experiments were performed in triplicate and results are expressed as mean ± SD (*n* = 3). The buffer for donors **4** and **5** also contained a 1.0 mM CTAB additive..... 285

222. **Figure 3.4**. Normalized fluorescence turn-on (F/F_0) of donor **3** (10 μM) upon incubation with analytes (100 μM) for 120 minutes in PBS buffer (10 mM, pH 7.4). Conditions from left to right: blank, PLE, CA, Cys + CA, Cys, Hcy, NAC, GSH, Pen, SO_3^{2-}, Ser, Lys, Gly, GSSG, O_2^{-}, H_2O_2, and SO_4^{2-}. λ_{ex} = 350 nm, λ_{em} = 370–600 nm, T = 25 °C, slit width = 2 nm. The experiments were performed in triplicate and results are expressed as mean ± SD (*n* = 3). 287

223. **Figure 3.5**. Live-cell imaging of fluorescence turn-on COS/H_2S donors **1**–**5** showing concurrent H_2S release and fluorescence turn-on. (a) Differential interference contrast (DIC) overlaid with Hoechst 33342 (5 μM) or NucRed (2 μM). (b) H_2S probe CT-MeRhoAz (2.5 μM) confirming cellular H_2S release. (c) COS/H_2S donor **1** (50 μM) and **2**–**5** (20 μM). Bar scale: 50 mm. 288

224. **Figure 3.6**. Live rat imaging of fluorescence turn-on COS/H_2S donor **5** loaded into alginate gels. (a) Alginate gels containing **5** (250 μM) before GSH tail vein injection and 180 minutes after GSH injection. Regions of interest are labeled with red circles. (b) Average radiant efficiency of alginate gels loaded with DMSO, DMSO with GSH, donor **5**, and donor **5** with GSH at 0 or 180 minutes. The experiments were performed in quadruplicate and results are expressed as mean ± SD (*n* = 4). **p < 0.001. 290

225. **Figure 4.1**. Perthiocarbonate reaction pathways when activated by (a) thiols,

(b) base, or (c) esterase. 294

226. **Figure 4.2**. General conditions for preparing persulfide donors **1**–**9** starting from either (a) chlorocarbonylsulfenyl chloride or (b) methoxycarbonylsulfenyl chloride. (c) Persulfide donors synthesized. 295

227. **Figure 4.3**. (a) Persulfide trapping assay with FDNB. (b) Synthetic route to prepare RSS-DNB adducts **10**–**16**. 297

228. **Figure 4.4**. Persulfide release from (a) persulfide donors **1**–**3** and (b) persulfide donors **1** and **4**–**6**. Experiments were performed in triplicate with results expressed in mean ± standard deviation (*n* = 3). 298

229. **Figure 4.5**. HPLC chromatograms showing (a) FDNB trapping assay results with persulfide donor **1** after 30 minutes, (b) 50 μM BnSS-DNB adduct, and (c) 50 μM benzyl trisulfide. In chromatogram (a) the peak at 3.096 minutes corresponds to residual persulfide donor **1**. 299

230. **Figure 4.6**. Alternate reaction pathways of persulfides produced by perthio-carbonate-based persulfide donors. All compounds are shown in the neutral state for simplicity. Pathways (a), (b), and (c) are likely most prevalent for high persulfides concentrations, small R^2 groups, and larger R^2 groups, respectively. 301

231. **Figure 4.7**. Investigation of persistence of persulfides released from donors **1** and **5**–**6** by use of the FDNB trapping assay (FT) or the modified FDNB trapping assay (MFT). Experiments were performed in triplicate with results expressed in mean ± standard deviation (*n* = 3). 303

232. **Figure 5.1**. Methods employed to generate persulfides *in situ* including (a) reaction of disulfides with H_2S, (b) reaction of trisulfides with thiols, or (c) persulfide donors activated by a specific trigger. (d) Examples of persulfide donors that are activated by hydrogen peroxide, esterase, light, S- to N-acyl transfer, or superoxide. 314

233. **Figure 5.2**. Activation and reaction free energies (kcal mol^{-1}) for H_2S release or transpersulfidation of substituted aryl persulfides with methyl thiolate..... 317

234. **Figure 5.3**. Hammett linear free energy relationship of the (a) thermodynamic and (b) kinetic preferences for transpersulfidation and H_2S release..... 318

235. **Figure 5.4**. Activation and reaction free energies (kcal mol^{-1}) for H_2S release or transpersulfidation of alkyl persulfides with methyl thiolate. 319

236. **Figure 5.5**. Computed H_2S release and transpersulfidation transition structures (TSs) for cysteine (Cys) and penicillamine (Pen) systems. 320

237. **Figure 5.6**. Computationally derived energetics of the reaction between the persulfide donor scaffold and cysteine thiolate at either the S^1, S^2, or carbonyl carbon position and (b) the generated penicillamine-based persulfide with cysteine thiolate at either the S^1 or S^2 positions. Calculations were performed at the ωB97X-D/aug-cc-pVDZ/SMD(water) // ωB97X-D or (M06-2X)/aug-cc-

pV(T+d)Z /SMD(water) level of theory. Free energies (in kcal mol^{-1}) of reaction are relative to the preceding intermediate. 323

238. **Figure 5.7**. (a) Proposed reaction pathway of the persulfide donor **1** with excess **2**. After treatment with the TME-IAM trapping agent, persulfides, thiols, and other hydrosulfide species form stable adducts. (b) Stacked HPLC chromatograms of the TME-IAM trapping experiment with persulfide donor **1** (100 μM), **2** (1.0 mM), and TME-IAM (10 mM) and (c) peak area plotted of identified compounds over 60 minutes. 324

239. **Figure 5.8**. (a) Hydrogen sulfide release vs. persulfide **3** and **6** release from persulfide donor **1** (100 μM) when treated with 2 (1.0 mM) compared over 60 minutes. Persulfide **3** and **6** were quantified with a calibration curve of the persulfide adduct analogues. (b) Hydrogen sulfide release from persulfide donor **1** (100 μM) when treated with **2** (1.0 mM) or **5** (1.0 mM) monitored at 670 nm by the methylene blue H_2S assay over 60 minutes in PBS buffer (10 mM, pH 7.4). 325

LIST OF TABLES

Table Page

1. **Table 3.1**. Spectroscopic properties of donors **1**–**5** and the corresponding fluorophores. 284

2. **Table 4.1**. Persulfide release from persulfide donors **1**–**6**. 298

LIST OF SCHEMES

Scheme Page

1. **Scheme 1.1**. General reaction of aryl azides with H_2S to form an amine. 42
2. **Scheme 1.2**. General pathway for coupling azide reduction to self-immolation cascades..... 60
3. **Scheme 1.3**. General pathway for azide reduction followed by intramolecular reaction..... 67
4. **Scheme 1.4**. General reaction of nitro group reduction by H_2S to form an amine..... 90
5. **Scheme 1.5**. General reaction of oxidized nitrogen-containing groups with H_2S to form an amine. 95
6. **Scheme 1.6**. Reactivity of an unsymmetric pyridyl disulfide with H_2S to remove a protecting group. 99
7. **Scheme 1.7**. H_2S-mediated reduction of selenoxides. 109
8. **Scheme 1.8**. General reaction scheme for cleavage of a 2,4-DNP group by H_2S. 111
9. **Scheme 1.9**. H_2S-medated DNP cleavage followed by intramolecular cyclization. 133
10. **Scheme 1.10**. Removal of DNBS protecting groups with H_2S. 137
11. **Scheme 1.11**. H_2S detection based on addition to an aldehyde and further cyclization. 171
12. **Scheme 1.12**. Addition of H_2S to an aldehyde and subsequent ester cleavage. 173
13. **Scheme 1.13**. Addition of H_2S to an electron poor styrene and subsequent ester cleavage..... 175
14. **Scheme 1.14**. Addition of H_2S to benzyl electrophiles and subsequent ester cleavage..... 176
15. **Scheme 1.15**. H_2S-mediated cleavage of thiophene-2-carboxylic acid esters..... 179
16. **Scheme 1.16**. H_2S-mediated deprotection of electrophilic cyanate esters. 181
17. **Scheme 1.17**. General approach for H_2S addition to electron poor conjugated systems and subsequent cyclization. 183
18. **Scheme 1.18**. General approach for H_2S addition to an α,β-unsaturated ketone. 186
19. **Scheme 1.19**. General approach H_2S addition into conjugated indolium motifs. 188
20. **Scheme 1.20**. General approach of H_2S addition to electron poor alkenes. 196

21. **Scheme 1.21**. Addition of H_2S to pyrilium cations. 203

22. **Scheme 1.22**. Schematic of H_2S-mediated precipitation from a metal-binding motif. 209

23. **Scheme 1.23**. General approach for developing responsive systems upon H_2S/ HS^- coordination to a metal. 232

24. **Scheme 1.24**. General approach for H_2S_n detection using *p*-nitrofluorobenzene electrophiles. 240

25. **Scheme 1.25**. General approach for H_2S_n detection by cleavage of 2-(benzoyl-thio)benzoate groups followed by intramolecular cyclization. 248

26. **Scheme 1.26**. Addition of H_2S_n or hydropolysulfides (RSSH) to pyrilium cations. 251

27. **Scheme 1.27**. Addition of H_2S_n to α,β-unsaturated esters and resultant cleavage 253

28. **Scheme 1.28**. Addition of H_2S_n to electron poor vinyl coumarins and subsequent cyclization. 254

29. **Scheme 1.29**. General approach to use nucleophilic probes for H_2S_n detection. 258

30. **Scheme 1.30**. General reaction of aryl nitro groups with H_2S_n to form an amine. 262

31. **Scheme 5.1**. Comparison of attack at the sulfenyl sulfur to generate a disulfide and H_2S and at the sulfhydryl sulfur to undergo a transpersulfidation reaction. RSS are shown in their neutral form for simplicity. 313

32. **Scheme 5.2**. Reactivity of the penicillamine-based acyl perthiol donor platform. Persulfide donor **1** with thiol **2** releases persulfide **3** that further react to release H_2S or can be trapped by treatment with trapping agent TME-IAM to form a stable persulfide adduct. 321

I. ACTIVITY-BASED FLUORESCENT PROBES FOR HYDROGEN SULFIDE AND RELATED REACTIVE SULFUR SPECIES

This chapter includes previously published and co-authored material from Fosnacht, K.G.; Pluth, M.D. Activity-Based Fluorescent Proves for Hydrogen Sulfide and Related Reactive Sulfur Species. *Chem. Rev.* **2024**, *124*, 4124–4257. This manuscript was written by Kaylin G. Fosnacht and Professor Michael D. Pluth.

1.1 Introduction

1.1.1 Background

Hydrogen sulfide (H_2S) is fundamentally intertwined with life on Earth. Prior to the rise of O_2 in Earth's atmosphere, H_2S functioned as a required primordial energy source and structural component of early life.[1] Remnants of the early role of H_2S in anoxygenic photosynthesis are still seen today in anerobic photosynthetic green and purple sulfur bacteria.[2-4] Similarly, the ability of H_2S to form transition metal sulfides, such as sphalerite (ZnS) and iron sulfur minerals and clusters (FeS_2, Fe_2S_2, Fe_3S_4, Fe_4S_4, etc.), likely provided early structural motifs and catalysts capable of carrying out organic transformations including electron transfer reactions and C-H bond activation.[5-8] Vestigial remnants of this past are found in present-day iron sulfur clusters cofactors that mediate electron transfer in contemporary biology, including within the mitochondrial respiratory chain.

Now most known for its characteristic "rotten egg" smell, H_2S is found in natural sources including volcanos, hot springs, and natural gas deposits, with the anaerobic microbial breakdown of organic matter by sulfate-reducing bacteria also providing a significant source of sulfide.[9] Contemporary anthropogenic sources of H_2S primarily stem from industrialization and agriculture, with modern oil production, urban sewage systems, and large-scale farming all contributing to H_2S generation, release, and exposure.[10] Highlighting this prevalence, poisonings by acute exposure to H_2S are still the second most common cause of fatal gas inhalation in occupational settings.[10-12] Even low ppm levels of H_2S can lead to nausea, with 20-50 ppm leading to ocular inflammation and lung irritation, 100-150 ppm leading to olfactory fatigue or paralysis, and 500+ ppm levels leading to possible pulmonary edema, serious ocular damage, immediate collapse, and/or death.[11] This significant toxicity profile may also explain the sub-ppm human olfactory threshold for H_2S

detection. Much of the toxicity of H_2S is linked to binding and inhibition of cytochrome c oxidase (complex IV) in the mitochondrial electron transport chain, which leads to disrupted cellular respiration and energy production.[13-16] When taken together, natural and anthropogenic H_2S generation coupled with the high toxicity has led to H_2S being viewed primarily as an industrial and environment toxic pollutant for most of recent history.

The perception of H_2S solely as a toxin began to change in the mid-20th century when better molecular understandings of possible pathways for endogenous H_2S generation and sulfur metabolism were beginning to emerge.[17, 18] This shift may not be overly surprising because natural sulfur-rich spring water has been used since ancient times in balneotherapy to treat skin, inflammation, and musculoskeletal conditions.[19, 20] Similarly, the health benefits of cruciferous vegetables, alliums, mushrooms, and other traditional medicine-based remedies, many of which contain organosulfur compounds capable of releasing H_2S, have been known for centuries.[21-23] The more widespread acknowledgement and appreciation of H_2S as a potentially important biomolecule was accelerated dramatically in 1996, when Abe and Kimura discovered that H_2S functions as an endogenous neuromodulator.[24] Since this discovery, the multifaceted roles that H_2S plays in mammalian biology and physiology have expanded exponentially and ushered in a new need for model systems, investigative tools, and systems-level understanding of how H_2S and related reactive sulfur species (RSS) participate in complex biological processes.

1.1.2 Properties and Biological Synthesis

H_2S is now a well-established small molecule bioregulator and joins nitric oxide (NO) and carbon monoxide (CO) in a group of molecules often referred to as "gasotransmitters."[20, 25-27] These endogenously produced gaseous molecules act on molecular targets at physiologically relevant concentrations within the organism of generation and have emerged as important targets for biological investigation and intervention. When compared to NO and CO, H_2S provides unique physical properties that differentiate it from other small molecule bioregulators. For example, H_2S is a weak acid with $pK_a(1) = 7.0$ and $pK_a(2) > 14$ for the equilibria $H_2S \rightleftharpoons HS^- + H^+$ and $HS^- \rightleftharpoons S^{2-} + H^+$, respectively, meaning that most (~80%) of H_2S is in the monoanionic HS^- form at physiological pH. Although S^{2-} was previously assumed to be a minor component of this equilibrium, recent work has demonstrated that S^{2-} is unlikely to exist in aqueous solution.[28] The ability of H_2S to readily equilibrate between H_2S and HS^- under physiological conditions means

that protonation can be used to modulate both the lipophilicity and nucleophilicity of this important molecule. As an example of this importance, the equilibrium speciation favors the more highly-reactive HS^- form in the slightly alkaline mitochondrial matrix (pH ~7.8-8), whereas the diprotic H_2S form is greatly favored in the acidic lysosome (pH ~4.5-5.5). Throughout this Review, we will use the term "H_2S" to describe the totality of the H_2S + HS^- distribution found in water, unless a specific protonation state is needed for clarity or differential reactivity.

Adding to the complexity of different protonation states, H_2S is only one component of a broader landscape of RSS that encompasses sulfur oxidation states from -2 to +6. H_2S, thiols, and sulfur atoms in iron sulfur clusters are examples of RSS in the -2 oxidation state. The activity of these species is inexorably linked with "redox labile" or "sulfane sulfur" RSS in the -1 and 0 oxidation states, with common examples including persulfides (RSSH), inorganic polysulfides ($H_2S_{n\geq2}$), hydropolysulfides ($RS_{n\geq2}H$), and organic polysulfides ($R_2S_{n>2}$). These sulfane sulfur species constitute both important storage platforms for reductant-labile sulfide and also contribute directly to both the protective and signaling roles of RSS.[29-31]

Endogenous H_2S production stems from both enzymatic and non-enzymatic pathways. Mammalian enzymatic production of H_2S mainly occurs during the transsulfuration pathway that involves the interconversion of methionine and cysteine by the pyridoxal-5′-phosphate (PLP)-dependent enzymes cystathionine β-synthase (CBS) and cystathionine γ-lyase (CSE) (Figure 1.1).[32-35] The enzyme 3-mercaptopyruvate (3-MST) along with either cysteine aminotransferase (CAT) or D-amino acid oxidase (DAO) is also involved in H_2S production, although likely contribute less to the H_2S pool than CBS or CSE.[36-38] In general, these enzymes use L-cysteine (Cys), homocysteine (Hcy), and/or cystine as substrates for H_2S generation.[39] Our focus will be on mammalian systems, but H_2S production in bacteria and plants is well established, with microbial H_2S generation contributing significantly to H_2S production in the gut.[40-42] Non-enzymatic H_2S production pathways are also prevalent, with many of such pathways stemming from the reduction of redox-labile sulfide sources, like polysulfides, persulfides, thiosulfate, and related molecules, by glutathione (GSH) or other cellular reductants.[43, 44]

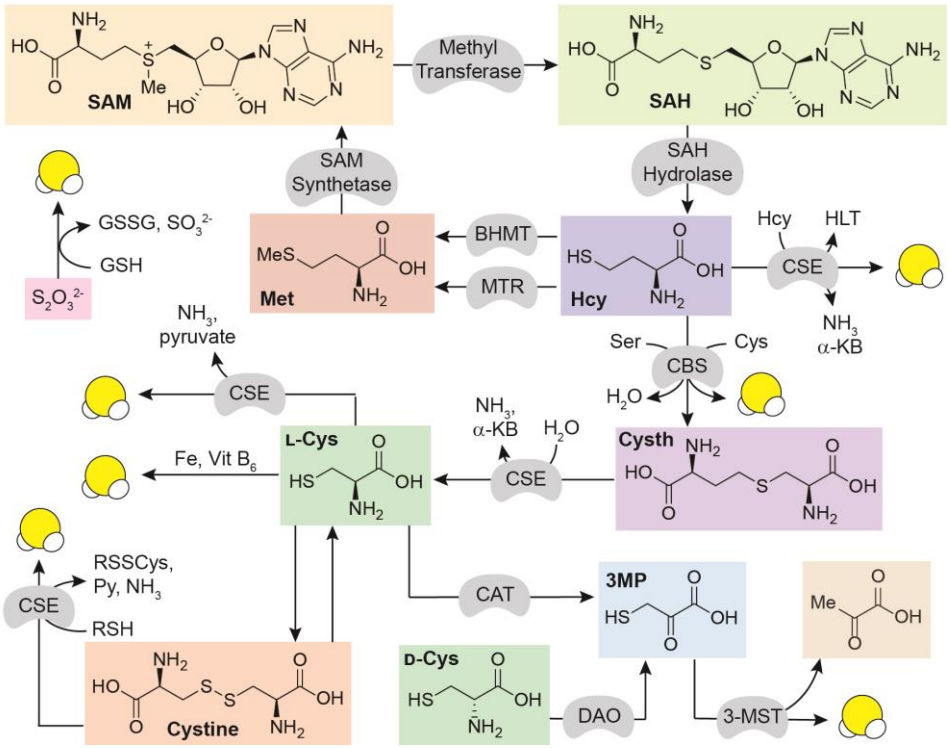


Figure 1.1. Simplified schematic of mammalian H_2S production pathways. Involved intermediates and enzymes include *S*-adenosyl methionine (SAM), *S*-adenosyl-L-homocysteine (SAH), betaine homocysteine *S*-methyltransferase (BHMT), methionine synthase (MTR), cystathionine γ-lyase (CSE), homolanthionine (HLT), α-ketobutyrate (α-KB), cystathionine β-synthase (CBS), cystathionine (Cysth), cysteine aminotransferase (CAT), D-amino acid oxidase (DAO), 3-mercaptopyruviate (3MP), and 3-mercaptopyruvate (3-MST).

1.1.3 Roles of H_2S and RSS in Biology

H_2S and related RSS play important roles in cell signaling and homeostasis, with direct impacts in a wide array of cellular processes including angiogenesis, inflammation, vasorelaxation, and regulation of oxidative stress.[45-50] Furthermore, imbalances in endogenous H_2S production are associated with different deleterious conditions, including neurodegenerative diseases, hypertension, diabetes, and liver cirrhosis.[51-58] For example, increasing evidence has shown that endogenous H_2S production within the brain decreases in individuals with Parkinson's disease, and exogenous H_2S treatment has been shown to prevent further neurodegeneration in rodent models.[59, 60] In addition to the direct role of H_2S in many of these pathways, small molecule and protein persulfides formed from oxidative posttranslational modification of Cys residues also play key roles in H_2S biological action.[29, 61-63] This rapid growth of established and speculated roles of H_2S in human health, as well as the molecular level appreciation for possible signaling pathways

involving RSS, has propelled both the need and development of innovative chemical approaches to measure and manipulate H_2S in biological contexts.

1.1.4 Tools for Investigating Biological H_2S

Modulating H_2S levels in complex systems has been accomplished by both biological and chemical approach. For example, the inhibition or knockout of H_2S-producing enzymes is commonly used to decrease H_2S levels in different model systems.[50] Complementing the above approaches, methods to increase H_2S levels using either overexpression of H_2S enzymes or by exogenous delivery of H_2S using synthetic donors, all allow for the impacts of differential H_2S levels to be investigated directly. In addition to H_2S modulation, direct detection and measurement also constitutes a critical need that has been accomplished with two primary approaches. The first approach is to use analytical methods for sulfide quantification. Common examples of this approach include electrophilic trapping assays (methylene blue assay, monobromobimane, iodoacetamide, etc.), H_2S-selective electrodes, or other instrumental approaches.[64-68] One challenge with these approaches is that they generally lack temporal resolution, do not allow for direct H_2S detection in intact samples, and cannot provide cellular-level spatiotemporal resolution for H_2S generation. For example, electrophilic trapping methods generally require sample homogenization prior to analysis, can alter the RSS pools, and fail to provide information on the precise locus of H_2S generation.[69] H_2S selective electrodes have been applied to tissue measurement to provide a temporal response, but generally lack sufficient spatial resolution for more complex studies.[70] Similarly, head-space analysis approaches lack spatial information and are further complicated by solution phase / gas phase H_2S equilibrium challenges.[71]

One approach to address these limitations is to use activity-based fluorescent probes. Such probes translate a specific chemical reaction to an optical response and allow for high spatiotemporal resolution. Activity-based probes have revolutionized our understanding of cellular roles of different reactive nitrogen species (RNS) and reactive oxygen species (ROS), in particular NO and H_2O_2 signaling.[72-78] Translating these opportunities to RSS, activity-based probes for H_2S now constitute a key pillar of detection and measurement approaches for investigating H_2S in biology. More broadly, activity-based fluorescent probes for H_2S directly address key limitations in the field and provide the ability track H_2S generation in real time in complex living systems with subcellular resolution. In addition, such probes can also be used with complementary

fluorescence microscopy approaches to investigate multiple analytes simultaneously or in response to different stimuli. Mirroring the rapid growth of biological investigations in H_2S, the development of different activity-based sensing approaches for H_2S has expanded significantly over the last decade (Figure 1.2).

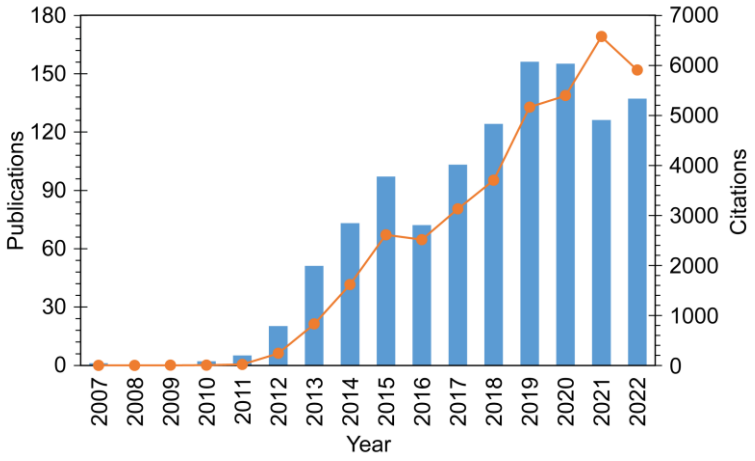


Figure 1.2. Annual publications (blue) and citations (orange) pertaining to fluorescent probes for hydrogen sulfide. Data from Web of Science.

A major challenge in developing activity-based probes for H_2S is addressing the needed selectivity for H_2S over competing analytes. For example, endogenous H_2S levels are in the low to mid nM ranges, yet other thiols are present at much higher concentrations, with reduced GSH levels reaching up to 5-10 mM in different environments. Effectively differentiating these low H_2S levels from other reactive analytes provides a fundamental challenge that will be highlighted throughout this Review. Most reported probes provide at least some selectivity data for H_2S over competing analytes, and in many cases the competing analytes are tested at biologically relevant concentrations, but in many cases they are not. For example, reporting the selectivity of a probe toward 100 μM H_2S (orders of magnitude above endogenous levels) and 100 μM GSH (order of magnitudes below endogenous levels) provides little information about the actual functional selectivity of a probe in a complex biological environment.

In general, the most challenging competing analytes for H_2S selectivity are thiols because they are also sulfhydryl-containing nucleophiles that are reductants and metallophilic. Similarly, nucleophilic sulfur oxides, like thiosulfate ($S_2O_3^{2-}$) and sulfite (SO_3^{2-}) often interfere with many electrophilic probes. Persulfides, polysulfides, and other nucleophilic redox-labile RSS share

many of these nucleophilic properties but are rarely screened as competing analytes. Reactive selenium species, such as selenocysteine (Sec), are also rarely screened, but are typically not found at the same levels as thiol counterparts. RNS, including NO, HNO, $ONOO^-$, and NO_2^- rarely activate probes for H_2S, although HNO can serve as a potential reductant for many metal-based H_2S sensing approaches. Similarly, ROS typically do not activate H_2S probes since they are primarily oxidants, although can contribute to probe degradation. Examples of common interferants that should be considered when developing or working with activity-based H_2S probes are provided in Figure 1.3. We also note that the nucleophilicity of different thiol nucleophiles may change based on local environment, particularly within protein environments, which is difficult to fully mimic or account for in most selectivity screens.

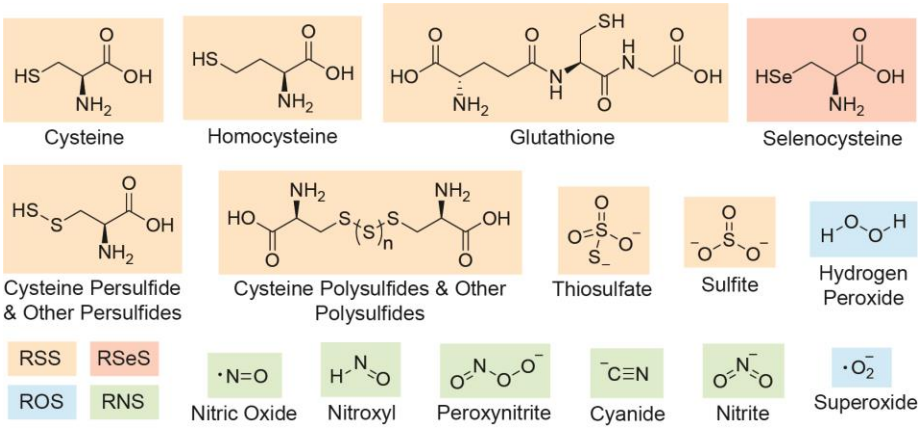


Figure 1.3. Examples of common competing analytes for H_2S including reactive sulfur species (RSS), reactive selenium species (RSeS), reactive oxygen species (ROS), and reactive nitrogen species (RNS).

1.1.5 Scope of the Review

Our goal in this Review is to highlight both the breadth and depth of approaches for activity-based H_2S and RSS sensing. Other analytical approaches for H_2S measurement, such as mass spectrometry (MS), high performance liquid chromatography (HPLC), gas chromatography (GC), colorimetry, etc, are also commonly used for H_2S detection but are outside the scope of this Review. Our coverage will focus on activity-based probes that function in aqueous solution and result in a change in fluorescent signal upon reaction with H_2S because such approaches are most compatible with live-cell biological applications. This coverage will include methods that utilize reduction, nucleophilic attack, and metal precipitation, with different approaches grouped and

highlighted within each category. To further the breadth of this Review, we also highlight key advances in reductant-labile sulfane sulfur probes, which in many cases either build from or parallel developments for activity-based H_2S probes. We have generally excluded investigations that solely provide colorimetric responses unless the chemistry is particularly unique from other examples. Similarly, we have focused on small molecule-based approaches and generally exclude macromolecular or solid state methods for simplicity. Most probes highlighted include either a demonstration that the developed approach can function in live cell environments or in aqueous samples. In general, we have excluded probes that function in purely organic solution without a demonstrated application in biological systems and probes that function through acid/base chemistry in unbuffered water, particularly if they are using already-established sensing mechanisms.

In addition to highlighting the fundamental chemistry that has enabled many different sensing approaches, our goal is to highlight differences that help define benefits and limitations of each strategy s and to further highlight specific case studies with particularly compelling biological applications. When including information on demonstrated biological applications of the developed probes we have tried to denote when exogenous H_2S is used in cellular experiments. Similarly, many reports use the addition of Cys or sodium nitroprusside (SNP), an NO donor, to stimulate endogenous H_2S production. In such cases, we typically refer these systems as generating Cys- or SNP-derived H_2S to differentiate from cases where inhibitors of enzymatic H_2S synthesis, such as propargylglycine (PAG) or aminooxyacetic acid (AOAA), are used. When highlighting the properties of activity-based probes discussed in this Review, we made a cognizant choice to not discuss reaction rates except within a few specific examples. It is well established that both organic solvent and surfactant addition can significantly impact the rate of many of the reactions discussed, which makes direct comparisons between probes difficult. Similarly, because most of the activity-based approaches rely on bimolecular reactions between the probe and analyte, increasing either (or both) concentrations has a significant effect on the measured rates of reaction. As an example, many published reports of ‘fast’ probes are merely faster because they are investigated at much higher, abiotic concentrations of H_2S or other analytes.

Similarly, we have intentionally excluded tabulation or discussion of H_2S detection limits for a number of reasons. First, many detection limit measurements are performed under different conditions, and reports rarely demonstrate that detection limits calculated by extrapolation can

actually be measured. Second, since our focus is on biological applications of these probes, reported detection limits in pristine buffer with only H_2S present have little relevance if there is even minor cross-reactivity with other analytes likely to be found in complex biological environments. Finally, we have excluded examples where H_2S detection and subsequent application is not the primary focus of the investigation. Most such examples appear in systems where H_2S is used to remove a metal from a ligand scaffold. If such reactivity is not the primary focus of the manuscript, or if such reactivity is only used in a selectivity screen for other analytes, then we have typically excluded such examples. As a whole, we hope that readers will find the significant breadth and diversity of chemistry used to develop activity-based H_2S and RSS detection to be inspiring and that the examples highlighted in this Review will stimulate future ideas, approaches, and applications.

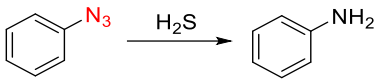
1.2 H_2S Fluorescent Probes: Reduction of Oxidized Nitrogen Motifs

One of the most common approaches for activity-based H_2S detection is to use H_2S to reduce oxidized nitrogen motifs. In many cases, H_2S reduces such motifs more quickly than competing thiols, which provides an initial source of selectivity for this approach. In addition, many fluorophores contain amine functional groups that are required for fluorescence, which provides a simple synthetic approach to develop fluorogenic systems that respond to H_2S.

1.2.1 Azide Reduction

Azides are a common functional group used in organic chemistry, often as synthetic intermediates that can be reduced to furnish amine products. Furthermore, azides have found significant utility in bioorthogonal and bioconjugation chemistry as a key reaction partner in both azide-alkyne Huisgen 1,3-dipolar cycloaddition reactions as well as in the Staudinger ligation between an azide and organophosphorus component.[79-82] Although azides are typically stable toward biological nucleophiles, they can readily be reduced by organophosphines and dithiol-reductants, such as dithiothreitol (DTT), to generate the parent amine. Early reports of azide protecting group reduction by H_2S were reported in the late 19th century, albeit in organic solution and at high concentrations.[83-85] Leveraging this fundamental chemistry, many activity-based fluorescent probes for H_2S have been developed that use fluorogenic azide reduction as an activation mechanism for probe response (Scheme 1.1). In most cases, converting an aryl amine

in a fluorophore to an azide results in fluorescence quenching. Such quenching can be abolished by reducing the azide to regenerate the parent amine-based fluorophore, although other cascade approaches that include azide reduction followed by a self-immolative pathways or intramolecular cyclization have also been reported.



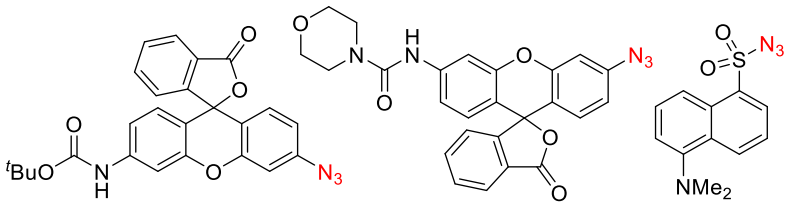
Scheme 1.1. General reaction of aryl azides with H_2S to form an amine.

Mechanistically, this reduction process requires two equivalents of H_2S per azide and proceeds through attack of nucleophilic HS^- on the azide to form an azidothiol intermediate, which further reacts with H_2S to fully reduce the azide to an amine and generate N_2 and hydrogen disulfide as byproducts.[86] In general, azide-based H_2S probes provide large fluorescent responses, relatively high selectivity for H_2S over other biologically relevant analytes, and are compatible with cell and animal studies. H_2S-mediated azide reduction is often slower than many activity-based H_2S detection methods, although examples of faster reactivity have been reported, albeit often at the cost of reduced selectivity. In addition, the rate of H_2S-mediated azide reduction is often increased by the use of organic co-solvents or other hydrophobic additives. Other practical considerations should also be taken into account when using azide-based probes. For example, aryl azides are inherently photosensitive and can be photoreduced to the parent amine, which may provide challenges for longer term imaging experiments. Azides are also incompatible with the commonly used reducing agents DTT and *tris*(2-carboxyethyl)phosphine (TCEP) and have also been reported to be reduced by certain reductases.[87] Despite these limitations, the application of H_2S-mediated reduction has been used broadly to develop diverse activity-based probes for H_2S detection, with the section below highlighting both key advances and the breadth of this simple approach.

1.2.1.1. Direct Azide Reduction

In 2011, Chang reported rhodamine-based probes **1** and **2** (SF1 and SF2) as first generation activity-based probes for H_2S that function through the H_2S-mediated reduction of an azide to generate a fluorescence response (Figure 1.4).[88] Upon reaction with H_2S, **1** and **2** provided a

fluorescence response at 525 nm, with 7- and 9-fold fluorescence turn-ons, respectively. Both probes showed a greater fluorescent response to H_2S over other reactive species, with **2** providing a higher selectivity although a minimal response was also observed for SO_3^{2-}. Both probes were also used to image exogenous H_2S in HEK293T cells, with **2** providing a larger response (Figure 1.5). Also in 2011, Wang reported dansyl-based probe **3** (DNS-Az) that exhibits a 40-fold fluorescence turn-on at 535 nm when treated with H_2S in buffer with 0.5% Tween-20.[89] This probe showed good selectivity for H_2S over other reactive species and anions, although a response was also observed for the abiological interferant PhSH. This probe showed a faster reaction profile than most azide-based probes and was used to investigate H_2S in biological media including fetal bovine serum (FBS) and mouse blood.



1 SF1 **2** SF2 **3** DNS-Az

Figure 1.4. Early examples of fluorescent H_2S probes based on azide group reduction.

This general approach for H_2S detection has been applied to a wide array of fluorogenic systems, including 1,8-naphthalimide-based probes that differ by substitution at the imide. In 2012, Pluth reported the 2-methoxyethyl substituted probe **4** (HSN2), that featured a 60-fold fluorescence turn-on at 542 nm when treated with H_2S (Figure 1.6).[90] This probe showed a greater fluorescence response for H_2S over other reactive species, including millimolar concentrations of Cys and GSH and was also used to image exogenous H_2S in HeLa cells. Following this, Lin reported propyl substituted probe **5** (Fl-H_2S), which provided a 38-fold fluorescence turn-on at 561 nm.[91] This probe used to image exogenous and Cys-derived H_2S in HeLa cells. Probe **5** was further used with two-photon imaging to image H_2S in mouse liver tissue at depths up to 126 μm and also to image H_2S generation *in vivo* in a mouse air pouch inflammation model.

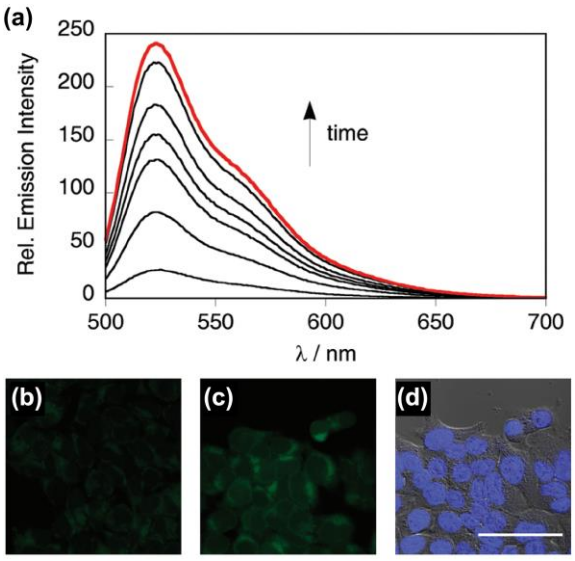


Figure 1.5. (a) Fluorescent response of 10 µM **2** treated with 100 µM H_2S at 25 °C in 20 mM pH 7.4 PIPES buffer. Cell images of HEK293T cells in (b) the absence of **2**, (c) with **2** + 250 µM H_2S, and (d) brightfield overlay with the Hoechst nuclear dye. Reproduced and modified with permission from ref [88]. Copyright 2011 American Chemical Society.

Adding a *N*-[2-(2-hydroxy)-ethoxy]ethyl group or extending the carbon chain to an *n*-butyl group, Zhang reported fluorescence turn-on probes **6** and **7** (SS1 and SS2) to investigate the impacts of water solubilizing groups.[92] Upon treatment with H_2S, **6** provided a 50-fold fluorescence turn-on at 540 nm, whereas **7** was noted as too insoluble to measure a response accurately. The reaction rate of **6** with H_2S was faster at higher pH values, slightly slower in anionic surfactant, and faster in cationic surfactant, all of which are consistent with HS^- being the active species for azide reduction. Probes **6** and **7** were shown to be selective for H_2S over other analytes, and both probes were used to investigate H_2S in FBS, with **7** shown to be slightly more sensitive than **6**. Probe **6** was also reported by Shi and Cai in 2014 and shown to provide a 25-fold fluorescence turn-on at 540 nm in 50% DMSO in buffer.[93] Here, **6** showed good selectivity for H_2S over competing RSS, metal cations, and ROS and was also used to investigate H_2S and spiked H_2S in tap, mineral, and lake water samples.

Using a shorter-chain alcohol motif, Lin reported probe **8** (Nap-N_3), which provided an 8-fold fluorescence turn-on at 546 nm with relatively good selectivity for H_2S over other competing analytes, although some response to Cys and GSH was observed.[94] Probe **8** was used to image exogenous and Cys-derived H_2S in HeLa cells. Probe **8** was also reported by Ji in 2022, and demonstrated a fluorescence turn-on at 530 nm in DMSO, good selectivity for H_2S over other

reactive species, and imaging of exogenous H_2S in SiHa cells.[95] Further expanding the water solubilizing groups, Ha and Lee reported **9** in 2016, which includes a hydrophilic poly(ethylene glycol) chain to increase solubility.[96] Incubation with H_2S resulted in a 70-fold fluorescence turn-on at 550 nm, and the probe showed good selectivity for H_2S over biological anions and thiols. Probe **9** was subsequently used to image exogenous and endogenous H_2S in Raw 264.7 cells and zebrafish embryos.

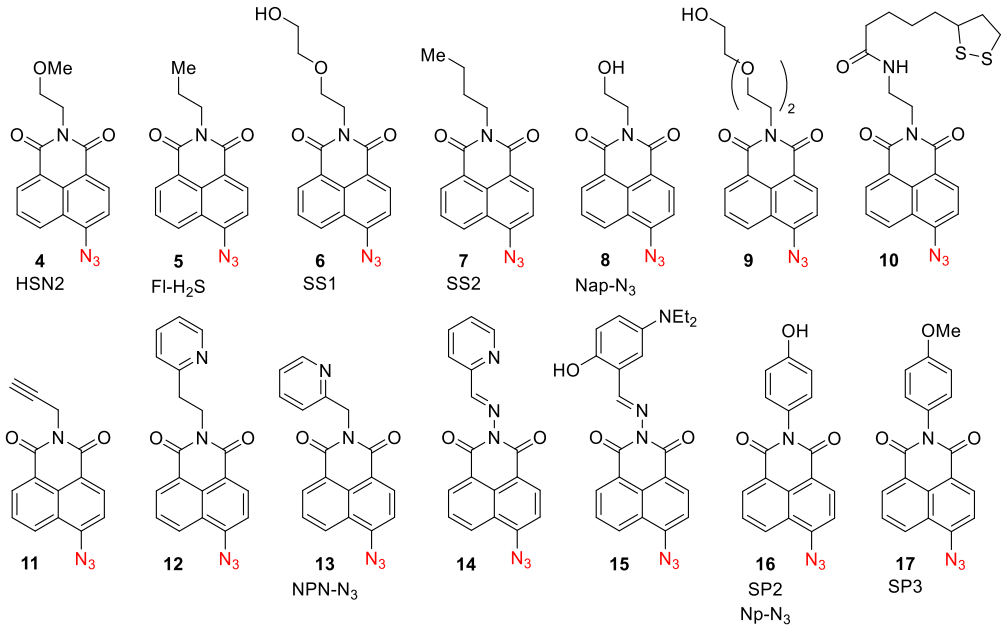


Figure 1.6. Examples of azide-based fluorescent H_2S probes based on 1,8-naphthalimides.

Further highlighting the impacts of naphthalimide functionalization, Xu reported probe **10**, which incorporates a dithiolane motif to impart dynamic thiol-disulfide exchange on the fluidic lipid bilayer of cytomembrane.[97] Treatment with H_2S resulted in a 131-fold fluorescence turn-on at 545 nm, and the probe showed good selectivity for H_2S over competing analytes. Moreover, this probe showed better cellular uptake compared to a non-dithiolane containing analogue and provided a good fluorescence response to both exogenous and endogenous H_2S in HeLa cells. Utilizing an alkyne that can be used to enable further reactivity beyond H_2S sensing, Zhengjun and Xicun reported **11** that responded to H_2S with a fluorescence turn-on at 539 nm in 50% MeCN in buffer and showed good selectivity for H_2S over other biologically relevant anions, amino acids, and thiols.[98]

Using a pyridine-linked naphthalimide, Su reported probe **12** that displayed a fluorescence turn-on at 532 nm toward H_2S in 50% MeCN in buffer without a response to other biologically relevant analytes.[99] This probe was also shown to be stable at neutral to basic pH solution and to image both exogenous and endogenous H_2S in live cells. Iyer reported a similar probe **13** where H_2S induces a fluorescent response at 523 nm with demonstrated selectivity for H_2S over other anions.[100] Probe **13** was further used to develop test paper strips, image exogenous H_2S in *E. coli*, and quantify H_2S in natural water, wine, and beer samples.

Expanding to aromatic functionalized motifs, Kang and Lee prepared a naphthalimide-hydrazone **14**, which displayed a large fluorescence turn-on response to H_2S in 40% DMSO in buffer and good selectivity for H_2S over biologically relevant metals, ROS, and RSS.[101] Similarly, Sahoo reported **15** that responded to H_2S with a 5-fold fluorescence turn-on at 524 nm with good selectivity for H_2S over various RNS, ROS, and thiols.[102] The probe was also was used to develop paper strips for measuring H_2S in different foods. Zhang reported phenol-substituted **16** (SP2), which showed a fluorescence turn-on at 552 nm in response to H_2S that was selective for H_2S over anions and thiols, although SO_3^{2-} did produce a minor response.[103] The probe was further used to construct a logic gate utilizing the reactivity with H_2S and SO_3^{2-} as well as to image exogenous and SNP-generated H_2S in HepG2 cells. Probe **16** was also reported by Wang where the azide could be reduced to the parent amine by either H_2S or 465 nm light in 70% DMF in buffer and was further used to image exogenous H_2S in HeLa cells.[104] Zhang reported **17** (SP3), which provides a turn-on at 557 nm with good selectivity for H_2S over competing analytes, although some response to Cys, GSH, HPO_4^{2-}, and H_2O_2 was also observed.[105] This probe was used to investigate H_2S levels in red wine and also to image exogenous H_2S in SW480 cells.

Different *bis*-(azido-naphthalimide) motifs have also been used for H_2S detection. For example, Huo reported a two-site H_2S probe **18** (ND-N_3), which provided a 20-fold fluorescence turn-on to H_2S in 80% DMSO in PBS buffer (Figure 1.7).[106] This probe showed good selectivity for H_2S over competing analytes and was used to image exogenous H_2S in HepG2 cells. Zhang reported probes **19** (NAN0-N_3) and **20** (NAN6-N_3) featuring linked *bis*-naphthalimides that bind to DNA and induce a fluorescent enhancement due to removal of intramolecular torsion or dimerization-caused quenching, respectively, to monitor DNA damage induced by H_2S overexpression.[107] Probes **19** and **20** exhibited a fluorescent response to H_2S at 556 nm and 565

nm, respectively, that was amplified by the addition of DNA. Both probes were used to image DNA damage induced by exogenous H_2S in live HepG2 and CHO cells.

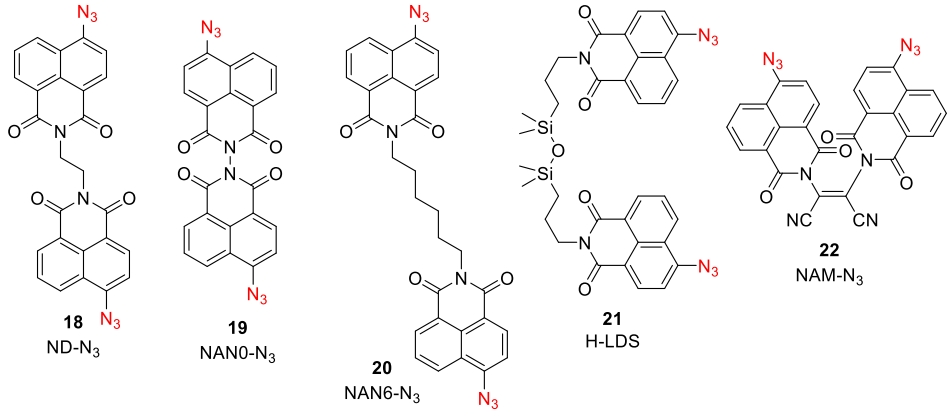


Figure 1.7. Examples of azide-based fluorescent H_2S probes based on *bis*-naphthalimides.

Lin also reported a related **21** (H-LDS) that incorporates two naphthalimide motifs linked through a siloxane that increased probe affinity to lipid droplets.[108] This probe provided a ~10-fold fluorescence turn-on in 10% EtOH in buffer and showed good selectivity for H_2S over competing analytes. The probe was demonstrated to localize in lipid droplets in HeLa cells and provided a response to exogenous H_2S. This general approach was also used by Iyer, who reported probe **22** (NAM-N_3) in which two azide-modified 1,8-naphthalimides are linked by a 2,3-diaminomalononitrile.[109] This probe provided a 6-fold fluorescent at 452 nm response in 50% DMSO in buffer with good selectivity over competing reactive species. Probe **22** was used to investigate H_2S in beer and wine samples and was demonstrated to detect exogenous H_2S in HeLa cells.

Expanding to other chromophores, Sun reported rhodamine-based probe **23** with dual azide functionalization in 2013 to impart better fluorescence quenching and higher sensitivity (Figure 1.8).[110] Treatment with H_2S resulted in a 120-fold fluorescence turn-on at 525 nm, and the probe showed excellent selectivity for H_2S over other competing analytes. This probe was subsequently used to image exogenous H_2S in HeLa cells. Using a hybrid rhodafluor scaffold, Pluth reported the methylrhodol **24** (MeRho-Az) in 2015.[111] This probe provided a 1200-fold fluorescence turn-on to H_2S at 516 nm and showed good selectivity over other reactive sulfur species. Moreover, **24** was shown to be less photosensitive than other commonly used azide-based probes and did not

undergo appreciable photoreduction. This probe was subsequently shown to respond to exogenous and endogenous H_2S in C6 cells and was also used to image H_2S released from diallyl trisulfide gavaged into the gut of larval zebrafish using light sheet microscopy (Figure 1.9).

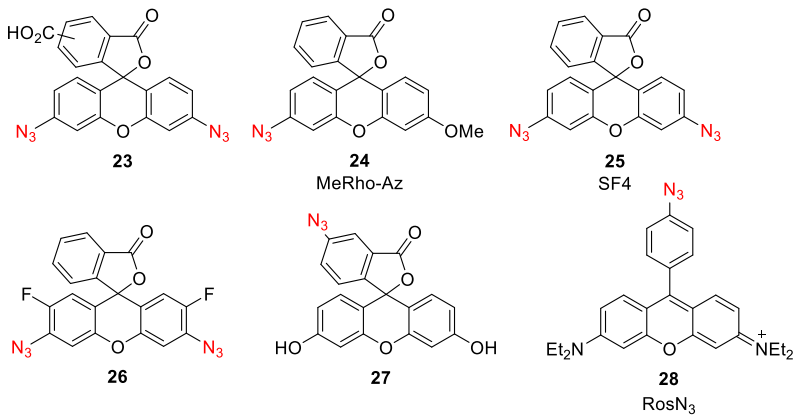


Figure 1.8. Examples of azide-based fluorescent H_2S probes based on xanthene dyes.

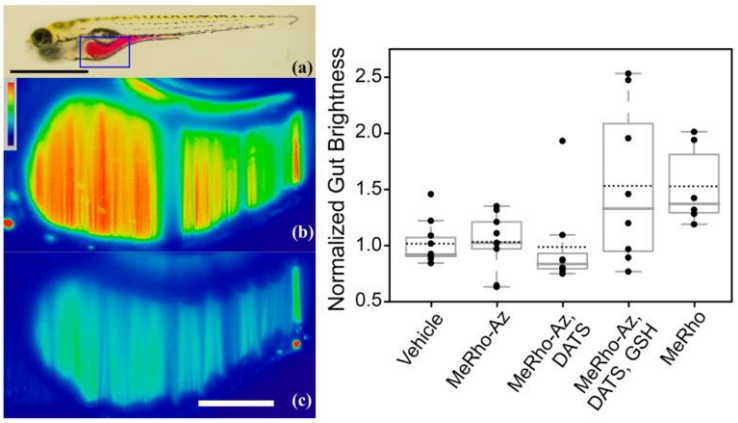


Figure 1.9. (left) Two-dimensional slices of light sheet fluorescent microscopy (LFSM) images of larval zebrafish gavaged with 5 μM **24** + 250 μM DATS + 250 μM GSH or **24** only. (right) Fluorescence quantification of larval zebrafish gavaged with different combinations of **24**, DATS, and GSH. Reproduced with permission from ref [111]. Copyright 2015 American Chemical Society.

In 2013, Chang reported *bis*-azide **25** (SF4) alongside other probes that will be discussed later in this review.[112] Probe **25** displayed a 40-fold fluorescence turn-on at 517 nm and good selectivity for H_2S over other biological analytes with further application to image H_2S in human umbilical vein endothelial cells (HUVECs). Following this, Yi and Xi developed **26** that showed a 700-fold fluorescence turn-on at 520 nm with addition of H_2S and a high selectively for H_2S over

biological anions and thiols.[113] Probe **26** was used to monitor CBS activity in situ and also to image exogenous and enzymatically produced H_2S in HEK293A. Also in 2015, Huo and Kang reported **27** that exhibited a 50-fold fluorescence turn-on at 531 nm with the addition of H_2S in 75% MeCN in buffer with demonstrated selectively for H_2S over anions and thiols.[114] The probe was also used to image exogenous H_2S in HepG2 cells. Building from the rhodamine xanthene core, Zhang and Ye developed the red-emitting rosamine-based probe **28** ($RosN_3$).[115] This probe provided a turn-off response to H_2S at 590 nm in 60% DMF in buffer and showed good selectivity for H_2S over other biological anions and thiols. The turn-off response of **28** was also demonstrated in MGC-803 cells treated with exogenous H_2S.

Expanding to other high quantum yield dyes, a number of BODIPY containing azide-based H_2S probes have also been reported. In 2013, Talukdar reported **29** featuring an azide-modified BODIPY that exhibited a 40-fold fluorescence turn-on at 520 nm with addition of H_2S (Figure 1.10).[116] This probe was shown to be selective for H_2S over biologically relevant anions and thiols and was further used to image both endogenous and exogenous H_2S in HeLa cells. Following this, Kumar reported probe **30** that features an azide-modified BODIPY derivative that also responds to changes in viscosity based on rotation of the phenyl substitution on the BODIPY.[117] This molecular rotor approach was used to detect viscosity changes associated with apoptosis. The probe fluorescence at 515 nm in 20% DMSO in buffer decreases upon addition of H_2S, and this response showed good selectivity for H_2S over biological analytes. In contrast to the response to H_2S, increasing the solution viscosity using glycerol resulted in a fluorescence increase. The fluorescence turn-off to H_2S was also confirmed in C6 cells. In addition, **30** was used to image changes in cellular viscosity attributed to H_2S-mediated apoptosis upon treatment with lipopolysaccharide (LPS).

Using a similar platform, Sarkar reported **31**, which resulted in a turn-off fluorescence at 516 nm in 33% MeOH in buffer.[118] This fluorescence turn-off response was selective for H_2S over other biologically relevant anions. This probe was used to develop H_2S test strips and the turn-off response to exogenous H_2S was confirmed in normal human oral fibroblast cells. In 2014, Akkaya reported ethylene glycol functionalized probe **32**, which provided a fluorescence turn-off at 670 nm when incubated with H_2S in 60% MeCN in buffer.[119] This fluorescence quenching was selective for H_2S over biological anions and thiols and probe **32** was also used to image exogenous H_2S in MCF-7 cells.

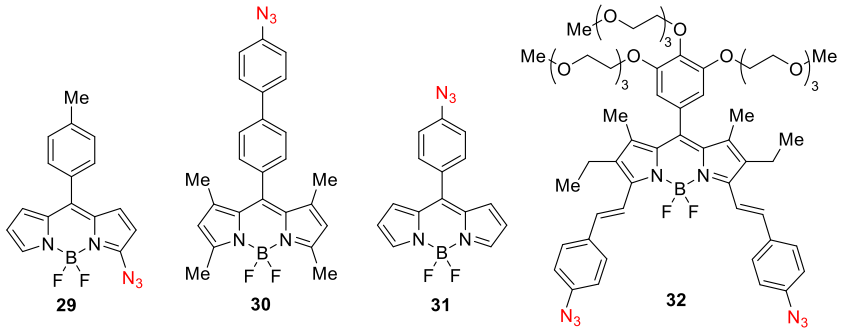


Figure 1.10. Examples of azide-based fluorescent H_2S probes based on BODIPY chromophores.

Coumarin-based systems for H_2S detection have also been widely reported. For example, Yu reported the two coumarin-based probes **33** and **34** in 2012 that include azides at the 3-position and either an alcohol or diethyl amine functionalization at the 7-position, respectively (Figure 1.11).[120] When treated with H_2S, the probes resulted in a 5- and 40-fold fluorescence turn-on at 483 and 515 nm, respectively. Probe **33** provided only a minimal response to H_2S with no appreciable selectivity for H_2S over other RSS, whereas **34** provided a fluorescence turn-on with only moderate selectivity against Cys and GSH. The probes were demonstrated to detect thiols in rabbit plasma, and **34** was shown to respond to exogenous H_2S in PC-3 cells.

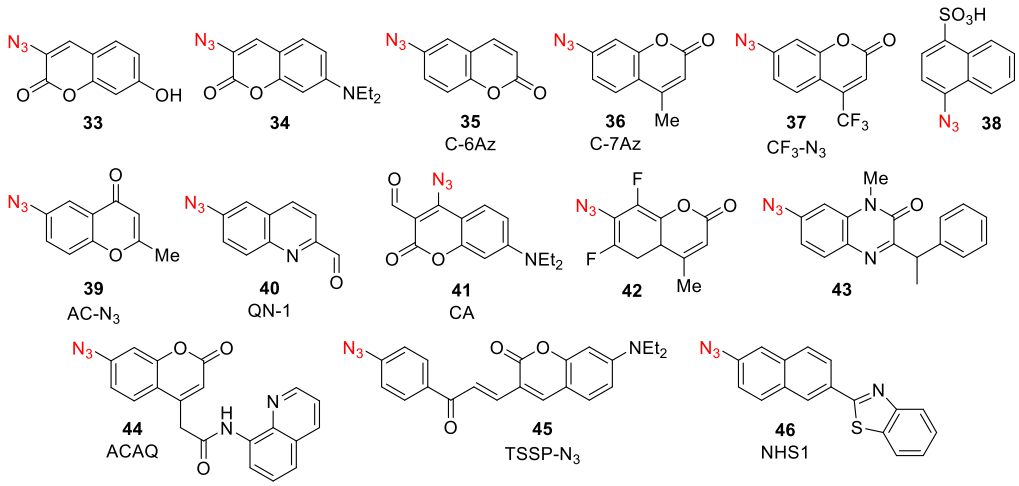


Figure 1.11. Examples of azide-based fluorescent H_2S probes based on coumarin, naphthalene, and related chromophores.

In 2013, Tang reported azide-functionalized coumarin derivatives **35** and **36** (C-6Az and C-7Az).[121] Treatment of **36** with H_2S resulted in a 108-fold fluorescence turn-on at 434 nm with

excellent selectivity for H_2S over other RSS, RNS, ROS, and anions and also showed good photostability. In contrast, **35** provided only an 8-fold turn-on for H_2S, albeit at a higher concentration than for **36**, and showed no selectivity for H_2S over other species. Probe **36** was also used to image exogenous H_2S as well as Cys and GSH-derived H_2S in HeLa cells using two-photon excitation at 720 nm and also used further to image H_2S in rat cardiac tissue. Using a related platform with trifluoromethyl modification, Huang and Qian reported **37** (CF_3-N_3), which provided a 137-fold fluorescence turn-on at 490 nm when incubated with H_2S.[122] This probe was selective for H_2S over other competing analytes and demonstrated to detect exogenous H_2S in K562 cells. Martínez-Máñez and Costero also reported **37** and naphthyl azide **38**, which provided 11-fold and 50-fold turn-on responses, with good selectivity for H_2S over other biological analytes.[123] Probe **37** was also used to image exogenous H_2S in HeLa cells.

Using a related scaffold, Zhang reported chromone derivative **39** (AC-N_3), which provides a turn-on response at 500 nm in 50% DMSO in buffer with good selectivity for H_2S over other competing analytes, including thiols.[124] This probe was also used to image exogenous H_2S in HeLa cells. Expanding to an azide-modified 6-azidoquinoline-2-carbaldehyde motif, Yin reported **40** (QN-1), which provides a fluorescence shift from 476 to 533 nm with an 11-fold increase in intensity upon treatment with H_2S.[125] This probe showed good selectivity for H_2S, with only a minimal response to Cys. Probe **40** was also used to image exogenous and SNP-derived H_2S in HepG2 cells. Also containing an aldehyde motif, Yang and Wang reported the coumarin aldehyde derivative **41** (CA), which provided a 217-fold fluorescence turn-on at 422 nm in 30% MeCN in unbuffered water.[126] The probe was selective for H_2S over competing analytes, and used to image exogenous H_2S in HeLa cells and zebrafish.

Wang and Yi reported **42** that featured a fluorinated azide-substituted coumarin derivative and exhibited a 160-fold fluorescence turn-on at 436 nm that was selective for H_2S over thiols and biologically relevant species.[127] The reactivity of the azide to various biorthogonal reaction conditions was also investigated. Sabot reported **43** that exhibited a 72-fold fluorescence turn-on at 489 nm when treated with H_2S that was selective for H_2S over other RSS and ascorbate.[128] In 2020, Zhao and Zhu reported **44** (ACAQ) featuring an azide modified coumarin linked to a quinoline that produced a fluorescence shift and enhancement from 496 nm to ~460 nm when treated with H_2S.[129] The probe was shown to be selective for H_2S over biothiols, anions, and metal ions and was further used to image exogenous H_2S in MCF-7 cells.

Qian and Zhang reported **45** (TSSP-N_3), which provided a fluorescence shift from 590 nm to 564 nm upon addition of H_2S and a fluorescence shift to 460 nm after addition of SO_3^{2-}, which was attributed to Michael addition to the α,β-unsaturated ketone.[130] The probe was shown to be selective for H_2S and SO_3^{2-} over other anions and thiols with SO_3^{2-} outcompeting H_2S. The probe was also used to image both H_2S and SO_3^{2-} in HeLa cells. Zhang and Tan reported the two-photon probe **46** (NSH1) that exhibited a 67-fold fluorescence turn-on at 480 nm in 80% DMF in buffer that was selective for H_2S over thiols, RNS, and ROS, although high concentrations of thiols did produce a minor response.[131] When excited at 760 nm, the TP excitation cross-section of the activated probe was 110.98 GM and **46** was used to image exogenous H_2S and endogenous H_2S confirmed by treatment with phorbol-12-myristate-13-acetate (PMA) in HeLa cells with two-photon imaging.

Expanding to longer wavelengths, Tang reported resorufamine-derived **47** (R-Az), which provides a 25-fold fluorescence turn-on at 590 nm upon addition of H_2S (Figure 1.12).[132] This probe showed good selectivity over competing RNS, ROS, anions, and thiols, and was used to image exogenous and GSH-derived H_2S in HeLa cells. In 2013, Ma reported the related cresyl violet-based probe **48**, which provides a ratiometric response with decrease at 566 nm and increase at 620 nm upon treatment with H_2S.[133] This probe was selective for H_2S over inorganic salts, ROS, NADH, and thiols. Probe **48** was also used for ratiometric imaging of exogenous H_2S in MCF-7 cells and zebrafish. In 2021, Diao reported phenoxazine-based **49** (BPO-N_3) that upon incubation with H_2S exhibited a 30-fold fluorescence emission ratio shift from 560 nm to 625 nm that was selective for H_2S over thiols and anions and further used to image exogenous H_2S in live HepG2 cells.[134]

As an additional two-photon excitation probe, Lin reported **50** (1-H_2S), which provides a 7-fold fluorescence turn-on at 635 nm to H_2S in 20% DMSO in buffer.[135] This probe showed good selectivity for H_2S over other analytes, but did show a minimal response to Hcy. Cell imaging experiment in HeLa cells showed initial localization the mitochondria with extended incubation times leading to nucleolar localization. Probe **50** was further used to image exogenous H_2S in live cells, liver tissues samples at up to 60 μm with a 760 nm excitation and also in live mice. In 2017, Zhou, Sun, and Liu reported **51** where the corresponding amine exhibited an emission at 725 nm and a two-photon excitation at 820 nm with a 180 GM TP cross section.[136] The probe was shown to be selective for H_2S over other biological analytes, have a low cytotoxicity, and was used to

image exogenous H_2S in live HeLa cells with TP microscopy and live mice with one-photon bioimaging.

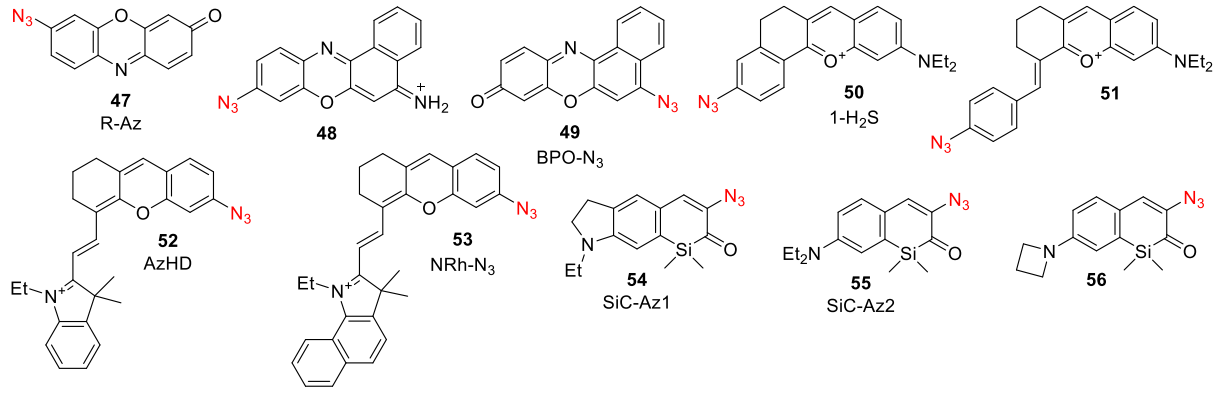


Figure 1.12. Additional examples of azide-based fluorescent H_2S probes based on various fluorophores.

Zhang and Xing reported **52** (AzHD) that was used as a ratiometric photoacoustic (PA) nanoprobe by encapsulating the probe within a liposome.[137] With the addition of H_2S, the PA signal at 532 nm decreased and the signal at 700 nm increased. The probe was selective for H_2S over other anions and was used to image H_2S in brain tissue from mouse models of Alzheimer's disease (AD) and also in live mice. In 2020, Liu developed **53** (NRh-N_3) that exhibited a weak fluorescence at 740 nm that intensified at 735 nm upon addition of H_2S.[138] This response was selective for H_2S over other biological relevant species, and the probe was further used to image exogenous H_2S in live U87 cells and BALB/c nude mice.

Adding to the diversity of chromophore platforms, Cui reported azide-modified Si-coumarin derivatives **54**–**56** (SiCAz1–3) that include different amine substitution.[139] Treatment with H_2S in 30% MeCN in buffer resulted in 14, 40 and 13-fold fluorescence turn-ons, respectively. Based on these results, **55** was investigated further and shown to have good selectivity for H_2S over other reactive species. In addition, this probe was used to image both exogenous and Cys-derived H_2S in live HeLa cells and zebrafish.

In 2013, Xu developed NIR probe **57** based on an azide modified dicyanomethylene-4*H*-chromene (Figure 1.13).[140] Treatment with H_2S in 50% MeCN in buffer resulted in a 96-fold fluorescence turn-on at 655 nm and a Job plot demonstrated that two equivalents of H_2S were needed to fully reduce the azide to the amine. The probe showed good selectivity for H_2S over

other analytes, with $S_2O_3^{2-}$ and $S_2O_4^{2-}$ producing only minimal responses. The probe was further used to image exogenous H_2S in HUVECs. Also in 2013, Fan and Peng reported the identical probe **57** for use as a two-photon excitation probe.[141] Treatment with H_2S resulted in a 65-fold fluorescence turn-on at 670 nm that was selective for H_2S over competing species. The probe was demonstrated to function in FBS and also used to image exogenous H_2S in MCF-7 cells. Probe **57** was also used to image exogenous H_2S in rat liver cancer tissues at depths of 60–220 μm and also exogenous H_2S in live mice.

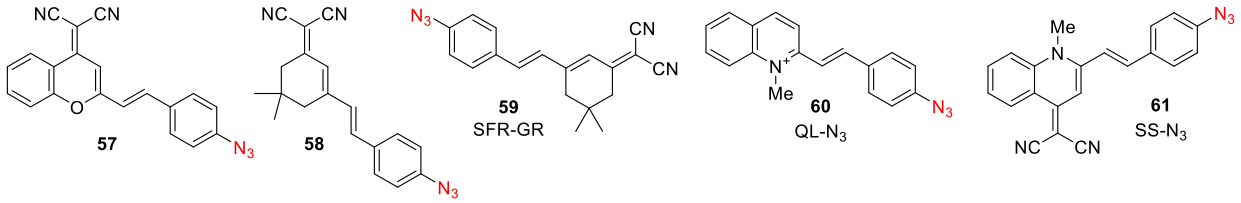


Figure 1.13. Examples of azide-based fluorescent H_2S probes based on dicyanoisophorone and related conjugated systems.

Tian and Zhang reported ratiometric fluorescence turn-on probe **58** in 2015, which utilizes an azide-modified dicyanoisophorone derivative with a large Stokes shift (163 nm).[142] Treatment with H_2S in 50% DMSO in buffer resulted in a fluorescence decrease at 562 nm and concomitant increase at 643 nm with good selectivity for H_2S over biologically relevant anions and thiols. This probe was used to investigate and quantify H_2S in natural waters as well as H_2S-doped samples. Also in 2015, Zhu and Qian reported ratiometric probe **59** (SFP-GR) that exhibited weak fluorescence at 558 nm that shifted to 637 nm upon H_2S addition.[143] This probe was selective for H_2S over biological analytes such as thiols, metal ions, and amino acids and also used to image exogenous H_2S in HeLa cells and zebrafish.

Using a similar extended conjugation approach, Wei and Zhang reported the ratiometric probe **60** (QL-N_3) based on an azide-modified *N*-methylquinolinium motif.[144] When treated with H_2S in 50% DMSO in buffer, the fluorescent signal at 525 nm decreased with a concomitant increase at 605 nm with good selectivity for H_2S over biological metal ions, anions, thiols, and ROS. Probe **60** was used to image exogenous H_2S in HeLa cells, and the two emission signals could be modulated by pretreatment of the cells with $ZnCl_2$ and subsequent addition of H_2S. Wei and Zhang also reported related **61** (SS-N_3), which provided a turn-on response to H_2S at 610 nm

in 60% DMSO in buffer.[145] This probe showed good selectivity over biothiols, amino acids, and other biologically relevant molecules and was used to image exogenous and endogenous H_2S in HeLa cells.

Liu and Zhang reported probes **62** and **63**, which are based on pomalidomide, a drug for multiple myeloma (Figure 1.14).[146] Based on fluorescence turn-on and pH stability investigations, probe **63** was used for further study and provided a fluorescence turn-on response to H_2S at 500 nm. This probe showed good selectivity for H_2S over competing analytes, although 1 mM of SO_3^{2-} did result in partial probe activation. The probe was used to detect H_2S in FBS and confirmed to respond to exogenous H_2S in U266 cells using flow cytometry. Song later reported the related phthalimide-based **64**, which provided a 196-fold fluorescence turn-on at 492 nm in buffer with CTAB.[147] The probe was selective for H_2S over biological analytes and was used to image exogenous H_2S in HNE-2 cells. In 2016, Cao reported **65** (AHS) that displayed a 17-fold fluorescence turn-on at 557 nm when treated with H_2S in 60% DMSO in buffer and was selective for H_2S over other biological analytes, although high concentrations of GSH did elicit a minor response.[148] This probe was further used to image exogenous H_2S in live U937 monocytic cells.

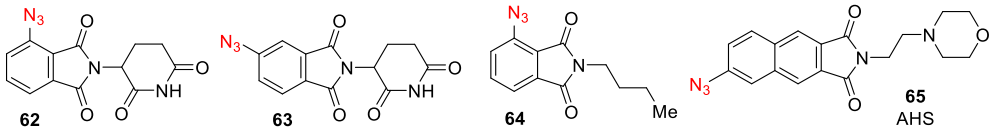


Figure 1.14. Examples of azide-based fluorescent H_2S probes based on phthalimides.

In 2012, Lin reported probe **66** (PI-N_3) utilizing a phenanthroimidazole scaffold that exhibited a 20-fold fluorescence turn-on at 423 nm when treated with H_2S in 30% EtOH in buffer (Figure 1.15).[149] This probe was selective for H_2S over competing analytes and was used to image exogenous H_2S in HeLa cells. Li later reported related probe **67** (P-N_3) that utilizes an excited state intramolecular proton transfer (ESIPT) mechanism for fluorescence modulation.[150] Addition of H_2S in 10% EtOH in buffer resulted in turn-on response at 436 nm. This probe showed good selectivity for H_2S over competing analytes and was used to image exogenous H_2S in HeLa cells.

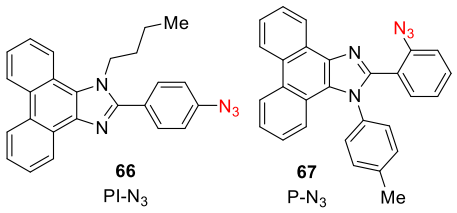


Figure 1.15. Examples of azide-based fluorescent H_2S probes based on phenanthroimidazole.

Rodembusch reported a series of (2′-hydroxyphenyl)benzothiazole (HBT) and (2′-hydroxyphenyl)benzoxazole (HBO) based ESIPT probes (**68**–**71**) with azide modifications at either the 5- or 6-position (Figure 1.16).[151] Treatment with H_2S in 50% EtOH in buffer resulted in a fluorescent response for each probe in the 425–500 nm range. The selectivity of these probes was not investigated, but each provided a fluorescent response in fixed T98G cells pre-treated with Cys. In 2014, Guo reported **72** that exhibited a 1150-fold fluorescence turn-on at 450 nm when incubated with H_2S and was selective for H_2S over anions, metals, RNS, ROS, and thiols.[152] This probe was also used to image both exogenous H_2S and endogenous H_2S by Cys and PMA addition melanoma B16 cells

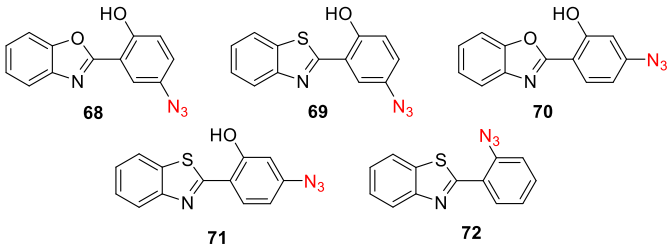


Figure 1.16. Examples of azide-based fluorescent H_2S probes based on benzoxazole and benzothiazole.

Qin and Tang groups designed **73** and **74** (TPE-Az and DPE-Az) in which the tetraphenylethylene-based **73** undergoes aggregation induced emission (AIE) upon azide reduction and **74** was used as a control compound in which the fluorescence of the probe did not involve AIE (Figure 1.17).[153] Treatment of **74** with H_2S in 20% DMSO in buffer resulted in a 60-fold luminescent turn-on at 493 nm. This probe was selective for H_2S over other biologically relevant anions and thiols. Focusing on a polycyclic aromatic hydrocarbon chromophore Sinha and Ghosh reported anthracene-derived **75**.[154] Treatment with H_2S in 50% DMSO in buffer resulted in a

fluorescence response at 505 nm, which was selective for H_2S over other biologically relevant anions, cations, and thiols.

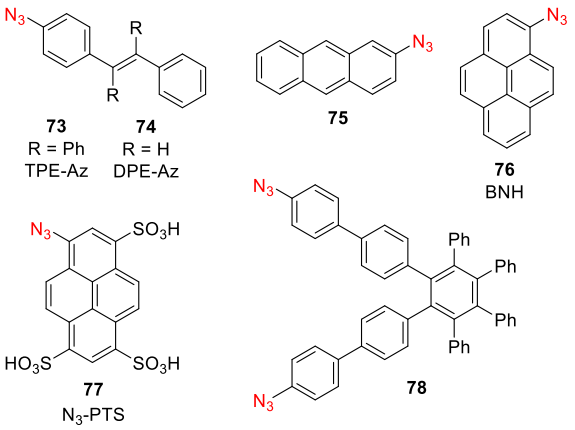


Figure 1.17. Examples of azide-based fluorescent H_2S probes based on conjugated and polyaromatic chromophores.

In 2017, Sun reported probe **76** (BTN) that exhibited a 20-fold fluorescence turn-on at 437 nm upon addition of H_2S in 80% DMSO in buffer.[155] The probe was shown to be selective for H_2S over other biological anions and thiols, although thiols did generate a minor fluorescent response. Probe **76** was then also used to develop paper test strips and used to detect H_2S spiked into red wine samples. In 2012, Hartman reported **77** (N_3-PTS) that exhibited a 7-fold fluorescence turn-on at 505 nm upon incubation with H_2S that was selective for H_2S over other anions.[156] The probe was used to quantify H_2S in FBS, although the sensitivity for the probe in FBS was lower than in buffer. Kumar also reported the two-photon excitation hydrophobic hexaphenylbenzene-based probe **78** that functions through AIE enhancement.[157] Treatment with H_2S in 30% DMSO in buffer resulted in a 30-fold fluorescence turn-on at 465 nm that was selective for H_2S over other competing analytes. The probe was further applied to develop paper test strips for H_2S and used to image exogenous H_2S in HeLa cells.

In 2012, Cho reported two-photon excitation probe **79** (FS1), which provides a 17- and 21-fold fluorescence turn-on at 548 nm for one- and two-photo excitation, respectively, with good selectivity for H_2S over other competing analytes (Figure 1.18).[158] Using two-photon excitation at 750 nm, probe **79** was used to image H_2S in HeLa cells in response to H_2S, Cys, and GSH. This probe was also used to image rat brain tissue samples at depths of up to 190 μm. In 2013, Chen

reported NBD-azide probe **80** that resulted in a 16-fold fluorescence turn-on at 550 nm upon treatment with H_2S that was selective for H_2S over other anions but was not evaluated with thiols.[159] The probe was also used to image exogenous H_2S in MCF-7 cells. The reported mechanism involves azide reduction, but it is also possible nucleophilic attack by H_2S to generate NBD-SH may be a competing process (*vide infra,* Section 4.3). In 2013, Xu, Xu, and Cui reported probe **81**, with provides a 55-fold turn-on response at 619 nm in 33% MeCN in buffer.[160] This probe showed good selectivity for H_2S over other biological anions, with small responses for both Cys and GSH, and was also used to image exogenous H_2S in HUVECs.

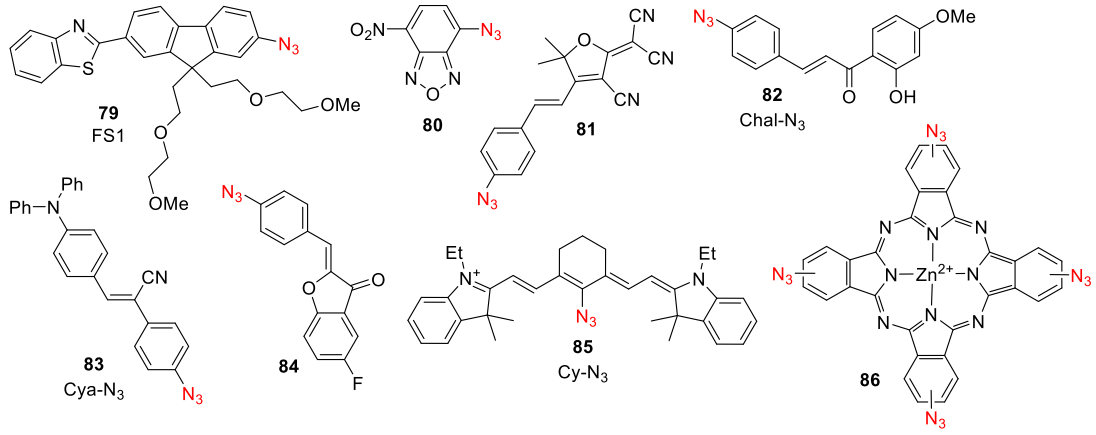


Figure 1.18. Additional examples of azide-based fluorescent H_2S probes based on various chromophores.

Also building from extended conjugated systems, Zhuang reported **82** (Chal-N_3), which was selective for H_2S over anions and thiols to produce a 258-fold fluorescence turn-on at 570 nm in 80% DMSO in buffer.[161] This probe was also used to quantify H_2S in various H_2S-spiked natural water samples. Hu and Liu reported ratiometric probe **83** (Cya-N_3) based on a cyanostilbene derivative that generates an AIE response.[162] Treatment with H_2S in 40% DMF in buffer resulted in a hypsochromic shift in fluorescence from 590 nm to 511 nm, which was selective for H_2S over other biologically relevant thiols and anions. Probe **83** was used to image exogenous H_2S in HeLa cells, which resulted in a shift from orange to green fluorescence upon H_2S-mediated AIE. Also working with an extended system, Miller and Handy reported aurone-based **84**, which reacted with H_2S to generate a fluorescence response at 560 nm.[163] This probe was selective for H_2S over Cys and GSH, but did provide a small response to 2-mercaptoethanol.

In 2012, Han reported cyanine-based **85** (Cy-N_3) that exhibited a ratiometric response with a decrease at 710 nm and increase at 750 nm upon H_2S addition and showed good selectivity for H_2S over other biological ROS, RNS, and RSS.[164] This probe was also used to quantify H_2S in water and FBS and additionally was used to image exogenous and endogenous H_2S stimulated by PMA in RAW264.7 cells. In 2020, Topal and Gürek developed **86** that utilized an aryl-azide functionalized Zn(II)-phthalocyanine that responded to H_2S with emission quenching at 698 nm and a fluorescence enhancement at 748 nm in DMSO and was selective for H_2S over other biological species although $S_2O_3^{2-}$ did produce a minor response.[165]

Wang reported the modified dansyl azide **87** (2,6-DNS-Az), which provides a 100-fold fluorescence turn-on at 525 nm when treated with H_2S (Figure 1.19).[166] The probe was selective for H_2S over other biological anions, including sulfur-containing reducing anions, and was further applied to measuring H_2S in FBS. Martínez-Máñez and Costero reported sulfonyl azide **88**, which when treated with H_2S, this probe provided a 20-fold turn-on responses with good selectivity for H_2S over other biological analytes.[123] Martínez-Máñez and Costero also reported related **89**, which provided a fluorescence response to H_2S at 557 nm in buffer with 50% MeCN in buffer and good selectivity for H_2S over biological anions and thiols.[167] This probe was also used to image exogenous H_2S in live HeLa cells. In 2020, Xiong and Kang reported **90** (DR-SO_2N_3) that can react with H_2S either by reduction of the sulfonyl azide and or by nucleophilic attack in the central ring system.[168] Treatment with one equivalent of H_2S resulted in new emissions at 435 nm and 584 nm, with the 435 nm signal increasing and the 584 nm signal decreasing with further H_2S addition. The probe was selective for H_2S over biothiols, amino acids, RNS, and ROS and further used to image exogenous H_2S in MCF-7 cells.

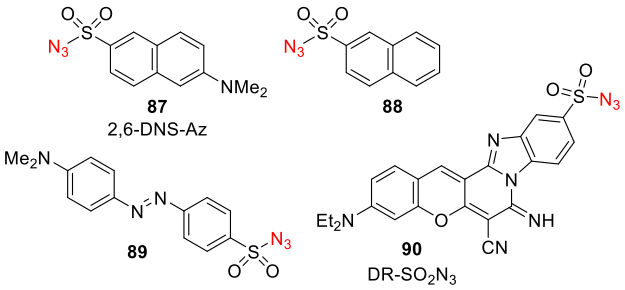
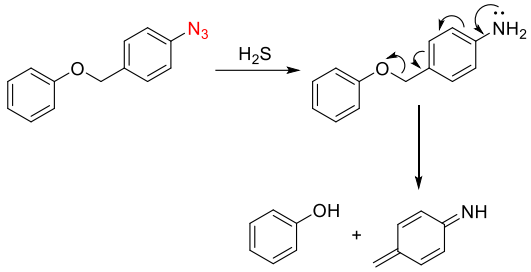


Figure 1.19. Examples of sulfonyl azide-based fluorescent H_2S probes.

1.2.1.2 Azide Reduction and Self-Immolation

In addition to direct incorporation of an azide on a fluorogenic nitrogen atom, other approaches have also been reported that use self-immolative or cascade reactions to translate azide reduction into fluorescent responses (Scheme 1.2). One benefit of this approach is that atoms other than nitrogen can be uncaged upon azide reduction, which broadens the palette of available fluorophores. Conversely, limitations of this approach include the addition of an extra reaction step to the activation process and the generation of an iminomethide (or similar) product, which likely reacts with water or possibly cellular nucleophiles to generate additional reaction byproducts.



Scheme 1.2. General pathway for coupling azide reduction to self-immolation cascades.

An early example of this strategy was reported in 2013 by Cho with **91** (TFCA), which generated a fluorescence turn-on at 750 nm, was compatible with two-photon excitation, and was selective for H_2S over other biologically relevant species in 50% EtOH in buffer (Figure 1.20).[169] Using two-photon imaging, **91** was further used to image and quantify exogenous and Cys/GSH-derived H_2S in HeLa cells and to investigate H_2S in rat colon tissue with a penetration depth of up to 146 μm. Following this, Song reported naphthalimide-based probes **92** (AcHS-1) and **93** (AcHS-2), which generated a ratiometric response with a fluorescence decrease at 468 nm with a concomitant increase at 530 nm and good selectivity for H_2S over other reactive species.[170] Both probes were used to image exogenous H_2S in SGC-7901 cells and were found to localize to the mitochondria. The same year Liu, Qian, and Zhao also reported **92** (NAP-1) and similarly observed a 24-fold enhancement of the emission intensity ratio (F_{541}/F_{474}) upon H_2S treatment, good selectivity for H_2S over biologically relevant analytes, and compatibility with imaging exogenous

H_2S in MCF-7 cells.[171] This probe was also used to image endogenous H_2S generated by SNP or PAG and also to measure H_2S in human plasma and mouse hippocampus.

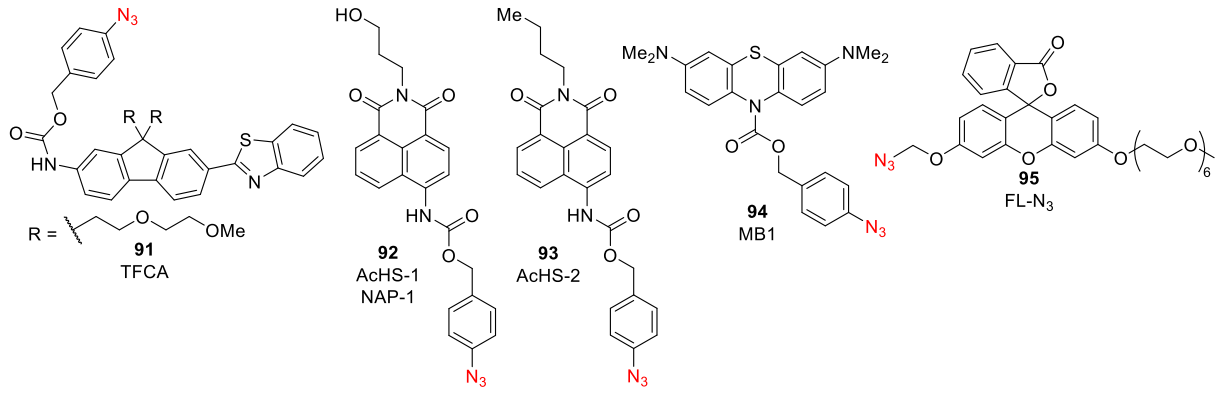


Figure 1.20. Examples of self-immolative azide-based fluorescent H_2S probes.

In 2019, Yin reported **94** (MB1), which exhibited a 49-fold fluorescence turn-on at 687 nm when treated with H_2S and was selective for H_2S over metal ions, amino acids, RSS, and ROS in 50% DMSO in buffer.[172] This probe was also used to image exogenous H_2S, endogenous H_2S stimulated with SNP, and H_2S levels in Ca^{2+}-treated HeLa cells. In 2023, Feng and Yang reported **95** (FL-N_3), which included a polyethylene glycol motif to increase water solubility.[173] This probe responded to H_2S with a 32-fold fluorescent turn-on at 515 nm, was selective for H_2S over thiols and biological anions, and was applied to image exogenous H_2S in MCF-7 cells.

In 2014, Chang reported ESIPT-based **96** that displayed an emission shift from 370 nm to 465 nm when incubated with H_2S, good selectivity for H_2S over other biological species, and compatibility with imaging exogenous H_2S in HeLa cells (Figure 1.21).[174] Dong reported a series of ESIPT probes (**97**–**99**) containing hydroxyl, tertiary amine, and quaternary ammonium groups to impart improved solubility.[175] Addition of H_2S to **97**–**99** resulted in a 3–20-fold fluorescence response at 475 nm, with probe **99** showing the highest response. This probe showed generally good selectivity for H_2S over competing analytes, with some probe activation from SO_4^{2-} and partial probe deactivation by $S_2O_5^{2-}$ and $S_2O_3^{2-}$, and the probe was subsequently used to image exogenous H_2S in HeLa cells.

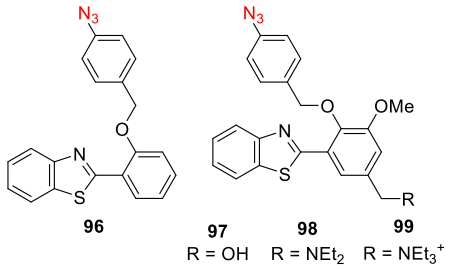


Figure 1.21. Examples of self-immolative azide-based fluorescent H_2S probes based on ESIPT chromophores.

Incorporating this approach into a BODIPY chromophore, Dong and Zhao reported pyridinium **100**, which releases the neutral pyridine-BODIPY construct after reaction with H_2S (Figure 1.22).[176] This probe provided a 27-fold turn-on at 517 nm with good selectivity for H_2S over other competing analytes. Probe **100** was also used to image exogenous H_2S in SMMC-7721 cells. Following this, Yin and Huo also reported **100** (BDP-N_3) as a viscosity sensitive H_2S probe.[177] Treatment with H_2S resulted in a fluorescent turn-on response at 515 nm in DMSO that was selective for H_2S over other analytes. The fluorescence of the probe also increases with increasing solvent viscosity as demonstrated by addition of glycerol. Probe **100** was further used to image both exogenous H_2S and changes in cellular viscosity after dexamethasone induced apoptosis. Gu reported **101** and **102** (N_3-BOD-E and N_3-BOD-C), both of which responded to H_2S with a fluorescence turn-on at 700 nm in buffer with CTAB, but only **101** was selective for H_2S over RNS, ROS, and thiols.[178] Probe **101** was further applied to image exogenous H_2S in cardiomyocytes.

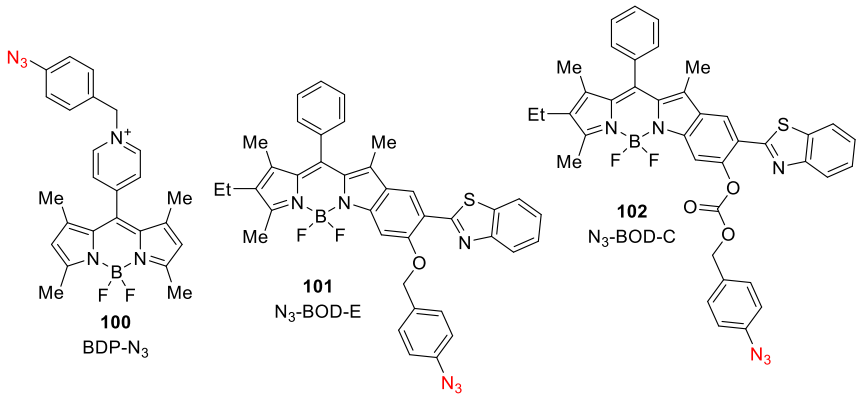


Figure 1.22. Examples of self-immolative azide-based fluorescent H_2S probes based on BODIPY chromophores.

Extended wavelength NIR probes have also been reported using azide reduction coupled with self-immolative linkers. For example, Kwon, Lee, and Yoon reported **103** (NIR-Az) that results in a 200-fold fluorescence turn-on at 720 nm when treated with H_2S (Figure 1.23).[179] This probe showed good selectivity for H_2S over competing analytes and was used to image exogenous H_2S in Raw 264.7 cells and live mice. Zhang reported the related sulfonated cyanine **104** ($CySO_3N_3$) to improve solubility.[180] Treatment with H_2S resulted in a fluorescent turn-on at 695 nm, and the probe showed good selectivity for H_2S with only a small activation by GSH. This probe was also used to image both exogenous and endogenous H_2S in HepG2 cells. Additionally, **104** was used to detect both endogenous and exogenous H_2S in H9C2 cells, H_2S increases after LPS treatment in Raw 264.7 cells, and exogenous H_2S in live mice. Moving to longer emission wavelengths, Shi, Zhang, and Song reported a self-immolative NIR-II emitting probe in **105** (BP-A), which upon reaction with H_2S generates a fluorescent response at 1032 nm with good selectivity for H_2S.[181] This probe was used to image exogenous H_2S in mice and also to image endogenous H_2S generation in subcutaneous tumors in 4T1 tumor-bearing mice.

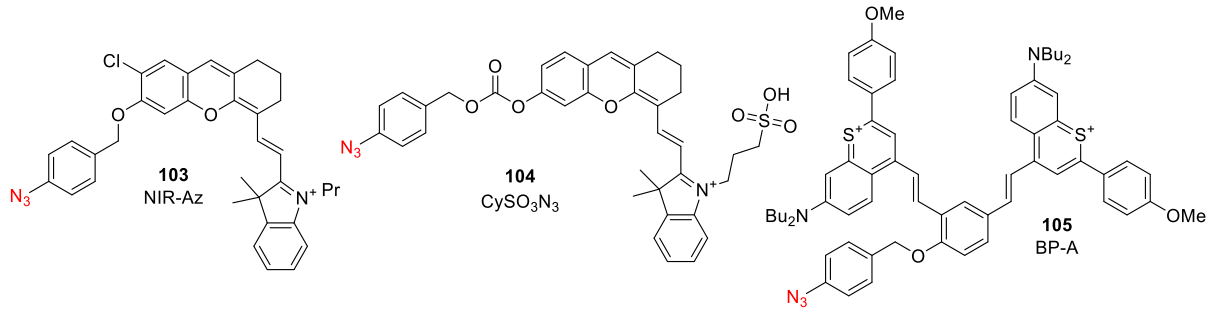


Figure 1.23. Examples of self-immolative azide-based fluorescent H_2S probes that function at extended wavelengths.

In 2018, Li and Li reported **106** (Mito-VS) that responds to increased viscosity with a red emission at 610 nm and responds to H_2S treatment with a green, 7-fold fluorescence turn-on at 510 nm (Figure 1.24).[182] The probe was shown to be selective for H_2S over thiols and ROS, found the localize in the mitochondria, and used to image viscosity and both exogenous and endogenous H_2S. In 2020, Wu, Peng, and Li reported **107** (Mito-HS), which also functioned as a dual responsive probe for both viscosity and H_2S with fluorescent responses at 750 nm and 585 nm, respectively.[183] The probe was selective for H_2S and viscosity changes over other biological

analytes. In addition, this probe was used to image changes in viscosity and exogenous H_2S in live HepG2 cells using both one- and two-photon microscopy and also to investigate the relationship between Cys-derived H_2S and local viscosity. In 2023, Wang reported **108** (NIR-H_2S) that responded to H_2S with a fluorescence turn-on centered at 693 nm and a large Stokes shift (258 nm) in 50% DMF in buffer.[184] The probe was selective for H_2S over other biological species, showed good photostability, and was used to image exogenous and endogenous H_2S in HeLa cells.

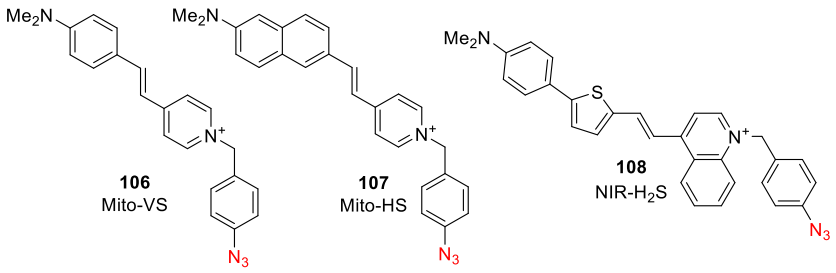


Figure 1.24. Additional examples of self-immolative azide-based fluorescent H_2S probes that also report on changes in viscosity.

Self-immolative H_2S-reporting approaches have also been developed that couple H_2S-mediated azide reduction with H_2S release. For example, in 2016 Pluth reported methylrhodol-based **109** (MeRho-TCA) that contains a thiocarbamate motif in the self-immolative linker (Figure 1.25). Upon reaction with H_2S, the self-immolative cascade reaction release carbonyl sulfide (COS), which is converted to H_2S by the ubiquitous enzyme carbonic anhydrase.[185] Reaction with H_2S resulted in 65-fold fluorescence turn-on at 515 nm with good selectivity for H_2S. We note that although this approach releases one equivalent of H_2S, two equivalents of H_2S are required for azide reduction, so this approach does not fully replace H_2S consumed by the probe. This 'analyte replacement' approach has also been applied to other small molecule reactive species like formaldehyde and CO,[186, 187] and the general approach of using the intermediate release of COS as a H_2S precursor has been expanded to develop a variety of H_2S donor motifs.[188-190]

Hu and James translated this approach to develop NIR **110** (HL-H_2S) that reports on both changes in local viscosity and H_2S.[191] In buffer containing 80% glycerol and 2% DMSO, **110** exhibited a 25-fold fluorescence turn-on at 670 nm when treated with H_2S and was selective for H_2S over other analytes. This probe was demonstrated to detect exogenous H_2S and later used to investigate ferroptosis in a cellular model and mouse model of middle cerebral artery occlusion in

mice. Importantly, the partial replacement of H_2S by probe **110** avoided inducing ferroptosis by minimally impacting the redox state of the system. In 2022, Zhang reported analyte replacement probe **111** (NP-SN_3) that exhibited a fluorescence turn-on at 520 nm upon incubation with H_2S and released H_2S after azide reduction.[192] This probe was used to image exogenous and endogenous H_2S in HepG2 cells pretreatment with Cys or PAG and exogenous H_2S in larval zebrafish. In addition, comparison of this probe to non-analyte replacement **93** revealed that **111** decreased the degree of liver fibrosis in a cell model, increased the hatch rate of zebrafish embryos, and generated lower liver toxicity in rats.

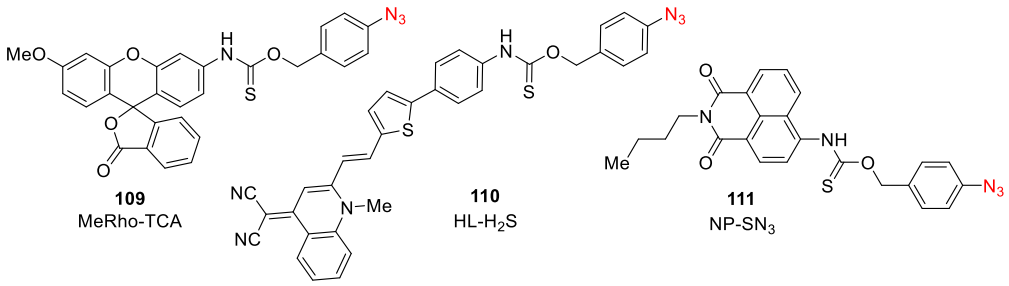


Figure 1.25. Examples of self-immolative "analyte replacement" azide-based fluorescent H_2S probes.

Zhu and Sun reported iminocoumarin benzothiazole-based probe **112** in 2015, which utilizes a self-immolative linker to release the parent phenol upon reaction with H_2S (Figure 1.26).[193] In this specific example, the resultant phenol subsequently attacks the proximal nitrile to generate the final iminocoumarin fluorescent product. Treatment with H_2S results in an 80-fold fluorescence turn-on at 520 nm with good selectivity for H_2S over other analytes, although minor activation with Cys was also observed. This probe was used further to image exogenous H_2S in HeLa cells. Talukdar also reported a similar approach in 2015 with probe **113**, which also forms an iminocoumarin product after reaction with H_2S and subsequent cyclization.[194] Addition of H_2S resulted in a 31-fold fluorescence increase at 480 nm with accompanying decrease at 580 nm. Probe **113** showed good selectivity for H_2S over competing analytes and was also used to image exogenous H_2S in HeLa cells. This approach was later also used by Song in the development of iminocoumarin-based **114**.[195] This probe generates a fluorescent response at 610 nm upon reaction with H_2S, provides good selectivity for H_2S over competing analytes, and was used to image exogenous and SNP-derived H_2S in HeLa cells. Using a related approach, Xu reported NBD-based

probe **115**, in which azide reduction initiates a self-immolative decay to release the amine fluorophore and CO_2.[196] Treatment with H_2S in 10% MeCN in buffer provided a fluorescence increase at 550 nm that was selective for H_2S over other reactive species. This probe was used further to image exogenous H_2S in HT-29 cells.

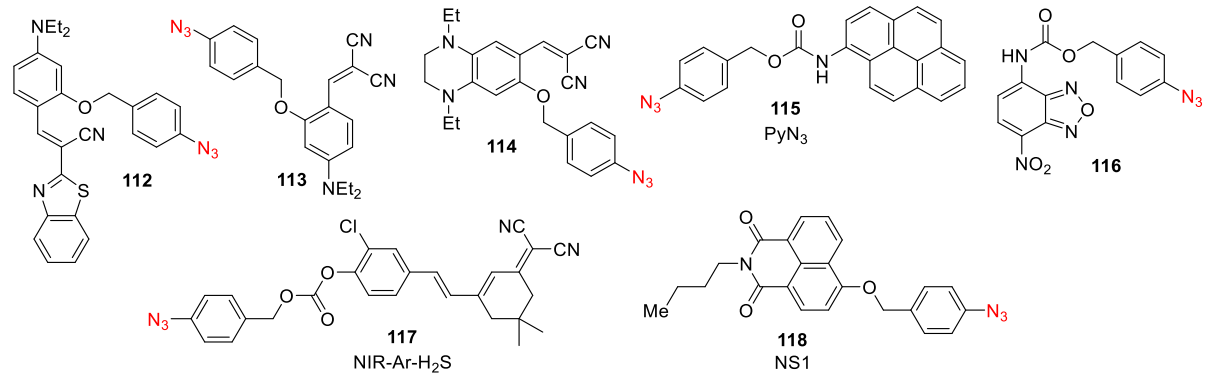


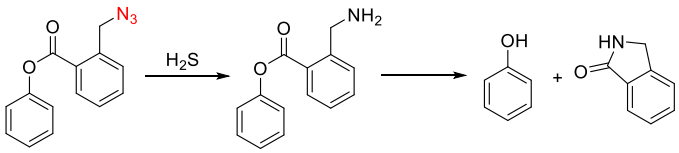
Figure 1.26. Additional examples of self-immolative azide-based fluorescent H_2S probes with various chromophores.

In 2017, Wu developed pyrene-based **116** (PyN_3) that responds to H_2S with a fluorescence turn-on at 346 nm that is selective for H_2S over other biological anions and thiols.[197] The probe was used to image exogenous and SNP-derived H_2S in MCF-7 cells and exogenous H_2S in larval zebrafish. In 2023, Lin reported **117** (NIR-Ar-H_2S) that exhibited a 40-fold fluorescence turn-on at 680 nm in response to H_2S that was selective for H_2S over biological species such as thiols, anions, cations, and ROS.[198] The probe was also used to image exogenous and endogenous H_2S confirmed by Cys or *N*-ethylmaleimide (NEM) pretreatment in HeLa cells. Furthermore, the probe was applied to mouse arthritis model to show decreases in H_2S levels in response to treatment with the arthritis drug methotrexate. Han and Xia also reported ratiometric probe **118** (NS1), which response to H_2S in 50% EtOH in buffer to provide a fluorescence decrease at 444 nm and increase at 539 nm.[199] This probe showed good selectivity for H_2S over competing species and was used to image exogenous H_2S in MCF-7 cells.

1.2.1.3 Azide Reduction and Intramolecular Reaction

Different approaches have also coupled H_2S-mediated azide reduction with subsequent cyclization to generate a fluorescent response. Examples of this approach include reduction to the parent amine followed by intramolecular cyclization to cleave an esterified fluorophore or attack

on a pendant electrophile to form a conjugated system. One such approach is shown in Scheme 1.3, in which reduction of an aliphatic azide generates a benzylamine product, which undergoes a subsequent cyclization to release a phenolic fluorophore. This approach has yielded a number of probes for H_2S, but we also note benzyl azides are good electrophiles, which may in some cases allow for nucleophilic displacement of the azide by H_2S to occur, akin to the approaches described in section 4.4.4. In our hands, the reduction of aliphatic azides by H_2S is significantly slower than aryl azides, and this difference is reflected often the abiological millimolar H_2S concentrations often used when screening many of the aliphatic azide systems.



Scheme 1.3. General pathway for azide reduction followed by intramolecular reaction.

In 2012, Han reported **119** (AzMB-coumarin), which reacts with H_2S to generate an amine intermediate that then undergoes intramolecular reaction to form the fluorescent coumarin product and isoindolinone (Figure 1.27).[200] Treatment with 1 mM H_2S in 20% MeCN in buffer resulted in a fluorescent turn-on at 450 nm, with good selectivity over representative biological thiols and other reactive species. This probe was further applied to image exogenous H_2S in HeLa cells. Koszelewski and Ufnal expanded on this approach to develop coumarin-based **120** and **121**, which undergo aliphatic azide reduction and intramolecular lactamization to produce a fluorescence response.[201] Treatment with H_2S in 20% MeCN in buffer provided a 1000-fold enhancement at 445 nm, but the selectivity against other analytes was not reported. Probe **120** was further applied to detecting exogenous and endogenous H_2S in saliva samples.

Talukdar later reported a similar approach in 2015 using a resorufin-based system to develop **122** (Reso-N_3).[202] Treatment with 5 mM H_2S resulted in a 614-fold fluorescence enhancement at 585 nm, and the probe showed good selectivity for H_2S over competing analytes, although a small response to Cys was observed. As shown in Figure 1.28, co-incubation of 5 mM **122** with equimolar GSH or Hcy was found to blunt the response of the probe to H_2S, which highlights the complexities of detecting low levels of H_2S in the presence of higher levels of competing thiols. This probe was also used to image exogenous H_2S in HeLa cells.

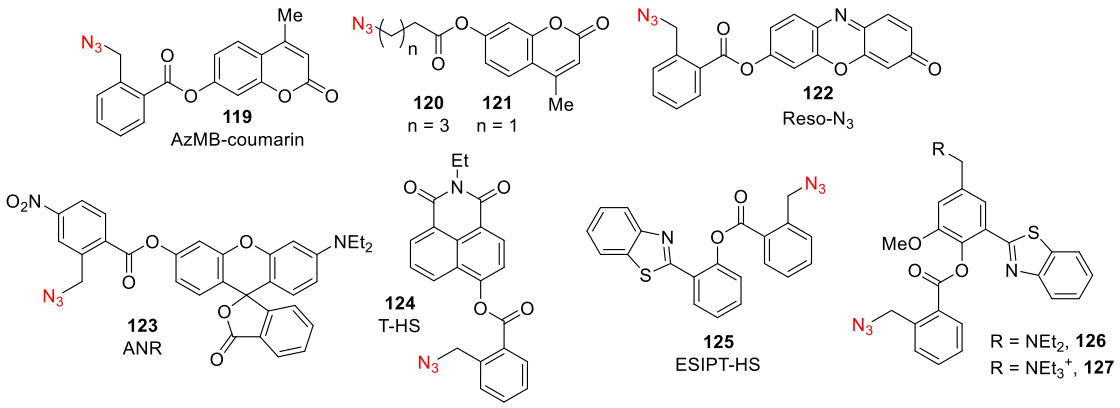


Figure 1.27. Examples of azide-based fluorescent H_2S probes that function through subsequent intramolecular cyclization to remove a protecting group.

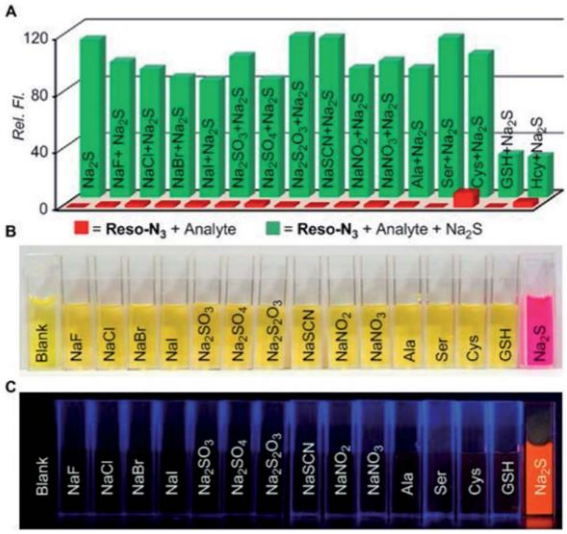


Figure 1.28. (a) Selectivity of 10 µM **122** in response to 5 mM of H_2S and different analytes. (b,c) Corresponding visible and fluorescent response, respectively, of 50 µM **122** in response to different analytes. Reproduced with permission from ref [202]. Copyright 2015 Royal Society of Chemistry.

In 2015 Zhan and Zhang developed **123** (ANR), which generated a fluorescence turn-on at 550 nm, was selective for H_2S over thiols and biological nucleophiles, and further used to image exogenous H_2S in 3T3 cells.[203] In 2023, Ren developed **124** (T-HS) that exhibited a fluorescence turn-on at 570 nm with H_2S treatment and was selective for H_2S although produced a minor response to other biological analytes.[204] The probe was used to image exogenous H_2S and endogenous H_2S by pre-incubating with Cys or PAG in HepG2 cells. Furthermore, the probe was used to image H_2S in mouse liver tissue with two-photon microscopy and also in zebrafish. The

same protecting group removal strategy was also used by Lin to develop **125** (ESIPT-HS).[205] Treatment with H_2S in 30% DMSO in buffer resulted in a 400-fold fluorescence turn-on at 462 nm. This probe showed good selectivity for H_2S over competing analytes and was used to image exogenous and Cys-derived H_2S in HeLa cells. Dong used a related chromophore system to develop **126** and **127** with functionalization to improve solubility.[175] Reaction with H_2S resulted 3–20-fold fluorescence turn-on at 475 nm, but the kinetics of these systems were found to be much slower than the related self-immolative scaffolds **97**–**99**, which is consistent with the lower sensitivity of aliphatic azides toward H_2S.

In 2019, Bandyopadhyay reported **128** and **129** that featured azide reduction followed by intramolecular cyclization with a resulting 70- and 10-fold fluorescent turn on responses at 445 and 440 nm, respectively.[206] These probes were selective for H_2S over biological oxidants, reductants, and nucleophiles. Probe **128** was then used to quantify H_2S in various water samples and image exogenous H_2S in *Drosophila* ovary. Also using an intramolecular cyclization approach, but without protecting group removal, Xu and Qian reported **130**, in which the amine formed upon azide reduction underwent a cascade reaction with the aldehyde to form an indole product (Figure 1.29).[207] Addition of H_2S resulted in a 10-fold turn-on response at 520 nm with good selectivity for H_2S over competing analytes. This probe was further used to image exogenous H_2S in HeLa cells. Yang and Guo used a related approach to develop NIR ratiometric probe **131**, in which a coumarin-benzopyrylium scaffold undergoes an intramolecular spirocyclization after azide reduction.[208] Treatment with H_2S resulted in a decrease in the 702 nm emission with concomitant increase at 478 nm with good selectivity for H_2S over other analytes. The ratiometric probe response to exogenous H_2S was also confirmed in HSC cells.

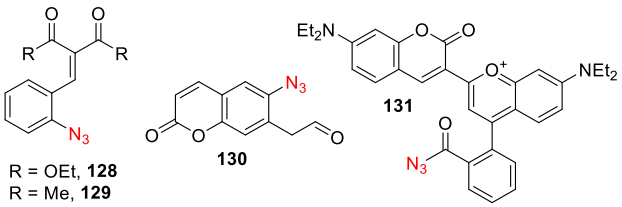


Figure 1.29. Additional examples of azide-based fluorescent H_2S probes that function through subsequent intramolecular cyclization.

1.2.1.4 Azide Reduction with Dual Reactivity

H_2S detection based on azide reduction has also been coupled with other analyte responsive groups to develop dual responsive probes. In some cases, this has included using different activity-based components to respond to multiple analytes, whereas in other cases has included sequential reactions at the same site on the probe. These probes are different than H_2S probes that contain multiple H_2S-reactive groups for the purpose of only sensing H_2S, and will refer to the latter as bifunctional probes for clarity. In this section, we highlight a number of compounds that use the above approaches to develop tools that respond to H_2S and a second analyte.

In 2014, Ramaiah reported *bis*-azide **132**, which detects H_2S through azide reduction and NO through subsequent amine oxidation (Figure 1.30).[209] Treatment with H_2S resulted in a 97-fold turn-on at 750 nm, with selectivity demonstrated for H_2S over other anions. Subsequent addition of NO or NO_2^- to the amine product resulted in a shift in the absorbance of the probe to form a green product that corresponded to the parent phenol. This final oxidation step required acidic conditions, so likely is not general for all azide-based probes at physiological pH.

Dual sensing approaches have also been used for detecting both H_2S and cellular oxidants. For example, Wang and Song reported **133** (Han-HClO-H_2S) that has a red signal at 640 nm and displays dual reactivity with H_2S and HClO to blue (450 nm) and green (520 nm) fluorescent responses, respectively, in 50% MeCN in buffer.[210] The probe was shown to be selective for H_2S/HClO over other biologically relevant species and was used to image exogenous H_2S and HClO in MCF-7 cells. Similarly, Lin reported **134** (Lyso-HA-HS) that responds to both H_2S and HClO with morpholine incorporation for lysosomal targeting.[211] H_2S addition results in azide reduction and coumarin-based fluorescence, whereas HClO addition results in hydrazine cleavage and rhodamine-based fluorescence. Upon addition of both H_2S and HClO, signals from both fluorophores are observed at 448 and 580 nm, respectively. This probe was further used to image exogenous H_2S and HClO in HeLa cells, both individually and in combination, as well as endogenous H_2S and HClO in HeLa and Raw 264.7 cells after treatment with Cys and LPS, respectively. Song and Wang developed **135** (TCAB) with a blue signal at 413 nm and displays dual reactivity with H_2S producing a new red emission at 627 nm and H_2O_2 reactions with the boronate to produce a new cyan emission at 486 nm in buffer with CTAB.[212] The probe was shown to be selective for H_2S/H_2O_2 over other ROS, anions, cations, and thiols. The probe was further

used to image both exogenous and endogenous H_2S/H_2O_2 from PMA and SNP treatment in HeLa cells and also to image exogenous H_2S/H_2O_2 in larval zebrafish.

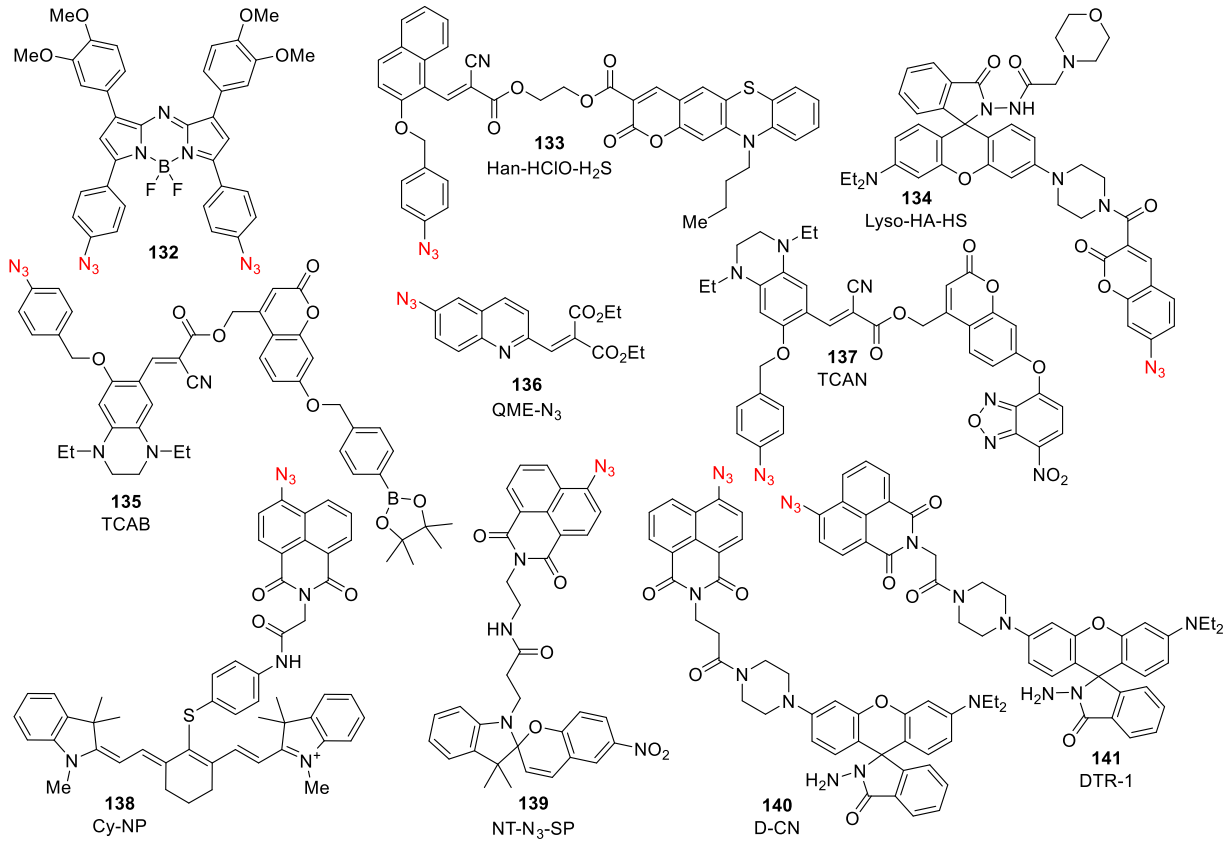


Figure 1.30. Examples of azide-based fluorescent H_2S probes that contain dual reaction sites to report on multiple types of species.

Expanding to different reaction sites for different analytes, Song reported probe **136** (QME-N_3), which has contains an azide and a α,β-unsaturated carbonyl group for reaction with H_2S and thiols, respectively.[213] Both H_2S and thiol addition are required for full probe activation, with treatment of Cys alone only generating a 2-fold fluorescence response at 455 nm. The probe was shown to be selective for H_2S / thiol combinations over other competing analytes and was subsequently used to image exogenous H_2S in MCF-7 cells using two-photon excitation at 700 nm. Further evidence for the requirement of both thiols and H_2S was provided by pretreatment of cells with thiol scavenger NEM, which reduced the overall fluorescence response.

Further focusing on separating the reactivity of different RSS, Yang and Song reported **137** (TCAN), which can be used to differentiate Cys/Hcy, GSH, and H_2S by utilizing an azide for H_2S

detection and NBD group for thiol differentiation (*vide infra,* section 4.3).[214] Depending on the analyte or analyte combination, different responses were observed in the blue, green, and red channels. For example, treatment with H_2S provided a "blue-red" response, whereas Cys/Hcy provided a 'blue-green" response, with GSH resulting solely in a "blue" response. The signal selectivity was confirmed using *in vitro* selectivity studies and also in HeLa cells and zebrafish. In addition, treatment with NEM abates the signal outputs due to thiol scavenging. The application of imaging different thiol/H_2S combinations is shown in Figure 1.31. Following this, Ding and Pu reported **138** (Cy-NP) that contains an azide-functionalized naphthalimide linked via thioether to a cyanine dye.[215] The probe responds to H_2S with a fluorescence turn-on at 450 nm and responds to Cys with a fluorescence turn-on at 560 nm and could sense both H_2S and Cys simultaneously. Probe **138** was shown to be selective for H_2S and Cys over other biological analytes including other biothiols and was used further to develop test strips for H_2S detection in food and also used to image H_2S/Cys in MCF-7 cells.

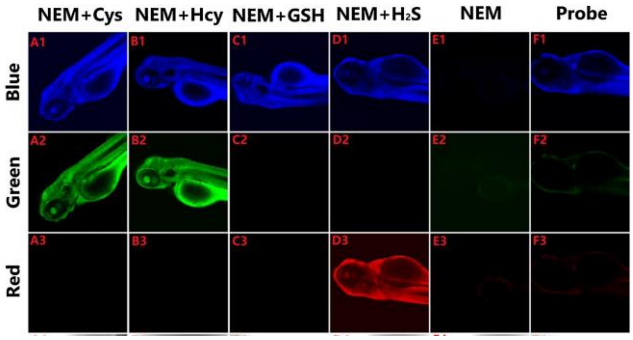


Figure 1.31. Fluorescent responses from **137** in zebrafish pretreated with NEM followed by different combination of Cys, Hcy, GSH, and H_2S. Reproduced with permission from ref [214]. Copyright 2019 Elsevier.

Also focusing on dual reactivity with RSS, Yin reported **139** (NT-N_3-SP), which utilizes an azide-modified naphthalimide and also spiropyran that converts to an SO_2-reactive merocyanine upon UV irradiation.[216] Addition of H_2S results in a fluorescence increase at 540 nm, and UV-activation followed by treatment with SO_3^{2-} results in fluorescence quenching at 630 nm. This probe was used to detect exogenous H_2S and SO_2 in HepG2 cells and also changes in intensity upon treatment with SNP and LPS.

Approaches for H_2S and Cu^{2+} detection have also been reported that utilize azides as the H_2S-detection motif. For example, Kong reported **140** (D-CN), which contains a naphthalimide azide and rhodamine-based hydrazine that can be cleaved by Cu^{2+} to generate rhodamine fluorescence.[217] Addition of H_2S results in a 40-fold fluorescence turn-on at 540 nm, and addition of $CuSO_4$ results in a 31-fold fluorescence increase at 586 nm. This turn-on response for both analytes was confirmed using exogenous H_2S and Cu^{2+} in HeLa cells and zebrafish, with further experiments also demonstrating Cys-derived H_2S production in HeLa cells. Pu reported probe **141** (DTR-1), which differs from **140** by one methylene unit and also responds to both Cu^{2+} and H_2S.[218] Treatment with H_2S in 90% DMF in buffer resulted in a 34-fold fluorescence turn-on at 560 nm and treatment with Cu^{2+} resulted in a turn-on response at 630 nm. This probe was also used to image exogenous H_2S and Cu^{2+} in HeLa cells.

1.2.1.5 FRET-Based Azide Reduction

Förster resonance energy transfer (FRET) is a process that occurs between two fluorophores in close proximity in which the emission of the donor fluorophore overlaps with absorption spectrum of the acceptor fluorophore. In such systems, excitation of the donor results in excited state transfer through nonradiative dipole–dipole coupling to the acceptor fluorophore and subsequent emission. A variety of FRET based systems have been developed in which H_2S-mediated azide reduction on either a donor or acceptor in a FRET pair allows for either a turn-on or ratiometric response. In some cases, such probes could also be included in other sections of this Review based on additional probe properties, but we have focused on highlighting several examples of this general principle in this subsection.

Huo and Yin later reported the coumarin-fluorescein probe **142** (Flu-N_3), which resulted in a 50-fold turn on when treated with H_2S in 90% MeCN in buffer (Figure 1.32).[219] This probe was also used to image exogenous H_2S in HepG2 cells and mice. Wang and Tang developed rhodamine-coumarin linked **143** (RPC-1) that responds to H_2S with a fluorescence turn-on at 445 nm and/or HClO with a fluorescence turn-on at 580 nm.[220] The probe was selective for H_2S and HClO over other biological analytes and was further used to image both exogenous and endogneous H_2S and HClO modulated with NAC, LPS, and PMA in Raw 264.7 and HepG2 cells. Further, H_2S and HClO were investigated in a mouse model of drug-induced liver injury. Using a rhodol-coumarin linked probe, Zhang and Zhang reported **144** (N_3-CR-PO_4) that responds to H_2S

with a blue fluorescence turn-on at 445 nm and to phosphatase with a green fluorescence turn-on at 545 nm.[221] The probe was selective for H_2S and phosphatase over other biological analytes and was further used to image both exogenous and endogenous H_2S and phosphatase levels modulated by AOAA, PMA, and Na_2VO_4, as well as to investigate the relationship between H_2S and phosphatase activity in HeLa cells.

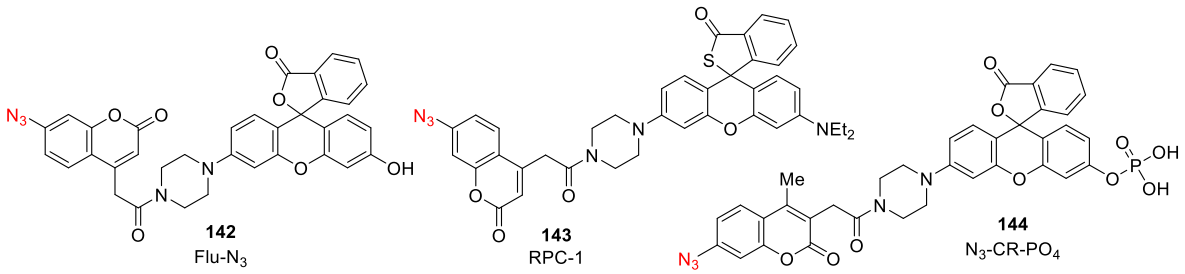


Figure 1.32. Examples of azide-based fluorescent H_2S probes that function through FRET mechanisms.

In 2015, Wei reported the ratiometric coumarin-naphthalimide adduct **145** (CN-N_3), which provides a 9-fold ratiometric response (F_{534}/F_{474}) toward H_2S in 50% EtOH in buffer (Figure 1.33).[222] This probe showed good selectivity toward H_2S over competing species, although some response to Cys and GSH was observed. Addition of H_2S or pre-incubation with Cys led to the expected ratiometric response in PC-3 cells. In 2019, Wu and Bhuniya reported coumarin-naphthalimide linked **146** (PHS1) that reacted with H_2O_2 to generate a 35-fold fluorescence turn-on at 390 nm and reacted with H_2S to generate a 32-fold fluorescence turn-on at 550 nm, with FRET occurring with co-incubation of both analytes.[223] The probe was selective for H_2S/H_2O_2 over other biological analytes and was used to image H_2S and H_2O_2 in HT29 and HeLa cells and larval zebrafish.

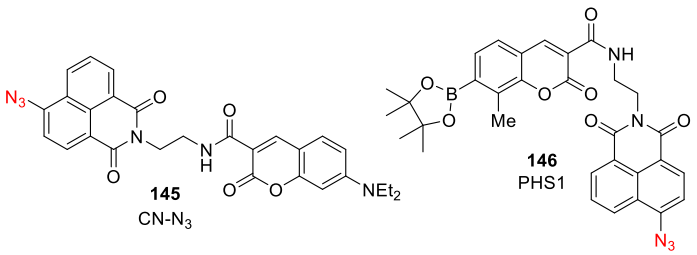


Figure 1.33. Examples of azide-based fluorescent H_2S probes based on coumarin / naphthalimide FRET pairs.

In 2015, Zeng and Wu reported the dual functional rhodamine-naphthalimide linked **147** (Naph-RhB) that responds to H_2S with a fluorescence turn-on at 539 nm and responds to NO with a fluorescence turn-on at 570 nm in 20% MeCN in buffer (Figure 1.34).[224] The probe was selective for H_2S and NO over other RSS, RNS, and ROS, although GSH and Cys did elicit a minor response at 539 nm. This probe was used to develop a logic gate response model and was also used to image exogenous H_2S and NO in L929 cells.

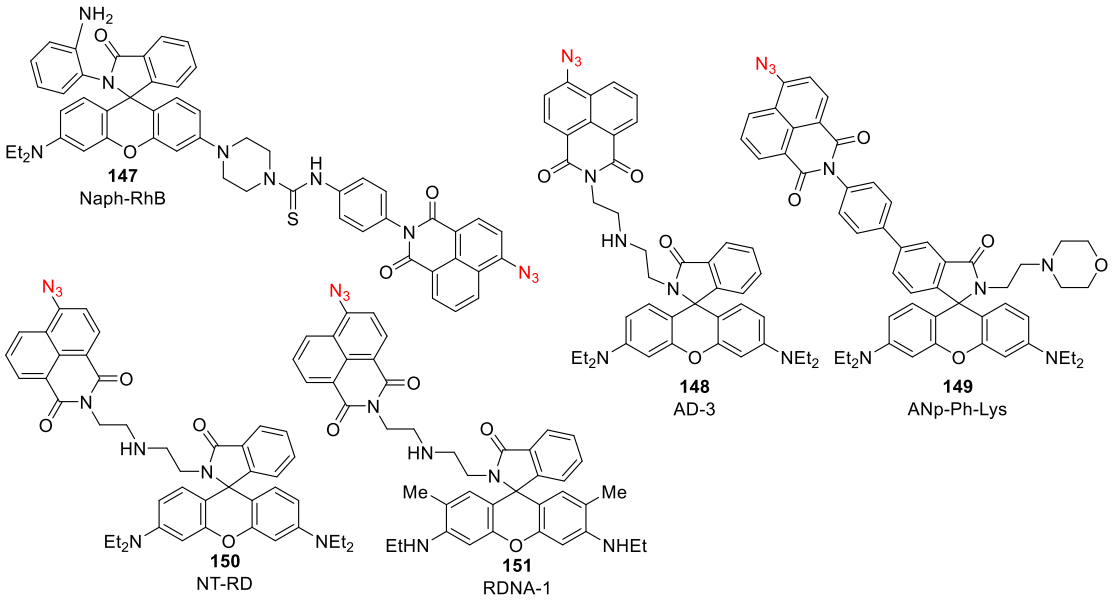


Figure 1.34. Examples of azide-based fluorescent H_2S probes based on naphthalimide / rhodamine FRET pairs.

In 2022, Jing and Wang developed rhodamine-naphthalimide linked **148** (AD-3) to respond to H_2S with a fluorescence turn-on at 528 nm and/or ATP with a fluorescence turn-on at 577 nm.[225] The probe was selective for H_2S and ATP over anions, thiols, amino acids, and metal ions. Furthermore, the probe was used to image exogenous and endogenous H_2S/ATP with stimulation with SNP and oligomycin using two-photon microscopy in HT22 cells. After confirming the probe can pass through the blood-brain barrier, this probe was also used to image H_2S/ATP in the brain of AD mice treated with various natural drugs. In 2020, Zhang and Zhang developed lysosome-targeted, rhodamine-naphthalimide linked **149** (Anp-Rh-Lys) that responds to H_2S with a fluorescence turn-on at 530 nm and responds to acidic pH with opening the spirolactam of the rhodamine to produce a new fluorescent signal at 580 nm.[226] The probe was shown to be selective

for H_2S and pH changes over biological anions, cations, thiols, and amino acids and was used to image H_2S and changes in pH in the lysosome of HeLa cells. Yin also reported H_2S/ATP responsive probe in **150** (NT-RD), which featured a fluorescence turn-on at 550 nm with the treatment of H_2S and/or a fluorescence turn-on at 585 with the treatment of ATP.[227] The probe was selective for H_2S and ATP over other biological species and was used to image exogenous H_2S/ATP and Cys-derived H_2S in HCT116 cells. Ye developed lysosome-targeted **151** (RDNA-1) that responded to H_2S with a fluorescence turn-on at 530 nm and/or ATP with a fluorescence turn-on at 560 nm in 10% DMSO in buffer.[228] The probe was selective for H_2S and ATP over other biological analytes, was demonstrated localize to the lysosome, and was used to image exogenous H_2S and ATP. The effect of anticancer drugs on H_2S and ATP levels in cells was also investigated, and the probe was used to image exogenous H_2S/ATP in larval zebrafish.

Also in 2014, Tang reported a series of FRET-based H_2S probes (**152**–**156**, FRET-P1–5) built from fluorescein isothiocyanate with different immolative linkers (Figure 1.35).[229] Of these constructs, **156** showed the highest sensitivity for H_2S with a 12-fold fluorescence turn-on at 538 nm in 40% DMF in buffer with good selectivity over other RSS. This probe also provided a fluorescent response in HeLa cells when treated with H_2S and GSH.

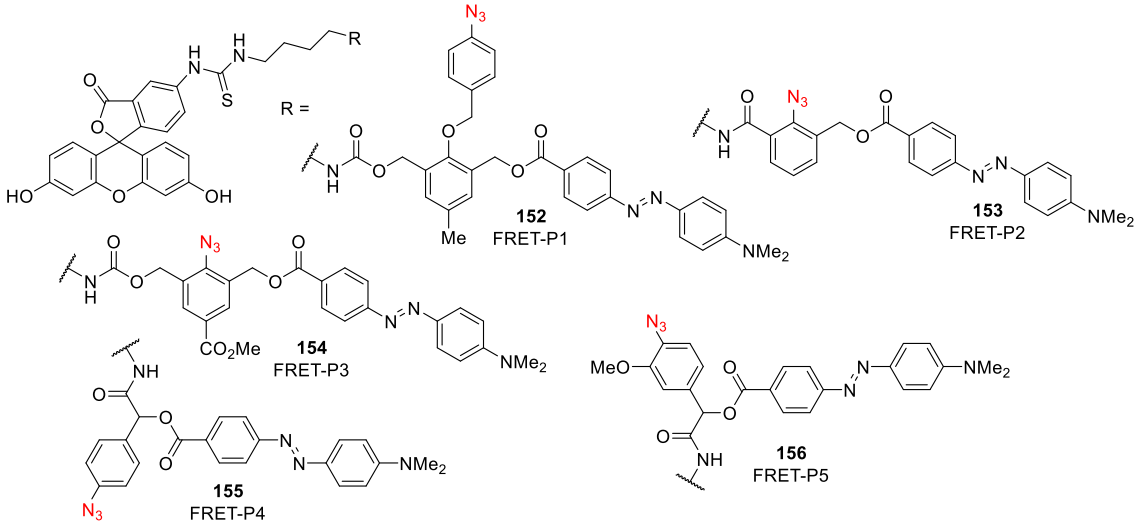


Figure 1.35. Examples of azide-based fluorescent H_2S probes based on fluorescein isothiocyanates.

Yi reported an early example of a FRET approach in H_2S detection in 2014 with coumarin-BODIPY probes **157** and **158** (Figure 1.36).[230] Treatment with H_2S results in amine reduction to form the parent aminocoumarin dye, which restores the FRET between the two chromophores and an increase in 508 nm emission when excited at 360 nm. This probe showed good selectivity for H_2S over other reactive species and was used to image both exogenous and D-Cys-derived H_2S in HEK293 cells. In 2021, Zhang, Yoon, and Ren reported methylene blue-naphthalimide linked **159** (MB-N-NAP) that showed dual reactivity and responded to H_2S with a 22-fold fluorescence turn-on at 533 nm and/or HClO with a 26-fold fluorescence turn-on at 690 nm in 60% DMSO in buffer.[231] The probe was selective for H_2S and HClO over other biological analytes, although HClO gave a minor response at 533 nm. The probe was used to image endogenous H_2S and HClO confirmed with AOAA and PMA in a variety of normal and cancer cells.

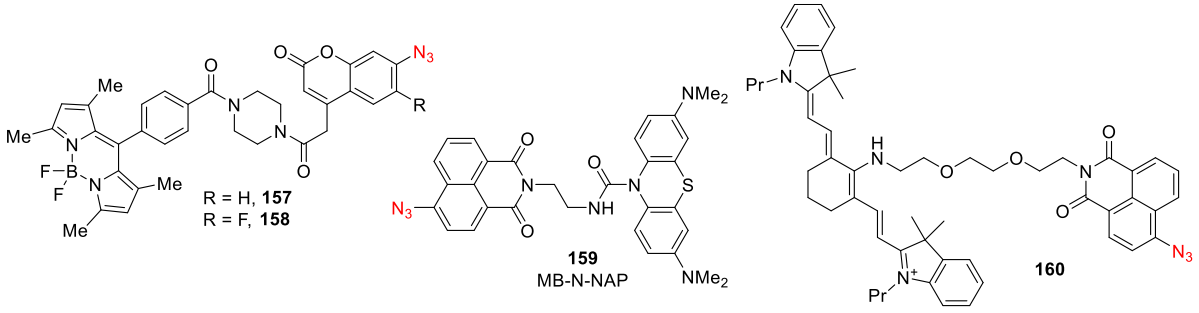


Figure 1.36. Additional examples of azide-based fluorescent H_2S probes that function through FRET mechanisms.

As an additional example, Liu and Shangguan reported mitochondria-targeted **160** based on the cyanine dye IR-780.[232] Upon treatment with H_2S this probe provided an increased F_{530}/F_{733} ratiometric response with conversion at different timepoints verified by HPLC. This probe was confirmed to detect both exogenous and endogenous H_2S in HeLa cells. Moreover, highlighting the benefits of ratiometric detection, this probe provided a linear ratiometric response to increasing exogenous H_2S level in live cells as shown in Figure 1.37.

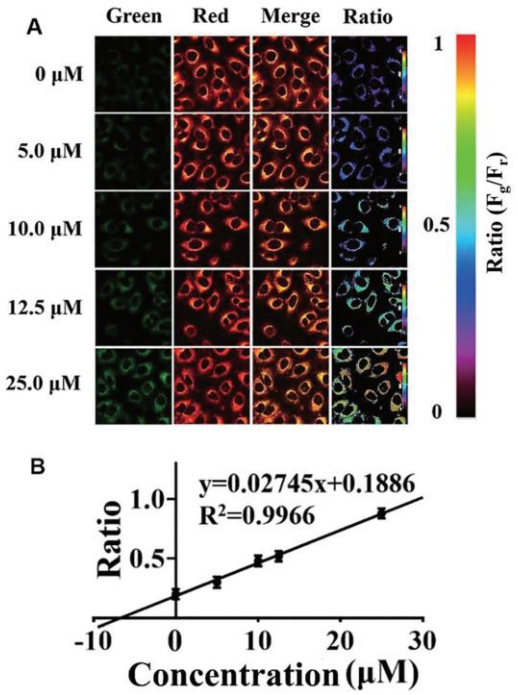


Figure 1.37. (top) Fluorescent images of **160** incubated with increasing amounts of H_2S in HeLa cells. (bottom) Linear relationship of the measured fluorescence ratio against H_2S concentration. Reproduced with permission from ref [232]. Copyright 2020 Royal Society of Chemistry.

1.2.1.6 Targeted Azide-Based Probes

Azide-based probes for H_2S detection have also been developed that contain functional groups that impart accumulation in specific subcellular organelles. Such probes provide useful tools to investigate the role of H_2S in specific organelles, which provides an important approach to better understand the H_2S generation, translocation, and action. As an early example of this approach, Yang reported the lysosome targeted probe **161** (SulpHensor), which uses a morpholine moiety to target the lysosome and a spirolactam moiety that only becomes fluorescent in acidic environments (Figure 1.38).[233] In a neutral solution, treatment of **161** with H_2S failed to generate a fluorescence response, whereas fluorescence was observed in mildly acidic conditions. This probe was further used to image exogenous H_2S in HeLa cells and confirmed to localize within lysosomes. A related approach was later reported by Liu and Miao with rhodamine-based probe **162** (MF-N_3).[234] Upon addition of H_2S, **162** displays a 16-fold fluorescence turn-on at 560 nm only at acidic pH values (<6.5), although some response to Cys and GSH was also observed. This probe was also used to image exogenous H_2S in HepG2 cells and confirmed to localize the lysosome.

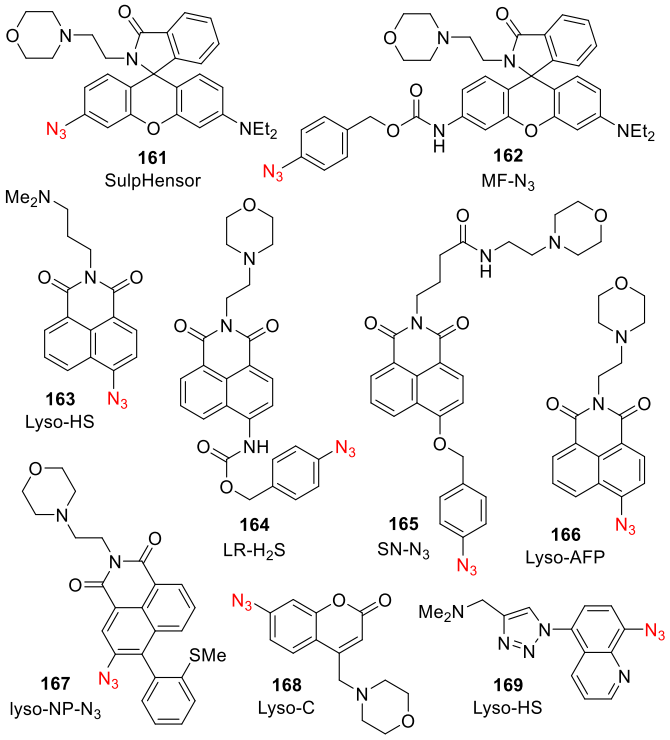


Figure 1.38. Examples of azide-based fluorescent H_2S probes targeted to the lysosome.

Lysosomal-targeted probes based on naphthalimide chromophores have also been reported. For example, Tang reported **163** (Lyso-HS), with a dimethyl amine motif to target the lysosome.[235] This probe provides a 14-fold fluorescent response at 540 nm when treated with H_2S, but also provides a small response to Cys and GSH. Lysosomal localization was confirmed in HeLa cells, and this probe was used to image exogenous and endogenous H_2S. Liu and Liu reported the two-photon probe **164** (LR-H_2S) that utilizes an azide-modified self-immolative linker and a morpholine moiety to impart lysosome localization.[236] Treatment with H_2S in 20% MeCN in buffer resulted a ratiometric response with a fluorescence decrease at 475 nm and concomitant increase at 541 nm when excited at 840 nm. The probe showed good selectivity for H_2S over competing species and was used to image H_2S in SGC-7901 cells. Using a related approach, Wang and Jiang used an ether-based self-immolative linker to develops **165** (SN-N_3).[237] When treated with H_2S in 50% DMF in buffer, this probe generates a ratiometric response with fluorescence decrease at 450 nm and increase at 550 nm with moderate selectivity for H_2S over Cys and GSH. This probe was also confirmed to localize to the lysosome and used to image exogenous H_2S in HepG2 cells.

In 2014, Cui and Xu reported **166** (Lyso-AFP) that responded to H_2S with a fluorescence turn-on at 535 nm, showed good selectivity for H_2S over other biological anions and thiols, and allowed for imaging of exogenous H_2S in the lysosomes of HeLa cells.[238] In 2022, Wu and Zhang reported **167** (lyso-NP-N_3) that upon incubation with H_2S exhibited a 45-fold fluorescence turn-on at 543 nm that was quenched with the addition of HBrO.[239] The probe was selective for H_2S and HBrO and over metal ions, anions, amino acids, and ROS and was able to monitor H_2S and HBrO at pH 5-10. This probe was also used to image exogenous and endogenous H_2S and HBrO sequentially in the lysosome of RAW264.7 cells. Lysosome-targeted probes have also been developed for other chromophores. For example, Kuang and Jiang reported coumarin-based **168** (Lyso-C), which reacts with H_2S to generate a fluorescent response at 458 nm with good selectivity for H_2S.[240] This probe was used to image exogenous H_2S in HepG2 cells. Building from a quinoline platform, Shen and Zhu reported **169** (Lyso-HS), which responded to H_2S in 10% DMSO in buffer to generate a 95-fold fluorescent turn-on.[241] This probe showed relatively good selectivity, although minor probe activation was observed with 10 equiv. of Cys and Hcy. This probe was used to image both exogenous and endogenous H_2S in RTE, A549, and HepG2 cells, with increased H_2S generation observed in cancerous cell lines.

In addition to lysosomal targeting, a variety of probes have been developed for specific localization to the mitochondria. In an early example, Joe, Cho, and Kim reported the ratiometric two-photon probes **170** and **171** (SHS-M1 and SHS-M2) that use an azide-modified self-immolative for H_2S detection and a triphenylphosphonium (TPP) moiety to impart mitochondrial localization (Figure 1.39).[242] Addition of H_2S to these probes results in a ratiometric response, with a decrease at 420 nm and increase at ~500 nm for both probes with good selectivity for H_2S over other analytes. Probe **171** was used in further imaging experiments due to its larger ratiometric response and was confirmed to localize to the mitochondria. Using two-photon microscopy, **171** was sufficiently sensitive to measure differences in the endogenous H_2S levels in primary astrocytes treated with CBS-specific siRNA. Moreover, this probe was also used to image changes in H_2S levels in murine astrocytes and brain slices deficient in the Parkinson's disease related gene DJ-1, which also correlated with decreases in measured CBS expression (Figure 1.40).

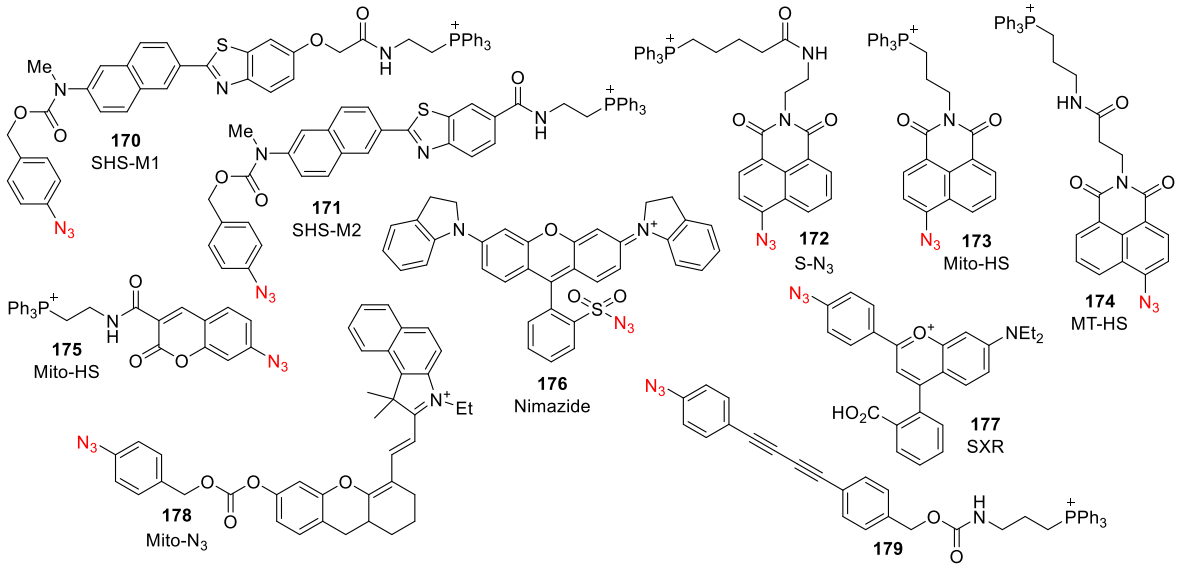


Figure 1.39. Examples of azide-based fluorescent H_2S probes targeted to the mitochondria.

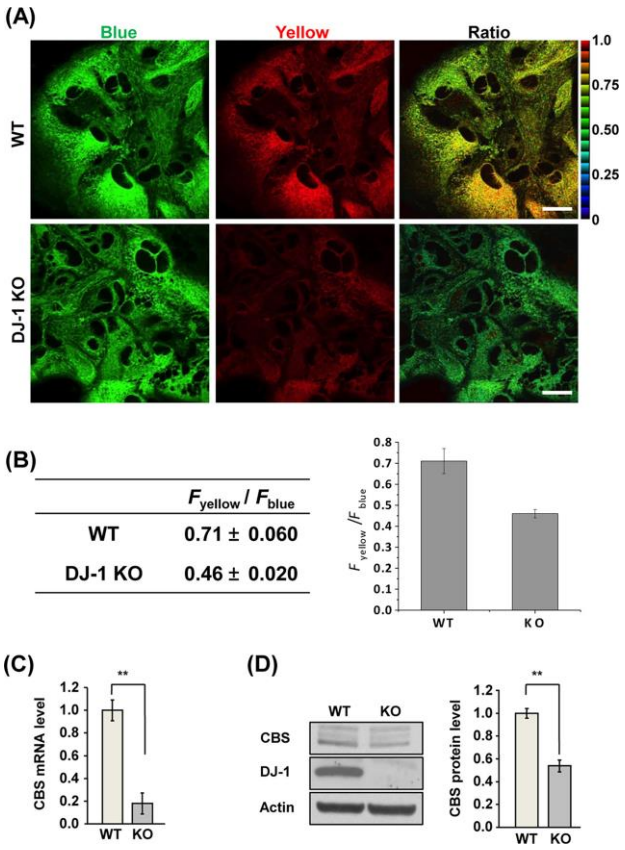


Figure 1.40. Example of using probe **171** to investigate H_2S generation in a Parkinson's disease model. (a,b) Ratiometric fluorescence response from **171** in cultured astrocytes from WT and DJ-1-KO mice. (c) Quantification of CBS mRNA. (d) CBS and DJ-1 quantification. Reproduced with permission from ref [242]. Copyright 2013 American Chemical Society.

Naphthalimide-based probes have also been used for mitochondrial targeting. For example, Qian and Ge report **172** (S-N_3), which reacts with H_2S to generate a fluorescent response at 545 nm with good selectivity over competing analytes.[243] This probe was used to image exogenous H_2S in MCF-7 cells and also confirmed to localize to the mitochondria. Using a related approach with modified linker, Tang reported **173** (Mito-HS), which provides a 21-fold turn on to H_2S at 540 nm.[235] After confirming mitochondrial localization, this probe was used to image both exogenous H_2S and endogenous H_2S with phorbol myristate acetate (PMA) in cells and was additionally applied to breast cancer tumors in BALB/C mice. Further expanding the naphthalimide platform, Lin reported the two-photon H_2S probe **174** (MT-HS), which reacts with H_2S to generate a 40-fold enhancement at 540 nm in 30% DMF in buffer.[244] This probe showed good selectivity for H_2S over competing analytes and was used to image exogenous H_2S in HeLa cells and also shown to enable imaging at depths of up to 80 μm in liver tissue. Mishra and Bhuniya reported the mitochondria-targeted coumarin derivative **175** (Mito-HS), which provides a 43-fold fluorescent response at 450 nm with good selectivity over competing analytes.[245] This response to exogenous H_2S was also confirmed in blood serum, cancer cells, and non-cancerous cells. Probe **175** was also used to image different endogenous H_2S levels in cancerous versus non-cancerous cells and was confirmed to localize to the mitochondria.

Shifting to longer wavelength detection, Ai reported the NIR fluorescence turn-off probe **176** (nimazide), which utilized an azide-modified QSY-21 derivative.[246] In glycerol, the probe exhibited a emission at 733 nm that was quenched upon H_2S addition, and this response was selective for H_2S over competing analytes. This probe was further used to image exogenous and endogenous H_2S in HEK 293T cells. Zhang and Liu also reported the red mitochondrially-targeted probe **177** (SXR), which reacts with H_2S to generate a fluorescent turn-on at 624 nm with good selectivity for H_2S over other analytes.[247] This probe was also used to image exogenous and Cys-derived H_2S in HeLa cells. Li and Yin reported the turn-on cyanine-based NIR probe **178** (Mito-N_3), which uses an azide-modified self immolative linker and cationic cyanine to impart mitochondrial localization.[248] Treatment with H_2S in 30% EtOH in buffer resulted in a ~15-fold fluorescent enhancement at 736 nm with good selectivity over other analytes and applied to image exogenous and SNP-derived H_2S in MCF-7 cells. Expanding to other detection approaches, Min reported diyne **179** that functions as a ratiometric Raman probe with a shift from shift from 2223 cm^{-1} to 2214 cm^{-1} when treated with H_2S.[249] This response was selective for H_2S over other

biological reactive species, and the probe was further used to image exogenous H_2S in the mitochondria of HeLa and COS-7 cells using stimulated Raman scattering imaging.

In addition to the more common approaches to target probes to the lysosome and mitochondria, other organelles have also been targeted for H_2S detection. For example, Lin reported endoplasmic reticulum (ER) targeted probe **180** (Na-H_2S-ER) in 2017 that utilizes *p*-toluenesulfonamide for ER targeting (Figure 1.41).[250] Treatment with H_2S results in a 45-fold fluorescence turn-on at 545 nm with good selectivity for H_2S. This probe was used to image both exogenous and endogenous H_2S in HeLa cells using both one- and two-photon excitation. In addition, two-photon imaging with **180** was demonstrated to detect exogenous H_2S at depths of up to 100 μm in liver slices and also exogenous H_2S in zebrafish. Xiao and Liu reported the identical compound later in 2021 (ER-N3), but reported a lower 11-fold turn on.[251] This probe was further used to image endogenous H_2S production in cells under ER stress as well as respond to exogenous H_2S in live mice using two-photon microscopy.

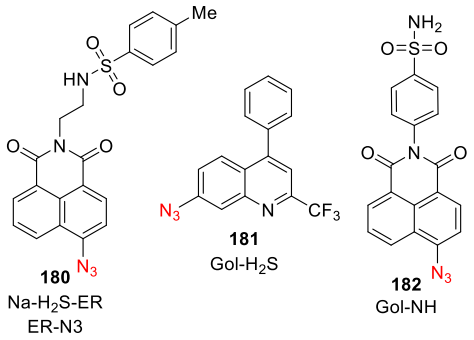


Figure 1.41. Examples of azide-based fluorescent H_2S probes targeted to the endoplasmic reticulum and Golgi apparatus.

Expanding to the Golgi apparatus, Liu, Sheng, and Zhu reported **181** (Gol-H_2S), which provided a turn-on response at 515 nm upon treatment with H_2S and was selective for H_2S over other competing analytes.[252] Cell imaging experiments confirmed Golgi localization and also detection of exogenous and endogenous H_2S in both live cells and zebrafish. In addition, **181** was used to image increased H_2S production under Golgi apparatus stress induced by Monensin. In 2020, Liu, Sheng, Huang, and Zhu developed **182** (Gol-NH) that utilized a phenylsulfonamide to impart Golgi targeting and responded to H_2S with a fluorescence turn-on at 550 nm.[253] In HeLa cells, the probe could detect both exogenous H_2S and endogenous H_2S stimulated with Cys and

removed with $ZnCl_2$. The probe was also confirmed to localize to the Golgi apparatus, was used to visualize H_2S during induced Golgi stress and H_2S in larval zebrafish.

Other functional groups have also been incorporated onto azide-based H_2S probes to impart different types of localization or uptake. For example, Wang reported hydrophobic naphthalimide **183** (ASNSN-N_3) that localized to cell membranes (Figure 1.42).[254] Upon treatment with H_2S, the probe exhibited a fluorescence turn-on at 545 nm in buffer with Triton-X surfactant, and showed good selectivity for H_2S over competing species. The probe was used to image both exogenous and endogenous H_2S in HeLa and Raw 264.7 cells and was also used to image endogenous H_2S in liver and blood vessel tissues using two-photon microscopy. In 2022, Liu and Zhu reported cell-membrane targeted **184** (PCM) that reacted with H_2S to produce a fluorescence turn-on response at 535 nm in buffer with CTAB that features a lipophilic alkyl chain and a large 115 nm Stokes shift.[255] The probe showed selectively for H_2S over other biological species and was used to image exogenous H_2S and endogenous H_2S modulated with Cys and $ZnCl_2$ in the cell membrane of HeLa cells and Cys-derived H_2S in larval zebrafish.

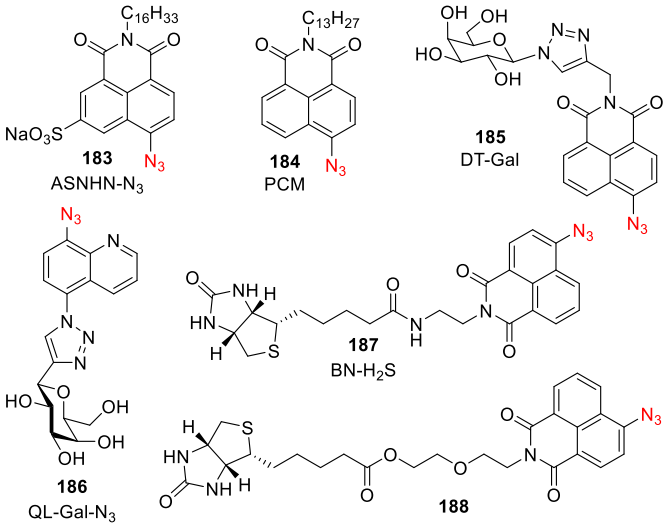


Figure 1.42. Additional examples of azide-based fluorescent H_2S probes based with different targeting groups.

In 2015, Li and He reported **185** (DT-Gal) that featured a glycosyl moiety as a hepatocyte cell targeting group and showed a fluorescence turn-on at ~550 nm when treated with H_2S and good selectively for H_2S over other biological anions and amino acids.[256] The probe responded to

exogenous H_2S only in in HepG2 cells overexpressing asialoglycoprotein receptors (ASGPR) but not in HCT116 cells, A549 cells, or HepG2 cells with a reduced ASGPR expression. Expanding to sugar ligation, Wang and Du reported the hepatocyte-targeted probe **186** (QL-Gal-N_3), which uses a tethered galactose to target ASGPR that are overexpressed in the liver.[257] This probe provided a 102-fold fluorescence turn-on at 521 nm upon treatment with H_2S with good selectivity, although a minor response to Cys was observed. In addition, this probe was shown to provide a larger fluorescent response in HepG2 cells than A549 or HeLa cells, which is consistent with the increased level of ASGPR in hepatic cells.

Also using a naphthalimide system, Lin two-photon fluorescent probe **187** (BN-H_2S) using a naphthalimide derivative with a biotin moiety to act as a cancer cell specific targeting group.[258] Upon the addition of H_2S, the probe exhibited a fluorescence increase at 544 nm that was selective for H_2S over other biological analytes. In live cell experiments, **187** showed a stronger fluorescent response in cancer cell lines when compared to non-cancerous cell lines, which was attributed to facilitated uptake by the biotin motif. Using a related approach but different linker, Lee later reported **188**, which provided similar turn-on and selectivity properties to **187** and was used to image both exogenous and endogenous H_2S in A549 cells.[259]

Complementing subcellular localization, probes that can be trapped inside of cells offer benefits for increased signal to noise when compared to non-trappable probes and and further enable longer time-course experiments by limiting passive probe diffusion out of cells during the course of an experiment. The most common approach to develop such cell trappable probes is to appending an ester that can be cleaved by intracellular esterases. Once the probe is internalized, cleavage of the ester generates a negatively charged carboxylate, which is typically cell impermeable and thus traps the probe within the cell. In 2013, Chang reported the two *bis*-azido rhodamine derivatives **189** and **190** (SF5-AM and SF7-AM) with acetoxymethyl (AM) esters to impart cell trappability (Figure 1.43).[112] Upon addition of H_2S, these probes exhibited a 4-fold and 20-fold fluorescence turn-on, respectively, with good selectivity for H_2S over competing analytes. In cell-based studies, **190** showed better cellular retention than **189**, which is likely due to the two AM esters in **189**. Highlighting the benefits of cell trappable probes, **190** shows a significantly brighter signal and better retention after 30 minutes in cells than non-trappable **2** and **25** or **189** (Figure 1.44). In addition, **190** was used to image endogenous H_2S in HUVECs stimulated with vascular endothelial growth factor (VEGF).

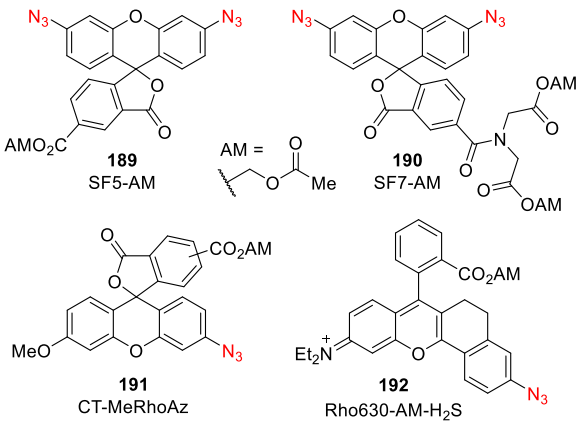


Figure 1.43. Examples of cell trappable azide-based fluorescent H_2S probes.

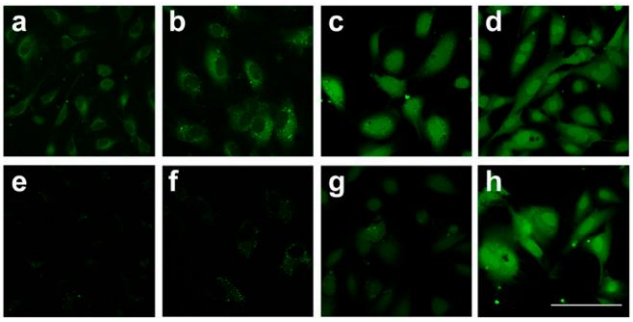


Figure 1.44. Fluorescent response of (a,e) 5 µM **2**, (b,f) 5 µM **25**, (c,g) 2.5 µM **189**, and (d,h) 2.5 µM **190** in HUVECs. Panels (a-d) show the response after incubation for 30 minutes, and panels (e-h) show the response after further incubation for 60 minutes after replacing the media showing the enhanced cellular retention of **190**. Reproduced with from ref [112]. Copyright 2013 National Academy of Science.

More recently, Pluth reported cell-trappable **191** (CT-MeRhoAz), which contains an azide-modified methyl rhodol with AM ester incorporation to impart cell trappability.[260] This probe provided a large 3000-fold fluorescence turn-on at 514 nm with good selectivity for H_2S over competing analytes. Probe **191** was used to image both exogenous and endogenous H_2S in HeLa cells and was shown to be retained in live cells longer than the non-cell trappable analogue **24**. Longer-wavelength cell trappable probes have also been reported. For example, Liu and Kong reported **192** (Rho630-AM-H_2S), which includes AM ester functionalization to a rhodamine 630 (Rho63) dye.[261] Treatment with H_2S results in a 20-fold fluorescent turn-on at 645 nm with good

selectivity for H_2S over other competing analytes. This probe was also used to image both exogenous and endogenous H_2S in HeLa cells and also in zebrafish.

1.2.1.7 Luminescent Azide Reduction

In addition to fluorescent reporters, a number of chemiluminescent, bioluminescent, or time-gated luminescent azide-based probes for H_2S have also been reported. Each of these approaches provides a useful method to decrease background fluorescence in biological systems by overcoming background autofluorescence from cellular milieu. For example, chemiluminescent and bioluminescent probes benefit from reduced background signal because biological material typically does not spontaneously emit light. Similarly, time-gated luminescence occurs at a timescale that is longer than typical fluorescent processes associated with organic and biological molecules and further benefits from reduced background luminescence. In addition, the lack of required excitation for chemiluminescent and bioluminescent azide-based probes limits unwanted photoactivation/photoreduction of the azide.

An early example of using a chemiluminescent reporter for H_2S detection was reported by Pluth in 2013. Probes **193** and **194** (CLSS-1 and CLSS-2) are based on the parent isomers of luminol, and azide reduction results in a luminescent response at 425 nm in the presence of HRP and H_2O_2 (Figure 1.45).[262] Probe **193** showed a 128-fold luminescent turn-on but had poor selectivity for H_2S over Cys-derived thiols, which was attributed to hydrogen bonding interactions between Cys and the probe as evidenced by NMR spectroscopy. In contrast, **194** provided a 45-fold luminescent response with good selectivity for H_2S over competing thiols. This probe was further used to detect enzymatically produced H_2S from isolated CSE.

Expanding to bioluminescent scaffolds, luciferin analogues have also been used for H_2S sensing. Such platforms provide a luminescent response after luciferin oxidation by the enzyme firefly luciferase in the presence of ATP, Mg^{2+}, and O_2. In 2015, Lu reported azidoluciferin **195** in which the amine of aminoluciferin was converted to an azide.[263] Importantly, **195** was a poor substate for luciferase prior to azide reduction, meaning that neither a background luminescent response nor probe consumption were observed prior to H_2S-mediated reduction. This probe provided an 8-fold luminescent response and was selective for H_2S over competing analytes. Probe **195** was also used to image exogenous and endogenous H_2S in Huh7 cells that constitutively expressed luciferase and also in Huh7 xenografts in live mice. Ke and Li later reported the same

azidoluciferin **195** and two additional derivatives, **196** and **197**, which incorporate self-immolative linkers.[264] Comparison of the three luciferin-derived probes showed 2- to 8-fold luminescence responses to H_2S, with the highest response and selectivity with probe **195**. This probe was further used to image exogenous H_2S in FVB-luc$^+$ mice.

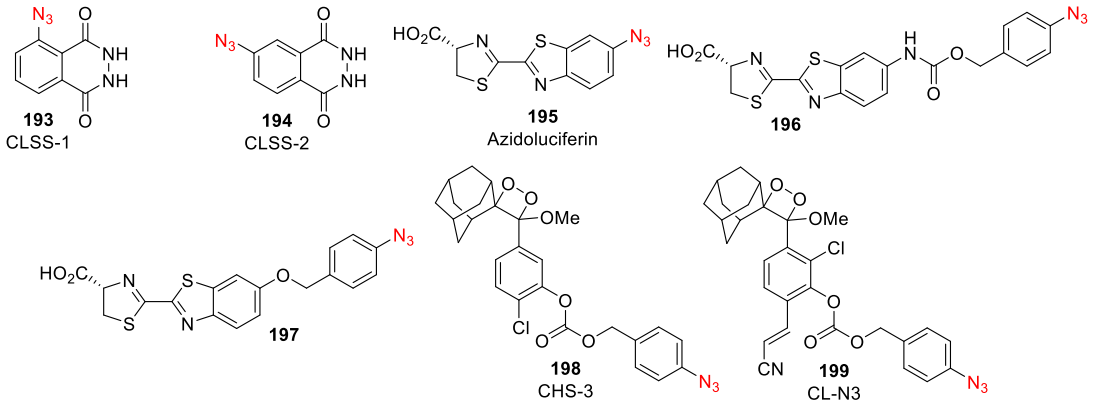


Figure 1.45. Examples of azide-based luminescent H_2S probes.

One limitation of the luminol and luciferin systems is the requirement of enzymatic activation for luminescence. To overcome these limitations, chemiluminescent probes based on 1,2-dioxetane motifs have also been reported, which do not require external enzymatic activity. In 2015, Lippert reported chemiluminescent probe **198** (CHS-3), which includes a self-immolative azide motif for H_2S detection coupled to a dioxetane chemiluminophore.[265] Probe **198** provided a 6-fold luminescent response to H_2S in buffer containing Emerald II Enhancer, with good selectivity for H_2S over competing analytes. This probe was further used to image exogenous H_2S in C6 brown mice. Pluth later modified this platform to incorporate a substituted 1,2-dioxetane reported by Shabat with significantly enhanced chemiluminescent efficiently[266] to prepare **199** (CL-N3).[267] Treatment with H_2S in THF resulted in a 2600-fold increase in luminescence that reduced to 7-fold increase observed in buffer, which was attributed to likely background hydrolysis of the probe leading to a reduced dynamic range.

More recently Song and Yuan reported the ratiometric lanthanide luminescent probes **200** and **201** (Golgi-ABTTA-Eu^{3+} and Golgi-ABTTA-Tb^{3+}), which contained both an azide-modified self-immolative linker and a sulfanilamide moiety to impart localization to the Golgi apparatus (Figure 1.46).[268] Addition of H_2S resulted in a luminescent decrease at 610 nm for Eu^{3+} in **200** but

increase at 540 nm for Tb^{3+} in **201**, which led to these probes being used in tandem for greater signal information. These probes were confirmed to localize to the Golgi and provide a ratiometric response to exogenous HeLa cells. In 2014, Tropiano and Faulkner reported **202** that responded to H_2S with a luminescent signal at about 615 nm that was improved by time-gating the luminescent signal and was selective for H_2S over anions, reducing agents, and thiols, although GSH did produce a minor response.[269]

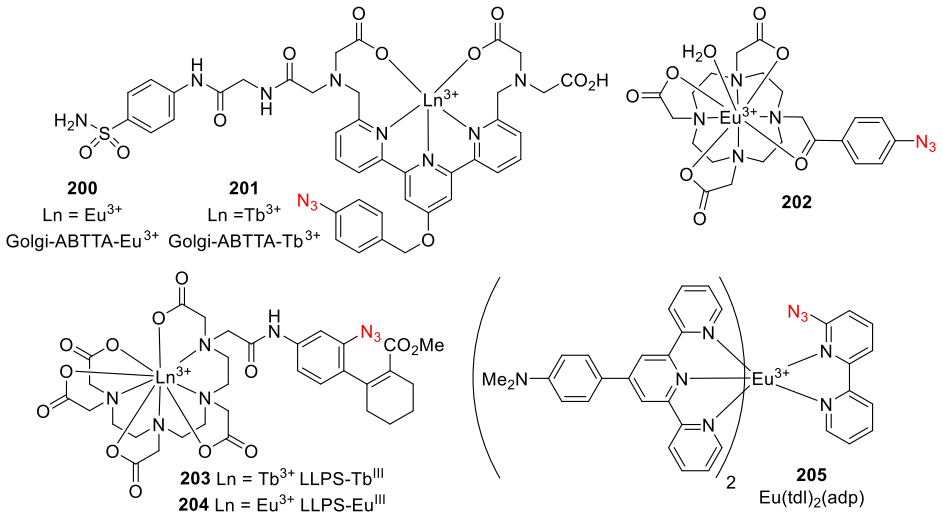
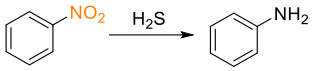


Figure 1.46. Examples of azide-based H_2S probes based on lanthanide luminescence.

Expanding the lanthanide luminescent platforms, Miller reported two lanthanide-based luminescence probes **203** and **204** (LLPS-Tb^{III} and LLPS-Eu^{III}) in 2016.[270] Reaction with H_2S resulted in azide reduction and subsequent reaction with the proximal carboxylic acid to form a quinolinone end product with an associated 3- to 8-fold turn-on depending on the time course of the experiment. This slower response time was attributed to the slower cyclization to form the quinolinone, and this response time could be increased with increasing temperature. These probes were used further to detect CSE-generated H_2S and to differentiate H_2S levels in the presence of CSE inhibitors. In 2022, Fan and Pu reported **205** ($Eu(tdl)_2adp$) that utilized europium with tripyridine-based ligands that showed a fluorescence turn-off at 575 nm when treated with H_2S in DMSO.[271] The probe was shown to be selective for H_2S over biological anions, cations, and thiols and was also used image exogenous H_2S in live HeLa cells and quantify H_2S in natural waters.

1.2.2 Nitro Reduction

The development of reduction-based H_2S probes is not solely limited to H_2S-mediated azide reduction, but has also included other oxidized nitrogen precursors (Scheme 1.4). For example, H_2S-mediated reduction of both aryl and alkyl nitro groups has also been used to develop activity-based probes for H_2S. This approach builds from earlier synthetic chemistry approaches to use H_2S as a reducing agent for nitro groups.[272, 273] One limitation of this approach is the potential of such probes to react with nitroreductases, which are often upregulated under hypoxic conditions,[274] although the specificity of such reductases for other oxidized nitrogen species used for H_2S detection has not yet been investigated in detail.



Scheme 1.4. General reaction of nitro group reduction by H_2S to form an amine.

An early report of H_2S detection using nitro group reduction was reported by Pluth in 2012 using nitrated naphthalimide **206** (HSN1, Figure 1.47).[90] Treatment with H_2S resulted in a 15-fold fluorescence turn-on at 542 nm. This probe was found to be selective for H_2S over 500 μM of different competing species, but the selectivity against 10 mM Cys and GSH was significantly eroded. When compared directly with azide analogue **4**, the reaction rate, turn-on response, and selectivity of the nitro-based probe **206** were blunted, with poor selectivity observed at mM concentrations of thiols (Figure 1.48). This probe was subsequently used to image exogenous H_2S in HeLa cells. Also in 2012, Li and Yu developed the ratiometric, 7-diethylamine coumarin-based probes **207**–**209** that included nitroolefin functionalization.[275] Treatment with H_2S in DMF failed to produce a fluorescent response for **207**, but resulted in ratiometric responses for both **208** and **209**. The selectivity of both probes for H_2S over competing analytes was good, although some response was observed for $S_xO_y^{n-}$ species. In the same year, Chen reported cyanine-based probe **210** (Cy-NO_2) that resulted in a 13-fold fluorescence turn-on at 789 nm when incubated with H_2S.[276] This probe showed good selectivity for H_2S over competing reactive species, and was shown to respond to exogenous H_2S in Raw 264.7 cells.

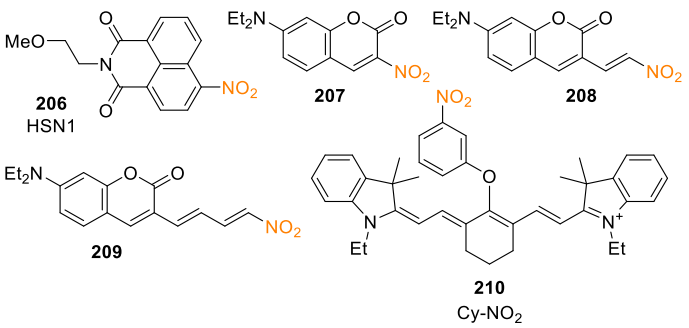


Figure 1.47. Examples of fluorescent H_2S probes based on nitro group reduction.

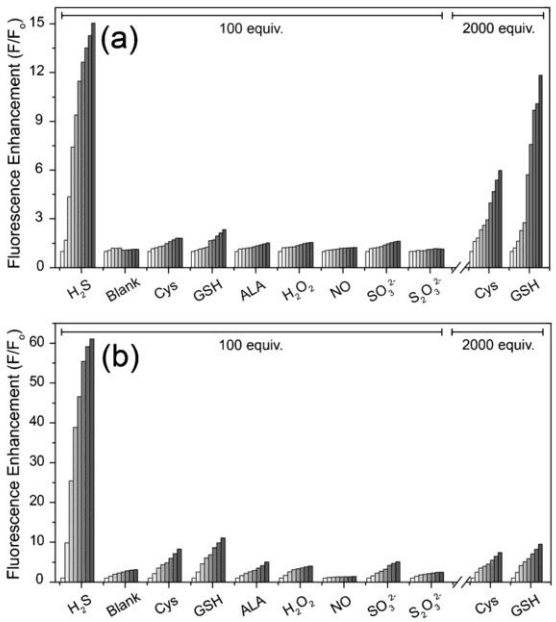


Figure 1.48. Selectivity of 5 μM (a) nitro-naphthalimide **206** and (b) azido-naphthalimide **4** showed the significantly reduced selectivity of the nitro functional group toward high concentrations of Cys and GSH. Reproduced with permission from ref [90]. Copyright 2012 Royal Society of Chemistry.

Chattopadhyay reported **211**–**213** (L^1–L^3) that exhibited fluorescence enhancements at 502 nm when incubated with H_2S (Figure 1.49).[277] Only **211** was selective for H_2S over other biological anions and was additionally used to image exogenous H_2S in *Bacillus subtilis* and *Candida sp.*. In 2014, Zhang and Meng developed **214** (RHP-2) that responded to H_2S treatment with a 27-fold fluorescence turn-on at 467 nm, was stable to visible light over 60 minutes, and is selective for H_2S over analytes including thiols, amino acids, RNS, and ROS.[278] This probe was used to image exogenous H_2S, SNP-induced H_2S, and PAG-induced H_2S inhibition in MCF-7 cells. In addition,

214 was also used to monitor H_2S in mouse hippocampus and chronic unpredictable mild stress-induced depression models. More recently, Singh reported **215** (PDI1) that exhibited a fluorescence increase at 526 nm, 561 nm, and 670 nm when incubated with H_2S, but also showed a fluorescent increase at 688 nm and a decrease at 560 nm when treated with Cys in 50% MeCN in buffer.[279] Thise probe also showed responses to exogenous H_2S when applied to a thin film, in solution, loaded onto silica, and when applied to A549 cells.

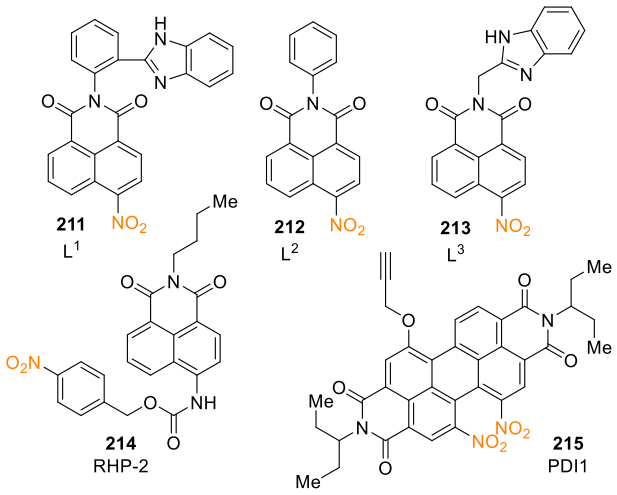


Figure 1.49. Additional examples of H_2S probes based on nitro group reduction with naphthalimide chromophores.

Expanding on the aryl nitro-based probes, Kumar reported the 2-hydroxynaphthalene derivatized **216**, which provides a 35-fold fluorescence turn-on at 462 nm upon treatment with H_2S (Figure 1.50).[280] This probe showed moderate selectivity over GSH and Cys, was used to develop H_2S test strips, and was used to image exogenous H_2S in PC3 cells. Jiang used this same approach to develop rhodol-based **217** (FD-NO_2), which reacts with H_2S to generate a 25-fold fluorescent enhancement at 518 nm with good selectivity for H_2S over competing anions, RSS, RNS, and ROS.[281] This probe was also used to image exogenous H_2S in NIH 3T3 cells. Expanding to more red-shifted platforms, Yin and Huo reported ratiometric probe **218** (IS-NO_2), which is based on a dicyanomethylene-4H-chromene scaffold.[282] Treatment with H_2S resulted in reduction of the signal at 565 nm with concomitant increase at 650 nm. The probe showed good selectivity for H_2S over competing analytes and was used to image exogenous and SNP-derived H_2S in HepG2 cells and exogenous H_2S in mice.

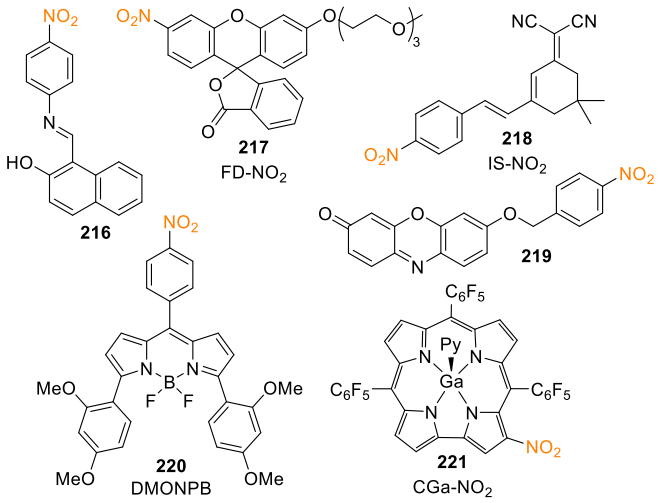


Figure 1.50. Additional examples of H_2S probes based on nitro group reduction with various chromophores.

In 2022, Zhao reported **219**, which exhibited a fluorescence turn-on at 586 nm that was selective for H_2S over anions, ROS, and thiols.[283] The probe was used to detect H_2S when loaded onto cellulose paper and also in live larval zebrafish. In 2019, Wang reported BODIPIY-based **220** (DMONPB) that responded to H_2S with a fluorescence turn-on at 627 nm and was selective for H_2S over other biological analytes.[284] The probe was also used to image exogenous H_2S and endogenous H_2S confirmed by PMA in both live HeLa and Raw 264.7 cells. In 2023, Santos and Maçôas reported **221** (CGa-NO_2) that showed a fluorescent shift from 750 nm to 612 nm in DMSO that was selective for H_2S over biological anions and thiols, but was unable to image exogenous H_2S in live HeLa cells.[285]

In 2016, Mahapatra reported **222** that featured nitro reduction followed by intramolecular cyclization to form a fluorescent coumarin derivative (Figure 1.51).[286] Incubation with H_2S led to an 800-fold fluorescence turn-on at 484 nm 10% DMSO in buffer that was selective for H_2S over RNS, ROS, and thiols. The probe was then used to develop paper strips for H_2S detection and used to image exogenous H_2S in Vero cells. Utilizing similar chemistry, Liang and Liang developed **223** (KOP) with the goal of distinguishing H_2S from nitroreductase (NTR).[287] After incubation with H_2S, the probe exhibited a fluorescence turn-on at 470 nm that was selective for H_2S over NTR or other biological analytes, although NTR and NADH did produce a response. Using HCT116 cells, the probe was used to investigate H_2S in a cellular hypoxia model and also changes with AOAA treatment.

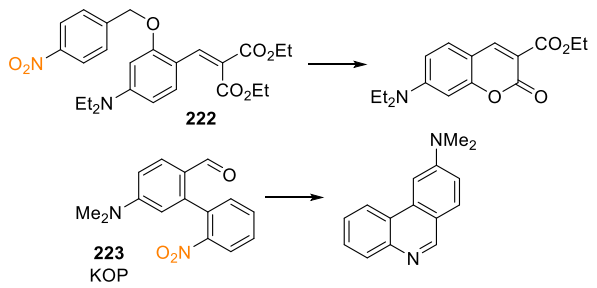


Figure 1.51. Examples of H_2S probes based on nitro group reduction and intramolecular cyclization.

Nitrated styryl isoxazoles have also been used to develop H_2S-reporting fluorescent probes. For example, Kanvah reported ratiometric probes **224**–**227** with conjugated benzene, naphthalene, anthracene, and pyrene scaffolds (Figure 1.52).[288] When treated with H_2S in 90% DMSO in buffer, each of the probes provided a shift in fluorescence with greater sensitivity for H_2S than other anions and thiols. Yin and Huo expanded this approach to report BODIPY-based **228**, which provides a ~16-fold fluorescent turn-on response at 522 nm when treated with H_2S in 10% DMSO in buffer.[289] This probe showed moderate selectivity for H_2S over 2 mM Cys and SO_4^{2-} and was subsequently used to image exogenous and SNP-generated H_2S in HepG2 cells.

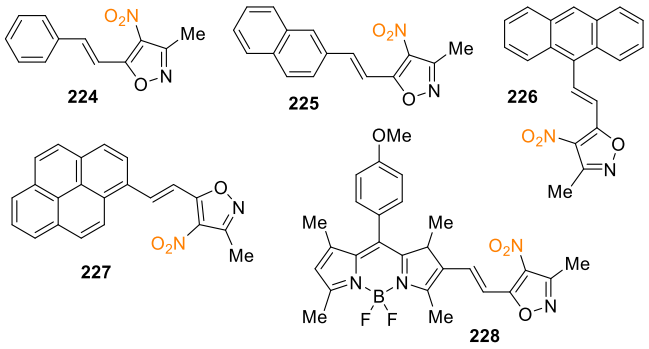


Figure 1.52. Additional examples of H_2S probes based on nitro group reduction with various chromophores.

Related hydrophobic scaffolds with pendant nitroolefins have also been used to develop H_2S-responsive systems. For example, Wang reported diketopyrrolopyrrole-based **229** (DPP-NO_2), which reacts with H_2S to generate a 800-fold fluorescence turn-on at 550 nm with good selectivity for H_2S over anions and thiols (Figure 1.53).[290] This probe was also used to image exogenous H_2S in HeLa cells. Using this same approach, Hua reported *N*-annulated perylene

probes **230**–**232** (NPNM, Mito-MPNM, and Lyso-MPNM), with contained an aliphatic side chain, a TPP motif to target the mitochondria, or a morpholine to target the lysosome.[291] Treatment of these probes with H_2S in 30% DMSO in buffer provided a fluorescence turn-on at 481 nm and were selective for H_2S over competing species, although minor probe activation was observed at higher thiol concentrations. These probes were further used to image exogenous H_2S in HeLa cells and FBS, and mitochondrial and lysosomal targeted was confirmed for **231** and **232**, respectively. Zhang also used the nitroolefin motif to develop carbazole-based **233**, which provided a turn-on fluorescence response to H_2S at 525 nm in 20% MeCN in buffer. This activated fluorophore could be oxidized and quenched by addition of *t*-BuO· and subsequently reactivated by addition of H_2S.[292] This probe was further used to image exogenous H_2S in HeLa cells.

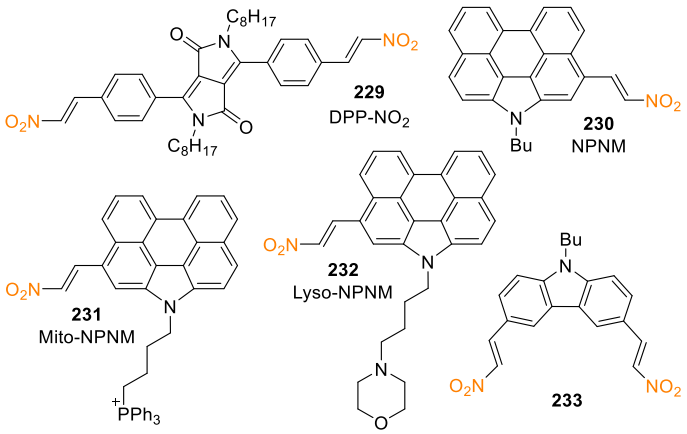
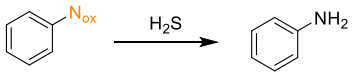


Figure 1.53. Additional examples of H_2S probes based on nitro group reduction with hydrophobic chromophores.

1.2.3 Other Oxidized Nitrogen Motifs



Scheme 1.5. General reaction of oxidized nitrogen-containing groups with H_2S to form an amine.

In addition to the H_2S-mediated reduction of azide and nitro groups discussed above, different partially oxidized nitrogen motifs have also been used for H_2S detection (Scheme 1.5). For example, Sabot and Renard reported that nitroso coumarin **234** could be reduced by H_2S,

although some background reduction was observed from Cys (Figure 1.54).[293] Following this, the Yang group also reported the nitroso-substituted **235**, which reacted with H_2S to generate a fluorescence turn-on at 625 nm.[294] This probe showed moderate selectivity for H_2S over Hcy, GSH, and Cys and was subsequently used to image exogenous and Cys-derived H_2S in SMMS-7721 cells. Gui reported that *tert*-butyl nitroxides could also be used to report on H_2S in pyrene-based probe **236** (TBP-NO).[295] Treatment with H_2S resulted in a fluorescence response at 458 nm, although some response for thiols was also noted, and Na_2S only provided a minimal response whereas NaSH provided full probe activation. Probe **236** was subsequently used to image exogenous H_2S in HeLa cells. Tang reported **237** (COU) that featured an aromatic dialkylamine *N*-oxide to impart a 10-fold fluorescence turn-on at 455 nm when incubated with H_2S with good selectivity over anions and thiols.[296] The probe was used to detect H_2S in buffer, mouse serum, and human plasma as well as to image exogenous H_2S in MCF-7 cells.

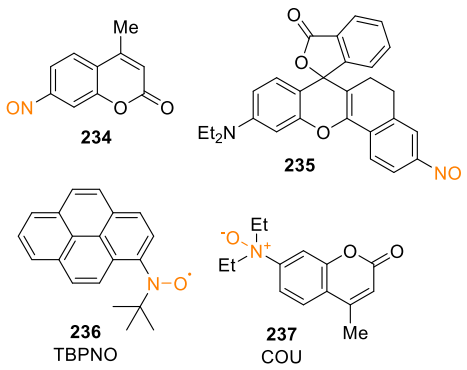


Figure 1.54. Examples of H_2S probes based on reduction of nitroso and *N*-oxide groups.

Hydroxylamines have also been used for H_2S detection. For example, Wang reported **238** in 2012 that showed a 13-fold fluorescence turn-on at 435 nm that was selective for H_2S over biological cations, anions, and ROS, although $S_2O_3^{2-}$, ascorbate, and thioacetic acid did produce minor signals (Figure 1.55).[297] The probe was also used to image exogenous H_2S in astrocytes. Sabot and Renard reported that hydroxylamine coumarin **239** could be reduced by H_2S, although some background reduction was observed from Cys.[293] The Han group also reported a hydroxylamine platform in **240** (PHS1), which reacted with H_2S to generate a 40-fold fluorescence turn-on at 486 nm with good and selectivity for H_2S over competing analytes.[298] This probe was also used to image exogenous H_2S in HeLa cells.

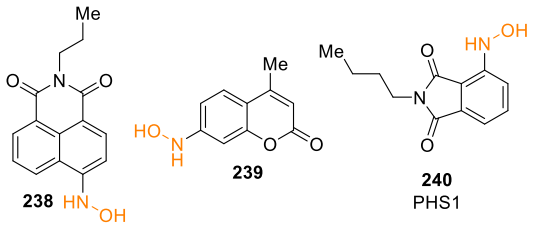


Figure 1.55. Examples of H_2S probes based on reduction of nitroso hydroxylamines.

Tetrazines have also been reported to react with H_2S to be reduced to the corresponding dihydro-tetrazine. For example, Yang reported BODIPY-based **241**–**243** (BODIPY-Tz-I, BODIPY-Tz-II, and Coumarin-Tz) that when incubated with H_2S displayed a 16, 23, and 31-fold fluorescence enhancements at 660 nm or 456 nm in 60% MeOH in buffer (Figure 1.56).[299] Coumarin-based **243** did not provide selectivity for H_2S over thiols, but both **241** and **242** showed good selectivity for H_2S over RNS, ROS, and thiols and were applied to image exogenous H_2S in live 3T3 fibroblast cells.

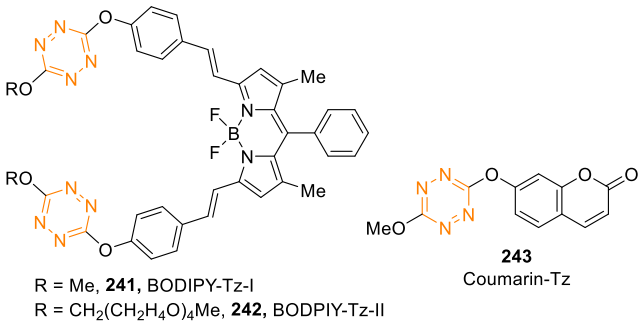


Figure 1.56. Examples of H_2S probes based on reduction of tetrazines.

Using a related approach, Li investigated a series of azo compounds (**244**–**250**) that reacted with H_2S to reduce the azo motif to the parent aniline. Of these compounds, the electron poor fluorinated **246** and **247** were reduced to the corresponding aniline by H_2S but not thiols (Figure 1.57).[300] This reactivity resulted in fluorescent responses at 517 nm for the probes, with the perfluorinated **246** showing faster reactivity.

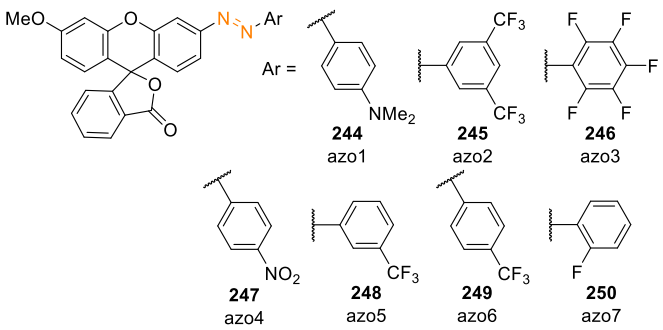
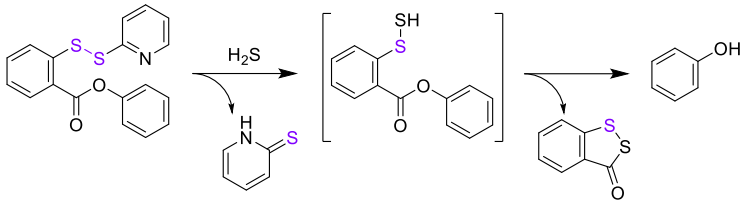


Figure 1.57. Examples of H_2S probes based on reduction of azo compounds.

1.3 H_2S Probes Based on Dichalcogenide Reduction or Exchange

1.3.1 Disulfide-Based H_2S Probes

Much like other sulfhydryl-containing species, H_2S can reduce disulfide bonds. This H_2S-mediated reduction results in disulfide cleavage to form a thiol and persulfide, both of which can undergo further chemistry to activate a fluorogenic system. Such chemistry has been leveraged to develop activity-based fluorescent probes in which the intermediate persulfide generated by disulfide cleave undergoes a subsequent intramolecular cyclization to unmask a caged fluorophore (Scheme 1.6). Unsymmetric pyridyl disulfides are commonly used to increase polarize and increase the electrophilicity of the disulfide at the distal sulfur from the pyridine, which results in efficacious persulfide formation. This persulfide can then undergo an intramolecular nucleophilic attack on the proximal ester to generate a 5-membered ring transition state and extrude the fluorophore and benzodithiolone as a byproduct. This general approach has also been applied to symmetric disulfides (*vide infra*) as well as to other hetero- and homo-dichalcogenides, all of which generate anionic and highly nucleophilic dichalcogenide intermediates.[301] Importantly, disulfide reduction by H_2S is the only pathway that generates a persulfide intermediate, which is required for the subsequent intramolecular cyclization and fluorophore release. In contrast, reaction with other thiols or reductants can result in thiol exchange and/or reduction, but neither of these pathways would generate the intermediate persulfide required for cyclization. Because of these points, the disulfide exchange approach generally shows high selectivity for H_2S, although the presence of other thiols or reductants may deactivate or slow further reactivity of such probes.



Scheme 1.6. Reactivity of an unsymmetric pyridyl disulfide with H_2S to remove a protecting group.

In 2011, Xian reported the first disulfide-exchange based H_2S probe **251** (WSP1), which contains a methoxyfluorescein fluorophore and showed good selectivity for H_2S over other thiols (Figure 1.58).[302] In addition, **251** was used to detect exogenous H_2S in plasma and in COS7 cells. Another early example of the disulfide-exchange approach was reported by Qian in 2012 in the development of HBT-based **252**, which provided a 30-fold fluorescence turn-on response upon treatment with H_2S.[303] The probe showed good selectivity for H_2S over thiols and was subsequently used to image exogenous H_2S in HeLa cells.

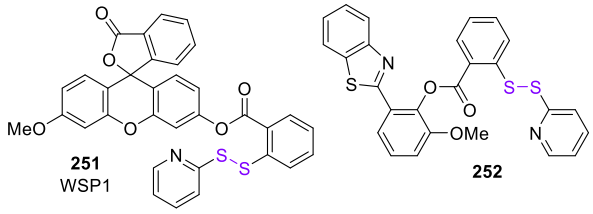


Figure 1.58. Early examples of disulfide-based fluorescent probes for H_2S.

In subsequent work, Xian expanded this approach to different wavelength probes and also to doubly-substituted reports in the series of probes with **253**–**256** (WSP2–5) (Figure 1.59).[304] This approach broadened the palette of fluorophores used with this activation approach, and depending on the system resulted in a 20-275 fold turn-on in response to H_2S. These probes showed good selectivity for H_2S over competing thiols but did show some signal attenuation with H_2S was co-incubated with thiols. In addition, **255** and **256** were used to image exogenous H_2S in live HeLa cells with **255** also being used to image Cys-mediated H_2S release from the synthetic H_2S donor YZ-4-074 (Figure 1.60).

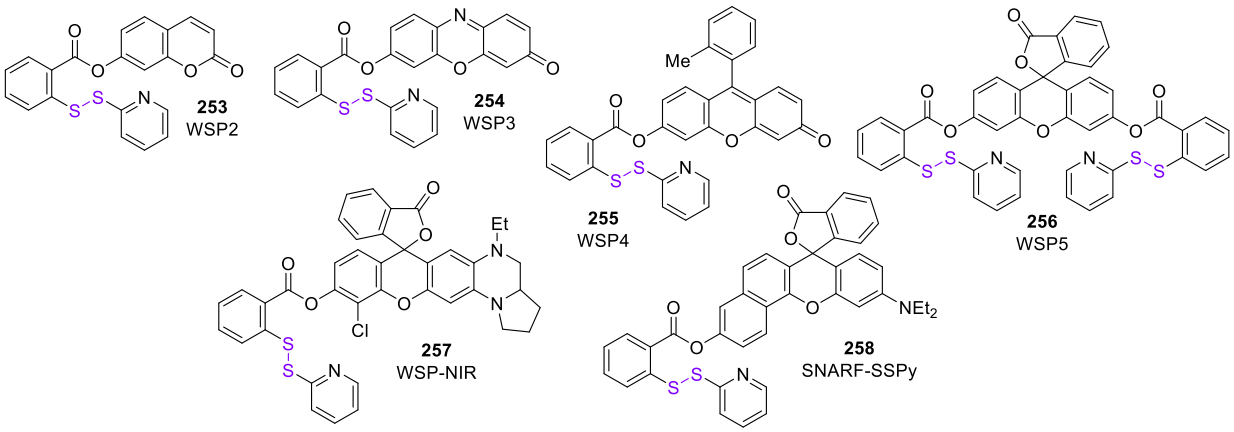


Figure 1.59. Additional examples of fluorescent H_2S probes based on disulfide cleavage and subsequent cyclization.

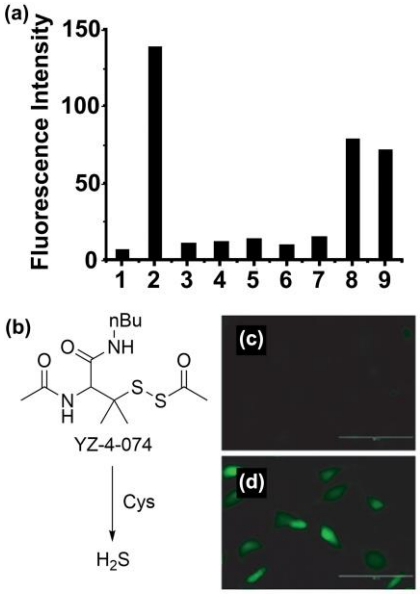


Figure 1.60. (a) Fluorescent response of 10 μM **255** with 1) control; 2) 50 μM NaHS; 3) 200 μM Cys; 4) 200 μM GSH; 5) 200 μM Hcy; 6) 200 μM Na_2SO_3; 7) 200 μM $Na_2S_2O_3$; 8) 50 μM NaHS + 200 μM Cys; 9) 50 μM NaHS + 200 μM GSH. (b) YZ-4-074 donor used for cell studies. Fluorescent response from **255** after incubation (c) with or (d) without 100 μM YZ-4-074. Reproduced and modified from ref [304]. Copyright 2014 John Wiley and Sons.

Expanding to longer wavelengths, Xian reported **257** (WSP-NIR) that responded to H_2S with a fluorescence turn-on at 706 nm but also showed no response to H_2S when pre-treated with biothiols.[305] As will be discussed later in this review, this study showed that probe **295** featuring a diselenide showed excellent selectivity for H_2S even in with high concentrations of biothiols. Liu,

Sun, and Yu developed naphthalmide **258** (SNARF-SSPy) using this same approach, which responded to H_2S with a fluorescence enhancement but treatment with high concentrations of biothiols completely deactivated this probe for subsequent reaction with H_2S.[306] Discussed later in this review, this study showed that probe **293** featuring a pyridyl selenenyl sulfide showed excellent selectivity for H_2S even in with high concentrations of biothiols.

Different naphthalimide-based probes have also been reported that use the H_2S-mediated disulfide cleavage approach. For example, Zhang reported ratiometric probe **259**, which showed a 30-fold ratio of fluorescence intensity (F_{550}/F_{442}) in response to H_2S in 10% DMF in buffer (Figure 1.61).[307] This probe showed good selectivity for H_2S over thiols, although this response was attenuated when the probe was co-incubated with thiols. Probe **259** was further used to image exogenous H_2S in HeLa cells. Using symmetric scaffolds, Ye group designed probes **260** and **261** (M2 and BHNP-DA) that either used amide and ester linkages, respectively, and also include a lysosome-targeted morpholine.[308] Treatment of amide **260** with H_2S resulted in a fluorescence turn-off for both H_2S and thiols, whereas treatment of ester **261** resulted in a fluorescence turn-on at 550 nm that is selective for H_2S over anions, thiols, and cations. Probe **261** was shown to localize to the lysosome and used to image exogenous H_2S in MCF-7 cells using two-photon microscopy.

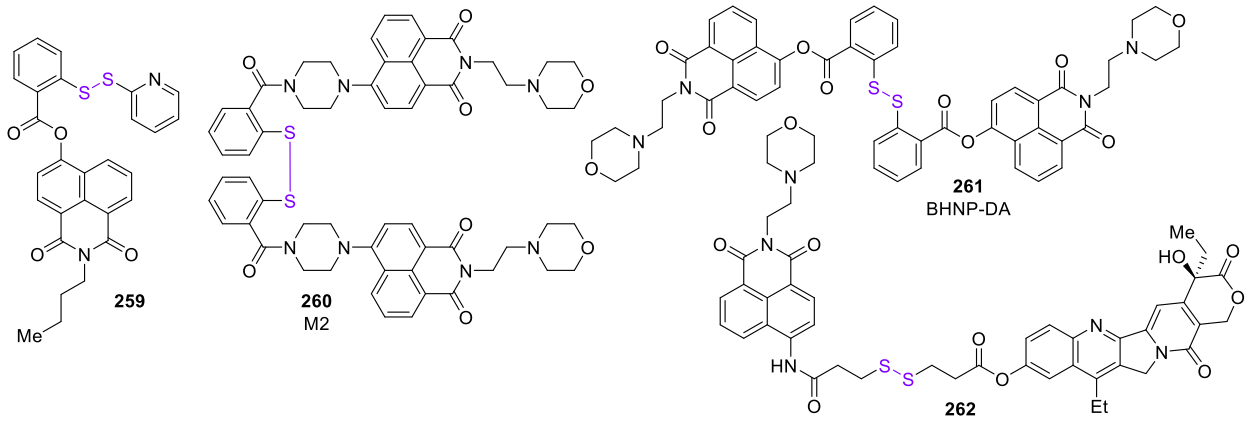


Figure 1.61. Additional examples of fluorescent H_2S probes based on disulfide cleavage and subsequent cyclization with naphthalimide chromophores.

Using an alkyl disulfide, Zhang and Zhou reported **262** that featured a ratiometric shift from 460 nm to 545 nm in 50% DMSO in buffer when treated with H_2S that also led to release of an anticancer drug SN-38.[309] The probe was shown to be selective for H_2S over other biological

anions although activation with Cys/GSH was also observed. As expected, the probe was cytotoxic to cancer HCT116 cells and was further used to image exogenous H_2S, SAM-derived H_2S, and cells treated with AOAA. The probe was also applied to image H_2S in *C. elegans* and determined to activate in tumor sites of mice.

Miao and Zhao developed a ratiometric, 3-hydroxyflavone-based probe **263** (HF-PBS) that showed a fluorescence shift from 380 nm to 250 nm in response to H_2S (Figure 1.62).[310] The probe was shown to be selective for H_2S over anions and thiols, but with eroded selectivity against Cys/Hcy after 24 hours. This probe was also used to image exogenous H_2S in HeLa cells. Qin and Guo reported related ratiometric probe **264**, which responds to H_2S with an emission shift from 495 nm to 525 nm, shows good selectivity for H_2S over other RSS, and was also used to image exogenous H_2S in HeLa cells.[311] Expanding to a coumarin platform, Yin reported the aminocoumarin **265** (HS-1), which also provides a ratiometric response to H_2S.[312] This probe showed good selectivity for H_2S over competing species and was used to image exogenous H_2S in live A549 cells. Gu and Zhu reported **266** (C359) that featured a fluorescence turn-on at 450 nm when treated with H_2S and was selective for H_2S over biological anions, thiols, and enzyme cofactors.[313] This probe was further used to evaluate different CSE inhibitors.

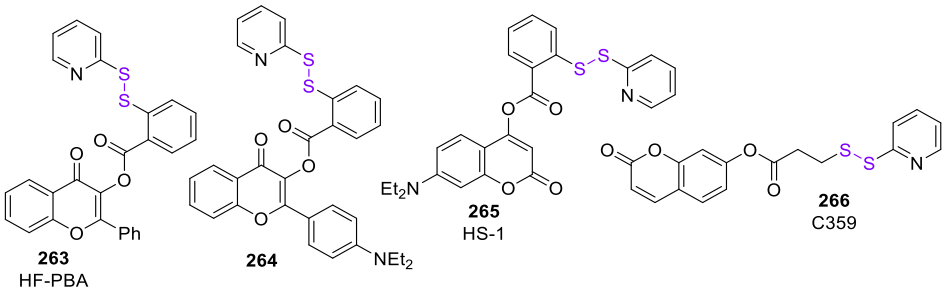


Figure 1.62. Additional examples of fluorescent H_2S probes based on disulfide cleavage and subsequent cyclization based on hydroxyflavone and coumarin chromophores.

Zhang and Dong used this same general approach to generate ratiometric probe **267** (DSPBP), which is based on a conjugated pyridinium system (Figure 1.63).[314] This cationic system showed high water solubility, good selectivity for H_2S over other competing analytes, and a shift in fluorescence from 450 to 520 nm upon reaction with H_2S. Probe **267** was also used to image exogenous H_2S in HeLa cells. Wang and Zha reported **268** (NIPY-PBA), which provides a 230-fold enhancement at 520 nm when treated with H_2S.[315] This probe also showed good selectivity

over competing thiols and was used to image exogenous H_2S in live A549 cells. Using the same pyridyl disulfide deprotection motif, Yin developed dicyanoisopentanone-based **269** (DCN-S), which provided a 6-fold fluorescence turn-on at 580 nm.[316] Working with a benzothiazole-based system, Zhao and Lin reported **270** (HBT-PBA) that exhibited a fluorescence turn-on at 430 nm when incubated with H_2S and showed selectivity for H_2S over biological anions and thiols.[317] The probe found to localize to both the lysosome and endoplasmic reticulum and was further applied to HeLa cells to image exogenous and Cys-derived H_2S as well as changes in signal from PAG and AOAA treatment.

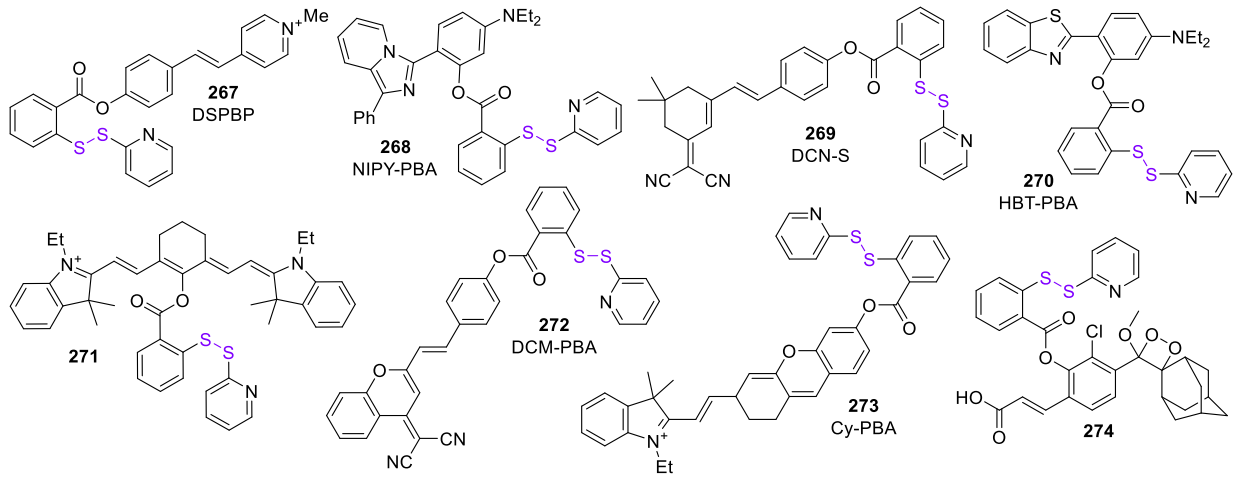


Figure 1.63. Additional examples of fluorescent H_2S probes based on disulfide cleavage and subsequent cyclization.

Expanding to longer wavelength approaches, Yin reported Cy7-based **271**, which reacts with H_2S to generate a 22-fold fluorescent turn-on at 639 nm with good selectivity for H_2S over other analytes.[318] Further advancing NIR probes using this approach, Zhou reported **272** (DCM-PBA), which provides a response at 680 nm and was used to image exogenous H_2S in HeLa cells.[319] Building from a semiheptamethine system, Zhang and Zha developed **273** (Cy-PBA), which extends the emission to 725 nm and allows for imaging of exogenous H_2S in both A549 cells and mice.[320] Using a different reporting approach, Spitz and Shabat developed chemiluminescent probe **274** that provided a 62-fold signal-to noise value when treated with H_2S-releasing β-lactam antibiotic cefalexin and was further used to detect biodegradation of β-lactam antibiotics by β-lactamases to produce H_2S.[321]

Complementing the above approach, unsymmetric aliphatic pyridyl disulfides with aliphatic motifs have also been reported. These systems have higher degrees of flexibility than the aryl esters described in the above section, which likely results in less efficient intramolecular cyclization. As an example of this modified approach, Zhao and Gu used a modified ester linker to generate **275** (NIRDCM-H_2S, Figure 1.64).[322] Treatment with H_2S resulted in a fluorescence response at 650 nm with good selectivity for H_2S over competing analytes. Gu also used this approach to develop BODPIY-based **276** (B601), which showed an 8-fold fluorescence turn-on at 575 nm with H_2S that was selective for H_2S over anions and thiols.[323] This probe was used to image both exogenous H_2S in Raw 264.7 macrophage cells and also to observe increases in endogenous H_2S levels after treatment with Fluvastatin, which could be attenuated by additional treatment with H_2S synthesis inhibitor DL-propargylglycine (PAG) (Figure 1.65). Kang and Lee developed **277** that undergoes a H_2S-triggered dimerization to produce a 53-fold AIE enhancement at 480 nm in 40% DMSO in buffer.[324] The probe was shown to be selective for H_2S over anions, metal ions, ROS, and RSS and was used to image exogenous H_2S, Cys/NAC-derived H_2S, and H_2S in PAG-treated HeLa cells. The probe was also coated onto silica gel TLC plates to develop a sensor for H_2S gas.

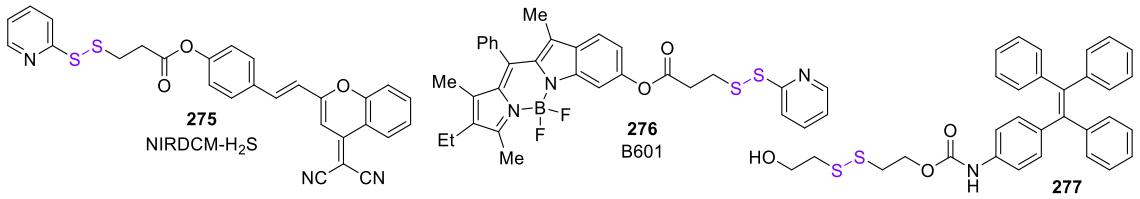


Figure 1.64. Examples of fluorescent H_2S probes based on unsymmetric disulfide cleavage and subsequent cyclization.

Symmetric disulfides lacking pyridyl motifs have also been reported. For example, Li reported two additional HBT-based probes **278** and **279** featured symmetric aryl and alkyl disulfides (Figure 1.66).[325] Aryl disulfide **278** provided a fluorescence turn-on response near 480 nm, whereas alkyl disulfide **279** provided a ratiometric response with an increase at 478 nm and decrease at 374 nm. A symmetric aryl disulfide was also reported by Yin in probe **280** (EW-H). This probe provided a turn-on response at 580 nm, good selectivity for H_2S over competing analytes, and was subsequently used to image exogenous H_2S in HepG2 cells.[326]

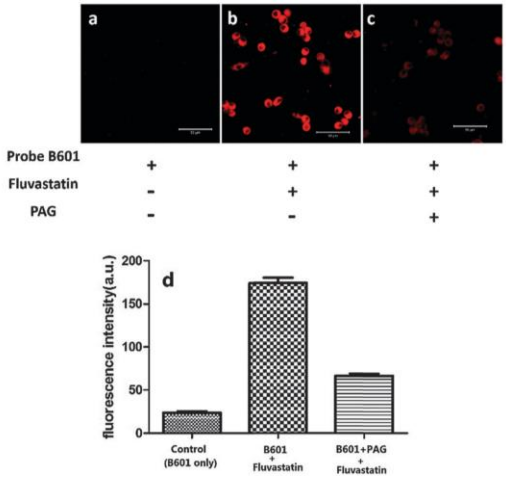


Figure 1.65. Fluorescent images and associated quantification of H_2S detection using 10 µM **276** in Raw 264.7 cells pre-treated with either 2 µM fluvastatin or fluvastatin with PAG. Reproduced with permission from ref [323]. Copyright 2015 Royal Society of Chemistry.

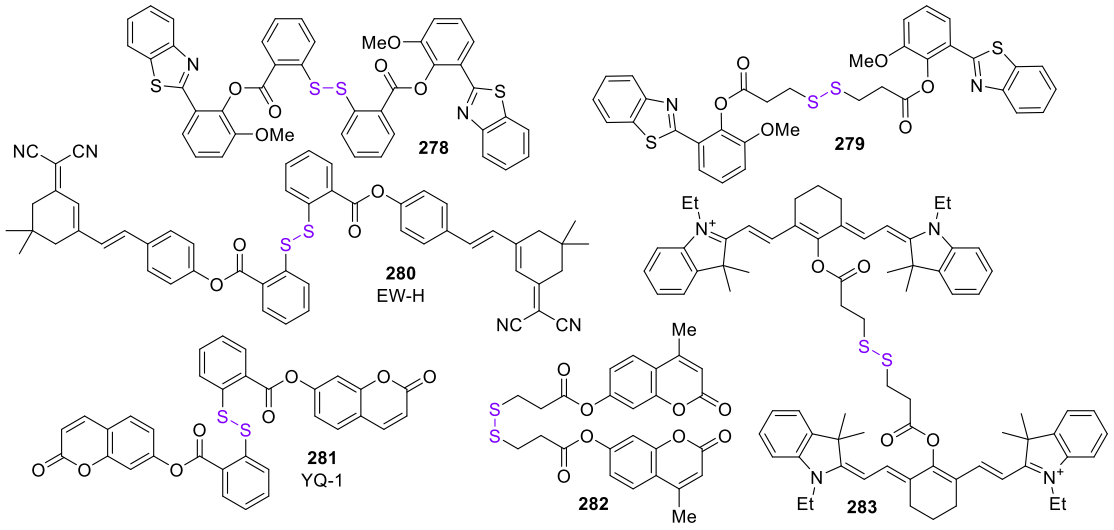


Figure 1.66. Examples of fluorescent H_2S probes based on symmetric disulfide cleavage and subsequent cyclization.

Focusing on a symmetric coumarin scaffold, Yin reported **281** (YQ-1) that exhibited a fluorescent response at 462 when treated with H_2S in 30% MeCN in buffer and was selective for H_2S over biological anions and thiols.[327] This probe was also used to image exogenous H_2S in live A549 cells. Zhou and Zhang reported a related approach with alkyl disulfide **282** that showed a 15-fold fluorescence turn-on at 453 nm when treated with H_2S that was selective for H_2S over other biological anions and thiols.[328] The probe was found to localize in the lysosome and used to image exogenous in H_2S in live HeLa cells, *C. elegans*, and *D. melanogaster*. Zhang and Zhou

reported an additional example of an aliphatic symmetric disulfide in cyanine-based **283**, which generated a 25-fold fluorescence turn-on at 633 nm with good selectivity for selective for H_2S over anions and thiols.[329] The probe was subsequently used to image exogenous H_2S in Hi5 insect cells and *C. elegans*.

1.3.2 Selenenyl Sulfide and Diselenide-Based H_2S Probes

A key component of the disulfide cleavage approach discussed above is the use of the 2-mercaptopyridine thiol motif to help polarize the disulfide bond to promote nucleophilic attack by H_2S. A related approach using selenenyl sulfide motifs was also reported by Xian that leverages the size, polarizability, and electronegativity of sulfur versus selenium to polarize the dichalcogenide motif. Based on these factors, the selenium atom on the selenenyl sulfides should be more electrophilic, and resultant attack by H_2S should form a reactive selenosulfide intermediate. This approach was used to develop **284**–**292** (SeSP1–9), which contain different thiol leaving groups (Figure 1.67).[330] From this group, aryl thiol containing **284**–**286** provided the best fluorescent response to H_2S, with addition of CTAB being required for optimal performance. The pyridyl heterodichalcogenide **284** showed both a faster rate of reaction and larger fluorescence turn-on when compared to **285** and **286**. The aliphatic probes **287**–**292** failed to provide a significant response to H_2S, highlighting the structural requirements for efficacious H_2S attack. Probes **284**–**286** showed good selectivity for H_2S over competing thiols and also showed limited signal attenuation when co-incubated with thiols, with **284** also being used to image exogenous H_2S in HeLa cells.

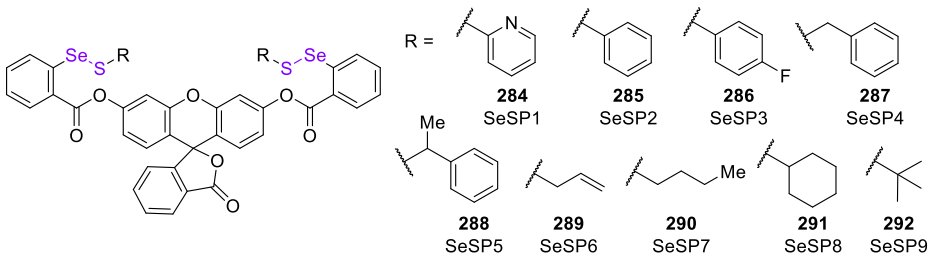


Figure 1.67. Examples of fluorescent H_2S probes based on selenenyl sulfide cleavage and subsequent cyclization.

This approach has also been applied to different chromophores. For example, Liu, Sun, and Yu developed **293** (SNARF-SeSPy) that responded to H_2S with a fluorescence enhancement at 635 nm with good selectivity for H_2S over amino acids, anions, cations, and thiols even when co-incubated with H_2S (Figure 1.68).[306] This probe was also used to image exogenous H_2S and SNP-derived H_2S in A549 cells and zebrafish. Spitz and Shabat also applied this approach to develop chemiluminescent probe **294** that provided a 15-fold signal-to noise value when treated with H_2S-releasing β-lactam antibiotic cefalexin.[321] Xian also further expanded this chemistry to develop **295** (SeSP-NIR), which responded to H_2S with a fluorescence turn-on at 706 nm and is selective for H_2S over amino acids, anions, and thiols even when co-incubated with H_2S.[305] The probe was also applied to HeLa cells to image changes in H_2S upon treatment with PAG or a *N*-(benzoylthio)benzamide-derived H_2S donor.

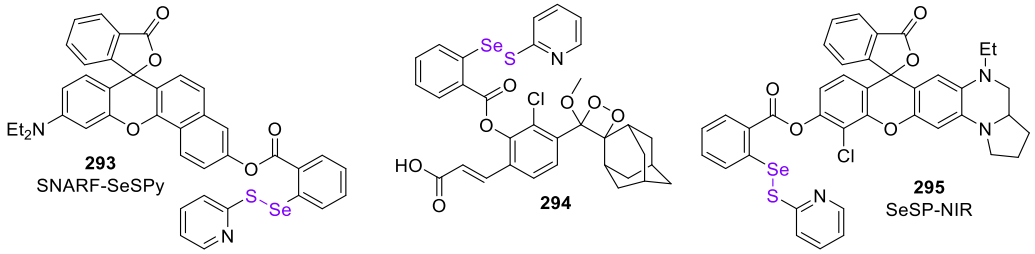


Figure 1.68. Additional examples of fluorescent H_2S probes based on selenenyl sulfide cleavage and subsequent cyclization.

Using the same approach but with alkyl selenosulfides, Lukesh developed **296**–**298** (AL1, AL2, AL4) with coumarin or resorufin-based fluorophores (Figure 1.69).[331] The inclusion of the *gem*-dimethyl groups greatly increased probe selectivity for H_2S, and the developed probes were selective for H_2S over various biothiols and nucleophiles even when co-incubated with H_2S. These probes were further used to image exogenous H_2S in HeLa and HEK293 cells.

Xian also reported diselenide based probes **299** and **300** (SeP1 and SeP2), which are based on coumarin and Tokyo Green, respectively (Figure 1.70).[332] These symmetric probes are reduced by H_2S to generate a selenosulfide, which then undergoes and intramolecular attack and results in ester cleavage. Probes **299** and **300** provided 35- and 15-fold fluorescent enhancements when treated with H_2S in 50% MeCN in buffer. Probe **300** was used to image exogenous H_2S in HeLa cells and also changes in H_2S levels in neuroblastoma cells treated with different H_2S production

substrates or inhibitors. Dong expanded on this approach to develop **301** (SeP3), which uses a naphthalimide derivative to impart a ratiometric response.[333] Upon incubation with H_2S in buffer with 10% DMF, the emission of the probe shifted from 435 nm to 550 nm with an 8-fold increase in fluorescence intensity ratio (F_{550}/F_{435}). Probe **301** was shown to be selective for H_2S over other RSS, to respond to H_2S in bovine plasma, and could be used to image exogenous H_2S in live HeLa cells.

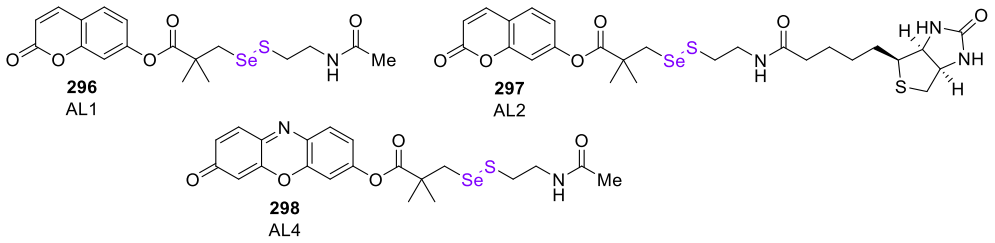


Figure 1.69. Examples of fluorescent H_2S probes based on alkyl selenenyl sulfide cleavage and subsequent cyclization.

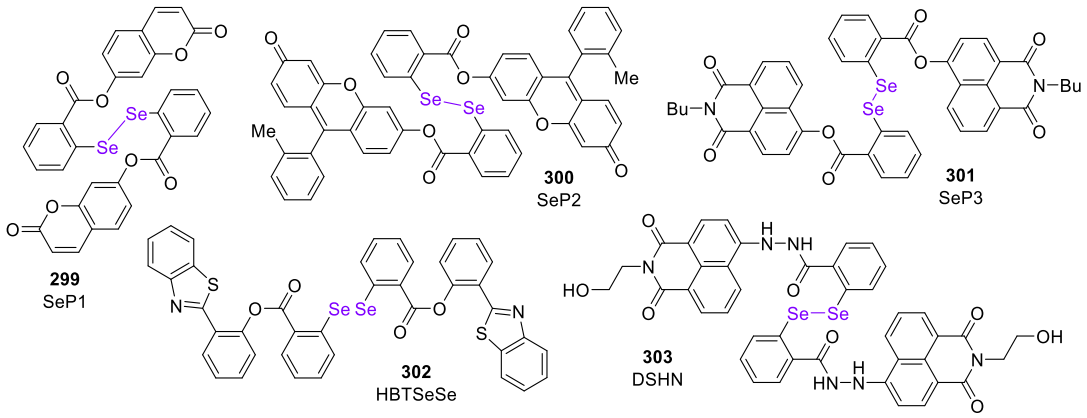


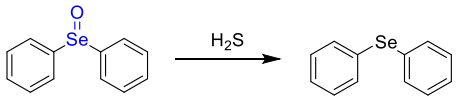
Figure 1.70. Examples of fluorescent H_2S probes based on diselenide cleavage and subsequent cyclization.

Xia and Guo also used this approach to report a HBT-based system to develop **302** (HBTSeSe), which showed a 47-fold fluorescence turn-on in response to H_2S and was also used to image exogenous H_2S in Raw 264.7 cells.[334] Using a different electrophilic linker, Zhang and Liu developed **303** (DSHN), which responded to H_2S with an enhanced emission at 551 nm in 10% DMSO in buffer with good selectivity for H_2S over biologically relevant anions, amino acids, and thiols, although thiols did interfere with the ability of the probe to sense H_2S.[335] This probe

was also used to image exogenous H_2S in GBC-SD cells as well as used to quantify H_2S in natural waters.

1.3.3 Selenoxide-Based H_2S Probes

Although not relating involving dichalcogenide bond cleavage, the reduction of selenoxide (Se=O) motifs has also been used for H_2S detection (Scheme 1.7). In the design of such probes, a key requirement is for the corresponding selenoether and selenoxide to have different optical properties. While this approach for H_2S sensing has been reported in a number of publications, similar chemistry has also been reported previously for the detection of GSH through Se=O reduction, which may highlight GSH as an important competing analyte in certain systems.[336, 337]



Scheme 1.7. H_2S-mediated reduction of selenoxides.

As an example of this approach, Han reported a BODIPY based probe **304** (diMPhSeO-BOD) with two selenoxide motifs (Figure 1.71).[338] The oxidized probe shows a strong fluorescence signal at 635 nm, which shifts to a weaker signal at 700 nm upon reduction by H_2S. The reduced probe can be re-oxidized by HOBr to regenerate **304**. The reduction of the Se=O motif was selective for H_2S over other thiols, and this probe was used to image H_2S and HOBr cycling in live Raw 264.7 cells. Han used a similar approach in the naphthalimide based system **305** (NI-SeO), which can be reduced by H_2S and re-oxidized by HClO.[339] Zeng and co-workers reported a rhodamine analogue **306** (PzSeO) containing a Se=O motif with a strong fluorescent signal at 600 nm that shifts and weakens to 730 nm upon H_2S-mediated reduction to the selenoether.[340] The reduced probe can be re-oxidized with HClO to regenerate **306**. This probe was used to image exogenous HClO and H_2S in live HeLa cells, endogenous ROS production induced by PMA, and changes in H_2S and HClO upon Ca^{2+} modulation in PC12 cells. Shen also reported a related approach using a benzothiazole motif coupled to a selenoxide to generate **307** (BT-SeO).[341] The oxidized BT-SeO could be reduced to BT-Se with H_2S, resulting in a fluorescence shift from 450 to 560 nm, and re-oxidized to **307** with HClO. This probe was used to image exogenous H_2S and HClO in Raw 264.7 cells. Ishii reported **308** and **309** (MbbSeO and

DbbSeO) that resulted in a fluorescence turn-on at 480 nm when incubated with H_2S in 50% MeCN in buffer and was also shown to be reduced by Cys/GSH, although at a much slower rate.[342] The reduced probe could be oxidized by HClO, H_2O_2, ^tBuOOH, and $ONOO^-$, with HClO having the fastest oxidation rate and leading to a fluorescence turn-off. Related chemistry has also been shown with sulfoxides, with a selected example shown from work by Sun who used a thioether/sulfoxide and H_2S/HClO reduction-oxidation cycle to demonstrate this reactivity with the luminescent Ru complex **310**.[343]

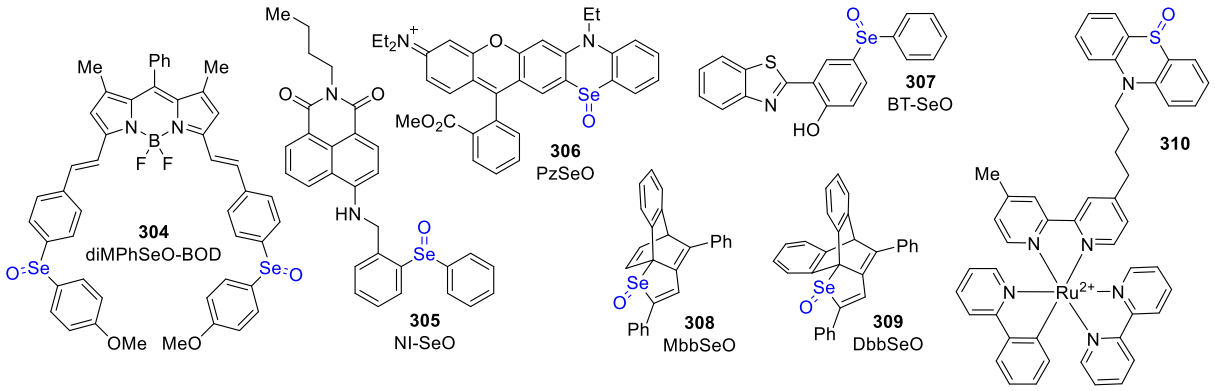


Figure 1.71. Examples of fluorescent H_2S probes based on selenoxide and sulfoxide reduction.

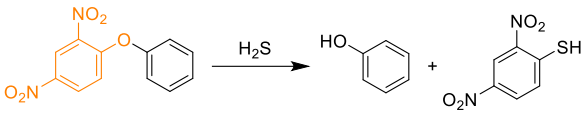
1.4 Electrophilic H_2S Probes

One of the significant differentiating factors between H_2S and other small molecule bioregulators like NO or CO is that H_2S exists primarily in an anionic form, namely HS^-, at physiological pH. In addition to promoting solubility, this anionic form is also significantly more nucleophilic than the diprotic form, which enables HS^- to act as a potent nucleophile. This high nucleophilicity was discussed in earlier sections in this Review briefly in the mechanism of H_2S-mediated azide reduction and dichalcogenide cleavage, but it is even more apparent in probes with specific electrophilic sites designed to react with sulfur nucleophiles. In many cases, fundamental approaches for thiol detection have been repurposed, and in some cases further refined, to enable selective H_2S detection. One challenge in many of these systems is overcoming competing reactions with high concentrations of Cys or GSH. Although the pK_a difference between H_2S and Cys/GSH means that a greater proportion of H_2S is deprotonated to the monoanionic form, the much higher levels of Cys and particularly GSH make this selectivity problem challenging for

many electrophilic probes, particularly at longer reaction times. Despite these challenges, the breadth of approaches that leverage the high nucleophilicity of HS^- to enable specific detection has grown considerably, and in addition to providing useful tools for H_2S-related biological research has also uncovered new fundamental reaction chemistry of this important small molecule.

1.4.1 2,4-Dinitrophenyl (DNP) Cleavage

2,4-Dinitrophenyl (DNP) ether motifs have been used broadly as protecting groups in peptide synthesis and also for cleavage by thiols such as often 2-mecaptoethanol. The electron withdrawing nitro groups in the 2- and 4- positions on the aromatic group activate the phenolic carbon for S_NAr attack by thiol-based nucleophiles. An added convenience of the 2,4-DNP group is that it can be readily attached to phenolic chromophores to generate turn-on probes for reactive sulfhydryl species (Scheme 1.8). Other versions of this approach use 2,4-dinitrobenzenesulfonate (DNBS) groups, which are also cleaved by sulfhydryl species, typically releasing SO_2 in the process are discussed later in this review. The H_2S-mediated reduction of nitro does not appear to be a competing reaction in DNP motifs, and if it is occurring it is much slower than nucleophilic cleavage of the DNP group. Based on the heightened nucleophilicity of HS^- by comparison to other biological thiols, these approaches have been used to provide turn-on fluorescence probes for H_2S. DNP and related groups have been used previously to develop thiol-activate probes that have found broad utility in the field.[344] The selectivity reported from various H_2S-reporting DNP platforms varies greatly, which is noted throughout this section and highlights that such probes may also response to other nucleophilic residues in more complex systems. In general, this class of probes often shows interference from thiols like Cys, Hcy, and GSH, but has been used to generate a wide array of probes for H_2S in different environments.



Scheme 1.8. General reaction scheme for cleavage of a 2,4-DNP group by H_2S.

Lin reported an early example of this approach in 2012 by appending a DNP group to a BODIPY platform to develop **311** (NIR-H_2S), which showed an 18-fold fluorescence turn on at

708 nm (Figure 1.72).[345] This probe showed relatively good selectivity over Cys and GSH and was used to image exogenous H_2S in MCF-7 cells. Other BODIPY motifs have also been reported using this strategy. For example, Li reported **312** (PS1), which provided good selectivity toward H_2S over a 20 minute incubation period, a 60-fold turn-on response at 570 nm, and was used to image exogenous H_2S in HeLa cells.[346] Wang also reported the BODIPY-based probe **313** (TMSDNPOB), which provided a fluorescence response at 592 nm in 50% DMSO in buffer.[347] This probe showed moderate selectivity over GSH and was used to image H_2S in HeLa cells. Jiang reported a related construct in **314**, which reacts with H_2S to generate a turn-off response at 615 nm with good selectivity over 10 μM Cys, Hcy, and GSH.[348] This turn-off response was confirmed with exogenous H_2S in HCT-116 and CT-26 cells. Adding a second DNP motif, Xue and Zhao reported **315** (LM-BDP), which generated a turn-off response to H_2S at 558 nm in 80% MeCN in buffer and also responded to exogenous H_2S in Raw 264.7 cells.[349]

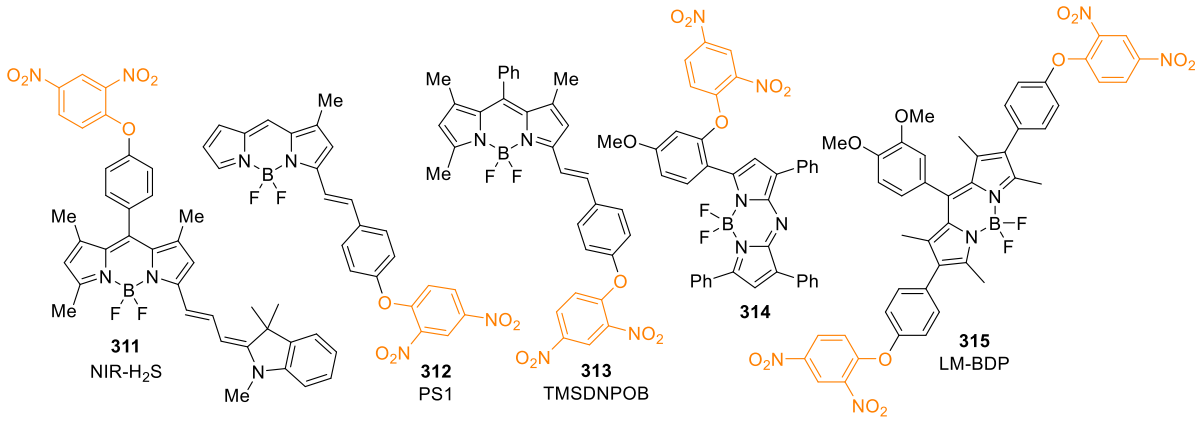


Figure 1.72. Examples of fluorescent H_2S probes based on DNP cleavage with BODIPY chromophores.

Expanding to other fluorophores, Cui and Xu also reported an early example of this approach in 2013 by appending the DNP group to the naphthalimide platform to report **316** (NI-NHS) (Figure 1.73).[350] This probe showed moderate selectivity over thiols in 10% MeCN in buffer and was used to image exogenous H_2S in MCF-7 cells using two-photon excitation at 810 nm. Hongmei reported a related systems with different naphthalimide functionalization in **317** (NTE-1) and also reported an adduct with two DNP groups in **318** (NTE-2).[351] NTE-1 showed poor selectivity over thiols, but this selectivity was moderately improved in NTE-2. Peng and co-

workers reported a naphthalimide amine version in **319** (NP-H_2S), which relies on quenching of the DNP group to modulate the naphthalimide fluorescence.[352] This probe showed good selectivity for H_2S over other analytes, although only 100 μM of thiols were tested. This probe was also used to image exogenous H_2S in HeLa cells and in inflamed tissue from mice using two-photon excitation at 780 nm. Wang, Wang, and Qu reported extended naphthalimide construct **320** (NI-SH), which provided a fluorescence increase at 540 nm with concomitant decrease at 465 nm that showed good selectivity over competing species, but a small response to Cys.[353] This response was further confirmed in HeLa cells treated with exogenous H_2S. One theme observed from these naphthalimide-based probes is that moving the DNP group so that it was not directly attached to the already electron deficient naphthalimide ring improved probe selectivity.

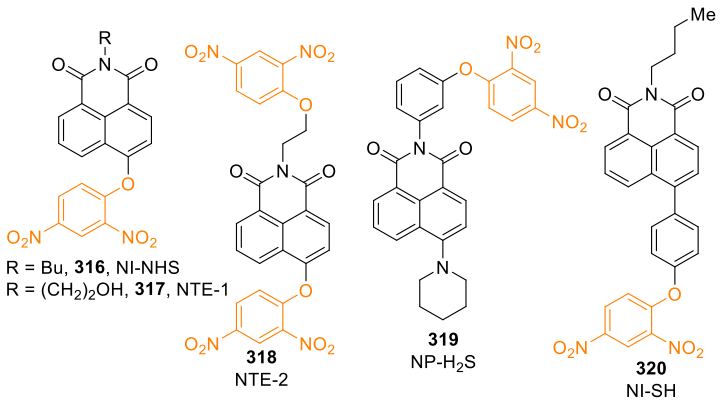


Figure 1.73. Examples of fluorescent H_2S probes based on DNP cleavage with naphthalimide chromophores.

A variety of coumarin derivatives incorporating DNP sensing groups have also been reported. For example, Yuan reported the coumarin benzothiazole adduct **321** (MC8), which provides a 491-fold turn-on response to H_2S at 491 nm and good selectivity of competing thiols (Figure 1.74).[354] This probe was used to image exogenous H_2S in Raw 264.7 cells and liver slices as well as to investigate H_2O_2-induced H_2S generation. Wang reported ester-functionalized **322** (DNPOCA), which provided good selectivity over GSH in 10% MeCN in buffer and was used to image exogenous H_2S in HepG2 cells.[355] Zhao and co-workers reported the aminocoumarin benzothiazole adduct **323** (CTN), which provided relatively good selectivity for H_2S over Cys and GSH, although some response to 100 μM GSH was observed. This probe was further used to image exogenous H_2S in HeLa cells.[356]

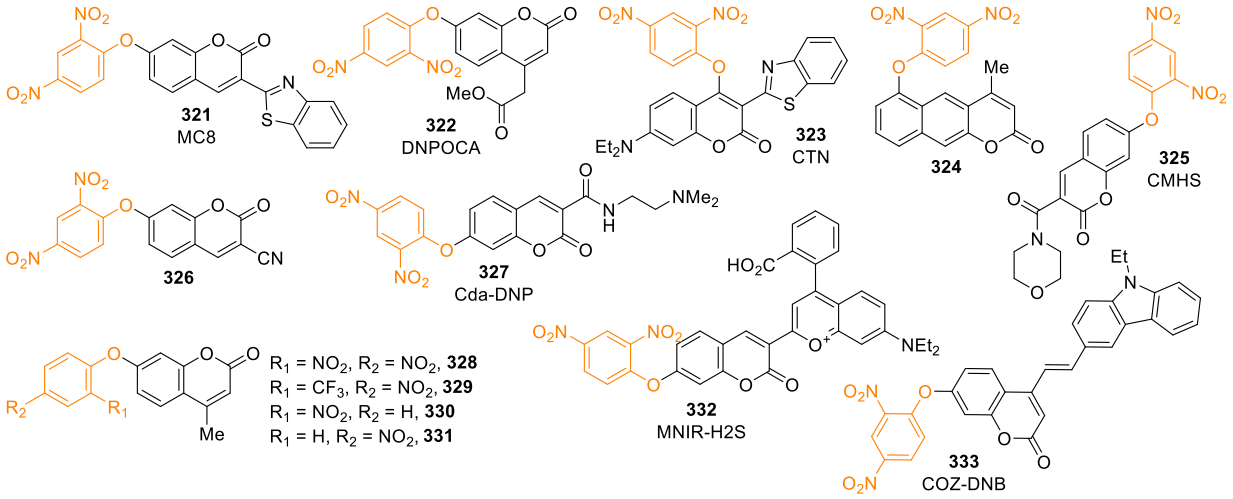


Figure 1.74. Examples of fluorescent H_2S probes based on DNP cleavage with coumarin chromophores.

Yin and Huo reported extended coumarin derivative **324**, which provided a 25-fold turn-on response at 530 nm with moderate selectivity for H_2S over other thiols in 50% DMSO in buffer and was further used to image exogenous H_2S in HeLa cells.[357] Similarly, Lin reported **325** (CMHS), which contains a coumarin fluorophore with pendant amide motif to enhance solubility.[358] This probe showed a 180-fold turn-on response at 455 nm, good selectivity for H_2S over thiols, and subsequently was used to image exogenous H_2S in HeLa cells. Peng and Dahaen reported the related cyanocoumarin **326**, which was used to image exogenous H_2S in MCF-7 cells and zebrafish.[359] Adding a dimethylamino motif to improve membrane permeability, Zhang reported **327**, which provided a turn-on response at 450 nm in 30% THF in buffer, with good selectivity over competing analytes, although a small response to 2 mM GSH was observed.[360] This probe was further used to image exogenous and endogenous H_2S in A549 cells, different cancer cell lines, and zebrafish. Expanding on the DNP functionalization, Shang reported a series of probes with different patterns of electron withdrawing groups on the S_NAr electrophile in **328**–**331**, with both the DNP (**328**) and *o*-CF_3 analogue (**329**) showing a response to H_2S.[361]

Extending to longer-wavelength coumarin motifs, Zhou reported **332** (MNIR-H_2S) with a coupled xanthene dye to allow for two-photon excitation at 810 nm.[362] This probe provided a ~150-fold fluorescence turn-on at 668 nm with good selectivity for H_2S over competing thiols, although a minor response was observed with 100 μM GSH and Cys. Probe **332** probe was further used to

image exogenous H_2S in a variety of systems, including HeLa cells, live mice, onion cells, and zebrafish. Using an extended coumarin-carbazole derivative, Hou reported **333** (COZ-DNB), which provided a turn-on response at 556 nm with good selectivity for H_2S.[363] This probe was further used to image exogenous and Cys-derived H_2S in HeLa cells and zebrafish.

Expanding to xanthene-based chromophores, Ge reported Nile red and Nile blue DNP probes **334** and **335** in 2014, which react with H_2S in 25% DMSO in buffer to provide an 18-fold turn-on response at 660 nm and gradual turn-off at 682 nm for the two probes, respectively (Figure 1.75).[364] Probe **334** showed relatively good selectivity for H_2S over thiols although a minor response to some analytes was observed, and this probe was further used to image exogenous H_2S in HeLa cells. Using a related platform, Yin and Zhang reported NIR probe **336** (NRDNP), which provides a fluorescence response at 610 nm upon treatment with H_2S in 10% DMSO in buffer.[365] This probe showed moderate selectivity for H_2S over other reactive analytes at equimolar concentrations to H_2S, and was used to image exogenous H_2S in Raw 264.7 cells. Zheng and Cui reported Nile red derivative **337** (NR-HS) in 2014, which provided a turn-on response at 655 nm upon reaction with H_2S.[366] This probe showed good selectivity toward H_2S over other reactive species in 10% DMSO in buffer and was used to image exogenous H_2S in MCF-7 cells. Hou later reported related derivative **338**, which provided a turn-on response at 640 nm with good selectivity over competing anions and thiols in 80% DMSO in buffer.[367] This probe was also used to image exogenous H_2S in MCF-7 cells and was determined to accumulate in the mitochondria.

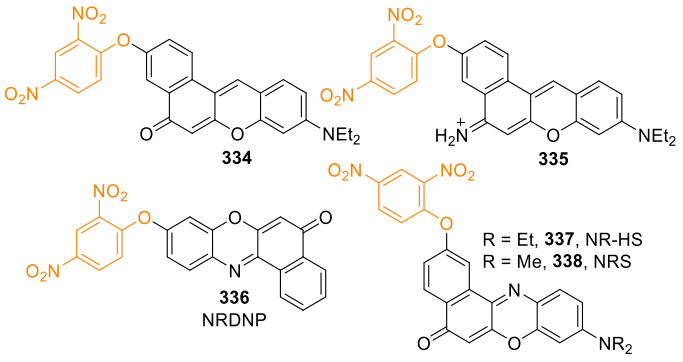


Figure 1.75. Examples of fluorescent H_2S probes based on DNP cleavage with Nile red and Nile blue chromophores.

Hou also reported a doubly DNP substituted probe **339**, with a 250-fold turn-on response at 510 nm in 25% DMSO and 1 mM CTAB in buffer (Figure 1.76). This probe showed some

activation by thiols, including by 50 μM GSH, and was used to image exogenous H_2S in SW480 cells.[368] In 2016, Zhang as well as Zhang and Zheng independently reported **340** (NIR-HS), which provides a turn-on fluorescence response ~720 nm and shows good selectivity for H_2S over other nucleophilic analytes.[369, 370] This probe was used to image H_2S production from sulfate reducing bacteria as well as exogenous H_2S and SNP-derived H_2S in MCF-7 cells. In addition, **340** was used to image exogenous H_2S in mice. Zeng and Wu reported similar probe **341** (CHO-OH-NO_2), which incorporates an *o*-aldehyde for increased selectivity and short polyethylene glycol motif for enhanced solubility.[371] This probe provided a turn-on response to H_2S at 718 nm and good selectivity for H_2S over competing analytes. Further applications included developing paper test strips for H_2S release from foodstuffs and monitoring H_2S generation in germinating wheat grains under Al^{3+} stress. Yang and Yin as well as Liu reported **342** (Mito-DNP, NFL-DNBr) in independent reports, which further extended the emission to 741 nm and showed good selectivity for H_2S against competing analytes.[372, 373] This probe was used to image exogenous H_2S in HepG2 and A549 cells, H_2S from the H_2S donor ADT-OH in A549, and also in mice.

Tian and co-workers reported aldehyde-containing **343** (QcyCHO) with an extended emission of 744 nm.[374] Careful selectivity studies in 50% MeCN in buffer showed some probe activation by 1 mM Cys, but less for GSH, and partial probe deactivation by SO_3^{2-}. This probe was used to image exogenous H_2S and Cys-derived H_2S in HeLa cells. Feng reported a similar platform incorporating a pyridinium motif to develop **344** (MI-H_2S), which has an emission maximum at 663 nm and showed good selectivity for H_2S over other thiols and nucleophiles.[375] This probe was used to image exogenous and Cys-derived H_2S in MCF-7 cells, as well as exogenous H_2S in zebrafish and mice. A similar approach was reported by Lin who reported quinolinium-functionalized **345** (PAP-H_2S), which provided a 9-fold enhancement at 715 nm.[376] This probe was subsequently used for photoacoustic imaging of H_2S and applied to investigate H_2S generation in a mouse air pouch inflammation model. A different quinolinium isomer was reported by Cheng and Xu with **346** (WFP-HS), which provided a further red-shifted emission of 750 nm and was used to image exogenous H_2S in SHSY5Y cells and mice.[377] Zhang reported a related platform with an additional H_2O_2 sensing motif in **347** (QM-RSH), which provided a response turn-off response to H_2S in the red channel, but turn-on response to sequential reaction with H_2O_2 and H_2S in the yellow channel.[378] This response was confirmed in HepG2 cells, and the probe was further used to investigate LPS-mediated inflammation responses in zebrafish.

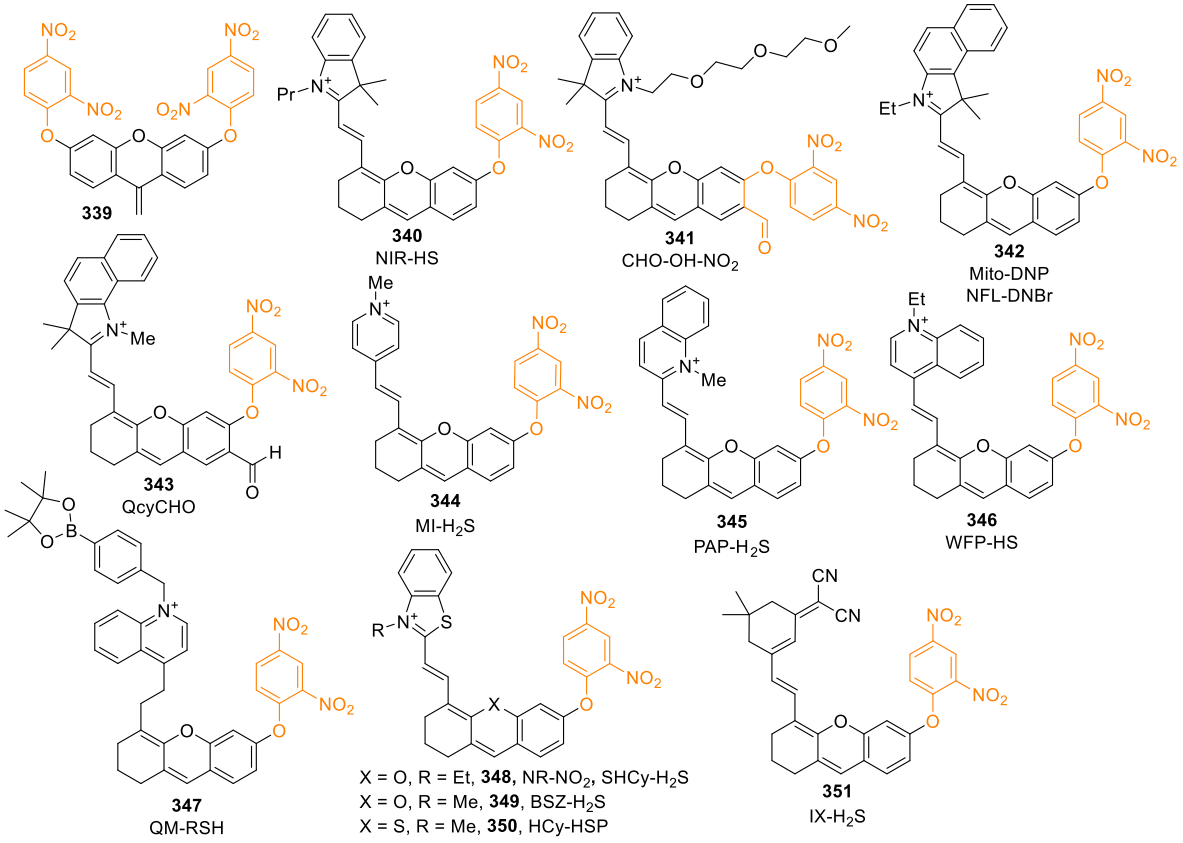


Figure 1.76. Examples of fluorescent H_2S probes based on DNP cleavage with red-shifted chromophores.

Xanthene-benzothiazolium fluorophores have also been used with this approach. Zeng and Wu reported **348** (NR-NO_2), which provides a turn-on response to H_2S at 725 nm with good selectivity for H_2S over competing analytes.[379] This probe was further used to image exogenous and endogenous H_2S in HCT-116 cells and intratumoral endogenous H_2S generation in tumor-bearing mice. In addition to a fluorescence readout, **348** was also used for optoacoustic imaging of H_2S generation from metformin-induced liver injury in mice. The same construct was later reported by Zeng and Gong (SHCy-H_2S), which was used to image exogenous and Cys-derived H_2S in HeLa cells.[380] Fu reported an almost identical platform with a methyl, rather than ethyl-benzothiazolium motif to report **349** (BSZ-H_2S). This probe was used to image exogenous H_2S in MCF-7 cells and zebrafish, as well as endogenous H_2S in rice roots.[381] Lin and co-workers reported **350** (Hcy-HSP), which is built from the same structure but includes a sulfur rather than oxygen atom in the xanthene core. This substitution resulted in a further red-shifted emission of 787 nm.[382]

This probe showed good selectivity for H_2S against competing analytes and was also used to image exogenous and endogenous H_2S in SH-SY5Y cells and LPS-mediated H_2S increases in live mice. Further applications of this probe were used to monitor endogenous upregulation of H_2S in mouse lungs following LPS injection in models of acute lung injury. Using a similar construct, Li reported **351** (IX-H_2S), which provided a response at 770 nm with good selectivity over competing ions, metals, amino acids, and thiols.[383] This probe was further used to image exogenous and endogenous H_2S in HCT116 cells, exogenous H_2S in nude mice, and differences in H_2S generation in the colon of mouse models of ulcerative colitis.

Also in 2014, Xu and Xu reported the doubly protected fluorescein derivative **352**, which showed excellent selectivity for H_2S over Cys, Hcy, NAC, and GSH and was used to image exogenous H_2S in HeLa cells (Figure 1.77).[384] This improvement in selectivity is possibly due to inclusion of two DNP ether groups, both of which must be cleaved for full probe activation. Expanding to lower-ring functionalization strategies, Yuan reported ratiometric probes **353** and **354** (Ratio-H_2S-1 and Ratio-H_2S-2), which differ by the positions of the amide linkage.[385] Probe **353** provided moderate selectivity for H_2S over Cys and GSH, was demonstrated to localize in the mitochondria, and was used to image exogenous H_2S in MCF-7 cells. Jiang reported the NIR probe **355** (Mito-NIR-SH), which showed a turn-on response at 720 nm with good selectivity for H_2S, although some response to GSH was also observed.[386] This probe was confirmed to localize to the mitochondria and was subsequently used to image exogenous H_2S in HeLa cells. Expanding to further xanthene functionalization, Jiang reported **356** (Mito-NSH), which provides a fluorescence response at 664 nm upon treatment with H_2S.[387] This probe showed good selectivity for H_2S over other competing thiols and was used to image exogenous H_2S in HeLa cells. Using a related approach, Jiang reported **357** (NIR-H_2S), which provided a turn-on response to H_2S at 736 nm, which showed good selectivity, only a small response to Cys, and was used to image exogenous H_2S in HeLa cells.[388]

Focusing on direct xanthene ring substitution on rhodafluor motifs, Wang, Yang, and Zhu reported **358** (Rho-HS), which also includes an *ortho*-chloro substitution adjacent to the DNP group.[389] This probe showed improved selectivity over thiols, but only moderate selectivity when tested against nucleophilic oxidized sulfur species like SO_3^{2-}, SO_4^{2-}, and $S_2O_4^{2-}$. This probe was used to image exogenous H_2S in MCF-7 cells and in *C. elegans*. Using a similar system but with an *ortho* aldehyde to improve selectivity (*vide infra*, section 4.1), Jin and co-workers reported **359**

(RCHO).[390] This probe was used to investigate H_2S in different water sources and also to image exogenous H_2S in HeLa cells. Martínez-Máñez and Costero reported methoxyfluoresceine-based **360**, which provided a turn-on response to H_2S at 515 nm with good selectivity for H_2S over other analytes, although a small response to GSH was also observed.[391]

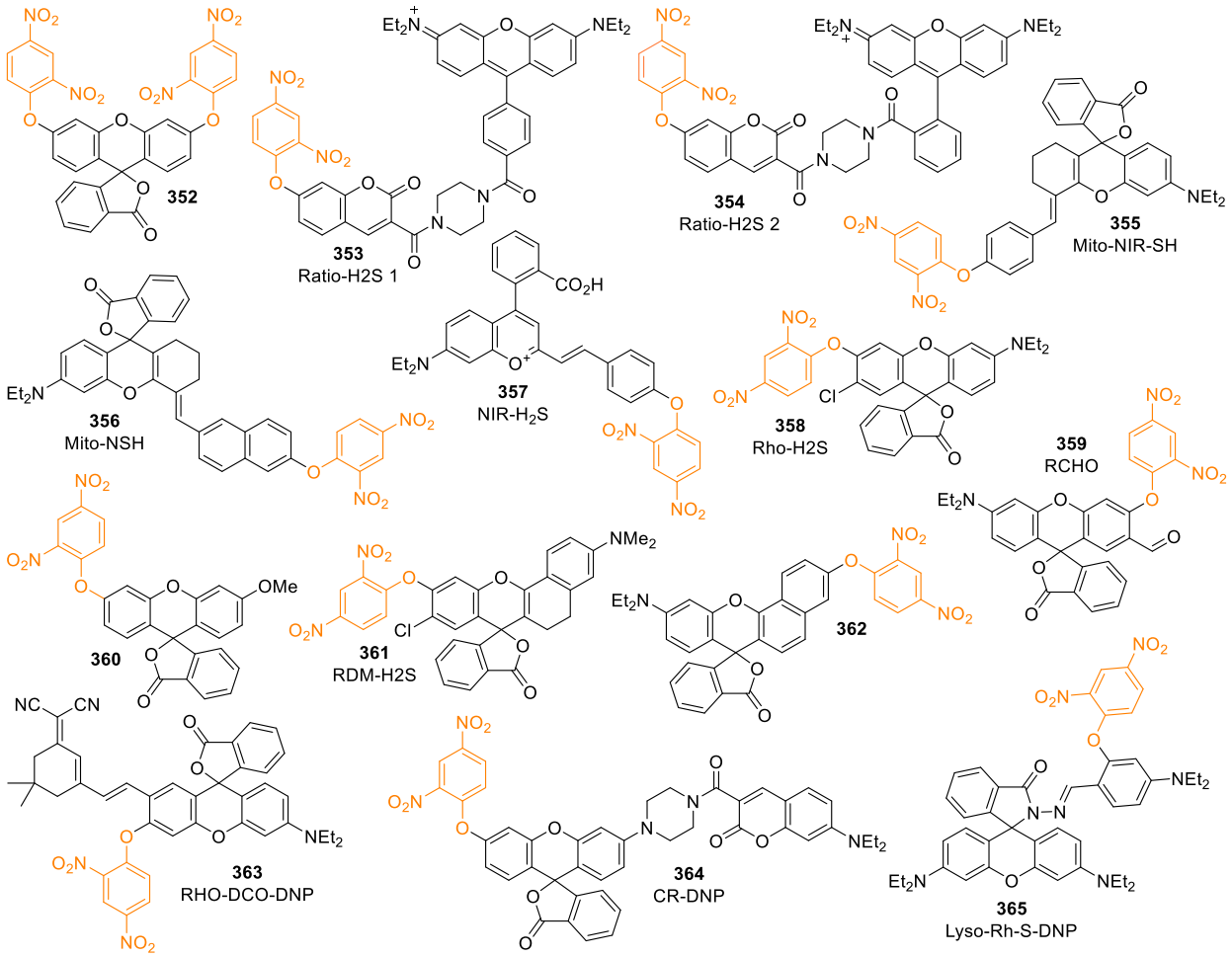


Figure 1.77. Examples of fluorescent H_2S probes based on DNP cleavage with xanthene-based chromophores.

Using the same with an extended emission system, Yang, Zhu, and Hu reported **361** (RDM-H_2S), which provides a turn-on response to H_2S at 620 nm and excellent selectivity over thiols and $S_xO_y^{n-}$ nucleophiles.[392] This probe was used to image exogenous and Cys-derived H_2S in cell and in 4T1-xenograft tumor mice, revealing an increased signal from the tumor when compared to other organs. In addition, this probe was used to image increases in endogenous H_2S in mice during

LPS-induced inflammation, with good differentiation between the probe and LPS-treated animals. Jin reported the seminaphtharhodafluor-based probe **362**, which provided a turn on response at 635 nm with good selectivity for H_2S, although a minor response to GSH was also observed. This probe was further applied to develop H_2S-responsive hydrogels and to detect exogenous H_2S in HeLa cells.[393] The same probe was later reported by Jiang and used to detect H_2S release from different glucosinolate and isothiocyanate compounds, including sulforaphane, and was also used to image H_2S in mouse brain tissue.[394]

Further extending the emission wavelength, Gao reported **363** (RHO-DCO-DNP), which responds to both H_2S and changes in viscosity with fluorescence at 760 and 585 nm, respectively.[395] This probe showed good selectivity for H_2S over other analytes in 40% MeCN in buffer and was used to image exogenous H_2S and Cys-derived H_2S in HeLa cells. In a final example of direct rhodafluor functionalization, Zeng reported the ratiometric reporter **364** (CR-DNP), in which FRET between a pendant aminocoumarin chromophore and the parent rhodafluor dye modulate the fluorescence.[396] Treatment with H_2S results in a fluorescent decrease at 474 nm and concomitant increase at 541 nm with good selectivity and further demonstration of imaging exogenous H_2S in HeLa cells. Zhao and Zhu used a related approach to combine the H_2S-mediated DNP cleavage with spiro-lactam opening of **365** (Lyso-Rh-S-DNP) to generate a fluorescent response at 777 nm.[397] This probe was subsequently confirmed to localize in the lysosome and was used to image exogenous H_2S in HeLa cells and zebrafish.

A variety of DNP adducts based on cyanine dyes have also been reported to further shift fluorescent responses to longer wavelengths. For example, in 2014 Govindaraju reported **366** (DNPOCy), which provides a ratiometric response to H_2S with increase at 695 nm and concomitant decrease at 555 nm (Figure 1.78).[398] This probe showed moderate selectivity for H_2S over Cys and GSH and was used to image exogenous H_2S in HEK293T cells. Zhao later reported an almost identical platform with **367** differing from **366** by one carbon in the sulfonate chain, which was used to image exogenous H_2S in HeLa and HepG2 cells as well as in mice.[399] Su and Yuan also reported non-sulfonated **368** (QCy7-HS), which showed a fluorescence response at 715 nm in 50% MeCN in buffer and good selectivity for H_2S over competing analytes.[400] This probe was used to image exogenous H_2S in HeLa cells and live mice, as well as NAC-derived H_2S in mice. Li also reported DNP adduct **369** (CyO-DNP), which has a significantly red-shifted emission at 793 nm upon reaction with H_2S and showed good selectivity for H_2S over other thiols and $S_xO_y^{n-}$

species.[401] This probe was used to image endogenous H_2S in HCT116 cells and exogenous H_2S in live mice, also showing increased signal from isolated tumor when compared to other organs (Figure 1.79). This probe provided a maximum signal at pH 5 rather than physiological pH, which may be beneficial for investigating H_2S in acidic microenvironments.

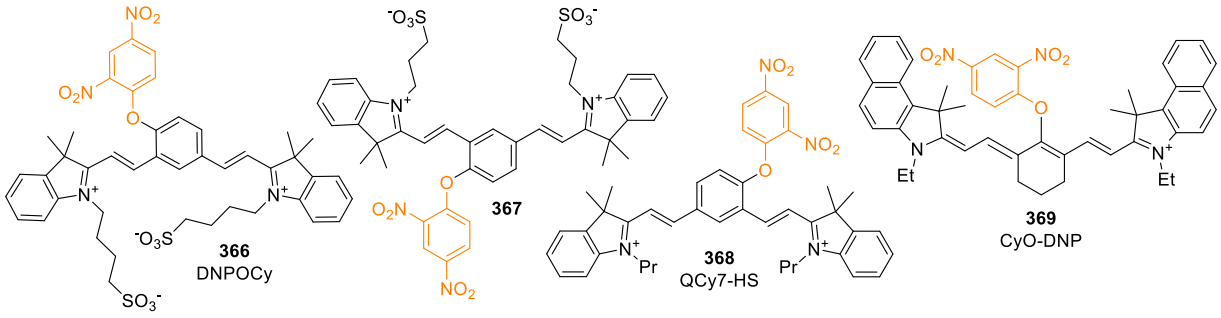


Figure 1.78. Examples of fluorescent H_2S probes based on DNP cleavage with cyanine-based chromophores.

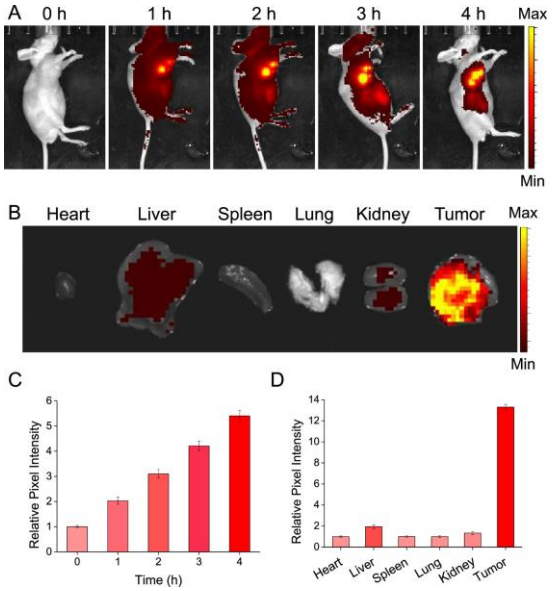


Figure 1.79. Fluorescence imaging of endogenous H_2S in HCT116 tumor-bearing mice through tail vein injection of **369**, including (a) time course, (b) *ex vivo* fluorescence imaging of isolated organs, (c) time course fluorescence quantification, and (d) organ fluorescence quantification. Reproduced and modified with permission from ref [400]. Copyright 2021 American Chemical Society.

Other extended wavelength fluorophores have also been used with the DNP sensing approach. For example, Zhou reported the tetrahydroxanthylium scaffold **370** (TP-NIR-HS),

which provided a 150-fold turn-on response at 665 nm upon reaction with H_2S and good selectivity over competing analytes (Figure 1.80).[402] This probe was used to image exogenous H_2S in A375 cells with two-photon excitation at 800 nm and also in live mice. Lu and Lu reported the related rhodamine hybrid **371** (FL-NO_2), which can be excited at 808 nm and emits in the NIR-II region with a maximum at 932 nm.[403] This probe showed good selectivity for H_2S over competing analytes and was used to image differential H_2S signals from CT-26 and HeLa implanted tumors in mice.

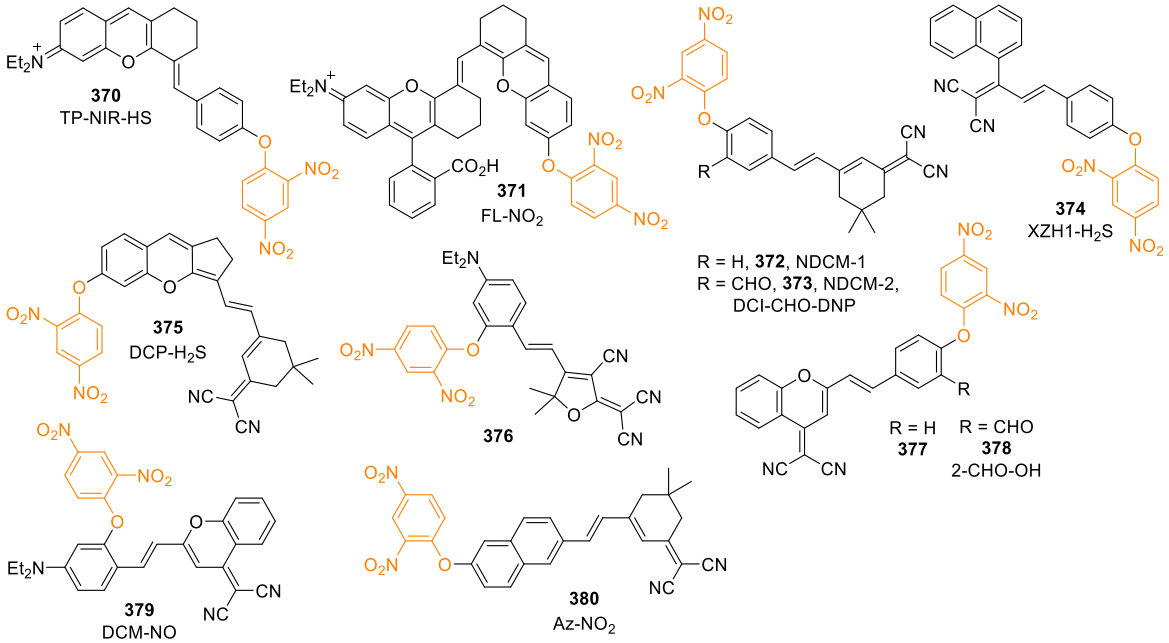


Figure 1.80. Additional examples of fluorescent H_2S probes based on DNP cleavage with extended wavelength chromophores.

Wang and Peng reported **372** and aldehyde-functionalized **373** (NDCM-1 and NDCM-2) to compare the selectivity of these two platforms. Probe **373** was found to react significantly faster than the parent probe, which was attributed to participation of the aldehyde in H_2S addition to the DNP group.[404] This probe provided a turn-on response at 660 nm with good selectivity for H_2S over competing analytes, and was further used to image exogenous and Cys-derived H_2S in MCF-7 cells as well as exogenous H_2S in Kunming mice. Feng later reported the same compound **373** (DCI-CHO-OH).[405] Interestingly, this platform also showed selectivity over highly nucleophilic selenocysteine, which highlights the fidelity of this selectivity-enhancing aldehyde inclusion

approach. This probe was also used to image both exogenous and endogenous H_2S in HeLa cells. Xu, Bo, and Zheng reported the naphthalene extended **374** (XZH1-H_2S), which showed a turn-on response at 585 nm with good selectivity over competing analytes.[406] This probe was subsequently used to image exogenous and endogenous H_2S in MCF-7 cells, exogenous H_2S in mice, and H_2S generation in different organism from tumor-bearing mice.

Mao and Li reported a related scaffold in **375** (DCP-H_2S), which shows a 15-fold turn-on response at 770 nm.[407] This probe showed good selectivity for H_2S over competing nucleophiles and was used to image differential endogenous H_2S production in 293T, Caco-2, and CT-26 cells. In addition, this system was used to image increased H_2S generation in tumor-bearing mice when compared to mice without tumor implantation. Tang also reported a similar scaffold **376**, which has an emission maximum at 640 nm.[408] This probe was selective against competing anions in 30% DMSO in buffer, although thiols were not investigated. The probe was used to investigate H_2S levels in different water samples and to image exogenous H_2S in MCF-7 cells. Xie and Guo reported DNP-based **377**, which provided a turn-on response at 712 nm in 90% DMF in water and was used to investigate sulfide levels in spiked tap water.[409] Li also incorporated an *ortho*-aldehyde to prepare **378** (2-CHO-OH), which provided good selectivity for H_2S over competing analytes in 50% DMSO in buffer and used to image exogenous and Cys-derived H_2S in HeLa cells.[410] Jin and She reported related isomer **379** (DCM-NO), which provided a fluorescent response to H_2S at 672 nm and showed moderate selectivity for H_2S over thiols.[411] This probe was used to image exogenous H_2S in HeLa cells and also to prepare PMMA nanofibrous films containing the probe, which were used to measure H_2S in water samples. Using a naphthalene core, Zhao reported **380** (AZ-NO_2), which provided moderate selectivity for H_2S over competing thiols in 50% DMSO in buffer at 620 nm. The probe was used to exogenous and SNP-generated H_2S in HepG2 cells and zebrafish.[412]

Several organelle targeted probes containing DNP motifs have also been reported. For example, Xu and Cui reported the naphthalimide probe **381** (Lyso-DNP) in 2013, which provides a 42-fold turn-on fluorescence response at 555 nm upon treatment with H_2S in 10% MeCN in buffer (Figure 1.81).[413] This probe was confirmed to localize to the lysosome and was used to image exogenous H_2S in MCF-7 cells. The resultant probe was demonstrated to localize to the lysosome and used to image exogenous H_2S in HeLa cells. Ou, Zhao, and Peng also reported a naphthalimide-based probe, but in this case the morpholine targeting group was directly attached

to the chromophore to generate **382**.[414] This probe showed a fluorescence response at pH 4.5 upon treatment with H_2S, was confirmed to localize to the lysosome, and was used to image differences in normal and inflamed excised mouse tissues. Li also reported a lysosomal based on a chromene-4-one derivative to prepare **383** (DMC), which provides a fluorescence response at 547 nm.[415] This probe showed good selectivity for H_2S over competing species, although with only 10 equivalence of thiols were tested. Wang and Xu reported chalcone-based probe **384**, which provided a fluorescence turn-on response to H_2S in 50% DMF in buffer, but also showed a sizeable response to HClO. This probe was used to image exogenous and Cys-derived H_2S in MCF-7 cells and larval zebrafish.[416]

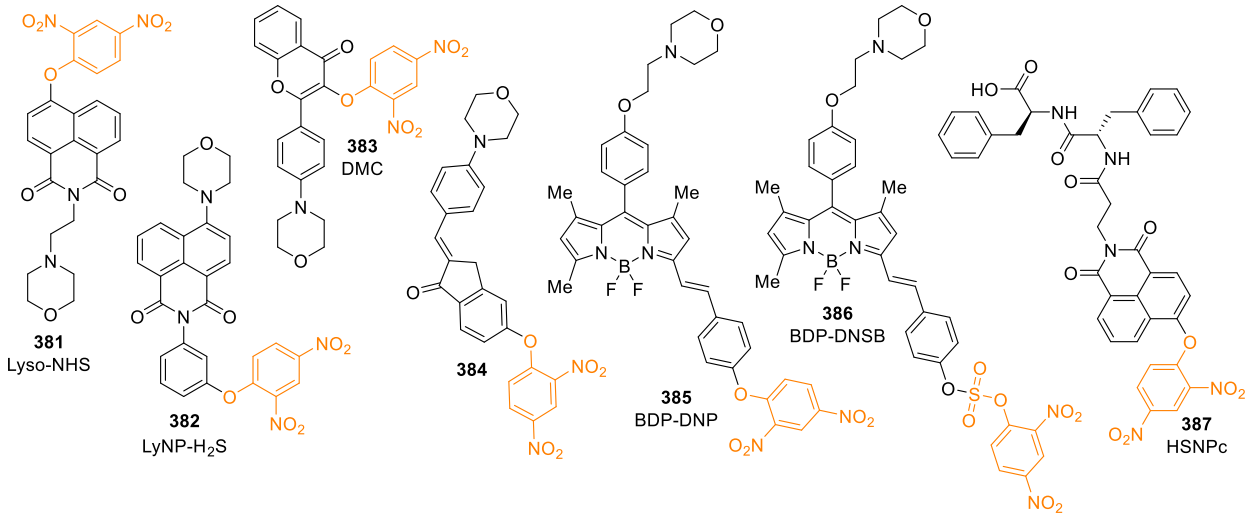


Figure 1.81. Examples of fluorescent H_2S probes based on DNP cleavage with targeting groups.

Zhang and Zhao reported a BODIPY-based probe that uses the DNP motif for H_2S recognition to prepare **385** (BDP-DNP) and also the sulfonate ester analogue (*vide infra*, section 4.2) **386** (BDP-DNPS).[417] Both probes provided a turn-on response at 587 nm, but **386** provided a significantly faster response. This probe showed moderate selectivity for H_2S over thiols, although the selectivity was only measured after 1 minute of incubation, and the probe was also used to image exogenous and Cys-derived H_2S in HeLa cells. Using a different localization approach, Joshi and Verma reported the naphthalimide-conjugate **387** (HSNPc), which contained a short diphenylalanine-based peptide to promote cellular uptake that selectively induced apoptosis in cancer cells and also reported on H_2S levels.[418]

Different cationic DNP-based H_2S probes have also been reported. Zhang and Dong reported **388** (DPPVP), which contains a pyridinium motif to improve water solubility (Figure 1.82).[419] This probe provides a turn-on response at 520 nm in 1 mM CTAB in buffer, showed moderate selectivity for H_2S over thiols, and was used to investigate exogenous H_2S in different vegetables. Using related quinolinium, Fu reported **389**, which provided a turn-off fluorescent response at 500 nm in 40% DMSO in buffer.[420] Modifying the central conjugation of these motifs, Chen and Liu reported related probe **390** (EMII-H_2S), that is compatible with both one- and two-photon excitation at 410 and 750 nm, respectively.[421] This probe was used to image exogenous H_2S in T24 cells and to investigate H_2S in liver slices at scanning depths up to 180 μm. As an additional example of this approach, Li, Cheng, and Tang reported **391**, which provided a turn-on response at 607 nm and good selectivity for H_2S over competing thiols in 40% DMF in buffer.[422] This probe was used to image exogenous H_2S in MCF-7 cells and to develop nanofiber-based test strips for H_2S.

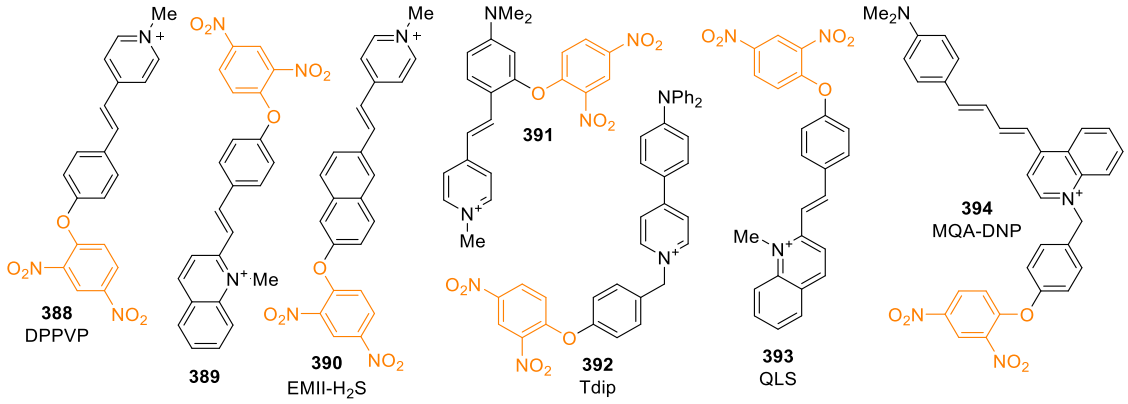


Figure 1.82. Examples of fluorescent H_2S probes based on DNP cleavage with cationic chromophores.

Hu and Zhang reported the benzylpyridinium construct **392** (Tdip), which upon reaction with H_2S results in DNP cleavage and a subsequent cascade elimination to release the neutral pyridine. This probe showed moderate selectivity for H_2S over $S_2O_3^{2-}$ in 70% DMSO in buffer. The resultant probe was used to investigate H_2S in wine samples and also to image exogenous H_2S in MCF-7 cells.[423] Liu reported a quinolinium-based **393** (QLS), which reacted with H_2S to cleave the DNP group to form a zwitterionic intermediate that ultimately converted to a neutral quinone-alkenone product.[424] This response of this probe was measured in 90% MeCN in buffer and later

applied to develop H_2S-responsive test strips for measurement in different food products. Fan and Shuang reported the extended quinolinium probe **394** (MQA-DNP), which provided a turn-on response at 634 nm and additional response to solvent viscosity / polarity >700 nm.[425] This probe was subsequently used to image exogenous and Cys-derived H_2S in HeLa cells, as well as to investigate H_2S and viscosity differences in malignant versus benign organ and tissue samples.

A variety of flavone-based DNP probes for H_2S have also been reported, many of which make use of the ESIPT fluorescence mechanism of this class of fluorophores. For example, Feng reported **395**, which reacts with H_2S to generate a fluorescence response at 538 nm in 20% DMSO in buffer with CTAB (Figure 1.83).[426] This probe provided moderate selectivity for H_2S over other competing thiols like GSH and NAC, although only 10 equiv. of competing analytes were tested, and the probe was subsequently used to investigate H_2S in different water samples.[427] Hou and Hou prepared related construct **396**, which also provided moderate selectivity for H_2S over competing thiols in 20% DMSO solution with 3 mM CTAB and was used to image exogenous H_2S in LoVo cells. Using the related fused coumarin system, Liu reported DNP **397** (YB), which reacted with both H_2S and GSH, with moderate signal for Cys and Hcy.[428] Adding additional hydrophobicity to the platform, Zeng and Wu developed tetraphenylethylene probe **398** (TPE-3), which provides an AIE response to H_2S. This probe provided a turn-on response at 550 nm with good selectivity for H_2S over competing anions and thiols.[429] The resultant construct was used to image exogenous H_2S in HeLa cells and zebrafish and also an increase in fluorescence in cells treated with GSH, which was attributed to endogenous H_2S formation.

Man, Hu and Wang, and co-workers reported a series of flavone-based probes containing either DNP ethers **399** and **400** (FlaN-DN and FlaO-DN) or sulfonate esters **401** and **402** (FlaN-DB and FlaO-DB).[430] The sulfonate-based probes were found to react with both H_2S and competing thiols, but better selectivity was observed for the DNP-ether probes **399** and **400**, with **399** being subsequently used to image exogenous and Cys-derived H_2S in HeLa cells. Further extending the conjugation of flavone systems, Song reported **403**, which provides a red-shifted fluorescence response at 612 nm, with moderate selectivity for H_2S over thiols and oxidized sulfur anions.[431] This probe was subsequently used to image exogenous H_2S in Raw 264.7 cells. Viswanathamurthi reported the triphenylamine and pyrene conjugates **404** and **405**, respectively, which provided fluorescence responses to H_2S a ~540 nm in 50% DMSO in buffer.[432] Both probes were additionally used to image exogenous H_2S in HeLa cells. A further extended flavanol-based

probe was reported by Zhang in **406** (Fla-DNP), which provides a turn-on response at 566 nm with moderate selectivity over thiols.[433] This probe was used to image exogenous H_2S in 4T1 cells and to develop H_2S test strips for food products.

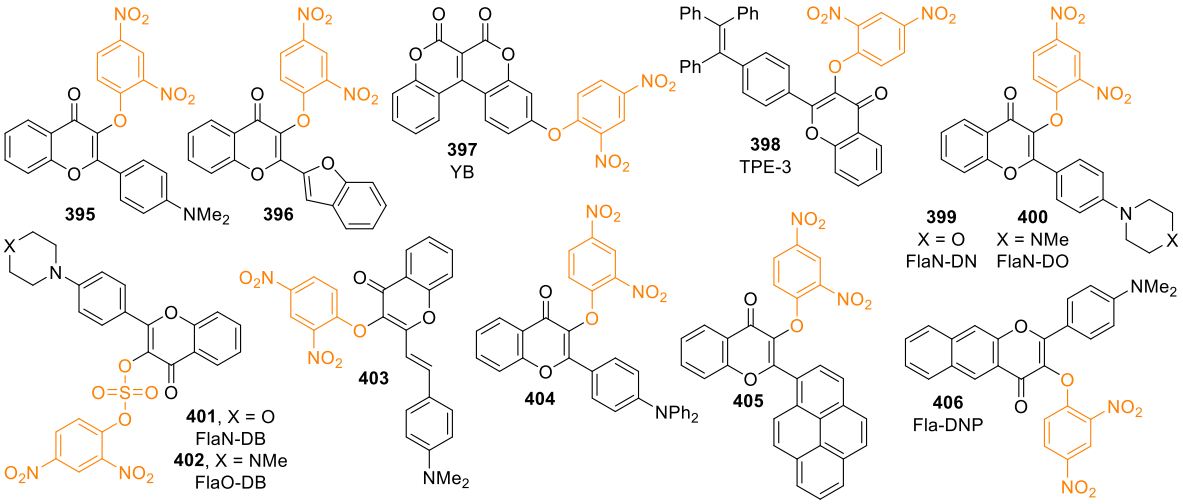


Figure 1.83. Examples of fluorescent H_2S probes based on DNP cleavage with flavone-based chromophores.

In one of the early example of DNP usage for H_2S sensing, Martínez-Máñez and Costero reported quinoline derivative **407**, which showed moderate selectivity for H_2S over thiols, provided a fluorescence turn-on at 514 nm, and was used to image exogenous H_2S in HeLa cells (Figure 1.84).[434] Using a naphthalene fluorophore, Yang reported the cyanonaphthalene derivative **408**, which provided a response at 432 nm, moderate selectivity over thiols, and was used to investigate H_2S in beer and wine samples.[435] The parent naphthalene-DNP adduct **409** was also reported by both Martínez-Máñez and Costero as well as Goswami, with the latter report also highlighting that inclusion of the *ortho*-aldehyde in **410** resulting in an increase in reactivity toward H_2S.[391, 436] Expanding to a benzothiazole motif, Liu reported **411** (EPS-H_2S), which showed only a minimal response to thiols, but also was only tested for 20 minutes of incubation time.[437] The resultant probe was used to image exogenous H_2S in HT22 cells and used to investigate H_2S in mouse hippocampal slices.

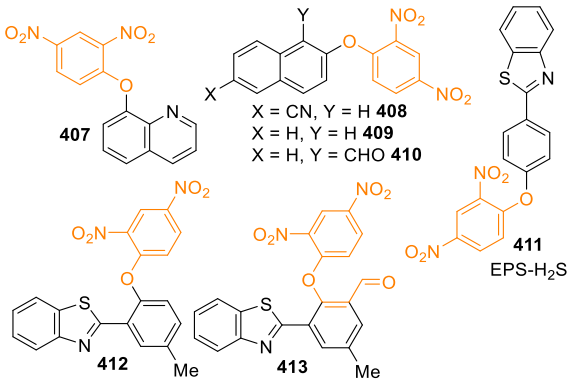


Figure 1.84. Additional examples of fluorescent H_2S probes based on DNP cleavage with small molecule chromophores.

In an important study on the selectivity of DNP-based probes, Feng investigated the role of an aldehyde group *ortho* to the DNP to improve both the selectivity and reaction rate of DNP-based probes in 2014.[438] When directly comparing **412** and aldehyde-containing **413**, they found that the parent probe **412** did not appreciably react with H_2S, but that aldehyde incorporation into **413** significantly increased the rate of reaction and improved the selectivity in 25% MeCN in buffer. This improved performance was attributed to initial attack of H_2S on the aldehyde and subsequent intramolecular attack on the DNP motif (Figure 1.85) and has been used by others as an approach to improve the selectivity and overall performance of DNP-based probes for H_2S as discussed elsewhere in this section.

Tang and Zhang reported a similar construct with an *o*-aldehyde for increased H_2S selectivity and a thioether for HClO detection in **414** (HSB-DNP) (Figure 1.86).[439] This probe provided a signal in the green, red, or yellow channel after reaction with HClO, H_2S, or H_2S followed by HClO, respectively. This response profile was further confirmed in HeLa cells treated with exogenous H_2S and HClO as well as in cell treated stimulated to produce H_2S with Cys, cells inhibited with PAG, and cells treated with HClO scavenger ebselen. Further extending this platform, Zeng reported **415** (HBTPP-S), which reacts with H_2S to generate a fluorescence response at 620 nm in 50% MeCN in buffer with moderate selectivity for H_2S over Cys and GSH.[440] This mechanism of this probe was later investigated in greater detail by Chu and co-workers and confirmed to occur through the accepted mechanism.[441] Zeng also reported the *para*-pyridinium isomer of this platform with **416** (HBTP-S), which also provided a turn-on response in 50% MeCN in buffer.[442] Using a similar construct, Ren and Chen later reported **417** (HBTP-H_2S),

which generated a fluorescence enhancement at 650 nm upon reaction with H_2S with good selectivity over competing analytes in 10% MeCN in buffer.[443] This probe was additional used to image exogenous and endogenous H_2S in HeLa cells, investigate H_2S levels upon Ca^{2+} addition, and image endogenous H_2S in rice roots under normal conditions and when exposed to Al^{3+} stress. Expanding to include a triphenylamine motif, Mahapatra reported **418** (TPB-NO_2), which generated a turn-on response at 483 nm in 50% DMSO in buffer with a minor response to Cys.[444] This probe was also used to image exogenous H_2S in MDA-MB 231 cells and to develop test strips for H_2S detection. Ali reported benzoxazole-based **419** (DPPB), which generated a fluorescent response at 400 nm in 60% DMSO in buffer, with good selectivity over competing anions and thiols and further demonstration of exogenous H_2S detection in HepG2 cells.[445]

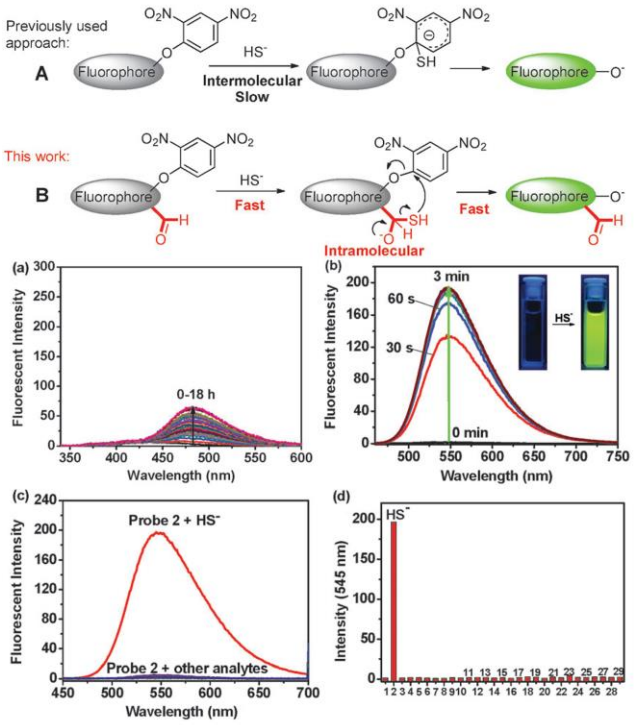


Figure 1.85. (top) Proposed mechanistic difference for the role of an *ortho* aldehyde in H_2S-mediated DNP cleavage. Bottom panels: (a) Reaction of **412** with 10 equiv. of H_2S. (b) Reaction of **413** with 10 equiv. of H_2S. (c,d) Selectivity of **413** for H_2S over competing analytes, including blank, HS^-, F^-, Cl^-, Br^-, I^-, SCN^-, CO_3^{2-}, AcO^-, NO_3^-, NO_2^-, PO_4^{3-}, HPO_4^{2-}, $H_2PO_4^-$, $S_2O_3^{2-}$, $S_2O_7^{2-}$, SO_4^{2-}, SO_3^{2-}, HSO_3^-, HSO_4^-, CN^-, GSH, Hcy, Cys, NAC, $C_6H_5NH_2$, $C_6H_5CH_2NH_2$, $H_2NCH_2CH_2NH_2$, and $HOCH_2CH_2NH_2$. Reproduced and modified with permission from ref [438]. Copyright 2014 Royal Society of Chemistry.

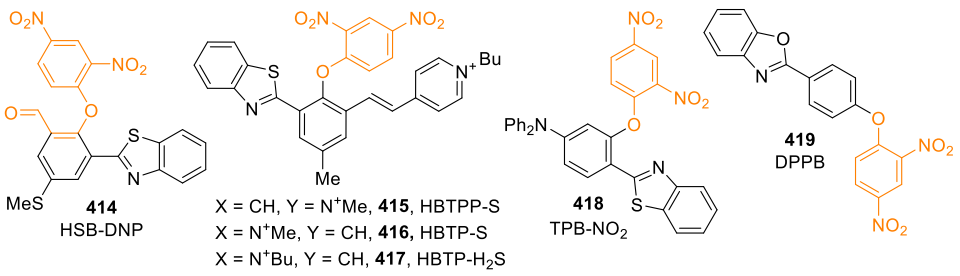


Figure 1.86. Examples of fluorescent H_2S probes based on DNP cleavage with benzothiazole and benzoxazole chromophores.

Using a related small molecule platform, Lin reported the two-photon platform **420** (GCTPOC-H_2S) with a two-photon excitation at 780 nm and resultant emission at 514 nm (Figure 1.87). This probe showed good selectivity over anions but significant activation by GSH in 20% EtOH in buffer, and was used to image exogenous H_2S in rat liver slices.[446] Expanding on related more conjugated systems, Yang developed naphthalene-based probe **421**, which was reported to respond to both H_2S and N_2H_4 based on cleavage of the DNP group and addition to the alkene, respectively.[447] Yang also reported a dual site reactive probe **422**, with a DNP group to react with H_2S and a cyanoalkene to react with both H_2S and SO_3^{2-}.[448] This probe provided different response for H_2S and SO_3^{2-}, with fluorescent signals at 480 and ~460 nm for the two analytes respectively, although primary differentiation of these analytes was accomplished by UV-vis spectroscopy. Yi and Yi reported the pyrene-based probe **423** (PCNP), which provides a turn-on response at 604 nm with a moderate response to glutathione and minor response to $S_2O_8^{2-}$ and $S_2O_4^{2-}$.[449] Yao reported **424** (YG-H_2S), which includes dichloro substitution on the phenol to shift the emission to 520 nm upon reaction with H_2S.[450] This probe showed good selectivity for H_2S over other competing analytes and was used to image both exogenous and endogenous H_2S in HeLa cells. In addition, this probe was used to image exogenous H_2S in mice, H_2S accumulation in different organs in 4T1-xenograft mice, and differential H_2S levels in normal, acute liver injury, and treatment groups. Including an electron withdrawn scaffold, Chen reported a cyanobiphenyl based probe **425** with a response at 508 nm and an aldehyde incorporation to improve selectivity.[451] This probe provided good selectivity for H_2S over competing analytes, and was used to image exogenous H_2S in MDA-MB-231 cells. Lin reported **426** (DFAN), which provided a signal at 510 nm and was use to image exogenous and Cys-derived H_2S in HepG2 cells as well as exogenous

H_2S in zebrafish.[452] The mechanism of this fluorescence response was also later investigated computationally by Wang and Gao.[453]

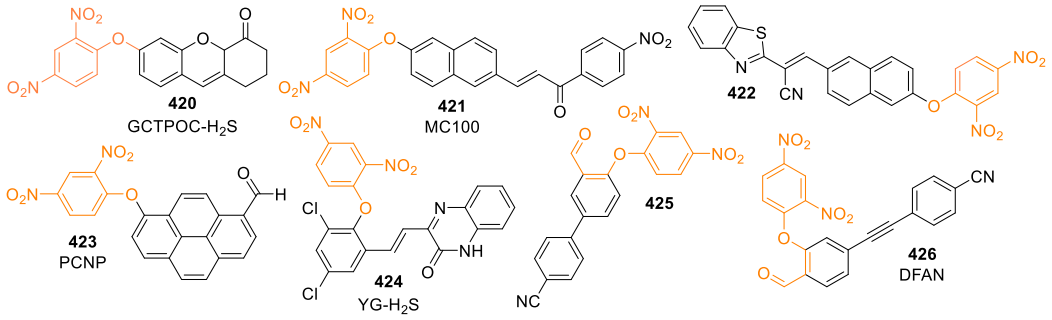


Figure 1.87. Additional examples of fluorescent H_2S probes based on DNP cleavage.

As further examples of DNP-based probes with amine-containing fluorophores, Sun, Li, and Tang reported the extended coumarin derivative **427**, which provides a red-shifted turn-on response to H_2S at 650 nm in 40% THF buffered solution and was subsequently used to image exogenous H_2S in MCF-7 cells (Figure 1.88).[454] A related conjugated dimethylamino styrene derivative **428** was also reported by Zhong and Zhu, which showed good selectivity for H_2S in 50% DMSO in buffer and was used to image exogenous H_2S in HeLa cells.[455] This probe was later further studied by computational investigations.[456] Hou reported **429** (NIPY-DNP), which provides a 273-fold turn-on at 505 nm upon treatment with H_2S, with minimal signal toward competing thiols at pH 7.0.[457] This probe was used to image exogenous H_2S in A549 cells. Guo and co-workers reported related probe **430** (PI-H_2S), which response to H_2S to provide a fluorescent signal at 465 nm with moderate selectivity for H_2S over Cys, and it was further used to image exogenous H_2S in HeLa cells.[458] Lin reported a related compound conjugated to a flavone to develop **431**.[459] The broad emission of this white-light emitting probe encompasses the blue, green, and red channels, which was used to image exogenous H_2S in MG63 cells. Long and Wang reported the related probe **432**, which was used to develop test strips for H_2S detection from different meat samples.[460] Expanding to other nitrogen heterocycles, Tang reported the oxadiazole-based **433** (OXDNP), which generates a fluorescence response at 418 and 556 in response to H_2S, with a small response to Cys/Hcy, but was not used for further applications.[461]

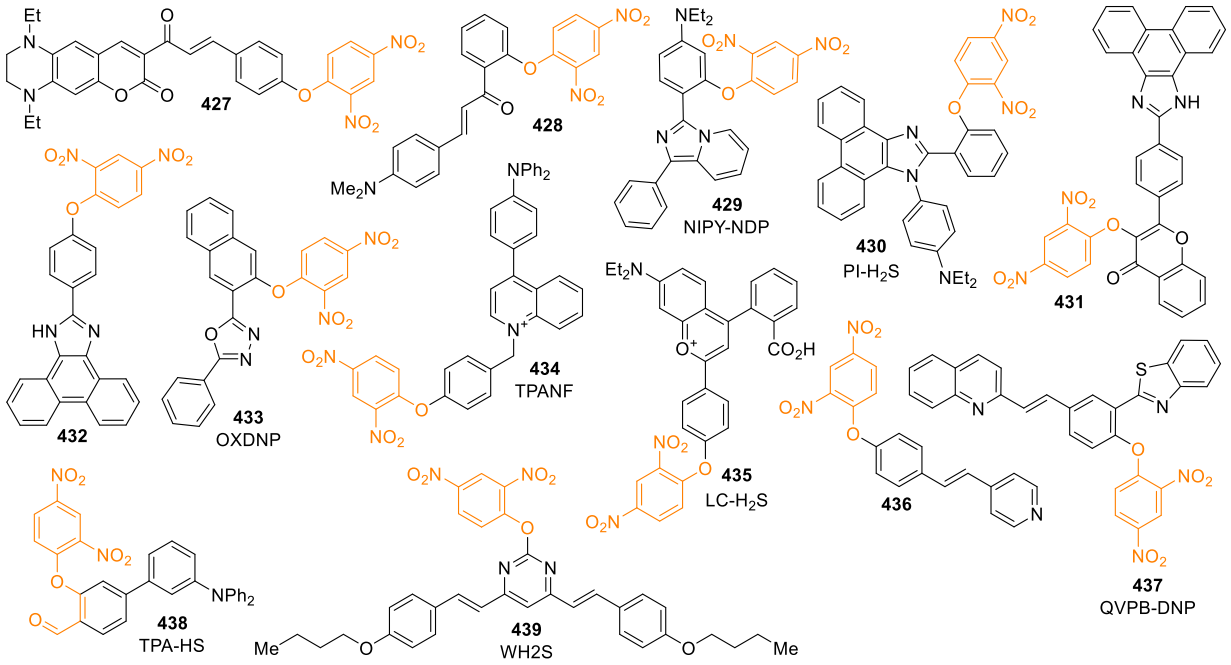
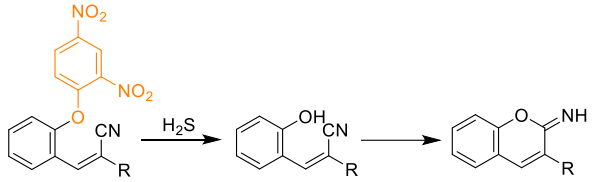


Figure 1.88. Additional examples of fluorescent H_2S probes based on DNP cleavage with amine-based chromophores.

Building on an extended triphenylamine motif, Zeng and Wu reported **434** (TPANF), in which with H_2S cleaves the DNP group to initiate a subsequent self-immolative cascade to release the fluorophore.[462] The response of this system is based on AIE and provides good selectivity for H_2S over other reactive species. This probe was further used to investigate H_2S release from different meats, exogenous and endogenous H_2S in L929, HeLa, and HCT-116 cells, as well as H_2S generation in mouse organs and tumor tissues. Jiang also reported **435** (LC-H_2S), which provides a fluorescence response at 644 nm, showed good selectivity for H_2S over other reactive species, and was used to image exogenous H_2S in HeLa cells.[463] This probe was further used to develop test strips for H_2S detection from foods. Incorporating a conjugated pyridine, Martínez-Máñez and Costero reported **436**, which showed good selectivity for H_2S over competing species and was used to image exogenous H_2S in HeLa cells.[391] Incorporating an extended quinoline, Liu reported **437** (QVPB-DNP), which provided a turn-on response at 605 nm in 70% DMSO in buffer with good selectivity over competing analytes.[464] Including a triphenylamine motif with an *o*-aldehyde to the DNP group, Tang and Yan reported **438** (TPA-HS), which provided a turn-on AIE response at 496 nm with good selectivity for H_2S over competing analytes.[465] This probe was further used to investigate H_2S in spiked water samples and to image exogenous H_2S in MCF-7

cells. Using a conjugated pyrimidine, Wu, Hu, and Lin reported **439** (WH2S), which was found to localize in the lysosome.[466] This probe provided a fluorescence enhancement at 506 nm and good selectivity for H_2S over competing analytes in 80% EtOH in buffer. In addition, this system was used to image Cys-derived H_2S in HeLa cells.

Approaches to couple H_2S-mediated DNP cleavage followed by cyclization have also been reported (Scheme 1.9). For example, Wang, Re, and Ye reported **440**, which responded to H_2S but also provided a significant signal to GSH (Figure 1.89).[467] This probe was used to image exogenous and Cys-derived H_2S in Ec1 cells and was found to localize to the ER. Similarly, Chen and Hu reported related probe **441** (DN-DM), which provided good selectivity against competing reactants, including GSH although only 20 equiv. of thiols were tested.[468] This probe provided a turn-on response at 618 nm and was used to image exogenous H_2S in HeLa cells. This approach was also used by Li and Tang who reported **442** (THQ-L), which provides a red-shifted emission at 652 nm upon reaction with H_2S.[469] This probe showed good selectivity for H_2S over competing species and was subsequently used to image exogenous H_2S in MCF-7 cells, measure spiked H_2S in various water and wine samples, and develop paper test strips for H_2S.



Scheme 1.9. H_2S-medated DNP cleavage followed by intramolecular cyclization.

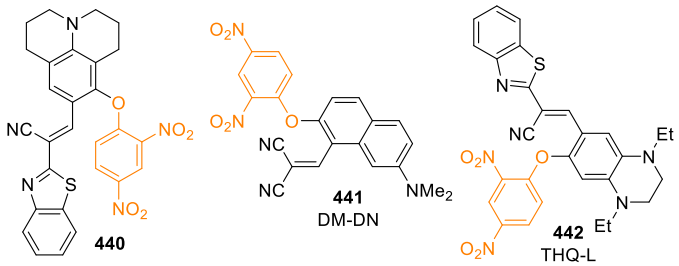


Figure 1.89. Examples of fluorescent H_2S probes based on DNP cleavage and subsequent intramolecular cyclization.

As additional examples of DNP-based probes that function through AIE mechanisms, Li and Tang reported **443** (TPE-NP), which is based on a tetraphenylethylene motif (Figure 1.90) and

showed good selectivity for H_2S over other analytes.[470] Although this probe showed a response for HS^- salts, it failed to produce a response for S^{2-} salts even though both species should provide the same H_2S related species in the 10% THF in buffer solution used in these experiments. The resultant probe was used to investigate H_2S in different water sources, as well as in HeLa cells and *C. elegans*. Viswanathamurthi also reported the hydrophobic platform **444** (DFI), which showed moderate selectivity over thiols and was used to image exogenous H_2S in HeLa cells.[471] Wang and Hu reported the tetrahydro[5]helicene derivative **445** (HD-DNP), which showed good selectivity for H_2S in 90% DMSO in buffer although the probe was not applied to imaging expeirments.[472]

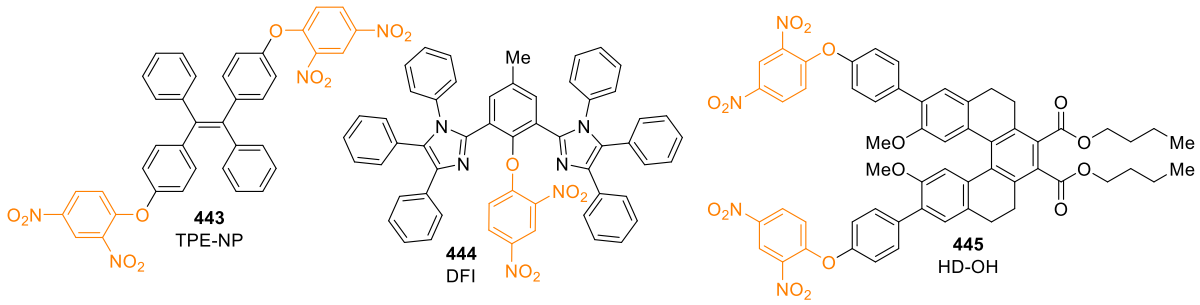


Figure 1.90. Examples of fluorescent H_2S probes based on DNP cleavage with AIE.

Incorporation of DNP motifs into other types of luminophores have also been reported. As brief examples, Yu and Yuan reported the Eu^{3+} and Tb^{3+} complexes **446** and **447** (HTTA-Eu^{3+}/Tb^{3+}) with pendant DNP motifs as lanthanide luminescence complexes (Figure 1.91).[473] These complexes showed characteristic time-gated emission spectra in the 475-600 nm range, with moderate selectivity for H_2S over GSH. This complex was used for time-gated luminescence imaging of exogenous H_2S in HepG2 cells. Expanding the chemiluminescent platforms, Sozmen reported **448**, which is based on a 1,2-dioxetane motif. This probe provided a chemiluminescent response at 468 nm to H_2S in 90% DMSO in buffer, with maximum luminosity at pH 12.4, although significant differences between H_2S and background chemiluminescence were not observed.[474] Pluth later reported a related 1,2-dioxetane with brighter chemiluminescence probe **449** (CL-DNP), which provided a 100-fold chemiluminescence turn on at 525 nm in 5% DMSO in buffer.[267] Neither of these platforms were applied to biological samples.

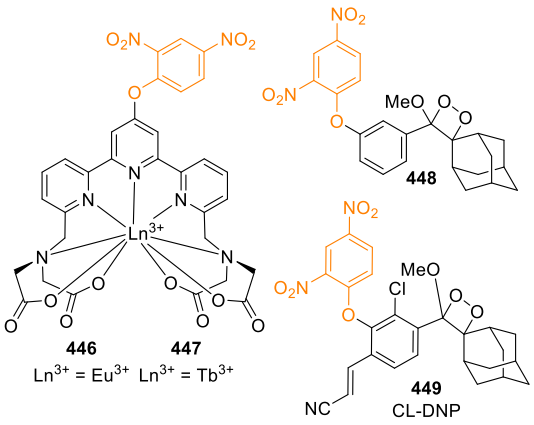


Figure 1.91. Examples of luminescent H_2S probes based on DNP cleavage.

An additional approach for H_2S detection that relies on cleavage of electron-poor protecting groups has been the cleavage of DNP thioethers adjacent to esters. Detailed investigations into this mechanism of this reaction have not been performed, but different reports have proposed direct H_2S-medated cleavage of the ester motif, followed by further fragmentation of the DNP thioester after subsequent reaction with H_2S. It is also possible that the thiol intermediate in the Meisenheimer complex formed by H_2S attack on the DNP motif could participate in subsequent attack on the ester (in similar fashion to the assistance of *ortho* aldehydes in DNP cleavage). Because of the mechanistic ambiguity of this reaction, we have chosen to include these examples here due to the presence of the DNP motifs, although it is possible that other H_2S-mediated chemistry may be operable.

As an example of this approach, Zhang and Yuan reported the Ru^{2+} luminescent complex **450** (Ru-MDB) with DNP-thioether linkage to provide a time-gated luminescence response at 612 nm (Figure 1.92).[475] This probe was used to measure H_2S in plasma and *ex vivo* organs of adult zebrafish, image exogenous H_2S in live zebrafish, and to image LPS- and Cys-derived H_2S in J774A.1 cells. This cleavage approach was also used by Li, Tang, and Zhang to develop the phosphorescent cyclometalated Ir^{3+} complex **451**, which generated a luminescent response to H_2S with good selectivity over competing analytes.[476] This probe was further used to image exogenous and LPS-derived H_2S in HeLa cells and mice. Moving away from metal-containing systems, Yin reported **452**, which generated a fluorescent response at 538 nm with good selectivity for H_2S over competing anions and thiols.[477] This probe was additionally used to image exogenous and endogenous H_2S in HepG2 cells as well as differences in H_2S levels in upon treatment with Ca^{2+},

AOAA, and PAG. Yin also reported a coumarin-based version of this approach in **453** (CDP), which was used to image exogenous and SNP-derived H_2S in HepG2 cells.[478] Lu expanded on this cleavage approach to develop **454** (DNPT-HS), which reacts with H_2S to release a bioluminescent aminoluciferin derivative.[479] This probe showed good selectivity for H_2S over competing analytes and was used to measure H_2S generation in luciferase-transfected Huh7 cells as well as differences in H_2S levels in cells treated with AOAA and PAG. Further use of this probe demonstrated the time-dependent bioluminescence H_2S generation in luciferase-transfected Huh7 xenografts in mice. Li and Zhou also used this approach to develop naphthalimide-based **455**, which showed good selectivity for H_2S over other analytes, including Cys, Hcy, and GSH.[480] This probe was shown to localize to the lysosme and was additionally used to image exogenous and endogenous H_2S in A549 cells.

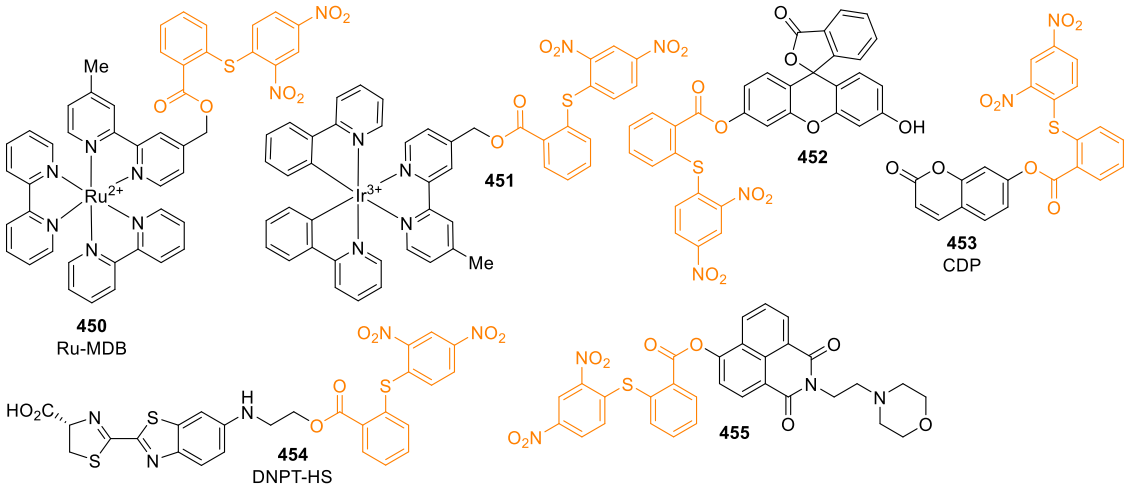
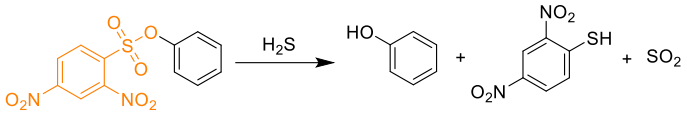


Figure 1.92. Examples of fluorescent H_2S probes based on cleavage of DNP thioethers adjacent to esters.

1.4.2 2,4-Dinitrobenzenesulfonate (DNBS) Cleavage

In addition to H_2S-mediated cleavage of DNP ethers, a variety of DNP sulfonyl esters, often referred to as 2,4-dinitrobenzenesulfonate (DNBS), have also been reported as an approach for H_2S detection. The fundamental chemistry of this approach is the same and proceeds through S_NAr addition of HS^- to the DNBS group to generate DNP-SH and SO_2 as byproducts (Scheme 1.10). This chemistry generally broadens the platform of scaffolds available for H_2S detection, but

also releases SO_2, which equilibrates in water to form H_2SO_3 / HSO_3^- / SO_3^{2-} depending on the pH of the solution.



Scheme 1.10. Removal of DNBS protecting groups with H_2S.

In an early report of this approach, Jiang and co-workers reported the BODIPY analogue **456**, which responded with a turn-on response at 633 nm to both H_2S and F^- in 20% acetone in buffer (Figure 1.93).[481] The resultant probe was used to image exogenous H_2S in HeLa cells. Quan, Ye, and Huang also reported a BODIPY analogue in **457** (DBT), which provided a fluorescence turn-on response at 716 nm in 80% THF in buffer, exhibited moderate selectivity over Cys, Hcy, and GSH, and was used to image H_2S in HCT116 cells.[482] Using a BF_2-derived chromophore, Zhang reported **458** (BF_2-DBS), which provided a fluorescence enhancement at 500 nm with good selectivity.[483] This probe was further used to image exogenous H_2S and PAG-inhibited H_2S synthesis in HeLa cells.

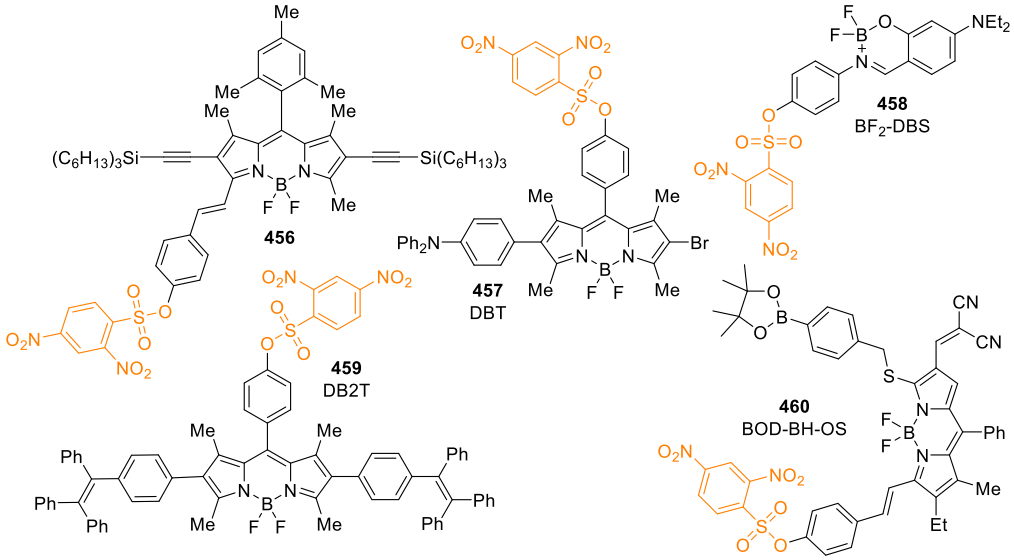


Figure 1.93. Examples of fluorescent H_2S probes based on DNBS cleavage with BODIPY chromophores.

Luo, Huang, and Ye expanded this approach with the related scaffold **459** (DB2T), which contains a tetraphenylethylene modified BODIPY and showed moderate selectivity against thiols.[484] This probe was used to image H_2S in HCT116 cells and also probe accumulation in mice bearing HCT116 implanted tumors. Also using a BODIPY platform, Zhao reported **460** (BOD-BH-OS), which provides responses to both H_2O_2 and H_2S through cleavage of the boronate and DNBS group, respectively.[485] Upon formation of the BODIPY thiol from H_2O_2 activation, the resultant sulfhydryl group can be oxidized by H_2O_2 to generate a SOH group, which can subsequently be reduced by H_2S to the parent thiol. This chemically reversible approach was demonstrated both in solution and in HeLa cells treated with exogenous H_2S and H_2O_2 as well as by treatment with PMA and AOAA.

A variety of blue chromophores using DNBS motifs for H_2S detection have also been reported. For example, Yang reported cyanonaphthalene **461**, which provided moderate selectivity for H_2S over GSH at 440 nm although only tested at 10 equiv., and was used to investigate H_2S in wine and beer samples (Figure 1.94).[486] A naphthaldehyde derivative was also reported in **462** by Yang that resulted in DNBS cleavage and also H_2S addition to the aldehyde to provide a turn-on response at 487 nm.[487] Although the initial testing was performed in DMSO, the probe was also used to investigate H_2S in different water sources. Hou reported the coumarin-carbazole adduct **463** (COZ-DNBS), which provides a turn-on response at 558 nm with moderate selectivity for H_2S over thiols after 1 minute incubation and was used to image exogenous H_2S in MCF-7 cells and zebrafish.[488]

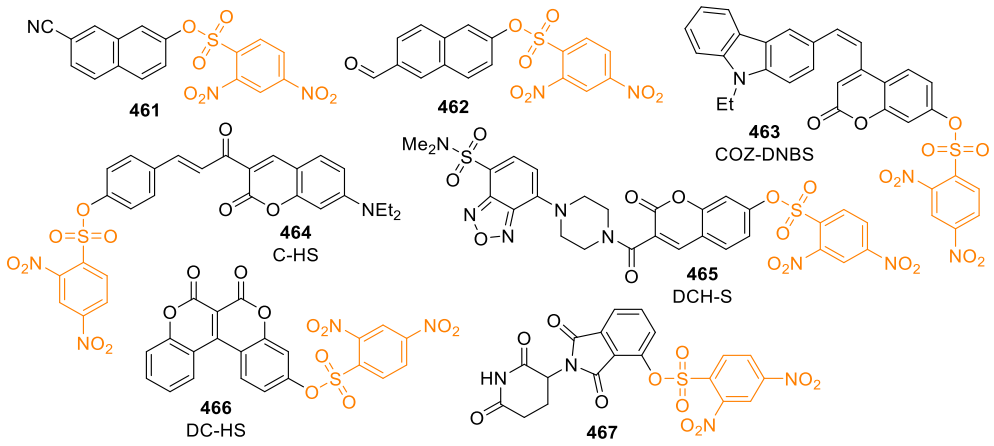


Figure 1.94. Examples of fluorescent H_2S probes based on DNBS cleavage with coumarin and related chromophores.

Lin reported the coumarin-chalcone platform **464** (C-HS), which generates a fluorescent response at 575 nm, with moderate to good selectivity over 50 μM Hcy, Cys, and GSH.[489] This probe was additionally used to image exogenous H_2S in HeLa cells as well as changes in H_2S response upon H_2S scavenging with $ZnCl_2$. Jiao reported the coumarin-SDB adduct **465** (DCH-S), which provides a turn-on response at 456 and 600 nm and shows moderate selectivity for H_2S over thiols. The probe was used to image exogenous and Cys-derived H_2S in MCF-7 cells.[490] Expanding to dicoumarin systems, Zhao prepared **466** (DC-HS), which provided a fluorescence response at 582 nm, provided moderate selectivity for H_2S over thiols and other nucleophilic anions in 25% EtOH in buffer, and was used to investigate H_2S in zebrafish.[491] Sun reported the hydroxy-thalidomide-based **467**, which provides a fluorescent response at 495 nm to H_2S in 20% MeCN in buffer, showed good selectivity for H_2S over competing thiols, and was used to image exogenous H_2S in HeLa cells.[492]

Naphthalimide-based DNBS-based probes have also been reported. For example, Qu and Zhou reported the AIE-based systems **468** and **469** (TPANI-DNs and PCZNI-DNs) and subsequent test strip formulations, which provided turn-on fluorescent responses at 575 and 530 nm, respectively, although both probes showed relatively poor selectivity against 10 equiv. of GSH and Cys in 30% DMSO in buffer (Figure 1.95).[493] Hu, Fu, and Zhu reported the naphthalimide conjugate **470** (DF), which provided a fluorescent turn on at 650 nm and good selectivity for H_2S over competing analytes. This probe was used to image exogenous H_2S in HeLa cells.[494] Sun and Zhang reported naphthalimide conjugate **471** (SDB), which was to prepare test strips for H_2S gas detection, although the selectivity of this platform was not investigated.[495] Using the parent naphthalimide, Wang reported **472** (NT-SH), which showed a response to H_2S but also ~50% activation by Cys and was further demonstrated to respond to H_2S in A549 cells and zebrafish.[496] Lin reported a benzothiazole modified naphthalimide in **473** (NP-S), which provided a turn-on response at 551 nm, but also showed full activation by GSH and Cys, with partial activation by Hcy.[497]

Mahapatra reported functionalized benzothiazole **474** (BNPT), which provided a turn-on response at 503 nm in 60% MeCN in buffer (Figure 1.96).[498] The fluorescence of the resultant product could be quenched by Zn^{2+} and regenerated by subsequent H_2S addition and ZnS precipitation. The turn-on response to H_2S was also demonstrated in HADF cells treated with exogenous H_2S. Lee and Han reported **475** (KF-DNBS) based on H_2S-medaited cleavage of the

DNBS group to release the KF fluorophore that is only weakly fluorescent unless complexed to human serum albumin (HSA).[499] This probe showed poor selectivity for H_2S over Cys or Hcy unless the samples were also treated with 2-formyl benzene boronic acid (2-FBBA) to scavenge the Cys and Hcy present in solution. Also using a benzothiazole motif, Li reported **476**, which provided a turn-on response at 479 nm and was further used to develop H_2S responsive test strips.[500] Further expanding on the benzothiazole platform, Wang and Wang reported **477** (NPS), which provides a fluorescent response at 520 nm with moderate responses from Cys and GSH.[501] This probe was additionally used to image exogenous H_2S in HeLa cells and zebrafish.

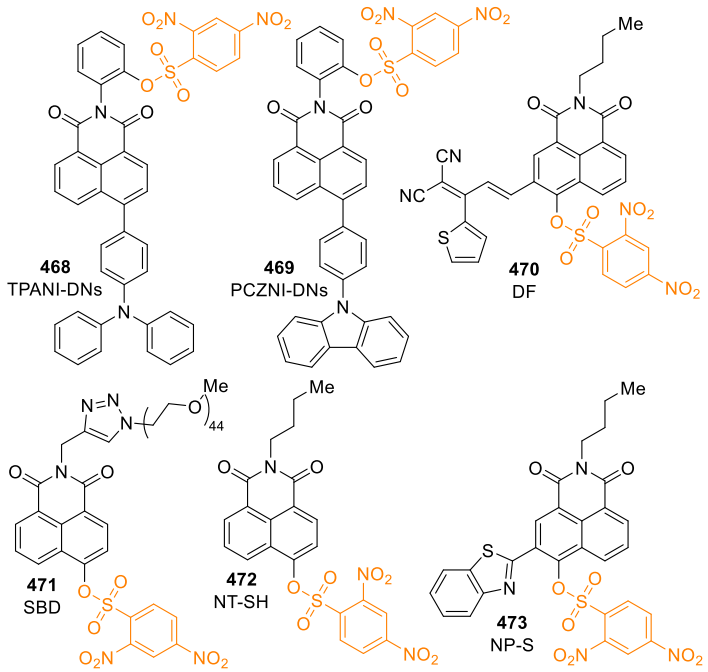


Figure 1.95. Examples of fluorescent H_2S probes based on DNBS cleavage with naphthalimide chromophores.

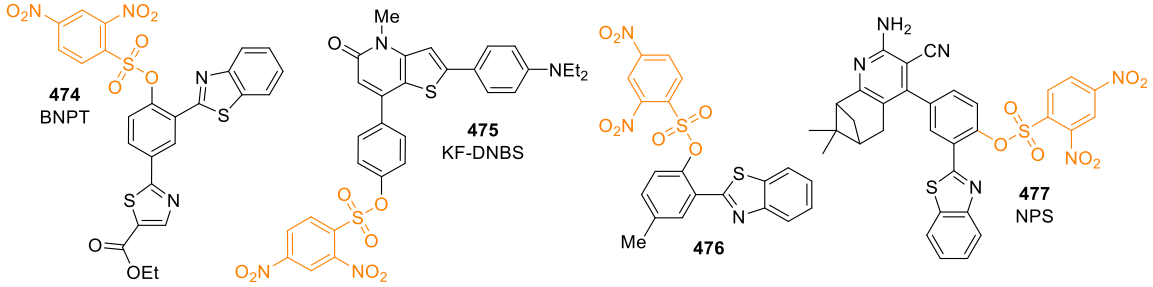


Figure 1.96. Additional examples of fluorescent H_2S probes based on DNBS cleavage with benzothiazole and related chromophores.

The DNBS approach has also been used with porphyrin and corrole derivates (Figure 1.97). For example, Zeng reported functionalized porphyrin **478** which generates a fluorescent response at 653 nm when treated with H_2S and good selectivity over competing analytes in 50% THF in buffer.[502] This turn-on response was also demonstrated in HeLa cells treated with exogenous H_2S. Chen and Zeng also used this approach with an *ortho* functionalized porphyrin to generate **479** with similar optical and responsive properties and increased selectivity attributed to an enhanced steric effect.[503] Expanding to a tetrasubstituted system, Jiang, Li, and Chen reported **480** (TDBP), which responded to both H_2S and GSH to generate a fluorescent response that was confirmed in HepG2 cells.[504] Expanding to corrole-based systems, Lu and co-workers reported the *p*-chlorophenyl **481** (COR-DNBS), phenyl **482** (DPC-DNBS), and naphthyl **483** (NPC-H_2S) derivatives in separate publications.[505-507] These probes provide a turn-on response ~650 nm and were found to be compatible with imaging exogenous H_2S in HeLa cells. DPC-DNBS was also shown to react with both H_2S and N_2H_4.

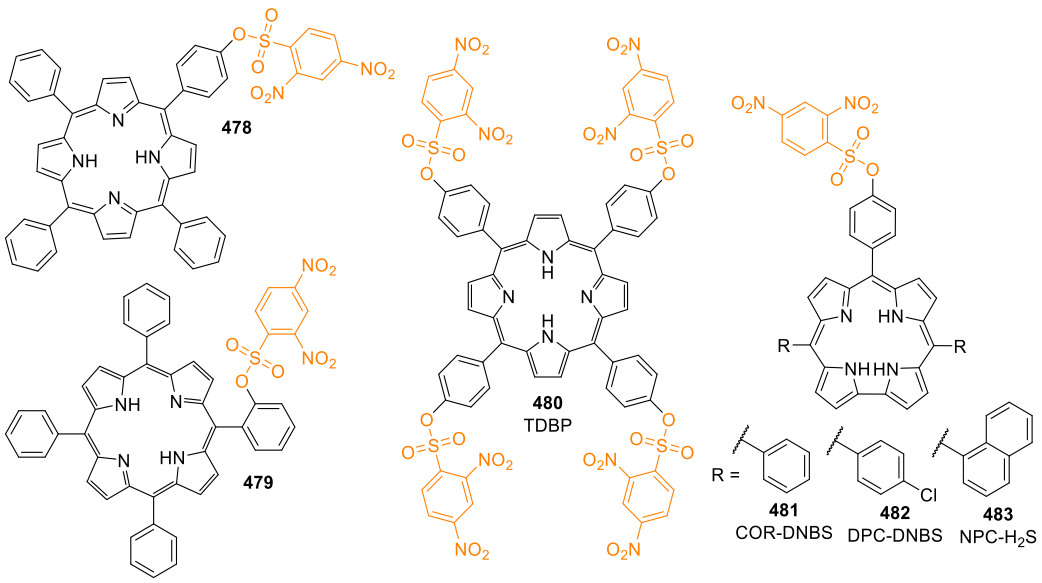


Figure 1.97. Examples of fluorescent H_2S probes based on DNBS cleavage with porphyrin and related chromophores.

Other fluorophores containing the DNBS motif have also been reported. Sureshkumar reported the napthofluorescein derivative **484**, which provided a fluorescence turn-on at 670 nm in 10% MeOH in buffer, and the resultant probe was used to investigate H_2S in different water sources (Figure 1.98).[508] Investigating the role of *ortho* aldehyde groups in DNBS selectivity for

H_2S, Chen reported compounds **485-487**, which contain 0, 1, and 2 aldehyde groups on the fluorescein scaffold, respectively.[509] The parent compound was found to have poor selectivity for H_2S over Cys, GSH, or Hcy, with the selectivity being significantly improved by inclusion of an aldehyde adjacent to each DNBS group in **487**. The resultant optimized probe was also used to image exogenous H_2S in HeLa cells. Also building from a fluorescein backbone, Zeng and Wu reported the poly(ethylene glycol) functionalized **488**, which provided a fluorescence turn on at 518 nm and was used to image exogenous H_2S in HeLa and L929 cells.[510] Thongyoo reported **489**, which contains a dabsyl-fluorescein motif.[511] This probe provided a response at 520 nm in 30% MeOH in buffer and good selectivity for H_2S over other competing species, although a moderate response was also observed for CO_3^{2-}. Further use of this probe included imaging exogenous H_2S in HeLa cells. Zhang, Gao, and Chen reported the AIE probe **490** (DNBS-DCM-SP), which reacts with H_2S to generate a fluorescence response at 592 nm.[512] This probe can also be photoswitched between AIE fluorescence and the ring-opened spiropyran using UV-vis irradiation and was used to image exogenous and Cys-derived H_2S in HeLa cells.

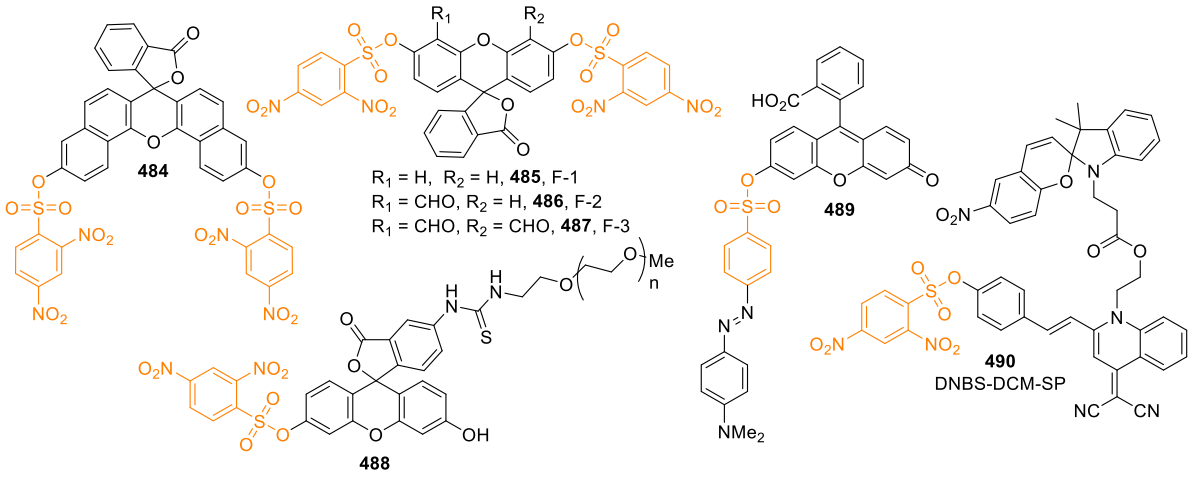


Figure 1.98. Examples of fluorescent H_2S probes based on DNBS cleavage with xanthene based chromophores.

Moving to longer emission wavelengths, Feng reported NIR probe **491** (DCIP-NIR-HS), which generates a fluorescent response at 666 nm, showed good selectivity for H_2S in 20% DMSO, and was used to image exogenous and Cys-derived H_2S in HeLa cells (Figure 1.99).[513] The NIR probe **492** (DDM-H_2S) was reported by Zhang and Wang, which provided a turn-on response at

770 nm, but was only tested against 5 equiv. of competing analytes.[514] The probe was used to develop H_2S test strips for gaseous H_2S and also used to image exogenous H_2S in HeLa cells and zebrafish. Xu and co-workers reported **493** (HCB-BT), which provided a turn-on fluorescent response at 745 nm in 67% DMSO in buffer.[515] This probe was used to image H_2S in SHSY5Y cells and also in mice. Hou and Yin reported a related probe in **494** (SP1), which generated a turn-on response at 644 nm with good selectivity over competing anions but showing a significant response to GSH. This probe was also used to image exogenous H_2S in MCF-7 cells and zebrafish.[516] Using a different isomer, Cuiling and Chunpo reported **495** (XXMU-H_2S), which showed a turn-on response at 686 nm with good selectivity over most amino acids and anions, although a moderate response to Cys, Hcy, and GSH was also observed.[517] The resultant probe was also demonstrated to detect exogenous H_2S in HepG2 cells and zebrafish.

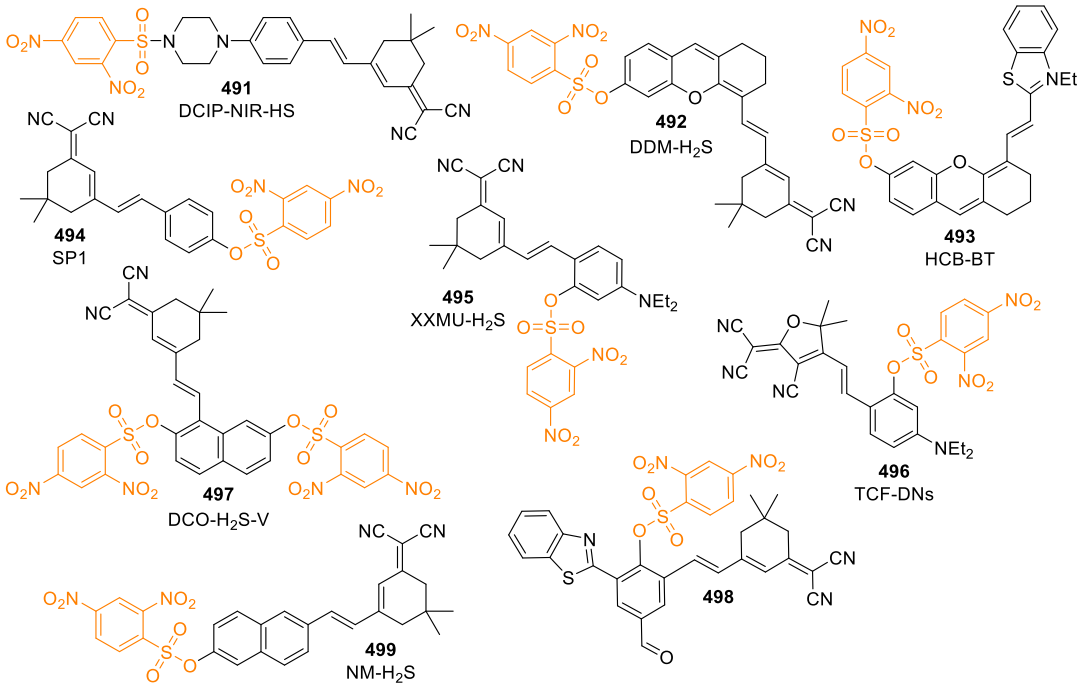


Figure 1.99. Examples of fluorescent H_2S probes based on DNBS cleavage with extended wavelength chromophores.

Using a similar construct, Li and Tang reported **496** (TCF-DNs), which generated a fluorescent turn-on response at 643 nm in 20% EtOH in buffer.[518] This response was attenuated by SO_3^{2-}, which was attributed to direct addition to the conjugated chromophore. The resultant system was used to develop H_2S-responsive test strips and also image exogenous H_2S in MCF-7

cells. Kong, Xu, and Tang reported the construct **497** (DCO-H_2S-V) with two DNBS motifs that provided a turn-on response at 630 nm in 10% glycerol in buffer with a maximal signal being observed at higher viscosities.[519] This probe showed good selectivity for H_2S over other analytes and was used to image H_2S and viscosity changes in in HeLa and PC12 cells. Also using a benzothiazole motif, Xu reported **498**, which responded to H_2S at 720 nm, with moderate activation by Cys, Hcy, and GSH.[520] This probe was further used to image exogenous H_2S in HeLa cells and to investigate both PAG-inhibited and exogenous H_2S in mice. He and Wang also reported extended system **499** (NM-H_2S), which generates a fluorescent response at 625 nm in 25% DMSO in buffer.[521] This probe showed good selectivity over competing analytes and was further used to image exogenous H_2S in HeLa cells and zebrafish.

Other chromophores have also been used with DNBS-based H_2S recognition motifs. For example, Yan and Wang reported the triazine based **500** (TzAr-H_2S), which provides a fluorescence response at 450 nm in 50% EtOH in buffer and was used to image Cys-derived H_2S in HeLa cells (Figure 1.100).[522] Song and Zhang reported imine-based **501** (BPI-DNBS), which provides a turn on response at 585 nm in 20% DMSO in buffer and good selectivity over competing thiols.[523] Building from symmetric substitution, Zhang reported **502** (LODNBS), which provided a fluorescence enhancement with H_2S at 596 nm in 20% DMSO in buffer, and showed good selectivity over competing analytes although only 10 equiv. of analytes were tested.[524] This system was further used to investigate H_2S in wine samples and to image exogenous H_2S in A594 cells. Fan and Pu reported **503** (TTPD), which generates a fluorescent response at 652 nm, with good selectivity over competing analytes.[525] This probe was used to investigate H_2S levels in different water samples, develop test strips for H_2S gas, and image exogenous and Cys-derived H_2S in HeLa cells.

Viswanathamurthi reported hydrophobic **504** (CNS), which provided a turn-on response at 560 nm in 10% DMSO in buffer, good selectivity over other anions and GSH, and was further used to image exogenous H_2S in HeLa cells.[526] Hong expanded this approach to cyclometalated Ir^{3+} complex **505**, which provided an electrochemiluminescent response to H_2S with moderate selectivity over thiols.[527] Both thiols and H_2S were found to cleave the DNBS group, but further addition of H_2S to the α,β-unsaturated ketone enhanced the response. Hu reported the tetrahydro[5]helicene derivative **506** (H-DNP), which was reported to have a faster reaction rate and the better detection limit than the DNP analogue with similar photophysical properties.[528] This

probe showed some activation by Cys and Hcy in 50% DMSO in buffer, and was additionally used to image exogenous H_2S in HeLa cells.

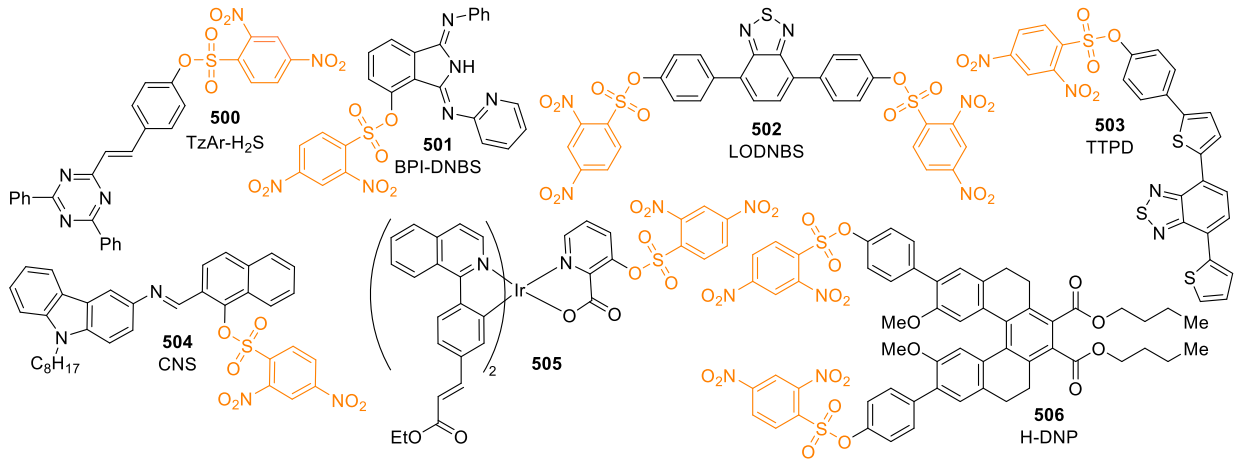


Figure 1.100. Additional examples of fluorescent H_2S probes based on DNBS cleavage.

Using a triphenylamine platform, Hu reported **507** (BOTD), which provided a turn-on response at 550 nm to H_2S with good selectivity over other anions and thiols (Figure 1.101). This probe was further used to image exogenous and SNP-derived H_2S in HeLa cells.[529] Incorporating a benzothiazole into a triphenylamine platform, Shi reported **508** (T-DNBS), which generated a fluorescent response at 686 nm in 20% DMSO in buffer and good selectivity over competing analytes.[530] This probe was also used to image exogenous H_2S in zebrafish. Li and Tang reported **509** (TPA-M), which includes an *ortho* aldehyde to improve selectivity.[531] This probe generated an AIE response to H_2S with good selectivity for H_2S over competing analytes and was further used to image exogenous H_2S in MCF-7 cells. Using a cationic triphenylamine motif, Fan and Pu reported **510** (DDMI), which responded at 623 nm in 50% DMSO/H_2O with good selectivity for H_2S over competing analytes.[532] The resultant probe was also used to image exogenous H_2S in HeLa cells.

Organelle-targeted version of DNBS probes have also been reported. For example, Zeng and Zhang prepared a BODIPY conjugated indole with a morpholine group for lysosomal targeting in **511** (DNBY) (Figure 1.102).[533] This probe provided a turn-on response at 635 nm in 30% EtOH in buffer, showed moderate selectivity over Cys, and was used to image exogenous H_2S in HeLa cells. Wu and Xu also reported a lysosomal targeted probe in **512** that provided a turn-on response at 580 nm, although the selectivity was only investigated with 3 equiv. of competing species.[534]

The resultant probe was used to image exogenous and Cys-derived H_2S in MCF-7 cells and exogenous and SNP-derived H_2S in zebrafish. Tang and Yan reported mitochondrial-targeted **513** (SPy-DNs), which provided a fluorescent response at 608 nm in 50% DMF in buffer, although the selectivity was only measured with 5 equivalents of competing species.[535] This probe was used to image exogenous H_2S in MCF-7 cells. Lin reported a lysosome targeted coumarin in **514**, which generated a fluorescent response at 460 nm with moderate selectivity for H_2S over GSH.[536] This system was also used to image differences in exogenous and NEM-scavenged H_2S in HeLa cells. Moving to the ER, Zhang, Wang, and Jiang reported **515** (FER-H_2S), which provided a response at 556 nm in 10% EtOH in buffer.[537] This probe provided relatively good selectivity for H_2S, with only a minimal response observed with 10 mM GSH and was used to image exogenous H_2S in HepG2 cells.

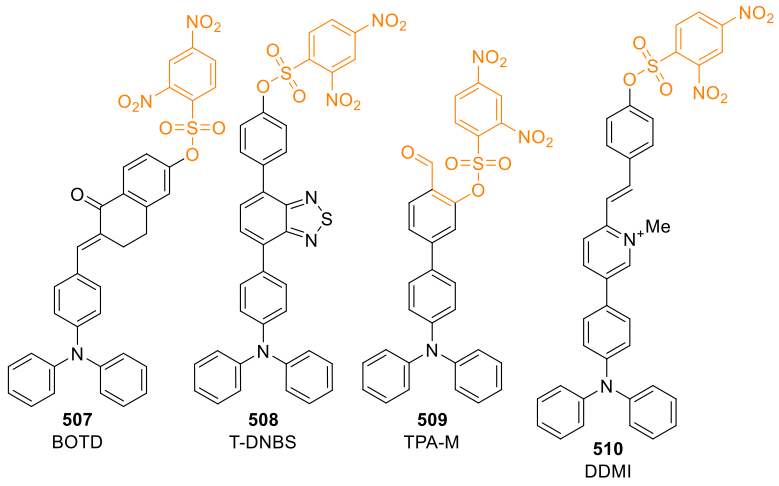


Figure 1.101. Examples of fluorescent H_2S probes based on DNBS cleavage with triphenylamine chromophores.

In addition to DNP and DNBS groups, a smaller number of reports have included 2,4-dinitrophenyl sulfonamides as H_2S-reactive groups (Figure 1.103). For example, Feng reported an iminosulfonyl cleavage in **516** (NIR-IC-H_2S), which reacts with H_2S at 652 nm and provided good selectivity over competing analytes in 50% DMF in buffer, although the selectivity was measured after only 5 minutes of incubation.[538] This probe was subsequently used to image exogenous and Cys-derived H_2S in Raw 264.7 cells as well as exogenous H_2S in mice. Wei and Zhang reported a 2,4-dinitrophenyl sulfonamide coupled to chromone to report **517** (BSNC), which provides a

fluorescent turn-on at 515 nm when investigated in pH 4 buffer.[539] This probe also provided a small response from Cys under these conditions and was used to image exogenous H_2S in HeLa cells. Wang and Hu also reported an coumarin-pyrazole derivative in **518** (CP2) results in cleavage of a DNP-sulfonamide.[540] This probe provides turn-on response at 500 nm in 10% DMSO with moderate selectivity for H_2S over Cys and was used to measure H_2S in different water samples as well as image exogenous H_2S in MCF-7 cells.

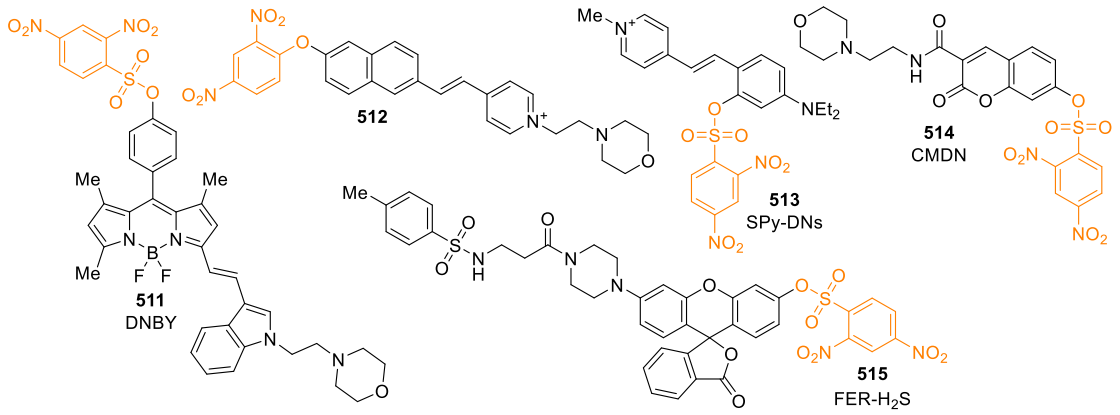


Figure 1.102. Examples of fluorescent H_2S probes based on DNBS cleavage with organelle targeting groups.

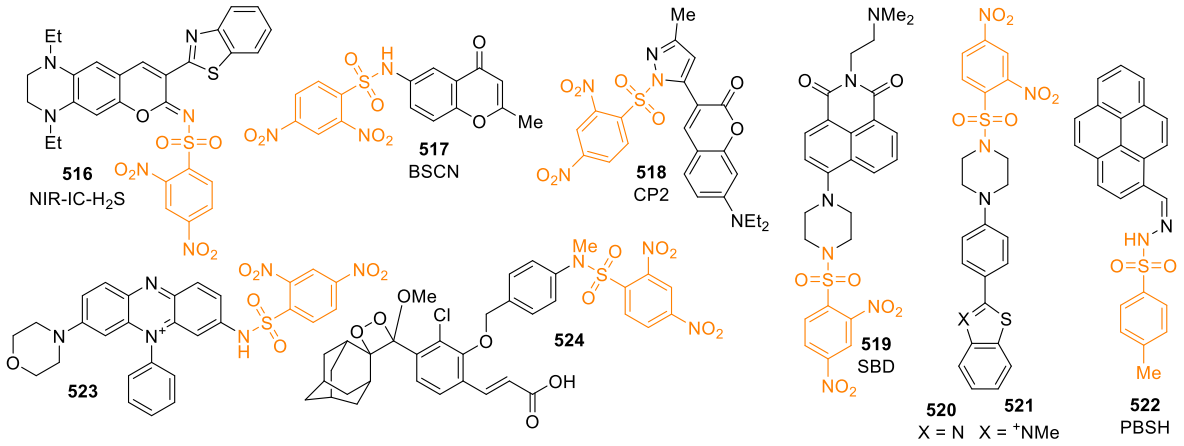


Figure 1.103. Examples of fluorescent H_2S probes based on 2,4-dinitrophenyl sulfonamides cleavage.

Expanding to a pyrazolesulfonamide motif, Zhang and Wu reported **519** (SDB), which contains a naphthalimide fluorophore.[541] This probe provided a turn-on response at 530 nm in 20% DMSO, also a moderate response to SO_3^{2-}, and was used to image exogenous H_2S in CaKi-1 cells.

Further applying this cleavage group, Zhao and Lin reported benzothiazole and benzothiazolium probes **520** and **521**, respectively.[542] When comparing the selectivity of these two probes in 30% dioxane in buffer, they found that **520** had significantly better selectivity than **521**, with the latter also providing significant response to arylthiols, and that **520** also reacted more quickly with H_2S than did **521**. Probe **521** was used to image exogenous and endogenous H_2S in HeLa cells. Wu and Velmathi reported pyrene-based **522** (PBSH), which provided a turn-off response to H_2S that was also confirmed in HeLa cells and zebrafish.[543] Lin, Xia, and Wang reported **523**, which responded to H_2S with an enhancement at 623 nm in 20% DMSO in buffer with good selectivity over competing anion and thiol analytes.[544] Expanding to a chemiluminescent platform, Spitz and Shabat reported **524**, which was used to detect H_2S release from the biodegradation of cefalexin by β-lactamase with a moderate signal-to-noise ratio over control compounds.[321]

1.4.3 Nitrobenzofurazan (NBD) Cleavage

Nitrobenzofurazans are pro-fluorogenic motifs that have been used extensively in biochemical studies to label primary and secondary amines.[545-547] The common "NBD" acronym for this functional group stems from the 7-nitro-1,2,3-benzoxadiazole core, which is often functionalized with a leaving group, such as F or Cl, to provide electrophilic labeling reagents. NBD electrophiles also react with nucleophilic thiols, although the resultant thioether is typically non-fluorescent, although in the case of Cys or Hcy can undergo a Smiles rearrangement in which the primary amine undergoes an intramolecular attack to displace the thiol and generate the more thermodynamically stable, and also fluorescent, NDB-amine product. In addition to producing H_2S responsive fluorescent probes in system with fluorogenic leaving groups, such platforms have also been used to differentiate Cys/Hcy from H_2S and GSH due to the presence or absence of a fluorescent NBD-containing product, respectively (*vide infra*).

In 2013, Pluth reported the use of NBD-Cl as a colorimetric approach for H_2S detection based on the formation of the highly colored NBD-SH product upon reaction with excess H_2S.[548] Simple NBD-ethers or thioethers could be cleaved by H_2S to generate the same NBD-SH product. The NBD-SH product is highly colored with an emission maximum at ~535 nm in aqueous buffer due to the high acidity of the SH motif (pK_a ~2.6), which has in many cases been used to differentiate the reaction products between H_2S and thiols. The general approach of using NBD-based electrophiles has been expanded significantly to develop activity-based probes for H_2S based

on the displacement of a pendant fluorophore from the NBD scaffold (Figure 1.104). As described in this section, this general approach has evolved significantly from the parent NBD-Cl system to include NBD ethers and improved H_2S selectivity by the use of NBD-piperazine adducts. Our discussion of probes using these approaches will be primarily grouped by chromophore functional group rather than by chronology to provide a better overview of the general types of tools that have become available using this approach.

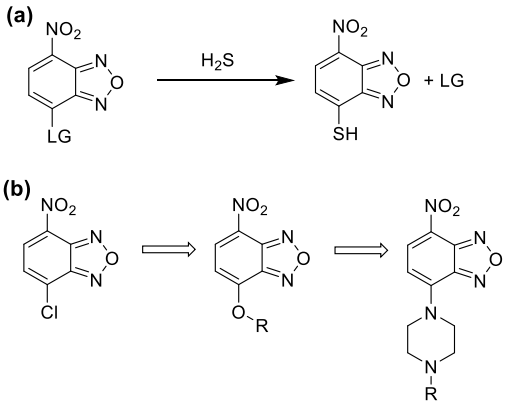


Figure 1.104. (a) General reactivity of NBD electrophiles with H_2S to generate NBD-SH. (b) Evolution from initial reported reactivity to fluorogenic ether-based probes to fluorogenic piperazine based systems with improved selectivity.

Building from NBD adducts with oxygen-based fluorogenic leaving groups, Chang reported **525** based on hydroxycoumarin in 2014 (Figure 1.105).[549] This probe reacted with H_2S to release the fluorescent coumarin product at 454 nm, but also showed reactivity with thiols to form different products. Also in 2014, Pluth reported **526** (NBD-Coum), which was used to measure H_2S and Cys/Hcy ratios based on differences in the products released after reaction of the probe with H_2S, Cys/Hcy, and GSH.[550] Yin reported aldehyde variant **527** (FCH-O-NBD), which also provided different response to H_2S, Cys/Hcy, and GSH, which was also demonstrated in HepG2 cells.[551] Yinhui and Yang further expanded the coumarin platform with benzothiazole functionalized coumarin **528** (TPP-H_2S), which reacted with H_2S to provide a signal at 500 nm and was also compatible with two-photon excitation at 800 nm.[552] This probe was reported to be selective for H_2S over Cys and GSH, which differed from prior reports with coumarin-NBD adducts. Probe **528** was further used to image exogenous H_2S in HeLa cells and also showed an increase upon Cys addition. Also building from a coumarin platform, Song reported **529** (NCQ),

which provided different responses to Cys/Hcy, GSH/H_2S, and PhSH.[553] This differentiation was based on PhSH-based cleavage of the DNP group, which is in contrast with the earlier-described approaches in this review focused on H_2S-mediated DNP cleavage. Probe **529** construct was additionally used to image different thiol and H_2S responses in NEM-pretreated HeLa cells.

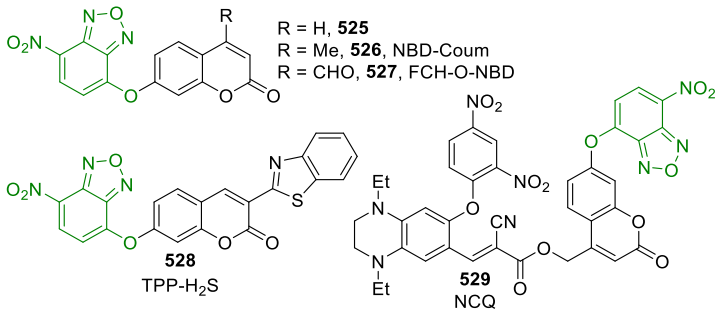


Figure 1.105. Examples of fluorescent H_2S probes based on NBD-ether cleavage with coumarin based chromophores.

Feng and co-workers also investigated the differential responses of H_2S, Cys, Hcy, and GSH using the HBT-derived **530**,[554] and later further functionalized the construct with aldehyde groups to generate **531** and **532** to improve selectivity for H_2S (Figure 1.106).[555] This increase in selectivity was attributed to possible H_2S addition into the aldehyde, followed by assisted intramolecular NBD cleavage from the resultant thiol. The presence of an aldehyde in the *ortho*, rather than *para* position to the NBD group resulted in faster overall reaction with H_2S, although the reason for additional selectivity from the *para*-aldehyde remains unclear. Probe **531** was also used to image exogenous H_2S in HeLa cells. Xing reported related NBD compounds **533**–**535** (BMNO-C1, BMNO-C2, BMNO), which were used to provide different fluorescent outputs for H_2S, Cys/H_2S, and GSH both in 50% MeCN in buffer and in HSC cells.[556]

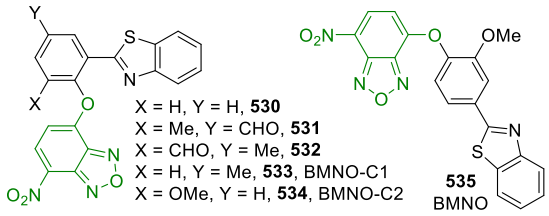


Figure 1.106. Examples of fluorescent H_2S probes based on NBD-ether cleavage with benzothiazole based chromophores.

Expanding to flavone-based systems, Hou reported NBD conjugate **536**, which provided a fluorescence response at 516 nm upon treatment with H_2S, showed some activation from equimolar Cys or GSH, and was used to image exogenous H_2S in A431 cells (Figure 1.107).[557] Liu also reported a similar compound but with dimethylamine substitution in **537** (FHS-1), which provided a fluorescent enhancement at 550 nm was used to investigate the role H_2S levels in apoptosis in MCF-7 cells.[521] Lu used a similar approach to develop NBD-corrole adduct **538** (DPC-O-NBD) in which the NBD motif effectively quenches corrole fluorescence through PET.[558] When comparing solvent systems, the authors observed the largest fluorescent turn-on in DMSO, which highlights the sensitivity of many of these reactions to organic solvent additives. Probe **538** provided a fluorescence turn on at 653 nm in 90% DMSO in buffer, shows some fluorescence response to Cys, GSH, and Hcy, and was used to image exogenous H_2S in HeLa cells. Chang and co-workers reported an NBD-dansyl adduct **539**, which provides a fluorescent response to H_2S, but selectivity with other thiols was not reported.[559] Interestingly, this probe showed additional reactivity toward N_3^- with increasing organic solvent composition. Probe **539** was used to develop test strips for both H_2S and N_3^-. Singh also used the general reactivity of NBD-ether motifs toward both H_2S and Cys to develop the perylenediimide benzoxadiazole system **540** (NBD-PDI).[560] This probe reacts with H_2S to diminish the fluorescent signal at 537 nm, whereas reaction with Cys results in an increase at 537 nm. This reactivity was translated to develop test strips for varying H_2S/Cys concentrations.

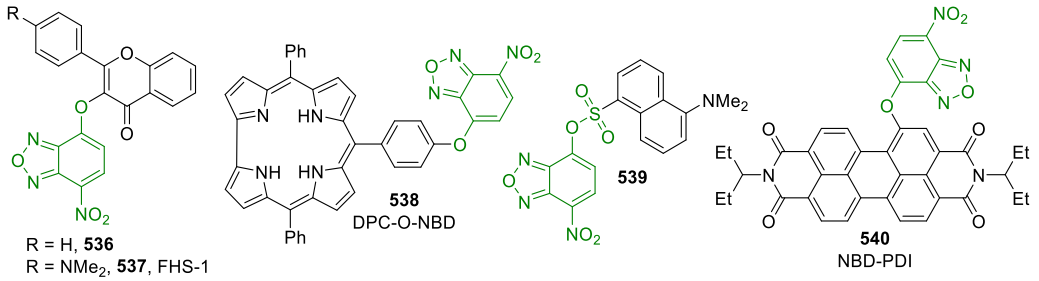


Figure 1.107. Additional examples of fluorescent H_2S probes based on NBD-ether cleavage.

NBD functionalization of xanthene-based systems has also been reported. For example, Yi reported both fluorescein-based **541** and naphthofluorescein-based **542** for H_2S detection (Figure 1.108).[561] Probes **541** and **542** provided fluorescent responses at 514 and 662 nm, respectively,

with both probes showing additional minor reactivity with Cys and GSH. Zhu and Sheng reported the seminaphthorhodafluor-NBD conjugate **543** (SNARF-NBD), which provided different signals for Cys/Hcy, GSH, and H_2S.[562] Based on the relative ratios of fluorescence at 643 and 543 nm, Cys/Hcy could be differentiated from GSH/H_2S and the general response profiles are shown in Figure 1.109. In addition, **543** was also demonstrated to image exogenous H_2S in Raw 264.7 cells. Zhou and Zhang also reported probe **543** in the same year, and used this probe to image exogenous H_2S in HeLa cells and mice.[563]

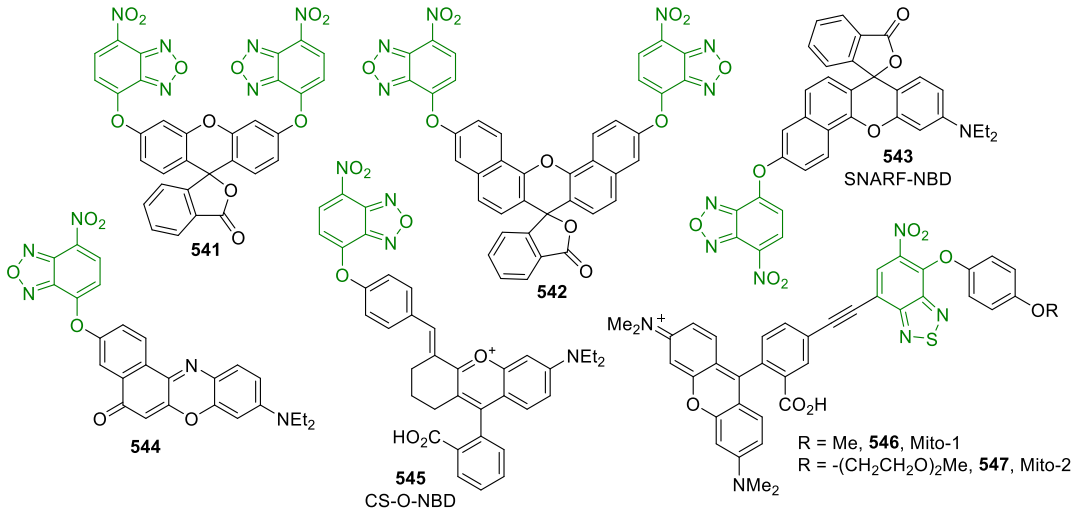


Figure 1.108. Examples of fluorescent H_2S probes based on NBD-ether cleavage with xanthene based chromophores.

Lin also used this approach to develop the probe **544**, which would differentiate Cys from GSH/H_2S using a Nile Red NBD conjugate based on different emission profiles between 500–550 and 663–738 nm.[564] The differentiation between Cys and GSH/H_2S was also demonstrated in live cells and mice with exogenous H_2S and thiols. Yin reported **545** (CS-O-NBD), which was also used to investigate different responses to H_2S, Cys/Hcy, GSH, and SO_3^{2-} depending on excitation at 395, 481, or 570 nm.[565] The different responses for each analyte were confirmed in solution, in HeLa cells, and in zebrafish. Using a modified benzothiadiazole platform, Feng reported **546** (Mito-1) and **547** (Mito-2), which provide different reaction kinetics with H_2S and GSH, and in which the H_2S derived thiol product can be further oxidized by H_2S/H_2O_2 to a sulfonate with concomitant reduction of the nitro group to an amine by H_2S.[566] This reaction scheme was leveraged to provide a response to the presence of both H_2S and H_2O_2. Both **546** and **547**, react

with H_2S/H_2O_2 to generate a fluorescent response at 590 nm, are localized to the mitochondria, and can be used to image exogenous H_2S/H_2O_2 in HeLa cells.

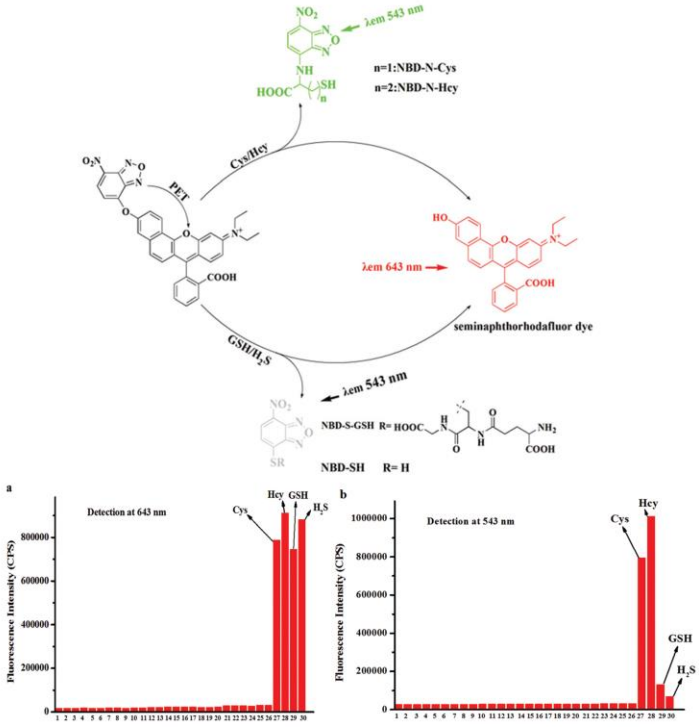


Figure 1.109. (top) Response mechanism from **543** in response to Cys/Hcy and GSH/H_2S. (bottom) Fluorescent response of **543** at 643 nm and 543 nm against different analytes, with Cys, Hcy, GSH, and H_2S highlighted. Reproduced and modified with permission from ref [562]. Copywrite 2019 Royal Society of Chemistry.

Phenolic NBD substitution has also been used to develop different BODIPY-based H_2S probes. For example, Shao reported **548** with a NBD-functionalized *meso* hydroxybenzyl motif.[567] Reaction with H_2S results in a fluorescence increase 510 nm, with some signal also occurring for Cys and GSH (Figure 1.110). The resultant probe was also used to image exogenous H_2S in HeLa cells. Huo and Yin reported both the single and double NBD adducts in **549** and **550** (BDP-N1 and BDP-N2), respectively.[568] Both probes provide a turn-on response to H_2S in 50% DMSO in buffer, with **549** having a maximum at 587 nm and **550** having a maximum at 674 nm. Both probes showed good general selectivity for H_2S, but also showed small signal enhancements for Cys, Hcy, and GSH. Probe **550** was used to detect exogenous H_2S in A549 cells.

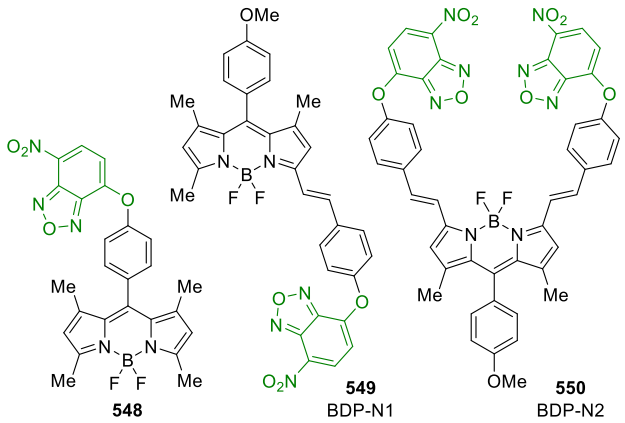


Figure 1.110. Examples of fluorescent H_2S probes based on NBD-ether cleavage with BODIPY chromophores.

NBD ethers have also been incorporated into other extended fluorophores to expand the spectral coverage of NBD-based probes for reactive sulfur species. For example, Lin reported **551** (CS-NBD), which provides a signal at 544 nm for Cys/Hcy and at 707 nm for H_2S (Figure 1.111).[569] This discrimination for Cys/Hcy and GSH/H_2S was also demonstrated in HeLa cells and larval zebrafish. Kim and Kim reported **552**, which reacts with H_2S to generate fluorescent response at 545 nm and was reported to be selective for H_2S over other analytes including Cys.[570] This probe was used to image different H_2S levels in H9C2 as well as cancerous cell lines HUH7, MDA231, and U87MG.

Zhao reported the NIR probe **553** (HZ-NBD), which provided a maximal fluorescent signal for H_2S and GSH at 672 nm, with the reaction with H_2S being faster, and also showed minor enhancement by Cys and Hcy.[571] The resultant probe was used to image exogenous H_2S and GSH in HepG2 cells and larval zebrafish. Feng reported **554** (DC-NBD), which was reported to react selectively with H_2S to generate a fluorescence turn on at 744 nm.[572] This probe was used to image exogenous H_2S in MCF-7 cells, endogenous H_2S generation from Cys, which could be abolished by incubation with the PAG, and exogenous H_2S in mice. Li also reported an extended construct in **555** (CX-N), which provided a turn-on response at 699 nm with good selectivity for H_2S over competing RSS and amino acids.[573] This probe was further used to demonstrate a dose-dependent response to exogenous H_2S in HeLa cells, Cys- or LPS-derived H_2S in HeLa cells, and Cys-derived H_2S in zebrafish, and in LPS-treated mice. Lu reported the related platforms **556** (Mito-HS-1) and **557** (Mito-HS-2), which provided fluorescent responses to H_2S at 720 and 730 nm, respectively.[574]

Both probes showed good selectivity for H_2S over thiols, were found to localize to the mitochondria, and responded to exogenous H_2S in in A549 cells. **557** was further used to image the time-dependent generation of H_2S from H_2S donor ADT-OH in A549 cells. Probe **558** was reported independently by Cao and Ye as well as Liu and Sheng for the discrimination between H_2S, Cys, and GSH.[575, 576] This probe was shown to provide different fluorescent responses depending on the analyte with an H_2S response at 652 nm, which was also demonstrated in MCF-7 and Raw 264.7 cells.

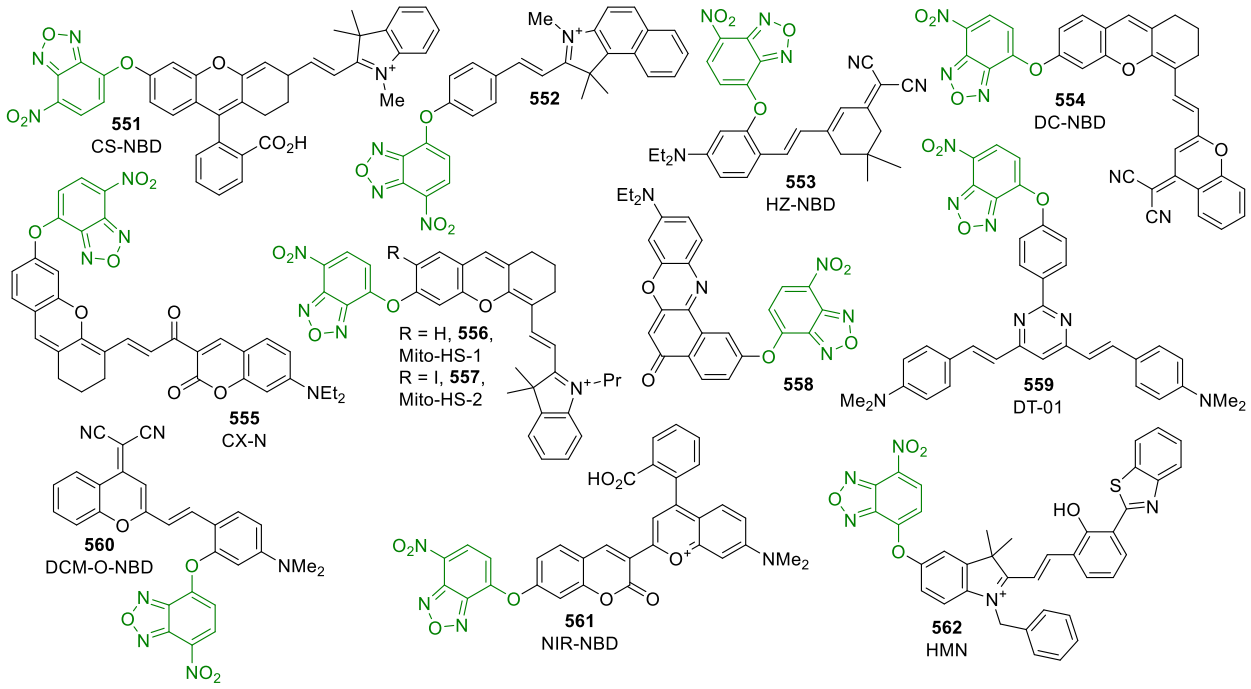


Figure 1.111. Examples of fluorescent H_2S probes based on NBD-ether cleavage with extended wavelength chromophores.

Also using this approach, Peng, Yu and Li reported **559**, which also provides different turn-on responses to H_2S and other biothiols with two-photon excitation at 760 nm.[577] This probe was further used to image exogenous thiols and H_2S in HeLa cells, mouse brain slices, and zebrafish. Wu and Tians reported related **560** (DCM-O-NBD), which was used for two-photon excitation experiments at 960 nm to generate a fluorescent response at 667 nm with only a minor response from Cys, Hcy, or GSH.[578] This probe was used to image both exogenous and endogenous H_2S in HeLa cells as well as activation in different organs in a metformin-induced liver injury model in mice. Dai and Zhou also reported a multifunctional **561** (NIR-NBD) probe that reacts with

Cys/Hcy, GSH, SO_2, and H_2S in different pathways to provide different fluorescent products, with different emission patterns depending on excitation at either 465 or 625 nm, which was used to image these different RSS in HepG2 cells.[579] This general approach was also expanded by Lin, who combined the H_2S/Cys/Hcy/GSH cleavage of NBD ethers with the H_2S addition to indolium motifs to generate **562** (HMN).[580] Using this approach, different signal patterns were observed with the probe was excited at 410, 470, or 550 nm, with the blue, green, and red channels reporting on H_2S, Cys/Hcy, and Cys/Hcy/GSH/H_2S, respectively. This probe was further used to image these analytes in HeLa cells, including the sequential addition of different analytes.

One of the major limitations of H_2S-mediated cleavage of NBD ethers is the general reactivity toward sulfhydryl nucleophiles. Although some of the reports described above highlight the potential to separate Cys/Hcy from GSH/H_2S reactivity, these systems in general are not efficacious for direct and selective H_2S detection. In further expanding NBD-based electrophiles for H_2S detection NBD-amine conjugates display significantly higher selectivity for H_2S over other competing nucleophiles. While some of this selectivity is empirical, Qiu and Yi provided a useful screen of different amine displacement rates, which helped identify piperazine as a particularly useful linkage motif that imparts both high reaction rates with H_2S and also good overall selectivity (Figure 1.112).[581]

Earlier in 2013, Yi reported the simple coumarin-based analogue **563**, which reacted with H_2S selectively over Cys or GSH to produce a fluorescence response at 480 nm (Figure 1.113).[582] A minor response to SO_3^{2-} was reported, although this response was <10% of the H_2S response. This probe was used to image exogenous H_2S in HEK293 cells. An extended coumarin-based system was also reported by Liu and co-workers who reported **564** (Cou-NBD). This probe was used to image exogenous and SNP-generated H_2S in A549 cells and also exogenous H_2S in zebrafish.[583] Romieu also reported a coumarin-based probe in **565**, which provided a rapid response to H_2S, $S_2O_5^{2-}$, and SO_3^{2-} at 465 nm with minimal signals for other thiols in buffer.[584] In an unusual selectivity profile, a response to Na_2S but not NaSH was observed in buffer even though both of these sources should provide the same speciation of sulfide. Xi and Yi also reported a coumarin-based probe with a triazole linker in probe **566**, which provided a response to H_2S at 486 nm with good selectivity for H_2S over competing thiols, but also a small response to SO_3^{2-}.[585] This probe was also used to image H_2O_2-induced H_2S generation in yeast cells. Yi and Xi also reported the related julolidine-fused coumarin probe **567**, which provided a turn-on response at 496 nm

with good selectivity for H_2S over competing species, but also a minor response to SO_3^{2-}.[586] This probe was further used to image exogenous H_2S in HEK293A and A549 cells as well as exogenous and Cys-derived H_2S in zebrafish. Expanding to a two-photon approach, Wei and Chen reported the benzocoumarin-NBD motif **568** (BCD), which provided a ratiometric response to H_2S with an increase at 440 nm and concomitant decrease at 555 nm.[587] This probe showed good selectivity for H_2S over competing analytes and was further used to image exogenous and Cys-derived H_2S in HeLa cells and zebrafish.

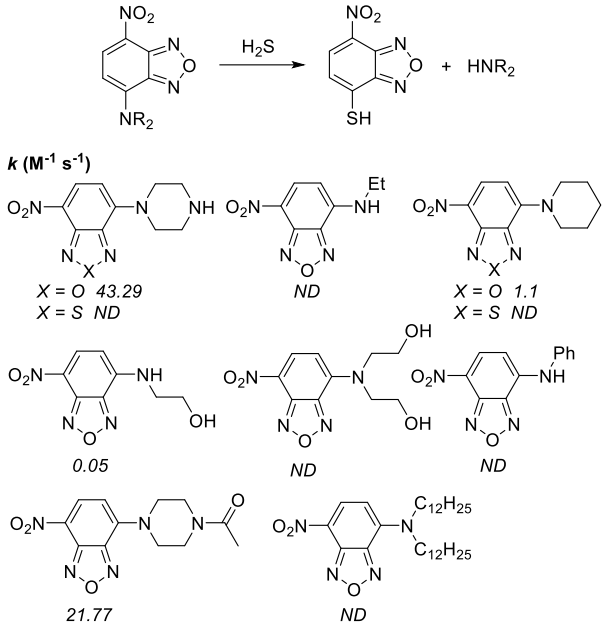


Figure 1.112. (top) General reactivity of NBD-amines with H_2S. (bottom) Second order rate constants for the reaction of H_2S with different NBD amines.

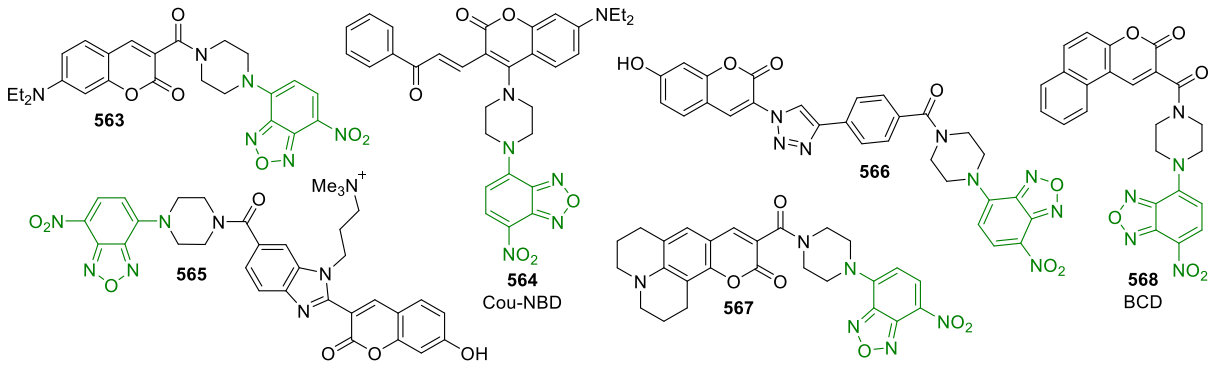


Figure 1.113. Examples of fluorescent H_2S probes based on NBD-amine cleavage with coumarin based chromophores.

Using the same approach, Chen, Liu, and Yin reported **569** (DP-NBD), which was based on a dansyl chromophore and provided a selective response to H_2S at 595 nm (Figure 1.114).[588] This probe was also used to image exogenous H_2S in HeLa cells. A variety naphthalimide-based NBD scaffolds have also been reported as H_2S probes. For example, Sureshkumara reported piperazine ligated NBD-naphthalimide conjugate **570**, which provided a fluorescence turn-on at 550 nm in 10% DMSO in buffer and was used to investigate H_2S levels in different water samples.[589] Lee reported a similar platform in **571**, which differs by a more solubilizing ether on the naphthalimide, which was used to image exogenous and Cys-derived H_2S and also to investigate the role of H_2O_2 on H_2S generation in HeLa cells.[590] A related platform incorporating a 7-chlorobenzofurazan-4-sulfonyl chloride (CBD) motif was reported by Li, Dong, and Han in **572**.[591] In this platform, reaction with H_2S at sulfonamide motif and Cys reaction a the CBD chloride position generated products with fluorescent responses at 535 and 571 nm for H_2S and Cys, respectively. In addition, this probe showed selectivity for Cys over Hcy and GSH due to the lack of subsequent Smiles rearrangement for the Hcy and GSH analogues. Probe **572** was used to image exogenous H_2S and Cys in MCF-7 cells. Du and Chen also used a naphthalimide scaffold to develop the dual reporting H_2S and HClO probe **573** (NB-NAP-NBD).[592] This probe reported a dual signal from NBD cleavage by H_2S and urea linker cleavage by HClO to release the naphthalimide and methylene blue components, respectively. This probe, along with a related azide compound used for comparison, was used to image exogenous H_2S in HeLa cells, endogenous H_2S and HClO stimulated by NAC and LPS administration, respectively, in Raw 264.7 cells and in zebrafish.

Moving the substituted naphthalene chromophores, Jiang reported aminonaphthalene construct **574** using this same approach of H_2S mediated cleavage of an NBD-piperazine motif to develop a two-photon imaging system (Figure 1.115).[593] This probe could be excited at either 365 or 780 nm, had an emission maximum at 468 nm, and was used to image exogenous H_2S in HeLa cells. Wu used a related acetylnaphthalene derivative **575** (NNE) to also develop a two-photon imaging approach for H_2S detection.[594] This probe used direct linkage of the NBD sensing motif to the secondary amine, underwent one- and two-photon excitation at 347 and 700 nm with an associated emission at 490 nm, and showed good selectivity for H_2S over other reactive anions and thiols in 30% DMSO in buffer. The probe was used to image exogenous and SNP-generated H_2S in HeLa cells and in zebrafish.

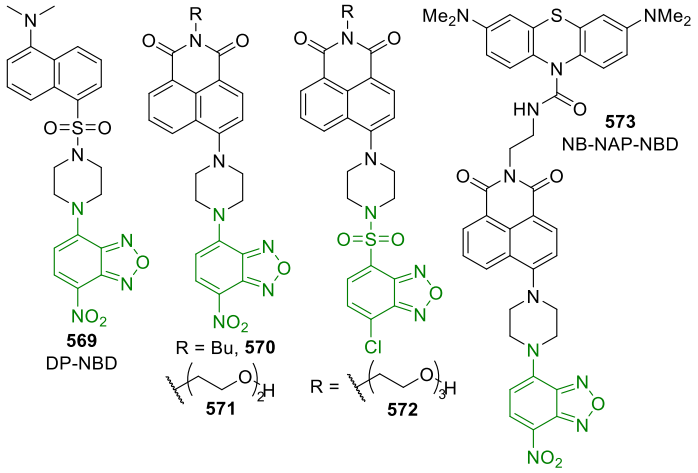


Figure 1.114. Examples of fluorescent H_2S probes based on NBD-amine cleavage with naphthalimide chromophores.

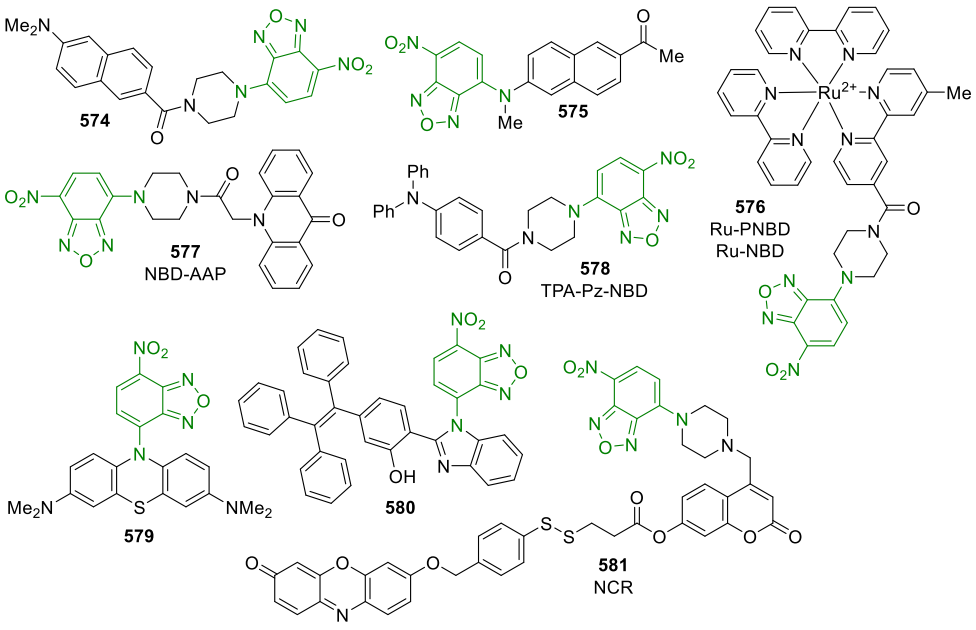


Figure 1.115. Additional examples of fluorescent H_2S probes based on NBD-amine cleavage.

Highlighting how this approach can be transfered to other chromophore scaffolds, both Yuan and Zhang as well as Ren and Yuan reported a Ru(II) complex with functionalized bipyridine ligand containing a piperazine-NBD H_2S sensing motif to prepare **576** (Ru-PNBD / Ru-NBD).[595, 596] This probe showed a turn on fluorescent response to H_2S at 638 nm and was selective for H_2S over other analytes, but did show small response to the nucleophilic anions SO_3^{2-}, S_4^{-}, and $S_2O_4^{2-}$

in the report by Yuan and Zhang. Yuan and Zhang demonstrated the use of this probe to image exogenous H_2S in HeLa cells and larval zebrafish, and Ren and Yuan reported both exogenous and endogenous H_2S imaging in HCT116 cells and cellular responses to different irradiation times. Sun and You reported acridone acetylpiperazine adduct **577** (NBD-AAP), which generates a ratiometric response to H_2S with a fluorescence decrease at 552 nm and concomitant increase at 427 nm.[597] The probe was used to investigate H_2S in water samples and exogenous H_2S in Daphnia magna. Using a triphenylamine motif, Zhang and Dong developed **578** (TPA-Pz-NBD).[598] This probe provides a ratiometric response with fluorescence turn on at 500 nm and concomitant turn-off at 545 nm and was also used to image exogenous H_2S in HeLa cells. Further demonstrating the different linkage opportunities of this approach, Zhao reported on a directly-functionalized leuco methylene blue adduct **579**.[599] This probe reacts with H_2S to generate non-fluorescent leuco methylene blue, which is subsequently oxidized under ambient conditions to form the fluorescent methylene blue product in 90% MeOH in buffer and was also demonstrated to detect exogenous H_2S in HCT-117 cells. Liu and Pu used a related NBD-cleavage approach to report **580**, which was used to detect H_2S and also Zn^{2+} after the initial H_2S-mediated NBD cleavage.[600] This probe provided a turn-on response at 445 nm in response to H_2S and was used to develop test strips for food spoilage. In addition, Wang and Shang reported an extended coumarin adduct with a NBD-piperazine motif for H_2S detection and disulfide cleavage site for Cys, Hcy, GSH, and H_2S activation to prepare **581** (NCR).[601] By exciting at 360 and 580 nm, the fluorescence signals for H_2S, Cys/Hcy, and GSH could be differentiated, and this differential response was also demonstrated with exogenous analytes in HeLa cells.

H_2S-mediated cleavage of NBD amines has also been used to develop different rhodamine and fluorescein derivatives. For example, Yi and Xi reported **582** and **583**, which include bottom ring functionalization of fluorescein and rhodamine chromophores, respectively (Figure 1.116).[602] In both cases, cleavage of the piperazine-NBD removes the NBD-based quenching of the fluorophore and results in a fluorescence response with good selectivity for H_2S over other competing species. Both **582** and **583** were used to image exogenous and Cys-derived H_2S in HEK293 cells, investigate H_2O_2-mediated H_2S formation, and **583** was also used to image exogenous H_2S in mice. Yi and Xi also reported the azetidine functionalized rhodamine derivative **584** with improved photophysical properties and emission at 585 nm.[603] This probe was used to image exogenous H_2S and Cys-derived H_2S in HEK293 cells and zebrafish. Moving to direct

functionalization of a rhodamine nitrogen, Lv and Guo reported **585**, which provided a 160-fold turn-on with moderate cross reactivity with SO_3^{2-} and was used to image exogenous H_2S in HeLa cells.[604] Yi and Xi reported **586**, which provided a turn-on response at 660 nm with good selectivity for H_2S over Cys, Hcy, and GSH, including when the analytes were co-incubated. This probe was further used to image both exogenous and endogenous H_2S in HeLa cells.[605] This same probe was later reported by Na, who further investigated the impacts of pH on this reaction using DFT calculations and MS experiments.[606] Li, Zhai, and Ye used a related approach to combine oxygen and nitrogen protection with NBD leaving groups to develop dual reactive probe **587** (NJB), which provides different responses to H_2S and Cys in both the fluorescence and absorption spectrum.[607] This probe was used to detect H_2S and Cys in MCF-7 cells.

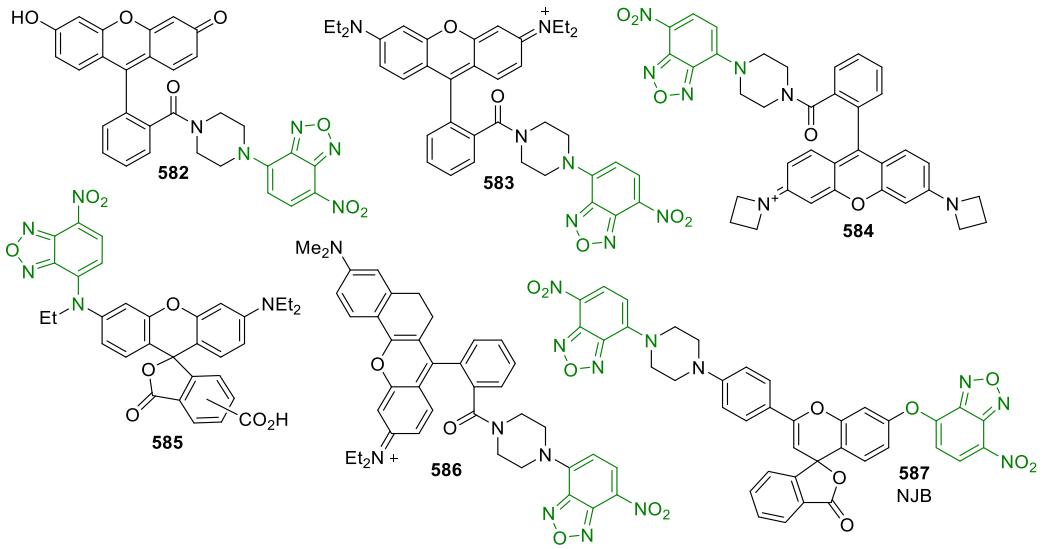


Figure 1.116. Additional examples of fluorescent H_2S probes based on NBD-amine cleavage with fluorescein and rhodamine based chromophores.

As examples of BODIPY-based probes incorporating NBD-amine approaches for H_2S detection, Chen, Dong, and Zhao reported **588** for the differentiation of H_2S/GSH and Cys/Hcy (Figure 1.117).[608] In this system, reaction at the NBD ether site results in self-immolation through the pyridinium core to release the BODIPY chromophore. Depending on the sulfhydryl nucleophile, different fluorescent signals are generated, which was confirmed both HeLa cells and mice. NBD-piperazine motifs have also been incorporated into BODIPY scaffolds, as demonstrated by Wang, Zhang, and Wei. All three *ortho*, *meta*, and *para* isomers **589**–**591** (*o*/*m*/*p*-

BNP) of phenyl linker were prepared, with the *ortho* isomer **589** showing the best response and being used for further investigations to image exogenous and Cys-generated H_2S in HeLa cells and in zebrafish.[609] Probe **589** was also reported by Xi who used this probe to image tobacco mosaic virus induced endogenous H_2S production in protoplasts and tobacco leaves.[610]

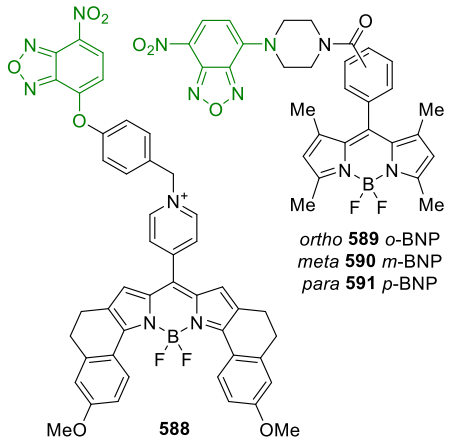


Figure 1.117. Examples of fluorescent H_2S probes based on NBD-amine cleavage with BODIPY chromophores.

Further red-shifted NBD conjugates have also been reported. For example, Zhao, Yang, and co-workers reported the heptamethine cyanine NBD derivative **592** (IR800-DPII) (Figure 1.118).[611] This probe shows a ~100-fold turn-on the H_2S at 800 nm in 30% DMSO in buffer, excellent selectivity for H_2S over other reactive species, and was used to image exogenous H_2S in HeLa cells. A related construct was also reported by Zhang and Yi in **593**, which also provided a turn-on response to H_2S at 796 nm and was investigated directly in buffer.[612] This probe was demonstrated to image exogenous H_2S in FHC, HCT116, and HT29 using a variety of inhibition experiments using AOAA and also siRNA with accompanying mRNA quantification for CBS, CSE, and 3MST (Figure 1.119). Probe **593** was further used to investigate differences in endogenous H_2S production from FHC, HCT116, and HT29 grafted in live mice, with the latter two example resulting in tumor growth and increased endogenous H_2S production. A further red-shifted analogue was reported by Wang, who reported **594** (NIH-H_2S), which has an emission maximum at 820 nm.[613] This probe showed minor activation by SO_3^{2-} and was used to image exogenous H_2S and Cys-derived H_2S in MCF-7 cells and also in mice.

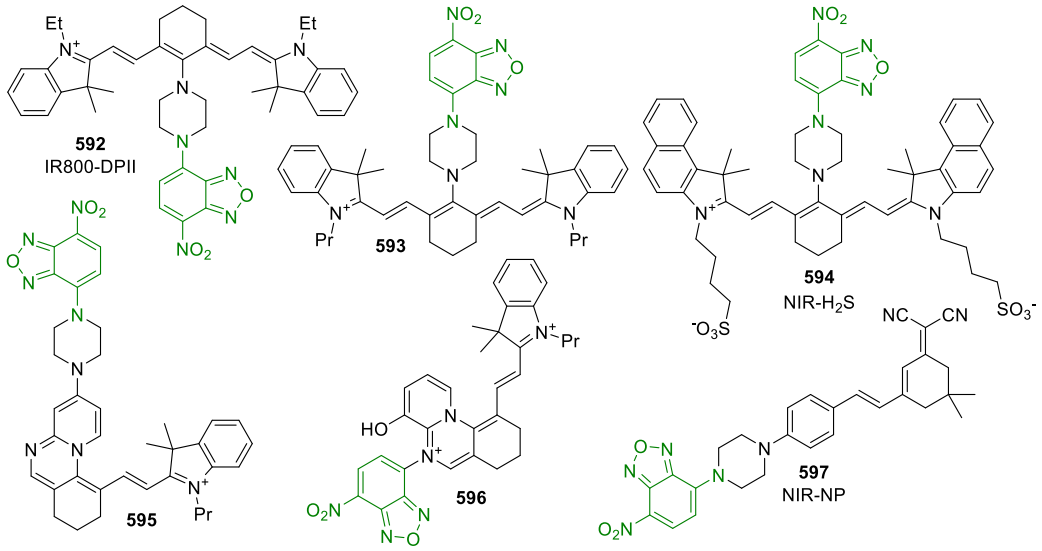


Figure 1.118. Additional examples of fluorescent H_2S probes based on NBD-amine cleavage with extended wavelength chromophores.

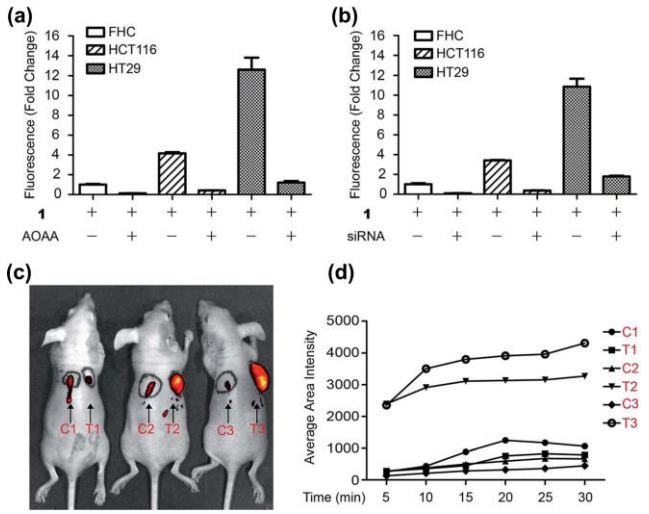


Figure 1.119. (a) Fluorescence response from FHC, HCT116, and HT29 cells treated with **593** and H_2S inhibitor AOAA. (b) Fluorescence response from FHC, HCT116, and HT29 cells treated with **593** and siRNAs for endogenous H_2S production. (d) *In vivo* images of mice with itratumoral injection of **593** differences from control (C1-C3) and tumor sites (T1-T3). (d) Quantified fluorescence from each site showing higher H_2S generation in T3 (HCT116) and T2 (HT29) tumoral sites. Reproduced and modified with permission from ref [612]. Copywrite 2017 Royal Society of Chemistry.

An azonia-cyanine NBD conjugate was also reported by Gao and Ge in **595** and **596** with emission maxima at 660 and 639 nm.[614] The structure of **596** is somewhat unusual in that it is a pyridinium-NBD conjugate, and it remains unclear why the more nucleophilic phenolic oxygen

was not ligated directly to the NBD motif. Both constructs were used to image exogenous H_2S in HeLa cells. Tan and Jiang reported dicyanoisophorone based NBD conjugate **597** (NIR-NP), which has a fluorescence maximum at 670 nm in 30% DMSO.[615] NIR-NP was used to investigate the H_2S response in HeLa, HepG2, MDA-MB-231, and SKOV-3 cells and exogenous H_2S in liver tissues.

The H_2S-mediated cleavage of NBD-piperazine motifs has also been incorporated in different probes for targeting different subcellular organelles (Figure 1.120). For example, Yi and Xi reported **598**, which contains a morpholine group targeted to the lysosome in 2015.[616] This probe showed high selectivity for H_2S over other analytes, including SO_3^{2-}, when tested at pH 6.0 to mimic the acidic environment of the lysosome. Lysosomal localization was confirmed using an organelle marker dye, and **598** was used to image exogenous H_2S in HEK-293 cells. The naphthalimide based probe **599** targeted to the lysosome was also reported independently by both Li and Li in 2018 as well as Wang and Liu in 2019.[617, 618] Probe **599** showed good selectivity for H_2S over other reactive analytes and provided a maximal fluorescence turn-on at 536 nm. Both studies demonstrated lysosomal co-localization and the two-photon imaging in cells, with additional applications in tissue slices and xenograft mice, respectively.

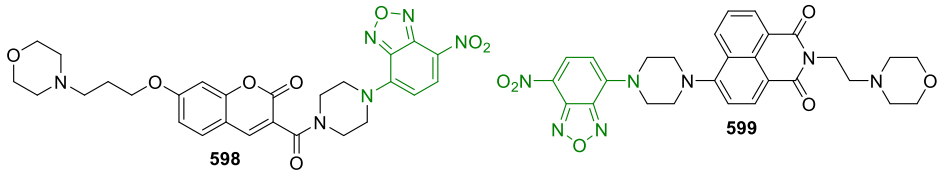


Figure 1.120. Examples of fluorescent H_2S probes based on NBD-amine cleavage targeted to the lysosome.

This approach has also been applied to different probes for H_2S detection in the ER. For example, Chen and Song reported an NBD-coumarin conjugate **600** (ER-CN), which provided a turn-on fluorescence response at 490 nm in 30% DMSO in buffer (Figure 1.121).[619] Subcellular localization was confirmed and the probe was used to image exogenous H_2S in HeLa cells. Yoon and Li reported NBD-naphthalimide conjugate **601** (ER-Nap-NBD), which provides a turn-on response at 530 nm in 50% EtOH in buffer.[620] This probe was confirmed to colocalize in the ER, demonstrated to image exogenous and Cys-derived H_2S in MCF-7 cells, and used to detect exogenous H_2S in live zebrafish. In an unusual example, Yan reported a turn-off response of

fluorophore-lacking **602**, which was characterized in 33% MeCN in buffer and also provided a turn-off response in HeLa cells.[621] Since this probe lacks an additional chromophore, the signal is likely derived from residual fluorescence from the NBD-piperazine motif, although this background fluorescence has not been reported by others. Also using a ER targeting motif but with a BODIPY chromophore, Cheng and Yi reported **603** (ER-BODIPY-NBD), which provided a turn-on response at 520 nm with good selectivity for H_2S over competing analytes.[622] This probe was confirmed to localize the ER and was additionally used to image increased H_2S generation from HClO or cisplatin administration in HeLa cells, which could be abated by treatment with the ROS-scavenger ebselen or H_2S synthesis inhibitor DL-PAG.

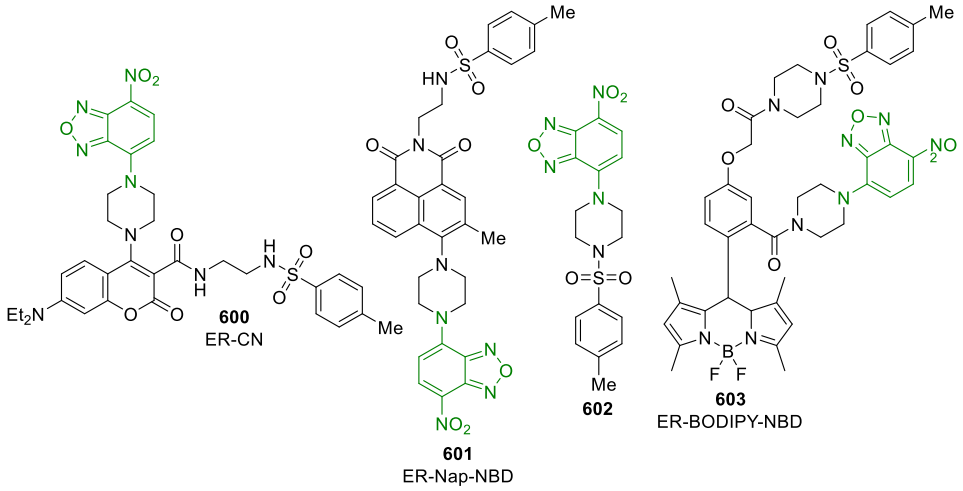


Figure 1.121. Examples of fluorescent H_2S probes based on NBD-amine cleavage targeted to the ER.

Mitochondrially-targeted NBD-piperazine motifs have also been reported. For example, Li, Lee, and Yoon prepared the TPP-naphthalimide **604**, which showed good selectivity for H_2S over other analytes, with a moderate response to SO_3^{2-}, and which was used to image exogenous H_2S in HeLa cells (Figure 1.122).[623] Wei and Li also used a TPP targeting motif, but in this case appended to a coumarin chromophore, to develop **605** (MR-1).[624] This probe provides a ratiometric response to H_2S with an increase at 415 nm and decrease at 565 nm and was further used to image exogenous H_2S in HeLa cells using the 565 nm turn-off response. Transitioning to a pyridinium motif for mitochondrial targeting, Dai and Zho reported **606** (MNOP-H_2S).[625] This probe provided a turn-on fluorescence response at 590 nm in 33% DMSO in buffer and was used to image

exogenous H_2S in HepG2 cells, investigate differences in H_2S levels in HUVECs incubated with vascular endothelial growth factor (VEGF) and PAG, and image exogenous H_2S in zebrafish.

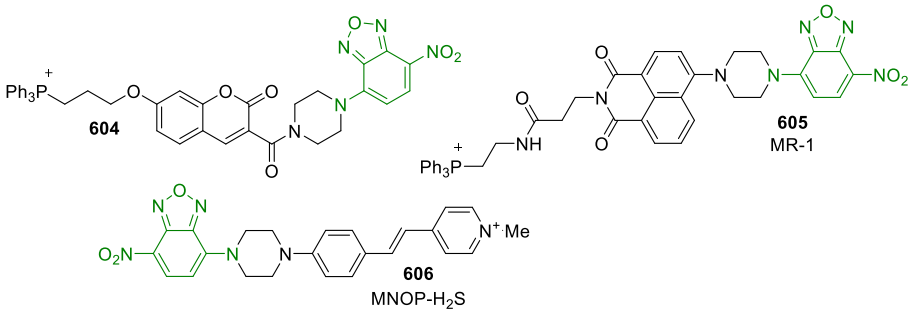


Figure 1.122. Examples of fluorescent H_2S probes based on NBD-amine cleavage targeted to the mitochondria.

Expanding to hepatocyte targeting, Wang, Qu, and Wei prepared the galactose functionalized naphthalimide **607** (GSP-H_2S) (Figure 1.123).[626] This probe provided a turn-on fluorescence response at 540 nm and was used to image H_2S production in HepG2 cells in the presence and absence of PAG as well as exogenous and Cys-generated H_2S in the liver of live zebrafish. Yi and Yang reported the biotin-functionalized NIR fluorescent probe **608** to target cancer cells.[627] This probe provides a turn-on response at 754 nm upon reaction with H_2S in 20% DMSO and shows goods selectivity over other competing analytes. This probe was used to image endogenous H_2S in HepG2 cells, including in the presence of H_2S scavenger NBD-S8.[628] Although not targeted to a specific organelle, Yi reported the cell-trappable probe **609** (AM-BODIPY-NBD), which provides a turn-on response at 520 nm with excellent selectivity over competing species.[629] The cell trappable version of this probe was shown to show good cellular retention over 3 hours, whereas the non-trappable version showed rapid loss withing 30 minutes. This probe was further used to image endogenous H_2S in LO-2 and HepG2 cells, to differentiate between different cancer cell lines based on H_2S generation, to detect endogenous H_2S production in tobacco mosaic virus-infected tobacco leaves and observed H_2S genesis in zebrafish upon tail amputation.

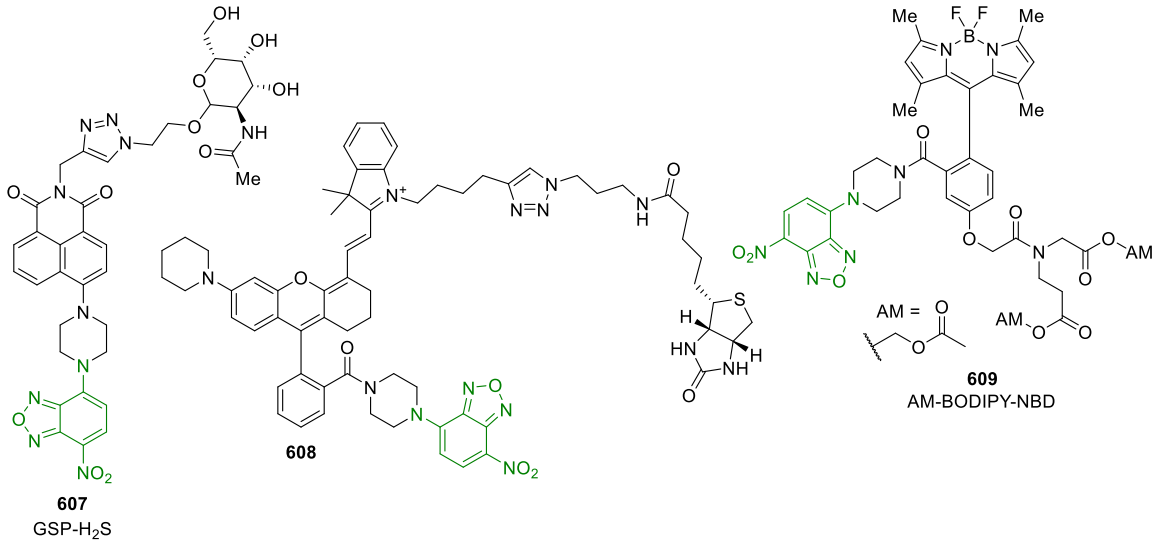


Figure 1.123. Examples of cell trappable fluorescent H_2S probes based on NBD-amine cleavage.

In addition to using different motifs to target NBD-amine systems to different cellular locales, different dual reactive NBD-based H_2S probes have also been reported (Figure 1.124). In general, the goal of including two different reactive sites is to provide responsiveness toward two separate analytes, or to improve sensitivity toward a single analyte if both reactive sites are targeted to only one analyte. As an example of this general approach, Li, Yi, and Xi reported **610** and **611** with both an H_2S-responsive NBD-piperazine motif and a quinone that is reduced by human NAD(P)H:quinone oxidoreductase 1 (hNQO1), which subsequently results in removal of the trimethyl lock motif.[630] Of these two probes, **611** was found to provide a larger signal when dual activation was present and was used to investigate the dual hNQO1 and H_2S response in different cell lines, and different responses upon treatment with H_2O_2, AOAA, or the hNQO1 inhibitor dicoumarol. Liu, Sheng, and Zhu used a related approach but installed the tyrosine kinase inhibitor crizotinib on an NBD-amine adduct for H_2S detection to develop **612** (CZ-NBD).[631] This probe provides a large turn-off response at 550 nm that was used in combination with a small fluorescence increase at 440 nm to provide a ratiometric response, which was used to monitor fluorescence responses in both tumor and non-tumor derived cell lines. Probe **612** also showed greater cytotoxicity toward tumor-derived cell lines. In an additional example, Niu, Qin, and Ye reported **613** (NJA), which reports on both H_2S and HNO using NBD and diphenylphosphine motifs, respectively.[632] Reaction of this probe with HNO only generates a weak fluorescent

response and requires additional H_2S-mediated NBD cleavage to generate full fluorescence, which was additionally confirmed by exogenous addition in MCF-7 cells.

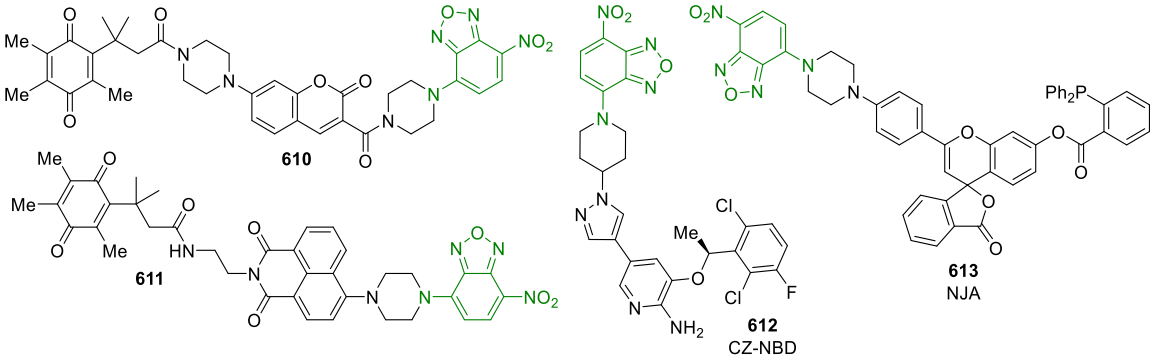


Figure 1.124. Examples of fluorescent H_2S probes based on NBD-amine cleavage with dual reactivity sites for other analytes.

Bifunctional probes with different H_2S-reactive groups have also been reported. The design principle of these probes is that having multiple quenching groups should increase the dynamic range of the probe and that using different activity-based methods for H_2S detection should improve the selectivity against competing analytes. Yi and Xi reported two coumarin-based platforms **614** and **615** with both NBD and azide reactive groups that provided higher selectivity than either of the two individual motifs (Figure 1.125).[633] Probe **615** provided a large 4000-fold turn-on for H_2S and was applied to image Cys-derived H_2S production in zebrafish as well as in a high-throughput assay for screening CBS inhibitors. A related approach was reported by Song and Chen who incorporated an azide and an NBD-thioether adduct into a sensing platform to generate **616**. Lacking the increased selectivity of the NBD-piperazine motif, the thio-NBD motif in **616** reacted with both H_2S and thiols, so was used to differentiate H_2S, Cys/Hcy, and GSH and also demonstrated to provide different fluorescent outputs for each analyte in HeLa cells.[634] Using a related approach, Xi and Yi including an NBD and DNP motif in a coumarin platform to develop **617**, which was used to image H_2S in HEK293A cells.[635] Sun and Li reported **618** with both NBD-ether and NBD-amine motifs, which provides different responses due to activation by H_2S and Cys/H_2S by monitoring different excitation and emission wavelengths. This differential signal was also demonstrated with H_2S and Cys in HeLa cells.[636] Xi and Yi reported naphthalimide based **619**, which also showed enhanced selectivity when compared to the mono-functionalized probes,

and was used to image exogenous H_2S in HEK293 cells.[637] Hou used a similar approach using an NBD thioether in combination with an H_2S responsive thiophene ester to develop **620** (COT-NBD), which provided responses to H_2S and Cys/Hcy, but not GSH, in different channels.[638] These differentiated responses were further demonstrated in MCF-7 cells and zebrafish.

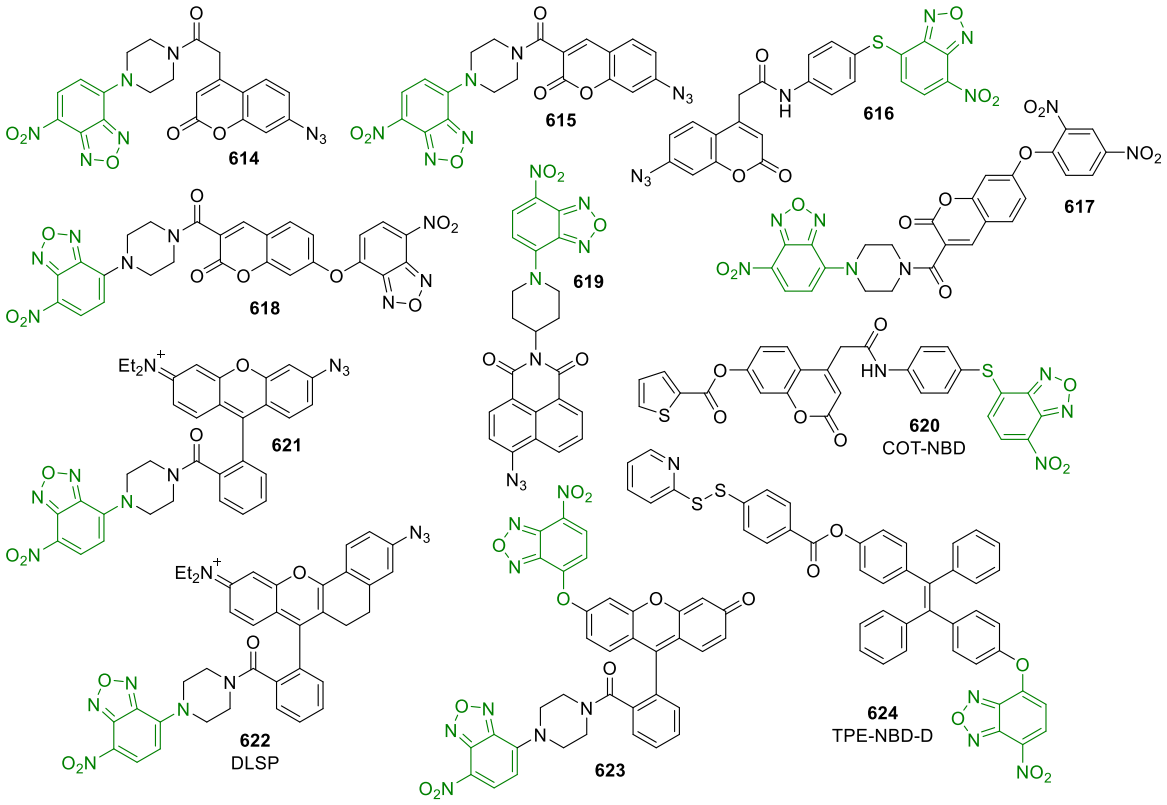


Figure 1.125. Examples of fluorescent H_2S probes based on NBD-amine cleavage with additional H_2S reactive groups.

Wei and Li also incorporated an azide and NBD-piperazine motif into a rhodamine platform to develop **621**.[639] This probe showed good selectivity for H_2S over other reactive analytes and was used to image Cys-derived H_2S in HEK293A cells and also exogenous H_2S in mice. Chen and Wei also used a bifunctional approach to develop **622** (DLSP), which showed enhanced selectivity when compared to the monofunctional adducts.[640] This probe was further used to image endogenous H_2S in HepG2, MCF-7, and HeLa cells, differences in H_2S levels between HepG2 and insulin-resistant HepG2 cells, and differences in H_2S generation in normal versus diabetic mice. The combination of NBD-ether and NBD-piperazine motifs was

demonstrated by Wang and Yi to develop probe **623**, which provided a signal from H_2S and GSH, but not Cys.[641] This probe was used to differentiate Cys metabolism of L-Cys versus D-Cys in the generation of Cys-derived H_2S and GSH products. Incorporating an NBD ether with a pyridyl disulfide ester motif, Maiti reported the dual functional probe **624** (TPE-NBD-D).[642] In this probe, the ester was reported to be cleaved by esterase, and moderate selectivity for H_2S over GSH and Cys were observed. The disulfide motif was proposed to release H_2S upon reaction with Cys/GSH, but a potential mechanism for this chemistry was not provided. This probe was further used to image exogenous and Cys-derived H_2S in SHSY5Y cells, responses in mice, and investigations into $A\beta_{1\text{-}42}$ deagglomeration.

A number of other functionalized NBDs lacking additional fluorophores have been reported as fluorescent sensors, often with turn-off responses.[643-648] This signal change is likely due to residual and minimal fluorescence of the NBD-piperazine constructs or in less selectivity systems some signal in complex environments may be due to adventitious reaction with Cys or Hcy to generate fluorescent responses.

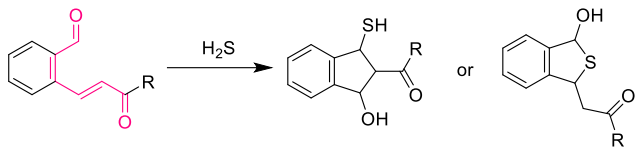
1.4.4 Other Electrophilic Platforms

The general nucleophilicity of H_2S has been used to develop H_2S probes using a variety of different strategies in addition to the broadly applied approaches discussed above. This section highlights the diversity of electrophilic system used to develop activity-based probes for H_2S. Some of these platforms contain single electrophilic sites, many of which have been tuned to favor reactivity toward H_2S over other competing thiols, whereas others rely on the ability of H_2S to participate in two sequential nucleophilic attacks to provide selectivity over thiols and other competing species.

1.4.4.1 Cyclization from Aldehydes and α,β-Unsaturated Ketones

In 2011, He reported a new strategy for H_2S detection and trapping based on the addition of H_2S to an aldehyde that is proximal to an unsaturated acrylate (Scheme 1.11).[649] This approaches relies on the initial addition of H_2S to the aldehyde to generate a hemithioacetal intermediate, which then undergoes subsequent Michael addition to an adjacent unsaturated acrylate to disrupt the conjugation of the system. One benefit of this approach is that the addition of a thiol to the aldehyde is likely reversible, thus providing additional selectivity and reducing irreversible probe

activity by thiols. Initial reports suggested that a thiofuran is formed as the end product of this tandem addition, whereas later NMR spectroscopy experiments in related systems suggest benzocyclopentane formation (*vide infra*).



Scheme 1.11. H_2S detection based on addition to an aldehyde and further cyclization.

In the initial proof-of-concept report of this approach, He reported **625** (SFP-1), which was based on a 1,3,5-triaryl-2-pyrazoline fluorophore and resulted in a >10-fold fluorescence turn-on at 391 nm upon treatment with H_2S (Figure 1.126).[649] An improved BODIPY-based **626** (SFP-2) using the same reporting strategy provided a 16-fold turn-on and a longer wavelength emission of 510 nm. Probe **626** showed some activation by Cys, GSH, and β-mercaptoethanol, was used to detect enzymatically generated H_2S from isolated CBS, and was further demonstrated to detect exogenous H_2S in live HeLa cells. Zhao later reported in 2015 a related approach to prepare functionalized BODIPY **627** (SFP-3) using an α,β-unsaturated phenyl ketone instead of an acrylate as the electrophile to increase the rate of reaction.[650] The resultant probe showed a ~70-fold fluorescence turn on at 500 nm upon treatment with H_2S in PBS buffer although the selectivity toward Cys and GSH was slightly eroded. Probe **627** was also used to measure H_2S in blood plasma and brain tissues, although the measured levels have been significantly refined by more recent analytical methods.

Li and Hu reported a related approach using functionalized BODIPY **628**.[651] Based on the elongated conjugation, the emission of this probe is shifted to 561 nm, and treatment with H_2S in 20% MeCN in PBS buffer resulted in a 62-fold fluorescence increase with good selectivity for H_2S over other amino acids and biothiols. The resultant probe was used to image phorbol myristate acetate (PMA) dependent H_2S levels in live Raw 264.7 cells. Qian and Zhu further expanded on this approach to develop BODIPY-coumarin conjugate **629** (SFP-BC).[652] This probe provided a 26-fold fluorescence turn-on upon treatment with H_2S in 40% MeCN in PBS buffer with a modest selectivity over Cys and GSH. Probe **629** was used to investigate H_2S in blood plasma and exogenous H_2S in B16-F1 cells.

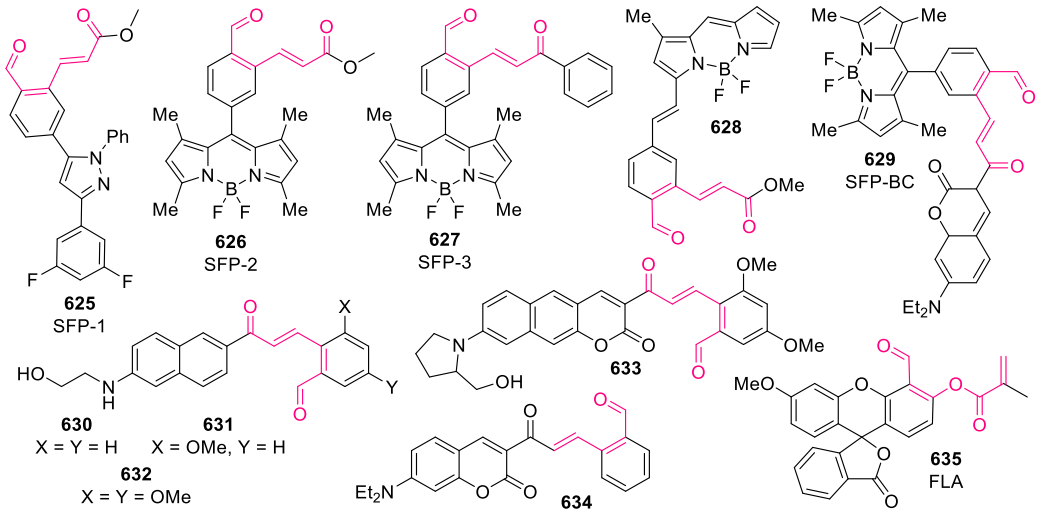


Figure 1.126. Examples of fluorescent H_2S probes based on tandem reactivity with an aldehyde and α,β-unsaturated ketone.

Using a conjugated naphthalene fluorophore, Ahn used a similar approach to prepare **630**–**632** with different substitution on the benzaldehyde motif.[653] The resultant probes show a 200-400 fold response to H_2S in buffer with high selectivity for H_2S over, and the selectivity toward H_2S over Cys could be modified by steric substitution of the probe. In addition, NMR spectroscopy investigations support that a benzocyclopentane product is formed rather than the earlier proposed benzothiofuran. Benzocyclopentane formation can be accounted for by H_2S addition to the aldehyde, sulfhydryl transfer to the enone, and subsequent aldol condensation to afford the final product (Figure 1.127). The probes **630** and **632** were also used to image H_2S in HeLa cells, using exogenous H_2S, PMA, and PAG in separate experiments.

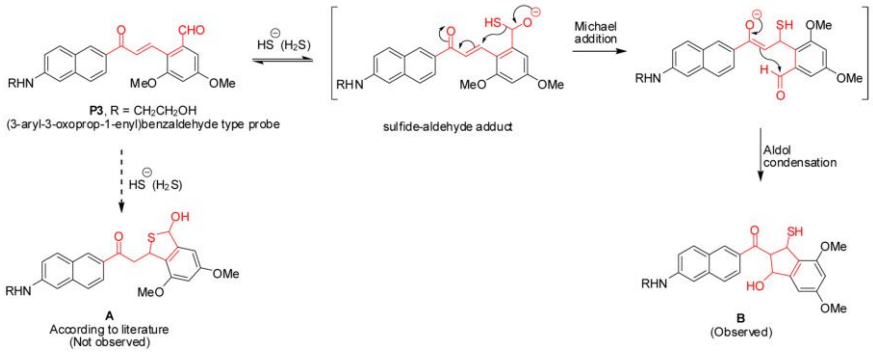
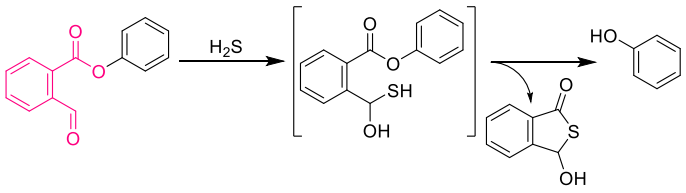


Figure 1.127. Competing pathways for addition of H_2S to aldehyde-containing α,β-unsaturated ketone systems. Reproduced with permission from ref [653]. Copyright 2015 American Chemical Society.

Singha and Ah also used a related approach to append the optimized aldehyde from **630** above to prepare an extended coumarin based probe **633** with H_2S responsive turn-on at 628 nm in 30% EtOH in H_2O.[654] The **633** probe was also used to image exogenous H_2S in HeLa cells using two-photon excitation at 900 nm. Also providing an example of a coumarin-based platform, Hou reported probe **634**, which provided different fluorescent responses to H_2S and GSH at 587 nm and 501 nm respectively in 50% DMSO in buffer.[655] Comparing the reaction rates between GSH and H_2S under identical conditions showed a significantly faster rate of reaction with GSH. This probe was further used to image exogenous H_2S in Raw 264.7 cells and mice. Using a related strategy but with a terminal acrylate rather than an internal α,β-unsaturated ketone, Upadhyay reported **635** (FLA), which also undergoes an intramolecular cyclization after H_2S addition to form a fluorescent product at 496 nm.[656] This probe showed good selectivity for H_2S over Cys, Hcy, GSH, and other oxidized sulfur anions and was subsequently used to image exogenous H_2S in HeLa cells.

1.4.4.2 Addition to Aldehydes and Subsequent Ester Cleavage

Addition of H_2S to aryl aldehydes to form a nucleophilic hemithioacetal intermediate has also been used as an approach to cleave esters and liberate a protected fluorophore (Scheme 1.12). Much like the above examples the addition of thiols to the aldehyde is likely reversible, although dependent on both the identity of the thiol and the aldehyde.



Scheme 1.12. Addition of H_2S to an aldehyde and subsequent ester cleavage.

In early example of this approach, Tang reported a 2-carboxybenzaldehyde functionalized cyanine probe **636** (HS-Cy), which upon reaction with H_2S resulted in ester cleavage to liberate the cyanine dye (Figure 1.128).[657] Upon reaction with H_2S, the fluorescence shifts from 780 to 625 nm, leading to a ratiometric response with good selectivity for H_2S over other thiols. Based on the

observed kinetics in this system, the initial addition of H_2S to the aldehyde is faster than the subsequent intramolecular cyclization and cleavage of the ester, which was supported by UV-vis and fluorescence measurements. Probe **636** was further used to monitor exogenous H_2S in HepG2 cells and H_2S generation on A549 cells after addition of SNP.

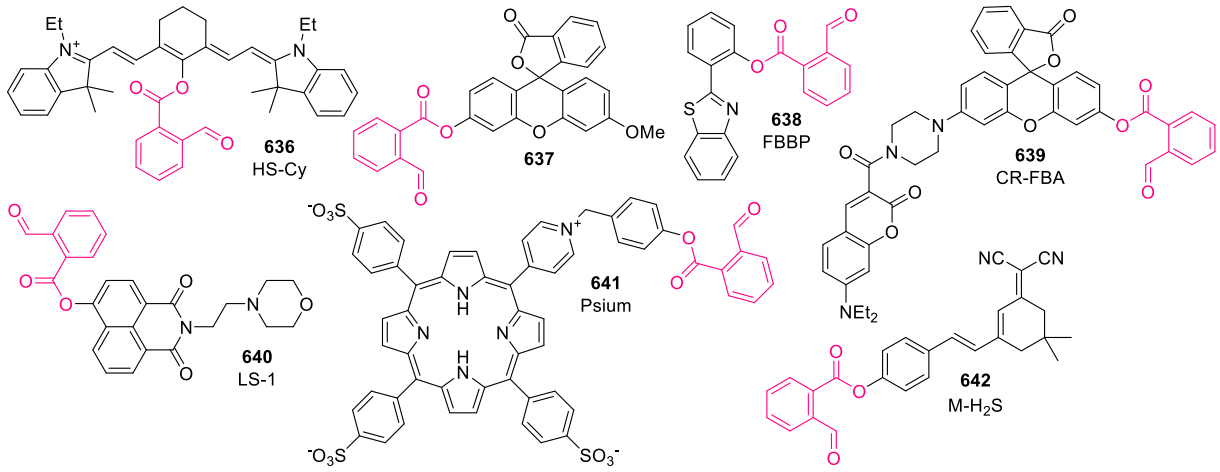


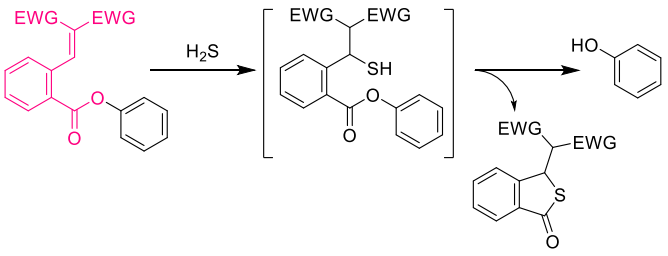
Figure 1.128. Examples of fluorescent H_2S probes based on cleavage of 2-carboxybenzaldehyde esters.

Using this same approach, Zhang reported methylfluorescein probe **637** using the 2-carboxybenzaldehyde group, which provided a 26-fold turn-on in 50% EtOH in buffer.[658] The resultant probe showed moderate selectivity over other anions and GSH and was also used to image exogenous H_2S in live HeLa cells. Goswami reported benzothiazole **638**, which provided a ratiometric response to H_2S in 20% MeCN in water and shift in emission from 359 to 462 nm.[659] This probe showed good selectivity for H_2S over other anions, Cys, and GSH although only 5 equiv. of analytes were tested and was subsequently used to image exogenous H_2S in yeast cells. Zeng reported a coumarin-rhodol platform in **639** (CR-FBA), which provides a ratiometric response upon reaction with H_2S in 10% MeCN in PBS buffer and was used to image exogenous H_2S in H9C2 cells.[660] Expanding the fluorophores that have been used with this approach, Wu and Bhuniya prepared naphthalimide **640** (LS-1), which also contains a morpholine group for lysosomal targeting.[661] The resultant probe provided a 15-fold fluorescence response at 560 nm and was used to image exogenous H_2S in MCF-7 cells as well as by two-photon excitation at 900 nm in HT-29 cells. The 2-carboxybenzaldehyde responsive group was also used with a functionalized porphyrin system by Sun and Lv to generate the probe **641** (Psium).[662] This system

relies on the H_2S mediated cleavage of the ester to generate a phenol, which then undergoes a self-immolative cascade to the release the free pyridine and result in a ~280-fold increase in fluorescence at 643 nm. Probe **641** was used to detect exogenous H_2S in HeLa cells and shown to accumulate in the mitochondria. A dicyanoisophorone-based ratiometric near-infrared probe **642** (M-H_2S) was reported by Jing and Zhang, which provided good selectivity for H_2S over other analytes and a shift in emission from 560 to 650.[663] Localization studies showed that this probe accumulated in the ER, and it was further used to detect endogenous H_2S in HeLa cells, increased H_2S production during ER stress, as well as H_2S generation in zebrafish.

1.4.4.3 Cyclization from Electron-Poor Styrenes

Using a related general approach of coupling H_2S addition with an intramolecular cyclization to cleave an esterified fluorophore, Xian reported a strategy for Michael addition of H_2S to an electron poor styrene followed by subsequent cyclization in 2012 (Scheme 1.13).[664] In this approach, addition of H_2S to the Michael acceptor generates an intermediate thiol, which then undergoes an intramolecular attack to cleave the ester of the protecting group and release the fluorophore. This approach shows good selectivity for H_2S over competing thiols because the resultant thioether formed after thiol addition cannot participate the subsequent nucleophilic cyclization.



Scheme 1.13. Addition of H_2S to an electron poor styrene and subsequent ester cleavage.

Xian applied this approach to develop **643**, which provided a 160-fold turn-on to H_2S and was used to image exogenous H_2S in COS7 cells (Figure 1.129).[664] Zeng later used this strategy to develop the ratiometric FRET-based probe **644** (H_2S-CR), which shifted emission from 470 to 541 nm upon reaction with H_2S.[665] The resultant probe showed good selectivity over competing analytes and was used to image exogenous H_2S in H9C2 cells. Zhang and Dong also expanded on

this approach to prepare the naphthalimide based probe **645**, which showed an emission maximum at 550 nm in 50% MeCN in buffer, but biological compatibility was not reported.[666]

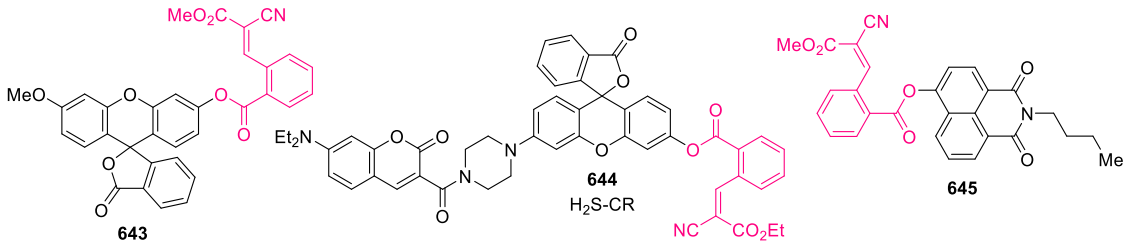
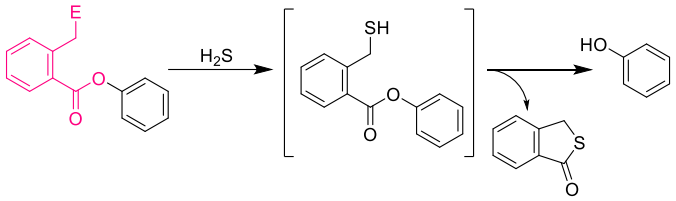


Figure 1.129. Examples of fluorescent H_2S probes based on addition to electron poor styrenes.

1.4.4.4 Addition to Benzyl Electrophiles and Subsequent Ester Cleavage

Different benzylic electrophiles have also been used to generate H_2S responsive probes using a similar nucleophilic addition, intramolecular cyclization, and protecting group removal strategy (Scheme 1.14). Unlike the earlier electrophilic dichalcogenide or Michael addition approaches, the nucleophilic displacement of benzylic electrophiles by thiols is an irreversible process. This difference means that benzylic electrophiles are more likely to be irreversibly consumed by reaction with competing thiols than other electrophilic approaches.



Scheme 1.14. Addition of H_2S to benzyl electrophiles and subsequent ester cleavage.

Guo reported benzyl iodide containing probe **646**, which reacts with H_2S to form a pendant benzyl thiol and undergoes an intramolecular cyclization to cleave the pendant ester and release a fluoresceine fluorophore (Figure 1.130).[667] This probe showed a turn-on fluorescence at 517 nm in buffer with 20 mM CTAB with good selectivity for H_2S over competing analytes, including co-incubation with Cys, Hcy, and GSH, and was further used to image exogenous H_2S in COS-7 cells. Li and Luo reported related probe **647**, which showed a 60-fold turn-on toward H_2S with an emission maximum at 466 nm, but showed eroded reactivity when H_2S was added in the presence

of thiols like Cys or GSH.[668] A related approach was reported by Niu who used a benzyl bromide electrophile and ESIPT probe to generate **648**.[669] This probe provided good selectivity toward H_2S over thiols and was used to image exogenous H_2S in HeLa cells, but the response to H_2S in the presence of Cys or GSH was not reported. Using a related approach, Kumar reported methoxyfluorescein based **649**, which contains a pendant bromide electrophile and a carbonate cleavage unit.[670] This system lacks the added electrophilicity of the prior benzyl electrophiles, but shows good selectivity for H_2S over other thiols. Probe **649** was used to image exogenous and LPS-stimulated generation of H_2S in C6 and BV-2 cells as well as in rat hippocampal slices and nematodes. Talukdar reported benzyl bromide and benzyl azide probes based on resorufin.[202] Probe **650** (Reso-Br) provides a fluorescence response at 585 nm upon treatment with H_2S. The probe shows good selectivity for H_2S over other analytes, but a significantly reduced response to H_2S in the presence of Cys, GSH, or Hcy even with 5 mM H_2S.

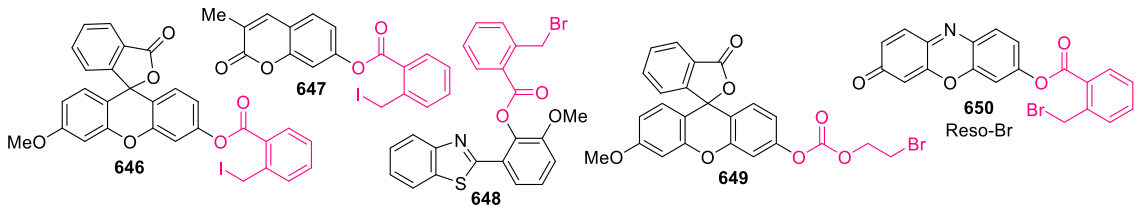


Figure 1.130. Examples of fluorescent H_2S probes based addition to aliphatic electrophiles.

1.4.4.5 Acrylate Cleavage

Acrylates have also been used as pendant electrophiles to provide turn-on responsive fluorescent probes for H_2S. For example, Chao reported cyclometalated Ir^{3+} complex **651** (IrOC) with pendant acrylic esters that are cleaved upon H_2S addition with moderate selectivity over competing analytes (Figure 1.131).[671] On the basis of the acrylate electrophilicity, the likely mechanism of activation involves Michael addition of H_2S to the acrylate and subsequent intramolecular cyclization, albeit through a 4-membered ring, to cleave the ester. Alternatively, direct H_2S-mediated ester cleavage may be operable. Probe **651** showed a luminescent response to H_2S at 500 nm, and acrylate cleavage was confirmed by mass spectrometry. This probe was also used to observe exogenous H_2S in HeLa cells. Yan and Chen also reported acrylate ester **651**, which generates fluorescence enhancement 663 nm at decrease at 800 nm in 30% EtOH in

buffer.[672] This probe showed good selectivity for H_2S over most competing analytes, although small responses to OH^-, CO_3^{2-}, Cys, and GSH were observed. The fluorescent response to H_2S was also confirmed in HeLa cells treated with exogenous H_2S. Yin and Huo reported **652**, which reacts with H_2S to generate a fluorescent response at 500 nm, whereas treatment with thiols results in a signal at 455 nm.[673] Selectivity studies also showed that **652** reacted with SO_3^{2-} to generate a larger fluorescent response at 500 nm than for H_2S, which is likely due to the more efficient 6-membered ring intramolecular cyclization for SO_3^{2-} than for the 4-membered ring for H_2S. The probe was also used to investigate SNP-derived H_2S in B16 cells and exogenous H_2S in mice.

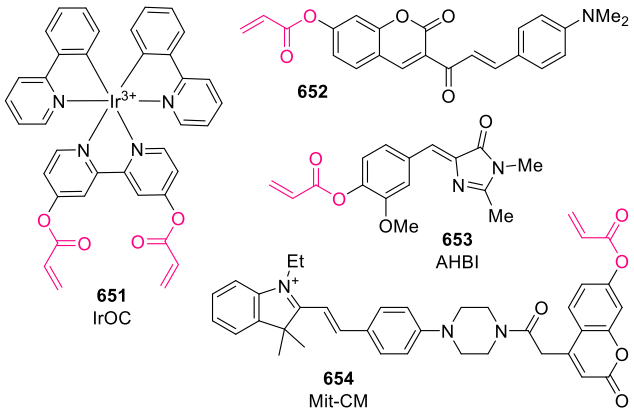
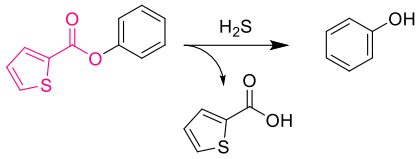


Figure 1.131. Examples of fluorescent H_2S probes based on acrylates cleavage.

Gore also reported a related approach using a chromophore related to that found in green fluorescent protein to develop **653** (AHBI).[674] Interestingly, ester cleavage was also observed with a methyl ester analogue, which suggests that 1,2-carbonyl attack, rather than a 1,4-Michael addition may be operable. These experiments were formed in unbuffered water, however, so it is also possible that the pH change upon NaSH addition impacts ester cleavage rates. Probe **653** provided a selective response for H_2S in unbuffered water over competing thiols and was used to image exogenous H_2S in HCT116 cells. Using a related approach, Qi reported ratiometric **654** (Mit-CM), which provided a turn-off response to H_2S at 596 nm and an increase in intensity at 468 upon Cys addition to the acrylate.[675] Different fluorescent responses were observed for H_2S and Cys addition, including abatement of signal with the thiol scavenger NEM, in both HepG2 cells and larval zebrafish.

1.4.4.6 Thiophene-2-carboxylic Acid Ester Cleavage

Direct H_2S-mediated ester cleavage has also been reported for thiophene-2-carboxylic acid esters (Scheme 1.15). Cleavage of thiophene ester shows empirical selectivity for H_2S over other thiols, including physiologically relevant concentrations of Cys and GSH, although the origin of this selectivity remains uncertain.



Scheme 1.15. H_2S-mediated cleavage of thiophene-2-carboxylic acid esters.

Li reported the symmetrically substituted fluorescein derivative **655**, which showed high selectivity toward H_2S over other mM concentrations of thiols and competing nucleophiles, with only minimal turn-on from ClO^-, H_2O_2, and $S_2O_3^-$ (Figure 1.132).[676] The resultant probe was used to image endogenous H_2S in live HepG2 and Raw 264.7 cells as well as exogenous H_2S in live mice. Yang used the same ester cleavage strategy to develop the coumarin-based probe **656**, which was used to investigate H_2S levels in wine and beer samples.[677] This approach was also used by Chen with coumarin derivative **657**, which showed good selectivity for H_2S over competing thiols, anions, and metal cations.[678] Probe **657** was also used to image exogenous H_2S in MCF-7 cells and mice. A similar approach was used by Yang who reported a probe **658**, which utilized a naphthalene rather than coumarin backbone and was used to investigate H_2S in wine and beer samples.[679]

The ratiometric reporter **659** (NBP-HS) based on coupling a thiophene-2-carboxylic acid esters to a merocyanine dye was reported by Zhao and provided a ratiometric response with fluorescence decrease at 520 nm and concomitant increase at 590 nm.[680] This probe was used to detect H_2S from different foodstuffs using filter paper test strips loaded with the NBP-HS dye, and the ratiometric response was also demonstrated in HeLa cells. Wang also a hepatocyte and mitochondrially targeted probe **660** (Dye-H_2S-Gal), which showed a strong fluorescent enhancement at 545 nm upon treatment with H_2S and good selectivity over competing analytes.[681] This probe was also used to investigate H_2S generation in HepG2, A549, HeLa, and SGC-7901

cells. Also using a targeting approach, Wang and Wang reported lysosome targeted **661** (Rh-Lyso-H_2S), which provides a fluorescence turn-on at 550 nm and good selectivity for H_2S over competing anions and thiols.[682] This probe was confirmed to localize to the lysosome and demonstrate to image exogenous H_2S in HepG2 cells.

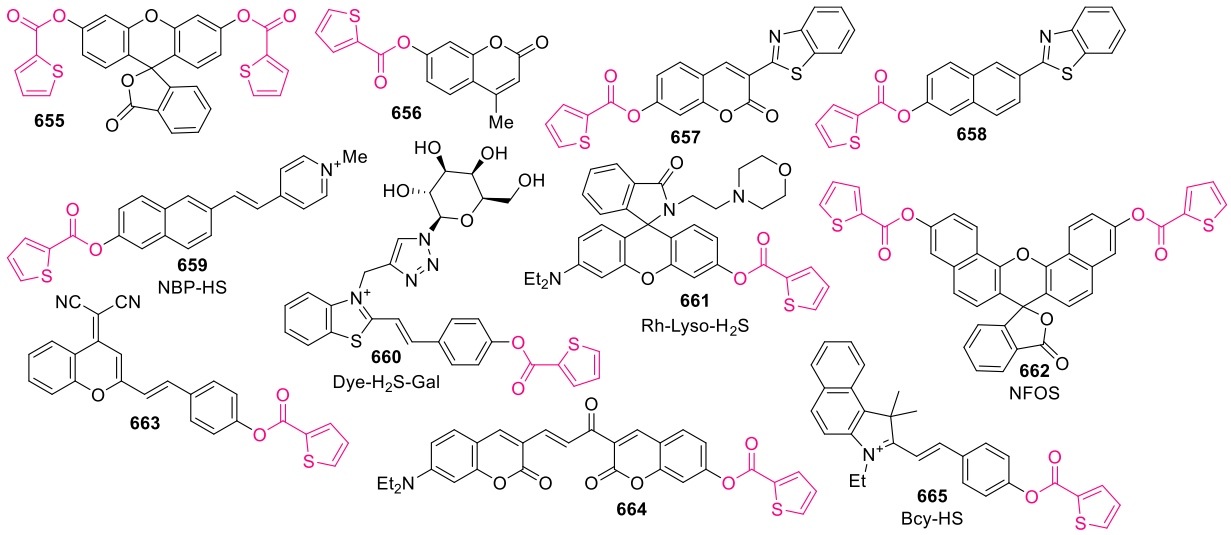


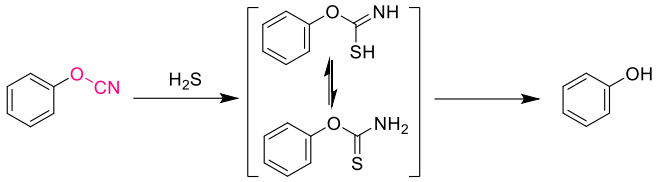
Figure 1.132. Examples of fluorescent H_2S probes based on thiophene-2-carboxylic acid ester cleavage.

Zhou and Jin used a similar activation approach to develop the naphthofluorescein based probe **662** (NFOS), which showed red-shifted emission at 680 nm and was used to image exogenous H_2S in HeLa cells.[683] A similarly red-shifted probe **663**, was reported by Jin and She.[684] This probe was used to image exogenous H_2S in HeLa cells and also used to prepare fluorescent nanofibrous films for detection of H_2S in different solutions. Wang and Long reported the coumarin derivative **664**, which also uses the thiophene ester for H_2S detection and an additional α,β-unsaturated ketone to react with thiols.[685] Upon addition of H_2S, a rapid fluorescence response at 585 nm was observed, and further reaction with thiols at the α,β-unsaturated ketone resulted in subsequent formation of a blue emissive adduct at 480 nm. Probe **664** was used to investigate H_2S and Cys responses in PC12 and HeLa cells as well as tissue from Chinese cabbage grown with different amounts of H_2S. Huang, Chen, and Lv also reported a red-shifted benzoindocyanine probe **665** (Bcy-Hs), which provides a fluorescent enhancement at 620 nm and good selectivity over different anions, cations, and thiols.[686] This probe was subsequently used to investigate

exogenous and endogenous H_2S in RLE-6TN and MRC-5 cells by fluorescence imaging and flow cytometry as well as to investigate H_2S levels in mouse models of pulmonary fibrosis in vivo.

1.4.4.7 Cyanate Ester Cleavage

Electrophilic cyanate esters have also been used as protecting groups to develop H_2S probes (Scheme 1.16). H_2S addition to the cyanate eseter results in formation of a thiocarbamate, which decomposes to produce the parent phenol product. Although not investigated directly, this intermediate is likely hydrolyzed by water to form thiocarbamic acid.



Scheme 1.16. H_2S-mediated deprotection of electrophilic cyanate esters.

As an example of this approach, Mrullahoğlu reported 3-hydroxyflavone based probe **666** (FLVN-OCN) as a selective reporter for H_2S in 2016 (Figure 1.133).[687] This probe provided good selectivity for H_2S over other competing anions and amino acids, although a small response to GSH was reported. The probe was also used to image exogenous H_2S is A549 cells. Expanding on this approach, Berreau reported flavonol based **667**, which reacts with H_2S to generate H_2S to generate a fluorescent response at 582 nm, which was further confirmed with exogenous H_2S in HUVECs.[688] The resultant alcohol product could also be phototriggered to release CO in the presence of O_2, which was further used to use this compound as a logic gate sensor. Yan reported naphthalimide **668**, which provides a ratiometric response with a fluorescence decrease at 448 nm and increase at 552 nm when treated with H_2S.[689] Probe **668** showed good selectivity toward competing analytes, including thiols, and was used to image exogenous H_2S in HeLa cells. Lv used this approach to report red shifted **669** (DCM-OCN), which reacts with H_2S to generate a response at ~690 nm.[690] This probe was found to provide a stronger fluorescence response in the presence of CTAB and was used to investigate H_2S levels in different water samples.

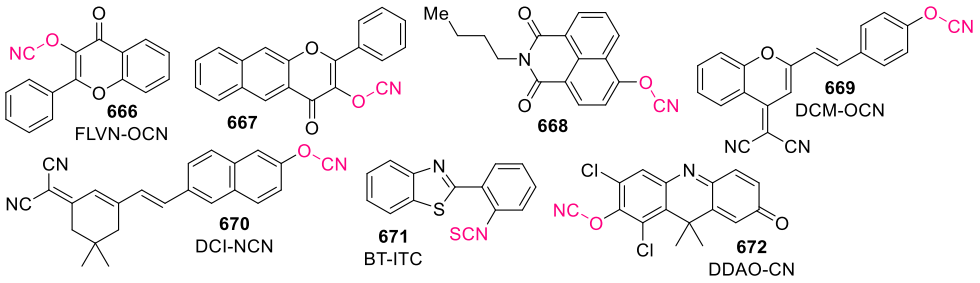
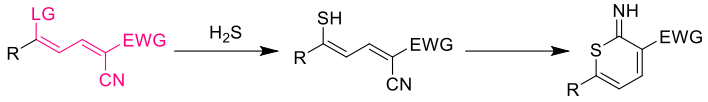


Figure 1.133. Examples of fluorescent H_2S probes based on cyanate ester and thiocyanate cleavage.

Using a dicyanoisophorone chromophore, Yang reported **670** (DCI-NCN), which provided a fluorescence response at 618 nm.[691] This probe was used to detect exogenous H_2S in MDA-MB-231 cells and Kunming mice. Building from a dichloroacridone scaffold, Gao and Zhou also used this strategy to generate **671** (DDAO-CN).[692] This probe provides a red-shifted fluorescence response at 658 nm in response to H_2S, and good selectivity for H_2S over other competing analytes although minor probe activation was observed for SCN^-. Probe **671** was also adsorbed to test strips to study H_2S generation from different foods and further used to image exogenous H_2S in HeLa cells. Modifying this general approach slightly, Jang also reported an isothiocyanate rather than a cyanate as an H_2S-responsive motif.[693] Conversion of an aminophenyl benzothiazole to the corresponding isothiocyanate generated **672** (BT-ITC), which provided a fluorescence response when treated with H_2S. A moderate fluorescence response was also observed from Cys, which matches prior work on known reactions of Cys with isothiocyanates.[694-696] This probe was also used to investigate H_2S in different water sources and image exogenous H_2S in HeLa cells.

1.4.4.8 Addition to Conjugated Systems and Cyclization

Electron poor conjugated systems have also been used as platforms for H_2S detection based on the nucleophilic addition of sulfide followed by intramolecular addition into a nitrile to incorporate the sulfur atom into a heterocyclic thiopyran imine product (Scheme 1.17). Related cyclization approaches have also been used with H_2S-selective cleavage groups as described earlier in this Review. The general benefit of the addition followed by cyclization approach is that the reaction should be subsequent intramolecular cyclization should be selective for H_2S over other thiols based the ability of H_2S to participate in two sequential nucleophilic additions.



Scheme 1.17. General approach for H_2S addition to electron poor conjugated systems and subsequent cyclization.

Wang and Zhang reported an early example of this approach with the conjugated coumarin **673**, with sites for both H_2S and GSH addition that resulted in fluorescent turn-on responses at 564 nm and 517 nm, respectively (Figure 1.134).[697] This different response was also demonstrated by exogenous addition of these analytes in MCF-7 cells. This same approach, but with a selenol leaving group, was reported by Song to develop **674** (PhSeCou), which also could differentiate between H_2S and GSH.[698] This probe was additionally used to image H_2S and Cys-derived H_2S in HepG2 cells. Han also provided two independent reports in 2018 of extending the conjugation outside of the fluorophore backbone with coumarin-based **675** (FZ-1)[699] and indole-based **677** [700] Probe **675** provides a different fluorescent responses for H_2S and thiols, with H_2S addition resulting in a response at 490 nm whereas GSH addition resulted in a signal at 505 nm. This probe was used to image GSH and H_2S independently in MCF-7 cells. Using modified **677**, reaction with H_2S results in formation of a red but non-fluorescent product, whereas reaction with Cys/Hcy provides a fluorescent signal.

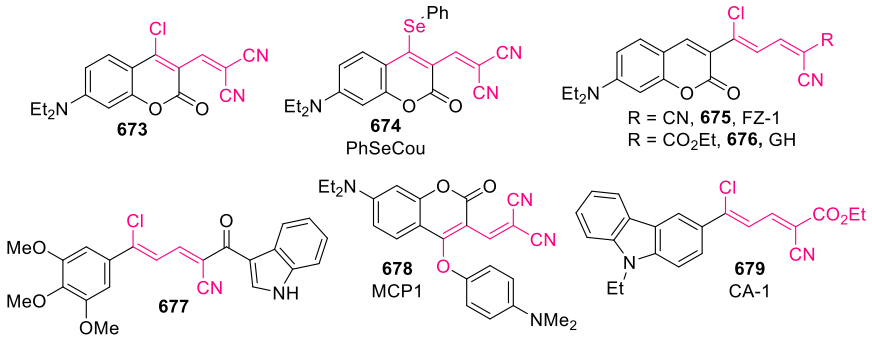


Figure 1.134. Examples of fluorescent H_2S probes based addition to electron poor conjugated systems and subsequent cyclization.

A similar coumarin motif using a ethyl ester rather than a nitrile was reported by Liu in probe **676** (GH), which had similar spectroscopic properties and was used to develop paper test strips for use with smartphone-based H_2S detection.[701] Chen, Sheng, and Song reported a related

approach in which the dicyanoethylene motif is directly attached to the chromophore to generate **678** (MCP1).[702] This probe provides different responses to H_2S, thiols, and polysulfides, with fluorescent enhancements at 508, 469, and 576 nm, respectively. Further applications were focused on investigating H_2S and polysulfide formation from LPS and Cys addition to Raw 264.7 cells. As a further example, Yin reported **679** (CA-1), which generated a turn-off response at 577 nm upon addition of H_2S.[703] This turn-off response was selective for H_2S and also demonstrated in HepG2 cells and Chlorella.

Also using an addition-cyclization approach, Zhang and reported a related system in which addition of H_2S into an electron poor phenothiazine ethylidene malononitriles results in reductive cleavage to form a thiophene product (Figure 1.135).[704] Using this approach, probes **680**–**683** (PTZ-P1–4) were prepared. For **682** and **683**, the inclusion of different fluorophores provided a fluorescent response upon reaction with H_2S at 540 and 628 nm, respectively, although a DMSO co-solvent was required for solubility. Both probes showed good selectivity for H_2S over competing analytes, and **683** was used to image exogenous H_2S in HeLa cells. In addition, this probe was used to image endogenous H_2S in *C. elegans*, including enhanced H_2S levels in germline-deficient *glp-1* mutants and decreased H_2S from cystathionine γ-lyase deletion *cth-1* mutants (Figure 1.136). Zhang further expanded on this approach to investigate structure-reactivity relationships for C=C bond substitution for the H_2S-mediated reductive cleavage including optimized compounds **684** and **685**, both of which were used to image exogenous H_2S in HeLa cells.[705]

In a related example, Mahapatra reported **686**, with a different electrophile arrangement that also resulted in H_2S-mediated addition and subsequent cyclization (Figure 1.137).[706] Reaction with H_2S generated a ratiometric response with a fluorescence decrease at 408 nm and concomitant increase at 463 nm. This approach showed good selectivity for H_2S over competing thiols and was also used to image exogenous H_2S in Vero cells.

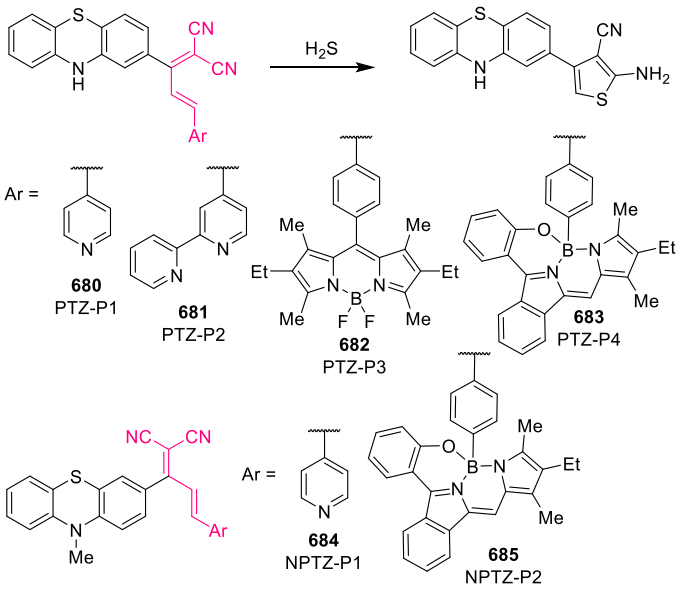


Figure 1.135. Examples of fluorescent H_2S probes based reductive cleavage followed by thiophene formation.

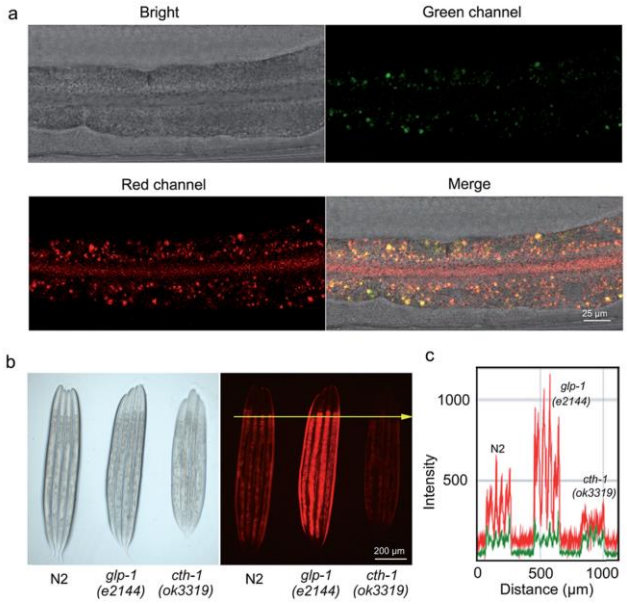


Figure 1.136. (a) Fluorescent images captured the H_2S distribution in *C. elegans* wild type N2 treated with 200 μM of **683**. (b) Fluorescence imaging of endogenous H_2S in wild type N2, germline-deficient *glp-1* and *cth-1* mutants. (c) Associated fluorescence intensities across the anterior of the intestine. Reproduced with permission from ref [704]. Copywrite 2018 Royal Society of Chemistry.

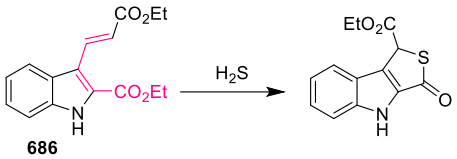
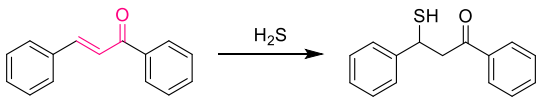


Figure 1.137. Additional example of H_2S mediated reductive cleavage followed by thiophene formation to form a fluorescent product.

1.4.4.9 Addition to α,β-Unsaturated Ketones

Continuing with the strategy of H_2S addition to electron-poor conjugated systems, the direct addition of H_2S to α,β-unsaturated ketones has also been used for H_2S detection (Scheme 1.18). The general approach of H_2S addition to α,β-unsaturated ketones followed by subsequent cyclization into a pendant electrophile has been discussed earlier as an H_2S sensing approach. In addition to these earlier methods, such H_2S addition has been used as a method to disrupt longer-range conjugation of a chromophore and provide a change in optical response. In such examples, the direct attack of HS^- to the alkene and subsequent tautomerization of the enolate intermediate results in formal addition of H_2S across the alkene.



Scheme 1.18. General approach for H_2S addition to an α,β-unsaturated ketone.

Using this approach, Ding and Zhu reported a benzimidazole conjugated to an electron poor α,β-unsaturated ketone to generate **687** (Figure 1.138).[707] This probe reacted with H_2S to abolish fluorescence quenching from the conjugated nitrobenzene motifs and provide a fluorescence enhancement at 450 nm with good selectivity for H_2S over competing thiols. Shang used this same approach to develop anthracene-based **688**, which was investigated in DMSO.[708] This probe provides a turn on response at 420 nm, which was attributed to the addition of 2 equiv. of H_2S addition across the alkene. Yang and co-workers reported a naphthalene based probe with the same H_2S reactive motif to generate **689**.[709] This probe also contains a thiocarbonate motif for Hg^{2+} detection, which was used to demonstrate different responses to H_2S and Hg^{2+}. In addition, hydrazine (N_2H_4) was shown to also react with the electron poor α,β-unsaturated ketone to provide

a different optical response. The resultant probe was used to develop test strips for these three analytes.

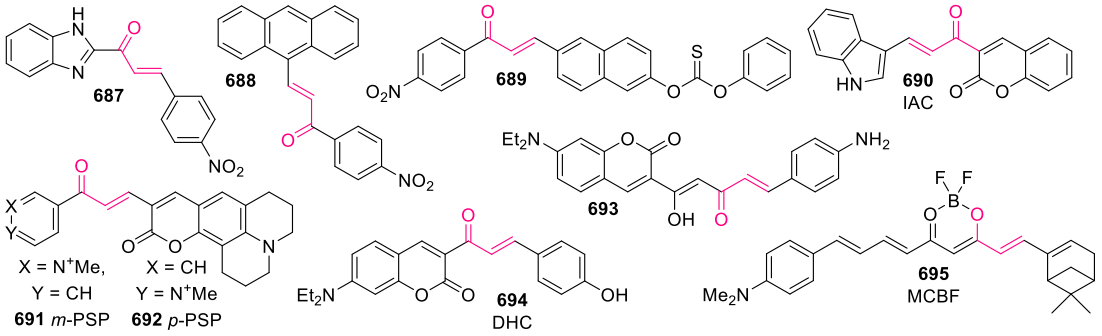
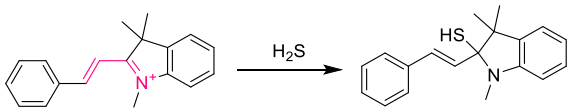


Figure 1.138. Examples of fluorescent H_2S probes based addition across an α,β-unsaturated ketone.

Expanding to other electrophiles, Bai and Wang reported coumarin indole adduct **690** (IAC), which showed a fluorescence response at 580 nm upon reaction with H_2S in 60% DMF in buffer.[710] Using pyridinium motifs instead of nitro groups as electron withdrawing motifs, Zhang and Qian reported the two probes **691** (*m*-PSP) and **692** (*p*-PSP), which generated turn-on fluorescent responses at ~510 nm upon reaction with both SO_3^{2-} and H_2S.[711] This response was selective for these two analytes over other competing thiols. Probe **692** was further used to image exogenous H_2S in L929 cells. Also using a coumarin-based platform but with an aniline motif, Wang and Yang reported **693**, which responds to both H_2S and Cu^{2+}.[712] Reaction with H_2S results in a shift in fluorescence from 577 nm to 452 nm, which was used to investigate H_2S levels in different water samples and also image exogenous H_2S in zebrafish. Liu further expanded coumarin platforms to phenol-based **694** (DHC).[713] This probe showed a decrease in fluorescence at 556 nm upon addition of H_2S in 50% EtOH in water, and this turn-off response was confirmed with exogenous H_2S in BHK cells. As an additional related example, Wang and Wang reported **695** (MCBF), which incorporates BF_2 addition to the dione of the probe.[714] Reaction with H_2S resulted in a fluorescent turn-on response at 620 nm, which showed good selectivity for H_2S over competing anions, GSH, Cys, and Hcy. This probe was further used to investigate H_2S levels in different wine samples.

1.4.4.10 Addition to Conjugated Indolium Motifs

The high nucleophilicity of HS^- has also been used to develop fluorescent probes for H_2S based on addition to conjugated indolium motifs and subsequent disruption of the extended conjugation. Different reactivity modes have been reported, including single and double Michael addition conjugated alkenes as well as direct addition to the indolium, with the latter being most prevalent and supported in the literature. It is possible that addition in different electrophilic positions may occur depending on the exact electronic structure of individual motifs, but for general simplicity we are focusing on direct addition to the electrophilic indolium C2 carbon (Scheme 1.19). We note that conjugated indolium moieties have been incorporated as fluorophore components in other classes of H_2S reported discussed elsewhere in this Review, so it is possible that the differences in the electrophilicity of specific indolium moieties may govern H_2S reactivity in these systems.



Scheme 1.19. General approach H_2S addition into conjugated indolium motifs.

As an example of this approach, He and Guo reported coumarin-indolium conjugate **696** (CouMC),[715] which reacts with H_2S to provide a ratiometric response with fluorescence decrease at 652 nm with concomitant growth of a new peak at 510 nm (Figure 1.139). This probe showed good selectivity for H_2S over other competing anions, nucleophiles, and thiols. With this design, the addition of HS^- to the indolium should be chemically reversible at sufficiently acidic pH. Such chemical reversibility was demonstrated by adjusting the pH to 2.5 after addition of H_2S, which resulted in regeneration of the parent probe. Probe **696** was also used to image exogenous H_2S in MCF-7 cells and were shown to accumulate in the mitochondria (Figure 1.140).

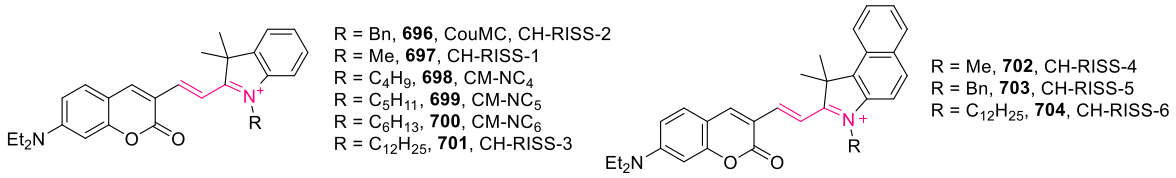


Figure 1.139. Examples of fluorescent H_2S probes based on addition into indolium motifs conjugated to coumarin chromophores.

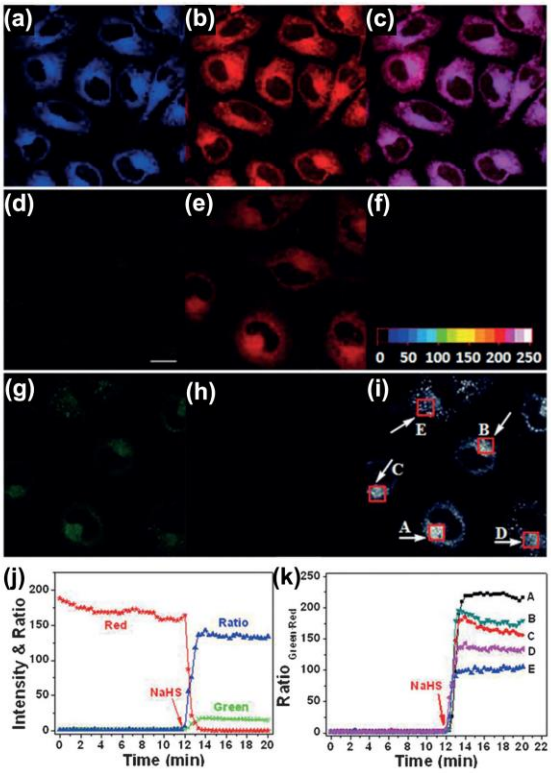


Figure 1.140. (a-c) MCF-7 cells treated with 10 μM of **696** and mitochondrial marker Deep red. (a) Pseudocolor image of 660-750 nm band excited at 488 nm, (b) image of 660-750 band exciting at 633 nm, and (c) overlay channels. (d-k) Images of MCF-7 cells monitoring dual emission mode of excitation at 488 nm. (d,f) Include incubation with 10 μM of **696**. (g-i) Include pre-incubation with 10 μM of **696** followed by 200 μM of NaSH. Panels (d,g) correspond to 500-560 nm), (e,h) correspond to 650-799 nm, and (f,i) correspond to ratiometric images. Panels (j) and (k) show temporal profiles of area of interest 'D' and other regions, respectively. Reproduced with permission from ref [715]. Copyright 2013 John Wiley and Sons.

Using a structurally similar motif, Yin and Huo reported **697**, which showed a similar response to **697** in MeOH in buffer and demonstrated to detect exogenous H_2S in HepG2 cells.[716] Chen and He later optimized performance of related coumarin-indolium derivatives by modifying the lipophilicity of the *N*-alkyl chain to report **698**–**700** (CM-NC_4, CM-NC_5, and CM-NC_6) with methyl, butyl, pentyl, and hexyl chains, respectively.[717] They found that increasing the lipophilicity of the alkyl chain resulted in faster reaction with H_2S. Each of these probes was used to investigate exogenous H_2S imaging in MCF-7 cells, and **700** was also demonstrated to image exogenous H_2S in live mice. Chen and Li later reported a series of coumarin hemicyanine scaffolds, including examples described above in **696**, **697**, and **700**–**704** (CH-RISS-1–6), that provided a ratiometric response with fluorescence decrease at 650–660 nm and increase at 480-505 nm depending on the

scaffold.[718] These probes were found to show responses to H_2S, polysulfides as well as $S_xO_y^{n-}$ anions and were used to image exogenous H_2S in L929 cells.

Chen and He also reported also reported amide-functionalized **705** (CouMa) for H_2S detection in the cytosol, which showed good selectivity for H_2S over Cys, Hcy, and GSH and was used to image exogenous and Cys, and SNP-derived H_2S in MCF-7 cells (Figure 1.141).[719] The scaffold was further elaborated by to develop **706** (CouPa) and **707** (CouDE), with the latter being found the localize in the mitrochondria. Probe **707** was used to image exogenous and endogenous H_2S in MCF-7 cells and Hep3B cells as well as differences in H_2S in HCT116 tumor-bearing mice.[720] Chen and He also used this approach to develop FRET based probes based on the coumarin-indolium core conjugated to a secondary chromophore based on either NBD or naphthalimide motifs **708** (NBD-CMC) and **709** (Nap-CMC), respectively.[721] Both systems provided a ratiometric response upon reaction with H_2S with an increase at 530 nm and decrease at 665 nm with good selectivity for H_2S over competing analytes. In addition, both probes were used to image exogenous and endogenous H_2S in HepG2 cells. Miao and Zhao expanded on this approach to introduce a piperazine linker between the coumarin and indolium motifs to develop **710** (CPC).[722] Much like related derivatives, this probe provided a ratiometric response with an increase at 474 nm and decrease at 587 nm. The resultant probe was used to image exogenous H_2S in HeLa cells and differences in endogenous H_2S levels upon treatment with Cys or CBS/CSE inhibitors PAG and AOAA.

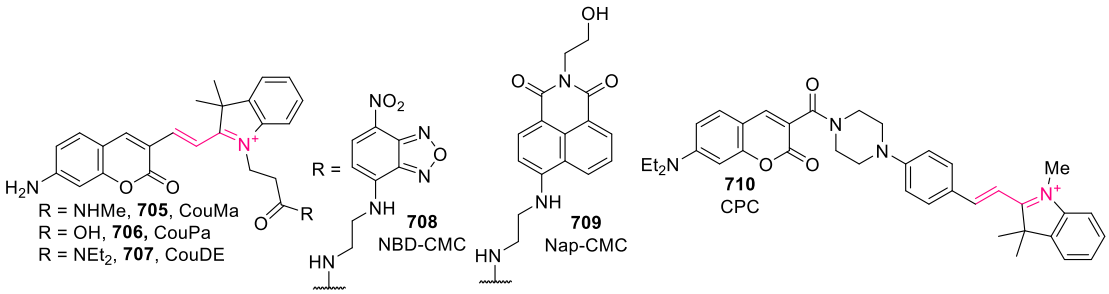


Figure 1.141. Additional examples of fluorescent H_2S probes based on addition into indolium motifs conjugated to coumarin chromophores.

Expanding to a conjugated naphthalimide, Li and Yu reported **711** (IDNA), which provides a ratiometric response to H_2S in 40% DMSO in buffer with an increase at 510 nm and concomitant decrease at 620 nm (Figure 1.142).[723] This probe was demonstrated to localize to the mitochondria

and also used to provide ratiometric imaging of exogenous H_2S in HeLa cells. Li used a related intramolecular charge transfer (ICT) approach to develop **712**, which provided a turn-off response upon reaction with H_2S.[724] This probe showed good selectivity for H_2S over competing anions and thiols, and the turn-off response to exogenous H_2S was confirmed in HeLa cells. Extending the conjugation with a quinoline system, Yin reported **713**, which provides a ratiometric response with increase at 470 nm and concomitant decrease at 572 nm.[725] This probe also showed good selectivity for H_2S over competing analytes and was subsequently used to image exogenous and SNP-derived H_2S in HeLa cells and also exogenous H_2S in mice. Adding an additional indolium motif, Sun and Ge reported **714**, which provided a turn-on response at 657 nm, showed good selectivity for H_2S over competing anions, amino acids, and thiols, and was subsequently used to image exogenous and Cys-derived H_2S in HeLa cells.[726]

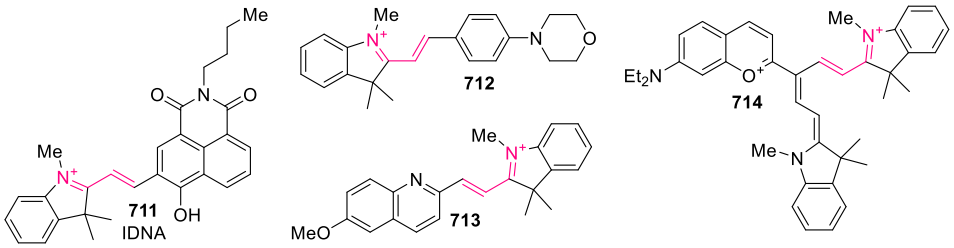


Figure 1.142. Additional examples of fluorescent H_2S probes based on addition into indolium motifs.

Wang and Wang reported a series of Si-rhodamine derivates including **715**–**717** (Indo-SiR, Mindo-SiR, Hindo-SiR) that provided similar fluorescent turn-on responses near 680 nm in response to H_2S (Figure 1.143).[698] These probes were further used to image H_2S in live mice and also investigate H_2S accumulation in different organs *ex vivo*. In addition, **716** was also used to investigate differences in H_2S levels in brains of normal and schizophrenic mouse models, with the latter group exhibiting higher H_2S levels. Expanding the fluorophore platforms for this approach, Lin reported a BODIPY conjugate based disruption of a twisted internal charge transfer (TICT) process to develop **718** (BH-HS).[727] The parent probe is non-fluorescent due to TICT from the BODIPY to the indolium motif, which is abolished upon reaction with H_2S to restore the fluorescence. This probe provided a fluorescence response at 535 nm in 50% DMF in buffer and was used to image exogenous and Cys-derived H_2S in HeLa cells. Using a related approach with different fluorophore partners, Goswami reported a benzothiazole-indolium adduct in **719** (BHD),

which reacts with H_2S to generate a ratiometric response in 40% MeCN in buffer with fluorescence increase at 428 nm and decrease at 570 nm.[728] The probe was used to image exogenous H_2S in Raw 264.7 cells and also used to develop paper test strips. Lu and Guo also used this approach to develop the dihydroxanthene indolium probe **720** (CyT), which also provided a ratiometric response to H_2S with an increase at 595 nm and decrease at 655 nm that was used to image exogenous H_2S in HeLa cells and zebrafish.[729] A related approach was reported by Zeng used a thiodihydroxanthene scaffold to generate **721**.[730] This probe also showed a turn-on rather than ratiometric response at 455 nm in a 50% EtOH in buffer and was used to image exogenous H_2S in HeLa cells and difference in H_2S levels upon treatment with H_2O_2 or PMA.

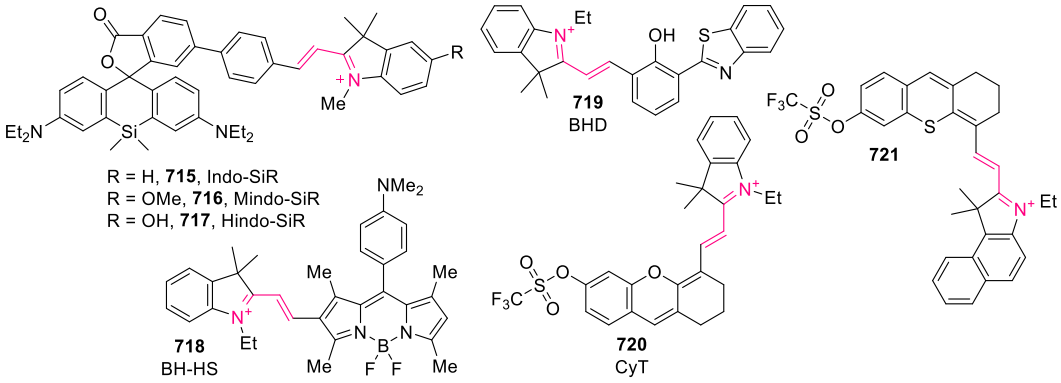


Figure 1.143. Additional examples of fluorescent H_2S probes based on addition into indolium motifs conjugated to choromophores.

Jiang reported the hydrophobic tetraphenylene **722** (TPE-indo), which reacts with H_2S to generate an AIE response (Figure 1.144).[731] The resultant aggregate system was used to image exogenous H_2S in HeLa cells and HUVECs. Wang and Wang used a related approach to incorporate two indolium motifs **723** (TBE-Indo), which also provided an AIE response and was used to image H_2S in HUVEC and MCF-7 cells as well 4T1 tumor-bearing mice.[732]

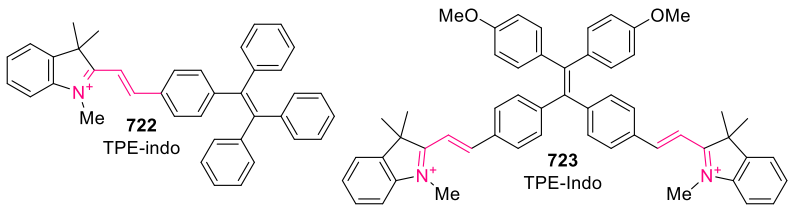


Figure 1.144. Examples of fluorescent H_2S probes based on addition into indolium motifs with an AIE response.

Expanding to two-photon excitation approaches, Lin reported **724** (TP-PMVC), which was also found to accumulate in the lysosome (Figure 1.145).[733] This probe provided a turn-on fluorescence response at 550 nm in pH 4.4 buffer, was used to investigate endogenous H_2S in the lysosomes of A549 cells, and was also used for two-photon imaging using excitation at 960 and 810 nm. Lin reported a similar pyridinium scaffold in **725** (TP-MIVC), which was designed to intercalate with RNA and also react with H_2S.[734] The probe showed a fluorescence response for H_2S and also for RNA but not DNA, and allowed for differentiation between H_2S and RNA signals based on the different excitation and emission profiles. This approach was expanded to investigate signals from RNA and H_2S in HeLa cells, zebrafish, mice, and excised mouse tumors.

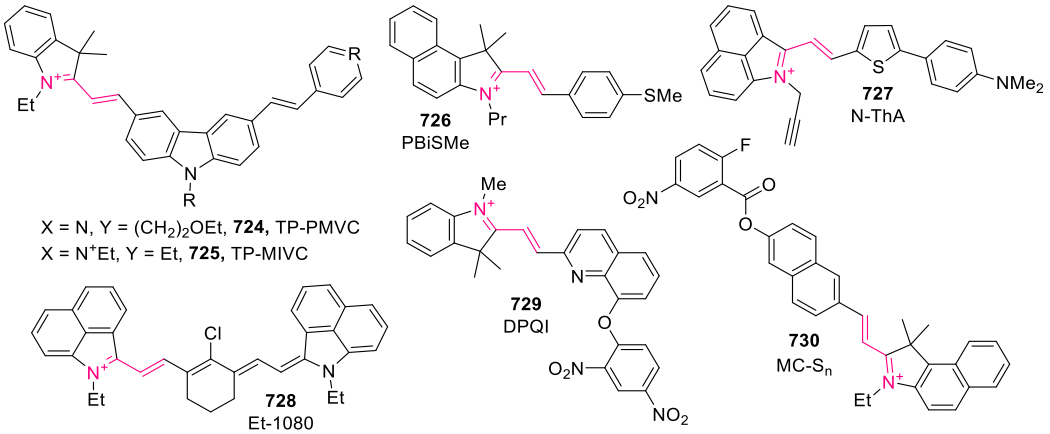


Figure 1.145. Additional examples of fluorescent H_2S probes based on addition into indolium motifs with additional reactivity.

Velmathi used a naphthyl indole to generate **726** (PBiSMe), which provided a fluorescence response to H_2S at 465 nm, although this probe also reacted with but did not provide a fluorescent response for CN^-.[735] This probe was also demonstrated to image exogenous H_2S in HCT-116 cells. As an additional example of sulfur incorporation, Yin reported thiophene conjugated **727** (N-ThA), which provides a response to both H_2S and changes in viscosity due to changes conjugation and free rotation around the extended chromophore upon H_2S addition and increased viscosity, respectively.[736] This probe was used to image exogenous H_2S in PC12 cells and also in tumor models in live mice. Expanding to longer conjugation, Chang reported **728** (Et-1080), which reacts with H_2S to abolish the fluorescent signal at 1060 nm.[737] This probe showed a high selectivity for H_2S, but was not used further for additional investigations. Further expanding this detection

approach, Mahapatra reported bifunctional probe **729** (DPQI) with two different site for H_2S detection.[738] Lower concentrations of H_2S cleave the DNP group, whereas higher concentrations resulted in addition to the indolium motif. This difference in reactivity also may suggest that the DNP group than the conjugated indolium toward H_2S. The resultant probe was used to investigate H_2S in water samples and also different concentrations of exogenous H_2S in Vero cells. Expanding to dual reactive probes, Qi reported **730** (MC-S_n) with a second reactive site for polysulfides (*vide infra*).[739] Reaction with H_2S generated a turn-on response at 519 nm, whereas reaction with polysulfides results in a response at 486 nm. This probe was demonstrated to detect exogenous H_2S and polysulfides in liver slices and also larval zebrafish using two-photon excitation at 780 nm.

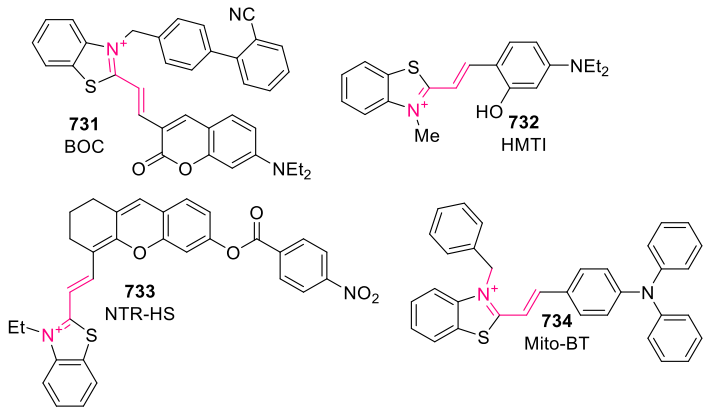


Figure 1.146. Examples of fluorescent H_2S probes based on addition into conjugated benzothiazolium motifs.

Modifying the indolium to a benzothiazolium group, Jiang and Zheng reported **731** (BOC), which provided a ratiometric response with fluorescence decrease at 652 nm and increase at 492 nm upon treatment with H_2S in 70% MeCN in buffer (Figure 1.146).[740] This probe showed good selectivity for H_2S over other analytes and was used to image exogenous H_2S in HeLa cells. Liao and Fan developed **732** (HMTI), which provided a turn-off response to H_2S in 50% DMSO in water and was used to image exogenous H_2S in HeLa cells.[741] In a related approach, Liu and Xu developed **733** (NTR-HS) with a red-shifted emission at 760 nm in response to H_2S.[742] This probe was confirmed to localize to the mitochondria and was further used to image H_2S in HeLa and HCT116 cells. Jiang and Zheng also reported a related triphenyl amine motif conjugate to develop **734** (Mito-BT), which provides a ratiometric response with fluorescence decrease at 645 nm and

increase at 525 nm in 75% EtOH in water.[743] This probe showed good selectivity for H_2S over other analytes, accumulated in the mitochondria, and was used to image exogenous H_2S in HeLa cells.

1.4.4.11 Additional Electrophilic Approaches

In an interesting and related example, Li reported a spiropyran functionalized fluorescent probe **735** (FMC) (Figure 1.147).[744] Spiropyrans are in equilibrium with indolium constructs, and this equilibrium has used previously as a light-activated photoswitch. Probe **735** is non-fluorescent in the spiropyran configuration but generates a fluorescent response at 525 nm upon addition of H_2S and generation of the parent fluorescein chromophore. This probe showed good selectivity for H_2S over competing analytes and was used to image differences in HEp-2 cells pretreated with PAG or Cys.

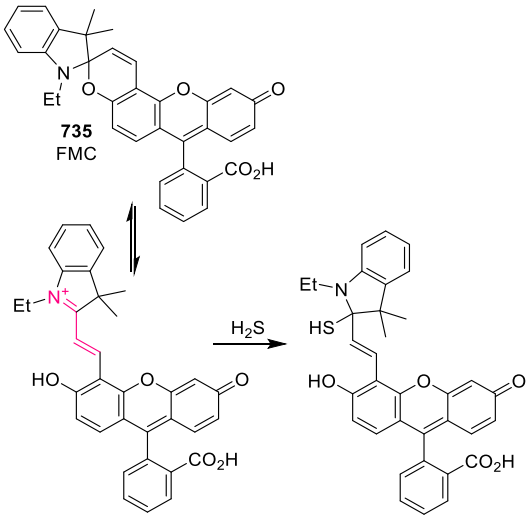
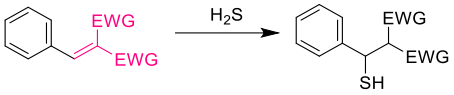


Figure 1.147. Examples of H_2S addition to a spiropyran based system.

Related approaches have also been used to disrupt conjugation by H_2S addition to highly electron withdrawn conjugated systems to modulate the fluorescent properties of the parent fluorophore (Scheme 1.20). This general approach is related to approaches described in section 4.4.3, but without the subsequent intramolecular attack to result in ester cleavage. Because the approach described in Scheme 1.20 disrupts conjugation, it generally results in ratiometric rather than turn-on responses, but can also be influenced by nucleophilic thiols.



Scheme 1.20. General approach of H_2S addition to electron poor alkenes.

As an example of this approach, Dong, Zheng, and Zhao reported BODIPY conjugate **736** (BDP-680), which reacts with H_2S to generate a 40-fold turn-on response at 683 nm in 80% MeCN in buffer (Figure 1.148).[745] This probe showed good selectivity for H_2S over competing anions and thiol analytes and was used to image exogenous H_2S in SMMC-7721 cells. Hong, Meng, and Zhang used a similar approach to develop **737** (PR), in which H_2S addition to the electron poor conjugated alkene abolishes ICT between the phenothiazine and electron poor motif.[746] Reaction with H_2S generates a 34-fold fluorescent response at 596 nm in 70% DMF in buffer, and this probe was used to investigate Cys-derived H_2S and also basal H_2S levels in inflammation models in mice. Tang also reported a related approach in which a dicyanoethylene motif was appended to a tetraphenylpyrazine to generate the aggregation induced luminogen **738** (TPP-PDCV) that was shown to function in 90% DMSO in buffer.[708] In this system, the turn-on response was attributed to H_2S addition and reductive cleavage to the alkene to form a thiol, which was subsequently oxidized to the disulfide. Zhou and Wang reported a related approach to generate **739** (SO-CN), which reacted with both H_2S and N_2H_4 to shift the initial fluorescence at 604 nm to 532 nm or 442 nm, respectively, in 60% DMSO in buffer.[747]

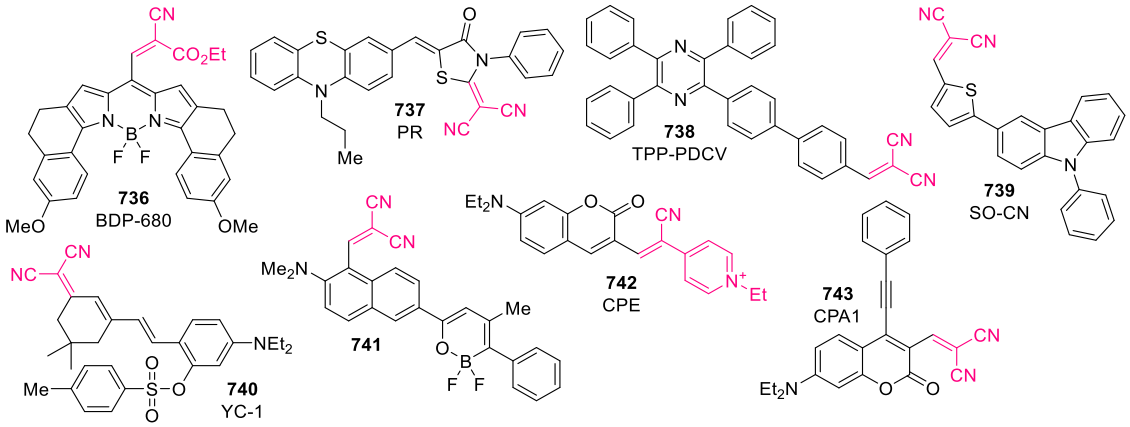


Figure 1.148. Examples of fluorescent H_2S probes based addition to electron poor alkenes.

Yin also reported a dicyanoethylene based **740** (YC-1), which contains a conjugated electron poor motif and pendant aryl sulfonate.[748] This probe shows a ratiometric response with an increase at 540 nm and decrease at 660 nm in 60% DMSO in buffer. The probe activation mechanism was proposed to be sulfonate cleavage, although this may be competitive with addition into electron poor Michael acceptor. Moderate selectivity for H_2S over Cys and other thiols was reported, and the resultant probe was used to detect exogenous or SNP-generated H_2S in HepG2 cells. Hong reported a derivatized oxazaborine with a dicyanoethylene motif in **741**, which provided a fluorescence turn-on to both SO_3^{2-} and H_2S with selectivity depending on the MeCN to buffer ratio.[749] By including an electron withdrawing pyridinium, Fang, Wang, and Dong developed the mitochondrially-targeted probe **742** (CPE), which provided a turn-off response to both H_2S and SO_3^{2-}.[750] This probe was also used in live cells to investigate changes in signal upon addition of the mitophagy inducer carbonyl cyanide *m*-chlorophenyl hydrazone (CCCP). Wang and Song also used the dicyanoethylene motif to generate probe **743** (CPA1), which reacted with both SO_3^{2-} and H_2S to generate fluorescent responses at 565 nm and 500 nm, respectively.[751] This difference in fluorescence was attributed to additional addition of H_2S across the alkyene. The resultant fluorescent responses to SO_3^{2-} and H_2S were different than the minor turn-off response to Cys, Hcy, and GSH. The different fluorescent response to SO_3^{2-} and H_2S was further demonstrated in HeLa cells and zebrafish with exogenous RSS.

In a different sequence of reactivity from the above systems, Xu and Wang reported the reaction of a 2,3-dicarbonitrile derivative **744** (OPD), which undergoes an interesting H_2S-mediated rearrangement that undergoes a subsequent oxidation to form a final fluorescent product (Figure 1.149).[752] This probe provided a fluorescent enhancement at 571 nm upon reaction with H_2S and was further used to image exogenous H_2S in HeLa cells.

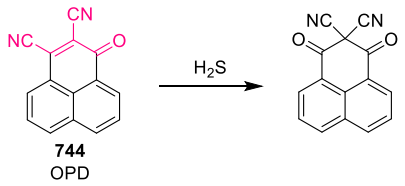


Figure 1.149. Example of an H_2S probe based on H_2S reaction with a 2,3-dicarbonitrile motif.

As an additional example of H_2S addition to an electron poor alkene, Kim and Yoon reported probe **745** (Figure 1.150) that functions by H_2S addition followed by subsequent bond cleavage to modify hydrogen bonding motifs.[753] In this system, the fused pyran does not allow ESIPT, but H_2S addition to the α,β-unsaturated ketone opens the central pyran ring to generate a phenol, which can now hydrogen bond with the benzothiazole and restore fluorescence. This probe provided an 80-fold fluorescence response at 540 nm with minor cross reactivity with thiols and SO_3^{2-} and was used to image exogenous H_2S in HeLa cells. Du also reported an ESIPT approach for H_2S detection in probe **746** (BTDI).[754] In this system, Michael addition of H_2S breaks conjugation with the dione motif, and also likely impacts the hydrogen bonding of the phenol due to the proximal thiol/thiolate. This probe generates a new emission feature at 542 nm in 50% MeCN in buffer upon reaction with H_2S, showed good selectivity for H_2S over competing anions and thiols, and was used to image exogenous and Cys-derived H_2S in HepG2 cells.

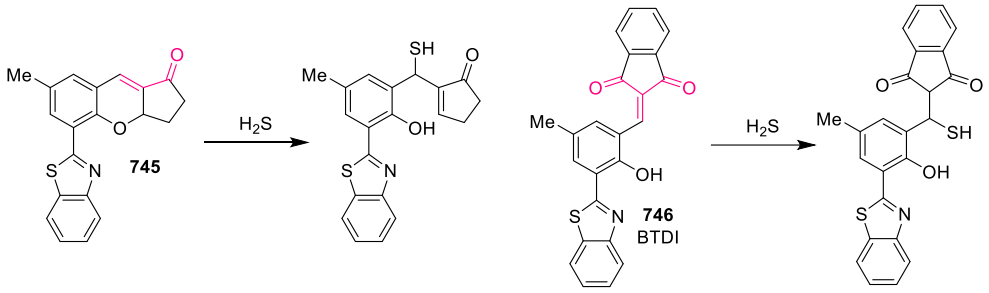


Figure 1.150. Examples of fluorescent H_2S probes based addition to an alkenes to modify hydrogen bonding.

In addition to H_2S addition to alkenes, a number of examples have also demonstrated the attack of H_2S aryl imines, typically with ortho hydroxyl groups. As an example of this approach, Sahoo reported an example of H_2S addition into an imine motifs in **747** (NSPI) (Figure 1.151).[755] Upon H_2S addition, the PET quenching between the two components of the probe is abolished to generate a fluorescent response. This approach showed good selectivity for H_2S over competing anions and Cys and was used to develop paper test strips for measuring H_2S levels in oil. Huang reported **748**, which was demonstrated to respond to both H_2S and Al^{3+} with a turn-on fluorescence response to H_2S at 495 nm in 10% MeOH in water.[756] The response to H_2S was attributed to H_2S addition to the imine, and the probe was used to investigate H_2S in different water sources. Lee reported related construct **749**, which provided a fluorescent response to H_2S at ~550 nm with

good selectivity over other anions and thiols in 40% DMSO in buffer.[757] Further investigations showed that the response toward H_2S could be cycled by sequential addition of H_2S and H^+, although the intensity variation diminished with cycle count. This compound was further used to develop test strips for detection and H_2S concentration measurements of water samples. Using a more conjugated system, He and Zhong reported **750** (DCI-SB) which showed good selectivity for H_2S over competing anions with a turn-on fluorescence response at 675 nm.[758] This probe was further demonstrated to respond to exogenous H_2S in HeLa cells and also zebrafish.

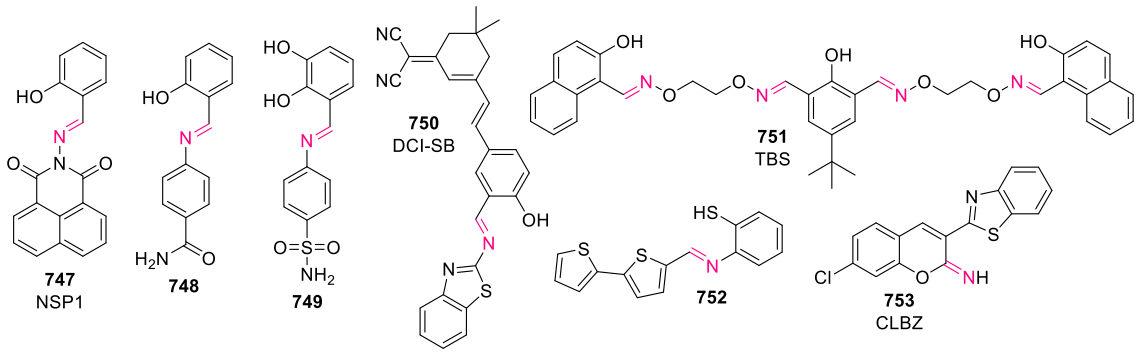


Figure 1.151. Examples of fluorescent H_2S probes based addition to imines.

Dong reported polyimine **751** (TBS) that provided a fluorescent turn-on response at 502 nm when treated with H_2S and was used to investigate H_2S levels in different water samples..[759] The authors attributed the turn-on response to sulfide-mediated phenol deprotonation, but we have grouped this example with other imine-based systems. Using a similar approach, Elango reported the bithiophene based **752**, which provided a turn-on response to both H_2S and CN^- at 461 nm in 40% DMSO in water.[760] NMR experiments showed the likely formation of an aldehyde product, which suggests that nucleophile addition may result in imine cleavage. This probe was further used to image exogenous H_2S in HeLa cells. Zhao reported a related imine in **753** (CLBZ), which provided a ratiometric response to H_2S at with fluorescence decrease at 475 and concomitant increase at 622 nm.[761] This response could be cycled by addition of Ag^+ and reintroduction of H_2S. We have grouped this example with other imines, although the authors also suggest possible conjugate addition at the α,β-unsaturated ring position. The resultant probe was used to develop test strips for H_2S detection, which were later applied to monitor the freshness of different food samples.

In a relatively recent electrophilic approach for H_2S detection, ebselen conjugates have also been appended to fluorophores to generate a fluorescent response (Figure 1.152). For example, in two reports in 2022, Zhang and Liu reported **754** (EHN) and **755** (BPHN), which tether ebselen to naphthalimide platforms. Initial attack by H_2S on the Se atom generates a selenosulfide intermediate, which subsequently results in cleavage of the ebselen motif from the chromophore.[762, 763] Depending on the fluorophore linkage, this approach resulted in either a turn-on or ratiometric response for **754** and **755**, respectively. Both platforms were also used to image exogenous H_2S in cells.

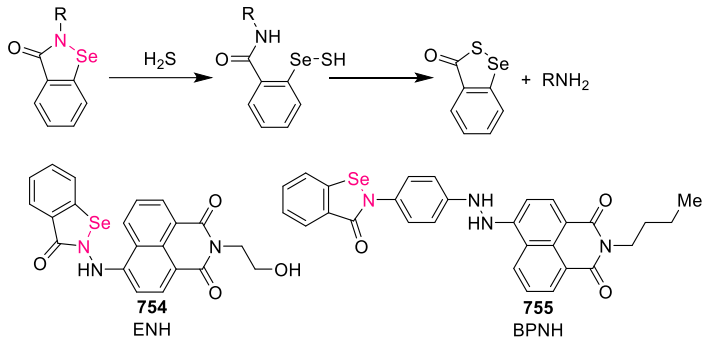


Figure 1.152. Examples of fluorescent H_2S probes based on ebselen derivatives

A variety of other approaches for electrophilic detection of H_2S have been reported. In some cases, these do not fall into a clear mechanistic category, and have typically been used in selected examples rather than broader adoption. In this subsection, we provide examples of such types of chemistry, and highlight the likely chemistry resulting in the probe activation.

Isolated aldehydes have been used for H_2S detection, but in many cases the selectivity over biothiols is eroded without additional directing or cascade chemistry utilizing the diprotic nature of H_2S. In general, the response to H_2S after thiol addition has not been broadly investigated. As brief examples of aldehydes being used for direct H_2S detection, Yin, Huo, and Zheng reported the reaction of H_2S with salicylaldehyde derivative **756**, which provides a fluorescent response for H_2S and SiO_3^{2-} at 555 nm and was used to image exogenous H_2S in HepG2 cells (Figure 1.153).[764] Similarly, Yang reported **757** with an aldehyde for H_2S recognition and thiocarbamate for Hg^{2+} detection in **757**.[765] This probe was also used to develop test strips for these two analytes for different water and drink samples. Liu also reported an ESIPT probe with an ester and aldehyde

motif for independent esterase and H_2S detection in **758**.[766] Esterase cleavage restores ESIPT fluorescence, and H_2S addition results in a ratiometric shift in response from 545 to 485 nm. Based on observed reactivity in other systems, this observed reactivity is likely due to H_2S addition to the aldehyde, rather than dearomatization of the benzothiazole as proposed by the authors. The resultant probe was confirmed to localize to the lysosome and was used to image exogenous changes in H_2S signals in SMCC-7721, HeLa, and MPC cells.

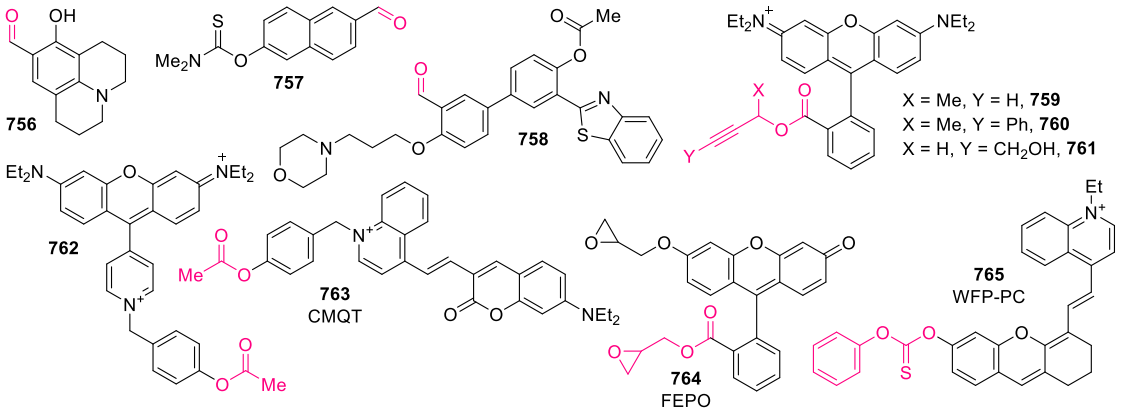


Figure 1.153. Additional examples of electrophilic fluorescent H_2S probes operating by various mechanisms.

In addition to the thiophene esters and acrylates discussed earlier, other esters have also been tuned to provide enhanced reaction rates with H_2S. For example, Han investigated different propargyl esters in rhodamines **759**–**761** (RB-PE-1–3) and found that the rate of non-fluorescent spirolactam formation could be increased by different substitutions when compared to the parent methyl ester.[767] This reduction in fluorescence was also observed in HeLa cells to image exogenous H_2S. Similarly, Sun and Ge also used ester hydrolysis as an H_2S activation approach on a pyridinium rosamine derivative **762**.[768] The proposed mechanism proceeded through H_2S-mediated cleavage of the ester to generate an intermediate phenol, which then undergoes an intermolecular cascade decomposition to release the neutral pyridine and the quinone methide. It is also possible that direct H_2S attack on the benzylpyridinium carbon could yield the same product. The probe was selective over most anions and amino acids, but did provide a small response to Arg, Lys, GSH, and N_2H_2, and was further used to image exogenous H_2S in HeLa cells. Using a similar approach, Zhou prepared a coumarin quinolinium adduct also with an ester cleave site in **763** (CMQT).[769] Dealkylation of the quinolinium by H_2S results in an increase in fluorescence at

570 nm, and this probe was also used to image exogenous H_2S in HepG2 cells and zebrafish. In addition to H_2S, this probe also showed a viscosity dependent enhanced emission at 721 nm. Wang reported the epoxide functionalized fluorescein **764** (FEPO), which provides a decrease in fluorescence upon treatment with H_2S.[770] The mechanism of activation remains unclear, but a possible mechanism could include epoxide opening by H_2S and subsequent intramolecular cyclization to cleave the lower ring ester and regenerate the carboxylate / lactone form of the dye. This probe construct was used to image exogenous H_2S in HeLa cells and larval zebrafish. Expanding to an electrophilic carbamate group, Fu and Xu reported probe **765** (WFP-PC), which reacted with H_2S in 80% DMSO in buffer to cleave the carbamate group and provide a feature at 745 nm.[771] Thiocarbonates have been used previously in the presence of H_2S in buffered solutions, so it is possible that the high DMSO content impacts the overall reactivity.[190] This probe was used to image exogenous H_2S in HeLa cells and mice.

Expanding to other electrophilic systems, Podsiadly reported naphthoquinone systems **766** (Nq-Cm) and **767** (Nq-2Cm), in which Michael addition into the alkene resulted in coumarin release and a concomitant fluorescent response (Figure 1.154).[772] Treatment of either the mono- or di-functionalized probes, respectively, with H_2S in 30% MeCN in buffer resulted in a fluorescence response at 448 nm. Unfortunately, these probes also showed significant response to other biothiols, which is consistent with the method of probe activation. Expanding to additional electrophilic carbonyl species, Huo reported the addition of H_2S to perylene anhydride **768** in 50% DMSO in buffer to generate a fluorescent thioacid product, which could be converted back to the parent anhydride by Hg^{2+}.[773] The selectivity of this probe was not investigated, but it was used to image exogenous H_2S in HepG2 cells.

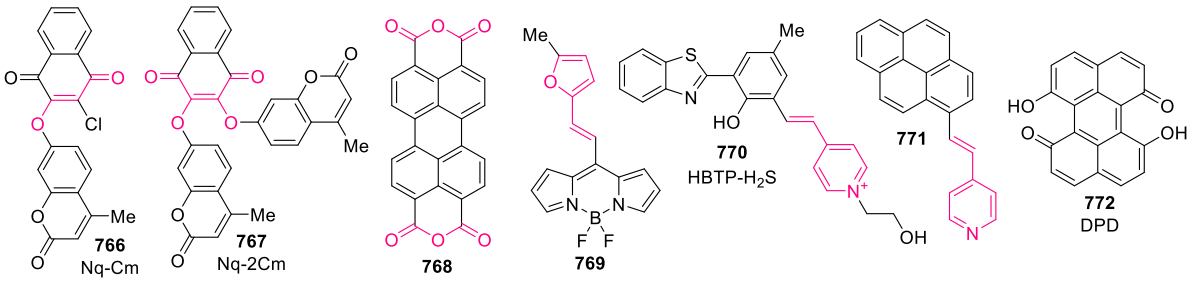
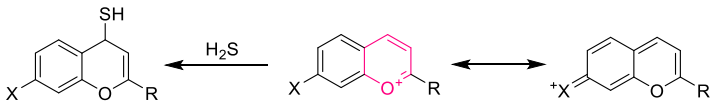


Figure 1.154. Additional examples of electrophilic fluorescent H_2S probes operating by various mechanisms.

Qin and Guo reported BODIPY construct **769**, which reacts with H_2S at the electrophilic alkene conjugated to the furan with proposed further opening of the furan.[774] This probe provided a fluorescent enhancement at 490 nm in response to H_2S, showed good selectivity for H_2S over competing RSS, and was used to image exogenous H_2S in HeLa cells. Also using an electrophilic alkene, Du reported pyridinium **770** (HBTP-H_2S), which reacted with H_2S to provide a ratiometric ESIPT response with decrease at 658 nm and increase at 470 nm in 50% MeCN in buffer.[775] This response was attributed to H_2S addition and dearomatization of the pyridine, which is almost certainly incorrect. More likely alternative mechanisms include either direct dealkylation of the pyridinium or addition into the electron poor alkene, as is observed in other related probes. This probe was used to image exogenous H_2S in HepG2 cells. Also using a conjugated electrophiles, Velmathi reported pyrene-based **771**, which provides a shift in fluorescence from 595 nm to 482 nm upon reaction with H_2S with good selectivity over competing cations, anions, and thiols.[776] This reaction could be chemically reversed by the addition of acid and was further used to develop H_2S responsive test strips. As an additional example, Hu reported perylenequinone-based **772**, which generates a fluorescent response at 462 nm when treated with H_2S.[777] This probe showed good selectivity over other competing species, but did show partial activation when treated with polysulfides and was further used to image exogenous H_2S in HeLa cells.

Complementing the approach of adding H_2S to different electrophilic sp^2 based systems, a variety of groups have also used the reaction of H_2S with pyrilium motifs to generate H_2S responsive probes. Earlier chemistry documented the reaction of H_2S with 2,4,6-trisubsituted pyrilium cations to form a thiopyrilium product, which has been used to demonstrate colorimetric response upon product acidification.[778] In the absence of functionalization at the 4-position, H_2S addition results in formation of an aryl thiol (Scheme 1.21), which has been used as an approach for H_2S detection.[779]



Scheme 1.21. Addition of H_2S to pyrilium cations.

As an example of this approach, Guo developed **773** (1-HS), which reacts with H_2S to provide a ratiometric response with a fluorescence increase at 485 nm and concomitant decrease at 690 nm in 30% MeCN in buffer (Figure 1.155).[779] This response was selective for H_2S over other competing anions and thiols, and the resultant probe was used to image exogenous H_2S in HeLa cells. Peng reported a similar approach to develop **774**, which provided a ratiometric response to H_2S with increase at 487 and decrease at 707 nm in 30% MeCN in buffer, which was further used to image exogenous H_2S in MCF-7 cells and also in live mice.[780] Using this approach with different coumarin motif, Zhang and Yu prepared **775** (HABA), which showed a similar ratiometric fluorescence response with an increase at 440 nm and decrease at 630 nm in 30% DMSO in buffer. [781] This probe was used to measure serum and urine spiked with H_2S and also exogenous H_2S in HeLa cells.

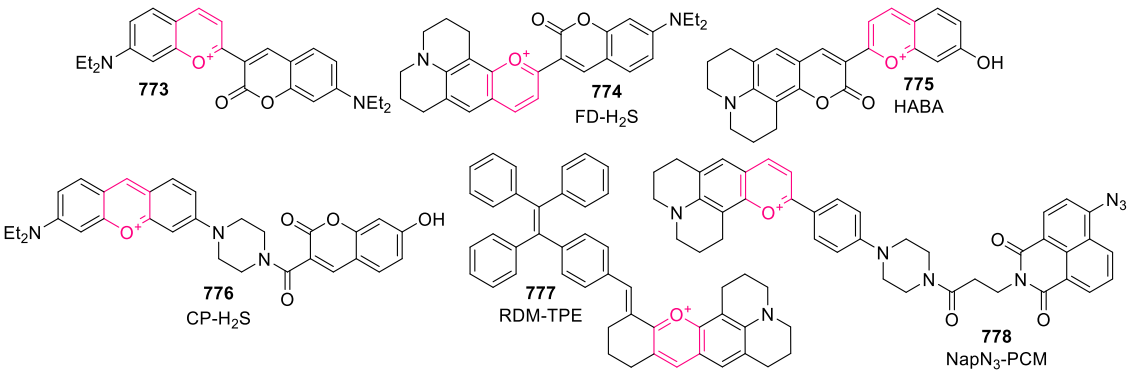


Figure 1.155. Examples of fluorescent H_2S probes based on addition to pyrilium motifs.

Lin expanded on this approach to develop a FRET based probe that functioned through a similar mechanism.[782] Probe **776** (CP-H_2S) provided a ratiometric response with increase at 454 nm and decrease at 573 nm in 5% DMF in buffer with high selectivity for H_2S over competing analytes, including thiols, and was used to provide ratiometric detection of exogenous H_2S in SMMC-7721 cells. Xie and Liu reported the TPE construct **777** (RDM-TPE), which results in a turn-off response to H_2S with moderate selectivity for H_2S over other amino acids.[783] The probe activation was attributed to H_2S addition to the alkene, but we have grouped it other pyrilium motifs. This probe was further used to investigate H_2S and pollution levels in different water sources. Lin also used a pyrilium adduct, in this case also incorporating an azide motif, to develop **778** (NapN_3-PCM), which provides a ratiometric response to different H_2S levels based on the

different sensitivities of the azide and pyrilium groups.[784] This approach showed good selectivity for H_2S below 200 μM, although moderate erosion of selectivity was observed at the higher 2 mM levels investigated. This probe and related approach was used to image exogenous H_2S in HeLa cells and zebrafish.

As further examples of electrophilic approaches that result in direct H_2S functionalization of aromatic rings, different BODIPY platforms with thio- and seleno-ether electrophiles have also been reported. For example, Qin and Guo reported the BODIPY selenoether **779** (BOD-PhSe), which reacts with H_2S sequentially to displace both selenoethers and generate the dithiol BODIPY product (Figure 1.156).[785] This nucleophilic displacement occurred in a stepwise manner, with each displacement reducing the fluorescence of the BODIPY probe. This turn off response at 610 nm was selective for H_2S over other thiols and was also maintained in BHK cells treated with exogenous H_2S.

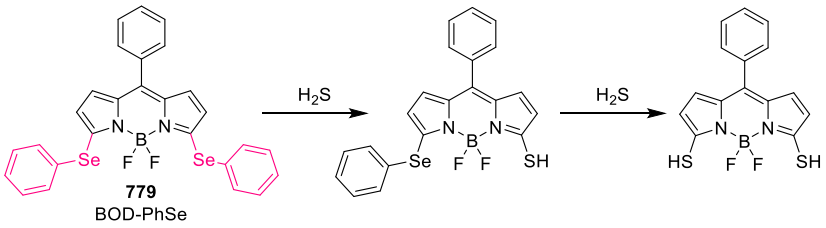


Figure 1.156. Examples of fluorescent H_2S probes based cleavage of BODIPY selenoethers.

More recently, Li and Zhao reported the 4-nitrothiophenol substituted BODIPY **780** (BOD-NH-SC), which reacts with H_2S to generate the BODIPY thiol (Figure 1.157).[786] Subsequent addition of NO under aerobic conditions results in reaction with both the secondary aryl amine and the BODIPY thiol to generate a nitrosamine and nitrosothiol, respectively. Interestingly, the nitrosothiol can react further with H_2S to regenerate the parent thiol and result in NO/H_2S cycling. This probe also benefits from NIR and NIR-II emission, with the nitrosamine product emitting at 655 nm and the resultant BODIPY thiol emitting at 936 nm, which could be cycled back to the nitrosothiol product at 645 nm upon subsequent NO addition (Figure 1.158). This probe was used to measure changes in exogenous NO and H_2S cycling in HepG2 cells.

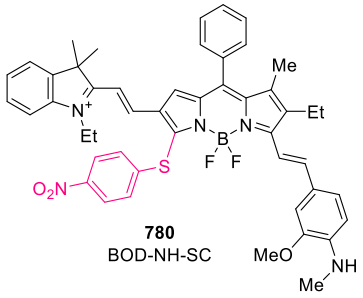


Figure 1.157. Example of a fluorescent H_2S probe based on cleavage of a BODIPY thioether.

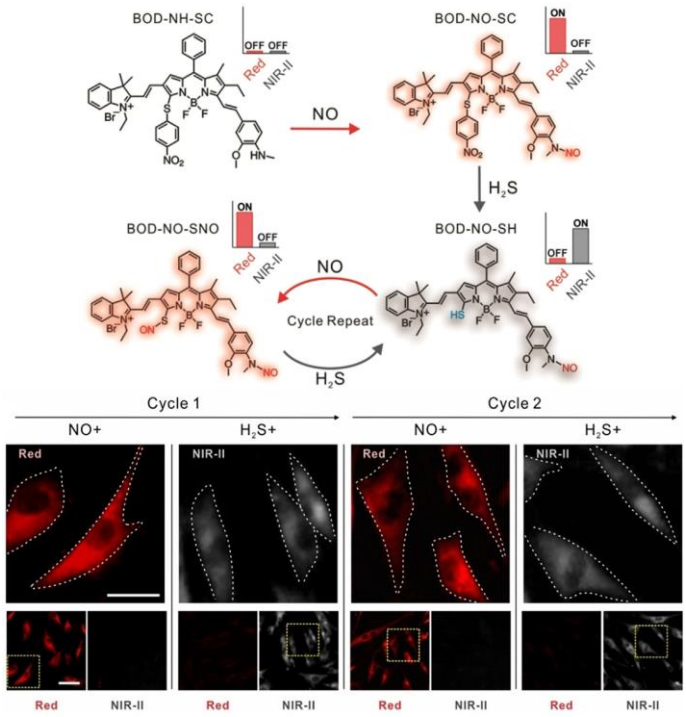


Figure 1.158. (top) Schematic of **780** reacting with both H_2S and NO. (bottom) Colonic smooth muscle cells treated with DEA·NONOate followed by **780** and NaSH in cycle 1. Cycle 2 included additional treatment with DEA·NONOate and NaSH. Reproduced with permission from ref [786]. Copyright 2021 John Wiley and Sons.

Other BODIPY electrophiles have also been reported. For example, Gu and Zhao reported the monochloro BODIPY triphenylethylene adduct **781** (TPE-BODIPY-Cl), which reacts with H_2S to generate a BODIPY thiol and provide luminescent response at 760 nm in a 40% MeCN in buffer solution (Figure 1.159).[787] This probe was used to image changes in H_2S levels in cells treated with either AOAA or SAM as well as in HCT116 subcutaneous xenografts in mice. A related approach was reported by Ye, Wang, and Li who reported monochloro BODIPY **782** with

a pendant aldehyde to react with the resultant BODIPY thiol formed after H_2S addition.[788] This probe provided a ratiometric response to H_2S in 50% DMSO in buffer, showed good selectivity for H_2S over competing analytes, and was used to image exogenous H_2S in HeLa cells. Wang and Zhao reported the doubly-cationic probe **783**, which generates a fluorescence turn on at 732 nm upon treatment with H_2S in buffer, with good selectivity for H_2S over competing anions and thiols, as well as maintenance of signal when H_2S was co-incubated with Cys, Hyc, or GSH.[789] This probe was further used to image exogenous and endogenous H_2S in HCT116 cells.

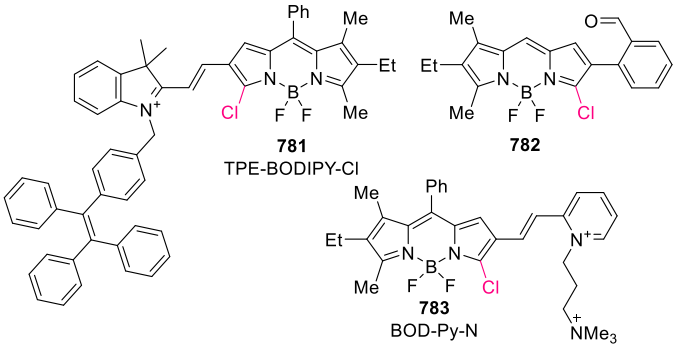


Figure 1.159. Additional examples of fluorescent H_2S probes based on addition to BODIPY electrophiles.

Other examples of direct H_2S addition to electrophile-substituted fluorophores have been reported, particularly with coumarin-based probes (Figure 1.160). For example, Chen, Sheng, and Song reported **784** (Lyso-RC), which provided different response to H_2S, Cys/Hcy, and GSH and was targeted to the lysosome.[790] The response to H_2S was based off of nucleophilic displacement of the resorufin dye. The approach allowed for different signals in the blue, green, and red channels for the different types of analytes, which was further confirmed by exogenous analyte treatment in HeLa cells. Chen and Song reported a related approach with a similar resorufin-functionalized coumarin in **785** (RC), which functioned by a similar mechanism but also allowed for differentiation of Cys and Hcy.[791] This general approach has also been used with more traditional electrophiles. For example, Li and Yang reported **786**, which generated a turn-off response to H_2S at 557 nm in buffer with 80% DMSO.[792] This probe was further used to develop test strips for H_2S detection.

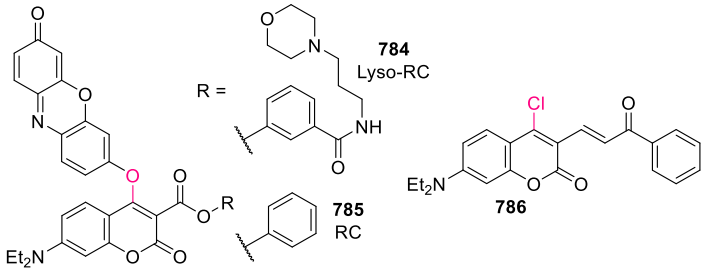


Figure 1.160. Examples of fluorescent H_2S probes based on electrophilic coumarins.

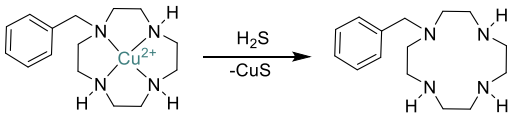
1.5 Metal-Based H_2S Probes

In addition to using H_2S mediated reactivity with organic molecules to develop activity-based probes, a number of strategies have been implemented that use transition metals to enable H_2S detection. Two primary approaches have emerged: H_2S-mediated precipitation of coordinated metal ions and coordination of H_2S, or more accurately HS^-, to metal centers. The former of these two approaches has been developed much more broadly due to the high affinity of sulfide for many metal ions in weak coordination environments. This section highlights fundamental approaches and advances in these two areas of complementary investigation.

1.5.1 Metal Precipitation

A common approach to develop H_2S-responsive probes is to use the H_2S-mediated removal of transition metals coordinated to fluorescent or fluorophore-ligated ligands to generate a fluorescent response. Different transition metals have been used for this approach, with Cu^{2+} being used most frequently due to the enhanced paramagnetic quenching from this ion when in close proximity to fluorophores. This fluorescence quenching from the unpaired electrons on the metal provides an "off" state for the fluorophore and fluorescence can be restored by removal of the Cu^{2+} ion.[793] This general approach is shown in Scheme 1.22 with a cyclen-Cu^{2+} binding motif but has been adapted to different chelators and metal systems. In such systems, the coordination of Cu^{2+} to the metal binding site quenches the fluorescence of the pendant fluorophore, and reaction with H_2S results in formation of insoluble CuS and release of the metal-free chromophore, which results in a fluorescence response. Although we have not focused on reaction rates throughout this Review, the precipitation of metal ions from such constructs is generally significantly faster than other methods of H_2S detection, with responses typically in the order of seconds. For practical

considerations, the choice of metal chelator is important and needs to have a sufficiently high binding affinity for the metal to ensure the metal remains ligated at the concentrations at which the probe will be used. Throughout this section we have deferred to the initial authors' reported metal coordination environment, unless this is significantly different from well-established binding modes in common ligands. In some cases, multiple coordination modes, geometries, or sites may be present and/or the precise binding environment may remain unknown. The metal precipitation approach has also been applied to different material, macromolecular systems, and surface-modification approaches, which are outside the scope of our general discussion. In general, the metal precipitation approach is less developed than organic molecule-derived activity-based probes, with comparatively fewer publications reporting detailed selectivity investigations or applications in more complex biological imaging experiments.



Scheme 1.22. Schematic of H_2S-mediated precipitation from a metal-binding motif.

1.5.1.1 Cu^{2+} Precipitation

In 2011, Nagano and co-workers reported **787** (HSip-1), which is based on a fluorescein motif conjugated to a Cu^{2+}-binding cyclen (Figure 1.161).[794] In the initial report, TACN, cyclam, cyclen, and TMcyclen were screened as metal binding units, with the best response coming from the cyclen derivative. Probe **787** showed a rapid response to H_2S and was also used to measure the Cys-mediated H_2S release from a thiol-activated H_2S donor. This probe showed good selectivity for H_2S over other analytes, with only minor signals for thiol-based reductants like Cys, GSH, Hcy, or DTT when these analytes were used in a large excess (Figure 1.162). Most reports of Cu^{2+}-precipitation based probes show good selectivity over RNS, but we also note that related Cu^{2+} systems have also been used for HNO and NO detection, resulting in formation of Cu(I)-NO species or in nitrosation of coordinated secondary amines, respectively.[795, 796] In general, this approach of H_2S-mediated metal precipitation has been used broadly in different systems to develop H_2S response fluorogenic probes.

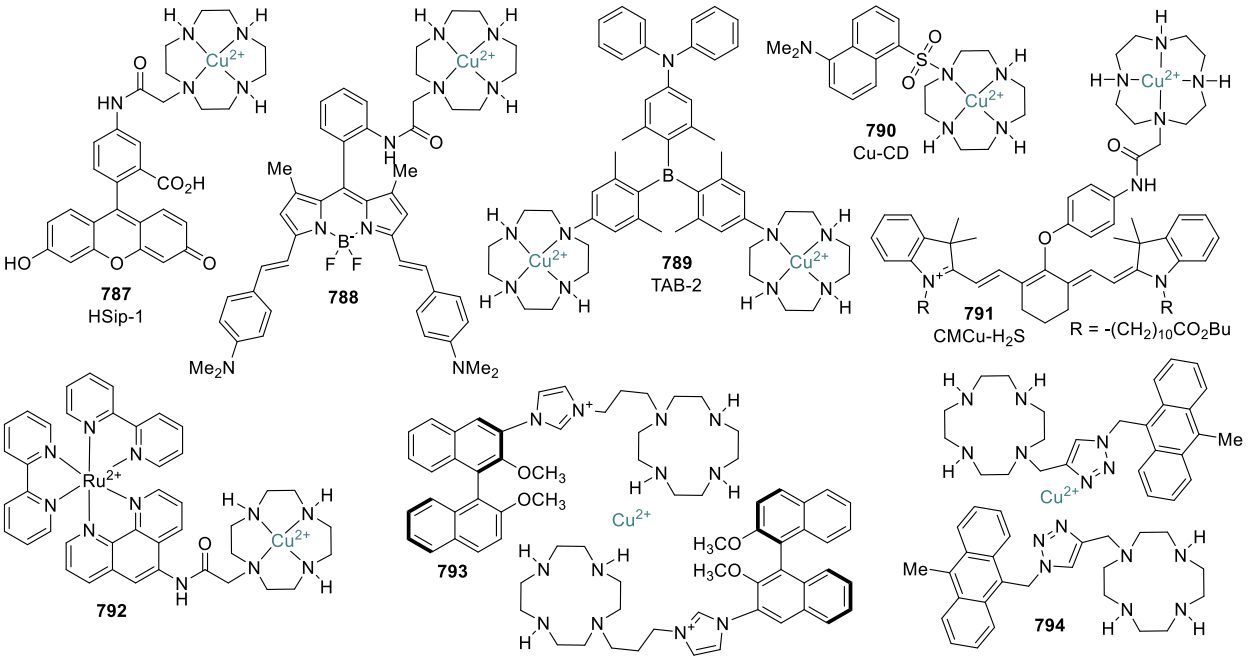


Figure 1.161. Examples of fluorescent H_2S probes based on Cu^{2+} precipitation from functionalized cyclen ligands.

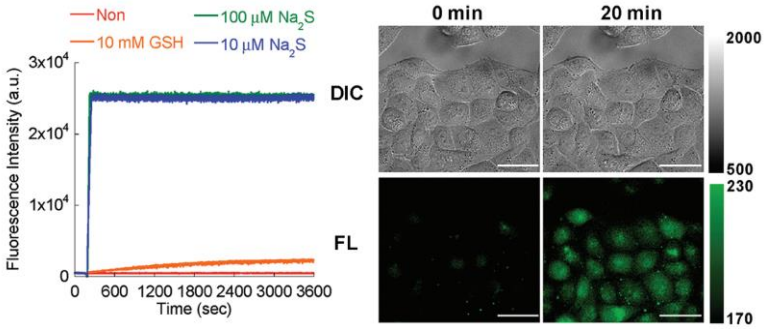


Figure 1.162. (left) Response from **787** upon treatment with H_2S and GSH. (right) Fluorescent response of **787** in HeLa cells treated with exogenous H_2S. Reproduced with permission from ref [794]. Copywrite 2011 American Chemical Society.

Deng and Huang reported a related BODIPY-cyclen motif **788** that provides a red-shifted emission at 716 nm upon treatment with H_2S.[797] This system was used to image exogenous H_2S in Raw 264.7 cells as well as endogenous H_2S from HEK293 cells overexpressing CSE, when compared to scrambled or CSE KO cells. In addition, **788** was also used to image exogenous H_2S in live mice. Li, Li, and Yang reported the *bis*(cyclen) **789** (TAB-2), which provides a fluorescence response at ~550 nm and is compatible with both one- and two-photon excitation.[798] This probe showed good selectivity toward H_2S although did produce a minimal response to thiols. Probe **789**

was subsequently used to image exogenous H_2S in NIH/373 cells as well as increased H_2S levels in cells pre-incubated with CBS.

Further extending the cyclen platform, Yoo reported a dansyl-cyclen adduct **790** (Cu-CD), which provided a turn-on response to H_2S at 491 nm in 10% DMSO in buffer.[799] This probe showed good selectivity over competing analytes and was used to image exogenous and Cys-derived H_2S in HeLa and EMT6 cells. Using a related strategy but moving to the NIR, Liang, Li, and Li reported the lipophilic and cell membrane-targeting probe **791** (CMCu-H_2S), which reacts with H_2S to generate a fluorescent response at 790 nm.[800] This probe was used to image H_2S near the membrane of live HepG2 cells using both exogenous and Cys-derived H_2S and also used to investigate H_2S levels during NFS1 inhibition or knockdown. Expanding to Ru-based luminescent systems, Ye and Yuan reported the Cu^{2+}-cyclen $Ru(bpy)_2$ motif **792**, which provided a fluorescence turn-on at 605 nm in response to H_2S.[801] This probe showed good selectivity over different anion, amino acid, and thiol competing analytes. Using a 2:1 binaphthyl-cyclen to Cu^{2+} complex, Li and Yu reported **793**, which provided a turn-on response to H_2S at 449 nm with good selectivity over competing analytes.[802] Chen and Wang also reported a 2:1 ligand:Cu^{2+} complex in anthracene-ligated Mat-cyclen **794**, which showed good selectivity for H_2S over other analytes and was used to image exogenous H_2S in HeLa cells and zebrafish.[803]

Other macrocycles have also been used for this H_2S detection approach. For example, Li reported macrocycle **795**, which responds to H_2S in 25% MeOH in buffer to generate a fluorescence response at 538 nm, with good selectivity for H_2S over other anions, although competing thiols were not investigated (Figure 1.163).[804] Martínez-Máñez and Costero reported the anthracene-ligated cyclen complex **796**, which provided a turn-on response at 417 nm with minimal response from thiols and was used to image exogenous H_2S in in HeLa cells.[805] Using a 5-coordinate macrocyclic cyclam complex, Pellecchia reported **797**, which reacts with H_2S to generate a fluorescence response at 404 nm, with moderate responses from $S_2O_3^{2-}$ and SO_3^{2-}.[806]

Expanding the list of Cu^{2+} binding motifs, the di(picolyl)amine (DPA) chelate has also been used broadly to develop Cu^{2+} ligated systems that respond to H_2S with a fluorescent response. In an early example of this approach in 2009, Chang reported the DPA fluorescein conjugate **798**, which provided a fluorescent response toward H_2S over other competing anions in water, but thiol-based reactants were not investigated (Figure 1.164).[807] Also in 2009, Xing reported a hemicyanine-carbazole platform **799** (CuHCD) that responded to both H_2S and HNO to generate

a fluorescent response at 595 nm, although selectivity against thiols was not reported.[808] Interestingly, the selectivity for H_2S or HNO could be modulated by using different concentrations of the surfactant SDS, with 1 mM SDS providing specificity for HNO and 5 mM SDS providing specificity for H_2S. More broadly, similar Cu-ligating motifs have also been developed previously as HNO reporters based on the HNO-mediated reduction of Cu^{2+}.[809, 810]

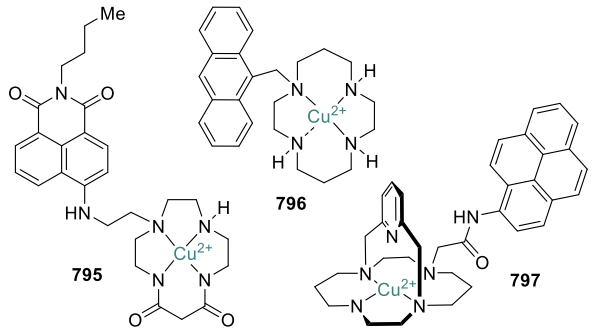


Figure 1.163. Examples of fluorescent H_2S probes based on Cu^{2+} precipitation from other macrocyclic ligands.

Zhu and Zhu reported the BODIPY-DPA conjugate **800** in 2011, which provided a colorimetric response to H_2S in 5% DMSO in buffer, although the fluorescent response of the BODIPY motif was not reported.[811] Kan and Yin reported the coumarin-DPA conjugate **801**, which provided a fluorescent response to H_2S, including in mixed H_2S/thiol solutions.[812] In addition, the ability to regenerate the probe with Cu^{2+} after addition of H_2S was demonstrated for a number of cycles. In the same year, Li and Yu reported the related coumarin complex **802**, which showed good selectivity for H_2S over competing anions.[813] This probe was subsequently used to image exogenous H_2S in HeLa cells. Li and Han reported the BODIPY-DPA conjugate **803** (ZS2), which provided a turn-on response at 546 nm to H_2S but not to other competing anions or Cys, although only 2 equivalents of competing anions were investigated.[814] This probe was also used to image exogenous H_2S in HeLa cells. Also using a BODIPY platform, Wang reported the BODIPY DPA adduct **804** (BC-DPA), which showed good selectivity for H_2S over competing anions, but did not result in a fluorescent turn-on in cells treated with H_2S.[815]

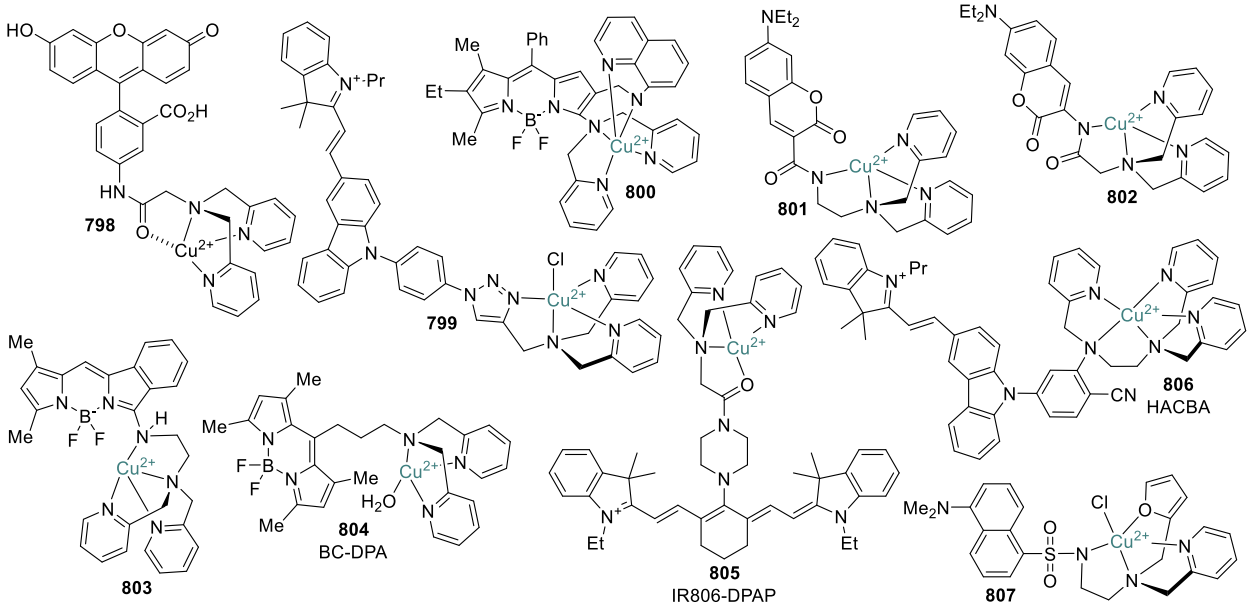


Figure 1.164. Examples of fluorescent H_2S probes based on Cu^{2+} precipitation from functionalized di(picolyl)amine and related ligands.

Expanding to longer wavelengths, Zhao and Wang reported the cyanine-DPA adduct **805** (IR806-DPAP), which provided a fluorescent response to H_2S at 806 nm in 40% EtOH in buffer, with good selectivity for H_2S over competing anions.[816] This probe was also used to image exogenous H_2S in HeLa cells. Adding an extra pyridyl binding motif, Xing reported the tri(2-pyridylmethyl)ethylenediamine (TPEA) carbazole-hemicyanine construct **806** (HACBA), which provided a fluorescent response to H_2S in buffer with 5 mM SDS, but also had a minor response to Cys and GSH.[817] Wang reported a dansyl conjugate **807** (DNS-Cu), which provided a turn-on response to H_2S and good selectivity over competing anions and was used to investigate H_2S in different water samples.[818]

In addition to the above Cu^{2+} chelating motifs, a variety of platforms have also used derivatized quinoline ligands for Cu^{2+} binding and subsequent H_2S detection. Lin reported the NIR probe **808**, which incorporates a cyanine dye and 8-aminoquinoline motif (Figure 1.165). This probe provides a turn-on response at 794 nm in response to H_2S in 40% EtOH in buffer with good selectivity over other anions.[819] Bai and Zeng reported the fluorescein quinoline motif **809**, which provided a fluorescent response to H_2S over other anions in 50% MeCN in buffer with good selectivity over competing anions but was not tested with thiols.[820] This probe was subsequently used to image exogenous H_2S in HeLa cells. Fang reported aminoquinoline probe **810** (DOQED),

which provided a fluorescent response at 420 nm with good selectivity over other anions but was not investigated with thiols.[821] Long reported probe **811**, which was investigated in 40% DMF in buffer to provide a fluorescent response at 451 nm with good selectivity for H_2S over competing species including thiols. This probe was subsequently used to image exogenous H_2S in MCF-7 cells.[822] Tang reported a quinoline-based benzohydrazide **812**, which also responded to H_2S at 468 nm in 10% DMSO in buffer. This probe showed only moderate selectivity for H_2S over other competing anions, but was demonstrated to cycle between the off to on state by sequential Cu^{2+} and H_2S additions.[823]

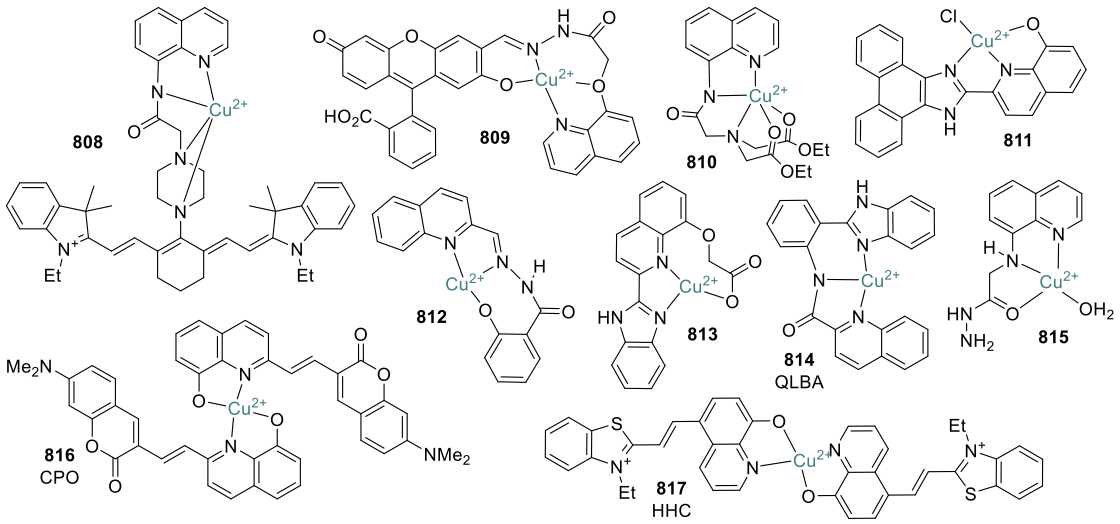


Figure 1.165. Examples of fluorescent H_2S probes based on Cu^{2+} precipitation from functionalized quinoline and related pyridine ligands.

Using a quinoline-benzimidazole motif, Zhang reported **813**, which reacted with H_2S to generate a response at 460 nm with good selectivity over other anions.[824] This probe was also used to image exogenous H_2S in SMC-7721 cells. Tan and Jiang reported the related scaffold **814** (QLBA), which also provided good selectivity over competing anions, and was further used to image exogenous H_2S in HeLa cells.[825] Ali reported a similar complex in **815**, which shows good selectivity over competing anions and also showed a turn-on response to HNO.[826] Zhou and Wu reported **816** (CPO), which responded to H_2S but not other competing anions, although a minor response from thiols and CN^- was observed.[827] This probe was also subsequently used to image exogenous H_2S in HeLa cells. Also using a 2:1 complex, Li reported the 2:1 complex **817** (HHC) based on a quinoline Cu^{2+} binding motif coupled to a benzothiazolium group. This probe provided

a turn-on response at 592 nm, with good selectivity for H_2S over competing anions and thiols, although only 5 equiv. of competing analytes were tested. This probe was subsequently used to image exogenous H_2S in HeLa cells and investigate H_2S in blood samples.[828]

In addition to direct Cu^{2+} chelating ligands, different Cu^{2+} binding peptides ligated to fluorophores have also been used. For example, Tang reported a peptide-based fluorescent probe for H_2S detection based on a fluorescein isothiocyanate (FITC) fluorophore linked to a Ser–Pro–Gly–His-NH_2 peptide in **818** (Figure 1.166).[829] This scaffold was found to bind 1 equiv. of Cu^{2+}, provide a signal at 525 nm upon treatment with H_2S, and be selective over other competing anions, although the selectivity against thiols was not investigated. Probe **818** was used to image exogenous H_2S in HeLa cells and zebrafish. Also using a FITC chromophore, Yang reported a Gly-His-Lys-NH_2 tripeptide **819**, which also bound 1 equiv. of Cu^{2+}.[830] This probe also showed good selectivity over competing anions, although thiols were not investigated. The resultant probe was used to image exogenous H_2S in RKO cells. Bian and Wu similarly reported a His-Glu-Phe-His-NH_2 tetrapeptide linked to FITC to report **820**.[831] This probe was investigated with thiols and provided a full turn-on response with H_2S, Cys, and GSH, and was used to image exogenous H_2S, Cys, and GSH in HeLa cells.

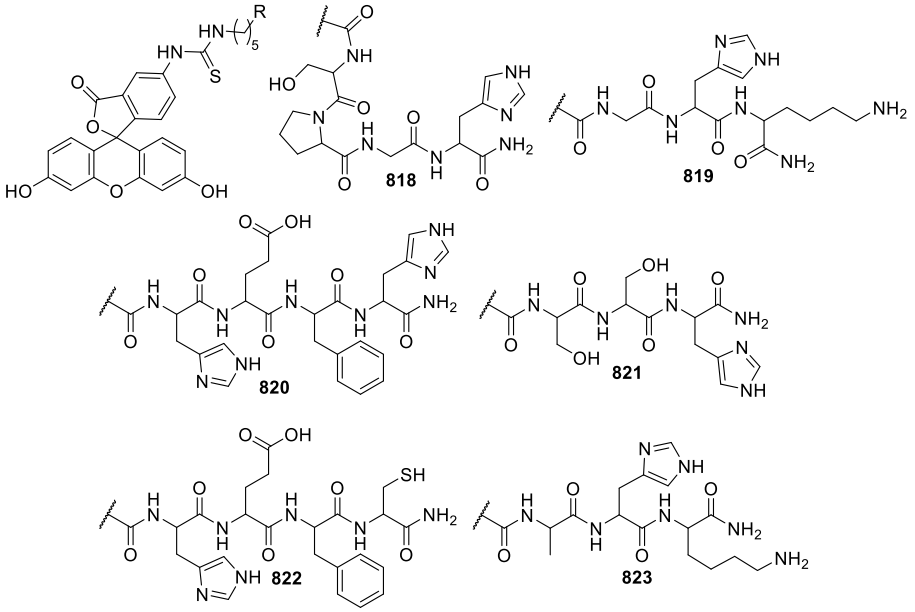


Figure 1.166. Examples of fluorescent H_2S probes based on Cu^{2+} precipitation Cu^{2+}-binding peptides ligated with fluorescein chromophores. Cu^{2+} ions have been omitted for clarity because local coordination environments were not identified.

Wang reported the related Ser-Ser-His-NH_2 tripeptide **821**, which also bound 1 equiv. of Cu^{2+}.[832] This probe showed good selectivity for H_2S over other anions and was further used to image exogenous H_2S in RKO cells. Wu reported Cys-containing His-Glu-Phe-Cys-NH_2 tetrapeptide **822**, which was found to bound to bind Cu^{2+} with a 2:1 ligand to Cu^{2+} ratio.[833] This peptide showed selectivity for H_2S over other competing anions and was also found to be non-toxic to BEL-7402 cells. Adding to the FITC functionalized peptides, Wang and Liao reported the Ala-His-Lys-NH_2 tripeptide **823**, which also bound with a 2:1 ligand to metal stoichiometry.[834] The resultant Cu^{2+}-peptide showed good selectivity for H_2S over competing anions and was used to image exogenous H_2S in RKO cells.

Peptide conjugates for H_2S detection have also been prepared using the dansyl chromophore (Figure 1.167). For example Wang and Yue reported **824** (DP5), which is based on Ser-Pro-Gly-His-Gly-NH_2 pentapeptide Cu^{2+} binding motif.[835] This probe was selective against competing anions but not investigated with thiols, but was subsequently used to image exogenous H_2S in HK2 cells. Using a related approach, Wang and Zhou reported **825** (DAHK), which also contains a dansyl reporter and in this case a Ala-His-Lys-NH_3 tripeptide.[836] This probe also was not tested against thiols, but provided good selectivity over competing anions and was subsequently used to image exogenous H_2S in RKO cells. Sun and Xiao reported the hexapeptide Asp-Asp-Gly-Gly-Glu-Glu **826**, which bound 1 equiv. of Cu^{2+} and provided a turn-on response to H_2S with good selectivity over competing anions.[837] The resultant Cu^{2+}-peptide construct was further used to image exogenous H_2S in HeLa cells and larval zebrafish. Wang, Yang, and Wen reported the related dansyl construct **827** (DGGH) with a Gly-Gly-His-NH_2 tripeptide motif, which showed good selectivity against anions and was used to investigate H_2S in water samples and also image exogenous H_2S in LNcap cells.[838] Peptides with two dansyl fluorophores have also been reported. For example, Wang, Yang, and An reported polypeptide **828** (DM), which was used to bind Hg^{2+} instead of Cu^{2+}, with the likely ligated through the methionine residues.[839] When treated with H_2S, this probe provided a fluorescent response that was selective for H_2S over competing anions. The Hg^{2+} conjugated probe was also used to image exogenous H_2S in HK2 cells. Other fluorophore-free approaches with Cu^{2+} ligated peptides using natural tryptophan fluorescence have also been reported, but overlap significantly with the background fluorescence of protein and peptide interferants.[840]

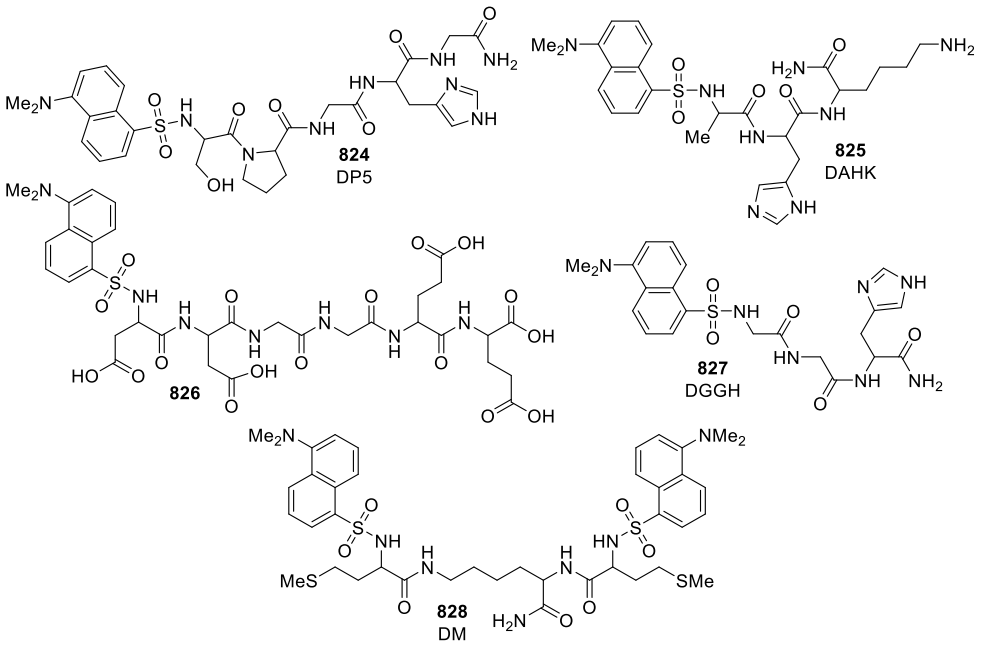


Figure 1.167. Examples of fluorescent H_2S probes based on metal precipitation metal-binding peptides ligated with dansyl chromophores. Metal ions have been omitted for clarity because local coordination environments were not identified.

The Cu^{2+} precipitation approach for H_2S detection has also been incorporated into various lanthanide-luminescence complexes. For example, in 2014 Wang and Xu reported this proof of concept approach with probe **829**, which is based on a Tb^{3+} complex that provided a time-gated luminescent at 545 nm upon treatment with H_2S and displacement of the Cu^{2+} (Figure 1.168).[841] Law and Wong reported a related approach with Eu^{3+} complex **830**, which responds to H_2S with only minor interference from Cys and good selectivity over other anions.[842] Miller also used this approach to develop Ln^{3+} complex **831**, which showed good selectivity for H_2S with only a minor signal from Cys and was used to measure differences in H_2S generated from isolated CSE in the presence and absence of an inhibitor.[843] Wu reported Eu^{3+} complex **832**, which provided good selectivity over competing anions, and was subsequently used to image exogenous H_2S using time-gated imaging in HepG2 cells.[844] Song and Yuan reported the combined Eu^{3+}/Tb^{3+} system **833**, which provided good selectivity for H_2S and competing anions with only a minor response for Cys and GSH.[845] This probe was subsequently used to image exogenous H_2S in HeLa cells and zebrafish using ratiometric imaging. Wu reported β-diketonate Eu^{3+} complex **834** (Eu^{3+}-BHHCT-BPED-Cu^{2+}), which reacted with H_2S to generate a luminescent response that was selective for H_2S over competing anions and subsequently used to image exogenous H_2S in HepG2 cells.[846]

Lanthanide-based systems have also been developed using the Cu^{2+}(DPA) ligated motifs. Barrios and Tuck reported the Tb^{3+} complex **835**, which provided good selectivity for H_2S over competing anions, although moderate response to cystamine was also observed.[847] Using a different luminescent approach, Yui, Zhang, and Ye reported the Ru^{2+} complex **836**, which provides a fluorescent response when treated with H_2S.[848] This compound was developed as an electrochemiluminescent sensor using a Nafion ion exchange membrane and was further used to investigate H_2S in rat brain tissue.

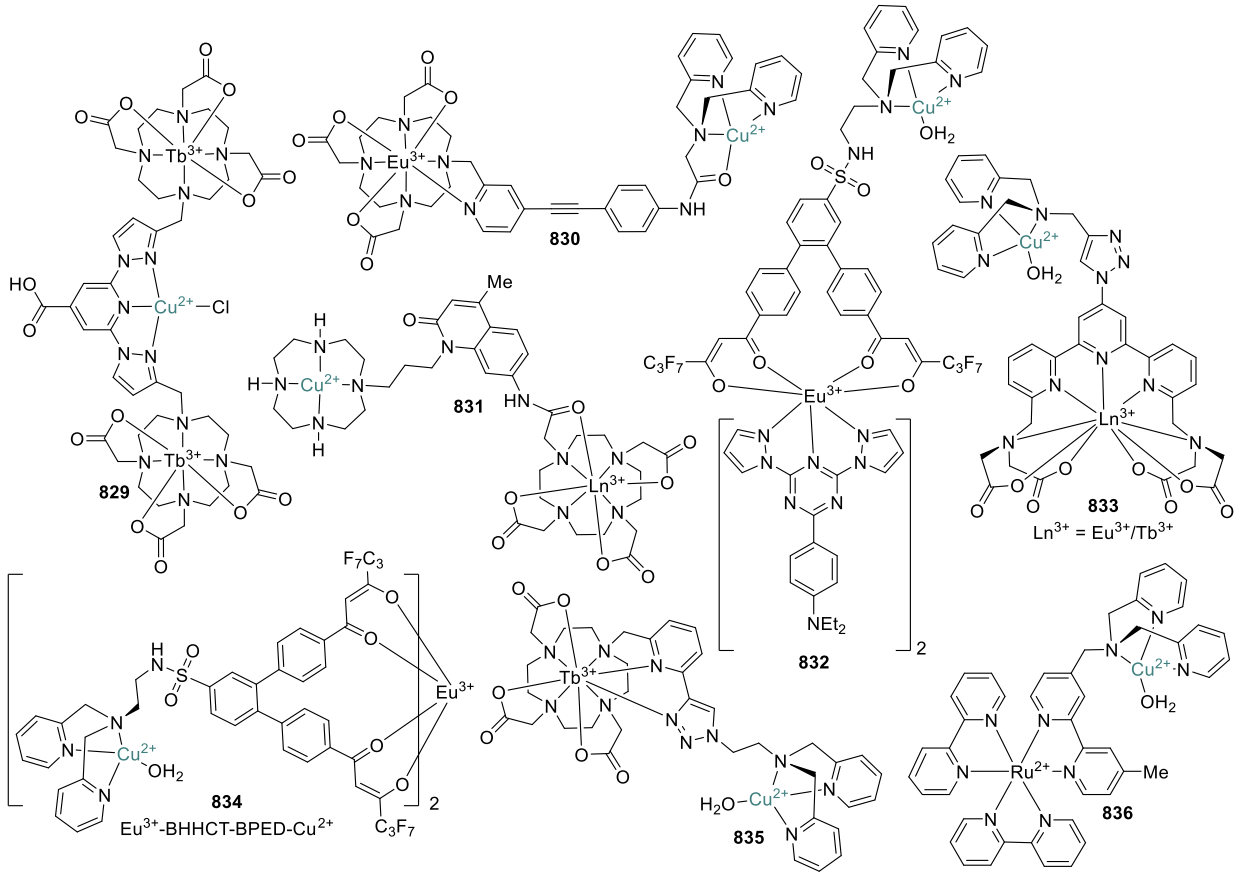


Figure 1.168. Examples of fluorescent H_2S probes based on Cu^{2+} precipitation with luminescent reporters.

Expanding to different coordinating ligands, a number of different hydrazine and hydrazide-based scaffolds for Cu^{2+} have also been developed. For example, Bai and Zeng reported **837**, which incorporates a fluorescein motif and provides a fluorescent response in 40% MeCN in buffer (Figure 1.169).[849] This probe showed good selectivity over other anions and only minimal

response to other RSS and ROS and was subsequently used to image exogenous H_2S in HepG2 cells. Also functionalizing the xanthene ring, Meng and Zhang reported the bis-fluorescein adduct **838**, which provided a turn-on response to H_2S with good selectivity for H_2S over competing anions with a minimal response to Hcy and GSH.[850] This probe was also demonstrated to image exogenous H_2S in MDA-MB-231 cells. Moving to bottom ring functionalization, Ramesh and Das reported a rhodamine adduct with a pendant indole in **839**, which provided a turn-off fluorescent response at 557 nm to H_2S and was used to image exogenous H_2S in HeLa cells.[851] Yan and Yao reported the related rhodamine derivative **840**, which provides good selectivity for H_2S over competing anions in 50% MeCN in buffer, but was not tested with thiols.[852] Cai reported a spiropyran functionalized rhodamine **841** (RB-SP2), which provided a fluorescent turn-off response to H_2S in 40% EtOH in buffer.[853] This probe was selective for H_2S over competing anions but was not tested with thiols, although the turn-off response to H_2S was confirmed in HeLa cells. Also using a rhodamine platform, Li reported **842**, which provided a fluorescent response to H_2S with selectivity over competing anions and thiols in 50% EtOH in buffer.[854] The resultant probe was used to image exogenous H_2S in MCF-7 cells and was used additionally to investigate Cu^{2+} in Aβ aggregation. Liu and Pu reported the dual chromophore system **843** that provided a turn-off response to H_2S at 610 nm in mixed MeCN and water samples.[855] As an additional example, Yoo reported a related fluorescein-based adduct in **844** (ATSM-FITC), which showed good selectivity for H_2S over competing thiols, with only a small signal from 1 mM Cys and was further used to exogenous H_2S in HeLa cells.[856] The $^{64}Cu^{2+}$ version of this probe was applied *in vivo* to image endogenous H_2S in mouse brain using PET imaging, including differences upon AOAA or LPS treatment, in models of neuroinflammation.

Hydrazine and hydrazide-based scaffolds have also been used with different chromophores. For example, Tang reported the acylhydrazone-based **845**, which provided a turn-on response to H_2S at 523 nm with good selectivity for H_2S over anions and also Cys, GSH, and Hcy (Figure 1.170).[857] Qian and Zhu reported an aminonaphthalene motif **846** (NJ1), which provided a turn-on fluorescence response to H_2S at 492 nm. This system showed moderate selectivity for H_2S over competing anions and amino acids and was subsequently used to image exogenous H_2S in HeLa cells.[858] Li and Yang used a related approach to develop chromone derived **847**, which showed good selectivity for H_2S over other anions although showed a diminished response in the presence of F^-.[859] This probe was further used to develop test strips for H_2S

detection. Also using a coumarin chromophore, Pei reported glucose-ligated probe **848** (GluC) to improve solubility, which showed good selectivity for H_2S over competing anions and was subsequently used to develop a smartphone approach for H_2S measurement from test strips.[834]

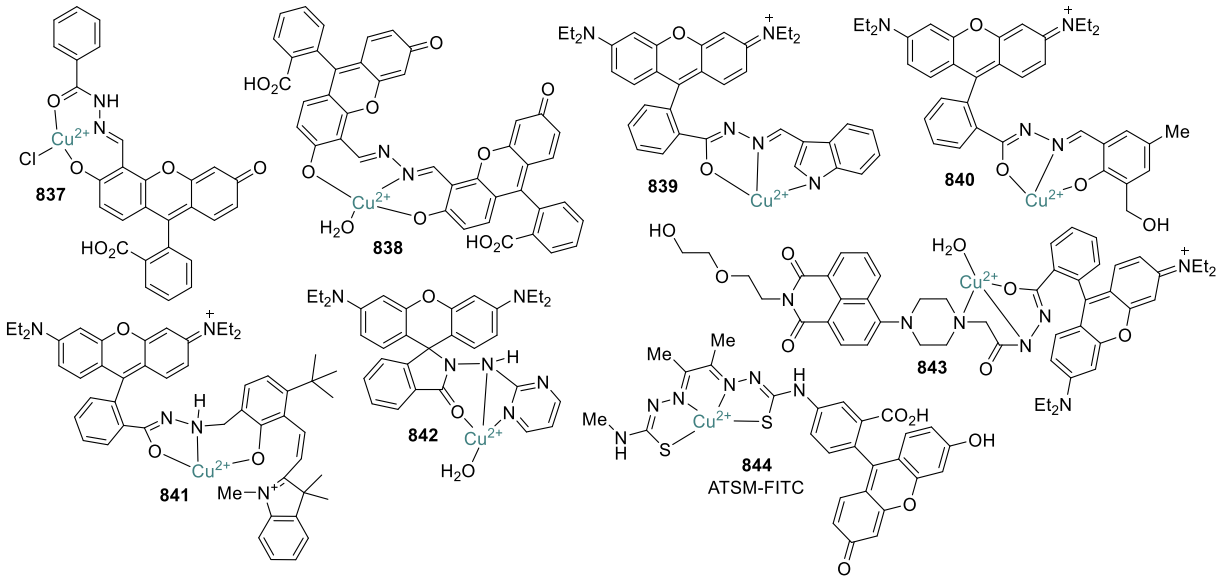


Figure 1.169. Examples of fluorescent H_2S probes based on Cu^{2+} precipitation from hydrazine and hydrazide ligands tethered to xanthene-based chromophores.

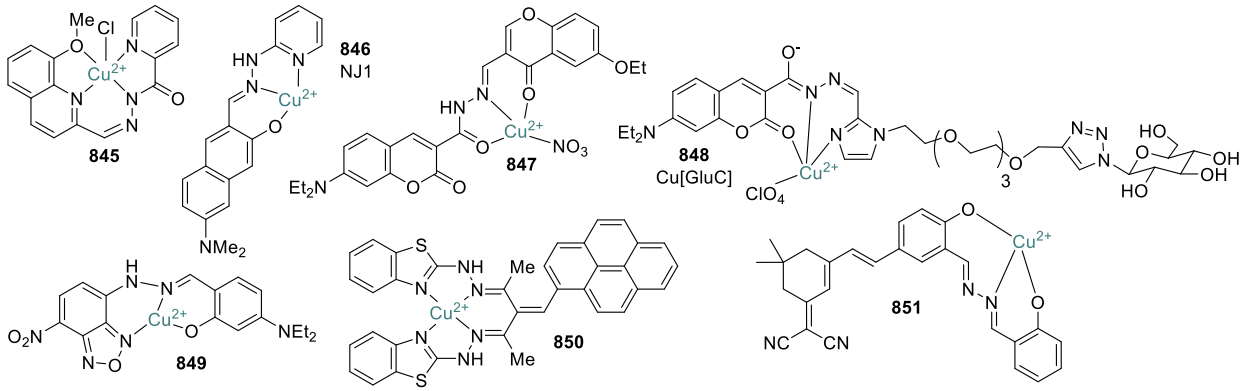


Figure 1.170. Additional examples of fluorescent H_2S probes based on Cu^{2+} precipitation from hydrazine and hydrazide ligands containing various chromophores.

Using similar chemistry with an NBD chromophore, Zhang and Zhang reported **849** (NL), which provided a turn-on response to H_2S at 519 nm in 30% THF in buffer. This probe provided good selectivity over competing species including Cys, Hcy, and GSH, although only 2 equiv. of each analyte was investigated.[860] The resultant probe was used to image exogenous H_2S in MDA-

MB-231 cells and also used to monitor responses using flow cytometry. Periasamy reported **850**, which includes a pyrene fluorophore and provides a turn-on response to H_2S at 510 nm with a change in fluorescence lifetime.[861] The resultant probe was subsequently used to investigate spiked H_2S levels in water samples and also used to image exogenous H_2S in A549 cells. Shifting to longer-wavelength emissions with a dicyanoisophorone-based fluorophore, Leng and Weng reported **851**, which provided a turn-on response at 659 nm and was used to develop paper test strips for H_2S.[862]

Similar ligand motifs have also been investigated with 2:1 Cu^{2+} to chromophore stoichiometry, including complex **852** from Tang and Tang (Figure 1.171). This probe provided a turn-on response at 652 nm in 70% DMSO in buffer and was also used to develop H_2S test strips.[863] Wang also reported a 2:1 complex in the triphenylamine based **853** (DPA-SAA), which provides a fluorescence turn-on at 492 nm and moderate selectivity over competing anions and thiols.[864] This probe was subsequently used to image exogenous H_2S in HeLa cells. Related amino-coumarin complexes were also reported by Liu, Xie, and Xu as well as Wang, Wu, and Xu that differed by inclusion of a quinoline or benzyl morpholine group in **854** and **855**, respectively. Both probes provided a turn-on response to H_2S at ~525 nm and were used to image exogenous H_2S in MCF-7 cells and zebrafish as well as HeLa cells, respectively.[865, 866]

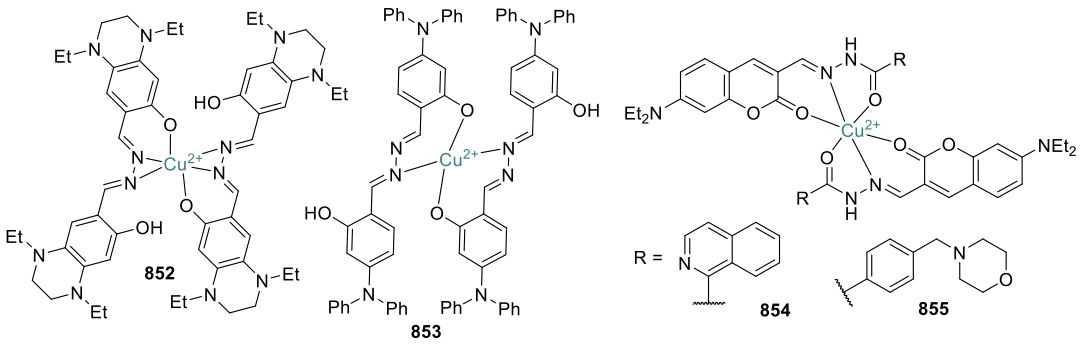


Figure 1.171. Examples of fluorescent H_2S probes based on Cu^{2+} precipitation from hydrazine and hydrazide ligands with a 2:1 ligand to Cu^{2+} stoichiometry.

Similar approaches have also been used with Cu^{2+}-imine motifs. For example, Liang reported **856** (AIE-S) in 2014, which contains a tetraphenylethylene motif that functioned by AIE and provided good selectivity for H_2S over competing anions and thiols in 10% THF in water (Figure 1.172).[867] This probe was subsequently used to image exogenous H_2S in HeLa cells. Shang

reported a series of phenylimine compounds with phenol, azo, and naphthyl functionalization in a series of papers to report compounds **857**–**860**.[868-870] These compounds were investigated in mixed DMSO buffer solutions and provided fluorescence responses between 391 and 490 nm with moderate selectivity over other anions by UV-vis spectroscopy. Dalai reported a related pyrene scaffold **861** that provided a fluorescent response at 429 nm and selectivity over other anions in mixed MeCN and water solutions.[871] Using a similar approach with a coumarin motif, Shang reported **862**, which provided selectivity against anions but also a significant response to Cys in mixed DMSO and water solutions.[872] Liu and Chen reported the related *tris*-Cu^{2+} complex **863** (TPI-H), which provided a fluorescent response to H_2S at 547 nm and good selectivity over competing anions.[873] This fluorescent response was also observed in MCF-7 cells treated with exogenous H_2S. Dong reported a related imine-based compound **864** with 1:1 stoichiometry, which exhibited moderate selectivity for H_2S over other anions.[874]

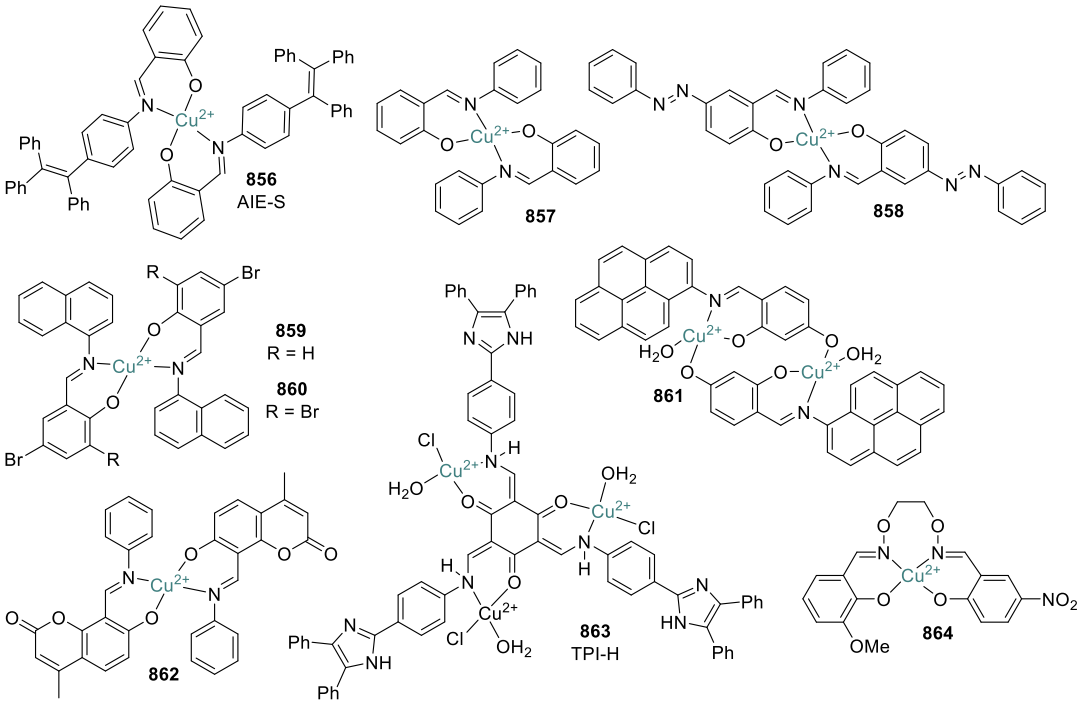


Figure 1.172. Examples of fluorescent H_2S probes based on Cu^{2+} precipitation from imine-based ligands.

Copper-benzimidazole complexes have also been used for H_2S detection. In 2014, Zang reported complex **865**, which showed a turn-on fluorescence response at 436 nm, showed good

selectivity for H_2S over competing anions, and was used to image exogenous H_2S in Ec-9706 cells (Figure 1.173).[875] Similarly, Huang and Wang reported a BINOL-benzimidazole motif **866**, which showed a turn-on response at 590 nm and minimal response to Cys in 20% DMF in buffer and was used further to develop H_2S test strips for gas detection.[876] Zhang and Fang also used this approach to develop the benzimidazole conjugate **867** (AQ-NS), which also contains two thioether motifs for Cu^{2+} binding. The resultant probe showed a turn-on response at 610 nm in 40% EtOH in buffer, with a moderate response when exposed to 10 equiv. of thiols.[877] Expanding to an AIE turn-on mechanism, Sun, Tang, and Yan reported the Cu-benzothiazole complex **868** (TPE-1), which generates a fluorescent response at 618 nm upon exposure to H_2S with good selectivity toward anions and thiols, although a minor response to CN^-, HPO_4^{2-}, and HCO_3^- was observed.[878] The resultant probe was used to investigate H_2S in food samples and also in MCF-7 cells.

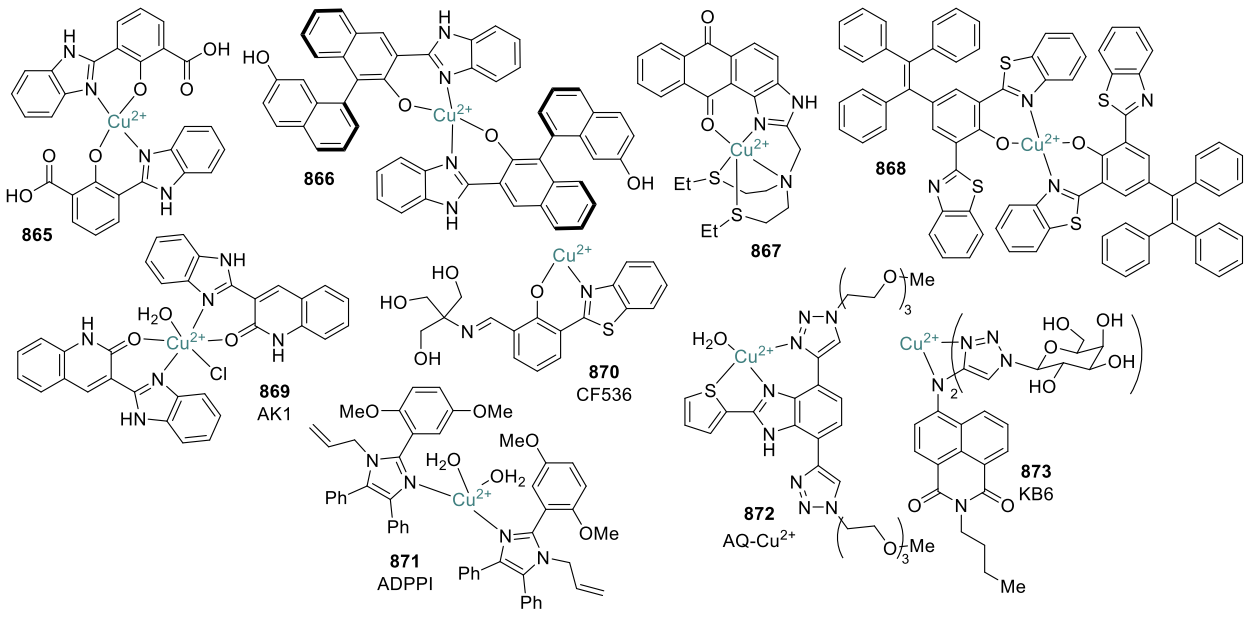


Figure 1.173. Examples of fluorescent H_2S probes based on Cu^{2+} precipitation benzimidazole, triazole, and benzothiazole ligands.

Elango reported coumarin-derived **869** (AK1), which provided a moderate fluorescent turn-on in response to H_2S with moderate selectivity over other anions and was further used to investigate H_2S in different water sources.[879] Using a related benzothiazole motif, Guo reported **870** (CF536), which provided a fluorescent response at 536 nm upon treatment with H_2S and good selectivity over other anions.[880] This probe was also used to image exogenous H_2S in HepG2 cells.

El-Wekil reported the imidazole construct **871** (ADPPI), which provided a turn-off response to H_2S at 447 nm in 50% iPrOH in buffer and was further used to measure H_2S levels in spiked water samples.[881] Incorporating a thiophene motif, Cai and Leung reported **872** (AQ-Cu^{2+}), which bound 1 equiv. of Cu^{2+}, provided a fluorescent turn-on response to H_2S, and showed good selectivity for H_2S over competing anions, with minor responses to $S_2O_5^{2-}$, $S_2O_8^{2-}$, and GSSG.[882] The resultant probe was further used to image exogenous H_2S in A549 cells. Han and He also reported a monomeric Cu^{2+} construct in **873** (KB6), which incorporated solubilizing β-D-galactoside groups.[883] The resulting probe showed a turn-on fluorescent response to H_2S at 535 nm and good selectivity over competing anions, and the probe was used further to investigate H_2S in water samples.

Other Cu^{2+} coordination environments have also been reported for use with H_2S sensing motifs. In an early example of this approach, Guo and Shen reported **874**, which forms a 2:1 complex with Cu^{2+} and a turn-on response to H_2S at 600 nm in 80% DMSO in water, but did show a moderate response to 10 equiv. of GSH (Figure 1.174).[884] This probe was also used to image exogenous H_2S in HeLa cells. Zeng and Wu reported a fluorescein-polyamine motif **875** that also provided a turn-on response to H_2S with good selectivity over other anions but also provided a response to GSH.[885] The resultant probe was used to investigate H_2S in water samples and also image exogenous H_2S in HeLa and L929 cells. Tang reported a piperazine based Cu^{2+}-binding motif in **876**, which reacts with H_2S to generate a fluorescent response an 495 nm, with some signal from stoichiometric addition of diphosphate ($P_2O_7^{4-}$) or GSH.[886] Tang and Nandhakumar reported probe **877**, which provided a turn-on response to H_2S at 475 nm with good selectivity for H_2S over competing anions, Cys, GSH, and Hcy.[887] The cyclability of this probe by sequential addition of Cu^{2+} and H_2S was also demonstrated. Koruda reported a functionalized imidazole scaffold in **878** (HPI) that also provided a turn-on response to H_2S and was used to investigate H_2S in water samples.[888] Paul and Pombeiro reported quinazoline scaffold **879**, which also binds Cu^{2+} and provides a turn-on response to H_2S at 425 nm in 50% DMF in buffer with minimal response to other anions except for CN^-.[889] This probe was subsequently used to image exogenous H_2S in DL cells.

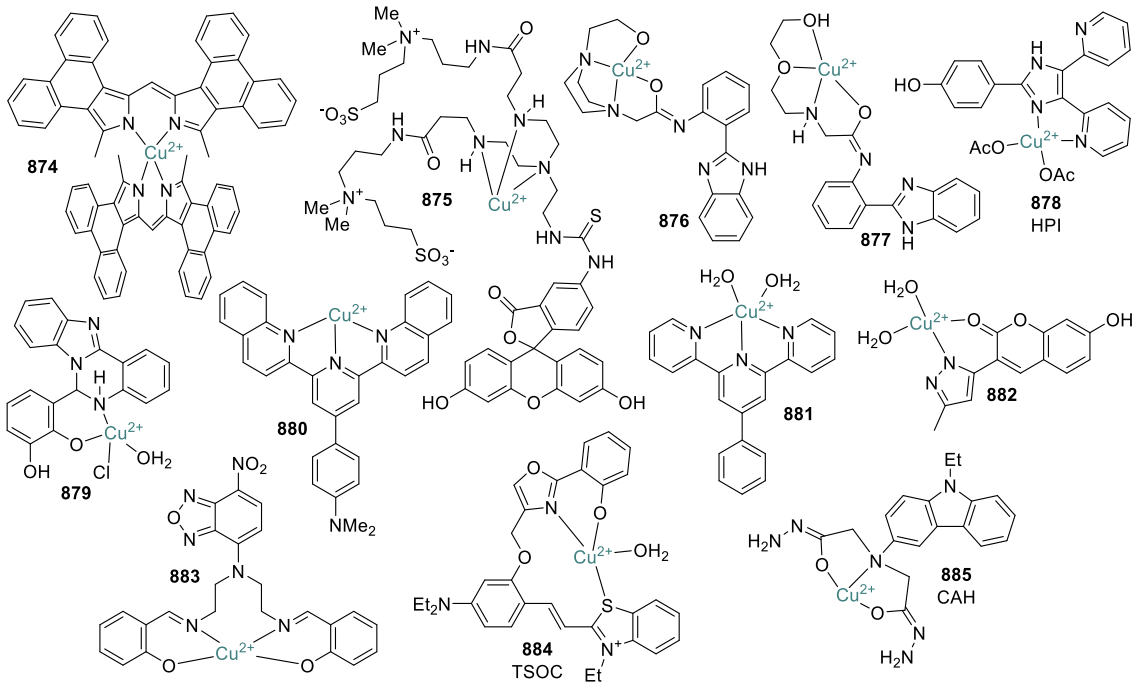


Figure 1.174. Examples of fluorescent H_2S probes based on Cu^{2+} precipitation from other nitrogen-based coordination environments.

Using a bis-quinoline pyridine scaffold, Liang reported **880**, which provided a fluorescent response to H_2S at 477 nm, minor responses to 5 equivalents of thiols, and was subsequently used to image exogenous H_2S in HepG2 cells.[890] Using a related approach, Jose reported a terpyridine system **881**, which provided a turn-on response to H_2S at 364 nm, but was also partially activated by Cys and GSH.[891] Expanding to comparing motifs, Wang and Xu reported **882**, which provided a turn-on response at 466 nm upon treatment with H_2S that was attributed to AIE.[892] This probe was further demonstrated to detect exogenous H_2S in both HeLa cells and zebrafish. A turn-off response was also reported for the Zn^{2+} adduct of **882**. Wang reported the NBD-Cu^{2+} complex **883**, which provided a turn-on response to H_2S at 540 nm with good selectivity over other anions and also Cys, GSH, and DTT and was further used to measure H_2S in different water samples.[893] Sun and Xu reported the Cu^{2+} benzothiazolium **884** (TSOC), which provides a red-shifted turn-on response to H_2S at 600 nm.[894] This probe showed good selectivity for H_2S over competing anions and was demonstrated to respond to exogenous H_2S in live SHSY5Y cells. Expanding to carbazole based systems, Liu and Jiang reported **885** (CAH), which provided a turn-on response at 425 nm with moderate activation by GSH, Cys, and Hcy, and was used to develop paper sensors for H_2S.[895]

Fewer examples of Cu^{2+} coordination for H_2S reporting involve primarily oxygen-based coordination spheres. In general, as the coordination environment gets weaker the selectivity for metal precipitation by H_2S rather than thiols is eroded. As examples of this approach, Wang and Jin reported a dihydroxy anthraquinone motif **886** (DHAQ), which provided a fluorescence response at 538 nm with good selectivity for H_2S over other anions, with only a small response to CN^- (Figure 1.175).[896] Using a catechol-functionalized coumarin, Li, Li, and Wu reported **887** (CMOH), which was found to bind Cu^{2+} with a 1:1 stoichiometry and provided a fluorescent response at 500 nm upon addition of H_2S.[897] This probe showed good selectivity over other anions although thiols were not investigated, and was demonstrated to be cyclable with repeated addition of Cu^{2+}/H_2S (Figure 1.176). Probe **887** was further used to image exogenous H_2S in HeLa cells. He also reported the hydroxy-naphthalene scaffold **888** (NA-LCX), which provided a turn-on response to H_2S at 575 nm in 60% DMSO in buffer.[898] This probe showed a moderate response toward 10 equivalents of Cys, Hcy, and GSH and was subsequently used to image exogenous H_2S in HepG2 cells. Building from a coumarin based system, Lu and Li reported **889** ($(BuCAC)_2Cu$), which provided a turn-on fluorescence response to H_2S in 80% MeCN in buffer with good selectivity for H_2S over competing anions.[899] This probe was further used to image exogenous H_2S in HeLa cells, soybean root tissues, and zebrafish.

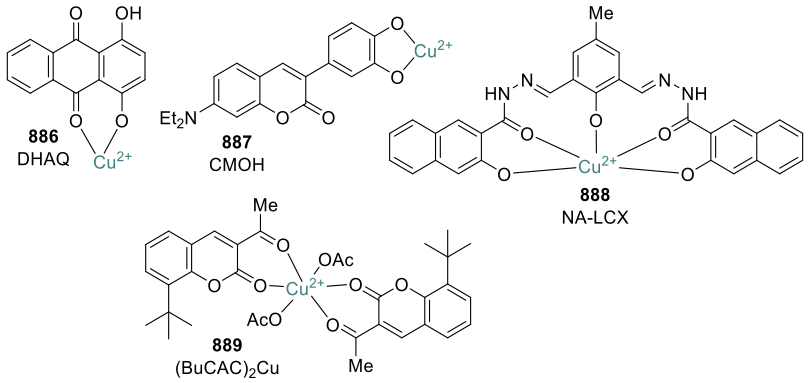


Figure 1.175. Examples of fluorescent H_2S probes based on Cu^{2+} precipitation from oxygen-based ligands.

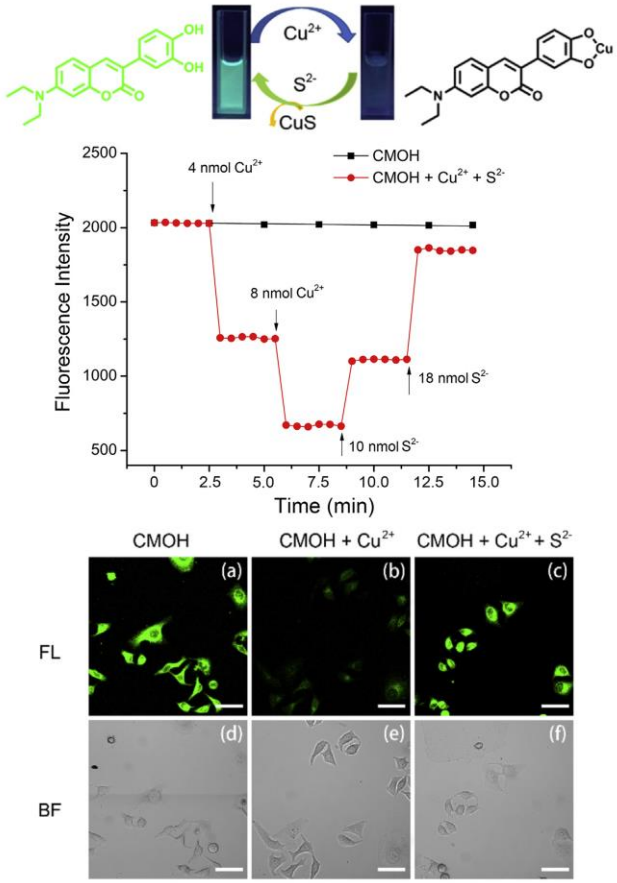


Figure 1.176. (top) Response of **887** upon addition of Cu^{2+} and H_2S. (bottom) Example of the fluorescent response of **887** in HeLa cells upon addition of Cu^{2+} followed by H_2S. Reproduced with permission from ref [897]. Copywrite 2019 Elsevier.

1.5.1.2 Zn^{2+} Precipitation

Although Cu^{2+} often provides an additional advantage of paramagnetic quenching upon coordination to fluorophores, other metals have also been used for precipitation-based H_2S reporters. For diamagnetic metals like Zn^{2+}, this approach often results in different fluorescent signals before and after removal of Zn^{2+} or a turn-off response. For example, the ligand-fluorophore conjugates are not fluorescent due to photoinduced electron transfer (PET) from the ligand lone pairs to the chromophore. Coordination of the Zn^{2+} ion lowers the energy of coordinating lone pairs and restores the fluorescence. In such a system, removal of Zn^{2+} by H_2S would result in a fluorescence turn-off response. Alternatively, Zn^{2+} coordination has been used to generate turn-on responses by disrupting hydrogen bonding or rotational components of a chromophore that are required for fluorescence. In contrast to the lighter Zn^{2+} congener,

coordination of heavy metals like Hg^{2+} often results in fluorescent quenching through spin orbit coupling, which can subsequently result in a fluorescent turn-on upon heavy metal removal by H_2S.

In an early example of this approach, Tang reported the Zn^{2+} conjugate of a DPA-benzimidazole motif in **890** (BMD), which provides a ratiometric response to H_2S with fluorescence increase at 502 nm and concomitant decrease at 424 nm in 20% MeCN in buffer (Figure 1.177).[900] This probe reported good selectivity for H_2S over 20 equiv. of competing anions and thiols. Using a more compact ligand system, Kim and Harrison reported a quinoline-based Zn^{2+} complex **891**, which provides a fluorescence turn-off response to H_2S, with good selectivity for other anions and cations, although Hg^{2+} also generated a turn-off response.[901] Jose reported a Zn^{2+} terpyridine motif in **892**, which also provided a turn-off fluorescence response to H_2S at 360 nm that also provided a significant response to Cys and GSH.[891]

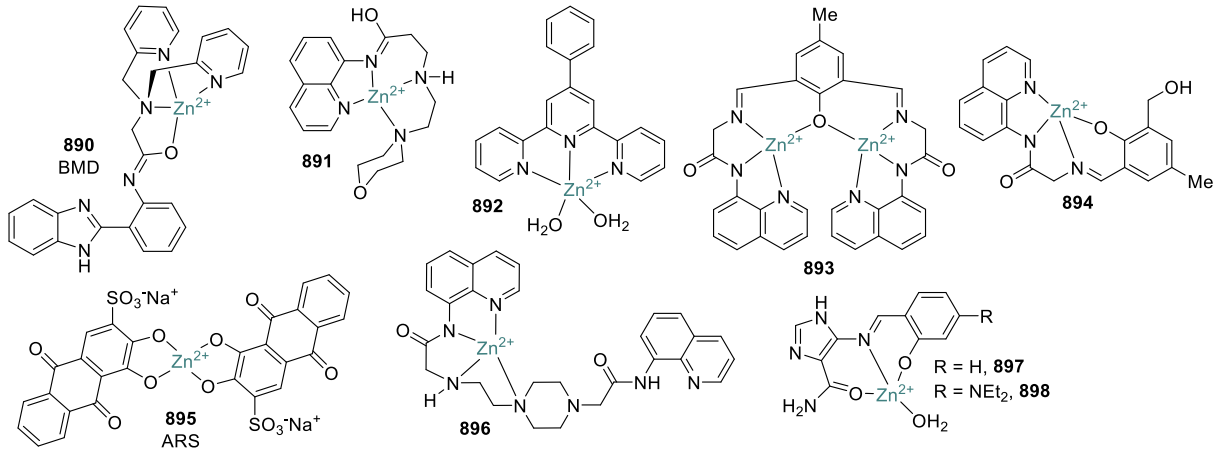


Figure 1.177. Examples of fluorescent H_2S probes based on Zn^{2+} precipitation.

Expanding to other coordination environments, Dong and Ma reported the 2:1 Zn^{2+} to ligand complex **893**, which provides a turn-off response to H_2S in 50% MeOH in buffer, with good selectivity for H_2S over 10 equiv. of other anions, Cys, and GSH.[902] Dong and Ma also reported a monomeric Zn^{2+} motif **894**, which provided a similar turn-off response and selectivity profile toward H_2S.[903] Using the Alizarin Red S Zn^{2+} complex **895** (ARS-Zn(II)), Jose also reported a turn-off response to H_2S in 75% MeOH in buffer.[904] This response was attenuated by Cys and GSH as well as phosphates, but the turn-off response was also confirmed using exogenous H_2S in

C6 cells. Kim and Kim reported the quinoline-based **896**, which reacts with H_2S to generate a turn-off response at 500 nm in buffer with good selectivity over other competing ions, including CN^- and SCN^-.[905] The turn-off response from the probe toward H_2S was also demonstrated in HeLa cells and live zebrafish. Kim also reported related Zn^{2+} adducts **897** and **898**, which reacts with H_2S to abolish the fluorescent signal at 484 nm with good selectivity for H_2S over competing anions.[906, 907] This turn-off response was also demonstrated in HeLa cells.

1.5.1.3 Cd^{2+}/Hg^{2+} Precipitation

Moving down group 12 on the periodic table, Cd^{2+} has also been used to develop H_2S responsive probes. Ojida reported the bis(DPA) xanthene motif **899**, which provided a ratiometric response to H_2S with a fluorescent decrease at 557 nm and moderate increase at 527 nm (Figure 1.178).[908] This probe was found to show only minor activation by GSH, and a related esterified version of the probe (**900**) was used to image a ratiometric response to exogenous H_2S in HeLa cells (Figure 1.179). Using a related pyronine-based system, Ojida also reported **901**, which provided a ratiometric response to H_2S with a fluorescence increase at 559 nm and moderate decrease at 619 nm.[909] This probe showed good selectivity for H_2S over GSH and was used to image both exogenous H_2S in HeLa cells and also endogenous H_2S in HUVECs after addition of VEGF.

Moving further down group 12, different Hg^{2+} complexes have also been used for H_2S detection. As an example of this approach, Sanz-Medel reported that the simple Hg^{2+} **902** reacted with H_2S in 1999 to generate a fluorescence response at 373 nm (Figure 1.180).[910] This compound was used to measure H_2S levels in exhaled breath in humans and correlated with breath malodor scores. As another example, Chattopadhyay reported the rhodamine Hg^{2+} complex **903**, which reacts with H_2S to generate a ratiometric response with fluorescence increase at 440 nm and decrease at 575 nm.[911] This probe showed good selectivity over other anions, but thiol interferants were not investigated. Probe **903** was subsequently used to image exogenous H_2S in HeLa cells. Wang reported a Hg^{2+} complex **904** (PIPT), which provided a turn-on response upon reaction with H_2S at 505 nm with good selectivity over other anions except for Br^- and selectivity against thiols was not reported.[912] The resultant probe was used to develop paper-based test strips for H_2S and to investigate H_2S in different water sources. Singaravadivel also reported a Hg^{2+} complex based on a phenothiazine-diaminomalenonitrile in **905**.[913] This probe provided a turn-on response to H_2S

in 60% EtOH in water and was demonstrated to image exogenous H_2S in HeLa cells. Using a bis-amide scaffold, Wang reported **906**, which reacts with H_2S to remove HgS and restore the fluorescence of the ligand.[914] This probe was selective for H_2S over competing RSS and RNS and was further used to measure H_2S in different spiked water samples. Zao and Ding reported Hg^{2+} complex **907** (*ol*-PIP), which results in a fluorescent turn-off at 495 nm in response to H_2S, which was confirmed with exogenous H_2S in HeLa cells.[915]

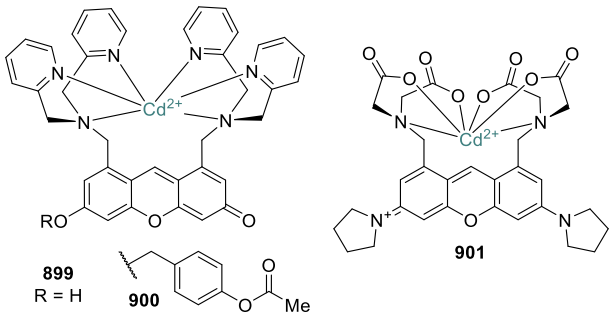


Figure 1.178. Examples of fluorescent H_2S probes based on Cd^{2+} precipitation.

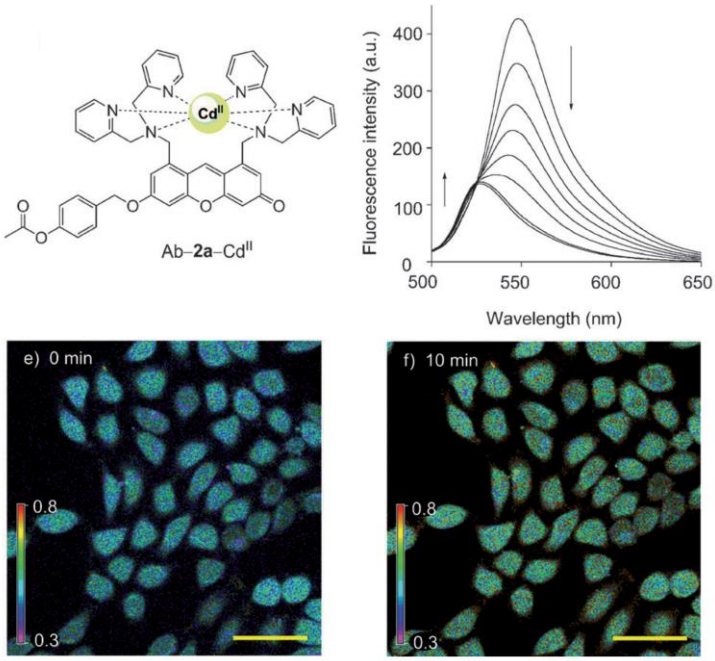


Figure 1.179. (top) Ratiometric response from **899** in response to H_2S. (bottom) Change in cellular fluorescence after treatment of HeLa cells incubated with **900** with H_2S. Reproduced with permission from ref [908]. Copyright 2014 John Wiley and Sons.

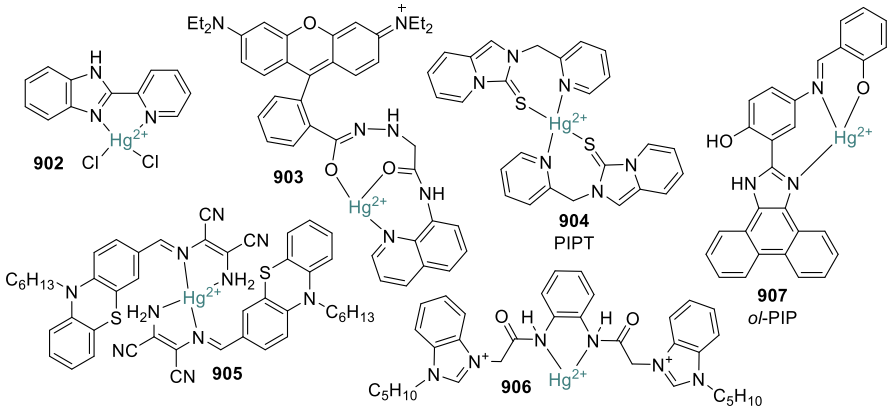


Figure 1.180. Examples of fluorescent H_2S probes based on Hg^{2+} precipitation.

1.5.1.4 Other Metals

As selected examples of other heavy metal precipitation approaches for H_2S detection, Ag^+, Sn^{4+}, and Pd^{2+} examples have also been reported. For example, Rarabi reported the 2:2 Ag^+ to ligand complex **908** that reacts with H_2S to generate a fluorescence response at 520 nm (Figure 1.181).[916] Moderate signal was also observed for I^-, Br^-, and Cl^-, likely due to the low solubility product of these anions with Ag^+. Wang also used an Ag^+ in with tetrasulfonated porphyrin **909** to provide a fluorescent turn-on toward H_2S, which provided good selectivity for H_2S over competing halides and anions.[917] This probe was further used to measure added H_2S in rabbit serum samples. In work with Sn^{4+}, Mahapatra reported the rhodamine-based adduct **910** (AR), which reacts with H_2S to provide a turn-off response at 582 nm in 80% MeOH in water.[918] This probe was subsequently used to image exogenous H_2S in Raw 264.7 cells. As an example of Pd^{2+} based approaches, Cardoso reported the bis(2-aminobenzoic) **911**, which reacts with H_2S to generate a fluorescent response at 410 nm with selectivity over gaseous interferants including NO_2 and SO_2.[919] This system was subsequently used to develop cellulose paper test systems for gaseous H_2S. Using a BODIPY-based system, He and Guo reported Pd^{2+} complex **912** (BDPA), which provided a fluorescent response at 632 nm in response to H_2S in 20% DMSO in buffer with good selectivity for H_2S over competing anions.[920] This complex was further applied to develop H_2S test strips, which were demonstrated to maintain the same selectivity observed in solution. Other metals, including Cr^{3+} have also been used for H_2S detection, with Yu, Li, and Zhang providing

example **913**, which provides a turn-off response when treated with H_2S that was also confirmed in HeLa cells treated with exogenous H_2S.[921]

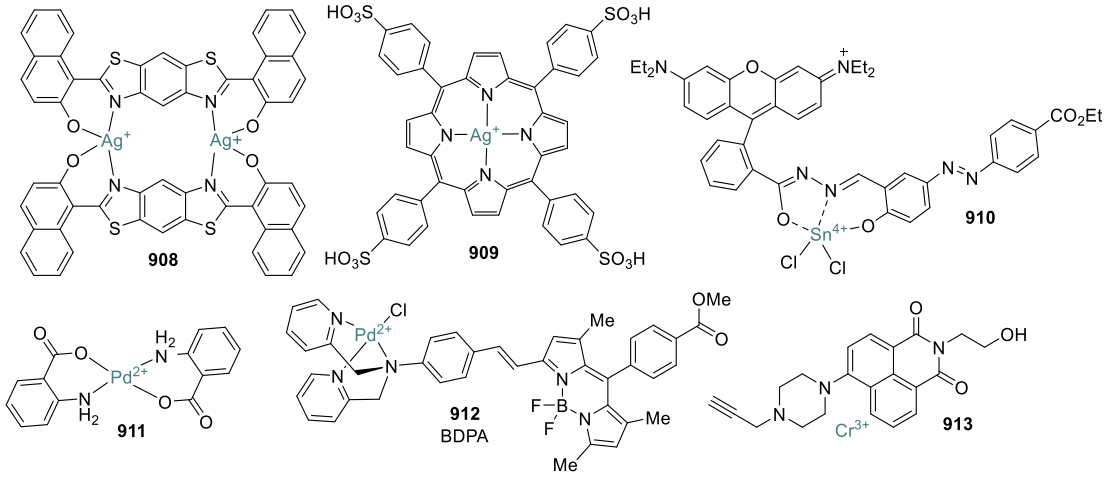
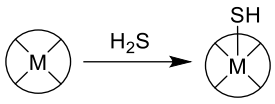


Figure 1.181. Examples of fluorescent H_2S probes based on precipitation of other metals.

1.5.2 Metal Coordination

The coordination of H_2S, or more commonly HS^-, to transition metal centers provides another platform on which metal complexes have been developed for H_2S reporters (Scheme 1.23). This approach offers the longer-term potential benefit of developing functionally-reversible probes for H_2S detection based on the reversible coordination of H_2S/HS^- to a metal center. Such approaches would need to overcome the significant concentration differences of thiols like GSH and Cys when compared to endogenously relevant H_2S levels, which poses a fundamentally challenging problem. In addition, the coordination chemistry of H_2S/HS^- is inherently challenging due to both the prevalence of forming insoluble metal-sulfide products and also the challenges in characterizing M-SH motifs.[922] Despite these challenges, a number of reports have focused on the development of different coordination approaches for H_2S detection.



Scheme 1.23. General approach for developing responsive systems upon H_2S/HS^- coordination to a metal.

1.5.2.1 Small Molecule Approaches

In an early example of developing platforms that provide a fluorescent response to H_2S, Galardon reported Zn^{2+} complexes **914** and **915** in 2009, which are based on coumarin coordination to a trispyrazolylborate Zn^{2+} complex (Figure 1.182).[923] Both the parent coumarin and thiocoumarin derivatives were prepared, but reactions with H_2S focused on thiocoumarin adduct **915**. Reaction of this complex with H_2S in 67% acetone in buffer resulted in a fluorescence turn-off, which was preserved in the presence of excess Cys or GSH. This general response profile is consistent with HS^- coordination to the Zn^{2+} center and displacement of the fluorophore, which in the case for the thiocoumarin derivative is minimally fluorescent in free solution. The formation of such Zn-SH species opens the door for potentially chemically reversible systems upon protonation and liberation of H_2S gas. Pluth reported examples of this approach in 2014 and 2016 with Zn phthalocyanine and pyridyl diamine complexes, respectively, but did not include fluorescence investigations nor studies in water.[924, 925] Strianese and Pellecchia expanded on this approach with a Zn^{2+} porphyrin complex **916** in 2017, which binds HS^- and results in a fluorescence decrease at 630 nm.[926] This fluorescence decrease could be rescued by addition of acetic acid, demonstrating the coupling of chemical reversibility with a fluorescence response.

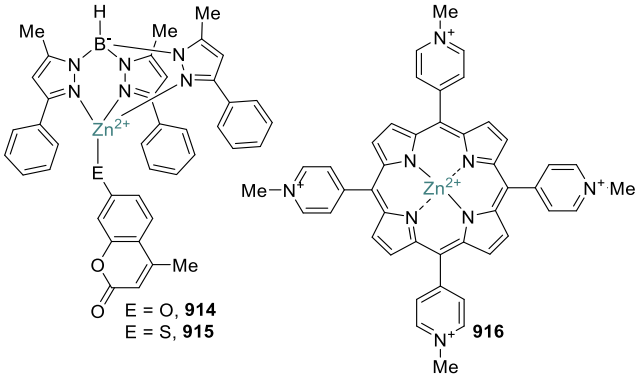


Figure 1.182. Examples of Zn^{2+} complexes that bind HS^- to provide a change in fluorescence response.

Strianese has further expanded on the Zn^{2+}/H_2S coordination approach with a number of different pyridoxal-based systems. The reaction of hydrosulfide with Zn^{2+} complexes **917**–**919** resulted in a negligible response from **917** and **918** in DMSO or pH 10 buffer, respectively (Figure 1.183). Compound **919**, however, provided a significant fluorescent shift from 500 to 380 nm upon

addition of H_2S in pH 7.4 buffer.[927] The selectivity of this response to H_2S over thiols was not reported.

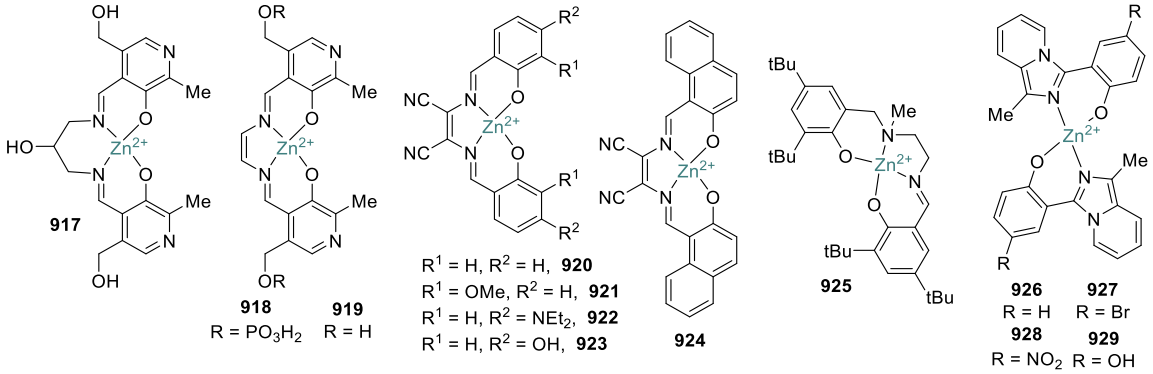


Figure 1.183. Additional examples of Zn^{2+} complexes investigated for HS^- binding to generate a fluorescence response.

Expanding on the salen platform, Strianese also reported derivatives **920**–**923**, which provided different responses to H_2S in DMSO.[928] Focusing on compound **923**, a turn-on response to H_2S was also observed at 630 nm in water, which could be reversed by addition of acetic acid. This compound was subsequently used to image exogenous H_2S in HepG2 cells (Figure 1.184). Probe **923** and also related **924**, which provides a fluorescent turn-off at ~650 nm upon treatment with H_2S, were used to develop sol-gel matrices on paper strips for both visible and fluorescence detection of H_2S in different samples in two separate reports.[929, 930] Using a similar Salalen ligand system, Strianese also reported **925**, which provides a fluorescent enhancement at 480 nm and increase in fluorescence lifetime upon treatment with H_2S.[931] This complex was also screened with Cys and GSH, both of which provided minimal responses. Using a related approach but different ligand scaffold, Strianese also reported the imidazo-pyridine system with ligand variants **926**–**929**, which also provide responses to H_2S in DMSO.[932] Focusing on **929**, the fluorescence response at 460 nm was maintained in water and could be reversed by acidification with acetic acid. The selectivity of this platform against other analytes was not investigated, but the probe was used to image exogenous H_2S in HepG2 cells.

Expanding to other transition metals, Strianese and Pellecchia reported Zn^{2+} and Co^{2+} complexes of a heteroscorpionate ligand in **930** and **931**, respectively (Figure 1.185).[933] Both **930** and **931** reacted with H_2S in CH_2Cl_2 to provide fluorescent turn-on responses at ~350 and ~325

nm, respectively. The chemistry associated with this response was not determined, but in the case of **931** was likely due to partial ligand hydrolysis due to the appearance of an aldehydic proton in the ^{1}H NMR spectrum. Nonetheless, these platforms provide a fluorescent response to H_2S, albeit by an unclear mechanism. Rurack also reported a Co^{2+} based approach with the BODIPY-cobaloxime complexes **932** and **933**.[934] Both of these complexes react with HS^- in MeCN to generate a fluorescent response at 527 nm due to BODIPY displacement, with a larger response for **933**. Complex **932** was also investigated in water/hydrogel solutions and demonstrated to provide a fluorescence response to H_2S, although significant fluorescent responses were also observed for HSO_3^- and Cys. Moving to a Cu^{2+} based system, Strianese and Pellecchia investigated the protoporphyrin **934** (CuPPIX).[935] At pH 12.6, a significant change in the fluorescence intensity was observed, with the appearance of a new emission band at 430 nm. This complex showed good selectivity for H_2S over GSH and Cys, but did show moderate responses for SCN^-, HSO_4^-, HSO_3^-, and leucine. The resultant response was attributed to coordination to the Cu^{2+} metal center. We note that prior work with CuPPIX in organic solution showed no reactivity toward H_2S or HS^-,[936] which when taken together with the work above highlights the likely importance of solvation environment and pH in H_2S reactivity.

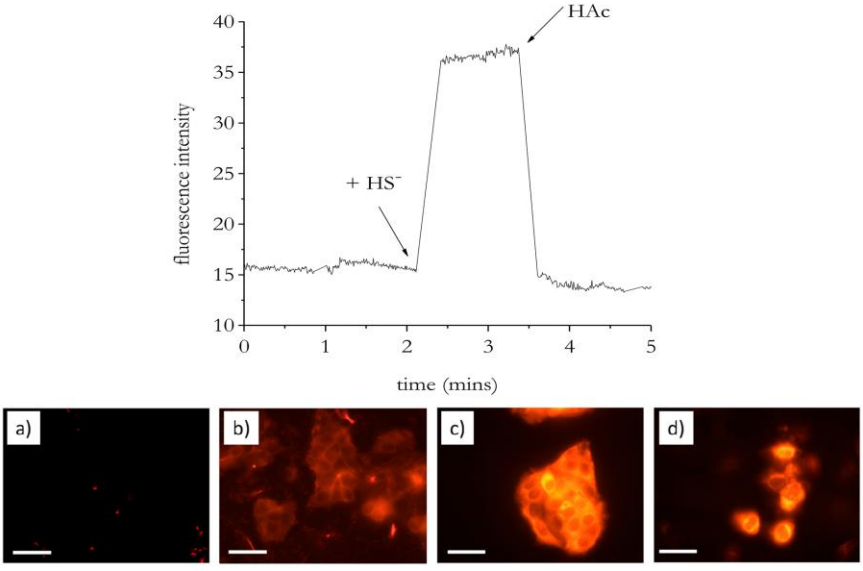


Figure 1.184. (top) Change in fluorescent response from **915** upon addition of H_2S and acetic acid. (bottom) Fluorescent response from HepG2 cells treated with (a) no addition, (b) 120 μM of **923**, (b)120 μM of **923**-SH, and (d) 120 μM of **923** with 250 μM NaSH. Reproduced with permission from ref [928]. Copyright 2020 American Chemical Society.

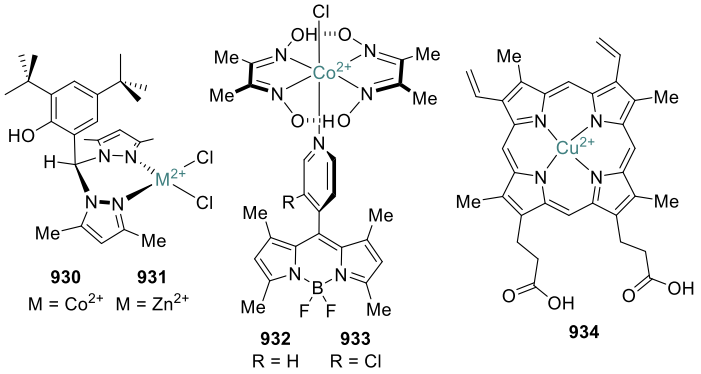


Figure 1.185. Additional examples of metal complexes used to investigate coordinative approaches for H_2S detection.

1.5.2.2 Protein Approaches

Although we have generally excluded protein-based systems for H_2S detection in this review, there are selected examples involving H_2S/HS^- coordination that we chose to highlight based on their relevance to H_2S/HS^- coordination to transition metal centers. In general, the reaction of H_2S with protein metal centers can either result in metal reduction with concomitant sulfide oxidation, or can result in coordination, and in some cases reversible binding. The most well know example of the latter reaction manifold is from the heme center in *Lucina pectinata*, a clam commonly found in sulfide-rich swamp waters.[937-939] Although this level of reversibility has to date eluded synthetic chemists, a number of approaches have leveraged different H_2S binding or reversible interactions with protein metal centers to develop different reporting strategies.

In an early report of this approach, D'Auria labeled the *N*-terminus of horse skeletal muscle myoglobin (Mb) with Atto620 and Cy3 dyes to develop FRET-based system **935**.[940] Upon reaction with H_2S, the Soret band at 409 nm shifts to 421 nm, and the weaker absorbances at 503 and 636 nm are quenched, with new absorbances appearing at 543, 581, and 617 nm. These changes in absorbance and spectral overlap with the ligated Atto620 (λ_{ex} = 620 nm, λ_{em} = 645 nm) and Cy3 (λ_{ex} = 550 nm, λ_{em} = 570 nm) dyes resulted in fluorescence turn-on and turn-off responses, respectively. In both cases, bubbling Ar through the solution reverses the response. System **935** was also demonstrated to function when immobilized in a sol-gel matrix for solid state measurements. Eventually, these systems are reduced to the more stable ferrous Mb, which stymies reversibility, but as a whole provides a useful proof of concept for reversible detection using protein motifs.

Using a related approach with recombinant HbI from *L. pectinata* (rHbI), Galardon used the spectral overlap between HbI in the presence and absence of H_2S with the absorbance of the Pacific Blue coumarin dye to develop a reversible H_2S sensing system in **936** (Figure 1.186).[941] rHbI has an absorbance band at 407 nm, which shifts to 425 nm upon H_2S binding, allowing for coupling to the excitation band of Pacific Blue at 404 nm. This system showed good selectivity for H_2S over Cys and GSH and the reversibility was demonstrated for multiple cycles when purged by Ar. This system was also used to detect exogenous H_2S, but not GSH, added to human plasma.

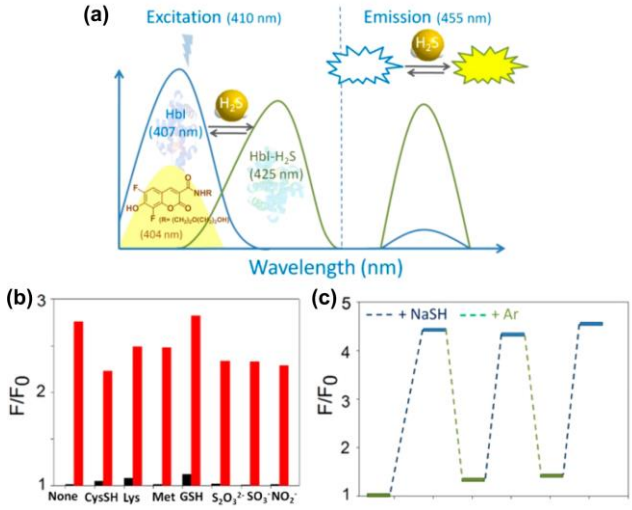


Figure 1.186. (a) General schematic for **936** in which a turn-on fluorescent response is generated using the change in rHbI absorbance upon H_2S binding to modulate the fluorescence of a Pacific Blue fluorophore. (b General selectivity of **936** against competing species, and (c) demonstration of reversibility up purging with Ar. Reproduced with permission from ref [941]. Copyright 2018 American Chemical Society.

Non-heme protein systems have also been leveraged for H_2S detection. For example, Strianese reported a cobalt peptide deformylase (Co-PDF) conjugate labeled with the Atto620 dye to generate conjugate **937**.[942] Reaction with H_2S resulted in irreversible sulfide coordination to the Co, which was supported by X-ray crystallography, and a broad increase in absorbance that overlapped with the Atto620 absorbance. This change in absorbance resulted in fluorescence turn-off from the Atto620 dye upon H_2S addition. Strianese and Palm reported a related example in investigating the reaction of H_2S with the metalloprotein Cu-azurin **938** as well as its Co^{2+} adduct **939**.[943] For **938**, addition of H_2S to a buffered aqueous solution bleached the 550–650 nm absorbance, which could be restored by addition of the oxidant $K_3[Fe(CN)_6]$, suggesting that

addition of H_2S results in Cu^{2+} reduction rather than Cu precipitation and formation of the apoprotein. When coupling the Atto620 dye to Cu-azurin a fluorescence enhancement was observed upon H_2S addition, which again could be bleached by oxidation by $K_3[Fe(CN)_6]$. Additional experiments were performed with Co-azurin **939**, which was labeled with Alexa350 to match the absorbance profile of the Co-azurin platform. Upon addition of H_2S, a fluorescence decrease from the Alexa350 dye was observed, which could be restored by oxidation by $K_3[Fe(CN)_6]$. Addition of Cys or GSH did not result in fluorescence modulation, highlighting the specificity of this approach for H_2S (Figure 1.187).

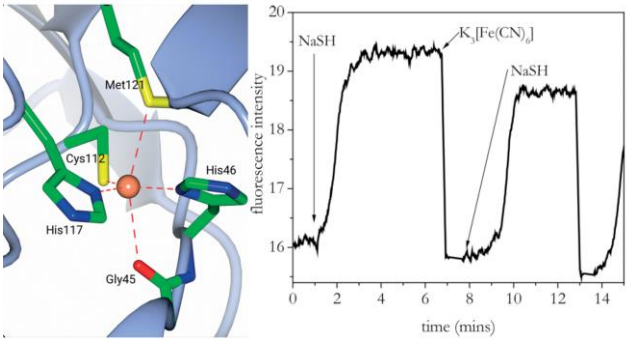


Figure 1.187. (left) Copper site in Cu-azurin. (b) Fluorescence response of Atto 620-labelled Cu-azurin **938** after addition of 50 μM NaSH and 80 μM $K_3[Fe(CN)_6]$. Reproduced with permission from ref [943]. Copyright 2019 American Chemical Society.

1.6 Fluorescent Probes for Sulfane Sulfur-Containing Species

In addition to developing activity-based fluorescent probes for H_2S, different researchers have also developed innovative approaches for detecting other RSS. For example, persulfides (RSSH), polysulfides (RSS_nSR), and hydropolysulfides (HSS_nSR or HSS_nH) are all important RSS that have chemical reactivities that can be targeted by activity-based probes. Different quantification approaches, such as the monobromobimane method for H_2S/H_2S_n/polysulfide quantification, have been reported, but these approaches do not provide the real-time response afforded by activity-based probes.[944-947] One characteristic of these partially oxidized RSS is that they contain both nucleophilic and electrophilic sulfur atoms, which has been leveraged to develop different approaches for detecting these species. In general, most of these probes report broadly on sulfane sulfur containing species, rather than one specific RSS, in part due to the rapid interconversion of many of these species. For example, many researchers use commercially

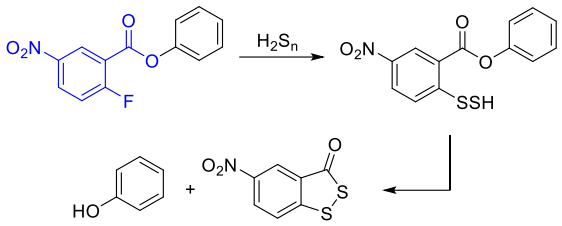
available polysulfide sources like Na_2S_2, Na_2S_3, or Na_2S_4, but these species can rapidly equilibrate in solution, and reactivity with these polysulfides is generally under Curtin−Hammett control.[948] Because of these equilibria, the general term of H_2S_n is commonly used to denote the complex milieu of partially oxidized sulfide species used to activate this family of probes.

1.6.1 Electrophilic Probes

One approach to develop activity-based probes for polysulfides is to use electrophilic groups that can react with nucleophilic RSS. Based on the enhanced nucleophilicity of polysulfide and persulfide due to the α-effect, weaker electrophiles can be used to intercept these species when compared to previously discussed electrophilic probes for H_2S.[949] A common approach to target H_2S_n species is to use an electrophilic protecting group coupled through an ester linkage appended to a chromophore. After initial H_2S_n reactivity, the subsequent intramolecular cyclization needed to cleave the ester can only occur if two sulfur atoms are present to form a 5-membered ring and elicit a fluorescent response. A drawback to the design of these probes is that although thiols cannot undergo the intramolecular cyclization necessary to generate a fluorescent response, they can react at the electrophilic sites and have been observed to degrade the reactivity of these probes to sulfane sulfur species. General examples of this approach are described below.

1.6.1.1 p-Nitrofluorobenzene Cleavage

Many sulfane sulfur probes feature a 2-fluoro-5-nitrobenzoic ester with a nitro group substituted para to the fluorine to activate these S_NAr electrophiles (Scheme 1.24). The first example of this chemistry was reported Xian in 2014 with three fluorescein-based probes **940**–**942** (DSP-1–3) (Figure 1.188).[950] Nucleophilic attack of H_2S_n on a *p*-nitrofluorobenzene moiety generates an aryl persulfide intermediate, which can then undergo an intramolecular attack on the ester to form the cyclized benzodithiolone product. Treatment of **940** and **942** with H_2S_n generated a strong fluorescent enhancement at 515 nm, whereas **941** provided a weaker response. Probe **942** showed good selectivity for sulfane sulfur-based species over other RSS, ROS, and anions, but co-incubation of sulfane sulfur sources with thiols decreased the overall response of the probe. When the probe was incubated with ROS and H_2S together, a fluorescent response was observed, which is consistent with H_2S oxidation to H_2S_n species. Probe **942** was further used to image exogenous H_2S_n in HeLa cells.



Scheme 1.24. General approach for H_2S_n detection using *p*-nitrofluorobenzene electrophiles.

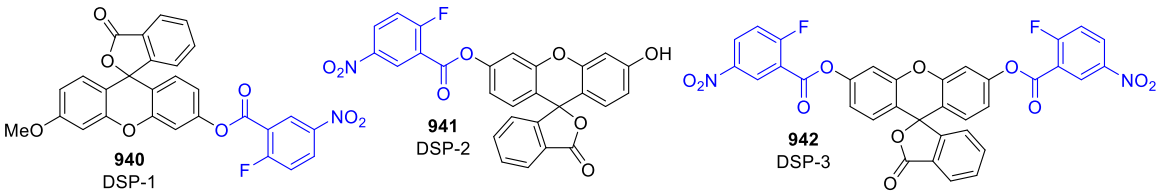


Figure 1.188. Early examples of fluorescent H_2S_n probes based on cleavage of *p*-nitrofluorobenzene esters.

Building from this approach, Liu reported the two-photon excitation probe **943** (QS_n), which provided a 24-fold fluorescence turn-on at 534 nm with H_2S_n incubation that was selective for H_2S_n over RNOS (Figure 1.189).[951] This probe was used to image H_2S_n in both live HeLa cells and zebrafish. Expanding to longer wavelength systems, Chen developed cyanine-based **944** (HCy-FN), which functioned as a dual responsive probe due to initial reactivity with superoxide to produce a fluorescent signal at 794 nm followed by reactivity with H_2S_n to produce a fluorescent response at 625 nm.[952] This probe was used to detect H_2S_n formation from reaction of ROS and H_2S, was used to detect superoxide and H_2S_n in Raw 264.7 cells, and was shown to localize within the mitochondria. In addition, this probe was used to image superoxide and H_2S_n in mice.

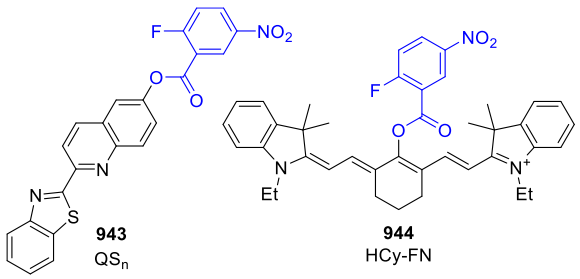


Figure 1.189. Additional examples of fluorescent H_2S_n probes based on cleavage of *p*-nitrofluorobenzene esters.

This general approach has also been adapted to different BODIPY-based probes. For example, Chen developed mitochondria-targeted **945** (Mito-ss), which uses a TPP cation to impart mitochondrial targeting (Figure 1.190).[953] This probe showed a 24-fold fluorescence turn-on with H_2S_n treatment, was selective for H_2S_n over other RSS, and was used to image H_2S_n in cells, mice, and organs. Chen also reported **946** (BD-ss), which provides a fluorescent response to H_2S_n at 737 nm with high selectivity for H_2S_n over other RSS or anions.[954] In addition, a fluorescent response was observed when **946** was incubated with H_2S, H_2O_2, and glutathione peroxidase, confirming polysulfides were produced. This probe was also used to image H_2S_n in Raw 264.7 cells and mice. Wang and Xu also reported a NIR probe in **947** (NIR-PHS1), which provided a fluorescent turn-on at 684 nm upon treatment with H_2S_n. This probe showed good selectivity for H_2S_n over other competing analytes and was used to image H_2S_n in both live cells and mice.[955] Ratiometric approaches have also been developed, with Liu reporting **948** (BDP-PHS), which generated a fluorescent decrease at 574 nm with concomitant increase at 618 nm upon incubation with H_2S_n.[956] This probe showed high selectivity for H_2S_n over other analytes and was used to image exogenous H_2S_n in HeLa cells.

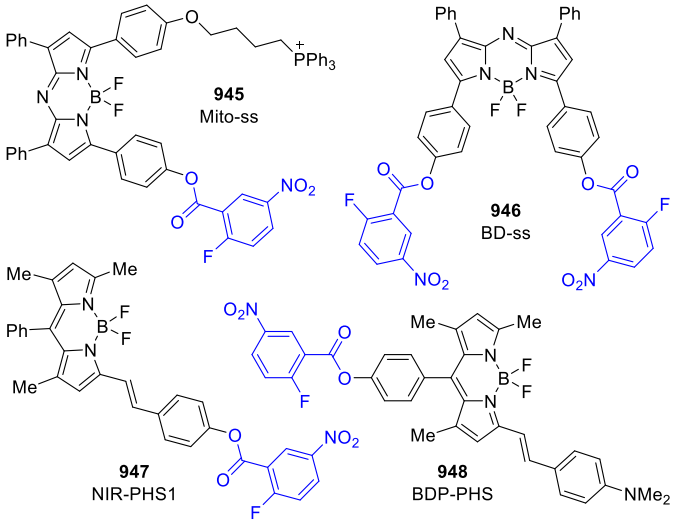


Figure 1.190. Examples of fluorescent H_2S_n probes based on cleavage of *p*-nitrofluorobenzene esters with BODIPY chromophores.

Using this same approach, a variety of naphthalimide-based probes have also been developed. For example, Liu reported two-photon ratiometric probe **949** (NRT-HP), which provided a shift in emission from 518 nm to 460 nm upon incubation with H_2S_n (Figure 1.191).[957]

This probe showed good selectivity for H_2S_n over other anions, and the probe was used to image H_2S_n in live cells using two-photon microscopy. Zhou also reported a two-photon probe in **950** (Np-S_n), which provided an 80-fold fluorescence turn-on at 550 nm with H_2S_n treatment, was selective for H_2S_n, and provided a fluorescent response to H_2S_n in cells.[958]

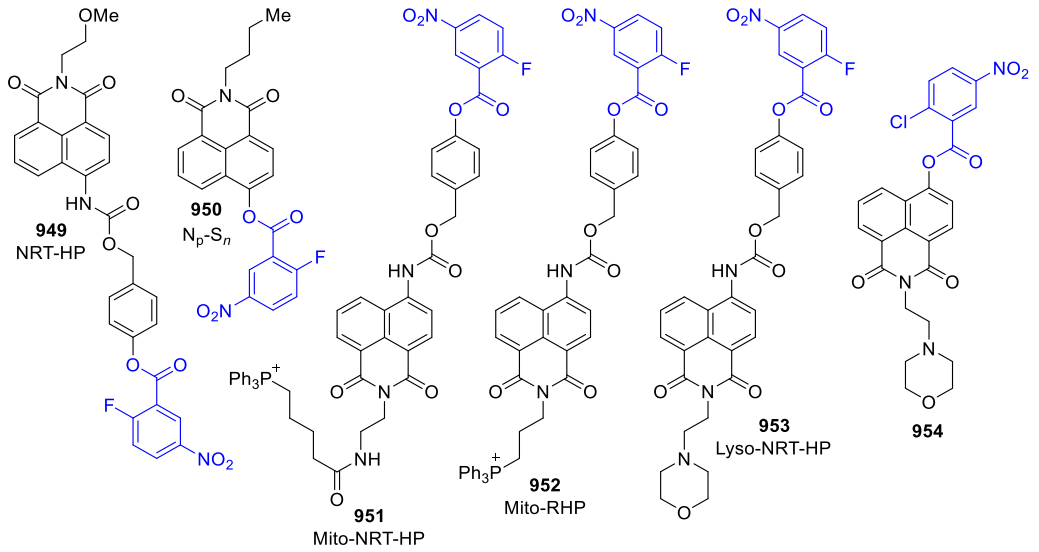


Figure 1.191. Examples of fluorescent H_2S_n probes based on cleavage of *p*-nitrofluorobenzene esters with naphthalimide chromophores.

Further functionalization of naphthalimide motifs has also been used to develop organelle-targeted H_2S_n probes. For example, Ru and Liu reported the mitochondria-targeted, ratiometric probe **951** (Mito-NRT-HP), which showed a 70-fold fluorescence ratio shift from 546 nm to 478 nm upon incubation with H_2S_n.[959] The probe was selective for H_2S_n over metal ions, biological anions, and thiols, and was determined to have a two-photon absorption value of 290 GM when excited at 810 nm. The probe was further used to image exogenous and LPS-derived H_2S_n in the mitochondria of live HeLa and BHK cells and also to image increased H_2S_n in an LPS-induced acute organ injury mouse model using two-photon microscopy. In a subsequent report, Han, Ru, and Wang reported the related probe **952** (Mito-RHP), which showed similar properties as **951** and was used to image both exogenous and endogenous H_2S_n in HeLa cells and zebrafish.[960]

Naphthalimide probes targeted to the lysosome have also been reported. For example, Wang, Ru, and Liu reported **953** (Lyso-NRT-HP), which also provided a ratiometric response to H_2S_n with a fluorescent decrease at 548 nm and concomitant increase at 472 nm with good

selectivity for H_2S_n over other RSS and anions.[961] This probe was used to image exogenous and endogenous H_2S_n in HeLa cells and at up to 100 μm depths in kidney tissue using two-photon excitation. This approach was modified by Yuan, who reported *p*-nitrochlorobenzene based **954**, which provided a 10-fold fluorescence turn-on at 548 nm when incubated with H_2S_n.[962] This probe showed good selectivity for H_2S_n over other biological species and was used to image exogenous H_2S_n in the lysosomes of live HeLa cells.

Ratiometric probes have also been reported using other chromophores. For example, Yin and Zhang reported **955** (TPR-S), which featured a rhodol-naphthalene FRET-pair and provided a ratiometric shift from 448 nm to 541 nm upon incubation with H_2S_n in 50% EtOH in buffer (Figure 1.192).[963] The probe was selective for H_2S_n over other RSS and anions and was also used to image H_2S_n in live cells, liver tissue, and organs. Ma and Wu reported the related coumarin-rhodol FRET probe **956**, which was selective for H_2S_n and exhibited a emission shift from 460 nm to 537 nm with H_2S_n treatment.[964] This ratiometric response was maintained in cell experiments. Combining this approach with an indolium motif, Qi developed the dual H_2S/H_2S_n probe **957** (MC-S_n), which resulted in an emission shift from 606 nm to 468 nm upon treatment with H_2S_n, but to 519 nm upon addition of H_2S.[739] This probe was selective for H_2S_n over other RSS and anions when monitored at 468 nm and was further used to image H_2S/H_2S_n in live cells, tissue, and zebrafish.

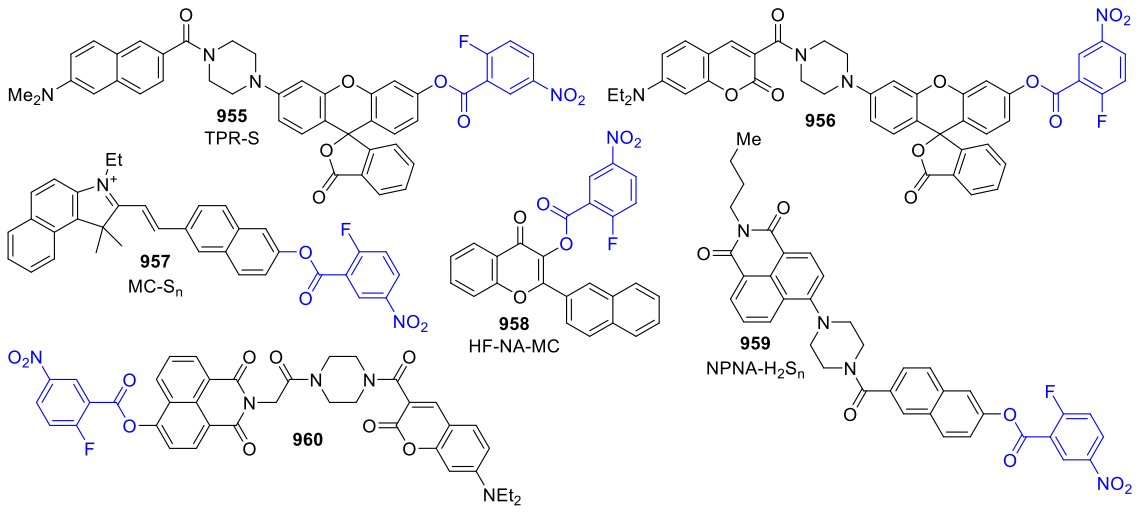


Figure 1.192. Examples of fluorescent H_2S_n probes based on cleavage of *p*-nitrofluorobenzene esters with ratiometric responses.

Building from a flavone backbone, Yang and He reported **958** (HF-NA-MC), which was selective for H_2S_n and resulted in a ratiometric shift from 450 nm to 540 nm that was further confirmed in HeLa cells.[965] Peng also reported the related probe **959** (NPNA-H_2S_n), which employed a naphthalene-naphthalimide FRET pair for an 8-fold fluorescence ratio enhancement (F_{450}/F_{256}) when treated with H_2S_n.[966] The probe was shown to be selective for H_2S_n and respond to H_2S_n in both HeLa cells and zebrafish. More recently, Ma reported **960**, which incorporates a coumarin-naphthalimide FRET pair to impart a ratiometric response from 473 nm to 550 nm when incubated with H_2S_n.[967] This probe was selective for H_2S_n over ROS, amino acids, and thiols, and it was further used to image exogenous H_2S_n and changes in H_2S_n levels with NEM addition in A549 cells.

This general approach for H_2S_n detection using *p*-nitrofluorobenzene cleavage has also been applied to other fluorophores to expand the library of probes suitable for polysulfide detection. For example, Lin reported **961** (GCTPOC-H_2S_2), which provides a fluorescent turn-on response at 512 nm when treated with H_2S_n, shows good selectivity for H_2S_n over other analytes, and was used to image exogenous H_2S_n in both MCF-7 cells and mice (Figure 1.193).[968] Wang and Zha developed imidazo[1,5-]pyridine-based probe **962** (NIPY-NF), which provided a selective fluorescence turn-on at 520 nm with H_2S_n, was found to accumulate in the lysosome, and was applied to image H_2S_n in A549 cells.[969] Using a benzothiazole motif, Chen reported **963**, which provided a 328-fold fluorescence turn-on at 534 nm upon treatment with H_2S_n, showed good selectivity over competing analytes, and was used to image H_2S_n in both A549 cells and zebrafish.[970] Yin further developed a resorufin-based probe in **964** (Re-SS), which featured a 40-fold fluorescence turn-on at 589 nm, good selectivity for H_2S_n over anions, and which was used to image H_2S_n in Raw 264.7 cells.[971]

Furthering the fluorophore diversity of this approach, Ma and Zhang reported naphthalene-based **965**, which was also selective for H_2S_n with an 18-fold fluorescent response. This probe was also used to image H_2S_n in HepG2 cells.[972] Using a related platform, Wang and Song reported **966** (JCCF), which provided a 25-fold fluorescence turn-on at 543 nm and was used to image H_2S_n in MCF-1 cells and zebrafish.[973] Fan and Pu reported coumarin-based **967** (QLB-CF), with a 7-fold fluorescence turn-on at 486 nm upon addition of H_2S_n that was selective for H_2S_n over other anions and further used to image H_2S_n in HeLa cells.[974] Expanding to triphenylamine-based systems, Liu reported **968** (TBF-SS), which responded to H_2S_n in 10% DMSO in buffer to provide a selective

fluorescence turn-on response at 575 nm.[975] This probe was further used to detect H_2S_n in tea samples and image exogenous H_2S_n in MCF-7 cells.

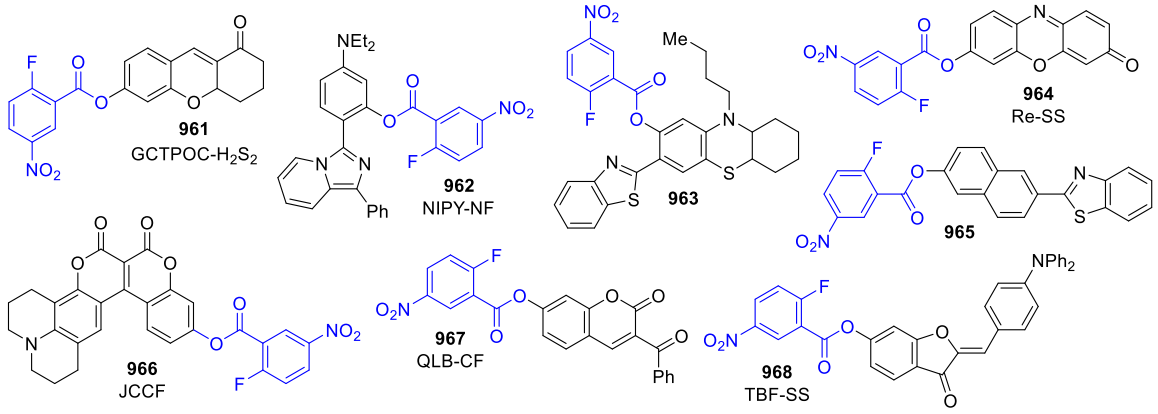


Figure 1.193. Additional examples of fluorescent H_2S_n probes based on cleavage of *p*-nitrofluorobenzene esters.

This sensing strategy has also been used to develop red-shifted and NIR fluorescent probes for H_2S_n. In 2017, Peng reported a semiheptamethine **969** (Cy-S_n) that exhibited a fluorescence turn-on at 720 nm with good selectivity for H_2S_n over other RSS and anions (Figure 1.194).[976] This probe was also used to image H_2S_n in Raw 264.7 cells and mice. Chen later reported **970** (BCy-FN) that responded to H_2S_n with a fluorescence enhancement at 727 nm, was selective for H_2S_n over other RSS and ROS, and was used to confirm H_2S_n production from reactions of H_2S with ROS.[977] The probe was also used to image exogenous and LPS-induced H_2S_n in the mitochondria of ZF_4 cells. In addition, probe **970** was used to investigate H_2S_n generation in cells treated with H_2S, PMA, NAC, and the GPx-inhibitor misonidazole, as well as the effect of H_2S_n on hypoxia/reperfusion induced damage. Expanding to animal studies, this probe was further applied to image H_2S_n in both zebrafish and BALB/c mice. Hu and Man developed berberrubine-based probe **971** (BER9SS) that responded to H_2S_n with a fluorescence turn-on at 615 nm that was non-competitive and selective for H_2S_n over other RSS, ROS, and RNS in buffer with 5% DMSO.[978] Probe **971** was used to detect pre-doped H_2S in a large variety of water and food samples and image exogenous H_2S_n and H_2S_n induced by β-lapachone/H_2S treatment in HeLa cells.

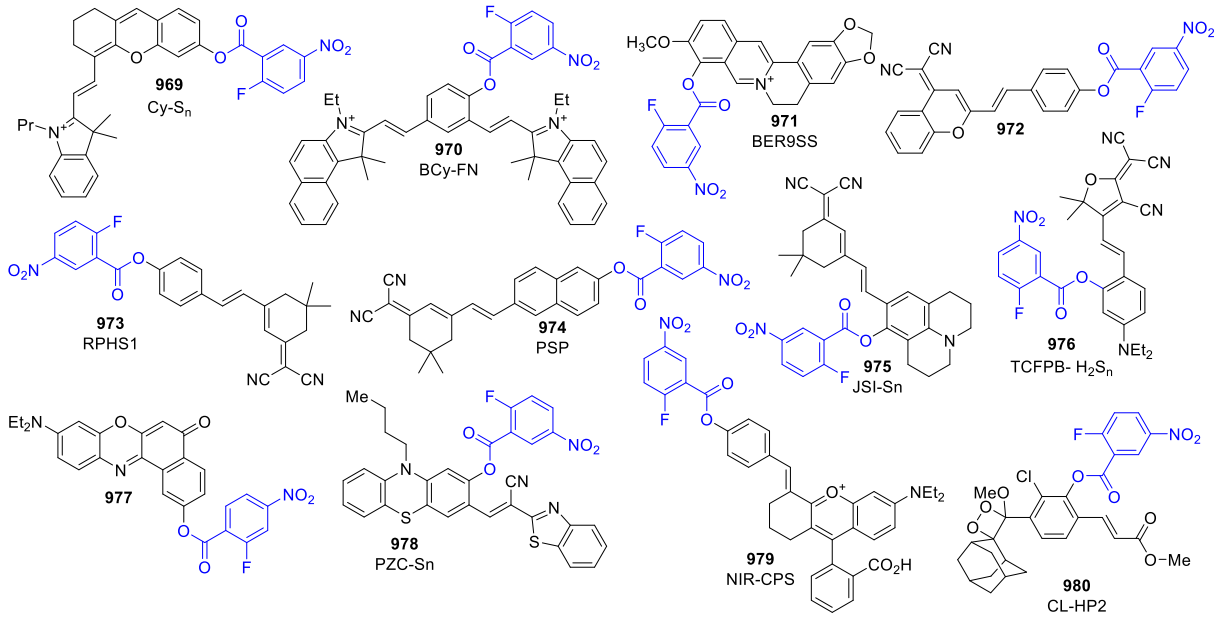


Figure 1.194. Examples of fluorescent H_2S_n probes based on cleavage of *p*-nitrofluorobenzene esters with extended wavelengths.

Also reporting at longer wavelengths, Han reported dicyanomethylene-benzopyran **972** that generated a 30-fold fluorescence turn-on at 682 nm when treated with H_2S_n with good selectivity for H_2S_n over other biological species.[979] The probe was further used to image H_2S_n in MCF-7 cells treated with exogenous H_2S_n and pre-treated with *N*-methylmaleimide. Zhang, Gong, and Liu reported isophorone-based **973** (RPHS1) that responded to H_2S_n with a decrease in fluorescence at 482 nm and a fluorescence enhancement at 577 nm and 655 nm in buffer with 0.4% Tween 80.[980] This probe selective for H_2S_n over other biological analytes including H_2S and Na_2S and was further used to image exogenous H_2S_n in HeLa cells. Qian reported the anthracene-based, two-photon probe **974** (PSP) that responds to H_2S_n with a 6-fold fluorescence turn-on at 640 nm in buffer with 5% DMSO and 1 mM CTAB and was selective for H_2S_n over other biological analytes, although Na_2S did activate the probe.[981] The probe was able detect H_2S_n at 640 nm using two-photon excitation at 880 nm. In HeLa cells, **974** was used to image exogenous and LPS-induced H_2S_n, changes in levels in cells pretreated with PAG or NEM and was further used to monitor H_2S_n during erastin-induced ferroptosis.

In 2020, Wang, Wang, and Song reported **975** (JSI-Sn) that generated a fluorescence turn-on at 701 nm that showed a large Stokes shift of 123 nm treatment with H_2S_n.[982] The probe was selective for H_2S_n over biological anions and thiols and was then used to image exogenous H_2S_n

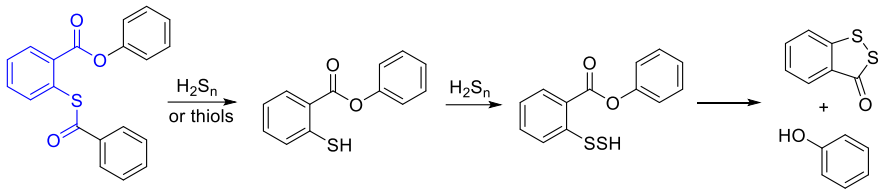
in live HeLa cells and larval zebrafish. Zhang, Gong, and Cai reported AIE-based **976** (TCFPB-H_2S_n) that showed an increased AIE with decreased solvent polarity and with addition of H_2S_n to exhibit a ratiometric shift from 751 nm to 619 nm.[983] The probe was selective for H_2S_n over other biological analytes including ROS and thiols. This construct was determined to localize to the lysosome, was used to image exogenous H_2S_n in HeLa cells, and was further used to image H_2S_n in mice.

Han reported Nile Red-based probe **977** (KB1) that responded to H_2S_n with a 17-fold fluorescence turn-on at 655 nm and was selective for H_2S_n over other biological analytes.[984] This probe was used to image exogenous H_2S_n in MCF-7 cells. Zhang and Chen reported **978** (PZC-S_n) that exhibited a fluorescence turn-on at 620 nm when incubated with H_2S_n and was selective for H_2S_n over other biological analytes in buffer with 1 mM CTAB.[985] The probe was further used to image exogenous and LPS-induced H_2S_n, changes in signal upon preincubation with NEM or PAG in Raw 264.7 cells, and exogenous and LPS-induced H_2S_n in larval zebrafish. Zhang and Xue reported **979** (NIR-CPS) that exhibited a 20-fold fluorescence turn-on at 670 nm when incubated with H_2S_n and was selective for H_2S_n over other biological analytes.[986] The probe used to image exogenous and LPS-induced H_2S_n, changes in signal upon pretreatment with NMM or PAG in MCF-7 cells, and image H_2S_n in mice. Using a different reporting approach, Lu reported chemiluminescent **980** (CL-HP2) using an adamantylidene–dioxetane system that emitted at 540 nm when incubated with H_2S_n and was selective for H_2S_n over biological analytes.[987] The probe used to image exogenous H_2S_n and changes in signal upon treatment with PAG and ferroptosis inducing agent imidazole ketone erastin in MDA-MB-231 cells. The probe was also used to image H_2S_n in healthy, LPS-treated, and ferroptosis-induced mice.

1.6.1.2 2-(Benzoylthio)benzoate Cleavage

One limitation of the 2-fluoro-5-nitrobenzoic ester platforms discussed above is that these platforms can also react with and be partially deactivated by thiols. Although this reactivity does not generate a fluorescent response, it does inactivate the probe and blunt the H_2S_n response range. One approach to abrogate this challenge is by using electrophilic thioesters with a proximal ester motif that is removed by subsequent intramolecular cyclization (Scheme 1.25). Similar to the electrophiles discussed in the previous section, H_2S_n can displace the thioester to form an aryl persulfide, which can then undergo an intramolecular cyclization to cleave the ester. Empirically,

this platform can also react with thiols, but this reactivity was shown to not deactivate the probe from further reaction with H_2S_n.



Scheme 1.25. General approach for H_2S_n detection by cleavage of 2-(benzoylthio)benzoate groups followed by intramolecular cyclization.

As a demonstration of this approach, Xian reported three fluorescein-based H_2S_n probes **981**–**983** (PSP-1–3) in 2015 based on the thioester cleavage strategy (Figure 1.195).[988] Probe **983** showed the best stability and response, including high selectivity for H_2S_n over RSS and anions. This probe was also used to image H_2S and H_2S_n in COS-7 cells. Following this initial report, additional fluorescein and rhodol-based probes were also reported. For example, Xian reported FRET-based bifunctional probe **984** (DDP-1), which used an azide-modified coumarin attached to a thioester-modified rhodol to impart dual H_2S/H_2S_n detection.[989] When **984** was treated with H_2S, fluorescent responses at both 452 nm and 542 nm were observed, whereas treatment with H_2S_n resulted in only a signal at 542 nm. This fluorescence turn-on behavior was shown to be selective for H_2S and H_2S_n and was used to image H_2S and H_2S_n in HeLa cells (Figure 1.196).

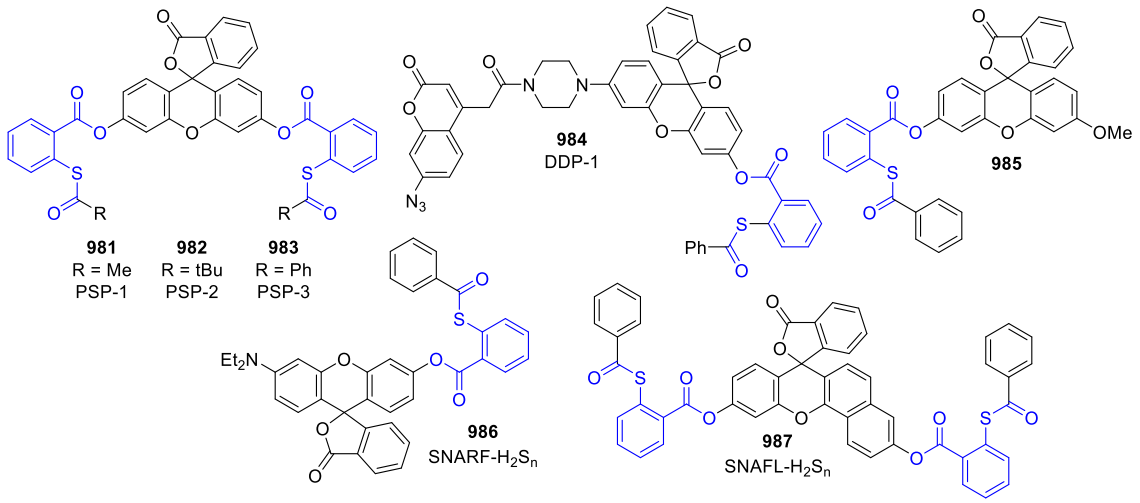


Figure 1.195. Examples of fluorescent H_2S_n probes based on thioesters cleavage and subsequent cyclization using xanthene based chromophores.

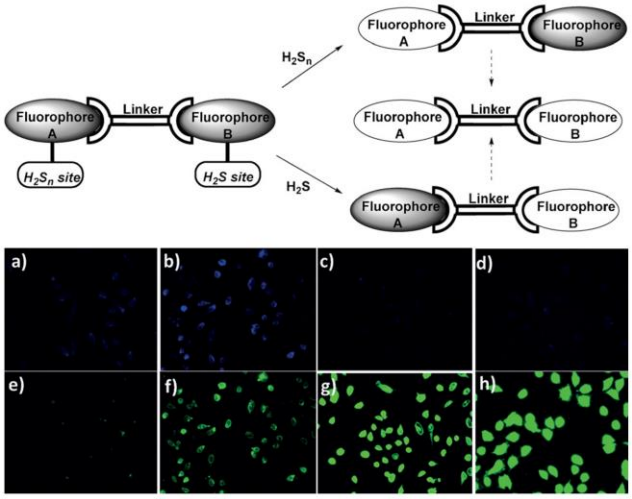


Figure 1.196. (top) General strategy for developing different fluorescent responses from both an H_2S_n and H_2S reactive site. (bottom) Blue (a-d) and green (e-h) channels of HeLa incubated with **984** followed by treatment with (a,e) vehicle; (b,f) Na_2S; (c,g) Na_2S and NaOCl; (d,h) Na_2S_2. Reproduced with permission from ref [989]. Copyright 2016 John Wiley and Sons.

Also using this cleavage strategy, Kang and Xu developed **985**, which provided both a turn-on fluorescence response and change in fluorescence lifetime upon treatment with H_2S_n. [990] Fluorescence lifetime imaging was used to image H_2S_n levels in HeLa cells and zebrafish. Liu and Yu reported **986** (SNARF-H_2S_n), which generated a 1000-fold fluorescence turn-on at 640 nm with H_2S_n incubation in 50% MeCN in buffer with good selectivity for H_2S_n. This probe was further used to image H_2S_n in both A549 cells and zebrafish.[991] Using a ditopic probe, Zhang, Wu, and Liu developed **987** (SNAFL-H_2S_n), which also provides a selective, 1000-fold fluorescence turn-on at 626 nm and was used to image H_2S_n in Raw 264.7 cells and zebrafish.[992]

As additional examples of this approach, Ma reported the NIR hemicyanine-based **988**, which showed a 44-fold fluorescence turn-on at 708 nm with H_2S_n and was selective for H_2S_n over thiols and anions (Figure 1.197).[993] This probe was also used to image H_2S_n in HeLa cells and BALB/c mice. Thomas and Das also prepared BODIPY-based **989** (MB-Sn), which that localized within the endoplasmic reticulum.[994] Upon treatment of H_2S_n, this probe provided a fluorescence turn-on at 584 nm that was selective for H_2S_n over ROS, thiols, and anions and was subsequently used to image H_2S_n in Raw 264.7 cells. Expanding the toolbox of different methods of polysulfide detection, Zhang reported bioluminescent luciferin-based probe **990** (BP-PS), which generates a 7.3-fold bioluminescent turn-on to H_2S_n in the presence of firefly luciferase (fLuc) with good

selectivity for H_2S_n over other RSS and anions.[995] This probe was also used to image H_2S_n in MDA-MB-231-luc and in murine models of inflammation and bacterial infection when co-injected with fLuc. Expanding to other model systems, Park and Kim reported the ratiometric and mitochondria-targeted **991** (SPS-M1), which upon treatment with H_2S_n exhibited a fluorescent shift from 471 nm to 506 nm that was selective for H_2S_n over other RSS and anions.[996] This probe was also used to image H_2S_n in HeLa cells and in a Parkinson's disease model by two-photon microscopy.

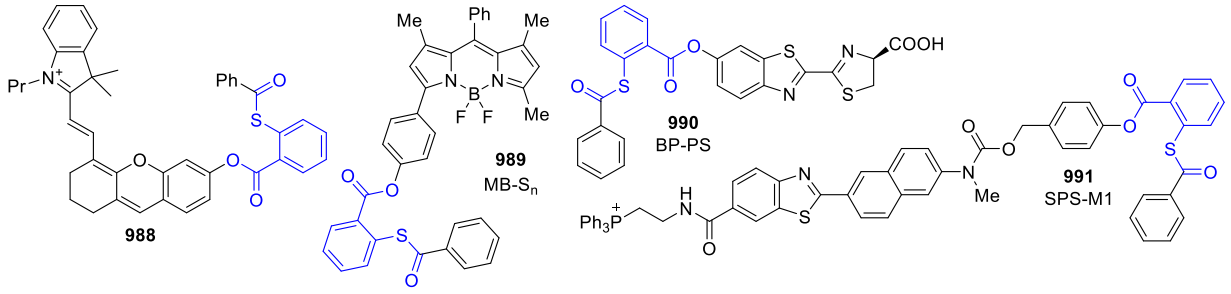


Figure 1.197. Additional examples of fluorescent H_2S_n probes based on thioesters cleavage and subsequent cyclization.

Further expanding on this approach, Chen and Yuan reported **992** (PP-PS), which showed a 20-fold fluorescence turn-on at 478 nm with H_2S_n treatment (Figure 1.198).[997] This probe was selective for H_2S_n over competing analytes, was found to localize to the lysosome, and was also used to image H_2S_n in A549 cells, tissues, and a mouse model of inflammation. Following this, Li and Xiao reported probe **993** (HQO-PSP), which used a cationic heptamethine cyanine to impart mitochondrial targeting.[998] This probe was shown to respond to H_2S_n with an 86-fold fluorescence turn-on at 633 nm, be selective for H_2S_n, and was used to image H_2S_n in mitochondria in live cells and animal lung tissue. Extending to other detection approaches, Zhao also used an extended platform in hemicyanine-based photoacoustic probe **994** (AP-S_n) that was shown to selectively respond to H_2S_n in buffer, Raw 264.7 cells, and mice.[999] Similarly, Lu reported chemiluminescent **995** (CL-HP1) that emitted at 540 nm when incubated with H_2S_n and was selective for H_2S_n over biological analytes.[987] This probe was significantly times less sensitive than the *p*-nitrofluorobenzene analogue **980** and was thus not applied to cell or animal investigations.

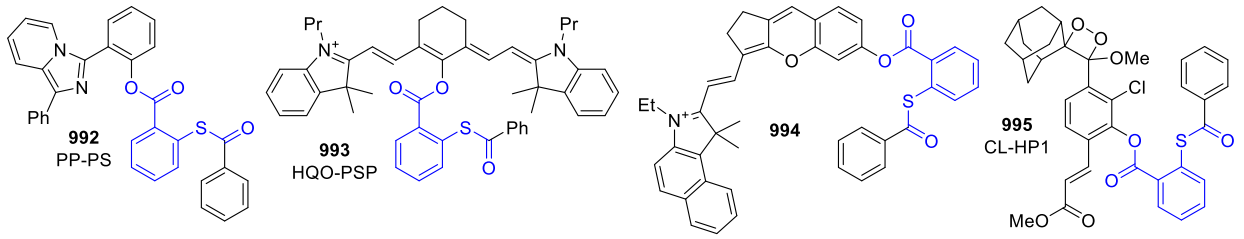
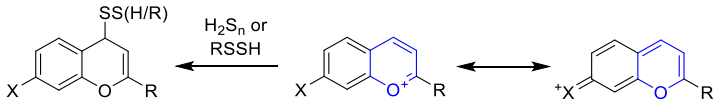


Figure 1.198. Additional examples of fluorescent and luminescent H_2S_n probes based on thioesters cleavage and subsequent cyclization.

1.6.1.3 Other Approaches

Another avenue to detect oxidized RSS like H_2S_n or persulfides is based on the increased nucleophilicity of these species when compared to H_2S. Using a related approach to earlier examples of H_2S detection, the direct addition of polysulfides or hydropolysulfides to pyrilium motifs has also been used for fluorescent probe development (Scheme 1.26). In general, this approach typically results in conversion of a fluorescent platform to a non-fluorescent product, which has been coupled with FRET pairs to develop both ratiometric and turn-on responses.



Scheme 1.26. Addition of H_2S_n or hydropolysulfides (RSSH) to pyrilium cations.

In 2017, Ojida reported coumarin-pyronine scaffolds **996** and **997**, which generate a ratiometric shift from 584 to 479 nm when treated with H_2S_n (Figure 1.199).[1000] The response of these probes was strongest for H_2S_n species and also provided a response to persulfides generated *in situ*. These responses could be reversed chemically by addition of NEM. Probe **997** was also used to image exogenous H_2S_n in A549 cells and differences in endogenous hydropersulfides generated through CSE and CBS inhibition by AOAA and TrxR inhibition by Auranofin. Using a related approach, Urano reported silicon-rhodamine platform **998** (QS10), which also reacts directly with poly- and persulfides to generate a fluorescent response.[1001] Much like the above example, this fluorescent response could be chemically reversed by the addition of NEM. This chemical reversibility was also demonstrated in A549 cells through repeated cycles of NEM and exogenous BnSSH addition (Figure 1.200). Furthermore, probe **998** was also demonstrated to

image endogenous hydropolysulfide generation through CSE/CBS inhibition and use of exogenous H_2O_2.

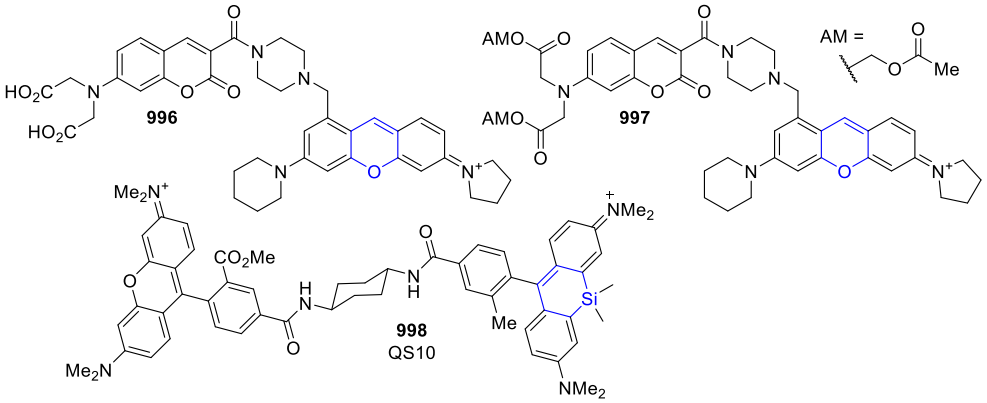


Figure 1.199. Examples of chemically reversible probes for H_2S_n/HSSR detection based on nucleophilic addition to a fluorophore core.

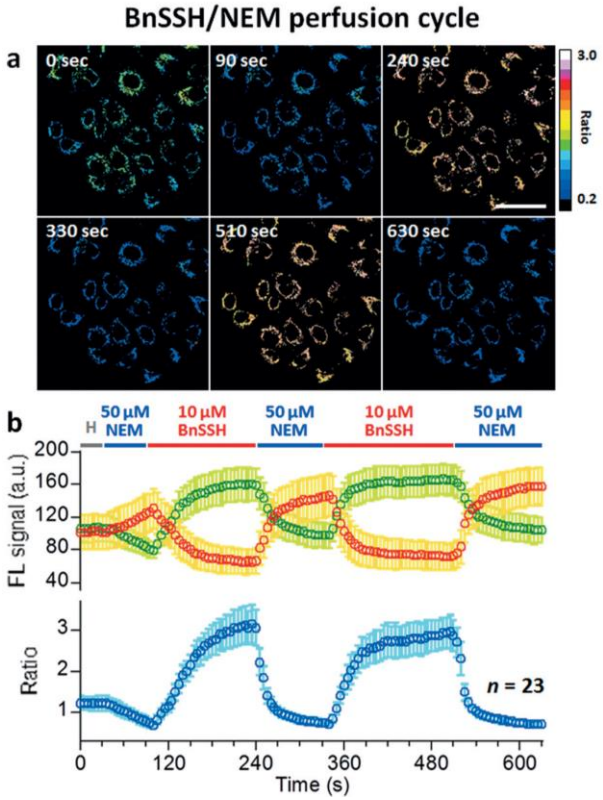
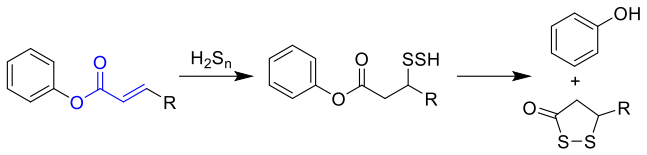


Figure 1.200. (top) Schematic of the reactivity of **998** with per-/poly-sulfides. (middle) Ratio images at different time points of the response from A549 cells treated with **998** followed by addition cycles of BnSSH and NEM. (bottom) Quantified fluorescent response at ratio after different cycles of BnSSH and NEM addition. Reproduced with permission from ref [1001]. Copyright 2018 John Wiley and Sons.

Also using a general approach discussed earlier for H_2S detection, a number of probes have also been developed for H_2S_n that rely on the addition to α,β-unsaturated esters. Unlike for the H_2S-responsive counterparts, in which H_2S conjugate addition was followed by a subsequent addition to a proximal electrophile (often an aldehyde), for the H_2S_n-responsive systems, the conjugate addition results in an intramolecular cyclization and subsequent ester cleavage (Scheme 1.27).



Scheme 1.27. Addition of H_2S_n to α,β-unsaturated esters and resultant cleavage.

As an example of this approach, Yang reported a rhodol-based **999** (DERC) in 2015, which uses a cinnamate ester to impart H_2S_n reactivity (Figure 1.201).[1002] Different esters were prepared and the 3-(trifluoromethyl) cinnamate ester derivative was determined to have the largest fluorescent response. When compared to the related H_2S sensing platforms built from α,β-unsaturated ketones discussed earlier, the higher nucleophilicity of polysulfides enables the use of less electrophilic Michael acceptors, which also likely enhances the stability of these platforms in biological environments. Treatment of **999** with H_2S_n resulted in a fluorescent turn-on at 548 nm in 10% EtOH in buffer. This probe was moderately selective for H_2S_n over other RSS, with a minor response from H_2S but a larger response from 5 mM GSH and was further used to image H_2S_n in SMMC-7721 cells. Using a related approach, Yang and Yang reported four hydroxycoumarin-based probes **1000**–**1003** (FP-H, FP-CH_3, FP-Ph, and FP-CF_3) with different α-substituted acrylates.[1003] The found that **1003** showed the largest fluorescence turn-on at 490 nm and the best selectivity for H_2S_n over other RSS. This probe was further used to image exogenous H_2S_n in HeLa cells with minimal interference from Cys and also to image increases in H_2S_n upon LPS stimulation in Raw 264.7 cells. As an additional example, Xiao reported **1004** (HQO-SSH) that showed a fluorescence turn-on at ~630 nm when treated with papain persulfide. This probe showed good selectivity for protein persulfides over amino acids, ROS, thiols, and H_2S, although inorganic sulfane sulfur species were not tested.[1004] The probe was also used to image H_2S_n in the mitochondria of live A549 and BEAS-2B cells treated with Na_2S, PAG, and Na_2S/DTT. As an

additional application, probe **1004** was also used to image mitochondrial protein persulfidation in mouse lung tissue, persulfidation of GAPDH in lung cells, and persulfidation during sulfur mustard-induced lung injury.

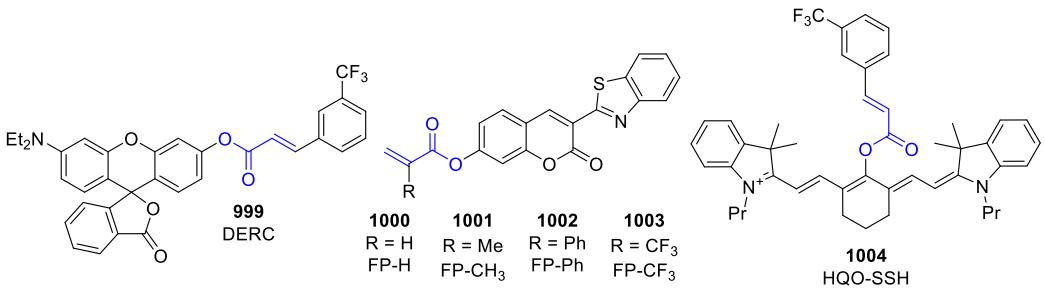
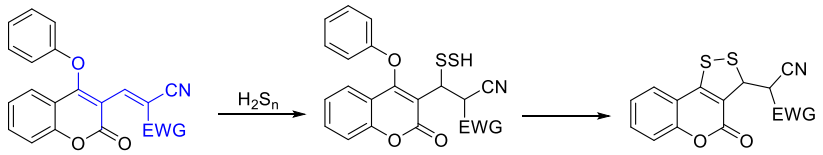


Figure 1.201. Examples of fluorescent H_2S_n probes based on cleavage of α,β-unsaturated esters.

Also sharing a similar background as earlier discussed H_2S probes based on Michael addition and subsequent cyclization, different coumarin adducts with pendant cyanoethylene motifs have been used for H_2S_n detection. Unlike the observed response for H_2S, which derived from subsequent addition to a pendant nitrile, reaction with H_2S_n results in leaving group displacement from the coumarin ring (Scheme 1.28).



Scheme 1.28. Addition of H_2S_n to electron poor vinyl coumarins and subsequent cyclization.

Chen, Sheng, and Song reported five coumarin-based probes **1005**–**1009** (MCP1–5), which all use an electron poor vinyl coumarin backbone for H_2S_n recognition, with **1005** showing general reactivity for H_2S_n, H_2S, and thiols as well as providing discreet emissions at 508, 576, or 469 nm, for each of these analytes, respectively (Figure 1.202).[702] Probe **1005** was also used to image exogenous H_2S/H_2S_n in Raw 264.7 cells. In an independent report, Chen, Yang, and Sheng later focused on methoxy-substituted **1006** (C-HPS), which had higher direct selectivity for H_2S_n over H_2S and thiols.[1005] This probe provided a 97-fold fluorescence turn-on at 576 nm in 20% DMSO

in buffer with good selectivity for H_2S_n over other RSS and anions. Probe **1006** was also used to image H_2S_n in MGC-803 cells.

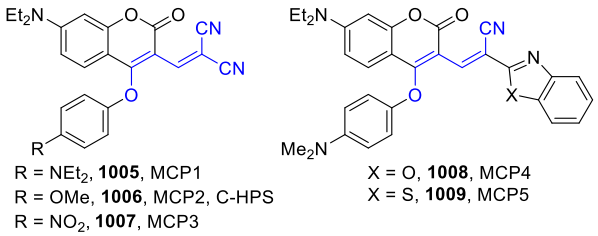


Figure 1.202. Examples of fluorescent H_2S_n probes based on addition to electron poor vinyl coumarins and subsequent cyclization.

Electrophilic coumarins have also been used for H_2S_n detection. For example, Chen and Sheng groups developed selenoether **1010** (ACC-SePh), which provided a response to H_2S_n and GSH and H_2S_n by different emission profiles (Figure 1.203).[1006] Reaction with H_2S_n resulted in selenol displacement and intramolecular cyclization to cleave the ester bond, whereas reaction with GSH resulted in selenol release without ester cleavage. Treatment with GSH resulted in a 16-fold fluorescence turn-on at 540 nm whereas H_2S_n treatment resulted in a 21-fold turn-on at 465 nm, and these different responses were also observed in Raw 264.7 cells. Similar approaches to differentiate H_2S_n from GSH using selenoethers were also reported by Liu in **1011** (DCM-Cou-SePh) and **1012** (DCI-Cou-SePh). These probes featured phenylselenides that were also reported to sense both GSH and H_2S_n through different fluorescent signals and demonstrated their application in live cells.[1007, 1008]

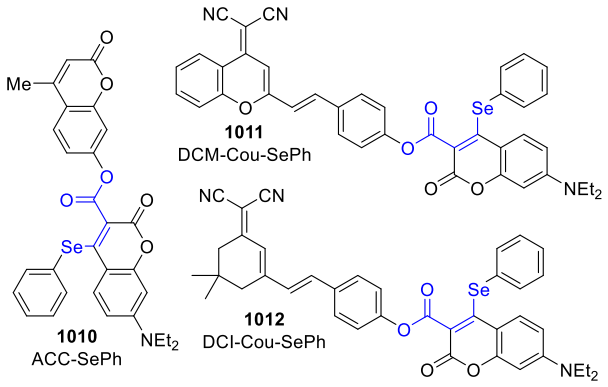


Figure 1.203. Examples of fluorescent H_2S_n probes that provide different responses for H_2S_n and GSH.

Chen reported a related approach using a chloro-coumarin derivative to develop ratiometric **1013** (ACC-Cl) (Figure 1.204).[1009] This probe reacts with H_2S_n to displace the chloride and subsequently cleave the ester through an intramolecular cyclization, but unlike the selenoethers described above, probe **1013** does not react with GSH. Investigations in 50% MeCN in buffer showed a ratiometric response with a fluorescent shift from 510 to 461 nm upon reaction with H_2S_n with good selectivity over other reactive species, including GSH. This probe was further used to image exogenous H_2S_n in Raw 264.7 cells. Also using H_2S_n-mediated ester cleavage, Ge, Zhang, and Li reported mitochondria-targeted **1014**, which contains a photocleavable ortho-nitrobenzyl (ONB) group.[1010] Photocleavage of the ONB group furnishes an aldehyde, which can react with H_2S_n and then undergo intramolecular cyclization to cleave the ester. Upon UV irradiation and H_2S_n treatment, a 50-fold fluorescence turn-on at 525 nm was observed that was selective for H_2S_n over RSS and ROS. This probe was subsequently used to image exogenous H_2S_n after probe photoactivation in HepG2 cells.

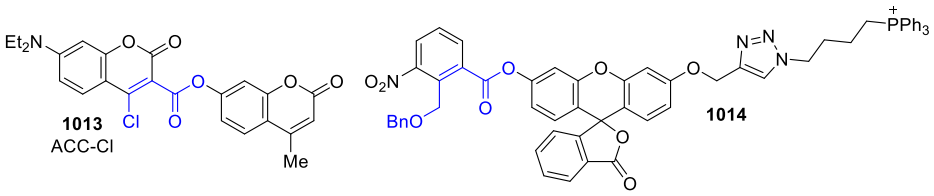


Figure 1.204. Examples of fluorescent H_2S_n probes based on ester cleavage.

Using a similar approach to the DNBS probes used for H_2S detection, less electrophilic substituted nitrobenzenesulfonyl groups have also been used for H_2S_n detection. For example, Tsukamoto and Maeda reported a series of probes in **1015**–**1027** to investigate overall reactivity toward H_2S_n (Figure 1.205).[1011] They observed that that higher electrophilicity resulted in faster reactivity with RSS, with 2-nitrobenzenesulfonyl containing **1018** showing the highest selectivity and response for H_2S_n over thiols and H_2S. This probe was subsequently used to image exogenous H_2S_n in HeLa cells. Song and Wu also developed a variety of electronically substituted H_2S probes, with **1027** (NR-BS4) being the most sensitive and selective, responding to H_2S_n with a fluorescence turn-on at 590 nm with good selectivity for H_2S_n over anions, H_2S, and thiols, although NaClO did decrease the sensitivity of the probe.[1012] The probe was further used to image

exogenous H_2S_n, LPS-induced H_2S_n, and PAG treatment in live HepG2 cells and exogenous H_2S_n in larval zebrafish.

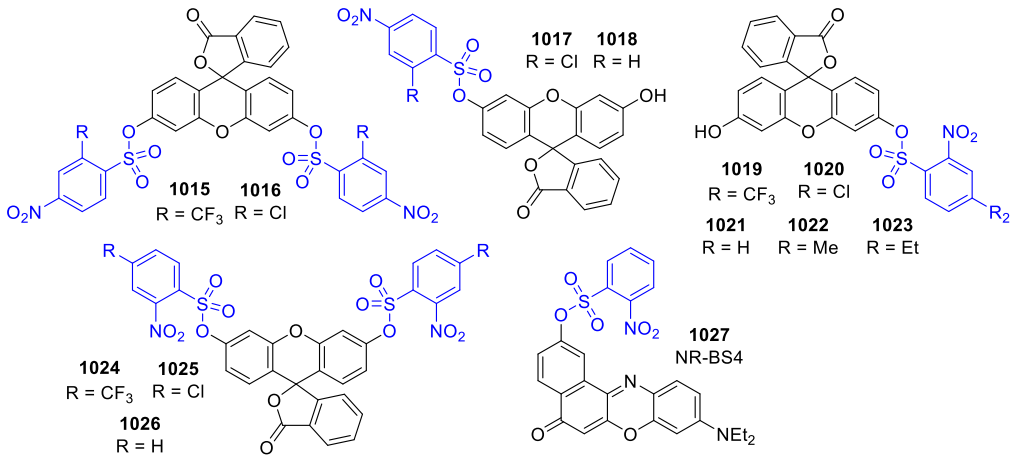


Figure 1.205. Examples of fluorescent H_2S_n probes based on cleavage of substituted nitrobenzenesulfonyl groups.

As an additional approach of leveraging earlier reactivity determined for H_2S detection to develop H_2S_n reporting systems, Xie and Guo reported NBD ether **1028**, which provides different responses to GSH, Cys/Hcy, and H_2S_n (Figure 1.206).[1013] Incubation of the probe with GSH, Cys/Hcy, and H_2S_n all resulted in a fluorescence turn-on at 468 nm that was selective for these analytes over other anions, although H_2S was noted to produce a weak fluorescent signal. The probe was further demonstrated to provide different signals in the green and blue channels when treated with Cys/Hcy or GSH and H_2S_n, respectively, in 786-O cells.

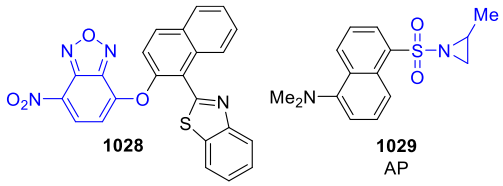


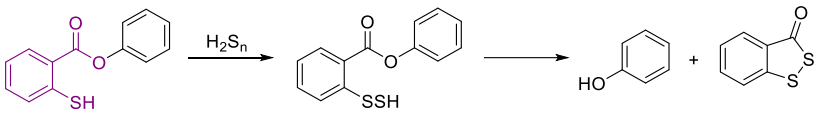
Figure 1.206. Examples of NBD ether probes for the discrimination of GSH, Cys/Hcy, and H_2S_n.

As an additional example of an electrophilic platform, Xian reported **1029** (AP) in 2015 that works through an H_2S_n mediated aziridine ring-opening reaction to generate a fluorescence turn-on at 530 nm in buffer with CTAB.[1014] The probe was shown to be selective for H_2S_n over

ROS, amino acids, and RSS such as thiols and H_2S, although the sensitivity of the probe was decreased when pre-treated with thiols. The probe was further used to detect H_2S_n in bovine plasma free of protein.

1.6.2 Nucleophilic Probes

The examples of H_2S_n probes described above leveraged the enhanced nucleophilicity of poly- and persulfides to generate a wide array of fluorescent probes. A complementary approach to differentiate H_2S_n and other sulfane-sulfur containing species from H_2S is to exploit the electrophilicity of sulfane sulfur motifs. The ambiphilic character provides a unique approach to develop platforms that differentiate H_2S_n and related sulfane sulfur species from H_2S by having a nucleophilic probe that initially reacts with the sulfane sulfur containing analyte to generate a nucleophilic intermediate that can then undergo further chemistry to generate a fluorescent response (Scheme 1.29).



Scheme 1.29. General approach to use a nucleophilic probes for H_2S_n detection.

The first example of this approach was reported by Xian in 2013 with coumarin and methylfluorescein-based probes **1030** and **1031** (SSP1 and SSP2), respectively (Figure 1.207).[1015] Both probes showed a fluorescence turn-on response to H_2S_n (25-fold and 50-fold, respectively) and are selective for H_2S_n over other RSS. In addition, **1031** was also used to image exogenous H_2S_n in H9c2 cells. Xian later further refined this platform to develop **1032** (SSP4),[1016] which uses a doubly-substituted fluorescein to enhance the performance of this probe and was used to image differences in intracellular sulfane sulfur levels in COS-7 cells overexpressing CSE and also in HEK293T CARS2 KO cells (Figure 1.208).[1017]

Following this same probe design, Chen reported BODIPY-based **1033** (BD-diSH), which provided a fluorescent turn-on at 734 nm with the addition of H_2S_n.[1018] This probe was shown to be selective for H_2S_n, such as Na_2S_2, Na_2S_4, Cys-based polysulfides, and S_8, over other RSS and anions. Probe **1033** was also used image H_2S_n in live cells and quantify H_2S_n levels in various mice

organs. Yu and Chen reported mitochondria-targeted **1034** (Mito-SH), which exhibited a 10-fold fluorescence turn-on with H_2S_n treatment and was selective for H_2S_n over other RSS.[1019] This probe was used to image H_2S_n in the mitochondria of different cell lines and also in an acute brain ischemia model with BALB/c mice. Using a different fluorophore, Yuan and Liu reported **1035** (SSNIP), which provided a fluorescence turn-on at 680 nm with H_2S_n treatment and is selective for H_2S_n over other RSS.[1020] This probe was shown to respond to exogenous Na_2S_2 and dimethyl trisulfide in HeLa cells, endogenous H_2S_n after TMSCN treatment, and also H_2S_n in live plant tissues. Chen, Li, and Xian further expanded the SSP series with **1036** (SSP5) that responded to H_2S_n with an fluorescence turn-on at 634 nm and was selective for sulfane sulfur over other RSS and metal ions.[1021] This selectivity profile was also confirmed on a smartphone-based device and used to detect H_2S_n in pre-doped urine samples.

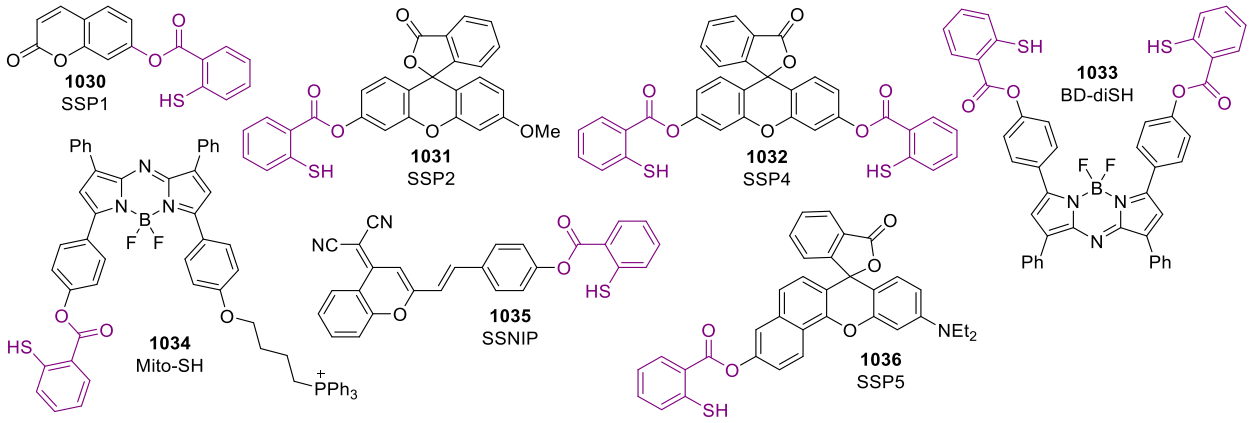


Figure 1.207. Examples of fluorescent H_2S_n probes based on nucleophilic thiol addition to sulfane sulfur species and subsequent cyclization using xanthene based chromophores.

Using a related nucleophilic approach, Urano reported thiol-modified rhodamine B **1037** (SSip-1) (Figure 1.209).[1022] This probe was prepared as the disulfide, but can be reduced to form the active thiol-based system. Prior to reaction with H_2S_n, this probe is non-emissive due to FRET between the two fluorophores. Upon addition of sulfane sulfur species, however, the pendant thiol is converted to a persulfide, which subsequently undergoes a spirocyclization to abolish the quenching mechanism and restore fluorescence. This probe provided a 15-fold fluorescence response to H_2S_n with good selectivity for H_2S_n over thiols and other RSS. In addition, the signal can be chemically reversed by the addition of GSH to reduce the persulfide. A cell permeable

diacetate version of this probe **1038** (SSip-1 DA) was subsequently used to image exogenous H_2S_n in A549 cells and in rat astrocytes.

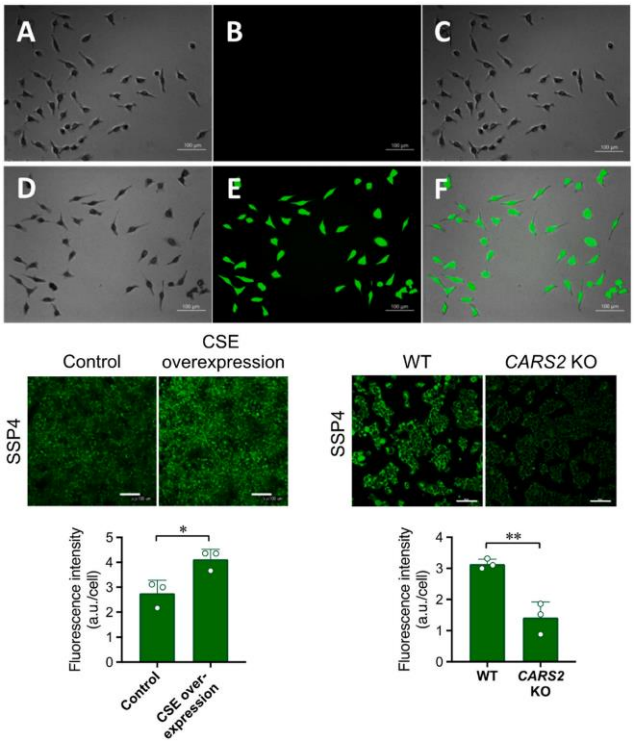


Figure 1.208. (top) Brightfield (A, D), fluorescence (B, E), and overlaid images (C, F) of HeLa cells treated with **1032** and Na_2S_2. (bottom) Differences in fluorescence from normal COS-7 and CSE overexpressing cells and also normal and CARS2 KO HEK293T cells. Reproduced with permission from ref [1017]. Copyright 2022 Elsevier.

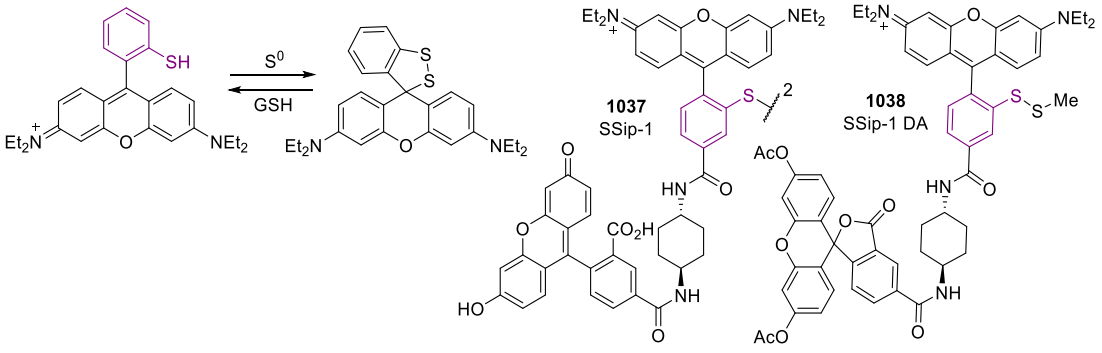


Figure 1.209. Nucleophilic probes based on sulfane sulfur mediated spirocyclization.

The general approach of using thiol-based nucleophiles to detect sulfane sulfur species has also been used with selenium-based nucleophiles. For example, Yu and Chen reported BODIPY-

based probes **1039** (MitoSeH) and **1040** (BD-*di*SeH) that featured nucleophilic selenol motifs (Figure 1.210).[1023, 1024] These probes reacts with sulfane sulfur to generate a selenosulfide intermediate that can subsequently attack and cleave the ester. Both probes were shown to be selective for H_2S_n over other RSS. Probe **1039** used a TPP motif to target the mitochondria and was used to image H_2S_n in live cells and tissues. Ditopic probe **1040** was used to image H_2S_n in live cells, tissues, live mice, and zebrafish.

Using a related approach Chen reported the diselenide system **1041** (Cy-Dise) that also contains a D-galactose for targeting the liver.[1025] When treated with Cys-SSH generated in situ, this probe showed a fluorescent shift from 797 nm to 749 nm with good selectivity for small molecule persulfides over protein-based persulfides. This probe showed good selectivity for small molecule persulfide analytes with only a minimal response to inorganic polysulfides and negligible response to GSH or Sec. Probe **1041** was further used to image persulfides in HepG2 and HL-7702, in live mice treated with persulfide precursors, and in excised organs in a murine hepatic carcinoma model. Building from a similar diselenide, Chen reported **1042** (TP-Dise) that provided a ratiometric response from 585 nm to 674 nm when treated with GSSH and was shown to be selective for sulfane sulfur over disulfides, thiols, and metal cations.[1026] The probe was also used to image changes in sulfane sulfur levels in SH-SY5Y and A549 cells when treated with various promoters and inhibitors of GSSH production. Furthermore, this probe was also used to investigate GSSH in Hg-stressed cells and also to image sulfane sulfur in mouse brain tissue exposed to Hg stress at depths up to 100 μm using two-photon microscopy.

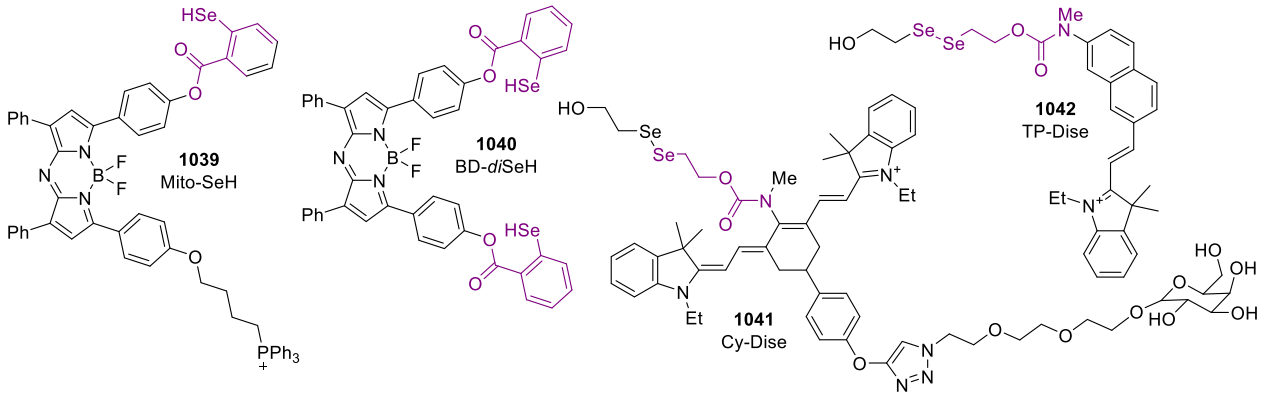
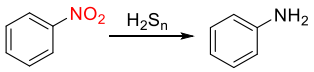


Figure 1.210. Examples of fluorescent H_2S_n probes based on nucleophilic selenol addition to sulfane sulfur species and subsequent cyclization using xanthene based chromophores.

1.6.3 Reduction-Based Probes

Nitro group reduction was discussed earlier as an approach to generate H_2S responsive activity-based probes. One limitation of this approach is the empirically slower reaction rates and lower selectivity when compared to other reduction-based approaches. Building on this prior work, a number of reports have highlighted the H_2S_n-mediated reduction nitro groups as an approach for H_2S_n detection (Scheme 1.30).



Scheme 1.30. General reaction of aryl nitro groups with H_2S_n to form an amine.

Yu and Chen reported an early example of this approach in 2015 with cyanine-based probes **1043** (Hcy-Mito) and **1044** (Hcy-Biot), which contain a *para*-chlorophenyl and a biotin moiety, respectively (Figure 1.211).[1027] These probes were designed as dual probes, where initial KO_2 treatment resulted in probe oxidation to the fluorescent form of the chromophore with a response at 780 nm that was further enhanced by H_2S_n-mediated nitro group reduction. When investigated in Raw 264.7 cell, treatment of **1043** with both KO_2 and H_2S_n treatment resulted in a fluorescent response and the probe was confirmed to localize in the mitochondria. The probe was further used to investigate the relationship between superoxide and sulfane sulfur under oxidative stress in cells and mice. This approach was also used by Yu, Ding, and Chen who reported cyanine-based probe **1045** (HCy-ONO), which also required initial oxidation by KO_2 to provide a fluorescence turn-on at 785 nm followed by a fluorescence shift to 635 nm upon treatment with H_2S_n.[1028] This probe was used to image both superoxide and H_2S_n in tissue as well as in a SH-SY5Y tumor-bearing mouse model.

Expanding to a flavylium-based system, Yang reported probe **1046**, which provides an 87-fold fluorescence turn-on at 568 nm, with good selectivity for H_2S_n over competing analytes, although a small response for H_2S was also observed.[1029] This probe was also demonstrated to respond to H_2S_n in both FBS and SMMC-7721 cells. Zhou also used this approach to develop naphthalimide-based **1047** (ER-H_2S_2), which provided a 160-fold fluorescence turn-on at 540 nm with H_2S_n in buffer with CTAB.[1030] The probe was selective for H_2S_n over other reactive species including H_2S, was found to localize to the ER, and responded to H_2S_n in both MCF-7 cells and

zebrafish. Kim and Yoon also used a naphthalimide-based system for two-photon imaging with **1048** (NI-H_2S_2).[1031] This probe provided good selectivity for H_2S_n and was used to image H_2S_n in live HeLa cells and hippocampal tissues slices with two-photon imaging.

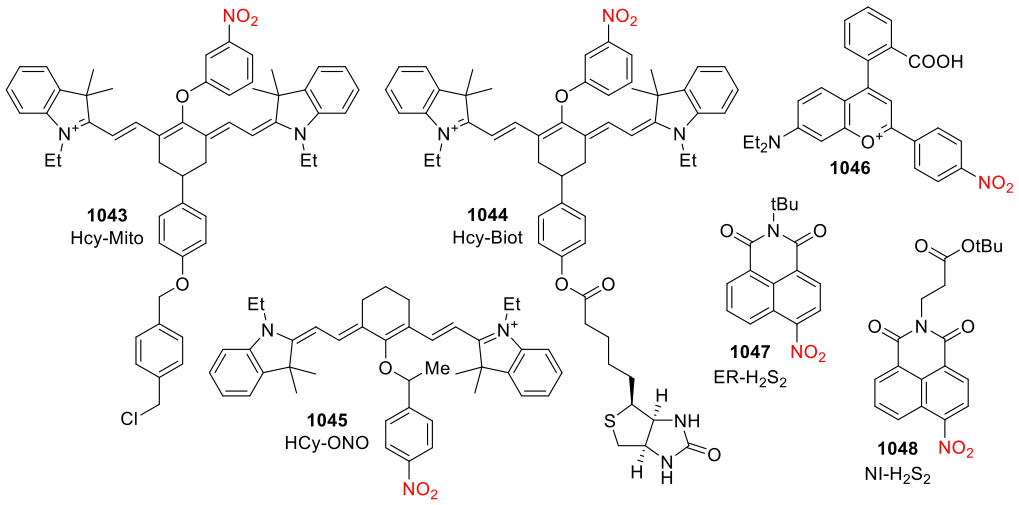


Figure 1.211. Examples of fluorescent H_2S_n probes based on nitro group reduction.

Using a different reduction approach, Luo and Zeng reported 6,7-dihydroxyperylene-1,12-quinone **1049** (DHPQ) as a reduction-based probe for H_2S_n (Figure 1.212).[1032] H_2S_n-mediated reduction of **1049** resulted in a fluorescence turn-on at 490 nm and was found to be selective over other biologically relevant species. This response could be chemically reversed by subsequent addition HClO to re-oxidize the probe. This cyclability was also demonstrated in HeLa cells.

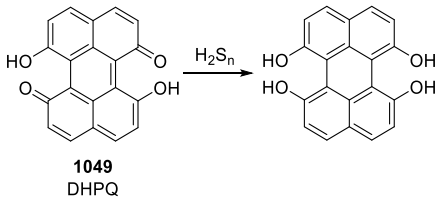


Figure 1.212. H_2S_n-mediated reduction of **1049**.

1.7 Conclusions and Future Perspectives

The development and rapid expansion of activity-based fluorescent probes for H_2S over the past decade has provided a key cornerstone of investigative tools for examining the roles of

H_2S in biology. The diversity of sensing approaches is in many ways enabled by the broad and complex reactivity of H_2S, which has been leveraged by researchers to couple selective chemical reactivity with fluorescent outputs. One apparent and important reality is that there is no singular "perfect" detection strategy for H_2S, with different approaches having specific benefits and detractions based on the fundamental chemistry from which these platforms are built. Since each approach has strengths and weaknesses, both must be considered when choosing different activity-based sensing approaches to apply to specific biological problems.

As highlighted through this Review, different activity-based H_2S probes have distinct selectivity profiles. For example, many of the approaches used to develop H_2S reporters, such as cleavage of NBD ethers, DNP groups, and metal precipitation from weaker field ligands, have moderate selectivity for H_2S over competing analytes. In many ways, understanding these selectivity challenges has enabled the discovery of fundamentally new chemistry and subsequent translation to new tools. Similarly, some functional groups, such as nitro groups and certain electrophiles, react with both H_2S and H_2S_n species. This duality likely limits the broad application of such approaches in complex redox environments. In addition, efforts to translate activity-based approaches for H_2S sensing to longer wavelength systems often relies on inclusion of indolium or dicyano alkenes, but these groups have also been used directly as H_2S reporters. One fundamental challenge in understanding these broad classes of reactivity is that most selectivity investigations are performed aerobically, which means that adventitious oxygen and trace metal impurities likely generate small amounts of sulfane sulfur species that can further complicate analysis or reproducibility. Based on these considerations, careful analysis is needed in choosing detection chemistry that is compatible with both the competing analytes and type of experiments being performed. This selectivity challenge should not be surprising nor underestimated based on the close connectivity between H_2S and other RSS.

Future expansions of activity-based H_2S probe development need to address critical problems in the field to avoid stagnation. Based on the breadth of reported probes and growing maturity of the field, simple adaptations of known approaches to include new chromophores are unlikely to make a significant impact unless they are coupled with fundamentally new outputs unavailable with current systems. In many ways, this field maturity highlights the opportunity to connect innovation with impact by addressing forward-looking critical needs in the field rather than lateral expansion. One of the most daunting challenges in the field is the development of

reversible H_2S probes. Such platforms would allow for both increases and decreases in H_2S levels to be monitored in real time in complex biological environments. Fundamentally, reversible probes would also significantly simplify problems with analyte consumption and interconversion to other RSS by different classes of probes. New approaches to address this challenge, such as chemically reversible or analyte replacement approaches highlighted throughout this Review are beginning to emerge, but application to endogenous H_2S fluxes remains elusive. Although currently less developed than other approaches, the use of reversible electrophiles or transition metal complexes to bind H_2S/HS^- both provide promising platforms for solving this challenge. Similarly, adjacent efforts in reversible binding of HS^- to synthetic purely organic platforms offer attractive and emerging approaches for developing reversible reporters.[1033-1037] Translating these proof-of-concept approaches to functional probes will require tuning the binding affinities of such platforms to match the concentration range of endogenous H_2S, which provides and additional level of complexity to the design of these platforms. In addition to the above challenges, probes that can selectively detect and differentiate specific RSS within the sulfane sulfur pool are still needed. For example, differentiation of Cys-SSH, GSSH, and inorganic polysulfides using activity-based approaches in intact samples would be a major advance. First-generation approaches for H_2S_n reporters have already made major impacts, but many of these systems rely on the interconversion of different sulfane sulfur species to activate specific probe designs. In general, a better understanding of the fundamental chemistry of these reactive and rapidly interconverting sulfane sulfur species is needed to better understand how it can be leveraged to generate new activity-based approaches.

This innate RSS interconnectivity likely contributes to why Nature chose these reactive molecules for important biological actions, yet also poses a significant challenge for engineering molecular selectivity and specificity into sensing approaches. For example, understanding the specific activities of H_2S, polysulfides, and persulfides with different activity-based platforms remains a muddy and mainly unmet challenge. In addition, the rapid interconversion between RSS makes dissecting individual contributions or equilibrium concentrations particularly challenging. In many cases, that addition of activity-based H_2S probes effectively siphon out specific species from these RSS equilibria, thereby perturbing both the RSS distribution and redox state of the system. An alternative although possibly less satisfying solution is that if Nature can select whichever RSS is needed for a specific biological action from a broader pool of RSS, then

specificity between components within such pools may not actually be needed. In this situation, the more important although equally challenging need would be to develop small molecule chemical tools that allow for the redox state of different RSS pools to be measured directly in complex environments. Such approaches would complement protein-based redox probes and broaden the potential application of such systems to broader types of environments.[1038-1040] In many ways, the development of such activity-based redox probes, tuned to different RSS equilibrium environments, pose a more daunting design challenge than for individual RSS.

Even with outstanding challenges in the field, the advent and expansion of activity-based probes for H_2S detection and imaging has advanced remarkably in the past decade and more importantly has positively impacted our understanding of how H_2S and related RSS function in biological contexts. In addition, many of these approaches have enabled new ideas on how to delineate reactivity and signals from molecules with remarkable similarity within RSS pools. For example, chemists have already begun to harness such interfacial chemistry to develop proof-of-concept activity-based approaches for detecting adjacent RSS like nitrosothiols, HSNO, and COS.[1041-1043] One benefit of developing activity-based approaches for H_2S and RSS detection is the relatively simple translation to other detection methods including photoacoustic imaging, ultra-sound, MRI, Raman, and other approaches. In addition, much of the chemistry highlighted throughout this Review is compatible with engineered protein-based systems including genetically encoded or fusion protein H_2S probes.[1044-1048] More broadly, the development and refinement of specific approaches to translate H_2S reactivity to an optical response has also expanded and honed our understanding of the fundamental reaction chemistry of this enigmatic small molecule. Much like these developed probes have illuminated new impacts of biological H_2S, they have also shed light on future challenges and opportunities that form the foundation for future advances in the field. Rising to meet these challenges in the development of new probes has the bright potential to further translate the unique biological activity of H_2S and related RSS into important chemical tools that can be applied directly to understanding RSS dynamics in human health and disease.

II. A CELL TRAPPABLE METHYL RHODOL-BASED FLUORESCENT PROBE FOR HYDROGEN SULFIDE DETECTION

This chapter includes previously published and co-authored material from Fosnacht, K.G.; Hammers, M.D.; Earp, M.S.; Gilbert, A.K.; Pluth, M.D. A Cell Trappable Methyl Rhodol-Based Fluorescent Probe for Hydrogen Sulfide Detection. *Chem. Asian J.* **2022**, *17*, e202200426. This manuscript was written by Kaylin G. Fosnacht with editorial assistance by Professor Michael D. Pluth. The project in this chapter was conceived by Matthew D. Hammers, and the experimental work was performed by Kaylin G. Fosnacht, Matthew D. Hammers, and Mary S. Earp.

2.1 Introduction

Hydrogen sulfide (H_2S) and related reactive sulfur species (RSS) are highly involved in the health and homeostasis of humans, animals, bacteria, and other organisms.[1] H_2S is one of three commonly recognized gasotransmitters and is produced endogenously by numerous processes, including the enzymatic breakdown of cysteine by cystathionine γ-lyase (CSE), cystathionine-β-synthase (CBS), and 3-mercaptopyruvate sulfurtransferase (3-MST).[2] Decreased H_2S levels have been observed in various diseases, such as Huntington's disease, asthma, and Crohn's disease.[3] Whether the downregulation of H_2S production is a contributing cause or a resulting symptom of different diseases remains an ongoing question. For example, the mutation that causes Huntington's disease also causes a decrease in brain CSE, which leads to decreased cysteine and H_2S production and ultimately increases oxidative stress and damage.[4] Disentangling the separate impacts of genetic mutation, oxidative damage, and Hcy/H_2S levels remains a challenge.

Aligned with the rapid expansion of the roles of H_2S and other RSS in biology, the last decade has seen a significant increase in the available tools for H_2S detection. These approaches can broadly be divided into two classes: those that allow for bulk H_2S measurement and quantification (e.g. colorimetric assays, H_2S-selective electrodes, electrophilic trapping, etc.) and those that allow for *in cellulo* or *in vivo* imaging (e.g. fluorescent probes).[5] Fluorescent probes for H_2S have been developed based on a number of strategies including electrophilic reactions with H_2S, azide reduction, metal precipitation, and other methods.[6] Of these approaches, azide reduction has emerged as the most commonly used approach, in part due to the ease of modifying chromophores with fluorogenic amines into azides and the established mechanism of H_2S-

mediated azide reduction.[7] Such approaches have generated a broad array of fluorescent probes with different properties, including different emission wavelengths, sensitivities, and targets.[8]

One challenge for many fluorescent probes, including those developed for H_2S, is that most such probes are freely membrane permeable and can diffuse both into and out of cells, making signals less reliable over longer time course experiments. A common approach to address this limitation is to append ester motifs to small molecule probes, which can be cleaved by intracellular esterase enzymes and converted into the corresponding carboxylate. The resulting negative charge of the carboxylate at physiological pH makes the probe cell impermeable, thus trapping the probe within the cell. Despite the high fidelity of this approach to impart trappability in other activity-based probes, relatively few examples of cell trappable H_2S fluorescent probes have been reported. These include BODIPY-, rhodamine-, and fluorescein-based fluorescent probes that incorporate acetoxymethyl ester (AM) groups[9] to impart cell trappability.[10] Key examples of azide-based cell trappable probes based on rhodamine fluorophores include SF5-AM and SF7-AM, developed by the Chang group in 2013,[10a] and Rho630-AM-H_2S, developed by the Kong group[10b] in 2019 (Figure 2.1). These platforms generated cell-trappable azide-based probes for H_2S detection and provide moderate fluorescence turn-on responses (4–20 fold) upon probe activation.

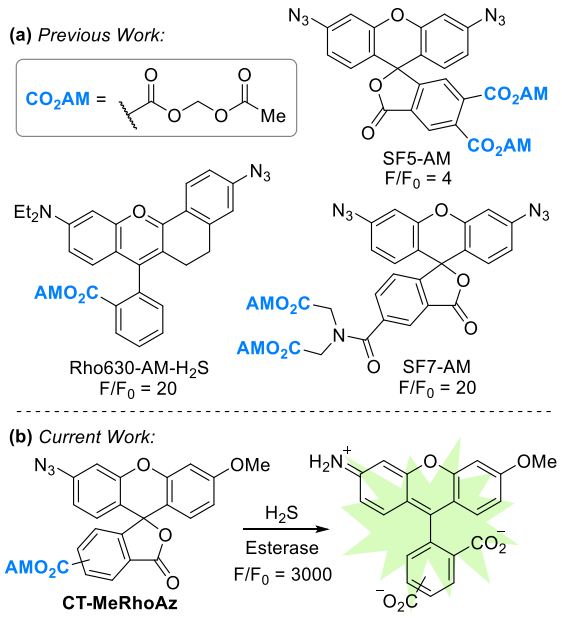


Figure 2.1. (a) Prior rhodamine-based cell-trappable H_2S probes based on azide reduction and associated fluorescent responses for H_2S (F/F_0). (b) This work reports a cell-trappable methylrhodolazide-based H_2S probe, **CT-MeRhoAz**.

Inspired by this approach, we viewed the addition of an enzyme-cleavable ester group onto a bright, otherwise non-trappable H_2S probe could increase the usefulness of this platform. In prior work, we reported the azide-based H_2S fluorescent probe methylrhodolazide (MeRhoAz), which has been used to detect endogenous H_2S both in cells and also investigate H_2S in larval zebrafish.[11] The azide motif in MeRhoAz locks the fluorophore in the closed, non-fluorescent lactone form until the azide is reduced to an amine to generate the fluorescent quinoidal form of the dye. Notably, MeRhoAz showed a 1200-fold fluorescence turn-on with H_2S and minimal unwanted photoactivation when compared to other common fluorogenic platforms. Building from the MeRhoAz platform, we report here a cell trappable methylrhodolazide probe (**CT-MeRhoAz**) by addition of an acetoxymethyl ester to the 5(6)-position of the benzene ring. The **CT-MeRhoAz** fluorescent probe for H_2S shows a high fluorescence response, excellent selectivity against other reactive species, and enhanced cell trappability when compared to the parent MeRhoAz platform.

2.2 Results and Discussion

2.2.1 Probe Design and Synthesis

To prepare **CT-MeRhoAz**, we first methylated 5(6)-carboxyfluorescein with methyl iodide to form the trimethylated precursor **1** (Figure 2.2). Basic hydrolysis of **1** removed the methyl esters to afford **2**, and the carboxylic acid was converted to the desired acetoxymethyl group using bromomethyl acetate under basic conditions to form **3**. Treatment of **3** with $PhN(Tf)_2$ afforded triflate **4**, which was converted to **CT-MeRho** using a Buchwald-Hartwig amination using $Ph_2C{=}NH$ as the initial coupling partner followed by acidic hydrolysis. Subsequent azidification using *tert*-butyl nitrite followed by trimethylsilyl azide addition afforded **CT-MeRhoAz**. Each step of the **CT-MeRhoAz** synthesis is moderate to high yielding (42–98%), which allows for relatively simple preparation of the final probe in good overall yield.

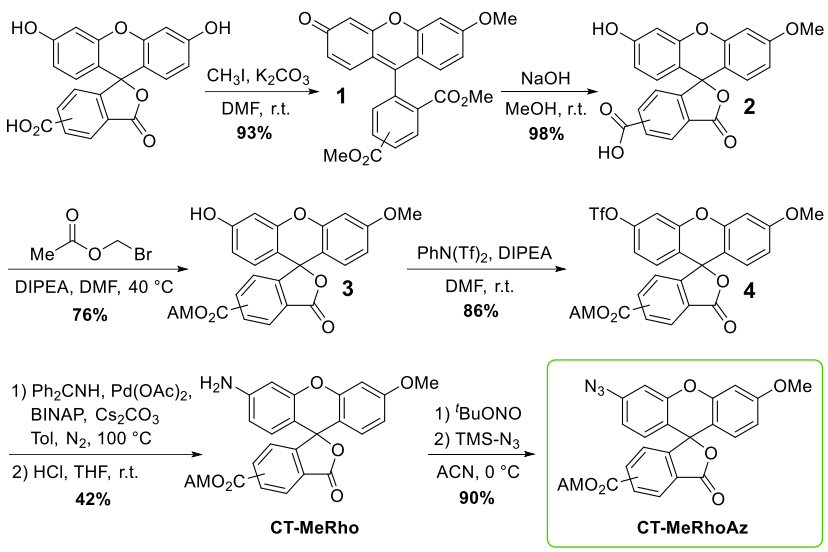


Figure 2.2. Synthesis of **CT-MeRhoAz**. Structures are shown in the closed lactone tautomer for simplicity.

2.2.2 Spectroscopic Properties and Selectivity

Having prepared **CT-MeRhoAz**, we next measured the spectroscopic properties of the probe in 50 mM PIPES buffer (100 mM KCl, pH 7.4). As expected, prior to reduction of the azide, **CT-MeRhoAz** is only minorly absorptive (λ_{max} = 286 nm, ε = 15,400 M^{-1} cm^{-1}) and non-fluorescent in the visible region due to the fluorescein unit being locked in the closed lactone tautomer (Figure A1). By contrast, **CT-MeRho** shows a prominent absorbance band in the visible region (λ_{max} = 480 nm, ε = 26,800 M^{-1} cm^{-1}) with a strong fluorescence (λ_{em} = 514 nm, ϕ = 0.45), exemplifying the fluorescence turn-on of this system (Figure A2). Treatment of **CT-MeRhoAz** (5 μM) in 50 mM PIPES buffer (100 mM KCl, pH 7.4) with excess H_2S (NaSH, 250 μM, 50 equiv.) at 37 °C and monitoring from 490–650 nm over 90 minutes resulted in a 2500-fold fluorescence turn-on (Figure 2.3). The detection limit of the probe was also calculated as 160 ± 30 nM using the blank + 3σ method (Figure A3, Table A1). Further, we tested the fluorescent response of **CT-MeRhoAz** in the presence of both H_2S and porcine liver esterase (PLE). When **CT-MeRhoAz** was treated with only PLE (10 U mL^{-1}) for 90 minutes, a minimal 16-fold enhancement was observed, which confirmed that PLE alone does not lead to a significant false signal increase (Figure A4). Treatment of **CT-MeRhoAz** with H_2S (NaSH, 250 μM, 50 equiv.) in the presence of PLE (10 U mL^{-1}) resulted in a 3000-fold turn-on response over the course of 90 minutes (Figure A4), which highlights the overall dynamic range of the carboxylate form of the probe.

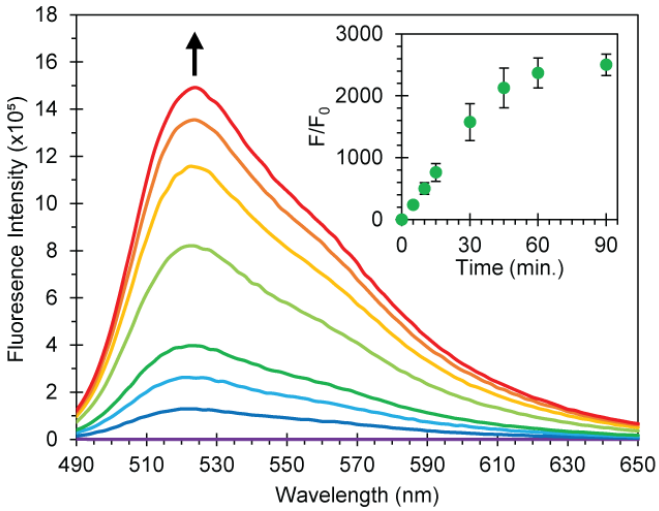


Figure 2.3. Fluorescence turn-on of **CT-MeRhoAz** (5 μM) in response to H_2S (250 μM NaSH, 50 equiv.) in 50 mM PIPES buffer (100 mM KCl, pH 7.4) at 37 °C. λ_{ex} = 480 nm, λ_{em} = 490–650 nm. Slit width: 0.4 mm. The experiments were performed in triplicate and results are expressed as mean ± SD (*n* = 3).

Having confirmed the response of **CT-MeRhoAz** with H_2S, we next investigated the selectivity of the probe against other biologically relevant analytes over a 90-minute incubation period at 37 °C. We tested the fluorescent response of **CT-MeRhoAz** against (250 μM, 50 equiv.) of L-cysteine, DL-homocysteine, and glutathione (5 mM) as well as the analytes $S_2O_3^{2-}$, SO_3^{2-}, SO_4^{2-}, H_2O_2, NO, O_2^-, and NO_2^- (Figure 2.4). No significant response was observed in the presence of any of these competing analytes, which is consistent with the significant body of literature reporting the high selectivity of azide reduction for H_2S. Additionally, in the presence of 5 mM glutathione, only a 16-fold turn-on was observed, which further highlights the selectivity of this platform.

2.2.3 Response to H_2S and Cell Trappability in Live Cells

After confirming the response and selectivity of **CT-MeRhoAz**, we next investigated H_2S detection in live cells. We first incubated HeLa cells with either vehicle or aminooxyacetic acid (AOAA, 20 μM) for 45 minutes. AOAA is a CBS/CSE inhibitor and reduces endogenous production of H_2S.[12] Next, cells were treated with 5 μM **CT-MeRhoAz**. After incubation for 45 minutes, the cells were treated with either the vehicle or 200 μM NaSH and incubated for 45 minutes and then imaged by fluorescence microscopy (Figure 2.5). As expected, treatment with

AOAA resulted in a reduction in background fluorescence, which is consistent with detection of endogenous H_2S by the probe. Similarly, treatment with NaSH resulted in a significant increase in fluorescence, confirming that **CT-MeRhoAz** can image H_2S in live cells.

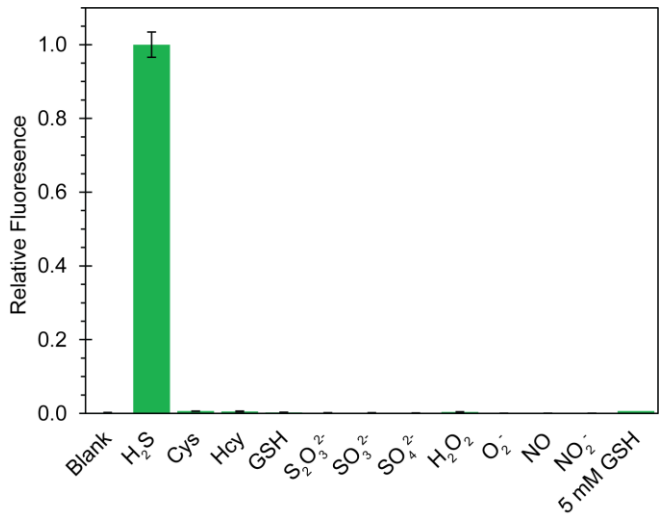


Figure 2.4. Selectivity of **CT-MeRhoAz** (5 μM) in the presence of competing analytes (250 μM, 50 equiv.) including NaSH, L-cysteine, DL-homocysteine, glutathione, $Na_2S_2O_3$, Na_2SO_3, Na_2SO_4, H_2O_2, KO_2, DEANONOate, $NaNO_2$, and 5 mM glutathione, respectively. λ_{ex} = 480 nm, λ_{em} = 490–640 nm. The experiments were performed in triplicate and results are expressed as mean ± SD (*n* = 3).

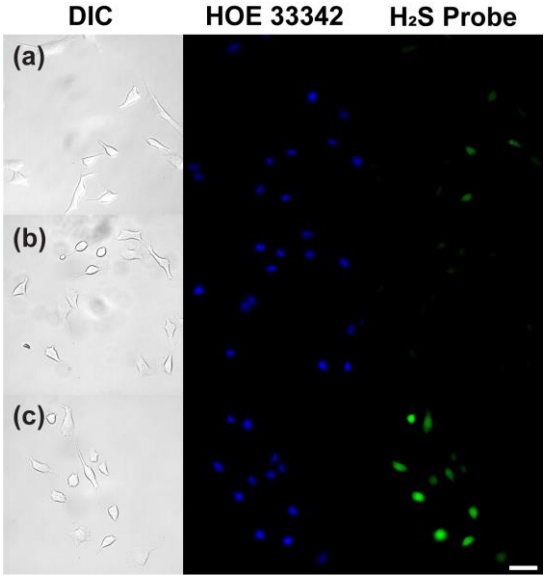


Figure 2.5. Fluorescence imaging of **CT-MeRhoAz** in HeLa cells. Cells were incubated with 5 μM **CT-MeRhoAz** for 45 minutes with either (a) vehicle, (b) pre-treatment with 20 μM AOAA, or (c) post-treatment with 200 μM NaSH and then imaged. Barscale: 50 μm.

We next compared the signal stability from **CT-MeRhoAz** and the non-cell trappable MeRhoAz to confirm addition of the acetoxymethyl ester group imparted cell trappability to the probe. HeLa cells were first incubated with the H_2S donor AP39[13] (100 nM) for 1 hour followed by incubation for 45 minutes with 5 μM of either **CT-MeRhoAz** or MeRhoAz (Figure 2.6). After the initial washing to remove any extracellular probe, the media was replaced every 10 minutes over the course of 1 hour. Cell images were acquired at 5, 30, and 60 minutes. Substantial loss of signal due to probe diffusion was observed for MeRhoAz, with minimal signal remaining at the end of the 60-minute time period. By contrast, using the same washing procedures, the signal from **CT-MeRhoAz** is retained after 60 minutes, confirming that the probe was trapped inside of the cells. Quantification of the cellular fluorescence further emphasized the attenuation of fluorescent signal **CT-MeRhoAz** displayed over MeRhoAz, with 54% of the initial fluorescent signal being retained for **CT-MeRhoAz** whereas MeRhoAz retains <0.1% of the original signal (Figure A10). Taken together, these cell experiments establish that **CT-MeRhoAz** is a cell trappable probe and can be used to detect H_2S in a cellular environment.

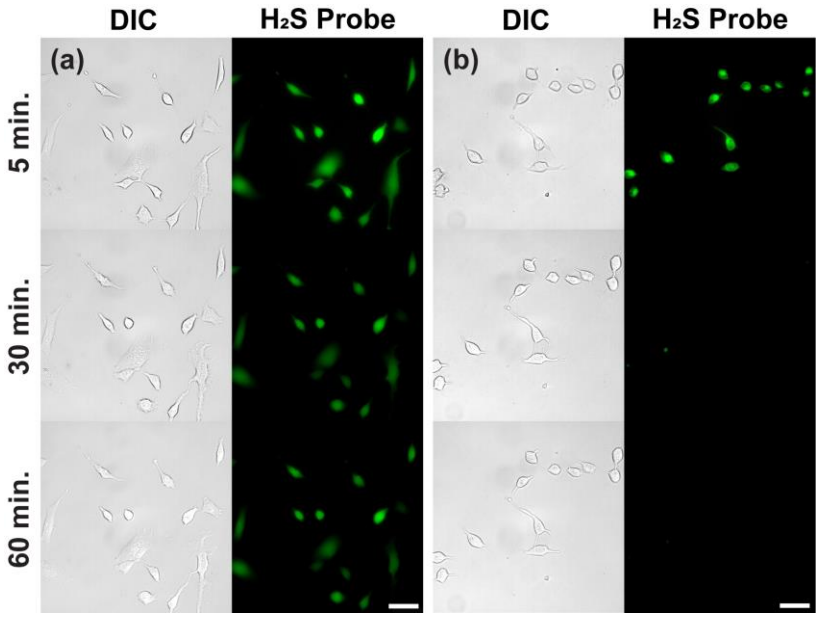


Figure 2.6. Cell trappability experiments of (a) **CT-MeRhoAz** and (b) MeRhoAz in HeLa cells. Cells were incubated with AP39 (100 nM) for 1 hour and then incubated with the probe (5 μM) for 45 minutes. Cells were washed with fresh media every 10 minutes and imaged at 5, 30, and 60 minutes. Bar scale: 50 μm.

2.3 Conclusion

We demonstrated that addition of an acetoxymethyl ester to the bright MeRhoAz scaffold imparts cell trappability to the **CT-MeRhoAz** probe. When treated with excess H_2S, **CT-MeRhoAz** generates a 2500-fold turn-on response over the course of 90 minutes, and a 3000-fold response with concurrent cleavage of the ester group with PLE. When compared to other cell trappable fluorescence probes for H_2S, **CT-MeRhoAz** has a greater fluorescence turn-on and is synthetically easier to prepare.[10] The selectivity profile against other biologically-relevant sulfur, nitrogen, and oxygen species is excellent, with a maximal turn-on of 16-fold observed for 5.0 mM GSH, which is significantly lower than the response to H_2S. Additionally, cell imaging experiments demonstrated that **CT-MeRhoAz** can respond to H_2S in a cellular environment and also confirmed enhanced cell trappability when compared to the parent MeRhoAz probe. In conclusion, **CT-MeRhoAz** is a bright, cell trappable fluorescent probe for H_2S with excellent selectivity that should be useful to advance imaging work related to H_2S detection in complex biological environments.

2.4 Experimental Section

Methods and Materials

Reagents were purchased from Sigma-Aldrich, Tokyo Chemical Industry (TCI), Fisher Scientific, Combi-Blocks, and VWR and used directly as received. AP39[1049] and MeRhoAz[111] were prepared as described in the literature. Silica gel (SiliaFlash F60, Silicycle, 230−400 mesh) was used for column chromatography. Deuterated solvents were purchased from Cambridge Isotope Laboratories (Tewksbury, Massachusetts, USA). ^{1}H and $^{13}C\{^{1}H\}$ NMR spectra were recorded on Bruker 500 MHz NMR or Bruker 600 MHz NMR instrument at the indicated frequencies. Chemical shifts are reported in ppm relative to residual protic solvent resonances. Compounds **1**–**4**, **CT-MeRho**, and **CT-MeRhoAz** are a combination of the 5- and 6-carboxyfluorescein isomers, which is reflected in the ^{1}H and $^{13}C\{^{1}H\}$ NMR spectra. Mass spectrometric measurements were performed by the University of Illinois, Urbana Champaign MS facility or on a Xevo Waters ESI LC/MS instrument. UV-visible spectra were acquired on a Cary 60 spectrometer and fluorescence spectra were obtained on a Quanta Master 40 spectrofluorometer (Photon Technology International).

*Synthesis of **CT-MeRhoAz***

Compound **1**. 5(6)-Carboxyfluorescein (1.02 g, 2.71 mmol, 1.0 equiv.) and potassium carbonate (1.12 g, 8.13 mmol, 3.0 equiv.) were added to 3 mL of DMF, after which methyl iodide (0.67 mL, 11 mmol, 4.0 equiv.) was added dropwise. The reaction mixture was stirred at room temperature for 21 hours, diluted with a saturated sodium bicarbonate solution (50 mL), and then extracted into ethyl acetate. The organic phase was washed with brine and then dried with $MgSO_4$. After removal of solvent under reduced pressure, the crude product was purified by column chromatography (1–2% methanol in DCM as the eluent) to afford **1** as an orange solid (1.06 g, 93.3%). ^{1}H NMR (500 MHz, DMSO-d_6) δ (ppm): 8.72 (s, 1 H), 8.38 (d, *J* = 7.9 Hz, 1H), 8.33 (m, 3H), 8.00 (s, 1H), 7.69 (d, *J* = 7.9 Hz, 1H), 7.26 (s, 2H), 6.88 (s, 4H), 6.83 (dd, *J* = 9.7, 4.1, 9.78 Hz, 2H), 6.40 (d, *J* = 9.7 Hz, 2H), 6.27 (s, 2H), 3.98 (s, 3H), 3.93 (s, 6H), 3.90 (s, 3H), 3.65 (s, 3H), 3.62 (s, 3H). ^{13}C{^{1}H} NMR (125 MHz, DMSO-d_6) δ (ppm): 184.2, 184.1, 165.5, 165.4, 165.1, 164.8, 164.6, 158.8, 158.8, 154.2, 154.1, 149.5, 139.0, 134.7, 133.9, 133.9, 133.9, 132.1, 131.9, 131.7, 131.6, 131.5, 131.0, 130.9, 130.8, 130.6, 129.8, 129.4, 129.4, 117.4, 117.0, 114.7, 114.4, 114.2, 105.2, 105.1, 101.1, 56.8, 53.3, 53.2, 53.2, 53.1. HRMS m/z $[M + H]^+$ calcd. for $[C_{24}H_{19}O_7]^+$ 419.1125; found 419.1136.

Compound **2**. Fluorescein derivative **1** (1.00 g, 2.44 mmol, 1.0 equiv.) was added to a mixture of 40 mL of methanol and 40 mL of 1.0 M NaOH. The reaction mixture was stirred for 18 hours, and then the methanol was removed under vacuum. This solution was then acidified to pH 4.0 with 1.0 M HCl and then extracted into ethyl acetate. The organic phase was washed with brine and then dried with $MgSO_4$. After removal of solvent under reduced pressure, compound **2** was isolated as a yellow solid (910 mg, 97.5%). ^{1}H NMR (500 MHz, DMSO-d_6) δ (ppm): 10.22 (s, 2H), 8.41 (s, 1H), 8.31 (d, *J* = 8.1 Hz, 1H), 8.24 (d, *J* = 8.0 Hz, 1H), 8.13 (d, *J* = 8.0 Hz, 1H), 7.67 (s, 1H), 7.41 (d, *J* = 8.0 Hz, 1H), 6.96 (s, 2H), 6.72 (s, 5H), 6.64 (dd, *J* = 2.0 Hz, 2H), 6.58 (dd, *J* = 9.0 Hz, 2H), 3.83 (s, 6H). ^{13}C{^{1}H} NMR (125 MHz, DMSO-d_6) δ (ppm): 168.3, 166.8, 161.7, 160.2, 156.6, 153.2, 152.4, 152.3, 152.2, 137.8, 136.6, 133.4, 131.5, 129.8, 129.8, 129.7, 129.7, 129.6, 127.1, 126.0, 125.8, 125.1, 124.9, 113.4, 112.5, 110.8, 110.8, 109.3, 109.2, 102.7, 101.3, 83.5, 56.2. HRMS m/z $[M + H]^+$ calcd. for $[C_{22}H_{15}O_7]^+$ 391.0812; found 391.0813.

Compound **3**. Fluorescein derivative **2** (910 mg, 2.31 mmol, 1.0 equiv.) was added to 3 mL of DMF, and then bromomethyl acetate (216 μL, 2.31 mmol, 1.0 equiv.) followed by DIPEA (403 μL, 2.31 mmol, 1.0 equiv.) were added dropwise. The reaction mixture was stirred at 40 °C for 25

hours and then diluted with water, extracted into ethyl acetate, washed with brine, and then dried with $MgSO_4$. After removal of solvent under reduced pressure, the crude product was purified by column chromatography (50–90% ethyl acetate in DCM as the eluent) to afford **3** as a yellow solid (792 mg, 75.8%). ^{1}H NMR (500 MHz, DMSO-d_6) δ (ppm): 10.22 (s, 2H), 8.44 (s, 1H), 8.33 (d, *J* = 8.0 Hz, 1H), 8.27 (d, *J* = 8.0 Hz, 1H), 8.19 (d, *J* = 8.1 Hz, 1H), 7.72 (s, 1H), 7.47 (d, *J* = 8.1 Hz, 1H), 6.96 (s, 2H), 6.72 (m, 8H), 6.58 (m, 2H), 6.00 (s, 2H), 5.88 (s, 2H), 3.83 (s, 6H), 2.14 (s, 3H), 2.07 (s, 3H). ^{13}C{^{1}H} NMR (125 MHz, DMSO-d_6) δ (ppm): 169.9, 169.8, 168.0, 163.9, 163.8, 161.7, 160.3, 157.4, 153.2, 152.4, 152.3, 152.2, 136.8, 131.7, 131.1, 130.8, 129.9, 129.8, 129.7, 129.7, 127.4, 126.5, 126.2, 125.5, 125.1, 113.4, 112.5, 110.6, 110.5, 109.1, 109.0, 102.8, 101.3, 83.7, 83.6, 80.6, 80.5, 56.2, 21.0. HRMS m/z [M + H]$^+$ calcd. for $[C_{25}H_{19}O_9]^+$ 463.1024; found 463.1029.

Compound **4**. Fluorescein derivative **3** (500 mg, 1.08 mmol, 1.0 equiv.) was added to 3.5 mL DMF and then DIPEA (755 μL, 4.33 mmol, 4.0 equiv.) followed by the $PhN(Tf)_2$ (386 mg, 1.08 mmol, 1.0 equiv.) were added dropwise. The reaction mixture was stirred at room temperature for 24 hours and then diluted with water, extracted into ethyl acetate, washed with brine, and then dried with $MgSO_4$. After removal of solvent under reduced pressure, the crude product was purified by column chromatography (25% ethyl acetate in hexanes as the eluent) to afford **4** as a white solid (532 mg, 85.7%). ^{1}H NMR (50 MHz, DMSO-d_6) δ (ppm): 8.48 (s, 1H), 8.36 (d, *J* = 8.1 Hz, 1H), 8.30 (d, *J* = 8.1 Hz, 1H) 8.24 (d, *J* = 8.0 Hz, 1H), 7.93 (s, 1H), 7.73 (d, *J* = 6.5 Hz, 2H), 7.59 (d, *J* = 8.1 Hz, 1H), 7.26 (m, 2H), 7.15 (m, 2H), 7.01 (s, 2H), 6.84 (m, 2H), 6.78 (m, 2H), 6.01 (s, 2H), 5.88 (s, 2H), 3.85 (s, 6H), 2.14 (s, 3H), 2.07 (s, 3H). ^{13}C{^{1}H} NMR (125 MHz, DMSO-d_6) δ (ppm): 169.9, 169.8, 167.8, 167.7, 163.7, 162.0, 162.0, 156.8, 152.6, 151.9, 151.8, 151.7, 151.7, 150.3, 150.3, 137.0, 135.8, 132.1, 131.5, 131.4, 131.3, 130.4, 130.0, 129.9, 129.9, 127.0, 126.8, 126.5, 125.6, 125.5, 123.4, 120.0, 120.0, 119.4, 117.9, 117.8, 117.4, 113.2, 113.2, 111.2, 111.2, 110.1, 109.9, 101.1, 82.0, 81.8, 80.6, 80.5, 56.3, 56.3, 21.0, 21.0. HRMS m/z [M + H]$^+$ calcd. for $[C_{26}H_{18}F_3O_{11}S]^+$ 595.0516; found 595.0522.

CT-MeRho. In a glovebox, compound **4** (265 mg, 0.446 mmol, 1.0 equiv.), $Pd(OAc)_2$ (10 mg, 0.045 mmol, 0.10 equiv.), rac-BINAP (41.62 mg, 0.067 mmol, 0.15 equiv.), and Cs_2CO_3 (436 mg, 1.34 mmol, 3.0 equiv.) were dissolved in toluene (10 mL) in a three-neck flask fitted with a reflux condenser. After the reaction vessel was sealed under N_2 and removed from the glovebox, benzophenone imine (89.8 μL, 0.535 mmol, 1.2 equiv.) was added via syringe. The reaction

mixture was heated and stirred at 140 °C for 5 min, and then the temperature was reduced to 100 °C for an additional 8 hours. After heating, the reaction mixture was allowed to cool to room temperature and was filtered through a plug of Celite. After removal of the solvent under reduced pressure, the residue was dissolved in a solution of THF (20 mL) and 1.0 M HCl (5 mL) and stirred at room temperature for 1 hour. The THF was removed under reduced pressure, the crude product was diluted with water, and then the pH was neutralized. The aqueous solution was extracted into EtOAc, and the organic phase was washed with brine and dried using $MgSO_4$. The crude product was purified using column chromatography (20–80% ethyl acetate in hexanes as the eluent) to afford **CT-MeRho** as a yellow solid (87.2 mg, 42.4%). ^{1}H NMR (500 MHz, DMSO-d_6) δ (ppm): 8.41 (s, 1H), 8.32 (d, *J* = 9.6 Hz, 1H), 8.25 (d, *J* = 9.4 Hz, 1H), 8.16 (d, *J* = 8.0 Hz, 1H), 7.68 (s, 1H), 7.44 (d, *J* = 8.1 Hz, 1H), 6.92 (s, 2H), 6.67 (m, 4H), 6.44 (m, 4H), 6.34 (m, 2H), 6.00 (s, 2H), 5.88 (s, 2H), 5.71 (s, 4H), 3.82 (s, 6H), 2.14 (s, 3H), 2.07 (s, 3H). ^{13}C{^{1}H} NMR (150 MHz, DMSO-d_6) δ (ppm): 169.1, 168.1, 136.8, 161.6, 157.5, 152.6, 152.1, 136.6, 130.9, 129.6, 129.2, 127.7, 126.3, 125.5, 112.1, 111.8, 110.9, 104.8, 101.3, 99.5, 84.6, 80.4, 56.1, 21.0. HRMS m/z [M + H]$^+$ calcd. for $[C_{25}H_{20}NO_8]^+$ 462.1183; found 462.1186.

CT-MeRhoAz. **CT-MeRho** (20 mg, 0.043 mmol, 1.0 equiv.) was dissolved in 1 mL of acetonitrile and then cooled to 0 °C in an ice bath. *tert*-Butyl nitrite (7.7 μL, 0.065 mmol, 1.5 equiv.) was added dropwise, and the solution was stirred for 5 minutes. Trimethylsilyl azide (8.6 μL, 0.065 mmol, 1.5 equiv.) was then added dropwise, and the solution was stirred for an additional 10 minutes. The reaction mixture was removed from the ice bath and stirred at room temperature for 5 hours. The crude product was purified using column chromatography (30% ethyl acetate in hexanes as the eluent) to afford **CT-MeRhoAz** as a white solid (19.0 mg, 90.4%). ^{1}H NMR (500 MHz, DMSO-d_6) δ (ppm): 8.46 (s, 1H), 8.34 (d, *J* = 8.1 Hz, 1H), 8.29 (d, *J* = 9.4 Hz, 1H), 8.22 (d, *J* = 8.1 Hz, 1H), 7.77 (s, 1H), 7.50 (d, *J* = 8.1 Hz, 2H), 7.14 (s, 2H), 6.97 (s, 2H), 6.92 (m, 2H), 6.91 (s, 2H), 6.80 (t, *J* = 9.11 Hz, 2H), 6.74 (m, 2H), 3.84 (s, 6H), 2.14 (s, 4H), 2.06 (s, 3H), 1.99 (s, 3H). ^{13}C{^{1}H} NMR (150 MHz, DMSO-d_6) δ (ppm): 169.9, 169.8, 168.0, 167.9, 163.9, 163.8, 161.9, 161.9, 157.2, 153.0, 152.0, 152.0, 151.9, 143.0, 142.9, 136.9, 135.6, 131.9, 131.3, 130.5, 129.8, 129.8, 127.1, 126.7, 126.4, 125.5, 125.2, 116.0, 115.2, 115.1, 112.9, 110.3, 110.2, 107.7, 107.7, 101.4, 101.4, 82.7, 82.6, 80.6, 80.5, 56.2, 56.2, 21.0, 21.0. HRMS m/z [M + H]$^+$ calcd. for $[C_{25}H_{18}N_3O_8]^+$ 488.1088; found 488.1094.

General Procedure for Fluorescence and Selectivity Measurements

A stock solution of **CT-MeRhoAz** (15 μL, 1.0 mM in DMSO) was added to 3.00 mL of 50 mM PIPES buffer (100 mM KCl, pH 7.4) under N_2 at 37 °C in a setup-capped cuvette. To start the experiment, a stock solution of the analyte (15 μL, 50 mM) was added. Scans were taken at 0, 1, 5, 10, 15, 30, 45, 60, and 90 minutes after injection. DEA NONOate was used to generate NO, and stock solutions were prepared in degassed 0.01 M NaOH. λ_{ex} = 480 nm, λ_{em} = 490–640 nm. Slit width: 0.4 mm. The experiments were performed in triplicate.

Quantum Yield Measurement

Quantum yields were determined according to published standard methods and are presented relative to fluorescein in 0.1 M NaOH (ϕ = 0.95).[1050]

Determination of Detection Limit

A stock solution of **CT-MeRhoAz** (15 μL, 1.0 mM in DMSO) was added to 3.00 mL of 50 mM PIPES buffer (100 mM KCl, pH 7.4). To start the experiment, the cuvettes were treated with various concentrations (10, 7.5, 5.0, 2.5, 0.1 μM) of NaSH and incubated at 37 °C for 90 minutes. The background-corrected fluorescence was fit to a linear regression, and the detection limit was determined as the point at which [$a + 3\sigma$] where a is the y-intercept and σ is the standard deviation of the blank.

Cell Culture and Imaging Experiments

HeLa cells (ATCC CCL-2) were cultured in high glucose Dulbecco's modified Eagle's medium (DMEM) supplemented with 10% fetal bovine serum (FBS) and 1% penicillin/streptomycin (PS) at 37 °C under 5% CO_2. Cells were seeded in 35 mm imaging dishes at 1.0 x 10^5 cells per dish and allowed to adhere for 24 hours prior to fluorescence imaging studies. Cells were then washed with 1x Phosphate Buffered Saline (2 × 2.0 mL) and treated with 2.0 mL of DMEM containing the vehicle or 20 μM AOAA for 45 minutes. Next, cells were washed with 1x Phosphate Buffered Saline (2 × 2.0 mL) and treated with 2.0 mL of DMEM containing the vehicle or 5 μM **CT-MeRhoAz**. After incubation for 45 minutes, the cells were washed again with 1x Phosphate Buffered Saline (2 × 2.0 mL) and treated with 2.0 mL of DMEM containing either the vehicle or 200 μM NaSH and incubated for 45 minutes. After incubation, cells were washed

with 1x Phosphate Buffered Saline (2 × 2.0 mL) and then the media was replaced with 2.0 mL of FluoroBrite DMEM. Cell imaging was performed on a Zeiss LSM 880 confocal microscope using a 40x objective with standard DAPI and GFP filter cubes equipped for imaging of Hoechst 33342 and **CT-MeRhoAz**, respectively. All images were processed using LasX.

For cell trappability experiments, HeLa cells were incubated with 100 nM AP39 for 1 hour followed by incubation with 5 μM **CT-MeRhoAz** or MeRhoAz for 45 minutes at 37 °C under 5% CO_2 in 35 mm imaging dishes as described above. After incubation, the cells were washed with 1x PBS (2 × 2.0 mL), and then the media was replaced with 2.0 mL of FluoroBrite DMEM. The media was exchanged every 10 minutes for 60 minutes, and the same section of cells was imaged at 5, 30, and 60 minutes after the initial media exchange. All images were processed using LasX and ImageJ was used to quantify cellular fluorescence.

III. AN EXPANDED PALETTE OF FLUORESCENT COS/H_2S-RELEASING DONORS FOR H_2S DELIVERY, DETECTION, AND IN VIVO APPLICATION

This chapter includes previously published and co-authored material from Fosnacht, K.G.; Dorogin, J.; Jefferis, P.M.; Hettiaratchi, M.H.; Pluth, M.D. An Expanded Palette of Fluorescent COS/H_2S-Releasing Donors for H_2S Delivery, Detection, and In Vivo Application. *Angew. Chem. Int. Ed.* **2024**, *63*, e202402353. This manuscript was written by Kaylin G. Fosnacht with editorial assistance by Professor Michael D. Pluth. The project in this chapter was conceived by Kaylin G. Fosnacht and Professor Michael D. Pluth. , and the experimental work was performed by Kaylin G. Fosnacht, Jonathan Dorogin, and Payton M. Jefferis.

3.1 Introduction

Reactive sulfur species (RSS), such as thiols, polysulfides, hydrogen sulfide (H_2S), and persulfides are important small molecules relevant to human health. H_2S is a known gasotransmitter, generally defined as an endogenously produced and membrane permeable gaseous molecule that is highly involved in biological pathways, cellular signaling, and cell function.[1, 1051] More recently, H_2S has been shown to be intertwined with various processes including cell apoptosis, cellular metabolism, endoplasmic reticulum stress, vasorelaxation, and oxidative stress.[1052-1057] For example, the observed vasorelaxation from H_2S stems from the reaction of H_2S with oxidized cysteine (Cys) residues of ATP-sensitive potassium channels to produce persulfides, which opens these channels and results in downstream effects of decreasing blood pressure.[47, 1058, 1059] As the fundamental understanding of H_2S and other RSS in biology continues to expand, tools are needed to monitor and perturb RSS in living systems to advance investigations into the biological functions of RSS.

Inspired by the beneficial biological effects associated with H_2S, a variety of compounds that release H_2S when activated by specific stimuli, such as light, enzymes, or nucleophiles, have been developed.[1060-1062] The direct addition of H_2S gas or sulfide salts to biological media results in an immediate bolus of H_2S delivery, which typically lacks physiological relevance.[1063] In contrast, donor compounds that release H_2S in response to specific stimuli or at consistent, low levels over time mimic endogenous H_2S production. H_2S donors can be used to release H_2S in cellular environments, but there are few non-destructive methods to monitor H_2S release from such compounds, and it remains impractical to use fluorescent H_2S probes in these contexts because the

probes consume the H_2S released by the donor.[64, 66, 68, 1064] Analyte replacement H_2S probes that release H_2S upon probe activation may offer one approach to overcome these challenges, but such systems do not result in full H_2S replacement and are useful as H_2S detection rather than delivery systems.[185, 191, 781] To more directly remedy this problem, small molecule H_2S donors that release both H_2S and a fluorescent marker provide an important tool to track temporal H_2S release in real time.

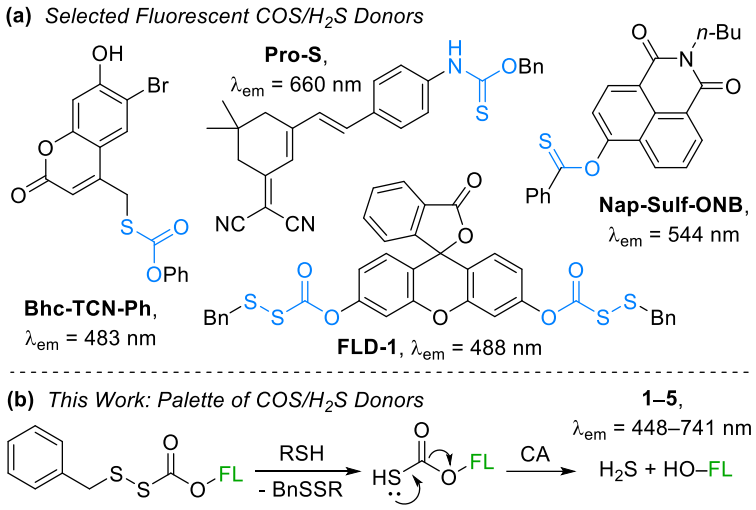


Figure 3.1. (a) Selected small molecule fluorogenic COS/H_2S donors that incorporate different fluorophores and H_2S-releasing scaffolds. (b) Activation mechanism for COS/H_2S and fluorophore (FL) release from donors **1**–**5**.

Fluorogenic H_2S donors with direct H_2S-releasing scaffolds, such as trisulfides and activated thioethers, or indirect COS/H_2S-releasing scaffolds, such as thioesters, thiocarbamates, thiocarbonates, and sulfenyl thiocarbonates, have been reported previously (Figure 3.1a).[185, 1065-1080] Indirect COS/H_2S donors function by the intermediate release of COS, which is rapidly converted to H_2S in cellular environments by the enzyme carbonic anhydrase (CA). These COS/H_2S donor scaffolds enable easy modification via addition of an alcohol or amine-modified fluorescent dye. From the available approaches for H_2S delivery coupled with a fluorescence response, there are a number of limitations. First, fluorogenic donors that utilize the same H_2S release chemistry across the palette of fluorophores have not been reported, which makes it difficult to compare the outcomes of different platforms across a series of samples. In addition, no near infrared (NIR) donors with emissions above 700 nm have been developed, which further

limits applications to *in vivo* use and imaging. Furthermore, fluorogenic donors have not yet been demonstrated in subcutaneous imaging in non-transparent organisms, which is a key step in advancing the biocompatibility of this important class of compounds. These as well as other factors are major limitations for translating this chemistry into more complex *in vivo* environments. Herein, we expand the palette to include fluorescent H_2S donors spanning the emission spectrum to include blue, yellow, orange, red, and NIR (>700 nm) donors, and demonstrate their use both in cell culture and subcutaneous *in vivo* animal work to advance this important class of compounds for studying H_2S in biology (Figure 3.1b).

3.2 Results and Discussion

3.2.1 Donor Synthesis

H_2S donors based on the sulfenyl thiocarbonate scaffold, also referred to as a sulfenyl thiocarbonate, were previously utilized by our group to develop a fluorescein-based H_2S donor.[1081] This study showed that the sulfenyl thiocarbonate scaffold can be activated by thiols to result in COS/H_2S release and a concurrent fluorescence turn-on response. Functionally, these donors undergo general activation by thiols rather than one specific activating analyte. This donor design is beneficial in complex biological systems since no single species is depleted and the overall RSS redox state is not significantly perturbed. Previous work provided a proof-of-concept for fluorogenic H_2S delivery and fluorescence responses, but neither chromophore diversification nor translation to *in vivo* applications were reported. To bridge this gap, we prepared five novel fluorogenic H_2S donors using fluorophores that spanned different emissive regions of the visible and NIR spectrum. Using these commercially or synthetically available fluorophores, we treated each precursor with readily prepared ((benzyl)dithio)carbonyl chloride in the presence of DIPEA to afford the corresponding donors **1**–**5** in moderate to high yields (34–98%, Figure 3.2).[372, 1081-1084] All compounds were characterized by ^{1}H and $^{13}C\{^{1}H\}$ NMR spectroscopy and mass spectrometry.

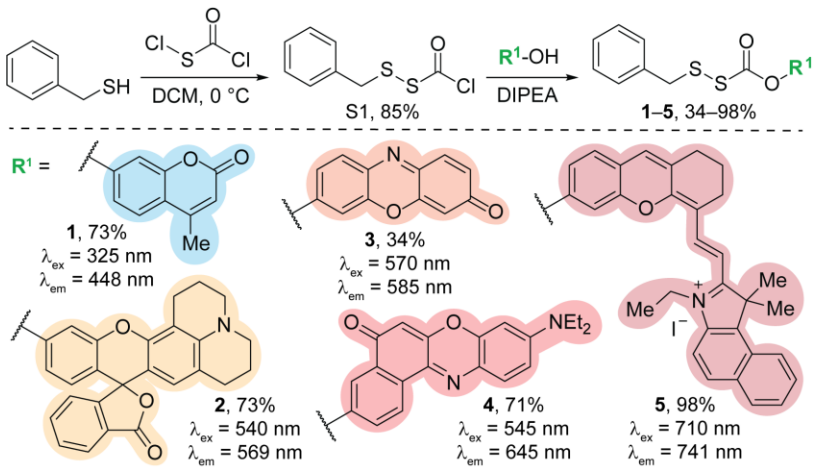


Figure 3.2. Synthetic pathway of fluorogenic COS/H_2S donors **1**–**5**.

3.2.2 Spectroscopic Properties and Response to Cys Activation

Following the synthesis of donors **1**–**5**, we next investigated the spectroscopic properties of each system in phosphate buffered saline (PBS) buffer (10 mM, pH 7.4). For donors **1**–**5**, alkylation of the alcohol significantly quenches the fluorescence and shifts the absorption from the original fluorophore (Table 3.1, Figures B5–B9). For donors **1**–**3** that contain smaller conjugated systems, this alkylation completely abolishes the fluorescence, whereas for larger, more conjugated donors **4** and **5**, this alkylation shifts the absorbance and results in a residual minor fluorescence at a shifted wavelength. Based on the documented low solubility and fluorescence of Nile Red, we used cetyltrimethylammonium bromide (CTAB, 1.0 mM) to increase the solubility and fluorescent response of **4** and **5** for *in situ* measurements.[1083, 1085, 1086] Overall, all synthesized donors displayed significantly decreased fluorescence when compared to the parent fluorophore, which matched our design principle in designing fluorogenic COS/H_2S releasing motifs.

After evaluating the photophysical properties of **1**–**5**, we next investigated the fluorescence turn-on and H_2S release from each donor. To carry out these experiments, we used 10 μM of each donor in the presence of CA (25 μg mL^{-1}) and 10 equiv. of Cys (100 μM) and monitored the fluorescence response and H_2S release over a 120-minute period (Figure 3.3, B17–B21, and B23–B27). We chose to use an H_2S responsive electrode for these measurements to have better time resolution than other H_2S measurement techniques. Importantly, this approach also allowed for the direct comparison of H_2S release and fluorescence response with high temporal resolution, which to the best of our knowledge has not been investigated previously.

Table 3.1. Spectroscopic properties of donors **1**–**5** and the corresponding fluorophores.

Compound	Parent Fluorophore				COS/H_2S Donor			
	λ_{max} (nm)	λ_{em} (nm)	ε (M^{-1} cm^{-1})	Φ[a]	λ_{max} (nm)	λ_{em} (nm)	ε (M^{-1} cm^{-1})	Φ[a]
1	325	448	14,900[1087]	0.36[1087]	–	–	–	–
2	540	569	29,300[1082]	0.46[1082]	–	–	–	–
3	570	585	56,000[1088]	0.74[1088]	–	–	–	–
4[b]	545	645	5,100 55,000[c]	0.08 0.67[c]	500	640	4,800	0.02
5[b]	710	744	54,000	0.12	610	737	27,000	0.06

[a] The Φ of **4** and **5** is referenced to rhodamine 101 and 1,1′,3,3,3′,3′-hexamethylindotricarbocyanine iodide, respectively. [b] In 1.0 mM CTAB in 10 mM PBS buffer (pH 7.4) unless otherwise noted. [c] Measured in EtOH.

For donor **1**, we observed a 310-fold fluorescence turn-on and quantitative H_2S release. For donors **2** and **3**, we observed an 84-fold fluorescence turn-on and 7.1 μM (71%) H_2S release and a 240-fold fluorescence turn-on and 9.7 μM (97%) H_2S release, respectively. We found that that donor **4** was incompatible with the H_2S-selective electrode due to unanticipated interactions between the Nile Red derivative and the semi-permeable electrode membrane, so H_2S release was measured using the methylene blue H_2S assay. Based on the lower sensitivity of the methylene blue method than the electrode-based experiments, we chose to use a higher donor concentration to ensure accurate H_2S measurement at early reaction time points (50 μM donor, 0.5 μM Cys, and 50 μg mL^{-1} CA), which also required a 20% MeCN co-solvent to ensure full solubility of the released fluorophore. Under these conditions, donor **4** resulted in a 15-fold fluorescence turn-on and 32.3 μM H_2S (65%) released over 120 minutes. For NIR donor **5**, we observed H_2S release of 6.0 μM (60%) over 30 minutes whereas the fluorescence instantaneously increased 4-fold after Cys addition. At sub-stoichiometric amounts of Cys, an increase in the fluorescent response of donor **5** with addition of Cys was observed, confirming that fluorescence of this donor is dependent on thiol concentration (Figure B22). Overall, donors **1**–**3** released H_2S at a similar rate with maximum H_2S release observed after 40 minutes, whereas the more red-shifted donors **4** and **5** released H_2S on very different timescales with maximum H_2S release being observed after 80 and 10 minutes, respectively.

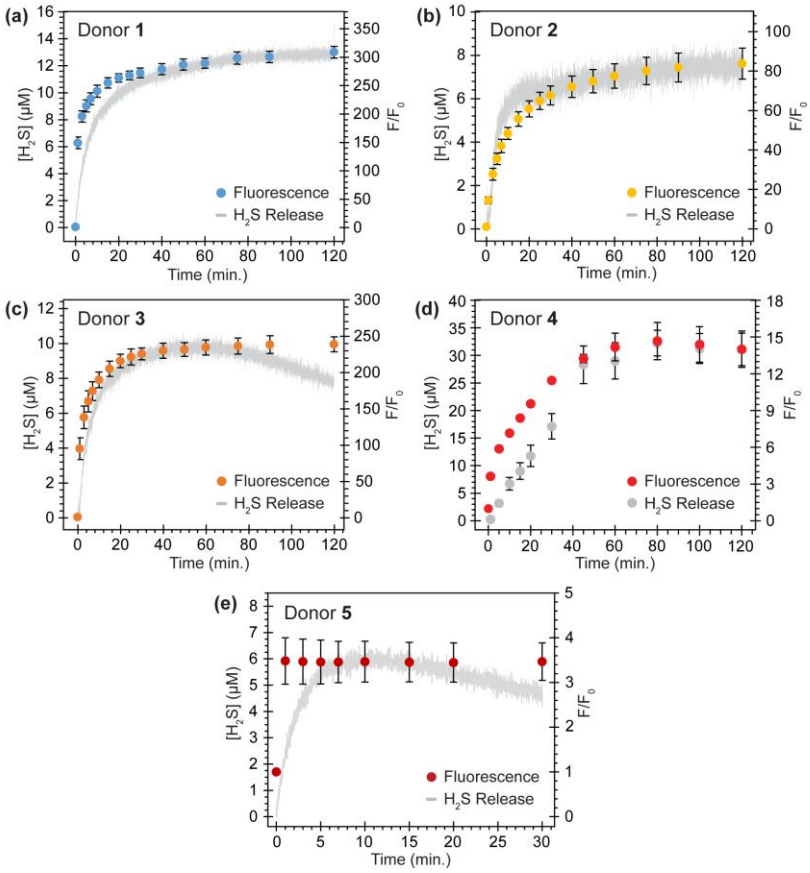


Figure 3.3. Fluorescence response (F/F_0) and H_2S release from COS/H_2S donors (a) **1**, (b) **2**, (c) **3**, (d) **4**, and (e) **5**. General conditions: **1**–**3** or **5** (10 mM) with Cys (100 mM) and CA (25 mg mL^{-1}) in PBS buffer (10 mM, pH 7.4) at 25 °C. Donor **4**: (50 mM) with Cys (500 mM) and CA (50 mg mL^{-1}) in PBS buffer (10 mM, pH 7.4) at 25 °C. The experiments were performed in triplicate and results are expressed as mean ± SD (n = 3). The buffer for donors **4** and **5** also contained a 1.0 mM CTAB additive.

As shown in Figure 3.3, the fluorescent donors efficiently release H_2S with a concomitant fluorescence response, which is consistent with the donor design. When comparing the electrode versus fluorimeter responses for **1**–**3**, as well as the fluorescence versus methylene blue response for **4**, we noticed slight differences in rates for these two processes. For donors **1** and **3**–**4**, the fluorescence turn-on increases at a faster rate than H_2S production at early timepoints, whereas the opposite is observed for donor **2**.

For donors **1**, **3**, and **4**, we attribute this trend to a longer lifetime of the thiocarbonate intermediate generated upon initial disulfide cleavage. Notably, each of these three donors have a fully conjugated π-system that could stabilize the thiocarbonate intermediate and potentially

provide a fluorescent intermediate, which would account for the observed small lag time in COS/H_2S release upon disulfide cleavage. In contrast, the lactone form of **2** reduces the overall conjugation of the system in the non-fluorescent state, which may lead to a shorter thiocarbonate intermediate lifetime prior to COS/H_2S release. Attempts to observe these transient thiocarbonate intermediates directly have proven unsuccessful, but we do note that Chakrapani and co-workers did observe a presumed arylthiocarbonate intermediate by HPLC from an esterase-activated *S*-alkyl thiocarbonate previously, which would be consistent with the above hypothesis.[1089]

Donor **5** releases H_2S the fastest of the presented donors, with full H_2S release being observed after only about 10 minutes. Consistent with the observed instantaneous fluorescence turn-on, this fast H_2S release rate could be due to either the donor releasing COS rapidly, which exceeds the rate of CA conversion of COS to H_2S, or the donor being activated to form a fluorescent intermediate. With the exception of donor **5** that releases H_2S very quickly, donors **1**–**4** release H_2S over a longer time period with full fluorescence turn-on and H_2S release observed after 40–80 minutes (Figure 3.3). Additionally, donors **1**–**3** result in large fluorescence turn-on responses (84–310-fold turn-on), and the more red-shifted donors **4** and **5** result in lower fluorescence turn-on responses (4–15-fold turn-on). This lower fluorescence response is likely due to the donor compounds themselves having minimal but observable latent fluorescence, as discussed previously. Overall, donors **1**–**5** resulted in concomitant fluorescence turn-on response and H_2S release with high COS/H_2S release efficiencies (>60%) observed.

3.2.3 Selectivity to Sulfur, Nitrogen, and Oxygen Species

After establishing the correlation of H_2S release and fluorescence response from these donors, we next investigated the activation of these donors by other biologically relevant sulfur, nitrogen, and oxygen species (Figure 3.4 and B28). For these selectivity experiments, we used donor **1** due to the high H_2S release efficiency, sizeable fluorescence response, and temporal correlation between fluorescence response and H_2S release. We first treated **1** (10 μM) with biologically relevant thiols (100 μM) including Cys, homocysteine (Hcy), *N*-acetyl cysteine (NAC), glutathione (GSH), and penicillamine (Pen). After 120 minutes, all thiols generated a fluorescence response from **1**. This activation of the donor by various biological thiols highlights that application of these donors to biological systems will not deplete one specific species and not greatly affect RSS. We also found that sulfite (SO_3^{2-}) generated a fluorescence turn-on, which is

consistent with the ability of SO_3^{2-} to reduce disulfides.[1090] Incubation of **1** with serine (Ser), lysine (Lys), glycine (Gly), oxidized glutathione (GSSG), superoxide (O_2^-), hydrogen peroxide (H_2O_2), or sulfate (SO_4^{2-}) failed to produce a significant fluorescent response. Donor **1** was also activated by both porcine liver esterase (PLE, 1.0 U mL^{-1}) and CA (25 μg mL^{-1}), which was previously observed with other sulfenyl thiocarbonates and further supports the generalized activation of this delivery platform.[1091] Although donor **1** is less stable in the presence of esterases, the rate of hydrolysis by CA is slower than the reactivity of Cys, with the analytes taking 120 minutes and 30 minutes to fully activate **1**, respectively (Figure B29). Additionally, the degradation of **1** by CA is likely significantly amplified by ester hydrolysis of the donor releasing a thiol byproduct, which increases the rate of donor activation and is magnified in the closed system of the cuvette. In addition to biological species, these donors were confirmed to be photostable, with minimal fluorescence turn-on being observed over 30 minutes of excitation (Figure B30 and B31).

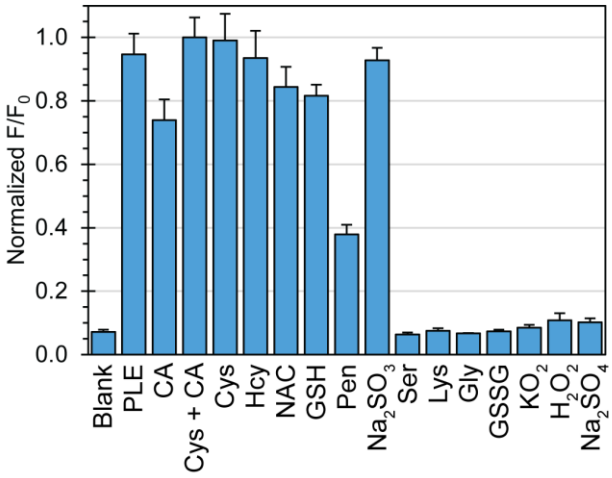


Figure 3.4. Normalized fluorescence turn-on (F/F_0) of donor **3** (10 mM) upon incubated with analytes (100 mM) for 120 minutes in PBS buffer (10 mM, pH 7.4). Conditions from left to right: blank, PLE, CA, Cys + CA, Cys, Hcy, NAC, GSH, Pen, SO_3^{2-}, Ser, Lys, Gly, GSSG, O_2^-, H_2O_2, and SO_4^{2-}. λ_{ex} = 350 nm, λ_{em} = 370–600 nm, T = 25 °C, slit width = 2 nm. The experiments were performed in triplicate and results are expressed as mean ± SD (*n* = 3).

3.2.4 Application to Live Cells

We next investigated whether donors **1**–**5** were compatible with live cell imaging using HeLa cells and co-incubation with the H_2S responsive and cell-trappable probe CT-MeRhoAz to detect H_2S in a cellular environment. We chose to use CT-MeRhoAz because its spectral window

does not overlap with donors **1**–**5** and the cell trappability increases signal retention. HeLa cells were incubated with either the vehicle, H_2S probe, H_2S donor, or both the H_2S probe and H_2S donor for 20 minutes and then imaged by fluorescence microscopy (Figure B32–B36). Cells were also co-incubated with the nuclear dyes NucRed (for **1**) or Hoechst 33342 (for **2**–**5**). For each of the donors investigated, we observed a fluorescent response from the released donor fluorophore in both the presence and absence of CT-MeRhoAz. These results confirmed that the donor response in live cell environments was not due to interaction with or channel bleed through from the CT-MeRhoAz probe. In the presence of CT-MeRhoAz, we only observed a significant fluorescent response in the presence of the COS/H_2S donors (Figure 3.5). Taken together, these results confirm that donors **1**–**5** release H_2S in a cellular environment, and that the H_2S release can be tracked by fluorescence microscopy.

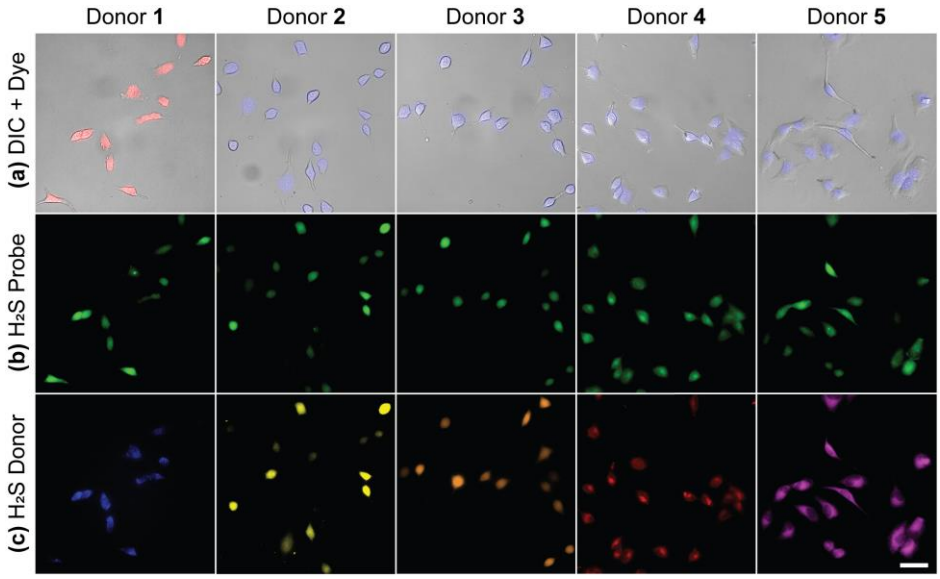


Figure 3.5. Live-cell imaging of fluorescence turn-on COS/H_2S donors **1**–**5** showing concurrent H_2S release and fluorescence turn-on. (a) Differential interference contrast (DIC) overlaid with Hoechst 33342 (5 mM) or NucRed (2 mM). (b) H_2S probe CT-MeRhoAz (2.5 mM) confirming cellular H_2S release. (c) COS/H_2S donor **1** (50 mM) and **2**–**5** (20 mM). Bar scale: 50 μm.

3.2.5 Application to Alginate Hydrogels for In Vivo Imaging

Based on the efficacy of these donors in live cell environments, we next wanted to translate this donor approach to live animal investigations. We chose to focus on NIR donor **5**, which should have significantly better tissue penetration than donors **1**–**4**. For live animal experiments, donor **5**

was loaded into a 2% (w/v) alginate hydrogel before administration into rats. We chose to use alginate hydrogels due to their biocompatibility and injectability, which allows for site injection rather than surgical implantation. As a proof-of-concept experiment to verify the stability of sulfenyl thiocarbonates in alginate gels, we loaded donors **1** and **5** into an alginate hydrogel and monitored the fluorescence over time (Figure B37 and B38). After loading **1** or **5** (10 μM) into the hydrogel and then soaking the hydrogel in PBS buffer (10 mM, pH 7.4) for 20 minutes, minimal fluorescence of the buffer was observed. Addition of buffer containing Cys (100 mM) followed by buffer replacement with agitation both led to an increase in fluorescence response, meaning that these donors are stable in the hydrogel until the addition of Cys activates the donor. To confirm that these donors are still releasing H_2S when loaded into an alginate hydrogel, we directly measured H_2S release from donors **1** and **5** loaded into 2% (w/v) alginate hydrogels using an H_2S selective electrode (Figure B39 and B40). When loaded into the alginate hydrogel, donors **1** and **5** showed slower rates of H_2S release, which is consistent with the expected reduced rate of Cys penetration into the hydrogel to activate the donors. Taken together, these studies show that the donors still respond to thiols with H_2S release and a fluorescent response when loaded into an alginate hydrogel.

Having confirmed the stability of the donors in hydrogels, we used donor **5** to investigate whether thiol-mediated donor activation could be observed *in vivo*. Alginate hydrogels were prepared containing either the vehicle (DMSO) or **5** and then injected into the subcutaneous shoulder or hip space of 5–6-week-old male Sprague Dawley rats to image the donor fluorescence over time under the skin. After initial imaging using a Perkin Elmer Spectrum In Vivo Imaging System (IVIS), rats were administered sterile GSH via tail vein injection and imaged over 3 hours. As expected, no observable fluorescent signal was observed for either of the alginate gels containing the vehicle with and without GSH administration (Figure B41 and B42). By contrast, inclusion of donor **5** in the alginate hydrogels resulted in a significant fluorescence response (Figure 3.6, B43, and B44). The fluorescence response is observed both in the absence and presence of exogenous GSH, which we attribute to local activation of the donor by endogenous thiols and other species, as was observed during the *in vitro* selectivity studies. This fluorescent signal increases appreciably over the first hour, followed by a plateau over the next 2 hours, which is likely due to donor activation followed by diffusion of the fluorophore. These results are highlighted by plotting the average radiant efficiency of regions of interest for all alginate gels

(Figure 3.6b). Overall, these studies confirmed that these donors are compatible with application to live animals and the fluorescent response can be observed within tissues.

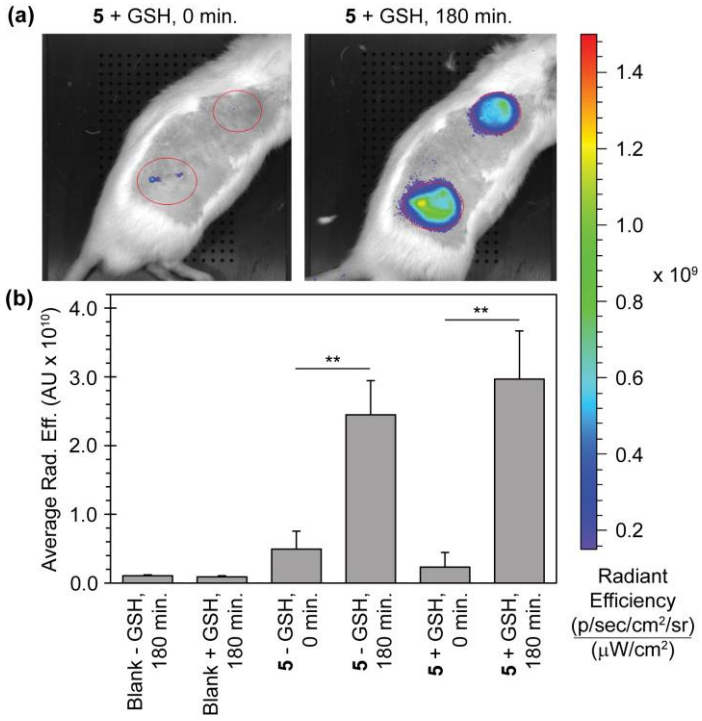


Figure 3.6. Live rat imaging of fluorescence turn-on COS/H_2S donor **5** loaded into alginate gels. (a) Alginate gels containing **5** (250 mM) before GSH tail vein injection and 180 minutes after GSH injection. Regions of interest are labeled with red circles. (b) Average radiant efficiency of alginate gels loaded with DMSO, DMSO with GSH, donor **5**, and donor **5** with GSH at 0 or 180 minutes. The experiments were performed in quadruplicate and results are expressed as mean ± SD (n = 4). $^{**}p < 0.001$.

3.3 Conclusion

We developed a suite of fluorescence turn-on COS/H_2S donors **1**–**5** that provide fluorescent responses upon release of H_2S across a broad palette of the fluorescence spectrum. Incubation of the donor scaffold with biologically relevant sulfur, nitrogen, and oxygen species confirmed the activation of the donors by a variety of thiol species in addition to sulfite and esterases. This activation profile matches the goal of these donors functioning as slow-releasing COS/H_2S motifs that can be activated by ubiquitous cellular components. By using combined fluorescence and H_2S-responsive electrode experiments, we directly correlated the temporal H_2S release and fluorescence output from each donor. Cell imaging experiments demonstrated that a fluorescence

turn-on and H_2S release is observed in a cellular environment for all donors. Additionally, we demonstrated *in vivo* donor activation in live rats using subcutaneous injections of alginate hydrogel containing the NIR donor **5**. Further, this study exemplified that the sulfenyl thiocarbonate scaffold can be applied to a wide variety of fluorophores, and hydroxyl substitutions beyond the specific dyes utilized in this paper are expected to be straightforward. In conclusion, COS/H_2S donors **1**–**5** exemplify the wide application and compatibility of the sulfenyl thiocarbonate scaffold for the development of H_2S donors with various fluorogenic responses and demonstrates the viability of using such donor constructs in both cellular and *in vivo* environments.

IV. ESTERASE-ACTIVATED PERTHIOCARBONATE PERSULFIDE DONORS PROVIDE INSIGHTS INTO PERSULFIDE PERSISTENCE AND STABILITY

This chapter includes previously published and co-authored material from Fosnacht, K.G.; Cerda, M.M.; Mullen, E.J.; Pigg, H.C.; Pluth, M.D. Esterase-Activated Perthiocarbonate Persulfide Donors Provide Insights into Persulfide Persistence and Stability. *ACS Chem. Bio.* **2022**, *17*, 331–339. This manuscript was written by Kaylin G. Fosnacht with editorial assistance by Professor Michael D. Pluth. The project in this chapter was conceived by Matthew M. Cerda, and the experimental work was performed by Kaylin G. Fosnacht.

4.1 Introduction

Important sulfur-containing biomolecules are found across all kingdoms of life. Although biological thiols, such as glutathione and cysteine, are well known bio-active sulfur species, recent studies have revealed the crucial role of other reactive sulfur species (RSS) in biological systems. Specifically, endogenously-produced H_2S has been discovered to regulate essential cellular processes like cell signaling and function, leading to the classification of H_2S as a gasotransmitter alongside CO and NO.[24, 1092] H_2S exerts many physiological effects, such as cytoprotection, anti-inflammation, and vasodilation, and for this reason H_2S is currently under investigation as a therapeutic for various disease pathologies.[1093-1095] H_2S cannot react directly with thiols, but many functions and actions of H_2S are proposed to be mediated by persulfides (RSSH) and related oxidized sulfur species.[1096-1098] H_2S can generate persulfides upon reaction with organic polysulfides (RSSR, RSSSR, etc.), oxidized thiols such as sulfenic acids (RSOH), or through O_2-mediated radical pathways.[1099-1103] Further, the oxidative posttranslational modification of cysteine by H_2S occurs through the reaction of H_2S and an oxidant with cysteine residues to form cysteine persulfide, providing cytoprotection against oxidative damage.[1098, 1102, 1104, 1105] This conversion of thiols to persulfides, known as *S*-persulfidation or *S*-sulfhydration, protects cysteine from irreversible oxidation.[1106] For example, the loss of persulfidated cysteine residues is suspected to be involved in various neurodegenerative diseases including Alzheimer's and Parkinson's disease.[1107-1110] Persulfides can be produced by both enzymatic and nonenzymatic processes. For example, 3-mercaptopyruvate sulfurtransferase, cystathionine β-synthase, and cystathionine γ-lyase all can generate persulfides, and persulfides have also been found as important intermediates

in enzyme function.[1104, 1111-1113] Additionally, micromolar levels of persulfides have been found in cells, tissues, and plasma, exemplifying the importance of persulfides in biological systems.[1096, 1104, 1114] Overall, there is a close relationship between H_2S and persulfides, but the inherent reactivity of these RSS makes dissecting biological outcomes from H_2S, persulfides, or other RSS difficult.

Persulfides are more nucleophilic when compared to the parent thiols due to the alpha effect, but can be electrophilic at both sulfur atoms.[1115-1117] Generally, the pK_a of persulfides is 1–3 pK_a units lower than the corresponding thiol analogues, meaning that the majority of persulfides are deprotonated at physiological pH. For example, glutathione has a pK_a of 8.49, whereas glutathione persulfide has a pK_a of 5.45.[949] Due to this heightened reactivity, isolated persulfides are generally unstable and are readily converted to other RSS, such as H_2S, thiols, polysulfides, and elemental sulfur.[1115, 1118] This reactivity makes it difficult to probe or deliver persulfides directly. One solution to this challenge is to develop and use readily-modifiable small molecule persulfide donors to generate persulfide species *in situ* and to use these systems to further investigate persulfides. Although many H_2S-releasing donors have been reported previously and have increased the fundamental understanding of H_2S in biology, significantly fewer persulfide donors have been developed. The current library of persulfide donors include synthetic polysulfides as well as persulfide donor scaffolds that release persulfides when activated by hydrogen peroxide, enzymes, base, and light, but these scaffolds often lack simple modification methods that allow insights into how structural and electronic effects impact persulfide release rate.[1119-1127]

Perthiocarbonates, also referred to as sulfenyl thiocarbonates, react with thiols to release carbonyl sulfide (COS) and an alcohol payload (Figure 4.1a).[1081, 1128] We recently used this reactivity to develop thiol-activated COS-releasing molecules that simultaneously release a fluorescent dye as the payload. In addition to the electrophilic disulfide motif that can react with thiols, perthiocarbonates also contain a cleavable ester that has been proposed to release persulfides upon activation by a base.[1128-1130] The Toscano group recently reported a perthiocarbonate-based persulfide donor using base-mediated hydrolysis of this ester motif (Figure 4.1b).[1131] The electronic effects of ester substitution were investigated by using esters with *p*-substituted phenols, which revealed a mild substituent effect where electron withdrawing groups increased persulfide release rate and electron donating groups decreased persulfide release rate.

Furthering our understanding of different pathways in which perthiocarbonates generate RSS, we report here the use of enzymatic esterase cleavage to provide controllable persulfide release (Figure 4.1c). Furthermore, our investigations into the structural factors that influence persulfide release rates reveal new insights into the stability and persistence of persulfides in the presence of biological nucleophiles.

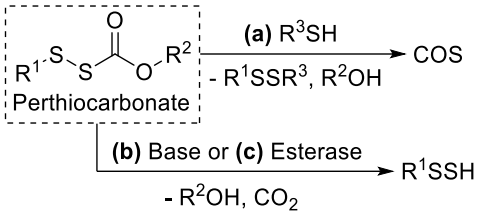


Figure 4.1. Perthiocarbonate reaction pathways when activated by (a) thiols, (b) base, or (c) esterase.

4.2 Results and Discussion

4.2.1 Donor Design and Synthesis

Perthiocarbonates can be modified at either the ester (R^1) or thiol (R^2) position (Figure 4.2). To better understand the effect of steric bulk on persulfide release rate and persulfide stability, we prepared persulfide donors **1**–**9**. To simplify these systems, a methyl ester at R^1 or benzyl thiol at R^2 were used as controls when modifying the opposite position, allowing for direct comparisons across a series. For example, persulfide donors **1**–**3** vary by the ester substituent (R^1), and **1** and **4**–**7** vary by the thiol substituent (R^2). Persulfide donors **7**–**9** are based on *N*-acetyl-L-cysteine, *N*-acetyl-L-cysteine methyl ester, and penicillamine derivatives, respectively.

Persulfide donors **1**–**3** were synthesized by treating benzyl mercaptan with chlorocarbonylsulfenyl chloride followed by addition of the corresponding alcohol (Figure 4.2a). Persulfide donors **4**–**9** were prepared in moderate to good yields (66–93%) by treating methoxycarbonylsulfenyl chloride with the desired thiol (Figure 4.2b). In general, these synthetic routes are simple, efficient, and require inexpensive starting materials to enable various substitutions on either side of the perthiocarbonate. All perthiocarbonate compounds were characterized by ^{1}H and ^{13}C{^{1}H} NMR spectroscopy and mass spectrometry.

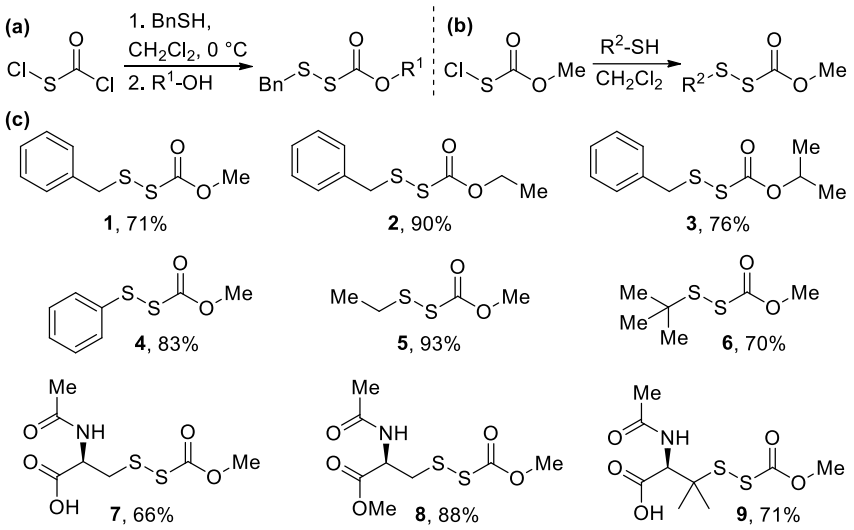


Figure 4.2. General conditions for preparing persulfide donors **1**–**9** starting from either (a) chlorocarbonylsulfenyl chloride or (b) methoxycarbonylsulfenyl chloride. (c) Persulfide donors synthesized.

4.2.2 Persulfide Release

Having prepared a small library of persulfide donors, we next measured persulfide release rates. Each persulfide donor (100 μM) was treated with porcine liver esterase (PLE, 1.0 U mL^{-1}) in PBS buffer (pH 7.4, 10 mM) containing 10% (v/v) MeCN at 25 °C. MeCN was added to increase the solubility of the more hydrophobic donors. We used a *p*-nitrophenyl acetate esterase activity assay to confirm that PLE maintained esterase activity with 10% MeCN co-solvent relative to esterase activity in PBS buffer (Figure C1). Persulfide release was quantified by trapping the released persulfide with an excess of electrophilic 1-fluoro-2,4-dinitrobenzene (FDNB, 4 mM) to form a highly absorptive RSS-DNB adduct (Figure 4.3a).[1124] Although persulfide trapping can be difficult due to the reactivity of the disulfide product formed, use of FDNB is a well-established method to accurately trap persulfides without trapping of similar nucleophiles such as thiols or alcohols.[1132] The formation of the RSS-DNB adduct was monitored over 60 minutes by removing reaction aliquots (500 μL) and diluting with MeCN (500 μL) to both ensure solubility of the final trapped product and stop PLE activity prior to HPLC analysis. We prepared and isolated RSS-DNB adducts **10**–**16** independently to confirm product formation from retention times and to generate calibration curves for each RSS-DNB adduct to ensure accurate quantification (Figure 4.3, Figure C2). Although the slope and absorbances correlated with the calibration curves of the

RSS-DNB adducts do not vary greatly by R^2-group identity, slight changes in the calibration curves are accounted for and ensures accurate quantification.

In addition to esterase activation, we also investigated whether persulfide release from these perthiocarbonate-based persulfide donors could be activated by base-mediated hydrolysis. When activated by PLE, persulfide donor **1** released 40.1 μM of persulfides after 60 minutes. To confirm that the persulfide release observed was due to esterase-mediated hydrolysis, the FDNB trapping assay was repeated with PLE that has been pre-incubated with the esterase inhibitor Parathion (10 μM).[1133] No persulfide production was observed over the course of three hours, which confirmed that PLE was mediating the observed persulfide release (Figure C3). Having verified that esterase-mediated hydrolysis was occurring, we next investigated the non-enzymatic hydrolysis of these persulfide donors by the FDNB trapping assay under neutral and basic conditions. At pH 7.4, neither persulfide release nor persulfide donor degradation was observed from persulfide donor **1** over three hours (Figure C3–C4). At pH 9.0, however, slow persulfide release was observed, although it only reached a maximum concentration of 16.1 μM after three hours (Figure C3). Although hydrolysis and resultant persulfide release increases with pH, the persulfides donors release persulfides significantly faster when activated by PLE. We also note that persulfide release has been reported previously from similar penicillamine-derived persulfide donors when activated by thiols through nucleophilic attack at the carbonyl carbon of the perthiocarbonate.[1131] We further investigated this reactivity with persulfide donor **6** due to the similar bulkiness at the thiol position to penicillamine. We carried out the FDNB trapping assay in the presence of *N*-acetyl-L-cysteine (NAC, 500 μM) and did not observe any persulfide release over three hours (Figure C5). Based on these results, persulfide donors **1**–**9** likely release COS or other RSS rather than persulfides when activated by thiols. With these control experiments completed, the persulfide release rates from persulfide donors **1**–**9** when activated by PLE was measured.

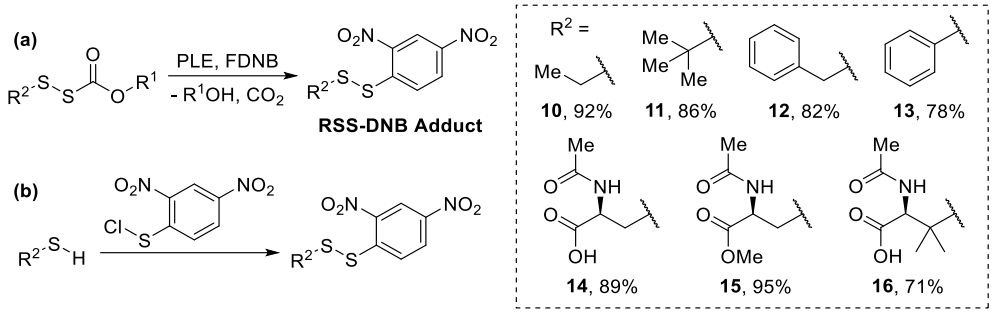


Figure 4.3. (a) Persulfide trapping assay with FDNB. (b) Synthetic route to prepare RSS-DNB adducts **10**–**16**.

To determine how structural modifications impact persulfide release from perthiocarbonate-based persulfide donors **1–9**, we fit the measured persulfide release curves from the FDNB trapping assay to a pseudo first-order equation to obtain k_{obs} (Figure 4.4, Table 4.1). According to the Jones model of the PLE active site, the alkoxy group of the perthiocarbonate does not enter the active site.[1134] Based on this model, increasing steric bulk at the ester for persulfide donors **1**–**3** should not impact persulfide release rate since the R^2 position of these donors are all benzyl groups. As expected, steric bulk on the ester of **1**–**3** had a negligible impact on the rate of persulfide release. As seen in Table 4.1, both $t_{1/2}$ and k_{obs} of persulfide donors **1**–**3** are statistically different from one another and are not correlated with steric bulk. Interestingly, we found that the persulfides trapped by FDNB of **1**–**3** increased with increasing steric bulk and electron donation at the ester position, suggesting that R^1 identity has an effect on persulfide release other than persulfide release kinetics. Based on these data, the ester group identity has a minor effect on persulfide release rate from the scaffold when activated by esterase likely through altering esterase binding.

After investigating the effect of ester group identity on persulfide release rate, we next focused on thiol group identity. As the steric bulk on the thiol increases in persulfide donors **1** and **4**–**6**, the rate of persulfide release and persulfide persistence also increases. For example, persulfide donor **6** contains the bulky *tert*-butyl group at the R^2 position and has both a high rate constant (0.17 ± 0.1 min^{-1}) and the highest persulfides trapped by FDNB (70%). This high efficiency of persulfide trapping is likely due to the bulkiness of the *tert*-butyl group, which increases the persulfide persistence and decreases potential side reactions of the persulfide. One outlier of this trend is persulfide donor **4**, which contains a phenyl group at the thiol position. This aromatic

group may be in conjugation with the disulfide of the perthiocarbonate, unlike the other persulfide donors investigated, which could account for the unexpected increase in rate constant (0.23 ± 0.5 min^{-1}) and decrease in percent persulfide trapped (32%) for **4**. In total, increased steric bulk at the R^2 position appears to have a minor effect on persulfide release rate and persistence.

Table 4.1. Persulfide release from persulfide donors **1**–**6**.

Persulfide Donor	$t_{1/2}$ (min)	k_{obs} (min^{-1})	RSSH Trapping Efficiency (%)
1	5.6 ± 0.9	0.13 ± 0.2	40
2	1.9 ± 0.3	0.37 ± 0.5	57
3	3.3 ± 0.8	0.23 ± 0.6	61
4	3.2 ± 0.7	0.23 ± 0.5	32
5	6.9 ± 0.9	0.10 ± 0.2	36
6	4.2 ± 0.3	0.17 ± 0.1	70

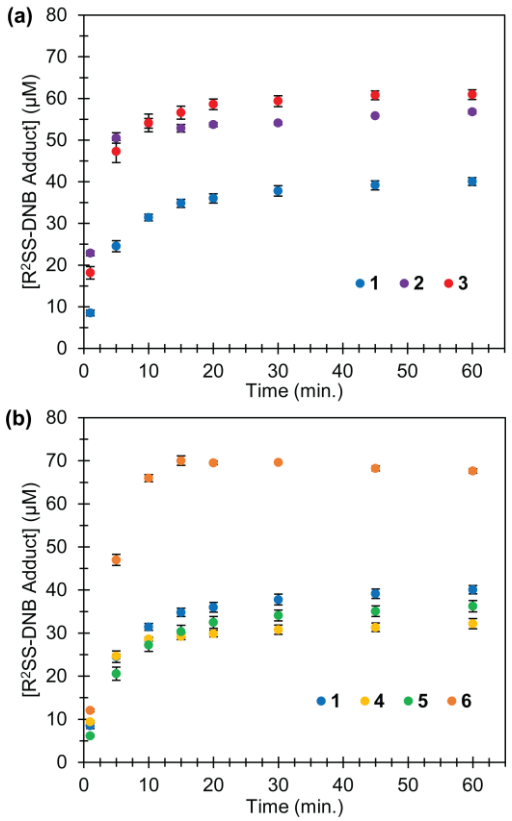


Figure 4.4. Persulfide release from (a) persulfide donors **1**–**3** and (b) persulfide donors **1** and **4**–**6**. Experiments were performed in triplicate with results expressed in mean ± standard deviation (*n* = 3).

Persulfide donors **7**–**9** were synthesized to investigate the viability of using our scaffold to release cysteine-derived persulfides, but FDNB trapping studies resulted in negligible trapped persulfides. To determine whether the ester motif of the perthiocarbonate was being cleaved, we monitored the reaction by ^{1}H NMR spectroscopy. Treatment of **7** (10 mM) with PLE (10 U mL^{-1}) failed to generate MeOH, which would be an expected product if the ester were cleaved (Figure C6). Treatment of **7** with *tert*-butoxide (10 mM) to activate persulfide release through hydrolysis, however, did result in MeOH formation (Figure C7). Additionally, we used a *p*-nitrophenyl acetate assay to determine whether the cysteine-based persulfide donors were acting as PLE inhibitors by completing the assay in the presence of **7** (100 μM). No change in esterase activity was observed when **7** was added, meaning the lack of persulfide release from this donor was not due to alteration of PLE activity by the persulfide donor. Taken together, these results suggest that the esterase cannot cleave the esters in **7**–**9**, leading to low persulfide release. We hypothesized that the bulky and hydrophilic nature of the cysteine-based persulfide donors interferes with the ability of esterase to properly envelop the persulfide donors within the active site and thus prevents the esterase from cleaving the ester.

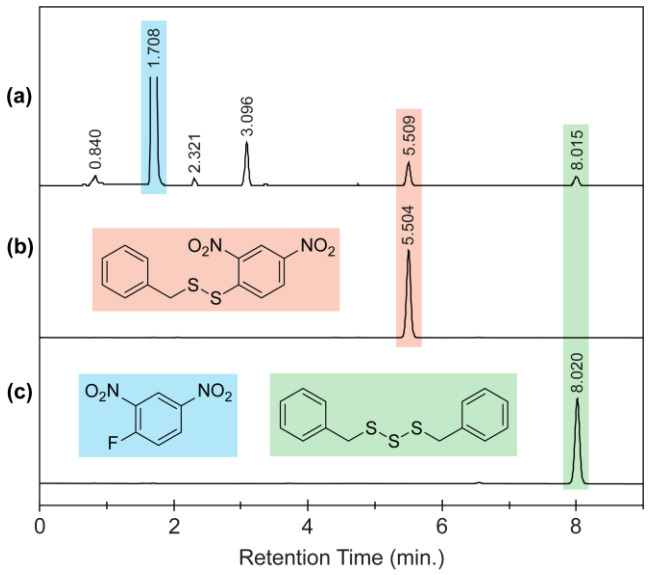


Figure 4.5. HPLC chromatograms showing (a) FDNB trapping assay results with persulfide donor **1** after 30 minutes, (b) 50 μM BnSS-DNB adduct, and (c) 50 μM benzyl trisulfide. In chromatogram (a) the peak at 3.096 minutes corresponds to residual persulfide donor **1**.

4.2.3 Persulfide Donor Side Reactivity and Byproduct Investigation

We next investigated whether other RSS were formed from the persulfide donors, which could account for the non-quantitative persulfide trapping by FDNB. We further analyzed the FDNB trapping assay results and found polysulfide formation occurring alongside RSS-DNB adduct formation. Specifically, in the case of **1**, we observed benzyl trisulfide (BnSSSBn) formation during the FDNB trapping experiments (Figure 4.5). The trisulfide can be formed by the direct reaction of two equivalents of benzyl persulfide to release H_2S, which has been demonstrated previously using isolated BnSSH (Figure 4.6a).[1118] To confirm H_2S release, we used the methylene blue (MB) H_2S assay. We first measured H_2S release in the presence of FDNB (4 mM) and PLE (1.0 U mL^{-1}), and only minimal H_2S release from **1** (100 μM) was observed. This outcome was expected because trisulfide formation and concomitant H_2S release should only be a minor side reaction in the presence of excess highly electrophilic FDNB trapping agent. In the absence of FDNB, we expected that more H_2S would be observed; however, we still observed minimal H_2S release from **1** (Figure C8). Because consumption of **1** is still observed in the absence of FDNB, we hypothesized the operable reaction pathway to generate the trisulfide does not release H_2S directly. One pathway that meets these requirements is persulfide attack at the α-sulfur atom of the perthiocarbonate to release COS and generate a trisulfide. Nucleophilic attack at this position of the perthiocarbonate has been observed previously in the thiol-mediated release of COS from perthiocarbonates.[1081] To test whether **1** was releasing COS rather than H_2S, we added carbonic anhydrase (CA, 50 μg mL^{-1}) to the MB assay to convert any generated COS to H_2S. Under these reaction conditions, we observed significant H_2S release reaching a maximum of 8.5 μM after 90 minutes (Figure C8). Based on these results, persulfide donor **1** can also release COS to form the trisulfide, likely stemming from persulfide attack on the α-sulfur atom of the perthiocarbonate (Figure 4.6b).

To test whether steric bulk at the thiol can be used to influence reactivity of the perthiocarbonates, we used **6** to investigate if the COS/trisulfide releasing pathway was also present even when the α-sulfur atom was sterically blocked. Similar to **1**, minimal H_2S release was observed in the presence of FDNB and PLE for persulfide donor **6**. In the absence of FDNB, however, significant H_2S release was observed in the absence of CA and reached a maximum of 9.3 μM after 45 minutes (Figure C8). Based on these results, we attribute H_2S release from **6** to

preferential persulfide attack at the β-sulfur atom of the perthiocarbonate due to the bulky *tert*-butyl group at the thiol position (Figure 4.6c). To support the proposed reaction pathway, we also performed a methylene blue assay with a decreased concentration of PLE (0.1 U mL^{-1}) since PLE levels should directly affect H_2S release. Under these conditions, H_2S release was decreased as expected, with only 5.3 μM H_2S observed after 90 minutes (Figure C9). Furthermore, the reactivity between **6** (10 mM) and PLE (10 U mL^{-1}) was monitored by $^{13}C\{^1H\}$ NMR spectroscopy over 12 hours and clearly shows the appearance of the expected ^{t}BuSH byproduct (Figure C10), which also supporting the pathway proposed in Figure 4.6c. Overall, these experimental results show that nucleophilic attack on the perthiocarbonate can be controlled by altering thiol group identity, where **1** has preferential attack at the α-sulfur atom and **6** has preferential attack at the β-sulfur atom. Based on these results, the steric bulk next to the perthiocarbonate thiol as well as the identity of the nucleophile determines whether perthiocarbonates function as H_2S, COS, or persulfide donors.

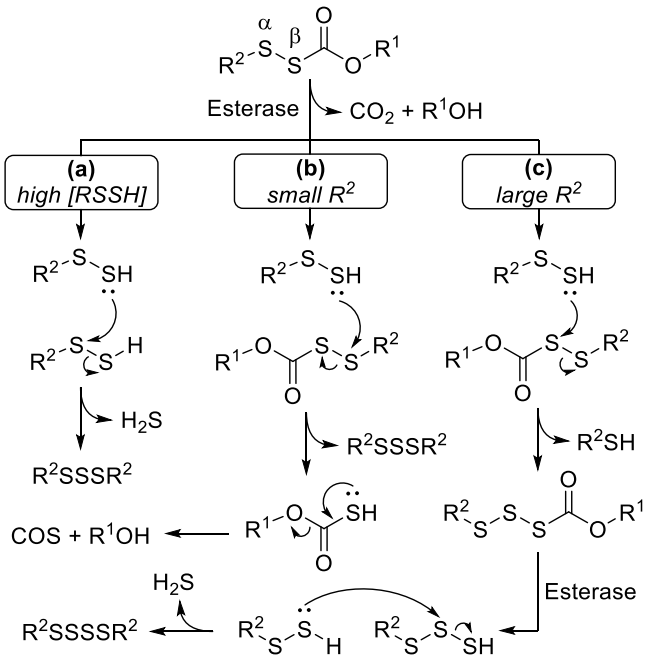


Figure 4.6. Alternate reaction pathways of persulfides produced by perthiocarbonate-based persulfide donors. All compounds are shown in the neutral state for simplicity. Pathways (a), (b), and (c) are likely most prevalent for high persulfides concentrations, small R^2 groups, and larger R^2 groups, respectively.

4.2.4 Persulfide Persistence

In general, the detection and delivery of persulfides is challenging because persulfides can function as both nucleophiles and electrophiles, which can lead to complex reaction pathways that generate RSS mixtures rather than one distinct product. Furthermore, the persulfide persistence, meaning how long a persulfide exists in solution before reacting with other species, remains an under-investigated and underappreciated challenge. Fundamental properties, such as the pK_a and steric bulk at the α-sulfur atom of the persulfide, should all contribute to persulfide persistence. Because persulfide donors **1**–**6** do not result in quantitative persulfide trapping, we suspected that persulfide persistence may be a contributing factor. To determine directly whether the steric bulk of R^2 impacts persulfide persistence, we next measured *in situ* persulfide concentration over time when persulfides were not trapped with FDNB directly after release. We modified the FDNB trapping assay so that FDNB was not present during the persulfide-generating reaction, but rather was added after aliquots were removed from the reaction mixture. This approach effectively tests the concentration of persulfides within the reaction vial at specific time points. Under these conditions, more reactive (or less persistent) persulfides will react more quickly to form other RSS upon generation, resulting in lower measured persulfide levels and equating to a lower persulfide persistence. Persulfide donors (100 μM) were treated with PLE (1.0 U mL^{-1}) in 10% MeCN in PBS buffer (pH 7.4, 10 mM) at 25 °C. At each time point, reaction aliquots were removed, diluted in acetonitrile containing FDNB (8 mM), and filtered before analysis by HPLC. For compounds **1** and **5**, HPLC analysis did not show any formation of the RSS-DNB adducts, meaning that persulfides generated in solution were consumed prior to FDNB addition (Figure 4.7). In contrast, persulfides were trapped from **6** with the total trapped persulfides peaking at 23.7 μM for a trapping efficiency of 47% after 5 minutes. Further, for persulfide donor **6** there is an initial increase in RSSH trapped before a decrease observed after 5 minutes. This trend is likely due to polysulfide concentration being high enough to initiate further reaction with persulfides only after 5 minutes. This observed difference in trapped persulfide levels suggests that *t*BuSSH released from **6** is significantly more persistent than persulfides released from **1** and **5**. We attribute the greater persistence of *t*BuSSH to the increased steric bulk of the *tert*-butyl group, which blocks nucleophilic attack at the α-sulfur.

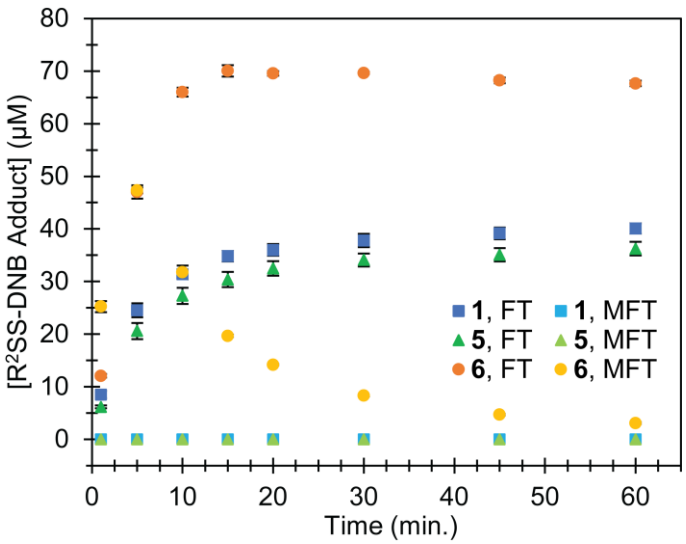


Figure 4.7. Investigation of persistence of persulfides released from donors **1** and 5–**6** by use of the FDNB trapping assay (FT) or the modified FDNB trapping assay (MFT). Experiments were performed in triplicate with results expressed in mean ± standard deviation (n = 3).

4.3 Conclusions

Perthiocarbonates can be cleaved by esterase to release persulfides, which were quantified by trapping with FDNB. We found that modification of the steric bulk of the ester (R^1) had little effect on persulfide release, whereas increased steric bulk at the thiol (R^2) generally led to an increase in persulfide release rate. Cysteine-based perthiocarbonates were also prepared but did not release appreciable persulfide due to incompatible interactions with the esterase. Investigations into alternate reaction pathways of the perthiocarbonate-based persulfide donors revealed that the thiol position (R^2 group) size directly influences what RSS are generated from perthiocarbonates. Perthiocarbonates release COS when a non-bulky group is at the thiol position, but release H_2S when a bulky group is at the thiol position. Furthermore, we used the perthiocarbonate-based donors to study persulfide persistence. These investigations showed that increased steric bulk at the R^2 position significantly increases persulfide persistence by blocking nucleophilic attack on the α-sulfur. Based on these results, perthiocarbonates can function as either H_2S, COS, or persulfide donors depending on the triggering mechanism and biological environment, which would likely result in the delivery of multiple RSS in complex environments. A benefit of these esterase-activated persulfide donors over other persulfide donors, such as those activated by base-mediated hydrolysis, is the ability to halt persulfide production by destruction of the esterase by addition of organic solvent, addition of an inhibitor, or other means. Overall, these persulfide

donors can be used to investigate persulfide fundamental properties or apply persulfides to specific biological isolates like enzymes to further understand the complex chemistry of persulfides.

4.4 Experimental Section

Methods and Materials

Reagents were purchased from Sigma-Aldrich, Tokyo Chemical Industry (TCI), Fisher Scientific, Combi-Blocks, and VWR and used directly as received. Silica gel (SiliaFlash F60, Silicycle, 230−400 mesh) was used for column chromatography. Deuterated solvents were purchased from Cambridge Isotope Laboratories. ^{1}H and $^{13}C\{^{1}H\}$ NMR spectra were recorded on Bruker 500 MHz NMR instruments at the indicated frequencies. Chemical shifts are reported in ppm relative to residual protic solvent resonances. Mass spectrometric measurements were performed by the University of Illinois, Urbana Champaign MS facility or on a Xevo Waters ESI LC/MS instrument. Methylene blue absorbance was monitored by a Cary 60 UV-Vis spectrometer. FDNB trapping assay analysis was conducted on an Agilent 1260 Infinity II HPLC.

*Synthesis of Persulfide Donors **1**–**9***

*General Procedure for Synthesis of Persulfide Donors **1** and **4**–**9***. Methoxy-carbonylsulfenyl chloride (2.2 mmol, 1.1 equiv.) was added to 10 mL CH_2Cl_2 containing the thiol starting material (2.0 mmol, 1.0 equiv.). The reaction mixture was stirred at room temperature until the completion of the reaction was indicated by TLC (about 1 hour). The reaction was quenched by adding water (10 mL) and then aqueous solution was extracted with CH_2Cl_2 (3 × 10 mL). The organic layers were combined, washed with brine, dried over $MgSO_4$, and then evaporated under vacuum. The product was then isolated after purification by column chromatography.

*General Procedure for Synthesis of Persulfide Donors **2** and **3***. The thiol starting material (2.0 mmol, 1.0 equiv.) was added to 10 mL CH_2Cl_2 and then cooled to 0 ºC in an ice bath under nitrogen. Chlorocarbonylsulfenyl chloride was added slowly (2.2 mmol, 1.1 equiv.). The reaction mixture was stirred at 0 ºC until the completion of the reaction was indicated by TLC (about 1 hour). Next, 15 mL of the alcohol starting material was added and the reaction was allowed to warm to room temperature over an hour. The reaction was quenched by adding water (10 mL) and then the aqueous solution was extracted with CH_2Cl_2 (3 × 10 mL). The organic layers were

combined, washed with brine, dried over $MgSO_4$, and then evaporated under vacuum. The product was then isolated after purification by column chromatography.

Persulfide Donor **1** was prepared by reacting methoxycarbonylsulfenyl chloride (403 μL, 4.43 mmol) with benzyl mercaptan (471 μL, 4.01 mmol) using the general synthetic procedure described above. Compound **1** was isolated as clear oil by column chromatography using ethyl acetate/hexanes (1/20, v/v) as the eluent (611 mg, 71.0% yield). ^{1}H NMR (500 MHz, DMSO-d_6) δ (ppm): 7.34 (m, 5H), 4.08 (s, 2H), 3.80 (s, 3H). ^{13}C{^{1}H} NMR (125 MHz, DMSO-d_6) δ (ppm): 168.9, 136.6, 129.9, 128.9, 128.1, 56.3, 42.6. HRMS m/z $[M]^+$ calcd. for $[C_9H_{10}O_2S_2]^+$ 214.0122; found 214.0114.

Persulfide donor **2** was prepared by reacting chlorocarbonylsulfenyl chloride (136 μL, 1.49 mmol) with benzyl mercaptan (189 μL, 1.61 mmol) using the general synthetic procedure described above. Compound **2** was isolated as clear oil by column chromatography using dichloromethane/hexanes (1/4, v/v) as the eluent (331 mg, 90.2% yield). ^{1}H NMR (500 MHz, DMSO-d_6) δ (ppm): 7.33 (m, 5H), 4.26 (m, 2H), 4.07 (s, 2H), 1.22 (t, J = 7.09 Hz, 3H). ^{13}C{^{1}H} NMR (125 MHz, DMSO-d_6) δ (ppm): 168.1, 136.6, 129.9, 128.9, 128.1, 65.8, 42.6, 14.5. HRMS m/z $[M + Na]^+$ calcd. for $[C_{10}H_{12}O_2S_2Na]^+$ 251.0171; found 251.0169.

Persulfide donor **3** was prepared by reacting chlorocarbonylsulfenyl chloride (136 μL, 1.49 1.49 mmol) with benzyl mercaptan (189 μL, 1.61 mmol) using the general synthetic procedure described above. Compound **3** was isolated as clear oil by column chromatography using dichloromethane/hexanes (1/4, v/v) as the eluent (297 mg, 76.2% yield). ^{1}H NMR (500 MHz, DMSO-d_6) δ (ppm): 7.32 (m, 5H), 5.01 (m, 1H), 4.06 (s, 2H), 1.24 (d, J = 6.26 Hz, 6H). ^{13}C{^{1}H} NMR (125 MHz, DMSO-d_6) δ (ppm): 167.5, 136.6, 129.9, 128.9, 128.0, 74.5, 42.5, 22.0. HRMS m/z $[M + Na]^+$ calcd. for $[C_{11}H_{14}O_2S_2Na]^+$ 265.0327; found 265.0329.

Persulfide donor **4** was prepared by reacting methoxycarbonylsulfenyl chloride (182 μL, 2.00 mmol) with phenyl mercaptan (185 μL, 1.82 mmol) using the general synthetic procedure described above. Compound **4** was isolated as a clear oil by column chromatography using ethyl acetate/hexanes (1/20, v/v) as the eluent (302 mg, 82.9% yield). ^{1}H NMR (500 MHz, DMSO-d_6) δ (ppm): 7.57 (d, J = 8.04 Hz, 2H), 7.43 (t, J = 7.45 Hz, 2H), 7.38 (m, 1H), 3.91 (s, 3H). ^{13}C{^{1}H} NMR (125 MHz, DMSO-d_6) δ (ppm): 168.5, 135.2, 130.0, 129.8, 129.1, 56.9. HRMS m/z $[M]^+$ calcd. for $[C_8H_8O_2S_2]^+$ 199.9966; found 199.9964.

Persulfide donor **5** was prepared by reacting methoxycarbonylsulfenyl chloride (239 μL, 2.00 mmol) with ethyl mercaptan (221 μL, 2.20 mmol) using the general synthetic procedure described above. Compound **5** was isolated as a clear oil by column chromatography using ethyl acetate/hexanes (1/20, v/v) as the eluent (284 mg, 93.4% yield). ^{1}H NMR (500 MHz, DMSO-d_6) δ (ppm): 3.87 (s, 3H), 2.82 (m, 2H), 1.25 (t, J = 7.27 Hz, 3H). ^{13}C{^{1}H} NMR (125 MHz, DMSO-d_6) δ (ppm): 169.5, 56.3, 32.2, 14.3. HRMS m/z $[M]^+$ calcd. for $[C_4H_8O_2S_2]^+$ 151.9966; found 151.9971.

Persulfide donor **6** was prepared by reacting methoxycarbonylsulfenyl chloride (1.99 mL mg, 4.02 mol) with *tert*-butyl mercaptan (1.44 mL, 4.43 mol) using the general synthetic procedure described above. Compound **6** was isolated as clear oil by column chromatography using ethyl acetate/hexanes (1/20, v/v) as the eluent (2.09 g, 69.6% yield). ^{1}H NMR (500 MHz, DMSO-d_6) δ (ppm): 3.86 (s, 3H), 1.30 (s, 9H). ^{13}C{^{1}H} NMR (125 MHz, DMSO-d_6) δ (ppm): 169.5, 56.7, 49.1, 29.5. HRMS m/z $[M]^+$ calcd. for $[C_6H_{12}O_2S_2]^+$ 180.0279; found 180.0277.

Persulfide donor **7** was prepared by reacting methoxycarbonylsulfenyl chloride (199.0 μL, 2.20 mmol) with *N*-acetyl-L-cysteine (326 mg, 2.00 mmol) using the general synthetic procedure described above. Compound **7** was isolated as white solid by column chromatography using 10% methanol, 40% DCM, and 50% hexane as the eluent (369 mg, 66.2% yield). ^{1}H NMR (500 MHz, DMSO-d_6) δ (ppm): 12.98 (s, 1H), 8.31 (d, J = 8.01 Hz, 1H), 4.49 (m, 1H), 3.89 (s, 3H), 3.20 (dd; J = 4.88, 13.80 Hz; 1H), 3.08 (dd; J = 8.71, 13.81 Hz; 1H), 1.87 (s, 3H). ^{13}C{^{1}H} NMR (125 MHz, DMSO-d_6) δ (ppm): 172.1, 169.8, 169.1, 56.5, 51.6, 22.8. HRMS m/z $[M + H]^+$ calcd. for $[C_7H_{12}NO_5S_2]^+$ 254.0151; found 254.0153.

Persulfide donor **8** was prepared by reacting methoxycarbonylsulfenyl chloride (199 μL, 2.20 mmol) with *N*-acetyl-L-cysteine methyl ester (354 mg, 2.00 mmol) using the general synthetic procedure described above. Compound **8** was isolated as white solid by column chromatography using 5% methanol, 40% dichloromethane, and 55% hexane as the eluent (464 mg, 87.7% yield). ^{1}H NMR (500 MHz, DMSO-d_6) δ (ppm): 8.47 (d, J = 7.78 Hz, 1H), 4.53 (m, 1H), 3.87 (s, 3H), 3.65 (s, 3H), 3.20 (dd; J = 5.16, 13.93 Hz; 1H), 3.10 (dd; J = 8.59, 13.94 Hz; 1H), 1.87 (s, 3H). ^{13}C{^{1}H} NMR (125 MHz, DMSO-d_6) δ (ppm): 171.2, 169.9, 169.0, 56.5, 52.7, 51.6, 22.8. HRMS m/z $[M + H]^+$ calcd. for $[C_8H_{14}NO_5S_2]^+$ 268.0308; found 268.0312.

Persulfide donor **9** was prepared by reacting methoxycarbonylsulfenyl chloride (131 μL, 1.10 mmol) with *N*-acetyl-D-penicillamine (191 mg, 1.00 mmol) using the general synthetic procedure described above. Compound **9** was isolated as white solid by column chromatography using first column had 1:4:5 methanol:dichloromethane:hexane as the solvent while the second column had 5% ethyl acetate in hexane as the eluent (76.3 mg, 27.9% yield). ^{1}H NMR (500 MHz, DMSO-d_6) δ (ppm): 12.97 (s, 1H), 8.23 (d, *J* = 9.22 Hz, 1H), 4.51 (d, *J* = 9.30 Hz, 1H), 3.85 (s, 3H), 1.91 (s, 3H). ^{13}C{^{1}H} NMR (125 MHz, DMSO-d_6) δ (ppm): 171.4, 169.9, 169.2, 58.3, 56.4, 53.3, 25.3, 23.7, 22.8. HRMS m/z $[M + H]^+$ calcd. for $[C_9H_{16}NO_5S_2]^+$ 282.0464; found 282.0464.

*General procedure for synthesis of RSSH-DNB adducts **10–16***

2,4-Dinitrophenylsuelfenyl chloride (1.5 mmol, 1.0 equiv.) was added to 10 mL CH_2Cl_2 and stirred momentarily. Next, the thiol starting material (1.5 mmol, 1.0 equiv.) was added dropwise, then this solution was stirred for 1 hour until the completion of the reaction was indicated by TLC. The reaction was quenched by adding water (10 mL) and then the aqueous solution was extracted with CH_2Cl_2 (3 × 10 mL). The organic layers were combined, washed with brine, dried over $MgSO_4$, and then evaporated under vacuum. The final product was then isolated after purification by column chromatography as a yellow solid.

Adduct **10** was prepared by reacting 2,4-dinitrophenylsulfenyl chloride (352 mg, 1.50 mmol) with ethyl mercaptan (86.3 μL, 1.50 mmol) using the general synthetic procedure described above. Compound **10** was isolated as yellow solid by column chromatography using ethyl acetate/hexanes (1/9, v/v) as the eluent (371 mg, 92.2% yield). ^{1}H NMR (500 MHz, DMSO-d_6) δ (ppm): 8.91 (d, *J* = 2.50, 1H), 8.62 (dd; *J* = 2.52, 8.97 Hz; 1H), 8.51 (d, *J* = 9.00 Hz, 1H), 2.92 (m, 2H), 1.27 (t, *J* = 7.39 Hz, 3H). ^{13}C{^{1}H} NMR (125 MHz, DMSO-d_6) δ (ppm): 145.8, 145.4, 145.2, 129.3, 128.6, 122.0, 32.3, 14.5. LRMS m/z $[M + H]^+$ calcd. for $[C_8H_9N_2O_4S_2]^+$ 260.9998; found 261.0070.

Adduct **11** was prepared by reacting 2,4-dinitrophenylsulfenyl chloride (352 mg, 1.50 mmol) with *tert*-butyl mercaptan (169 μL, 1.50 mmol) using the general synthetic procedure described above. Compound **11** was isolated as a light-yellow solid by column chromatography using ethyl acetate/hexanes (1/9, v/v) as the eluent (370 mg, 85.5% yield). ^{1}H NMR (500 MHz, DMSO-d_6) δ (ppm): 8.90 (s, 1H), 8.58 (m, 2H), 1.35 (s, 9H). ^{13}C{^{1}H} NMR (125 MHz, DMSO-

d_6) δ (ppm): 145.8, 145.3, 139.8, 128.2, 121.8, 51.5, 29.9. LRMS m/z $[M + H]^+$ calcd. for $[C_{10}H_{13}N_2O_4S_2]^+$ 289.0311; found 289.0367.

Adduct **12** was prepared by reacting 2,4-dinitrophenylsulfenyl chloride (379 mg, 1.61 mmol) with benzyl mercaptan (189 μL, 1.61 mmol) using the general synthetic procedure described above. Compound **12** was isolated as yellow solid by column chromatography using ethyl acetate/hexanes (1/9, v/v) as the eluent (416 mg, 81.7% yield). ^{1}H NMR (500 MHz, DMSO-d_6) δ (ppm): 8.83 (d, *J* = 2.44 Hz, 1H), 8.45 (dd; *J* = 2.47, 8.97 Hz; 1H), 8.26 (d, *J* = 8.98 Hz, 1H), 7.31 (d, *J* = 6.58 Hz, 2H), 7.24 (m, 3H), 4.16 (s, 2H). ^{13}C{^{1}H} NMR (125 MHz, DMSO-d_6) δ (ppm): 145.6, 145.2, 144.8, 136.3, 130.0, 129.5, 129.0, 128.1, 121.7, 42.2. LRMS m/z $[M + H]^+$ calcd. for $[C_{13}H_{11}N_2O_4S_2]^+$ 323.0155; found 323.0264.

Adduct **13** was prepared by reacting 2,4-dinitrophenylsulfenyl chloride (352 mg, 1.50 mmol) with phenyl mercaptan (153 μL, 1.50 mmol) using the general synthetic procedure described above. Compound **13** was isolated as yellow solid by column chromatography using ethyl acetate/hexanes (1/9, v/v) as the eluent (362 mg, 78.4% yield). ^{1}H NMR (500 MHz, DMSO-d_6) δ (ppm): 8.93 (d, *J* = 2.49 Hz, 1H), 8.62 (dd; *J* = 2.47, 8.99 Hz; 1H), 8.46 (d, *J* = 8.98 Hz, 1H), 7.60 (d, *J* = 8.02 Hz, 2H), 7.35 (m, 3H). ^{13}C{^{1}H} NMR (125 MHz, DMSO-d_6) δ (ppm): 146.2, 145.2, 143.8, 133.9, 130.2, 129.0, 122.1. LRMS m/z $[M + H]^+$ calcd. for $[C_{12}H_9N_2O_4S_2]^+$ 308.9998; found 309.0074.

Adduct **14** was prepared by reacting 2,4-dinitrophenylsulfenyl chloride (352 mg, 1.50 mmol) with *N*-acetyl-L-cysteine (245 mg, 1.50 mmol) using the general synthetic procedure described above. Compound **14** was isolated as a pale-yellow solid by column chromatography using a gradient of 10-60% ethyl acetate/hexanes as the eluent (337 mg, 88.7% yield). ^{1}H NMR (500 MHz, DMSO-d_6) δ (ppm): 13.01 (s, 1H), 8.91 (d, *J* = 2.43 Hz, 1H), 8.61 (d; *J* = 2.46, 9.00 Hz; 1H), 8.51 (d, *J* = 8.98 Hz, 1H), 8.46 (d, *J* = 8.02 Hz, 1H), 4.47 (m, 1H), 3.27 (dd; *J* = 4.54, 13.76 Hz; 1H), 3.16 (dd; *J* = 9.03, 13.71 Hz; 1H), 1.87 (s, 3H). ^{13}C{^{1}H} NMR (125 MHz, DMSO-d_6) δ (ppm): 172.0, 170.0, 145.9, 145.3, 144.9, 129.4, 128.6, 129.4, 128.6, 121.9, 51.8, 22.9. HRMS m/z $[M + H]^+$ calcd. for $[C_{11}H_{12}N_3O_7S_2]^+$ 362.0111; found 362.0107.

Adduct **15** was prepared by reacting 2,4-dinitrophenylsulfenyl chloride (352 mg, 1.50 mmol) with *N*-acetyl-L-cysteine methyl ester (266 mg, 1.50 mmol) using the general synthetic procedure described above. Compound **15** was isolated as a pale-yellow solid by column chromatography using a gradient of 10-60% ethyl acetate/hexanes as the eluent (378 mg, 95.4%

yield). ^{1}H NMR (500 MHz, DMSO-d_6) δ (ppm): 8.91 (d, *J* = 2.43 Hz, 1H), 8.61 (dd; *J* = 2.48, 8.98 Hz; 1H), 8.56 (d, *J* = 7.87 Hz, 1H), 8.49 (d, *J* = 8.99 Hz, 1H), 4.55 (m, 1H), 3.62 (s, 3H), 3.25 (dd; *J* = 4.81, 13.89 Hz; 1H), 3.15 (dd; *J* = 8.93, 13.86 Hz; 1H), 1.88 (s, 3H). ^{13}C{^{1}H} NMR (125 MHz, DMSO-d_6) δ (ppm): 171.0, 170.0, 145.9, 145.3, 144.7, 129.4, 128.7, 122.0, 52.7, 51.7, 22.8. HRMS m/z $[M + H]^+$ calcd. for $[C_{12}H_{14}N_3O_7S_2]^+$ 376.0268; found 376.0271.

Adduct **16** was prepared by reacting 2,4-dinitrophenylsulfenyl chloride (176 mg, 0.75 mmol) with *N*-acetyl-D-penicillamine (112 mg, 0.75 mmol) using the general synthetic procedure described above. Compound **16** was isolated as a yellow solid by column chromatography using a gradient of 10-60% ethyl acetate/hexanes as the eluent (206 mg, 70.5% yield). ^{1}H NMR (500 MHz, DMSO-d_6) δ (ppm): 8.90 (s, 1H), 8.56 (s, 2H), 8.37 (d, *J* = 9.25 Hz, 1H), 4.58 (d, *J* = 9.16 Hz, 1H), 1.92 (s, 3H), 1.37 (s, 6H). ^{13}C{^{1}H} NMR (125 MHz, DMSO-d_6) δ (ppm): 171.3, 170.0, 145.8, 145.7, 145.4, 130.1, 128.2, 121.8, 58.7, 55.4, 25.6, 24.0, 22.8. HRMS m/z $[M + H]^+$ calcd. for $[C_{13}H_{16}N_3O_7S_2]^+$ 390.0424; found 390.0421.

Esterase Activity in Solvent System

A freshly prepared *p*-nitrophenyl acetate stock solution (15 μL, 15 mM in acetonitrile) was added to 3 mL of PBS buffer (pH 7.4, 10 mM) in a quartz cuvette. The esterase stock solution (6 μL, 500 U mL^{-1} in PBS buffer) was added to begin the experiment and the absorbance was measured at 405 nm on a UV-Vis spectrophotometer over 15 minutes. This procedure was repeated using 10% (v/v) acetonitrile in PBS buffer and 20% (v/v) acetonitrile in PBS buffer as the solvents to determine esterase activity at varying levels of organic solvents as seen in **Fig. S1**.

Esterase Activity with Parathion

A freshly prepared esterase stock solution (6 μL, 500 U mL^{-1} in PBS buffer) and Parathion stock solution (30.0 μL, 1.0 mM in acetonitrile) was added to 3 mL of PBS buffer (pH 7.4, 10 mM) in a quartz cuvette and incubated for 30 minutes. The *p*-nitrophenyl acetate stock solution (15 μL, 15 mM in acetonitrile) was added to begin the experiment, and the absorbance was measured at 405 nm on a UV-Vis spectrophotometer over 15 minutes as seen in Fig. C1.

General Persulfide Trapping FDNB Assay Procedure

A freshly prepared 1-fluoro-2,4-dinitrobenzene stock solution (20 μL, 4.0 M in acetonitrile) was added to 20 mL of 10% (v/v) acetonitrile in 10 mM PBS buffer (pH 7.4) containing PLE (1.0 U mL^{-1}) in a vial. This solution was then stirred for 30 minutes at 25 °C. A persulfide donor stock solution (20 μL, 100 μM in acetonitrile) was added to begin the experiment and 500 μL aliquots were taken at 1, 5, 10, 15, 20, 30, 45, and 60 minutes and then added to 2 mL GC vials containing 500 μL of acetonitrile. After filtering, these solutions were run on a reverse-phase HPLC. The HPLC method is as follow: Mobile phase A (5% methanol in water) and mobile phase B (acetonitrile); Flow rate of 1 mL/min; Injection volume of 5 μL; Detection wavelength of 250 nm; Column used was InfinityLab Poroshell 120 EC-C18, 4.6 x 100 mm, 2.7 μm, analytical LC column; Gradient method with 40% A from 0 to 5 min, 40% to 10% A from 5 to 10 minutes, 10% to 0% A from 10 to 15 minutes, 0% A from 15 to 17 minutes, 0% to 40% A from 17 to 20 minutes, and then 40% A from 20 to 22 minutes.

*Calibration Curves with RSS-DNB Adducts **10**–**16***

Calibration curves were created by first preparing a 10 mM stock solution of the RSS-DNB adduct in acetonitrile and then serial diluting to obtain 5, 2.5, 1.25, 0.625, and 0.3125 mM solutions. Next 10 μL volume of these solutions were added to vials containing 990 μL of 50% acetonitrile in PBS buffer (pH 7.4, 10 mM) to obtain final RSS-DNB adduct concentrations of 100, 75, 50, 25, 12.5, 6.25, and 3.125 μM. These solutions were filtered and then run on a reverse-phase HPLC using the same method as described above for the FDNB trapping assay. The calibration curves of **10**–**16** are plotted in Fig. C2.

^{1}H NMR Spectroscopy Experiments Monitoring Ester Cleavage by Esterase or tert-Butoxide:

To monitor ester cleavage by esterase, a freshly prepared stock solution of FDNB (8.33 μL, 300 mM in acetonitrile-d_3) was added to 442 μL of D_2O along with 16.67 μL of acetonitrile-d_3 and a PLE stock solution (8 μL, 625 U mL^{-1} in D_2O). A stock solution of persulfide donor **7** (25 μL, 200 mM in acetonitrile-d_3) was added, the tube was inverted to mix, and then ^{1}H NMR spectra were taken at t = 5 m, 30 m, 1 h, 2 h, 4 h, 6 h, 10 h, and 18 h.

To monitor ester cleavage by *tert*-butoxide, a freshly prepared stock solution of FDNB (50 μL, 200 mM in THF-d_8) was added to 250 μL of 20 mM KO*t*Bu in THF-d_8 along with 50 μL D_2O and 100 μL THF-d_8. A stock solution of persulfide donor 7 (50 μL, 100 mM in THF-d_8) was added, the tube was inverted to mix, and then ^{1}H NMR spectra were taken at t = 5 m, 30 m, 1 h, 2 h, 4 h, 6 h, 10 h, and 18 h. ^{1}H NMR spectra are shown in Fig. C6 and Fig. C7.

*Methylene Blue Assay Experiments with Persulfide Donors **1** and **6***

Four experiments were completed: (1) MB assay of persulfide donor **1** with PLE, (2) MB assay of persulfide donor **1** with PLE and CA, (3) MB assay of persulfide donor **6** with PLE, and (4) MB assay of persulfide donor **6** with PLE and CA. MB assays were also completed in the presence of FDNB, but this data is omitted due to negligible H_2S being released, as expected. A stock solution of the persulfide donor (20 μL, 100 mM) was added to 20 mL of degassed 10% acetonitrile in PBS buffer (pH 7.4, 10 mM) containing PLE (1.0 U mL^{-1}) as well as CA (50 μg mL^{-1}) for experiments 2 and 4. At 1, 5, 10, 15, 20, 30, 45, 60, and 90 minutes 500 μL aliquots were taken and placed in cuvettes containing 500 μL of 2:2:1 iron (III) chloride/*N*,*N*-dimethyl-*p*-phenylenediamine/zinc acetate and then filtered. After 1 hour the absorbance at 670 nm was measured using a UV-Vis spectrophotometer and was converted to H_2S concentration by using an H_2S calibration curve. Quantified H_2S release from persulfide donors **1** and **6** with and without CA present are plotted in Fig. C8.

*^{13}C NMR Spectroscopy Monitoring the Reactivity of Persulfide Donor **6** and PLE*

A freshly prepared stock solution of **6** (25 μL, 200 mM in CD_3CN) was added to solution of 442 μL of D_2O and 25 μL of CD_3CN. A stock solution of PLE (8 μL, 625 U mL^{-1} in PBS buffer) was added, the tube was inverted to mix, and then ^{1}H NMR spectra were taken at t = 1, 3, 6, 12 hours. The ^{13}C NMR spectra are shown in Fig. C10.

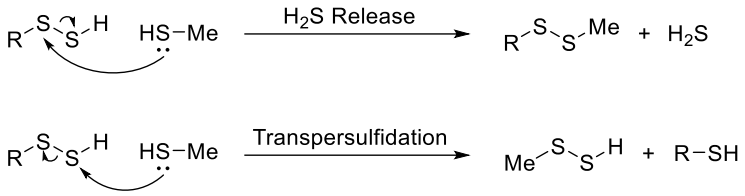
V. TRANSPERSULFIDATION OR H_2S RELEASE? UNDERSTANDING THE LANDSCAPE OF PERSULFIDE CHEMICAL BIOLOGY

This chapter includes previously published and co-authored material from Fosnacht, K.G.; Sharma, J.; Champagne, P.A.; Pluth, M.D. Transpersulfidation or H_2S release? Understanding the landscape of persulfide chemical biology. *J. Am. Chem. Soc.* **2024**, *Accepted*. This manuscript was written by Kaylin G. Fosnacht with editorial assistance by Professor Michael D. Pluth. The project in this chapter was conceived by Kaylin G. Fosnacht, the computational work was performed by Jyoti Sharma, and the experimental work was performed by Kaylin G. Fosnacht.

5.1 Introduction

Reactive sulfur species (RSS) play critical roles in biological chemistry, including roles in redox homeostasis and small molecule signaling pathways. This important class of compounds encompasses a wide array of oxidation states, with molecules containing sulfur atoms in the –2 to +6 oxidation state including such as H_2S, persulfides (RSSH), polysulfides (RSS_nSR), sulfenic acids (RSOH), and sulfate (SO_4^{2-}).[1135-1137] These redox active species are involved in diverse biological functions across all kingdoms of life, and the fundamental chemistry by which RSS exert action is a rapidly-expanding area of investigation. Building from the discovery that endogenous H_2S participates in various mammalian signaling pathways in the late 1990's, significant effort has expanded our understanding of how H_2S and other RSS are intertwined in complex pathways associated with RSS generation, translocation, and action.[24, 25] More recent work has further clarified that many cellular signaling processes initially attributed to H_2S alone are likely due to persulfides.[29, 61, 1138] Similar to H_2S, persulfides are generated endogenously through both enzymatic and non-enzymatic processes, and cellular persulfide levels are generally found in the low micromolar range, although elevated glutathione persulfide levels have also been found in specific environments, such as brain tissue.[1102, 1104, 1111, 1139-1141] Persulfides protect essential protein Cys residues from irreversible oxidation, are soluble sources of redox-labile sulfur, and are versatile intermediates in important cellular processes.[1106, 1107, 1142] For example, persulfide intermediates have been observed during processes including Fe-S cluster formation, sulfur homeostasis maintenance by thioredoxin, sulfur transfer by 3-mercaptopyruvate sulfur

transferase, prevention against Tau hyperphosphorylation, as well as other systems.[37, 1105, 1114, 1143-1146]



Scheme 5.1. Comparison of attack at the sulfenyl sulfur to generate a disulfide and H_2S and at the sulfhydryl sulfur to undergo a transpersulfidation reaction. RSS are shown in their neutral form for simplicity.

Despite the broad importance of persulfide chemistry, understanding the fundamental chemistry of this functional group remains challenging because both the local environment and protonation state directly impact persulfide reactivity. For example, although other RSS such as H_2S or thiols exclusively function as nucleophiles, persulfides are both nucleophilic and electrophilic with an additional propensity to participate in one electron chemistry. Persulfides are more acidic than the corresponding thiol by 1–4 pK_a units (e.g. pK_a GSH = 8.94, GSSH = 5.45), and are also significantly better nucleophiles than thiols due to the α-effect. [949, 1147] In their neutral protic form, persulfides are electrophilic at either sulfur atom and reactivity with nucleophiles such as thiolates, cyanide, sulfite, phosphines, and amines has been observed previously.[1148-1151] More specifically, reaction with a thiolate at the inner sulfenyl sulfur (R<u>S</u>SH) results in disulfide formation and H_2S release whereas reaction at the outer sulfhydryl sulfur (RS<u>S</u>H) results in sulfur transfer, or transpersulfidation, to the incoming nucleophile (Scheme 5.1). Both of these reaction manifolds are common in RSS chemical biology, with select reported H_2S donors generating an intermediate persulfide and transpersulfidation observed during enzymatic processes.[1061, 1115] Despite the increasing literature examples of this bifurcated reactivity between persulfides and thiols, approaches to control or understand these pathways remain elusive.

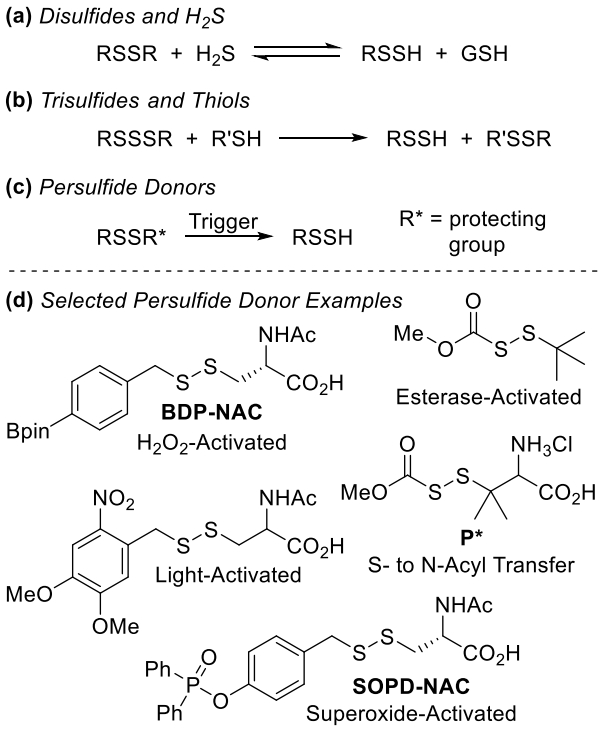


Figure 5.1. Methods employed to generate persulfides *in situ* including (a) reaction of disulfides with H_2S, (b) reaction of trisulfides with thiols, or (c) persulfide donors activated by a specific trigger. (d) Examples of persulfide donors that are activated by hydrogen peroxide, esterase, light, S- to N-acyl transfer, or superoxide.

To further understand the reactivity and biological roles of persulfides, different approaches have been developed to generate persulfides. Methods used to isolate low molecular weight (LMW) model persulfides have been helpful for exploring fundamental persulfide reactivity, however the organic solvent environments used in these investigations does not map to persulfide reactivity in aqueous systems.[29, 301, 1118, 1152-1157] Alternatively, persulfides can be produced *in vitro* through the upregulation of persulfide-producing enzymes or by exogenous treatment of enzyme substrates.[1104, 1112] Other approaches to generate LMW persulfides include the treatment of oxidized thiols with H_2S, disulfides with H_2S, or trisulfides with thiols, although such reactions are reversible and typically generate RSS mixtures (Figure 5.1a–b).[1099, 1102, 1103, 1158, 1159] Another commonly used approach is the use of persulfide donors, also known as persulfide prodrugs or protected persulfides, that release persulfides when activated by specific conditions or stimuli.[1160] Examples include persulfide donors activated by hydrolysis, nucleophiles, enzymes, or light (Figure 5.1c–d).[1091, 1122, 1127, 1161, 1162] Although persulfide donors provide an important approach

for generating and investigating the biological impacts of persulfides, the specific reactivity of the structurally-diverse released persulfides are generally not investigated directly and may depend on the characteristics of the released persulfides. Expanding the fundamental understanding of structural impacts on persulfide stability, persistence, and reactivity would significantly advance our understanding of whether released persulfides participate primarily in H_2S release, transpersulfidation, or a mixture of both pathways.

Initial insights into persulfide persistence were obtained during prior work from our lab using an esterase-activated persulfide donor where the sterically bulky *tert*-butyl persulfide was more persistent in buffer than the less bulky ethyl or benzyl persulfides.[1091] Other reports have postulated similar impacts of bulk on persulfide reactivity, but experimental investigations into this hypothesis are primarily lacking.[1118, 1163] With the goal of bridging this major gap in knowledge, we report here a combined computational and experimental approach to examine how both electronic and steric components influence persulfide properties and can be used to tune H_2S release versus transpersulfidation pathways. Importantly, computational investigations are a key component of this approach because they allow for specific molecular entities to be investigated without unwanted interference from other generated RSS and also because they allow for motifs to be investigated that would not be possible experimentally due to cross reactivity, synthetic challenges, or persulfide stability issues. Using this approach, we demonstrate here how the electronic structure of persulfides influences the linear free energy relationship for both the thermodynamic and kinetic preferences for H_2S release versus transpersulfidation. Moreover, translating this approach to the persulfide local steric environment, we use these computational insights to experimentally monitor and measure transpersulfidation from a bulky penicillamine-based persulfide and a cysteine-based thiol, which to the best of our knowledge is the first direct observation of transpersulfidation between low molecular weight species.

5.2 Results and Discussion

5.2.1 Computational Investigation of Persulfide Reactivity with Thiols

To overcome the experimental limitations of working with a broad array of functionalized persulfides, we used computational approaches to investigate the fundamental energetics of persulfide reaction manifolds. Importantly, this approach allows for individual reaction pathways to be probed directly without potential interference from competing pathways and also removes

the need to synthesize these otherwise unstable molecules. In addition, computational investigations can be used to identify target systems that can be prepared experimentally to validate the predicted reactivity from computational approaches.

5.2.1.1 Effect of Electronic Effects on Persulfide Reactivity

To investigate how persulfide electron density impacts the intrinsic energy landscape of persulfides for competing pathways of H_2S release and transpersulfidation, we first investigated a series of phenyl persulfides substituted with electron donating or withdrawing groups in the *para* position. DFT calculations were performed at the ωB97X-D/aug-cc-pV(T+*d*)Z/SMD(H_2O) level of theory, which provides accurate results for nucleophilic substitution reactions involving S–S bonds.[1164, 1165] To investigate the intrinsic energy landscape of persulfides for competing pathways of H_2S release and transpersulfidation, we used methyl thiolate as a model nucleophile to simplify possible conformations and protonation states. In each system we calculated the thermodynamic (ΔG_{rxn}) and activation ($\Delta G^{\ddagger}$) free energy for both the H_2S release ($\Delta G_{rxn}(H_2S)$, $\Delta G^{\ddagger}_{H2S}$) and transpersulfidation pathways (ΔG_{rxn}(persulf), $\Delta G^{\ddagger}_{persulf}$). When comparing the energetics of these systems (Figure 5.2), in all cases transpersulfidation is kinetically favored over H_2S release, and the selectivity for transpersulfidation over H_2S release increases as electron withdrawing groups are added to the persulfide. For example, transpersulfidation is kinetically favored over H_2S release by 2.1 kcal mol^{-1} for the electron-donating NMe_2 persulfide, versus by 3.5 kcal mol^{-1} for electron-withdrawing NO_2 persulfide. Interestingly, transpersulfidation for electron-poor persulfides is more exergonic than H_2S release, which we attribute to the different basicities of the aryl thiolate products.

Using the reaction energetics obtained in Figure 5.2, we next used this data to investigate the Hammett linear free energy relationship to better understand the factors influencing both the kinetic and thermodynamic preferences for transpersulfidation and H_2S release. We converted the $\Delta G_{rxn}(H_2S)$ and ΔG_{rxn}(persulf) values to K_{eq} values at 298 K to generate the Hammett plot in Figure 5.3a. Because the negative charge of the product thiolate can be stabilized through resonance, we used the modified para substituent constant (σ_p^-) values in our analysis.[1166] When looking at the sensitivity constants (ρ) acquired, electronic substitution has a major impact on transpersulfidation (ρ = 4.14), which is likely driven by the different pK_a values of the resultant aryl thiolate products.

By contrast, there is only minimal dependence upon electronic substitution for H_2S release (ρ = 0.23). We attribute this lower sensitivity to the lack of charge buildup in the disulfide product formed after H_2S release. The significant difference in ρ values for the H_2S release and transpersulfidation pathways shows that the thermodynamic favorability for transpersulfidation can be greatly favored by including electron withdrawing groups on the persulfide.

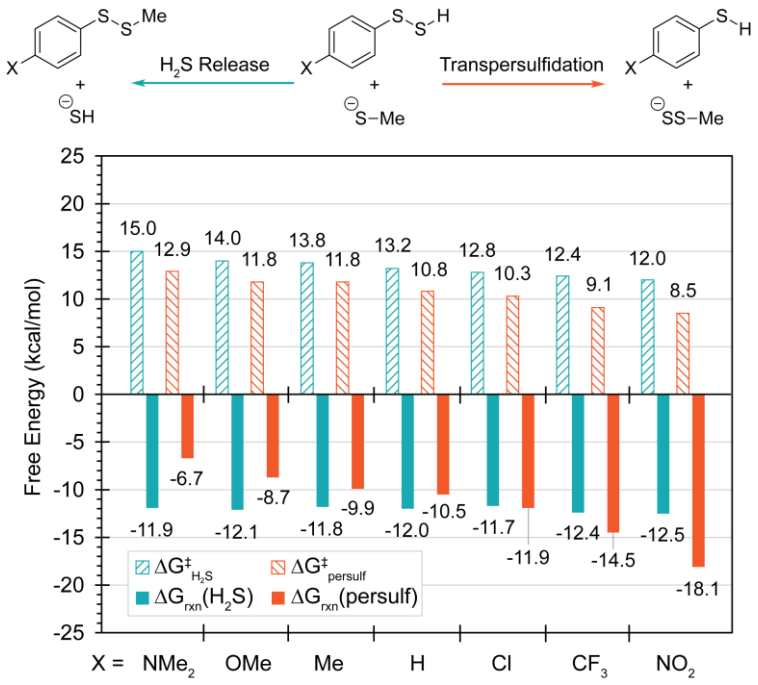


Figure 5.2. Activation and reaction free energies (kcal mol^{-1}) for H_2S release or transpersulfidation of substituted aryl persulfides with methyl thiolate.

To complement these thermodynamic insights, we also used $\Delta G^{\ddagger}_{H2S}$ and $\Delta G^{\ddagger}_{persulf}$ to generate a Hammett plot to understand how electronic structure impacts the barriers for these competing reaction pathways (Figure 5.3b). For the transition state structures we found the best correlation with σ_p values, which suggests a lower degree of overall charge delocalization in the transition state.[1166] The Hammett plot for both reaction pathways is consistent with partial negative charge character on the sulfenyl sulfur, with a larger charge buildup for the transpersulfidation reaction, which is consistent with the aryl thiol acting as a leaving group. The transpersulfidation pathway (ρ = 2.08) shows a greater sensitivity to negative charge buildup than the H_2S release pathway (ρ = 1.36), which again highlights that transpersulfidation can be favored by inclusion of electron withdrawing substituents.

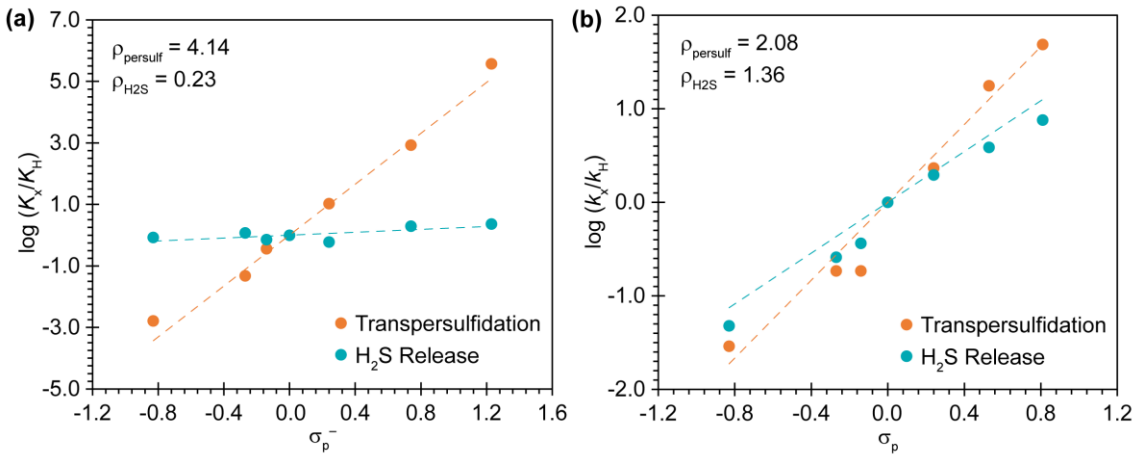


Figure 5.3. Hammett linear free energy relationship of the (a) thermodynamic and (b) kinetic preferences for transpersulfidation and H_2S release.

5.2.1.2 Effect of Steric Substitutions on Persulfide Reactivity

Having demonstrated the impact of electronic donating and withdrawing substituents on persulfide reactivity, we next investigated the energy landscape for the competing H_2S and transpersulfidation reactions of alkyl persulfides with different steric profiles (Me, Et, allyl, Bn, *i*Pr, *t*Bu). We first compared $\Delta G^{\ddagger}$ for H_2S release and transpersulfidation for alkyl persulfides with increasing steric bulk (Figure 5.4). Our expectation was that more steric bulk on the persulfide would increase the barrier for attack by MeS^-. Consistent with this expectation, we observed an increase in $\Delta G^{\ddagger}$ for both reaction pathways going from primary (Et) to secondary (*i*Pr) to tertiary (*t*Bu) persulfides. This increase is more significant for the H_2S releasing pathway because the thiolate needs to attack the sulfenyl sulfur atom, which is more impacted by the steric hinderance of the alkyl group. Indeed, all aliphatic primary persulfides (Me, Et, allyl, Bn) have similar barriers for both pathways, which is supported by prior computational work with MeSSH that showed little preference for nucleophilic attack on either sulfur atom.[1167] Increasing in steric bulk, both *i*PrSSH and *t*BuSSH show lower barriers for transpersulfidation over H_2S release by 2.7 and 7.7 kcal mol^{-1}, respectively. Additionally, we used this data to investigate the Taft linear free energy relationship between sterics and kinetic preference, and although both pathways are sensitive to steric effects ($\delta > 0$), the H_2S releasing pathway has a much higher steric sensitivity (Figure D9).[1168] Taken together, these data support that primary persulfides function as both H_2S and transpersulfidation reagents, whereas bulkier persulfides have a significant kinetic preference for transpersulfidation

over H_2S release. More broadly, this chemistry is consistent with prior experimental work with primary persulfides, such as diallyl trisulfide, which is a naturally occurring polysulfide from garlic and alliums that is well established to release H_2S in the presence of thiols through the intermediate release of the allyl persulfide followed by subsequent reaction with a thiol to release H_2S.[1169-1172]

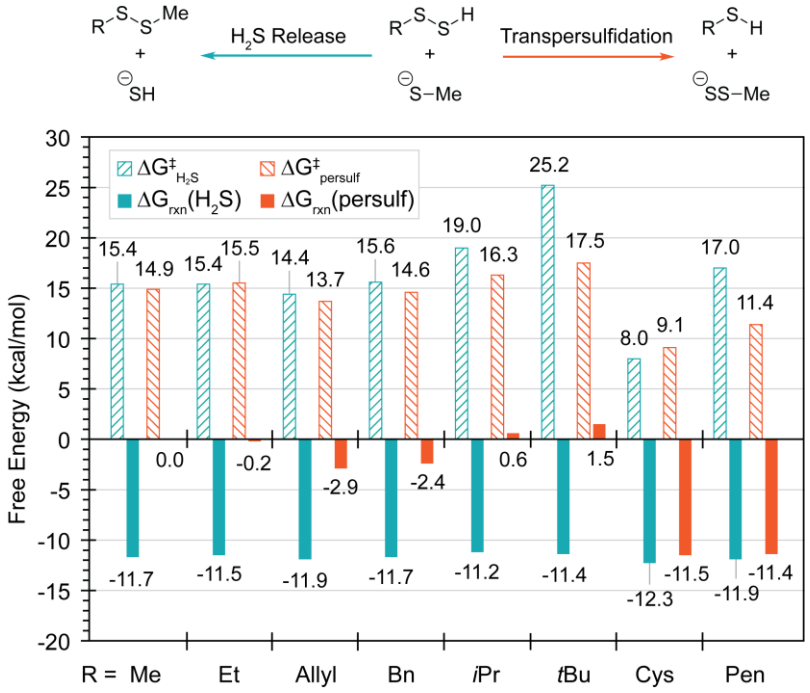


Figure 5.4. Activation and reaction free energies (kcal mol^{-1}) for H_2S release or transpersulfidation of alkyl persulfides with methyl thiolate.

The steric effects are also apparent when comparing the reactivity of penicillamine and cysteine persulfides. Although $\Delta G^{\ddagger}_{persulf}$ values are similar for both persulfides (11.4 vs. 9.1 kcal mol^{-1}), the bulkier penicillamine persulfide has a much larger $\Delta G^{\ddagger}_{H2S}$ than cysteine persulfide (17.0 vs. 8.0 kcal mol^{-1}). This difference is due to the tertiary carbon next to the sulfenyl sulfur atom, which distorts the S_N2-like transition state angle from the near linear 174° for cysteine persulfide to a much more bent 165° for the penicillamine derivative (Figure 5.5). These results are especially interesting, as penicillamine persulfides are commonly used as cysteine analogues in persulfide donors due to the increased stability of the donor itself. Although these structures are commonly used interchangeably, the steric bulk of the penicillamine alters the reactivity of the persulfide considerably from that of cysteine persulfide.

To further probe this system with more biologically-relevant nucleophiles, we also investigated the reaction of cysteine persulfide with methyl thiolate, cysteine thiolate, and a bulky penicillamine-based thiolate as the nucleophiles (Figure D7). We found that as the nucleophile increases in size, the preference for the H_2S releasing pathway over transpersulfidation is eroded. For example, the cysteine thiolate nucleophile results in a 0.3 kcal mol^{-1} kinetic preference for transpersulfidation over H_2S release, which increases to 0.6 kcal mol^{-1} for the penicillamine-based system. Although increased nucleophile steric bulk does affect reaction preference for transpersulfidation over H_2S release, persulfide steric bulk has a much larger effect on reaction energetics.

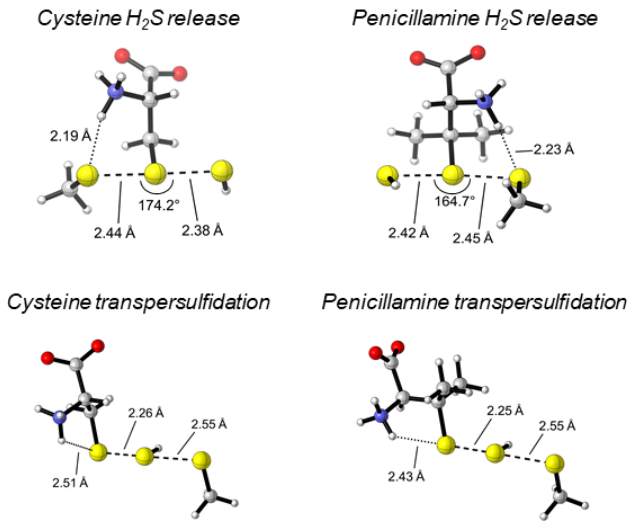


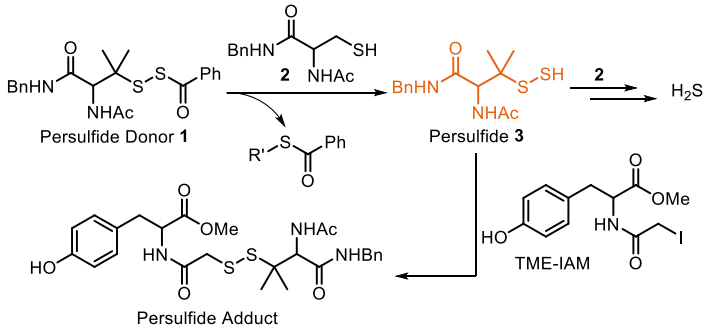
Figure 5.5. Computed H_2S release and transpersulfidation transition structures (TSs) for cysteine (Cys) and penicillamine (Pen) systems.

5.2.2 Experimental Transpersulfidation Observation and Measurement

After demonstrating through computational methods that transpersulfidation between persulfides and thiols can be influenced directly by persulfide steric bulk, we next aimed to translate these DFT results into experimental solution reactivity. As mentioned previously, the reversible reaction between LMW persulfides and thiols resulting in H_2S release and disulfide formation is well established, and adaptations of this chemistry have been used to generate GSSH *in situ* by the reaction of GSSG with H_2S.[949] Further dissecting the direct reaction of a persulfide with a thiol, either H_2S release and disulfide formation or transpersulfidation can occur. Prior work on this reaction has attributed the favorable release of H_2S to the leaving group ability of H_2S (pK_a

= 6.98) versus a thiol such as GSH (pK_a = 8.94), with transpersulfidation being accessible in specific environments within proteins.[39, 1115] Indeed, transpersulfidation has primarily been observed between proteins or between a protein and LMW species in select systems, although this reactivity is also hypothesized to occur more broadly during other cellular processes.[1173-1176] One report did observe an increase in GSSH with increased cysteine persulfide production through enzymatic means in cell lysates, but it is unclear if the increase in GSSH is due to direct reaction of CysSSH with GSH or through other pathways.[1104] Expanding beyond these systems, to the best of our knowledge the direct transpersulfidation between LWM persulfides and thiols has not previously been directly observed experimentally.

For probe this question directly, we built from the computational insights from above by modifying a penicillamine-based acyl perthiol donor platform reported by Xian in 2013.[1177] These acyl perthiols react with Cys or GSH to form an intermediate persulfide, which subsequently reacts further with excess thiol to release H_2S (Scheme 5.2). In addition, these systems demonstrated good activity against myocardial ischemia-reperfusion injury in mouse models, demonstrating the efficacy of this system in more complex environments.



Scheme 5.2. Reactivity of the penicillamine-based acyl perthiol donor platform. Persulfide donor **1** with thiol **2** releases persulfide **3** that further react to release H_2S or can be trapped by treatment with trapping agent TME-IAM to form a stable persulfide adduct.

To better understand the specific reactivity of the tertiary persulfide intermediate formed in this reaction, we modified both the parent donor platform and thiol reactant with benzyl groups to improve HPLC detection. With this modified system, reaction of acyl perthiol **1** with *N*-acetyl cysteine derived **2** results in release of the analogous penicillamine-based persulfide **3** (Scheme 5.2). Since persulfides have a short persistence in solution due to their reaction with other thiols

or persulfides, we used a persulfide trapping agent to form a stable persulfide adduct to aid in analysis. After screening different trapping agents, we chose to use the iodoacetamide derivative *N*-iodoacetyl L-tyrosine methyl ester (TME-IAM), which has been used previously to trap and stabilize persulfides and other sulfhydryl species in complex RSS solutions.[1178] Specifically, we used TME-IAM to trap and measure both penicillamine-derived persulfide **3** as well as the associated transpersulfidation product **6** by HPLC (*vide infra*)

Before beginning experimental studies, we confirmed that the expected reactivity of the persulfide donor scaffold was not significantly altered by the presence of the other functional groups on the penicillamine backbone. Specifically, we investigated the attack on different electrophilic sites including thiol attack at the carbonyl carbon and also at the sulfenyl sulfur atom (S^1) or sulfhydryl sulfur atom (S^2) of the perthiol (Figure 5.6a). DFT calculations were performed using a deprotonated cysteine as the model nucleophile and simplifying the structure of **1** by replacing the benzyl group with a methyl group. The values shown below were obtained with the ωB97X-D or M06-2X methods, using the aug-cc-pV(T+d)Z basis set and SMD solvation model for water, with the M06-2X results being represented in parentheses for energy tabulations below. These investigations demonstrated that nucleophilic attack by cysteine thiolate at the carbonyl carbon is kinetically favored by 3.6 (3.4) kcal mol^{-1} over attack at the S^1 site and by 5.6 (6.7) kcal mol^{-1} over attack at the S^2 site (Figure 5.6a). Additionally, we hypothesized that the bulky persulfide released from the persulfide donor would prefer transpersulfidation with the less bulky cysteine rather than direct H_2S release, whereas the less bulky cysteine persulfide could then react through the H_2S releasing pathway. To investigate this question directly, we compared the activation barriers for these two processes from the generated persulfide intermediate. We found that cysteine thiolate attack at the S^2 site, which results in transpersulfidation and formation of cysteine persulfide, was kinetically favored by 6.0 (5.2) kcal mol^{-1} over the H_2S releasing pathway occurring through attack at S^1. Although this reaction is reversible, with a positive free energy of reaction of 2.8 (3.5) kcal mol^{-1}, H_2S release from cysteine persulfide by reaction with a cysteine thiolate is the most kinetically favored (15.0 (12.8) kcal mol^{-1}) pathway of cysteine persulfide reactivity (Figure 5.6b).

To test these computational predictions experimentally, persulfide donor **1** (100 μM) was added to a solution containing **2** (1.0 mM, 10 equiv.) in PBS buffer (10 mM, pH 7.4, 10% MeCN). Excess thiol was used to ensure fast donor activation and subsequent reaction of the released

persulfide with the thiol rather than through an alternative pathway.[1179] Aliquots of the resultant solution were removed at specified timepoints, quenched with TME-IAM (10 mM, 100 equiv.), and analyzed by HPLC (Figure 5.7 and D10). Treatment with excess TME-IAM was required to measure persistent persulfides and other RSS in solution and also trap unreacted thiols that could perturb RSS equilibria. Authentic samples of trapped persulfide analogues **S4** and **S5** and side product **4** were prepared to allow for HPLC quantification (Figure D11–D15) and disulfides **7** and **8** were prepared *in situ* to confirm peak identity (Figure D16). Trapped persulfide identity was additionally confirmed by treatment of a 5-minute experiment timepoint with tris(2-carboxyethyl)phosphine (TCEP) to ablate peaks correlated with trapped persulfides as well as HPLC purification of hypothesized persulfide adduct peaks followed by MS analysis (Figure D17 and D18).

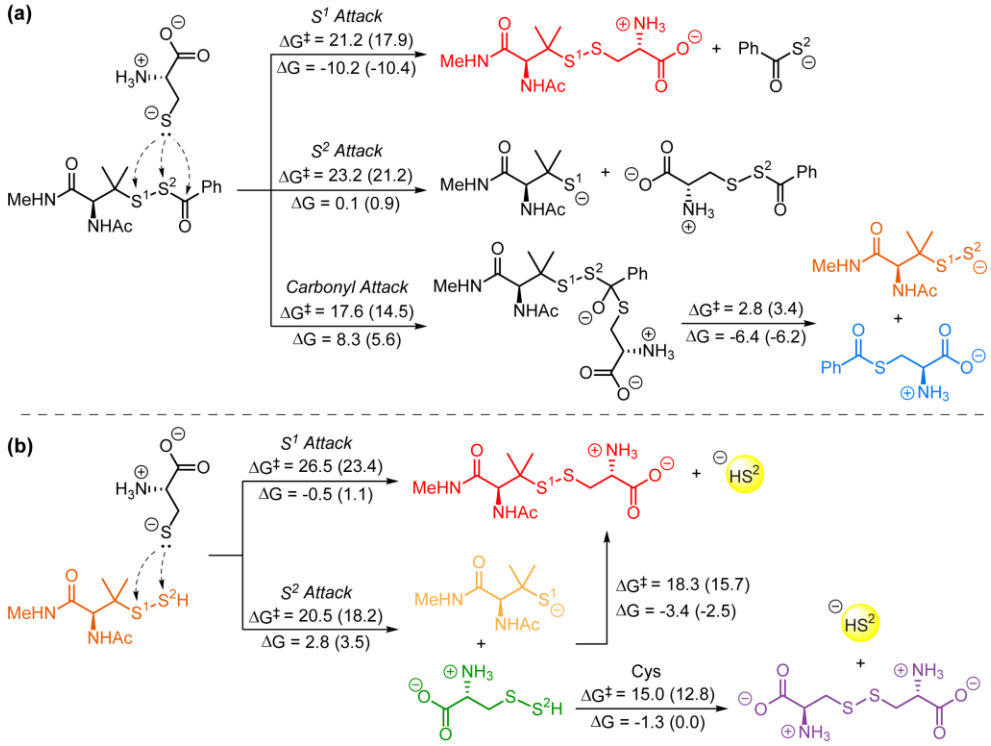


Figure 5.6. Computationally derived energetics of the reaction between the persulfide donor scaffold and cysteine thiolate at either the S^1, S^2, or carbonyl carbon position and (b) the generated penicillamine-based persulfide with cysteine thiolate at either the S^1 or S^2 positions. Calculations were performed at the ωB97X-D/aug-cc-pVDZ/SMD(water) // ωB97X-D or (M06-2X)/aug-cc-pV(T+d)Z /SMD(water) level of theory. Free energies (in kcal mol^{-1}) of reaction are relative to the preceding intermediate.

Through HPLC analysis, we showed that donor **1** was fully activated within the first minute of the experiment, with the appearance of both persulfide **3** and the expected side product **4** (Figure 5.7). The concentration of persulfide **3** then diminishes over time with concomitant growth of persulfide **6** formed from transpersulfidation, which reaches a maximum concentration at 5 minutes. Further evidence of transpersulfidation includes the appearance of tertiary thiol **5** produced during transpersulfidation. In addition, disulfides **7** and **8** are observed later in the reaction due to the reaction of persulfide **6** with either thiol **2** or **5**. It is possible that different thiols or persulfides with different pK_a values may show different initial speciation or reaction rates, based on the specific properties and relative concentrations of reactants in a specific system. Overall, this experiment shows that the more bulky penicillamine-based persulfide **3** undergoes a transpersulfidation reaction with the less bulky cysteine-based **2** to produce persulfide **6** before releasing H_2S.

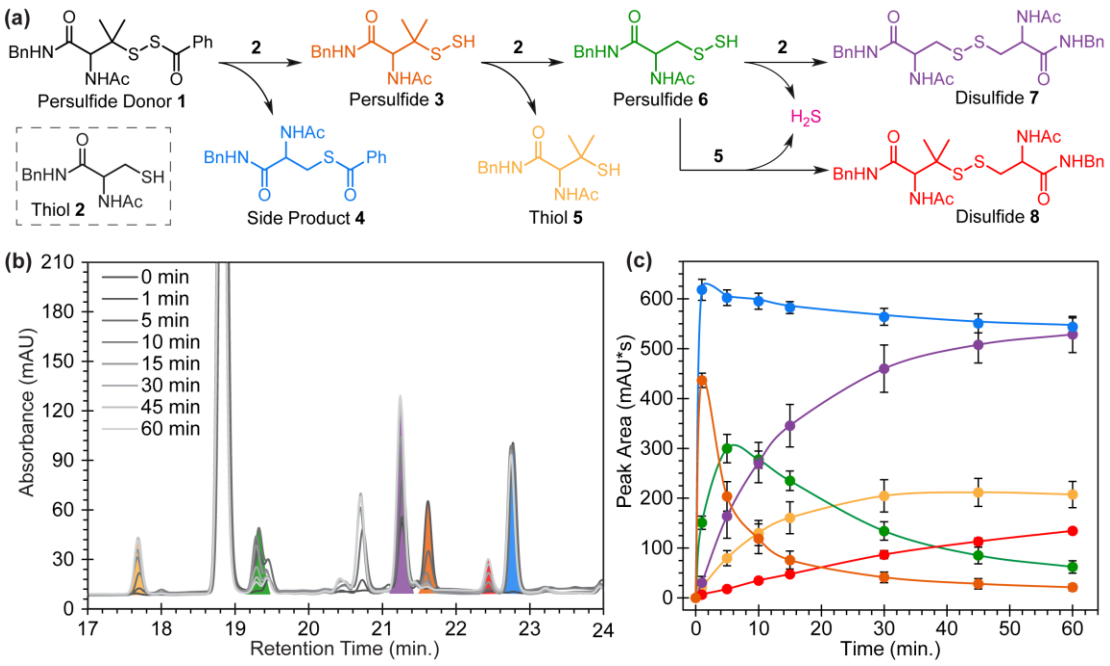


Figure 5.7. (a) Proposed reaction pathway of the persulfide donor **1** with excess **2**. After treatment with the TME-IAM trapping agent, persulfides, thiols, and other hydrosulfide species form stable adducts. (b) Stacked HPLC chromatograms of the TME-IAM trapping experiment with persulfide donor **1** (100 µM), **2** (1.0 mM), and TME-IAM (10 mM) and (c) peak area plotted of identified compounds over 60 minutes.

Having demonstrated direct experimental evidence for transpersulfidation, we next wanted to measure H_2S release, which should be generated during reaction of persulfide **6** with a thiol (Figure 5.7a). H_2S release was measured using the methylene blue H_2S assay under the same conditions used for the persulfide trapping experiments. Treatment of persulfide donor **1** (100 mM) with excess **2** resulted in 86 mM of H_2S release (86%), which reached a maximum at 45 minutes (Figure 5.8). Interestingly, although the HPLC trapping experiments showed full persulfide donor activation at 1 minute, no H_2S was observed at early reaction time points. This result suggests that H_2S release is more efficient from the less bulky persulfide and that efficient H_2S release does not occur until transpersulfidation from the tertiary to the primary persulfide occurs. As expected, when persulfide donor **1** was treated with **5** instead of **2** minimal H_2S release was observed, which is consistent with the decreased nucleophilicity of the bulkier tertiary thiol **5** (Figure 5.8b).

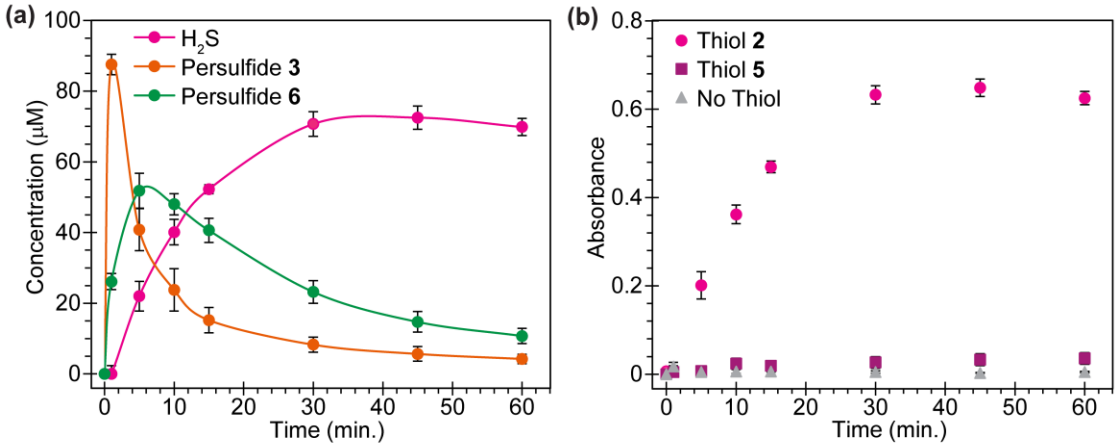


Figure 5.8. (a) Hydrogen sulfide release vs. persulfide **3** and **6** release from persulfide donor **1** (100 μM) when treated with **2** (1.0 mM) compared over 60 minutes. Persulfide **3** and **6** were quantified with a calibration curve of the persulfide adduct analogues. (b) Hydrogen sulfide release from persulfide donor **1** (100 μM) when treated with **2** (1.0 mM) or **5** (1.0 mM) monitored at 670 nm by the methylene blue H_2S assay over 60 minutes in PBS buffer (10 mM, pH 7.4).

Furthermore, in the absence of thiol, persulfide donor **1** did not release H_2S, which confirms that this donor is stable in solution until activated by a thiol. These results are particularly important in the design of persulfide donors with tertiary persulfides, such as those derived from penicillamine, because these platforms likely primarily function as transpersulfidation agents and the observed H_2S release is due to subsequent transpersulfidation to primarily thiols like Cys or

GSH. In addition, the increased pK_a of penicillamine (~10.5) when compared to primary thiols like Cys (8.5) or GSH (~8.9) also means that more of the tertiary persulfide is in the neutral, protonated, and electrophilic form at physiological pH, which further preferences reactivity through the transpersulfidation manifold.

5.3 Conclusion

Using a combined computational and experimental approach, we demonstrated the persulfide characteristics that govern transpersulfidation versus H_2S release. Our computational work demonstrated that the reaction of electrophilic persulfides with thiolates can be modulated by both steric and electronic modifications. Inclusion of electron withdrawing groups on *p*-substituted aryl persulfides increased both the kinetic and thermodynamic preference for transpersulfidation over H_2S release. Persulfides with limited steric bulk can react through either the H_2S releasing or the transpersulfidation pathways, whereas bulkier tertiary persulfides favor transpersulfidation over H_2S release. We confirmed this computational prediction using solution-based experimental transpersulfidation measurements from a tertiary penicillamine-based persulfide to generate a cysteine-based persulfide. H_2S release from the system was confirmed to derive from the resultant and less-hindered cysteine-based persulfide, which is likely the main H_2S releasing pathway for these types of penicillamine-based persulfide donors. Overall, this work revises the prior assumption that persulfides primarily react to directly release H_2S and rather can undergo transpersulfidation first followed by subsequent H_2S release. These results also suggest that the preference for transpersulfidation can be influenced by the electronic and steric components of persulfide, which is particularly relevant for applications of synthetic persulfide donors. Taken together, we anticipate that these results will not only help guide the design of future persulfide donors and bioanalytical trapping approaches, but also positively contribute to our fundamental understanding of biological persulfide reactivity within complex systems.

VI. CONCLUDING REMARKS

Overall, H_2S, persulfides, and other reactive sulfur species are biologically relevant molecules that have been discovered to be involved in the function of various biological processes. Interestingly, a change in RSS has been shown to occur with diseases although it is unclear if these changes in endogenous RSS are the cause of the disease or is a downstream effect. Because of this gap in knowledge, tools are needed to better understand and study the role of RSS in homeostasis and perturbation in biology, and donors and probes of RSS are methods of providing tools for these studies.

In this dissertation, I developed a cell-trappable H_2S probe for H_2S detection, a palette of fluorescent H_2S donors for detection of released H_2S, an esterase-activated persulfide donor scaffold, and investigated the fundamental reactivity of persulfides with thiolates. Chapter II featured the cell-trappable H_2S probe **CT-MeRhoAz** that contains an acetoxymethyl ester group to impart cell trappability. Here I showed the probe responds to H_2S with a 3000-fold fluorescence turn-on, is selective for H_2S over other biologically relevant species, and detects H_2S in live cells over a longer time scale than the analogous non-cell-trappable MeRhoAz. Chapters III and IV feature donors of RSS, with H_2S or persulfides being released, respectively. Specifically, Chapter III details a palette of fluorescence turn-on H_2S donors that span from the blue to NIR region. The synthesis, fluorescence turn-on, H_2S release, activation by thiols, and ability to release H_2S with a fluorescence signal in live cells was shown. Further, the NIR donor **5** was loaded into an alginate gel, injected subcutaneously into live rats, and then imaged to show a fluorescence turn-on through the skin, being the first study with a H_2S donor being imaged subcutaneously in non-transparent organisms. Utilizing the same perthioester group, Chapter IV details the synthesis and investigation of esterase-activated persulfide donors where the donor scaffold was modified to determine if structural changes could be used to alter persulfide release. The kinetics of persulfide release and side reactivity of the donor scaffold was investigated, but more interestingly a modified FDNB trapping assay was used to show the bulky, *tert*-butyl persulfide had an increased persistence in solution over other less bulky persulfides. This study inspired the work details in Chapter V where the reactivity between persulfides and thiols were computationally and experimentally investigated. With DFT calculations, we demonstrated that increasing steric bulk or electron withdrawal near the persulfide can direct persulfide reactivity through the

transpersulfidation pathway. Experimentally, we used a persulfide donor and persulfide trapping agent to experimentally monitor and measure transpersulfidation from a bulky penicillamine-based persulfide to a cysteine-based thiol, which is the first direct observation of transpersulfidation between low molecular weight species.

APPENDIX A

SUPPLEMENTARY CONTENT FOR CHAPTER II

Appendix A is the supplementary appendix for Chapter II of this dissertation. It includes all spectra and experimental information relevant to the material in Chapter II.

*Molar Absorptivity of **CT-MeRhoAz** and **CT-MeRho***

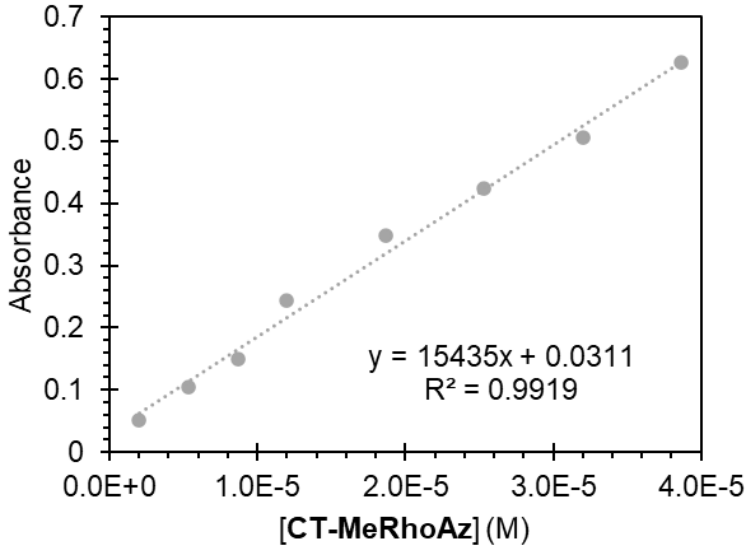


Figure A1. Molar absorptivity determination with 2.0, 5.3, 8.7, 12.0, 18.7, 25.3, 32.0, and 38.7 nM **CT-MeRhoAz** at 286 nm in 50 mM PIPES buffer (100 mM KCl, pH 7.4).

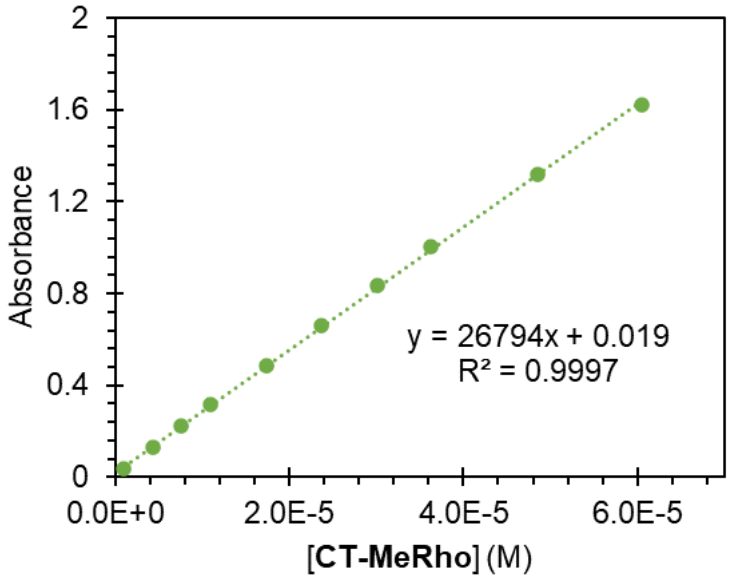


Figure A2. Molar absorptivity determination with 1.0, 4.3, 7.6, 10.9, 17.4, 23.8, 30.1, 3.63, 4.85, and 60.4 nM **CT-MeRho** at 480 nm in 50 mM PIPES buffer (100 mM KCl, pH 7.4).

*Detection Limit of **CT-MeRhoAz***

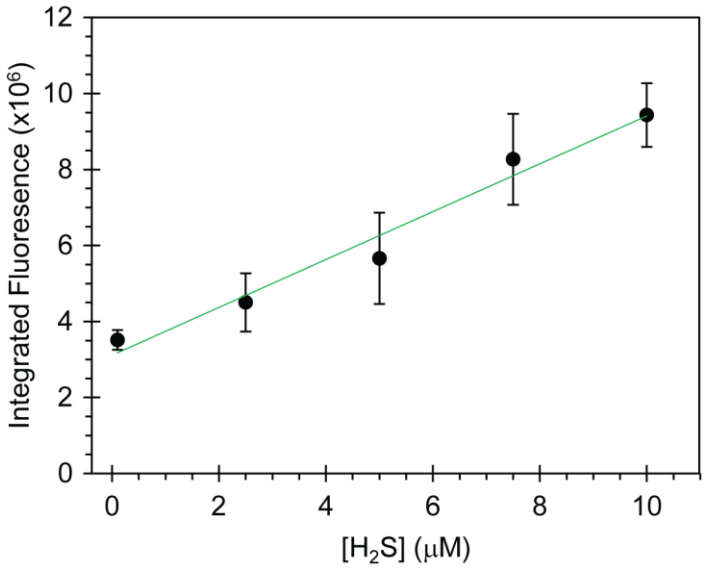


Figure A3. Fluorescence turn-on response of **CT-MeRhoAz** (5 μM) incubated with 10, 7.5, 5.0, 2.5, and 0.1 μM NaSH in 50 mM PIPES buffer (100 mM KCl, pH 7.4) at 37 °C for 90 minutes. λ_{ex} = 480 nm, λ_{em} = 490–640 nm. Slit width: 0.4 mm. The experiments were performed in triplicate and results are expressed as mean ± SD (n = 3).

*Tabulated Integrated Fluorescence of **CT-MeRhoAz** Detection Limit*

Table A1. Tabulated integrated fluorescence values for detection limit determination of **CT-MeRhoAz** (5 μM) incubated with 10, 7.5, 5.0, 2.5, 0.1, and 0 μM NaSH in 50 mM PIPES buffer (100 mM KCl, pH 7.4) at 37 °C for 90 minutes. λ_{ex} = 480 nm, λ_{em} = 490–640 nm. Slit width: 0.4 mm. The experiments were performed in triplicate.

[H_2S] (μM)	Integrated Fluorescence	Standard Deviation
10	9431385	838286
7.5	8269222	1198115
5.0	5661683	1203733
2.5	4503959	765610
0.1	3516142	255550
Blank	310695	31145

*Fluorescence Turn-on Response of **CT-MeRhoAz** with H_2S and Esterase*

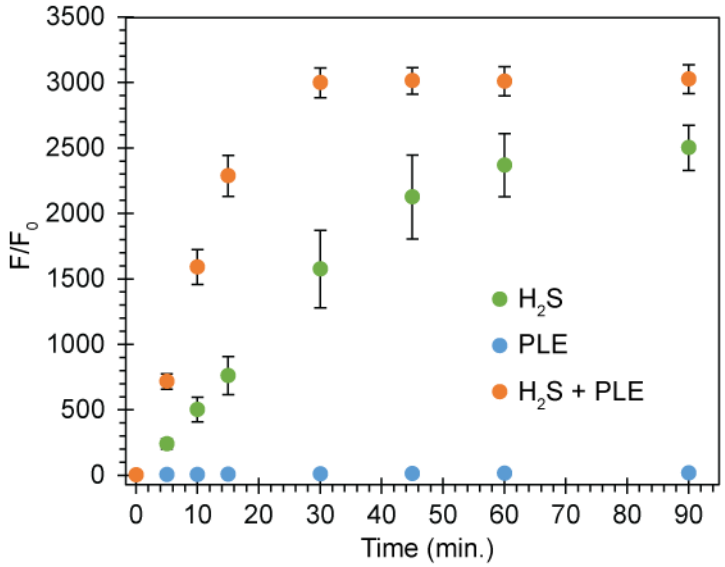


Figure A4. Comparison of the fluorescence turn-on response of **CT-MeRhoAz** with either NaSH (250 μM), PLE (5.0 U mL^{-1}), or with both NaSH (50 μM) and PLE (5.0 U mL^{-1}) in 50 mM PIPES buffer (100 mM KCl, pH 7.4) at 37 °C for 90 minutes. λ_{ex} = 480 nm, λ_{em} = 490–640 nm. Slit width: 0.4 mm. The experiments were performed in triplicate and results are expressed as mean ± SD (n = 3).

*Fluorescent Signal of Selectivity Experiments with **CT-MeRhoAz***

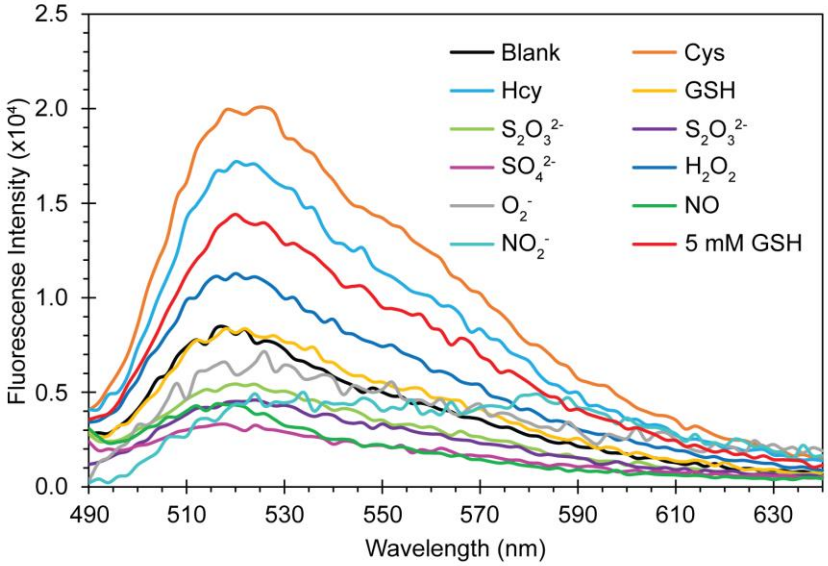


Figure A5. Fluorescence intensity of **CT-MeRhoAz** (5 μM) incubated with various analytes (250 μM, 50 equiv.) in 50 mM PIPES buffer (100 mM KCl, pH 7.4) at 37 °C after 90 minutes. λ_{ex} = 480 nm, λ_{em} = 490–640 nm. Slit width: 0.4 mm.

*Cell Experiments with **CT-MeRhoAz***

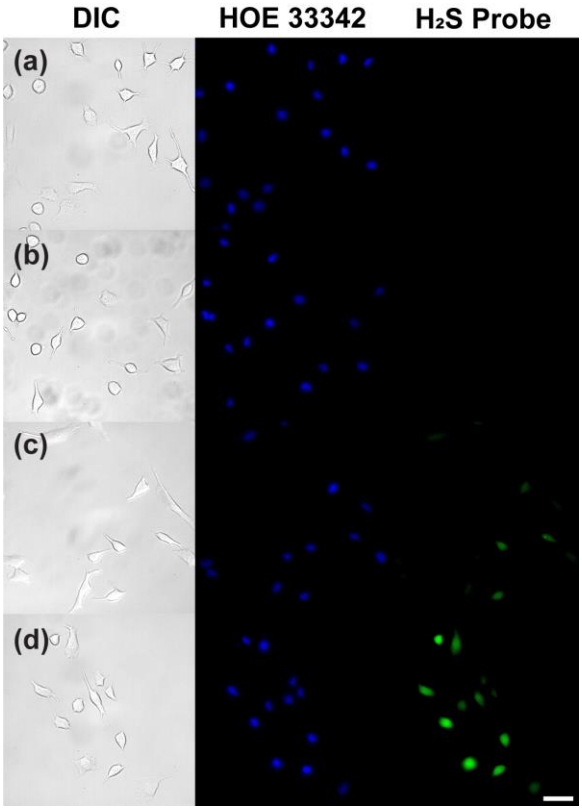


Figure A6. Fluorescence imaging of **CT-MeRhoAz** in HeLa cells. Cells were incubated with Hoechst 33342 (5 μM) and (a) vehicle, (b) NaSH (200 μM), (c) **CT-MeRhoAz** (5 μM), or (d) **CT-MeRhoAz** (5 μM) and NaSH (200 μM). Cells were incubated with vehicle for 45 minutes, the vehicle or **CT-MeRhoAz** for 45 minutes, and then either the vehicle or NaSH and Hoechst 33342 for 45 minutes followed by imaging. Bar scale: 50 μm.

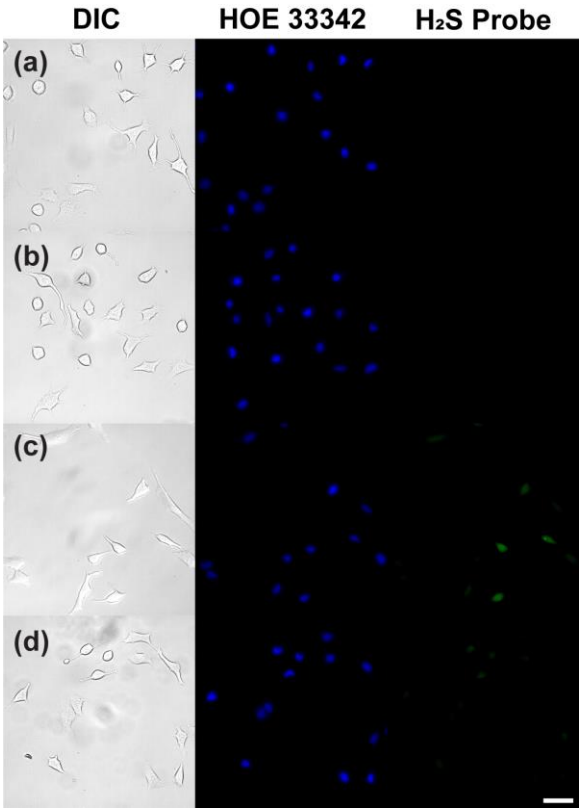


Figure A7. Fluorescence imaging of **CT-MeRhoAz** in HeLa cells. Cells were incubated with Hoechst 33342 (5 μM) and (a) vehicle, (b) AOAA (20 μM), (c) **CT-MeRhoAz** (5 μM), or (d) AOAA (20 μM) and **CT-MeRhoAz** (5 μM). Cells were incubated with either vehicle or AOAA for 45 minutes, the vehicle or **CT-MeRhoAz** for 45 minutes, and then the vehicle and Hoechst 33342 for 45 minutes followed by imaging. Bar scale: 50 μm.

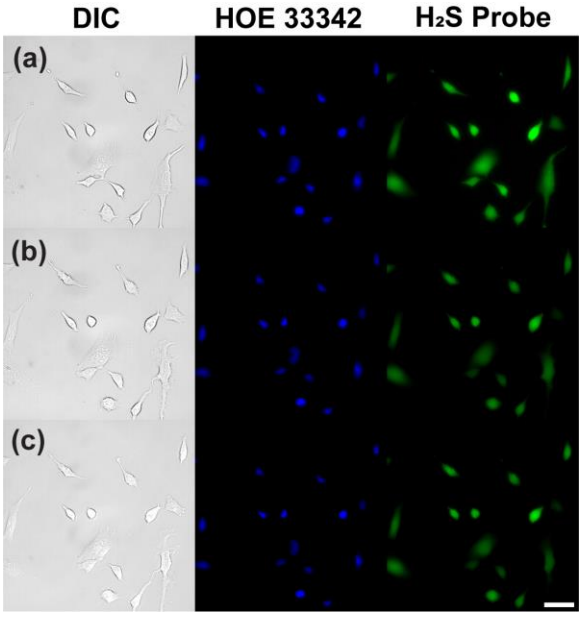


Figure A8. Cell trapping experiment with **CT-MeRhoAz** in HeLa cells. Cells were incubated with AP39 (100 nM) for 1 hour, washed, and then incubated with **CT-MeRhoAz** (5 μM) for 45 minutes. Cells were washed with fresh media every 10 minutes and cells were imaged at (a) 5 minutes, (b) 30 minutes, and (c) 60 minutes. Bar scale: 50 μm.

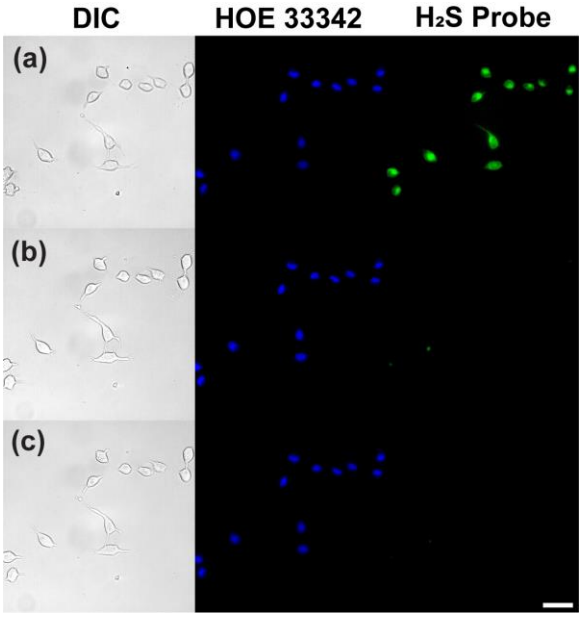


Figure A9. Cell trapping experiment with **MeRhoAz** in HeLa cells. Cells were incubated with AP39 (100 nM) for 1 hour, washed, and then incubated with **MeRhoAz** (5 μM) for 45 minutes. Cells were washed with fresh media every 10 minutes and cells were imaged at (a) 5 minutes, (b) 30 minutes, and (c) 60 minutes. Bar scale: 50 μm.

*Quantified Fluorescence of Cell Trapping with **CT-MeRhoAz** and **MeRhoAz***

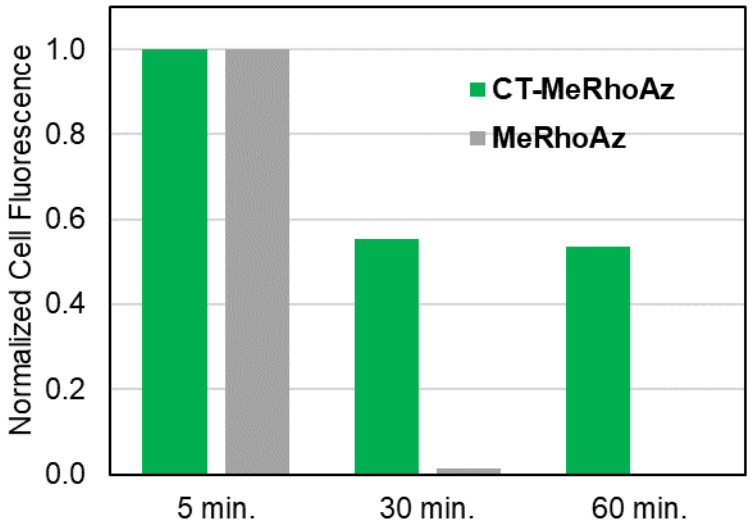


Figure A10. Quantified and normalized cell fluorescence at 5, 30, and 60 minutes for both **CT-MeRhoAz** and **MeRhoAz**.

^{1}H and ^{13}C NMR Spectra of Synthesized Compounds

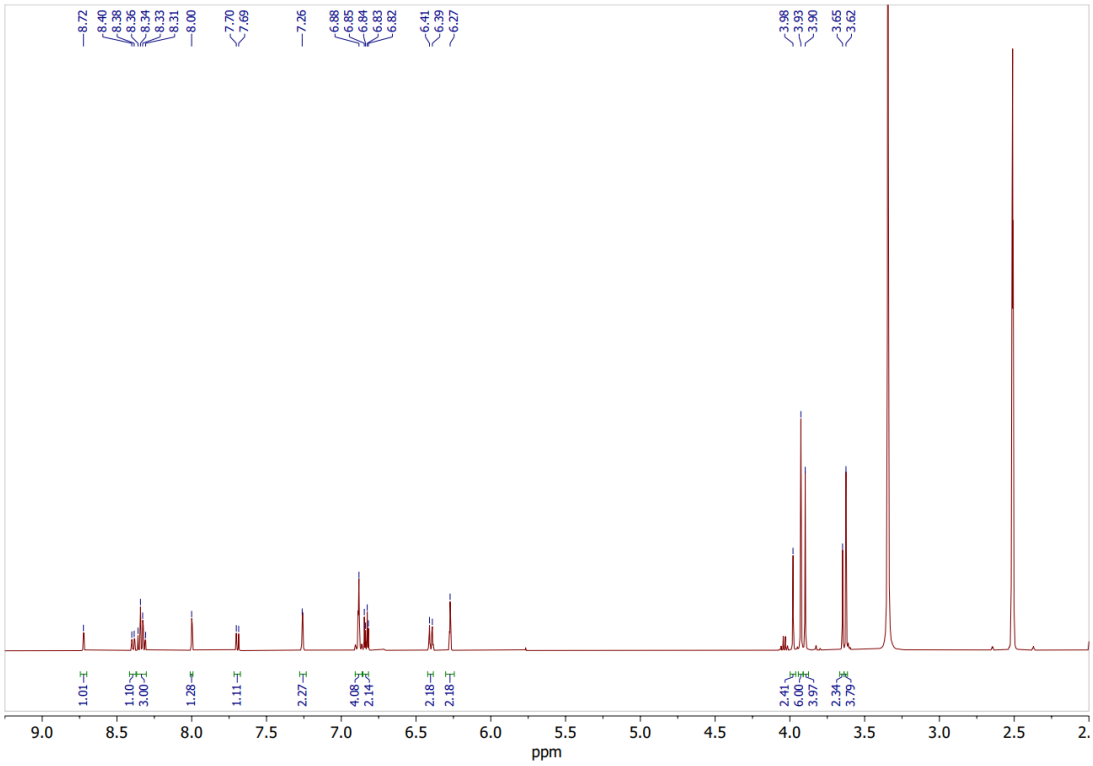


Figure A11. ^{1}H NMR (500 MHz, DMSO-d_6) spectrum of **1**.

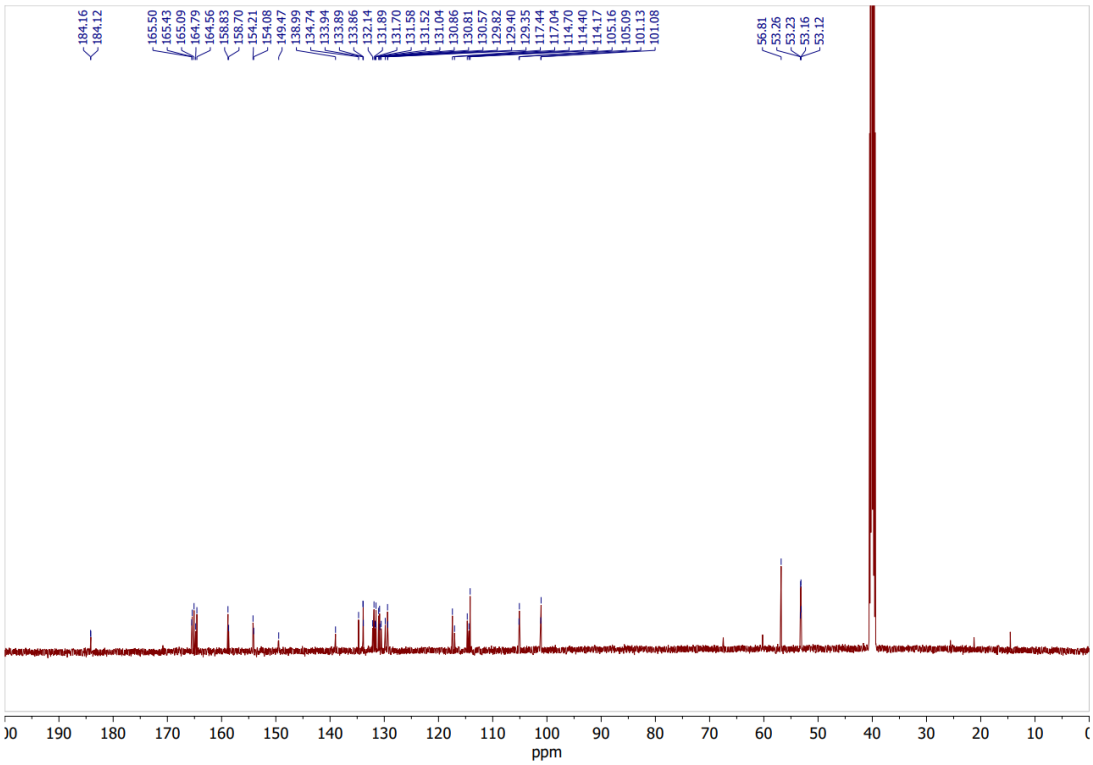


Figure A12. $^{13}C\{^{1}H\}$ NMR (125 MHz, DMSO-d_6) spectrum of **1**.

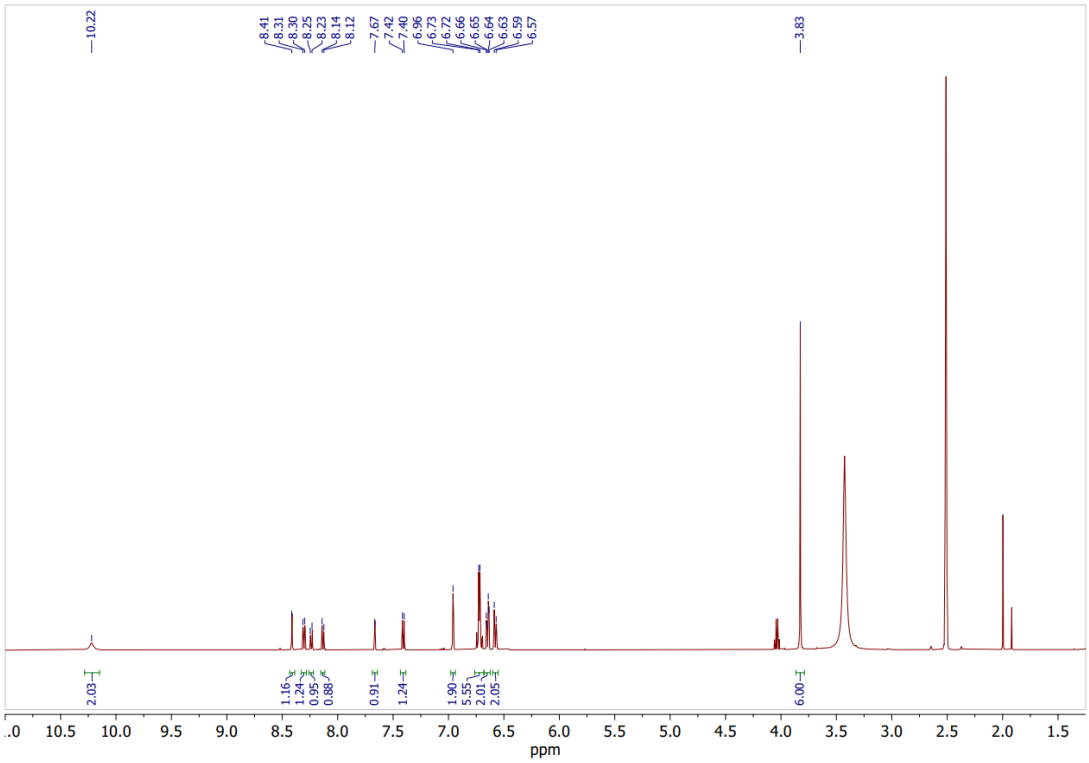


Figure A13. ^{1}H NMR (500 MHz, DMSO-d_6) spectrum of **2**.

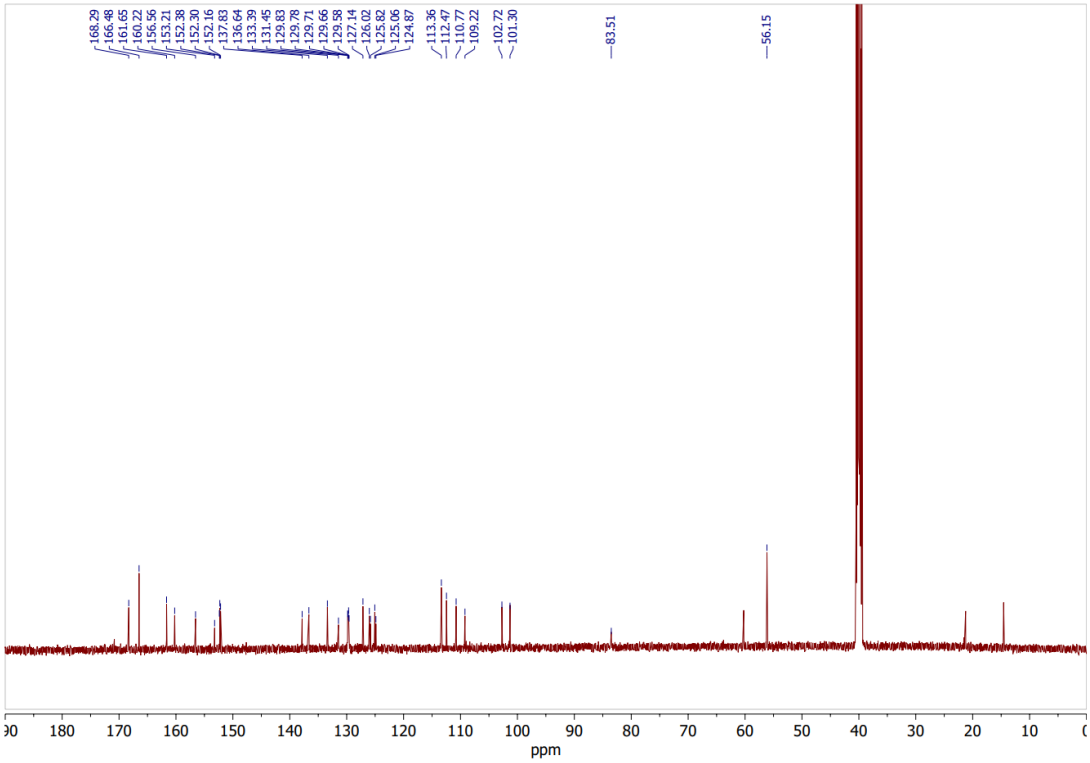


Figure A14. $^{13}C\{^{1}H\}$ NMR (125 MHz, DMSO-d_6) spectrum of **2**.

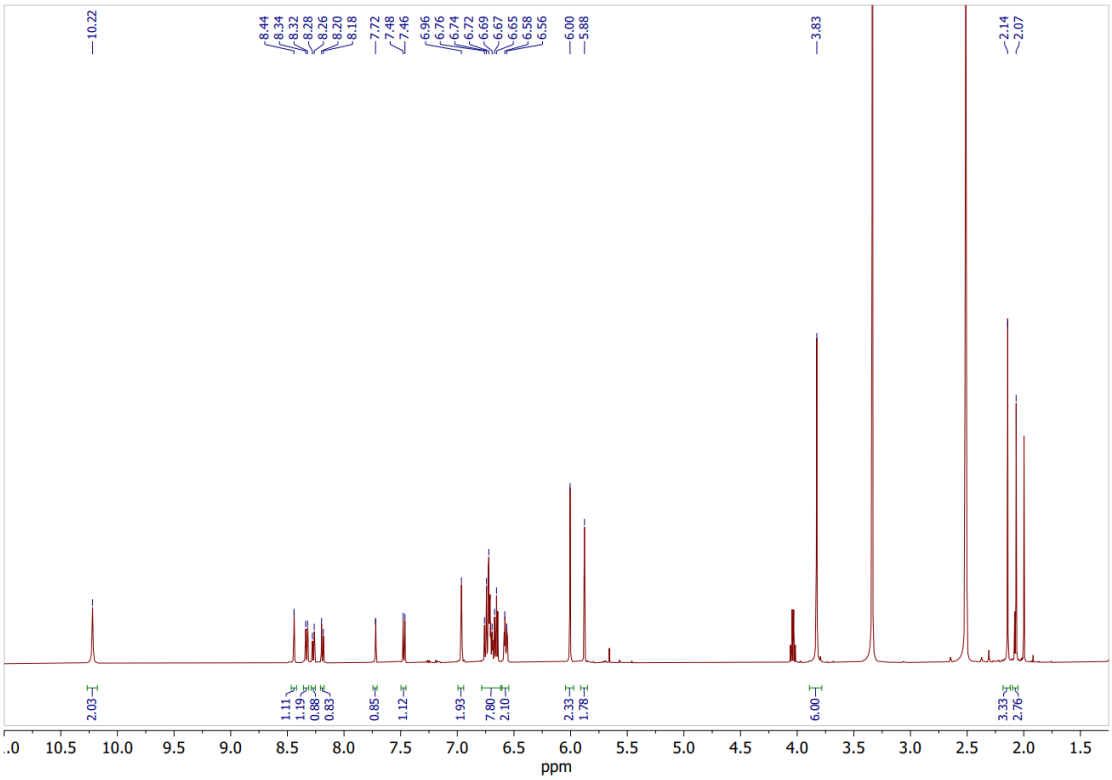


Figure A15. ^{1}H NMR (500 MHz, DMSO-d_6) spectrum of **3**.

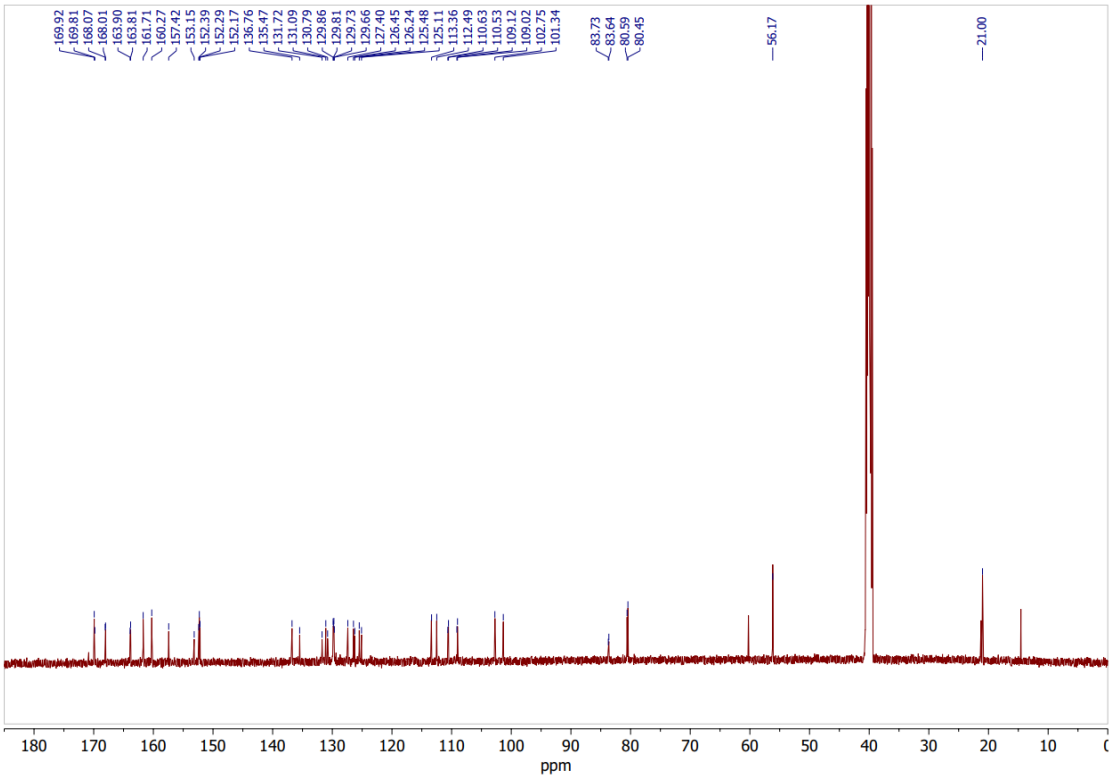


Figure A16. $^{13}C\{^{1}H\}$ NMR (125 MHz, DMSO-d_6) spectrum of **3**.

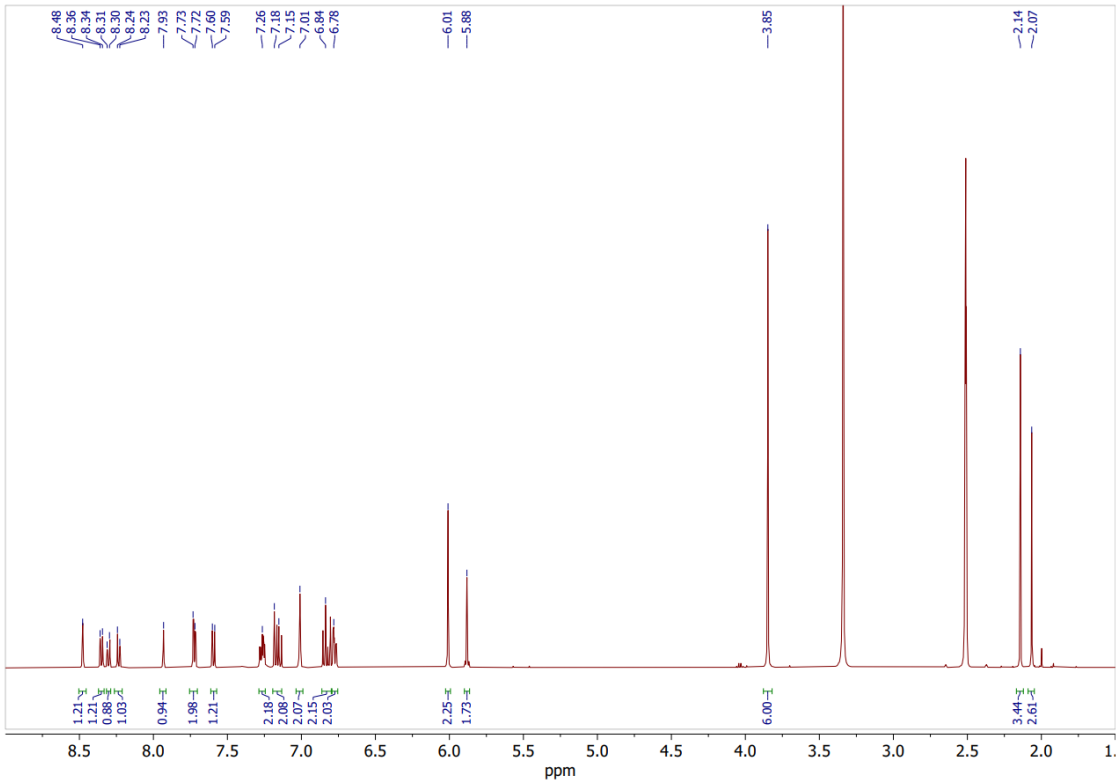


Figure A17. ^{1}H NMR (500 MHz, DMSO-d_6) spectrum of **4**.

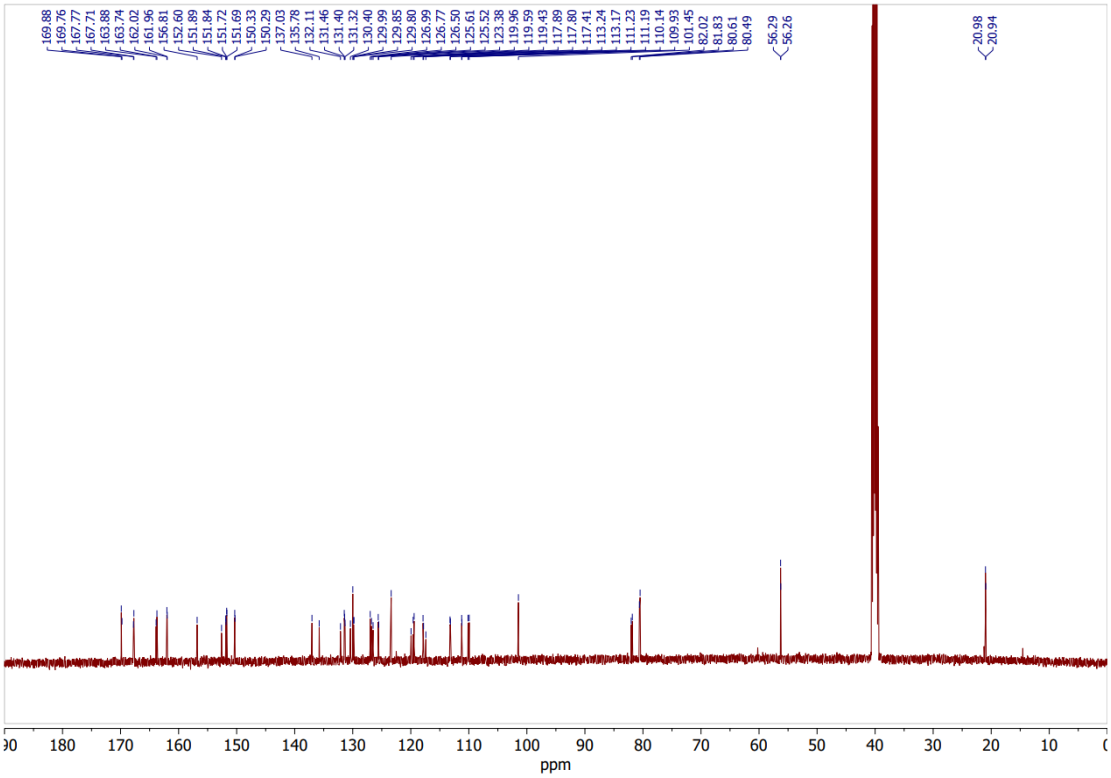


Figure A18. $^{13}C\{^{1}H\}$ NMR (125 MHz, DMSO-d_6) spectrum of **4**.

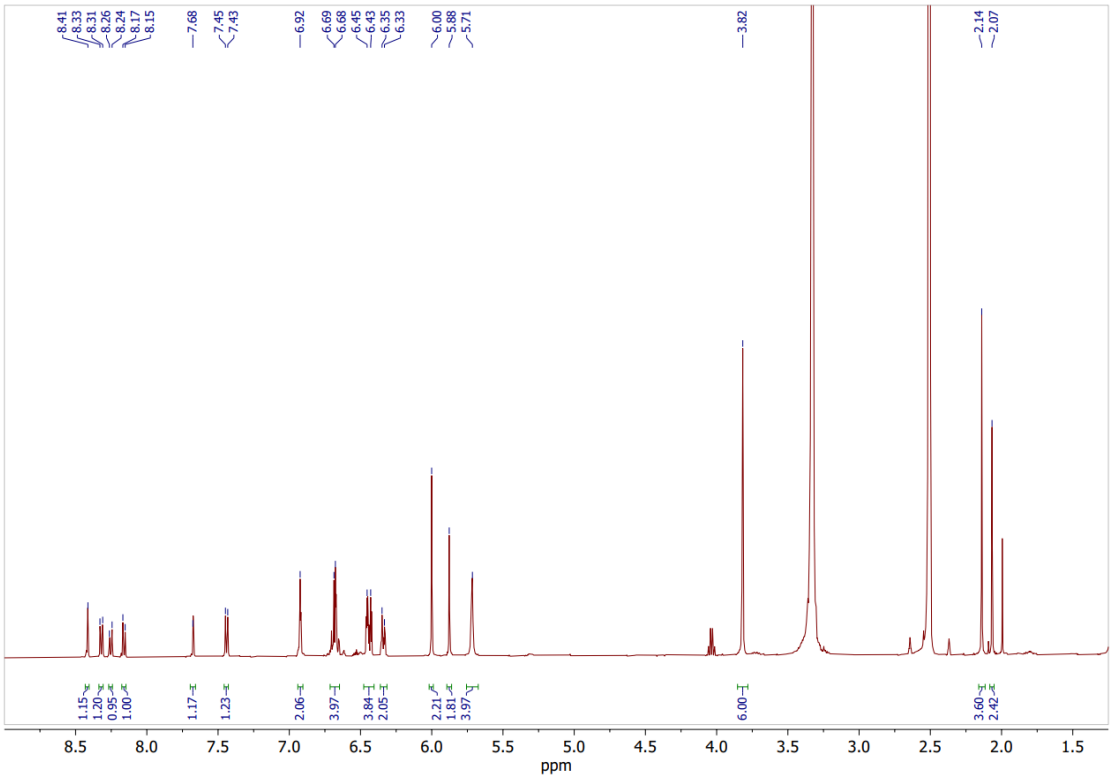


Figure A19. ^{1}H NMR (500 MHz, DMSO-d_6) spectrum of **CT-MeRho**.

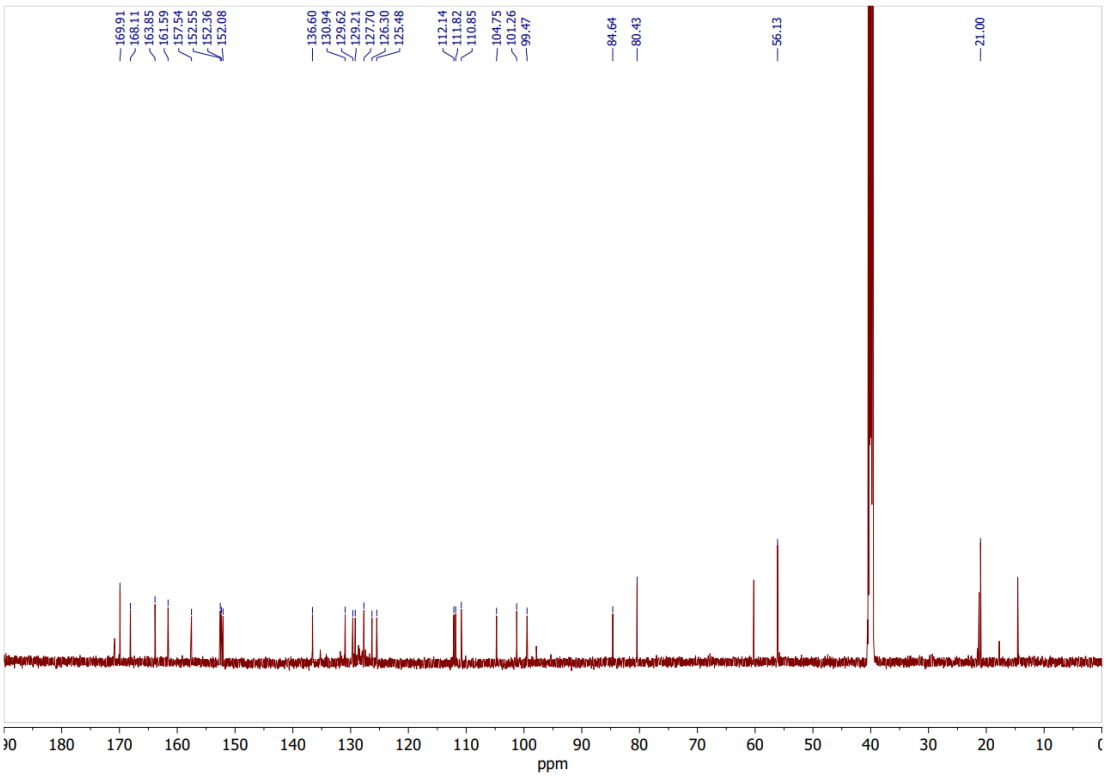


Figure A20. $^{13}C\{^{1}H\}$ NMR (150 MHz, DMSO-d_6) spectrum of **CT-MeRho**.

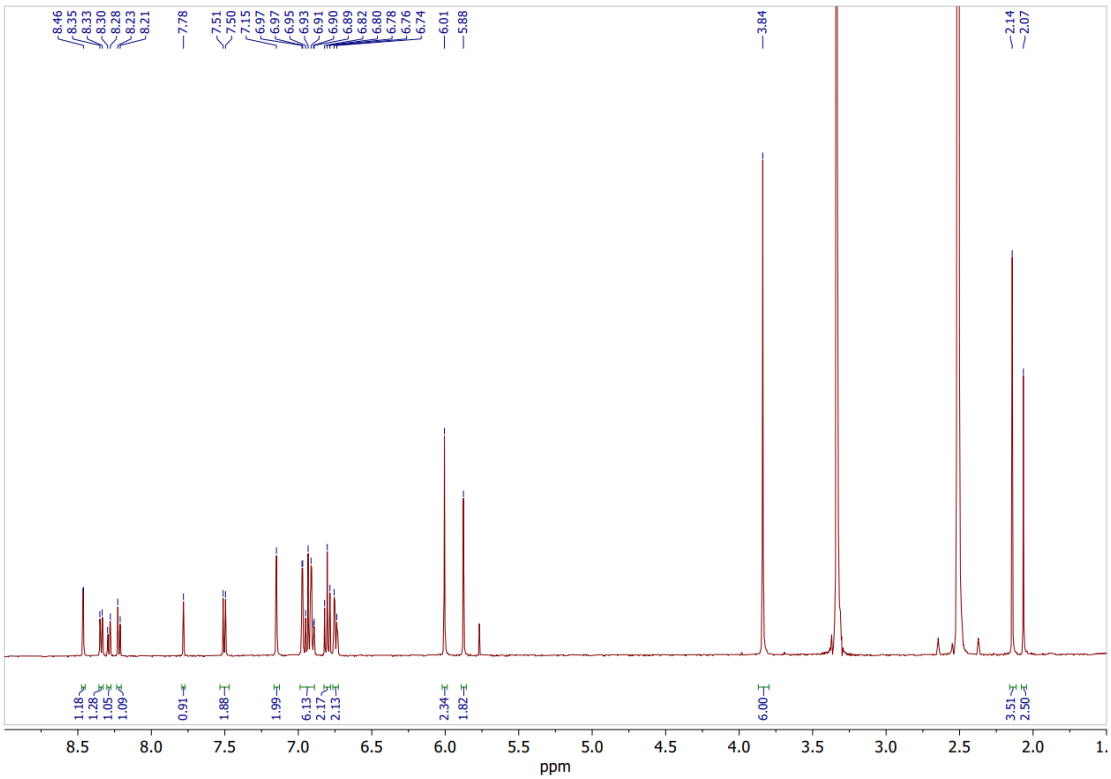


Figure A21. ^{1}H NMR (500 MHz, DMSO-d_6) spectrum of **CT-MeRhoAz**.

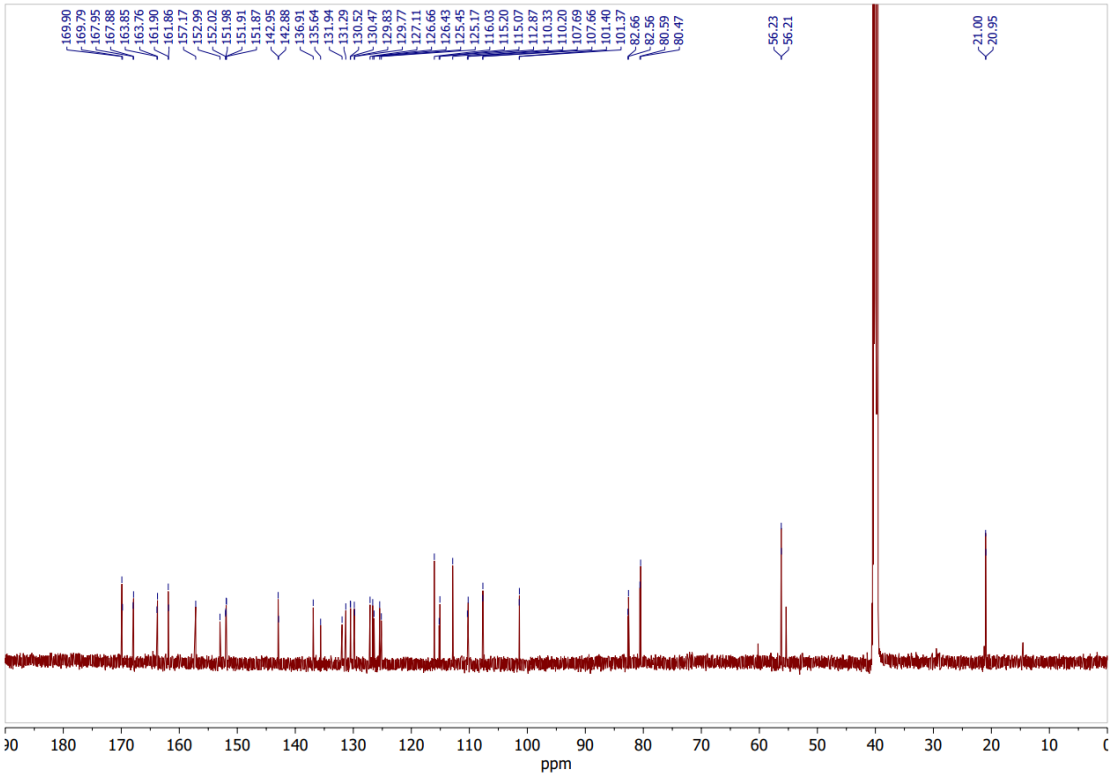


Figure A22. $^{13}C\{^{1}H\}$ NMR (125 MHz, DMSO-d_6) spectrum of **CT-MeRhoAz**.

APPENDIX B

SUPPLEMENTARY CONTENT FOR CHAPTER III

Appendix B is the supplementary appendix for Chapter III of this dissertation. It includes all spectra and experimental information relevant to the material in Chapter III.

Methods and Materials

Reagents were purchased from Sigma-Aldrich, Tokyo Chemical Industry (TCI), Fisher Scientific, Combi-Blocks, and VWR and used directly as received. Silica gel (SiliaFlash F60, Silicycle, 230−400 mesh) was used for column chromatography. Deuterated solvents were purchased from Cambridge Isotope Laboratories (Tewksbury, Massachusetts, USA). ^{1}H and $^{13}C\{^{1}H\}$ NMR spectra were recorded on Bruker 500 MHz NMR instruments at the indicated frequencies. Chemical shifts are reported in ppm relative to residual protic solvent resonances. Mass spectrometric measurements were performed by the University of Illinois, Urbana Champaign MS facility or on a Xevo Waters ESI LC/MS instrument. Fluorescence spectra were measured on a Photon Technology International fluorimeter and absorbance spectra were measured on an Agilent Cary 60 UV-Vis spectrophotometer. H_2S release was quantified on a Unisense electrode.

All surgical procedures were conducted according to the University of Oregon Institutional Animal Care and Use Committee protocols. The experiments were conducted under the approved protocol “IPROTO2023-0014 - Stimuli-Responsive Biomaterials”.

General Procedure for Fluorescence Measurements

A stock solution of donors **1**–**5** (3 μL, 10 mM in MeCN) was added to 3 mL of PBS buffer (10 mM, pH 7.4) in a septum-capped cuvette along with CA (3 μL, 25 mg mL^{-1}). To start the experiment, a stock solution of cysteine (6 μL, 50 mM) was added. Scans were taken at 0, 1, 3, 5, 7, 10, 15, 20, 25, 30, 40, 50, 60, 75, 90, and 120 minutes after injection. The experiments were completed in triplicate.

General Procedure for Selectivity Experiments

A stock solution of donor **1** (3 μL, 10 mM in MeCN) was added to 3 mL of PBS buffer (10 mM, pH 7.4) in a septum-capped cuvette. To start the experiment, a stock solution of the analyte (6 μL, 50 mM) was added. Scans were taken initially before analyte injection and then 120 minutes after the injection. The experiments were completed in triplicate.

General Procedure for H_2S Release Measurements via Electrode

The Unisense electrode was inserted through a rubber stopper into a 20 mL vial of PBS buffer (10 mM, pH 7.4) under N_2. Stock solutions of donors **1**–**3** or **5** (20 μL, 10 mM in MeCN) and CA (20 μL, 25 mg mL^{-1}) were added, and the electrode signal was allowed to equilibrate (~5 minutes). To start the experiment, a stock solution of cysteine (40 μL, 50 mM) was added, and the signal was measured over 120 minutes. The experiments were completed in triplicate and electrode H_2S calibration curves were conducted the same day as experiments.

*Methylene Blue Assay H_2S Release Measurement with Donor **4***

A stock solution of **4** (6 μL, 100 mM in MeCN) was added to 20 mL of degassed 1.0 mM CTAB in PBS buffer (10 mM, pH 7.4, 20% MeCN) containing CA (50 μg mL^{-1}). To start the experiment, a stock solution of cysteine (40 μL, 200 mM) was added. At 0, 1, 5, 10, 15, 20, 30, 45, 60, 80, 100, 120, 150 and 180 minutes 350 μL aliquots were taken and placed in cuvettes containing 350 μL of 2:2:1 iron (III) chloride/N,N-dimethyl-p-phenylenediamine/zinc acetate and then filtered. After 1 hour the absorbance at 745 nm was measured using a UV-Vis spectrophotometer and was converted to H_2S concentration by using an H_2S calibration curve.

*Titration of NIR Donor **5** with Cysteine*

A stock solution of donor **5** (3 μL, 10 mM in MeCN) was added to 3 mL of 1.0 mM CTAB in PBS buffer (10 mM, pH 7.4) in a septum-capped cuvette and the fluorescence was measured. To start the experiment, a stock solution of Cys (1.0 mM) was slowly titrated into the cuvette and scans were taken after each Cys addition.

Quantum Yield Measurement

Quantum yields of S5, **4**, S9, and **5** were determined according to published standard methods and are presented relative to rhodamine 101 (Φ = 0.951) and 1,1′,3,3,3′,3′-hexamethylindotricarbocyanine iodide (Φ = 0.3), respectively.

*Stability of Blue Donor **1** in Alginate Hydrogel*

A 500 μL 2% (w/v) alginate hydrogel was prepared by mixing 250 μL of 4% (w/v) sodium alginate dissolved in PBS (10 mM, pH 7.4) with 250 μL of 50 mM $CaCl_2$ loaded with 10 μM blue donor **1**. The hydrogel was incubated for 20-minute increments in 3.5 mL PBS buffer followed by removal/replacement of the buffer. Fluorescence of the incubated buffer was monitored (1) after initial hydrogel formation, (2) soak with no agitation, (3) addition of Cys (100 μM), and then followed by (4) addition of 10 equiv. Cys (100 μM) with sonication.

Cell Culture and Imaging Experiments

HeLa cells (ATCC CCL-2) were cultured in high glucose Dulbecco's modified Eagle's medium (DMEM) supplemented with 10% fetal bovine serum (FBS) and 1% penicillin/streptomycin (PS) at 37 °C under 5% CO_2. Cells were seeded in 32 mm culture dish at 1.0 x 10^5 cells per well and allowed to adhere for 24 hours prior to fluorescence imaging studies. Cells were then washed with 1x Phosphate Buffered Saline (2 x 2 mL) and treated with 2 mL of DMEM containing a nuclear dye (Hoechst 3342 or NucRed) and either the vehicle (DMSO), CT-MeRhoAz (2.5 μM), H_2S donor (20–50 μM), or both the CT-MeRhoAz (2.5 μM) and H_2S donor (20–50 μM). After a 20-minute incubation, cells were washed with 1x Phosphate Buffered Saline (2 x 2 mL) and then the media was replaced with 2 mL of FluoroBrite DMEM. Cell imaging was performed on a Zeiss LSM 880 confocal microscope using a 40x objective. All images were processed using LasX.

*In Vivo Visualization of NIR Fluorescent COS/H_2S-Releasing Donor **5***

The efficacy of NIR donor **5** *in vivo* was assessed by subcutaneous injection in rats and subsequent in vivo imaging. The 2% (w/v) injectable sodium alginate hydrogels were prepared by mixing 200 μL of 4% (w/v) sodium alginate dissolved in PBS (10 mM, pH 7.4) with 200 μL of 50

mM $CaCl_2$ dissolved in a 1:9 DMSO:PBS solution. Donor-containing hydrogels were prepared by supplementing the DMSO in the $CaCl_2$ solution with **5** for a final concentration of 250 μM. To ensure sterility, all solutions were sterile syringe filtered using a 0.2 mm filter and handled in a biosafety cabinet using aseptic technique and single use syringes and needles.

Male Sprague Dawley (Charles River Laboratory) rats (5-7 weeks) on an alfalfa-free diet were anesthetized with isoflurane and shaved. 400 mL alginate hydrogels were injected using a 18G needle in the subcutaneous shoulder or hip space of the rats and imaged using a Perkin Elmer Spectrum In Vivo Imaging System (IVIS). **5** was visualized using 675 nm excitation and 760 nm emission filters with a small aperture setting. Subsequently, rats were administered 200 mL of 1 mM sterile glutathione solution (GSH) via tail vein injection using a 25 G needle. Fluorescent images were taken for 3 hours after the tail vein injection. Regions of interest (ROIs) were drawn to contour each hydrogel.

Synthetic Procedures

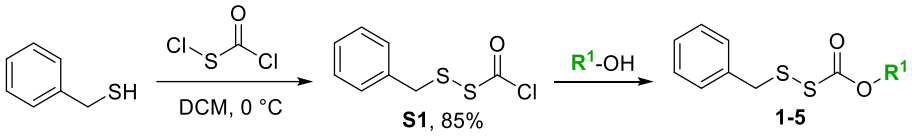


Figure B1. Synthetic route for **S1** and fluorescence turn-on COS/H_2S donors **1**–**5**.[1081]

Compound **S1**. Dichloromethane (10 mL) was cooled to 0 °C in an ice bath, and then benzyl mercaptan (432 mL, 3.69 mmol, 1.0 equiv.) followed by chlorocarbonylsulfenyl chloride (311 mL, 3.69 mmol, 1.0 equiv.) were added dropwise. The reaction mixture was stirred for 1 hour, the solvent was removed under vacuum, and then the crude material was purified by column chromatography (5% ethyl acetate in hexanes) to isolate the final product as a colorless liquid (685.6 mg, 85.0%). ^{1}H NMR (500 MHz, CD_2Cl_2) δ (ppm): 7.39 (m, 5H), 4.14 (s, 2H). $^{13}C\{^1H\}$ NMR (125 MHz, CD_2Cl_2) δ (ppm): 166.6, 135.6, 129.9, 129.2, 128.6, 43.7.

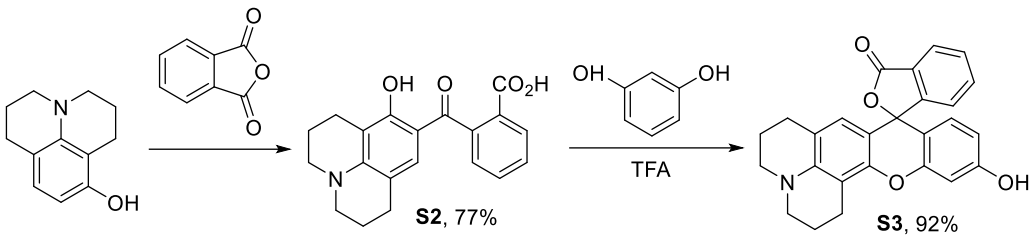


Figure B2. Synthetic route of **S2** and **S3** to yield the yellow-emitting fluorophore.[1082]

Compound **S2**. Phthalic anhydride (197.8 mg, 1.34 mmol, 1.0 equiv.) and 8-hydroxyjulolidine (255.8 mg, 1.35 mmol, 1.0 equiv.) were dissolved in 12 mL of toluene. The reaction mixture was refluxed at 110 °C for 24 hours. The solvent was removed under vacuum, and then **S2** was isolated after purification by column chromatography (5% methanol in dichloromethane as the eluent) as a yellow solid (348.9 mg, 77.44%). ^{1}H NMR (500 MHz, CD_2Cl_2) δ (ppm): 12.78 (s, 2H), 8.07 (d, *J* = 7.7 Hz, 1H), 7.64 (t, *J* = 7.5 Hz, 1H), 7.55 (t, *J* = 7.5 Hz, 1H), 7.34 (d, *J* = 7.5 Hz, 1H), 6.48 (s, 1H), 3.25 (m, 4H), 2.70 (t, *J* = 6.4 Hz, 2H), 2.46 (t, *J* = 6.3 Hz, 2H), 1.93 (p, *J* = 6.2 Hz, 2H), 1.85 (p, *J* = 6.1 Hz, 2H). ^{13}C{^{1}H} NMR (125 MHz, $CDCl_3$) δ (ppm): 169.3, 160.9, 148.9, 141.4, 132.6, 131.3, 130.5, 129.2, 128.5, 128.0, 113.2, 77.2, 61.0, 50.4, 50.0, 27.4, 21.7, 21.2, 20.8, 20.0, 14.3. HRMS m/z $[M + H]^+$ calcd. for $[C_{20}H_{20}NO_4]^+$ 338.1387; found 338.1390.

Compound **S3**. Resorcinol (82.6 mg, 0.75 mmol, 1.0 equiv.) and **S2** (250.0 mg, 0.74 mmol, 1.0 equiv.) were dissolved in 1.5 mL of methane sulfonic acid in a pressure flask and then stirred for 3 hours at 90 °C. After cooling to room temperature, the reaction mixture was basified with 1.0 M NaOH. The solvent was removed under vacuum, and then the crude product was purified by column chromatography (4.5:4.5:2 EtOAc:DCM:MeOH as the mobile phase) to isolate **S3** as a red solid (350.5 mg, 91.8%). ^{1}H NMR (500 MHz, $(CD_3)_2SO$) δ (ppm): 7.97 (d, *J* = 7.6 Hz, 1H), 7.66 (m, 2H), 7.18 (d, *J* = 7.4 Hz, 1H), 6.51 (m, 2H), 6.39 (d, *J* = 8.9 Hz, 1H), 6.13 (s, 1H), 3.21 (t, J = 5.6 Hz, 2H), 3.17 (t, *J* = 5.6 Hz, 2H), 2.85 (t, *J* = 6.5 Hz, 2H), 1.94 (m, 2H), 1.78 (m, 2H). ^{13}C{^{1}H} NMR (125 MHz, $(CD_3)_2SO$) δ (ppm): 175.5, 172.7, 168.9, 148.0, 145.2, 133.4, 129.4, 126.1, 125.6, 124.6, 117.5, 110.4, 105.8, 102.5, 49.2, 48.7, 39.5, 26.8, 21.9, 21.1, 20.4. HRMS m/z $[M + H]^+$ calcd. for $[C_{26}H_{22}NO_4]^+$ 412.1543; found 412.1539.

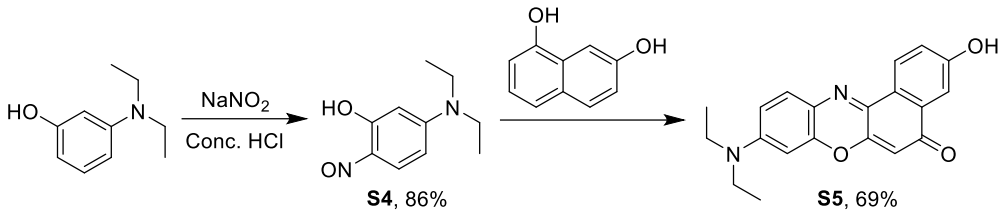


Figure B3. Synthetic route of **S4** and **S5** to yield the red-emitting fluorophore.[1083]

Compound **S4**. *N*,*N*-Diethyl-3-aminophenol (1.500 g, 9.08 mmol, 1.0 equiv.) was dissolved in a mixture of deionized water (2.0 mL) and concentrated hydrochloric acid (3.5 mL). The solution was cooled to 0 °C, and a solution of sodium nitrite (0.6225 g, 9.02 mmol, 1.0 equiv.) in deionized water (5 mL) was added dropwise over 30 minutes. The solution was then stirred at 0 °C for 3 hours. The solution was then filtered to yield **S4** as a brown solid (1.5135 g, 85.84%). ^{1}H NMR (500 MHz, $(CD_3)_2SO$) δ (ppm): 7.29 (d, *J* = 9.9 Hz, 1H), 6.88 (d, *J* = 12.5 Hz, 1H), 5.74 (s, 1H), 3.59 (m, 4H), 1.18 (t, *J* = 7.1 Hz, 6H). $^{13}C\{^{1}H\}$ NMR (125 MHz, $(CD_3)_2SO$) δ (ppm): 168.8, 157.1, 149.2, 134.4, 115.4, 95.1, 45.6, 14.0, 12.0. HRMS m/z $[M + H]^+$ calcd. for $[C_{10}H_{15}N_2O_2]^+$ 195.1128; found 195.1132.

Compound **S5**. Compound **S4** (230.0 mg, 1.18 mmol, 1.6 equiv.) and 1,7-dihydroxynapthalene (161.0 mg, 0.74 mmol, 1.0 equiv.) were combined in 8 mL of DMF and then refluxed at 140 °C for 3.5 hours. After cooling to room temperature, the solvent was removed under vacuum, and the crude product was purified by column chromatography (50% ethyl acetate in dichloromethane) to isolate **S5** as a dark blue solid (157.3 mg, 63.9%). ^{1}H NMR (500 MHz, $(CD_3)_2SO$) δ (ppm): 10.37 (s, 1H), 8.41 (d, *J* = 8.7 Hz, 1H), 7.59 (d, *J* = 9.0 Hz, 1H), 7.45 (d, *J* = 2.6 Hz, 1H), 7.21 (d, *J* = 8.7 Hz, 1H), 6.81 (dd, *J* = 9.1, 2.7 Hz, 1H), 6.65 (d, *J* = 2.7 Hz, 1H), 6.27 (s, 1H), 3.48 (q, *J* = 7.0 Hz, 4H), 1.16 (t, *J* = 7.0 Hz, 6H). $^{13}C\{^{1}H\}$ NMR (125 MHz, $(CD_3)_2SO$) δ (ppm): 181.9, 159.7, 151.4, 150.1, 146.0, 138.8, 133.0, 130.4, 125.8, 124.1, 123.4, 120.1, 110.1, 109.9, 104.6, 96.0, 44.4, 39.5, 12.4, 9.9. HRMS m/z $[M + H]^+$ calcd. for $[C_{20}H_{19}N_2O_3]^+$ 335.1390; found 335.1395.

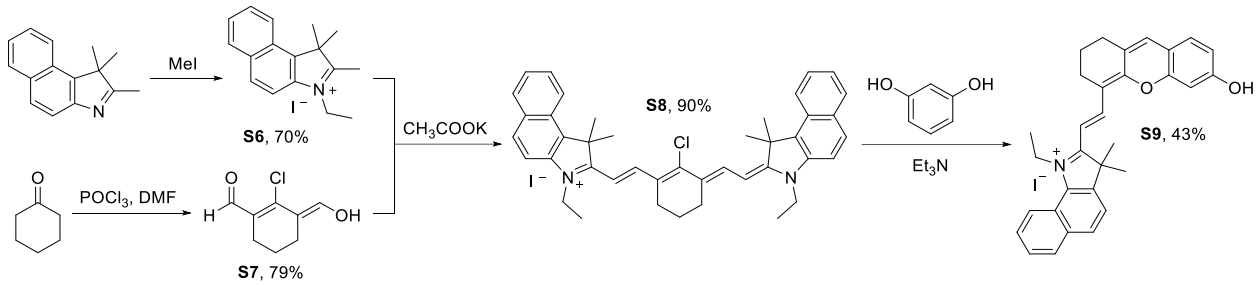


Figure B4. Synthetic route of **S6**–**S9** to yield the NIR-emitting fluorophore.[372]

Compound **S6**. 1,1,2-Trimethyl-1H-benzo[*e*]indole (1.0460 g, 5.00 mmol, 1.0 equiv.) and iodoethane (0.8599 g, 5.00 mmol, 1.0 equiv.) were dissolved in 3 mL of toluene and then refluxed at 100 °C for 20 hours. The reaction was then cooled to room temperature and filtered to yield **S6** as a light brown solid (1.2220 g, 69.72%). ^{1}H NMR (500 MHz, $CDCl_3$) δ (ppm): 8.11 (m, 3H), 7.77 (m, 2H), 7.69 (m, 1H), 4.93 (q, *J* = 7.5 Hz, 2H), 3.24 (s, 3H), 1.88 (s, 6H), 1.68 (m, 6H). ^{13}C{^{1}H} NMR (125 MHz, $CDCl_3$) δ (ppm): 195.3, 138.0, 137.4, 134.0, 131.8, 130.3, 128.9, 138.1, 127.9, 123.0, 56.0, 45.5, 22.9, 16.0, 13.8. HRMS m/z $[M + H]^+$ calcd. for $[C_{17}H_{20}N]^+$ 238.1590; found 238.1597.

Compound **S7**. A solution of $POCl_3$ (0.925 mL, 9.93 mmol, 7.6 equiv.) in 1 mL dichloromethane was slowly added to a flask containing DMF (1.00 mL, 12.9 mmol, 9.8 equiv.) and dichloromethane (1 mL) in an ice bath and then stirred for 30 minutes. Cyclohexanone (136 mL, 1.31 mmol, 1.0 equiv.) was then added dropwise, and the reaction mixture was refluxed for 4 hours at 80 °C. After the reaction cooled to room temperature, the mixture was poured over ice water, stirred for 30 minutes, and then filtered to afford **S7** as a yellow solid (180.2 mg, 78.56%).

Compound **S8**. Compound **S6** (1.000 g, 2.84 mmol, 2.0 equiv.), **S7** (249 mg, 1.42 mmol, 1.0 equiv.), and potassium acetate (279.0 mg, 2.84 mmol, 2.0 equiv.) were added to 5.5 mL of acetic anhydride and heated to 70 °C for 30 minutes. Once the reaction mixture had cooled to room temperature, the crude material was poured over ice water and then filtered to yield **S8** as a green-red solid (964.9 mg, 89.5%). ^{1}H NMR (500 MHz, $CDCl_3$) δ (ppm): 8.45 (d, *J* = 14.2 Hz, 2H), 8.12 (d, *J* = 9.7 Hz, 2H), 7.96 (t, *J* = 7.8 Hz, 4H), 7.62 (t, *J* = 7.7 Hz, 2H), 7.47 (m, 4H), 6.26 (d, *J* = 14.2 Hz, 2H), 4.37 (q, *J* = 7.3 Hz, 4H), 2.80 (t, *J* = 6.2 Hz, 4H), 2.03 (s, 12H), 1.53 (t, *J* = 7.3 Hz, 6H). ^{13}C{^{1}H} NMR (125 MHz, $CDCl_3$) δ (ppm): 174.5, 173.3, 150.0, 143.6, 139.4, 134.1, 132.1,

131.0, 130.3, 128.3, 127.9, 127.7, 125.3, 122.2, 110.7, 100.8, 77.2, 51.3, 40.4, 27.8, 27.0, 22.3, 21.0, 20.8, 13.0. HRMS m/z $[M + H]^+$ calcd. for $[C_{42}H_{44}ClN_2]^+$ 611.3188; found 611.3188.

Compound **S9**. Compound **S8** (550.0 mg, 0.74 mmol, 1.0 equiv.), resorcinol (935.0 mg, 8.49 mmol, 11.4 equiv.), and triethylamine (0.99 mL, 7.19 mmol, 9.6 equiv.) were dissolved in 8.25 mL of dry DMF and then heated to 110 °C for 30 minutes. After the reaction cooled to room temperature, the mixture was poured into a large amount of ice water, stirred for 30 minutes, filtered, and then the resulting solid was purified by column chromatography (10% methanol in dichloromethane) to isolate **S9** as a dark blue solid (183.7 mg, 42.88%). ^{1}H NMR (500 MHz, CD_3OD) δ (ppm): 8.80 (d, *J* = 15.0 Hz, 1H), 8.32 (d, *J* = 8.7 Hz, 1H), 8.09 (m, 2H), 7.71 (m, 2H), 7.57 (t, J = 7.6 Hz, 1H), 7.38 (m, 2H) 6.84 (m, 2H), 6.43 (d, *J* = 14.8 Hz, 1H), 4.45 (q, *J* = 7.3, 8.0 Hz, 2H), 2.75 (m, 4H), 2.06 (s, 6H), 1.94 (m, 2H), 1.53 (t, *J* = 7.3 Hz, 3H). ^{13}C{^{1}H} NMR (125 MHz, CD_3OD) δ (ppm): 178.7, 165.6, 163.2, 156.6, 145.1, 140.2, 136.6, 136.4, 134.1, 132.2, 131.2, 130.4, 129.2, 129.1, 127.0, 126.8, 123.6, 116.7, 116.2, 115.5, 112.4, 103.2, 102.7, 53.4, 49.0, 41.4, 29.9, 28.0, 25.1, 21.8, 13.0. HRMS m/z $[M + H]^+$ calcd. for $[C_{31}H_{30}NO_2]^+$ 448.2271; found 448.2275.

Compound **1**. Compound **S1** (51.5 mg, 0.235 mmol, 2.0 equiv.) was added to 10 mL of DCM and stirred momentarily. Next, 4-methylumbelliferone (20.7 mg, 0.118 mmol, 1.0 equiv.) was added followed by DIPEA (36.6 mL, 0.235 mmol, 2.0 equiv.) dropwise. The reaction was stirred at room temperature until the completion of the reaction was indicated by TLC (about 1 hour). The reaction was quenched by adding water (10 mL), and then aqueous solution was extracted with DCM (3 × 10 mL). The organic layers were combined, washed with brine, and then dried over $MgSO_4$. After removal of solvent under reduced pressure, the crude product was purified by column chromatography (30% ethyl acetate in hexanes as the eluent) to afford **1** as a white solid (31.7 mg, 72.5%). ^{1}H NMR (500 MHz, $(CD_3)_2SO$) δ (ppm): 7.84 (d, *J* = 8.7 Hz, 1H), 7.36 (m, 6H), 7.22 (d, *J* = 8.7 Hz, 2H), 6.43 (s, 1H), 4.18 (s, 2H), 2.44 (s, 3H). ^{13}C{^{1}H} NMR (125 MHz, $(CD_3)_2SO$) δ (ppm): 167.3, 159.4, 153.5, 152.8, 136.1, 129.6, 128.5, 127.3, 126.7, 118.2, 117.6, 114.2, 109.7, 42.0, 18.2. HRMS m/z $[M + H]^+$ calcd. for $[C_{18}H_{15}O_4S_2]^+$ 359.0406; found 359.0402.

Compound **2**. **S3** (50.0 mg, 0.12 mmol, 1.0 equiv.), **S1** (83.6 mg, 0.38 mmol, 3.1 equiv.), and DIPEA (68 mL, 0.37 mmol, 3.0 equiv.) were combined in 20 mL of anhydrous dichloromethane at room temperature for 1 hour. The solvent was then removed under vacuum

and then the crude product was purified by column chromatography (30% ethyl acetate in hexanes as the mobile phase) to yield compound **2** as a white solid (52.7 mg, 73.0%). ^{1}H NMR (500 MHz, CD_2Cl_2) δ (ppm): 7.97 (d, *J* = 7.8 Hz, 1H), 7.69 (t, *J* = 6.9 Hz, 1H), 7.63 (t, *J* = 7.5 Hz, 1H), 7.34 (m, 5H), 7.17 (d, *J* = 7.6 Hz, 1H), 7.08 (d, *J* = 2.2 Hz, 1H), 6.75 (m, 2H), 6.15 (s, 1H), 4.07 (s, 2H), 3.17 (m, 4H), 2.94 (m, 2H), 2.52 (m, 2H), 2.03 (m, 2H), 1.86 (m, 2H). ^{13}C{^{1}H} NMR (125 MHz, CD_2Cl_2) δ (ppm): 170.1, 168.9, 153.8, 153.2, 153.0, 148.5, 145.6, 136.6, 135.8, 130.5, 129.9, 129.5, 128.8, 127.9, 125.6, 125.4, 124.9, 119.2, 118.7, 116.8, 110.6, 108.0, 105.3, 84.6, 50.6, 50.2, 44.1, 28.2, 22.6, 22.0, 21.8. HRMS m/z $[M + H]^+$ calcd. for $[C_{35}H_{30}NO_5S_2]^+$ 594.1403; found 594.1417.

Compound **3**. Resorufin (31.1 mg, 0.15 mmol, 1.0 equiv.) was added to a mixture of 500 mL DCM and 100 mL acetonitrile and then cooled to 0 °C in an ice bath. Next, **S1** (92.3 mg, 0.42 mmol, 2.9 equiv.) was added followed by DIPEA (65.5 mL, 0.42 mmol, 2.9 equiv.). The reaction mixture was stirred for 1 hour at room temperature. The solvent was removed under reduced pressure until about 50 mL of solvent remained, and then the reaction was quenched with water (50 mL), extracted with DCM (3 x 50 mL), and then dried with $MgSO_4$. After removal of solvent under reduced pressure, the crude product was purified by column chromatography (10–30% ethyl acetate in DCM as the eluent) to afford **3** as an orange solid (19.8 mg, 34.3%). ^{1}H NMR (500 MHz, $(CD_3)_2SO$) δ (ppm): 7.79 (d, *J* = 8.5 Hz, 1H), 7.42 (d, *J* = 9.9 Hz, 1H), 7.34 (m, 5H), 7.13 (m, 2H), 6.81 (d, *J* = 9.9 Hz, 1H), 6.29 (s, 1H), 4.09 (s, 2H). ^{13}C{^{1}H} NMR (125 MHz, CD_2Cl_2) δ (ppm): 186.4, 168.4, 154.0, 149.7, 149.3, 144.8, 136.1, 135.6, 135.2, 132.0, 131.6, 130.0, 129.1, 128.4, 118.8, 109.5, 107.6, 43.6. HRMS m/z $[M + H]^+$ calcd. for $[C_{20}H_{14}NO_4S_2]^+$ 396.0359; found 396.0359.

Compound **4**. Compound **S5** (157.3 mg, 0.47 mmol, 1.0 equiv.), **S1** (307.3 mg, 1.41 mmol, 3.0 equiv.), and DIPEA (246.5 mL, 1.58 mmol, 3.4 equiv.) were combined in 50 mL of DCM and then stirred for 2 hours. The solvent was then removed under vacuum, and the crude product was purified by column chromatography (1-5% methanol in dichloromethane) followed by recrystallization in hexanes to isolate compound **4** as a purple solid (172.4 mg, 70.94%). ^{1}H NMR (500 MHz, CD_2Cl_2) δ (ppm): 8.71 (d, *J* = 8.7 Hz, 1H), 8.01 (s, 1H), 7.66 (d, J = 9.1 Hz, 1H), 7.49 (dd, J = 2.8, 8.7, 2H), 7.40 (m, 5H), 6.77 (dd, *J* = 2.7, 9.1 Hz, 1H), 6.57 (d, J = 2.8, 1H), 6.39 (s, 1H), 4.14 (s, 2H), 3.53 (q, *J* = 7.1 Hz, 4H), 1.30 (t, *J* = 7.1 Hz, 6H). ^{13}C{^{1}H} NMR (125 MHz, CD_2Cl_2) δ (ppm): 182.3, 168.7, 153.1, 152.8, 151.6, 147.4, 139.1, 136.2, 133.64, 131.5, 130.7,

130.0, 129.1, 128.4, 126.0, 125.5, 124.6, 117.8, 110.6, 105.7, 96.6, 45.6, 43.7, 12.8. HRMS m/z $[M + H]^+$ calcd. for $[C_{28}H_{25}N_2O_4S_2]^+$ 517.1250; found 517.1250.

Compound **5**. Compound **S9** (10.0 mg, 0.02 mmol, 1.0 equiv.) and DIPEA (8.8 mL, 0.052 mmol, 3.0 equiv.) were combined in 1 mL anhydrous DCM. Next, **S1** (11.4 mg, 0.052 mmol, 3.0 equiv.) was added dropwise and then the reaction was stirred for 10 minutes. The reaction mixture was then immediately purified by column chromatography (2-6% methanol in dichloromethane) to isolate compound **5** as a dark blue solid (12.9 mg, 98%). ^{1}H NMR (500 MHz, CD_2Cl_2) δ (ppm): 8.78 (d, *J* = 15.2 Hz, 1H), 8.24 (d, *J* = 8.4 Hz, 1H), 8.11 (d, *J* = 8.8 Hz, 1H), 8.06 (d, *J* = 8.2 Hz, 1H), 7.74 (t, *J* = 8.4 Hz, 1H), 7.68 (d, *J* = 8.8 Hz, 1H), 7.64 (d, *J* = 7.1 Hz, 1H), 7.44 (d, *J* = 8.5 Hz, 1H), 7.37 (m, 5H), 7.23 (d, *J* = 2.2 Hz, 1H), 7.15 (s, 1H), 7.05 (dd, *J* = 8.5, 2.2 Hz, 1H), 6.58 (d, *J* = 15.2 Hz, 1H), 4.58 (q, *J* = 7.4 Hz, 2H), 4.13 (s, 2H), 2.77 (m, 4H), 2.08 (s, 6H), 1.97 (m, 2H). ^{13}C{^{1}H} NMR (125 MHz, $(CD_3)_2SO$) δ (ppm): 179.8, 168.7, 160.0, 153.4, 153.3, 146.0, 138.7, 137.1, 136.1, 133.6, 131.9, 131.1, 130.9, 130.7, 130.4, 130.0, 129.8, 129.1, 129.0, 128.7, 128.7, 128.4, 128.1, 127.9, 127.1, 122.9, 120.7, 118.6, 115.6, 112.0, 109.3, 105.6, 103.2, 43.7, 42.2, 29.9, 28.1, 27.9, 24.6, 20.7, 13.6. HRMS m/z $[M + H]^+$ calcd. for $[C_{39}H_{36}NO_3S_2]^+$ 630.2131; found 630.2130.

UV-Vis and Fluorescence Spectra

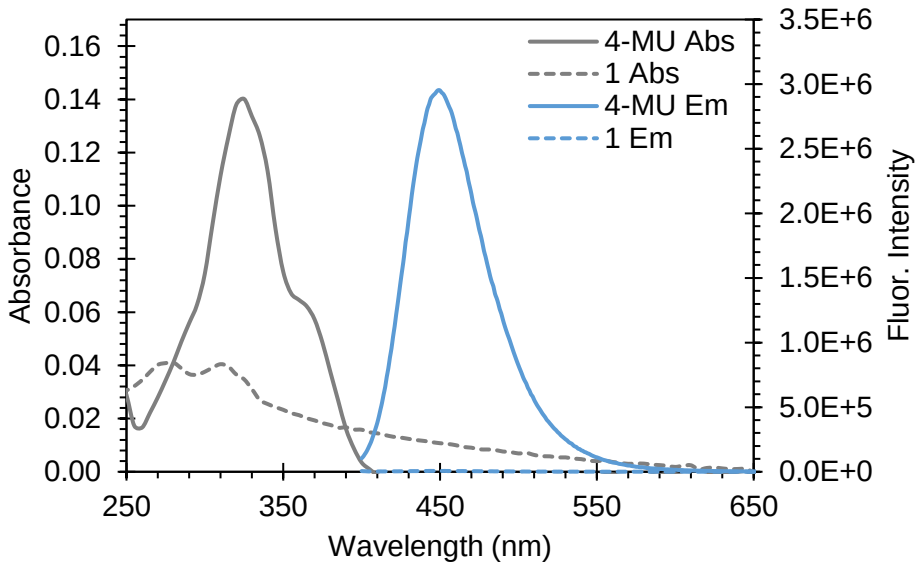


Figure B5. Absorption and emission (λ_{ex} = 350 nm) spectra of the blue-emitting fluorophore 4-methylumbelliferone (4-MU, 10 μM) and the blue fluorescence turn-on COS/H_2S donor **1** (10 μM) in PBS buffer (10 mM, pH 7.4).

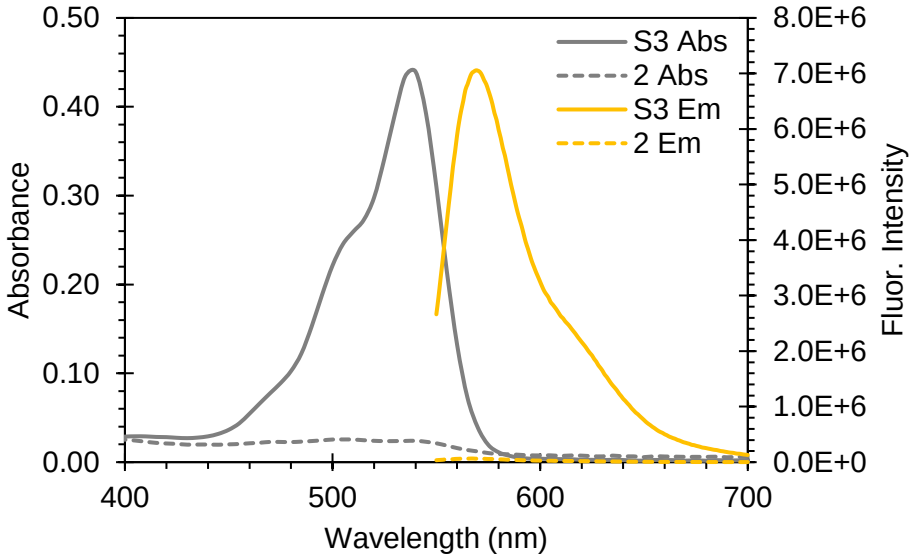


Figure B6. Absorption and emission (λ_{ex} = 540 nm) spectra of the yellow-emitting fluorophore **S3** (10 μM) and the yellow fluorescence turn-on COS/H_2S donor **2** (10 μM) in PBS buffer (10 mM, pH 7.4).

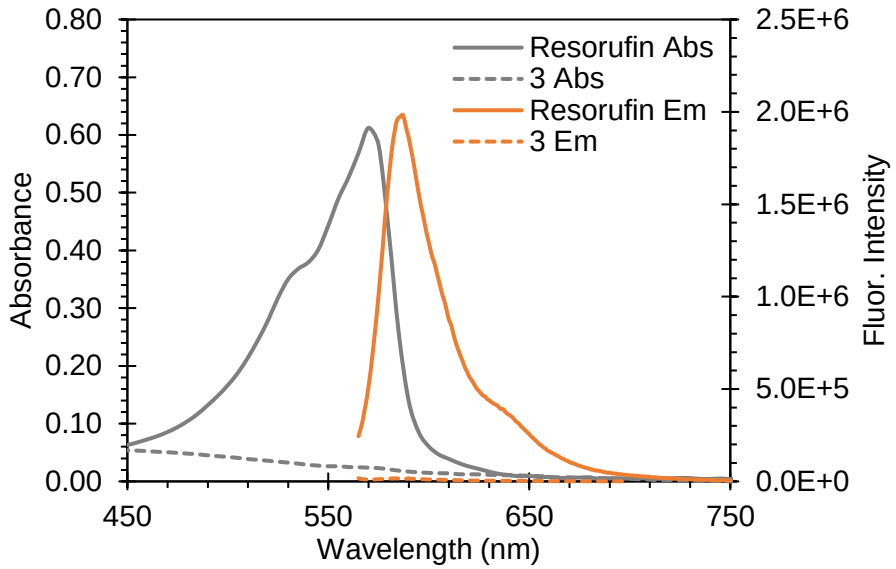


Figure B7. Absorption and emission (λ_{ex} = 560 nm) spectra of the orange-emitting fluorophore resorufin (10 μM) and the orange fluorescence turn-on COS/H_2S donor **3** (10 μM) in PBS buffer (10 mM, pH 7.4).

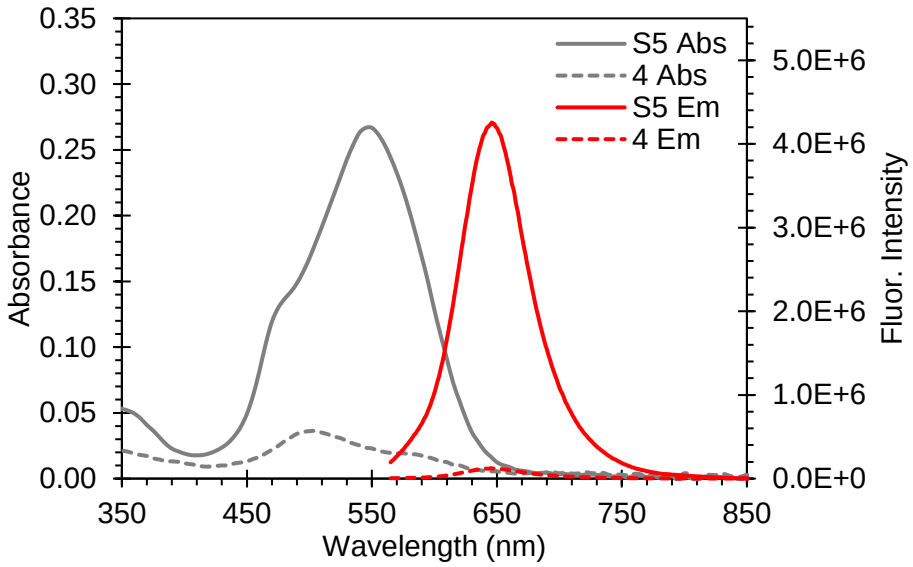


Figure B8. Absorption and emission (λ_{ex} = 550 nm) spectra of the red-emitting fluorophore **S5** (10 μM) and the red fluorescence turn-on COS/H_2S donor **4** (10 μM) in 1.0 mM CTAB in PBS buffer (10 mM, pH 7.4).

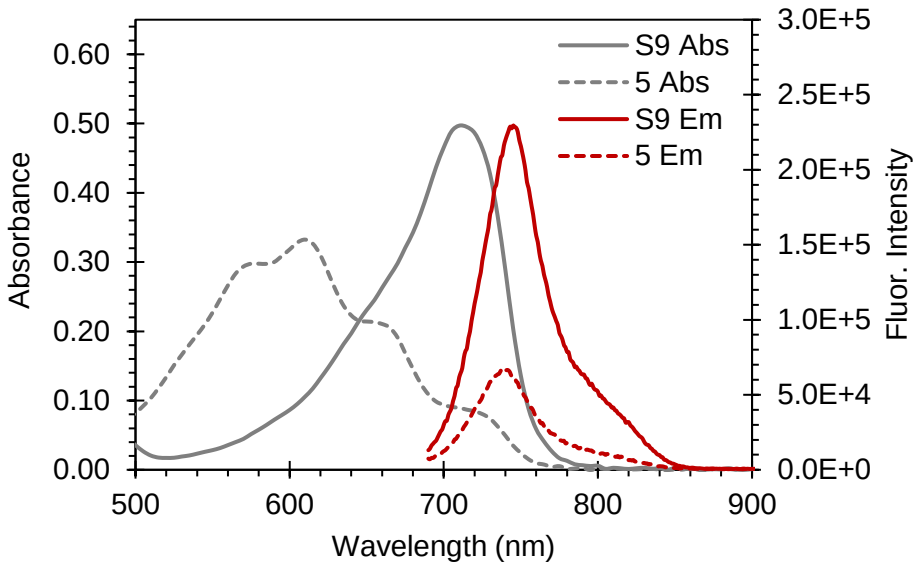


Figure B9. Absorption and emission (λ_{ex} = 645 nm) spectra of the NIR-emitting fluorophore **S9** (10 μM) and the NIR fluorescence turn-on COS/H_2S donor **5** (10 μM) in 1.0 mM CTAB in PBS buffer (10 mM, pH 7.4).

Molar Absorptivity & Quantum Yield

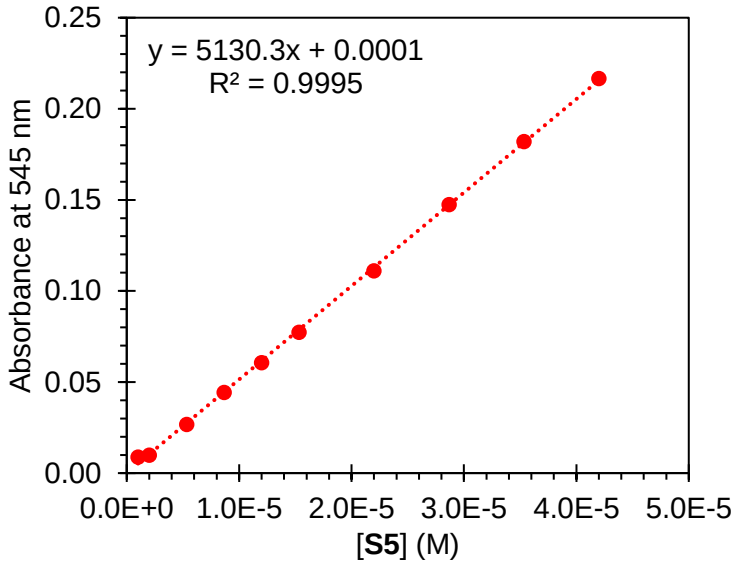


Figure B10. Molar absorptivity of the red fluorophore **S5** in 1.0 mM CTAB in PBS buffer (10 mM, pH 7.4) at 545 nm.

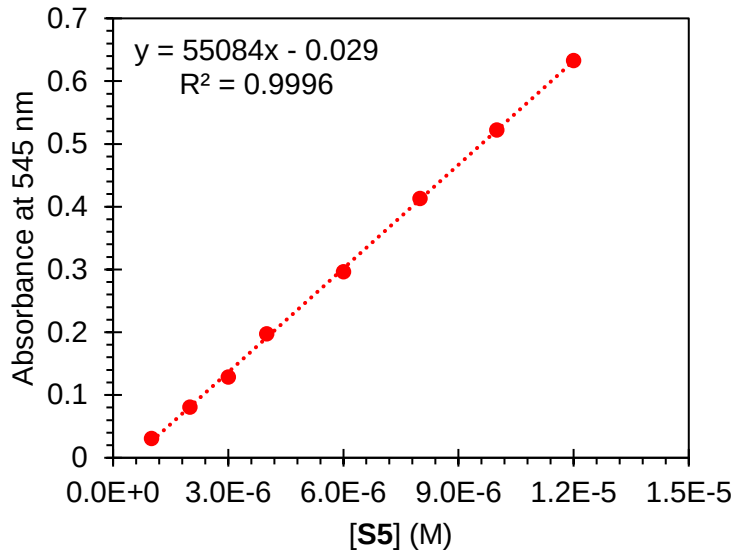


Figure B11. Molar absorptivity of the red fluorophore **S5** in ethanol at 545 nm.

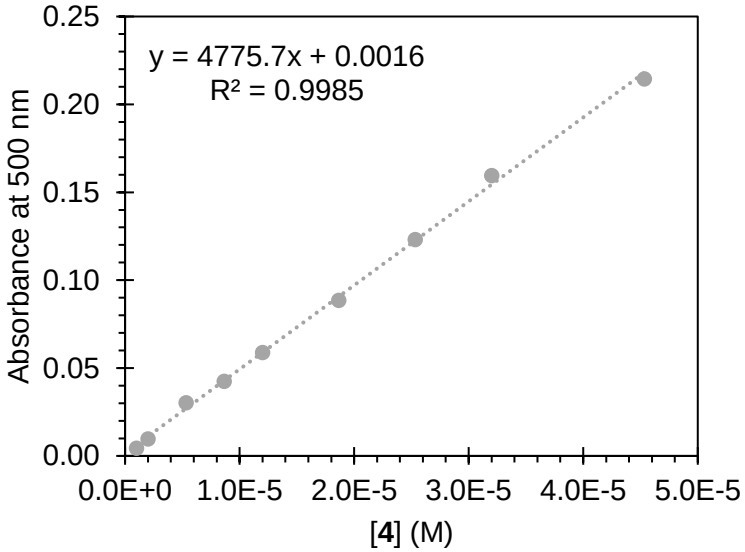


Figure B12. Molar absorptivity of the red COS/H_2S donor **4** in 1.0 mM CTAB in PBS buffer (10 mM, pH 7.4) at 500 nm.

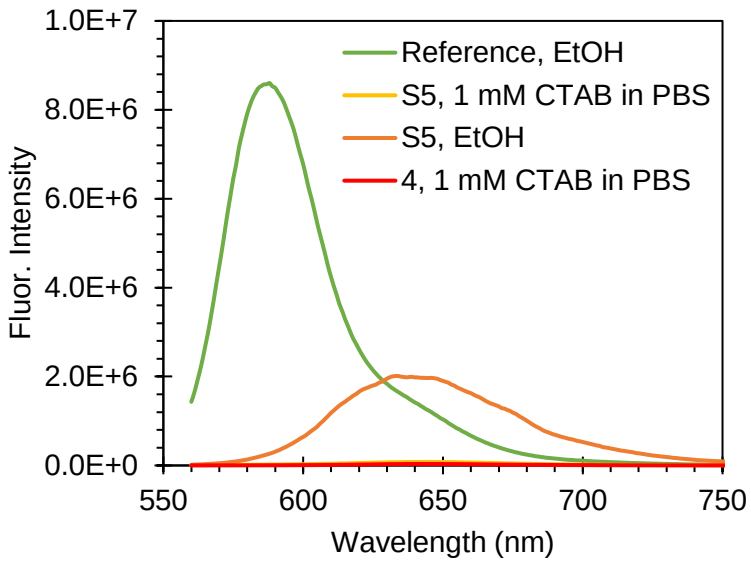


Figure B13. Quantum yield of the red fluorophore **S5** and the red COS/H_2S donor **4** in 1.0 mM CTAB in PBS buffer (10 mM, pH 7.4) compared to the reference. Excitation wavelength: 545 nm, slit width: 3 nm.

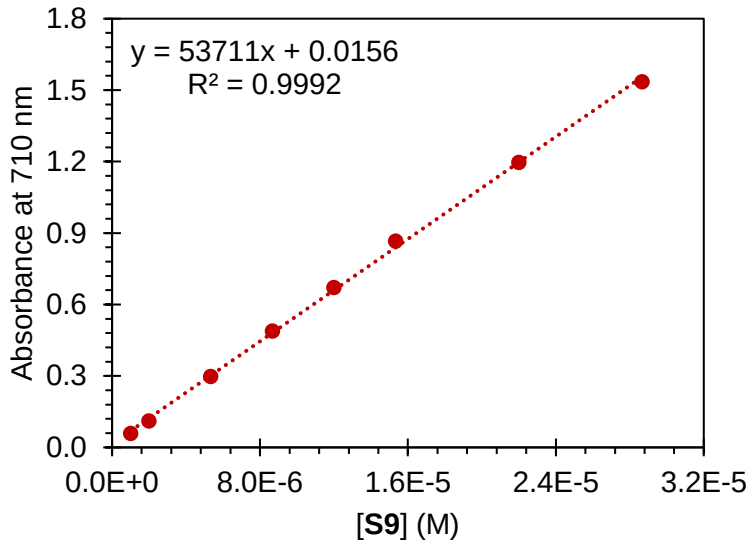


Figure B14. Molar absorptivity of the NIR fluorophore **S9** in 1.0 mM CTAB in PBS buffer (10 mM, pH 7.4) at 710 nm.

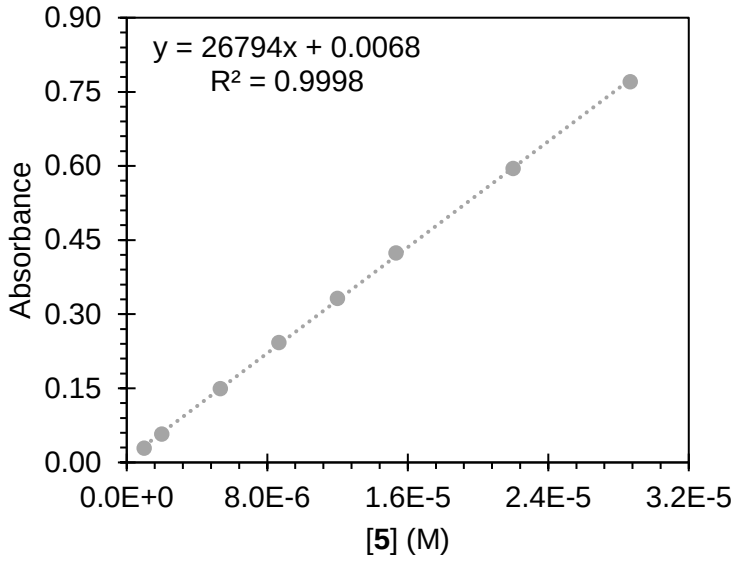


Figure B15. Molar absorptivity of the NIR COS/H_2S donor **5** in 1.0 mM CTAB in PBS buffer (10 mM, pH 7.4) at 610 nm.

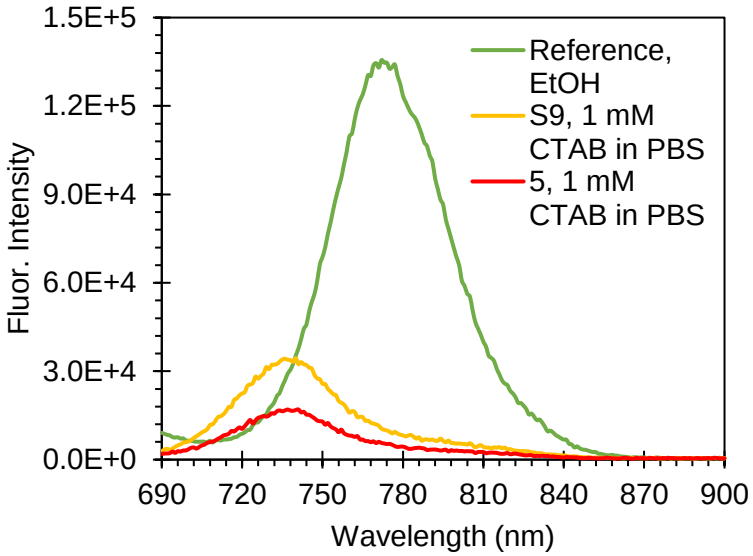


Figure B16. Quantum yield of the NIR fluorophore **S9** and the NIR COS/H_2S donor **5** in 1.0 mM CTAB in PBS buffer (10 mM, pH 7.4) compared to the reference. Excitation wavelength: 645 nm, slit width: 3 nm.

*Fluorescence Turn-on of Donors **1**–**5***

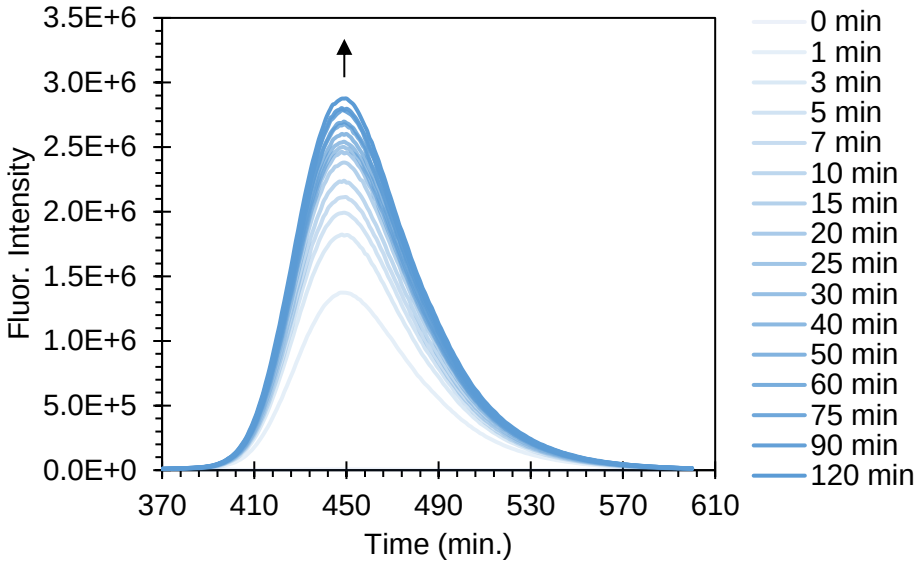


Figure B17. Fluorescence turn-on of the blue COS/H_2S donor **1** (10 μM) when activated by cysteine (100 μM, 10 equiv.) over 120 minutes. Excitation wavelength: 350 nm, slit width: 2 nm.

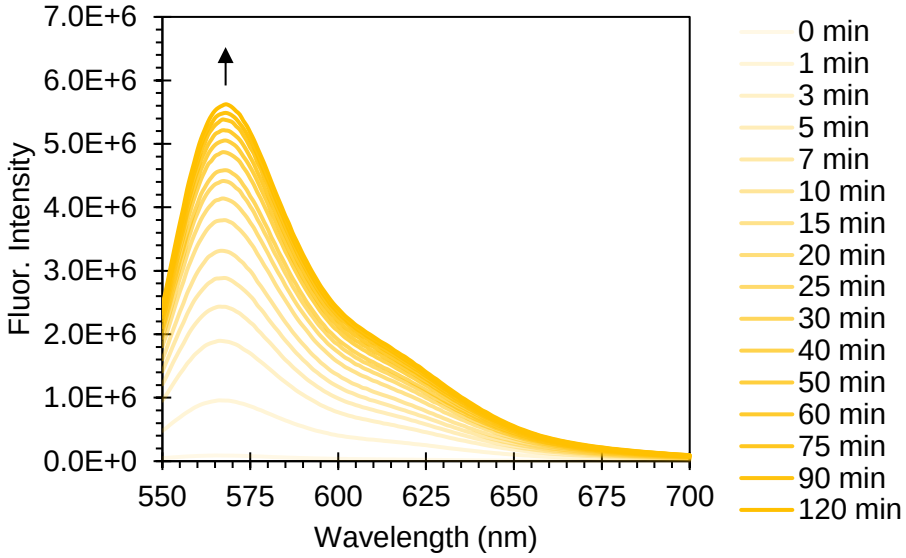


Figure B18. Fluorescence turn-on of the yellow COS/H_2S donor **2** (10 μM) when activated by cysteine (100 μM, 10 equiv.) over 120 minutes. Excitation wavelength: 540 nm, slit width: 2 nm.

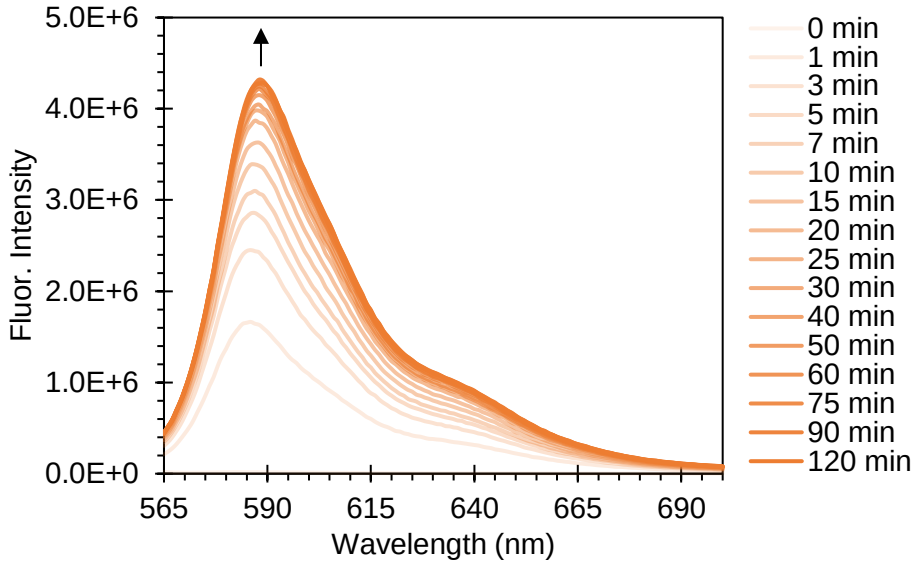


Figure B19. Fluorescence turn-on of the orange COS/H_2S donor **3** (10 μM) when activated by cysteine (100 μM, 10 equiv.) over 120 minutes in PBS buffer (10 mM, pH 7.4). Excitation wavelength: 560 nm, slit width: 2 nm.

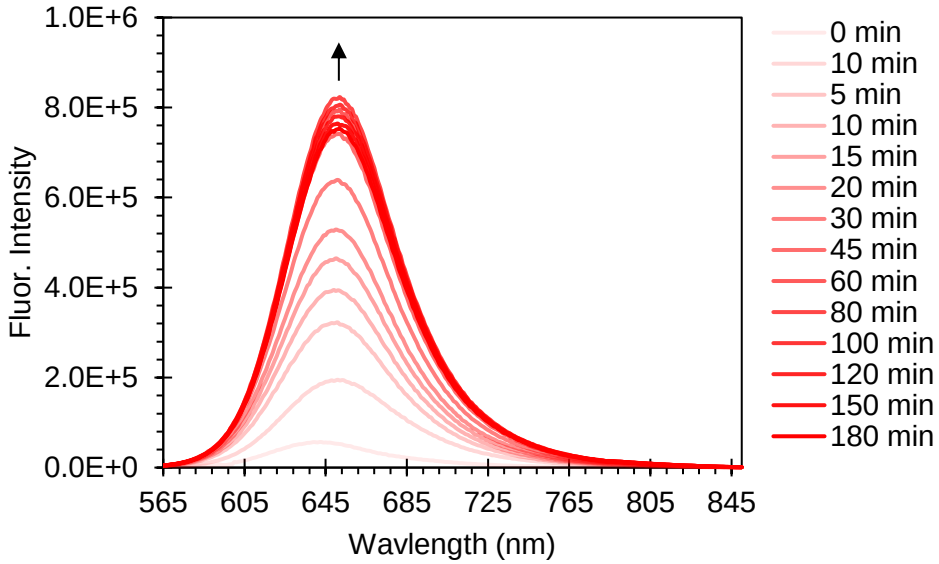


Figure B20. Fluorescence intensity of the red COS/H_2S donor **4** (50 μM) when activated by cysteine (500 μM, 10 equiv.) over 180 minutes in 1.0 mM CTAB in PBS buffer (10 mM, pH 7.4). Excitation wavelength: 545 nm, slit width: 3 nm.

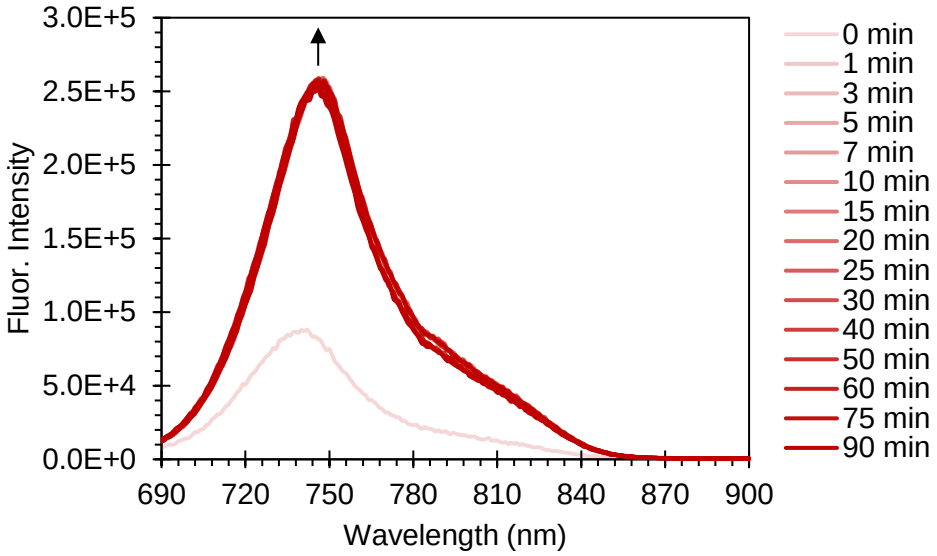


Figure B21. Emission spectra of the NIR COS/H_2S donor **5** (10 μM) when activated by cysteine (100 μM, 10 equiv.) over 90 minutes in 1.0 mM CTAB in PBS buffer (10 mM, pH 7.4). Excitation wavelength: 645 nm, slit width: 3 nm.

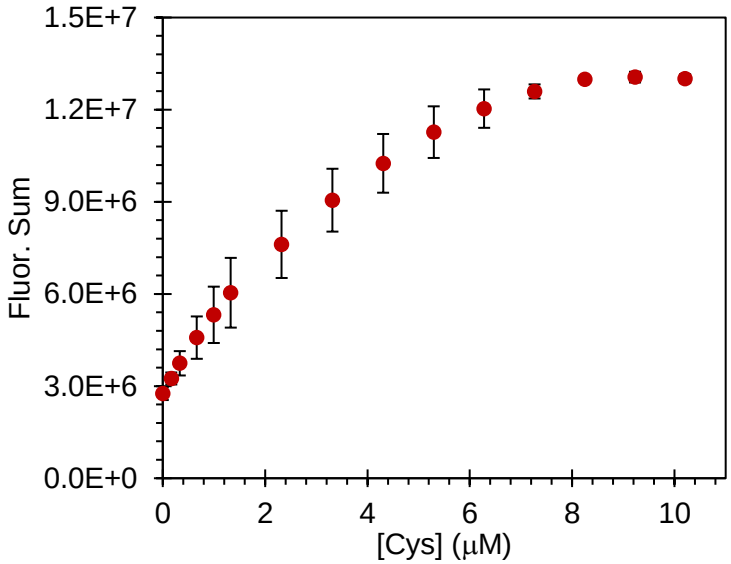


Figure B22. Sum of the fluorescence intensity (from 690–900 nm) of the NIR COS/H_2S donor **5** (10 μM) when activated by various concentrations of cysteine (0-10 μM) in 1.0 mM CTAB in PBS buffer (10 mM, pH 7.4). The experiments were performed in triplicate and results are expressed as mean ± SD (n = 3). Excitation wavelength: 645 nm, slit width: 3 nm.

*H_2S Release from Donors **1**–**5***

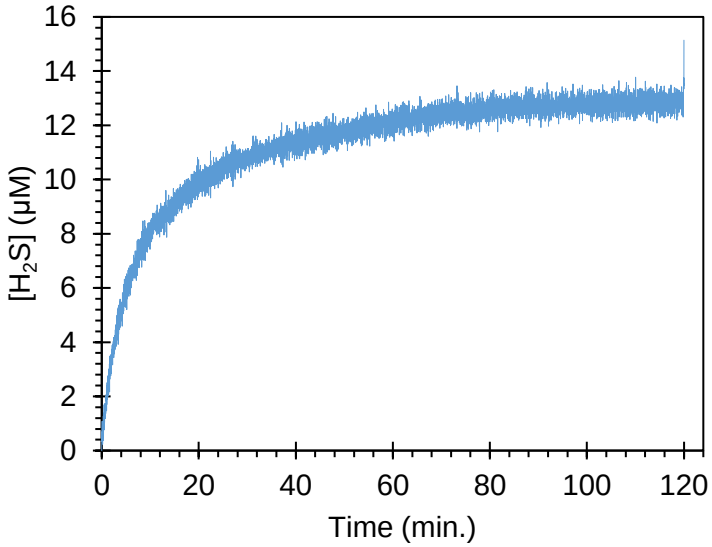


Figure B23. H_2S release from the blue COS/H_2S donor **1** (10 μM) in the presence of CA (25 μg mL^{-1}) when activated by cysteine (100 μM, 10 equiv.) over 120 minutes measured by a Unisense H_2S-selective electrode.

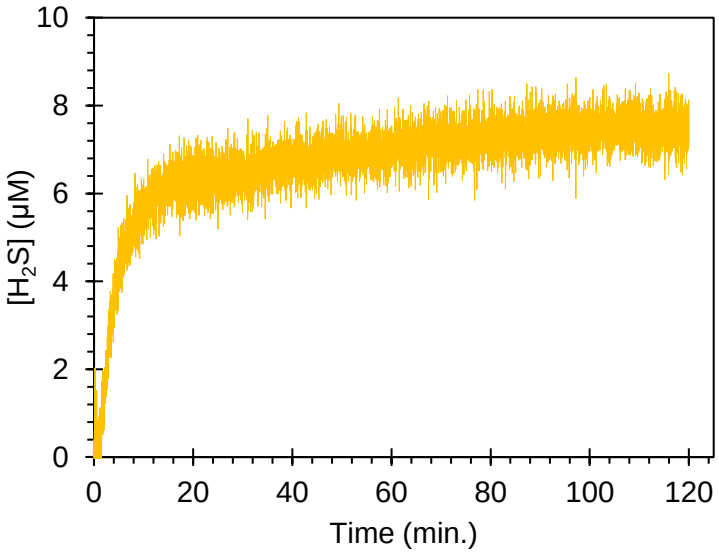


Figure B24. H_2S release from the yellow COS/H_2S donor **2** (10 μM) in the presence of CA (25 μg mL^{-1}) when activated by cysteine (100 μM, 10 equiv.) over 120 minutes measured by a Unisense H_2S-selective electrode.

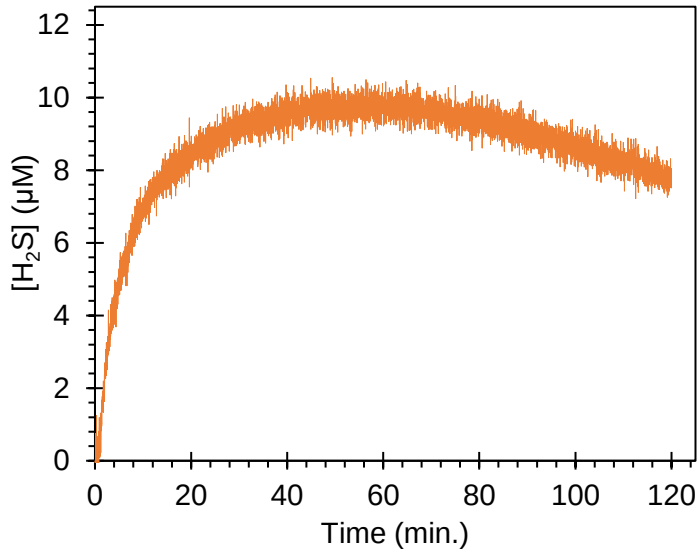


Figure B25. H_2S release from the orange COS/H_2S donor **3** (10 μM) in the presence of CA (25 μg mL^{-1}) when activated by cysteine (100 μM, 10 equiv.) over 120 minutes measured by a Unisense H_2S-selective electrode.

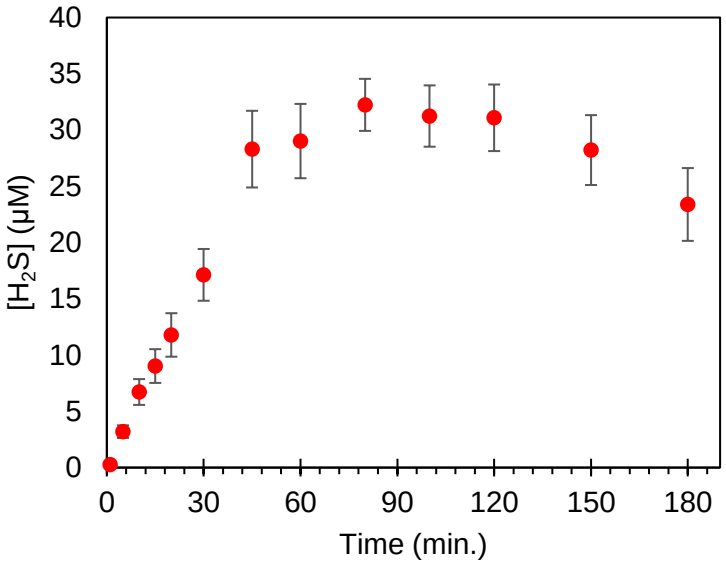


Figure B26. H_2S release from the red COS/H_2S donor **4** (50 μM) in the presence of CA (25 μg mL^{-1}) when activated by cysteine (500 μM, 10 equiv.) over 180 minutes measured by the methylene blue assay. The experiments were performed in triplicate and results are expressed as mean ± SD (n = 3).

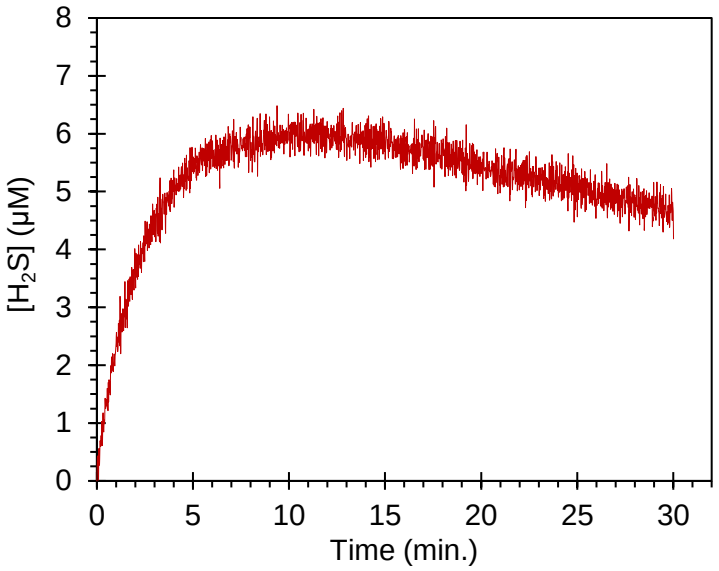


Figure B27. H_2S release from the NIR COS/H_2S donor **5** (10 μM) in the presence of CA (25 μg mL^{-1}) when activated by cysteine (100 μM, 10 equiv.) over 30 minutes measured by a Unisense H_2S-selective electrode.

*Fluorescence Turn-on of Donor **1** with Various Analytes*

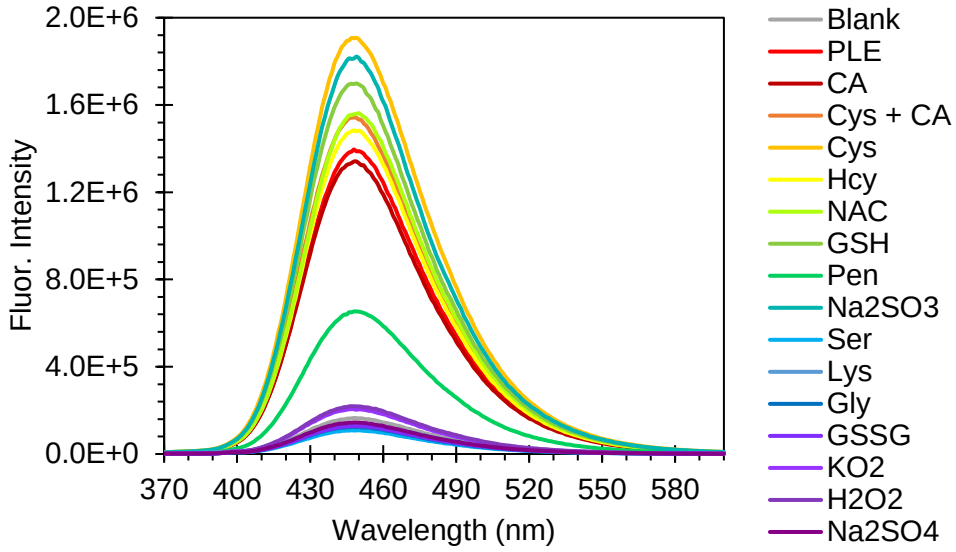


Figure B28. Emission spectra of the blue COS/H_2S donor **1** (10 μM) when activated by various analytes (100 μM, 10 equiv.) after 120 minutes. Conditions from top to bottom: blank, PLE (1.0 U mL^{-1}), CA (25 μg mL^{-1}), Cys + CA, Cys, Hcy, NAC, GSH, Pen, SO_3^{2-}, Ser, Lys, Gly, GSSG, O_2^{-}, H_2O_2, and SO_4^{2-}. Excitation wavelength: 350 nm, slit width: 2 nm.

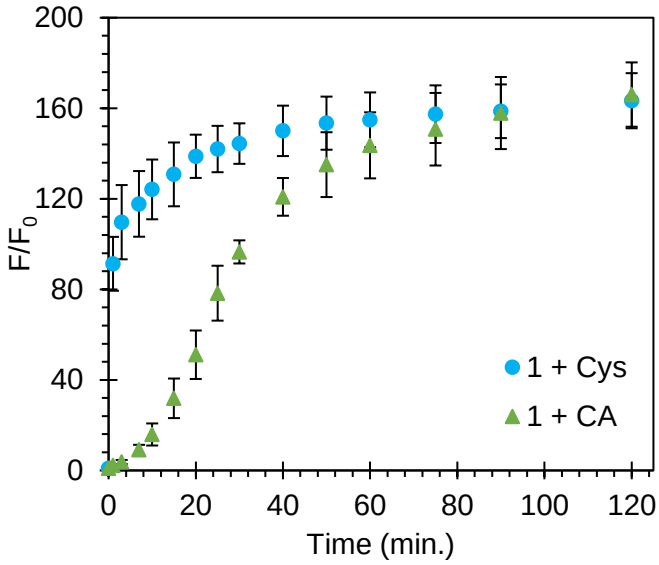


Figure B29. Fluorescence turn-on over time of the blue COS/H_2S donor **1** (10 μM) when activated by either cysteine (100 μM, 10 equiv.) or CA (25 μg mL^{-1}) over 120 minutes. The experiments were performed in triplicate and results are expressed as mean ± SD (n = 3). Excitation wavelength: 350 nm, slit width: 2 nm.

*Photostability of Donors **1**–**5***

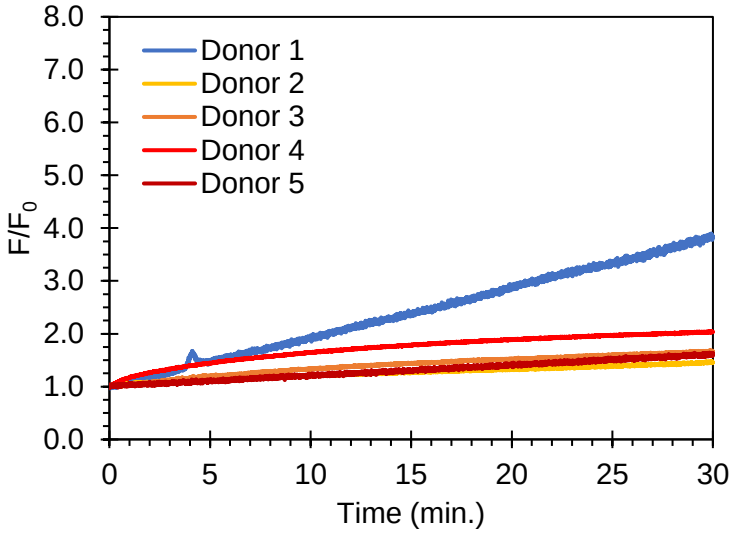


Figure B30. Fluorescence turn-on of donors **1**–**5** (10 μM) when irradiated over 30 minutes. Donor fluorescence turn-on is quantified by F/F_0 at the emission maxima. Excitation wavelength: 350, 540, 560, 545, and 645 nm, respectively. Emission wavelength: 448, 569, 585, 645, and 744 nm, respectively.

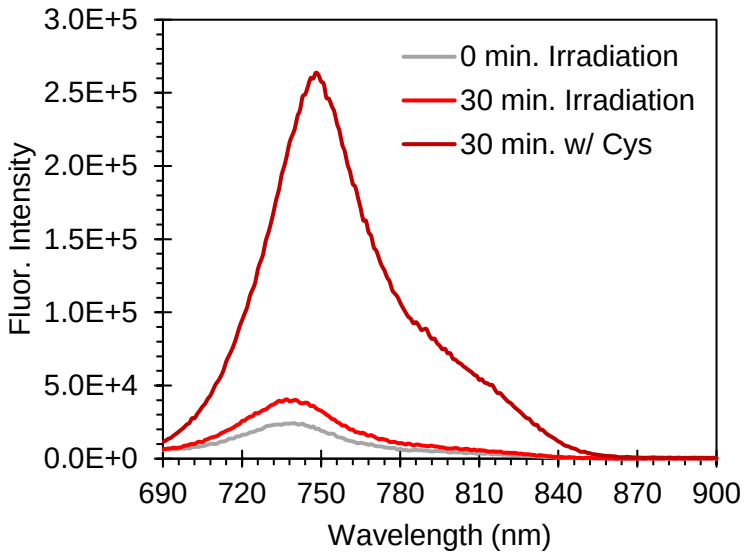


Figure B31. Emission spectra of the NIR COS/H_2S donor **5** (10 μM) with irradiation at 645 nm versus cysteine (100 μM, 10 equiv.) addition after 30 minutes in 1.0 mM CTAB in PBS buffer (10 mM, pH 7.4). Excitation wavelength: 645 nm, slit width: 3 nm.

*Cell Experiments of Donors **1**–**5** and CT-MeRhoAz*

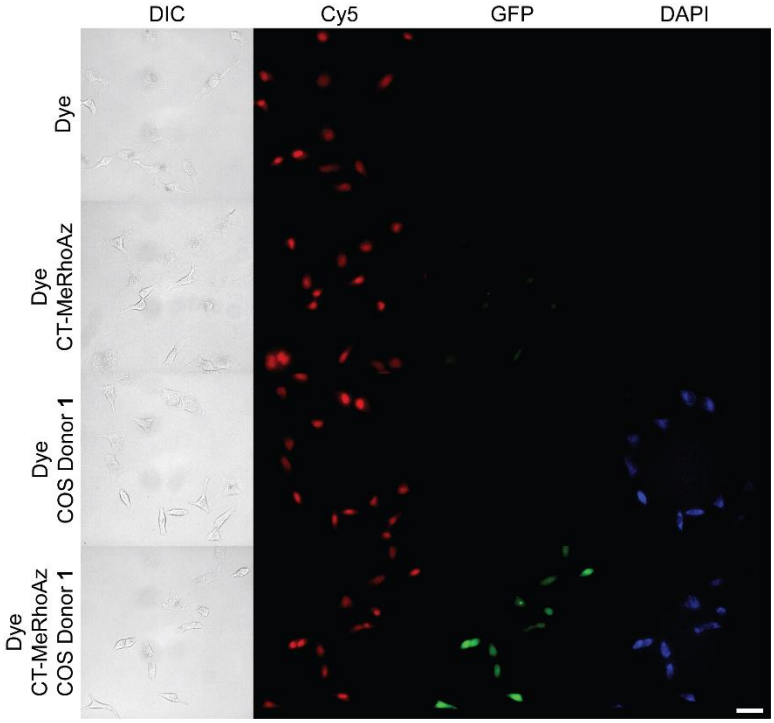


Figure B32. Fluorescence imaging of the blue fluorescence turn-on COS/H_2S donor **1** in HeLa cells. Cells were incubated with (a) NucRed (2 μM); (b) NucRed (2 μM) and CT-MeRhoAz (2.5 μM); (c) NucRed (2 μM) and COS/H_2S donor **1** (50 μM); and (d) NucRed (2 μM), CT-MeRhoAz (2.5 μM), and COS/H_2S donor **1** (50 μM). Cells were incubated with NucRed and either CT-MeRhoAz, COS/H_2S donor **1**, or both for 20 minutes and then imaged. Bar scale: 50 mm.

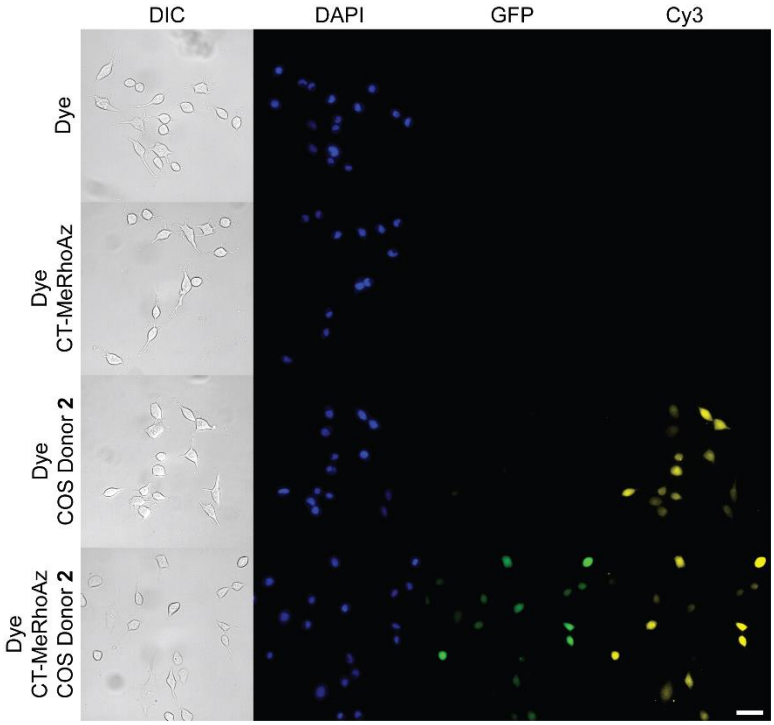


Figure B33. Fluorescence imaging of yellow fluorescence turn-on COS/H_2S donor **2** in HeLa cells. Cells were incubated with (a) Hoechst 33342 (5 μM); (b) Hoechst 33342 (5 μM) and CT-MeRhoAz (2.5 μM); (c) Hoechst 33342 (5 μM) and COS/H_2S donor **2** (20 μM); and (d) Hoechst 33342 (5 μM), CT-MeRhoAz (2.5 μM), and COS/H_2S donor **2** (20 μM). Cells were incubated with Hoechst 33342 and either CT-MeRhoAz, COS/H_2S donor **2**, or both for 20 minutes and then imaged. Bar scale: 50 mm.

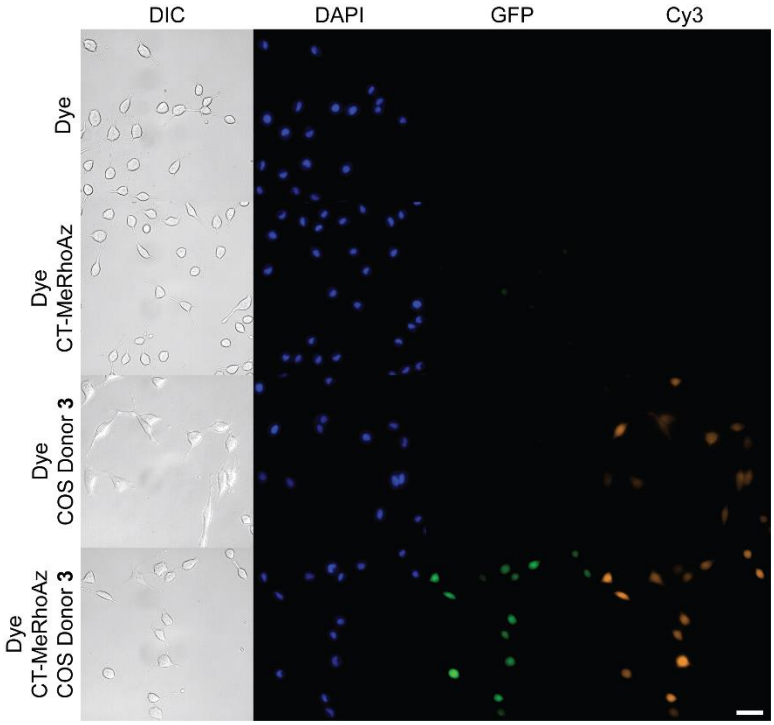


Figure B34. Fluorescence imaging of orange fluorescence turn-on COS/H_2S donor **3** in HeLa cells. Cells were incubated with (a) Hoechst 33342 (5 μM); (b) Hoechst 33342 (5 μM) and CT-MeRhoAz (2.5 μM); (c) Hoechst 33342 (5 μM) and COS/H_2S donor **3** (20 μM); and (d) Hoechst 33342 (5 μM), CT-MeRhoAz (2.5 μM), and COS/H_2S donor **3** (20 μM). Cells were incubated with Hoechst 33342 and either CT-MeRhoAz, COS/H_2S donor **3**, or both for 20 minutes and then imaged. Bar scale: 50 mm.

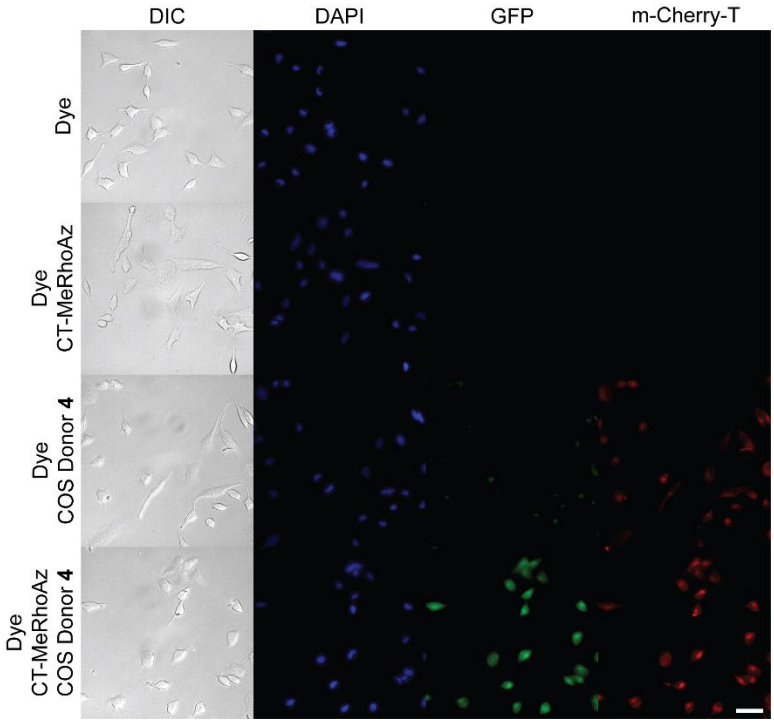


Figure B35. Fluorescence imaging of red fluorescence turn-on COS/H_2S donor **4** in HeLa cells. Cells were incubated with (a) Hoechst 33342 (5 μM); (b) Hoechst 33342 (5 μM) and CT-MeRhoAz (2.5 μM); (c) Hoechst 33342 (5 μM) and COS/H_2S donor **4** (20 μM); and (d) Hoechst 33342 (5 μM), CT-MeRhoAz (2.5 μM), and COS/H_2S donor **4** (20 μM). Cells were incubated with Hoechst 33342 and either CT-MeRhoAz, COS/H_2S donor **4**, or both for 20 minutes and then imaged. Bar scale: 50 mm.

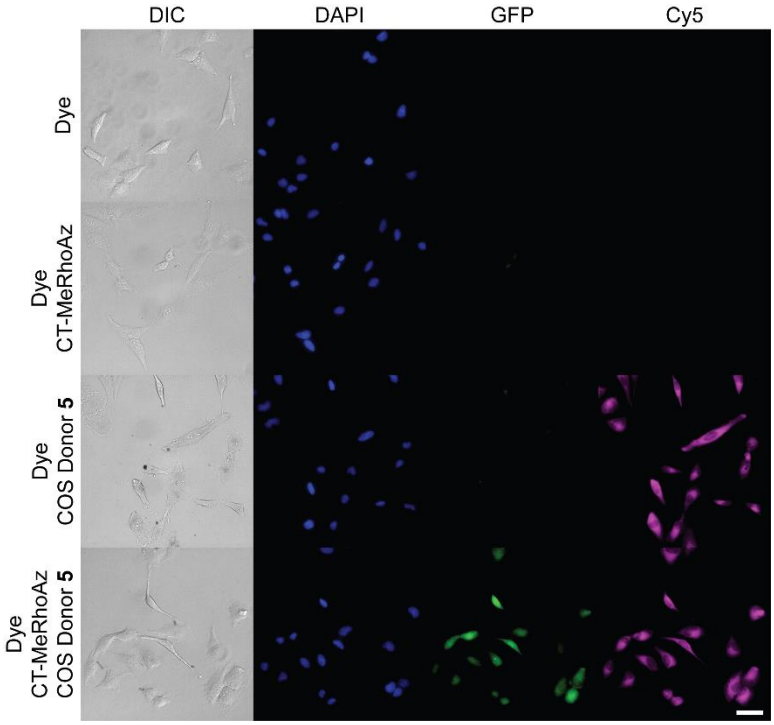


Figure B36. Fluorescence imaging of NIR fluorescence turn-on COS/H_2S donor **5** in HeLa cells. Cells were incubated with (a) Hoechst 33342 (5 μM); (b) Hoechst 33342 (5 μM) and CT-MeRhoAz (2.5 μM); (c) Hoechst 33342 (5 μM) and COS/H_2S donor **5** (20 μM); and (d) Hoechst 33342 (5 μM), CT-MeRhoAz (2.5 μM), and COS/H_2S donor **5** (20 μM). Cells were incubated with Hoechst 33342 and either CT-MeRhoAz, COS/H_2S donor **5**, or both for 20 minutes and then imaged. Bar scale: 50 mm.

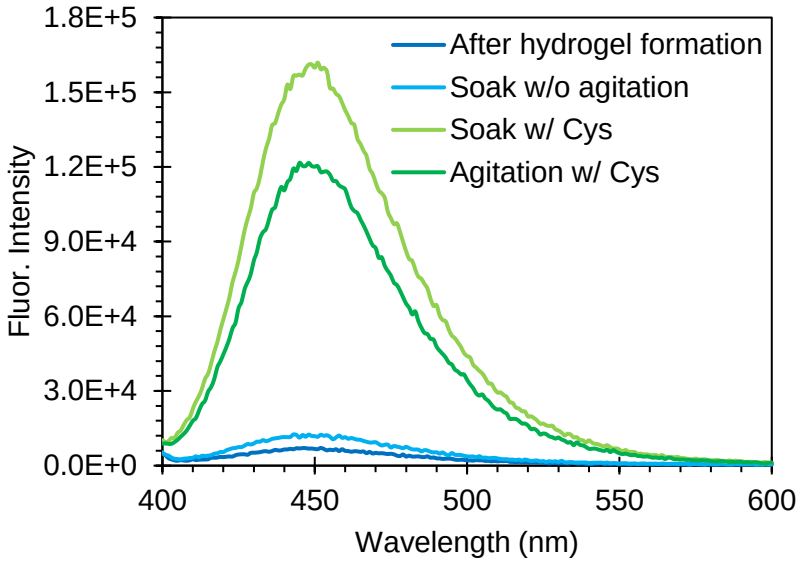


Figure B37. Fluorescence intensity of the blue COS/H_2S donor **1** (10 μM) when loaded into a 2% (w/v) alginate hydrogel under various conditions. Excitation wavelength: 350 nm, slit width: 2 nm.

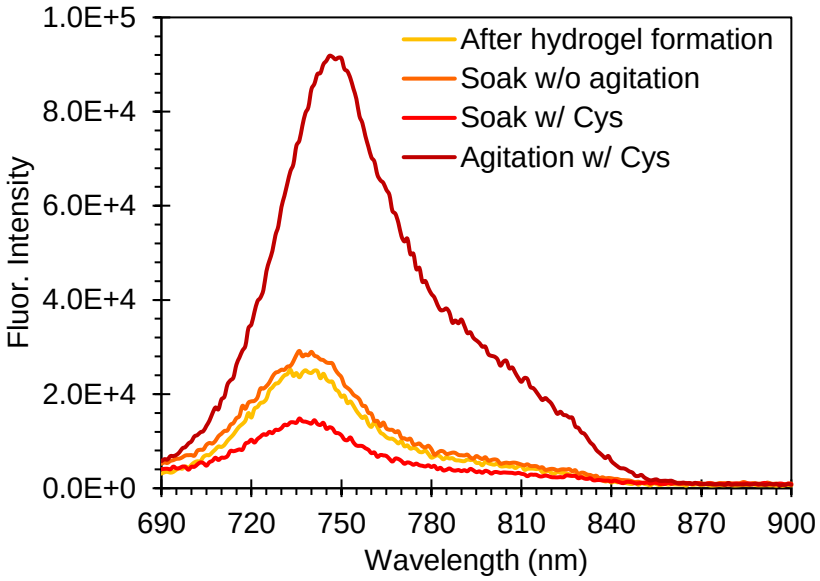


Figure B38. Fluorescence intensity of the NIR COS/H_2S donor **5** (10 μM) when loaded into a 2% (w/v) alginate hydrogel under various conditions. Excitation wavelength: 700 nm, slit width: 4 nm.

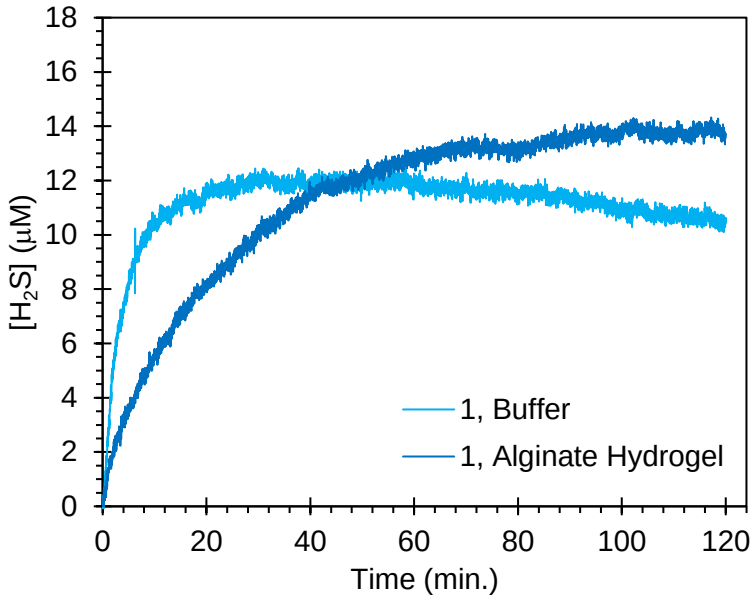


Figure B39. H_2S release from the blue COS/H_2S donor **1** (10 μM) in the presence of CA (25 μg mL^{-1}) when activated by cysteine (100 μM, 10 equiv.) either in buffer or loaded into an alginate hydrogel (2%, 800 μL) over 120 minutes measured by a Unisense H_2S-selective electrode.

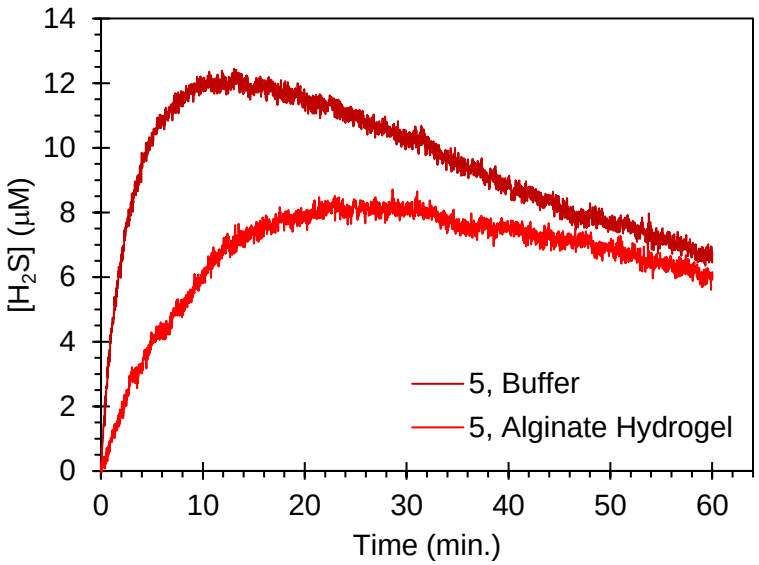


Figure B40. H_2S release from the NIR COS/H_2S donor **5** (10 μM) in the presence of CA (25 μg mL^{-1}) when activated by cysteine (100 μM, 10 equiv.) either in buffer or loaded into an alginate hydrogel (2%, 800 μL) over 120 minutes measured by a Unisense H_2S-selective electrode.

*Alginate Hydrogel Loaded with DMSO or Donor **5** in Rats*

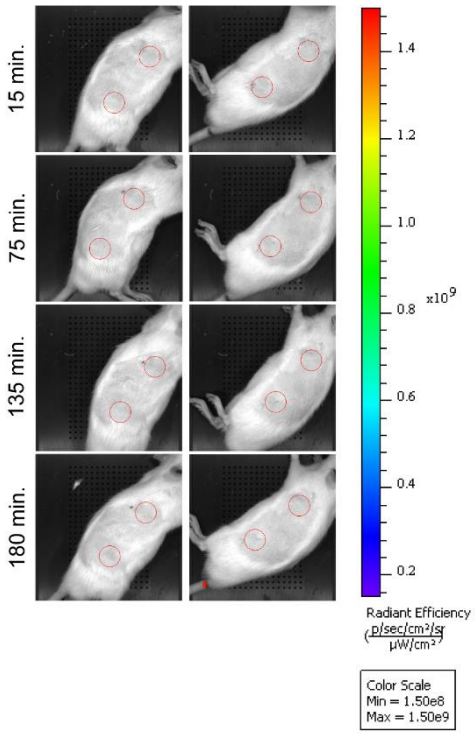


Figure B41. Fluorescence of the blank, DMSO-loaded alginate gel without GSH over 180 minutes in a live rat. The experiments were performed in quadruplicate with the regions of interest highlighted by the red circle.

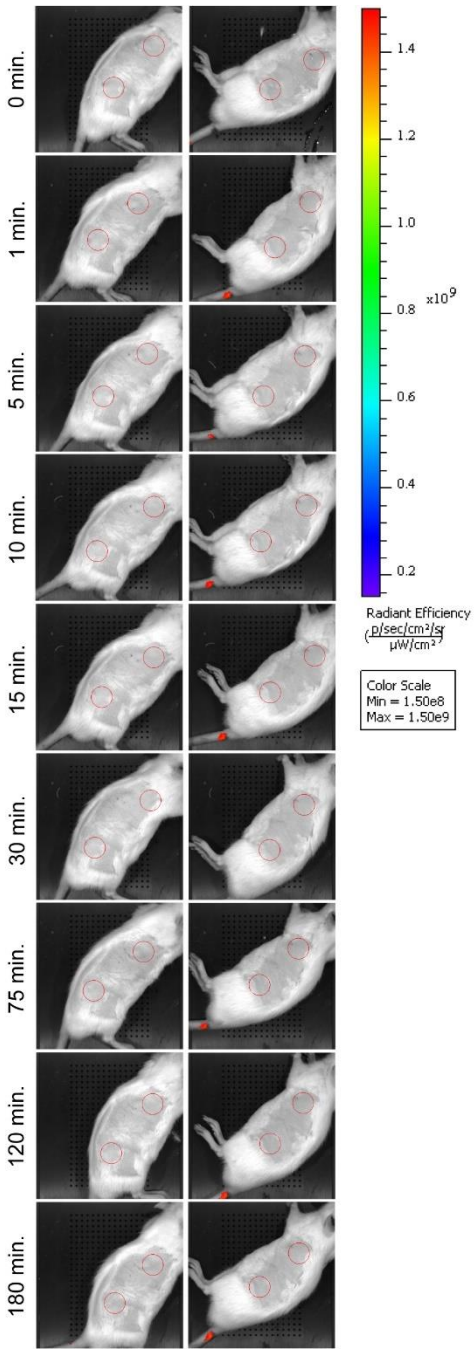


Figure B42. Fluorescence of the blank, DMSO-loaded alginate gel with GSH injection over 180 minutes in a live rat. The experiments were performed in quadruplicate with the regions of interest highlighted by the red circle.

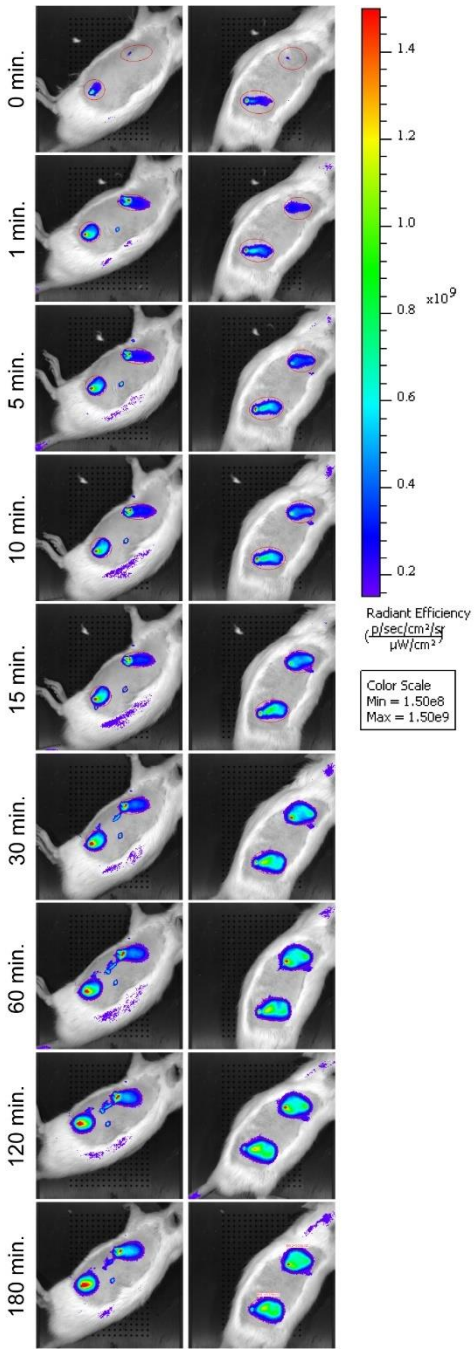


Figure B43. Fluorescence of the donor-loaded alginate gel (250 μM donor **5**) without GSH injection over 180 minutes in a live rat. The experiments were performed in quadruplicate with the regions of interest highlighted by the red circle.

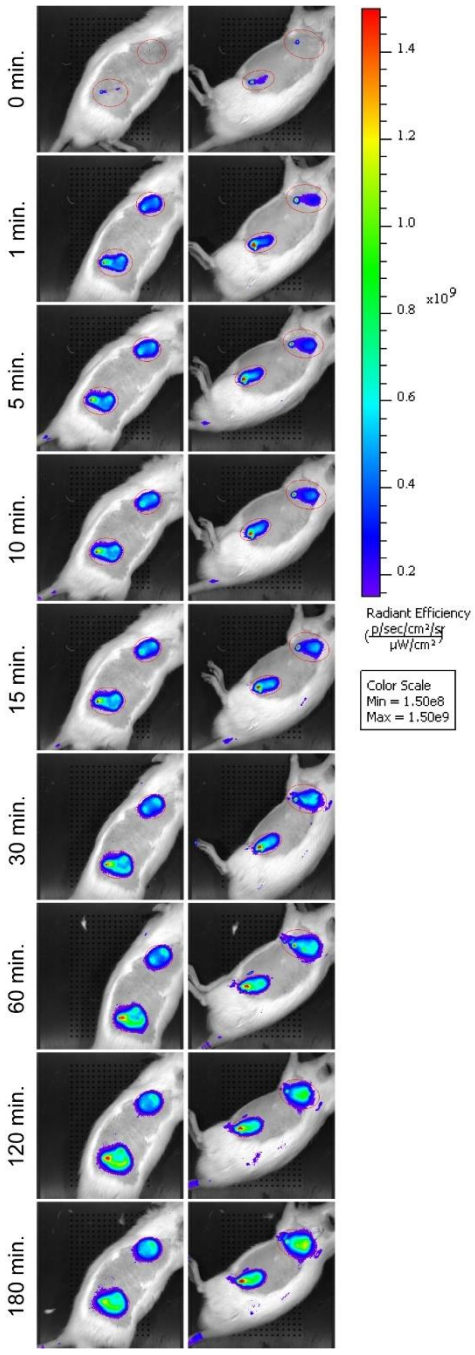


Figure B44. Fluorescence of the donor-loaded alginate gel (250 μM donor **5**) with GSH injection over 180 minutes in a live rat. The experiments were performed in quadruplicate with the regions of interest highlighted by the red circle.

*^{1}H and ^{13}C NMR spectra of compounds **1**–**5** and **S1**–**S9***

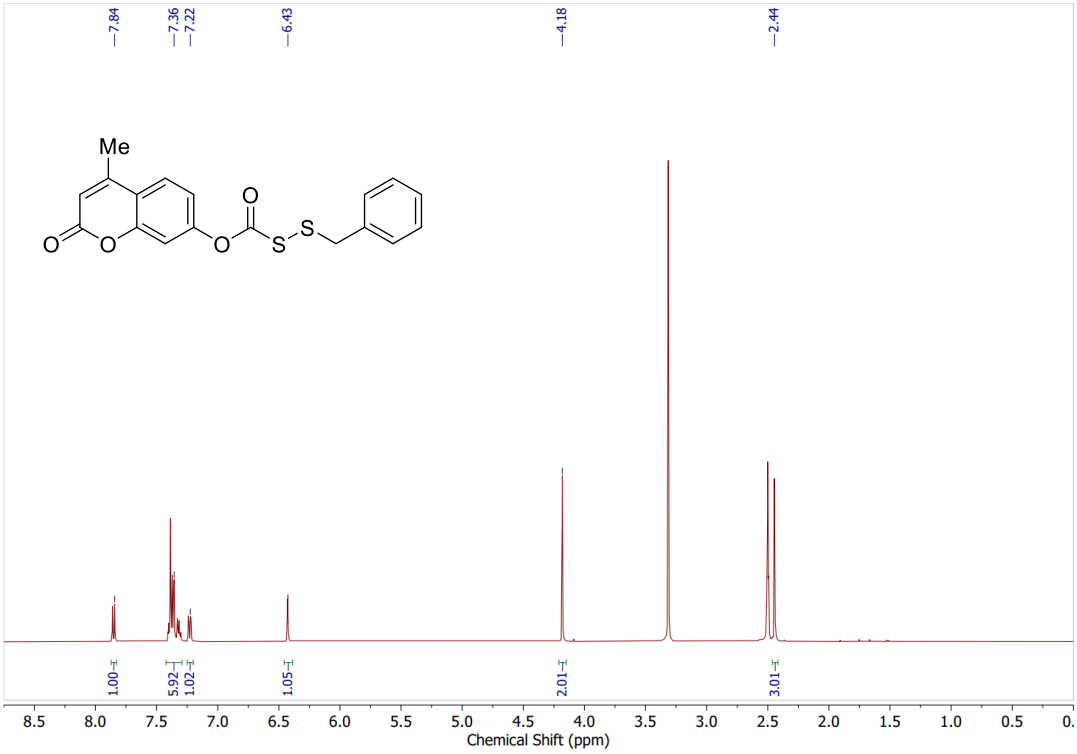


Figure B45. ^{1}H NMR (500 MHz, $(CD_3)_2SO$) spectrum of **1**.

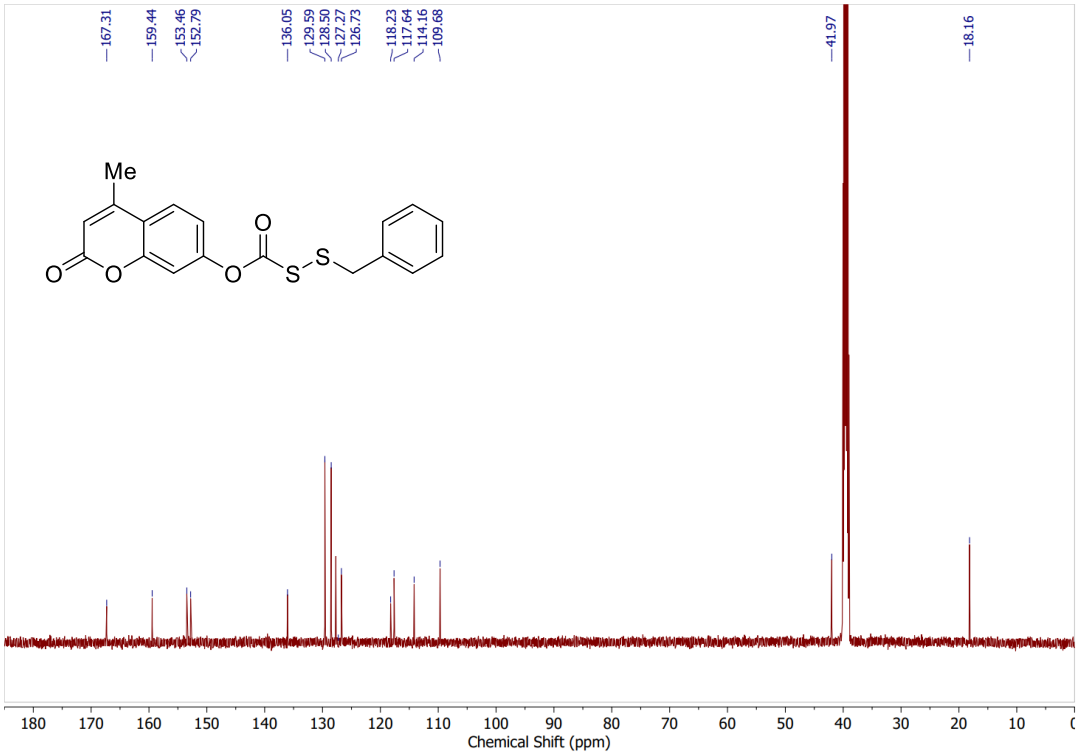


Figure B46. ^{13}C NMR (125 MHz, $(CD_3)_2SO$) spectrum of **1**.

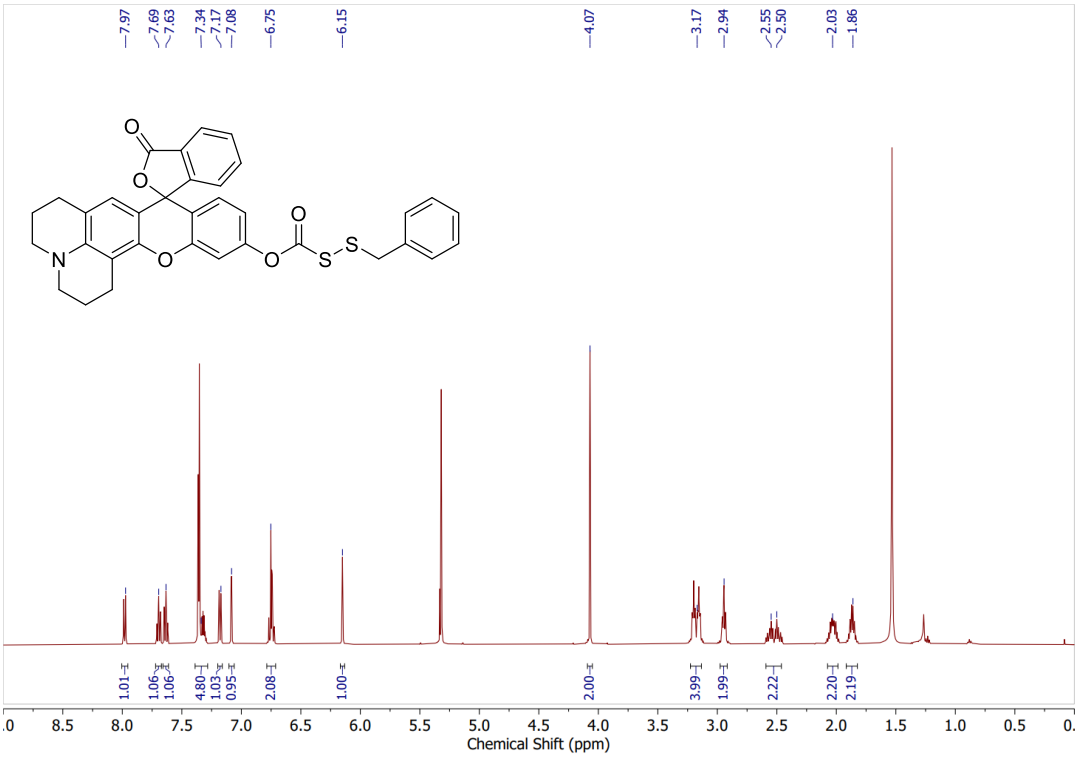


Figure B47. ^{1}H NMR (500 MHz, CD_2Cl_2) spectrum of **2**.

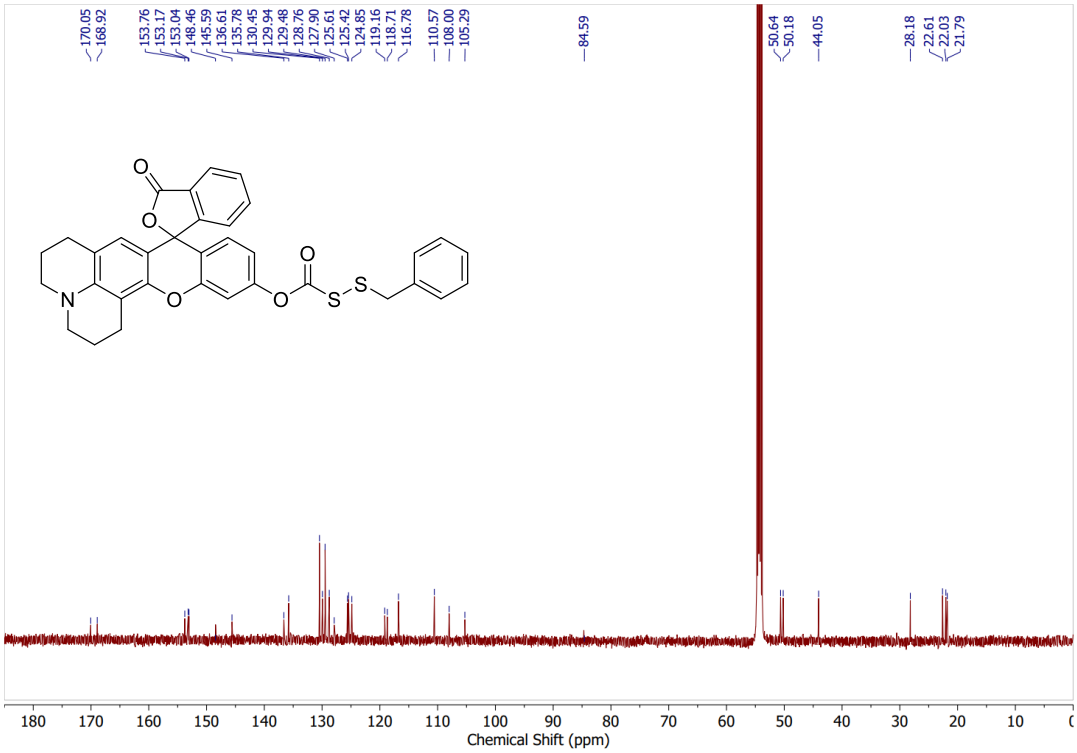


Figure B48. ^{13}C NMR (125 MHz, CD_2Cl_2) spectrum of **2**.

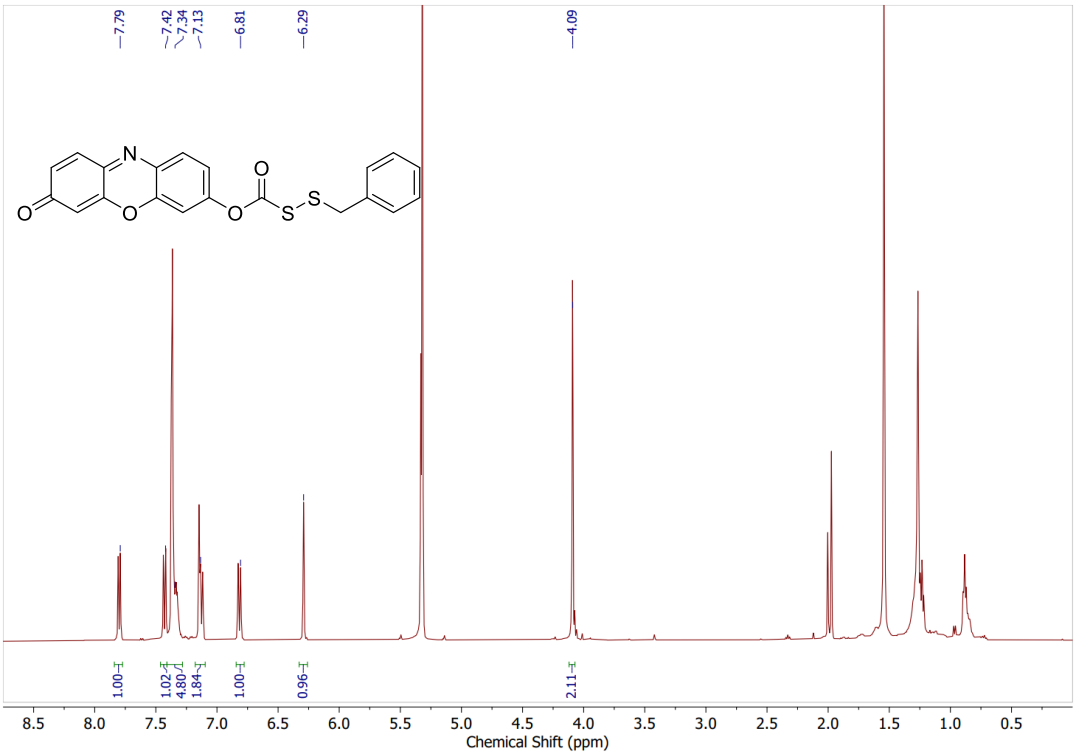


Figure B49. ^{1}H NMR (500 MHz, CD_2Cl_2) spectrum of **3**.

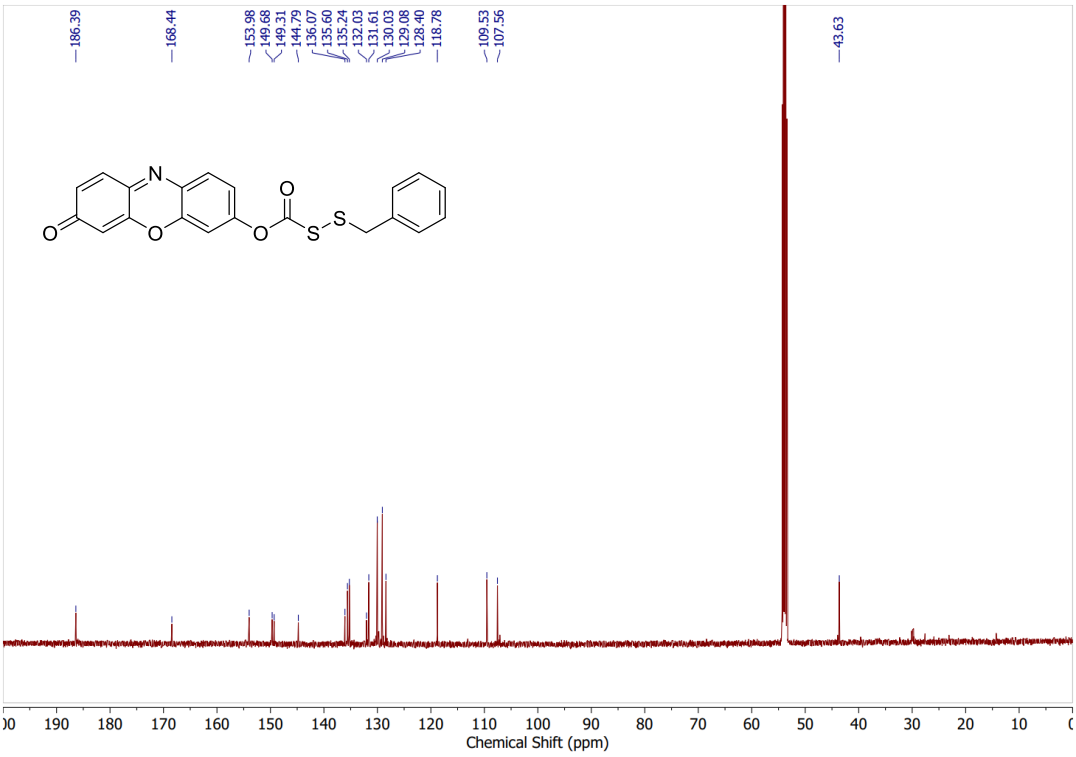


Figure B50. ^{13}C NMR (125 MHz, CD_2Cl_2) spectrum of **3**.

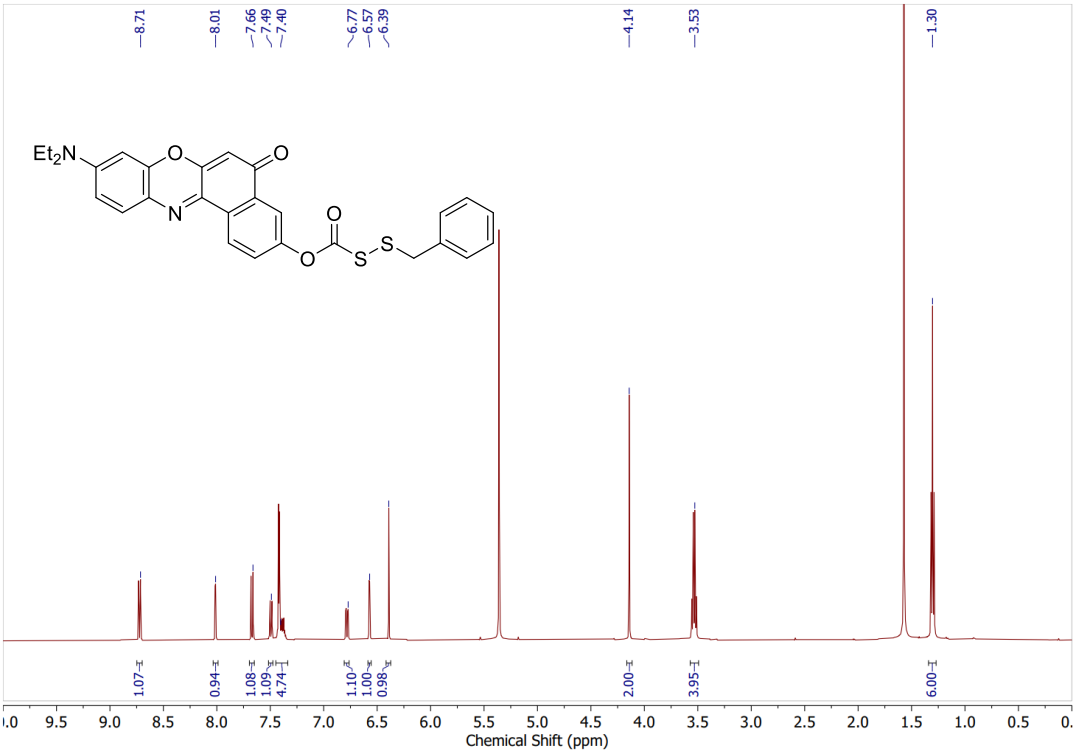


Figure B51. ^{1}H NMR (500 MHz, CD_2Cl_2) spectrum of **4**.

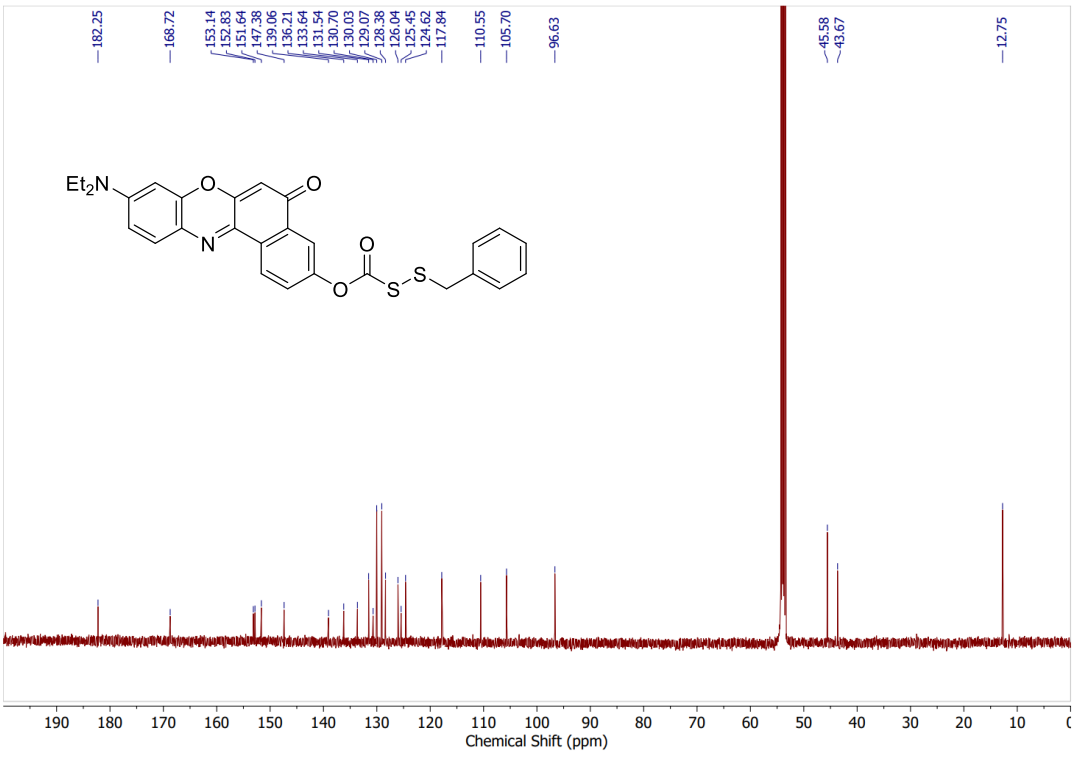


Figure B52. ^{13}C NMR (125 MHz, CD_2Cl_2) spectrum of **4**.

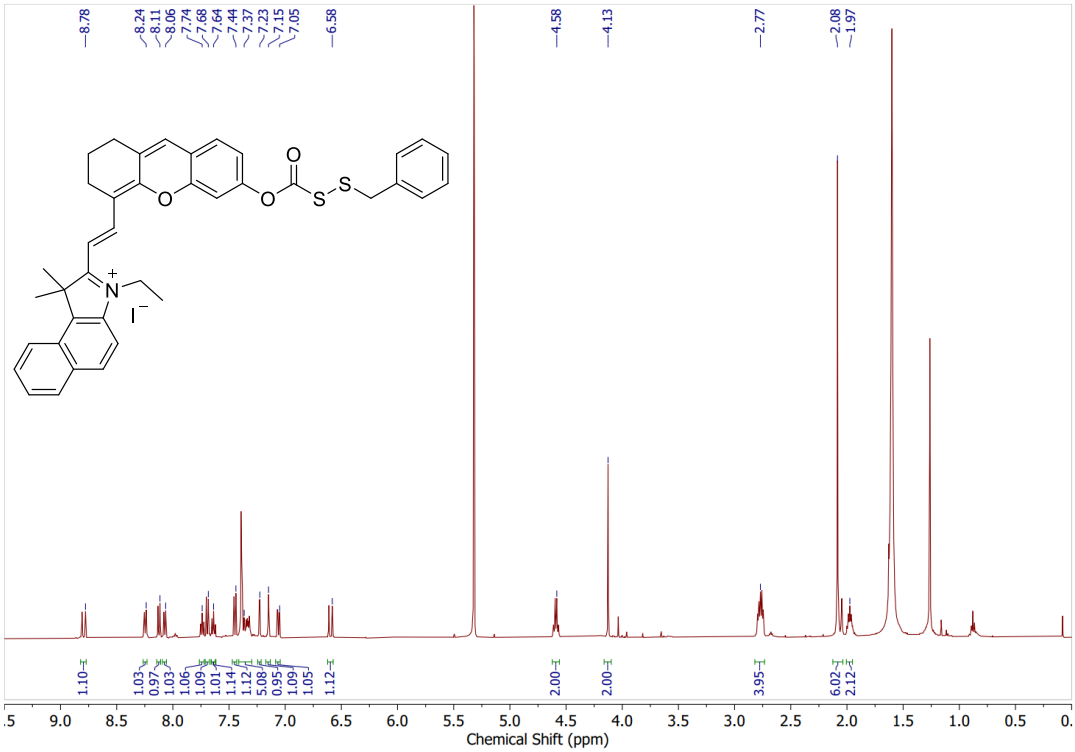


Figure B53. ^{1}H NMR (500 MHz, CD_2Cl_2) spectrum of **5**.

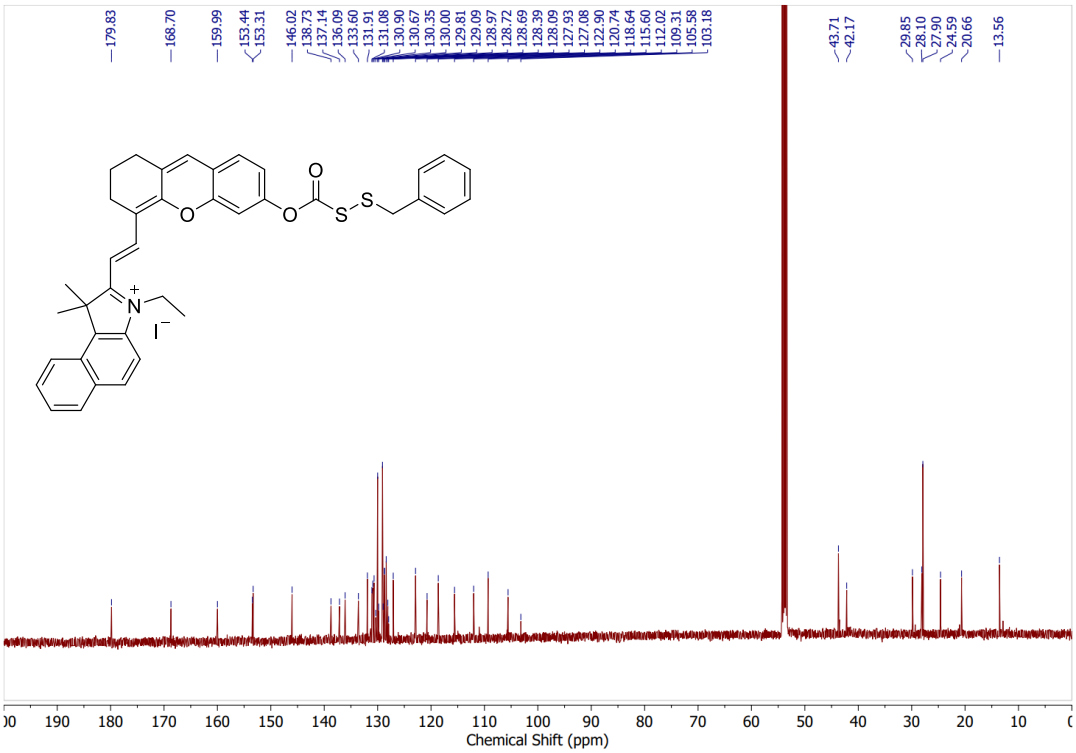


Figure B54. ^{13}C NMR (125 MHz, CD_2Cl_2) spectrum of **5**.

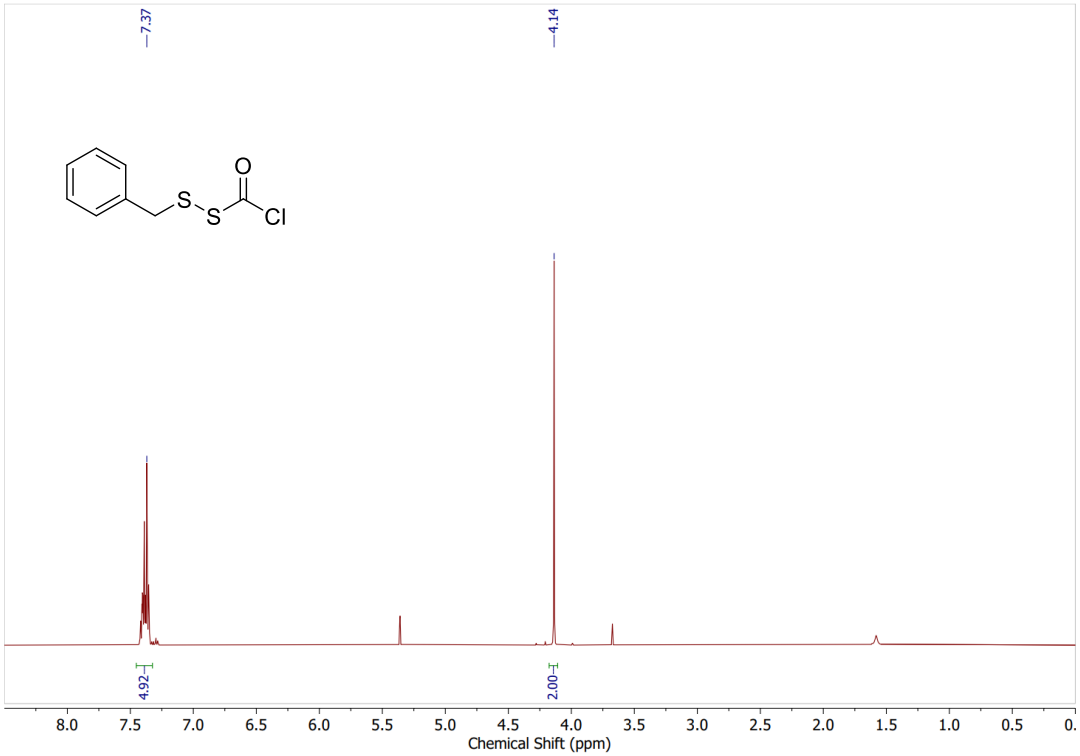


Figure B55. ^{1}H NMR (500 MHz, CD_2Cl_2) spectrum of **S1**.

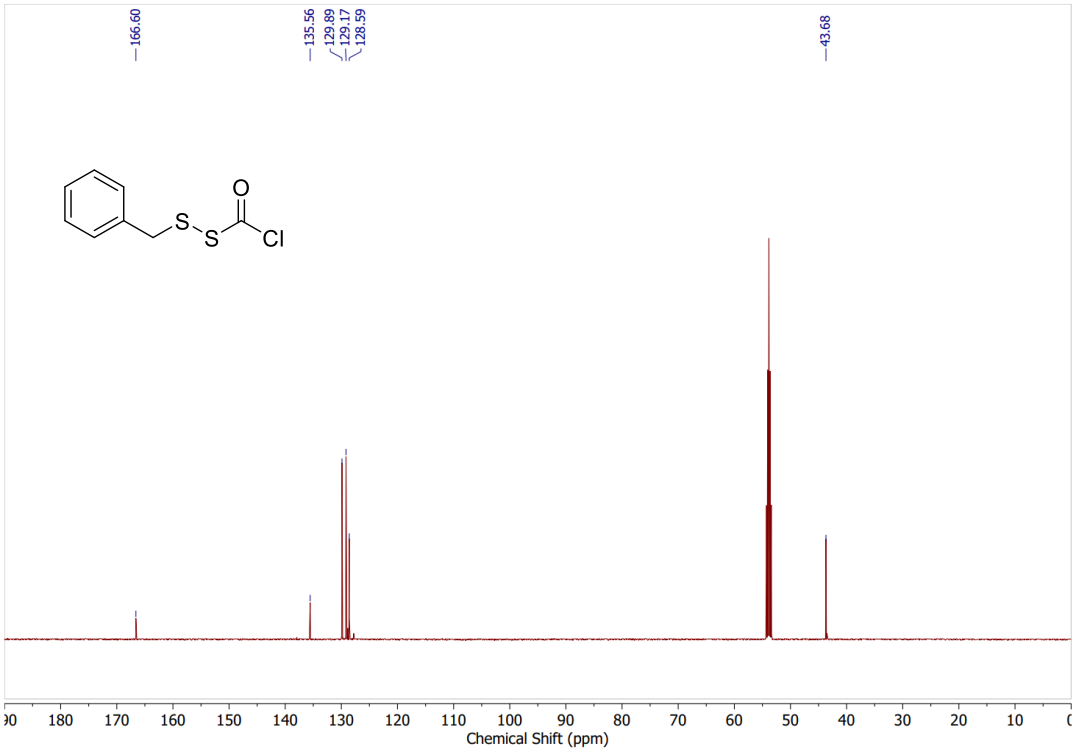


Figure B56. ^{13}C NMR (125 MHz, CD_2Cl_2) spectrum of **S1**.

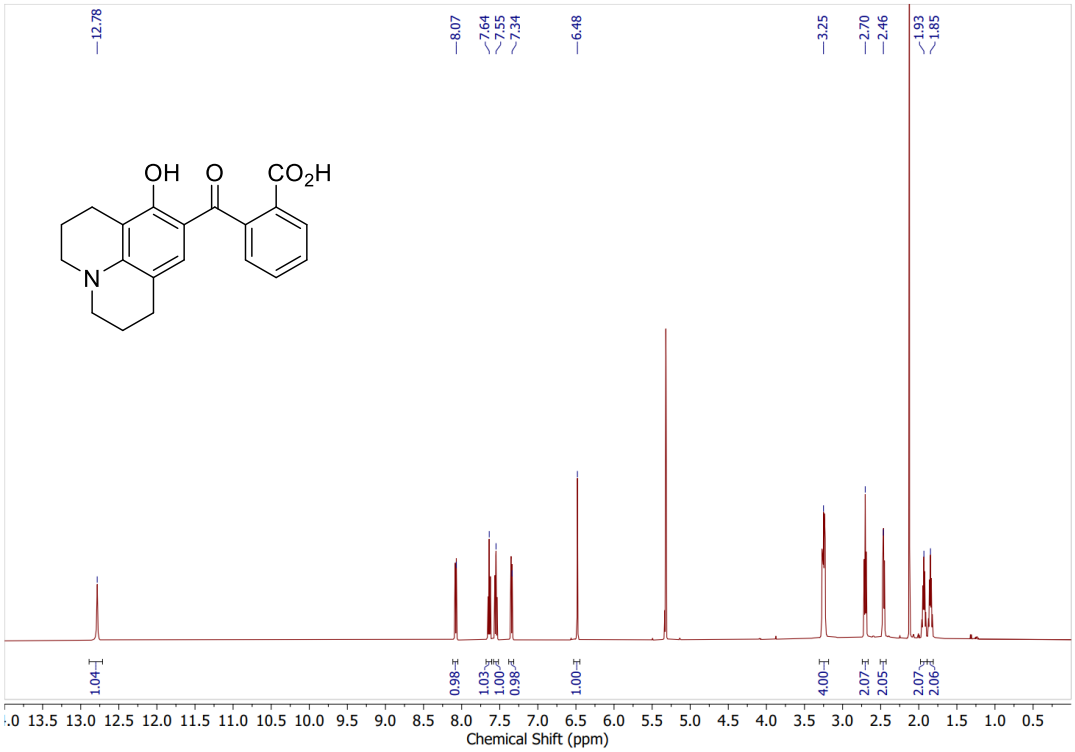


Figure B57. ^{1}H NMR (500 MHz, CD_2Cl_2) spectrum of **S2**.

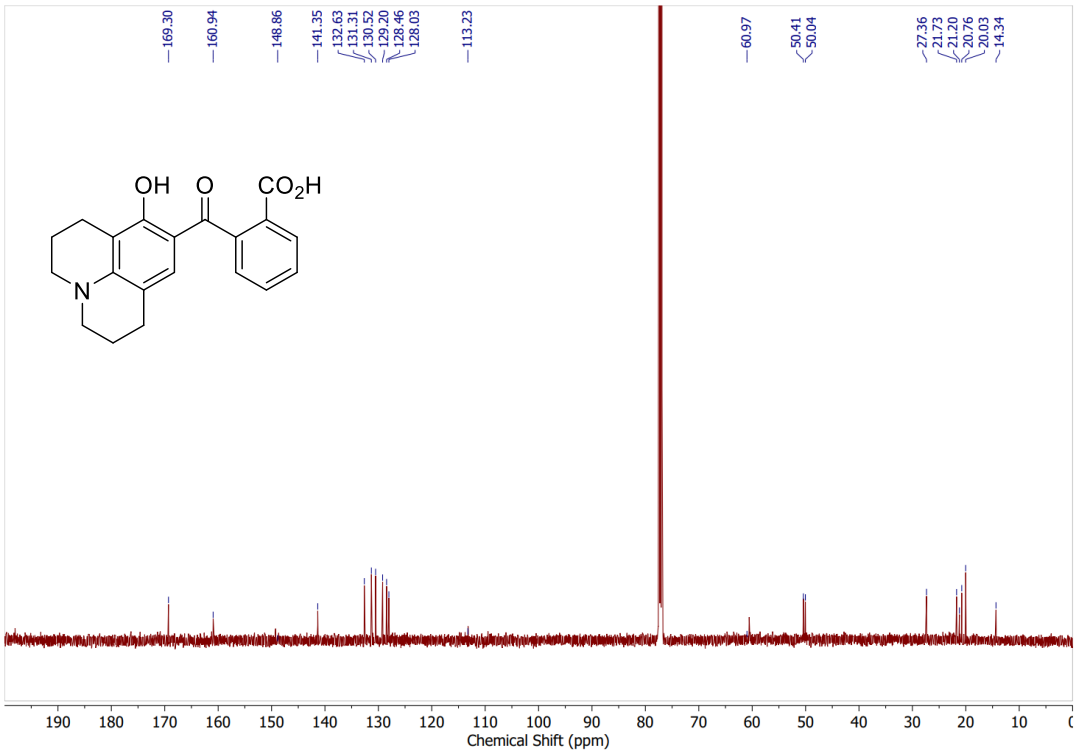


Figure B58. ^{13}C NMR (125 MHz, $CDCl_3$) spectrum of **S2**.

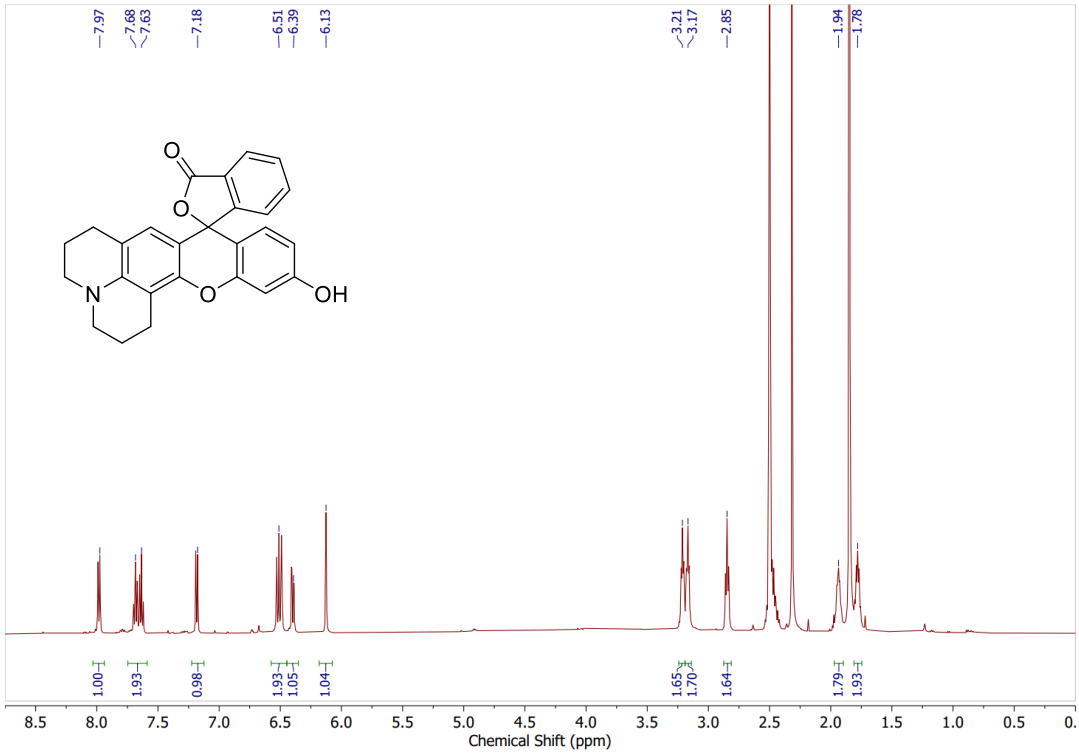


Figure B59. ^{1}H NMR (500 MHz, $(CD_3)_2SO$) spectrum of **S3**.

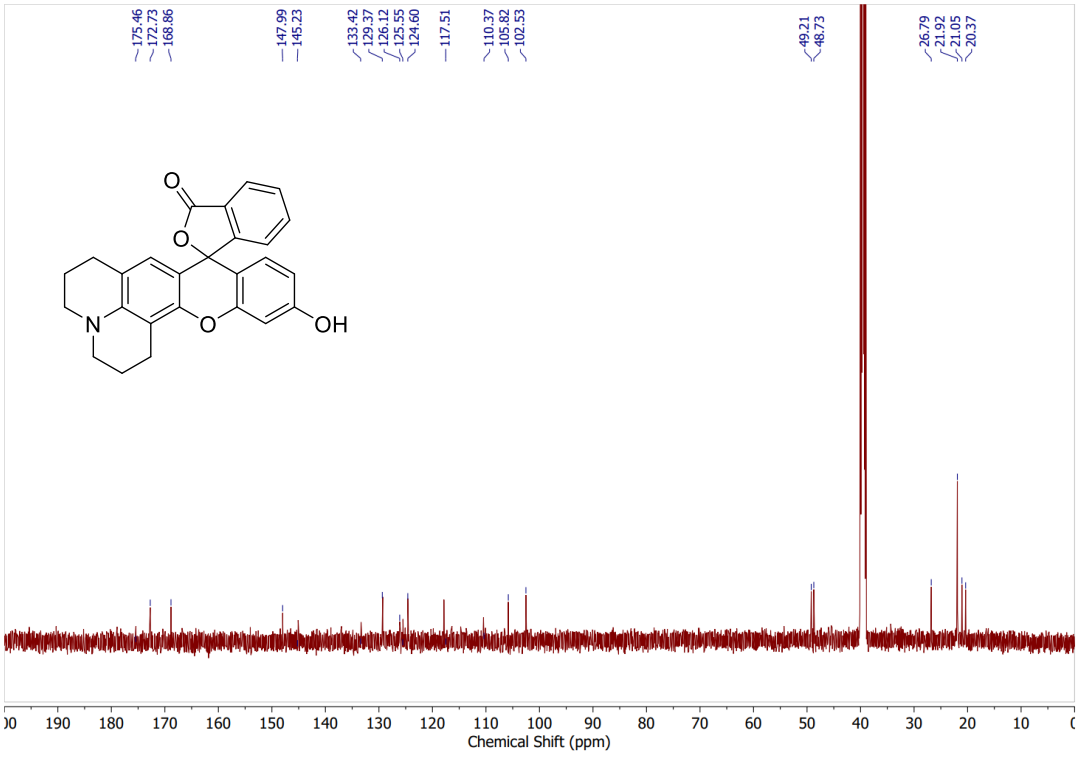


Figure B60. ^{13}C NMR (125 MHz, $(CD_3)_2SO$) spectrum of **S3**.

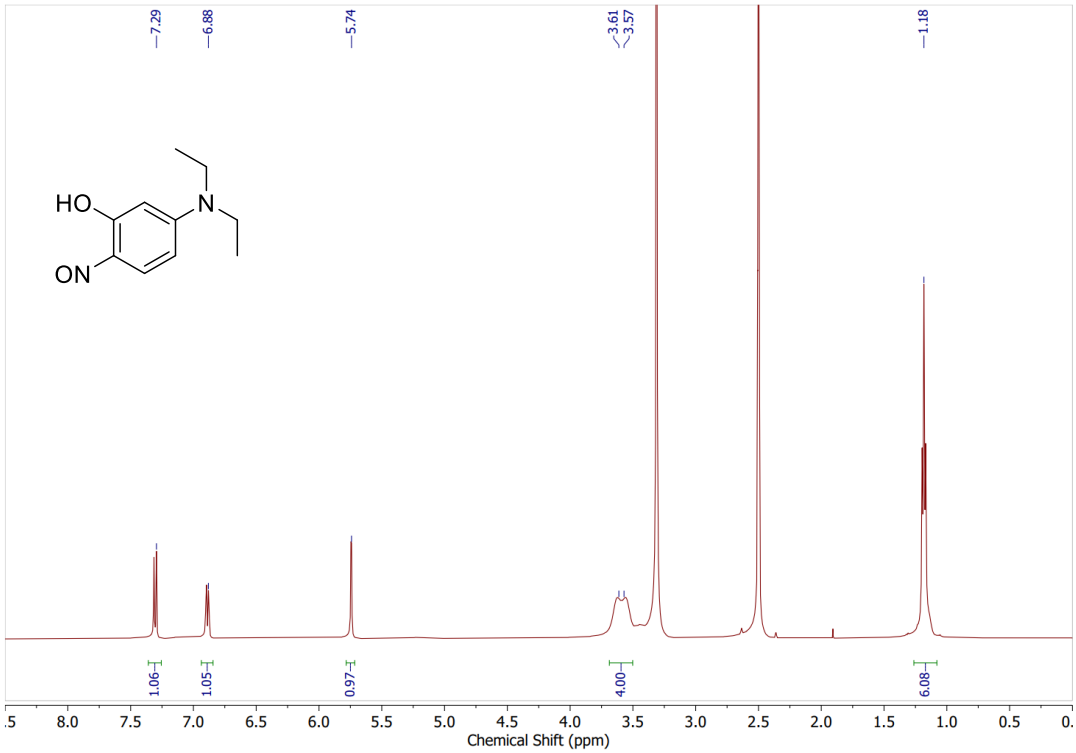


Figure B61. ^{1}H NMR (500 MHz, $(CD_3)_2SO$) spectrum of **S4**.

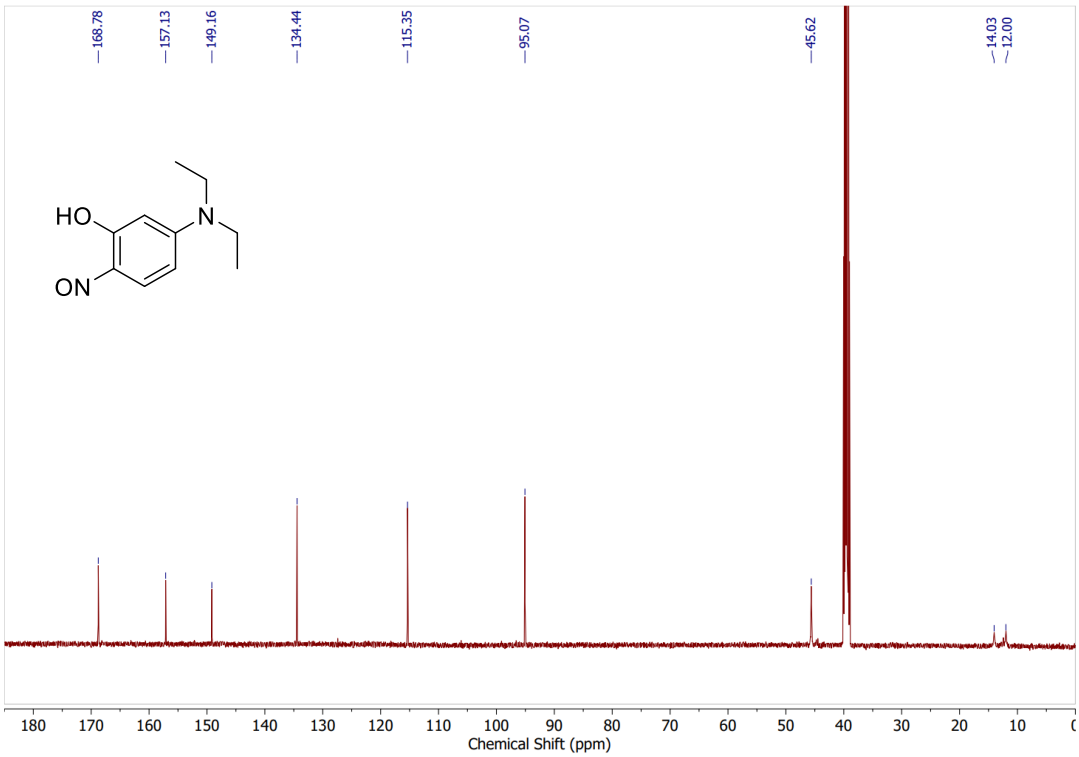


Figure B62. ^{13}C NMR (125 MHz, $(CD_3)_2SO$) spectrum of **S4**.

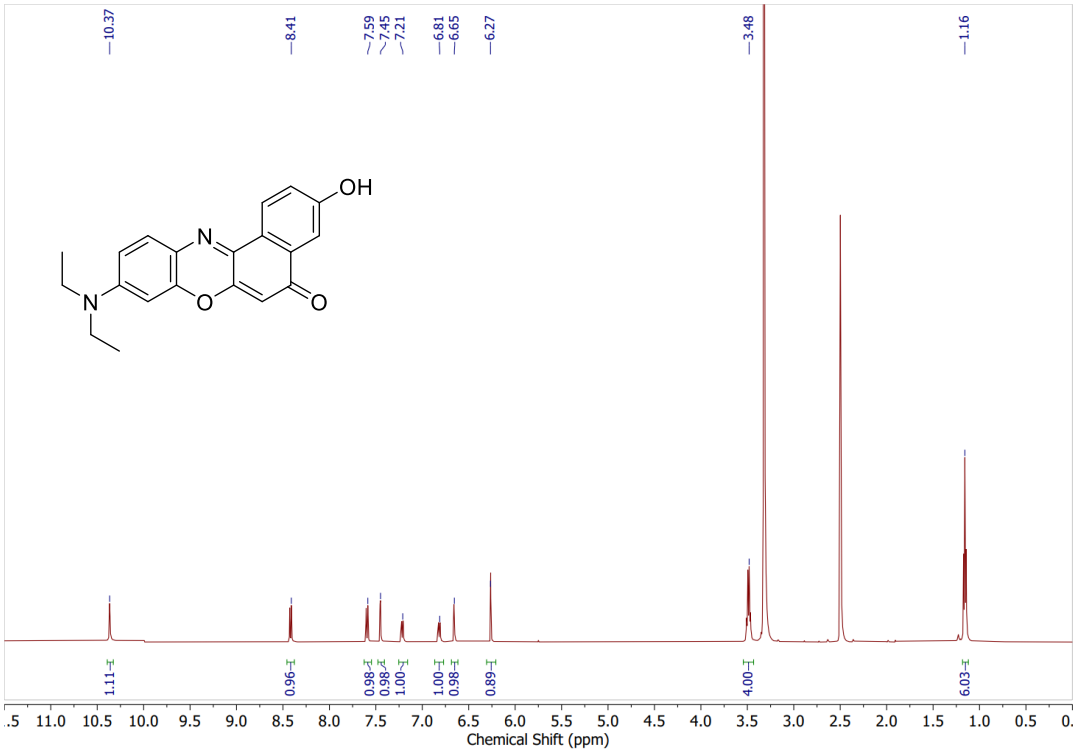


Figure B63. ^{1}H NMR (500 MHz, $(CD_3)_2SO$) spectrum of **S5**.

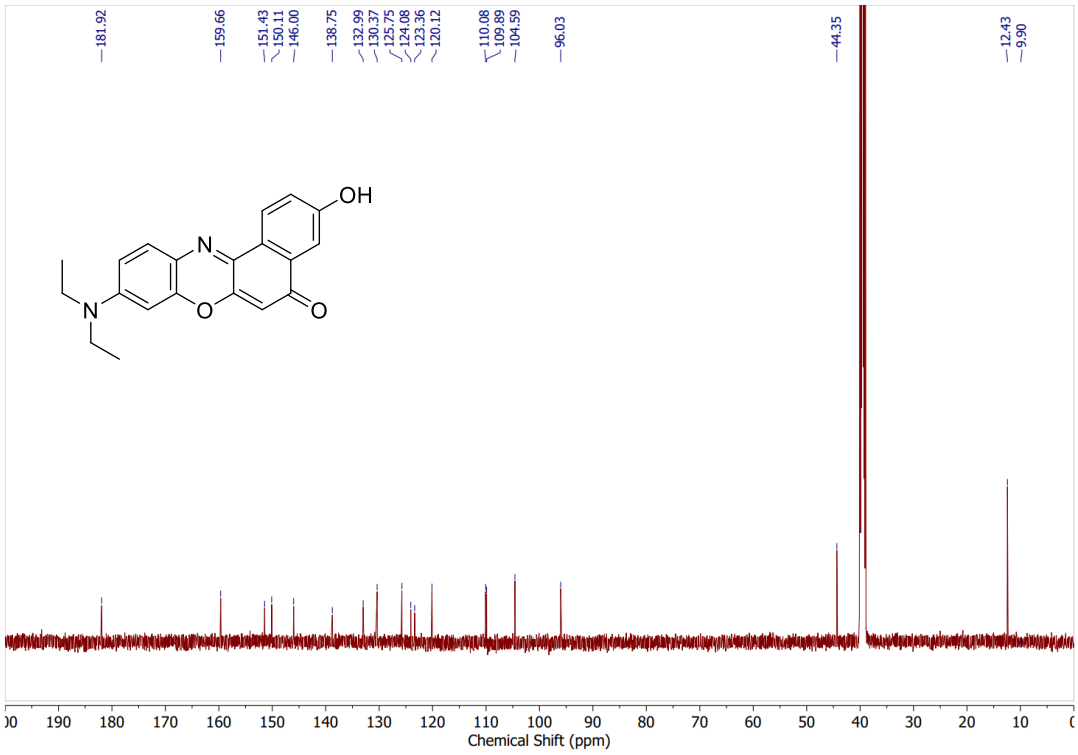


Figure B64. ^{13}C NMR (125 MHz, $(CD_3)_2SO$) spectrum of **S5**.

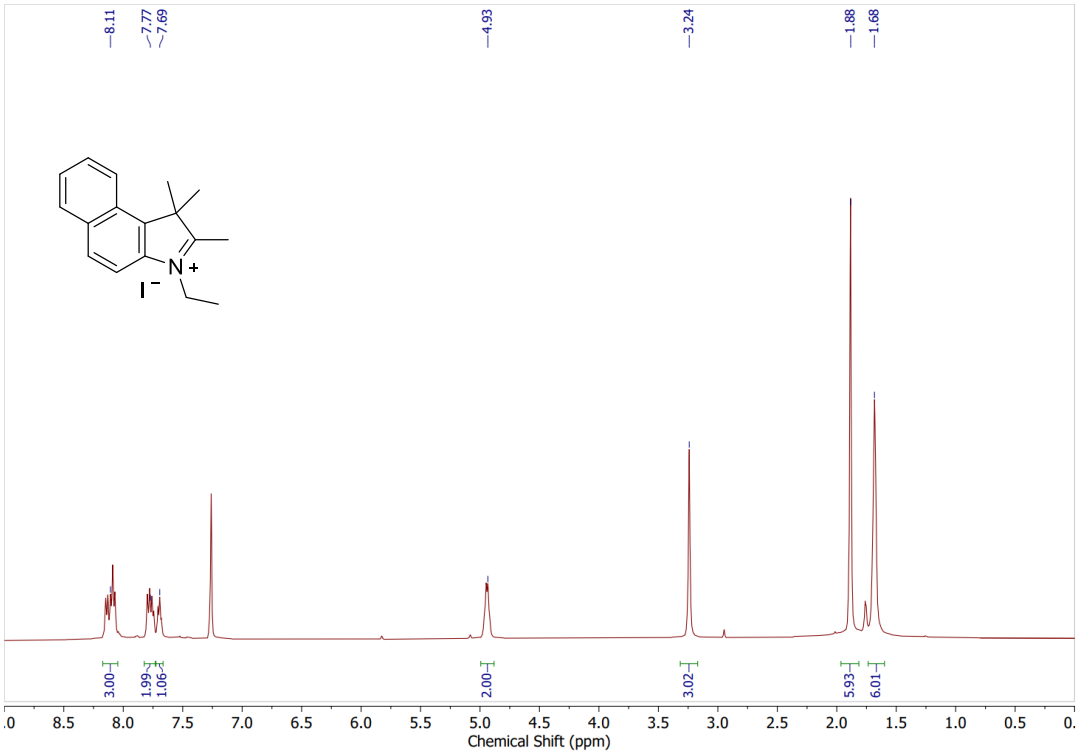


Figure B65. ^{1}H NMR (500 MHz, $CDCl_3$) spectrum of **S6**.

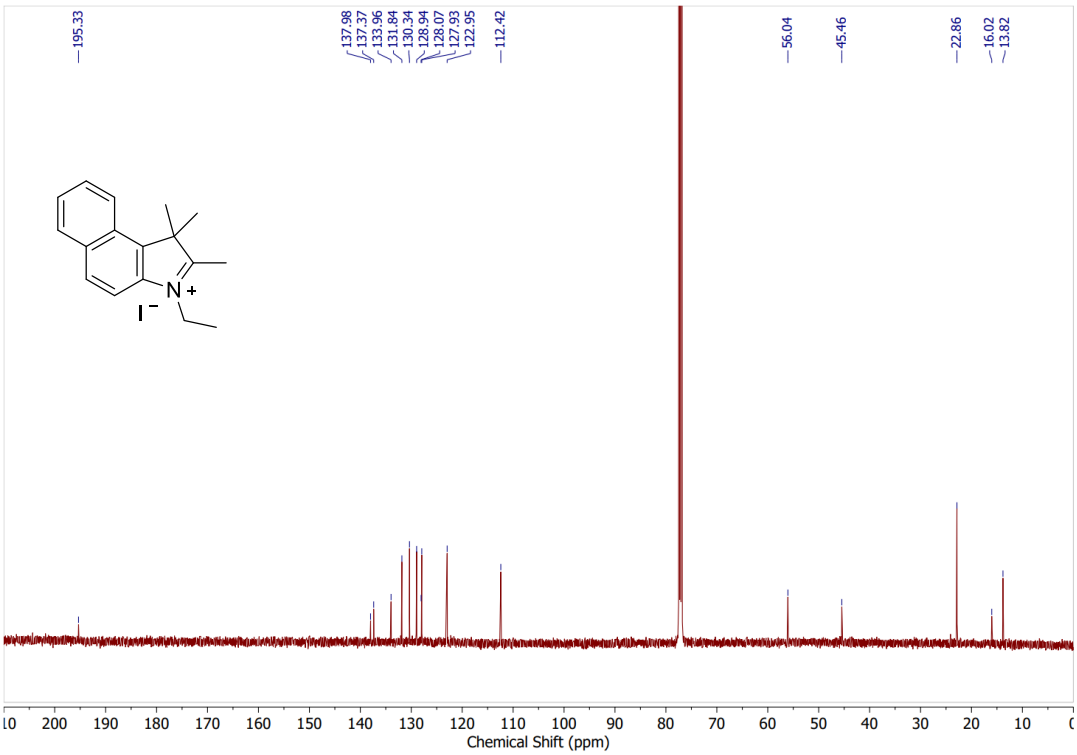


Figure B66. ^{13}C NMR (125 MHz, $CDCl_3$) spectrum of **S6**.

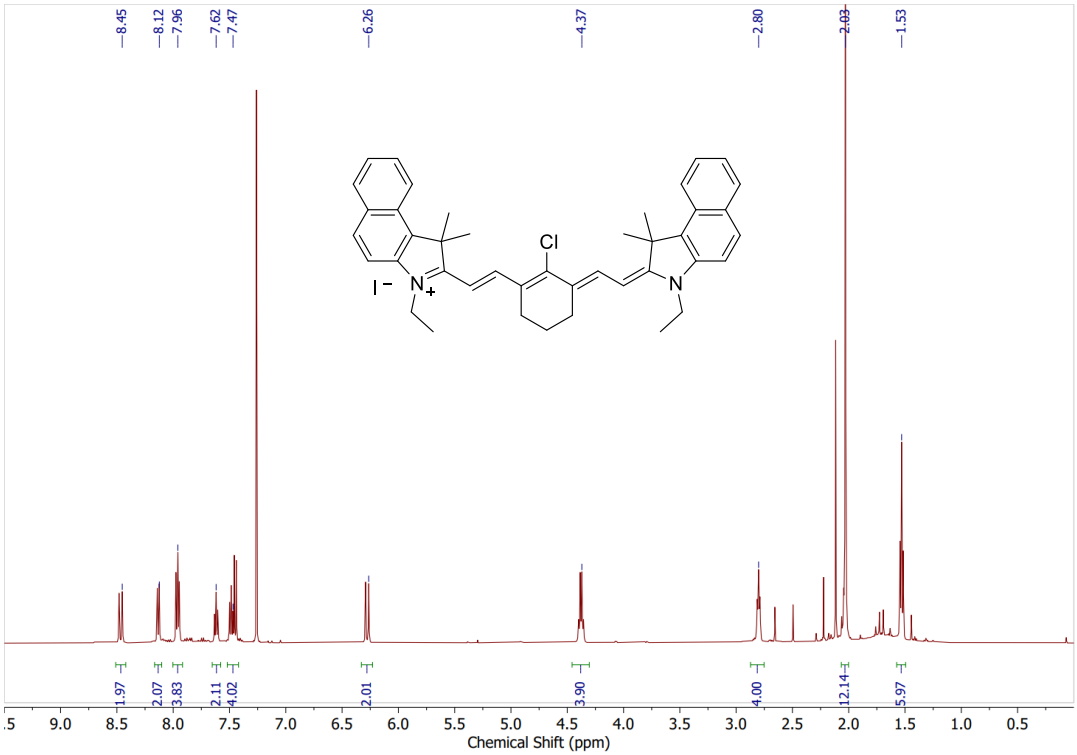


Figure B67. ^{1}H NMR (500 MHz, $CDCl_3$) spectrum of **S8**.

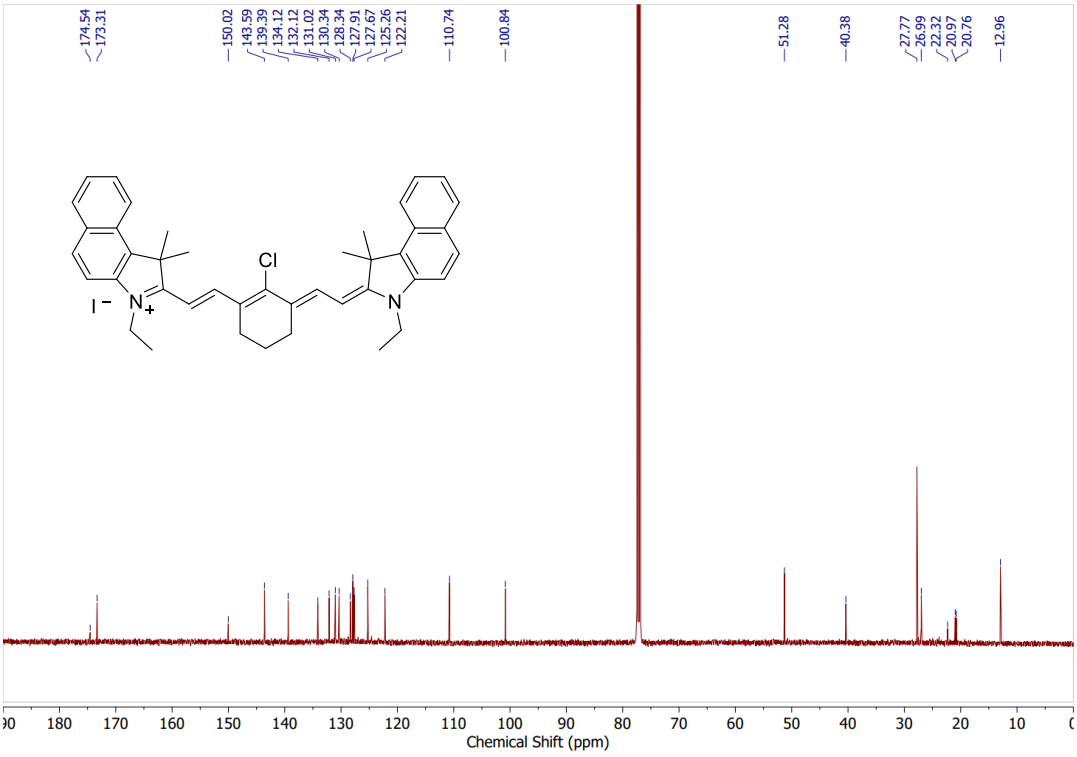


Figure B68. ^{13}C NMR (125 MHz, $CDCl_3$) spectrum of **S8**.

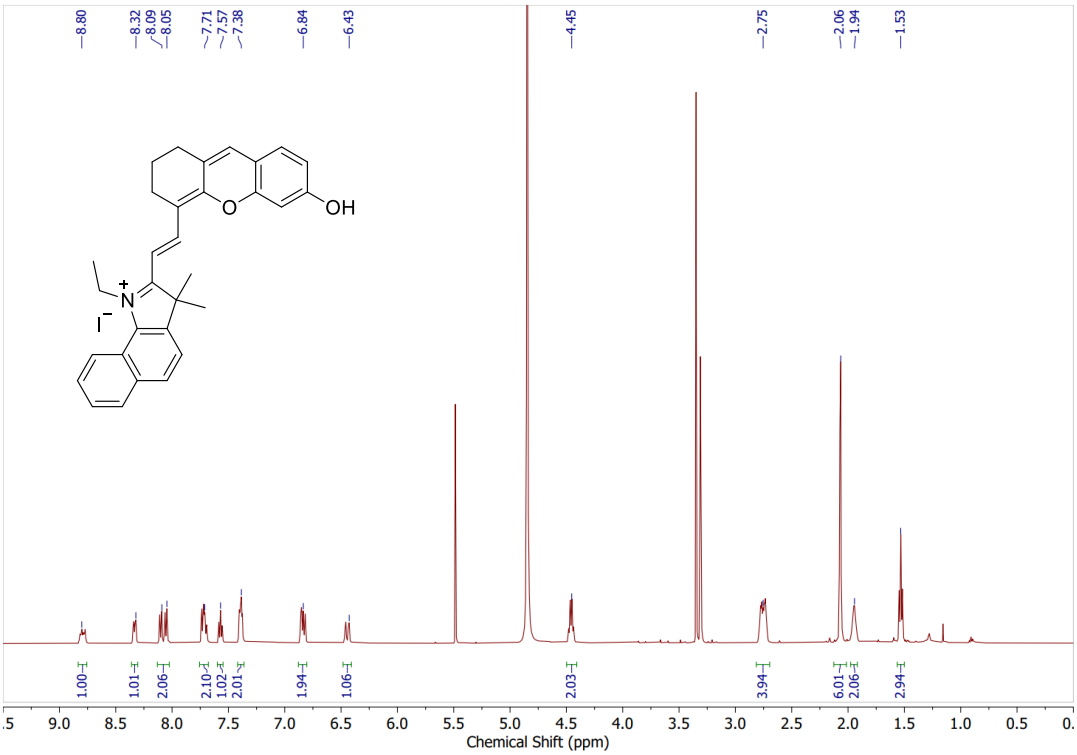


Figure B69. ^{1}H NMR (500 MHz, CD_3OD) spectrum of **S9**.

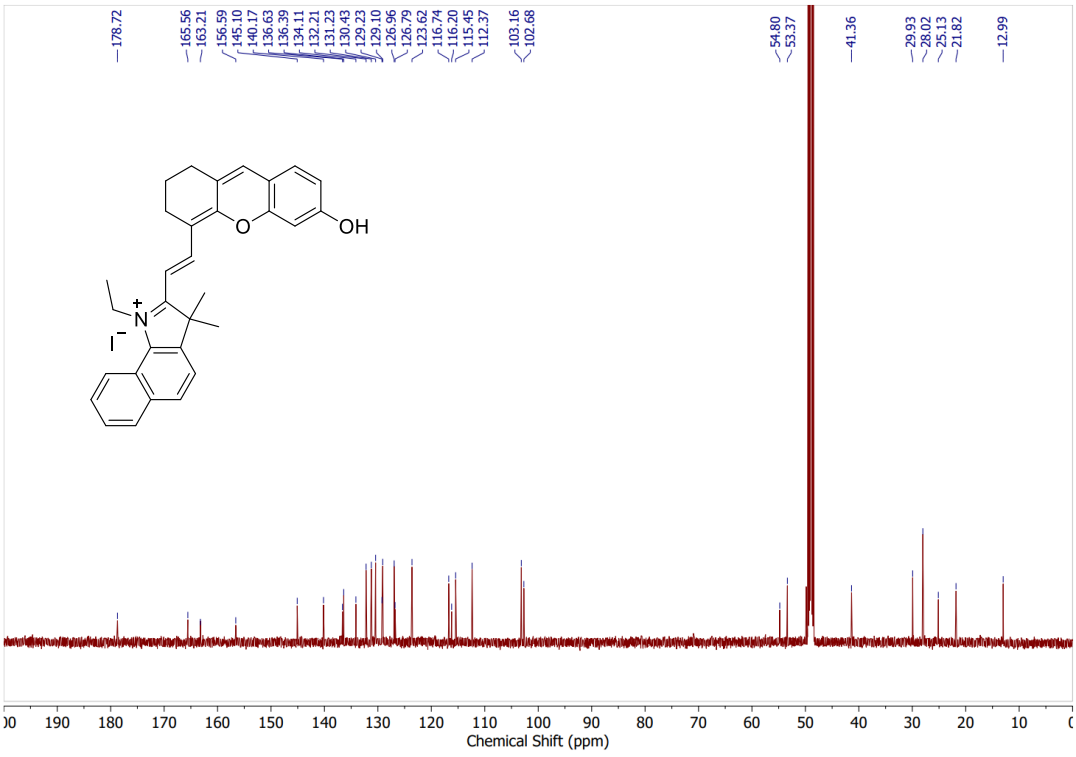


Figure B70. ^{13}C NMR (125 MHz, CD_3OD) spectrum of **S9**.

APPENDIX C

SUPPLEMENTARY CONTENT FOR CHAPTER IV

Appendix C is the supplementary appendix for Chapter IV of this dissertation. It includes all spectra and experimental information relevant to the material in Chapter IV.

Esterase Activity Measured by p-Nitrophenyl Acetate Assay

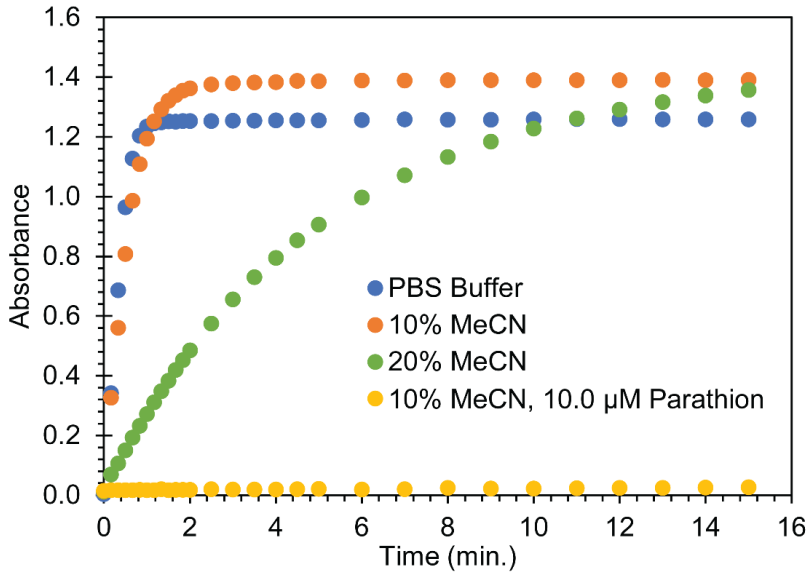


Figure C1. Esterase activity measured by *p*-nitrophenol absorbance at 405 nm.

*Calibration Curves for RSS-DNB Adducts **10**–**16***

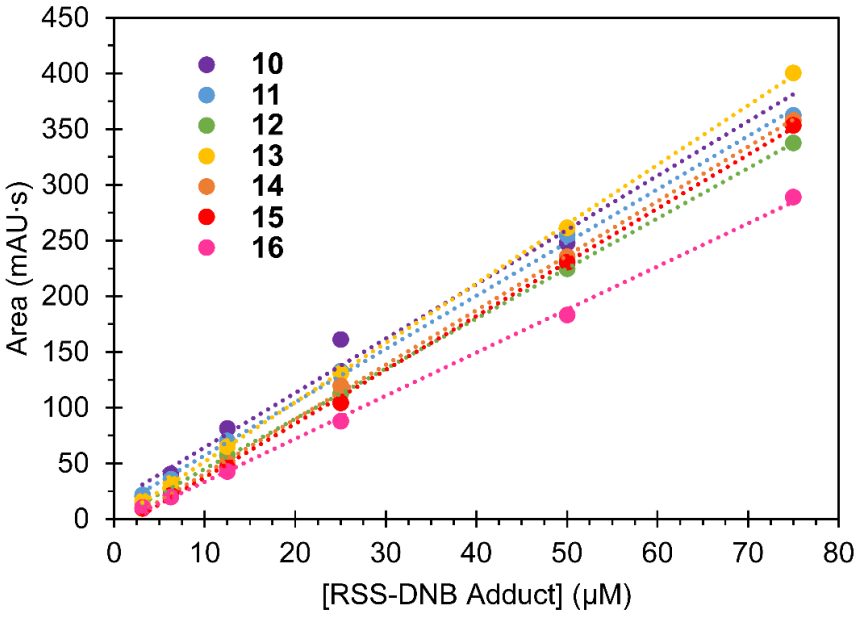


Figure C2. Calibration curves for RSS-DNB adducts **10**–**16**.

*Persulfide Release Control Experiments with Persulfide Donor **1***

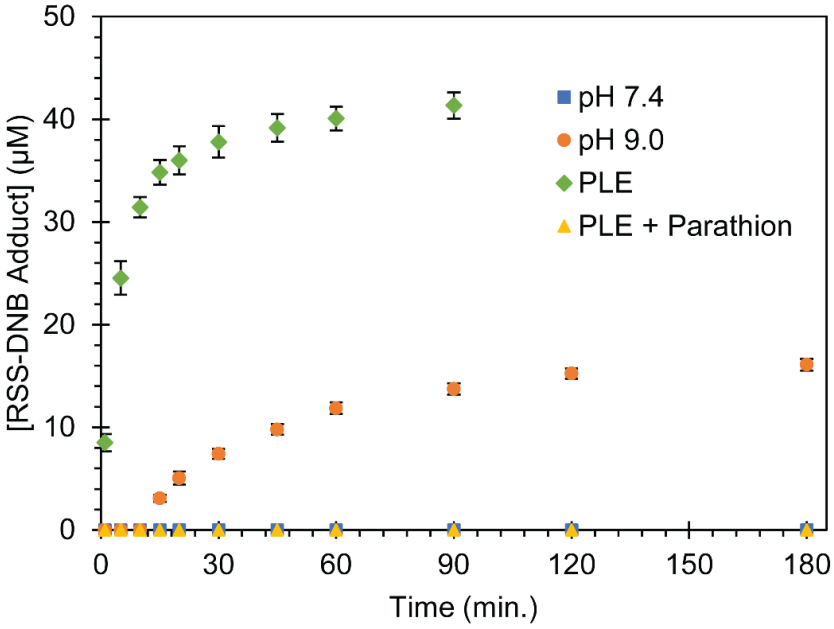


Figure C3. Persulfide release from donor **1** without PLE at pH 7.4, without PLE at pH 9.0, and with PLE in the presence of Parathion compared to persulfide release with PLE at pH 7.4. Experiments were performed in triplicate with results expressed in mean ± standard deviation (*n* = 3).

*Persulfide Donor **1** Stability at pH 7.4*

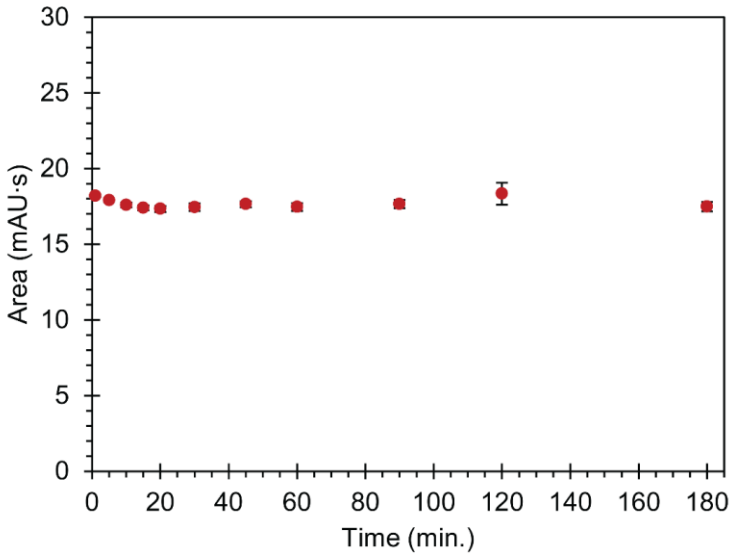


Figure C4. Persulfide donor **1** stability over three hours in 10% (v/v) MeCN in 10 mM PBS buffer (pH 7.4). Experiments were performed in triplicate with results expressed in mean ± standard deviation (n = 3).

*Persulfide Release from Persulfide Donor **6** with N-Acetyl-L-Cysteine*

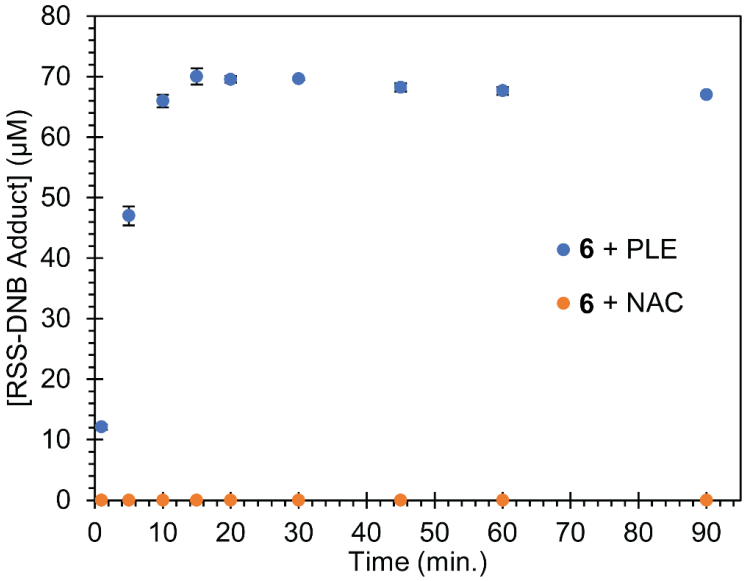


Figure C5. Persulfide release from persulfide donor **6** when activated by either PLE or *N*-acetyl-L-cysteine. Experiments were performed in triplicate with results expressed in mean ± standard deviation (n = 3).

*^{1}H NMR Spectroscopy Experiment with Persulfide Donor **7** and PLE*

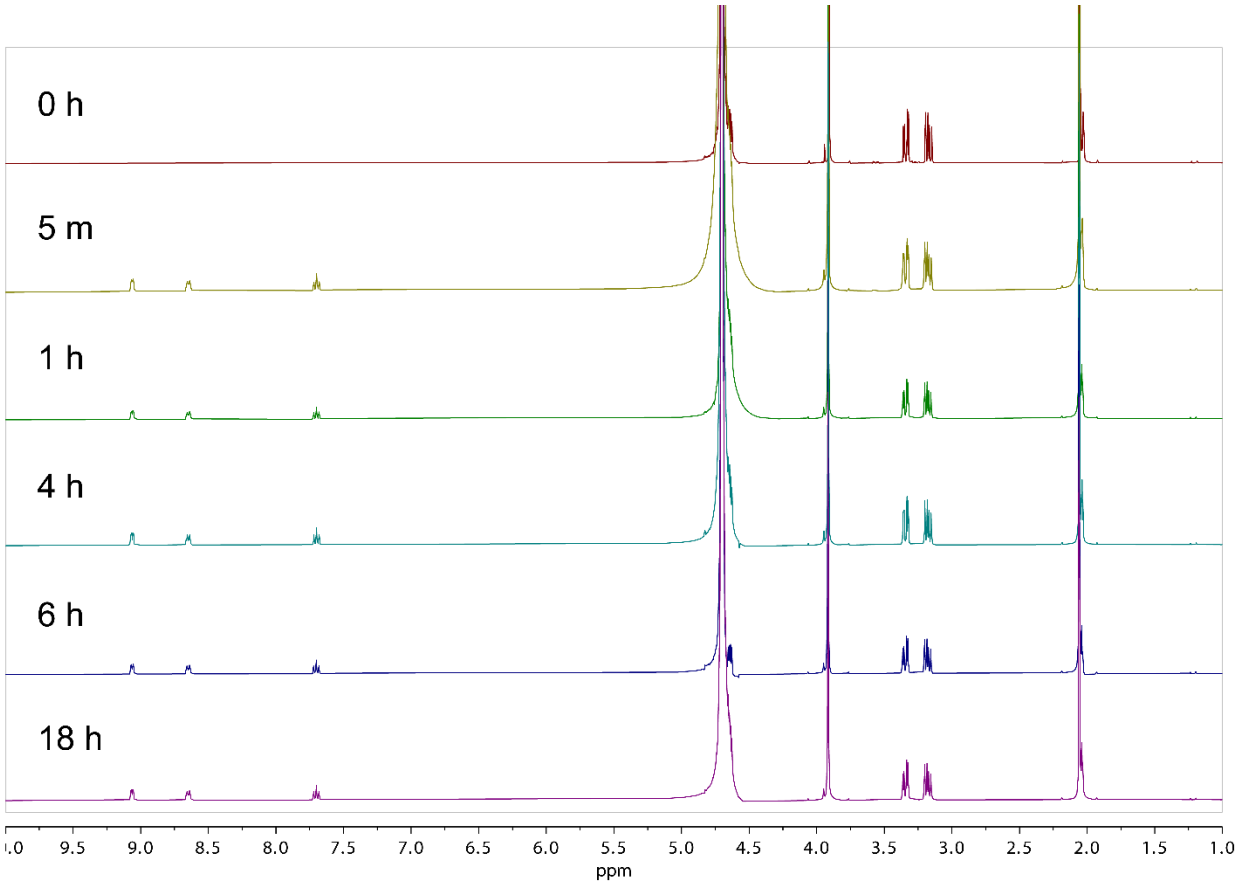


Figure C6. ^{1}H NMR spectra of persulfide donor **7** with PLE at various time points.

*^{1}H NMR Spectroscopy Experiment with Persulfide Donor **7** and tBuOK*

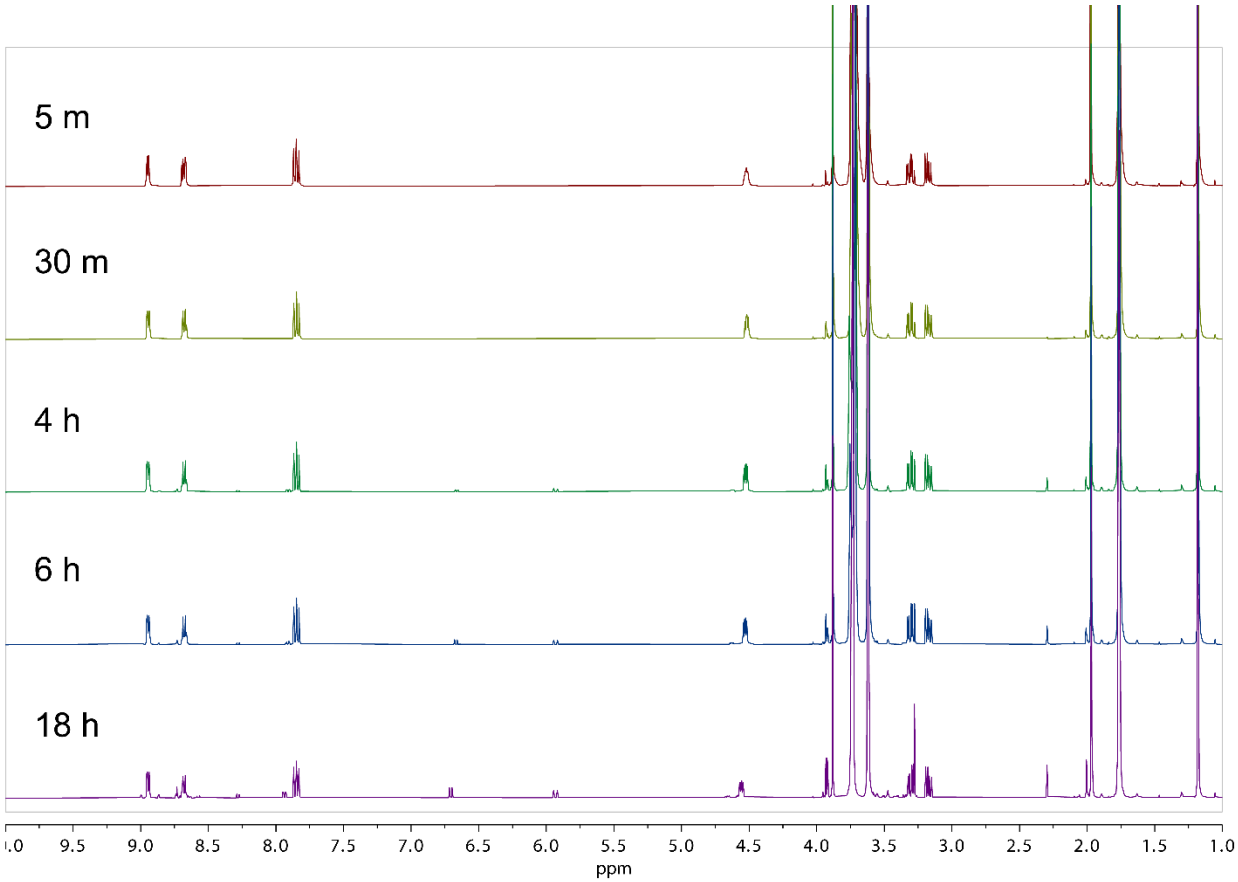


Figure C7. ^{1}H NMR spectra of persulfide donor **7** with *t*BuOK at various time points.

*Methylene Blue Assay Experiments with Persulfide Donors **1** and **6***

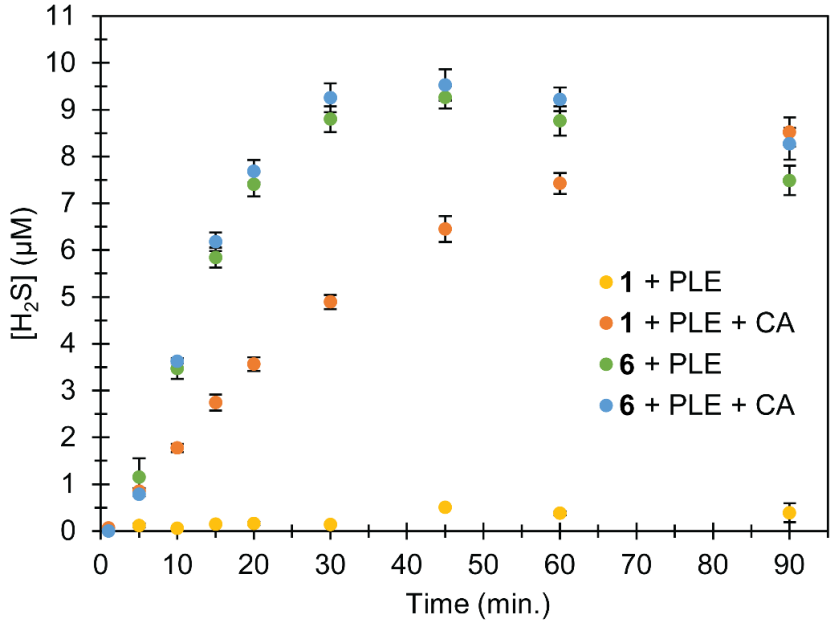


Figure C8. Methylene blue assay experiments of persulfide donors **1** and **6** activated by PLE with and without the addition of carbonic anhydrase (CA). Experiments were performed in triplicate with results expressed in mean ± standard deviation (n = 3).

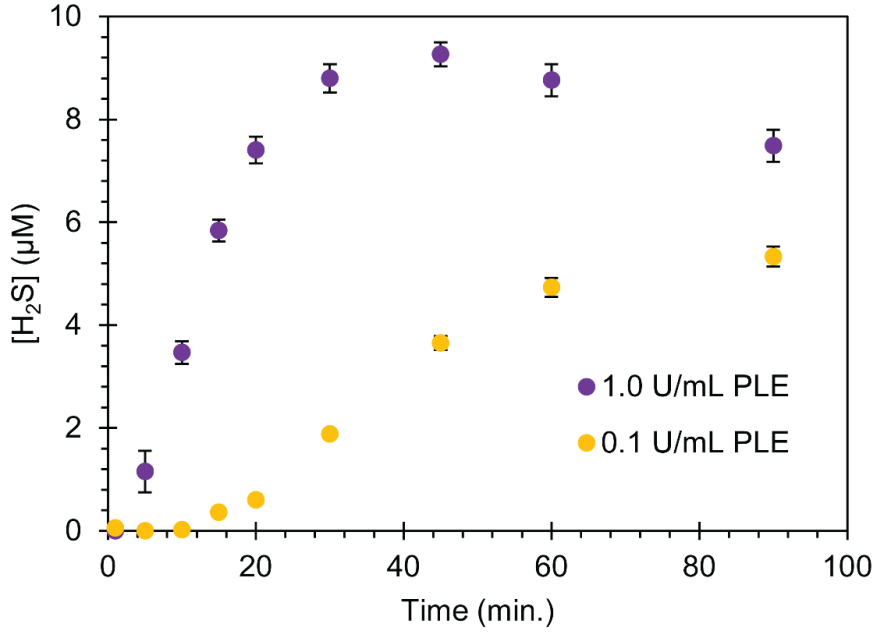


Figure C9. Methylene blue assay experiments of persulfide donor **6** activated by varying concentrations of PLE. Experiments were performed in triplicate with results expressed in mean ± standard deviation (n = 3).

*^{13}C NMR Spectroscopy Experiment with Persulfide Donor **6** and PLE*

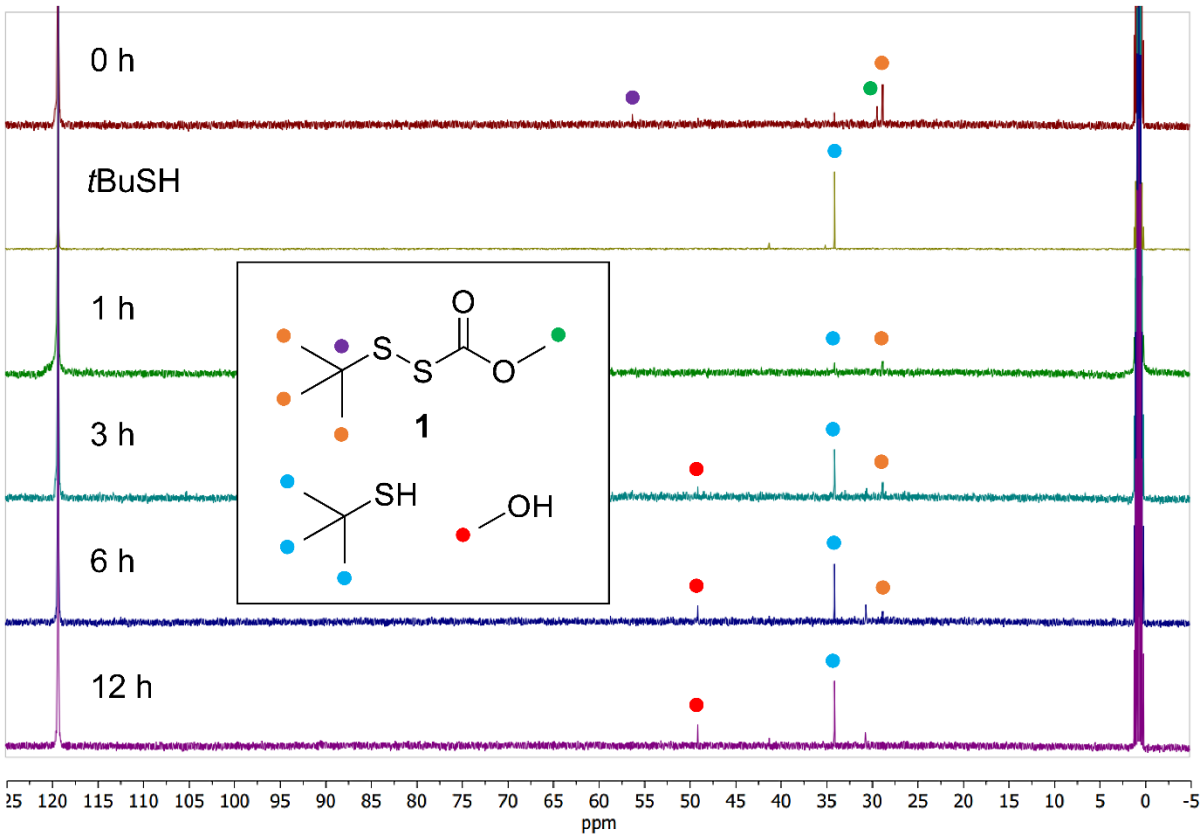


Figure C10. ^{13}C NMR spectroscopy experiment with persulfide donor **6** and PLE at 0, 1, 3, 6, and 12 hours showing the appearance of *tert*-butyl mercaptan and methanol over time.

*^{1}H and ^{13}C NMR Spectra of Compounds **1**–**16***

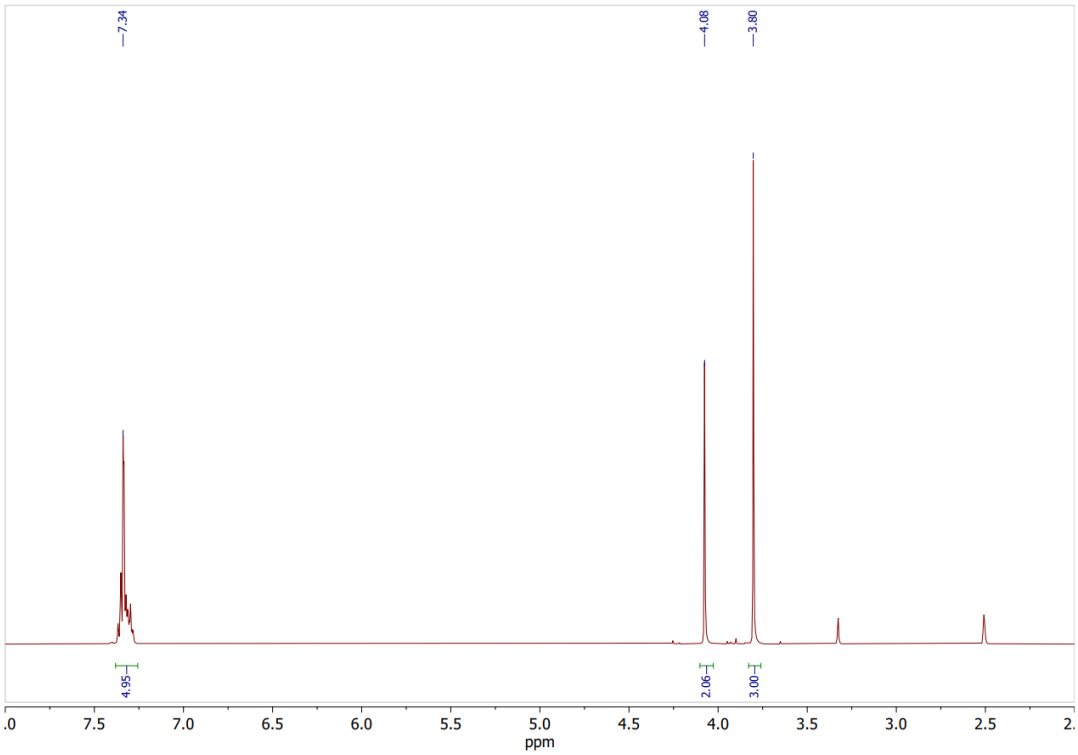


Figure C11. ^{1}H NMR (500 MHz, DMSO-d_6) spectrum of persulfide donor **1**.

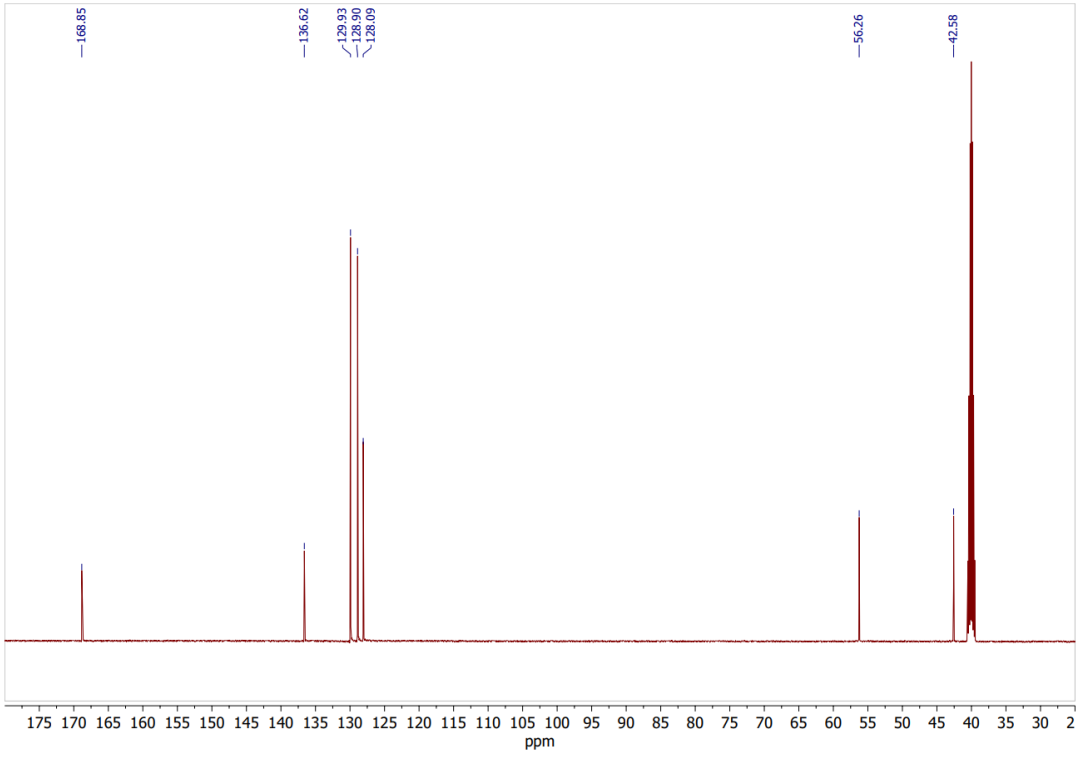


Figure C12. $^{13}C\{^{1}H\}$ NMR (125 MHz, DMSO-d_6) spectrum of persulfide donor **1**.

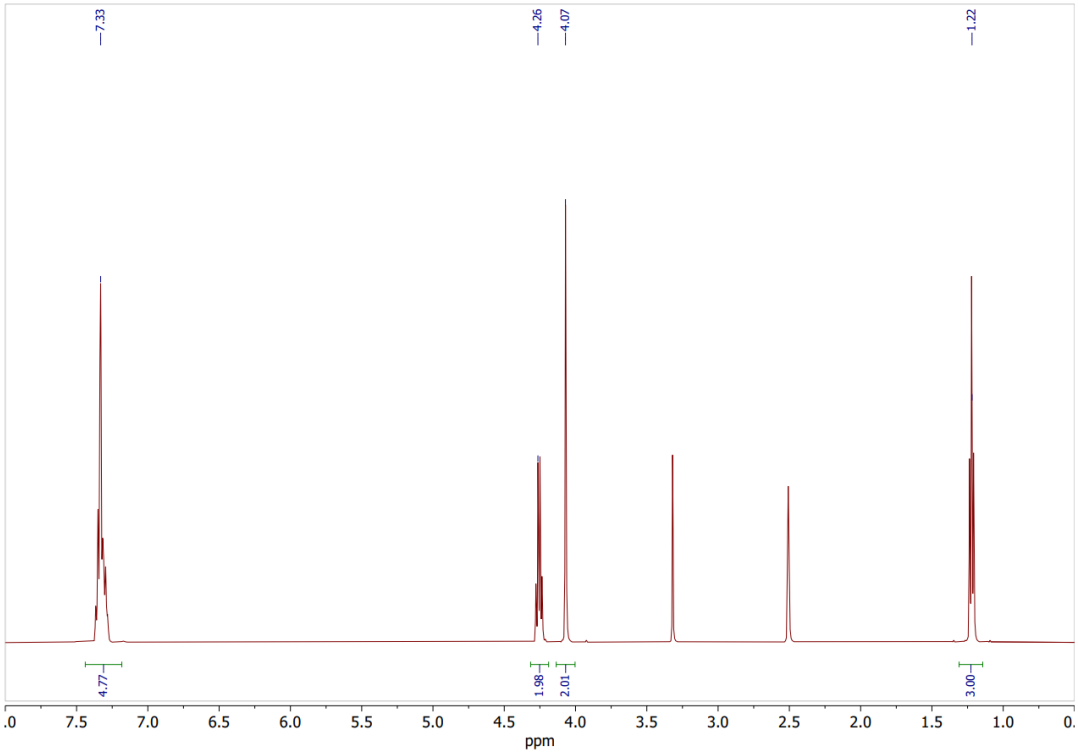


Figure C13. ^{1}H NMR (500 MHz, DMSO-d_6) spectrum of persulfide donor **2**.

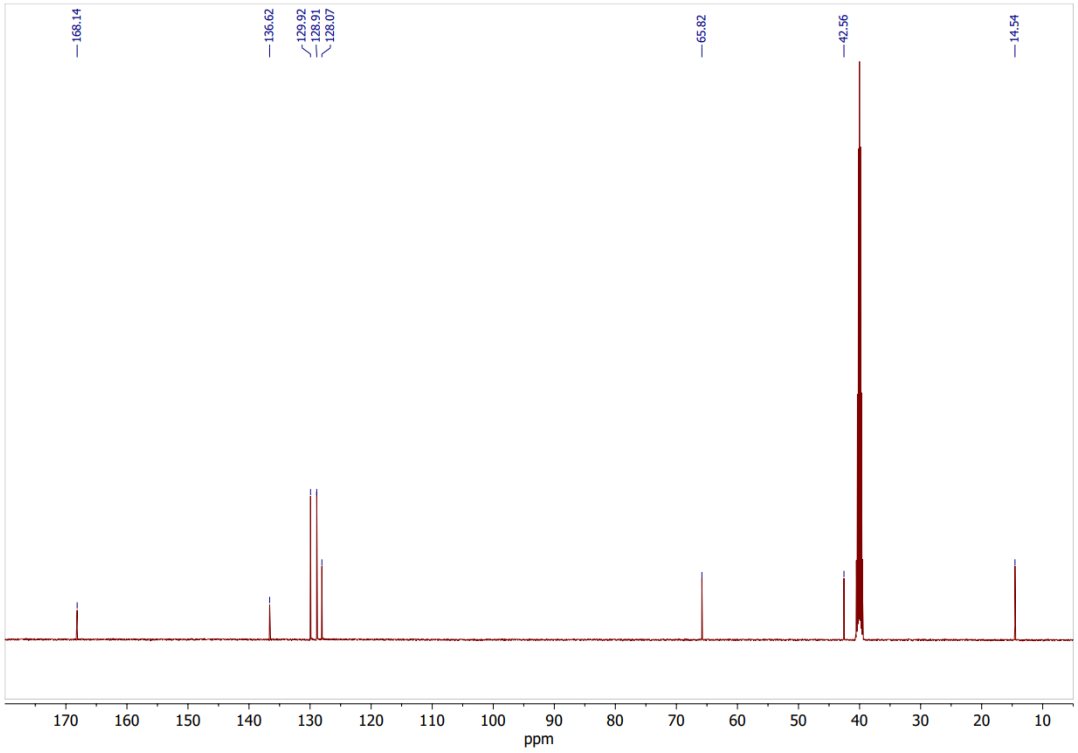


Figure C14. ^{13}C{^{1}H} NMR (125 MHz, DMSO-d_6) spectrum of persulfide donor **2**.

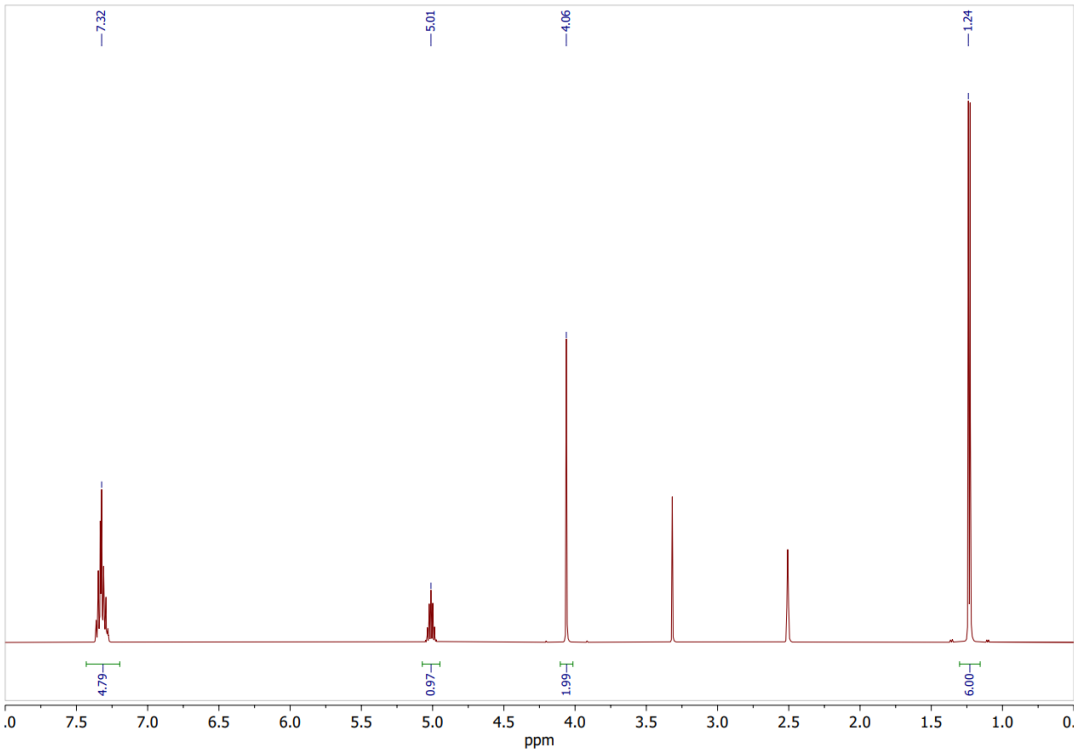


Figure C15. ^{1}H NMR (500 MHz, DMSO-d_6) spectrum of persulfide donor **3**.

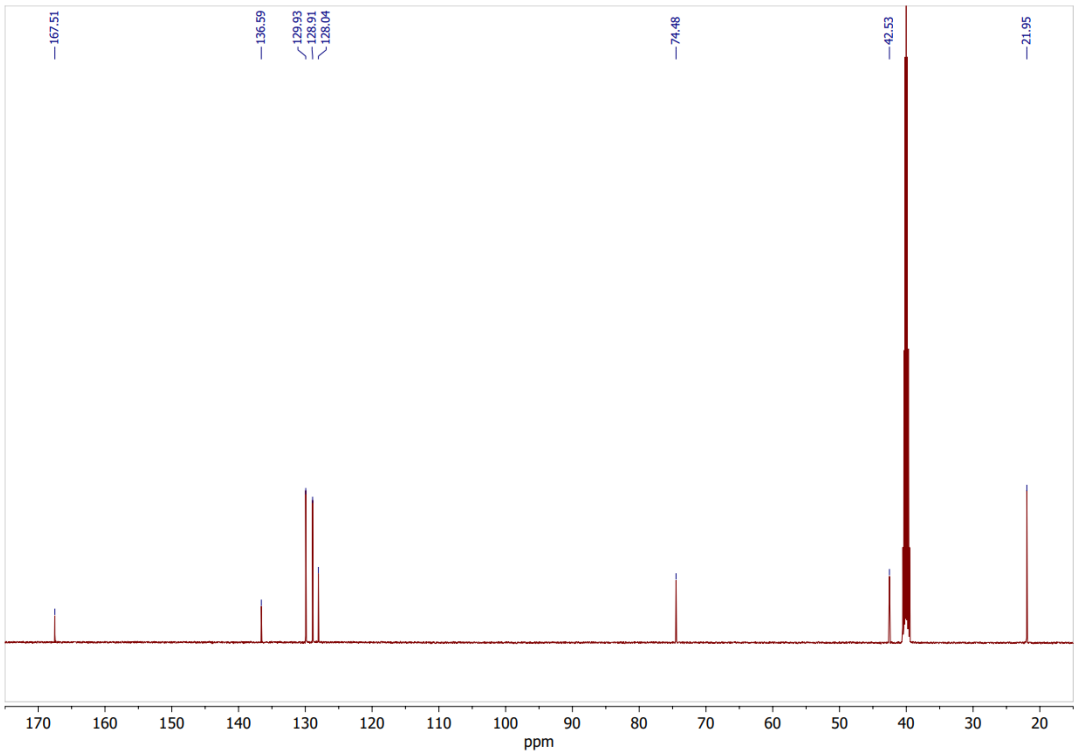


Figure C16. ^{13}C{^{1}H} NMR (125 MHz, DMSO-d_6) spectrum of persulfide donor **3**.

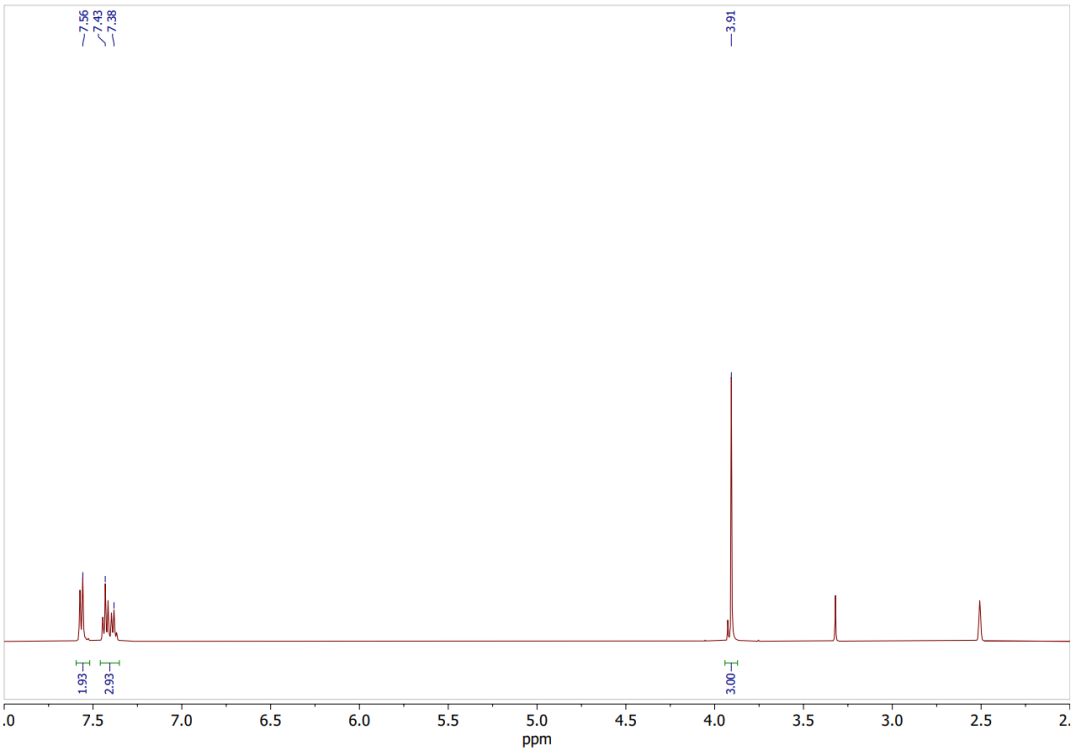


Figure C17. ^{1}H NMR (500 MHz, DMSO-d_6) spectrum of persulfide donor **4**.

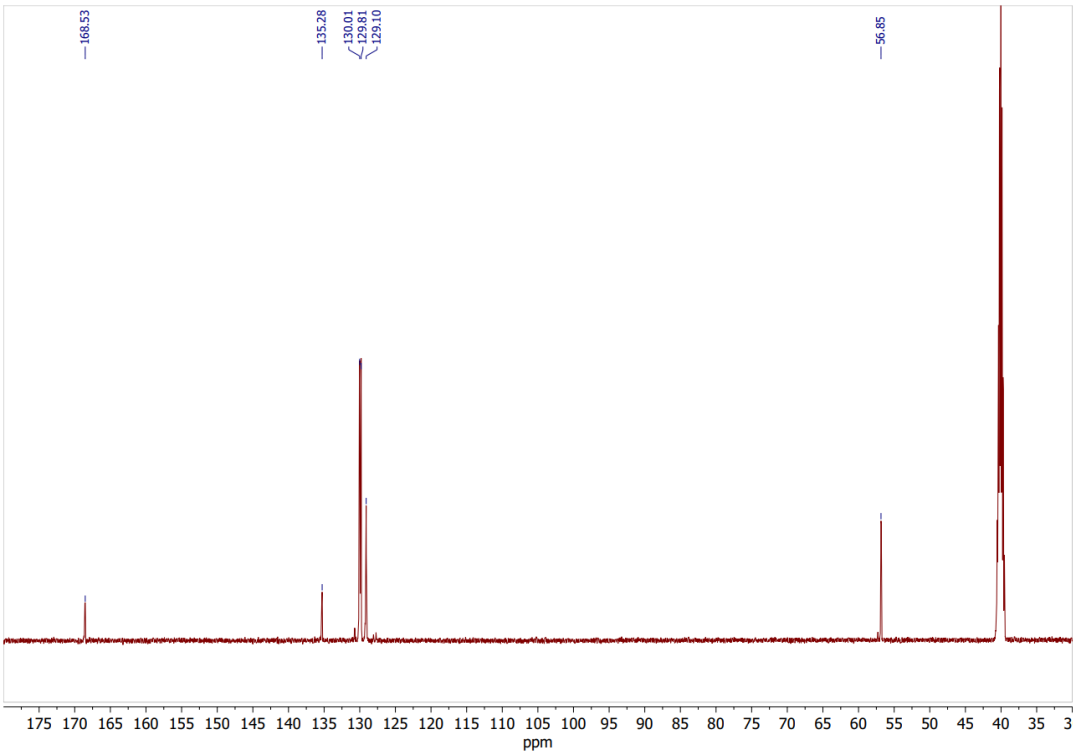


Figure C18. ^{13}C{^{1}H} NMR (125 MHz, DMSO-d_6) spectrum of persulfide donor **4**.

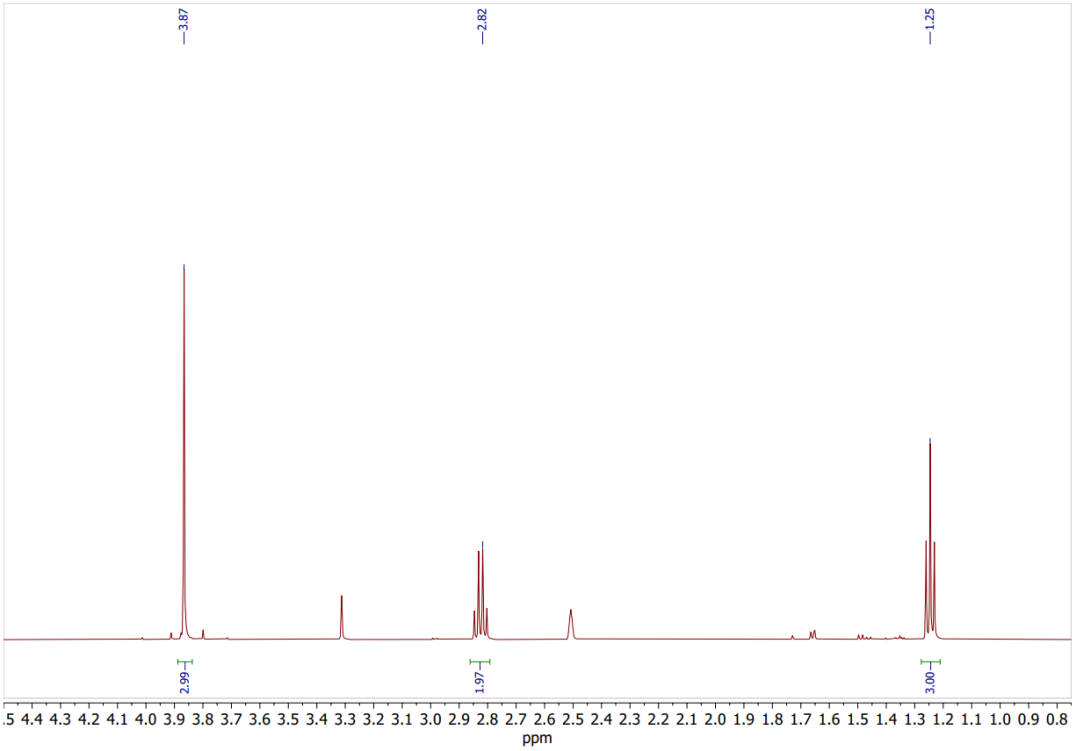


Figure C19. ^{1}H NMR (500 MHz, DMSO-d_6) spectrum of persulfide donor **5**.

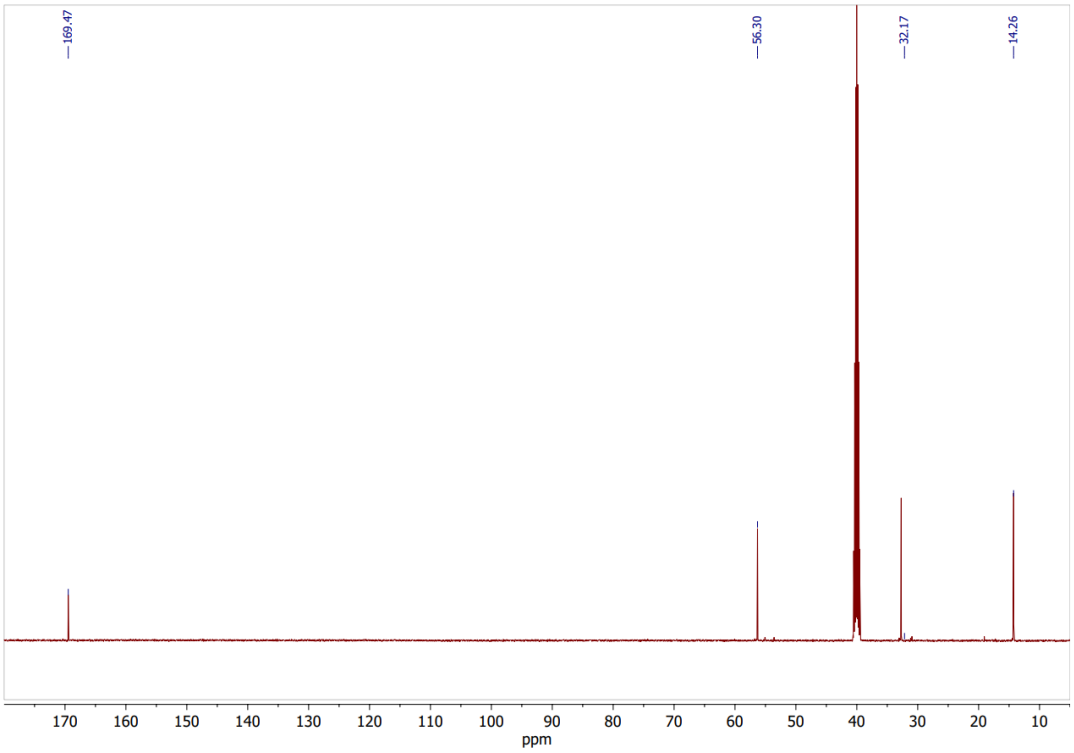


Figure C20. ^{13}C{^{1}H} NMR (125 MHz, DMSO-d_6) spectrum of persulfide donor **5**.

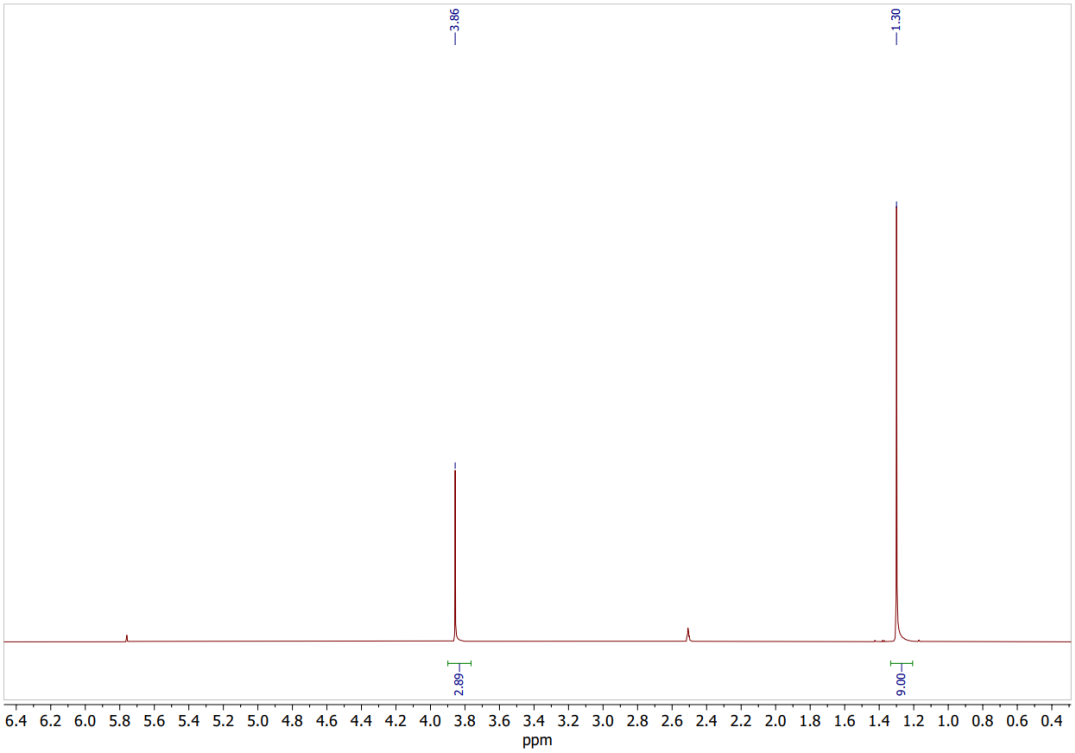


Figure C21. ^{1}H NMR (500 MHz, DMSO-d_6) spectrum of persulfide donor **6**.

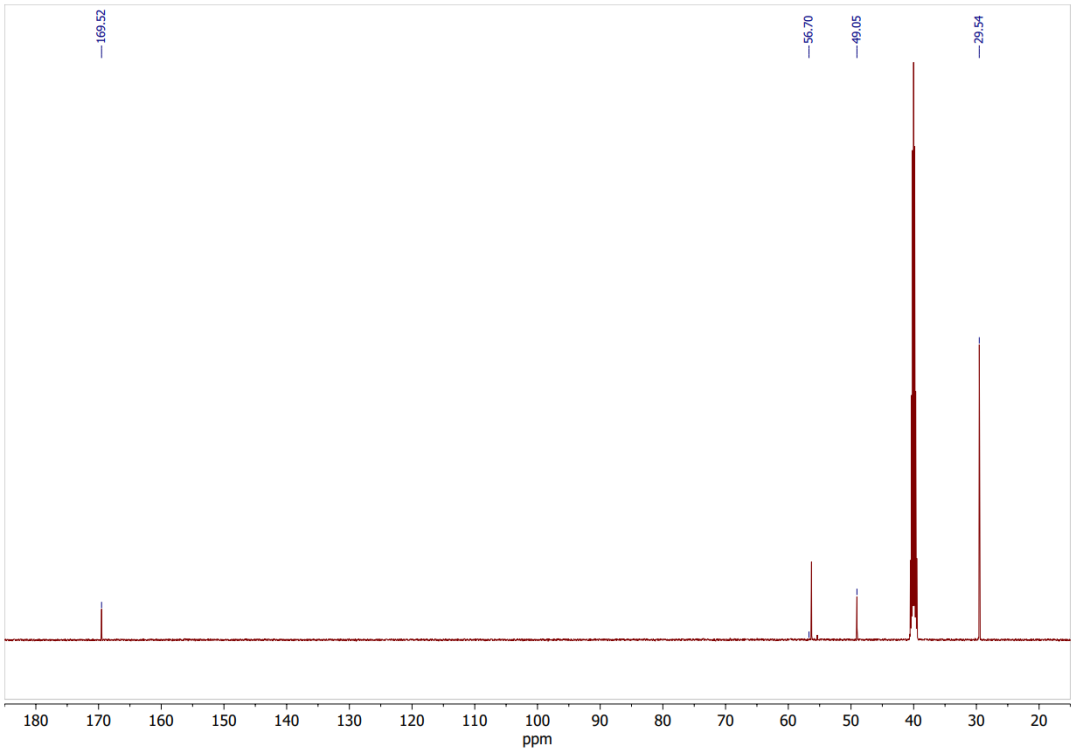


Figure C22. ^{13}C{^{1}H} NMR (125 MHz, DMSO-d_6) spectrum of persulfide donor **6**.

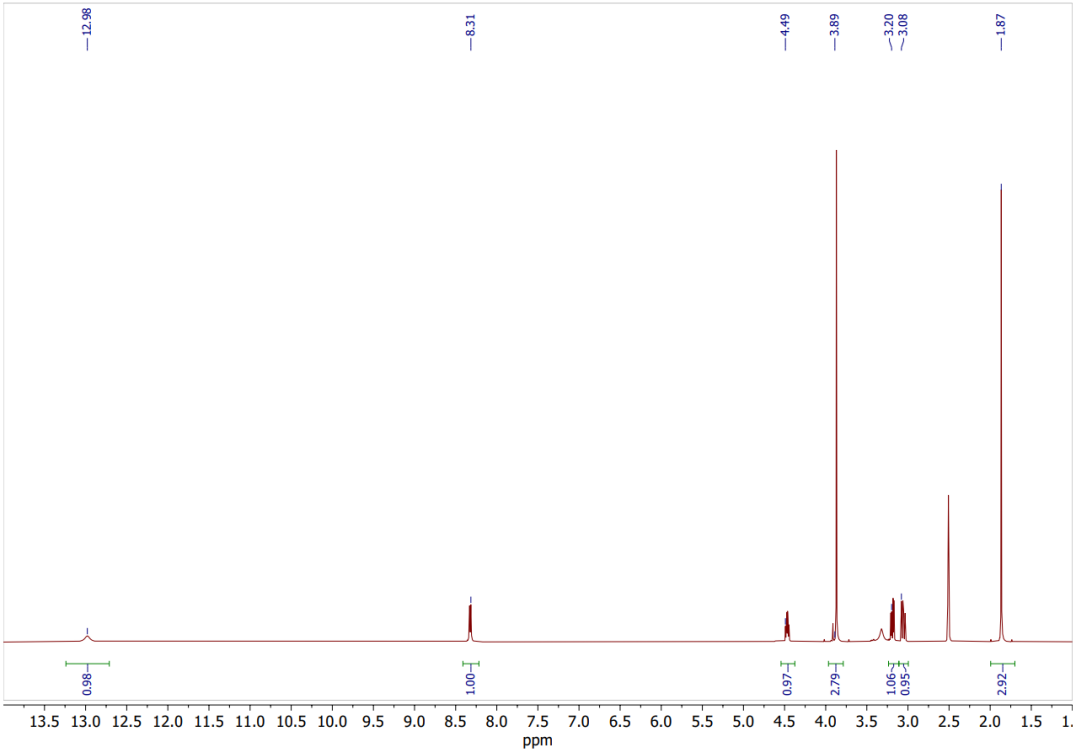


Figure C23. ^{1}H NMR (500 MHz, DMSO-d_6) spectrum of persulfide donor **7**.

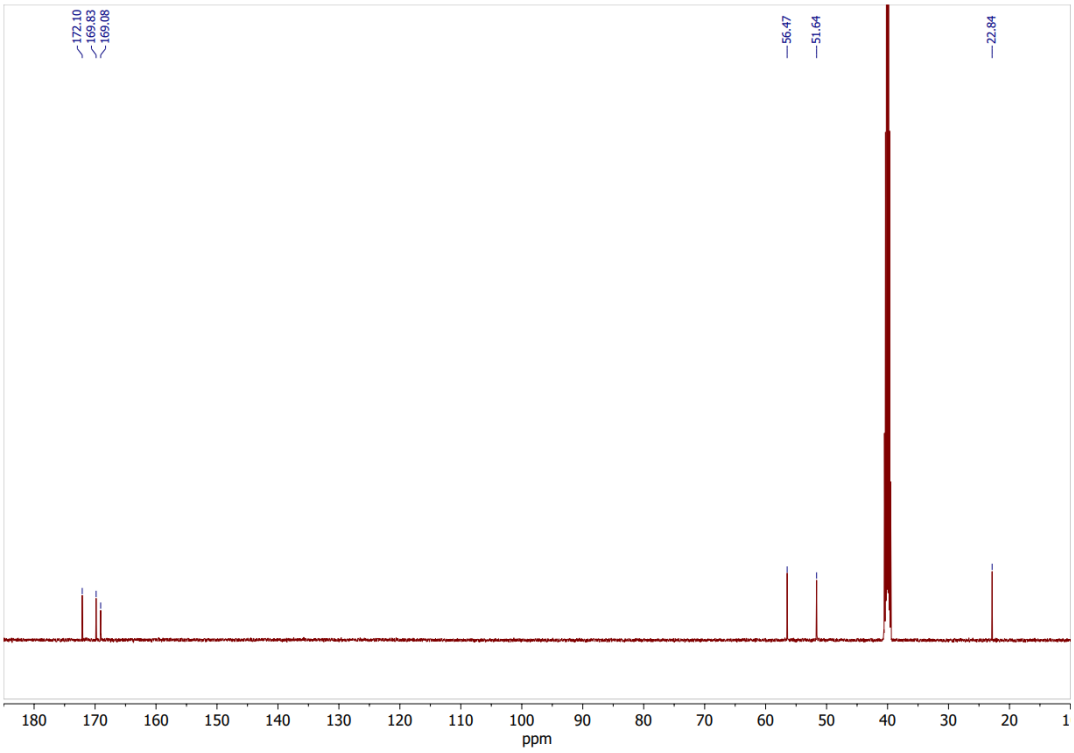


Figure C24. ^{13}C{^{1}H} NMR (125 MHz, DMSO-d_6) spectrum of persulfide donor **7**.

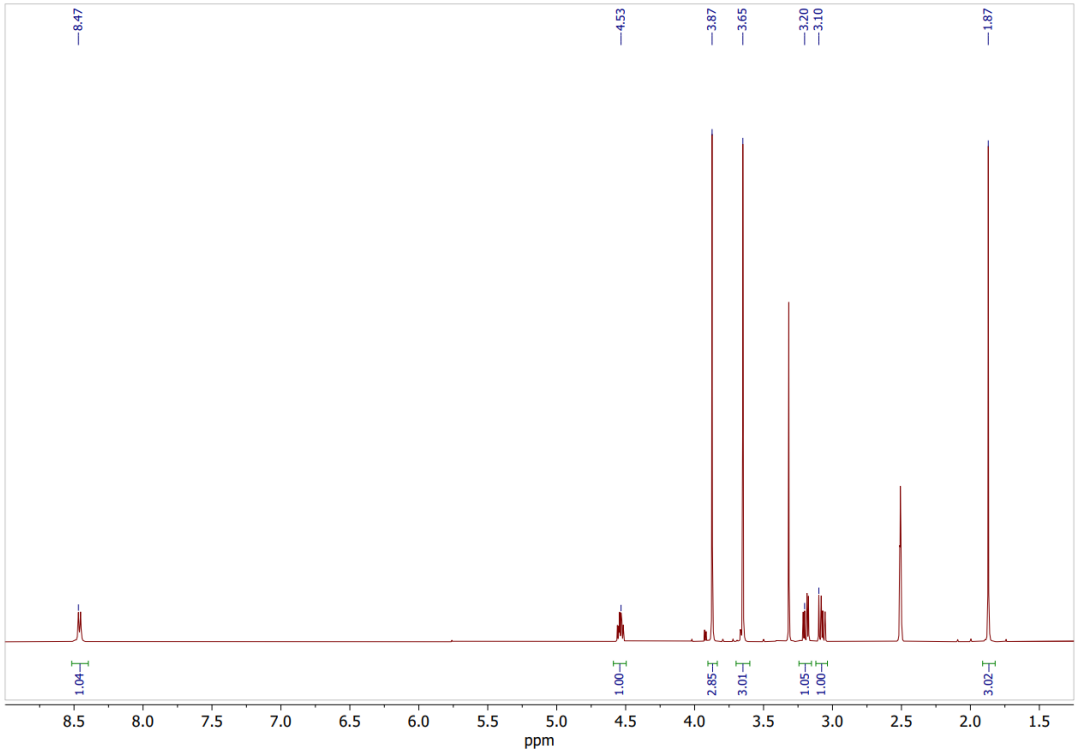


Figure C25. ^{1}H NMR (500 MHz, DMSO-d_6) spectrum of persulfide donor **8**.

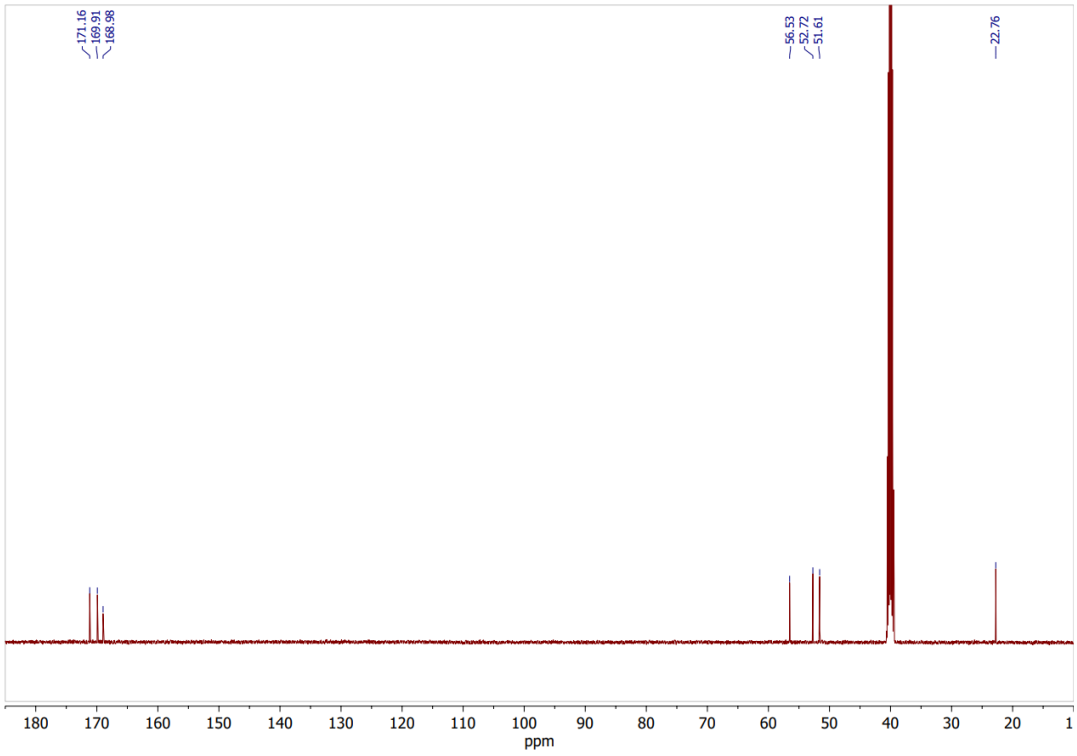


Figure C26. ^{13}C{^{1}H} NMR (125 MHz, DMSO-d_6) spectrum of persulfide donor **8**.

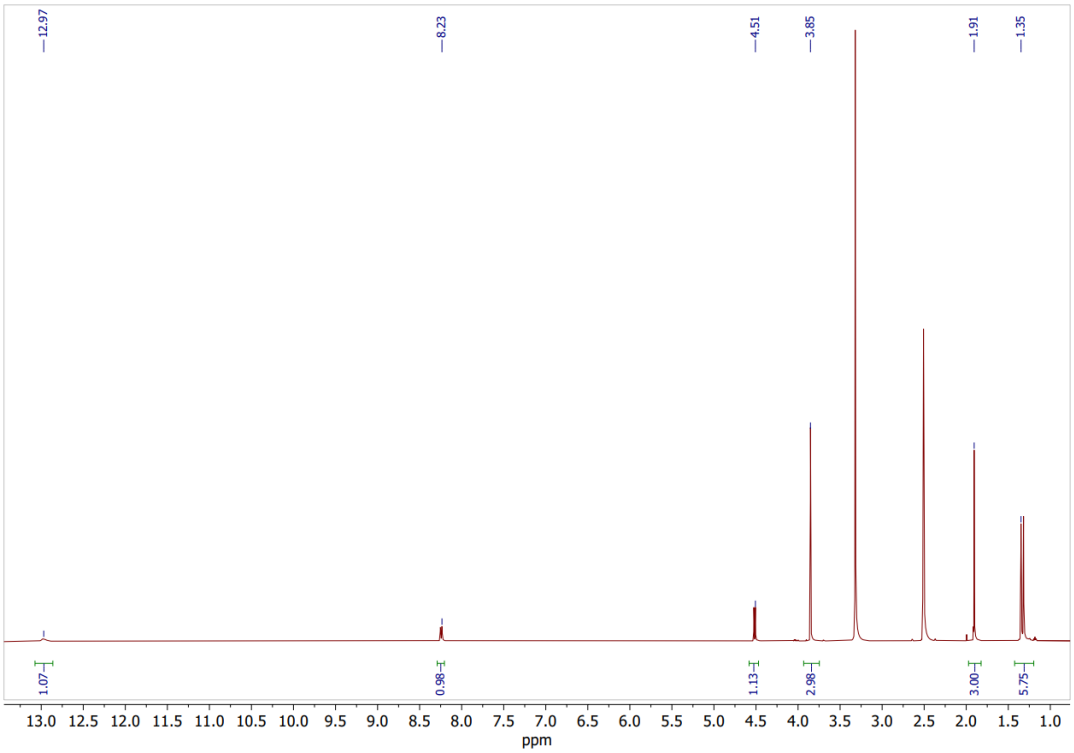


Figure C27. ^{1}H NMR (500 MHz, DMSO-d_6) spectrum of persulfide donor **9**.

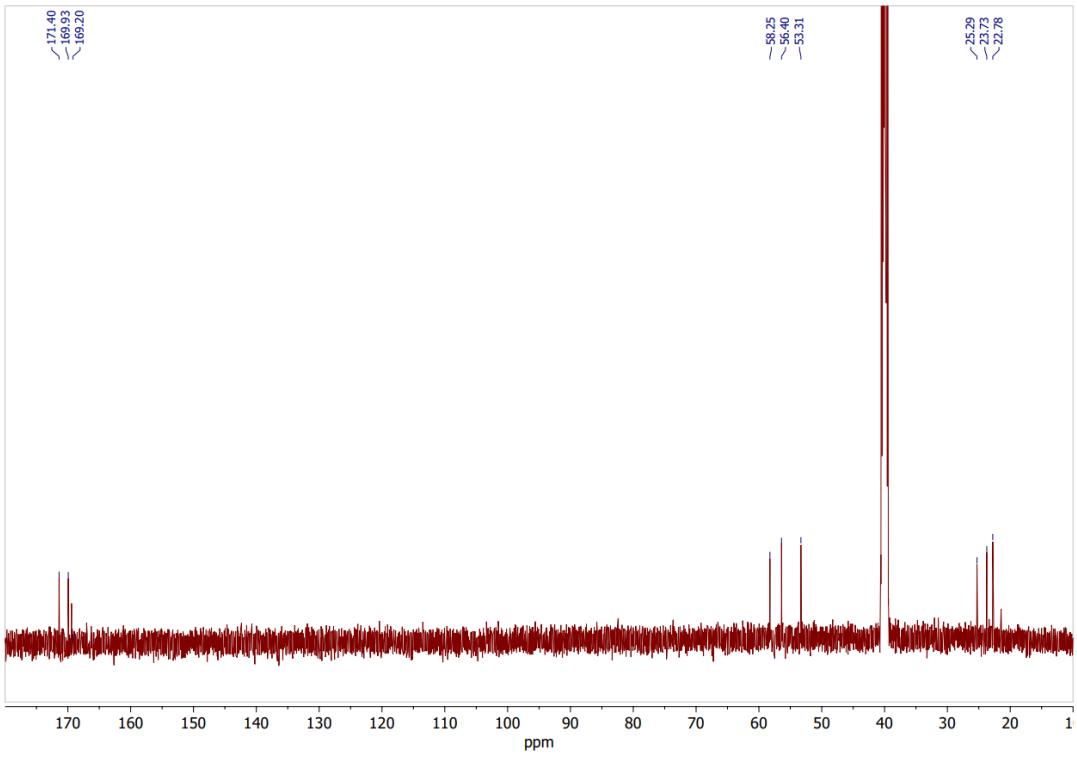


Figure C28. ^{13}C{^{1}H} NMR (125 MHz, DMSO-d_6) spectrum of persulfide donor **9**.

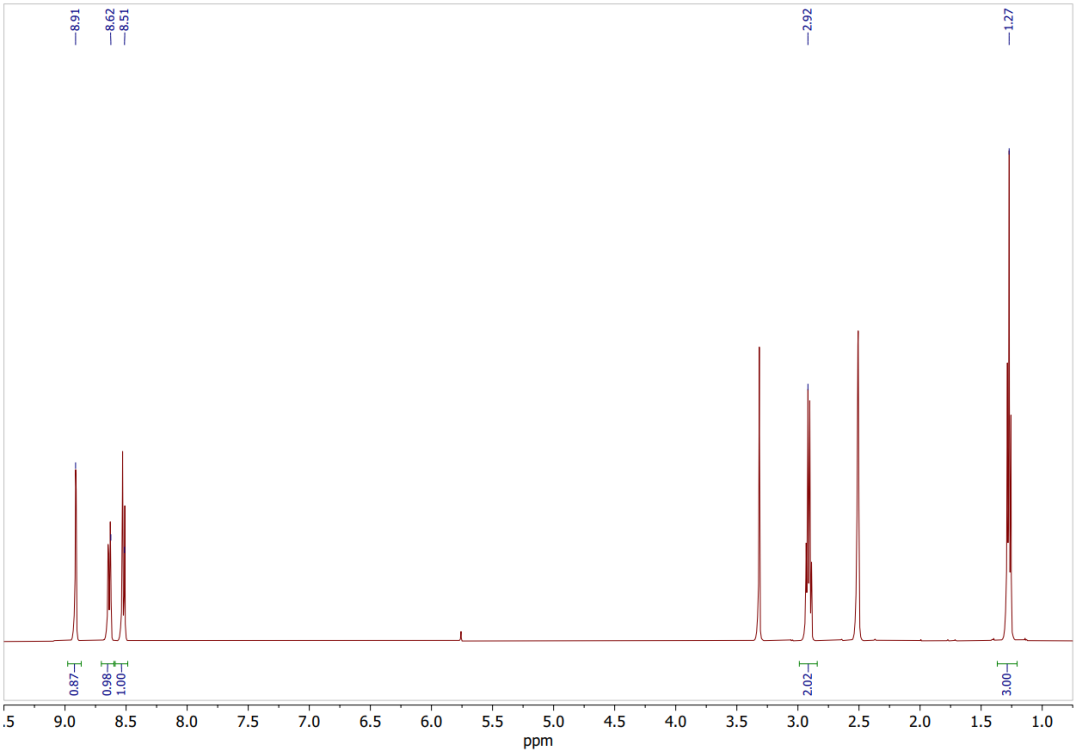


Figure C29. ^{1}H NMR (500 MHz, DMSO-d_6) spectrum of **10**.

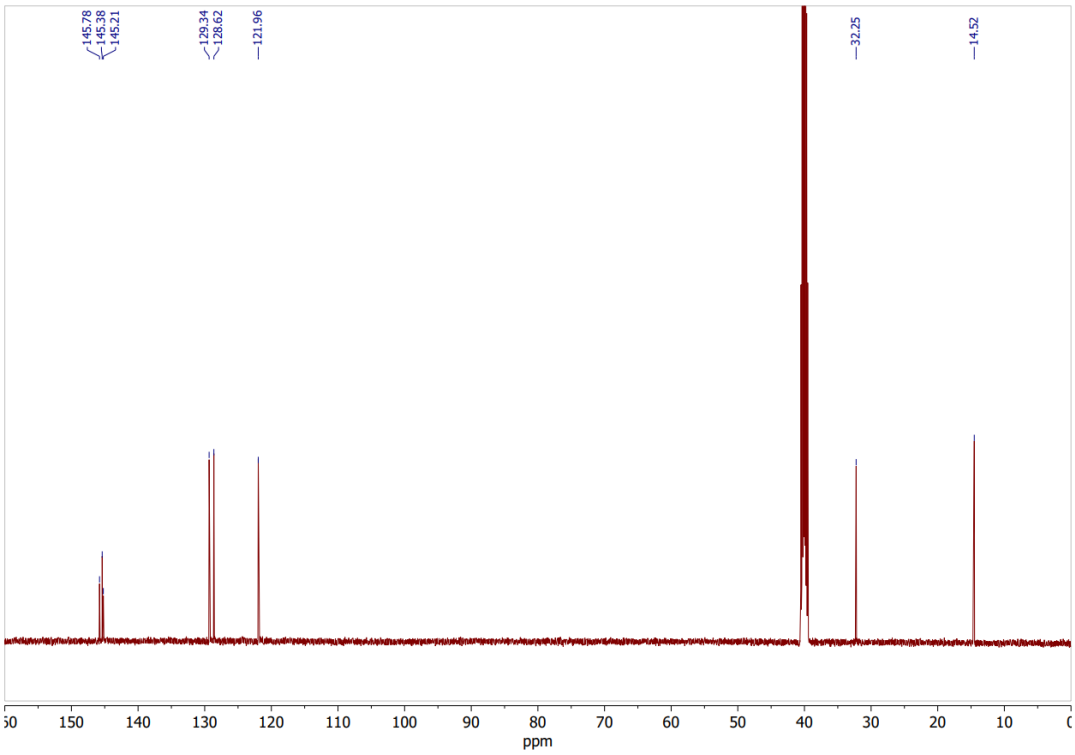


Figure C30. ^{13}C{^{1}H} NMR (125 MHz, DMSO-d_6) spectrum of **10**.

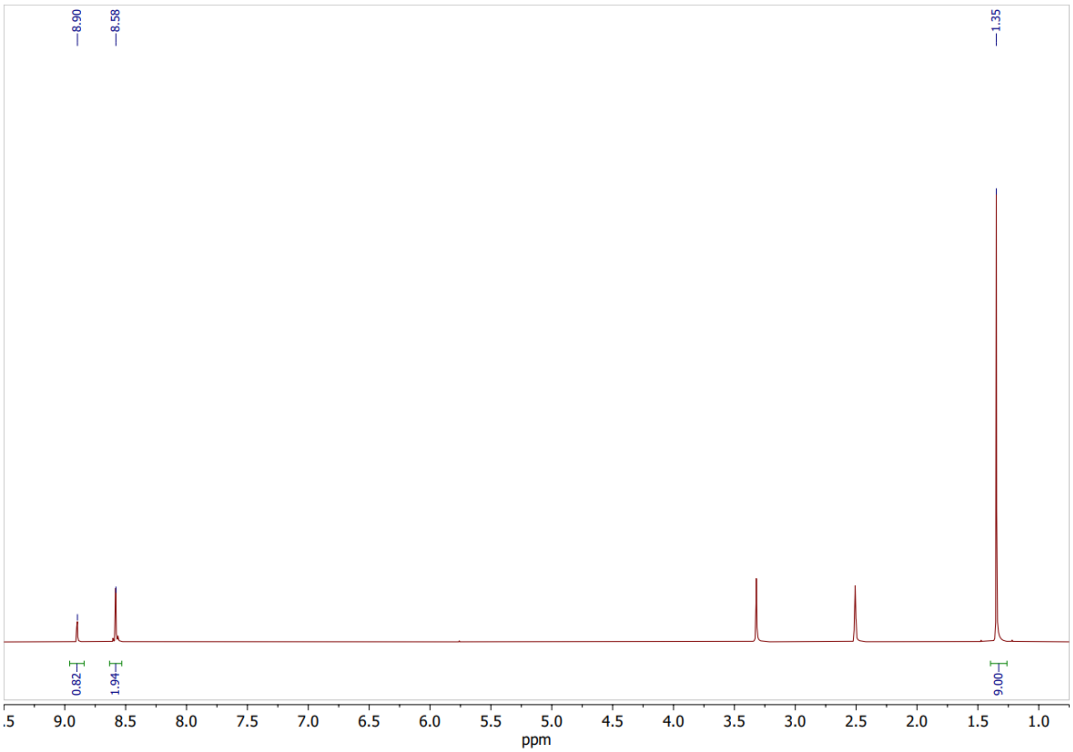


Figure C31. ^{1}H NMR (500 MHz, DMSO-d_6) spectrum of **11**.

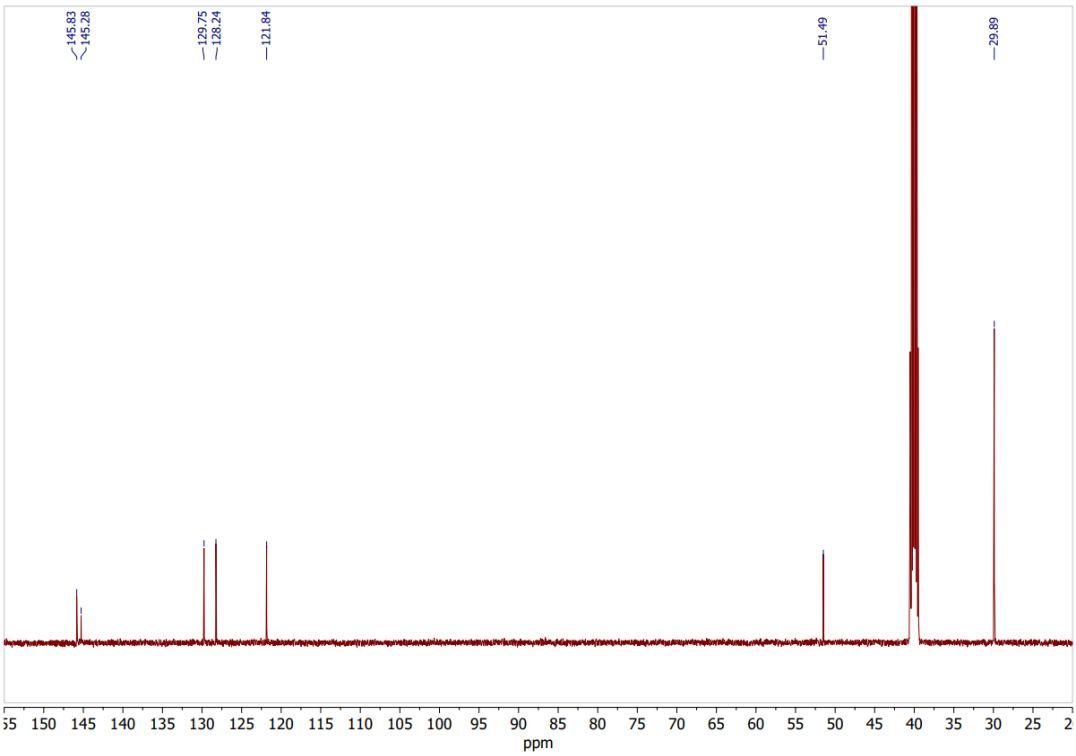


Figure C32. ^{13}C{^{1}H} NMR (125 MHz, DMSO-d_6) spectrum of **11**.

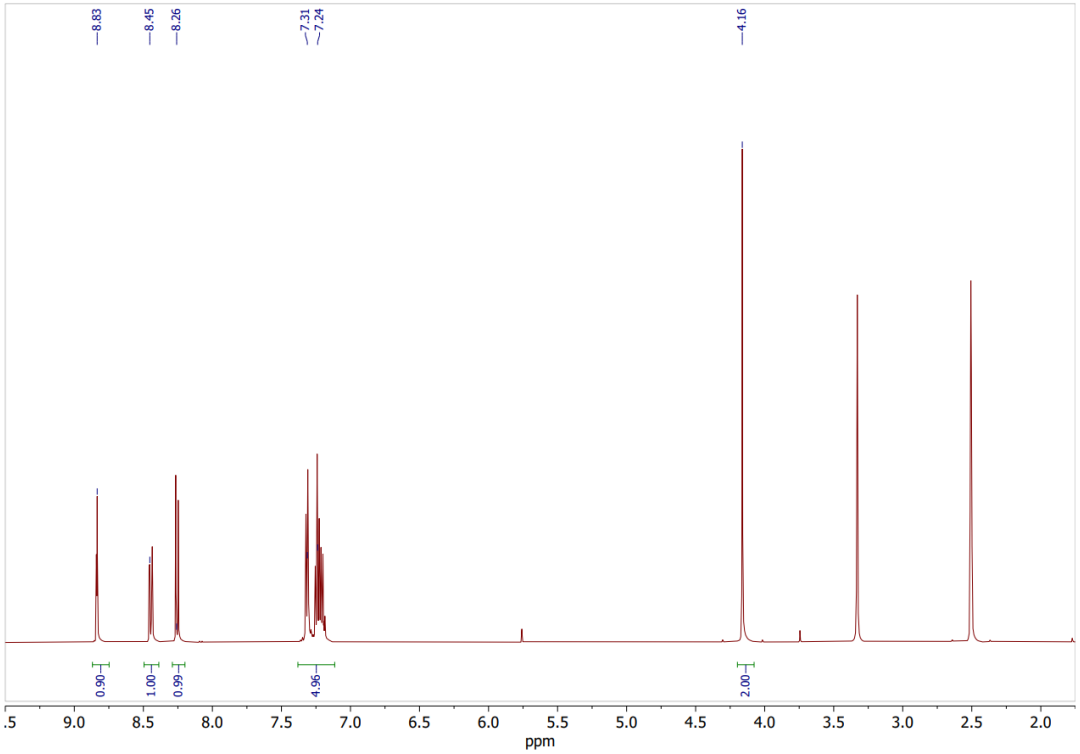


Figure C33. ^{1}H NMR (500 MHz, DMSO-d_6) spectrum of **12**.

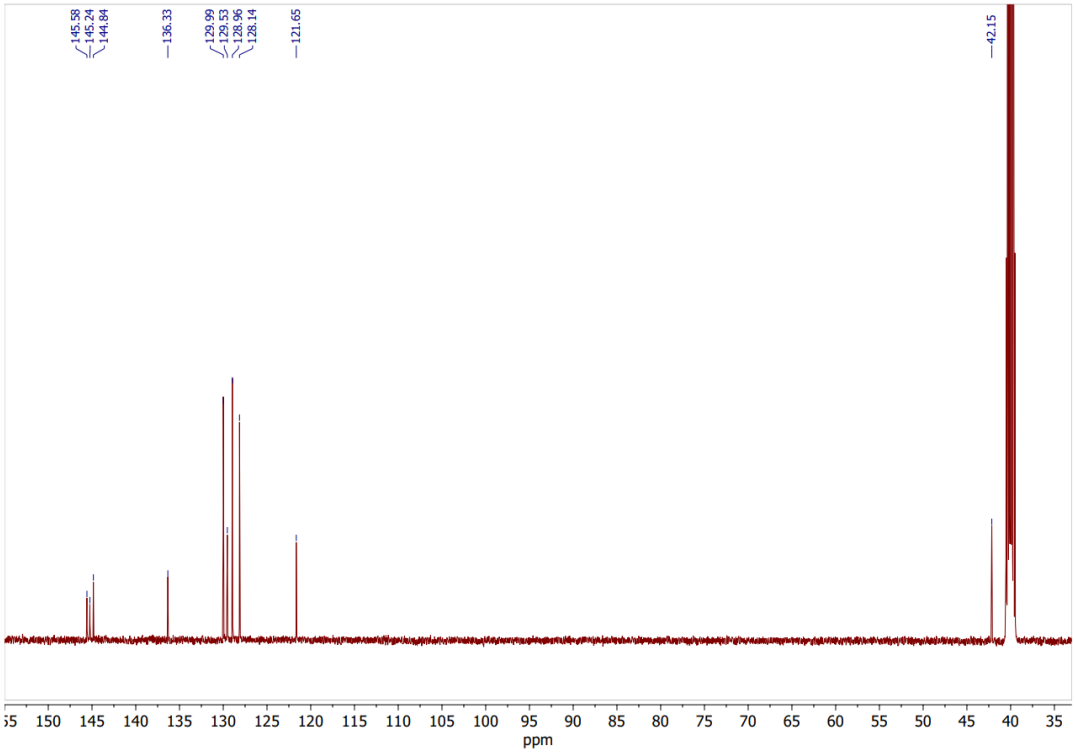


Figure C34. ^{13}C{^{1}H} NMR (125 MHz, DMSO-d_6) spectrum of **12**.

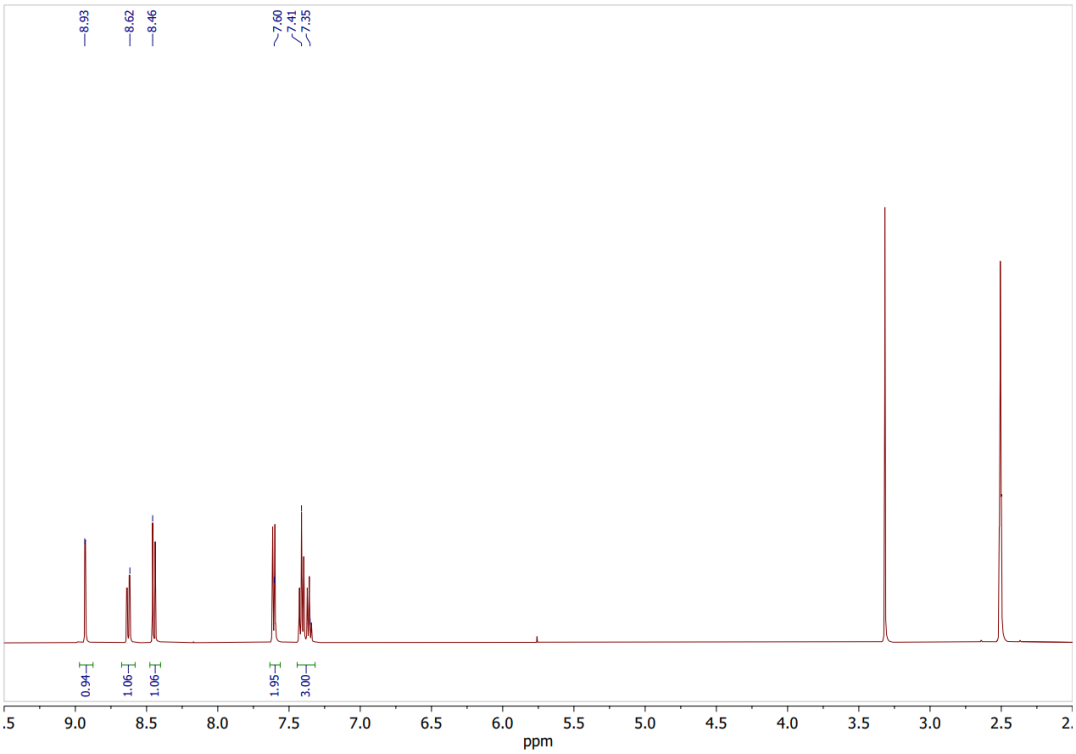


Figure C35. ^{1}H NMR (500 MHz, DMSO-d_6) spectrum of **13**.

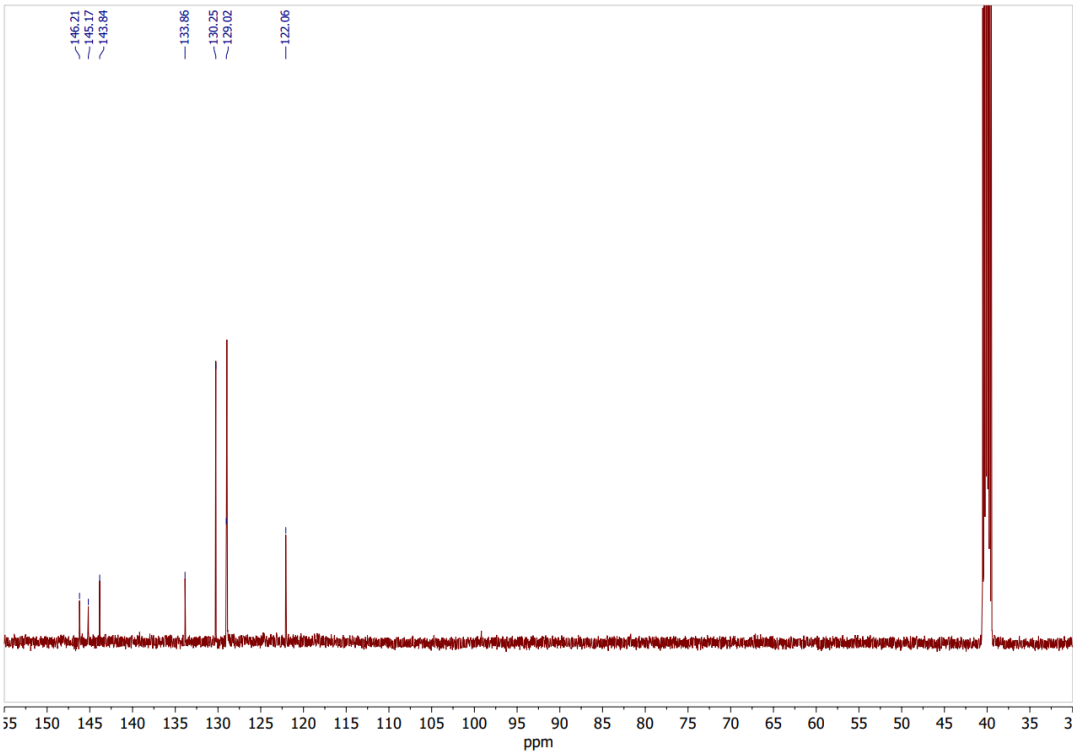


Figure C36. ^{13}C{^{1}H} NMR (125 MHz, DMSO-d_6) spectrum of **13**.

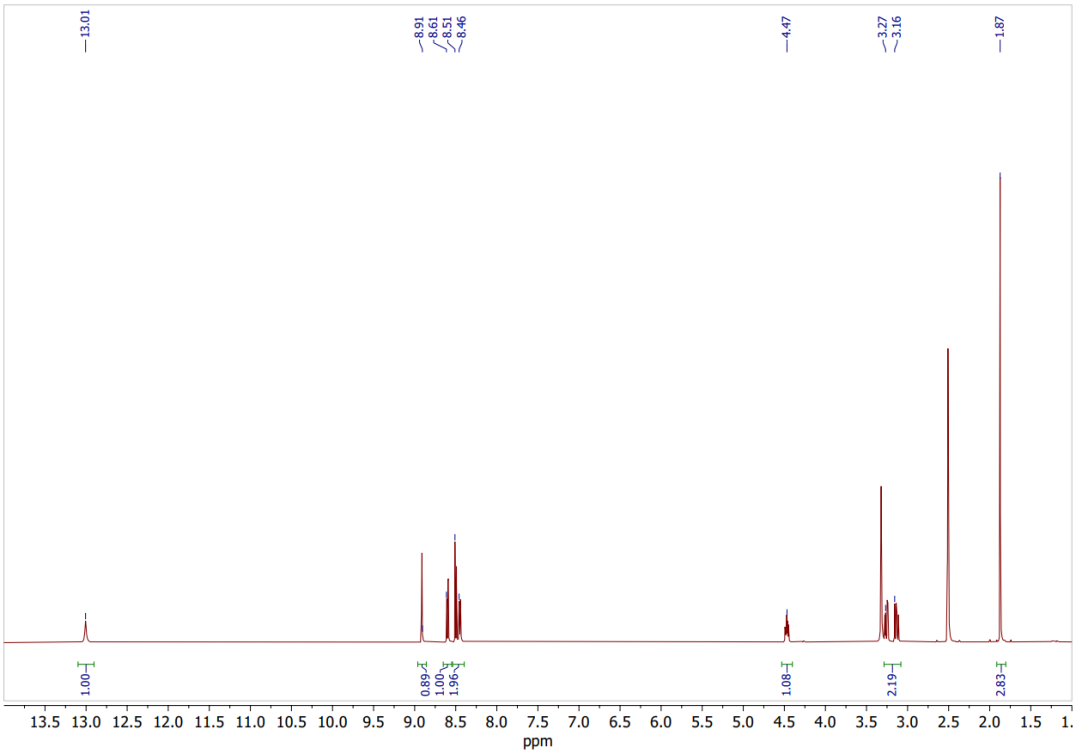


Figure C37. $^{13}C\{^{1}H\}$ NMR (500 MHz, DMSO-d_6) spectrum of **14**.

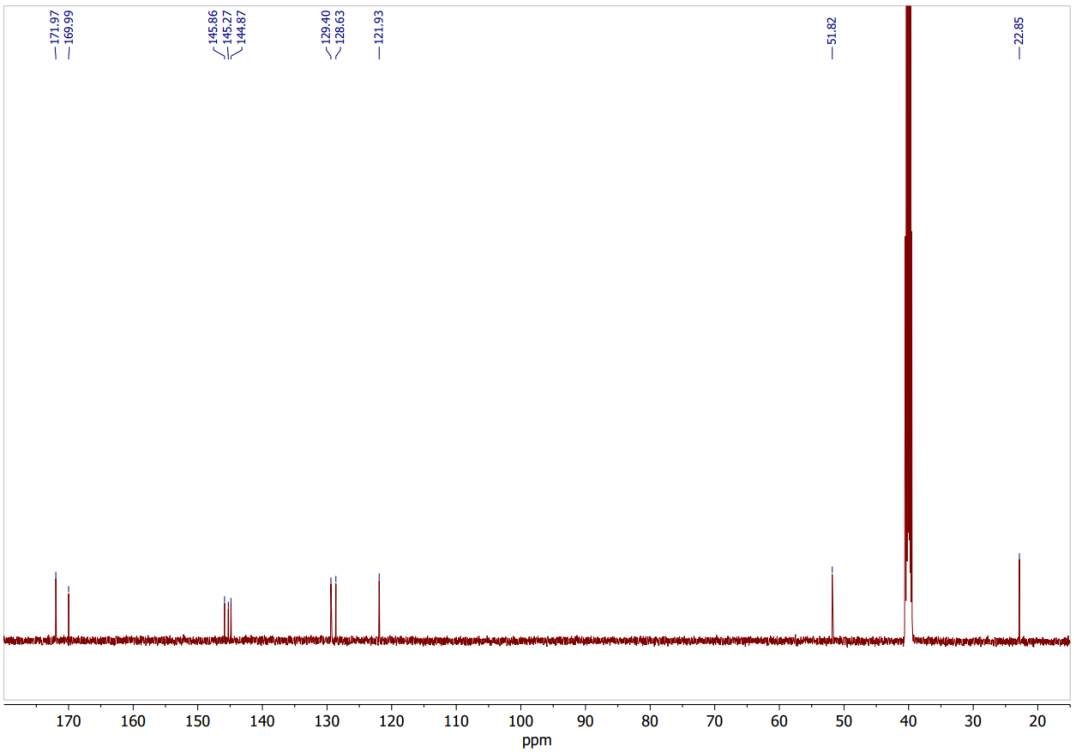


Figure C38. $^{13}C\{^{1}H\}$ NMR (125 MHz, DMSO-d_6) spectrum of **14**.

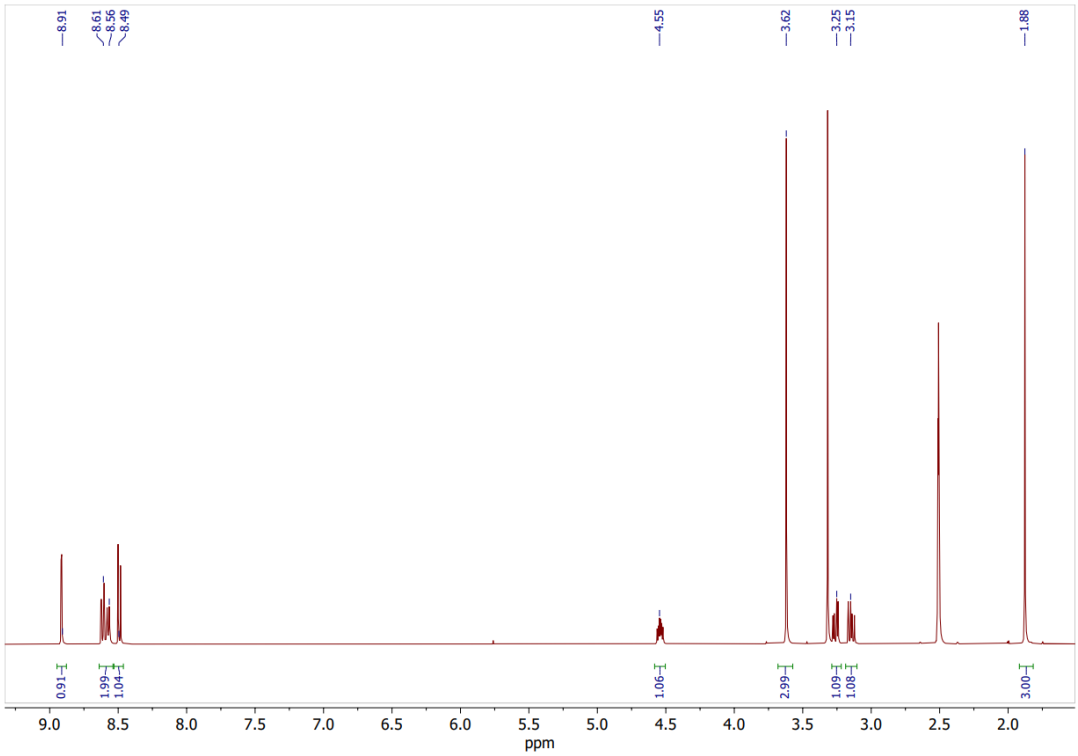


Figure C39. ^{1}H NMR (500 MHz, DMSO-d_6) spectrum of **15**.

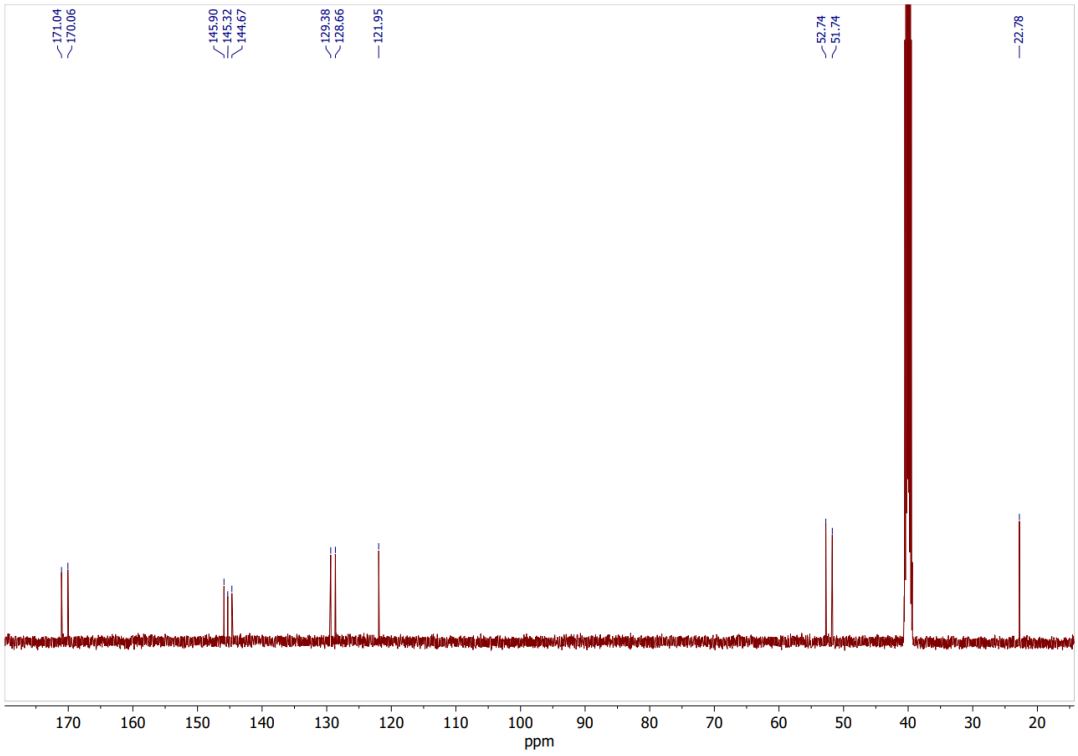


Figure C40. ^{13}C{^{1}H} NMR (125 MHz, DMSO-d_6) spectrum of **15**.

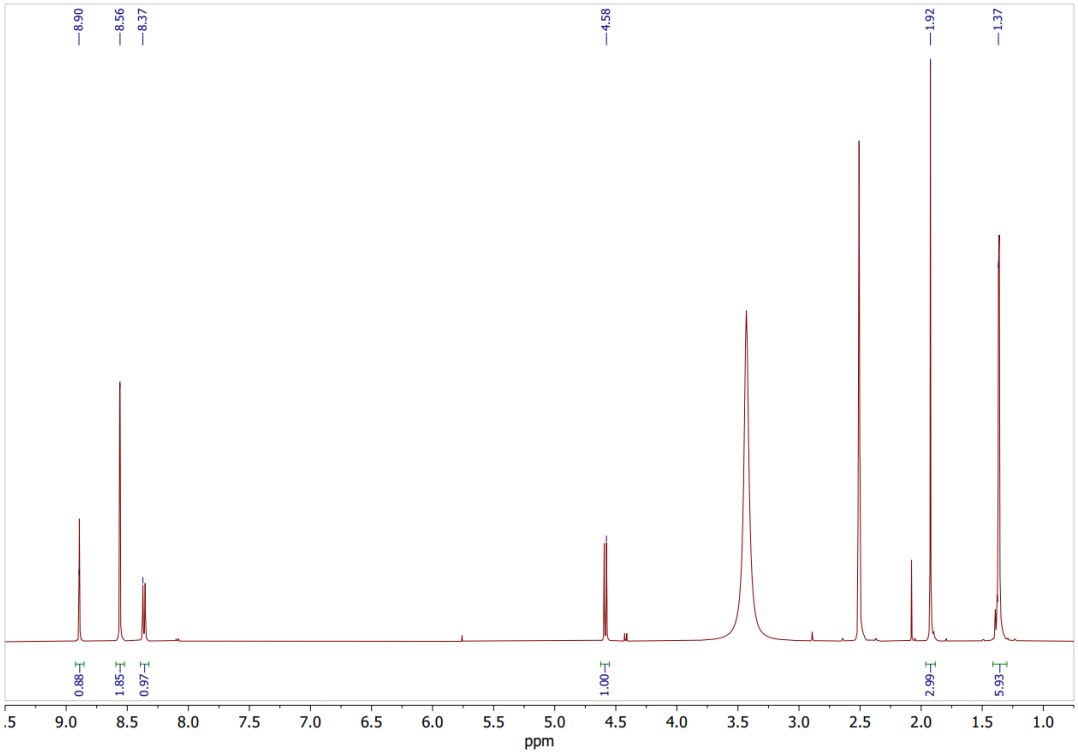


Figure C41. ^{1}H NMR (500 MHz, DMSO-d_6) spectrum of **16**.

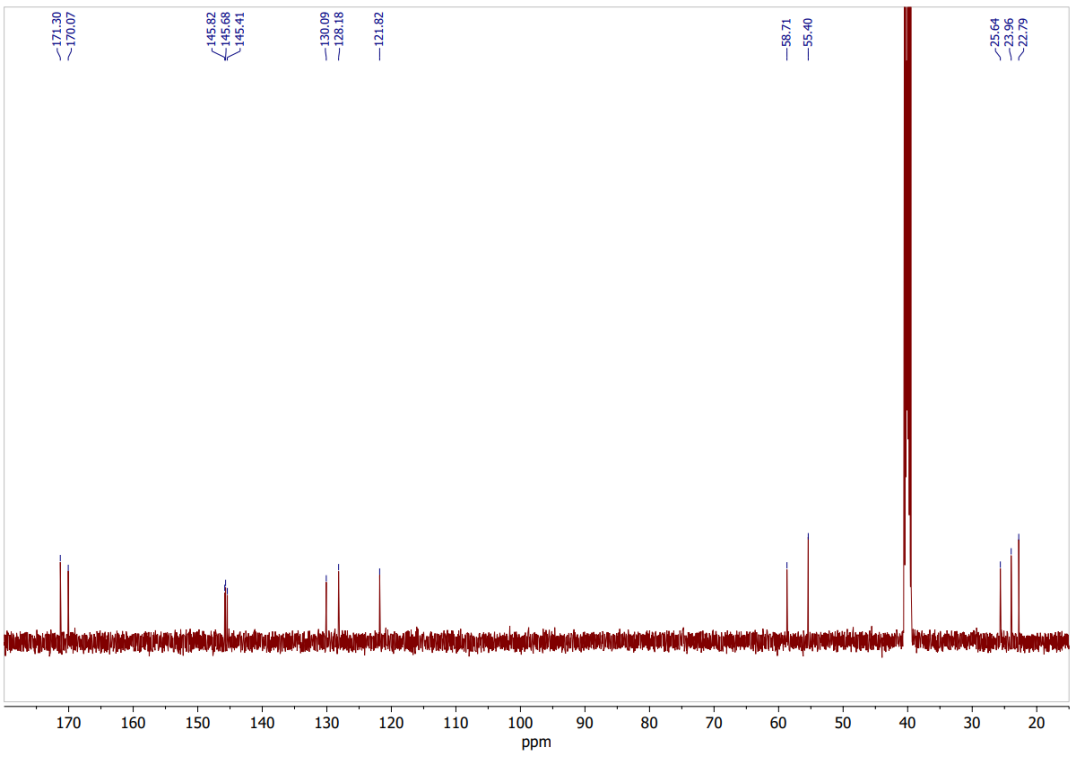


Figure C42. ^{13}C{^{1}H} NMR (125 MHz, DMSO-d_6) spectrum of **16**.

APPENDIX D

SUPPLEMENTARY CONTENT FOR CHAPTER V

Appendix D is the supplementary appendix for Chapter V of this dissertation. It includes all spectra and experimental information relevant to the material in Chapter V.

Computational Details

Gaussian 16 was used to perform all Density Functional Theory (DFT) calculations.[1180] Geometry optimizations were conducted with the ωB97X-D[1181] method using the aug-cc-pV(T+d)Z basis set for the H_2S versus transpersulfidation studies shown in Figures 2–5.[1182] For the penicillamine-derived persulfide precursor calculations in Figure 6, which are much larger systems, the optimization employed the aug-cc-pVDZ basis set and was followed by single-point energy refinements using the ωB97X-D or M06-2X functional and the aug-cc-pV(T+d)Z basis set. The SMD implicit solvation model for water was used at all stages to consider solvation effects.[1183] By default, an "ultrafine" pruned (99,590) grid in Gaussian 16 was used for numerical integrations, which eliminated most orientation-specific issues.[1184] Frequency calculations were performed at the level of theory used for optimization to confirm stationary points as minima or first-order saddle points and to obtain corrections for zero-point energy, enthalpy, and free energy at a standard state of 1 atm pressure and 298 K temperature using Goodvibes v3.0.1.[1185] Grimme's scheme for the treatment of small frequencies was applied, setting frequencies below 100 cm^{-1} to 100 cm^{-1}.[1186] The final free energies were computed by adding the free energy corrections obtained from the frequency analysis to the single-point electronic energies. Conformational analysis was performed manually on all flexible structures to locate the lowest-energy conformer for each stationary point. CYLview was used to prepare visualizations of the computed structures.[1187]

Methods and Materials:

Reagents were purchased from Sigma-Aldrich, Tokyo Chemical Industry (TCI), Fisher Scientific, Combi-Blocks, and VWR and were used directly as received. Silica gel (SiliaFlash F60, Silicycle, 230−400 mesh) and preparatory TLC plates (SiliaPlate Prep TLC, Silicycle, 1000 μm

thickness) were used for column chromatography. Deuterated solvents were purchased from Cambridge Isotope Laboratories (Tewksbury, Massachusetts, USA). ^{1}H and $^{13}C\{^{1}H\}$ NMR spectra were recorded on a Bruker 500 MHz NMR instrument at the indicated frequencies. Chemical shifts are reported in ppm relative to residual protic solvent resonances. Mass spectrometric measurements were performed by the University of Illinois, Urbana Champaign MS facility or on a Xevo Waters ESI LC/MS instrument. Methylene blue absorbance was monitored by a Cary 60 UV-Vis spectrometer. TME-IAM trapping assay analysis was conducted on an Agilent 1260 Infinity II HPLC with an analytical LC column (Eclipse XDB-C18, 4.6 x 250 mm, 5 μm).

Synthetic Procedures

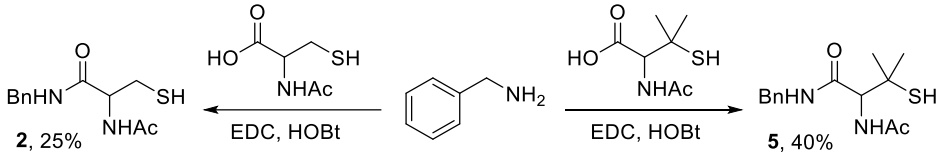


Figure D1. Synthetic routes for thiols **2** and **5**.

*Compound **2***. *N*-Acetyl-L-cysteine (258 mg, 1.58 mmol, 1.0 equiv.) was added to a mixture of CH_2Cl_2 (13 mL) and DMF (2 mL), and the reaction mixture was cooled to 0 °C. Next, *N*-hydroxybenzotriazole (236 mg, 1.75 mmol, 1.1 equiv.), benzylamine (246 μL, 2.25 mmol, 1.4 equiv.), and then *N*-(3-dimethylaminopropyl)-*N*′-ethylcarbodiimide (337 mg, 1.75 mmol, 1.1 equiv.) were added sequentially, and the reaction was stirred at room temperature overnight. After the solvent was removed under vacuum, the crude product was recrystallized in MeCN/water and filtered to yield the final product as a white solid (97.5 mg, 24.5%). ^{1}H NMR (500 MHz, DMSO-d_6) δ (ppm): 8.50 (t, *J* = 6.2 Hz, 1H), 8.10 (d, *J* = 8.0 Hz, 1H), 7.26 (m, 5H), 4.42 – 4.36 (m, 1H), 4.29 (d, *J* = 6.0 Hz, 2H), 2.80 (m, 1H), 2.72 – 2.65 (m, 1H), 2.28 (t, *J* = 8.4 Hz, 1H), 1.88 (s, 3H). $^{13}C\{^{1}H\}$ NMR (125 MHz, CD_2Cl_2) δ (ppm): 170.4, 170.0, 139.7, 128.7, 127.6, 127.2, 55.7, 42.6, 26.6, 23.1. HRMS m/z $[M + H]^+$ calcd. for $[C_{12}H_{16}N_2O_2SNa]^+$ 275.0825; found 275.0824.

*Compound **5***. Compound **5** was prepared according to a modified version of a reported procedure.[1188] *N*-Acetylpenicillamine (300 mg, 1.57 mmol, 1.0 equiv.) was added to a mixture of CH_2Cl_2 (13 mL) and DMF (2 mL) at 0 °C. Next, *N*-hydroxybenzotriazole (235 mg, 1.74 mmol, 1.1 equiv.), benzylamine (246 μL, 2.25 mmol, 1.4 equiv.), and *N*-(3-dimethylaminopropyl)-*N*′-

ethylcarbodiimide (332 mg, 2.14 mmol, 1.4 equiv.) were added sequentially, and the reaction was stirred at room temperature overnight. After the solvent was removed under vacuum, the crude product was recrystallized in MeCN/water and filtered to yield the final product as a yellow solid (215 mg, 40.0%). ^{1}H NMR (500 MHz, DMSO-d_6) δ (ppm): 8.63 (t, *J* = 5.9 Hz, 1H), 7.97 (d, *J* = 9.5 Hz, 1H), 7.27 (m, 5H), 4.54 (d, *J* = 9.5 Hz, 1H), 4.28 (dd, *J* = 6.0, 2.2 Hz, 2H), 2.75 (s, 1H), 1.92 (s, 3H), 1.34 (d, *J* = 18.7 Hz, 6H). ^{13}C{^{1}H} NMR (125 MHz, CD_2Cl_2) δ (ppm): 169.30, 169.19, 139.09, 128.20, 127.35, 126.76, 60.71, 46.09, 42.12, 30.05, 29.14, 22.49. HRMS m/z [M + H]$^+$ calcd. for $[C_{14}H_{20}N_2O_2SNa]^+$ 303.1138; found 303.1142.

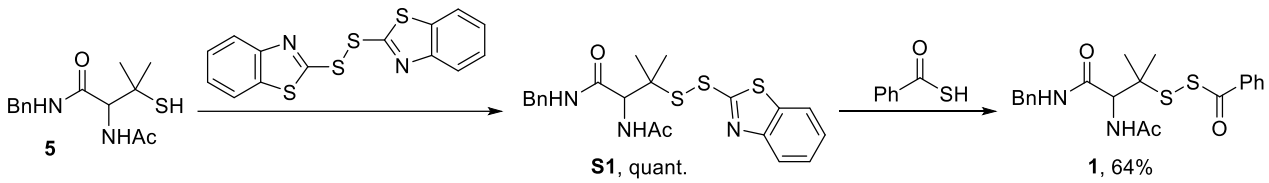


Figure D2. Synthetic route for the thiol-activated persulfide donor.

Persulfide donor **1** was prepared according to a modified version of a reported procedure.[1177]

*Compound **S1***. 2,2′-Dibenzothiazolyl disulfide (236 mg, 0.711 mmol, 1.0 equiv.) was dissolved into CH_2Cl_2 (50 mL) followed by **S1** (427 mg, 1.52 mmol, 2.1 equiv.). The reaction mixture was then stirred at room temperature for 44 hours. Next, the solvent was removed under vacuum, and the crude product was purified by column chromatography (3% MeOH in DCM) to yield the final product as yellow solid (374 mg, 99.8%). ^{1}H NMR (500 MHz, DMSO-d_6) δ (ppm): 8.94 (t, *J* = 6.1 Hz, 1H), 8.32 (d, *J* = 9.6 Hz, 1H), 8.03 (d, *J* = 7.9 Hz, 1H), 7.83 (d, *J* = 7.6 Hz, 1H), 7.48 (m, 1H), 7.40 (m, 1H), 7.26 (m, 5H), 4.77 (d, *J* = 9.6 Hz, 1H), 4.27 (m, 2H), 1.93 (s, 3H), 1.42 (s, 3H), 1.38 (s, 3H). ^{13}C{^{1}H} NMR (125 MHz, DMSO-d_6) δ (ppm): 173.5, 169.5, 168.3, 154.4, 138.9, 135.2, 128.3, 127.5, 126.9, 126.6, 124.9, 121.9, 121.7, 57.6, 56.1, 42.3, 25.5, 22.9, 22.5. HRMS m/z [M + H]$^+$ calcd. for $[C_{21}H_{24}N_3O_2S_3]^+$ 446.1025; found 446.1037.

*Compound **1***. Thiobenzoic acid (528 mg, 3.82 mmol, 4.3 equiv.) and **S3** (396 mg, 0.889 mmol, 1.0 equiv.) were added to chloroform (1.3 mL) and stirred at room temperature for 10 minutes. The reaction was then quenched with water, washed with sodium bicarbonate, and the organic layer was dried over $MgSO_4$ and evaporated under vacuum. The crude product was

purified by column chromatography (1% MeOH in DCM) to yield the final product as white solid (218 mg, 63.7%). ^{1}H NMR (500 MHz, DMSO-d_6) δ (ppm): 8.84 (t, *J* = 6.0 Hz, 1H), 8.22 (d, *J* = 9.5 Hz, 1H), 8.01 (d, *J* = 1.3 Hz, 2H), 7.76 (t, *J* = 7.6 Hz, 1H), 7.62 (t, *J* = 7.7 Hz, 2H), 7.28 (m, 5H), 4.66 (d, *J* = 9.5 Hz, 1H), 4.28 (m, 2H), 1.94 (s, 3H), 1.35 (s, 3H), 1.28 (s, 3H). ^{13}C{^{1}H} NMR (125 MHz, DMSO-d_6) δ (ppm): 189.9, 169.3, 168.5, 139.0, 135.2, 134.6, 129.4, 128.3, 127.5, 126.9, 57.8, 54.7, 42.2, 25.5, 23.2, 22.5. HRMS m/z [M + H]$^{+}$ calcd. for [$C_{21}H_{25}N_2O_3S_2$]$^{+}$ 417.1301; found 417.1302.

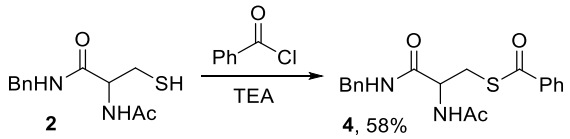


Figure D3. Synthetic route for the persulfide donor side product **4**.

*Compound **4***. Benzyl chloride (4.6 μL, 0.040 mmol, 1.0 equiv.) and **2** (10 mg, 0.036 mmol, 1.0 equiv.) were combined in anhydrous CH_2Cl_2 (5 mL), and then triethylamine (5.5 μL, 0.039 mmol, 1.0 equiv.) was added dropwise. After 2 hours, the reaction was concentrated and then loaded onto a preparatory TLC plate for purification using 5% MeOH in DCM as the mobile phase. The final product was isolated as a white solid (8.3 mg, 58%). ^{1}H NMR (500 MHz, CD_2Cl_2) δ (ppm): 7.96 (d, *J* = 7.0 Hz, 2H), 7.63 (t, *J* = 7.5 Hz, 1H), 7.48 (t, *J* = 7.9 Hz, 2H), 7.35 – 7.20 (m, 5H), 6.82 (s, 1H), 6.51 (d, *J* = 7.5 Hz, 1H), 4.69 – 4.61 (m, 1H), 4.41 (dd, *J* = 5.9, 2.3 Hz, 2H), 3.50 (d, *J* = 5.6 Hz, 2H), 1.95 (s, 3H). ^{13}C{^{1}H} NMR (125 MHz, CD_2Cl_2) δ (ppm): 193.05, 171.01, 170.08, 138.58, 136.88, 134.35, 129.19, 128.99, 127.89, 127.77, 43.85, 30.84, 23.30. HRMS m/z [M + H]$^{+}$ calcd. for [$C_{19}H_{20}N_2O_3SNa$]$^{+}$ 379.1087; found 379.1094.

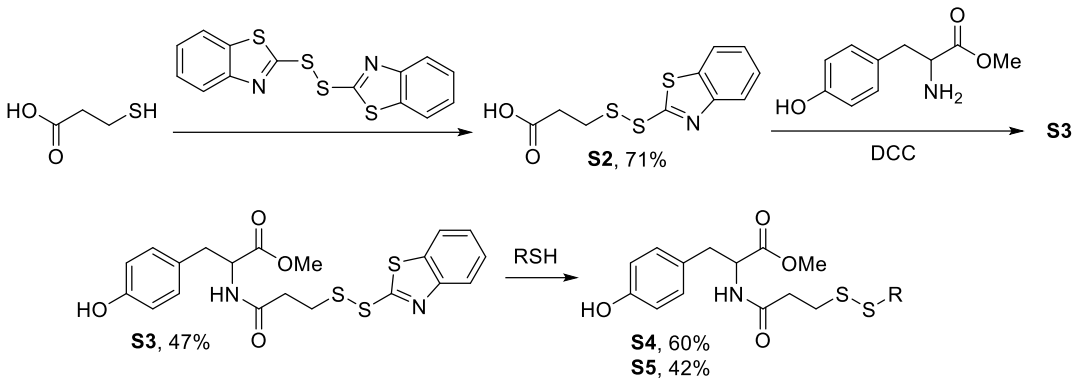


Figure D4. General synthetic route for the trapped persulfide adduct analogues **S4** and **S5**.

*Compound **S2***. 2,2′-Dibenzothiazolyl disulfide (874 mg, 2.63 mmol, 1.4 equiv.) was dissolved into CH_2Cl_2 (20 mL) and then 3-mercaptopropionic acid (156 μL, 1.88 mmol, 1.0 equiv.) was added dropwise. The reaction mixture was stirred at room temperature overnight. Next, the reaction was quenched with water, and then the aqueous solution was extracted with DCM, washed with brine, dried over $MgSO_4$, and then evaporated under vacuum. The crude solid was first purified by column chromatography using 1−5% MeOH in DCM as the mobile phase to yield the desired product as a white solid (361 mg, 70.5%). ^{1}H NMR (500 MHz, CD_2Cl_2) δ (ppm): 7.86 (m, 2H), 7.46 (t, *J* = 7.7 Hz, 1H), 7.37 (t, *J* = 7.6 Hz, 1H), 3.22 (t, *J* = 6.8 Hz, 2H), 2.89 (t, *J* = 6.8 Hz, 2H). ^{13}C{^{1}H} NMR (125 MHz, CD_2Cl_2) δ (ppm): 173.1, 171.9, 155.0, 136.4, 126.8, 125.3, 122.4, 121.7, 35.0, 33.9. HRMS m/z $[M + H]^+$ calcd. for $[C_{10}H_{10}NO_2S_3]^+$ 271.9868; found 271.9870.

*Compound **S3***. Compound **S2** (502 mg, 1.85 mmol, 1.0 equiv.), L-tyrosine methyl ester (363 mg, 1.85 mmol, 1.0 equiv.), and DCC (836 mg, 4.06 mmol, 2.2 equiv.) were dissolved in anhydrous DMF (4 mL) at 0 °C. This mixture was then stirred for 2 hours at 0 °C followed by 1 hour at room temperature. Next, the reaction was quenched with water, and then the aqueous solution was extracted with DCM, washed with 1% LiCl, dried over $MgSO_4$, and then evaporated under vacuum. The crude solid was first purified by column chromatography using 1-7% MeOH in DCM as the mobile phase. Since DCC/DCU still remained, the crude product was dissolved in minimal DCM and then chilled in the freezer overnight. After filtering, the resulting filtrate was then purified by column chromatography with 2−5% MeOH in DCM as the mobile phase to yield the final product as a white solid (390 mg, 46.9%). ^{1}H NMR (500 MHz, CD_2Cl_2) δ (ppm): 7.84 (d, *J* = 8.1 Hz, 2H), 7.45 (m, 1H), 7.36 (m, 1H), 6.95 (d, *J* = 8.5 Hz, 2H), 6.71 (d, *J* = 8.5 Hz, 2H),

6.12 (d, *J* = 7.9 Hz, 1H), 5.24 (s, 1H), 4.80 (m, 1H), 3.71 (s, 3H), 3.20 (t, *J* = 6.9 Hz, 2H), 3.08 (dd, *J* = 14.1, 5.8 Hz, 1H), 2.99 (dd, *J* = 14.0, 6.1 Hz, 1H), 2.68 (t, *J* = 7.0 Hz, 1H). $^{13}C\{^{1}H\}$ NMR (125 MHz, CD_2Cl_2) δ (ppm): 172.9, 171.3, 170.9, 169.5, 156.0, 138.3, 130.7, 129.0, 128.1, 127.8, 127.7, 116.0, 59.1, 52.8, 52.7, 44.0, 37.1, 35.8, 35.8, 25.7, 24.2, 23.4. HRMS m/z $[M + H]^+$ calcd. for $[C_{20}H_{21}N_2O_4O_3]^+$ 449.0658; found 449.0664.

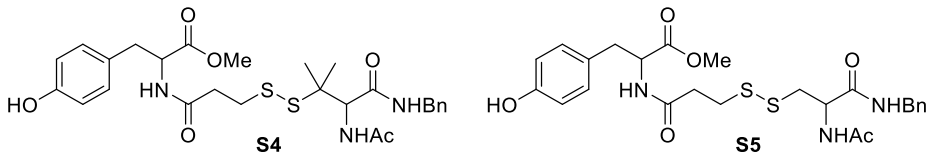


Figure D5. Structures of compounds **S4** and **S5**.

*Compound **S4***. Compound **S3** (30 mg, 0.066 mmol, 1.0 equiv.) and **5** (21 mg, 0.076 mmol, 1.0 equiv.) were dissolved in MeCN (10 mL) and then stirred for 1 hour at room temperature. Next, the reaction was concentrated and then loaded onto a preparatory TLC plate for purification using 5% MeOH in DCM as the mobile phase. The final product was isolated as a white solid (22 mg, 60%). ^{1}H NMR (500 MHz, CD_2Cl_2) δ (ppm): 7.29 (m, 7H), 6.94 (d, *J* = 8.4 Hz, 2H), 6.72 (d, *J* = 8.4 Hz, 2H), 6.65 (d, *J* = 9.1 Hz, 1H), 6.59 (d, *J* = 7.9 Hz, 1H), 4.70 (m, 2H), 4.44 (dd, *J* = 14.8, 5.9 Hz, 1H), 4.35 (dd, *J* = 14.9, 5.6 Hz, 1H), 3.66 (s, 3H), 3.04 (dd, *J* = 14.1, 5.3 Hz, 1H), 2.88 (m, 3H), 2.52 (m, *J* = 15.3, 6.6 Hz, 1H), 2.40 (dt, *J* = 15.2, 7.1 Hz, 1H), 2.00 (s, 3H), 1.39 (s, 3H), 1.36 (s, 3H). $^{13}C\{^{1}H\}$ NMR (125 MHz, CD_2Cl_2) δ (ppm): 172.9, 171.3, 170.9, 169.5, 156.0, 138.3, 130.7, 129.0, 128.1, 127.8, 127.7, 116.0, 59.1, 52.8, 52.9, 44.0, 37.1, 35.8, 35.8, 25.7, 24.2, 23.4. HRMS m/z $[M + H]^+$ calcd. for $[C_{27}H_{36}N_3O_6S_2]^+$ 562.2040; found 562.2049.

*Compound **S5***. Compound **S3** (30 mg, 0.067 mmol, 1.0 equiv.) and **2** (18 mg, 0.070 mmol, 1.0 equiv.) were dissolved in DCM (4 mL) and then stirred for 2 hours at room temperature. Next, the reaction was concentrated and then loaded onto a preparatory TLC plate for purification using 5% MeOH in DCM as the mobile phase. The final product was isolated as a white solid (16 mg, 42%). ^{1}H NMR (500 MHz, CD_2Cl_2) δ (ppm): 7.31 (m, 5H), 7.13 (m, 1H), 6.87 (d, *J* = 8.5 Hz, 2H), 6.82 (s, 1H), 6.72 (d, *J* = 8.5 Hz, 2H), 6.52 (d, *J* = 8.2 Hz, 1H), 6.19 (d, *J* = 8.6 Hz, 1H), 4.68 (d, *J* = 13.7 Hz, 2H), 4.47 (dd, *J* = 14.8, 6.1 Hz, 1H), 4.38 (dd, *J* = 14.8, 5.6 Hz, 1H), 3.74 (s, 3H), 3.11 (dd, *J* = 13.9, 5.4 Hz, 2H), 2.87 (d, *J* = 8.1 Hz, 3H), 2.74 (dd, *J* = 13.9, 8.8 Hz, 1H), 2.51 (d,

J = 5.9 Hz, 1H), 2.44 (d, *J* = 8.1 Hz, 1H), 2.04 (s, 3H). $^{13}C\{^{1}H\}$ NMR (125 MHz, CD_2Cl_2) δ (ppm): 172.5, 171.4, 170.6, 170.3, 156.1, 138.6, 130.8, 129.0, 128.2, 128.0, 127.8, 116.3, 52.7, 44.1, 41.2, 37.9, 35.6, 34.6, 23.5. HRMS m/z $[M + H]^+$ calcd. for $[C_{25}H_{32}N_3O_6S_2]^+$ 534.1727; found 534.1735.

TME-IAM was prepared according to a previously reported procedure.[1178]

Persulfide trapping with TME-IAM monitored by HPLC

Under inert conditions, a freshly prepared persulfide donor **1** stock solution (100 μL, 20 mM in acetonitrile) was added to 20 mL of 10% acetonitrile in PBS buffer (pH 7.4, 10 mM) containing **2** (1.0 mM) to begin the experiment. Individual 500 μL aliquots were taken at 0, 1, 5, 10, 15, 30, 45, and 60 minutes and added to GC vials containing 500 μL of TME-IAM (20 mM in acetonitrile). After filtering, these solutions were analyzed on by reverse-phase HPLC. The HPLC method is as follow: Mobile phase A (5% methanol in water) and mobile phase B (methanol); Flow rate of 1 mL/min; Injection volume of 10 μL; Detection wavelength of 210 nm; Column used was Eclipse XDB-C18, 4.6 x 250 mm, 5 μm, analytical LC column; Gradient method with 80% A from 0–2 min, 80–20% A from 2–22 min, 20% A from 22-24 min, 20–80% A from 24–29 min, and 80% A from 29–30 min.

*Persulfide adduct analogues **S4** and **S5** HPLC calibration curve*

A 100 μM stock solution of the persulfide adduct analogue was prepared and then serially diluted to 50, 25, 12.5, 6.25, 3.125, and 1.5625 μM in 1:1 MeOH/water. After filtering, these solutions were run on a reverse-phase HPLC instrument using the same method as described above for the TME-IAM trapping assay.

Symmetric and asymmetric disulfide formation for HPLC analysis

Disulfides were formed using the following conditions: (1) **5** (200 μM) and iodine (200 μM); (2) **5** (100 μM), **2** (100 μM), and iodine (200 μM); and (3) **2** (200 μM) and iodine (200 μM) in 1:1 MeOH/water. Samples were let sit for 10 minutes before filtering and analyzing by HPLC. Using these samples, the retention times of all disulfides were identified.

Methylene blue assay to monitor H_2S release

Under inert conditions, a stock solution of the persulfide donor **1** (100 μL, 20 mM) was added to 20 mL of 10% acetonitrile in PBS buffer (pH 7.4, 10 mM) containing **2** (1.0 mM). At 1, 5, 10, 15, 20, 30, 45, and 60 minutes, 500 μL aliquots were taken and placed in cuvettes containing 500 μL of 2:2:1 iron (III) chloride/*N*,*N*-dimethyl-*p*-phenylenediamine/zinc acetate and then filtered. After 1 hour the absorbance at 670 nm was measured using a UV-Vis spectrophotometer and was converted to H_2S concentration by using an H_2S calibration curve.

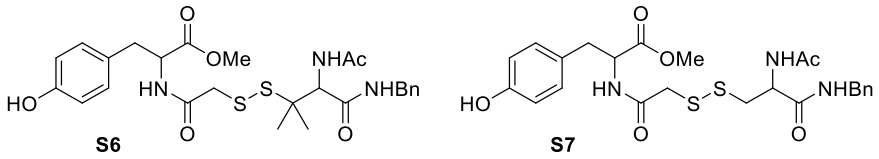


Figure D6. Structures of compounds **S6** and **S7**.

*Isolation of persulfide adducts **S6** and **S7***

Under inert conditions, a stock solution of the persulfide donor **1** (25 μL, 20 mM) was added to 2.5 mL of 10% acetonitrile in PBS buffer (pH 7.4, 10 mM) containing **2** (2.0 mM). After 5 minutes, a solution of TME-IAM (1250 μL, 40 mM) was added to the reaction mixture to trap any persulfide/RSS species and stop the reaction. The solution was then concentrated and purified by HPLC using a semi-prep column (Zorbax SB-C18, 5 μM, 9.5 x 200 mm). Both the trapped persulfide **3** as adduct **S6** and trapped persulfide **6** as adduct **S7** were isolated and analyzed by MS to confirm their identity. Adduct **S6**: HRMS m/z [M + H]+ calcd. for $[C_{26}H_{34}N_3O_6S_2]^+$ 548.1884; found 548.1886. Adduct **S7**: HRMS m/z $[M + H]^+$ calcd. for $[C_{24}H_{30}N_3O_3S_2]^+$ 520.1571; found 520.1580.

Energetics of Cysteine Persulfide Reactivity with Nucleophiles

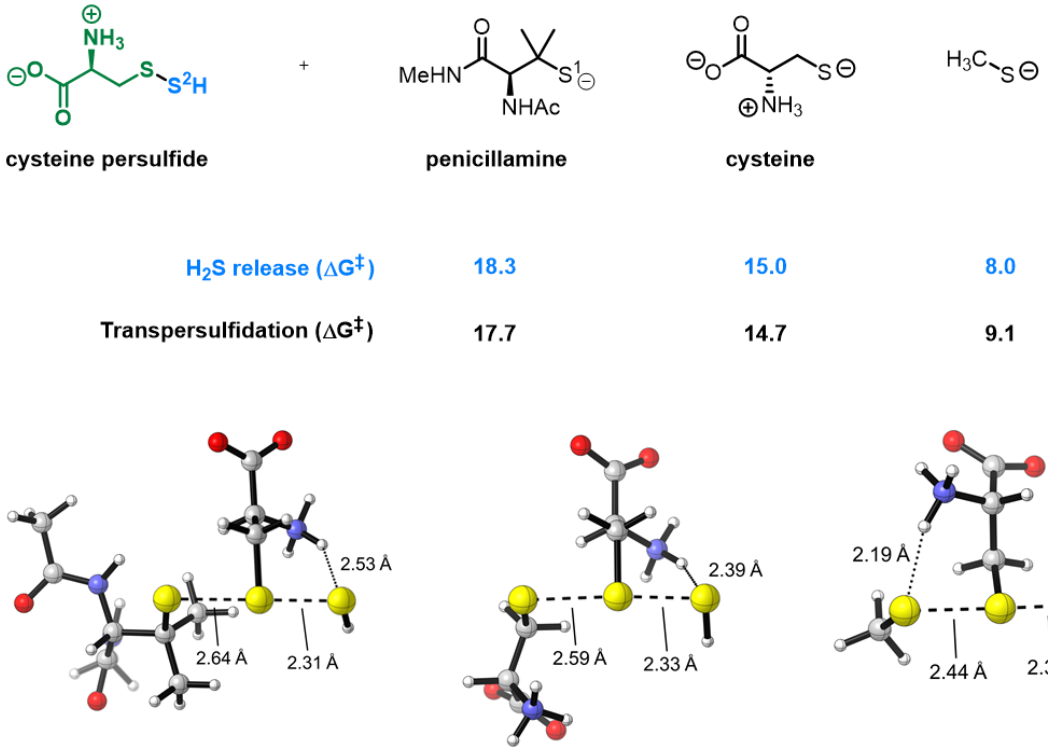


Figure D7. Impact of nucleophile steric bulk on the H_2S release and transpersulfidation activation free energies (kcal mol^{-1}) of cysteine persulfide.

Free Energy of H_2S Release and Transpersulfidation Pathways

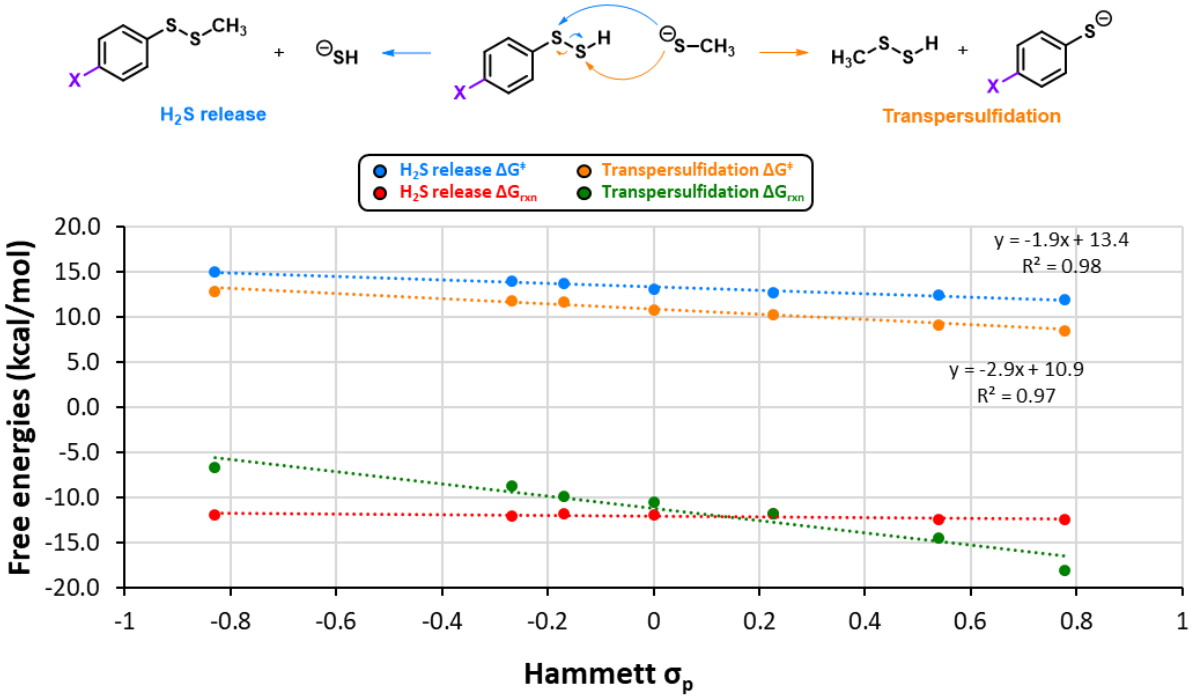


Figure D8. Free energies of activation and reaction as a function of Hammett σ_p values, for the transpersulfidation or H_2S release reactions of substituted aryl persulfides with methyl thiolate. The favorability of transpersulfidation increases with electron withdrawing substituents.

Taft Linear Free Energy Relationship

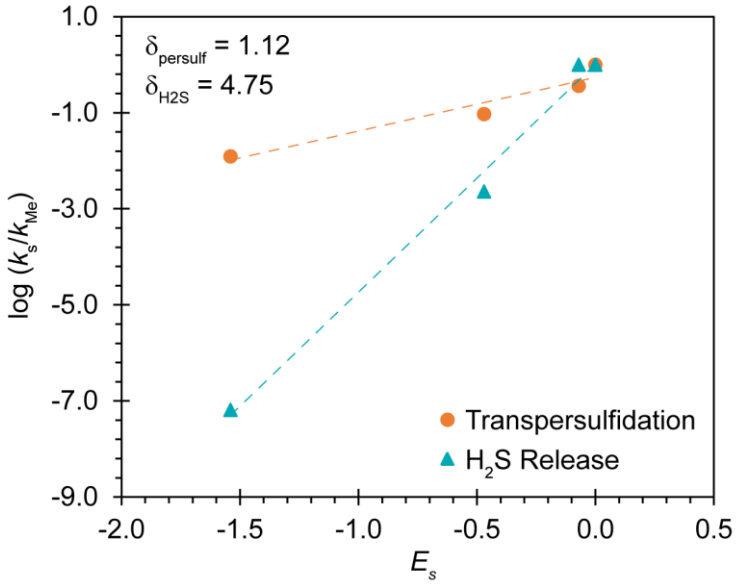


Figure D9. Taft linear free energy relationship of the steric sensitivity factor (δ) for transpersulfidation or H_2S release for MeSSH, EtSSH, *i*PrSSH, and *t*BuSSH.

*HPLC Chromatograms of the HPLC Trapping Assay with Persulfide Donor **1***

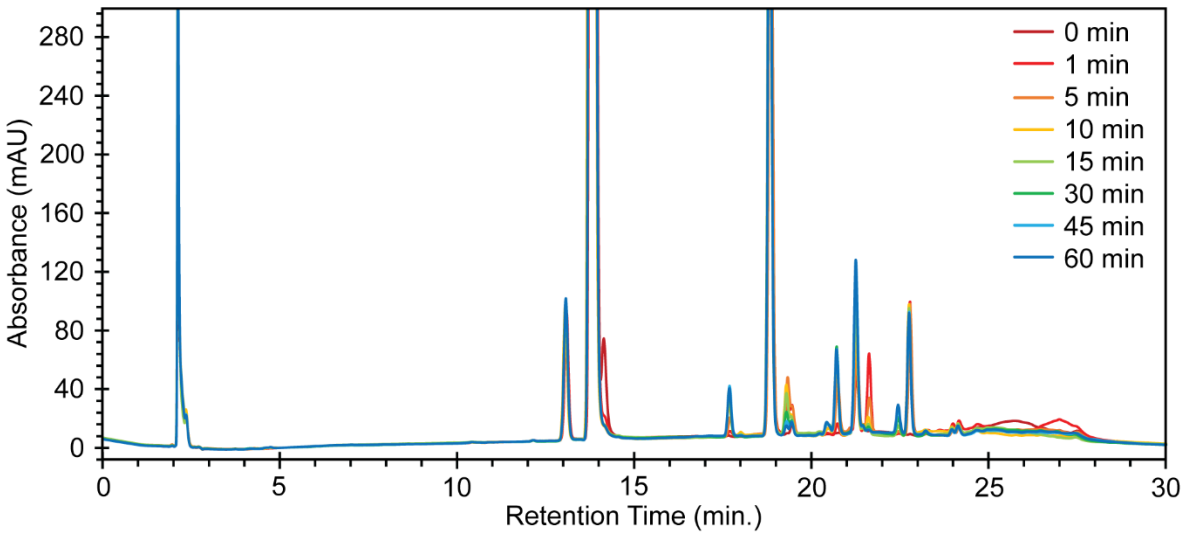


Figure D10. Full HPLC chromatograms of the TME-IAM persulfide trapping assay with the thiol-activated persulfide donor **1** (100 μM), **2** (1 mM), and TME-IAM (10 mM) over 60 minutes.

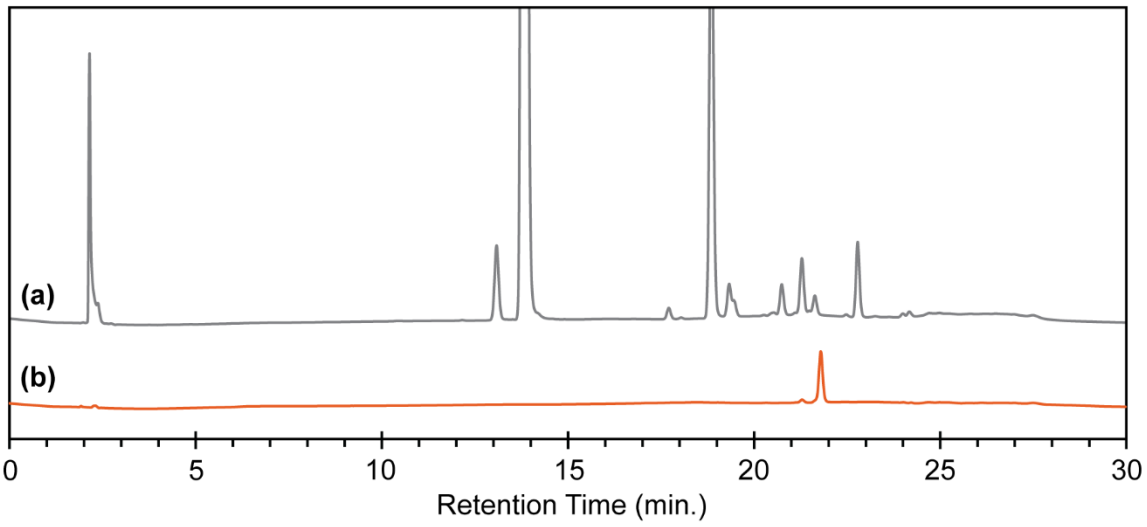


Figure D11. Stacked HPLC chromatograms of (a) the 5-minute timepoint of the TME-IAM persulfide trapping experiment and (b) the persulfide adduct analogue **S4**.

*Calibration Curves and HPLC Chromatograms of Trapped Persulfide Adducts **S4** and **S5***

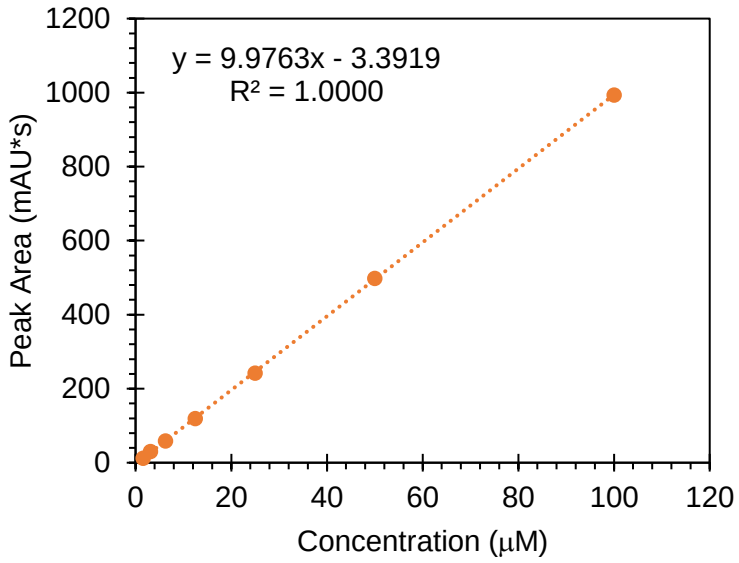


Figure D12. HPLC calibration curve of compound **S4** at various concentrations.

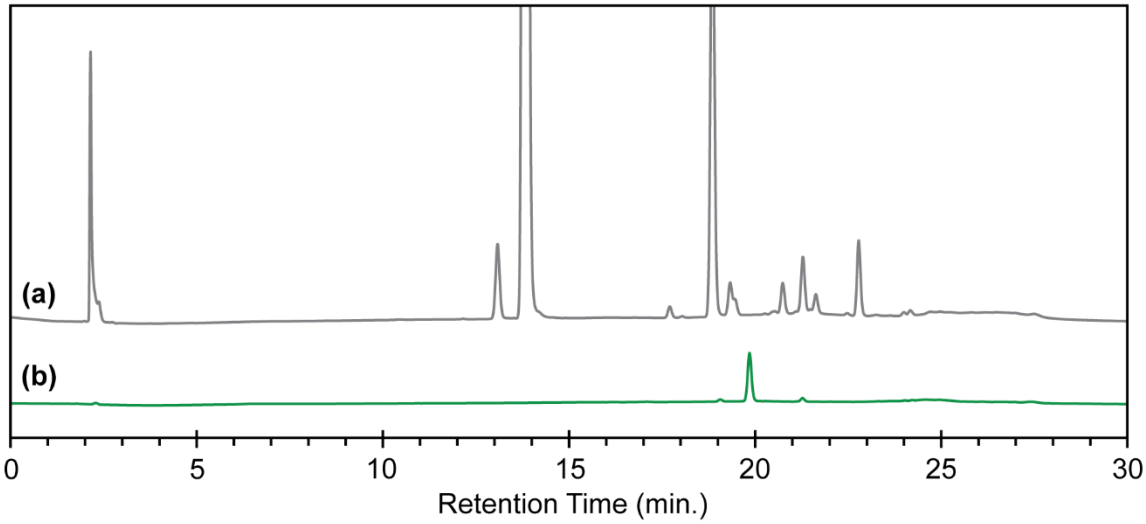


Figure D13. Stacked HPLC chromatograms of (a) the 5-minute timepoint of the TME-IAM persulfide trapping experiment and (b) the persulfide adduct analogue **S5**.

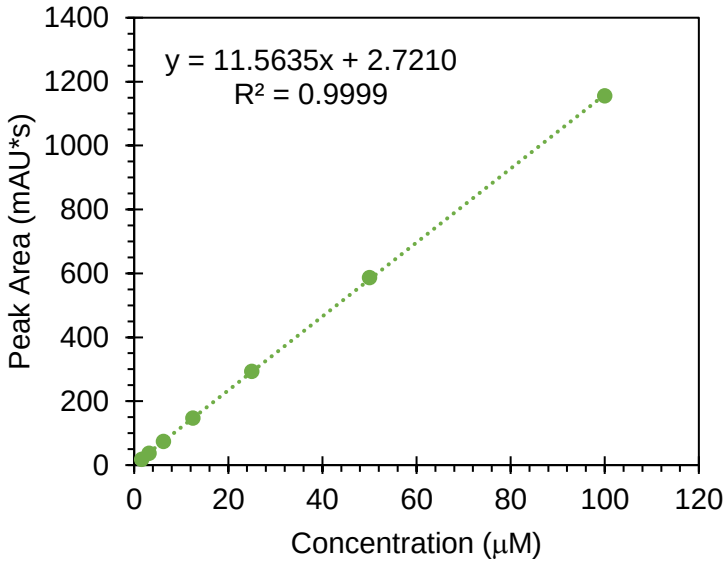


Figure D14. HPLC calibration curve of compound **S5** at various concentrations.

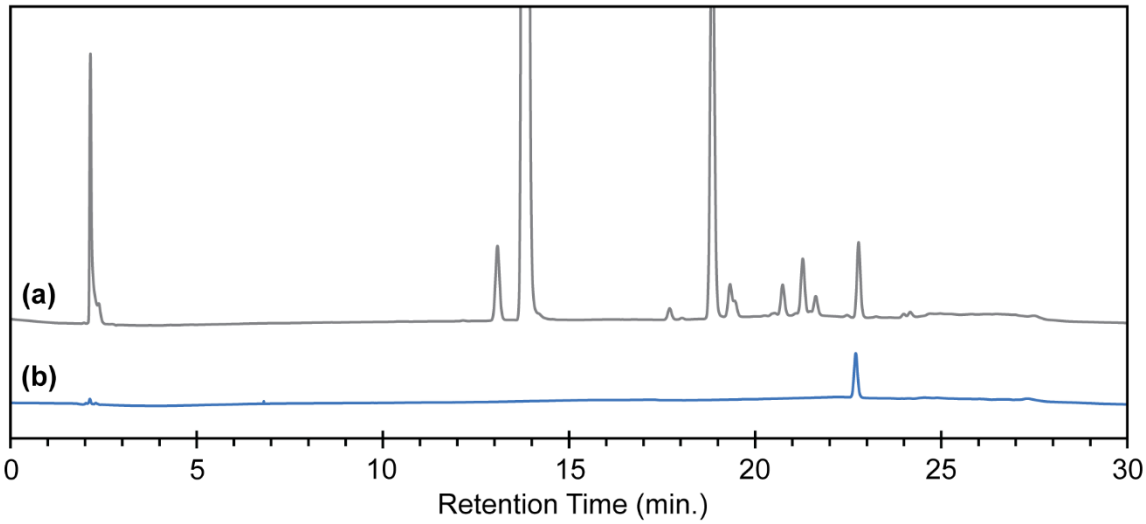


Figure D15. Stacked HPLC chromatograms of (a) the 5-minute timepoint of the TME-IAM persulfide trapping experiment and (b) the side product **4**.

HPLC Chromatograms of Symmetric and Unsymmetric Disulfides

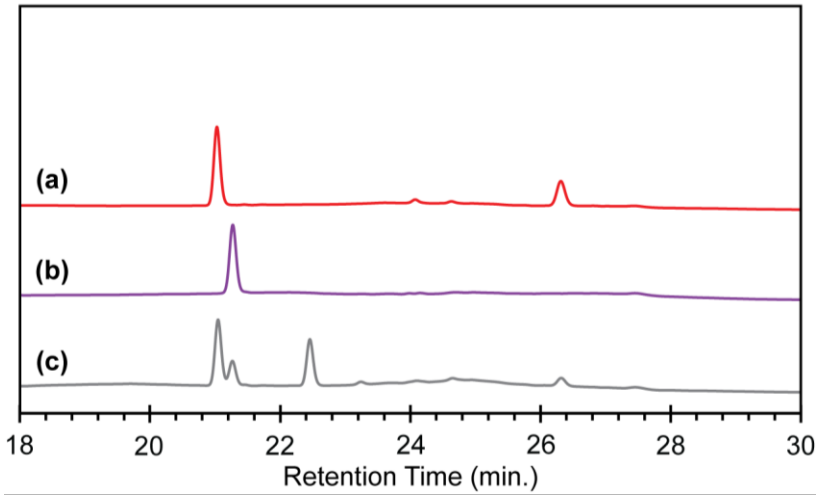


Figure D16. Stacked HPLC chromatograms of (a) thiol **5**, (b) thiol **2**, or (c) thiols **5** and **2** with iodine to form symmetric and unsymmetric disulfides for identification.

HPLC Chromatogram of Trapping Experiment Timepoint Treated with TCEP

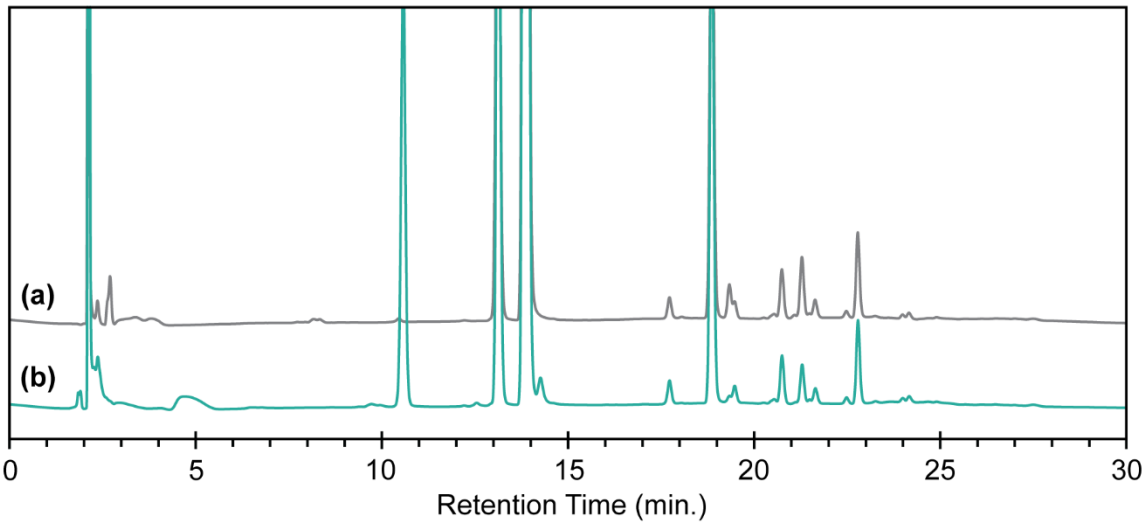


Figure D17. Stacked HPLC chromatograms of (a) the 5-minute timepoint of the TME-IAM persulfide trapping experiment and (b) after treatment with TCEP.

*HPLC Chromatograms of HPLC Purified Persulfide Adducts **S6** and **S7***

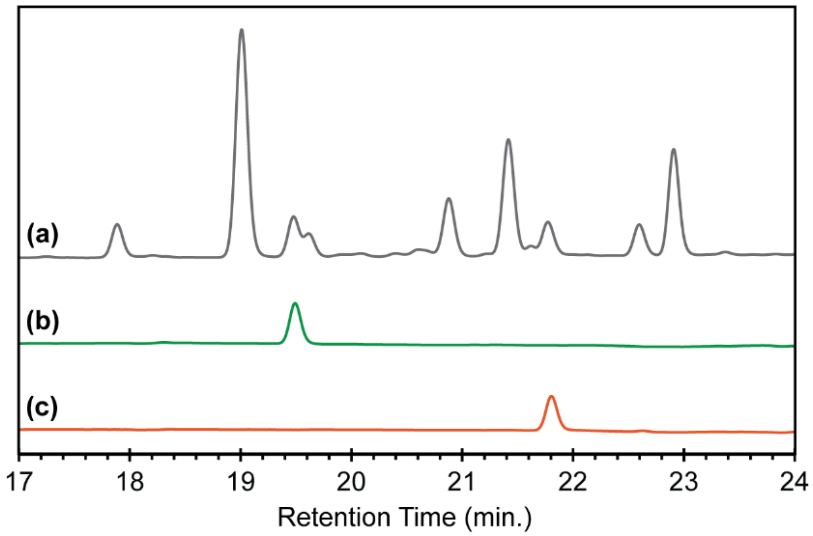


Figure D18. Stacked HPLC chromatograms of (a) the reaction between persulfide donor **1** and **2** quenched with TME-IAM after 5 minutes, (b) isolated persulfide adduct **S7**, and (c) isolated persulfide adduct **S6**.

^{1}H and $^{13}C\{^{1}H\}$ NMR Spectra

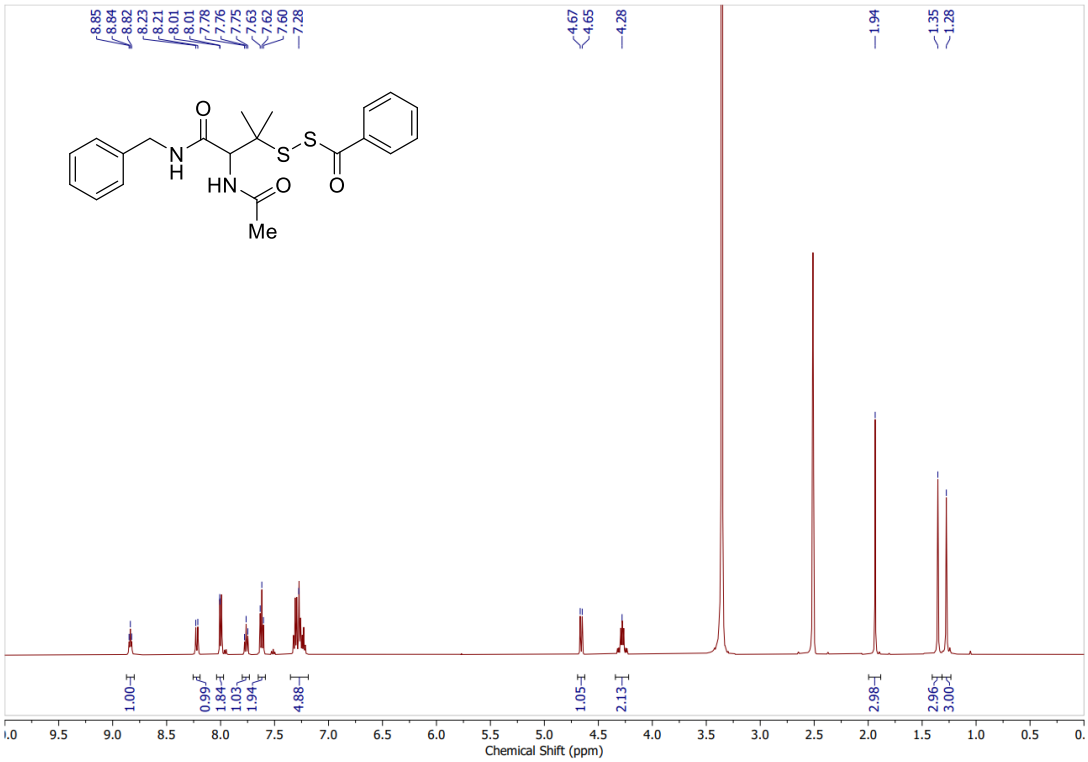


Figure D19. ^{1}H NMR (500 MHz, DMSO-d_6) spectrum of **1**.

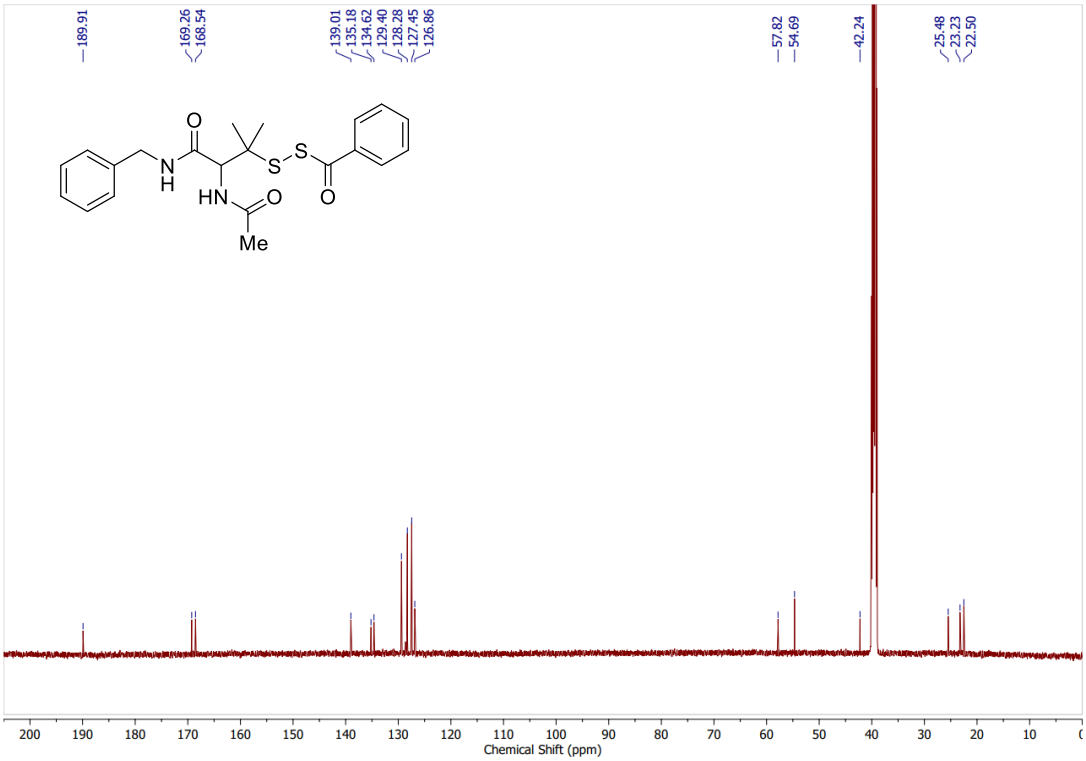


Figure D20. $^{13}C\{^{1}H\}$ NMR (125 MHz, DMSO-d_6) spectrum of **1**.

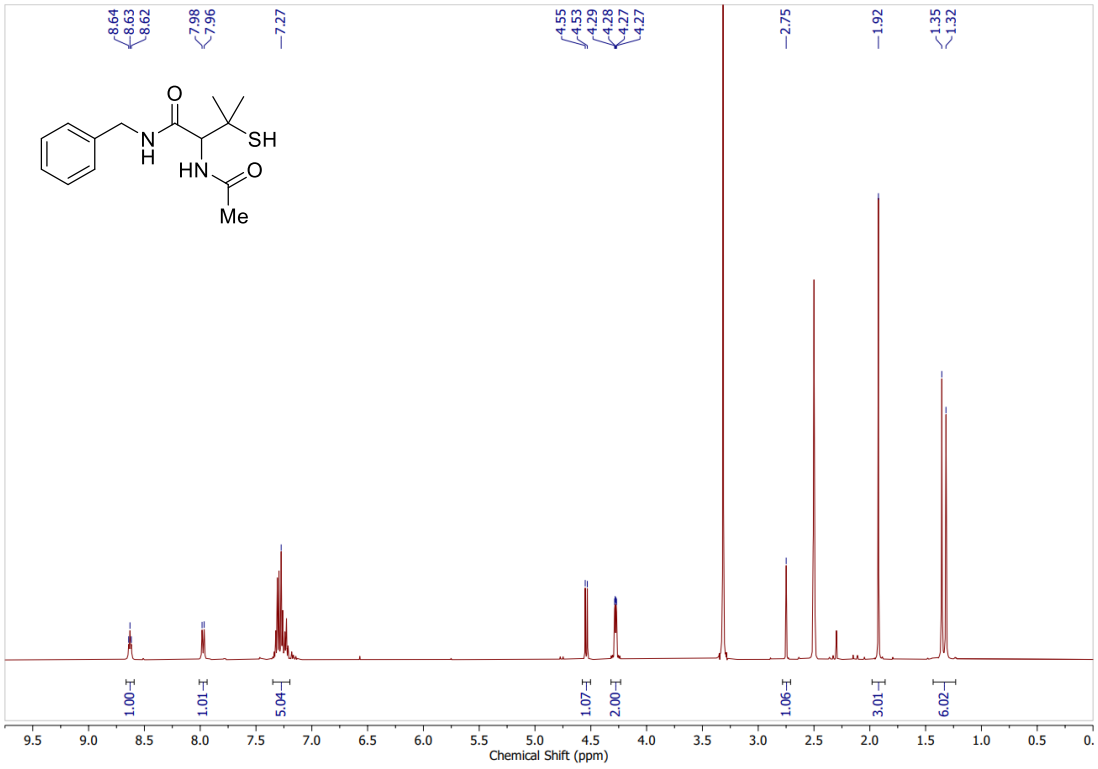


Figure D21. ^{1}H NMR (500 MHz, DMSO-d_6) spectrum of **5**.

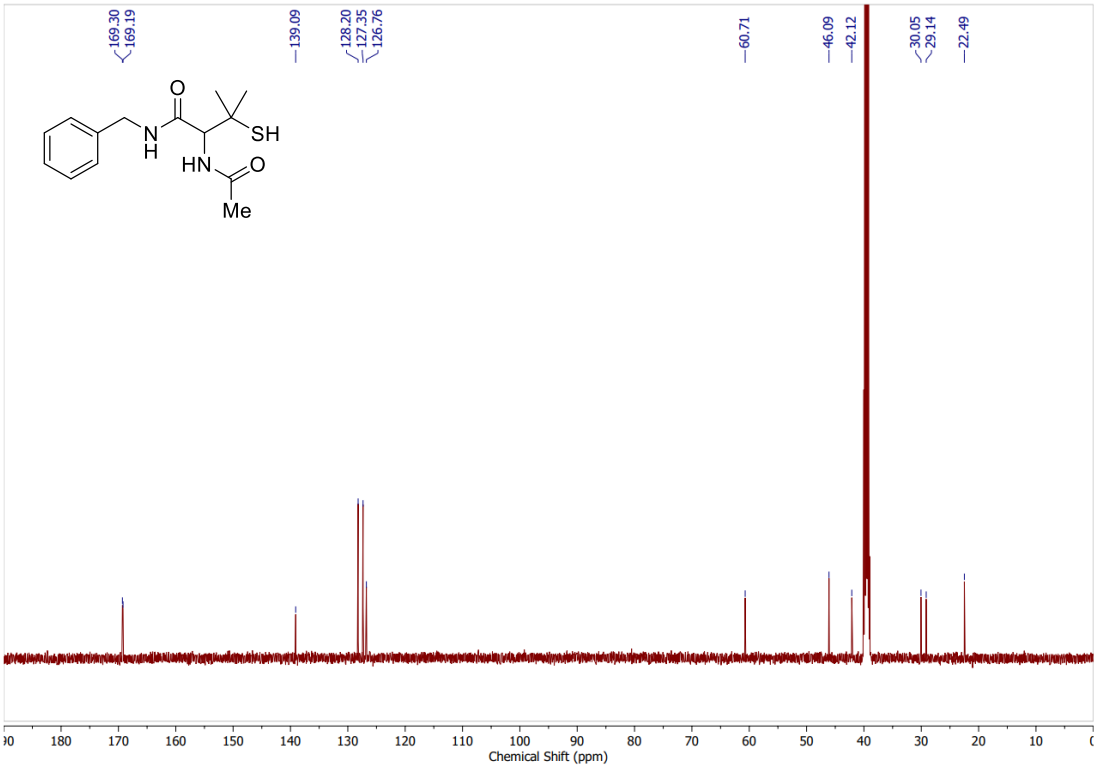


Figure D22. ^{13}C{^{1}H} NMR (125 MHz, DMSO-d_6) spectrum of **5**.

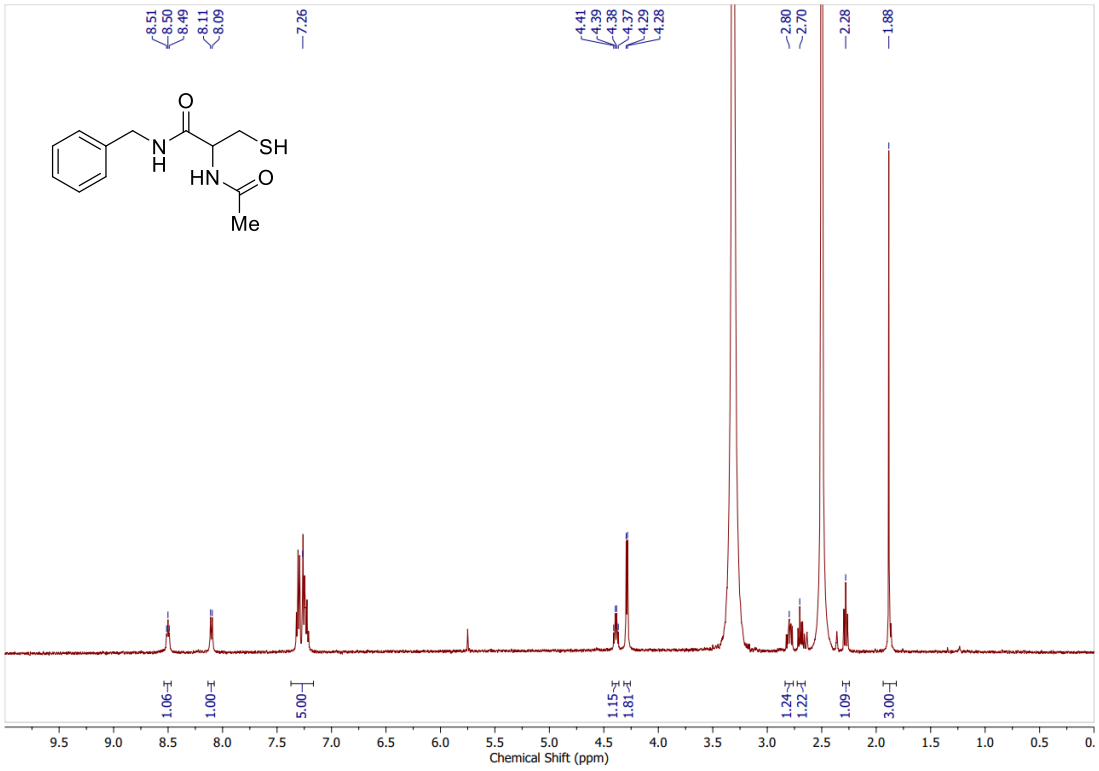


Figure D23. ^{1}H NMR (500 MHz, DMSO-d_6) spectrum of **2**.

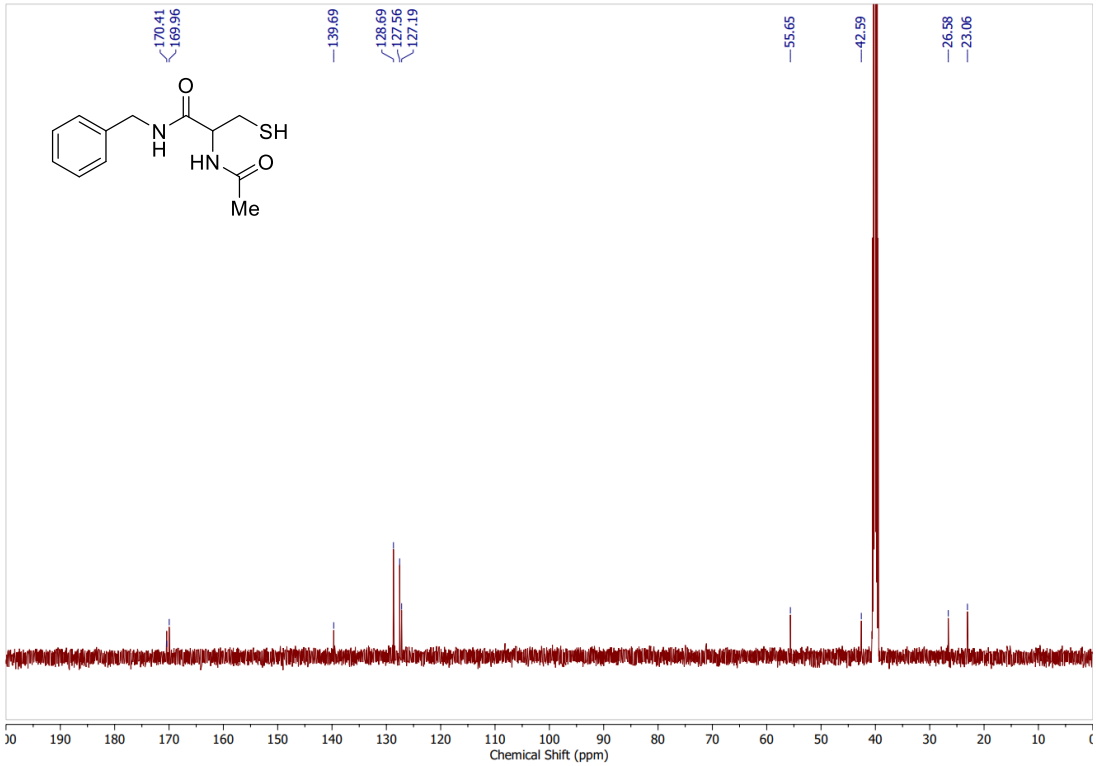


Figure D24. ^{13}C{^{1}H} NMR (125 MHz, DMSO-d_6) spectrum of **2**.

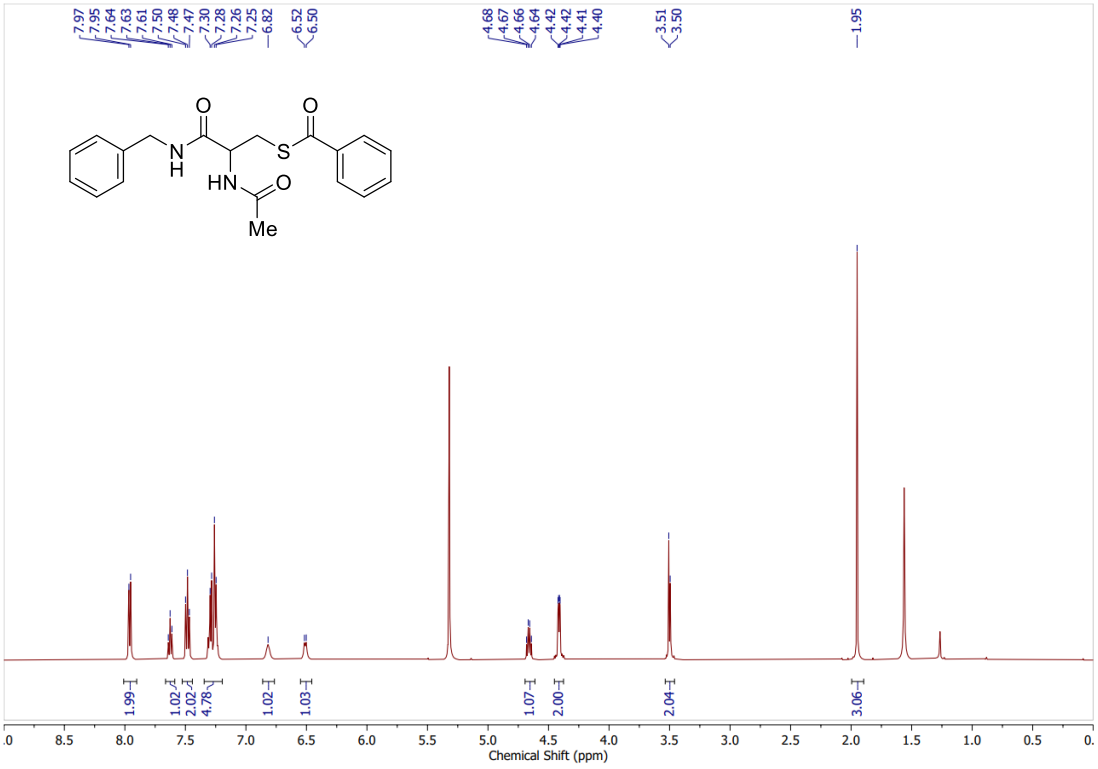


Figure D25. ^{1}H NMR (500 MHz, CD_2Cl_2) spectrum of **4**.

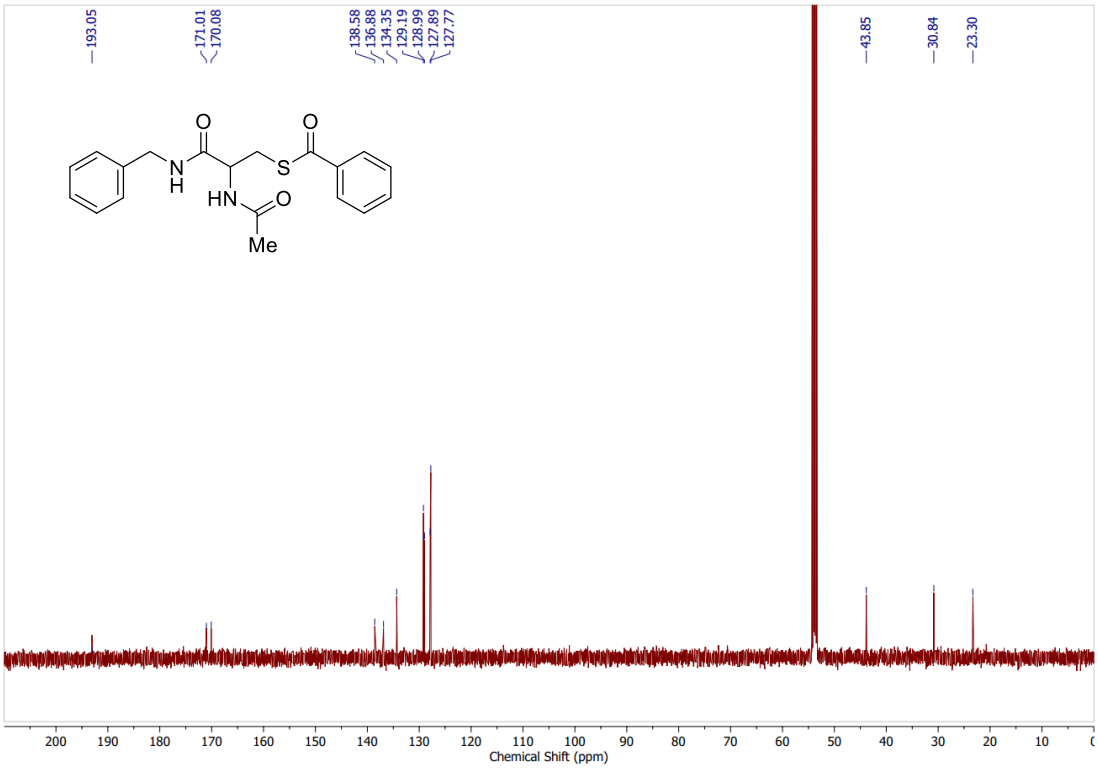


Figure D26. $^{13}C\{^{1}H\}$ NMR (125 MHz, CD_2Cl_2) spectrum of **4**.

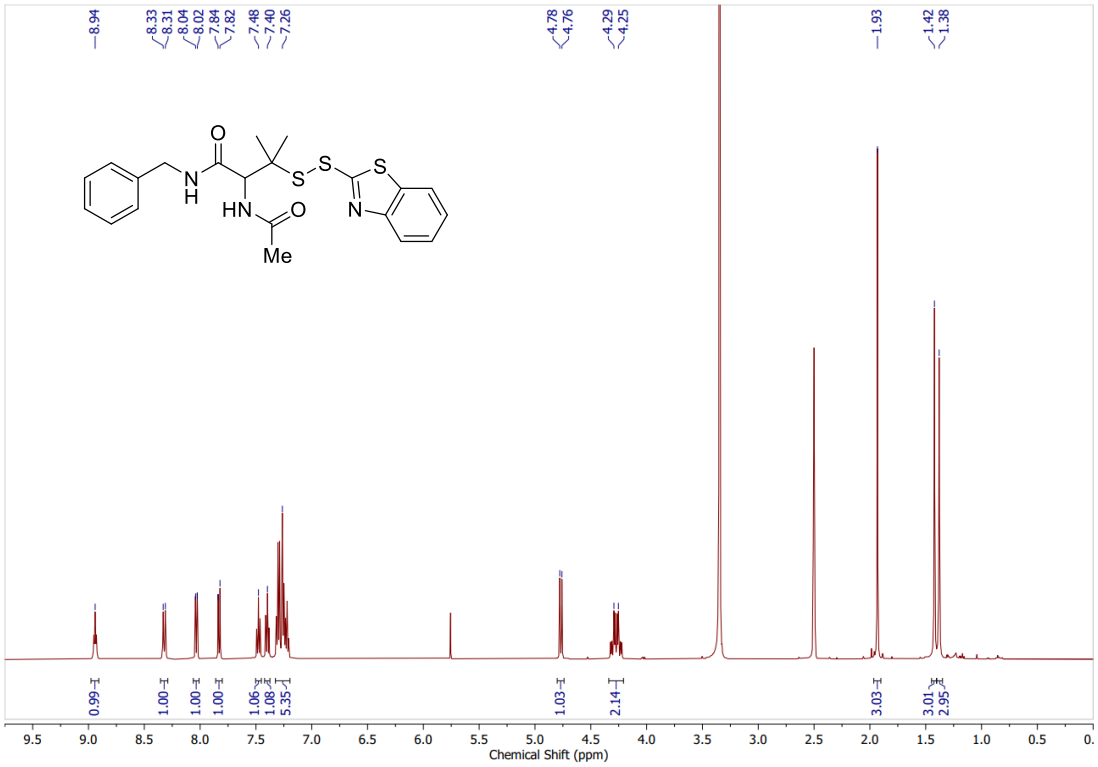


Figure D27. ^{1}H NMR (500 MHz, DMSO-d_6) spectrum of **S1**.

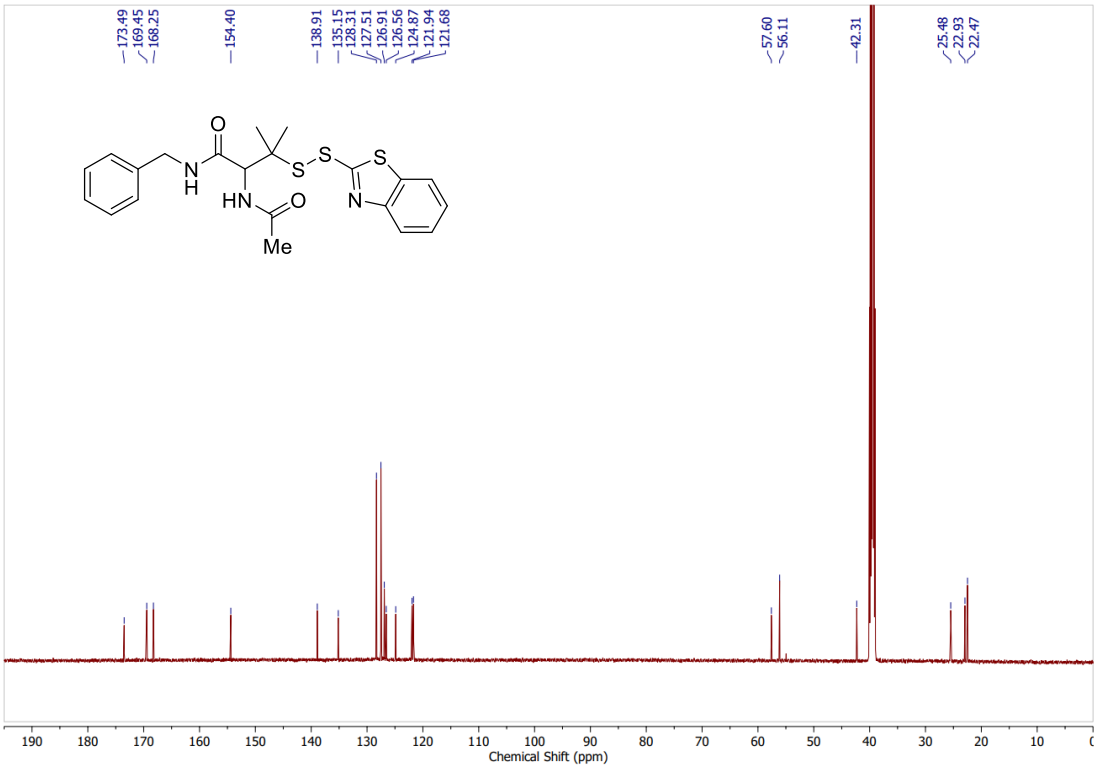


Figure D28. ^{13}C{^{1}H} NMR (125 MHz, DMSO-d_6) spectrum of **S1**.

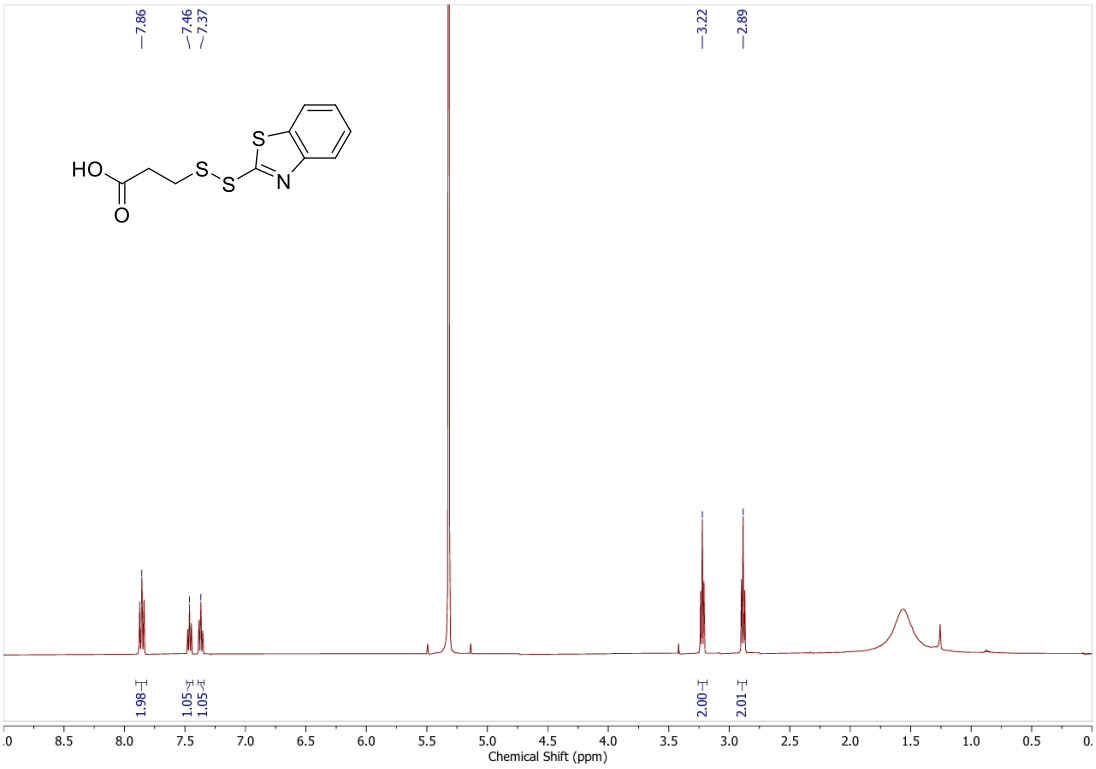


Figure D29. ^{1}H NMR (500 MHz, $CDCl_3$) spectrum of **S2**.

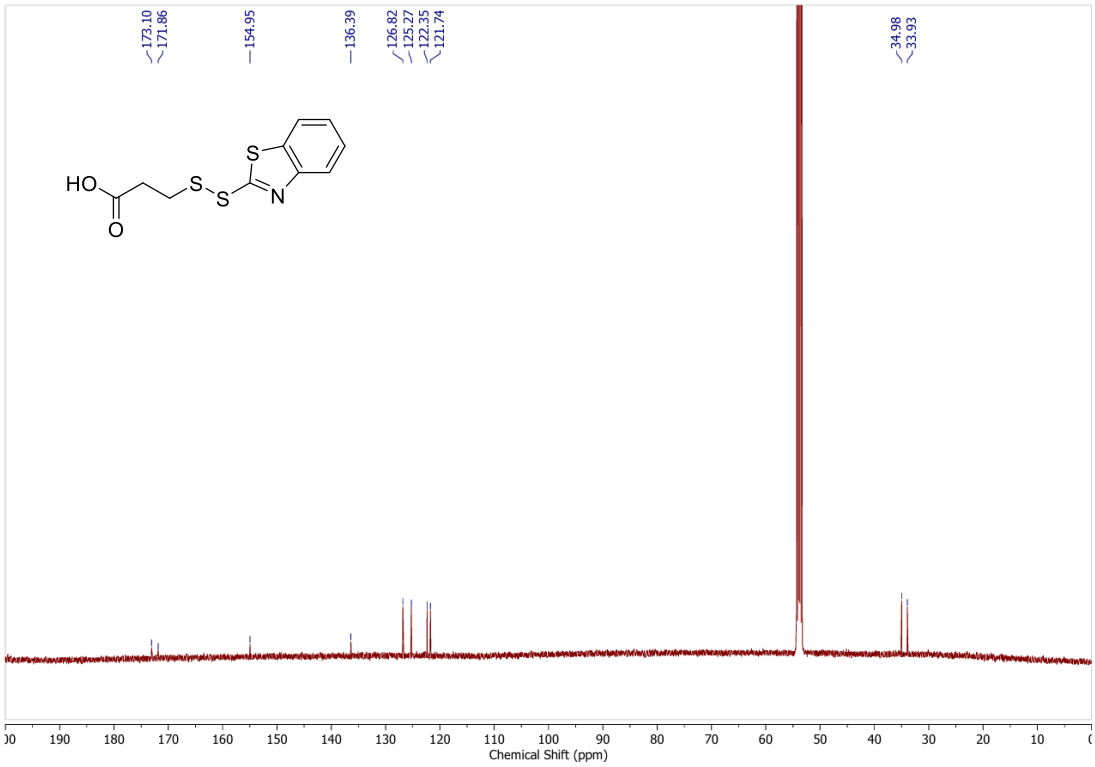


Figure D30. $^{13}C\{^{1}H\}$ NMR (125 MHz, DMSO-d_6) spectrum of **S2**.

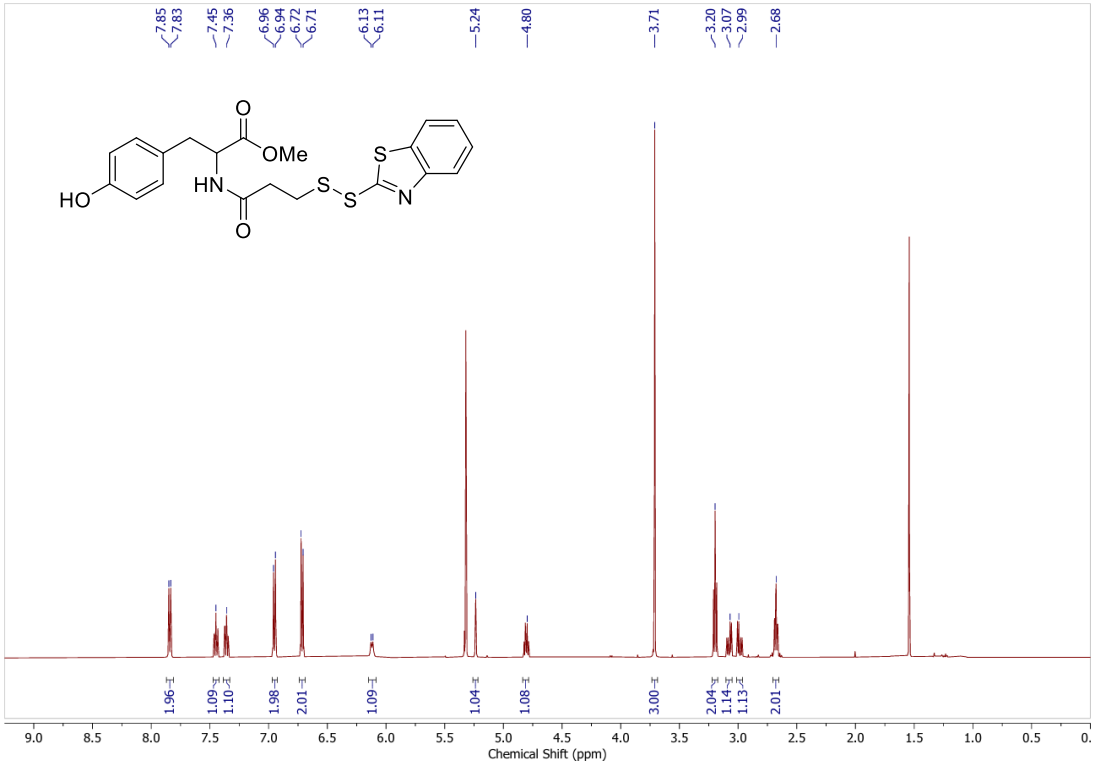


Figure D31. ^{1}H NMR (500 MHz, DMSO-d_6) spectrum of **S3**.

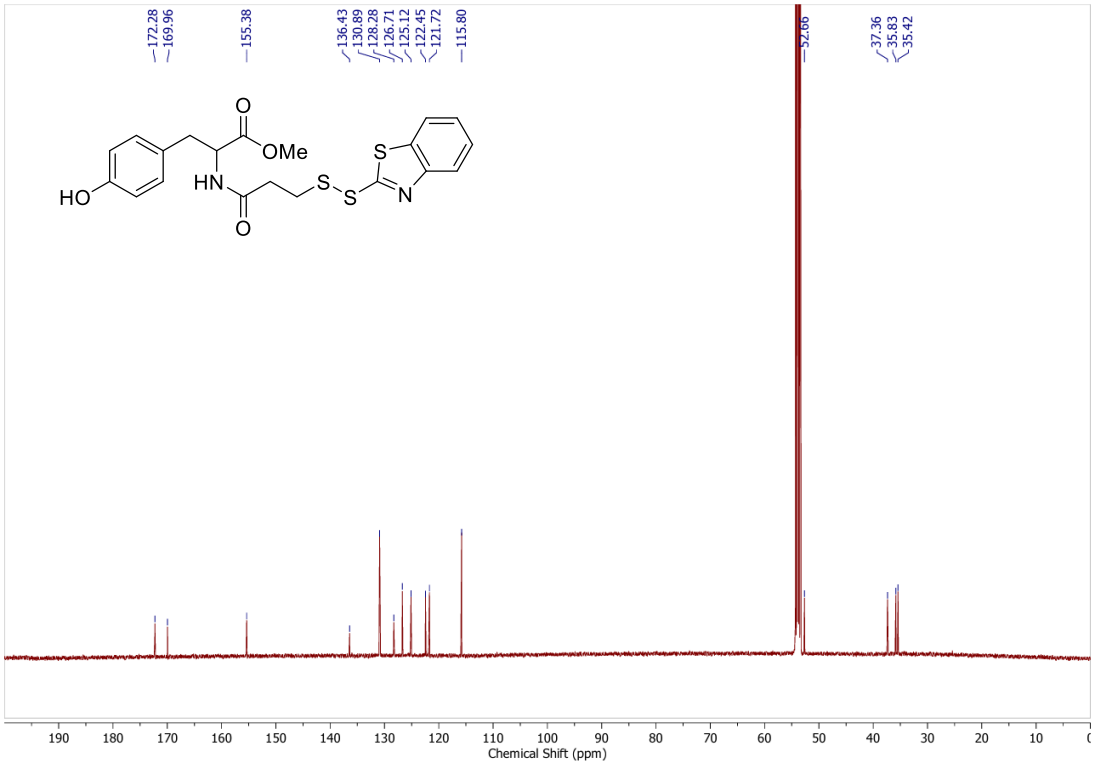


Figure D32. ^{13}C{^{1}H} NMR (125 MHz, DMSO-d_6) spectrum of **S3**.

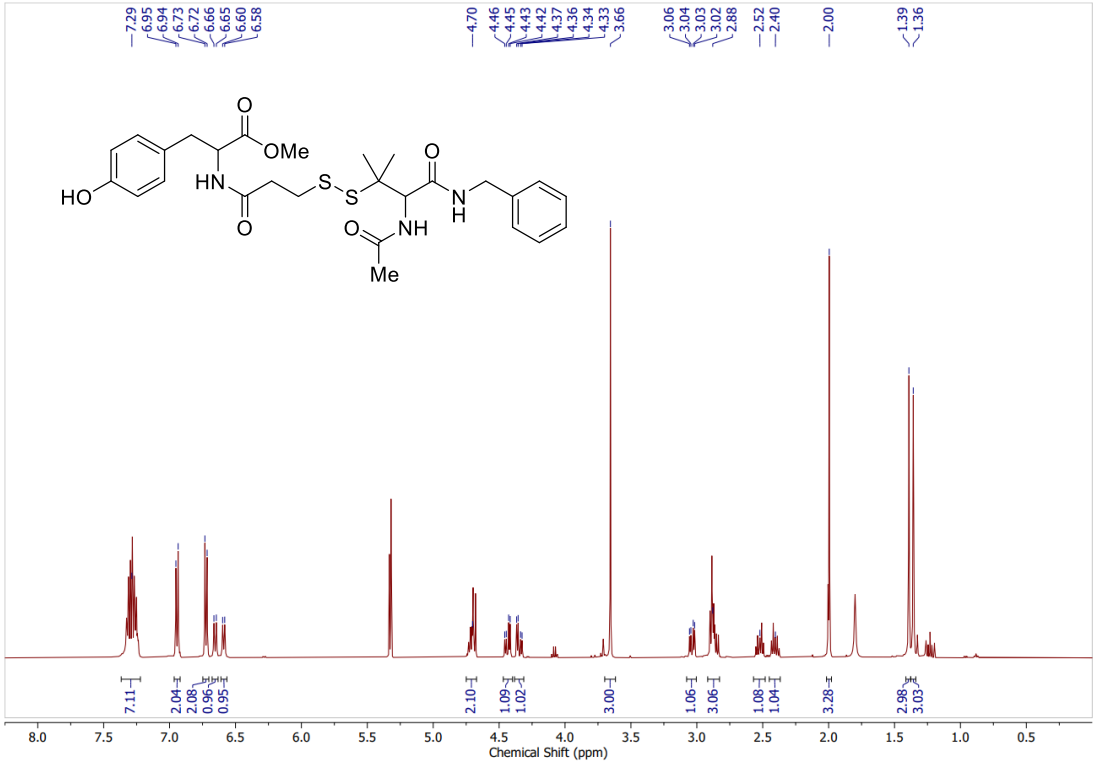


Figure D33. ^{1}H NMR (500 MHz, CD_2Cl_2) spectrum of **S4**.

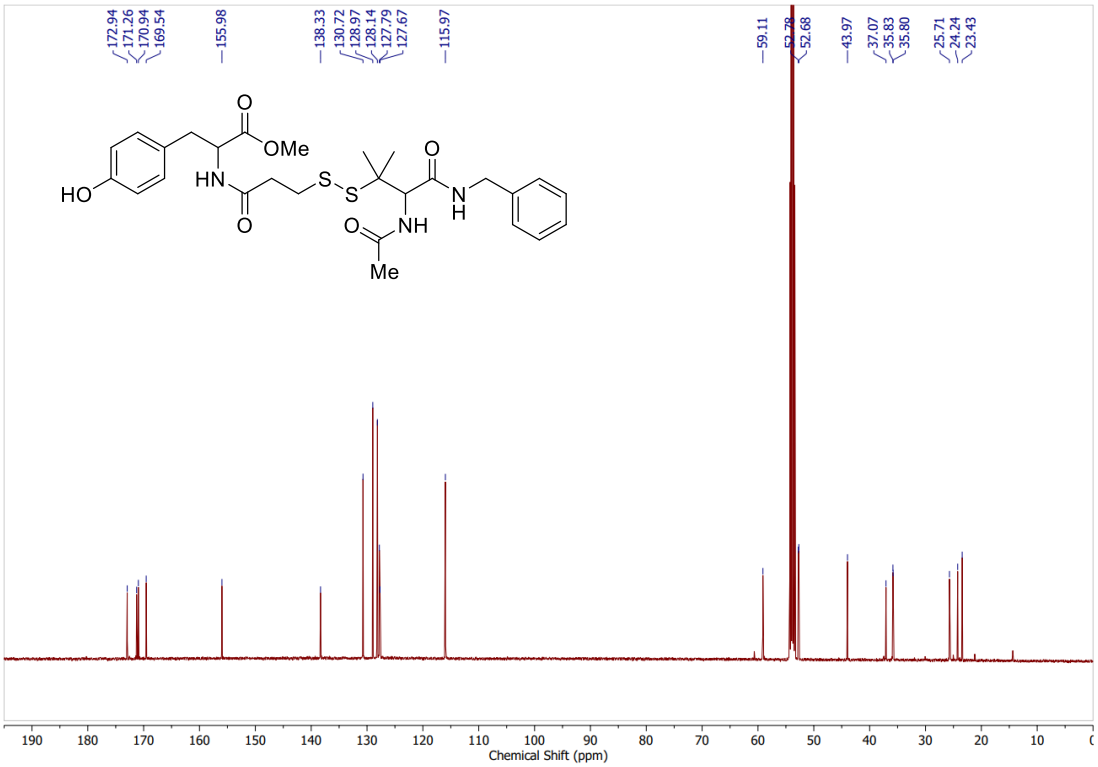


Figure D34. $^{13}C\{^{1}H\}$ NMR (125 MHz, CD_2Cl_2) spectrum of **S4**.

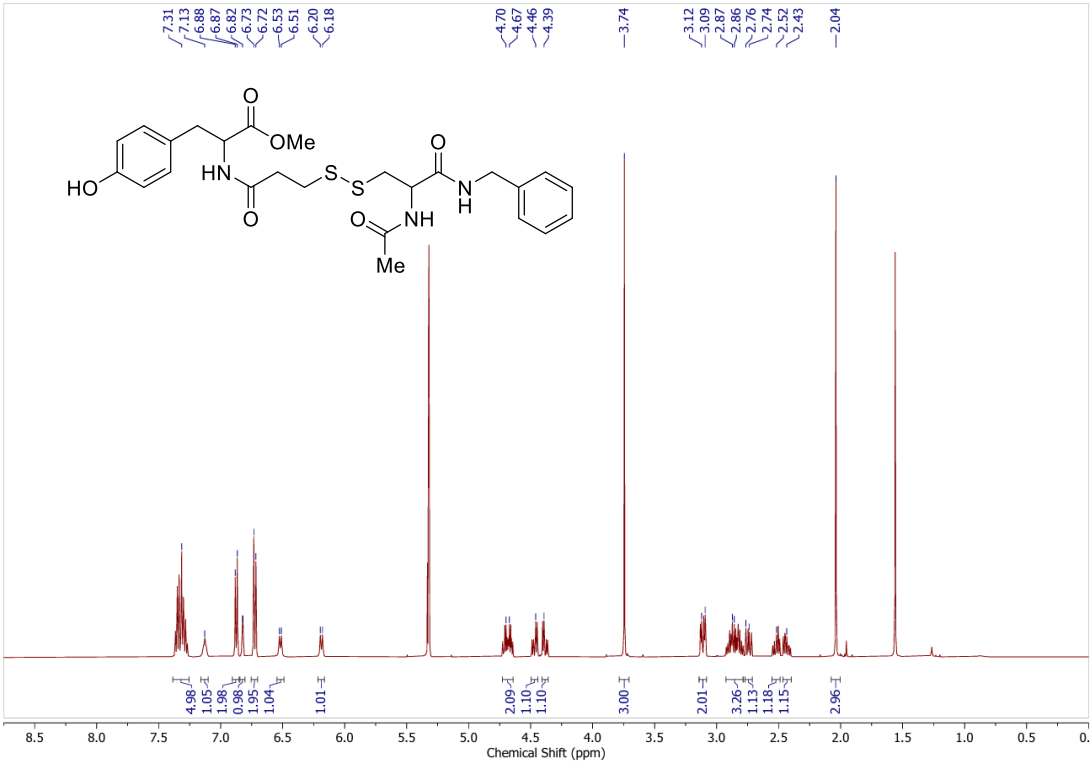


Figure D35. ^{1}H NMR (500 MHz, DMSO-d_6) spectrum of **S5**.

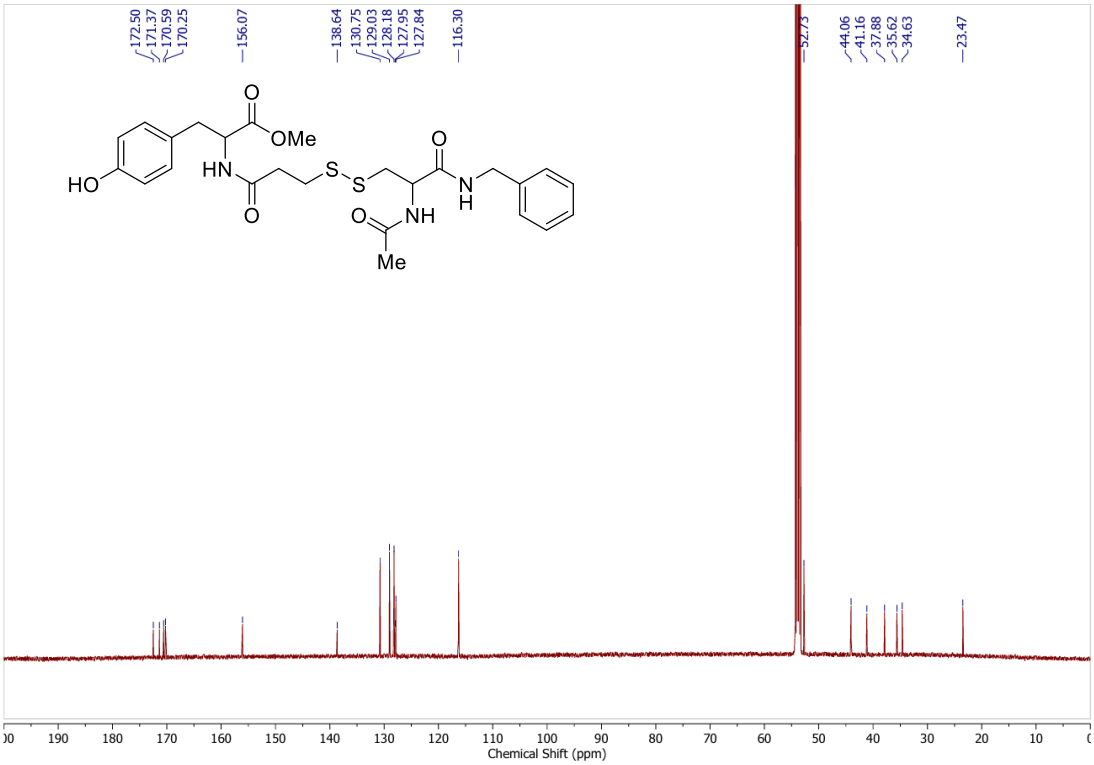


Figure D36. ^{13}C{^{1}H} NMR (125 MHz, DMSO-d_6) spectrum of **S5**.

Energies and Thermochemical Corrections of all Computed Structures

The energies and thermochemical corrections of Table S1 were obtained at the ωB97X-D/aug-cc-pV(T+*d*)Z/SMD(water) level of theory at the standard state of 1 atm and 298.15 K, using Grimme's quasiharmonic corrections. E: electronic energy; H: enthalpy; G: quasi-harmonic-corrected free energy.

Table D1. Energies, enthalpies, and free energies (in hartrees) for alkyl and aryl persulfides attacked by methyl thiolate.

Structure	E	H	G
ALKYL PERSULFIDES			
Methyl persulfide			
CH_3S-	-438.237552	-438.196883	-438.224467
SH-	-398.942523	-398.933045	-398.95419
CH_3SSCH_3	-876.25658	-876.171481	-876.208892
CH_3SH	-438.724276	-438.67348	-438.702244
CH_3SS-	-836.468042	-836.423696	-836.456279
CH_3SSH	-836.940393	-836.886457	-836.919892
TS-methyl-transpersulfidation	-1275.171839	-1275.076199	-1275.120567
TS-methyl-H_2S	-1275.170379	-1275.075224	-1275.11976
Ethyl persulfide			
C_2H_5SS-	-875.784299	-875.709937	-875.745984
C_2H_5SSH	-876.257098	-876.173087	-876.209928
C_2H_5SH	-478.041714	-477.960987	-477.993216
C_2H_5S-	-477.554248	-477.48366	-477.514795
$C_2H_5SSCH_3$	-915.573205	-915.457973	-915.49861
TS-ethyl-transpersulfidation	-1314.488063	-1314.362423	-1314.409725
TS-ethyl-H_2S	-1314.487892	-1314.362891	-1314.409894
Isopropyl persulfide			
$(CH_3)_2CHS$-	-516.871088	-516.77117	-516.805355
$(CH_3)_2CHSS$-	-915.101541	-914.997896	-915.036814
$(CH_3)_2CHSSH$	-915.575686	-915.46226	-915.501764
$(CH_3)_2CHSH$	-517.359135	-517.249051	-517.284436
$(CH_3)_2CHSSCH_3$	-954.89142	-954.746772	-954.789844
TS-isopropyl-transpersulfidation	-1353.805832	-1353.650822	-1353.700283
TS-isopropyl-H_2S	-1353.801131	-1353.646612	-1353.696007
tert-butyl persulfide			
$(CH_3)_3CSSH$	-954.893334	-954.75086	-954.792845
$(CH_3)_3CSH$	-556.676482	-556.537289	-556.575186
$(CH_3)_3CSSCH_3$	-994.209254	-994.035677	-994.081267
$(CH_3)_3CS$-	-556.187335	-556.058354	-556.095078
$(CH_3)_3CSS$-	-954.418236	-954.285551	-954.326899

TS-t-butyl-transpersulfidation	-1393.121905	-1392.937813	-1392.989407
TS-t-butyl-H_2S	-1393.10948	-1392.925689	-1392.977103
Allyl persulfide			
CH_2CHCH_2SS-	-913.861475	-913.781137	-913.819233
CH_2CHCH_2SH	-516.118055	-516.0314	-516.065943
CH_2CHCH_2SSH	-914.332694	-914.242656	-914.281516
$CH_2CHCH_2SSCH_3$	-953.649055	-953.527948	-953.570721
CH_2CHCH_2S-	-515.63379	-515.557224	-515.590732
TS-allyl-transpersulfidation	-1352.566587	-1352.435115	-1352.484224
TS-allyl-H_2S	-1352.565292	-1352.434256	-1352.483051
Benzyl persulfide			
$PhCH_2SS$-	-1067.518577	-1067.387346	-1067.430967
$PhCH_2SSH$	-1067.989775	-1067.848883	-1067.893348
$PhCH_2SH$	-669.773877	-669.636324	-669.676825
$PhCH_2SSCH_3$	-1107.306091	-1107.134131	-1107.182199
$PhCH_2S$-	-669.289718	-669.162237	-669.201687
TS-benzyl-transpersulfidation	-1506.222462	-1506.039982	-1506.094614
TS-benzyl-H_2S	-1506.220733	-1506.038905	-1506.092994
*(*R*)-Cysteine persulfide*			
$CysSSCH_3$	-1159.540618	-1159.386852	-1159.436233
$CysS^-$	-721.537766	-721.428939	-721.469375
CysSSH	-1120.223616	-1120.100496	-1120.146422
TS transpersulfidation CysSSH	-1558.464915	-1558.300781	-1558.356442
TS H_2S CysSSH	-1558.467098	-1558.30398	-1558.358182
*(*S*)-Penicillamine persulfide*			
Pen-$SSCH_3$	-1238.172295	-1237.959806	-1238.013763
Pen-SSH	-1198.856175	-1198.674538	-1198.724568
Pen-S^-	-800.169115	-800.002102	-800.047345
TS transpersulfidation PenSSH	-1637.093776	-1636.870795	-1636.930836
TS H_2S PenSSH	-1637.085808	-1636.863495	-1636.922022
ARYL PERSULFIDES			
Phenyl persulfide			
PhSS-	-1028.204267	-1028.103281	-1028.143631
PhSSH	-1028.669616	-1028.558865	-1028.600329
PhSH	-630.455931	-630.348473	-630.385798
$PhSSCH_3$	-1067.986612	-1067.844677	-1067.889661
PhS-	-629.983544	-629.886158	-629.921673
TS-H-transpersulfidation	-1466.908515	-1466.756081	-1466.807571
TS-H-H_2S	-1466.903948	-1466.752177	-1466.803815
p-NO_2-C_6H_4 persulfide			
$PhNO_2SS$-	-1232.728515	-1232.622584	-1232.668824

$PhNO_2SSH$	-1233.187464	-1233.071777	-1233.119075
$PhNO_2SH$	-834.974971	-834.862554	-834.905917
$PhNO_2SSCH_3$	-1272.505341	-1272.358512	-1272.409269
$PhNO_2S$-	-834.512342	-834.410175	-834.452434
TS-NO_2-transpersulfidation	-1671.430069	-1671.272743	-1671.329922
TS-NO_2-H_2S	-1671.42361	-1671.266867	-1671.32442
p-CF_3-C_6H_4 persulfide			
$PhCF_3SS$-	-1365.296007	-1365.186863	-1365.235969
$PhCF_3SSH$	-1365.75844	-1365.639502	-1365.689345
$PhCF_3SH$	-967.54534	-967.429749	-967.476323
$PhCF_3SSCH_3$	-1405.075982	-1404.926111	-1404.979408
$PhCF_3S$-	-967.076965	-966.971569	-967.016986
TS-CF_3-transpersulfidation	-1803.999265	-1803.838905	-1803.899261
TS-CF_3-H_2S	-1803.993927	-1803.83407	-1803.893982
p-Cl-C_6H_4 persulfide			
PhClSS-	-1487.824094	-1487.731498	-1487.775047
PhClSSH	-1488.288031	-1488.18571	-1488.230589
PhClSH	-1090.07453	-1089.975467	-1090.016041
$PhClSSCH_3$	-1527.605136	-1527.471617	-1527.519579
PhClS-	-1089.604289	-1089.515268	-1089.554069
TS-Cl-transpersulfidation	-1926.528018	-1926.384002	-1926.438596
TS-Cl-H_2S	-1926.523433	-1926.38006	-1926.434715
p-NMe_2-C_6H_4 persulfide			
NMe_2-Ph_SS-	-1162.177843	-1161.998772	-1162.04864
NMe_2-Ph_SSH	-1162.650536	-1162.46178	-1162.512168
NMe_2-Ph_SH	-764.433372	-764.248246	-764.295478
NMe_2-Ph_$SSCH_3$	-1201.967309	-1201.7475	-1201.801375
NMe_2-Ph_S-	-763.958069	-763.784035	-763.827451
TS-$(CH_3)_2N$-transpersulfidation	-1600.886146	-1600.655838	-1600.716037
TS-$(CH_3)_2N$-H_2S	-1600.882244	-1600.652559	-1600.712741
p-OCH_3-C_6H_4 persulfide			
OCH_3PhSS-	-1142.735668	-1142.599315	-1142.645452
OCH_3PhSSH	-1143.204153	-1143.058052	-1143.105016
OCH_3PhSH	-744.988404	-744.845665	-744.889169
$OCH_3PhSSCH_3$	-1182.521274	-1182.344114	-1182.394518
OCH_3PhS-	-744.514413	-744.381586	-744.423457
TS-OMe-transpersulfidation	-1581.441206	-1581.253484	-1581.310632
TS-OMe-H_2S	-1581.437363	-1581.250224	-1581.307215
p-Me-C_6H_4 persulfide			
$PhCH_3SS$-	-1067.518097	-1067.38765	-1067.432732
$PhCH_3SSH$	-1067.989064	-1067.849091	-1067.894813

$PhCH_3S$-	-669.774665	-669.638006	-669.679657
$PhCH_3SSCH_3$	-1107.306192	-1107.135062	-1107.183905
$PhCH_3S$-	-669.301077	-669.1745	-669.215149
TS-Me-transpersulfidation	-1506.227077	-1506.045392	-1506.100527
TS-Me-H_2S	-1506.222803	-1506.041812	-1506.09732

The energies and thermochemical corrections of Table S2 were obtained at the ωB97X-D/aug-cc-pVDZ/SMD(water) level of theory at the standard state of 1 atm and 298.15 K, using Grimme's quasiharmonic corrections. Single-point energies (SPE) at the ωB97X-D or M06-2X/aug-cc-pV(T+*d*)Z/SMD(water) level. E: electronic energy; H: enthalpy; G: quasi-harmonic-corrected free energy.

Table D2. Energies, enthalpies, and free energies (in hartrees) for perthioester-based persulfide donor reactions.

Structure	**E**	**H**	**G**	**ωB97XD SPE**	**M06-2X SPE**
ATTACK ON DONOR **1**					
(S) penicillamine persulfide S-COPh (**1**)	-1715.115812	-1714.753481	-1714.830044	-1715.356548	-1715.260614
(R) cysteine ZI thiolate anion	-721.450922	-721.342688	-721.382861	-721.537118	-721.500747
TS S1 cysteine thiolate on **1**	-2436.566599	-2436.093931	-2436.184919	-2436.887686	-2436.760648
(S) penicillamine (R) cysteine ZI disulfide	-1693.329847	-1692.967455	-1693.043611	-1693.569024	-1693.460958
Benzothiolate	-743.25412	-743.144979	-743.185911	-743.341504	-743.317603
TS S2 cysteine thiolate on **1**	-2436.557574	-2436.085597	-2436.1797	-2436.880749	-2436.751705
(R) cysteine ZI persulfide S-COPh	-1464.43374	-1464.212087	-1464.27169	-1464.616461	-1464.552545
(S) penicillamine thiolate anion	-972.132177	-971.883233	-971.940623	-972.276815	-972.207129
TS1 tetrahedral cysteine thiolate on **1**	-2436.56693	-2436.09546	-2436.187551	-2436.891254	-2436.763742
(S)-**1** (R) cysteine ZI tetrahedral int	-2436.582732	-2436.11095	-2436.202677	-2436.906692	-2436.778745
TS2 tetrahedral cysteine thiolate on **1**	-2436.576396	-2436.10517	-2436.197852	-2436.900655	-2436.771825
(R) cysteine ZI S-COPh	-1066.238339	-1066.020055	-1066.075632	-1066.4041	-1066.35193
(S) penicillamine persulfide anion	-1370.339659	-1370.086913	-1370.148143	-1370.500095	-1370.419659
DECOMPOSITION OF PENICILLAMINE PERSULFIDE					
(R) cysteine ZI	-721.917758	-721.798668	-721.840251	-722.008891	-721.965074
(S) penicillamine persulfide	-1370.801094	-1370.538254	-1370.60087	-1370.967293	-1370.879429
TS S1 cysteine thiolate on penicillamine persulfide	-2092.239024	-2091.866456	-2091.946676	-2092.486317	-2092.367034
(S) penicillamine (R) cysteine ZI disulfide	-1693.329847	-1692.967455	-1693.043611	-1693.569024	-1693.460958
HS- anion	-398.929633	-398.920216	-398.941382	-398.942424	-398.923735

TS S2 cysteine thiolate on penicillamine persulfide	-2092.244369	-2091.871704	-2091.953265	-2092.494502	-2092.373996
(R) cysteine ZI persulfide	-1120.114897	-1119.992546	-1120.038239	-1120.22302	-1120.167388
(R) cysteine ZI persulfide anion	-1119.660902	-1119.549221	-1119.593144	-1119.763187	-1119.715132
TS S1 penicillamine thiolate on cysteine persulfide	-2092.245928	-2091.873563	-2091.954406	-2092.494027	-2092.372832
TS S1 cysteine thiolate on cysteine persulfide	-1841.566933	-1841.335684	-1841.401445	-1841.75695	-1841.668583
TS S2 cysteine thiolate on cysteine persulfide	-1841.565965	-1841.334235	-1841.400444	-1841.757477	-1841.669303
(R) cysteine ZI disulfide dimer	-1442.644474	-1442.422657	-1442.482444	-1442.825379	-1442.749939

XYZ Coordinates and Imaginary Frequencies

The following geometries for methyl sulfide attack on persulfides were optimized at the ωB97X-D/aug-cc-pV(T+*d*)Z/SMD(water) level of theory. Imaginary frequencies are provided for transition structures. Minima had no imaginary frequencies.

ALKYL PERSULFIDES

Methyl persulfide

CH_3SSCH_3

C	1.80258	0.82187	-0.36835
S	0.90885	-0.51101	0.46297
S	-0.90885	-0.51101	-0.46297
C	-1.80258	0.82187	0.36835
H	2.79486	0.85116	0.08254
H	1.30939	1.77725	-0.20496
H	1.89529	0.61645	-1.43202
H	-2.79486	0.85116	-0.08254
H	-1.30939	1.77725	0.20496
H	-1.89529	0.61645	1.43203

CH_3SSH

C	-1.64562	0.67513	-0.00883
S	-0.47175	-0.69672	0.01766
S	1.34835	0.23921	-0.08799
H	1.54245	0.48486	1.21970
H	-2.63664	0.22018	-0.00988
H	-1.52251	1.27059	-0.91014
H	-1.53522	1.29381	0.87852

CH_3SS^-

C	-1.62983	0.66114	-0.00001
S	-0.43611	-0.69330	-0.00005
S	1.40070	0.27148	0.00005
H	-2.62902	0.22190	-0.00010
H	-1.51267	1.28025	-0.88948
H	-1.51277	1.28010	0.88958

CH_3SH

C	0.04819	1.15003	0.00000
S	0.04819	-0.66248	0.00000
H	-0.43585	1.53878	0.89168
H	-0.43585	1.53878	-0.89168
H	1.09101	1.45931	0.00000
H	-1.27955	-0.83738	0.00000

CH_3S^-

C	-1.12389	-0.00001	-0.00002
S	0.70712	0.00000	0.00000
H	-1.52353	-0.93612	-0.39467
H	-1.52350	0.80995	-0.61324
H	-1.52355	0.12623	1.00799

HS^-

S	0.00000	0.00000	0.07889
H	-0.00000	-0.00000	-1.26223

TS H2S from methyl-SSH

Imaginary frequency: -194.27 cm^{-1}

C	0.64713	1.74461	0.04361
S	0.37443	-0.05149	-0.04571
S	2.60690	-0.62233	-0.07083
H	2.83405	-0.60079	1.24977
H	0.41370	2.11593	1.03984
H	0.01336	2.24433	-0.68545
H	1.68871	1.94711	-0.18461
S	-2.09172	0.46228	-0.01771
C	-2.53032	-1.29616	0.04741
H	-2.12920	-1.83271	-0.81417
H	-3.61377	-1.41492	0.04385
H	-2.14133	-1.76492	0.95274

TS Tranpersulfidation from methyl-SSH

Imaginary frequency: -195.76 cm^{-1}

C	-3.06541	0.85296	0.27732
S	-2.26225	-0.73424	-0.07938

S	-0.00001	-0.00011	-0.24870
H	0.00003	-0.00011	1.08030
H	-4.14580	0.71406	0.32639
H	-2.84799	1.58204	-0.50362
H	-2.72816	1.25513	1.23300
S	2.26216	0.73426	-0.07942
C	3.06556	-0.85280	0.27735
H	4.14594	-0.71376	0.32637
H	2.84821	-1.58197	-0.50353
H	2.72840	-1.25496	1.23306

Ethyl persulfide

EtSS-

C	1.12204	0.63801	0.00036
S	-0.10556	-0.70189	0.00013
S	-1.92727	0.29017	-0.00014
C	2.53234	0.07325	-0.00031
H	0.95465	1.25699	0.88272
H	0.95414	1.25778	-0.88134
H	2.71527	-0.54068	0.88289
H	3.26026	0.88581	-0.00018
H	2.71474	-0.53990	-0.88417

EtSSH

C	-1.14834	0.65693	-0.00423
S	0.06042	-0.70583	0.01916
S	1.86498	0.25649	-0.08978
H	2.06161	0.50058	1.21777
C	-2.54887	0.06996	-0.00460
H	-0.97215	1.25438	-0.89639
H	-0.98312	1.27546	0.87583
H	-2.72191	-0.55065	-0.88428
H	-3.27672	0.88115	-0.01582
H	-2.73094	-0.53269	0.88574

EtSH

C	0.49572	0.64312	0.09131
S	-1.15905	-0.09795	-0.07923
C	1.63080	-0.35078	-0.05394
H	0.54537	1.16051	1.04698
H	0.53676	1.39865	-0.69253
H	-1.06707	-0.94890	0.95232
H	1.58186	-1.11540	0.72229
H	2.58874	0.16393	0.03892
H	1.60001	-0.84565	-1.02459

EtSSCH$_3$

C	-1.42442	0.44364	-0.50368
S	-0.35099	-0.67889	0.45080
S	1.47803	-0.44508	-0.41924
C	-2.83639	0.37551	0.05095
C	2.12263	1.05530	0.35651
H	-1.39637	0.13589	-1.54699
H	-1.02294	1.45200	-0.42143
H	-3.24576	-0.63261	-0.02218
H	-3.48129	1.04275	-0.52095
H	-2.87083	0.68731	1.09526
H	3.11335	1.21734	-0.06885
H	2.20834	0.92377	1.43237
H	1.49196	1.91043	0.12507

EtS-

C	-0.00000	0.77977	0.00000
S	-0.88772	-0.82256	0.00000
C	1.51583	0.65204	0.00000
H	-0.30480	1.35963	0.87422
H	-0.30480	1.35963	-0.87422
H	1.86058	0.10786	0.88158
H	1.99689	1.63516	0.00000
H	1.86058	0.10786	-0.88158

TS H2S FROM ETHYL-SSH

Imaginary frequency: -198.69 cm^{-1}

C	-0.74171	1.31999	-0.56461
S	-0.22167	-0.37684	-0.12205
S	-2.39858	-1.13948	0.12128
H	-2.67655	-1.37250	-1.16913
C	-1.00906	2.21080	0.63174
H	-1.62997	1.22301	-1.18379
H	0.05130	1.73148	-1.18535
H	-1.81090	1.80350	1.24905
H	-1.30883	3.20817	0.30211
H	-0.11546	2.30990	1.24850
S	2.16498	0.37349	-0.24441
C	2.76476	-1.19977	0.42595
H	2.43005	-2.03953	-0.18579
H	2.40630	-1.35509	1.44479
H	3.85445	-1.20981	0.44429

TS transpersulfidation FROM ETHYL-SSH
Imaginary frequency: -194.93 cm^{-1}

C	2.61224	-0.64747	0.13949
S	1.70185	0.90962	-0.11744
S	-0.52000	0.05745	-0.26495
H	-0.48914	0.00661	1.06253
C	4.11740	-0.44336	0.18579
H	2.35545	-1.33553	-0.66726
H	2.27155	-1.10064	1.07182
H	4.48519	-0.01256	-0.74682
H	4.62687	-1.39725	0.34078
H	4.40030	0.22540	1.00024
S	-2.73815	-0.80219	-0.07619
C	-3.61714	0.72937	0.34028
H	-4.68707	0.53075	0.40926
H	-3.45763	1.48904	-0.42533
H	-3.27984	1.12478	1.29876

Isopropyl persulfide

iPrSH

C	-0.40572	0.00000	-0.39716
S	1.38723	0.00000	-0.01784
C	-1.08476	-1.26052	0.11384
C	-1.08476	1.26052	0.11384
H	-0.42099	0.00000	-1.48793
H	1.26269	0.00000	1.31773
H	-1.03828	-1.30670	1.20380
H	-0.61800	-2.15830	-0.28892
H	-2.13666	-1.25843	-0.17863
H	-1.03828	1.30670	1.20380
H	-2.13666	1.25843	-0.17863
H	-0.61800	2.15830	-0.28892

iPrSS-

C	1.02379	0.15444	0.36580
S	-0.36619	-0.81030	-0.33443
S	-2.08153	0.23167	0.18534
C	2.29012	-0.67528	0.20702
C	1.16667	1.52260	-0.27684
H	0.80443	0.27704	1.42827
H	2.50686	-0.85919	-0.84781
H	2.20829	-1.63768	0.71298
H	3.14082	-0.13905	0.63180
H	1.43417	1.42569	-1.33151
H	1.95065	2.09667	0.22315

H	0.23489	2.08408	-0.20733

iPrSSH

C	-1.04923	0.16088	-0.37955
S	0.31906	-0.82281	0.34833
S	2.01748	0.15976	-0.23530
H	2.09595	1.07470	0.74651
C	-2.31263	-0.66516	-0.18150
C	-1.16040	1.53848	0.24415
H	-0.83080	0.24580	-1.44342
H	-2.52555	-0.81160	0.87927
H	-2.23870	-1.64126	-0.66063
H	-3.15746	-0.13366	-0.62065
H	-1.38523	1.46461	1.30950
H	-1.96732	2.09213	-0.23940
H	-0.24211	2.11298	0.12179

iPrS-

C	-0.35156	0.00024	0.38628
S	1.43054	0.00063	-0.06019
C	-1.07092	1.24784	-0.11338
C	-1.06875	-1.24898	-0.11309
H	-0.41190	0.00028	1.47772
H	-1.04180	1.29414	-1.20515
H	-0.60571	2.15568	0.27203
H	-2.12117	1.24646	0.19651
H	-1.03813	-1.29588	-1.20480
H	-2.11983	-1.24942	0.19474
H	-0.60265	-2.15595	0.27304

iPrSSCH$_3$

C	-1.40326	0.14773	-0.39571
S	-0.12511	-0.94063	0.35184
S	1.63280	-0.41073	-0.53358
C	-2.73312	-0.31762	0.18118
C	-1.15230	1.62145	-0.14128
C	2.33656	0.83417	0.57452
H	-1.38337	-0.05138	-1.46657
H	-2.77263	-0.15304	1.25967
H	-2.91515	-1.37414	-0.01646
H	-3.54043	0.25602	-0.27543
H	-1.12242	1.83444	0.92853
H	-1.95993	2.20658	-0.58563
H	-0.21710	1.95288	-0.59089
H	3.31783	1.07780	0.16597
H	2.45757	0.42605	1.57500

H	1.72536	1.73206	0.60150

TS H2S FROM Isopropyl-SSH
Imaginary frequency: -203.57 cm^{-1}

C	0.77719	1.25744	-0.01483
S	0.27594	-0.51766	-0.20925
S	2.44476	-1.31963	-0.16886
H	2.61863	-1.31911	1.15995
C	0.08220	2.20549	-0.98010
C	0.65001	1.71359	1.42937
H	1.83016	1.22700	-0.28001
H	-0.96542	2.35630	-0.72220
H	0.13711	1.84348	-2.00654
H	0.57974	3.17747	-0.93590
H	-0.39089	1.68075	1.75320
H	1.00811	2.74121	1.52995
H	1.24059	1.08225	2.09422
S	-2.18692	0.07122	-0.17111
C	-2.59745	-1.61238	0.36177
H	-2.14807	-2.35436	-0.30123
H	-3.67765	-1.75771	0.34289
H	-2.24452	-1.80502	1.37591

TS Transpersulfidation FROM Isopropyl-SSH
Imaginary frequency: -192.75 cm^{-1}

C	-2.43513	0.33515	-0.25367
S	-1.40796	-1.10220	0.22774
S	0.78860	-0.28187	-0.25775
H	0.71037	0.35864	0.90335
C	-3.88557	-0.08838	-0.44296
C	-2.32786	1.47500	0.74956
H	-2.04666	0.68124	-1.21397
H	-4.30416	-0.46650	0.49257
H	-3.97813	-0.87063	-1.19665
H	-4.49153	0.76457	-0.75989
H	-2.71349	1.16550	1.72366
H	-2.90870	2.33819	0.41272
H	-1.29398	1.79595	0.88002
S	2.95460	0.67432	-0.45891
C	3.88329	-0.44920	0.62092
H	4.94142	-0.18703	0.59772
H	3.77779	-1.48222	0.28871
H	3.53483	-0.37704	1.65149

Tert-butyl persulfide

tBuSSH

C	-0.98294	0.12501	0.00254
S	0.50010	-0.98847	-0.02109
S	2.13069	0.24292	0.08844
H	2.27727	0.52975	-1.21666
C	-2.15111	-0.85675	-0.06882
C	-0.97678	1.04141	-1.21183
C	-1.03454	0.92756	1.29389
H	-2.12474	-1.44706	-0.98568
H	-3.08395	-0.29078	-0.05887
H	-2.15919	-1.53410	0.78620
H	-0.95136	0.46961	-2.13965
H	-0.12201	1.71853	-1.19536
H	-1.88348	1.64990	-1.20728
H	-1.06300	0.27325	2.16520
H	-1.93549	1.54460	1.29699
H	-0.17450	1.59174	1.38293

tBuSH

C	0.34752	-0.00373	0.00000
S	-1.49824	0.08757	-0.00000
C	0.82815	-0.72830	-1.25234
C	0.82815	-0.72830	1.25235
C	0.83471	1.44216	-0.00000
H	-1.72504	-1.23363	0.00000
H	0.46089	-1.75504	-1.27841
H	1.92031	-0.75930	-1.25806
H	0.49533	-0.21823	-2.15612
H	0.46089	-1.75504	1.27841
H	0.49533	-0.21823	2.15612
H	1.92031	-0.75930	1.25806
H	0.49329	1.97855	-0.88621
H	1.92602	1.44957	-0.00000
H	0.49329	1.97855	0.88621

tBuSSCH$_3$

C	-1.27745	0.15902	0.07055
S	0.10085	-0.81694	-0.70014
S	1.75329	-0.50818	0.44985
C	-2.44452	-0.06322	-0.88906
C	-0.92240	1.63661	0.15095
C	-1.60600	-0.39223	1.45076
C	2.57201	0.91086	-0.31771
H	-2.23089	0.33932	-1.87996

H	-3.32448	0.44988	-0.49733
H	-2.68915	-1.12210	-0.98578
H	-0.65745	2.03741	-0.82741
H	-0.09250	1.80668	0.83721
H	-1.78455	2.19078	0.52844
H	-1.89943	-1.44076	1.39786
H	-2.43454	0.17594	1.87930
H	-0.75326	-0.30195	2.12443
H	3.51154	1.04198	0.21999
H	1.97400	1.81273	-0.22107
H	2.78463	0.70579	-1.36408

tBuS-

C	-0.28423	-0.00012	-0.00021
S	1.56230	0.00024	0.00117
C	-0.81878	0.25360	1.41084
C	-0.81564	-1.34991	-0.48671
C	-0.81576	1.09596	-0.92600
H	-0.47757	-0.51835	2.10247
H	-1.91447	0.25324	1.41687
H	-0.47950	1.21937	1.78875
H	-0.47426	-2.15972	0.16010
H	-0.47363	-1.56166	-1.50103
H	-1.91132	-1.35769	-0.49007
H	-0.47527	2.08026	-0.60031
H	-1.91145	1.10131	-0.93250
H	-0.47286	0.94222	-1.95045

tBuSS-

C	-0.96094	0.10934	-0.00006
S	0.54494	-0.96937	-0.00009
S	2.20287	0.27408	0.00020
C	-2.13643	-0.86442	-0.00017
C	-0.99871	0.97937	-1.24949
C	-0.99880	0.97918	1.24950
H	-2.12583	-1.50208	-0.88578
H	-3.07415	-0.30387	-0.00015
H	-2.12588	-1.50223	0.88534
H	-1.02518	0.36805	-2.15279
H	-0.12059	1.62451	-1.29598
H	-1.88900	1.61372	-1.23798
H	-1.02531	0.36773	2.15271
H	-1.88909	1.61353	1.23803
H	-0.12068	1.62433	1.29615

TS H2S from tbut-SSH
Imaginary frequency: -233.76 cm^{-1}

C	0.93313	-1.03948	-0.00424
S	-0.12341	0.53184	-0.00805
S	1.70791	2.06146	-0.07407
H	1.90538	2.16277	1.24644
C	0.06266	-2.29291	0.06716
C	1.84996	-1.03675	1.21652
C	1.75123	-1.10155	-1.29153
H	-0.53197	-2.32674	0.97810
H	0.72884	-3.15958	0.06600
H	-0.60298	-2.37929	-0.78926
H	1.27014	-0.99608	2.13946
H	2.54115	-0.19679	1.20182
H	2.43703	-1.95883	1.22453
H	1.09915	-1.14442	-2.16469
H	2.36813	-2.00411	-1.28356
H	2.40997	-0.24072	-1.38908
S	-2.38723	-0.49819	0.01704
C	-3.09847	1.16563	-0.01091
H	-4.18623	1.09811	-0.01101
H	-2.79197	1.71259	-0.90427
H	-2.79404	1.74168	0.86470

TS transpersulfidation from tbut-SSH
Imaginary frequency: -196.22 cm^{-1}

C	2.34324	0.17781	0.08266
S	1.15253	-1.20561	-0.20751
S	-1.02386	-0.16752	-0.31471
H	-0.95106	-0.11943	1.01066
C	3.74537	-0.42474	0.15409
C	2.02755	0.88282	1.40020
C	2.28223	1.18462	-1.06382
H	3.82626	-1.14034	0.97369
H	4.48382	0.36555	0.31983
H	4.00177	-0.93733	-0.77431
H	2.07901	0.18677	2.23862
H	1.03035	1.32430	1.38291
H	2.74771	1.68671	1.57947
H	2.54141	0.71232	-2.01241
H	2.98739	2.00212	-0.88610
H	1.28361	1.61243	-1.15615
S	-3.17581	0.78248	-0.09244
C	-4.11718	-0.69422	0.38026
H	-5.17357	-0.43960	0.46982
H	-3.77554	-1.08375	1.33950

H	-4.01422	-1.47706	-0.37141

Allyl persulfide

Allyl-SH

C	0.03179	0.75578	-0.15479
S	1.56763	-0.21695	0.02191
C	-1.14416	0.08464	0.46891
C	-2.20932	-0.31503	-0.21089
H	-0.14161	0.96533	-1.20799
H	0.25404	1.69698	0.34883
H	1.14959	-1.29820	-0.65033
H	-1.08935	-0.07759	1.54042
H	-2.28217	-0.16839	-1.28272
H	-3.04241	-0.79921	0.28197

Allyl-SSH

C	3.08633	0.06939	-0.40628
C	2.08445	0.03537	0.46053
C	0.74821	0.65125	0.20519
S	-0.45567	-0.70729	-0.03908
S	-2.25502	0.26534	-0.14639
H	-2.55369	0.31458	1.16367
H	4.04172	-0.38532	-0.17863
H	2.98424	0.55999	-1.36756
H	2.20953	-0.46488	1.41505
H	0.75836	1.27685	-0.68462
H	0.41687	1.23400	1.06303

Allyl-SS-

C	0.71638	-0.62020	0.21763
S	-0.51148	0.70485	-0.05993
S	-2.32654	-0.29421	-0.05876
C	2.06032	-0.01664	0.45125
C	3.07280	-0.09192	-0.40241
H	0.72706	-1.28613	-0.64561
H	0.39150	-1.18392	1.09318
H	2.18585	0.52660	1.38290
H	2.97833	-0.62304	-1.34320
H	4.02859	0.36878	-0.18704

Allyl-$SSCH_3$

C	1.05936	0.34850	0.54492
S	-0.04235	-0.59898	-0.57284
S	-1.85330	-0.51601	0.36019
C	2.35378	0.57784	-0.16237

C	3.48594	-0.03229	0.15787
C	-2.51576	1.08404	-0.15693
H	1.19864	-0.21753	1.46337
H	0.56563	1.29361	0.76646
H	2.33221	1.28131	-0.98818
H	3.53232	-0.74260	0.97561
H	4.40323	0.16594	-0.38131
H	-3.49388	1.17614	0.31557
H	-2.63069	1.12041	-1.23741
H	-1.87674	1.89398	0.18728

Allyl-S-

C	0.07804	0.75587	0.05974
S	1.59685	-0.26953	-0.09348
C	-1.10746	-0.05640	0.45520
C	-2.19140	-0.24710	-0.28937
H	-0.12861	1.26628	-0.88285
H	0.24853	1.52621	0.81534
H	-1.04314	-0.53641	1.42838
H	-2.28967	0.20943	-1.26883
H	-3.01176	-0.86732	0.05018

TS H2S from allyl-SSH

Imaginary frequency: -188.78 cm^{-1}

C	0.74899	3.04732	-0.44628
C	1.24924	1.83344	-0.25932
C	0.79714	0.89008	0.80157
S	0.13155	-0.67619	0.11537
S	2.20986	-1.65729	-0.06396
H	2.58904	-1.09729	-1.22080
H	1.11646	3.69466	-1.23257
H	-0.04509	3.43335	0.18335
H	2.04406	1.47479	-0.90683
H	0.01678	1.33411	1.41512
H	1.62836	0.60801	1.44416
S	-2.18594	0.29708	0.25809
C	-2.90407	-1.17255	-0.52343
H	-3.98723	-1.07194	-0.59018
H	-2.68372	-2.07240	0.05357
H	-2.51380	-1.31055	-1.53316

TS Transpersulfidation from allyl-SSH

Imaginary frequency: -199.70 cm^{-1}

C	-2.84625	-1.99447	-0.07880
C	-3.04784	-0.69686	-0.26950
C	-2.57708	0.38108	0.64614

S	-1.39019	1.52401	-0.14813
S	0.58265	0.22771	-0.19506
H	0.73042	0.56728	1.08126
H	-3.20856	-2.73268	-0.78331
H	-2.31030	-2.35993	0.79034
H	-3.58345	-0.36367	-1.15381
H	-2.11951	-0.04598	1.53943
H	-3.42419	0.99117	0.96554
S	2.66666	-0.95106	0.09033
C	3.80671	0.45726	-0.01294
H	4.83647	0.10337	0.04502
H	3.63942	1.15647	0.80701
H	3.68055	0.99137	-0.95516

Benzyl persulfide

BnSSH

C	0.60771	0.02077	0.86745
S	1.61380	-0.00584	-0.66298
S	3.53813	-0.08302	0.03384
H	3.76348	1.23300	0.19283
C	-0.83651	0.01027	0.46171
C	-1.51737	1.20507	0.24487
C	-2.84682	1.19614	-0.14952
C	-3.50873	-0.00932	-0.33637
C	-2.83610	-1.20510	-0.12578
C	-1.50679	-1.19467	0.26845
H	0.85696	0.92177	1.42315
H	0.86235	-0.85661	1.45728
H	-1.00217	2.14590	0.39286
H	-3.36675	2.13103	-0.30936
H	-4.54596	-0.01696	-0.64261
H	-3.34789	-2.14743	-0.26710
H	-0.98332	-2.12791	0.43442

BnS-

C	-1.50738	0.00060	0.85835
S	-2.66111	-0.00027	-0.57540
C	-0.06378	0.00028	0.45141
C	0.62352	-1.19544	0.24822
C	1.95031	-1.19883	-0.15783
C	2.61975	-0.00031	-0.36675
C	1.95071	1.19849	-0.15832
C	0.62390	1.19569	0.24775
H	-1.70310	-0.87709	1.47602
H	-1.70302	0.87910	1.47488

H	0.10868	-2.13506	0.41014
H	2.46433	-2.13928	-0.30868
H	3.65430	-0.00055	-0.68269
H	2.46502	2.13872	-0.30955
H	0.10938	2.13555	0.40932

BnSS-

C	-0.64682	0.00026	0.83660
S	-1.68233	-0.00002	-0.67010
S	-3.61719	-0.00006	0.06473
C	0.80146	0.00012	0.45086
C	1.48364	-1.19789	0.25182
C	2.81686	-1.19994	-0.13152
C	3.48752	-0.00016	-0.32553
C	2.81707	1.19976	-0.13168
C	1.48384	1.19799	0.25166
H	-0.89604	-0.88532	1.42067
H	-0.89597	0.88611	1.42030
H	0.96399	-2.13577	0.40469
H	3.33340	-2.13934	-0.27717
H	4.52750	-0.00027	-0.62281
H	3.33377	2.13905	-0.27745
H	0.96435	2.13598	0.40440

BnSH

C	1.45720	-0.03340	0.88289
S	2.62589	-0.04473	-0.52387
C	0.01881	-0.02222	0.46015
C	-0.66502	-1.21107	0.22256
C	-1.98931	-1.19313	-0.18793
C	-2.64695	0.01638	-0.36759
C	-1.97351	1.20626	-0.13001
C	-0.64899	1.18567	0.28203
H	1.68773	0.82184	1.51328
H	1.69390	-0.93875	1.43923
H	2.24240	1.12325	-1.05783
H	-0.15470	-2.15609	0.36184
H	-2.50981	-2.12465	-0.36578
H	-3.68007	0.03089	-0.68725
H	-2.48083	2.15239	-0.26301
H	-0.12629	2.11580	0.46881

$BnSSCH_3$

C	0.25925	-0.15998	0.82359
S	1.23639	-0.38202	-0.71180
S	3.15285	-0.52894	-0.03411

C	-1.18554	-0.02715	0.44436
C	-1.72424	1.22019	0.14020
C	-3.05536	1.34179	-0.22865
C	-3.86305	0.21523	-0.30088
C	-3.33307	-1.03248	-0.00328
C	-2.00133	-1.15240	0.36470
C	3.64428	1.19426	0.20467
H	0.61774	0.73582	1.32563
H	0.42600	-1.02643	1.45910
H	-1.09571	2.10004	0.19876
H	-3.46336	2.31715	-0.45709
H	-4.90206	0.30967	-0.58601
H	-3.95828	-1.91363	-0.05468
H	-1.58953	-2.12610	0.59897
H	4.67482	1.17060	0.55968
H	3.01979	1.67144	0.95627
H	3.59725	1.73996	-0.73447

TS H2S from Benzyl-SSH
Imaginary frequency: -199.41 cm^{-1}

C	-0.01129	0.27053	1.16177
S	-1.35291	0.68661	-0.01370
S	-0.37808	2.73154	-0.59250
H	-0.81503	3.44669	0.45337
C	1.26980	-0.19739	0.53254
C	1.29806	-1.31748	-0.29708
C	2.48863	-1.75932	-0.85056
C	3.67612	-1.08698	-0.58569
C	3.65960	0.02808	0.23733
C	2.46343	0.46815	0.79076
H	-0.41939	-0.50484	1.80740
H	0.16882	1.15018	1.77360
H	0.37282	-1.83933	-0.50869
H	2.49245	-2.63163	-1.49087
H	4.60543	-1.43151	-1.01904
H	4.57732	0.56095	0.44852
H	2.45637	1.34106	1.43143
S	-2.46997	-1.47152	0.47548
C	-3.82431	-1.09947	-0.66781
H	-4.53845	-1.92240	-0.68093
H	-3.45089	-0.95804	-1.68340
H	-4.35428	-0.19406	-0.36738

TS Transpersulfidation from benzyl-SSH
Imaginary frequency: -187.79 cm^{-1}

C	0.85447	-0.13437	-0.61242

S	-0.08221	0.10374	0.94085
S	-2.27099	-0.25157	0.15023
H	-2.23969	1.00393	-0.28473
C	2.33335	-0.05295	-0.37659
C	3.00136	1.16667	-0.45808
C	4.36556	1.24771	-0.21968
C	5.08561	0.10602	0.10476
C	4.43107	-1.11561	0.18569
C	3.06675	-1.19227	-0.05306
H	0.54625	0.63103	-1.32436
H	0.59251	-1.10787	-1.02614
H	2.44452	2.06001	-0.71355
H	4.86826	2.20319	-0.29092
H	6.14971	0.16705	0.28907
H	4.98513	-2.01168	0.43238
H	2.56093	-2.14805	0.00982
S	-4.51291	-0.28639	-0.75091
C	-5.36895	0.60421	0.57877
H	-6.43826	0.64254	0.36874
H	-5.00094	1.62721	0.66384
H	-5.22599	0.10372	1.53692

(R)-cysteine persulfide

Cys-$SSCH_3$

C	-1.47876	-0.27290	0.38259
H	-1.45283	-0.28767	1.47126
C	-2.62785	0.69073	-0.01920
O	-2.43723	1.89976	0.20265
O	-3.65144	0.15256	-0.49927
N	-1.86012	-1.64314	-0.06747
H	-1.35294	-1.92736	-0.90385
H	-1.71995	-2.34945	0.65071
C	-0.14203	0.15912	-0.18587
H	0.00598	1.20984	0.04439
H	-0.12246	0.02200	-1.26684
S	1.21935	-0.80333	0.55915
S	2.82675	-0.23310	-0.55256
C	3.29455	1.35212	0.17890
H	3.55309	1.22912	1.22758
H	4.17086	1.69143	-0.37394
H	2.49589	2.08059	0.06248
H	-2.86044	-1.57650	-0.31050

Cys-S-

C	0.23736	0.07238	0.47767
H	0.13164	-0.17620	1.52984
C	1.67589	-0.18396	0.01418
O	2.19225	-1.25805	0.39709
O	2.19969	0.67263	-0.73706
N	-0.10150	1.50687	0.32429
H	-1.13810	1.53672	0.22602
H	0.19849	2.06465	1.11808
C	-0.75975	-0.74523	-0.35542
H	-0.61508	-1.79099	-0.09127
H	-0.50121	-0.63568	-1.41130
S	-2.48609	-0.22437	-0.07660
H	0.35564	1.86759	-0.51450

Cys-SSH

C	1.24366	0.57049	0.69329
H	1.73477	0.76948	1.64290
C	2.02266	-0.54943	-0.03036
O	2.44802	-0.29353	-1.17672
O	2.14293	-1.61415	0.60904
N	1.32934	1.83233	-0.09570
H	0.78960	2.57795	0.34245
H	0.99319	1.69690	-1.04905
C	-0.20240	0.20605	0.98764
H	-0.21305	-0.60006	1.71598
H	-0.72944	1.06367	1.40173
S	-1.08208	-0.33747	-0.52176
S	-3.04164	-0.00041	-0.05001
H	-3.31207	-1.16341	0.56852
H	2.29997	2.13383	-0.16618

TS H2S from R-cysteine ZI

Imaginary frequency: -232.44 cm^{-1}

C	1.29495	-0.08231	-0.48413
H	1.43604	0.77872	-1.13207
C	2.64299	-0.41969	0.19060
O	3.04070	-1.60477	0.09842
O	3.21032	0.52012	0.78359
N	0.88554	-1.24114	-1.32617
H	1.01741	-1.05707	-2.31617
H	-0.11149	-1.49492	-1.15502
C	0.23621	0.22584	0.56208
H	0.03911	-0.65218	1.17404
H	0.61350	1.00568	1.21309
S	-1.35077	0.82327	-0.12358

S	-0.61124	3.09009	-0.08849
H	-0.71696	3.30099	1.23054
S	-2.16735	-1.45952	-0.39865
C	-2.10723	-2.18169	1.26527
H	-2.77942	-3.03754	1.30830
H	-1.10426	-2.52195	1.52006
H	-2.43193	-1.45168	2.00639
H	1.49941	-2.01930	-1.05335

TS Transpersulfidation from R-cysteine ZI
Imaginary frequency: -174.21 cm^{-1}

C	1.97267	-0.16503	0.29309
H	1.18778	-0.82214	0.65660
C	3.19593	-0.99475	-0.13227
O	4.31890	-0.57449	0.22822
O	2.95437	-2.00113	-0.83177
N	2.35185	0.73608	1.41067
H	2.38380	0.23871	2.29776
H	1.67056	1.49887	1.47907
C	1.46254	0.66542	-0.88107
H	2.27252	1.28385	-1.27306
H	1.14907	-0.01632	-1.66835
S	0.09907	1.78612	-0.45269
S	-1.55865	0.34265	0.07836
H	-1.85023	0.22122	-1.21381
S	-3.54870	-1.23735	0.29507
C	-4.84088	-0.01496	-0.08057
H	-5.82834	-0.47360	-0.01679
H	-4.80839	0.81764	0.62360
H	-4.72024	0.38636	-1.08805
H	3.28522	1.11095	1.22986

(S)-penicillamine persulfide

Pen-S-

C	-0.39890	-0.35131	-0.58661
H	-0.29528	-0.19640	-1.65687
C	-1.82391	0.04142	-0.15257
O	-2.37732	-0.68779	0.70599
O	-2.31691	1.05995	-0.68538
N	-0.21536	-1.80153	-0.33431
H	-0.68222	-2.04957	0.53857
H	-0.60574	-2.37101	-1.07884
C	0.74114	0.43160	0.13598
S	2.33947	-0.41545	-0.23615
C	0.76758	1.86307	-0.39572

H	0.90053	1.87779	-1.47785
H	-0.15332	2.39690	-0.15302
H	1.59946	2.40262	0.05647
C	0.49900	0.46624	1.64787
H	-0.41955	1.00760	1.89124
H	0.42744	-0.53539	2.07406
H	1.32907	0.97514	2.13627
H	0.82020	-1.93316	-0.27005

Pen-SS-

C	1.10667	0.37928	-0.55235
H	1.05365	0.30016	-1.63531
C	2.46544	-0.18670	-0.07366
O	3.01843	0.42729	0.86857
O	2.89216	-1.19867	-0.66356
N	1.09132	1.83011	-0.20657
H	1.60429	1.94466	0.67260
H	1.56309	2.38192	-0.91918
C	-0.11238	-0.33144	0.07660
S	-1.57308	0.52192	-0.71558
C	-0.12968	-1.80537	-0.30462
H	0.00542	-1.94078	-1.37759
H	0.65328	-2.35588	0.21766
H	-1.09233	-2.23042	-0.01904
C	-0.14275	-0.18190	1.59235
H	0.69751	-0.71301	2.04205
H	-0.10751	0.85914	1.91600
H	-1.06689	-0.61309	1.97441
S	-3.26980	-0.12699	0.25403
H	0.12791	2.16552	-0.11073

Pen-SSH

C	-1.12423	-0.37455	-0.54620
H	-1.04424	-0.27329	-1.62604
C	-2.48344	0.23103	-0.09769
O	-3.05984	-0.36209	0.84084
O	-2.87365	1.23854	-0.71488
N	-1.18115	-1.83178	-0.23300
H	-1.68962	-1.93704	0.65103
H	-1.70413	-2.33030	-0.95097
C	0.09103	0.29138	0.13942
S	1.52836	-0.44521	-0.80289
C	0.08438	1.79745	-0.08386
H	-0.06008	2.04849	-1.13359
H	-0.70844	2.26323	0.50069
H	1.03294	2.21849	0.24963

C	0.16872	-0.02720	1.62622
H	-0.72481	0.35007	2.12379
H	0.25812	-1.09348	1.83284
H	1.02958	0.47082	2.06755
S	3.20595	0.04449	0.24816
H	3.43695	1.25624	-0.28707
H	-0.25800	-2.25947	-0.15628

Pen-SH

C	0.42159	0.36028	-0.56636
H	0.28523	0.21637	-1.63487
C	1.84672	-0.11647	-0.17871
O	2.42586	0.55461	0.70504
O	2.28517	-1.11378	-0.78175
N	0.36874	1.82501	-0.29902
H	0.92555	2.00891	0.54139
H	0.78566	2.34671	-1.06750
C	-0.69964	-0.37816	0.20318
S	-2.28743	0.28298	-0.50279
H	-3.03239	0.09183	0.59348
C	-0.62928	-1.87797	-0.06420
H	-0.61013	-2.09269	-1.13200
H	0.26255	-2.30548	0.39317
H	-1.50070	-2.36335	0.37267
C	-0.65175	-0.10781	1.70461
H	0.28598	-0.48089	2.11705
H	-0.73993	0.95078	1.94748
H	-1.46802	-0.63408	2.19782
H	-0.59011	2.15317	-0.16842

Pen-$SSCH_3$

C	-1.44657	-0.26626	-0.59610
H	-1.29561	-0.04194	-1.64917
C	-2.74477	0.44572	-0.12485
O	-3.43076	-0.17491	0.71778
O	-2.98570	1.55631	-0.63204
N	-1.69867	-1.73247	-0.47841
H	-2.26763	-1.87984	0.36177
H	-2.23527	-2.06780	-1.27632
C	-0.19797	0.14847	0.21704
S	1.18946	-0.67089	-0.73368
C	-0.01066	1.65906	0.18826
H	-0.00007	2.04626	-0.82952
H	-0.81071	2.14987	0.74179
H	0.92914	1.91558	0.67465
C	-0.24690	-0.34883	1.65590

H	-1.09436	0.10480	2.17042
H	-0.33250	-1.43264	1.73264
H	0.65994	-0.04974	2.17831
S	2.88247	-0.43358	0.36498
C	3.63512	1.06542	-0.31224
H	4.59488	1.16460	0.19563
H	3.80510	0.95499	-1.38010
H	3.02934	1.94357	-0.10909
H	-0.84035	-2.28140	-0.41712

TS H_2S from S-penicillamine
Imaginary frequency: -215.74 cm^{-1}

C	-1.21957	-0.19680	-0.63004
H	-1.17445	0.64855	-1.31031
C	-2.69886	-0.61776	-0.45125
O	-2.92159	-1.85089	-0.38849
O	-3.54397	0.29743	-0.39084
N	-0.51221	-1.34397	-1.26969
H	0.44395	-1.47720	-0.88231
H	-1.07557	-2.17889	-1.07417
C	-0.51391	0.19668	0.68666
S	1.25293	0.68591	0.23544
S	0.68858	2.92685	-0.49438
H	1.56637	2.78979	-1.49468
S	2.22240	-1.54790	0.45652
C	3.50050	-1.12380	-0.75163
H	3.06552	-0.93457	-1.73293
H	4.19990	-1.95476	-0.83425
H	4.05629	-0.23968	-0.43793
H	-0.44997	-1.22387	-2.27655
C	-0.52240	-0.94979	1.70324
H	0.07814	-0.68325	2.57123
H	-1.54854	-1.10746	2.03841
H	-0.15581	-1.89472	1.31061
C	-1.22709	1.37281	1.35534
H	-1.44886	2.17952	0.66329
H	-2.16886	1.02624	1.77982
H	-0.61272	1.75989	2.16715

TS Transpersulfidation from S-penicillamine ZI
Imaginary frequency: -180.18 cm^{-1}

C	2.49487	0.41624	-0.45434
H	2.51895	0.58550	-1.52717
C	3.71466	-0.44980	-0.05655
O	4.27561	-0.15633	1.02490
O	4.03538	-1.36073	-0.84551

N	2.66130	1.73921	0.21170
H	3.08118	1.57798	1.13124
H	3.29120	2.33943	-0.31573
C	1.13079	-0.20389	-0.06459
S	-0.13356	1.02481	-0.65522
C	0.92621	-1.52567	-0.79613
H	1.07406	-1.41275	-1.86995
H	1.61596	-2.28544	-0.42773
H	-0.08900	-1.88234	-0.62260
C	1.02462	-0.42136	1.44262
H	1.76468	-1.15251	1.77192
H	1.17171	0.49795	2.01058
H	0.03712	-0.80737	1.68794
S	-2.11544	0.34099	0.16968
H	-2.22842	-0.52127	-0.83680
S	-4.43513	-0.57211	0.69410
C	-5.26353	0.08938	-0.78255
H	-6.32143	-0.17557	-0.77601
H	-4.82123	-0.31548	-1.69441
H	-5.18681	1.17691	-0.82110
H	1.75551	2.20854	0.30499

ARYL PERSULFIDES

Ph persufide

PhSSH

C	-0.25697	-0.29675	0.12793
S	1.40118	-0.90150	0.36188
S	2.62891	0.54753	-0.39833
H	2.76941	1.30840	0.70124
C	-0.60543	1.03867	0.28475
C	-1.93071	1.42138	0.14834
C	-2.91098	0.47671	-0.12283
C	-2.55954	-0.85706	-0.26768
C	-1.23337	-1.24684	-0.15281
H	0.14944	1.78006	0.50794
H	-2.19770	2.46299	0.26375
H	-3.94380	0.78015	-0.22357
H	-3.31550	-1.59903	-0.48519
H	-0.96137	-2.28555	-0.28718

$PhSSCH_3$

C	-0.53377	-0.29024	0.42546
S	1.09420	-0.71385	1.00899
S	2.29015	-0.33078	-0.61126

C	-1.28595	-1.21109	-0.29780
C	-2.55644	-0.87105	-0.73357
C	-3.08034	0.38245	-0.44507
C	-2.33266	1.29776	0.28057
C	-1.05851	0.96435	0.71746
C	2.45548	1.46640	-0.57686
H	-0.87635	-2.18727	-0.51938
H	-3.14010	-1.58707	-1.29577
H	-4.07330	0.64383	-0.78450
H	-2.73877	2.27394	0.50735
H	-0.47217	1.67559	1.28298
H	3.11062	1.72730	-1.40850
H	2.90574	1.79442	0.35690
H	1.48799	1.94187	-0.72372

PhS-

C	0.00000	0.00000	0.57794
S	0.00000	0.00000	2.33476
C	0.00000	1.19473	-0.16160
C	0.00000	1.19436	-1.54827
C	-0.00000	0.00000	-2.25782
C	-0.00000	-1.19436	-1.54827
C	-0.00000	-1.19473	-0.16160
H	0.00000	2.13795	0.36981
H	0.00000	2.13820	-2.07936
H	-0.00000	0.00000	-3.33934
H	-0.00000	-2.13820	-2.07936
H	-0.00000	-2.13795	0.36981

PhSS-

C	0.22573	-0.31537	-0.00010
S	-1.42359	-0.94925	-0.00007
C	0.53860	1.04006	-0.00006
C	1.86604	1.45184	-0.00006
C	2.89591	0.52455	-0.00010
C	2.58522	-0.83199	-0.00013
C	1.26701	-1.25073	-0.00014
S	-2.72908	0.63958	0.00032
H	-0.26492	1.76456	-0.00003
H	2.09175	2.51051	-0.00003
H	3.92733	0.84935	-0.00010
H	3.37716	-1.56958	-0.00016
H	1.04031	-2.31013	-0.00017

PhSH

C	-0.50377	-0.00490	0.00000
S	-2.27283	-0.08387	-0.00000
C	0.18702	1.20296	0.00000
C	1.57377	1.20385	0.00000
C	2.27991	0.00958	0.00000
C	1.58732	-1.19281	-0.00000
C	0.20114	-1.20530	-0.00000
H	-2.49638	1.23708	-0.00000
H	-0.35223	2.14082	0.00000
H	2.10256	2.14742	0.00000
H	3.36102	0.01580	0.00000
H	2.12638	-2.13045	-0.00000
H	-0.32846	-2.14904	-0.00000

TS H2S from phenyl-SSH

Imaginary frequency: -160.03 cm^{-1}

C	-0.66072	-0.00908	-0.01547
S	0.96947	0.71462	-0.03828
S	0.19163	2.86196	-0.11067
H	-0.07558	3.01037	1.19428
C	-1.31505	-0.21462	1.19428
C	-2.58791	-0.76583	1.21616
C	-3.21608	-1.11904	0.02985
C	-2.56326	-0.91924	-1.17876
C	-1.29046	-0.36753	-1.20221
H	-0.82710	0.06129	2.11955
H	-3.08910	-0.91954	2.16256
H	-4.20880	-1.54795	0.04708
H	-3.04567	-1.19288	-2.10769
H	-0.78373	-0.21155	-2.14500
S	1.86870	-1.66869	0.00544
C	3.58326	-1.08009	0.07959
H	4.27384	-1.92353	0.07738
H	3.76134	-0.50038	0.98691
H	3.81932	-0.44957	-0.77962

TS Tranpersulfidation from phenyl-SSH

Imaginary frequency: -171.50 cm^{-1}

C	-1.73798	-0.45583	0.10956
S	-0.37839	-1.58529	0.21448
S	1.45329	-0.39790	-0.29852
H	1.56244	0.02593	0.95781
C	-1.62340	0.89462	0.43781
C	-2.72745	1.73172	0.36840
C	-3.96570	1.23724	-0.01620

C	-4.08832	-0.10771	-0.33773
C	-2.98545	-0.94604	-0.28289
H	-0.66761	1.29440	0.74757
H	-2.61709	2.77759	0.62339
H	-4.82476	1.89214	-0.06604
H	-5.04621	-0.50785	-0.64297
H	-3.09088	-1.98998	-0.54860
S	3.63180	0.96142	-0.49318
C	4.61238	-0.06819	0.64033
H	5.63099	0.31359	0.71925
H	4.66390	-1.09952	0.28822
H	4.17746	-0.07287	1.64138

p-$CF_3C_6H_4$ persulfide

CF_3PhSS^-

C	1.30651	0.45073	-0.00038
S	3.02303	0.82954	0.00057
C	0.79698	-0.84362	-0.00106
C	-0.57293	-1.06025	-0.00225
C	-1.44814	0.01245	-0.00302
C	-0.94687	1.31420	-0.00170
C	0.41250	1.53150	-0.00057
C	-2.92848	-0.18783	-0.00028
F	-3.52854	0.40854	-1.05259
F	-3.28599	-1.47891	-0.03986
S	4.07371	-0.93343	0.00053
F	-3.51494	0.33790	1.09728
H	1.48290	-1.67942	-0.00086
H	-0.94869	-2.07358	-0.00278
H	-1.62395	2.15826	-0.00188
H	0.78980	2.54622	-0.00003

CF_3PhSSH

C	-0.97802	1.30786	0.06351
C	0.38490	1.52231	0.04550
C	1.25668	0.43875	-0.05600
C	0.75752	-0.85106	-0.13656
C	-0.61230	-1.06326	-0.10828
C	-1.47785	0.01256	-0.01082
H	-1.65063	2.15096	0.14300
H	0.76707	2.53233	0.11370
H	1.42431	-1.69698	-0.21876
H	-0.99221	-2.07247	-0.16844
S	2.98241	0.85766	-0.12334
S	4.01195	-0.87019	0.21658

H	4.06661	-1.33256	-1.04529
C	-2.96371	-0.18494	0.01824
F	-3.32299	-1.47111	-0.07584
F	-3.57785	0.46358	-0.99017
F	-3.51341	0.28820	1.15382

CF_3PhSH

C	0.07346	1.20772	-0.02159
C	-1.30987	1.20324	-0.00889
C	-2.00164	-0.00380	-0.00273
C	-1.29645	-1.20508	-0.00865
C	0.08516	-1.19682	-0.02185
C	0.77207	0.00972	-0.03152
H	0.60033	2.15097	-0.02564
H	-1.84518	2.14258	-0.00505
H	-1.82298	-2.14975	-0.00445
H	0.62283	-2.13457	-0.02592
S	-3.76472	-0.08283	0.01086
C	2.27007	0.00474	-0.00131
F	2.79343	-0.98545	-0.74403
F	2.75107	-0.16961	1.24759
F	2.80106	1.15049	-0.45359
H	-3.98642	1.23887	0.01670

$CF_3PhSSCH_3$

C	-0.93363	0.63887	-0.05867
S	-2.63595	1.15272	-0.03371
S	-3.74522	-0.47185	-0.54056
C	-0.50772	-0.65421	-0.31977
C	0.84595	-0.94997	-0.30978
C	1.77185	0.04391	-0.03931
C	1.34651	1.33954	0.22948
C	-0.00136	1.63727	0.22027
C	3.23683	-0.26780	0.01035
F	3.68631	-0.38315	1.27762
F	3.54560	-1.41616	-0.60742
F	3.98086	0.69429	-0.56251
C	-3.88083	-1.38390	1.01415
H	-1.22145	-1.43556	-0.53754
H	1.16806	-1.96057	-0.51498
H	2.06404	2.11937	0.44311
H	-0.32500	2.64909	0.42663
H	-4.50880	-2.24837	0.79851
H	-4.35552	-0.77111	1.77598
H	-2.90324	-1.72390	1.34727

CF_3PhS-

C	0.03500	1.20188	-0.02676
C	-1.34626	1.19727	-0.01121
C	-2.08725	0.00028	-0.00293
C	-1.34354	-1.19544	-0.01117
C	0.03731	-1.19678	-0.02719
C	0.74041	0.00350	-0.03916
H	0.56439	2.14526	-0.03133
H	-1.87608	2.14047	-0.00685
H	-1.87142	-2.13973	-0.00647
H	0.56933	-2.13891	-0.03175
S	-3.83092	-0.00191	0.01598
C	2.23005	0.00086	-0.00228
F	2.76606	-1.05288	-0.64564
F	2.72178	-0.05460	1.26045
F	2.76931	1.10239	-0.55425

TS H2S from Para CF_3 phenyl-SSH
Imaginary frequency: -147.29 cm^{-1}

C	-1.40078	-0.05795	-1.18477
C	-0.02826	0.10414	-1.19933
C	0.67071	0.28082	-0.00877
C	-0.02068	0.28526	1.19559
C	-1.39705	0.12362	1.21639
C	-2.08482	-0.04554	0.02534
H	-1.93791	-0.19343	-2.11393
H	0.50517	0.09644	-2.13933
H	0.51686	0.42027	2.12376
H	-1.92369	0.13107	2.15944
S	2.43868	0.50946	-0.02681
S	2.29847	2.77382	-0.11956
H	2.10661	3.00553	1.18669
C	-3.57155	-0.23430	0.01008
F	-4.13052	-0.10050	1.21987
F	-3.92131	-1.45596	-0.44205
F	-4.18634	0.64967	-0.79965
S	2.58358	-2.04450	0.03677
C	4.39723	-1.98671	0.04469
H	4.80815	-2.99628	0.05640
H	4.77030	-1.46055	0.92503
H	4.77758	-1.47848	-0.84317

TS Transpersulfidation from Para CF_3Ph-SSH
Imaginary frequency: -152.53 cm^{-1}

C	2.55597	1.29331	-0.08800
C	1.30057	1.86512	-0.09043

C	0.15514	1.07264	0.04554
C	0.30586	-0.30484	0.17997
C	1.56644	-0.88032	0.17382
C	2.69296	-0.08511	0.04304
H	3.43064	1.92110	-0.19430
H	1.20444	2.93696	-0.20072
H	-0.56400	-0.93652	0.28771
H	1.65986	-1.95178	0.27757
S	-1.40908	1.88979	0.07271
S	-2.94540	0.35428	-0.35579
H	-2.97416	-0.03020	0.91864
C	4.06654	-0.67718	0.02439
F	4.07327	-1.99778	0.25034
F	4.87281	-0.12331	0.95257
F	4.68691	-0.48801	-1.15971
S	-4.85948	-1.44028	-0.42319
C	-5.91227	-0.61597	0.81066
H	-6.81804	-1.19570	0.99266
H	-6.21015	0.37797	0.47317
H	-5.38940	-0.50663	1.76286

p-Cl-C$_6$H$_4$ persulfide

ClPhSS-

C	-0.65782	0.43176	0.00005
S	-2.37210	0.85004	0.00000
C	-0.17861	-0.87374	0.00027
C	1.18618	-1.12773	0.00025
C	2.07424	-0.06974	-0.00001
C	1.62109	1.24176	-0.00025
C	0.26131	1.48674	-0.00022
Cl	3.79371	-0.38413	-0.00002
S	-3.45478	-0.89626	-0.00002
H	-0.88327	-1.69429	0.00048
H	1.54801	-2.14642	0.00044
H	2.32212	2.06443	-0.00045
H	-0.08807	2.51170	-0.00040

ClPhSSH

C	0.61739	0.40331	-0.17311
S	2.34023	0.80534	-0.35596
S	3.35424	-0.76802	0.47172
H	3.44575	-1.55630	-0.61361
C	-0.24612	1.44761	0.13637
C	-1.61099	1.22263	0.21754
C	-2.09501	-0.05580	0.00566

C	-1.24640	-1.10822	-0.29569
C	0.11375	-0.87184	-0.39537
Cl	-3.80848	-0.35001	0.12438
H	0.13890	2.44130	0.32138
H	-2.28277	2.03342	0.45856
H	-1.63932	-2.10090	-0.46097
H	0.77443	-1.69060	-0.64427

ClPhSH

C	1.37842	-0.00477	0.00007
S	3.14526	-0.07856	0.00016
C	0.68189	1.19915	0.00005
C	-0.70344	1.20445	-0.00002
C	-1.38639	0.00108	-0.00007
C	-0.70957	-1.20609	-0.00004
C	0.67512	-1.20552	0.00003
Cl	-3.13094	0.00540	-0.00016
H	3.36329	1.24337	0.00017
H	1.21237	2.14145	0.00008
H	-1.24063	2.14180	-0.00004
H	-1.25127	-2.14074	-0.00008
H	1.20183	-2.15034	0.00005

ClPhSSCH$_3$

C	0.33420	-0.47544	0.49835
S	2.04641	-0.79943	0.85677
S	3.01479	-0.06603	-0.79443
C	-0.40574	-1.36077	-0.27845
C	-1.73969	-1.10695	-0.54540
C	-2.32252	0.03669	-0.02330
C	-1.60594	0.92660	0.75698
C	-0.26984	0.66429	1.01656
Cl	-4.00157	0.35943	-0.35587
C	3.01210	1.71558	-0.50565
H	0.05914	-2.25038	-0.68004
H	-2.31790	-1.79185	-1.14822
H	-2.07821	1.81204	1.15668
H	0.30129	1.35227	1.62400
H	3.54754	2.15966	-1.34521
H	3.52632	1.95657	0.42157
H	1.99395	2.09860	-0.49078

ClPhS-

C	0.00000	0.00000	-1.46100
S	0.00000	0.00000	-3.21302
C	0.00000	1.19352	-0.71917

C	0.00000	1.20180	0.66622
C	0.00000	0.00000	1.35333
C	-0.00000	-1.20180	0.66622
C	-0.00000	-1.19352	-0.71917
Cl	0.00000	0.00000	3.10419
H	0.00000	2.13914	-1.24513
H	0.00000	2.13987	1.20429
H	-0.00000	-2.13987	1.20429
H	-0.00000	-2.13914	-1.24513

TS H2S from P Cl phenyl-SSH
Imaginary frequency: -153.35 cm^{-1}

C	0.07483	0.23766	-0.02098
S	1.83065	0.54012	-0.03235
S	1.60354	2.80475	-0.11677
H	1.38362	3.02238	1.18738
C	-0.61281	0.02174	-1.20928
C	-1.98040	-0.20311	-1.20454
C	-2.65447	-0.21109	0.00441
C	-1.99145	-0.00182	1.20127
C	-0.62360	0.22041	1.18054
Cl	-4.37731	-0.49202	0.02025
H	-0.07889	0.02992	-2.14929
H	-2.51126	-0.36940	-2.13090
H	-2.53117	-0.01241	2.13729
H	-0.09825	0.38590	2.11107
S	2.10401	-1.99901	0.02328
C	3.91168	-1.85442	0.08519
H	4.37066	-2.84303	0.10143
H	4.23306	-1.31849	0.97991
H	4.29275	-1.32050	-0.78724

TS Transpersulfidation from parachloro phenyl-SSH
Imaginary frequency: -160.02 cm^{-1}

C	0.85788	0.91582	0.11142
S	-0.66146	1.81759	0.19281
S	-2.26704	0.36035	-0.30283
H	-2.34377	-0.04683	0.96193
C	2.01589	1.59457	-0.27108
C	3.24097	0.94998	-0.30993
C	3.30831	-0.39155	0.02406
C	2.17518	-1.09043	0.40054
C	0.95636	-0.43266	0.44852
Cl	4.84720	-1.21494	-0.03287
H	1.96306	2.63972	-0.54544
H	4.12993	1.48796	-0.60690

H	2.23815	-2.13722	0.66194
H	0.07618	-0.98212	0.75129
S	-4.24516	-1.33110	-0.47740
C	-5.36564	-0.41285	0.62279
H	-6.31732	-0.93576	0.72529
H	-5.56907	0.58521	0.23168
H	-4.93469	-0.30371	1.61977

p-Me-C_6H_4 persulfide

MePhSS-

C	-0.28391	0.09860	-0.44427
S	-2.01697	0.18907	-0.84242
C	0.38689	-1.12244	-0.44996
C	1.73911	-1.18569	-0.15544
C	2.46493	-0.03503	0.14720
C	1.79005	1.18164	0.15023
C	0.43476	1.25054	-0.14071
C	3.93709	-0.10749	0.43395
S	-2.99089	-0.20289	0.95738
H	-0.15665	-2.02888	-0.68296
H	2.24186	-2.14515	-0.16271
H	2.33076	2.09008	0.38591
H	-0.07045	2.20750	-0.12758
H	4.18692	-1.01332	0.98590
H	4.27001	0.75361	1.01196
H	4.50980	-0.12361	-0.49581

MePhSSH

C	0.24124	0.25280	-0.37429
S	1.96295	0.50086	-0.73619
S	2.94448	-0.42068	0.82167
H	3.01203	-1.66506	0.31845
C	-0.52399	1.31419	0.08907
C	-1.88003	1.13779	0.32677
C	-2.49100	-0.09306	0.11746
C	-1.70744	-1.15104	-0.34613
C	-0.35891	-0.98392	-0.59818
C	-3.95587	-0.29102	0.37395
H	-0.06446	2.27700	0.26708
H	-2.46859	1.97169	0.68698
H	-2.16557	-2.11699	-0.51767
H	0.23117	-1.81364	-0.96448
H	-4.41284	0.61000	0.77927
H	-4.11835	-1.10707	1.07919
H	-4.47630	-0.55314	-0.54857

MePhSH

C	-0.99347	-0.00505	0.00072
S	-2.76394	-0.07992	0.00585
C	-0.29535	1.19700	-0.00394
C	1.09101	1.19235	-0.01039
C	1.81434	0.00364	-0.01089
C	1.09928	-1.19057	-0.01029
C	-0.28624	-1.20277	-0.00369
C	3.31589	0.00798	0.01460
H	-2.98423	1.24145	0.00850
H	-0.82765	2.13907	-0.00570
H	1.61908	2.13774	-0.01749
H	1.63378	-2.13227	-0.01729
H	-0.81274	-2.14847	-0.00515
H	3.71602	0.90573	-0.45523
H	3.72160	-0.86228	-0.50029
H	3.68452	-0.01770	1.04230

MePhSSCH$_3$

C	-0.05697	-0.42520	0.47193
S	1.62942	-0.79818	0.89237
S	2.68784	-0.14724	-0.73983
C	-0.81858	-1.32118	-0.27216
C	-2.13355	-1.02050	-0.58107
C	-2.71987	0.17014	-0.15417
C	-1.94755	1.05621	0.59062
C	-0.62874	0.76574	0.90505
C	-4.15582	0.47144	-0.46797
C	2.74829	1.64055	-0.49780
H	-0.38040	-2.24961	-0.61292
H	-2.71704	-1.72230	-1.16348
H	-2.38160	1.98857	0.92860
H	-0.04243	1.46599	1.48447
H	-4.43323	0.08697	-1.44888
H	-4.34925	1.54285	-0.44497
H	-4.81253	-0.00005	0.26613
H	3.33711	2.03981	-1.32405
H	3.23242	1.88576	0.44447
H	1.74758	2.06544	-0.53659

MePhS-

C	1.07149	0.00027	0.00034
S	2.83202	-0.00038	0.00747
C	0.32859	1.19016	-0.00484
C	-1.05874	1.18727	-0.01126

C	-1.78627	0.00057	-0.01159
C	-1.05879	-1.18666	-0.01129
C	0.32807	-1.18980	-0.00484
C	-3.28950	-0.00043	0.01704
H	0.85475	2.13657	-0.00703
H	-1.58761	2.13382	-0.01795
H	-1.58794	-2.13309	-0.01798
H	0.85425	-2.13619	-0.00701
H	-3.69461	0.90159	-0.44172
H	-3.66508	-0.04162	1.04232
H	-3.69525	-0.86326	-0.51157

TS H2S from Para methyl phenyl-SSH
Imaginary frequency: -163.22 cm^{-1}

C	0.27322	0.18029	0.02059
S	-1.46411	0.57762	0.02959
S	-1.12017	2.83867	0.12055
H	-0.87249	3.04591	-1.18019
C	0.94957	-0.07797	1.20490
C	2.30525	-0.37643	1.18911
C	3.01776	-0.42549	-0.00430
C	2.32849	-0.16686	-1.18803
C	0.97577	0.12984	-1.17910
C	4.48319	-0.75362	-0.02897
H	0.41612	-0.04383	2.14546
H	2.81668	-0.57305	2.12334
H	2.86021	-0.19876	-2.13132
H	0.46055	0.32889	-2.10958
H	4.66210	-1.69331	-0.55448
H	4.88427	-0.84869	0.97898
H	5.04820	0.02012	-0.55054
S	-1.90451	-1.92911	-0.03206
C	-3.69997	-1.67167	-0.07445
H	-4.22041	-2.62938	-0.09117
H	-3.99612	-1.11120	-0.96288
H	-4.03803	-1.12008	0.80471

TS Transpersulfidation from Para methyl pheny-SSH
Imaginary frequency: -173.32 cm^{-1}

C	1.26371	0.77848	0.15971
S	-0.20431	1.76126	0.28670
S	-1.88504	0.37195	-0.26523
H	-1.96438	-0.06727	0.98767
C	2.40310	1.31907	-0.43465
C	3.57972	0.58834	-0.50716
C	3.65781	-0.70846	-0.00875

C	2.51529	-1.24432	0.58025
C	1.33958	-0.51617	0.67136
C	4.92024	-1.51359	-0.12746
H	2.37005	2.32074	-0.84343
H	4.45166	1.03545	-0.96905
H	2.54701	-2.24879	0.98490
H	0.47418	-0.95905	1.14624
H	5.79902	-0.86980	-0.14891
H	4.92051	-2.10059	-1.04863
H	5.02334	-2.21092	0.70362
S	-3.88222	-1.22418	-0.51422
C	-5.04470	-0.25334	0.49184
H	-6.01790	-0.74413	0.53166
H	-5.18562	0.74459	0.07406
H	-4.68110	-0.14476	1.51511

p*-$N(CH_3)_2C_6H_4$ *persulfide

NMe_2PhS-

C	-1.84600	0.00001	-0.00572
S	-3.60756	0.00002	0.09413
C	-1.09678	-1.18177	-0.04305
C	0.28852	-1.18915	-0.11402
C	1.02574	-0.00003	-0.16156
C	0.28857	1.18911	-0.11379
C	-1.09675	1.18176	-0.04282
N	2.42956	-0.00005	-0.28780
C	3.10169	-1.20683	0.16715
C	3.10171	1.20687	0.16672
H	-1.61409	-2.13281	-0.00945
H	0.78783	-2.14646	-0.13598
H	0.78791	2.14641	-0.13553
H	-1.61402	2.13281	-0.00903
H	2.81875	-2.06853	-0.43352
H	2.88928	-1.43479	1.22014
H	4.17504	-1.07432	0.05479
H	2.81866	2.06837	-0.43420
H	4.17504	1.07435	0.05426
H	2.88941	1.43515	1.21966

NMe_2PhS-

C	-1.07200	0.00013	-0.53093
S	-2.83052	0.00022	-0.77591
C	-0.35632	-1.18969	-0.43815
C	1.01623	-1.19831	-0.26231
C	1.74499	0.00003	-0.18140

C	1.01627	1.19843	-0.26190
C	-0.35628	1.18990	-0.43772
N	3.12828	-0.00005	-0.05265
C	3.74991	-1.22036	0.43485
C	3.75009	1.22014	0.43491
S	-3.65088	-0.00027	1.14194
H	-0.88221	-2.13407	-0.49806
H	1.51703	-2.15168	-0.19343
H	1.51708	2.15176	-0.19266
H	-0.88214	2.13432	-0.49731
H	3.58912	-2.04753	-0.25389
H	3.37654	-1.51491	1.42290
H	4.82261	-1.06250	0.50566
H	3.58916	2.04744	-0.25364
H	4.82282	1.06222	0.50537
H	3.37702	1.51453	1.42312

NMe_2PhSSH

C	-1.02764	-0.04213	-0.53027
S	-2.77157	-0.06294	-0.80858
S	-3.61249	-0.00102	1.07851
H	-3.63854	1.33126	1.25258
C	-0.31265	-1.22820	-0.39006
C	1.05435	-1.21685	-0.20138
C	1.77210	-0.00591	-0.15730
C	1.03482	1.18718	-0.28625
C	-0.33194	1.16242	-0.47479
N	3.14051	0.00931	-0.01263
C	3.79421	-1.19794	0.46377
C	3.77926	1.25897	0.36343
H	-0.83201	-2.17690	-0.42230
H	1.56457	-2.16082	-0.09143
H	1.52886	2.14506	-0.24305
H	-0.86645	2.09820	-0.57341
H	3.65143	-2.02399	-0.23106
H	3.42944	-1.50753	1.44929
H	4.86209	-1.01320	0.53469
H	3.61523	2.02752	-0.39006
H	4.85081	1.09664	0.43384
H	3.42082	1.63665	1.32735

NMe_2PhSH

C	-1.76449	-0.00001	-0.00757
S	-3.54119	0.00000	-0.12882
C	-1.05147	1.19291	0.01237
C	0.32960	1.19957	0.07294

C	1.06103	-0.00003	0.12180
C	0.32958	-1.19963	0.07284
C	-1.05149	-1.19293	0.01227
N	2.43988	0.00001	0.23024
C	3.14324	1.22421	-0.11459
C	3.14341	-1.22415	-0.11440
H	-3.82434	0.00011	1.18275
H	-1.57946	2.13645	-0.02305
H	0.83536	2.15226	0.08214
H	0.83531	-2.15233	0.08193
H	-1.57950	-2.13646	-0.02323
H	2.86019	2.04108	0.54675
H	2.95738	1.53546	-1.14902
H	4.21016	1.06139	0.00936
H	2.86032	-2.04100	0.54694
H	4.21029	-1.06122	0.00974
H	2.95777	-1.53547	-1.14885

$NMe_2PhSSCH_3$

C	-0.72561	-0.44543	-0.60451
S	-2.45372	-0.67815	-0.90231
S	-3.35435	-0.12275	0.86054
C	0.05251	-1.45598	-0.04691
C	1.40242	-1.27480	0.17558
C	2.04019	-0.06653	-0.16509
C	1.24077	0.95148	-0.71652
C	-0.10947	0.75809	-0.93481
N	3.39654	0.10416	0.01534
C	4.08941	-0.81963	0.89753
C	3.91948	1.46009	0.00352
C	-3.32307	1.68053	0.78107
H	-0.40408	-2.39837	0.22599
H	1.96261	-2.08476	0.61558
H	1.67115	1.90385	-0.98357
H	-0.69378	1.56042	-1.36564
H	4.02348	-1.84139	0.52804
H	3.69573	-0.79481	1.91990
H	5.14197	-0.55275	0.92705
H	3.76310	1.93514	-0.96352
H	4.99089	1.42418	0.17835
H	3.46300	2.08901	0.77602
H	-3.82579	2.03599	1.68094
H	-3.85677	2.03681	-0.09691
H	-2.29808	2.04515	0.77945

TS H2S from para NMe2 Phenyl-SSH
Imaginary frequency: -176.16 cm^{-1}

C	0.40842	0.21560	-0.01957
S	2.15789	0.52641	-0.03808
S	1.93796	2.81327	-0.18142
H	1.68105	3.06071	1.11034
C	-0.29150	-0.03547	-1.19235
C	-1.65631	-0.26515	-1.18198
C	-2.38401	-0.26462	0.01911
C	-1.67021	0.00471	1.19800
C	-0.30492	0.23050	1.17183
N	-3.74674	-0.54378	0.04299
C	-4.47302	-0.39763	-1.20761
C	-4.49038	-0.10604	1.21283
H	0.23504	-0.04596	-2.13775
H	-2.14989	-0.44940	-2.12361
H	-2.17462	0.03520	2.15137
H	0.21109	0.43228	2.10167
H	-4.10951	-1.09660	-1.95836
H	-4.40296	0.61747	-1.61690
H	-5.52091	-0.62635	-1.03302
H	-4.14027	-0.60677	2.11328
H	-5.53630	-0.37012	1.08208
H	-4.42308	0.97717	1.37087
S	2.51200	-1.98722	0.07514
C	4.31599	-1.79605	0.10333
H	4.80110	-2.77163	0.13876
H	4.63737	-1.22750	0.97779
H	4.66916	-1.27635	-0.78926

TS Transpersulfidation from para NMe2 Phenyl-SSH
Imaginary frequency: -178.95 cm^{-1}

C	0.41921	1.20334	0.28667
S	-1.16478	1.98203	0.40283
S	-2.59728	0.34162	-0.26379
H	-2.56010	-0.17877	0.95952
C	1.28288	1.46908	-0.77293
C	2.52389	0.86209	-0.87026
C	2.96665	-0.04877	0.10063
C	2.08482	-0.33110	1.15650
C	0.85128	0.28884	1.24572
N	4.23282	-0.62560	0.03504
C	4.89162	-0.61814	-1.26067
C	4.43708	-1.85200	0.78859
H	0.97986	2.16261	-1.54670
H	3.14628	1.10772	-1.71693

H	2.35831	-1.03510	1.92745
H	0.20551	0.04701	2.08042
H	5.08148	0.39810	-1.60061
H	4.30835	-1.13755	-2.03086
H	5.85449	-1.11315	-1.16649
H	4.31814	-1.68360	1.85699
H	5.45512	-2.19642	0.62742
H	3.74857	-2.65001	0.48493
S	-4.23393	-1.56138	-0.62947
C	-5.60574	-0.86814	0.34027
H	-6.47182	-1.52983	0.30024
H	-5.90528	0.10642	-0.04777
H	-5.32290	-0.74575	1.38698

p-$NO_2C_6H_4$ persulfide

NO_2PhSS-

C	-0.92857	0.44471	-0.00005
S	-2.62535	0.83420	-0.00009
S	-3.70311	-0.90178	0.00026
C	-0.43166	-0.86239	0.00018
C	0.92671	-1.09410	0.00017
C	1.80224	-0.01666	-0.00004
C	1.33158	1.29591	-0.00026
C	-0.02191	1.52069	-0.00028
N	3.21962	-0.25817	-0.00003
O	3.62319	-1.41414	-0.00011
O	3.98129	0.70056	0.00004
H	-1.12716	-1.68955	0.00036
H	1.30674	-2.10423	0.00035
H	2.02330	2.12403	-0.00044
H	-0.39092	2.53786	-0.00047

NO_2PhSSH

C	-0.87812	0.43457	0.03869
S	-2.59390	0.87253	0.09128
S	-3.64706	-0.85316	-0.17930
H	-3.70183	-1.26181	1.10106
C	-0.39560	-0.86697	0.08189
C	0.96664	-1.09623	0.05973
C	1.82858	-0.01549	0.00305
C	1.36597	1.29061	-0.03494
C	0.00585	1.51312	-0.01991
N	3.26448	-0.25692	-0.01795
O	3.65961	-1.40906	0.00972
O	4.01272	0.70359	-0.06240

H	-1.07288	-1.70650	0.13111
H	1.34973	-2.10410	0.09130
H	2.05577	2.11856	-0.08163
H	-0.36529	2.52847	-0.05756

NO_2PhSH

C	1.64094	-0.00441	0.00001
S	3.39690	-0.07858	-0.00002
C	0.94646	1.20485	0.00001
C	-0.43278	1.20949	0.00003
C	-1.10913	0.00027	0.00005
C	-0.43817	-1.21221	0.00005
C	0.94048	-1.21108	0.00003
N	-2.56257	0.00352	0.00006
O	-3.14190	1.07621	-0.00007
O	-3.14642	-1.06672	-0.00010
H	3.61510	1.24406	-0.00003
H	1.48012	2.14453	-0.00001
H	-0.97494	2.14208	0.00003
H	-0.98408	-2.14251	0.00006
H	1.47103	-2.15293	0.00003

$NO_2PhSSCH_3$

C	-0.55173	0.61645	-0.07574
S	-2.23764	1.16268	-0.07790
S	-3.37928	-0.45782	-0.52529
C	-0.15357	-0.69945	-0.27772
C	1.18812	-1.02570	-0.24574
C	2.11722	-0.02753	-0.00936
C	1.73998	1.29065	0.19556
C	0.39964	1.60968	0.16276
N	3.53037	-0.37193	0.02656
O	3.84950	-1.53486	-0.14940
O	4.33920	0.51641	0.23135
C	-3.53844	-1.30323	1.06447
H	-0.88334	-1.47338	-0.46423
H	1.50511	-2.04502	-0.40158
H	2.48026	2.05408	0.37592
H	0.09544	2.63555	0.32136
H	-4.18319	-2.16234	0.87906
H	-4.00386	-0.65114	1.79873
H	-2.56925	-1.64976	1.41481

NO_2PhS^-

C	1.72719	0.00000	-0.00000
S	3.44661	-0.00000	0.00000

C	0.98138	-1.20486	0.00015
C	-0.39010	-1.21123	0.00013
C	-1.08399	0.00000	-0.00001
C	-0.39010	1.21123	-0.00014
C	0.98138	1.20486	-0.00015
N	-2.50745	0.00000	-0.00000
O	-3.10713	-1.07330	-0.00038
O	-3.10713	1.07330	0.00039
H	1.51391	-2.14571	0.00030
H	-0.93095	-2.14546	0.00027
H	-0.93095	2.14546	-0.00027
H	1.51391	2.14571	-0.00030

TS H2S from paranitro phenyl-SSH
Imaginary frequency: -135.68 cm^{-1}

C	0.33029	0.26317	-0.02064
S	2.09121	0.53045	-0.03130
S	1.89478	2.78021	-0.12104
H	1.71565	3.00640	1.18809
C	-0.36362	0.24477	1.18640
C	-1.73132	0.05388	1.20566
C	-2.39358	-0.12048	0.00121
C	-1.72713	-0.11082	-1.21354
C	-0.35956	0.08140	-1.21629
N	-3.83612	-0.32003	0.01226
O	-4.41407	-0.32904	1.08544
O	-4.41086	-0.46991	-1.05215
H	0.16985	0.38435	2.11564
H	-2.27388	0.04091	2.13795
H	-2.26632	-0.25053	-2.13741
H	0.17734	0.09239	-2.15370
S	2.24580	-2.03092	0.03546
C	4.05861	-1.95801	0.07609
H	4.41107	-1.42304	0.95951
H	4.45145	-1.45348	-0.80830
H	4.47625	-2.96452	0.10281

TS Transpersulfidation from paranitro phenyl-SSH
Imaginary frequency: -119.84 cm^{-1}

C	0.57241	0.98501	0.00462
S	-0.95004	1.86371	0.01104
S	-2.52711	0.42014	-0.40623
H	-2.60023	0.03861	0.86866
C	0.66451	-0.40772	0.01226
C	1.89679	-1.02806	0.02602
C	3.04435	-0.25130	0.03862

C	2.98199	1.13561	0.03498
C	1.74846	1.74653	0.01547
N	4.33887	-0.90137	0.05709
O	4.38089	-2.12135	0.05529
O	5.34173	-0.20553	0.07387
H	-0.23167	-1.01005	0.00533
H	1.96494	-2.10490	0.03144
H	3.88512	1.72569	0.04285
H	1.69310	2.82645	0.00694
S	-4.57642	-1.35029	-0.41505
C	-5.43365	-0.56351	0.98608
H	-6.33934	-1.11307	1.24597
H	-5.72008	0.46231	0.74820
H	-4.79684	-0.53659	1.87309

p-OMeC$_6$H$_4$ persulfide

MeOPhSS-

C	0.66527	0.37562	-0.00015
S	2.35066	0.92726	0.00037
C	0.28252	-0.96244	0.00002
C	-1.05670	-1.31550	0.00004
C	-2.04456	-0.33840	-0.00014
C	-1.67659	1.00327	-0.00038
C	-0.33281	1.34783	-0.00044
O	-3.33876	-0.78141	-0.00021
S	3.56392	-0.73629	-0.00011
C	-4.36900	0.19217	0.00044
H	1.04636	-1.72872	0.00012
H	-1.34681	-2.35812	0.00018
H	-2.41890	1.78749	-0.00036
H	-0.06620	2.39788	-0.00059
H	-5.30512	-0.35956	0.00087
H	-4.32112	0.82080	-0.89125
H	-4.32013	0.82062	0.89221

MeOPhSSH

C	0.65613	0.14113	-0.47030
S	2.38360	0.05779	-0.85581
S	3.30316	-0.23730	0.96670
H	3.22214	-1.57751	1.02665
C	0.06090	1.36002	-0.14500
C	-1.28958	1.42515	0.12263
C	-2.07079	0.26993	0.06525
C	-1.48671	-0.94972	-0.26372
C	-0.12675	-1.00360	-0.52953

O	-3.38634	0.43045	0.34109
C	-4.22684	-0.71487	0.29335
H	0.65978	2.25941	-0.10055
H	-1.75878	2.36583	0.37576
H	-2.07279	-1.85420	-0.31651
H	0.32420	-1.95327	-0.78396
H	-5.22347	-0.36379	0.54418
H	-3.91078	-1.46352	1.02149
H	-4.23592	-1.15246	-0.70614

MeOPhSH

C	1.40427	-0.02487	0.00001
S	3.15798	-0.28898	-0.00004
C	0.83843	1.24819	-0.00002
C	-0.53375	1.40111	-0.00001
C	-1.36860	0.28628	0.00002
C	-0.81134	-0.98591	0.00004
C	0.57016	-1.13251	0.00003
O	-2.70687	0.53888	0.00004
C	-3.59024	-0.57176	-0.00005
H	3.51696	1.00142	0.00037
H	1.46849	2.12764	-0.00005
H	-0.97233	2.38970	-0.00002
H	-1.43017	-1.87023	0.00007
H	0.98762	-2.13102	0.00007
H	-4.59432	-0.15714	-0.00010
H	-3.45135	-1.18548	0.89206
H	-3.45123	-1.18542	-0.89218

MeOPhSSCH$_3$

C	0.36323	-0.53396	0.46778
S	2.07558	-0.73301	0.88542
S	3.06830	0.04090	-0.73672
C	-0.30679	-1.50135	-0.28198
C	-1.64019	-1.34315	-0.59131
C	-2.33128	-0.21220	-0.15256
C	-1.67448	0.75524	0.60018
C	-0.33087	0.58590	0.90468
O	-3.63768	-0.14335	-0.50398
C	-4.38582	0.98874	-0.08258
C	2.93539	1.82254	-0.47897
H	0.22146	-2.38039	-0.62543
H	-2.16594	-2.08928	-1.17103
H	-2.18993	1.63543	0.95253
H	0.17701	1.33983	1.49065
H	-5.39023	0.84349	-0.46941

H	-3.96787	1.90953	-0.49264
H	-4.42111	1.05225	1.00617
H	3.47360	2.29156	-1.30306
H	3.39298	2.11107	0.46433
H	1.89411	2.13638	-0.51094

MeOPhS-

C	1.48405	-0.02790	-0.00006
S	3.23716	-0.21903	-0.00008
C	0.87591	1.23882	0.00001
C	-0.49805	1.39635	0.00003
C	-1.33559	0.28524	-0.00004
C	-0.77068	-0.98184	-0.00012
C	0.61439	-1.12270	-0.00012
O	-2.68508	0.53716	-0.00008
C	-3.55749	-0.57902	0.00040
H	1.50173	2.12206	0.00007
H	-0.93562	2.38667	0.00009
H	-1.38733	-1.86897	-0.00017
H	1.02881	-2.12281	-0.00018
H	-4.56658	-0.17553	0.00063
H	-3.41471	-1.19379	0.89187
H	-3.41527	-1.19414	-0.89092

TS H2S from para OMe Phenyl-SSH

Imaginary frequency: -167.02 cm^{-1}

C	-0.08477	0.22924	0.09291
S	-1.83456	0.52945	-0.02907
S	-1.62686	2.81208	0.02097
H	-1.27996	2.99860	-1.26005
C	0.52246	0.03721	1.33198
C	1.88189	-0.18686	1.42531
C	2.66526	-0.22423	0.27312
C	2.07259	-0.03626	-0.96967
C	0.70296	0.18632	-1.04669
O	3.99492	-0.45009	0.46032
C	4.82717	-0.50383	-0.68792
H	-0.07623	0.06463	2.23239
H	2.35245	-0.33545	2.38793
H	2.65595	-0.06057	-1.87760
H	0.24851	0.33274	-2.01751
H	5.83243	-0.69217	-0.32157
H	4.81119	0.44279	-1.23130
H	4.52664	-1.31423	-1.35470
S	-2.15254	-1.99710	-0.04734
C	-3.95277	-1.82821	-0.19685

H	-4.42505	-2.81017	-0.22928
H	-4.22290	-1.29398	-1.10948
H	-4.36778	-1.28258	0.65255

TS Transpersulfidation from para OMe Phenyl-SSH
Imaginary frequency: -178.18 cm^{-1}

C	0.81272	1.08217	0.23125
S	-0.72698	1.90870	0.51445
S	-2.25123	0.41495	-0.22855
H	-2.16209	-0.25785	0.91583
C	1.63946	1.44714	-0.83380
C	2.84315	0.80570	-1.05446
C	3.24936	-0.22969	-0.21606
C	2.43901	-0.60995	0.84767
C	1.23623	0.05015	1.06225
O	4.44676	-0.80732	-0.51201
C	4.89538	-1.86845	0.31648
H	1.33445	2.24443	-1.49837
H	3.47863	1.09540	-1.88061
H	2.72880	-1.40737	1.51511
H	0.61643	-0.25188	1.89638
H	5.85324	-2.18189	-0.08909
H	4.19931	-2.70907	0.29240
H	5.03021	-1.53415	1.34692
S	-4.00612	-1.39935	-0.68876
C	-5.20267	-0.85882	0.56869
H	-6.08737	-1.49655	0.55334
H	-5.52277	0.16848	0.38864
H	-4.76958	-0.90915	1.56918

The following geometries related to the penicillamine-derived persulfide precursor were optimized at the ωB97X-D/aug-cc-pVDZ/SMD(water) level of theory. Imaginary frequencies are provided for transition structures. Minima had no imaginary frequencies.

Benzothiolate

S	2.55269	-0.79278	-0.00016
C	1.39698	0.49369	0.00009
O	1.71585	1.70046	0.00024
C	-0.08786	0.17118	0.00005
C	-0.57382	-1.14257	0.00016
C	-1.01113	1.22699	-0.00010
C	-1.94447	-1.39634	0.00013
H	0.13570	-1.96821	0.00028
C	-2.38228	0.97594	-0.00016
H	-0.65040	2.25445	-0.00018

C	-2.85405	-0.33767	-0.00005
H	-2.30349	-2.42582	0.00022
H	-3.08565	1.80907	-0.00030
H	-3.92623	-0.53593	-0.00009

2

HS-anion

S	-0.00000	-0.00000	0.07971
H	0.00000	0.00000	-1.27540

R-cysteine-ZI

C	-0.39470	0.54229	-0.29717
H	-0.18270	0.57827	-1.37222
C	-1.14489	-0.78215	-0.02050
O	-2.40171	-0.71947	-0.07259
O	-0.45103	-1.80272	0.19580
N	-1.34590	1.66068	-0.02575
H	-1.11607	2.49755	-0.56445
H	-2.28824	1.32552	-0.26545
C	0.88406	0.76112	0.50391
H	0.73035	0.48378	1.55307
H	1.15534	1.82357	0.46647
S	2.33861	-0.11486	-0.16574
H	1.81242	-1.35702	-0.05544
H	-1.35242	1.91136	0.96688

R-cysteine-ZI S-COPh

C	-0.61596	-0.42329	-0.57154
O	-0.23594	-1.55815	-0.83043
C	-2.01499	-0.12642	-0.16870
C	-2.80991	-1.19786	0.26410
C	-2.55104	1.16767	-0.20749
C	-4.12457	-0.97394	0.65826
H	-2.38904	-2.20132	0.29895
C	-3.86963	1.38521	0.18308
H	-1.95658	2.00995	-0.55948
C	-4.65561	0.31714	0.61744
H	-4.73765	-1.80732	0.99972
H	-4.28499	2.39137	0.14424
H	-5.68689	0.49095	0.92451
S	0.49387	0.96902	-0.61706
C	1.98384	0.23308	-1.38084
C	2.95825	-0.43357	-0.41929
H	1.66619	-0.46121	-2.16666
H	2.49229	1.07705	-1.85709
H	3.88644	-0.62238	-0.96929
C	3.31166	0.44473	0.80385

N	2.45582	-1.74999	0.07314
O	3.72140	1.60053	0.55019
O	3.16771	-0.08524	1.93618
H	3.01997	-2.52678	-0.27160
H	2.52562	-1.71047	1.10308
H	1.47447	-1.90775	-0.20629

R-cysteine-ZI disulfide-dimer

S	-0.57214	0.96769	-0.36616
C	-1.73131	0.78545	1.03995
C	-2.94161	-0.11532	0.81741
H	-3.65451	0.08489	1.62464
C	-3.64352	0.13468	-0.53145
O	-3.67315	-0.81817	-1.34871
N	-2.58103	-1.55776	0.93838
H	-2.08664	-1.74349	1.81492
S	0.50343	-0.82460	-0.39618
C	1.63194	-0.68075	1.04150
C	2.88887	0.14207	0.81024
H	1.93091	-1.71333	1.25469
H	1.07185	-0.31402	1.90957
H	3.54433	0.00503	1.67807
C	3.69980	-0.27704	-0.43839
N	2.60633	1.60614	0.71420
O	3.91994	-1.50242	-0.56871
O	4.08895	0.65541	-1.18904
H	3.24115	1.96703	-0.01652
H	1.64228	1.80030	0.41960
H	2.77083	2.09100	1.59726
H	-3.42507	-2.13526	0.91668
H	-1.99122	-1.86384	0.15938
O	-4.11988	1.28592	-0.68170
H	-1.17678	0.48649	1.93761
H	-2.09676	1.80660	1.20324

R-cysteine-ZI persulfide-anion

C	0.96849	0.31655	0.87107
H	1.57654	0.45067	1.77466
C	1.94404	-0.02805	-0.27433
O	2.50703	-1.14736	-0.20572
O	2.12337	0.85299	-1.15730
N	0.32485	1.62915	0.57093
H	0.89261	2.07848	-0.15960
H	-0.64906	1.48778	0.20096
C	-0.07472	-0.76216	1.13722
H	-0.69879	-0.48095	1.99511

H	0.45201	-1.69077	1.38709
S	-1.15797	-1.15006	-0.28460
S	-2.47904	0.50747	-0.34592
H	0.27481	2.22909	1.39403

R-cysteine-ZI persulfide

C	-1.13109	0.29955	-0.35712
H	-1.13333	0.41007	-1.44857
C	-2.39603	-0.52998	-0.00119
O	-2.36202	-1.74839	-0.27841
O	-3.35207	0.11690	0.50060
N	-1.31238	1.66583	0.21664
H	-0.80615	1.78887	1.09699
H	-1.03160	2.41107	-0.42238
C	0.15037	-0.36044	0.12535
H	0.14414	-1.40711	-0.18932
H	0.22293	-0.30413	1.21869
S	1.61518	0.47251	-0.61542
S	3.17959	-0.36151	0.47187
H	3.37070	-1.47676	-0.28136
H	-2.32305	1.73829	0.42648

R-cysteine-ZI persulfide S-COPh

S	-0.55193	-1.62710	-0.35207
S	1.29509	-1.88514	0.53614
C	2.41978	-0.81913	-0.46583
H	3.15187	-1.47760	-0.94257
H	1.82802	-0.32426	-1.24460
C	3.16317	0.20099	0.38874
H	3.65474	-0.28310	1.23738
C	4.23510	0.90563	-0.47964
O	3.96791	2.07344	-0.86022
O	5.25812	0.23103	-0.74078
C	-1.21051	-0.15801	0.47745
C	-2.61629	0.16093	0.13145
C	-3.02673	1.49782	0.24139
C	-3.52361	-0.82029	-0.29047
C	-4.33341	1.84870	-0.07815
H	-2.31477	2.25566	0.56463
C	-4.83359	-0.46261	-0.59867
H	-3.22992	-1.86766	-0.35294
C	-5.23710	0.86907	-0.49700
H	-4.65001	2.88824	-0.00148
H	-5.54160	-1.22754	-0.91467
H	-6.26221	1.14558	-0.74309
O	-0.53039	0.52616	1.21655

N	2.23220	1.23023	0.92017
H	1.28086	0.86639	1.10154
H	2.59247	1.63792	1.78484
H	2.18866	1.98687	0.22467

R-cysteine-ZI thiolate-anion

C	0.32272	0.38321	0.78830
H	0.77265	0.56532	1.77231
C	1.39370	-0.30673	-0.07863
O	1.66963	-1.49748	0.21219
O	1.94134	0.38735	-0.97860
N	0.00621	1.70222	0.18301
H	0.80778	2.01404	-0.37453
H	-0.80403	1.51407	-0.45277
C	-0.98108	-0.40908	0.93411
H	-1.55677	0.02757	1.76238
H	-0.71371	-1.43139	1.22416
S	-1.97479	-0.38324	-0.61380
H	-0.25264	2.40337	0.87677

S-penicillamine-donor R-cysteine-ZI tetrahedral-int

S	-1.03540	1.14688	-0.53355
S	0.73508	0.69403	-1.49493
C	2.07153	0.58348	-0.03599
O	1.64063	-0.04348	1.01526
C	-1.99542	-0.47695	-0.47001
C	-1.19031	-1.54727	0.25762
H	-0.99525	-1.27395	1.30018
H	-1.72637	-2.50406	0.23240
H	-0.23384	-1.68613	-0.25696
C	-3.26179	-0.10217	0.34893
H	-2.93660	0.24207	1.33871
C	-2.30956	-0.94616	-1.89013
H	-1.37126	-1.10764	-2.43438
H	-2.84526	-1.90368	-1.86043
H	-2.90944	-0.22738	-2.46160
C	-4.13903	-1.33327	0.63533
O	-3.93262	-2.02614	1.64340
N	-5.10662	-1.60882	-0.24226
H	-5.21879	-1.00260	-1.04272
C	-5.98475	-2.75304	-0.08752
H	-6.54636	-2.68713	0.85292
H	-6.68892	-2.76255	-0.92360
H	-5.41085	-3.68836	-0.09051
C	2.57630	2.00885	0.21069
C	3.09714	2.81645	-0.81024

C	2.51892	2.52137	1.50866
C	3.55396	4.10257	-0.53449
H	3.13958	2.44518	-1.83366
C	2.96827	3.81517	1.78519
H	2.11919	1.90152	2.30861
C	3.48956	4.60965	0.76644
H	3.95828	4.71555	-1.34039
H	2.91094	4.19957	2.80397
H	3.84323	5.61844	0.98047
N	-4.01547	0.96312	-0.28663
H	-3.81601	1.21825	-1.24400
C	-4.99262	1.62936	0.36225
O	-5.29590	1.34991	1.53259
C	-5.69073	2.71734	-0.40223
H	-6.76174	2.48333	-0.44194
H	-5.56870	3.66058	0.14458
H	-5.30403	2.83300	-1.42013
S	3.49106	-0.29516	-0.97129
C	2.82411	-1.98314	-1.18985
C	3.03795	-2.94321	-0.02386
H	1.75468	-1.91178	-1.42477
H	3.32632	-2.39215	-2.07224
H	2.76033	-3.94891	-0.36276
C	4.50153	-3.02517	0.45428
N	2.15915	-2.59866	1.12291
O	5.36192	-3.25338	-0.43194
O	4.71176	-2.89173	1.68884
H	2.66621	-2.82465	1.98428
H	1.28273	-3.11894	1.09135
H	1.92400	-1.54379	1.11509

S-penicillamine R-cysteine-ZI disulfide

S	-0.43447	-0.76069	-0.22973
C	0.81148	0.65545	-0.23708
C	0.31337	1.78578	0.65839
H	0.16484	1.45093	1.69164
H	1.03536	2.61123	0.65311
H	-0.63229	2.18085	0.26972
C	2.07368	-0.00706	0.38148
H	1.81852	-0.34594	1.39314
C	1.02218	1.16318	-1.66197
H	0.06652	1.50996	-2.07307
H	1.70781	2.02000	-1.65339
H	1.42364	0.40008	-2.33993
C	3.20833	1.01164	0.59348
O	3.27853	1.65088	1.65386

N	4.08660	1.16183	-0.40030
H	3.96487	0.61519	-1.24127
C	5.18926	2.10164	-0.31951
H	5.84170	1.86068	0.52912
H	5.76747	2.03469	-1.24466
H	4.81945	3.12790	-0.20014
N	2.50403	-1.15614	-0.39276
H	2.17665	-1.27611	-1.34155
C	3.40222	-2.04235	0.08866
O	3.88636	-1.91628	1.22328
C	3.78208	-3.17650	-0.81899
H	4.85901	-3.11403	-1.01985
H	3.58731	-4.12185	-0.29799
H	3.23300	-3.15940	-1.76613
S	-2.20594	0.10787	-0.84912
C	-2.98861	0.70820	0.71092
C	-4.33650	0.05421	0.96042
H	-2.29940	0.50661	1.53750
H	-3.13103	1.78942	0.62999
H	-4.78727	0.52091	1.84465
C	-5.35599	0.20181	-0.19302
N	-4.18593	-1.39191	1.27962
O	-5.38779	1.31653	-0.76477
O	-6.08326	-0.79735	-0.42572
H	-5.09652	-1.84426	1.13709
H	-3.52455	-1.84470	0.64064
H	-3.86118	-1.53980	2.23716

S-penicillamine persulfide-anion

S	-2.42240	-0.69370	-0.60613
C	-0.70753	-1.29302	-0.15202
C	-0.53821	-2.57159	-0.97737
H	-0.63747	-2.37541	-2.05360
H	0.44968	-3.01489	-0.80128
H	-1.29727	-3.30694	-0.68349
C	0.34527	-0.23585	-0.60287
H	0.31842	-0.18209	-1.69935
C	-0.61670	-1.61591	1.33654
H	-1.43516	-2.28868	1.61979
H	0.33273	-2.12279	1.55566
H	-0.68709	-0.71686	1.95977
C	1.77560	-0.67635	-0.25878
O	2.41267	-1.40732	-1.03663
N	2.28081	-0.26268	0.90633
H	1.70672	0.32778	1.49162

C	3.59704	-0.66132	1.36460
H	4.37067	-0.33999	0.65550
H	3.78351	-0.18772	2.33225
H	3.65788	-1.75121	1.48158
N	0.04258	1.07351	-0.05174
H	-0.85308	1.18800	0.43701
C	0.68253	2.17542	-0.48169
O	1.64076	2.11344	-1.27348
C	0.19735	3.49227	0.05735
H	-0.07025	4.13935	-0.78724
H	-0.66584	3.38252	0.72246
H	1.02014	3.97064	0.60371
S	-3.02115	0.71068	0.85300

S-penicillamine persulfide

S	-2.12124	0.84164	-0.32880
C	-0.95142	-0.58845	0.04420
C	-1.37298	-1.80842	-0.76811
H	-1.34010	-1.60795	-1.84553
H	-0.71418	-2.65629	-0.54407
H	-2.39195	-2.10527	-0.49228
C	0.41182	-0.04157	-0.46411
H	0.31039	0.19132	-1.53164
C	-0.95632	-0.91335	1.53560
H	-1.96733	-1.20114	1.84736
H	-0.29600	-1.76803	1.73015
H	-0.63615	-0.07320	2.16374
C	1.51129	-1.11778	-0.40964
O	1.66914	-1.89411	-1.36344
N	2.26251	-1.16672	0.69250
H	2.08764	-0.49713	1.42878
C	3.32411	-2.14192	0.85727
H	4.07900	-2.03073	0.06858
H	3.79617	-1.97606	1.82916
H	2.92424	-3.16309	0.82136
N	0.79450	1.16874	0.23814
H	0.33731	1.41478	1.10509
C	1.79417	1.96185	-0.20392
O	2.41994	1.69156	-1.23981
C	2.10878	3.17384	0.62463
H	2.04200	4.06243	-0.01485
H	1.43525	3.28531	1.48063
H	3.14277	3.08914	0.98236
S	-3.99115	0.15797	0.25805
H	-4.33957	-0.49663	-0.88083

S-penicillamine persulfide S-COPh (**1**)

S	-0.12920	-1.30947	0.18498
S	1.75130	-0.93973	0.93921
C	2.71085	-0.46842	-0.53799
O	2.24333	-0.51216	-1.65240
C	-1.01028	0.35682	0.31055
C	-0.24361	1.41485	-0.47556
H	-0.16911	1.15858	-1.53778
H	-0.74836	2.38333	-0.37688
H	0.76490	1.53462	-0.06279
C	-2.37200	0.05191	-0.37318
H	-2.17167	-0.27028	-1.40237
C	-1.14576	0.77499	1.77235
H	-0.15173	0.89169	2.22008
H	-1.64964	1.74801	1.83104
H	-1.70604	0.05308	2.37818
C	-3.22873	1.32182	-0.53010
O	-3.09304	2.04213	-1.52982
N	-4.10171	1.59338	0.44235
H	-4.16242	0.96404	1.23045
C	-4.95604	2.76565	0.40263
H	-5.59685	2.74781	-0.48793
H	-5.58590	2.76334	1.29593
H	-4.35641	3.68447	0.38747
C	4.11739	-0.08533	-0.24487
C	4.50788	0.43347	0.99621
C	5.06332	-0.24472	-1.26777
C	5.83765	0.78941	1.21002
H	3.78006	0.59086	1.79151
C	6.39110	0.10230	-1.04400
H	4.75309	-0.65035	-2.22969
C	6.77865	0.62065	0.19411
H	6.13769	1.20416	2.17152
H	7.12711	-0.03020	-1.83632
H	7.81900	0.89663	0.36588
N	-3.08279	-1.01255	0.30934
H	-2.84262	-1.25122	1.26210
C	-4.13511	-1.64007	-0.26148
O	-4.52005	-1.34026	-1.40097
C	-4.80914	-2.70781	0.55118
H	-4.79421	-3.64300	-0.02182
H	-4.33127	-2.86651	1.52351
H	-5.85667	-2.41838	0.70201

S-penicillamine thiolate-anion

S	1.50947	-1.21745	1.47570

C	1.19001	-1.09308	-0.35365
C	0.90211	-2.48617	-0.92761
H	0.02524	-2.94593	-0.45471
H	0.72228	-2.42982	-2.01330
H	1.76256	-3.14490	-0.75417
C	-0.05090	-0.19395	-0.65141
H	-0.32887	-0.33030	-1.70402
C	2.39965	-0.50279	-1.08552
H	3.25917	-1.17731	-0.98466
H	2.18403	-0.38064	-2.15952
H	2.69139	0.47385	-0.67845
C	0.23992	1.30557	-0.50703
O	0.19572	2.06084	-1.49531
N	0.53575	1.73354	0.72549
H	0.80229	0.98733	1.37934
C	0.98233	3.09153	0.96767
H	0.20952	3.80924	0.66808
H	1.17414	3.20835	2.03828
H	1.90375	3.31809	0.41238
N	-1.16319	-0.61055	0.17925
H	-0.89179	-1.06573	1.04954
C	-2.44142	-0.28417	-0.05277
O	-2.78820	0.38009	-1.04913
C	-3.45088	-0.76909	0.95141
H	-4.18539	-1.39975	0.43472
H	-2.99276	-1.33815	1.76737
H	-3.98012	0.09933	1.36357

TS1 tetrahedral cysteine-thiolate-on-**1**
Imaginary frequency: -195.18 cm^{-1}

S	1.61300	-1.57486	0.28332
S	-0.17961	-1.64802	-0.70893
C	-1.46032	-1.12157	0.59249
O	-1.08075	-0.90229	1.74368
C	2.30219	0.16542	0.06114
C	1.61923	1.10087	1.05609
H	1.78402	0.78076	2.09141
H	2.00121	2.12365	0.93668
H	0.54236	1.11855	0.85347
C	3.80087	-0.02944	0.43384
H	3.85054	-0.51328	1.41921
C	2.08941	0.67354	-1.36115
H	1.01602	0.77431	-1.55566
H	2.53938	1.66820	-1.46738
H	2.50824	0.01381	-2.13037
C	4.51583	1.31698	0.64346

O	4.56323	1.82783	1.77260
N	5.06036	1.89337	-0.43046
H	4.98944	1.42240	-1.32151
C	5.75314	3.16575	-0.35224
H	6.61038	3.09978	0.32971
H	6.11135	3.42507	-1.35191
H	5.07937	3.95522	0.00376
C	-2.80135	-1.76567	0.32782
C	-3.21901	-2.17287	-0.94710
C	-3.65270	-1.96486	1.41899
C	-4.46647	-2.76241	-1.12405
H	-2.58580	-2.00725	-1.81808
C	-4.91059	-2.54564	1.23819
H	-3.32884	-1.66200	2.41305
C	-5.32100	-2.94659	-0.03176
H	-4.77991	-3.07126	-2.12091
H	-5.56802	-2.68643	2.09575
H	-6.30133	-3.40042	-0.17463
N	4.48821	-0.86276	-0.53415
H	4.00460	-1.15587	-1.37124
C	5.72946	-1.33916	-0.31072
O	6.35569	-1.04723	0.72041
C	6.31585	-2.22607	-1.37183
H	6.58377	-3.18639	-0.91421
H	5.62900	-2.39779	-2.20734
H	7.23575	-1.75919	-1.74548
S	-1.99850	1.01729	-0.38910
C	-3.16315	1.53730	0.91679
C	-4.57090	1.81698	0.38531
H	-3.22024	0.74329	1.67665
H	-2.81057	2.44195	1.42209
H	-5.27394	1.90713	1.22203
C	-4.68666	3.10815	-0.45064
N	-5.01904	0.67524	-0.45247
O	-4.22373	4.15286	0.06916
O	-5.26868	3.01868	-1.56532
H	-5.70453	1.01055	-1.13626
H	-5.40097	-0.09539	0.09994
H	-4.18534	0.33584	-0.96574

TS2 tetrahedral cysteine-thiolate-on-**1**
Imaginary frequency: -176.07 cm^{-1}

S	1.06394	1.19420	0.63921
S	-0.68554	0.85612	1.69027
C	-2.36270	0.61445	-0.18691
O	-1.75494	-0.01382	-1.07428

C	1.95888	-0.46085	0.54784
C	1.07710	-1.49082	-0.15109
H	0.87726	-1.21434	-1.19245
H	1.54843	-2.48183	-0.12872
H	0.12402	-1.55854	0.38405
C	3.21018	-0.14810	-0.31811
H	2.86532	0.21326	-1.29579
C	2.30558	-0.94837	1.95369
H	1.38312	-1.02678	2.54172
H	2.76398	-1.94499	1.91019
H	2.98748	-0.27344	2.48590
C	4.01463	-1.41882	-0.63387
O	3.75130	-2.08991	-1.64427
N	4.97991	-1.76000	0.22317
H	5.14306	-1.16676	1.02466
C	5.79294	-2.94659	0.03642
H	6.34125	-2.89681	-0.91297
H	6.51005	-3.00619	0.85944
H	5.17061	-3.85047	0.03661
C	-2.60510	2.08814	-0.34543
C	-3.33866	2.84518	0.57782
C	-2.08378	2.71640	-1.48207
C	-3.54394	4.20514	0.36622
H	-3.73268	2.38006	1.48009
C	-2.28253	4.08166	-1.68751
H	-1.52211	2.13108	-2.20781
C	-3.01351	4.83007	-0.76578
H	-4.11487	4.78348	1.09258
H	-1.86783	4.56022	-2.57479
H	-3.17219	5.89643	-0.92705
N	4.03787	0.87372	0.29763
H	3.78316	1.23178	1.20799
C	5.05533	1.46365	-0.35997
O	5.37099	1.11503	-1.50916
C	5.79110	2.55000	0.37136
H	6.84433	2.25678	0.46327
H	5.74489	3.46788	-0.22759
H	5.37765	2.74121	1.36729
S	-3.65833	-0.22894	0.79689
C	-2.89702	-1.85380	1.13393
C	-3.05821	-2.93156	0.06937
H	-1.83733	-1.68055	1.35813
H	-3.37755	-2.20485	2.05226
H	-2.74471	-3.88404	0.51296
C	-4.50935	-3.12277	-0.41907
N	-2.17676	-2.68199	-1.10293

O	-5.38044	-3.25590	0.47388
O	-4.69012	-3.16112	-1.66454
H	-2.68609	-2.99256	-1.93906
H	-1.29073	-3.18164	-1.02509
H	-1.96677	-1.65492	-1.18684

TS S1 cysteine-thiolate-on-cysteine-persulfide
Imaginary frequency: -187.48 cm^{-1}

S	-1.94738	2.87034	-0.80146
H	-0.93501	3.01702	-1.68809
S	-0.69999	1.52745	0.64347
C	-2.05154	0.28212	0.77913
C	-1.93013	-0.86550	-0.21292
H	-3.01032	0.79954	0.65853
H	-2.00782	-0.12767	1.78923
H	-0.99582	-1.40850	-0.04229
C	-3.09529	-1.86894	-0.06334
N	-1.92021	-0.37162	-1.62246
O	-3.81120	-2.06333	-1.08201
O	-3.21886	-2.40802	1.06144
H	-2.70217	-0.85669	-2.09329
H	-1.04567	-0.58910	-2.10042
S	0.84281	-0.05849	1.98432
C	1.69627	-0.78498	0.53581
C	3.16379	-0.34963	0.42747
H	1.16630	-0.47730	-0.37813
H	1.68001	-1.87909	0.58619
H	3.74828	-0.76813	1.25166
C	3.75147	-0.79466	-0.92095
N	3.23585	1.12978	0.53789
O	3.84580	0.08077	-1.82165
O	4.04703	-2.01221	-1.01993
H	2.53050	1.42610	1.23428
H	3.03361	1.54147	-0.37954
H	4.16084	1.44922	0.82798
H	-2.06893	0.64903	-1.66927

TS S1 cysteine-thiolate-on-penicillamine-persulfide
Imaginary frequency: -214.27 cm^{-1}

S	0.13427	1.83456	-0.43163
C	-1.42203	0.92553	-1.06005
C	-1.27551	0.70082	-2.56818
H	-0.45340	0.02256	-2.80928
H	-2.20708	0.27986	-2.96706
H	-1.10096	1.66325	-3.06424
C	-1.48838	-0.42473	-0.29399

H	-0.60015	-1.00629	-0.56807
C	-2.68956	1.76257	-0.85153
H	-2.55899	2.76593	-1.27281
H	-3.51408	1.28142	-1.39386
H	-2.98900	1.85921	0.19622
C	-2.67712	-1.28939	-0.73141
O	-2.58458	-2.01625	-1.73451
N	-3.79064	-1.21959	0.00282
H	-3.79353	-0.60921	0.80790
C	-4.98513	-1.97070	-0.33159
H	-4.77820	-3.04844	-0.33579
H	-5.74887	-1.75795	0.42101
H	-5.36508	-1.68190	-1.32003
N	-1.48149	-0.19212	1.13939
H	-1.44720	0.77102	1.46274
C	-1.12221	-1.15974	2.00531
O	-0.96776	-2.33661	1.63938
C	-0.91162	-0.74107	3.43285
H	0.15492	-0.85639	3.66724
H	-1.20958	0.29685	3.61589
H	-1.47900	-1.40985	4.09017
S	-0.96353	3.31692	1.10929
H	0.12917	3.25273	1.90396
S	1.76996	0.18850	-1.43674
C	2.09096	-0.67856	0.14514
C	3.52212	-0.48560	0.64222
H	1.40044	-0.28118	0.90172
H	1.90592	-1.75296	0.04648
H	3.61405	-0.88014	1.66107
C	4.59801	-1.18120	-0.21470
N	3.82568	0.96875	0.70362
O	4.40857	-2.39727	-0.46266
O	5.59348	-0.48906	-0.55785
H	4.83746	1.10537	0.61221
H	3.36558	1.41144	-0.11010
H	3.47682	1.40171	1.55983

TS S1 penicillamine-thiolate-on-cysteine-persulfide
Imaginary frequency: -167.17 cm^{-1}

S	-4.45328	-2.23276	-0.10093
H	-3.87405	-2.90217	0.92389
S	-2.47159	-1.34989	-0.89462
C	-3.05100	0.39374	-0.75006
C	-2.61921	1.07475	0.53763
H	-4.14221	0.39954	-0.84835
H	-2.62960	0.94683	-1.59080

H	-1.52595	1.08460	0.58926
C	-3.10954	2.53586	0.62270
N	-3.12192	0.34624	1.74113
O	-3.77305	2.85337	1.64664
O	-2.78856	3.28539	-0.32960
H	-3.58493	1.06062	2.32695
H	-2.36480	-0.09510	2.26471
S	-0.13661	-0.34398	-1.60869
H	-3.80365	-0.38199	1.49054
C	0.99243	-1.07610	-0.32151
C	1.05753	-2.59481	-0.50322
C	2.40660	-0.45972	-0.56702
C	0.48207	-0.76502	1.09134
H	1.46695	-2.86053	-1.48596
H	1.67651	-3.06485	0.27428
H	0.04630	-3.01270	-0.42611
H	2.74467	-0.78161	-1.56093
C	3.45913	-0.99966	0.40751
N	2.33528	0.99007	-0.52206
H	-0.54051	-1.14341	1.19582
H	1.10106	-1.26563	1.84832
H	0.47592	0.31093	1.30794
O	4.09869	-2.02948	0.13185
N	3.63819	-0.33493	1.55250
H	1.40125	1.38630	-0.52670
C	3.35811	1.77397	-0.91224
H	3.08420	0.49435	1.71348
C	4.57372	-0.77820	2.56742
O	4.47728	1.30402	-1.18029
C	3.08523	3.25038	-0.98343
H	5.59510	-0.81457	2.16722
H	4.54320	-0.06883	3.39889
H	4.30623	-1.77621	2.93821
H	3.33759	3.60490	-1.99037
H	2.04213	3.49615	-0.75829
H	3.74206	3.76222	-0.26862

TS S2 cysteine-thiolate-on-cysteine-persulfide
Imaginary frequency: -148.31 cm^{-1}

S	-1.68436	1.77713	0.25210
S	0.10250	0.26049	-0.18810
H	-0.10204	-0.27804	1.02954
S	1.90283	-1.40542	-0.34861
C	2.96007	-0.89963	1.06022
C	3.92553	0.23811	0.74761
H	2.32711	-0.60965	1.91074

H	3.55661	-1.76125	1.38008
H	4.50460	0.47668	1.64800
C	4.93849	-0.08826	-0.36961
N	3.19062	1.47876	0.35852
O	5.61231	-1.13537	-0.22115
O	5.02955	0.74079	-1.31563
H	3.67827	1.85213	-0.47104
H	2.21316	1.27015	0.10164
H	3.18515	2.17611	1.10261
C	-3.07177	0.90921	-0.56860
C	-4.03089	0.22459	0.40924
H	-3.65564	1.62924	-1.15200
H	-4.53967	0.96823	1.02994
C	-5.06641	-0.61574	-0.35745
N	-3.26158	-0.65289	1.33019
O	-5.99125	0.02823	-0.91308
O	-4.88224	-1.85992	-0.39332
H	-3.83285	-0.96430	2.11747
H	-2.94283	-1.48730	0.82780
H	-2.45007	-0.13243	1.68799
H	-2.65784	0.16475	-1.26307

TS S1 cysteine-thiolate-on-**1**
Imaginary frequency: -217.64 cm^{-1}

S	-0.59830	0.06900	-1.58363
S	1.36765	-1.21583	-1.62518
C	2.37559	-0.22166	-0.58756
O	2.06081	0.89735	-0.17783
C	-1.84653	-1.29120	-1.10736
C	-1.31317	-2.69520	-1.39772
H	-0.42309	-2.95551	-0.81943
H	-2.10240	-3.41883	-1.14990
H	-1.08650	-2.80685	-2.46501
C	-2.19555	-1.11716	0.40893
H	-2.40225	-0.05748	0.58760
C	-3.09942	-1.08952	-1.96995
H	-2.81532	-1.05925	-3.02835
H	-3.77832	-1.93970	-1.82700
H	-3.63146	-0.16887	-1.71853
C	-1.07072	-1.59620	1.33557
O	-1.09703	-2.73396	1.83201
N	-0.08454	-0.73061	1.59134
H	-0.03771	0.11023	1.02808
C	1.10125	-1.13511	2.32368
H	1.62655	-1.95145	1.80951
H	1.76634	-0.27224	2.40763

H	0.83050	-1.47252	3.33036
C	3.71121	-0.79198	-0.21953
C	3.93886	-2.17096	-0.13483
C	4.74912	0.10039	0.08035
C	5.19073	-2.65015	0.24483
H	3.13199	-2.87203	-0.34213
C	6.00337	-0.38178	0.44470
H	4.57155	1.17301	0.01755
C	6.22537	-1.75778	0.52956
H	5.35786	-3.72414	0.32209
H	6.81004	0.31691	0.66524
H	7.20554	-2.13487	0.82169
N	-3.38943	-1.85510	0.76448
H	-3.29886	-2.85725	0.86257
C	-4.60102	-1.30331	0.96091
O	-4.80224	-0.07933	0.89520
C	-5.72036	-2.26115	1.26368
H	-5.37907	-3.29706	1.36236
H	-6.21460	-1.94551	2.19025
H	-6.45394	-2.19869	0.44944
S	-2.26449	2.03023	-1.36353
C	-1.46536	2.75402	0.11399
C	-0.34829	3.75061	-0.20681
H	-2.21590	3.28398	0.70944
H	-1.06022	1.94989	0.74344
H	-0.76917	4.63370	-0.70025
C	0.39172	4.20198	1.06239
N	0.60467	3.14191	-1.17104
O	-0.30456	4.83191	1.90089
O	1.61083	3.91066	1.16956
H	1.32220	3.80945	-1.45506
H	1.07797	2.31029	-0.76906
H	0.07236	2.84109	-1.99625

TS S2 cysteine-thiolate-on-**1**
Imaginary frequency: -140.94 cm^{-1}

S	0.94253	0.42428	0.38028
S	-1.12388	-0.54976	-0.61764
C	-1.40015	1.13912	-1.28241
O	-1.00726	1.43759	-2.38971
C	2.32102	-0.24973	-0.67831
C	2.16313	0.24524	-2.11624
H	2.19964	1.34029	-2.17035
H	2.95269	-0.16557	-2.76011
H	1.19917	-0.09094	-2.51376
C	3.64078	0.31899	-0.07222

H	3.59897	1.41337	-0.14665
C	2.29331	-1.78207	-0.66494
H	1.31584	-2.13207	-1.01638
H	3.05648	-2.19018	-1.34152
H	2.45821	-2.19716	0.33735
C	4.87771	-0.08435	-0.88642
O	5.27530	0.63683	-1.81676
N	5.48132	-1.23180	-0.56507
H	5.10818	-1.77168	0.20275
C	6.63765	-1.72540	-1.28773
H	7.46751	-1.00933	-1.23043
H	6.95072	-2.66971	-0.83431
H	6.39482	-1.89828	-2.34405
C	-2.19888	2.07783	-0.44031
C	-2.96896	3.04793	-1.09446
C	-2.22414	1.99793	0.95623
C	-3.77306	3.91314	-0.35730
H	-2.95362	3.10433	-2.18196
C	-3.01262	2.87817	1.69197
H	-1.61586	1.26010	1.47547
C	-3.79537	3.82984	1.03613
H	-4.38605	4.65327	-0.87085
H	-3.01992	2.81732	2.77962
H	-4.42421	4.50863	1.61207
N	3.77430	-0.06553	1.32190
H	2.98942	-0.53763	1.75329
C	4.72373	0.45608	2.12188
O	5.60883	1.20590	1.67619
C	4.67593	0.06679	3.57256
H	5.59328	-0.48506	3.81401
H	4.65925	0.97947	4.18058
H	3.80626	-0.55278	3.81580
S	-3.19203	-1.13466	-1.56321
C	-4.46132	-0.60851	-0.34772
C	-4.51402	-1.40961	0.94661
H	-4.34282	0.45684	-0.11244
H	-5.42930	-0.72293	-0.84798
H	-5.37928	-1.07345	1.53099
C	-4.66471	-2.93089	0.74902
N	-3.30958	-1.14954	1.78916
O	-5.61487	-3.30049	0.01805
O	-3.85289	-3.67047	1.36600
H	-3.13165	-1.98674	2.35626
H	-2.47420	-0.98535	1.20267
H	-3.43499	-0.33229	2.38902

TS S2 cysteine-thiolate-on-penicillamine-persulfide
Imaginary frequency: -150.40 cm^{-1}

S	0.63550	0.72296	-0.77315
C	1.83802	-0.58807	-0.21456
C	1.59921	-1.87530	-1.00698
H	1.75846	-1.71789	-2.08112
H	2.26555	-2.68039	-0.66721
H	0.56686	-2.21330	-0.85508
C	3.26582	-0.04220	-0.52954
H	3.34729	0.07900	-1.61779
C	1.65265	-0.87191	1.28028
H	0.60806	-1.14405	1.46948
H	2.28313	-1.71267	1.60136
H	1.89177	0.00001	1.90304
C	4.36826	-1.04191	-0.15763
O	4.75641	-1.88281	-0.98674
N	4.86674	-0.97813	1.08013
H	4.50364	-0.27268	1.70532
C	5.88316	-1.89689	1.55431
H	6.78862	-1.82779	0.93781
H	6.13393	-1.63261	2.58507
H	5.51907	-2.93217	1.52842
N	3.47254	1.24108	0.11813
H	2.65897	1.67052	0.54358
C	4.53700	2.02049	-0.15050
O	5.47377	1.62319	-0.86455
C	4.54743	3.38654	0.47595
H	3.63223	3.59761	1.03917
H	5.41214	3.45522	1.14826
H	4.67292	4.13474	-0.31634
S	-1.62654	-0.21221	-0.18125
H	-1.44964	-0.95622	-1.28764
S	-3.72188	-1.20459	0.08732
C	-4.75021	-0.27512	-1.11377
C	-5.66362	0.74944	-0.45030
H	-4.08785	0.23078	-1.82738
H	-5.37740	-0.97491	-1.67532
H	-6.16935	1.34133	-1.22310
C	-6.76286	0.14496	0.44921
N	-4.85818	1.69890	0.36361
O	-7.42512	-0.80166	-0.04004
O	-6.92977	0.68030	1.57710
H	-5.46511	2.10828	1.08234
H	-4.11780	1.17359	0.84766
H	-4.42790	2.42960	-0.20516

REFERENCES CITED

[1] Olson, K. R.; Straub, K. D., The Role of Hydrogen Sulfide in Evolution and the Evolution of Hydrogen Sulfide in Metabolism and Signaling. *Physiology* **2016,** *31* (1), 60-72.

[2] Frigaard, N.-U.; Bryant, D. A., Seeing green bacteria in a new light: genomics-enabled studies of the photosynthetic apparatus in green sulfur bacteria and filamentous anoxygenic phototrophic bacteria. *Archives of Microbiology* **2004,** *182* (4), 265-276.

[3] Gregersen, L. H.; Bryant, D. A.; Frigaard, N. U., Mechanisms and evolution of oxidative sulfur metabolism in green sulfur bacteria. *Frontiers in Microbiology* **2011,** *2*, 116.

[4] Xiong, J.; Fischer, W. M.; Inoue, K.; Nakahara, M.; Bauer, C. E., Molecular Evidence for the Early Evolution of Photosynthesis. *Science* **2000,** *289* (5485), 1724-1730.

[5] Shipp, J. A.; Gould, I. R.; Shock, E. L.; Williams, L. B.; Hartnett, H. E., Sphalerite is a geochemical catalyst for carbon−hydrogen bond activation. *Proceedings of the National Academy of Sciences* **2014,** *111* (32), 11642-11645.

[6] Rickard, D.; Luther, G. W., Chemistry of Iron Sulfides. *Chemical Reviews* **2007,** *107* (2), 514-562.

[7] Drobner, E.; Huber, H.; Wächtershäuser, G.; Rose, D.; Stetter, K. O., Pyrite formation linked with hydrogen evolution under anaerobic conditions. *Nature* **1990,** *346* (6286), 742-744.

[8] Nitschke, W.; McGlynn, S. E.; Milner-White, E. J.; Russell, M. J., On the antiquity of metalloenzymes and their substrates in bioenergetics. *Biochimica et Biophysica Acta (BBA) - Bioenergetics* **2013,** *1827* (8), 871-881.

[9] Jorgensen, B. B.; Findlay, A. J.; Pellerin, A., The Biogeochemical Sulfur Cycle of Marine Sediments. *Frontiers in Microbiology* **2019,** *10*, 849.

[10] Habeeb, O. A.; Kanthasamy, R.; Ali, G. A. M.; Sethupathi, S.; Yunus, R. B. M., Hydrogen sulfide emission sources, regulations, and removal techniques: a review. *Reviews in Chemical Engineering* **2018,** *34* (6), 837-854.

[11] Guidotti, T. L., Hydrogen Sulfide: Advances in Understanding Human Toxicity. *International Journal of Toxicology* **2010,** *29* (6), 569-581.

[12] Zhang, L.; De Schryver, P.; De Gusseme, B.; De Muynck, W.; Boon, N.; Verstraete, W., Chemical and biological technologies for hydrogen sulfide emission control in sewer systems: A review. *Water Research* **2008,** *42* (1), 1-12.

[13] Petersen, L., The effect of inhibitors on the oxygen kinetics of cytochrome c oxidase. *Biochim Biophys Acta* **1977,** *460* (2), 299-307.

[14] Hill, B. C.; Woon, T. C.; Nicholls, P.; Peterson, J.; Greenwood, C.; Thomson, A. J., Interactions of sulphide and other ligands with cytochrome c oxidase. An electron-paramagnetic-resonance study. *Biochemical Journal* **1984,** *224* (2), 591-600.

[15] Goubern, M.; Andriamihaja, M.; Nübel, T.; Blachier, F.; Bouillaud, F., Sulfide, the first inorganic substrate for human cells. *The FASEB Journal* **2007,** *21* (8), 1699-1706.

[16] Módis, K.; Coletta, C.; Erdélyi, K.; Papapetropoulos, A.; Szabo, C., Intramitochondrial hydrogen sulfide production by 3-mercaptopyruvate sulfurtransferase maintains mitochondrial electron flow and supports cellular bioenergetics. *The FASEB Journal* **2013,** *27* (2), 601-611.

[17] Meister, A.; Fraser, P. E.; Tice, S. V., Enzymatic Desulfuration of β-Mercaptopyruvate to Pyruvate. *Journal of Biological Chemistry* **1954,** *206* (2), 561-575.

[18] Gregory, J. D.; Robbins, P. W., Metabolism of Sulfur Compounds (Sulfate Metabolism). *Annual Review of Biochemistry* **1960,** *29* (1), 347-364.

[19] Costantino, M.; Izzo, V.; Conti, V.; Manzo, V.; Guida, A.; Filippelli, A., Sulphate mineral waters: A medical resource in several disorders. *Journal of Traditional and Complementary Medicine* **2020,** *10* (4), 320-326.

[20] Carbajo, J. M.; Maraver, F., Sulphurous Mineral Waters: New Applications for Health. *Evidence-Based Complementary and Alternative Medicine* **2017,** *2017*, 8034084.

[21] Cao, X.; Cao, L.; Zhang, W.; Lu, R.; Bian, J.-S.; Nie, X., Therapeutic potential of sulfur-containing natural products in inflammatory diseases. *Pharmacology & Therapeutics* **2020,** *216*, 107687.

[22] Ruhee, R. T.; Roberts, L. A.; Ma, S.; Suzuki, K., Organosulfur Compounds: A Review of Their Anti-inflammatory Effects in Human Health. *Frontiers in Nutrition* **2020,** *7*, 64.

[23] Miekus, N.; Marszalek, K.; Podlacha, M.; Iqbal, A.; Puchalski, C.; Swiergiel, A. H., Health Benefits of Plant-Derived Sulfur Compounds, Glucosinolates, and Organosulfur Compounds. *Molecules* **2020,** *25* (17), 3804.

[24] Abe, K.; Kimura, H., The possible role of hydrogen sulfide as an endogenous neuromodulator. *The Journal of Neuroscience* **1996,** *16* (3), 1066-1071.

[25] Wang, R., Two's company, three's a crowd: can H_2S be the third endogenous gaseous transmitter? *The FASEB Journal* **2002,** *16* (13), 1792-1798.

[26] Wu, L. Y.; Wang, R., Carbon monoxide: Endogenous production, physiological functions, and pharmacological applications. *Pharmacological Reviews* **2005,** *57* (4), 585-630.

[27] Wang, R., Physiological Implications of Hydrogen Sulfide: A Whiff Exploration that Blossomed. *Physiological Reviews* **2012,** *92* (2), 791-896.

[28] May, P. M.; Batka, D.; Hefter, G.; Königsberger, E.; Rowland, D., Goodbye to S^{2-} in aqueous solution. *Chemical Communications* **2018,** *54* (16), 1980-1983.

[29] Filipovic, M. R.; Zivanovic, J.; Alvarez, B.; Banerjee, R., Chemical Biology of H_2S Signaling through Persulfidation. *Chemical Reviews* **2018,** *118* (3), 1253-1337.

[30] Kolluru, G. K.; Shen, X. G.; Kevil, C. G., Reactive Sulfur Species A New Redox Player in Cardiovascular Pathophysiology. *Arteriosclerosis Thrombosis and Vascular Biology* **2020,** *40* (4), 874-884.

[31] Pedre, B.; Barayeu, U.; Ezerina, D.; Dick, T. P., The mechanism of action of N-acetylcysteine (NAC): The emerging role of H_2S and sulfane sulfur species. *Pharmacology & Therapeutics* **2021,** *228*, 107916.

[32] Stipanuk, M. H.; Beck, P. W., Characterization of the enzymic capacity for cysteine desulphhydration in liver and kidney of the rat. *Biochemical Journal* **1982,** *206* (2), 267-277.

[33] Griffith, O. W., Mammalian sulfur amino acid metabolism: An overview. In *Methods in Enzymology*, Academic Press: 1987; Vol. 143, pp 366-376.

[34] Chiku, T.; Padovani, D.; Zhu, W.; Singh, S.; Vitvitsky, V.; Banerjee, R., H_2S Biogenesis by Human Cystathionine γ-Lyase Leads to the Novel Sulfur Metabolites Lanthionine and Homolanthionine and Is Responsive to the Grade of Hyperhomocysteinemia. *Journal of Biological Chemistry* **2009,** *284* (17), 11601-11612.

[35] Singh, S.; Padovani, D.; Leslie, R. A.; Chiku, T.; Banerjee, R., Relative Contributions of Cystathionine β-Synthase and γ-Cystathionase to H_2S Biogenesis via Alternative Trans-sulfuration Reactions. *Journal of Biological Chemistry* **2009,** *284* (33), 22457-22466.

[36] Shibuya, N.; Tanaka, M.; Yoshida, M.; Ogasawara, Y.; Togawa, T.; Ishii, K.; Kimura, H., 3-Mercaptopyruvate Sulfurtransferase Produces Hydrogen Sulfide and Bound Sulfane Sulfur in the Brain. *Antioxidants & Redox Signaling* **2009,** *11* (4), 703-714.

[37] Yadav, P. K.; Yamada, K.; Chiku, T.; Koutmos, M.; Banerjee, R., Structure and Kinetic Analysis of H_2S Production by Human Mercaptopyruvate Sulfurtransferase. *Journal of Biological Chemistry* **2013,** *288* (27), 20002-20013.

[38] Shibuya, N.; Koike, S.; Tanaka, M.; Ishigami-Yuasa, M.; Kimura, Y.; Ogasawara, Y.; Fukui, K.; Nagahara, N.; Kimura, H., A novel pathway for the production of hydrogen sulfide from D-cysteine in mammalian cells. *Nature Communications* **2013,** *4* (1), 1366.

[39] Hughes, M. N.; Centelles, M. N.; Moore, K. P., Making and working with hydrogen sulfide: The chemistry and generation of hydrogen sulfide in vitro and its measurement in vivo: A review. *Free Radical Biology and Medicine* **2009,** *47* (10), 1346-1353.

[40] Vojtovič, D.; Luhová, L.; Petřivalský, M., Something smells bad to plant pathogens: Production of hydrogen sulfide in plants and its role in plant defence responses. *Journal of Advanced Research* **2021,** *27*, 199-209.

[41] Tomasova, L.; Konopelski, P.; Ufnal, M., Gut Bacteria and Hydrogen Sulfide: The New Old Players in Circulatory System Homeostasis. *Molecules* **2016,** *21* (11), 1558.

[42] Blachier, F.; Beaumont, M.; Kim, E., Cysteine-derived hydrogen sulfide and gut health: a matter of endogenous or bacterial origin. *Current Opinion in Clinical Nutrition & Metabolic Care* **2019,** *22* (1).

[43] Yang, J.; Minkler, P.; Grove, D.; Wang, R.; Willard, B.; Dweik, R.; Hine, C., Non-enzymatic hydrogen sulfide production from cysteine in blood is catalyzed by iron and vitamin B6. *Communications Biology* **2019,** *2* (1), 194.

[44] Olson, K. R.; DeLeon, E. R.; Gao, Y.; Hurley, K.; Sadauskas, V.; Batz, C.; Stoy, G. F., Thiosulfate: a readily accessible source of hydrogen sulfide in oxygen sensing. *American Journal of Physiology-Regulatory, Integrative and Comparative Physiology* **2013,** *305* (6), R592-R603.

[45] Szabó, C.; Papapetropoulos, A., Hydrogen sulphide and angiogenesis: mechanisms and applications. *British Journal of Pharmacology* **2011,** *164* (3), 853-865.

[46] Whiteman, M.; Winyard, P. G., Hydrogen sulfide and inflammation: the good, the bad, the ugly and the promising. *Expert Review of Clinical Pharmacology* **2011,** *4* (1), 13-32.

[47] Zhao, W.; Zhang, J.; Lu, Y.; Wang, R., The vasorelaxant effect of H_2S as a novel endogenous gaseous KATP channel opener. *The EMBO Journal* **2001,** *20* (21), 6008-6016.

[48] Chen, T.; Tian, M.; Han, Y., Hydrogen sulfide: a multi-tasking signal molecule in the regulation of oxidative stress responses. *Journal of Experimental Botany* **2020,** *71* (10), 2862-2869.

[49] Cirino, G.; Szabo, C.; Papapetropoulos, A., Physiological roles of hydrogen sulfide in mammalian cells, tissues, and organs. *Physiological Reviews* **2023,** *103* (1), 31-276.

[50] Yang, G.; Wu, L.; Jiang, B.; Yang, W.; Qi, J.; Cao, K.; Meng, Q.; Mustafa, A. K.; Mu, W.; Zhang, S.; Snyder, S. H.; Wang, R., H_2S as a Physiologic Vasorelaxant: Hypertension in Mice with Deletion of Cystathionine γ-Lyase. *Science* **2008,** *322* (5901), 587-590.

[51] Tabassum, R.; Jeong, N. Y.; Jung, J., Therapeutic importance of hydrogen sulfide in age-associated neurodegenerative diseases. *Neural Regeneration Research* **2020,** *15* (4).

[52] Tripathi, S. J.; Chakraborty, S.; Miller, E.; Pieper, A. A.; Paul, B. D., Hydrogen sulfide signalling in neurodegenerative diseases. *British Journal of Pharmacology* **2023**, 1-18.

[53] Gheibi, S.; Jeddi, S.; Kashfi, K.; Ghasemi, A., Regulation of vascular tone homeostasis by NO and H_2S: Implications in hypertension. *Biochemical Pharmacology* **2018,** *149*, 42-59.

[54] Meng, G.; Ma, Y.; Xie, L.; Ferro, A.; Ji, Y., Emerging role of hydrogen sulfide in hypertension and related cardiovascular diseases. *British Journal of Pharmacology* **2015,** *172* (23), 5501-5511.

[55] Zhao, H.; Liu, H.; Yang, Y.; Wang, H., The Role of H_2S Regulating NLRP3 Inflammasome in Diabetes. *International Journal of Molecular Sciences* **2022,** *23* (9), 4818.

[56] Szabo, C., Roles of Hydrogen Sulfide in the Pathogenesis of Diabetes Mellitus and Its Complications. *Antioxidants & Redox Signaling* **2012,** *17* (1), 68-80.

[57] Mani, S.; Cao, W.; Wu, L.; Wang, R., Hydrogen sulfide and the liver. *Nitric Oxide* **2014,** *41*, 62-71.

[58] Sun, H.-J.; Wu, Z.-Y.; Nie, X.-W.; Wang, X.-Y.; Bian, J.-S., Implications of hydrogen sulfide in liver pathophysiology: Mechanistic insights and therapeutic potential. *Journal of Advanced Research* **2021,** *27*, 127-135.

[59] Hu, L.-F.; Lu, M.; Tiong, C. X.; Dawe, G. S.; Hu, G.; Bian, J.-S., Neuroprotective effects of hydrogen sulfide on Parkinson's disease rat models. *Aging Cell* **2010,** *9* (2), 135-146.

[60] Kida, K.; Yamada, M.; Tokuda, K.; Marutani, E.; Kakinohana, M.; Kaneki, M.; Ichinose, F., Inhaled Hydrogen Sulfide Prevents Neurodegeneration and Movement Disorder in a Mouse Model of Parkinson's Disease. *Antioxidants & Redox Signaling* **2011,** *15* (2), 343-352.

[61] Ono, K.; Akaike, T.; Sawa, T.; Kumagai, Y.; Wink, D. A.; Tantillo, D. J.; Hobbs, A. J.; Nagy, P.; Xian, M.; Lin, J.; Fukuto, J. M., Redox chemistry and chemical biology of H_2S, hydropersulfides, and derived species: Implications of their possible biological activity and utility. *Free Radical Biology and Medicine* **2014,** *77*, 82-94.

[62] Paul, B. D.; Snyder, S. H., H_2S signalling through protein sulfhydration and beyond. *Nature Reviews Molecular Cell Biology* **2012,** *13* (8), 499-507.

[63] Gupta, R.; Sahu, M.; Tripathi, R.; Ambasta, R. K.; Kumar, P., Protein S-sulfhydration: Unraveling the prospective of hydrogen sulfide in the brain, vasculature and neurological manifestations. *Ageing Research Reviews* **2022,** *76*, 101579.

[64] Ibrahim, H.; Serag, A.; Farag, M. A., Emerging analytical tools for the detection of the third gasotransmitter H_2S, a comprehensive review. *Journal of Advanced Research* **2021,** *27*, 137-153.

[65] Xu, T.; Scafa, N.; Xu, L.-P.; Zhou, S.; Abdullah Al-Ghanem, K.; Mahboob, S.; Fugetsu, B.; Zhang, X., Electrochemical hydrogen sulfide biosensors. *Analyst* **2016,** *141* (4), 1185-1195.

[66] Lin, V. S.; Chen, W.; Xian, M.; Chang, C. J., Chemical probes for molecular imaging and detection of hydrogen sulfide and reactive sulfur species in biological systems. *Chemical Society Reviews* **2015,** *44* (14), 4596-4618.

[67] Li, H.; Fang, Y.; Yan, J.; Ren, X.; Zheng, C.; Wu, B.; Wang, S.; Li, Z.; Hua, H.; Wang, P.; Li, D., Small-molecule fluorescent probes for H_2S detection: Advances and perspectives. *TrAC Trends in Analytical Chemistry* **2021,** *134*, 116117.

[68] Smith, H. M.; Pluth, M. D., Advances and Opportunities in H2S Measurement in Chemical Biology. *JACS Au* **2023,** *3* (10), 2677-2691.

[69] Sawa, T.; Takata, T.; Matsunaga, T.; Ihara, H.; Motohashi, H.; Akaike, T., Chemical Biology of Reactive Sulfur Species: Hydrolysis-Driven Equilibrium of Polysulfides as a Determinant of Physiological Functions. *Antioxidants & Redox Signaling* **2022,** *36* (4-6), 327-336.

[70] Elise, R. H.; Anja, G.; Anna, K. W.; Daniel, D. R. A.; Mathilde, A.; Nirthika, S. R.; Mark, E. W.; Matthew, W.; Nini, S.; Ulf, S., Involvement of Potassium Channels and Calcium-Independent Mechanisms in Hydrogen Sulfide–Induced Relaxation of Rat Mesenteric Small Arteries. *Journal of Pharmacology and Experimental Therapeutics* **2016,** *356* (1), 53-63.

[71] Vitvitsky, V.; Banerjee, R., Chapter Seven - H_2S Analysis in Biological Samples Using Gas Chromatography with Sulfur Chemiluminescence Detection. In *Methods in Enzymology*, Cadenas, E.; Packer, L., Eds. Academic Press: 2015; Vol. 554, pp 111-123.

[72] Gomes, A.; Fernandes, E.; Lima, J. L. F. C., Fluorescence probes used for detection of reactive oxygen species. *Journal of Biochemical and Biophysical Methods* **2005,** *65* (2), 45-80.

[73] Wu, L.; Sedgwick, A. C.; Sun, X.; Bull, S. D.; He, X.-P.; James, T. D., Reaction-Based Fluorescent Probes for the Detection and Imaging of Reactive Oxygen, Nitrogen, and Sulfur Species. *Accounts of Chemical Research* **2019,** *52* (9), 2582-2597.

[74] Nagano, T.; Yoshimura, T., Bioimaging of Nitric Oxide. *Chemical Reviews* **2002,** *102* (4), 1235-1270.

[75] Pluth, M. D.; Tomat, E.; Lippard, S. J., Biochemistry of Mobile Zinc and Nitric Oxide Revealed by Fluorescent Sensors. *Annual Review of Biochemistry* **2011,** *80* (1), 333-355.

[76] Miller, E. W.; Chang, C. J., Fluorescent probes for nitric oxide and hydrogen peroxide in cell signaling. *Current Opinion in Chemical Biology* **2007,** *11* (6), 620-625.

[77] Geng, Y.; Wang, Z.; Zhou, J.; Zhu, M.; Liu, J.; James, T. D., Recent progress in the development of fluorescent probes for imaging pathological oxidative stress. *Chemical Society Reviews* **2023,** *52* (11), 3873-3926.

[78] Messina, M. S.; Quargnali, G.; Chang, C. J., Activity-Based Sensing for Chemistry-Enabled Biology: Illuminating Principles, Probes, and Prospects for Boronate Reagents for Studying Hydrogen Peroxide. *ACS Bio & Med Chem Au* **2022,** *2* (6), 548-564.

[79] Lutz, J.-F.; Zarafshani, Z., Efficient construction of therapeutics, bioconjugates, biomaterials and bioactive surfaces using azide–alkyne "click" chemistry. *Advanced Drug Delivery Reviews* **2008,** *60* (9), 958-970.

[80] Presolski, S. I.; Hong, V. P.; Finn, M. G., Copper-Catalyzed Azide–Alkyne Click Chemistry for Bioconjugation. *Current Protocols in Chemical Biology* **2011,** *3* (4), 153-162.

[81] Köhn, M.; Breinbauer, R., The Staudinger Ligation—A Gift to Chemical Biology. *Angewandte Chemie International Edition* **2004,** *43* (24), 3106-3116.

[82] Schilling, C. I.; Jung, N.; Biskup, M.; Schepers, U.; Bräse, S., Bioconjugation viaazide–Staudinger ligation: an overview. *Chemical Society Reviews* **2011,** *40* (9), 4840-4871.

[83] Thiele, J., Ueber Nitro- und Amidoguanidin. *Justus Liebigs Annalen der Chemie* **1892,** *270* (1-2), 1-63.

[84] Lieber, E.; Levering, D. R., The Reaction of Nitrous Acid with Diaminoguanidine in Acetic Acid Media. Isolation and Structure Proof of Reaction Products. *Journal of the American Chemical Society* **1951,** *73* (3), 1313-1317.

[85] Adachi, T.; Yamada, Y.; Inoue, I.; Saneyoshi, M., An Alternative Method for the Selective Reduction of Unsaturated Nucleoside Azides to the Amines. *Synthesis* **1977,** *1977* (01), 45-46.

[86] Henthorn, H. A.; Pluth, M. D., Mechanistic Insights into the H_2S-Mediated Reduction of Aryl Azides Commonly Used in H_2S Detection. *Journal of the American Chemical Society* **2015,** *137* (48), 15330-15336.

[87] O'Connor, L. J.; Mistry, I. N.; Collins, S. L.; Folkes, L. K.; Brown, G.; Conway, S. J.; Hammond, E. M., CYP450 Enzymes Effect Oxygen-Dependent Reduction of Azide-Based Fluorogenic Dyes. *Acs Central Science* **2017,** *3* (1), 20-30.

[88] Lippert, A. R.; New, E. J.; Chang, C. J., Reaction-Based Fluorescent Probes for Selective Imaging of Hydrogen Sulfide in Living Cells. *Journal of the American Chemical Society* **2011,** *133* (26), 10078-10080.

[89] Peng, H.; Cheng, Y.; Dai, C.; King, A. L.; Predmore, B. L.; Lefer, D. J.; Wang, B., A Fluorescent Probe for Fast and Quantitative Detection of Hydrogen Sulfide in Blood. *Angewandte Chemie International Edition* **2011,** *50* (41), 9672-9675.

[90] Montoya, L. A.; Pluth, M. D., Selective turn-on fluorescent probes for imaging hydrogen sulfide in living cells. *Chemical Communications* **2012,** *48* (39), 4767-4769.

[91] Ding, D.; Li, J.; Xu, L.; Wang, J.; Tan, D.; Lin, W., Development of an activatable hydrogen sulfide-specific two-photon fluorescent probe for bioimaging in an air pouch inflammation model. *Journal of Materials Chemistry B* **2022,** *10* (24), 4568-4574.

[92] Tian, H.; Qian, J.; Bai, H.; Sun, Q.; Zhang, L.; Zhang, W., Micelle-induced multiple performance improvement of fluorescent probes for H_2S detection. *Analytica Chimica Acta* **2013,** *768*, 136-142.

[93] Guo, Y.; Zeng, T.; Shi, G.; Cai, Y.; Xie, R., Highly selective naphthalimide-based fluorescent probe for direct hydrogen sulfide detection in the environment. *RSC Advances* **2014,** *4* (63), 33626-33628.

[94] Xu, Q.; He, L.; Wei, H.; Lin, W., An ICT-Based Hydrogen Sulfide Sensor with Good Water Solubility for Fluorescence Imaging in Living Cells. *Journal of Fluorescence* **2018,** *28* (1), 5-11.

[95] Yan, Y.; Zhu, S.; Chen, Z.; Ji, Y., A Novel Turn-On the Fluorescence Sensor for H_2S and its Applications in Bioimaging. *Journal of Applied Spectroscopy* **2022,** *89* (1), 191-200.

[96] Choi, S.-A.; Park, C. S.; Kwon, O. S.; Giong, H.-K.; Lee, J.-S.; Ha, T. H.; Lee, C.-S., Structural effects of naphthalimide-based fluorescent sensor for hydrogen sulfide and imaging in live zebrafish. *Scientific Reports* **2016,** *6* (1), 26203.

[97] Feng, G.; Li, Z.; Zhang, X.; Huang, H.; Zhai, P.; Jiang, Y.; Fan, M.; Xu, Z.; Wang, X.; Ying, M.; Yang, C.; Dong, B.; Yong, K.-T.; Shao, Y.; Xu, G., A dynamic thiol-disulfide exchange assisted high cell-penetrating fluorescent probe for intracellular H_2S detection. *Dyes and Pigments* **2022,** *207*, 110740.

[98] Jihua, Z.; Hao, Z.; Min, L.; Jingjiang, L.; Yuan, L.; Zhengjun, Q.; Xicun, W., An Intramolecular Charge Transfer (ICT)-Based Fluorescent Probe of Hydrogen Sulphide under pH Control Strategy. *Chinese Journal of Organic Chemistry* **2020,** *40* (4), 1043-1049.

[99] Su, S., Design and application of a fluorescent probe for rapid detection of H_2S. *Journal of Physics: Conference Series* **2021,** *2009* (1), 012077.

[100] Jothi, D.; Iyer, S. K., A highly sensitive naphthalimide based fluorescent "turn-on" sensor for H_2S and its bio-imaging applications. *Journal of Photochemistry and Photobiology A: Chemistry* **2022,** *427*, 113802.

[101] Yoo, S. Y.; Gopala, L.; Kang, C.; Lee, M. H., Hydrogen sulfide-activatable fluorescence turn-on azide-containing naphthalimide derivative. *Bulletin of the Korean Chemical Society* **2022,** *43* (11), 1231-1235.

[102] Ghosh, A.; Das, S.; Sarkar, H. S.; Kundu, S.; Sahoo, P., Consumption of H_2S from Our Daily Diet: Determination by a Simple Chemosensing Method. *ACS Omega* **2018,** *3* (9), 11617-11623.

[103] Zhang, Y.; Zhang, L., A novel "turn-on" fluorescent probe based on hydroxy functionalized naphthalimide as a logic platform for visual recognition of H_2S in environment and living cells. *Spectrochimica Acta Part A: Molecular and Biomolecular Spectroscopy* **2020,** *235*, 118331.

[104] Zhu, J.; Miao, C.; Wang, X., An ICT-PET dual-controlled strategy for improving molecular probe sensitivity: Application to photoactivatable fluorescence imaging and H_2S detection. *Journal of Photochemistry and Photobiology A: Chemistry* **2023,** *440*, 114659.

[105] Zhang, Y.; Zhang, L., A novel "turn-on" fluorescent probe based on naphthalimide for monitoring H_2S levels in living cells and red wine. *Microchemical Journal* **2020,** *159*, 105394.

[106] Shi, X.; Yin, C.; Wen, Y.; Huo, F., A dual-sites fluorescent probe based on symmetric structure of naphthalimide derivative to detect H_2S. *Dyes and Pigments* **2019,** *165*, 38-43.

[107] Wang, Y.; Zhao, X.; Chen, Y.; James, T. D.; Wang, G.; Zhang, H., Synergistically activated dual-locked fluorescent probes to monitor H_2S-induced DNA damage. *Chemical Communications* **2022,** *58* (75), 10500-10503.

[108] Wang, X.; Zuo, Y.; Zhang, Y.; Yang, T.; Lin, W., An ICT-based fluorescent probe with bridging Si–O–Si bonds for visualizing hydrogen sulfide in lipid droplets and its application. *Analytical Methods* **2020,** *12* (8), 1064-1069.

[109] Jothi, D.; Munusamy, S.; Iyer, S. K., A new sensitive "turn-on" fluorescent probe based on naphthalimide: Application in visual recognition of hydrogen sulfide in environmental samples and living cells. *Journal of Photochemistry and Photobiology A: Chemistry* **2021,** *420*, 113491.

[110] Zhang, H.; Wang, P.; Chen, G.; Cheung, H.-Y.; Sun, H., A highly sensitive fluorescent probe for imaging hydrogen sulfide in living cells. *Tetrahedron Letters* **2013,** *54* (36), 4826-4829.

[111] Hammers, M. D.; Taormina, M. J.; Cerda, M. M.; Montoya, L. A.; Seidenkranz, D. T.; Parthasarathy, R.; Pluth, M. D., A Bright Fluorescent Probe for H_2S Enables Analyte-Responsive, 3D Imaging in Live Zebrafish Using Light Sheet Fluorescence Microscopy. *Journal of the American Chemical Society* **2015,** *137* (32), 10216-10223.

[112] Lin, V. S.; Lippert, A. R.; Chang, C. J., Cell-trappable fluorescent probes for endogenous hydrogen sulfide signaling and imaging H_2O_2-dependent H_2S production. *Proceedings of the National Academy of Sciences* **2013,** *110* (18), 7131-7135.

[113] Wei, L.; Zhu, Z.; Li, Y.; Yi, L.; Xi, Z., A highly selective and fast-response fluorescent probe for visualization of enzymatic H_2S production in vitro and in living cells. *Chemical Communications* **2015,** *51* (52), 10463-10466.

[114] Huo, F.-J.; Kang, J.; Yin, C.; Chao, J.; Zhang, Y., Highly selective fluorescent and colorimetric probe for live-cell monitoring of sulphide based on bioorthogonal reaction. *Scientific Reports* **2015,** *5* (1), 8969.

[115] Cheng, J.; Song, J.; Niu, H.; Tang, J.; Zhang, D.; Zhao, Y.; Ye, Y., A new rosamine-based fluorescent chemodosimeter for hydrogen sulfide and its bioimaging in live cells. *New Journal of Chemistry* **2016,** *40* (7), 6384-6388.

[116] Saha, T.; Kand, D.; Talukdar, P., A colorimetric and fluorometric BODIPY probe for rapid, selective detection of H_2S and its application in live cell imaging. *Organic & Biomolecular Chemistry* **2013,** *11* (47), 8166-8170.

[117] Gupta, N.; Reja, S. I.; Bhalla, V.; Gupta, M.; Kaur, G.; Kumar, M., A bodipy based dual functional probe for the detection of hydrogen sulfide and H_2S induced apoptosis in cellular systems. *Chemical Communications* **2015,** *51* (54), 10875-10878.

[118] Paul, N.; Sarkar, R.; Sarkar, R.; Barui, A.; Sarkar, S., Detection of hydrogen sulfide using BODIPY based colorimetric and fluorescent on-off chemosensor. *Journal of Chemical Sciences* **2020,** *132* (1), 21.

[119] Ozdemir, T.; Sozmen, F.; Mamur, S.; Tekinay, T.; Akkaya, E. U., Fast responding and selective near-IR Bodipy dye for hydrogen sulfide sensing. *Chemical Communications* **2014,** *50* (41), 5455-5457.

[120] Li, W.; Sun, W.; Yu, X.; Du, L.; Li, M., Coumarin-based Fluorescent Probes for H_2S Detection. *Journal of Fluorescence* **2013,** *23* (1), 181-186.

[121] Chen, B.; Li, W.; Lv, C.; Zhao, M.; Jin, H.; Jin, H.; Du, J.; Zhang, L.; Tang, X., Fluorescent probe for highly selective and sensitive detection of hydrogen sulfide in living cells and cardiac tissues. *Analyst* **2013,** *138* (3), 946-951.

[122] Qiu, Q.; Deng, X.; Jiao, L.; Zhao, T.; Meng, F.; Huang, W.; Qian, H., A High-Sensitivity Coumarin-Based Fluorescent Probe for Monitoring Hydrogen Sulfide in Living Cells. *Chemical Biology & Drug Design* **2015,** *86* (2), 173-179.

[123] Elsayed, S.; de la Torre, C.; Santos-Figueroa, L. E.; Marín-Hernández, C.; Martínez-Máñez, R.; Sancenón, F.; Costero, A. M.; Gil, S.; Parra, M., Azide and sulfonylazide functionalized fluorophores for the selective and sensitive detection of hydrogen sulfide. *Sensors and Actuators B: Chemical* **2015,** *207*, 987-994.

[124] Qiao, Z.; Zhang, H.; Wang, K.; Zhang, Y., A highly sensitive and responsive fluorescent probe based on 6-azide-chroman dye for detection and imaging of hydrogen sulfide in cells. *Talanta* **2019,** *195*, 850-856.

[125] Ma, T.; Huo, F.; Wen, Y.; Glass, T. E.; Yin, C., A novel water-soluble fluorescence probe based on ICT lighten for detecting hydrogen sulfide and its application in bioimaging. *Spectrochimica Acta Part A: Molecular and Biomolecular Spectroscopy* **2019,** *214*, 355-359.

[126] Fang, Q.; Xiong, H.; Yang, L.; Wang, B.; Song, X., An instantaneous fluorescent probe for detecting hydrogen sulfide in biological systems. *New Journal of Chemistry* **2019,** *43* (34), 13594-13599.

[127] Zhang, J.; Gao, Y.; Kang, X.; Zhu, Z.; Wang, Z.; Xi, Z.; Yi, L., *o*,*o*-Difluorination of aromatic azide yields a fast-response fluorescent probe for H_2S detection and for improved bioorthogonal reactions. *Organic & Biomolecular Chemistry* **2017,** *15* (19), 4212-4217.

[128] Renault, K.; Renard, P.-Y.; Sabot, C., Photophysical properties of quinoxalin-2(1H)-ones: application in the preparation of an azide-based fluorogenic probe for the detection of hydrogen sulfide. *New Journal of Chemistry* **2017,** *41* (18), 10432-10437.

[129] Muthusamy, S.; Rajalakshmi, K.; Xu, Q.; Chen, Y.; Zhao, L.; Zhu, W., An azido coumarin-quinoline conjugated fluorogenic dye: Utilizing amide-iminol tautomerism for H_2S detection in live MCF-7 cells. *Spectrochimica Acta Part A: Molecular and Biomolecular Spectroscopy* **2020,** *238*, 118345.

[130] Tian, H.; Qian, J.; Sun, Q.; Jiang, C.; Zhang, R.; Zhang, W., A coumarin-based fluorescent probe for differential identification of sulfide and sulfite in CTAB micelle solution. *Analyst* **2014,** *139* (13), 3373-3377.

[131] Mao, G.-J.; Wei, T.-T.; Wang, X.-X.; Huan, S.-y.; Lu, D.-Q.; Zhang, J.; Zhang, X.-B.; Tan, W.; Shen, G.-L.; Yu, R.-Q., High-Sensitivity Naphthalene-Based Two-Photon Fluorescent

Probe Suitable for Direct Bioimaging of H_2S in Living Cells. *Analytical Chemistry* **2013,** *85* (16), 7875-7881.

[132] Chen, B.; Lv, C.; Tang, X., Chemoselective reduction-based fluorescence probe for detection of hydrogen sulfide in living cells. *Analytical and Bioanalytical Chemistry* **2012,** *404* (6), 1919-1923.

[133] Wan, Q.; Song, Y.; Li, Z.; Gao, X.; Ma, H., In vivo monitoring of hydrogen sulfide using a cresyl violet-based ratiometric fluorescence probe. *Chemical Communications* **2013,** *49* (5), 502-504.

[134] Lv, L.; Luo, W.; Diao, Q., A novel ratiometric fluorescent probe for selective detection and imaging of H_2S. *Spectrochimica Acta Part A: Molecular and Biomolecular Spectroscopy* **2021,** *246*, 118959.

[135] Liu, K.; Liu, C.; Shang, H.; Ren, M.; Lin, W., A novel red light emissive two-photon fluorescent probe for hydrogen sulfide (H_2S) in nucleolus region and its application for H_2S detection in zebrafish and live mice. *Sensors and Actuators B: Chemical* **2018,** *256*, 342-350.

[136] Zhou, L.; Wang, Q.; Tan, Y.; Lang, M. J.; Sun, H.; Liu, X., Rational Development of Near-Infrared Fluorophores with Large Stokes Shifts, Bright One-Photon, and Two-Photon Emissions for Bioimaging and Biosensing Applications. *Chemistry – A European Journal* **2017,** *23* (36), 8736-8740.

[137] Ma, T.; Zheng, J.; Zhang, T.; Xing, D., Ratiometric photoacoustic nanoprobes for monitoring and imaging of hydrogen sulfide in vivo. *Nanoscale* **2018,** *10* (28), 13462-13470.

[138] Yao, X.; Liu, W.; Zhu, W.; Tiemuer, A.; Zhou, F.; Yang, S.; Yu, H.; Qian, X.; Liu, Y., Near-infrared fluorescent chemodosimeter for real-time in vivo evaluation of H_2S-release efficiency of prodrug. *Chemical Communications* **2020,** *56* (58), 8111-8114.

[139] Sun, Y.; Li, C.; Feng, X.; Wang, C.; Wang, N.; Zhu, J.; Wang, T.; Cui, X., Si-coumarin-based fluorescent probes for ultrafast monitoring H_2S in vivo. *Dyes and Pigments* **2021,** *186*, 109059.

[140] Zheng, Y.; Zhao, M.; Qiao, Q.; Liu, H.; Lang, H.; Xu, Z., A near-infrared fluorescent probe for hydrogen sulfide in living cells. *Dyes and Pigments* **2013,** *98* (3), 367-371.

[141] Sun, W.; Fan, J.; Hu, C.; Cao, J.; Zhang, H.; Xiong, X.; Wang, J.; Cui, S.; Sun, S.; Peng, X., A two-photon fluorescent probe with near-infrared emission for hydrogen sulfide imaging in biosystems. *Chemical Communications* **2013,** *49* (37), 3890-3892.

[142] Xiang, K.; Liu, Y.; Li, C.; Tian, B.; Tong, T.; Zhang, J., A colorimetric and ratiometric fluorescent probe with a large stokes shift for detection of hydrogen sulfide. *Dyes and Pigments* **2015,** *123*, 78-84.

[143] Liu, T.; Lin, J.; Li, Z.; Lin, L.; Shen, Y.; Zhu, H.; Qian, Y., Imaging of living cells and zebrafish in vivo using a ratiometric fluorescent probe for hydrogen sulfide. *Analyst* **2015,** *140* (21), 7165-7169.

[144] An, B.; Zhang, H.; Peng, J.; Zhu, W.; Wei, N.; Zhang, Y., A highly sensitive ratiometric fluorescent probe for imaging endogenous hydrogen sulfide in cells. *New Journal of Chemistry* **2020,** *44* (46), 20253-20258.

[145] Peng, J.; Ju, Q.; An, B.; Yin, Z.; Wei, N.; Zhang, Y., A super sensitive fluorescent probe for imaging endogenous hydrogen sulfide in living cells. *Talanta* **2022,** *250*, 123741.

[146] Liu, K.; Zhang, S., Design and characterization of 3-azidothalidomide as a selective hydrogen sulfide probe. *Tetrahedron Letters* **2014,** *55* (40), 5566-5569.

[147] Yang, L.; Liu, X.; Gao, L.; Qi, F.; Tian, H.; Song, X., A selective and sensitive phthalimide-based fluorescent probe for hydrogen sulfide with a large Stokes shift. *RSC Advances* **2015,** *5* (119), 98154-98159.

[148] Kim, G.; Jang, E.; Page, A. M.; Ding, T.; Carlson, K. A.; Cao, H., Investigation of a sensing approach based on a rapid reduction of azide to selectively measure bioavailability of H_2S. *RSC Advances* **2016,** *6* (98), 95920-95924.

[149] Zheng, K.; Lin, W.; Tan, L., A phenanthroimidazole-based fluorescent chemosensor for imaging hydrogen sulfide in living cells. *Organic & Biomolecular Chemistry* **2012,** *10* (48), 9683-9688.

[150] Gu, B.; Mi, N.; Zhang, Y.; Yin, P.; Li, H.; Yao, S., A tetraphenylimidazole-based fluorescent probe for the detection of hydrogen sulfide and its application in living cells. *Analytica Chimica Acta* **2015,** *879*, 85-90.

[151] Brito da Silva, C.; Gil, E. S.; da Silveira Santos, F.; Morás, A. M.; Steffens, L.; Bruno Gonçalves, P. F.; Moura, D. J.; Lüdtke, D. S.; Rodembusch, F. S., Proton-Transfer-Based Azides with Fluorescence Off–On Response for Detection of Hydrogen Sulfide: An Experimental, Theoretical, and Bioimaging Study. *The Journal of Organic Chemistry* **2018,** *83* (24), 15210-15224.

[152] Zhang, J.; Guo, W., A new fluorescent probe for gasotransmitter H_2S: high sensitivity, excellent selectivity, and a significant fluorescence off–on response. *Chemical Communications* **2014,** *50* (32), 4214-4217.

[153] Cai, Y.; Li, L.; Wang, Z.; Sun, J. Z.; Qin, A.; Tang, B. Z., A sensitivity tuneable tetraphenylethene-based fluorescent probe for directly indicating the concentration of hydrogen sulfide. *Chemical Communications* **2014,** *50* (64), 8892-8895.

[154] Biswas, B.; Venkateswarulu, M.; Gaur, P.; Sharma, Y.; Sinha, S.; Ghosh, S., Triggered emission for rapid detection of hydrogen sulfide chaperoned by large Stokes shift. *Journal of Photochemistry and Photobiology A: Chemistry* **2019,** *371*, 264-270.

[155] Chen, Q.; Xing, P.; Xu, Y.; Li, H.; Sun, S., A Selective Fluorescent Sensor for Fast Detection of Hydrogen Sulfide in Red Wine. *Chinese Journal of Chemistry* **2017,** *35* (4), 477-482.

[156] Hartman, M. C. T.; Dcona, M. M., A new, highly water-soluble, fluorescent turn-on chemodosimeter for direct measurement of hydrogen sulfide in biological fluids. *Analyst* **2012,** *137* (21), 4910-4912.

[157] Pramanik, S.; Bhalla, V.; Kim, H. M.; Singh, H.; Lee, H. W.; Kumar, M., A hexaphenylbenzene based AIEE active two photon probe for the detection of hydrogen sulfide with tunable self-assembly in aqueous media and application in live cell imaging. *Chemical Communications* **2015,** *51* (85), 15570-15573.

[158] Das, S. K.; Lim, C. S.; Yang, S. Y.; Han, J. H.; Cho, B. R., A small molecule two-photon probe for hydrogen sulfide in live tissues. *Chemical Communications* **2012,** *48* (67), 8395-8397.

[159] Zhou, G.; Wang, H.; Ma, Y.; Chen, X., An NBD fluorophore-based colorimetric and fluorescent chemosensor for hydrogen sulfide and its application for bioimaging. *Tetrahedron* **2013,** *69* (2), 867-870.

[160] Chen, T.; Zheng, Y.; Xu, Z.; Zhao, M.; Xu, Y.; Cui, J., A red emission fluorescent probe for hydrogen sulfide and its application in living cells imaging. *Tetrahedron Letters* **2013,** *54* (23), 2980-2982.

[161] Zhang, X.; Weng, X.; Yang, Z.; Zhao, P.; Chen, W.; Wu, Z.; Zhuang, X., A Chalcone-based Fluorescence Probe for H_2S Detecting Utilizing ESIPT Coupled ICT Mechanism. *Journal of Fluorescence* **2023**, doi: 10.1007/s10895-023-03327-8.

[162] Zhao, B.; Yang, B.; Hu, X.; Liu, B., Two colorimetric and ratiometric fluorescence probes for hydrogen sulfide based on AIE strategy of α–cyanostilbenes. *Spectrochimica Acta Part A: Molecular and Biomolecular Spectroscopy* **2018,** *199*, 117-122.

[163] Kafle, A.; Bhattarai, S.; Miller, J. M.; Handy, S. T., Hydrogen sulfide sensing using an aurone-based fluorescent probe. *RSC Advances* **2020,** *10* (73), 45180-45188.

[164] Yu, F.; Li, P.; Song, P.; Wang, B.; Zhao, J.; Han, K., An ICT-based strategy to a colorimetric and ratiometric fluorescence probe for hydrogen sulfide in living cells. *Chemical Communications* **2012,** *48* (23), 2852-2854.

[165] Albakour, M.; Zeyrek Ongun, M.; Topal, S. Z.; Gürek, A. G., Zn(II) phthalocyanines tetra substituted by aryl and alkyl azides: design, synthesis and optical detection of H_2S. *New Journal of Chemistry* **2020,** *44* (16), 6285-6296.

[166] Wang, K.; Peng, H.; Ni, N.; Dai, C.; Wang, B., 2,6-Dansyl Azide as a Fluorescent Probe for Hydrogen Sulfide. *Journal of Fluorescence* **2014,** *24* (1), 1-5.

[167] Santos-Figueroa, L. E.; de laTorre, C.; El Sayed, S.; Sancenón, F.; Martínez-Máñez, R.; Costero, A. M.; Gil, S.; Parra, M., A Chemosensor Bearing Sulfonyl Azide Moieties for Selective Chromo-Fluorogenic Hydrogen Sulfide Recognition in Aqueous Media and in Living Cells. *European Journal of Organic Chemistry* **2014,** *2014* (9), 1848-1854.

[168] Fu, D.; Zhi, W.; Lv, L.; Luo, Y.; Xiong, X.; Kang, X.; Hou, W.; Yan, J.; Zhao, H.; Zheng, L., Construction of ratiometric hydrogen sulfide probe with two reaction sites and its applications in solution and in live cells. *Spectrochimica Acta Part A: Molecular and Biomolecular Spectroscopy* **2020,** *224*, 117391.

[169] Lim, C. S.; Das, S. K.; Yang, S. Y.; Kim, E. S.; Chun, H. J.; Cho, B. R., Quantitative Estimation of the Total Sulfide Concentration in Live Tissues by Two-Photon Microscopy. *Analytical Chemistry* **2013,** *85* (19), 9288-9295.

[170] Liu, X.-L.; Du, X.-J.; Dai, C.-G.; Song, Q.-H., Ratiometric Two-Photon Fluorescent Probes for Mitochondrial Hydrogen Sulfide in Living Cells. *The Journal of Organic Chemistry* **2014,** *79* (20), 9481-9489.

[171] Zhang, L.; Li, S.; Hong, M.; Xu, Y.; Wang, S.; Liu, Y.; Qian, Y.; Zhao, J., A colorimetric and ratiometric fluorescent probe for the imaging of endogenous hydrogen sulphide in living cells and sulphide determination in mouse hippocampus. *Organic & Biomolecular Chemistry* **2014,** *12* (28), 5115-5125.

[172] Wen, Y.; Huo, F.; Wang, J.; Yin, C., Molecular isomerization triggered by H_2S to an NIR accessible first direct visualization of Ca^{2+}-dependent production in living HeLa cells. *Journal of Materials Chemistry B* **2019,** *7* (43), 6855-6860.

[173] Feng, W.; Xiao, Q.; Wang, L.; Yang, Y., A New Fluorescent Probe for Hydrogen Sulfide Detection in Solution and Living Cells. *Molecules* **2023,** *28* (17), 6195.

[174] Jiang, Y.; Wu, Q.; Chang, X., A ratiometric fluorescent probe for hydrogen sulfide imaging in living cells. *Talanta* **2014,** *121*, 122-126.

[175] Liu, Z.; Wang, Q.; Wang, H.; Lan, Y.; Dong, S., A quaternary ammonium modified fluorescent probe for hydrogen sulfide detection in living cells. *Journal of Photochemistry and Photobiology A: Chemistry* **2020,** *389*, 112213.

[176] Zhang, J.; Peng, F.; Dong, X.; Zhao, W., Water-soluble BODIPY Derivative as a Highly Selective "Turn-on" Fluorescent Probe for Hydrogen Sulfide in Living Cells. *Chemistry Letters* **2015,** *44* (11), 1524-1526.

[177] Zhao, Q.; Yin, C.; Kang, J.; Wen, Y.; Huo, F., A viscosity sensitive azide-pyridine BODIPY-based fluorescent dye for imaging of hydrogen sulfide in living cells. *Dyes and Pigments* **2018,** *159*, 166-172.

[178] Fei, Q.; Li, M.; Chen, J.; Shi, B.; Xu, G.; Zhao, C.; Gu, X., Design of BODIPY-based near-infrared fluorescent probes for H_2S. *Journal of Photochemistry and Photobiology A: Chemistry* **2018,** *355*, 305-310.

[179] Park, C. S.; Ha, T. H.; Choi, S.-A.; Nguyen, D. N.; Noh, S.; Kwon, O. S.; Lee, C.-S.; Yoon, H., A near-infrared "turn-on" fluorescent probe with a self-immolative linker for the in vivo quantitative detection and imaging of hydrogen sulfide. *Biosensors and Bioelectronics* **2017,** *89*, 919-926.

[180] Zhang, J.; Mu, S.; Wang, Y.; Li, S.; Shi, X.; Liu, X.; Zhang, H., A water-soluble near-infrared fluorescent probe for monitoring change of hydrogen sulfide during cell damage and repair process. *Analytica Chimica Acta* **2022,** *1195*, 339457.

[181] Yang, L.; Jiang, L.; Xu, F.; Zheng, H.; Liu, M.; Shi, P.; Zhang, S.; Song, X., Hydrogen sulfide activatable NIR-II fluorescent probe for highly specific imaging of breast cancer. *Sensors and Actuators B: Chemical* **2023,** *379*, 133251.

[182] Li, S.-J.; Li, Y.-F.; Liu, H.-W.; Zhou, D.-Y.; Jiang, W.-L.; Ou-Yang, J.; Li, C.-Y., A Dual-Response Fluorescent Probe for the Detection of Viscosity and H_2S and Its Application in Studying Their Cross-Talk Influence in Mitochondria. *Analytical Chemistry* **2018,** *90* (15), 9418-9425.

[183] Fang, Z.; Su, Z.; Qin, W.; Li, H.; Fang, B.; Du, W.; Wu, Q.; Peng, B.; Li, P.; Yu, H.; Li, L.; Huang, W., Two-photon dual-channel fluorogenic probe for in situ imaging the mitochondrial H_2S/viscosity in the brain of drosophila Parkinson's disease model. *Chinese Chemical Letters* **2020,** *31* (11), 2903-2908.

[184] Fang, W.-L.; He, S.; Guo, X.-F.; Wang, H., A novel near infrared probe with large Stokes shift for detection of H_2S in living cells. *Sensors and Actuators B: Chemical* **2023,** *375*, 132961.

[185] Steiger, A. K.; Pardue, S.; Kevil, C. G.; Pluth, M. D., Self-Immolative Thiocarbamates Provide Access to Triggered H2S Donors and Analyte Replacement Fluorescent Probes. *Journal of the American Chemical Society* **2016,** *138* (23), 7256-7259.

[186] Xu, H.; Xu, H.; Ma, S.; Chen, X.; Huang, L.; Chen, J.; Gao, F.; Wang, R.; Lou, K.; Wang, W., Analyte Regeneration Fluorescent Probes for Formaldehyde Enabled by Regiospecific Formaldehyde-Induced Intramolecularity. *Journal of the American Chemical Society* **2018,** *140* (48), 16408-16412.

[187] Popova, M.; Lazarus, L. S.; Benninghoff, A. D.; Berreau, L. M., CO Sense and Release Flavonols: Progress toward the Development of an Analyte Replacement PhotoCORM for Use in Living Cells. *ACS Omega* **2020,** *5* (17), 10021-10033.

[188] Zhao, Y.; Pluth, M. D., Hydrogen Sulfide Donors Activated by Reactive Oxygen Species. *Angewandte Chemie International Edition* **2016,** *55* (47), 14638-14642.

[189] Powell, C. R.; Foster, J. C.; Okyere, B.; Theus, M. H.; Matson, J. B., Therapeutic Delivery of H_2S via COS: Small Molecule and Polymeric Donors with Benign Byproducts. *Journal of the American Chemical Society* **2016,** *138* (41), 13477-13480.

[190] Levinn, C. M.; Cerda, M. M.; Pluth, M. D., Development and Application of Carbonyl Sulfide-Based Donors for H_2S Delivery. *Accounts of Chemical Research* **2019,** *52* (9), 2723-2731.

[191] Liang, T.; Qiang, T.; Ren, L.; Cheng, F.; Wang, B.; Li, M.; Hu, W.; James, T. D., Near-infrared fluorescent probe for hydrogen sulfide: high-fidelity ferroptosis evaluation in vivo during stroke. *Chemical Science* **2022,** *13* (10), 2992-3001.

[192] Zhang, J.; Mu, S.; Wang, W.; Sun, H.; Li, S.; Shi, X.; Liu, Y.; Liu, X.; Zhang, H., Design strategy for an analyte-compensated fluorescent probe to reduce its toxicity. *Chemical Communications* **2022,** *58* (65), 9136-9139.

[193] Zhang, H.; Xie, Y.; Wang, P.; Chen, G.; Liu, R.; Lam, Y.-W.; Hu, Y.; Zhu, Q.; Sun, H., An iminocoumarin benzothiazole-based fluorescent probe for imaging hydrogen sulfide in living cells. *Talanta* **2015,** *135*, 149-154.

[194] Mishra, P. K.; Saha, T.; Talukdar, P., Hydrogen sulfide mediated cascade reaction forming an iminocoumarin: applications in fluorescent probe development and live-cell imaging. *Organic & Biomolecular Chemistry* **2015,** *13* (27), 7430-7436.

[195] Yang, L.; Su, Y.; Sha, Z.; Geng, Y.; Qi, F.; Song, X., A red-emitting fluorescent probe for hydrogen sulfide in living cells with a large Stokes shift. *Organic & Biomolecular Chemistry* **2018,** *16* (7), 1150-1156.

[196] Zhao, M.; Li, H.; Li, H.; Qiao, Q.; Cao, C.; Xu, Z., A turn-on fluorescent probe for hydrogen sulfide and its application in living cells. *RSC Advances* **2015,** *5* (105), 86355-86358.

[197] Thirumalaivasan, N.; Venkatesan, P.; Wu, S.-P., Highly selective turn-on probe for H_2S with imaging applications in vitro and in vivo. *New Journal of Chemistry* **2017,** *41* (22), 13510-13515.

[198] Li, Y.; Quan, W.; Song, W.; Zhan, J.; Lin, W., Near-infrared fluorescent probe for visualizing hydrogen sulfide fluctuations during arthritis and its treatment. *Microchemical Journal* **2023,** *191*, 108856.

[199] Wang, J.; Chen, Y.; Yang, C.; Wei, T.; Han, Y.; Xia, M., An ICT-based colorimetric and ratiometric fluorescent probe for hydrogen sulfide and its application in live cell imaging. *RSC Advances* **2016,** *6* (39), 33031-33035.

[200] Wu, Z.; Li, Z.; Yang, L.; Han, J.; Han, S., Fluorogenic detection of hydrogen sulfide *via* reductive unmasking of *o*-azidomethylbenzoyl-coumarin conjugate. *Chemical Communications* **2012,** *48* (81), 10120-10122.

[201] Zaorska, E.; Konop, M.; Ostaszewski, R.; Koszelewski, D.; Ufnal, M., Salivary Hydrogen Sulfide Measured with a New Highly Sensitive Self-Immolative Coumarin-Based Fluorescent Probe. *Molecules* **2018,** *23* (9), 2241.

[202] Saha, T.; Kand, D.; Talukdar, P., Performance comparison of two cascade reaction models in fluorescence off–on detection of hydrogen sulfide. *RSC Advances* **2015,** *5* (2), 1438-1446.

[203] Yang, Q.; Zhan, F.; Wang, Q.; Zhuang, Z.; Zhang, G.; Zheng, G., Construction of a turn-on probe for fast detection of H_2S in living cells based on a novel H_2S trap group with an electron rich dye. *RSC Advances* **2015,** *5* (128), 106156-106160.

[204] Xu, C.; Zhang, Y.; Sun, H.; Ai, J.; Ren, M., Development of a two-photon fluorescent probe for imaging hydrogen sulfide (H_2S) in living cells and zebrafish. *Analytical Methods* **2023,** *15* (16), 1948-1952.

[205] Deng, B.; Ren, M.; Kong, X.; Zhou, K.; Lin, W., An ESIPT based fluorescent probe for imaging hydrogen sulfide with a large turn-on fluorescence signal. *RSC Advances* **2016,** *6* (67), 62406-62410.

[206] Ghosh, S.; Roy, B.; Bandyopadhyay, S., Formation or Cleavage of Rings via Sulfide-Mediated Reduction Offers Background-Free Detection of Sulfide. *The Journal of Organic Chemistry* **2019,** *84* (18), 12031-12039.

[207] Zhou, J.; Luo, Y.; Li, Q.; Shen, J.; Wang, R.; Xu, Y.; Qian, X., Assembly of indole fluorophore in situ for hydrogen sulfide signaling through substrate triggered intramolecular reduction–cyclization cascade: a sensitive and selective probe in aqueous solution. *New Journal of Chemistry* **2014,** *38* (7), 2770-2773.

[208] Duan, Y.-W.; Yang, X.-F.; Zhong, Y.; Guo, Y.; Li, Z.; Li, H., A ratiometric fluorescent probe for gasotransmitter hydrogen sulfide based on a coumarin-benzopyrylium platform. *Analytica Chimica Acta* **2015,** *859*, 59-65.

[209] Adarsh, N.; Krishnan, M. S.; Ramaiah, D., Sensitive Naked Eye Detection of Hydrogen Sulfide and Nitric Oxide by Aza-BODIPY Dyes in Aqueous Medium. *Analytical Chemistry* **2014,** *86* (18), 9335-9342.

[210] Yue, X.; Wang, J.; Han, J.; Wang, B.; Song, X., A dual-ratiometric fluorescent probe for individual and continuous detection of H_2S and HClO in living cells. *Chemical Communications* **2020,** *56* (19), 2849-2852.

[211] Ren, M.; Li, Z.; Deng, B.; Wang, L.; Lin, W., Single Fluorescent Probe Separately and Continuously Visualize H_2S and HClO in Lysosomes with Different Fluorescence Signals. *Analytical Chemistry* **2019,** *91* (4), 2932-2938.

[212] Yang, L.; Zhang, Y.; Ren, X.; Wang, B.; Yang, Z.; Song, X.; Wang, W., Fluorescent Detection of Dynamic H_2O_2/H_2S Redox Event in Living Cells and Organisms. *Analytical Chemistry* **2020,** *92* (6), 4387-4394.

[213] Dai, C.-G.; Liu, X.-L.; Du, X.-J.; Zhang, Y.; Song, Q.-H., Two-Input Fluorescent Probe for Thiols and Hydrogen Sulfide Chemosensing and Live Cell Imaging. *ACS Sensors* **2016,** *1* (7), 888-895.

[214] Qi, F.; Zhang, Y.; Wang, B.; Chen, W.; Yang, L.; Yang, Z.; Song, X., A fluorescent probe for the dicriminatory detecion of Cys/Hcy, GSH and H_2S in living cells and zebrafish. *Sensors and Actuators B: Chemical* **2019,** *296*, 126533.

[215] Yue, L.; Ai, Y.; Liu, G.; Ding, H.; Pu, S., A dual-response NIR fluorescent probe for separately and continuously recognizing H_2S and Cys with different fluorescence signals and its applications. *Analyst* **2023,** *148* (19), 4829-4836.

[216] Zhang, W.; Huo, F.; Yin, C., Photocontrolled Single-/Dual-Site Alternative Fluorescence Probes Distinguishing Detection of H_2S/SO_2 in vivo. *Organic Letters* **2019,** *21* (13), 5277-5280.

[217] Ren, M.; Xu, Q.; Bai, Y.; Wang, S.; Kong, F., Construction of a dual-response fluorescent probe for copper (II) ions and hydrogen sulfide (H_2S) detection in cells and its application in exploring the increased copper-dependent cytotoxicity in present of H_2S. *Spectrochimica Acta Part A: Molecular and Biomolecular Spectroscopy* **2021,** *249*, 119299.

[218] Ai, Y.; Zhu, Z. F.; Ding, H. C.; Fan, C. B.; Liu, G.; Pu, S. Z., A dual-responsive fluorescent probe for detection of H_2S and Cu^{2+} based on rhodamine-naphthalimide and cell imaging. *Journal of Photochemistry and Photobiology a-Chemistry* **2022,** *427*, 113801.

[219] Zhao, Q.; Huo, F.; Kang, J.; Zhang, Y.; Yin, C., A novel FRET-based fluorescent probe for the selective detection of hydrogen sulfide (H_2S) and its application for bioimaging. *Journal of Materials Chemistry B* **2018,** *6* (30), 4903-4908.

[220] Jiao, X.; Xiao, Y.; Li, Y.; Liang, M.; Xie, X.; Wang, X.; Tang, B., Evaluating Drug-Induced Liver Injury and Its Remission via Discrimination and Imaging of HClO and H_2S with a Two-Photon Fluorescent Probe. *Analytical Chemistry* **2018,** *90* (12), 7510-7516.

[221] Ou, P.; Zhang, R.; Liu, Z.; Tian, X.; Han, G.; Liu, B.; Hu, Z.; Zhang, Z., Gasotransmitter Regulation of Phosphatase Activity in Live Cells Studied by Three-Channel Imaging Correlation. *Angewandte Chemie International Edition* **2019,** *58* (8), 2261-2265.

[222] He, L.; Lin, W.; Xu, Q.; Wei, H., A new strategy to construct a FRET platform for ratiometric sensing of hydrogen sulfide. *Chemical Communications* **2015,** *51* (8), 1510-1513.

[223] Velusamy, N.; Thirumalaivasan, N.; Bobba, K. N.; Podder, A.; Wu, S.-P.; Bhuniya, S., FRET-based dual channel fluorescent probe for detecting endogenous/exogenous H_2O_2/H_2S formation through multicolor images. *Journal of Photochemistry and Photobiology B: Biology* **2019,** *191*, 99-106.

[224] Zhang, P.; Li, J.; Li, B.; Xu, J.; Zeng, F.; Lv, J.; Wu, S., A logic gate-based fluorescent sensor for detecting H_2S and NO in aqueous media and inside live cells. *Chemical Communications* **2015,** *51* (21), 4414-4416.

[225] Sun, P.; Chen, H.-C.; Lu, S.; Hai, J.; Guo, W.; Jing, Y.-H.; Wang, B., Simultaneous Sensing of H_2S and ATP with a Two-Photon Fluorescent Probe in Alzheimer's Disease: toward Understanding Why H_2S Regulates Glutamate-Induced ATP Dysregulation. *Analytical Chemistry* **2022,** *94* (33), 11573-11581.

[226] Liu, Y.; Zhang, Y.; Zhang, X.-B., Engineering of a dual-site molecular probe for logical bioimaging of lysosomal H_2S and pH. *Talanta* **2020,** *219*, 121286.

[227] Zhang, W.; Lv, Y.; Huo, F.; Zhang, Y.; Yin, C., Dual-site fluorescent probe for bioimaging of upregulated adenosine triphosphate under the stresses of endogenous and exogenous H_2S. *Dyes and Pigments* **2022,** *204*, 110442.

[228] Yang, X.; Xie, P.; Liu, J.; Han, X.; Zhang, D.; Ye, Y.; Zhao, Y., Dual-site fluorescent sensor for tracking lysosomal ATP and H_2S during liver injury. *Chemical Engineering Journal* **2022,** *442*, 136141.

[229] Chen, B.; Wang, P.; Jin, Q.; Tang, X., Chemoselective reduction and self-immolation based FRET probes for detecting hydrogen sulfide in solution and in cells. *Organic & Biomolecular Chemistry* **2014,** *12* (30), 5629-5633.

[230] Wei , C.; Wang , R.; Wei , L.; Cheng , L.; Li, Z.; Xi , Z.; Yi , L., *o*-Fluorination of Aromatic Azides Yields Improved Azido-Based Fluorescent Probes for Hydrogen Sulfide: Synthesis, Spectra, and Bioimaging. *Chemistry – An Asian Journal* **2014,** *9* (12), 3586-3592.

[231] Chen, Y.; Lim, J.-Y.; Wu, X. H.; Heo, J. S.; FengyingYuan; Zhang, J. F.; Yoon, D. W.; Ren, W. X., Development of H_2S and HClO dual-responsive fluorescent probe for cancer recognition. *Dyes and Pigments* **2021,** *195*, 109666.

[232] Liu, J.; Liu, X.; Lu, S.; Zhang, L.; Feng, L.; Zhong, S.; Zhang, N.; Bing, T.; Shangguan, D., Ratiometric detection and imaging of hydrogen sulfide in mitochondria based on a cyanine/naphthalimide hybrid fluorescent probe. *Analyst* **2020,** *145* (20), 6549-6555.

[233] Yang, S.; Qi, Y.; Liu, C.; Wang, Y.; Zhao, Y.; Wang, L.; Li, J.; Tan, W.; Yang, R., Design of a Simultaneous Target and Location-Activatable Fluorescent Probe for Visualizing Hydrogen Sulfide in Lysosomes. *Analytical Chemistry* **2014,** *86* (15), 7508-7515.

[234] Zhu, L.; Liao, W.; Chang, H.; Liu, X.; Miao, S., A Novel Fluorescent Probe for Detection of Hydrogen Sulfide and Its Bioimaging Applications in Living Cells. *ChemistrySelect* **2020,** *5* (2), 829-833.

[235] Wu, Z.; Liang, D.; Tang, X., Visualizing Hydrogen Sulfide in Mitochondria and Lysosome of Living Cells and in Tumors of Living Mice with Positively Charged Fluorescent Chemosensors. *Analytical Chemistry* **2016,** *88* (18), 9213-9218.

[236] Feng, W.; Mao, Z.; Liu, L.; Liu, Z., A ratiometric two-photon fluorescent probe for imaging hydrogen sulfide in lysosomes. *Talanta* **2017,** *167*, 134-142.

[237] Gao, C.; Liu, X.; Chen, W.; Wang, F.; Jiang, J.-K., A naphthalene-based fluorescent probe for ratiometric imaging of lysosomal hydrogen sulfide in living cells. *Methods and Applications in Fluorescence* **2019,** *7* (1), 014002.

[238] Qiao, Q.; Zhao, M.; Lang, H.; Mao, D.; Cui, J.; Xu, Z., A turn-on fluorescent probe for imaging lysosomal hydrogen sulfide in living cells. *RSC Advances* **2014,** *4* (49), 25790-25794.

[239] Mu, S.; Zhang, J.; Gao, H.; Wang, Y.; Rizvi, S. F. A.; Ding, N.; Liu, X.; Wu, L.; Zhang, H., Sequential detection of H_2S and HOBr with a novel lysosome-targetable fluorescent probe and its application in biological imaging. *Journal of Hazardous Materials* **2022,** *422*, 126898.

[240] Xie, Q.-L.; Liu, W.; Liu, X.-J.; Ouyang, F.; Kuang, Y.-Q.; Jiang, J.-H., An azidocoumarin-based fluorescent probe for imaging lysosomal hydrogen sulfide in living cells. *Analytical Methods* **2017,** *9* (19), 2859-2864.

[241] Dou, Y.; Gu, X.; Ying, S.; Zhu, S.; Yu, S.; Shen, W.; Zhu, Q., A novel lysosome-targeted fluorogenic probe based on 5-triazole-quinoline for the rapid detection of hydrogen sulfide in living cells. *Organic & Biomolecular Chemistry* **2018,** *16* (5), 712-716.

[242] Bae, S. K.; Heo, C. H.; Choi, D. J.; Sen, D.; Joe, E.-H.; Cho, B. R.; Kim, H. M., A Ratiometric Two-Photon Fluorescent Probe Reveals Reduction in Mitochondrial H_2S Production in Parkinson's Disease Gene Knockout Astrocytes. *Journal of the American Chemical Society* **2013,** *135* (26), 9915-9923.

[243] Shi, W.; Pan, M.; Qiang, H.; Qiu, Q.; Huang, W.; Lin, H.; Qian, H.; Ge, L., A novel mitochondria-targeting fluorescent probe for hydrogen sulfide in living cells. *Chemical Biology & Drug Design* **2017,** *90* (2), 167-174.

[244] Deng, B.; Ren, M.; Wang, J.-Y.; Zhou, K.; Lin, W., A mitochondrial-targeted two-photon fluorescent probe for imaging hydrogen sulfide in the living cells and mouse liver tissues. *Sensors and Actuators B: Chemical* **2017,** *248*, 50-56.

[245] Velusamy, N.; Binoy, A.; Bobba, K. N.; Nedungadi, D.; Mishra, N.; Bhuniya, S., A bioorthogonal fluorescent probe for mitochondrial hydrogen sulfide: new strategy for cancer cell labeling. *Chemical Communications* **2017,** *53* (62), 8802-8805.

[246] Ji, A.; Fan, Y.; Ren, W.; Zhang, S.; Ai, H.-w., A Sensitive Near-Infrared Fluorescent Sensor for Mitochondrial Hydrogen Sulfide. *ACS Sensors* **2018,** *3* (5), 992-997.

[247] Song, X.; Wang, Y.; Ru, J.; Yang, Y.; Feng, Y.; Cao, C.; Wang, K.; Zhang, G.; Liu, W., A mitochondrial-targeted red fluorescent probe for detecting endogenous H_2S in cells with high selectivity and development of a visual paper-based sensing platform. *Sensors and Actuators B: Chemical* **2020,** *312*, 127982.

[248] Zhou, T.; Yang, Y.; Zhou, K.; Jin, M.; Han, M.; Li, W.; Yin, C., Efficiently mitochondrial targeting fluorescent imaging of H_2S in vivo based on a conjugate-lengthened cyanine NIR fluorescent probe. *Sensors and Actuators B: Chemical* **2019,** *301*, 127116.

[249] Zeng, C.; Hu, F.; Long, R.; Min, W., A ratiometric Raman probe for live-cell imaging of hydrogen sulfide in mitochondria by stimulated Raman scattering. *Analyst* **2018,** *143* (20), 4844-4848.

[250] Tang, Y.; Xu, A.; Ma, Y.; Xu, G.; Gao, S.; Lin, W., A turn-on endoplasmic reticulum-targeted two-photon fluorescent probe for hydrogen sulfide and bio-imaging applications in living cells, tissues, and zebrafish. *Scientific Reports* **2017,** *7* (1), 12944.

[251] Ma, Q.; Xiao, H.; Wang, K.; Liu, X.; Liu, Y., Determination of Hydrogen Sulfide in Endoplasmic Reticulum by Two-Photon Fluorescence. *Analytical Letters* **2021,** *54* (17), 2687-2699.

[252] Zhu, H.; Liang, C.; Cai, X.; Zhang, H.; Liu, C.; Jia, P.; Li, Z.; Yu, Y.; Zhang, X.; Sheng, W.; Zhu, B., Rational Design of a Targetable Fluorescent Probe for Visualizing H_2S Production under Golgi Stress Response Elicited by Monensin. *Analytical Chemistry* **2020,** *92* (2), 1883-1889.

[253] Zhu, H.; Liu, C.; Liang, C.; Tian, B.; Zhang, H.; Zhang, X.; Sheng, W.; Yu, Y.; Huang, S.; Zhu, B., A new phenylsulfonamide-based Golgi-targeting fluorescent probe for H_2S and its bioimaging applications in living cells and zebrafish. *Chemical Communications* **2020,** *56* (29), 4086-4089.

[254] Fu, Y.-J.; Yao, H.-W.; Zhu, X.-Y.; Guo, X.-F.; Wang, H., A cell surface specific two-photon fluorescent probe for monitoring intercellular transmission of hydrogen sulfide. *Analytica Chimica Acta* **2017,** *994*, 1-9.

[255] Zhu, H.; Sheng, W.; Liu, C.; Zhang, H.; Liang, C.; Zhang, X.; Wang, K.; Li, X.; Yu, Y.; Fan, D.; Zhu, B., Rational design of a fluorescent probe and its applications of imaging and distinguishing between exogenous and endogenous H_2S in living cells. *Spectrochimica Acta Part A: Molecular and Biomolecular Spectroscopy* **2022,** *266*, 120407.

[256] Shi, D.-T.; Zhou, D.; Zang, Y.; Li, J.; Chen, G.-R.; James, T. D.; He, X.-P.; Tian, H., Selective fluorogenic imaging of hepatocellular H_2S by a galactosyl azidonaphthalimide probe. *Chemical Communications* **2015,** *51* (17), 3653-3655.

[257] Shen, D.; Liu, J.; Sheng, L.; Lv, Y.; Wu, G.; Wang, P.; Du, K., Design, synthesis and evaluation of a novel fluorescent probe to accurately detect H_2S in hepatocytes and natural waters. *Spectrochimica Acta Part A: Molecular and Biomolecular Spectroscopy* **2020,** *228*, 117690.

[258] Song, X.; Dong, B.; Kong, X.; Wang, C.; Zhang, N.; Lin, W., A cancer cell-specific two-photon fluorescent probe for imaging hydrogen sulfide in living cells. *RSC Advances* **2017,** *7* (26), 15817-15822.

[259] Cha, Y.; Gopala, L.; Lee, M. H., A bio-friendly biotin-coupled and azide-functionalized naphthalimide for real-time endogenous hydrogen sulfide analysis in living cells. *Spectrochimica Acta Part A: Molecular and Biomolecular Spectroscopy* **2023,** *291*, 122385.

[260] Fosnacht, K. G.; Hammers, M. D.; Earp, M. S.; Gilbert, A. K.; Pluth, M. D., A Cell Trappable Methyl Rhodol-Based Fluorescent Probe for Hydrogen Sulfide Detection. *Chemistry-an Asian Journal* **2022,** *17* (16), e202200426.

[261] Lin, X.; Chen, Y.; Wang, S.; Liu, K.; Kong, F., Construction of a novel cell-trappable fluorescent probe for hydrogen sulfide (H_2S) and its bio-imaging application. *Analytical and Bioanalytical Chemistry* **2019,** *411* (27), 7127-7136.

[262] Bailey, T. S.; Pluth, M. D., Chemiluminescent Detection of Enzymatically Produced Hydrogen Sulfide: Substrate Hydrogen Bonding Influences Selectivity for H_2S over Biological Thiols. *Journal of the American Chemical Society* **2013,** *135* (44), 16697-16704.

[263] Tian, X.; Li, Z.; Lau, C.; Lu, J., Visualization of in Vivo Hydrogen Sulfide Production by a Bioluminescence Probe in Cancer Cells and Nude Mice. *Analytical Chemistry* **2015,** *87* (22), 11325-11331.

[264] Ke, B.; Wu, W.; Liu, W.; Liang, H.; Gong, D.; Hu, X.; Li, M., Bioluminescence Probe for Detecting Hydrogen Sulfide in vivo. *Analytical Chemistry* **2016,** *88* (1), 592-595.

[265] Cao, J.; Lopez, R.; Thacker, J. M.; Moon, J. Y.; Jiang, C.; Morris, S. N. S.; Bauer, J. H.; Tao, P.; Mason, R. P.; Lippert, A. R., Chemiluminescent probes for imaging H_2S in living animals. *Chemical Science* **2015,** *6* (3), 1979-1985.

[266] Green, O.; Eilon, T.; Hananya, N.; Gutkin, S.; Bauer, C. R.; Shabat, D., Opening a Gateway for Chemiluminescence Cell Imaging: Distinctive Methodology for Design of Bright Chemiluminescent Dioxetane Probes. *ACS Central Science* **2017,** *3* (4), 349-358.

[267] Levinn, C. M.; Pluth, M. D., Direct comparison of triggering motifs on chemiluminescent probes for hydrogen sulfide detection in water. *Sensors and Actuators B: Chemical* **2021,** *329*, 129235.

[268] Kong, D.; Song, B.; Yuan, J., A Golgi Apparatus-Targetable Probe Based on Lanthanide Complexes for Ratiometric Time-Gated Luminescence Detection of Hydrogen Sulfide. *European Journal of Inorganic Chemistry* **2023,** *26* (1), e202200642.

[269] Tropiano, M.; Faulkner, S., A lanthanide based sensor for the time-gated detection of hydrogen sulfide. *Chemical Communications* **2014,** *50* (36), 4696-4698.

[270] Yao, Y.; Kong, C.; Yin, L.; Jain, A. D.; Ratia, K.; Thatcher, G. R. J.; Moore, T. W.; Driver, T. G.; Miller, L. W., Time-Gated Detection of Cystathionine γ-Lyase Activity and Inhibition with a Selective, Luminogenic Hydrogen Sulfide Sensor. *Chemistry – A European Journal* **2017,** *23* (4), 752-756.

[271] Chen, X.; Cai, W.; Liu, G.; Tu, Y.; Fan, C.; Pu, S., A highly selective colorimetric and fluorescent probe $Eu(tdl)_2abp$ for H_2S sensing: Application in live cell imaging and natural water. *Spectrochimica Acta Part A: Molecular and Biomolecular Spectroscopy* **2022,** *282*, 121657.

[272] Anschutz, R.; Heusler, F., Ueber die schrittweise Amidirung von mehrfach nitrirten aromatischen Substanzen mittelst Zinnchlorür. *Chem. Ber.* **1886,** *19*, 2161.

[273] Cope, O. J.; Brown, R. K., The Reduction of Nitrobenzene by Sodium Sulphide in Aqueous Ethanol. *Canadian Journal of Chemistry* **1961,** *39* (8), 1695-1710.

[274] Cenas, N.; Prast, S.; Nivinskas, H.; Sarlauskas, J.; Arnér, E. S. J., Interactions of Nitroaromatic Compounds with the Mammalian Selenoprotein Thioredoxin Reductase and the Relation to Induction of Apoptosis in Human Cancer Cells. *Journal of Biological Chemistry* **2006,** *281* (9), 5593-5603.

[275] Wu, M.-Y.; Li, K.; Hou, J.-T.; Huang, Z.; Yu, X.-Q., A selective colorimetric and ratiometric fluorescent probe for hydrogen sulfide. *Organic & Biomolecular Chemistry* **2012,** *10* (41), 8342-8347.

[276] Wang, R.; Yu, F.; Chen, L.; Chen, H.; Wang, L.; Zhang, W., A highly selective turn-on near-infrared fluorescent probe for hydrogen sulfide detection and imaging in living cells. *Chemical Communications* **2012,** *48* (96), 11757-11759.

[277] Lohar, S.; Maji, A.; Pal, S.; Mukhopadhyay, S. K.; Nag, D.; Demitri, N.; Chattopadhyay, P., Naphthalimide-Based Turn-On Fluorosensor for Aqueous Sulfide Ions for Staining in Living Cells. *ChemistrySelect* **2017,** *2* (31), 9977-9983.

[278] Zhang, L.; Meng, W.-q.; Lu, L.; Xue, Y.-S.; Li, C.; Zou, F.; Liu, Y.; Zhao, J., Selective detection of endogenous H_2S in living cells and the mouse hippocampus using a ratiometric fluorescent probe. *Scientific Reports* **2014,** *4* (1), 5870.

[279] Kaur, N.; Kour, R.; Gasso, S.; Singh Marok, S.; Kaur, S.; Mahajan, A.; Singh, P., Near-IR intracellular ratiometric 'turn-on' discrimination of H_2S/Cys and low-cost test kits for ppm level detection of H_2S gas. *Journal of Photochemistry and Photobiology A: Chemistry* **2023,** *435*, 114345.

[280] Reja, S. I.; Kumar, N.; Sachdeva, R.; Bhalla, V.; Kumar, M., d-PET coupled ESIPT phenomenon for fluorescent turn-on detection of hydrogen sulfide. *RSC Advances* **2013,** *3* (39), 17770-17774.

[281] Zhu, D.; Xue, L.; Li, G.; Che, Y.; Jiang, H., A turn-on fluorescent probe for detection of hydrogen sulfide in aqueous solution and living cells. *Organic Chemistry Frontiers* **2014,** *1* (5), 501-505.

[282] Wu, Q.; Yin, C.; Wen, Y.; Zhang, Y.; Huo, F., An ICT lighten ratiometric and NIR fluorogenic probe to visualize endogenous/exogenous hydrogen sulphide and imaging in mice. *Sensors and Actuators B: Chemical* **2019,** *288*, 507-511.

[283] Sun, Y.; Tang, X.; Zhang, K.; Liu, K.; Li, Z.; Zhao, L., Hydrogen sulfide detection and zebrafish imaging by a designed sensitive and selective fluorescent probe based on resorufin. *Spectrochimica Acta Part A: Molecular and Biomolecular Spectroscopy* **2022,** *264*, 120265.

[284] Zhu, X.-Y.; Wu, H.; Guo, X.-F.; Wang, H., Novel BODIPY-based fluorescent probes with large Stokes shift for imaging hydrogen sulfide. *Dyes and Pigments* **2019,** *165*, 400-407.

[285] Santos, C. I. M.; Santiago, A. M.; Araújo, A. R. L.; Pinto, S.; Agostinho, R. R.; Simão, S.; Azevedo, T. P.; Antunes, C.; Faustino, M. A. F.; Araújo, I. M.; Neves, M. G. P. M. S.; Martinho, J. M. G.; Maçôas, E. M. S., New fluorescent probes based on gallium(III) corrole complexes for the recognition of hydrogen sulfide: A journey from solution to intracellular site. *Dyes and Pigments* **2023,** *216*, 111304.

[286] Maiti, K.; Mahapatra, A. K.; Maji, R.; Mondal, S.; Ali, S. S.; Gangopadhyay, A.; Manna, S. K.; Mandal, S., A Fluorophore-Free Chemodosimeter for H_2S with Luminescence Turn–on Response: Hyrdogen Sulphide Sensing in Garlic Extract. *ChemistrySelect* **2016,** *1* (15), 5066-5073.

[287] Xiong, J.; Wang, Y.; Jiang, X.; Liang, X.; Liang, Q., Kinetically Orthogonal Probe for Simultaneous Measurement of H_2S and Nitroreductase: A Refined Method to Predict the Invasiveness of Tumor Cells. *Analytical Chemistry* **2022,** *94* (3), 1769-1777.

[288] Katla, J.; Kanvah, S., Styrylisoxazole-based fluorescent probes for the detection of hydrogen sulfide. *Photochemical & Photobiological Sciences* **2018,** *17* (1), 42-50.

[289] Zhou, N.; Yin, C.; Chao, J.; Zhang, Y.; Huo, F., An isoxazole-accelerated nitro oxidation type fluorescent detection and imaging for hydrogen sulfide in cells. *Sensors and Actuators B: Chemical* **2019,** *287*, 131-137.

[290] Wang, L.; Chen, X.; Cao, D., A nitroolefin functionalized DPP fluorescent probe for the selective detection of hydrogen sulfide. *New Journal of Chemistry* **2017,** *41* (9), 3367-3373.

[291] Zhang, X.; Tan, H.; Yan, Y.; Hang, Y.; Yu, F.; Qu, X.; Hua, J., Targetable *N*-annulated perylene-based colorimetric and ratiometric near-infrared fluorescent probes for the selective detection of hydrogen sulfide in mitochondria, lysosomes, and serum. *Journal of Materials Chemistry B* **2017,** *5* (11), 2172-2180.

[292] Dong, J.; Hu, J.; Zhang, H., A fast-responsed fluorescent probe for the selective detection hydrogen sulfide and tert-butoxy radical. *Tetrahedron* **2020,** *76* (28), 131317.

[293] Renault, K.; Sabot, C.; Renard, P.-Y., Fast-Responsive Nitroso-Based Turn-On Probe for Hydrogen Sulfide. *European Journal of Organic Chemistry* **2015,** *2015* (36), 7992-7996.

[294] Chen, H.; Gong, X.; Liu, X.; Li, Z.; Zhang, J.; Yang, X.-F., A nitroso-based fluorogenic probe for rapid detection of hydrogen sulfide in living cells. *Sensors and Actuators B: Chemical* **2019,** *281*, 542-548.

[295] Nie, J.; Yang, D.; Tang, X.; Zhang, L.; Ni, Z.; Gui, X., A new pyrene-based tert-butylnitroxide radical "off-on" fluorescent probe for H_2S detection in living cells. *Dyes and Pigments* **2019,** *170*, 107644.

[296] Wu, Z.; Feng, Y.; Geng, B.; Liu, J.; Tang, X., Fluorogenic sensing of H_2S in blood and living cells *via* reduction of aromatic dialkylamino *N*-oxide. *RSC Advances* **2014,** *4* (57), 30398-30401.

[297] Xuan, W.; Pan, R.; Cao, Y.; Liu, K.; Wang, W., A fluorescent probe capable of detecting H_2S at submicromolar concentrations in cells. *Chemical Communications* **2012,** *48* (86), 10669-10671.

[298] Chen, B.; Huang, J.; Geng, H.; Xuan, L.; Xu, T.; Li, X.; Han, Y., A new ESIPT-based fluorescent probe for highly selective and sensitive detection of hydrogen sulfide and its application in live-cell imaging. *New Journal of Chemistry* **2017,** *41* (3), 1119-1123.

[299] Zhao, Z.; Cao, L.; Zhang, T.; Hu, R.; Wang, S.; Li, S.; Li, Y.; Yang, G., Novel Reaction-Based Fluorescence Probes for the Detection of Hydrogen Sulfide in Living Cells. *ChemistrySelect* **2016,** *1* (11), 2581-2585.

[300] Li, X.; Cheng, J.; Gong, Y.; Yang, B.; Hu, Y., Mapping hydrogen sulfide in rats with a novel azo-based fluorescent probe. *Biosensors and Bioelectronics* **2015,** *65*, 302-306.

[301] Li, K.; Zakharov, L. N.; Pluth, M. D., Taming the Dichalcogenides: Isolation, Characterization, and Reactivity of Elusive Perselenide, Persulfide, Thioselenide, and Selenosulfide Anions. *Journal of the American Chemical Society* **2023,** *145* (24), 13435-13443.

[302] Liu, C.; Pan, J.; Li, S.; Zhao, Y.; Wu, L. Y.; Berkman, C. E.; Whorton, A. R.; Xian, M., Capture and Visualization of Hydrogen Sulfide by a Fluorescent Probe. *Angewandte Chemie International Edition* **2011,** *50* (44), 10327-10329.

[303] Xu, Z.; Xu, L.; Zhou, J.; Xu, Y.; Zhu, W.; Qian, X., A highly selective fluorescent probe for fast detection of hydrogen sulfide in aqueous solution and living cells. *Chemical Communications* **2012,** *48* (88), 10871-10873.

[304] Peng, B.; Chen, W.; Liu, C.; Rosser, E. W.; Pacheco, A.; Zhao, Y.; Aguilar, H. C.; Xian, M., Fluorescent Probes Based on Nucleophilic Substitution–Cyclization for Hydrogen Sulfide Detection and Bioimaging. *Chemistry – A European Journal* **2014,** *20* (4), 1010-1016.

[305] Chen, W.; Xu, S.; Day, J. J.; Wang, D.; Xian, M., A General Strategy for Development of Near-Infrared Fluorescent Probes for Bioimaging. *Angewandte Chemie International Edition* **2017,** *56* (52), 16611-16615.

[306] Zhang, X.; Qu, W.; Liu, H.; Ma, Y.; Wang, L.; Sun, Q.; Yu, F., Visualizing hydrogen sulfide in living cells and zebrafish using a red-emitting fluorescent probe via selenium-sulfur exchange reaction. *Analytica Chimica Acta* **2020,** *1109*, 37-43.

[307] Zhang, C.; Zhang, G.; Feng, L.; Li, J., A ratiometric fluorescent probe for sensitive and selective detection of hydrogen sulfide and its application for bioimaging. *Sensors and Actuators B: Chemical* **2015,** *216*, 412-417.

[308] Li, G.; Ma, S.; Tang, J.; Ye, Y., Lysosome-targeted two-photon fluorescent probes for rapid detection of H_2S in live cells. *New Journal of Chemistry* **2019,** *43* (3), 1267-1274.

[309] Wu, X.; Lu, Y.; Liu, B.; Chen, Y.; Zhang, J.; Zhou, Y., A H_2S-triggered two-photon ratiometric fluorescent theranostic prodrug for bio-imaging. *Chinese Chemical Letters* **2021,** *32* (8), 2380-2384.

[310] Li, D.-P.; Zhang, J.-F.; Cui, J.; Ma, X.-F.; Liu, J.-T.; Miao, J.-Y.; Zhao, B.-X., A ratiometric fluorescent probe for fast detection of hydrogen sulfide and recognition of biological thiols. *Sensors and Actuators B: Chemical* **2016,** *234*, 231-238.

[311] Cao, T.; Teng, Z.; Gong, D.; Qian, J.; Liu, W.; Iqbal, K.; Qin, W.; Guo, H., A ratiometric fluorescent probe for detection of endogenous and exogenous hydrogen sulfide in living cells. *Talanta* **2019,** *198*, 185-192.

[312] Kang, J.; Huo, F.; Yin, C., A novel ratiometric fluorescent H_2S probe based on tandem nucleophilic substitution/cyclization reaction and its bioimaging. *Dyes and Pigments* **2017,** *146*, 287-292.

[313] Gu, X.; Zhu, H.; Yang, S.; Zhu, Y.-C.; Zhu, Y.-Z., Development of a highly selective H_2S fluorescent probe and its application to evaluate CSE inhibitors. *RSC Advances* **2014,** *4* (91), 50097-50101.

[314] Zhang, H.; Li, M.; Zhang, C.; Zhang, G.; Chao, J.; Shi, L.; Yao, Q.; Shuang, S.; Dong, C., The design of hydrogen sulfide fluorescence probe based on dual nucleophilic reaction and its application for bioimaging. *Spectrochimica Acta Part A: Molecular and Biomolecular Spectroscopy* **2019,** *207*, 150-155.

[315] Ren, Y.; Zhang, L.; Zhou, Z.; Wang, S.; Xu, Y.; Gu, Y.; Zha, X., A new fluorescent probe for quick and highly selective detection of hydrogen sulfide and its application in living cells. *New Journal of Chemistry* **2018,** *42* (16), 13884-13888.

[316] Wang, J.; Wen, Y.; Huo, F.; Yin, C., A highly sensitive fluorescent probe for hydrogen sulfide based on dicyanoisophorone and its imaging in living cells. *Sensors and Actuators B: Chemical* **2019,** *294*, 141-147.

[317] Liu, T.-Z.; Wang, S.; Zhao, K.-L.; Miao, J.-Y.; Zhao, B.-X.; Lin, Z.-M., A simple benzothiazole-based turn-on fluorescent probe for detecting H_2S in HeLa cells. *Dyes and Pigments* **2023,** *217*, 111418.

[318] Wang, J.; Wen, Y.; Huo, F.; Yin, C., Based 'successive' nucleophilic substitution mitochondrial-targeted H_2S red light emissive fluorescent probe and its imaging in mice. *Sensors and Actuators B: Chemical* **2019,** *297*, 126773.

[319] Men, J.; Yang, X.; Zhang, H.; Zhou, J., A near-infrared fluorescent probe based on nucleophilic substitution–cyclization for selective detection of hydrogen sulfide and bioimaging. *Dyes and Pigments* **2018,** *153*, 206-212.

[320] Zhang, X.; Sun, R.; Duan, G.; Zhou, Z.; Luo, Y.; Li, W.; Zhang, L.; Gu, Y.; Zha, X., A highly sensitive near-infrared fluorescent probe for the detection of hydrogen sulfide and its application in living cells and mice. *New Journal of Chemistry* **2018,** *42* (24), 19795-19800.

[321] Gholap, S. P.; Yao, C.; Green, O.; Babjak, M.; Jakubec, P.; Malatinský, T.; Ihssen, J.; Wick, L.; Spitz, U.; Shabat, D., Chemiluminescence Detection of Hydrogen Sulfide Release by β-Lactamase-Catalyzed β-Lactam Biodegradation: Unprecedented Pathway for Monitoring β-Lactam Antibiotic Bacterial Resistance. *Bioconjugate Chemistry* **2021,** *32* (5), 991-1000.

[322] Zhang, L.-L.; Zhu, H.-K.; Zhao, C.-C.; Gu, X.-F., A near-infrared fluorescent probe for monitoring fluvastatin-stimulated endogenous H_2S production. *Chinese Chemical Letters* **2017,** *28* (2), 218-221.

[323] Zhang, L.; Zhu, H.; Li, M.; Gu, X., A novel fluorescent probe for imaging endogenous hydrogen sulphide via the CSE enzymatic pathway. *Chemical Communications* **2015,** *51* (66), 13135-13137.

[324] Chang, M. J.; Kim, K.; Kang, C.; Lee, M. H., Enhanced Aggregability of AIE-Based Probe through H_2S-Selective Triggered Dimerization and Its Applications to Biological Systems. *ACS Omega* **2019,** *4* (4), 7176-7181.

[325] Huang, Q.; Yang, X.-F.; Li, H., A ratiometric fluorescent probe for hydrogen sulfide based on an excited-state intramolecular proton transfer mechanism. *Dyes and Pigments* **2013,** *99* (3), 871-877.

[326] Wu, Q.; Huo, F.; Wang, J.; Yin, C., Fluorescent probe for detecting hydrogen sulfide based on disulfide nucleophilic substitution-addition. *Spectrochimica Acta Part A: Molecular and Biomolecular Spectroscopy* **2020,** *238*, 118437.

[327] Zhao, Q.; Kang, J.; Wen, Y.; Huo, F.; Zhang, Y.; Yin, C., "Turn-on" fluorescent probe for detection of H_2S and its applications in bioimaging. *Spectrochimica Acta Part A: Molecular and Biomolecular Spectroscopy* **2018,** *189*, 8-12.

[328] Zou, X. J.; Ma, Y. C.; Guo, L. E.; Liu, W. X.; Liu, M. J.; Zou, C. G.; Zhou, Y.; Zhang, J. F., A lysosome-targeted fluorescent chemodosimeter for monitoring endogenous and

exogenous hydrogen sulfide by in vivo imaging. *Chemical Communications* **2014,** *50* (89), 13833-13836.

[329] Wang, H.; Yang, D.; Tan, R.; Zhou, Z. J.; Xu, R.; Zhang, J. F.; Zhou, Y., A cyanine-based colorimetric and fluorescence probe for detection of hydrogen sulfide in vivo. *Sensors and Actuators B: Chemical* **2017,** *247*, 883-888.

[330] Wang, Y.; Yang, C.-t.; Xu, S.; Chen, W.; Xian, M., Hydrogen Sulfide Mediated Tandem Reaction of Selenenyl Sulfides and Its Application in Fluorescent Probe Development. *Organic Letters* **2019,** *21* (18), 7573-7576.

[331] Suarez, S. I.; Ambrose, R.; Kalk, M. A.; Lukesh III, J. C., Selenosulfides Tethered to gem-Dimethyl Esters: A Robust and Highly Versatile Framework for H_2S Probe Development. *Chemistry – A European Journal* **2019,** *25* (69), 15736-15740.

[332] Peng, B.; Zhang, C.; Marutani, E.; Pacheco, A.; Chen, W.; Ichinose, F.; Xian, M., Trapping Hydrogen Sulfide (H_2S) with Diselenides: The Application in the Design of Fluorescent Probes. *Organic Letters* **2015,** *17* (6), 1541-1544.

[333] Zhang, C.; Peng, B.; Chen, W.; Shuang, S.; Xian, M.; Dong, C., A ratiometric fluorescent probe for hydrogen sulfide based on the nucleophilic substitution-cyclization of diselenides. *Dyes and Pigments* **2015,** *121*, 299-304.

[334] Guan, H.; Zhang, A.; Li, P.; Xia, L.; Guo, F., ESIPT Fluorescence Probe Based on Double-Switch Recognition Mechanism for Selective and Rapid Detection of Hydrogen Sulfide in Living Cells. *ACS Omega* **2019,** *4* (5), 9113-9119.

[335] Zhang, C.-l.; Li, X.-l.; Jiang, Y.-h.; Zhang, Y.-n.; Xie, Y.-x.; Li, Y.-z.; Liu, C., A turn-on colorimetric dual-response fluorescent probe for rapid detecting and its application in bio-imaging and real water samples. *Optical Materials* **2022,** *131*, 112625.

[336] Yu, F.; Li, P.; Li, G.; Zhao, G.; Chu, T.; Han, K., A Near-IR Reversible Fluorescent Probe Modulated by Selenium for Monitoring Peroxynitrite and Imaging in Living Cells. *Journal of the American Chemical Society* **2011,** *133* (29), 11030-11033.

[337] Zhang, W.; Liu, W.; Li, P.; Kang, J.; Wang, J.; Wang, H.; Tang, B., Reversible two-photon fluorescent probe for imaging of hypochlorous acid in live cells and in vivo. *Chemical Communications* **2015,** *51* (50), 10150-10153.

[338] Wang, B.; Li, P.; Yu, F.; Chen, J.; Qu, Z.; Han, K., A near-infrared reversible and ratiometric fluorescent probe based on Se-BODIPY for the redox cycle mediated by hypobromous acid and hydrogen sulfide in living cells. *Chemical Communications* **2013,** *49* (51), 5790-5792.

[339] Lou, Z.; Li, P.; Pan, Q.; Han, K., A reversible fluorescent probe for detecting hypochloric acid in living cells and animals: utilizing a novel strategy for effectively modulating the

fluorescence of selenide and selenoxide. *Chemical Communications* **2013,** *49* (24), 2445-2447.

[340] Liu, C.; Jiao, X.; Cai, S.; He, S.; Zhao, L.; Zeng, X., Reversible fluorescent probe for visually monitoring the concentration-dependent dynamic correlations among HOCl, H_2S, and Ca^{2+} in neurons. *Sensors and Actuators B: Chemical* **2021,** *329*, 129213.

[341] Shen, Y.; Zhang, X.; Zhang, C.; Tang, Y., An ESIPT-based reversible ratiometric fluorescent sensor for detecting HClO/H_2S redox cycle in living cells. *Spectrochimica Acta Part A: Molecular and Biomolecular Spectroscopy* **2023,** *285*, 121881.

[342] Annaka, T.; Nakata, N.; Ishii, A., A reversible and turn-on type fluorescence behaviour of hydrogen sulfide via a redox cycle between selenoxide and selenide. *New Journal of Chemistry* **2019,** *43* (29), 11643-11652.

[343] Liu, F.; Gao, Y.; Wang, J.; Sun, S., Reversible and selective luminescent determination of ClO^-/H_2S redox cycle in vitro and in vivo based on a ruthenium trisbipyridyl probe. *Analyst* **2014,** *139* (13), 3324-3329.

[344] Maeda, H.; Matsuno, H.; Ushida, M.; Katayama, K.; Saeki, K.; Itoh, N., 2,4-Dinitrobenzenesulfonyl Fluoresceins as Fluorescent Alternatives to Ellman's Reagent in Thiol-Quantification Enzyme Assays. *Angewandte Chemie International Edition* **2005,** *44* (19), 2922-2925.

[345] Cao, X.; Lin, W.; Zheng, K.; He, L., A near-infrared fluorescent turn-on probe for fluorescence imaging of hydrogen sulfide in living cells based on thiolysis of dinitrophenyl ether. *Chemical Communications* **2012,** *48* (85), 10529-10531.

[346] Cheng, J.; Shao, B.; Zhang, S.; Hu, Y.; Li, X., Selective and sensitive detection of hydrogen sulfide in live cells. *RSC Advances* **2015,** *5* (80), 65203-65207.

[347] Ji, Y.; Xia, L.-J.; Chen, L.; Guo, X.-F.; Wang, H.; Zhang, H.-J., A novel BODIPY-based fluorescent probe for selective detection of hydrogen sulfide in living cells and tissues. *Talanta* **2018,** *181*, 104-111.

[348] Fang, T.; Jiang, X.-D.; Sun, C.; Li, Q., BODIPY-based naked-eye fluorescent on-off probe with high selectivity for H_2S based on thiolysis of dinitrophenyl ether. *Sensors and Actuators B: Chemical* **2019,** *290*, 551-557.

[349] Wu, J.; Chan, C.; Li, J.; Shi, Y.; Xue, Z.; Zhao, L., A BODIPY-based fluorescent chemosensor with 2,6-substitution for visual and highly selective detection of S^{2-}. *Spectrochimica Acta Part A: Molecular and Biomolecular Spectroscopy* **2023,** *297*, 122741.

[350] Liu, T.; Zhang, X.; Qiao, Q.; Zou, C.; Feng, L.; Cui, J.; Xu, Z., A two-photon fluorescent probe for imaging hydrogen sulfide in living cells. *Dyes and Pigments* **2013,** *99* (3), 537-542.

[351] Ma, Y.; Zhang, J.; Qu, H., Synthesis and Properties of Novel Fluorescence Probe Based on 1,8-Naphthalimide for Detection of Hydrogen Sulfide. *Chemical Research in Chinese Universities* **2019,** *35* (1), 5-11.

[352] Ou, P.; Wang, Y.; Hao, C.; Peng, Y.; Zhou, L.-y., Naphthalimide-based a highly selective two-photon fluorescent probe for imaging of hydrogen sulfide in living cells and inflamed tissue of mouse model. *Spectrochimica Acta Part A: Molecular and Biomolecular Spectroscopy* **2021,** *245*, 118886.

[353] Luo, F.; Wang, L.; Zhang, X.; Xu, P.; Wang, X.; Qu, Y., Ratiometric H_2S probe that can be recognized by the naked eye and its application in cell imaging. *Phosphorus, Sulfur, and Silicon and the Related Elements* **2023,** *198* (10), 836-843.

[354] Yuan, L.; Zuo, Q.-P., Reaction-based fluorescent probe for hydrogen sulfide with large signal-to-noise ratio in living cells and tissues. *Sensors and Actuators B: Chemical* **2014,** *196*, 151-155.

[355] Chen, S.; Ma, C.; Wang, D.-E.; Han, X.; Zhang, L.; Wang, J., Highly sensitive and selective coumarin probe for hydrogen sulfide imaging in living cells. *Analytical Methods* **2015,** *7* (18), 7646-7652.

[356] Cui, J.; Zhang, T.; Sun, Y.-Q.; Li, D.-P.; Liu, J.-T.; Zhao, B.-X., A highly sensitive and selective fluorescent probe for H_2S detection with large fluorescence enhancement. *Sensors and Actuators B: Chemical* **2016,** *232*, 705-711.

[357] Yang, J.; Yin, C.; Wen, Y.; Zhang, Y.; Huo, F., A photostable fluorescent probe based on PET off for the detection of hydrogen sulfide and its application in bioimaging. *New Journal of Chemistry* **2020,** *44* (17), 7091-7095.

[358] Ou, L.; Guo, R.; Lin, W., A coumarin-based "off–on" fluorescent probe for highly selective detection of hydrogen sulfide and imaging in living cells. *Analytical Methods* **2021,** *13* (12), 1511-1516.

[359] Fang, Y.; Luo, F.; Cao, Z.; Peng, C.; Dehaen, W., Umbelliferone-Based Fluorescent Probe for Selective Recognition of Hydrogen Sulfide and Its Bioimaging in Living Cells and Zebrafish. *Chemosensors* **2022,** *10* (10), 427.

[360] Yang, L.; Zhao, J.; Yu, X.; Zhang, R.; Han, G.; Liu, R.; Liu, Z.; Zhao, T.; Han, M.-Y.; Zhang, Z., Dynamic mapping of spontaneously produced H_2S in the entire cell space and in live animals using a rationally designed molecular switch. *Analyst* **2018,** *143* (8), 1881-1889.

[361] Chen, Y.; Shang, X.; Li, C.; Xue, Z.; Chen, H.; Wu, H.; Wang, T., The synthesis, crystal, hydrogen sulfide detection and cell assement of novel chemsensors based on coumarin derivatives. *Scientific Reports* **2018,** *8* (1), 16159.

[362] Yang, Q.; Zhou, L.; Peng, L.; Yuan, G.; Ding, H.; Tan, L.; Zhou, Y., A smart mitochondria-targeting TP-NIR fluorescent probe for the selective and sensitive sensing of H_2S in living cells and mice. *New Journal of Chemistry* **2021,** *45* (16), 7315-7320.

[363] Tong, X.; Hao, L.; Song, X.; Wu, S.; Zhang, N.; Li, Z.; Chen, S.; Hou, P., Construction of novel coumarin-carbazole-based fluorescent probe for tracking of endogenous and exogenous H_2S in vivo with yellow-emission and large Stokes shift. *Spectrochimica Acta Part A: Molecular and Biomolecular Spectroscopy* **2022,** *279*, 121445.

[364] Liu, X.-D.; Fan, C.; Sun, R.; Xu, Y.-J.; Ge, J.-F., Nile-red and Nile-blue-based near-infrared fluorescent probes for in-cellulo imaging of hydrogen sulfide. *Analytical and Bioanalytical Chemistry* **2014,** *406* (28), 7059-7070.

[365] Yin, W.; Wang, H.; Ma, F.; Xu, Z.; Lu, Y.; Zhou, M.; Deng, B.; Wang, H.; Zhang, J., A benzophenoxazine-based NIR fluorescent probe for the detection of hydrogen sulfide and imaging in living cells. *Analyst* **2022,** *147* (20), 4547-4552.

[366] Tang, C.; Zheng, Q.; Zong, S.; Wang, Z.; Cui, Y., A long-wavelength-emitting fluorescent turn-on probe for imaging hydrogen sulfide in living cells. *Sensors and Actuators B: Chemical* **2014,** *202*, 99-104.

[367] Yu Haibo, L. H., Zhang Xinfu, Xiao Yi, Fang Peiju, Lv Chunjiao, Hou Wei, A Mitochondrial-Targetable and Turn-On Fluorescent Probe based on Nile Red and Monitoring for H_2S in Living Cells. *Acta Chimica Sinica* **2015,** *73* (5), 450-456.

[368] Liu, J.; Chen, X.; Zhang, Y.; Gao, G.; Zhang, X.; Hou, S., A novel xanthene-based colorimetric and fluorescence probe for detection of H_2S in living cells. *Journal of Luminescence* **2018,** *204*, 480-484.

[369] Qi, P.; Zhang, D.; Sun, Y.; Wan, Y., A selective near-infrared fluorescent probe for hydrogen sulfide and its application in sulfate-reducing bacteria detection. *Analytical Methods* **2016,** *8* (16), 3339-3344.

[370] Zhang, L.; Zheng, X. E.; Zou, F.; Shang, Y.; Meng, W.; Lai, E.; Xu, Z.; Liu, Y.; Zhao, J., A highly selective and sensitive near-infrared fluorescent probe for imaging of hydrogen sulphide in living cells and mice. *Scientific Reports* **2016,** *6* (1), 18868.

[371] Liang, K.; Li, Y.; Zeng, F.; Wu, S., A near-infrared fluorescent probe for detection of H_2S and its application in monitoring meat freshness and plant growth under aluminium-induced stress. *New Journal of Chemistry* **2023,** *47* (5), 2643-2650.

[372] Zhou, K.; Yang, Y.; Zhou, T.; Jin, M.; Yin, C., Design strategy of multifunctional and high efficient hydrogen sulfide NIR fluorescent probe and its application in vivo. *Dyes and Pigments* **2021,** *185*, 108901.

[373] Yang, S.; Zhou, F.; Yao, X.; Liu, W.; Zhu, W.; Qian, X.; Liu, Y., A novel near-infrared fluorescent probe to in vivo evaluate the release efficiency of H_2S prodrug. *Sensors and Actuators B: Chemical* **2021,** *339*, 129881.

[374] Zhang, K.; Meng, J.; Bao, W.; Liu, M.; Wang, X.; Tian, Z., Mitochondrion-targeting near-infrared fluorescent probe for detecting intracellular nanomolar level hydrogen sulfide with high recognition rate. *Analytical and Bioanalytical Chemistry* **2021,** *413* (4), 1215-1224.

[375] Gong, S.; Zheng, Z.; Guan, X.; Feng, S.; Feng, G., Near-Infrared Mitochondria-Targetable Fluorescent Probe for High-Contrast Bioimaging of H_2S. *Analytical Chemistry* **2021,** *93* (14), 5700-5708.

[376] Li, J.; Ding, D.; Wang, J.; Huang, L.; Zhan, J.; Lin, W., An activatable photoacoustic probe for imaging upregulation of hydrogen sulfide in inflammation. *Sensors and Actuators B: Chemical* **2022,** *367*, 132097.

[377] Wang, M.; Gu, X.; Chen, J.; Yang, X.; Cheng, P.; Xu, K., A novel near-infrared colorimetric-fluorescent probe for hydrogen sulfide and application in bioimaging. *Journal of Photochemistry and Photobiology A: Chemistry* **2023,** *437*, 114438.

[378] Wang, Y.; Li, S.; Zhu, X.; Shi, X.; Liu, X.; Zhang, H., A novel H_2O_2 activated NIR fluorescent probe for accurately visualizing H_2S fluctuation during oxidative stress. *Analytica Chimica Acta* **2022,** *1202*, 339670.

[379] Sun, L.; Wu, Y.; Chen, J.; Zhong, J.; Zeng, F.; Wu, S., A Turn-On Optoacoustic Probe for Imaging Metformin-Induced Upregulation of Hepatic Hydrogen Sulfide and Subsequent Liver Injury. *Theranostics* **2019,** *9* (1), 77-89.

[380] Liu, C.; Liu, Q.; Cai, S.; Ding, H.; He, S.; Zhao, L.; Zeng, X.; Gong, J., Novel near-infrared spectroscopic probe for visualizing hydrogen sulfide in lysosomes. *Spectrochimica Acta Part A: Molecular and Biomolecular Spectroscopy* **2022,** *271*, 120917.

[381] Lin, Y.-M.; He, Q.; Wang, X.-Y.; Hua, F.-F.; Liu, X.-Y.; Fu, Y.-L., Near-Infrared Fluorescent Probe for Imaging Upregulated Hydrogen Sulfide Levels in Rice under Salt and Drought Stress. *Journal of Agricultural and Food Chemistry* **2023,** *70* (13), 5154-5161.

[382] Su, W.; Huang, L.; Zhu, L.; Lin, W., A novel fluorescent probe for imagining hydrogen sulfide upregulation in acute lung injury. *Sensors and Actuators B: Chemical* **2022,** *369*, 132297.

[383] Qin, C.-K.; Yan, L.; Wang, Z.-Q.; Yu, G.; Mao, G.-J.; Xu, F.; Li, C.-Y., A near-infrared fluorescent probe for detecting hydrogen sulfide with high selectivity in cells and ulcerative colitis in mice. *Analyst* **2023,** *148* (22), 5724-5730.

[384] Liu, H.-Y.; Zhao, M.; Qiao, Q.-L.; Lang, H.-J.; Xu, J.-Z.; Xu, Z.-C., Fluorescein-derived fluorescent probe for cellular hydrogen sulfide imaging. *Chinese Chemical Letters* **2014,** *25* (7), 1060-1064.

[385] Yuan, L.; Zuo, Q.-P., FRET-Based Mitochondria-Targetable Dual-Excitation Ratiometric Fluorescent Probe for Monitoring Hydrogen Sulfide in Living Cells. *Chemistry – An Asian Journal* **2014,** *9* (6), 1544-1549.

[386] Zhao, X.-j.; Li, Y.-t.; Jiang, Y.-r.; Yang, B.-q.; Liu, C.; Liu, Z.-h., A novel "turn-on" mitochondria-targeting near-infrared fluorescent probe for H_2S detection and in living cells imaging. *Talanta* **2019,** *197*, 326-333.

[387] Zhao, X.-j.; Jiang, Y.-r.; Li, Y.-t.; Yang, B.-q.; Liu, C.; Liu, Z.-h., A novel "turn-on" mitochondria-targeting near-infrared fluorescent probe for determination and bioimaging cellular hydrogen sulfide. *Spectrochimica Acta Part A: Molecular and Biomolecular Spectroscopy* **2019,** *212*, 71-77.

[388] Wang, Z.; Li, Y.; Zhang, Q.; Jing, C.; Jiang, Y.; Yang, T.; Han, T.; Xiong, F., A highly selective and easily acquisitive near-infrared fluorescent probe for detection and imaging of hydrogen sulfide in cells. *Spectrochimica Acta Part A: Molecular and Biomolecular Spectroscopy* **2023,** *293*, 122428.

[389] Guo, M.-Y.; Wang, W.; Ainiwaer, D.; Yang, Y.-S.; Wang, B.-Z.; Yang, J.; Zhu, H.-L., A fluorescent Rhodol-derived probe for rapid and selective detection of hydrogen sulfide and its application. *Talanta* **2022,** *237*, 122960.

[390] Gao, Z.; Zhang, L.; Liu, H.; Yan, M.; Lu, S.; Lian, H.; Zhang, P.; Zhu, J.; Jin, M., A novel rhodol-based fluorescence turn-on probe for selective hydrogen sulfide detection in environment water and living cells. *Journal of Photochemistry and Photobiology A: Chemistry* **2022,** *423*, 113598.

[391] El Sayed, S.; de la Torre, C.; Santos-Figueroa, L. E.; Martínez-Máñez, R.; Sancenón, F.; Orzáez, M.; Costero, A. M.; Parra, M.; Gil, S., 2,4-dinitrophenyl ether-containing chemodosimeters for the selective and sensitive 'in vitro' and 'in vivo' detection of hydrogen sulfide. *Supramolecular Chemistry* **2015,** *27* (4), 244-254.

[392] Wang, K.; Yang, X.; Guo, M.-Y.; Chen, X.-Y.; Li, T.; Yan, R.; Yang, Y.-S.; Zhu, H.-L.; Hu, Z.-G., Imaging the dynamic processes of hydrogen sulfide using a rapid "turn-on" mitochondria-targeting fluorescent probe. *Sensors and Actuators B: Chemical* **2022,** *369*, 132285.

[393] Weixing, C.; Ting, W.; Yunfei, Z.; Shuying, L.; Hongwei, Z.; Yanlin, J.; Xilang, J., A Seminaphthorhodafluor-Based Fluorescent Probe for H_2S Detection and Its Application. *Chinese Journal of Organic Chemistry* **2020,** *40* (9), 2956-2962.

[394] Wu, K.; Wang, X.; Gong, L.; Zhai, X.; Wang, K.; Qiu, X.; Zhang, H.; Tang, Z.; Jiang, H.; Wang, X., Screening of H2S donors with a red emission mitochondria-targetable fluorescent probe: Toward discovering a new therapeutic strategy for Parkinson's disease. *Biosensors and Bioelectronics* **2023,** *237*, 115521.

[395] Liu, M.; Qiu, J.; Xiong, X.; Fu, S.; Guan, L.; He, M.; Gao, Y., A near infrared two-channel fluorescent probe for the detection of hydrogen sulfide and viscosity with a negligible crosstalk influence. *Bioorganic Chemistry* **2023,** *132*, 106379.

[396] Huang, K.; Liu, M.; Liu, Z.; Cao, D.; Hou, J.; Zeng, W., Ratiometric and colorimetric detection of hydrogen sulfide with high selectivity and sensitivity using a novel FRET-based fluorescence probe. *Dyes and Pigments* **2015,** *118*, 88-94.

[397] Muthusamy, S.; Rajalakshmi, K.; Zhu, D.; Zhao, L.; Wang, S.; Zhu, W., A novel lysosome targeted fluorophore for H_2S sensing: Enhancing the quantitative detection with successive reaction sites. *Sensors and Actuators B: Chemical* **2020,** *320*, 128433.

[398] Maity, D.; Raj, A.; Samanta, P. K.; Karthigeyan, D.; Kundu, T. K.; Pati, S. K.; Govindaraju, T., A probe for ratiometric near-infrared fluorescence and colorimetric hydrogen sulfide detection and imaging in live cells. *RSC Advances* **2014,** *4* (22), 11147-11151.

[399] Lin, X.; Lu, X.; Zhou, J.; Ren, H.; Dong, X.; Zhao, W.; Chen, Z., Instantaneous fluorescent probe for the specific detection of H_2S. *Spectrochimica Acta Part A: Molecular and Biomolecular Spectroscopy* **2019,** *213*, 416-422.

[400] Su, D.; Cheng, D.; Lv, Y.; Ren, X.; Wu, Q.; Yuan, L., A unique off-on near-infrared QCy7-derived probe for selective detection and imaging of hydrogen sulfide in cells and in vivo. *Spectrochimica Acta Part A: Molecular and Biomolecular Spectroscopy* **2020,** *226*, 117635.

[401] She, Z.-P.; Wang, W.-X.; Jiang, W.-L.; Wang, Z.-Q.; Mao, G.-J.; Fei, J.; Li, Y.; Li, C.-Y., Accurate Fluorescence Diagnosis of Cancer Based on Sequential Detection of Hydrogen Sulfide and pH. *Analytical Chemistry* **2021,** *93* (34), 11826-11835.

[402] Zhou, L.; Lu, D.; Wang, Q.; Liu, S.; Lin, Q.; Sun, H., Molecular engineering of a mitochondrial-targeting two-photon in and near-infrared out fluorescent probe for gaseous signal molecules H_2S in deep tissue bioimaging. *Biosensors and Bioelectronics* **2017,** *91*, 699-705.

[403] Wang, Z.; Li, X.; Sun, X.; Zhang, X.; He, C.; Li, Y.; Lu, F.; Lu, X.; Fan, Q., Highly selective imaging of intratumoral hydrogen sulfide by NIR-II emissive fluorescent probes. *Sensors and Actuators B: Chemical* **2023,** *384*, 133627.

[404] Qian, M.; Zhang, L.; Pu, Z.; Xia, J.; Chen, L.; Xia, Y.; Cui, H.; Wang, J.; Peng, X., A NIR fluorescent probe for the detection and visualization of hydrogen sulfide using the aldehyde group assisted thiolysis of dinitrophenyl ether strategy. *Journal of Materials Chemistry B* **2018,** *6* (47), 7916-7925.

[405] Hong, J.; Zhou, E.; Gong, S.; Feng, G., A red to near-infrared fluorescent probe featuring a super large Stokes shift for light-up detection of endogenous H_2S. *Dyes and Pigments* **2019,** *160*, 787-793.

[406] Xu, Z.; Zheng, Y.; Qiao, R.; Cao, S.; Fang, Y.; Bo, X.; Zhu, H.; Ying, C.; Sun, Y.; Zheng, J., Organic fluorescent probe for concurrent imaging and apoptosis induction in cancer cells in vivo and in vitro by utilizing endogenous hydrogen sulfide. *Chemical Engineering Journal* **2023,** *456*, 141000.

[407] Yan, L.; Gu, Q.-S.; Jiang, W.-L.; Tan, M.; Tan, Z.-K.; Mao, G.-J.; Xu, F.; Li, C.-Y., Near-Infrared Fluorescent Probe with Large Stokes Shift for Imaging of Hydrogen Sulfide in Tumor-Bearing Mice. *Analytical Chemistry* **2022,** *94* (14), 5514-5520.

[408] Zhong, K.; Chen, L.; Pan, Y.; Yan, X.; Hou, S.; Tang, Y.; Gao, X.; Li, J.; Tang, L., A colorimetric and near-infrared fluorescent probe for detection of hydrogen sulfide and its real multiple applications. *Spectrochimica Acta Part A: Molecular and Biomolecular Spectroscopy* **2019,** *221*, 117135.

[409] Xie, P.; Zhu, Y.; Huang, X.; Gao, G.; Guo, F.; Yang, G., A new near-infrared fluorescent chemodosimeter for discrimination of sulfide from disulfide. *Research on Chemical Intermediates* **2018,** *44* (4), 2823-2837.

[410] Gu, B.; Su, W.; Huang, L.; Wu, C.; Duan, X.; Li, Y.; Xu, H.; Huang, Z.; Li, H.; Yao, S., Real-time tracking and selective visualization of exogenous and endogenous hydrogen sulfide by a near-infrared fluorescent probe. *Sensors and Actuators B: Chemical* **2018,** *255*, 2347-2355.

[411] Jin, X.; Ma, X.; Zhou, H.; Chen, J.; Li, M.; Yang, J.; Bai, H.; She, M., Construction of DCM-based NIR fluorescent probe for visualization detection of H_2S in solution and nanofibrous film. *Spectrochimica Acta Part A: Molecular and Biomolecular Spectroscopy* **2021,** *257*, 119764.

[412] Zhang, H.; Zhu, M.; Jiang, D.-Y.; Xue, X.-Y.; Zhang, J.; Zhang, G.-N.; Wang, Y.-C.; Zhao, H., Ultrafast response fluorescent probe with red-emission for monitoring hydrogen sulfide in vivo and in vitro. *Journal of Photochemistry and Photobiology A: Chemistry* **2019,** *382*, 111974.

[413] Liu, T.; Xu, Z.; Spring, D. R.; Cui, J., A Lysosome-Targetable Fluorescent Probe for Imaging Hydrogen Sulfide in Living Cells. *Organic Letters* **2013,** *15* (9), 2310-2313.

[414] Wan, D.; Pan, T.; Ou, P.; Zhou, R.; Ouyang, Z.; Luo, L.; Xiao, Z.; Peng, Y., Construct a lysosome-targeting and highly selective fluorescent probe for imaging of hydrogen sulfide in living cells and inflamed tissues. *Spectrochimica Acta Part A: Molecular and Biomolecular Spectroscopy* **2021,** *249*, 119311.

[415] Wu, C.; Hu, X.; Gu, B.; Yin, P.; Su, W.; Li, Y.; Lu, Q.; Zhang, Y.; Li, H., A lysosome-targeting colorimetric and fluorescent dual signal probe for sensitive detection and bioimaging of hydrogen sulfide. *Analytical Methods* **2018,** *10* (6), 604-610.

[416] Zhang, L.; Yan, J.-L.; Wu, W.-N.; Zhao, X.-L.; Wang, Y.; Fan, Y.-C.; Xu, Z.-H., A "turn-on" chalcone-based probe for hydrogen sulfide and imaging applications in lysosomes of living cells and zebrafish. *Microchemical Journal* **2022,** *183*, 107941.

[417] Yue, J.; Tao, Y.; Zhang, J.; Wang, H.; Wang, N.; Zhao, W., BODIPY-based Fluorescent Probe for Fast Detection of Hydrogen Sulfide and Lysosome-targeting Applications in Living Cells. *Chemistry – An Asian Journal* **2021,** *16* (7), 850-855.

[418] Singh, N.; Sharma, S.; Singh, R.; Rajput, S.; Chattopadhyay, N.; Tewari, D.; Joshi, K. B.; Verma, S., A naphthalimide-based peptide conjugate for concurrent imaging and apoptosis induction in cancer cells by utilizing endogenous hydrogen sulfide. *Chemical Science* **2021,** *12* (48), 16085-16091.

[419] Kang, N.; Pei, S.; Zhang, C.; Zhang, G.; Zhou, Y.; Shi, L.; Wang, W.; Shuang, S.; Dong, C., A turn-on fluorescence probe for hydrogen sulfide in absolute aqueous solution. *Spectrochimica Acta Part A: Molecular and Biomolecular Spectroscopy* **2020,** *233*, 118156.

[420] Fu, D., A novel quinoline-based colorimetric fluorescent probe for hydrogen sulfide. *Journal of Chemical Research* **2021,** *45* (1-2), 76-79.

[421] Chen, G.; Xu, J.; Zhan, Z.; Gao, X.; Jiao, M.; Ren, M.; Lv, L.; Chen, T.; Li, Y.; Liu, Y., A bright two-photon fluorescence probe with large stokes shift for deep tissue imaging of H_2S during metabolism. *Dyes and Pigments* **2020,** *172*, 107850.

[422] Zhong, K.; Zhou, S.; Yan, X.; Li, X.; Hou, S.; Cheng, L.; Gao, X.; Li, Y.; Tang, L., A simple H_2S fluorescent probe with long wavelength emission: Application in water, wine, living cells and detection of H_2S gas. *Dyes and Pigments* **2020,** *174*, 108049.

[423] Yang, Y.; Chen, L.; Hu, X.; Zhong, K.; Li, S.; Yan, X.; Zhang, J.; Tang, L., Synthesis of a Turn-On Fluorescent Probe for Hydrogen Sulfide and Its Application in Red Wine and Living Cells. *Chinese Journal of Organic Chemistry* **2023,** *43* (1), 308-312.

[424] Hu, Y.; Chen, Z.; Ma, L.; Zhang, Z.; Zhang, H.; Yi, F.; Liu, C., A quinolinium-phenol vinylic conjugated fluorescent probe for H_2S detection based on H_2S-triggered release of protected group. *Tetrahedron* **2022,** *117-118*, 132837.

[425] Zan, Q.; Fan, L.; Ma, L.; Yang, Q.; Zhao, K.; Huang, Y.; Dong, C.; Shuang, S., Dual-channel fluorescent probe for simultaneously detecting H_2S and viscosity/polarity and its application in non-alcoholic fatty liver, tumor tissue, and food spoilage. *Sensors and Actuators B: Chemical* **2023,** *397*, 134596.

[426] Liu, Y.; Feng, G., A visible light excitable colorimetric and fluorescent ESIPT probe for rapid and selective detection of hydrogen sulfide. *Organic & Biomolecular Chemistry* **2014,** *12* (3), 438-445.

[427] Liu, J.; Chen, X.; Zhang, Y.; Gao, G.; Zhang, X.; Hou, S.; Hou, Y., A novel 3-hydroxychromone fluorescent probe for hydrogen sulfide based on an excited-state intramolecular proton transfer mechanism. *New Journal of Chemistry* **2018,** *42* (15), 12918-12923.

[428] Yu, B.; Chen, C.; Ru, J.; Luo, W.; Liu, W., A multifunctional two-photon fluorescent probe for detecting H_2S in wastewater and GSH in vivo. *Talanta* **2018,** *188*, 370-377.

[429] Zhang, P.; Nie, X.; Gao, M.; Zeng, F.; Qin, A.; Wu, S.; Tang, B. Z., A highly selective fluorescent nanoprobe based on AIE and ESIPT for imaging hydrogen sulfide in live cells and zebrafish. *Materials Chemistry Frontiers* **2017,** *1* (5), 838-845.

[430] Sun, T.-T.; Man, R.-J.; Shi, J.-Y.; Wang, X.; Zhao, M.; Hu, H.-Y.; Wang, C.-Y., A selective fluorescent probe for hydrogen sulfide from a series of flavone derivatives and intracellular imaging. *Spectrochimica Acta Part A: Molecular and Biomolecular Spectroscopy* **2023,** *299*, 122840.

[431] Chen, S.; Hou, P.; Song, X., A red-emitting fluorescent probe for imaging hydrogen sulphide with a large Stokes shift. *Sensors and Actuators B: Chemical* **2015,** *221*, 951-955.

[432] Dhivya, R.; Kavitha, V.; Gomathi, A.; Keerthana, P.; Santhalakshmi, N.; Viswanathamurthi, P.; Haribabu, J., Dinitrobenzene ether reactive turn-on fluorescence probes for the selective detection of H_2S. *Analytical Methods* **2022,** *14* (1), 58-66.

[433] Hong, L.-X.; Sun, L.; Li, C.; Zhang, R.-L.; Zhao, J.-S., Multiple Applications of a Novel Fluorescence Probe with Large Stokes Shift and Sensitivity for Rapid H_2S Detection. *Journal of Fluorescence* **2023**, DOI: 10.1007/s10895-023-03377-y.

[434] El Sayed, S.; Torre, C. d. l.; Santos-Figueroa, L. E.; Pérez-Payá, E.; Martínez-Máñez, R.; Sancenón, F.; Costero, A. M.; Parra, M.; Gil, S., A new fluorescent "turn-on" chemodosimeter for the detection of hydrogen sulfide in water and living cells. *RSC Advances* **2013,** *3* (48), 25690-25693.

[435] Wang, H.; Wang, J.; Yang, S.; Tian, H.; Liu, Y.; Sun, B., Highly selective and rapidly responsive fluorescent probe for hydrogen sulfide detection in wine. *Food Chemistry* **2018,** *257*, 150-154.

[436] Das, A. K.; Goswami, S.; Quah, C. K.; Fun, H.-K., Neighbouring group participation of thiol through aldehyde group assisted thiolysis of active ether: ratiometric and vapor phase fast detection of hydrogen sulfide in mixed aqueous media. *New Journal of Chemistry* **2015,** *39* (7), 5669-5675.

[437] Liu, Y.; Ding, Y.; Huang, J.; Zhang, X.; Fang, T.; Zhang, Y.; Zheng, X.; Yang, X., A benzothiazole-based fluorescent probe for selective detection of H_2S in living cells and mouse hippocampal tissues. *Dyes and Pigments* **2017,** *138*, 112-118.

[438] Huang, Z.; Ding, S.; Yu, D.; Huang, F.; Feng, G., Aldehyde group assisted thiolysis of dinitrophenyl ether: a new promising approach for efficient hydrogen sulfide probes. *Chemical Communications* **2014,** *50* (65), 9185-9187.

[439] Gu, B.; Dai, C.; Zhou, Z.; Tang, S.; Zhang, Y., Rational construction of an AIE-active fluorescent probe bearing three reaction sites for individual and continuous detection of H_2S and HClO with single-wavelength excitation. *Sensors and Actuators B: Chemical* **2023,** *375*, 132900.

[440] Xu, P.; Liu, M.; Gao, T.; Zhang, H.; Li, Z.; Huang, X.; Zeng, W., An ESIPT-based highly selective and sensitive probe for the detection of hydrogen sulfide. *Tetrahedron Letters* **2015,** *56* (26), 4007-4010.

[441] Li, Y.; Chu, T.-S., DFT/TDDFT Study on the Sensing Mechanism of a Fluorescent Probe for Hydrogen Sulfide: Excited State Intramolecular Proton Transfer Coupled Twisted Intramolecular Charge Transfer. *The Journal of Physical Chemistry A* **2017,** *121* (28), 5245-5256.

[442] Xu, P.; Gao, T.; Liu, M.; Zhang, H.; Zeng, W., A novel excited-state intramolecular proton transfer (ESIPT) dye with unique near-IR keto emission and its application in detection of hydrogen sulfide. *Analyst* **2015,** *140* (6), 1814-1816.

[443] Wang, J.; Xie, H.; Li, H.; Wang, R.; Zhang, B.; Ren, T.; Hua, J.; Chen, N., NIR Fluorescent Probe for In Situ Bioimaging of Endogenous H_2S in Rice Roots under Al^{3+} and Flooding Stresses. *Journal of Agricultural and Food Chemistry* **2021,** *69* (47), 14330-14339.

[444] Banik, D.; Karak, A.; Halder, S.; Banerjee, S.; Mandal, M.; Maiti, A.; Jana, K.; Mahapatra, A. K., A turn-on fluorescent probe for selective detection of H_2S in environmental samples and bio-imaging in human breast cancer cells. *Organic & Biomolecular Chemistry* **2023,** *21* (39), 8020-8030.

[445] Pal, K.; Islam, A. S. M.; Prodhan, C.; Bhunya, S.; Paul, A.; Ali, M., A Benzooxazole-Based Probe for the Sensitive Detection of Hydrogen Sulfide: Kinetic and Transition-State Studies and In vitro Application in HepG2 Cells. *ChemistrySelect* **2018,** *3* (25), 7283-7290.

[446] Zheng, K.; Lin, W.; Tan, L.; Cheng, D., A two-photon fluorescent probe with a large turn-on signal for imaging hydrogen sulfide in living tissues. *Analytica Chimica Acta* **2015,** *853*, 548-554.

[447] Wang, H.; Li, Y.; Yang, S.; Tian, H.; Liu, Y.; Sun, B., A dual-function fluorescent probe for discriminative detection of hydrogen sulfide and hydrazine. *Journal of Photochemistry and Photobiology A: Chemistry* **2019,** *377*, 36-42.

[448] Wang, H.; Wu, X.; Yang, S.; Tian, H.; Liu, Y.; Sun, B., A dual-site fluorescent probe for separate detection of hydrogen sulfide and bisulfite. *Dyes and Pigments* **2019,** *160*, 757-764.

[449] Zhou Chan, Q. B., Zeng Yi, Chen Jinping, Yu Tianjun, Li Yi, A Reaction-Based Chemsensor for Hydrogen Sulfide Detection with Fluorescence Enhancement. *Chinese Journal of Organic Chemistry* **2017,** *37* (1), 92-96.

[450] Wang, K.; Guo, R.; Chen, X.-Y.; Li, X.-L.; Hu, Z.-G.; Wang, X.; Wang, C.-Y.; Qin, Y.-J.; Yao, K.; Yang, Y.-S., A novel fluorescent probe for imaging endogenous hydrogen sulfide in living cells and mice models of acute liver injury. *Chemical Engineering Journal* **2023,** *468*, 143611.

[451] Chen, S.; Hou, P.; Wang, J.; Fu, S.; Liu, L., A rapid and selective fluorescent probe with a large Stokes shift for the detection of hydrogen sulfide. *Spectrochimica Acta Part A: Molecular and Biomolecular Spectroscopy* **2018,** *203*, 258-262.

[452] Lu, Y.; Dong, B.; Song, W.; Kong, X.; Mehmood, A. H.; Lin, W., A PET and ESIPT based fluorescent probe for the imaging of hydrogen sulfide (H_2S) in live cells and zebrafish. *Analytical Methods* **2019,** *11* (26), 3301-3306.

[453] Liu, X.; Qi, Y.; Pu, S.; Wang, Y.; Gao, Z., Sensing mechanism of a new fluorescent probe for hydrogen sulfide: photoinduced electron transfer and invalidity of excited-state intramolecular proton transfer. *RSC Advances* **2021,** *11* (36), 22214-22220.

[454] Zhong, K.; Deng, L.; Zhao, J.; Yan, X.; Sun, T.; Li, J.; Tang, L., A novel near-infrared fluorescent probe for highly selective recognition of hydrogen sulfide and imaging in living cells. *RSC Advances* **2018,** *8* (42), 23924-23929.

[455] Zhang, X.; Jin, X.; Zhang, C.; Zhong, H.; Zhu, H., A fluorescence turn-on probe for hydrogen sulfide and biothiols based on PET & TICT and its imaging in HeLa cells. *Spectrochimica Acta Part A: Molecular and Biomolecular Spectroscopy* **2021,** *244*, 118839.

[456] Cao, Y.; Wang, L.; Liu, Z.; Sun, C.; Li, Y., Theoretical study on the sensing mechanism of chalcone-based fluorescence probe for detecting hydrogen sulfide and biothiols. *New Journal of Chemistry* **2021,** *45* (36), 16906-16912.

[457] Chen, S.; Li, H.; Hou, P., A novel imidazo[1,5-α]pyridine-based fluorescent probe with a large Stokes shift for imaging hydrogen sulfide. *Sensors and Actuators B: Chemical* **2018,** *256*, 1086-1092.

[458] Peng, S.; Zhong, T.; Guo, T.; Shu, D.; Meng, D.; Liu, H.; Guo, D., A novel fluorescent probe for selective detection of hydrogen sulfide in living cells. *New Journal of Chemistry* **2018,** *42* (7), 5185-5192.

[459] Wang, J.; Lin, W.; Li, W., Three-channel fluorescent sensing via organic white light-emitting dyes for detection of hydrogen sulfide in living cells. *Biomaterials* **2013,** *34* (30), 7429-7436.

[460] Long, L.; Cao, S.; Jin, B.; Yuan, X.; Han, Y.; Wang, K., Construction of a Novel Fluorescent Probe for On-site Measuring Hydrogen Sulfide Levels in Food Samples. *Food Analytical Methods* **2019,** *12* (4), 852-858.

[461] Tang, L.; Zheng, Z.; Zhong, K.; Bian, Y., A 2,5-diaryl-1,3,4-oxadiazole-based fluorescent probe for rapid and highly selective recognition of hydrogen sulfide with a large Stokes shift through switching on ESIPT. *Tetrahedron Letters* **2016,** *57* (12), 1361-1364.

[462] Xu, L.; Ni, L.; Sun, L.; Zeng, F.; Wu, S., A fluorescent probe based on aggregation-induced emission for hydrogen sulfide-specific assaying in food and biological systems. *Analyst* **2019,** *144* (22), 6570-6577.

[463] Li, Y.-t.; Zhao, X.-j.; Jiang, Y.-r.; Yang, B.-q., A novel long-wavelength fluorescent probe for selective detection of hydrogen sulfide in living cells. *New Journal of Chemistry* **2018,** *42* (24), 19478-19484.

[464] Ma, L.; Chen, Z.; Hu, Y.; Zhang, Z.; Huang, Y.; Zhang, H.; Liu, C., A new highly selective fluorescent probe design for visualizing hydrogen sulfide in food sample. *Tetrahedron Letters* **2023,** *122*, 154508.

[465] Li, J.; Zhong, K.; Tang, L.; Yan, X., A triphenylamine derived fluorescent probe for efficient detection of H_2S based on aggregation-induced emission. *New Journal of Chemistry* **2021,** *45* (30), 13399-13405.

[466] Wang, H.; Hu, L.; Xu, B.; Chen, H.; Cai, F.; Yang, N.; Wu, Q.; Uvdal, K.; Hu, Z.; Li, L., Endoplasmic reticulum-targeted fluorogenic probe based on pyrimidine derivative for visualizing exogenous/endogenous H_2S in living cells. *Dyes and Pigments* **2020,** *179*, 108390.

[467] Zhang, Y.; Zhang, B.; Li, Z.; Wang, L.; Ren, X.; Ye, Y., Endoplasmic reticulum targeted fluorescent probe for the detection of hydrogen sulfide based on a twist-blockage strategy. *Organic & Biomolecular Chemistry* **2019,** *17* (38), 8778-8783.

[468] Zhang, W.; Jia, Q.; Meng, Y.; Chen, S.; Zhang, Y.; Wang, K.-P.; Gan, L.-H.; Hu, Z.-Q., Dimethylamino naphthalene-based fluorescent probes for hydrogen sulfide detection and living cell imaging. *Spectrochimica Acta Part A: Molecular and Biomolecular Spectroscopy* **2020,** *228*, 117835.

[469] Zhong, K.; He, Y.; Deng, L.; Yan, X.; Li, X.; Tang, Y.; Hou, S.; Tang, L., A near-infrared fluorescent probe for H_2S based on tandem reaction to construct iminocoumarin-benzothiazole and its application in food, water, living cells. *Analytica Chimica Acta* **2020,** *1127*, 49-56.

[470] Zhang, W.; Kang, J.; Li, P.; Wang, H.; Tang, B., Dual Signaling Molecule Sensor for Rapid Detection of Hydrogen Sulfide Based on Modified Tetraphenylethylene. *Analytical Chemistry* **2015,** *87* (17), 8964-8969.

[471] Asaithambi, G.; Periasamy, V., Hydrogen sulfide detection by ESIPT based fluorescent sensor: Potential in living cells imaging. *Journal of Photochemistry and Photobiology A: Chemistry* **2019,** *369*, 97-105.

[472] Lei, Y.; Wang, K.-P.; Chen, S.; Zhang, Q.; Hu, Z.-Q., A fluorescent probe based on tetrahydro[5]helicene for highly selective recognition of hydrogen sulfide. *Spectrochimica Acta Part A: Molecular and Biomolecular Spectroscopy* **2018,** *204*, 295-300.

[473] Dai, Z.; Tian, L.; Song, B.; Ye, Z.; Liu, X.; Yuan, J., Ratiometric Time-Gated Luminescence Probe for Hydrogen Sulfide Based on Lanthanide Complexes. *Analytical Chemistry* **2014,** *86* (23), 11883-11889.

[474] Simsek Turan, I.; Sozmen, F., A chromogenic dioxetane chemosensor for hydrogen sulfide and pH dependent off–on chemiluminescence property. *Sensors and Actuators B: Chemical* **2014,** *201*, 13-18.

[475] Du, Z.; Song, B.; Zhang, W.; Duan, C.; Wang, Y.-L.; Liu, C.; Zhang, R.; Yuan, J., Quantitative Monitoring and Visualization of Hydrogen Sulfide In Vivo Using a Luminescent Probe Based on a Ruthenium(II) Complex. *Angewandte Chemie International Edition* **2018,** *57* (15), 3999-4004.

[476] Liu, B.; Long, J.; Zhang, M.; Cheng, K.; Gao, X.; Zhou, Y.; Li, Y.; Tang, Z.; Zhang, W., Mitochondria-targeted phosphorescent cyclometalated iridium(III) complex for bioimaging of H_2S. *Journal of Inorganic Biochemistry* **2022,** *226*, 111626.

[477] Kang, J.; Huo, F.; Yao, Y.; Yin, C., A high signal-to-background ratio H_2S-specific fluorescent probe based on nucleophilic substitution and its bioimaging for generation H_2S induced by Ca^{2+} in vivo. *Dyes and Pigments* **2019,** *171*, 107755.

[478] Zhao, Q.; Huo, F.; Zhang, Y.; Wen, Y.; Yin, C., HS^- induced thiolysis reaction to regulate UV- and fluorescence spectra change and their bioimaging in living cells. *Spectrochimica Acta Part A: Molecular and Biomolecular Spectroscopy* **2019,** *215*, 297-302.

[479] Li, X.; Wang, A.; Wang, J.; Lu, J., Efficient Strategy for the Synthesis and Modification of 2-Hydroxyethylluciferin for Highly Sensitive Bioluminescence Imaging of Endogenous Hydrogen Sulfide in Cancer Cells and Nude Mice. *Analytical Chemistry* **2019,** *91* (24), 15703-15708.

[480] Wang, T.; Huang, X.; Yang, S.; Hu, S.; Zheng, X.; Mao, G.; Li, Y.; Zhou, Y., Monitoring H_2S fluctuation during autophagic fusion of lysosomes and mitochondria using a lysosome-targeting fluorogenic probe. *Analytica Chimica Acta* **2023,** *1265*, 341356.

[481] Fu, L.; Tian, F.-F.; Lai, L.; Liu, Y.; Harvey, P. D.; Jiang, F.-L., A ratiometric "two-in-one" fluorescent chemodosimeter for fluoride and hydrogen sulfide. *Sensors and Actuators B: Chemical* **2014,** *193*, 701-707.

[482] Li, Q.; Wang, Z.; Zhao, M.; Hong, Y.; Jin, Q.; Yao, S.; Zheng, C.; Quan, Y.-Y.; Ye, X.; Huang, Z.-S., A NIR fluorescent probe for the detection and visualization of hydrogen sulfide in colorectal cancer cell. *Sensors and Actuators B: Chemical* **2019,** *298*, 126898.

[483] Zhang, W.; Xun, Q.; Xing, W.; Xu, F.; Liu, X., A Highly Selective Fluorescent Probe for Imaging Hydrogen Sulfide in Living HeLa Cells. *Journal of Fluorescence* **2023,** *33* (4), 1603-1608.

[484] Quan, Y.-Y.; Fan, L.; Shen, H.; Wu, B.; Kong, S.; Luo, Y.; Huang, Z.-S.; Ye, X., A multifunctional BODIPY based fluorescent probe for hydrogen sulfide detection and photodynamic anticancer therapy in HCT116 colon cancer cell. *Dyes and Pigments* **2022,** *197*, 109897.

[485] Gao, J.; Wang, R.; Yin, K.; Zhu, T.; Sun, J.; Dong, C.; Dong, X.; Zhao, M.; Gu, X.; Zhao, C., Visualizing hydrogen peroxide and hydrogen sulfide fluctuations in living cells via dynamic-reversible fluorescent probes. *Chemical Engineering Journal* **2023,** *466*, 143102.

[486] Wang, H.; Wang, J.; Yang, S.; Tian, H.; Sun, B.; Liu, Y., A Reaction-Based Novel Fluorescent Probe for Detection of Hydrogen Sulfide and Its Application in Wine. *Journal of Food Science* **2018,** *83* (1), 108-112.

[487] Wang, H.; Li, Y.; Yang, S.; Tian, H.; Liang, S.; Sun, B., Dual-Function Fluorescent Probe for Detection of Hydrogen Sulfide and Water Content in Dimethyl Sulfoxide. *ACS Omega* **2019,** *4* (6), 10695-10701.

[488] Tong, X.; Hao, L.; Song, X.; Wu, S.; Zhang, N.; Li, Z.; Chen, S.; Hou, P., A fast-responsive fluorescent probe based on a styrylcoumarin dye for visualizing hydrogen sulfide in living MCF-7 cells and zebrafish. *RSC Advances* **2022,** *12* (28), 17846-17852.

[489] Chi, H.; Gu, L.; Zhang, Q.; Tang, Y.; Guo, R.; Lin, W., Development of a New Hydrogen Sulfide Fluorescent Probe Based on Coumarin-Chalcone Fluorescence Platform and Its Imaging Application. *Chemosensors* **2023,** *11* (8), 428.

[490] Li, M.; Jiao, Y.; Duan, C., A dual-emission fluorescence-enhanced probe for hydrogen sulfide and its application in biological imaging. *New Journal of Chemistry* **2022,** *46* (21), 10184-10190.

[491] Hong, T.; Cheng, S.; Zhong, X.; Zuo, Y.; Dong, Y.; Shi, Z.; Zhao, Z., Novel fluorescent probe based on dicoumarin for detection of hydrogen sulfide in real samples. *Journal of the Chinese Chemical Society* **2023,** *70* (2), 136-144.

[492] Liu, X.; Li, W.; Bai, S.; Cui, Y.; Sun, G., Off-label use of old drug: A 3-hydroxythalidomide-based fluorescent probe for the detection of hydrogen sulfide (H_2S) and bioimaging in HeLa cells. *Microchemical Journal* **2020,** *158*, 105144.

[493] Liu, L.; Qu, H.; Li, X.; Zhou, X.; Zhang, J.; Sun, Y.; Cheng, J.; Zhou, L., Novel naphthalimide derived fluorescent probe based on aggregation-induced emission for turn-on detection of hydrogen sulfide. *Tetrahedron* **2021,** *81*, 131923.

[494] Shen, W.; Wang, P.; Xie, Z.; Zhou, H.; Hu, Y.; Fu, M.; Zhu, Q., A bifunctional probe reveals increased viscosity and hydrogen sulfide in zebra fish model of Parkinson's disease. *Talanta* **2021,** *234*, 122621.

[495] Xiao, P.; Liu, J.; Wang, Z.; Tao, F.; Yang, L.; Yuan, G.; Sun, W.; Zhang, X., A color turn-on fluorescent probe for real-time detection of hydrogen sulfide and identification of food spoilage. *Chemical Communications* **2021,** *57* (41), 5012-5015.

[496] Sun, Q.; Liu, H.; Qiu, Y.; Chen, J.; Wu, F.-S.; Luo, X.-G.; Wang, D.-W., A highly sensitive and selective fluorescence turn-on probe for the sensing of H_2S in vitro and in vivo. *Spectrochimica Acta Part A: Molecular and Biomolecular Spectroscopy* **2021,** *254*, 119620.

[497] Xu, K.; He, L.; Yang, Y.; Lin, W., A PET-based turn-on fluorescent probe for sensitive detection of thiols and H_2S and its bioimaging application in living cells, tissues and zebrafish. *New Journal of Chemistry* **2019,** *43* (7), 2865-2869.

[498] Karmakar, P.; Manna, S.; Ali, S. S.; Guria, U. N.; Sarkar, R.; Datta, P.; Mandal, D.; Mahapatra, A. K., Reaction-based ratiometric fluorescent probe for selective recognition of sulfide anions with a large Stokes shift through switching on ESIPT. *New Journal of Chemistry* **2018,** *42* (1), 76-84.

[499] Lee, S.; Sung, D.-B.; Lee, J. S.; Han, M. S., A Fluorescent Probe for Selective Facile Detection of H_2S in Serum Based on an Albumin-Binding Fluorophore and Effective Masking Reagent. *ACS Omega* **2020,** *5* (50), 32507-32514.

[500] Li, Z.; Wang, J.; Peng, X.; Chen, Y.; Geng, M., A highly selective fluorescent probe for detection of H_2S based-on benzothiazole and its application. *Inorganica Chimica Acta* **2023,** *548*, 121378.

[501] Li, M.; Gao, M.; Fu, Q.; Chen, X.; Xu, K.; Gong, S.; Liang, Y.; Wang, Z.; Wang, S., Novel 2-Benzo[d]thiazolyl-4-quinolinylphenol Skeleton-Based Turn-on Fluorescent Probe for H_2S Detection and its Multiple Applications in Water Environment, Foodstuffs, and Living Organisms. *Journal of Agricultural and Food Chemistry* **2023,** *71* (1), 780-788.

[502] Cheng, F.; Wu, X.; Liu, M.; Lon, Y.; Chen, G.; Zeng, R., A porphyrin-based near-infrared fluorescent sensor for sulfur ion detection and its application in living cells. *Sensors and Actuators B: Chemical* **2016,** *228*, 673-678.

[503] Chen, G.; Tang, M.; Fu, X.; Cheng, F.; Zou, X.; Wang, J.; Zeng, R., A highly sensitive and selective fluorescent sensor for detection of sulfide anion based on the steric hindrance effect. *Journal of Molecular Structure* **2018,** *1151*, 230-235.

[504] Huang, K.; Xie, S.; Jiang, L.; Li, J.; Chen, J., A glutathione and hydrogen sulfide responsive photosensitizer for enhanced photodynamic therapy. *Dyes and Pigments* **2022,** *205*, 110529.

[505] Lu, G.; Yu, S.; Meng, S.; Wang, X.; Jiang, J.; Zhang, D.; Duan, L., Synthesis and applications of a corrole-based dual-responsive fluorescent probe for separate detection of hydrazine and hydrogen sulfide. *Spectrochimica Acta Part A: Molecular and Biomolecular Spectroscopy* **2023,** *296*, 122678.

[506] Lu, G.; Gao, Y.; Wang, X.; Zhang, D.; Meng, S.; Yu, S.; Zhuang, Y.; Duan, L., A near-infrared fluorescent probe based on corrole derivative with large Stokes shift for detection of hydrogen sulfide in water and living cells. *Dyes and Pigments* **2022,** *204*, 110445.

[507] Lu, G.; Duan, L.; Meng, S.; Cai, P.; Ding, S.; Wang, X., Development of a colorimetric and turn-on fluorescent probe with large Stokes shift for H_2S detection and its multiple applications in environmental, food analysis and biological imaging. *Dyes and Pigments* **2023,** *220*, 111687.

[508] Sureshkumar, K.; Ramakrishnappa, T., A near infrared fluorescent probe for naked eye visualization and selective detection of hydrogen sulfide. *Materials Today: Proceedings* **2022,** *49*, 597-602.

[509] Lv, J.; Wang, F.; Qiang, J.; Ren, X.; Chen, Y.; Zhang, Z.; Wang, Y.; Zhang, W.; Chen, X., Enhanced response speed and selectivity of fluorescein-based H_2S probe via the cleavage of nitrobenzene sulfonyl ester assisted by ortho aldehyde groups. *Biosensors and Bioelectronics* **2017,** *87*, 96-100.

[510] Zheng, F.; Wen, M.; Zeng, F.; Wu, S., A water-soluble, low-cytotoxic and sensitive fluorescent probe based on poly(ethylene glycol) for detecting sulfide anion in aqueous media and imaging inside live cells. *Polymer* **2013,** *54* (21), 5691-5697.

[511] Sontisiri, P.; Yingyuad, P.; Thongyoo, P., A highly selective "Turn On" fluorescent probe based on FRET mechanism for hydrogen sulfide detection in living cells. *Journal of Photochemistry and Photobiology A: Chemistry* **2020,** *391*, 112401.

[512] Hong, Y.; Zhang, P.; Wang, H.; Yu, M.; Gao, Y.; Chen, J., Photoswitchable AIE nanoprobe for lysosomal hydrogen sulfide detection and reversible dual-color imaging. *Sensors and Actuators B: Chemical* **2018,** *272*, 340-347.

[513] Hong, J.; Feng, W.; Feng, G., Highly selective near-infrared fluorescent probe with rapid response, remarkable large Stokes shift and bright fluorescence for H_2S detection in living cells and animals. *Sensors and Actuators B: Chemical* **2018,** *262*, 837-844.

[514] Yang, X.; Lu, X.; Wang, J.; Zhang, Z.; Du, X.; Zhang, J.; Wang, J., Near-Infrared Fluorescent Probe with a Large Stokes Shift for Detection of Hydrogen Sulfide in Food Spoilage, Living Cells, and Zebrafish. *Journal of Agricultural and Food Chemistry* **2022,** *70* (9), 3047-3055.

[515] Li, B.; Mei, H.; Wang, M.; Gu, X.; Hao, J.; Xie, X.; Xu, K., A near-infrared fluorescent probe for imaging of endogenous hydrogen sulfide in living cells and mice. *Dyes and Pigments* **2021,** *189*, 109231.

[516] Huo, F.; Zhang, Y.; Ning, P.; Meng, X.; Yin, C., A novel isophorone-based red-emitting fluorescent probe for selective detection of sulfide anions in water for in vivo imaging. *Journal of Materials Chemistry B* **2017,** *5* (15), 2798-2803.

[517] Cuiling, S.; Huayu, W.; Tianjun, N.; Kaiwen, C.; Chunpo, G., A dicyanoisophorone-based near-infrared fluorescent probe with fast detection for H_2S in living cells and zebrafish. *Journal of Luminescence* **2022,** *243*, 118669.

[518] Zhong, K.; Chen, L.; Yan, X.; Tang, Y.; Hou, S.; Li, X.; Tang, L., Dual-functional multi-application probe: Rapid detection of H_2S and colorimetric recognition of HSO_3^- in food and cell. *Dyes and Pigments* **2020,** *182*, 108656.

[519] Kong, F.; Wang, X.; Bai, J.; Li, X.; Yang, C.; Li, Y.; Xu, K.; Tang, B., A "double-locked" probe for the detection of hydrogen sulfide in a viscous system. *Chemical Communications* **2021,** *57* (54), 6604-6607.

[520] Gu, X.; Yun, L.; Chen, K.; He, S.; Cheng, P.; Xu, K., A novel near-infrared fluorescence probe for hydrogen sulfide detection and application in cell and mice imaging. *Journal of Molecular Structure* **2023,** *1286*, 135576.

[521] Liu, J.; Wang, X.; Cheng, Y.; Yu, Y.; Zhao, M.; Huang, J.; Yu, P.; Fu, Q.; Song, Y.; Liu, Y., Application of a fluorescent H_2S probe based on excited-state intramolecular proton transfer for detecting latent mechanism of H_2S-induced MCF-7 apoptosis. *Future Medicinal Chemistry* **2022,** *14* (9), 647-663.

[522] Zhang, Z.-H.; Li, S.; Yan, Y.; Qu, J.; Wang, J.-Y., A novel fast-responsive fluorescent probe based on 1,3,5-triazine for endogenous H_2S detection with large Stokes shift and its application in cell imaging. *New Journal of Chemistry* **2021,** *45* (22), 9756-9760.

[523] Chen, W.; Chen, S.; Zhou, B.; Wang, H.; Song, X.; Zhang, H., Highly selective red-emitting H_2S fluorescent probe with a large Stokes shift. *Dyes and Pigments* **2015,** *113*, 596-601.

[524] Zhang, L.; Luo, S.; Chen, Z.; Cui, L., A highly sensitive and selective fluorescent probe for tracking hydrogen sulfide in red wine. *Zeitschrift für anorganische und allgemeine Chemie* **2021,** *647* (20-21), 1986-1991.

[525] Xie, L.; Fan, T.; Yao, R.; Mu, Y.; Wang, R.; Fan, C.; Pu, S., Highly selective near-infrared fluorescent probe with large Stokes shift and sensitivity for H_2S detection in water, foodstuff and imaging in living cells. *Dyes and Pigments* **2022,** *208*, 110828.

[526] Kavitha, V.; Viswanathamurthi, P.; Haribabu, J.; Echeverria, C., An active ESIPT based molecular sensor aided with sulfonate ester moiety to track the presence of H_2S analyte in realistic samples and HeLa cells. *Microchemical Journal* **2023,** *188*, 108484.

[527] Kim, H. J.; Kim, T.; Hong, J.-I., Selective electrochemiluminescent detection of sulfide based on a dual-quenching cyclometalated Ir(III) complex. *Sensors and Actuators B: Chemical* **2020,** *307*, 127656.

[528] Wang, K.-P.; Zhang, Q.-L.; Wang, X.; Lei, Y.; Zheng, W.-J.; Chen, S.; Zhang, Q.; Hu, H.-Y.; Hu, Z.-Q., A fluorescent probe based on tetrahydro[5]helicene derivative with large Stokes shift for rapid and highly selective recognition of hydrogen sulfide. *Spectrochimica Acta Part A: Molecular and Biomolecular Spectroscopy* **2019,** *214*, 487-495.

[529] Wang, L.; Yang, W.; Song, Y.; Hu, Y., Novel turn-on fluorescence sensor for detection and imaging of endogenous H_2S induced by sodium nitroprusside. *Spectrochimica Acta Part A: Molecular and Biomolecular Spectroscopy* **2020,** *243*, 118775.

[530] Tan, X.; Hong, T.; Jiang, Y.; Zhao, Z.; Shi, Z., Synthesis and application of a novel fluorescent probe for detection of hydrogen sulfide in real samples. *International Journal of Environmental Analytical Chemistry* **2022**, 1-14.

[531] Meng, Y.; Yao, X.; Zhong, K.; Li, Y.; Tang, L., An Aggregation-Induced Emission-Based Fluorescence Turn-On Probe for Efficient Detection of HS^- in Water, Wine, and Living Cells. *European Journal of Organic Chemistry* **2023,** *26* (18), e202300022.

[532] Xie, L.; Wang, R.; Fan, C.; Tu, Y.; Liu, G.; Pu, S., Mitochondria-targeted fluorescent probe with long wavelength emission for detecting H_2S and its application in foodstuff, water and living cells. *Food Chemistry* **2023,** *410*, 135411.

[533] Pan, J.; Xu, J.; Zhang, Y.; Wang, L.; Qin, C.; Zeng, L.; Zhang, Y., A novel fluorescent probe for rapid and sensitive detection of hydrogen sulfide in living cells. *Spectrochimica Acta Part A: Molecular and Biomolecular Spectroscopy* **2016,** *168*, 132-138.

[534] Guo, F.-F.; Han, X.-F.; Zhao, X.-L.; Wang, Y.; Fan, Y.-C.; Wu, W.-N.; Xu, Z.-H., A ratiometric fluorescent probe for hydrogen sulfide in neat aqueous solution and its application in lysosome-targetable cell imaging. *Spectrochimica Acta Part A: Molecular and Biomolecular Spectroscopy* **2022,** *270*, 120835.

[535] Zhong, K.; Hu, X.; Zhou, S.; Liu, X.; Gao, X.; Tang, L.; Yan, X., Mitochondria-Targeted Red-Emission Fluorescent Probe for Ultrafast Detection of H_2S in Food and Its Bioimaging Application. *Journal of Agricultural and Food Chemistry* **2021,** *69* (16), 4628-4634.

[536] Jing, X.; Yu, F.; Lin, W., A PET-based lysosome-targeted turn-on fluorescent probe for the detection of H_2S and its bioimaging application in living cells and zebrafish. *New Journal of Chemistry* **2019,** *43* (43), 16796-16800.

[537] Zhou, L.; Cheng, Z.-Q.; Li, N.; Ge, Y.-X.; Xie, H.-X.; Zhu, K.; Zhou, A.; Zhang, J.; Wang, K.-M.; Jiang, C.-S., A highly sensitive endoplasmic reticulum-targeting fluorescent probe for the imaging of endogenous H_2S in live cells. *Spectrochimica Acta Part A: Molecular and Biomolecular Spectroscopy* **2020,** *240*, 118578.

[538] Feng, S.; Xia, Q.; Feng, G., Iminocoumarin-based red to near-infrared fluorescent turn-on probe with a large Stokes shift for imaging H_2S in living cells and animals. *Dyes and Pigments* **2019,** *163*, 447-453.

[539] Hou, F.; Zhu, L.; Zhang, H.; Qiao, Z.; Wei, N.; Zhang, Y., A highly selective and sensitive fluorescent probe based on the chromone fluorophore for imaging hydrogen sulfide in living cells. *New Journal of Chemistry* **2020,** *44* (4), 1537-1541.

[540] Shi, G.-J.; Wang, Y.-D.; Yu, Z.-X.; Zhang, Q.; Chen, S.; Xu, L.-Z.; Wang, K.-P.; Hu, Z.-Q., The coumarin-pyrazole dye for detection of hydrogen sulfide in cells. *Spectrochimica Acta Part A: Molecular and Biomolecular Spectroscopy* **2023,** *285*, 121898.

[541] Shi, J.; Zhang, D.; Li, M.; Wang, Y.; Liu, L.; Wang, T.; Guo, F.; Wu, X., A new fluorescent probe for hydrogen sulfide based on naphthalimide derivatives and its biological application. *Inorganic Chemistry Communications* **2022,** *146*, 110087.

[542] Liu, T.-Z.; Cui, X.-L.; Sun, W.-L.; Miao, J.-Y.; Zhao, B.-X.; Lin, Z.-M., Two simple but effective turn-on benzothiazole-based fluorescent probes for detecting hydrogen sulfide in real water samples and HeLa cells. *Analytica Chimica Acta* **2022,** *1189*, 339225.

[543] Naha, S.; Thirumalaivasan, N.; Garai, S.; Wu, S.-P.; Velmathi, S., Nanomolar Detection of H_2S in an Aqueous Medium: Application in Endogenous and Exogenous Imaging of HeLa Cells and Zebrafish. *ACS Omega* **2020,** *5* (31), 19896-19904.

[544] Zhao, F.; Chen, G.; Lin, X.; Jiang, J.; Xia, Y.; Li, X.; Wang, K., Novel 3RAX-based fluorescent probe for hydrogen sulfide detection and photodynamic therapy. *Journal of Luminescence* **2023,** *263*, 119990.

[545] Ghosh, P. B.; Whitehouse, M. W., 7-Chloro-4-nitrobenzo-2-oxa-1,3-diazole - A new fluorogenic reagent for amino acids and other amines. *Biochemical Journal* **1968,** *108* (1), 155-156.

[546] Imai, K.; Uzu, S.; Kanda, S.; Baeyens, W. R. G., Availabaility of fluorogenic reagents having a benzofurazan structure in the biosciences. *Analytica Chimica Acta* **1994,** *290* (1-2), 3-20.

[547] Imai, K.; Uzu, S.; Toyooka, T., Fluorogenic reagents, having benzafurazan structure, in liquid-chromatography. *Journal of Pharmaceutical and Biomedical Analysis* **1989,** *7* (12), 1395-1403.

[548] Montoya, L. A.; Pearce, T. F.; Hansen, R. J.; Zakharov, L. N.; Pluth, M. D., Development of Selective Colorimetric Probes for Hydrogen Sulfide Based on Nucleophilic Aromatic Substitution. *The Journal of Organic Chemistry* **2013,** *78* (13), 6550-6557.

[549] Bae, J.; Choi, J.; Park, T. J.; Chang, S.-K., Reaction-based colorimetric and fluorogenic signaling of hydrogen sulfide using a 7-nitro-2,1,3-benzoxadiazole–coumarin conjugate. *Tetrahedron Letters* **2014,** *55* (6), 1171-1174.

[550] Hammers, M. D.; Pluth, M. D., Ratiometric Measurement of Hydrogen Sulfide and Cysteine/Homocysteine Ratios Using a Dual-Fluorophore Fragmentation Strategy. *Analytical Chemistry* **2014,** *86* (14), 7135-7140.

[551] Zhang, Y.; Wang, J.; Yue, Y.; Chao, J.; Huo, F.; Yin, C., A new strategy for the fluorescence discrimination of Cys/Hcy and GSH/H_2S simultaneously colorimetric detection for H_2S. *Spectrochimica Acta Part A: Molecular and Biomolecular Spectroscopy* **2020,** *227*, 117537.

[552] Chen, Q.; Yang, J.; Li, Y.; Zheng, J.; Yang, R., Sensitive and rapid detection of endogenous hydrogen sulfide distributing in different mouse viscera via a two-photon fluorescent probe. *Analytica Chimica Acta* **2015,** *896*, 128-136.

[553] Yang, L.; Su, Y.; Geng, Y.; Zhang, Y.; Ren, X.; He, L.; Song, X., A Triple-Emission Fluorescent Probe for Discriminatory Detection of Cysteine/Homocysteine, Glutathione/Hydrogen Sulfide, and Thiophenol in Living Cells. *ACS Sensors* **2018,** *3* (9), 1863-1869.

[554] Ding, S.; Feng, G., Smart probe for rapid and simultaneous detection and discrimination of hydrogen sulfide, cysteine/homocysteine, and glutathione. *Sensors and Actuators B: Chemical* **2016,** *235*, 691-697.

[555] Ding, S.; Feng, W.; Feng, G., Rapid and highly selective detection of H_2S by nitrobenzofurazan (NBD) ether-based fluorescent probes with an aldehyde group. *Sensors and Actuators B: Chemical* **2017,** *238*, 619-625.

[556] Liu, T.-T.; Li, S.-J.; Zhang, X.-S.; Wang, J.; Deng, Y.-X.; Sun, X.-J.; Xing, Z.-Y.; Wu, R.-F., A Facile Probe for Fluorescence Turn-on and Simultaneous Naked-Eyes Discrimination of H_2S and biothiols (Cys and GSH) and Its Application. *Journal of Fluorescence* **2022,** *32* (1), 175-188.

[557] Hou, P.; Li, H.; Chen, S., A highly selective and sensitive 3-hydroxyflavone-based colorimetric and fluorescent probe for hydrogen sulfide with a large Stokes shift. *Tetrahedron* **2016,** *72* (24), 3531-3534.

[558] Lu, G.; Gao, Y.; Wang, X.; Zhang, D.; Meng, S.; Yu, S.; Zhuang, Y., A corrole-based fluorescent probe for detection of sulfur ion and its application in living cells. *Dyes and Pigments* **2022,** *197*, 109941.

[559] Jeong, Y. A.; Chang, I. J.; Chang, S.-K., Discriminative sensing of sulfide and azide ions in solution by a nitrobenzoxadiazole-dansyl dyad by simply tuning the water content. *Sensors and Actuators B: Chemical* **2016,** *224*, 73-80.

[560] Sharma, P.; Kumar, K.; Kaur, S.; Kaur, S.; Bhargava, G.; Kumar, S.; Singh, P., Near-IR discriminative detection of H_2S and Cysteine with 7-nitro-2,1,3-benzoxadiazole-perylenediimide conjugate in water, live cells and solid state: Mimicking IMP, INH and NOR/OR complimentary logic. *Journal of Photochemistry and Photobiology A: Chemistry* **2020,** *388*, 112151.

[561] Wei, C.; Zhu, Q.; Liu, W.; Chen, W.; Xi, Z.; Yi, L., NBD-based colorimetric and fluorescent turn-on probes for hydrogen sulfide. *Organic & Biomolecular Chemistry* **2014,** *12* (3), 479-485.

[562] Zhu, H.; Liu, C.; Yuan, R.; Wang, R.; Zhang, H.; Li, Z.; Jia, P.; Zhu, B.; Sheng, W., A simple highly specific fluorescent probe for simultaneous discrimination of cysteine/homocysteine and glutathione/hydrogen sulfide in living cells and zebrafish using two separated fluorescence channels under single wavelength excitation. *Analyst* **2019,** *144* (14), 4258-4265.

[563] Jin, X.; Zhao, S.; Wang, T.; Si, L.; Liu, Y.; Zhao, C.; Zhou, H.; Leng, X.; Zhang, X., Near-infrared fluorescent probe for selective detection of H_2S and its application in living animals. *Analytical and Bioanalytical Chemistry* **2019,** *411* (23), 5985-5992.

[564] Zhu, L.; Zhang, T.; Ma, Y.; Lin, W., Discriminating Cys from GSH/H_2S in vitro and in vivo with a NIR fluorescent probe. *Sensors and Actuators B: Chemical* **2020,** *305*, 127202.

[565] Zhang, Y.; Wen, L.; Zhang, W.; Yue, Y.; Chao, J.; Huo, F.; Yin, C., Sulphide activity-dependent multicolor emission dye and its applications in in vivo imaging. *Analyst* **2021,** *146* (18), 5517-5527.

[566] Sun, J.; Li, X.; Cao, J.; Sun, Q.; Zhang, Y.; Wang, X.; Wu, T.; Hu, X.; Feng, F., Mitochondria Targeting Fluorescent Probes Based on through Bond-Energy Transfer for Mutually Imaging Signaling Molecules H_2S and H_2O_2. *Chemistry – A European Journal* **2019,** *25* (39), 9164-9169.

[567] Wang, J.; Yu, H.; Li, Q.; Shao, S., A BODIPY-based turn-on fluorescent probe for the selective detection of hydrogen sulfide in solution and in cells. *Talanta* **2015,** *144*, 763-768.

[568] Kang, J.; Huo, F.; Ning, P.; Meng, X.; Chao, J.; Yin, C., Two red-emission single and double 'arms' fluorescent materials stemed from 'one-pot' reaction for hydrogen sulfide vivo imaging. *Sensors and Actuators B: Chemical* **2017,** *250*, 342-350.

[569] Yang, X.; He, L.; Xu, K.; Lin, W., A fluorescent dyad with large emission shift for discrimination of cysteine/homocysteine from glutathione and hydrogen sulfide and the application of bioimaging. *Analytica Chimica Acta* **2017,** *981*, 86-93.

[570] Fortibui, M. M.; Yoon, D. W.; Lim, J.-Y.; Lee, S.; Choi, M.; Heo, J. S.; Kim, J.; Kim, J., A cancer cell-specific benzoxadiazole-based fluorescent probe for hydrogen sulfide detection in mitochondria. *Dalton Transactions* **2021,** *50* (7), 2545-2554.

[571] Zhang, H.; Xia, X.; Zhao, H.; Zhang, G.-N.; Jiang, D.-Y.; Xue, X.-Y.; Zhang, J., A near-infrared fluorescent probe based on S_NAr reaction for H_2S/GSH detection in living cells and zebrafish. *Dyes and Pigments* **2019,** *163*, 183-189.

[572] Gong, S.; Zhou, E.; Hong, J.; Feng, G., Nitrobenzoxadiazole Ether-Based Near-Infrared Fluorescent Probe with Unexpected High Selectivity for H_2S Imaging in Living Cells and Mice. *Analytical Chemistry* **2019,** *91* (20), 13136-13142.

[573] Wang, W.-X.; Wang, Z.-Q.; Tan, Z.-K.; Mao, G.-J.; Chen, D.-H.; Li, C.-Y., A nitrobenzoxadiazole-based near-infrared fluorescent probe for the specific imaging of H_2S in inflammatory and tumor mice. *Analyst* **2022,** *147* (12), 2712-2717.

[574] Li, X.; Zang, L.; Zhao, H.; Qi, F.; Lau, C.; Lu, J., Modulation of Near-Infrared Mitochondria-Targetable fluorescent probe for H_2S bioimaging through the modification of heavy atom iodine. *Spectrochimica Acta Part A: Molecular and Biomolecular Spectroscopy* **2023,** *298*, 122767.

[575] Niu, H.; Ni, B.; Chen, K.; Yang, X.; Cao, W.; Ye, Y.; Zhao, Y., A long-wavelength-emitting fluorescent probe for simultaneous discrimination of H_2S/Cys/GSH and its bio-imaging applications. *Talanta* **2019,** *196*, 145-152.

[576] Zhu, H.; Liu, C.; Zhang, H.; Jia, P.; Li, Z.; Zhang, X.; Yu, Y.; Sheng, W.; Zhu, B., A Simple Long-wavelength Fluorescent Probe for Simultaneous Discrimination of Cysteine/Homocysteine and Glutathione/Hydrogen Sulfide with Two Separated Fluorescence Emission Channels by Single Wavelength Excitation. *Analytical Sciences* **2020,** *36* (2), 255-259.

[577] Zhang, D.; Du, W.; Peng, B.; Ni, Y.; Fang, H.; Qiu, X.; Zhang, G.; Wu, Q.; Yu, C.; Li, L.; Huang, W., Two-photon small molecular fluorogenic probe visualizing biothiols and sulfides in living cells, mice brain slices and zebrafish. *Sensors and Actuators B: Chemical* **2020,** *323*, 128673.

[578] Liu, M.; Bao, W.; Feng, X.; Meng, J.; Liu, S.; Cui, W.; Wu, Y.; Tian, Z., A double donor-π-acceptor type hydrogen sulfide fluorescent probe with nanomolar level sensitivity and second level response time for evaluating metformin-induced hepatotoxicity. *Sensors and Actuators B: Chemical* **2022,** *359*, 131572.

[579] Zheng, Y.-L.; Chai, Z.-H.; Tang, W.; Yan, S.; Dai, F.; Zhou, B., A multi-signal mitochondria-targetable fluorescent probe for simultaneously discriminating Cys/Hcy/H_2S, GSH, and SO_2 and visualizing the endogenous generation of SO_2 in living cells. *Sensors and Actuators B: Chemical* **2021,** *330*, 129343.

[580] He, L.; Yang, X.; Xu, K.; Kong, X.; Lin, W., A multi-signal fluorescent probe for simultaneously distinguishing and sequentially sensing cysteine/homocysteine, glutathione, and hydrogen sulfide in living cells. *Chemical Science* **2017,** *8* (9), 6257-6265.

[581] Song, F.; Li, Z.; Li, J.; Wu, S.; Qiu, X.; Xi, Z.; Yi, L., Investigation of thiolysis of NBD amines for the development of H_2S probes and evaluating the stability of NBD dyes. *Organic & Biomolecular Chemistry* **2016,** *14* (47), 11117-11124.

[582] Wei, C.; Wei, L.; Xi, Z.; Yi, L., A FRET-based fluorescent probe for imaging H_2S in living cells. *Tetrahedron Letters* **2013,** *54* (50), 6937-6939.

[583] Niu, P.; Liu, J.; Rong, Y.; Liu, X.; Wei, L., A fluorescent probe for selective and instantaneous detection of hydrogen sulfide in living cells and zebrafish. *Tetrahedron* **2021,** *89*, 132174.

[584] Roubinet, B.; Bailly, L.; Petit, E.; Renard, P.-Y.; Romieu, A., A FRET-based probe for fluorescence sensing of sulfide/sulfite analytes, using a novel long-wavelength water-soluble 7-hydroxycoumarin as reporter fluorophore. *Tetrahedron Letters* **2015,** *56* (8), 1015-1019.

[585] Huang, Y.; Zhang, C.; Xi, Z.; Yi, L., Synthesis and characterizations of a highly sensitive and selective fluorescent probe for hydrogen sulfide. *Tetrahedron Letters* **2016,** *57* (10), 1187-1191.

[586] Ismail, I.; Wang, D.; Wang, Z.; Wang, D.; Zhang, C.; Yi, L.; Xi, Z., A julolidine-fused coumarin-NBD dyad for highly selective and sensitive detection of H_2S in biological samples. *Dyes and Pigments* **2019,** *163*, 700-706.

[587] Gao, J.; Jia, X.; Guo, Z.; Yang, S.; Wei, L.; Zhang, P.; Wei, C.; Chen, G.; Li, X., A two-photon benzocoumarin-NBD dyad for highly selective and sensitive ratiometric detection of H_2S in biological samples. *Dyes and Pigments* **2021,** *185*, 108906.

[588] Zhang, Y.; Chen, H.; Chen, D.; Wu, D.; Chen, X.; Liu, S. H.; Yin, J., A fluorescent turn-on H2S-responsive probe: design, synthesis and application. *Organic & Biomolecular Chemistry* **2015,** *13* (38), 9760-9766.

[589] Sureshkumar, K.; Ramakrishnappa, T.; Samrat, D., Piperazine appended napthalimide scaffold as turn on fluorescent probe for hydrogen sulfide. *Microchemical Journal* **2020,** *157*, 105019.

[590] Yoon, S. A.; Gopala, L.; Lee, M. H., Biocompatible 7-nitro-2,1,3-benzoxadiazole-embedded naphthalimide for exploring endogenous H_2S in living cells. *Spectrochimica Acta Part A: Molecular and Biomolecular Spectroscopy* **2023,** *295*, 122582.

[591] Li, K.-B.; Qu, W.-B.; Shen, Q.; Zhang, S.; Shi, W.; Dong, L.; Han, D.-M., 1,8-Naphthalimide-based dual-response fluorescent probe for highly discriminating detection of cys and H_2S. *Dyes and Pigments* **2020,** *173*, 107918.

[592] Cheng, W.; Xue, X.; Gan, L.; Jin, P.; Zhang, B.; Guo, M.; Si, J.; Du, H.; Chen, H.; Fang, J., Individual and successive detection of H_2S and HClO in living cells and zebrafish by a dual-channel fluorescent probe with longer emission wavelength. *Analytica Chimica Acta* **2021,** *1156*, 338362.

[593] Tang, Y.; Jiang, G.-F., A novel two-photon fluorescent probe for hydrogen sulfide in living cells using an acedan–NBD amine dyad based on FRET process with high selectivity and sensitivity. *New Journal of Chemistry* **2017,** *41* (14), 6769-6774.

[594] Yang, W.-Y.; Anusuyadevi, K.; Lu, P.-H.; Thirumalaivasan, N.; Hsuan Lin, W.; Velmathi, S.; Wu, S.-P., A two photon fluorescent probe for highly selective detection and endogenous imaging of hydrogen sulfide. *Spectrochimica Acta Part A: Molecular and Biomolecular Spectroscopy* **2022,** *273*, 121043.

[595] Liu, C.; Liu, J.; Zhang, W.; Wang, Y.-L.; Gao, X.; Song, B.; Yuan, J.; Zhang, R., A Ruthenium(II) complex-based probe for colorimetric and luminescent detection and imaging of hydrogen sulfide in living cells and organisms. *Analytica Chimica Acta* **2021,** *1145*, 114-123.

[596] Yuan, J.; Ren, T.-B.; Xu, S.; Wang, C.-J.; Zhang, X.-B.; Yuan, L., A Unique Multifunctional Luminescent Probe for Self-Monitoring Photodynamic Therapy by Detecting H_2S in Cancer Cells. *ACS Applied Bio Materials* **2021,** *4* (8), 6016-6022.

[597] Yang, L.; Wang, F.; Luo, X.; Kong, X.; Sun, Z.; You, J., A FRET-based ratiometric fluorescent probe for sulfide detection in actual samples and imaging in Daphnia magna. *Talanta* **2020,** *209*, 120517.

[598] Pei, S.; Li, J.; Zhang, C.; Liang, W.; Zhang, G.; Shi, L.; Wang, W.; Shuang, S.; Dong, C., Development of a piperazinyl-NBD-based fluorescent probe and its dual-channel detection for hydrogen sulfide. *Analyst* **2021,** *146* (7), 2138-2143.

[599] Wei, H.-G.; Liu, Y.-J.; Zhao, X.-D., Methylene blue-based 7-nitro-1,2,3-benzoxadiazole NIR fluorescent probe triggered by H_2S. *Bioorganic & Medicinal Chemistry Letters* **2020,** *30* (13), 127221.

[600] Yi, S.; Liu, H.; Chen, Z.; Fan, C.; Liu, G.; Pu, S., Novel fluorescent probes based on NBD-substituted imidazole amino to sequentially detect H_2S and Zn^{2+}. *Dyes and Pigments* **2023,** *214*, 111211.

[601] Qiao, D.; Shen, T.; Zhu, M.; Liang, X.; Zhang, L.; Yin, Z.; Wang, B.; Shang, L., A highly selective and sensitive fluorescent probe for simultaneously distinguishing and sequentially detecting H_2S and various thiol species in solution and in live cells. *Chemical Communications* **2018,** *54* (94), 13252-13255.

[602] Wang, R.; Li, Z.; Zhang, C.; Li, Y.; Xu, G.; Zhang, Q.-Z.; Li, L.-Y.; Yi, L.; Xi, Z., Fast-Response Turn-on Fluorescent Probes Based on Thiolysis of NBD Amine for H_2S Bioimaging. *ChemBioChem* **2016,** *17* (10), 962-968.

[603] Ismail, I.; Wang, D.; Wang, D.; Niu, C.; Huang, H.; Yi, L.; Xi, Z., A mitochondria-targeted red-emitting probe for imaging hydrogen sulfide in living cells and zebrafish. *Organic & Biomolecular Chemistry* **2019,** *17* (13), 3389-3395.

[604] Wang, Y.; Lv, X.; Guo, W., A reaction-based and highly selective fluorescent probe for hydrogen sulfide. *Dyes and Pigments* **2017,** *139*, 482-486.

[605] Ismail, I.; Chen, Z.; Ji, X.; Sun, L.; Yi, L.; Xi, Z., A Fast-Response Red Shifted Fluorescent Probe for Detection of H_2S in Living Cells. *Molecules* **2020,** *25* (3), 437.

[606] Guan, X.; Lu, H.; Ge, X.; Yin, Y.; Ouyang, J.; Na, N., Near-Infrared Fluorescent Probe for H_2S Detection: Will pH Affect the Intracellular Sensing? *ACS Sensors* **2022,** *7* (8), 2483-2491.

[607] Niu, H.; Duan, Y.; Zhang, Y.; Hua, X.; Xu, C.; Li, Z.; Ma, J.; Qin, F.; Zhai, Y.; Ye, Y.; Zhao, Y., A bifunctional fluorescent probe based on PET & ICT for simultaneously recognizing Cys and H_2S in living cells. *Journal of Photochemistry and Photobiology B: Biology* **2022,** *230*, 112441.

[608] Zhang, J.; Ji, X.; Zhou, J.; Chen, Z.; Dong, X.; Zhao, W., Pyridinium substituted BODIPY as NIR fluorescent probe for simultaneous sensing of hydrogen sulphide/glutathione and cysteine/homocysteine. *Sensors and Actuators B: Chemical* **2018,** *257*, 1076-1082.

[609] Xin, Y.; Wang, M.; Liu, M.; Chen, Y.; Zhao, H.; Zhang, P.; Li, X.; Wei, C., BODIPY-NBD dyad for highly selective and sensitive detection of hydrogen sulfide in cells and zebrafish. *Spectrochimica Acta Part A: Molecular and Biomolecular Spectroscopy* **2022,** *272*, 121007.

[610] Pang, Z.; Ye, H.; Ma, D.; Tu, X.; Yi, L.; Xi, Z., A H_2S-Specific Ultrasensitive Fluorogenic Probe Reveals TMV-Induced H_2S Production to Limit Virus Replication. *ChemBioChem* **2021,** *22* (13), 2292-2299.

[611] Yang, X.; Zhang, C.; Shen, L.; Bao, H.; Xu, J.; Fang, X.; Zhao, Y.; Yang, W., A near-infrared fluorescent probe for sulfide detection. *Sensors and Actuators B: Chemical* **2017,** *242*, 332-337.

[612] Zhang, K.; Zhang, J.; Xi, Z.; Li, L.-Y.; Gu, X.; Zhang, Q.-Z.; Yi, L., A new H_2S-specific near-infrared fluorescence-enhanced probe that can visualize the H_2S level in colorectal cancer cells in mice. *Chemical Science* **2017,** *8* (4), 2776-2781.

[613] Xiong, J.; Xia, L.; Huang, Q.; Huang, J.; Gu, Y.; Wang, P., Cyanine-based NIR fluorescent probe for monitoring H_2S and imaging in living cells and in vivo. *Talanta* **2018,** *184*, 109-114.

[614] Wu, M.-X.; Sha, X.-L.; Wei, X.-R.; Sun, R.; Chen, Y.; Gao, J.; Xu, Y.-J.; Ge, J.-F., Fluorescent hydrogen sulfide probes based on azonia-cyanine dyes and their imaging applications in organelles. *Analytica Chimica Acta* **2019,** *1068*, 60-69.

[615] Huang, X.; Liu, H.; Zhang, J.; Xiao, B.; Wu, F.; Zhang, Y.; Tan, Y.; Jiang, Y., A novel near-infrared fluorescent hydrogen sulfide probe for live cell and tissue imaging. *New Journal of Chemistry* **2019,** *43* (18), 6848-6855.

[616] Zhang, J.; Wang, R.; Zhu, Z.; Yi, L.; Xi, Z., A FRET-based ratiometric fluorescent probe for visualizing H_2S in lysosomes. *Tetrahedron* **2015,** *71* (45), 8572-8576.

[617] Ou-Yang, J.; Jiang, W.-L.; Tan, K.-Y.; Liu, H.-W.; Li, S.-J.; Liu, J.; Li, Y.-F.; Li, C.-Y., Two-photon fluorescence probe for precisely detecting endogenous H_2S in lysosome by employing a dual lock system. *Sensors and Actuators B: Chemical* **2018,** *260*, 264-273.

[618] Luo, W.; Xue, H.; Ma, J.; Wang, L.; Liu, W., Molecular engineering of a colorimetric two-photon fluorescent probe for visualizing H_2S level in lysosome and tumor. *Analytica Chimica Acta* **2019,** *1077*, 273-280.

[619] Zhang, H.; Chen, J.; Xiong, H.; Zhang, Y.; Chen, W.; Sheng, J.; Song, X., An endoplasmic reticulum-targetable fluorescent probe for highly selective detection of hydrogen sulfide. *Organic & Biomolecular Chemistry* **2019,** *17* (6), 1436-1441.

[620] Kafuti, Y. S.; Zeng, S.; Liu, X.; Han, J.; Qian, M.; Chen, Q.; Wang, J.; Peng, X.; Yoon, J.; Li, H., Observing hydrogen sulfide in the endoplasmic reticulum of cancer cells and zebrafish by using an activity-based fluorescent probe. *Chemical Communications* **2023,** *59* (17), 2493-2496.

[621] Xu, Z.-y.; Wu, Z.-y.; Tan, H.-y.; Yan, J.-w.; Liu, X.-l.; Li, J.-y.; Xu, Z.-y.; Dong, C.-z.; Zhang, L., Piperazine-tuned NBD-based colorimetric and fluorescent turn-off probes for hydrogen sulfide. *Analytical Methods* **2018,** *10* (27), 3375-3379.

[622] Ye, H.; Liu, S.; Chen, Z.; Cheng, L.; Yi, L., A highly selective and sensitive endoplasmic reticulum-targeted probe reveals $HOCl^-$ and cisplatin-induced H_2S biogenesis in live cells. *Journal of Materials Chemistry B* **2023,** *11* (23), 5163-5169.

[623] Pak, Y. L.; Li, J.; Ko, K. C.; Kim, G.; Lee, J. Y.; Yoon, J., Mitochondria-Targeted Reaction-Based Fluorescent Probe for Hydrogen Sulfide. *Analytical Chemistry* **2016,** *88* (10), 5476-5481.

[624] Jia, X.; Li, W.; Guo, Z.; Guo, Z.; Li, Y.; Zhang, P.; Wei, C.; Li, X., An NBD-Based Mitochondrial Targeting Ratiometric Fluorescent Probe for Hydrogen Sulfide Detection. *ChemistrySelect* **2019,** *4* (29), 8671-8675.

[625] Ma, B.; Tian, D.-H.; Yan, S.; Li, X.-C.; Dai, F.; Zhou, B., Developing a styrylpyridinium-based fluorescent probe with excellent sensitivity for visualizing basal H_2S levels in mitochondria. *Sensors and Actuators B: Chemical* **2021,** *327*, 128937.

[626] Yao, M.; Jia, X.; Wang, M.; Li, X.; Wang, X.; Qu, H.; Li, X.; Wei, C., Visualizing hydrogen sulfide in HepG2 cells exposed to OGD/R and in the liver of zebrafish with a hepatocyte-targeting fluorescent probe. *Dyes and Pigments* **2021,** *188*, 109151.

[627] Cai, X.; Zhang, Z.; Dong, Y.; Hao, T.; Yi, L.; Yang, X., A biotin-guided near-infrared fluorescent probe for imaging hydrogen sulfide and differentiating cancer cells. *Organic & Biomolecular Chemistry* **2023,** *21* (2), 332-338.

[628] Ismail, I.; Chen, Z.; Sun, L.; Ji, X.; Ye, H.; Kang, X.; Huang, H.; Song, H.; Bolton, S. G.; Xi, Z.; Pluth, M. D.; Yi, L., Highly efficient H_2S scavengers via thiolysis of positively-charged NBD amines. *Chemical Science* **2020,** *11* (30), 7823-7828.

[629] Ye, H.; Sun, L.; Pang, Z.; Ji, X.; Jiao, Y.; Tu, X.; Huang, H.; Tang, X.; Xi, Z.; Yi, L., Cell-Trappable BODIPY-NBD Dyad for Imaging of Basal and Stress-Induced H_2S in Live Biosystems. *Analytical Chemistry* **2022,** *94* (3), 1733-1741.

[630] Zhang, C.; Zhang, Q.-Z.; Zhang, K.; Li, L.-Y.; Pluth, M. D.; Yi, L.; Xi, Z., Dual-biomarker-triggered fluorescence probes for differentiating cancer cells and revealing synergistic antioxidant effects under oxidative stress. *Chemical Science* **2019,** *10* (7), 1945-1952.

[631] Liu, C.; Zhang, Y.; Sun, W.; Zhu, H.; Su, M.; Wang, X.; Rong, X.; Wang, K.; Yu, M.; Sheng, W.; Zhu, B., H_2S-activated fluorescent probe enables dual-channel fluorescence tracking of drug release in tumor cells. *Bioorganic Chemistry* **2023**, 106498.

[632] Niu, H.; Mi, X.; Hua, X.; Zhang, Y.; Zhai, Y.; Qin, F.; Ye, Y.; Zhao, Y., A bifunctional fluorescent probe based on "AND logic" for the simultaneous recognition of H_2S/HNO and its bioimaging applications. *Analytica Chimica Acta* **2022,** *1192*, 339341.

[633] Wei, C.; Wang, R.; Zhang, C.; Xu, G.; Li, Y.; Zhang, Q.-Z.; Li, L.-Y.; Yi, L.; Xi, Z., Dual-Reactable Fluorescent Probes for Highly Selective and Sensitive Detection of Biological H_2S. *Chemistry – An Asian Journal* **2016,** *11* (9), 1376-1381.

[634] Zhang, H.; Li, W.; Chen, J.; Li, G.; Yue, X.; Zhang, L.; Song, X.; Chen, W., Simultaneous detection of Cys/Hcy and H_2S through distinct fluorescence channels. *Analytica Chimica Acta* **2020,** *1097*, 238-244.

[635] Zhang, C.; Wei, L.; Wei, C.; Zhang, J.; Wang, R.; Xi, Z.; Yi, L., A FRET–ICT dual-quenching fluorescent probe with large off–on response for H_2S: synthesis, spectra and bioimaging. *Chemical Communications* **2015,** *51* (35), 7505-7508.

[636] Jiang, Y.; Ji, X.; Zhang, C.; Xi, Z.; Sun, L.; Yi, L., Dual-quenching NBD-based fluorescent probes for separate detection of H_2S and Cys/Hcy in living cells. *Organic & Biomolecular Chemistry* **2019,** *17* (36), 8435-8442.

[637] Zhang, C.; Wang, R.; Cheng, L.; Li, B.; Xi, Z.; Yi, L., A Redox-Nucleophilic Dual-Reactable Probe for Highly Selective and Sensitive Detection of H_2S: Synthesis, Spectra and Bioimaging. *Scientific Reports* **2016,** *6* (1), 30148.

[638] Liu, X.; Fu, S.; Zhang, H.; Li, S.; Zhu, Z.; Chen, S.; Hou, H.; Chen, W.; Hou, P., Rational design of a GSH silent fluorescent probe for simultaneous detection of H_2S and Cys/Hcy from distinct channels. *Microchemical Journal* **2023,** *184*, 108187.

[639] Ma, C.; Wei, C.; Li, X.; Zheng, X.; Chen, B.; Wang, M.; Zhang, P.; Li, X., A mitochondria-targeted dual-reactable fluorescent probe for fast detection of H_2S in living cells. *Dyes and Pigments* **2019,** *162*, 624-631.

[640] Li, Z.; Gao, J.; Guo, Z.; Zhao, H.; Liu, L.; Wang, M.; Zhang, P.; Chen, G.; Li, X.; Wei, C., Monitoring the fluctuation of H_2S in insulin-resistant HepG2 cells and diabetic mice with a dual-locked NIR fluorescent probe. *Sensors and Actuators B: Chemical* **2022,** *353*, 131141.

[641] Ye, H.; Cheng, L.; Tu, X.; Wang, D.-W.; Yi, L., Rational design of a dual-reactive probe for imaging the biogenesis of both H_2S and GSH from l-Cys rather than d-Cys in live cells. *RSC Chemical Biology* **2022,** *3* (7), 848-852.

[642] Ramya, A. N.; Joseph, M. M.; Karunakaran, V.; Ahammed, C. V. S.; Samanta, A.; Maiti, K. K., An efficient molecular luminophore based on tetraphenylethylene (TPE) enabling intracellular detection and therapeutic benefits of hydrogen sulfide in Alzheimer's disease. *Sensors and Actuators B: Chemical* **2022,** *355*, 131118.

[643] Zhang, C.; Zhang, J.; Xu, Z.; Zang, K.; Liu, F.; Yin, J.; Tan, Y.; Jiang, Y., A biotin-guided hydrogen sulfide fluorescent probe and its application in living cell imaging. *RSC Advances* **2020,** *10* (59), 36135-36140.

[644] Kim, H. W.; Choi, M. G.; Park, H.; Lee, J. W.; Chang, S.-K., Single molecular multianalyte signaling of sulfide and azide ions by a nitrobenzoxadiazole-based probe. *RSC Advances* **2015,** *5* (6), 4623-4627.

[645] Ma, Z.; Lin, Y.; Chen, H.; Du, L.; Li, M., A novel NBD-based pH "on–off" fluorescent probe equipped with the N-phenylpiperazine group for lysosome imaging. *RSC Advances* **2016,** *6* (104), 102773-102777.

[646] Kang, J. H.; Yang, M.; Yun, D.; Kim, M.; Lee, H.; Kim, K.-T.; Lim, M. H.; Kim, C., A dual-response sensor based on NBD for the highly selective determination of sulfide in living cells and zebrafish. *New Journal of Chemistry* **2019,** *43* (10), 4029-4035.

[647] Zhang, J.; Wen, G.; Wang, W.; Cheng, K.; Guo, Q.; Tian, S.; Liu, C.; Hu, H.; Zhang, Y.; Zhang, H.; Wang, L.; Sun, H., Controllable Cleavage of C–N Bond-Based Fluorescent and Photoacoustic Dual-Modal Probes for the Detection of H2S in Living Mice. *ACS Applied Bio Materials* **2021,** *4* (3), 2020-2025.

[648] Chen, R.; Ye, H.; Fang, T.; Liu, S.; Yi, L.; Cheng, L., An NBD tertiary amine is a fluorescent quencher and/or a weak green-light fluorophore in H_2S-specific probes. *Organic & Biomolecular Chemistry* **2022,** *20* (20), 4128-4134.

[649] Qian, Y.; Karpus, J.; Kabil, O.; Zhang, S.-Y.; Zhu, H.-L.; Banerjee, R.; Zhao, J.; He, C., Selective fluorescent probes for live-cell monitoring of sulphide. *Nature Communications* **2011,** *2* (1), 495.

[650] Qian, Y.; Zhang, L.; Ding, S.; Deng, X.; He, C.; Zheng, X. E.; Zhu, H.-L.; Zhao, J., A fluorescent probe for rapid detection of hydrogen sulfide in blood plasma and brain tissues in mice. *Chemical Science* **2012,** *3* (10), 2920-2923.

[651] Li, X.; Zhang, S.; Cao, J.; Xie, N.; Liu, T.; Yang, B.; He, Q.; Hu, Y., An ICT-based fluorescent switch-on probe for hydrogen sulfide in living cells. *Chemical Communications* **2013,** *49* (77), 8656-8658.

[652] Qian, Y.; Yang, B.; Shen, Y.; Du, Q.; Lin, L.; Lin, J.; Zhu, H., A BODIPY–coumarin-based selective fluorescent probe for rapidly detecting hydrogen sulfide in blood plasma and living cells. *Sensors and Actuators B: Chemical* **2013,** *182*, 498-503.

[653] Singha, S.; Kim, D.; Moon, H.; Wang, T.; Kim, K. H.; Shin, Y. H.; Jung, J.; Seo, E.; Lee, S.-J.; Ahn, K. H., Toward a Selective, Sensitive, Fast-Responsive, and Biocompatible Two-Photon Probe for Hydrogen Sulfide in Live Cells. *Analytical Chemistry* **2015,** *87* (2), 1188-1195.

[654] Ryu, H. G.; Singha, S.; Jun, Y. W.; Reo, Y. J.; Ahn, K. H., Two-photon fluorescent probe for hydrogen sulfide based on a red-emitting benzocoumarin dye. *Tetrahedron Letters* **2018,** *59* (1), 49-53.

[655] Li, J.; Yin, C.; Zhang, Y.; Yongkang, y.; Chao, J.; Huo, F., High selective distinguishable detection GSH and H_2S based on steric configuration of molecular in vivo. *Dyes and Pigments* **2020,** *172*, 107826.

[656] Asthana, S. K.; Kumar, A.; Neeraj; Shweta; Upadhyay, K. K., Efficient visualization of H_2S via a fluorescent probe with three electrophilic centres. *Organic & Biomolecular Chemistry* **2016,** *14* (15), 3690-3694.

[657] Wang, X.; Sun, J.; Zhang, W.; Ma, X.; Lv, J.; Tang, B., A near-infrared ratiometric fluorescent probe for rapid and highly sensitive imaging of endogenous hydrogen sulfide in living cells. *Chemical Science* **2013,** *4* (6), 2551-2556.

[658] Liu, C.; Wu, H.; Han, B.; Zhu, B.; Zhang, X., A highly selective fluorescent chemodosimeter for imaging hydrogen sulfide in living cells. *Dyes and Pigments* **2014,** *110*, 214-218.

[659] Goswami, S.; Manna, A.; Mondal, M.; Sarkar, D., Cascade reaction-based rapid and ratiometric detection of H_2S/S^{2-} in the presence of bio-thiols with live cell imaging: demasking of ESIPT approach. *RSC Advances* **2014,** *4* (107), 62639-62643.

[660] Huang, K.; Liu, M.; Wang, X.; Cao, D.; Gao, F.; Zhou, K.; Wang, W.; Zeng, W., Cascade reaction and FRET-based fluorescent probe for the colorimetric and ratiometric signaling of hydrogen sulfide. *Tetrahedron Letters* **2015,** *56* (24), 3769-3773.

[661] Velusamy, N.; Thirumalaivasan, N.; Bobba, K. N.; Wu, S.-P.; Bhuniya, S., A hydrogen sulfide triggered self-immolative fluorescent probe for lysosome labeling in live cells. *New Journal of Chemistry* **2018,** *42* (3), 1590-1594.

[662] Li, Z.-Q.; Zhou, Z.; Chen, D.-X.; Wang, K.; Ye, N.-Y.; Sun, X.-Y.; Lv, Y.-Y., Mitochondrial-targeted red-fluorescent chemodosimeter for hydrogen sulfide signaling and visualizing. *Sensors and Actuators B: Chemical* **2022,** *369*, 132357.

[663] Shu, W.; Zang, S.; Wang, C.; Gao, M.; Jing, J.; Zhang, X., An Endoplasmic Reticulum-Targeted Ratiometric Fluorescent Probe for the Sensing of Hydrogen Sulfide in Living Cells and Zebrafish. *Analytical Chemistry* **2020,** *92* (14), 9982-9988.

[664] Liu, C.; Peng, B.; Li, S.; Park, C.-M.; Whorton, A. R.; Xian, M., Reaction Based Fluorescent Probes for Hydrogen Sulfide. *Organic Letters* **2012,** *14* (8), 2184-2187.

[665] Huang, K.; Yu, L.; Xu, P.; Zhang, X.; Zeng, W., A novel FRET-based ratiometric fluorescent probe for highly sensitive detection of hydrogen sulfide. *RSC Advances* **2015,** *5* (23), 17797-17801.

[666] Gao, B.; Cui, L.; Pan, Y.; Xue, M.; Zhu, B.; Zhang, G.; Zhang, C.; Shuang, S.; Dong, C., A highly selective fluorescent probe based on Michael addition for fast detection of hydrogen sulfide. *Spectrochimica Acta Part A: Molecular and Biomolecular Spectroscopy* **2017,** *173*, 457-461.

[667] Zhang, J.; Sun, Y.-Q.; Liu, J.; Shi, Y.; Guo, W., A fluorescent probe for the biological signaling molecule H_2S based on a specific H_2S trap group. *Chemical Communications* **2013,** *49* (96), 11305-11307.

[668] Yang, Y.; Liu, Y. U.; Yang, L.; Liu, J. U. N.; Li, K. U. N.; Luo, S., A coumarin-based colorimetric fluorescent probe for hydrogen sulfide. *Journal of Chemical Sciences* **2015,** *127* (3), 359-363.

[669] Zheng, H.-R.; Niu, L.-Y.; Chen, Y.-Z.; Wu, L.-Z.; Tung, C.-H.; Yang, Q.-Z., Cascade reaction-based fluorescent probe for detection of H_2S with the assistance of CTAB micelles. *Chinese Chemical Letters* **2016,** *27* (12), 1793-1796.

[670] Reja, S. I.; Sharma, N.; Gupta, M.; Bajaj, P.; Bhalla, V.; Parihar, R. D.; Ohri, P.; Kaur, G.; Kumar, M., A Highly Selective Fluorescent Probe for Detection of Hydrogen Sulfide in Living Systems: in vitro and in vivo Applications. *Chemistry – A European Journal* **2017,** *23* (41), 9872-9878.

[671] Zhang, Y.; Zhao, M.; Chao, D., A cyclometalated iridium(III) complex for selective luminescent detection of hydrogen sulfide. *Sensors and Actuators B: Chemical* **2017,** *248*, 19-23.

[672] Jiang, Y.; Jin, D.; Li, Y.; Yan, X.; Chen, L., A near-infrared fluorescent probe for rapid and selective detection of hydrosulfide and imaging in live cells. *Research on Chemical Intermediates* **2017,** *43* (5), 2945-2957.

[673] Xie, X.; Yin, C.; Yue, Y.; Chao, J.; Huo, F., Fluorescent probe detect distinguishly sulfite/hydrogen sulfide and thiol via two emission channels in vivo. *Sensors and Actuators B: Chemical* **2018,** *277*, 647-653.

[674] Mittapelli, L. L.; Nawale, G. N.; Gholap, S. P.; Varghese, O. P.; Gore, K. R., A turn-on fluorescent GFP chromophore analog for highly selective and efficient detection of H_2S in aqueous and in living cells. *Sensors and Actuators B: Chemical* **2019,** *298*, 126875.

[675] Zhao, X.; Ji, H.; Hasrat, K.; Misal, S.; He, F.; Dai, Y.; Ma, F.; Qi, Z., A mitochondria-targeted single fluorescence probe for separately and continuously visualizing H_2S and Cys with multi-response signals. *Analytica Chimica Acta* **2020,** *1107*, 172-182.

[676] Jin, X.; Wu, S.; She, M.; Jia, Y.; Hao, L.; Yin, B.; Wang, L.; Obst, M.; Shen, Y.; Zhang, Y.; Li, J., Novel Fluorescein-Based Fluorescent Probe for Detecting H_2S and Its Real Applications in Blood Plasma and Biological Imaging. *Analytical Chemistry* **2016,** *88* (22), 11253-11260.

[677] Wang, J.; Wang, H.; Yang, S.; Tian, H.; Liu, Y.; Sun, B., A Novel Fluorescent Probe for Detecting Hydrogen Sulfide in Wine. *Food Analytical Methods* **2018,** *11* (5), 1398-1404.

[678] Jin, X.; Wu, X.; Xie, P.; Liu, S.; Wu, J.; Wang, T.; Zhou, H.; Leng, X.; Chen, W., Reaction-based fluorescent probes for rapid detection of hydrogen sulfide in vivo. *Analytical Methods* **2018,** *10* (33), 4079-4084.

[679] Chen, H.; Wu, X.; Yang, S.; Tian, H.; Liu, Y.; Sun, B., A Visible Colorimetric Fluorescent Probe for Hydrogen Sulfide Detection in Wine. *Journal of Analytical Methods in Chemistry* **2019,** *2019*, 2173671.

[680] Wang, B.; Wang, X.; Zeng, A.; Leng, J.; Zhao, W., Engineering a mitochondria-targeted ratiometric fluorescent probe with a large Stokes shift for H_2S-specific assaying in foodstuffs and living cells. *Sensors and Actuators B: Chemical* **2021,** *343*, 130095.

[681] Yi, L.; Wang, Y.; Luo, T.; Hu, W.; Wang, M.; Wang, J., Design, synthesis and evaluation of a novel hepatocyte-targeting fluorescent probe to accurately detect H_2S in mitochondria. *Dyes and Pigments* **2019,** *166*, 460-466.

[682] Liao, L.; Li, Z.; Hu, W.; Huang, Y.; Liu, B.-m.; Wang, L.; Wang, M.; Wang, J., Design, synthesis and evaluation of a novel fluorescent probe to accurately detect H_2S in lysosomes. *Tetrahedron Letters* **2018,** *59* (27), 2683-2687.

[683] Chen, W.; Xie, P.; Shan, X.; Zhao, H.; Wu, Y.; Zhou, H.; Jin, X., A near-infrared naphthofluorescein-based fluorescent probe for hydrogen sulfide detection. *Journal of Molecular Structure* **2020,** *1207*, 127822.

[684] Ma, X.; Jin, X.; Zhou, H.; Wang, D.; Zhou, X.; Chen, J.; Li, M.; Du, H.; She, M., Near-infrared fluorescent probe for rapid detecting H_2S and its application in nanofibrous film and living cells. *Dyes and Pigments* **2021,** *188*, 109221.

[685] Chen, X.; He, D.; Yang, X.; Yuan, F.; Yang, S.; Yang, Y.; Wang, K.; Qian, J.; Long, L., Construction of bifunctional fluorescent probe for two-step cascade recognition of

hydrogen sulfide and biothiols in biological system. *Sensors and Actuators B: Chemical* **2023,** *381*, 133440.

[686] Hou, J.; Huang, Y.; Fu, L.; Sun, M.; Wang, L.; Guo, R.; Chen, L.; Lv, C., Evaluating the Effect of Hydrogen Sulfide in the Idiopathic Pulmonary Fibrosis Model with a Fluorescent Probe. *Analytical Chemistry* **2023,** *95* (13), 5514-5521.

[687] Karakuş, E.; Üçüncü, M.; Emrullahoğlu, M., Electrophilic Cyanate As a Recognition Motif for Reactive Sulfur Species: Selective Fluorescence Detection of H_2S. *Analytical Chemistry* **2016,** *88* (1), 1039-1043.

[688] Soboleva, T.; Benninghoff, A. D.; Berreau, L. M., An H_2S-Sensing/CO-Releasing Flavonol That Operates via Logic Gates. *ChemPlusChem* **2017,** *82* (12), 1408-1412.

[689] Yang, G.; Zhang, J.; Zhu, S.; Wang, Y.; Feng, X.; Yan, M.; Yu, J., Fast response and highly selective detection of hydrogen sulfide with a ratiometric two-photon fluorescent probe and its application for bioimaging. *Sensors and Actuators B: Chemical* **2018,** *261*, 51-57.

[690] Jin, Y.; Liu, R.; Zhan, Z.; Lv, Y., Fast response near-infrared fluorescent probe for hydrogen sulfide in natural waters. *Talanta* **2019,** *202*, 159-164.

[691] Zhou, R.; Cui, G.; Qi, Q.; Huang, W.; Yang, L., The synthesis and bioimaging of a biocompatible hydrogen sulfide fluorescent probe with high sensitivity and selectivity. *Analyst* **2020,** *145* (6), 2305-2310.

[692] Ma, Y.; Wang, X.; Wang, Z.; Zhang, G.; Chen, X.; Zhang, Y.; Luo, Y.; Gao, G.; Zhou, X., A water-soluble NIR fluorescent probe capable of rapid response and selective detection of hydrogen sulfide in food samples and living cells. *Talanta* **2023,** *256*, 124303.

[693] Kim, J. K.; Bong, S. Y.; Park, R.; Park, J.; Jang, D. O., An ESIPT-based fluorescent turn-on probe with isothiocyanate for detecting hydrogen sulfide in environmental and biological systems. *Spectrochimica Acta Part A: Molecular and Biomolecular Spectroscopy* **2022,** *278*, 121333.

[694] Martelli, A.; Testai, L.; Citi, V.; Marino, A.; Bellagambi, F. G.; Ghimenti, S.; Breschi, M. C.; Calderone, V., Pharmacological characterization of the vascular effects of aryl isothiocyanates: Is hydrogen sulfide the real player? *Vascular Pharmacology* **2014,** *60* (1), 32-41.

[695] Lin, Y.; Yang, X.; Lu, Y.; Liang, D.; Huang, D., Isothiocyanates as H_2S Donors Triggered by Cysteine: Reaction Mechanism and Structure and Activity Relationship. *Organic Letters* **2019,** *21* (15), 5977-5980.

[696] Zhang, M.; Wang, S.; Fu, Y.; Meng, M.; Jin, H.; Zhao, W., An isothiocyanate-functionalized self-immolative near-infrared fluorescence probe for cysteine sensing and bioimaging in living systems. *Sensors and Actuators B: Chemical* **2022,** *366*, 132013.

[697] Li, H.; Peng, W.; Feng, W.; Wang, Y.; Chen, G.; Wang, S.; Li, S.; Li, H.; Wang, K.; Zhang, J., A novel dual-emission fluorescent probe for the simultaneous detection of H_2S and GSH. *Chemical Communications* **2016,** *52* (25), 4628-4631.

[698] Geng, Y.; Zhang, G.; Chen, Y.; Peng, Y.; Wang, X.; Wang, Z., Si-Rhodamine Derivatives for Brain Fluorescence Imaging and Monitoring of H_2S in the Brain of Schizophrenic Mice before and after Treatment. *Analytical Chemistry* **2022,** *94* (3), 1813-1822.

[699] Chen, F.; Han, D.; Liu, H.; Wang, S.; Li, K.-B.; Zhang, S.; Shi, W., A tri-site fluorescent probe for simultaneous sensing of hydrogen sulfide and glutathione and its bioimaging applications. *Analyst* **2018,** *143* (2), 440-448.

[700] Chen, F.; Han, D.; Gao, Y.; Liu, H.; Wang, S.; Zhou, F.; Li, K.; Zhang, S.; Shao, W.; He, Y., A turn-on fluorescent probe for simultaneous sensing of cysteine/homocysteine and hydrogen sulfide and its bioimaging applications. *Talanta* **2018,** *187*, 19-26.

[701] Feng, Y.; Hu, S.; Wang, Y.; Song, X.; Cao, C.; Wang, K.; Jing, C.; Zhang, G.; Liu, W., A multifunctional fluorescent probe for visualizing H_2S in wastewater with portable smartphone via fluorescent paper strip and sensing GSH in vivo. *Journal of Hazardous Materials* **2021,** *406*, 124523.

[702] Chen, W.; Fu, L.; Chen, C.; Xiao, J.; Li, W.; Zhang, L.; Xiao, Q.; Huang, C.; Sheng, J.; Song, X., Unexpected reaction patterns enable simultaneous differentiation of H_2S, H_2S_n and biothiols. *Chemical Communications* **2019,** *55* (56), 8130-8133.

[703] Chao, J.; Xu, M.; Zhang, Y.; Huo, F.; Liu, Y.; Wang, X.; Yin, C., HS^- facilitated sulfur pyran realizing hydrogen sulfide detection and imaging in HepG2 cells and chlorella. *Spectrochimica Acta Part A: Molecular and Biomolecular Spectroscopy* **2019,** *214*, 227-232.

[704] Wang, C.; Cheng, X.; Tan, J.; Ding, Z.; Wang, W.; Yuan, D.; Li, G.; Zhang, H.; Zhang, X., Reductive cleavage of C=C bonds as a new strategy for turn-on dual fluorescence in effective sensing of H_2S. *Chemical Science* **2018,** *9* (44), 8369-8374.

[705] Wang, C.; Tan, J.; Zhang, X., Structure–reactivity relationship of probes based on the H2S-mediated reductive cleavage of the C=C bond. *New Journal of Chemistry* **2020,** *44* (27), 11667-11677.

[706] Samanta, S. K.; Ali, S. S.; Gangopadhyay, A.; Maiti, K.; Pramanik, A. K.; Guria, U. N.; Ghosh, A.; Datta, P.; Mahapatra, A. K., A highly selective ratiometric fluorescent probe for H_2S based on new heterocyclic ring formation and detection in live cells. *Supramolecular Chemistry* **2019,** *31* (5), 349-360.

[707] Ding, J.; Ge, Y.; Zhu, B., A Highly Selective Fluorescent Probe for Quantitative Detection of Hydrogen Sulfide. *Analytical Sciences* **2013,** *29* (12), 1171-1175.

[708] Shang, X.; Li, J.; Feng, Y.; Chen, H.; Guo, W.; Zhang, J.; Wang, T.; Xu, X., Low-Cytotoxicity Fluorescent Probes Based on Anthracene Derivatives for Hydrogen Sulfide Detection. *Frontiers in Chemistry* **2018,** *6*.

[709] Wu, X.; Li, Y.; Yang, S.; Tian, H.; Sun, B., A multiple-detection-point fluorescent probe for the rapid detection of mercury(II), hydrazine and hydrogen sulphide. *Dyes and Pigments* **2020,** *174*, 108056.

[710] Jin, L.; Tan, X.; Dai, L.; Bai, H.; Wang, Q., Modulation of fluorescence sensing properties of coumarin-based fluorescent probe for H_2S and its application in cell imaging. *Spectrochimica Acta Part A: Molecular and Biomolecular Spectroscopy* **2019,** *221*, 117187.

[711] Pei, X.; Tian, H.; Zhang, W.; Brouwer, A. M.; Qian, J., Colorimetric and fluorescent determination of sulfide and sulfite with kinetic discrimination. *Analyst* **2014,** *139* (20), 5290-5296.

[712] Wang, X.; Meng, Z.; Wang, S.; Kou, J.; Wang, Z.; Yang, Y., A dual-functional coumarin-based fluorescent probe for turn off detection of Cu^{2+} and ratiometric detection of H_2S and its applications in environmental samples and bioimaging samples. *Journal of Molecular Structure* **2023,** *1294*, 136390.

[713] Yang, Y.; Feng, Y.; Jiang, Y.; Qiu, F.; Wang, Y.; Song, X.; Tang, X.; Zhang, G.; Liu, W., A coumarin-based colorimetric fluorescent probe for rapid response and highly sensitive detection of hydrogen sulfide in living cells. *Talanta* **2019,** *197*, 122-129.

[714] Shen, Z.; Gao, Y.; Li, M.; Zhang, Y.; Xu, K.; Gong, S.; Wang, Z.; Wang, S., Development and application of a novel β-diketone difluoroboron-derivatized fluorescent probe for sensitively detecting H_2S. *Spectrochimica Acta Part A: Molecular and Biomolecular Spectroscopy* **2022,** *281*, 121609.

[715] Chen, Y.; Zhu, C.; Yang, Z.; Chen, J.; He, Y.; Jiao, Y.; He, W.; Qiu, L.; Cen, J.; Guo, Z., A Ratiometric Fluorescent Probe for Rapid Detection of Hydrogen Sulfide in Mitochondria. *Angewandte Chemie International Edition* **2013,** *52* (6), 1688-1691.

[716] Yang, Y.; Yin, C.; Huo, F.; Zhang, Y.; Chao, J., A ratiometric colorimetric and fluorescent chemosensor for rapid detection hydrogen sulfide and its bioimaging. *Sensors and Actuators B: Chemical* **2014,** *203*, 596-601.

[717] Fang, H.; Chen, Y.; Shi, X.; Bai, Y.; Chen, Z.; Han, Z.; Zhang, Y.; He, W.; Guo, Z., Tuning lipophilicity for optimizing the H_2S sensing performance of coumarin–merocyanine derivatives. *New Journal of Chemistry* **2019,** *43* (37), 14800-14805.

[718] Wu, L.; Chen, L.; Kou, M.; Dong, Y.; Deng, W.; Ge, L.; Bao, H.; Chen, Q.; Li, D., The ratiometric fluorescent probes for monitoring the reactive inorganic sulfur species (RISS)

signal in the living cell. *Spectrochimica Acta Part A: Molecular and Biomolecular Spectroscopy* **2020,** *231*, 118141.

[719] He, L.; He, L.-H.; Xu, S.; Ren, T.-B.; Zhang, X.-X.; Qin, Z.-J.; Zhang, X.-B.; Yuan, L., Engineering of Reversible NIR-II Redox-Responsive Fluorescent Probes for Imaging of Inflammation In Vivo. *Angewandte Chemie International Edition* **2022,** *61* (46), e202211409.

[720] Zhang, Y.; Chen, Y.; Fang, H.; Shi, X.; Yuan, H.; Bai, Y.; He, W.; Guo, Z., A ratiometric fluorescent probe for imaging enzyme dependent hydrogen sulfide variation in the mitochondria and in living mice. *Analyst* **2020,** *145* (15), 5123-5127.

[721] Zhang, Y.; Chen, Y.; Bai, Y.; Xue, X.; He, W.; Guo, Z., FRET-based fluorescent ratiometric probes for the rapid detection of endogenous hydrogen sulphide in living cells. *Analyst* **2020,** *145* (12), 4233-4238.

[722] Feng, X.; Zhang, T.; Liu, J.-T.; Miao, J.-Y.; Zhao, B.-X., A new ratiometric fluorescent probe for rapid, sensitive and selective detection of endogenous hydrogen sulfide in mitochondria. *Chemical Communications* **2016,** *52* (15), 3131-3134.

[723] Bu, D.; Wang, Y.; Wu, N.; Feng, W.; Wei, D.; Li, Z.; Yu, M., A mitochondrial-targeted ratiometric probe for detecting intracellular H_2S with high photostability. *Chinese Chemical Letters* **2021,** *32* (5), 1799-1802.

[724] Li, Y.; Gu, B.; Su, W.; Duan, X.; Xu, H.; Huang, Z.; Li, H.; Yao, S., A simple and efficient fluorescent probe for the rapid detection of H_2S in living cells and on agar gels. *Analytical Methods* **2017,** *9* (22), 3290-3295.

[725] Shi, Y.; Huo, F.; Yue, Y.; Yin, C., N-Positive ion activated rapid addition and mitochondrial targeting ratiometric fluorescent probes for in vivo cell H_2S imaging. *Frontiers of Chemical Science and Engineering* **2022,** *16* (1), 64-71.

[726] Sha, X.-L.; Xiao, J.-W.; Yin, D.-H.; Sun, R.; Xu, Y.-J.; Ge, J.-F., Preparation of a photostable tribrachia cyanine dye and its high chemical activity towards hydrosulfide. *Dyes and Pigments* **2018,** *149*, 505-511.

[727] Ren, M.; Deng, B.; Kong, X.; Zhou, K.; Liu, K.; Xu, G.; Lin, W., A TICT-based fluorescent probe for rapid and specific detection of hydrogen sulfide and its bio-imaging applications. *Chemical Communications* **2016,** *52* (38), 6415-6418.

[728] Paul, S.; Goswami, S.; Das Mukhopadhyay, C., A remarkable ratiometric fluorescent chemodosimeter for very rapid detection of hydrogen sulfide in the vapour phase and living cells. *New Journal of Chemistry* **2015,** *39* (11), 8940-8947.

[729] Ma, J.; Li, F.; Li, Q.; Li, Y.; Yan, C.; Lu, X.; Guo, Y., Naked-eye and ratiometric fluorescence probe for fast and sensitive detection of hydrogen sulfide and its application in bioimaging. *New Journal of Chemistry* **2018,** *42* (23), 19272-19278.

[730] Cai, S.; Liu, C.; He, S.; Zhao, L.; Zeng, X., Mitochondria-targeted fluorescent probe for imaging endogenous hydrogen sulfide in cellular antioxidant stress. *Analytical Methods* **2020,** *12* (42), 5061-5067.

[731] Zhang, Y.; Huang, X.; Liu, W.; Zhang, G.; Zhang, D.; Jiang, X., Organic nanoparticles formed by aggregation-induced fluorescent molecules for detection of hydrogen sulfide in living cells. *Science China Chemistry* **2016,** *59* (1), 106-113.

[732] Ma, Y.; Wang, H.; Su, S.; Chen, Y.; Li, Y.; Wang, X.; Wang, Z., A red mitochondria-targeted AIEgen for visualizing H_2S in living cells and tumours. *Analyst* **2019,** *144* (10), 3381-3388.

[733] Liu, Y.; Meng, F.; He, L.; Liu, K.; Lin, W., A dual-site two-photon fluorescent probe for visualizing lysosomes and tracking lysosomal hydrogen sulfide with two different sets of fluorescence signals in the living cells and mouse liver tissues. *Chemical Communications* **2016,** *52* (43), 7016-7019.

[734] Liu, Y.; Niu, J.; Wang, W.; Ma, Y.; Lin, W., Simultaneous Imaging of Ribonucleic Acid and Hydrogen Sulfide in Living Systems with Distinct Fluorescence Signals Using a Single Fluorescent Probe. *Advanced Science* **2018,** *5* (7), 1700966.

[735] Magesh, K.; Vijay, N.; Wu, S. P.; Velmathi, S., Dual-Responsive Benzo-Hemicyanine-Based Fluorescent Probe for Detection of Cyanide and Hydrogen Sulfide: Real-Time Application in Identification of Food Spoilage. *Journal of Agricultural and Food Chemistry* **2023,** *71* (2), 1190-1200.

[736] Li, S.; Huo, F.; Yin, C., NIR fluorescent probe for dual-response viscosity and hydrogen sulfide and its application in Parkinson's disease model. *Dyes and Pigments* **2022,** *197*, 109825.

[737] Zhao, S.; Xue, Y.; Hu, L.; Sun, F.; Nie, J.; Chang, Y., A NIR-II Fluorescent Probe for Hydrogen Sulfide Detection Based on Blocking Intramolecular Charge Transfer. *ChemistrySelect* **2023,** *8* (12), e202300554.

[738] Guria, U. N.; Maiti, K.; Ali, S. S.; Samanta, S. K.; Mandal, D.; Sarkar, R.; Datta, P.; Ghosh, A. K.; Mahapatra, A. K., Reaction-based bi-signaling chemodosimeter probe for selective detection of hydrogen sulfide and cellular studies. *New Journal of Chemistry* **2018,** *42* (7), 5367-5375.

[739] Zhao, X.; He, F.; Dai, Y.; Ma, F.; Qi, Z., A single fluorescent probe for one- and two-photon imaging hydrogen sulfide and hydrogen polysulfides with different fluorescence signals. *Dyes and Pigments* **2020,** *172*, 107818.

[740] Wang, B.; Jiang, N.; Sun, W.; Wang, Q.; Zheng, G., A ratiometric fluorescence probe for detection of hydrogen sulfide in cells. *RSC Advances* **2016,** *6* (43), 36906-36909.

[741] Xie, L.; Yuan, K.; Tao, B.; Liu, G.; Liao, G.; Chen, S.; Fan, C., Engineering a mitochondria-targeted fluorescent probe with long wavelength for rapid detection of H_2S in beer, water and living cells. *Journal of Photochemistry and Photobiology A: Chemistry* **2023,** *444*, 114993.

[742] Li, B.; Wang, M.; Gu, X.; Chen, J.; Yang, X.; Liu, X.; Xu, K., A hemicyanidin-based NIR fluorescent probe for detection of H_2S and imaging study in cells and mice. *Microchimica Acta* **2022,** *189* (8), 291.

[743] Jiang, N.; Wang, B.; Liu, T.; Liu, Q.; Wei, Q.; Xing, Y.; Zheng, G., Fast and sensitive fluorescent probe for ratiometric detection of hydrogen sulfide in mitochondria. *Analytical Methods* **2019,** *11* (2), 232-235.

[744] Liu, Q.; Zhao, Y.; Zhang, Y.; Xie, K.; Liu, R.; Ren, B.; Yan, Y.; Li, L., A spiropyran functionalized fluorescent probe for mitochondria targeting and imaging of endogenous hydrogen sulfide in living cells. *Analyst* **2020,** *145* (24), 8016-8021.

[745] Zhang, J.; Zhou, J.; Dong, X.; Zheng, X.; Zhao, W., A near-infrared BODIPY-based fluorescent probe for the detection of hydrogen sulfide in fetal bovine serum and living cells. *RSC Advances* **2016,** *6* (56), 51304-51309.

[746] Hu, Y.; Shang, Z.; Wang, J.; Hong, M.; Zhang, R.; Meng, Q.; Zhang, Z., A phenothiazine-based turn-on fluorescent probe for the selective detection of hydrogen sulfide in food, live cells and animals. *Analyst* **2021,** *146* (24), 7528-7536.

[747] Li, X.; Gu, J.; Huang, H.; Zhou, Z.; Gao, J.; Wang, Q., Carbazole based new organic dye recognizes hydrazine and hydrogen sulfide via signal difference protocols. *Dyes and Pigments* **2020,** *181*, 108545.

[748] Ma, T.; Huo, F.; Yin, C., A 'naked-eye' ratiometric and NIR fluorescent detection for hydrogen sulphide with quick response and high selectivity for and its bioimaging. *Dyes and Pigments* **2019,** *165*, 31-37.

[749] Su, C.-C.; Kim, K.-R.; Hong, J.-I., Dual-functional turn-on fluorescent probe for discriminative sulfite and sulfide detection via organic/aqueous ratio tuning and its application in real samples. *Dyes and Pigments* **2022,** *206*, 110669.

[750] Hu, M.; Wang, B.; Zhang, H.; Wang, H.; Li, H.; Zhang, X.; Zhang, J.; Lu, Q.; Fang, G.; Wang, J.; Dong, B., A Dual-Labeling Probe for Super-Resolution Imaging to Detect Mitochondrial Reactive Sulfur Species in Live Cells. *Frontiers in Pharmacology* **2022,** *13*, 871059.

[751] Han, S.; Zhang, H.; Wang, J.; Yang, L.; Lan, M.; Wang, B.; Song, X., Rational Development of Dual-Ratiometric Fluorescent Probes for Distinguishing between H_2S and SO_2 in Living Organisms. *Analytical Chemistry* **2021,** *93* (45), 15209-15215.

[752] Wang, S.; Xu, S.; Hu, G.; Bai, X.; James, T. D.; Wang, L., A Fluorescent Chemodosimeter for Live-Cell Monitoring of Aqueous Sulfides. *Analytical Chemistry* **2016,** *88* (2), 1434-1439.

[753] Chen, L.; Wu, D.; Lim, C. S.; Kim, D.; Nam, S.-J.; Lee, W.; Kim, G.; Kim, H. M.; Yoon, J., A two-photon fluorescent probe for specific detection of hydrogen sulfide based on a familiar ESIPT fluorophore bearing AIE characteristics. *Chemical Communications* **2017,** *53* (35), 4791-4794.

[754] Du, Y.; Wang, H.; Qin, L.; Zhao, M.; Pan, C., Rational development of an ESIPT-based fluorescent probe with large Stokes shift for imaging of hydrogen sulfide in live cells. *Bioorganic Chemistry* **2022,** *129*, 106158.

[755] Kundu, S.; Sahoo, P., Estimation of hydrogen sulfide from crude petroleum: a unique invention using a simple chemosensor. *New Journal of Chemistry* **2019,** *43* (31), 12369-12374.

[756] Zong, Z.; Wang, J.; Bin, Y.; Wu, Y.; Huang, G., A bifunctional fluorescent probe for sensing of Al^{3+} and H_2S. *Analytical Methods* **2021,** *13* (18), 2157-2164.

[757] Thai, D. A.; Lee, N. Y., A paper-based colorimetric chemosensor for rapid and highly sensitive detection of sulfide for environmental monitoring. *Analytical Methods* **2021,** *13* (11), 1332-1339.

[758] Huang, X.; Lan, N.; Jiang, F.; He, H.; Zhong, J., Synthesis of a Near-Infrared Fluorescence Turn-On Probe Based on Dicyanoisophorone for HS^--Detection in Cancer Cells and Zebrafish in Pure Water Media. *ChemistrySelect* **2022,** *7* (17), e202201070.

[759] Guo, W.-T.; Dou, L.; Yan, Y.-J.; Li, R.-Y.; Dong, W.-K., A naphthol-functionalized bis(salamo)-like chromogenic and fluorogenic probe for monitoring hydrogen sulfide and application in water samples. *Phosphorus, Sulfur, and Silicon and the Related Elements* **2022,** *197* (9), 899-908.

[760] Mahalakshmi, G.; Saravana Kumar, P.; Sivaraman, G.; Seenivasa Perumal, M.; Elango, K. P., A simple imine as a dual-channel chemosensor for detection of CN^- and HS^- ions via different mechanisms in organic and aquo-organic media. *Journal of Photochemistry and Photobiology A: Chemistry* **2021,** *406*, 113021.

[761] Wang, B.; Leng, J.; Wang, X.; Zhao, W., Reversible AIE-active fluorescent probe with a large emission peak shift for ratiometric detection of food freshness indicator H_2S. *Food Chemistry* **2022,** *386*, 132768.

[762] Zhang, C.; Wang, Y.; Li, X.; Liu, C.; Nie, S.; Li, Y.; Liu, C., A simple and efficient fluorescent probe based on 1,8-naphthalimide – Ebselen for selectively detecting H_2S in living cells. *Tetrahedron Letters* **2022,** *110*, 154199.

[763] Zhang, C.; Zhang, L.; Li, Y.; Ren, Z.; Li, L.; Zhang, Y.; Li, Y.; Liu, C., A simple and efficient fluorescent probe for rapidly detecting H2S in GBC-SD cells based on 1,8-naphthalimide-ebselen. *Journal of Molecular Structure* **2022,** *1250*, 131777.

[764] Yang, Y.; Yin, C.; Huo, F.; Chu, Y.; Tong, H.; Chao, J.; Cheng, F.; Zheng, A., pH-sensitive fluorescent salicylaldehyde derivative for selective imaging of hydrogen sulfide in living cells. *Sensors and Actuators B: Chemical* **2013,** *186*, 212-218.

[765] Wu, X.; Duan, N.; Li, Y.; Yang, S.; Tian, H.; Sun, B., A dual-mode fluorescent probe for the separate detection of mercury(II) and hydrogen sulfide. *Journal of Photochemistry and Photobiology A: Chemistry* **2020,** *388*, 112209.

[766] Guan, P.; Shi, S.; Zhang, T.; Chai, J.; Yang, B.; Liu, B., A strategy to distinguish cancers from normal cells through lysosomal targeted double site fluorescent probe for lipase and hydrogen sulfide. *Dyes and Pigments* **2022,** *205*, 110545.

[767] Chen, X.; Wu, S.; Han, J.; Han, S., Rhodamine–propargylic esters for detection of mitochondrial hydrogen sulfide in living cells. *Bioorganic & Medicinal Chemistry Letters* **2013,** *23* (19), 5295-5299.

[768] Wang, Y.; Yang, L.; Wei, X.-R.; Sun, R.; Xu, Y.-J.; Ge, J.-F., Fluorescent probe based on rosamine with pyridinium unit for hydrogen sulfide detection in mitochondria. *Analytical Methods* **2018,** *10* (44), 5291-5296.

[769] Cui, Y.; Hu, G.; Wu, T.; Yang, J.; Nie, Y.; Zhou, Y., Construction of an in vivo NIR fluorescent probe for revealing the correlation between inflammation and mitochondrial hydrogen sulfide and viscosity. *Bioorganic Chemistry* **2022,** *129*, 106107.

[770] Sathyadevi, P.; Chen, Y.-J.; Wu, S.-C.; Chen, Y.-H.; Wang, Y.-M., Reaction-based epoxide fluorescent probe for in vivo visualization of hydrogen sulfide. *Biosensors and Bioelectronics* **2015,** *68*, 681-687.

[771] Wang, M.; Chen, J.; Gu, X.; Yang, X.; Fu, J.; Xu, K., A novel near-infrared fluorescent probe with large Stokes shift for imagining hydrogen sulfide. *Spectrochimica Acta Part A: Molecular and Biomolecular Spectroscopy* **2023,** *295*, 122587.

[772] Słowiński, D.; Świerczyńska, M.; Grzelakowska, A.; Szala, M.; Kolińska, J.; Romański, J.; Podsiadły, R., Hymecromone naphthoquinone ethers as probes for hydrogen sulfide detection. *Dyes and Pigments* **2021,** *196*, 109765.

[773] Yang, Y.; Yin, C.; Huo, F.; Chao, J.; Zhang, Y., Highly selective relay recognition of hydrogen sulfide and Hg(II) by a commercially available fluorescent chemosensor and its application in bioimaging. *Sensors and Actuators B: Chemical* **2014,** *204*, 402-406.

[774] Qian, J.; Gong, D.; Teng, Z.; Wang, J.; Cao, T.; Iqbal, K.; Liu, W.; Iqbal, A.; Qin, W.; Guo, H., 2-Vinylfuran substituted BODIPY H_2S fluorescent turn on probe based on hydrolysis of furfural and nucleophilic addition of double bond. *Sensors and Actuators B: Chemical* **2019,** *297*, 126712.

[775] Du, Y.; Wang, H.; Zhang, T.; Wen, W.; Li, Z.; Bi, M.; Liu, J., An ESIPT-based fluorescent probe with fast-response for detection of hydrogen sulfide in mitochondria. *Spectrochimica Acta Part A: Molecular and Biomolecular Spectroscopy* **2022,** *265*, 120390.

[776] Magesh, K.; Singh, S.; Wu, S. P.; Velmathi, S., One-step synthesis of a pH switched pyrene-based fluorescent probe for ratiometric detection of HS^- in real water samples. *Analytical Methods* **2023,** *15* (33), 4159-4167.

[777] Chen, J.-P.; Duan, Y.-M.; Zheng, W.-J.; Zhang, Q.; Zong, Q.; Chen, S.; Wang, K.-P.; Hu, Z.-Q., Perylenequinone-based "turn on" fluorescent probe for hydrogen sulfide with high sensitivity in living cells. *Spectrochimica Acta Part A: Molecular and Biomolecular Spectroscopy* **2019,** *218*, 206-212.

[778] Jiménez, D.; Martínez-Máñez, R.; Sancenón, F.; Ros-Lis, J. V.; Benito, A.; Soto, J., A New Chromo-chemodosimeter Selective for Sulfide Anion. *Journal of the American Chemical Society* **2003,** *125* (30), 9000-9001.

[779] Liu, J.; Sun, Y.-Q.; Zhang, J.; Yang, T.; Cao, J.; Zhang, L.; Guo, W., A Ratiometric Fluorescent Probe for Biological Signaling Molecule H_2S: Fast Response and High Selectivity. *Chemistry – A European Journal* **2013,** *19* (15), 4717-4722.

[780] Li, H. D.; Yao, Q. C.; Fan, J. L.; Jiang, N.; Wang, J. Y.; Xia, J.; Peng, X. J., A fluorescent probe for H_2S in vivo with fast response and high sensitivity. *Chemical Communications* **2015,** *51* (90), 16225-16228.

[781] Liu, W.; Bu, D.; Zhang, H.; Zhang, M.; Ren, H.; Li, Z.; Yu, M., A mitochondrial and lysosomal targeted ratiometric probe for detecting intracellular H_2S. *Analytical Methods* **2022,** *14* (2), 101-105.

[782] He, L.; Yang, X.; Liu, Y.; Weiying, L., Colorimetric and ratiometric fluorescent probe for hydrogen sulfide using a coumarin–pyronine FRET dyad with a large emission shift. *Analytical Methods* **2016,** *8* (45), 8022-8027.

[783] Hao, Y.; Shen, J.; Zhang, Y.; Xie, P.; Liu, Y., Assessing the pollution level of a subtropical lake by using a novel hydrogen sulfide fluorescence technology. *Environmental Research* **2023,** *229*, 115916.

[784] Yang, Y.; He, L.; Xu, K.; Lin, W., A ratiometric fluorescent chemosensor for the convenient monitoring of hydrogen sulfide concentration by the dual fluorescence fluctuation mode of two distinct emission bands in living cells and zebrafish. *New Journal of Chemistry* **2019,** *43* (27), 10926-10931.

[785] Gong, D.; Zhu, X.; Tian, Y.; Han, S.-C.; Deng, M.; Iqbal, A.; Liu, W.; Qin, W.; Guo, H., A Phenylselenium-Substituted BODIPY Fluorescent Turn-off Probe for Fluorescence Imaging of Hydrogen Sulfide in Living Cells. *Analytical Chemistry* **2017,** *89* (3), 1801-1807.

[786] Zhu, T.; Ren, N.; Liu, X.; Dong, Y.; Wang, R.; Gao, J.; Sun, J.; Zhu, Y.; Wang, L.; Fan, C.; Tian, H.; Li, J.; Zhao, C., Probing the Intracellular Dynamics of Nitric Oxide and Hydrogen Sulfide Using an Activatable NIR II Fluorescence Reporter. *Angewandte Chemie International Edition* **2021,** *60* (15), 8450-8454.

[787] Wang, R.; Gao, W.; Gao, J.; Xu, G.; Zhu, T.; Gu, X.; Zhao, C., A Förster Resonance Energy Transfer Switchable Fluorescent Probe With H_2S-Activated Second Near-Infrared Emission for Bioimaging. *Frontiers in Chemistry* **2019,** *7*.

[788] Xiang, H.; Ye, T.; Li, Y.; Lin, Y.; Liu, D.; Zhou, H.; Wang, J.; Li, L., A New Ratiometric Fluorescent Probe Based on BODIPY for Highly Selective Detection of Hydrogen Sulfide. *Molecules* **2022,** *27* (21), 7499.

[789] Fang, J.; Dong, X.; Sun, L.; Sun, J.; Dong, C.; Wang, R.; Zhao, C., Specific imaging of intracellular hydrogen sulfide by a positively charged NIR fluorescent probe. *Bioorganic & Medicinal Chemistry Letters* **2023,** *96*, 129495.

[790] Zhang, H.; Xu, L.; Chen, W.; Huang, J.; Huang, C.; Sheng, J.; Song, X., A Lysosome-Targetable Fluorescent Probe for Simultaneously Sensing Cys/Hcy, GSH, and H_2S from Different Signal Patterns. *ACS Sensors* **2018,** *3* (12), 2513-2517.

[791] Zhang, H.; Xu, L.; Chen, W.; Huang, J.; Huang, C.; Sheng, J.; Song, X., Simultaneous Discrimination of Cysteine, Homocysteine, Glutathione, and H_2S in Living Cells through a Multisignal Combination Strategy. *Analytical Chemistry* **2019,** *91* (3), 1904-1911.

[792] Li, H.; Yang, Y.; Wu, X.; Jia, R.; Zhao, P.; Wang, Y., A novel reactive chemosensor for sulfide detection with high selectivity and sensitivity based on 4-Cl coumarin derivatives. *Dyes and Pigments* **2021,** *191*, 109373.

[793] Que, E. L.; Domaille, D. W.; Chang, C. J., Metals in Neurobiology: Probing Their Chemistry and Biology with Molecular Imaging. *Chemical Reviews* **2008,** *108* (5), 1517-1549.

[794] Sasakura, K.; Hanaoka, K.; Shibuya, N.; Mikami, Y.; Kimura, Y.; Komatsu, T.; Ueno, T.; Terai, T.; Kimura, H.; Nagano, T., Development of a Highly Selective Fluorescence Probe

for Hydrogen Sulfide. *Journal of the American Chemical Society* **2011,** *133* (45), 18003-18005.

[795] Rivera-Fuentes, P.; Lippard, S. J., Metal-Based Optical Probes for Live Cell Imaging of Nitroxyl (HNO). *Accounts of Chemical Research* **2015,** *48* (11), 2927-2934.

[796] Lim, M. H.; Lippard, S. J., Metal-Based Turn-On Fluorescent Probes for Sensing Nitric Oxide. *Accounts of Chemical Research* **2007,** *40* (1), 41-51.

[797] Wu, H.; Krishnakumar, S.; Yu, J.; Liang, D.; Qi, H.; Lee, Z.-W.; Deng, L.-W.; Huang, D., Highly Selective and Sensitive Near-Infrared-Fluorescent Probes for the Detection of Cellular Hydrogen Sulfide and the Imaging of H_2S in Mice. *Chemistry – An Asian Journal* **2014,** *9* (12), 3604-3611.

[798] Liu, J.; Guo, X.; Hu, R.; Liu, X.; Wang, S.; Li, S.; Li, Y.; Yang, G., Molecular Engineering of Aqueous Soluble Triarylboron-Compound-Based Two-Photon Fluorescent Probe for Mitochondria H_2S with Analyte-Induced Finite Aggregation and Excellent Membrane Permeability. *Analytical Chemistry* **2016,** *88* (1), 1052-1057.

[799] Kim, J. Y.; Sarkar, S.; Bobba, K. N.; Huynh, P. T.; Bhise, A.; Yoo, J., Development of dansyl based copper(II) complex to detect hydrogen sulfide in hypoxia. *Organic & Biomolecular Chemistry* **2019,** *17* (29), 7088-7094.

[800] Wang, H.; Mu, W.; Liu, Y.; Lu, Y.; Qiu, Y.; Ma, Q., An innovative study on the "on–off–on" detection of sulfur ions based on a TSPP–riboflavin fluorescent probe. *RSC Advances* **2022,** *12* (10), 5871-5877.

[801] Ye, Z. Q.; An, X.; Song, B.; Zhang, W. Z.; Dai, Z. C.; Yuan, J. L., A novel dinuclear ruthenium(II)-copper(II) complex-based luminescent probe for hydrogen sulfide. *Dalton Transactions* **2014,** *43* (34), 13055-13060.

[802] Wang, M. Q.; Li, K.; Hou, I. T.; Wu, M. Y.; Huang, Z.; Yu, X. Q., BINOL-Based Fluorescent Sensor for Recognition of Cu(II) and Sulfide Anion in Water. *Journal of Organic Chemistry* **2012,** *77* (18), 8350-8354.

[803] Palanisamy, S.; Lee, L. Y.; Wang, Y. L.; Chen, Y. J.; Chen, C. Y.; Wang, Y. M., A water soluble and fast response fluorescent turn-on copper complex probe for H_2S detection in zebra fish. *Talanta* **2016,** *147*, 445-452.

[804] Lou, X. D.; Mu, H. L.; Gong, R.; Fu, E. Q.; Qin, J. G.; Li, Z., Displacement method to develop highly sensitive and selective dual chemosensor towards sulfide anion. *Analyst* **2011,** *136* (4), 684-687.

[805] Santos-Figueroa, L. E.; de la Torre, C.; El Sayed, S.; Sancenón, F.; Martínez-Máñez, R.; Costero, A. M.; Gil, S.; Parra, M., Highly Selective Fluorescence Detection of Hydrogen

Sulfide by Using an Anthracene-Functionalized Cyclam–Cu(II) Complex. *European Journal of Inorganic Chemistry* **2014,** *2014* (1), 41-45.

[806] Mirra, S.; Strianese, M.; Pellecchia, C., A Cyclam-Based Fluorescent Ligand as a Molecular Beacon for Cu^{2+} and H_2S Detection. *European Journal of Inorganic Chemistry* **2017,** (33), 3900-3907.

[807] Choi, M. G.; Cha, S.; Lee, H.; Jeon, H. L.; Chang, S. K., Sulfide-selective chemosignaling by a Cu^{2+} complex of dipicolylamine appended fluorescein. *Chemical Communications* **2009,** (47), 7390-7392.

[808] Lv, H. J.; Ma, R. F.; Zhang, X. T.; Li, M. H.; Wang, Y. T.; Wang, S.; Xing, G. W., Surfactant-modulated discriminative sensing of HNO and H_2S with a Cu^{2+}-complex-based fluorescent probe. *Tetrahedron* **2016,** *72* (35), 5495-5501.

[809] Rosenthal, J.; Lippard, S. J., Direct Detection of Nitroxyl in Aqueous Solution Using a Tripodal Copper(II) BODIPY Complex. *Journal of the American Chemical Society* **2010,** *132* (16), 5536-5537.

[810] Zhou, Y.; Liu, K.; Li, J.-Y.; Fang, Y.; Zhao, T.-C.; Yao, C., Visualization of Nitroxyl in Living Cells by a Chelated Copper(II) Coumarin Complex. *Organic Letters* **2011,** *13* (6), 1290-1293.

[811] Gu, X. F.; Liu, C. H.; Zhu, Y. C.; Zhu, Y. Z., Development of a boron-dipyrromethene-Cu^{2+} ensemble based colorimetric probe toward hydrogen sulfide in aqueous media. *Tetrahedron Letters* **2011,** *52* (39), 5000-5003.

[812] Wu, X.; Li, H.; Kan, Y.; Yin, B., A regeneratable and highly selective fluorescent probe for sulfide detection in aqueous solution. *Dalton Transactions* **2013,** *42* (46), 16302-16310.

[813] Hou, J.-T.; Liu, B.-Y.; Li, K.; Yu, K.-K.; Wu, M.-B.; Yu, X.-Q., Two birds with one stone: Multifunctional and highly selective fluorescent probe for distinguishing Zn^{2+} from Cd^{2+} and selective recognition of sulfide anion. *Talanta* **2013,** *116*, 434-440.

[814] Li, X.; Gong, Y.; Wu, K.; Liang, S. H.; Cao, J.; Yang, B.; Hu, Y.; Han, Y., A highly sensitive and water soluble fluorescent probe for rapid detection of hydrogen sulfide in living cells. *RSC Advances* **2014,** *4* (68), 36106-36109.

[815] Wu, S.; Ma, X.; Wang, Y.; Zhou, J.; Li, X.; Wang, X., A novel fluorescent BODIPY-based probe for detection of Cu^{2+} and H_2S based on displacement approach. *Spectrochimica Acta Part A: Molecular and Biomolecular Spectroscopy* **2021,** *249*, 119330.

[816] Yang, X.; Shen, L.; Bao, H.; Fang, X.; Xu, J.; Zhao, Y.; Yang, W., A tricarbocyanine near-infrared fluorescent probe for sulfide through a copper displacement mechanism. *Sensors and Actuators B: Chemical* **2015,** *220*, 1361-1367.

[817] Xu, Q. C.; Gu, Z. Y.; Xing, G. W., Design and synthesis of a Cu(II)-complex-based carbazole-hemicyanine hybrid for fluorescent sensing of H_2S in SDS micellar solution. *Tetrahedron* **2017,** *73* (15), 2123-2130.

[818] Yan, Y.; Chen, L.; Liu, R.; Zheng, Y.; Wang, S., A turn-on fluorescent probe with a dansyl fluorophore for hydrogen sulfide sensing. *RSC Advances* **2019,** *9* (47), 27652-27658.

[819] Cao, X. W.; Lin, W. Y.; He, L. W., A Near-Infrared Fluorescence Turn-On Sensor for Sulfide Anions. *Organic Letters* **2011,** *13* (17), 4716-4719.

[820] Hou, F.; Huang, L.; Xi, P.; Cheng, J.; Zhao, X.; Xie, G.; Shi, Y.; Cheng, F.; Yao, X.; Bai, D.; Zeng, Z., A Retrievable and Highly Selective Fluorescent Probe for Monitoring Sulfide and Imaging in Living Cells. *Inorganic Chemistry* **2012,** *51* (4), 2454-2460.

[821] Zhang, L.; Sun, J.; Liu, S.; Cui, X.; Li, W.; Fang, J., Aminoquinoline-based fluorescent probe for detection of Cu^{2+} and hydrogen sulfide. *Inorganic Chemistry Communications* **2013,** *35*, 311-314.

[822] Wang, J.; Long, L.; Xie, D.; Zhan, Y., Highly selective fluorescence turn-on sensor for hydrogen sulfide and imaging in living cells. *Journal of Luminescence* **2013,** *139*, 40-46.

[823] Gao, C. J.; Liu, X.; Jin, X. J.; Wu, J.; Xie, Y. J.; Liu, W. S.; Yao, X. J.; Tang, Y., A retrievable and highly selective fluorescent sensor for detecting copper and sulfide. *Sensors and Actuators B-Chemical* **2013,** *185*, 125-131.

[824] Yao, X.; Guo, Y. Y.; Ru, J. X.; Xu, C.; Liu, Y. M.; Qin, W. W.; Zhang, G. L.; Tang, X. L.; Liu, W. S., Reversible fluorescent detection for sulfide with quinoline-ligated copper complexes and its application in living cells. *Sensors and Actuators B-Chemical* **2014,** *198*, 20-25.

[825] Liu, H. Y.; Wu, F. X.; Zhang, B. B.; Tan, C. Y.; Chen, Y. Z.; Hao, G. F.; Tan, Y.; Jiang, Y. Y., A simple quinoline-derived fluorescent sensor for the selective and sequential detection of copper(II) and sulfide ions and its application in living-cell imaging. *Rsc Advances* **2016,** *6* (81), 77508-77514.

[826] Dutta, A.; Alam, R.; Islam, A. S. M.; Dutta, A.; Ali, M., A dual response fluorescent sensor for HNO and S^{2-} ions using a Cu(II) complex based probe assisted by detailed DFT studies. *Dalton Transactions* **2018,** *47* (33), 11563-11571.

[827] Li, C. M.; Liu, Z. X.; Miao, Y.; Zhou, X.; Wu, X., A reversible fluorescent chemosensor for selective and sequential detection of copper ion and sulfide. *Dyes and Pigments* **2016,** *125*, 292-298.

[828] Li, H., A regenerated "turn on" fluorescent probe for sulfide detection in live cells and read samples based on dihydroxyhemicyanine-Cu^{2+} dye. *Analytica Chimica Acta* **2018,** *1010*, 69-75.

[829] Wang, P.; Wu, J.; Di, C. X.; Zhou, R.; Zhang, H.; Su, P. R.; Xu, C.; Zhou, P. P.; Ge, Y. S.; Li, D. A.; Liu, W. S.; Tang, Y., A novel peptide-based fluorescence chemosensor for selective imaging of hydrogen sulfide both in living cells and zebrafish. *Biosensors & Bioelectronics* **2017,** *92*, 602-609.

[830] Wang, P.; Xue, S. R.; Yang, X. P., Highly selective and sensitive detection of hydrogen sulfide in aqueous medium and live cells using peptide-based bioprobe to mimic the binding sites of the ceruloplasmin for Cu(II) ions. *Biosensors & Bioelectronics* **2020,** *163*, 112283.

[831] Hao, C.; Li, Y.; Fan, B.; Zeng, G.; Zhang, D.; Bian, Z.; Wu, J., A new peptide-based chemosensor for selective imaging of copper ion and hydrogen sulfide in living cells. *Microchemical Journal* **2020,** *154*, 104658.

[832] Wang, P.; Sun, L.; Wu, J.; Yang, X.; Lin, P.; Wang, M., A dual-functional colorimetric and fluorescent peptide-based probe for sequential detection of Cu^{2+} and S^{2-} in 100% aqueous buffered solutions and living cells. *Journal of Hazardous Materials* **2021,** *407*, 124388.

[833] Hao, C.; Guo, X.; Lai, Q.; Li, Y.; Fan, B.; Zeng, G.; He, Z.; Wu, J., Peptide-based fluorescent chemical sensors for the specific detection of Cu^{2+} and S^{2-}. *Inorganica Chimica Acta* **2020,** *513*, 119943.

[834] Xiao, L.; Wei, P.; He, F.; Gou, Y.; Ge, Y.; Liu, Y.; Wang, P.; Liao, Y., Peptide-based fluorescent and colorimetric dual-functional probe for visual detection of Cu^{2+}, Hg^{2+} and S^{2-} in 100% aqueous media, living cells and paper test strips. *Journal of Photochemistry and Photobiology A: Chemistry* **2022,** *433*, 114178.

[835] An, Y.; Wang, P.; Yue, Z., A sequential and reversibility fluorescent pentapeptide probe for Cu(II) ions and hydrogen sulfide detections and its application in two different living cells imaging. *Spectrochimica Acta Part A: Molecular and Biomolecular Spectroscopy* **2019,** *216*, 319-327.

[836] Wei, P.; Xiao, L.; Gou, Y.; He, F.; Zhou, D.; Liu, Y.; Xu, B.; Wang, P.; Zhou, Y., Fluorescent "on–off–on" probe based on copper peptide backbone for specific detection of Cu(II) and hydrogen sulfide and its applications in cell imaging, real water samples and test strips. *Microchemical Journal* **2022,** *182*, 107848.

[837] Hu, Y.; Quan, S.; Zhao, C.; Li, J.; Sun, X.; Xiao, J., An "on–off–on" fluorescent peptide probe for the specific detection of Cu^{2+} and S^{2-} in living cells and zebrafish. *New Journal of Chemistry* **2022,** *46* (16), 7663-7668.

[838] Wang, Q.; Guo, Z.; Zhou, D.; Wu, J.; Wang, P.; Yang, X.; Wen, S., A novel fluorescent probe for highly selective and sensitive detection of sulfur ions in real samples and living

cells based on the tripeptide-Cu^{2+} ensemble system. *Microchemical Journal* **2021,** *169*, 106612.

[839] Wen, S.; Wang, Q.; Guo, Z.; Chen, B.; Liu, Y.; Wang, P.; Yang, X.; An, Y., A rapid "on-off-on" peptide-based fluorescent probe for selective and consecutive detection of mercury and sulfide ions in aqueous systems and live cells. *Journal of Photochemistry and Photobiology A: Chemistry* **2021,** *417*, 113354.

[840] Zhang, Y.; Cai, Y.; He, Y.; Lin, Q.; Ren, J.; Cao, D.; Zhang, L., A label-free fluorescent peptide probe for sensitive and selective determination of copper and sulfide ions in aqueous systems. *RSC Advances* **2021,** *11* (13), 7426-7435.

[841] Xiao, Y. M.; Yang, Y. Q.; Zhao, G. Y.; Fang, X. X.; Zhao, Y. X.; Guo, P. R.; Yang, W.; Xu, J. W., A terbium-based time-resolved luminescent probe for sulfide ions mediated by copper in aqueous solution. *Inorganic Chemistry Communications* **2014,** *50*, 31-34.

[842] Yip, Y.-W.; Law, G.-L.; Wong, W.-T., A highly selective on–off–on responsive lanthanide(III) based probe for recognition of copper and hydrogen sulfide. *Dalton Transactions* **2016,** *45* (3), 928-935.

[843] Yao, Y.; Delgado-Rivera, L.; Samareh Afsari, H.; Yin, L.; Thatcher, G. R. J.; Moore, T. W.; Miller, L. W., Time-Gated Luminescence Detection of Enzymatically Produced Hydrogen Sulfide: Design, Synthesis, and Application of a Lanthanide-Based Probe. *Inorganic Chemistry* **2018,** *57* (2), 681-688.

[844] Wang, Y. R.; Wang, H.; Yang, M.; Yuan, J. L.; Wu, J., A visible-light-excited europium(III) complex-based luminescent probe for visualizing copper ions and hydrogen sulfide in living cells. *Optical Materials* **2018,** *75*, 243-251.

[845] Tang, Z.; Song, B.; Ma, H.; Shi, Y.; Yuan, J., A ratiometric time-gated luminescence probe for hydrogen sulfide based on copper(II)-coupled lanthanide complexes. *Analytica Chimica Acta* **2019,** *1049*, 152-160.

[846] Wang, Y.; Wang, H.; Zhao, X.; Jin, Y.; Xiong, H.; Yuan, J.; Wu, J., A β-diketonate–europium(iii) complex-based fluorescent probe for highly sensitive time-gated luminescence detection of copper and sulfide ions in living cells. *New Journal of Chemistry* **2017,** *41* (13), 5981-5987.

[847] Aulsebrook, M. L.; Biswas, S.; Leaver, F. M.; Grace, M. R.; Graham, B.; Barrios, A. M.; Tuck, K. L., A luminogenic lanthanide-based probe for the highly selective detection of nanomolar sulfide levels in aqueous samples. *Chemical Communications* **2017,** *53* (36), 4911-4914.

[848] Yue, X.; Zhu, Z.; Zhang, M.; Ye, Z., Reaction-Based Turn-on Electrochemiluminescent Sensor with a Ruthenium(II) Complex for Selective Detection of Extracellular Hydrogen Sulfide in Rat Brain. *Analytical Chemistry* **2015,** *87* (3), 1839-1845.

[849] Hou, F.; Cheng, J.; Xi, P.; Chen, F.; Huang, L.; Xie, G.; Shi, Y.; Liu, H.; Bai, D.; Zeng, Z., Recognition of copper and hydrogen sulfide in vitro using a fluorescein derivative indicator. *Dalton Transactions* **2012,** *41* (19), 5799-5804.

[850] Meng, Q.; Zhang, R.; Jia, H.; Gao, X.; Wang, C.; Shi, Y.; Everest-Dass, A. V.; Zhang, Z., A reversible fluorescence chemosensor for sequentially quantitative monitoring copper and sulfide in living cells. *Talanta* **2015,** *143*, 294-301.

[851] Kar, C.; Adhikari, M. D.; Ramesh, A.; Das, G., NIR- and FRET-Based Sensing of Cu^{2+} and S^{2-} in Physiological Conditions and in Live Cells. *Inorganic Chemistry* **2013,** *52* (2), 743-752.

[852] Guo, D.; Dong, Z. P.; Luo, C.; Zan, W. Y.; Yan, S. Q.; Yao, X. J., A rhodamine B-based "turn-on" fluorescent sensor for detecting Cu^{2+} and sulfur anions in aqueous media. *Rsc Advances* **2014,** *4* (11), 5718-5725.

[853] Zhou, Q.; Zhu, Y.; Sheng, P. T.; Wu, Z. M.; Cai, Q. Y., A highly selective and reversible fluorescent Cu^{2+} and S^{2-} probe under physiological conditions and in live cells. *Rsc Advances* **2014,** *4* (87), 46951-46954.

[854] Ma, S.; Qiang, J.; Li, L.; Mo, Y.; She, M.; Yang, Z.; Liu, P.; Zhang, S.; Li, J., An efficient biosensor for monitoring Alzheimer's disease risk factors: modulation and disaggregation of the Aβ aggregation process. *Journal of Materials Chemistry B* **2019,** *7* (26), 4124-4132.

[855] Wang, S.; Ding, H.; Wang, Y.; Fan, C.; Tu, Y.; Liu, G.; Pu, S., An ‘‘off–on–off’’ sensor for sequential detection of Cu^{2+} and hydrogen sulfide based on a naphthalimide–rhodamine B derivative and its application in dual-channel cell imaging. *RSC Advances* **2018,** *8* (58), 33121-33128.

[856] Nam, B.; Lee, W.; Sarkar, S.; Kim, J.-H.; Bhise, A.; Park, H.; Kim, J. Y.; Huynh, P. T.; Rajkumar, S.; Lee, K.; Ha, Y. S.; Cho, S. H.; Lim, J. E.; Kim, K. W.; Lee, K. C.; Suk, K.; Yoo, J., In vivo detection of hydrogen sulfide in the brain of live mouse: application in neuroinflammation models. *European Journal of Nuclear Medicine and Molecular Imaging* **2022,** *49* (12), 4073-4087.

[857] Tang, L., Zhou, P., Qi, Z., Huang, Z., Zhao, J., & Cai, M., A New Quinoline-Based Acylhydrazone for Highly Selective Fluorescence Recognition of Cu(II) and Sulfide in Aqueous Solution. *Bulletin of the Korean Chemical Society* **2013,** *34* (8), 2256-2260.

[858] Qian, Y.; Lin, J.; Liu, T.; Zhu, H., Living cells imaging for copper and hydrogen sulfide by a selective “on–off–on” fluorescent probe. *Talanta* **2015,** *132*, 727-732.

[859] Liu, C.; Tian, L.; Liu, K.; Xue, J.; Fan, L.; Li, T.; Yang, Z.-y., A chromone derivative as a colorimetric and “ON-OFF-ON” fluorescent probe for highly sensitive and selective detection of Cu^{2+} and S^{2-}. *Inorganica Chimica Acta* **2021,** *519*, 120280.

[860] Meng, Q. T.; Shi, Y.; Wang, C. P.; Jia, H. M.; Gao, X.; Zhang, R.; Wang, Y. F.; Zhang, Z. Q., NBD-based fluorescent chemosensor for the selective quantification of copper and sulfide in an aqueous solution and living cells. *Organic & Biomolecular Chemistry* **2015,** *13* (10), 2918-2926.

[861] Rajasekaran, D.; Venkatachalam, K.; Periasamy, V., "On–off–on" pyrene-based fluorescent chemosensor for the selective recognition of Cu^{2+} and S^{2-} ions and its utilization in live cell imaging. *Applied Organometallic Chemistry* **2020,** *34* (3), e5342.

[862] Li, J.-Z.; Leng, T.-H.; Wang, Z.-Q.; Zhou, L.; Gong, X.-Q.; Shen, Y.-J.; Wang, C.-Y., A large Stokes shift, sequential, colorimetric fluorescent probe for sensing Cu^{2+}/S^{2-} and its applications. *Journal of Photochemistry and Photobiology A: Chemistry* **2019,** *373*, 146-153.

[863] Zhong, K. L.; Zhao, J.; Li, Q. Y.; Hou, S. H.; Tang, Y. W.; Bian, Y. J.; Tang, L. J., Synthesis of Multifunctional Long-Wavelength-Emitting Fluorescent Probe Based on Hydrazine Dihydrazone and Its Copper Complex for Detection of H_2S. *Chinese Journal of Organic Chemistry* **2018,** *38* (7), 1786-1791.

[864] Qiao, Y.-J.; Xu, F.-Z.; Chen, Y.; Wang, Z.-Q.; Gong, X.-Q.; Wang, C.-Y., A sensitive "on-off-on" fluorescent probe for sequential Cu^{2+}/S^{2-} detection in actual water samples and living cells. *Tetrahedron* **2022,** *115*, 132791.

[865] Yan, X.-J.; Wang, Z.-G.; Wang, Y.; Huang, Y.-Y.; Liu, H.-B.; Xie, C.-Z.; Li, Q.-Z.; Xu, J.-Y., A dual-functional fluorescent probe for sequential determination of Cu^{2+}/S^{2-} and its applications in biological systems. *Spectrochimica Acta Part A: Molecular and Biomolecular Spectroscopy* **2020,** *243*, 118797.

[866] Gao, L. L.; Wang, B. B.; Chen, X.; Wang, Y.; Wu, W. N.; Zhao, X. L.; Yan, L. L.; Fan, Y. C.; Xu, Z. H., Hydrazone derivative bearing coumarin for the relay detection of Cu^{2+} and H_2S in an almost neat aqueous solution and bioimaging in lysosomes. *Spectrochimica Acta Part a-Molecular and Biomolecular Spectroscopy* **2021,** *255*.

[867] Li, X.; Yang, C.; Wu, K.; Hu, Y.; Han, Y.; Liang, S. H., A highly specific probe for sensing hydrogen sulfide in live cells based on copper-initiated fluorogen with aggregation-induced emission characteristics. *Theranostics* **2014,** *4* (12), 1233-8.

[868] Ren, K.; Shang, X.; Fu, J.; Zhao, P.; Zhang, J., Copper complex based on 2-(phenylimino-methyl)-phenol as a high selective fluoresencent probe for hydrogen sulfide. *Polyhedron* **2016,** *104*, 99-105.

[869] Ren, K.; Shang, X. F.; Chen, Y. M.; Zhang, X. L.; Fu, J. J.; Zhao, P. P.; Zhang, J. L., Synthesis and crystal structure of a highly selective colorimetric and fluorometric sensor for hydrogen sulfide. *Luminescence* **2017,** *32* (5), 765-771.

[870] Shang, X.; Yue, X.; Chen, Y.; Li, C.; Chen, H.; Wang, T., Design, synthesis, crystal structure and cytotoxicity studies of colorimetric fluorescent "OFF-ON" probes for rapid detection of hydrogen sulfide based on Cu(II) complex. *Inorganic Chemistry Communications* **2019,** *99*, 1-10.

[871] Dalbera, S.; Kulovi, S.; Dalai, S., Pyrene-based Schiff Base as Selective Chemosensor for Copper(II) and Sulfide Ions. *ChemistrySelect* **2018,** *3* (23), 6561-6569.

[872] Chen, Y.; Shang, X.; Pan, W.; Li, C.; Wang, T., Highly selective probe of a copper(II) complex based on a coumarin derivative for hydrogen sulfide detection. *Journal of Coordination Chemistry* **2018,** *71* (21), 3487-3499.

[873] Wang, Y.; Qiu, D.; Li, M.; Liu, Y.; Chen, H.; Li, H., A new "on-off-on" fluorescent probe containing triarylimidazole chromophore to sequentially detect copper and sulfide ions. *Spectrochimica Acta Part A: Molecular and Biomolecular Spectroscopy* **2017,** *185*, 256-262.

[874] Wei, Z. L.; Wang, L.; Guo, S. Z.; Zhang, Y.; Dong, W. K., A high-efficiency salamo-based copper(II) complex double-channel fluorescent probe. *Rsc Advances* **2019,** *9* (70), 41298-41304.

[875] Fu, Y.; Feng, Q. C.; Jiang, X. J.; Xu, H.; Li, M.; Zang, S. Q., New fluorescent sensor for Cu^{2+} and S^{2-} in 100% aqueous solution based on displacement approach. *Dalton Transactions* **2014,** *43* (15), 5815-5822.

[876] Sun, M.; Yu, H.; Li, H.; Xu, H.; Huang, D.; Wang, S., Fluorescence Signaling of Hydrogen Sulfide in Broad pH Range Using a Copper Complex Based on BINOL–Benzimidazole Ligands. *Inorganic Chemistry* **2015,** *54* (8), 3766-3772.

[877] Hu, Y. S.; Kang, J.; Zhou, P. P.; Han, X.; Sun, J. Y.; Liu, S. D.; Zhang, L. W.; Fang, J. G., A selective colorimetric and red-emitting fluorometric probe for sequential detection of Cu^{2+} and H_2S. *Sensors and Actuators B-Chemical* **2018,** *255*, 3155-3162.

[878] Pan, Y.; Li, Y.; Sun, X.; Tang, L.; Yan, X., An "AIE+ESIPT" characteristic fluorescent probe for relay recognition of Cu^{2+} and H_2S and its application in food samples and cell imaging. *Dyes and Pigments* **2023,** *210*, 110985.

[879] Kalavathi, A.; Saravana Kumar, P.; Satheeshkumar, K.; Vennila, K. N.; Ciattini, S.; Chelazzi, L.; Elango, K. P., Spectroscopic and TD-DFT studies on sequential fluorescent detection of Cu(II) and HS^- ions in an aqueous solution. *Inorganica Chimica Acta* **2023,** *550*, 121447.

[880] Wang, H.; Shi, D.-L.; Li, J.; Tang, H.-Y.; Li, J.; Guo, Y., A facile fluorescent probe with a large Stokes shift for sequentially detecting copper and sulfide in 100% aqueous solution and imaging them in living cells. *Sensors and Actuators B: Chemical* **2018,** *256*, 600-608.

[881] Mahnashi, M. H.; Mahmoud, A. M.; Alkahtani, S. A.; Ali, R.; El-Wekil, M. M., A novel imidazole derived colorimetric and fluorometric chemosensor for bifunctional detection of copper (II) and sulphide ions in environmental water samples. *Spectrochimica Acta Part A: Molecular and Biomolecular Spectroscopy* **2020,** *228*, 117846.

[882] Kwan, C.-S.; Wang, T.; Chan, S.-M.; Cai, Z.; Leung, K. C.-F., Selective detection of sulfide in human lung cancer cells with a blue-fluorescent "ON–OFF–ON" benzimidazole-based chemosensor ensemble. *Dalton Transactions* **2020,** *49* (17), 5445-5453.

[883] Li, K.-B.; Jia, W.-P.; Han, D.-M.; Liang, D.-X.; He, X.-P.; Chen, G.-R., Fluorogenic bis-triazolyl galactoprobe–metal complex for full-aqueous analysis of sulfide ion. *Sensors and Actuators B: Chemical* **2017,** *246*, 197-201.

[884] Qu, X.; Li, C.; Chen, H.; Mack, J.; Guo, Z.; Shen, Z., A red fluorescent turn-on probe for hydrogen sulfide and its application in living cells. *Chemical Communications* **2013,** *49* (68), 7510-7512.

[885] Zheng, F.; Wen, M.; Zeng, F.; Wu, S., A robust, water-soluble and low cytotoxic fluorescent probe for sulfide anion achieved through incorporation of betaine. *Sensors and Actuators B: Chemical* **2013,** *188*, 1012-1018.

[886] Tang, L. J.; Dai, X.; Cai, M. J.; Zhao, J.; Zhou, P.; Huang, Z. L., Relay recognition of Cu^{2+} and S^{2-} in water by a simple 2-(2'-aminophenyl)benzimidazole derivatized fluorescent sensor through modulating ESIPT. *Spectrochimica Acta Part a-Molecular and Biomolecular Spectroscopy* **2014,** *122*, 656-660.

[887] Tang, L. J.; Cai, M. J.; Huang, Z. L.; Zhong, K. L.; Hou, S. H.; Bian, Y. J.; Nandhakumar, R., Rapid and highly selective relay recognition of Cu(II) and sulfide ions by a simple benzimidazole-based fluorescent sensor in water. *Sensors and Actuators B-Chemical* **2013,** *185*, 188-194.

[888] El-Maghrabey, M. H.; Watanabe, R.; Kishikawa, N.; Kuroda, N., Detection of hydrogen sulfide in water samples with 2-(4-hydroxyphenyl)-4,5-di(2-pyridyl)imidazole-copper(II) complex using environmentally green microplate fluorescence assay method. *Analytica Chimica Acta* **2019,** *1057*, 123-131.

[889] Paul, A.; Anbu, S.; Sharma, G.; Kuznetsov, M. L.; da Silva, M.; Koch, B.; Pombeiro, A. J. L., Intracellular detection of Cu^{2+} and S^{2-} ions through a quinazoline functionalized benzimidazole-based new fluorogenic differential chemosensor. *Dalton Transactions* **2015,** *44* (38), 16953-16964.

[890] Hai, Z.; Bao, Y.; Miao, Q.; Yi, X.; Liang, G., Pyridine–Biquinoline–Metal Complexes for Sensing Pyrophosphate and Hydrogen Sulfide in Aqueous Buffer and in Cells. *Analytical Chemistry* **2015,** *87* (5), 2678-2684.

[891] Kaushik, R.; Ghosh, A.; Jose, D. A., Simple terpyridine based Cu(II)/Zn(II) complexes for the selective fluorescent detection of H_2S in aqueous medium. *Journal of Luminescence* **2016,** *171*, 112-117.

[892] Zhang, L.; Han, X.-F.; Wu, W.-N.; Zhao, X.-L.; Wang, Y.; Fan, Y.-C.; Xu, Z.-H., A novel fluorescence aggregation-induced emission active chemosensor for sequential determination of Cu^{2+} and S^{2-} in an almost neat aqueous solution. *Microchemical Journal* **2022,** *183*, 107974.

[893] Li, H. H.; Yu, H.; Sun, M. T.; Alamry, K. A.; Asiri, A. M.; Wang, S. H., Simultaneous removal and measurement of sulfide on the basis of turn-on fluorimetry. *International Journal of Environmental Science and Technology* **2018,** *15* (6), 1193-1200.

[894] Cheng, S.; Sun, R.; Wu, Z.; Mei, H.; Yang, H.; Kong, Q.; Xu, K., A novel reversible fluorescent probe for Cu^{2+} and S^{2-} ions and imaging in living cells. *Methods and Applications in Fluorescence* **2022,** *10* (3), 035009.

[895] Yang, L. L.; Wang, J. P.; Yang, L.; Zhang, C.; Zhang, R. L.; Zhang, Z. P.; Liu, B. H.; Jiang, C. L., Fluorescent paper sensor fabricated by carbazole-based probes for dual visual detection of Cu^{2+} and gaseous H_2S. *Rsc Advances* **2016,** *6* (61), 56384-56391.

[896] Wang, Y.; Sun, H. H.; Hou, L. J.; Shang, Z. B.; Dong, Z. M.; Jin, W. J., 1,4-Dihydroxyanthraquinone-Cu^{2+} ensemble probe for selective detection of sulfide anion in aqueous solution. *Analytical Methods* **2013,** *5* (20), 5493-5500.

[897] Liu, Z.; Liu, L. J.; Li, J. L.; Qin, Y. Y.; Zhao, C. Y.; Mi, Y.; Li, G. P.; Li, T. S.; Wu, Y. J., A new coumarin-based fluorescent probe for selective recognition of Cu^{2+} and S^{2-} in aqueous solution and living cells. *Tetrahedron* **2019,** *75* (30), 3951-3957.

[898] Mao, G.; Liu, C.; Yang, N.; Yang, L.; He, G., Design and Synthesis of a Fluorescent Probe Based on Copper Complex for Selective Detection of Hydrogen Sulfide. *Journal of Sensors* **2021,** *2021*, 8822558.

[899] Lu, W.; Shi, J.; Chen, J.; Sun, L.; Shao, L.; Ren, H.; Huang, M.; Wang, Y.; Yang, S.; Li, X., A coumarin-based reversible fluorescent probe for Cu^{2+} and S^{2-} and its applicability in vivo and for organism imaging. *New Journal of Chemistry* **2021,** *45* (27), 11983-11991.

[900] Tang, L. J.; Cai, M. J.; Zhou, P.; Zhao, J.; Zhong, K. L.; Hou, S. H.; Bian, Y. J., A highly selective and ratiometric fluorescent sensor for relay recognition of zinc(II) and sulfide ions based on modulation of excited-state intramolecular proton transfer. *Rsc Advances* **2013,** *3* (37), 16802-16809.

[901] Jung, J. M.; Lee, J. J.; Nam, E.; Lim, M. H.; Kim, C.; Harrison, R. G., A zinc fluorescent sensor used to detect mercury (II) and hydrosulfide. *Spectrochimica Acta Part a-Molecular and Biomolecular Spectroscopy* **2017,** *178*, 203-211.

[902] Dong, Z.; Le, X.; Zhou, P.; Dong, C.; Ma, J., Sequential recognition of zinc ion and hydrogen sulfide by a new quinoline derivative with logic gate behavior. *RSC Advances* **2014,** *4* (35), 18270-18277.

[903] Dong, Z.; Le, X.; Zhou, P.; Dong, C.; Ma, J., An "off–on–off" fluorescent probe for the sequential detection of Zn^{2+} and hydrogen sulfide in aqueous solution. *New Journal of Chemistry* **2014,** *38* (4), 1802-1808.

[904] Kaushik, R.; Kumar, P.; Ghosh, A.; Gupta, N.; Kaur, D.; Arora, S.; Jose, D. A., Alizarin red S-zinc(II) fluorescent ensemble for selective detection of hydrogen sulphide and assay with an H_2S donor. *Rsc Advances* **2015,** *5* (97), 79309-79316.

[905] Jung, J. M.; Kang, J. H.; Han, J.; Lee, H.; Lim, M. H.; Kim, K.-T.; Kim, C., A novel "off-on" type fluorescent chemosensor for detection of Zn^{2+} and its zinc complex for "on-off" fluorescent sensing of sulfide in aqueous solution, in vitro and in vivo. *Sensors and Actuators B: Chemical* **2018,** *267*, 58-69.

[906] Yun, J. Y.; Jo, T. G.; Han, J.; Jang, H. J.; Lim, M. H.; Kim, C., A highly sensitive and selective fluorescent chemosensor for the sequential recognition of Zn^{2+} and S^{2-} in living cells and aqueous media. *Sensors and Actuators B: Chemical* **2018,** *255*, 3108-3116.

[907] Yun, J. Y.; Chae, J. B.; Kim, M.; Lim, M. H.; Kim, C., A multiple target chemosensor for the sequential fluorescence detection of Zn^{2+} and S^{2-} and the colorimetric detection of $Fe^{3+/2+}$ in aqueous media and living cells. *Photochemical & Photobiological Sciences* **2019,** *18* (1), 166-176.

[908] Takashima, I.; Kinoshita, M.; Kawagoe, R.; Nakagawa, S.; Sugimoto, M.; Hamachi, I.; Ojida, A., Design of Ratiometric Fluorescent Probes Based on Arene–Metal-Ion Interactions and Their Application to CdII and Hydrogen Sulfide Imaging in Living Cells. *Chemistry – A European Journal* **2014,** *20* (8), 2184-2192.

[909] Kawagoe, R.; Takashima, I.; Usui, K.; Kanegae, A.; Ozawa, Y.; Ojida, A., Rational Design of a Ratiometric Fluorescent Probe Based on Arene–Metal-Ion Contact for Endogenous Hydrogen Sulfide Detection in Living Cells. *ChemBioChem* **2015,** *16* (11), 1608-1615.

[910] Rodriguez-Fernandez, J.; Costa, J. M.; Pereiro, R.; Sanz-Medel, A., Simple detector for oral malodour based on spectrofluorimetric measurements of hydrogen sulphide in mouth air. *Analytica Chimica Acta* **1999,** *398* (1), 23-31.

[911] Sen, B.; Mukherjee, M.; Pal, S.; Dhara, K.; Mandal, S. K.; Khuda-Bukhsh, A. R.; Chattopadhyay, P., A water soluble FRET-based ratiometric chemosensor for Hg(II) and S^{2-} applicable in living cell staining. *Rsc Advances* **2014,** *4* (29), 14919-14927.

[912] Ma, F.; Sun, M.; Zhang, K.; Yu, H.; Wang, Z.; Wang, S., A turn-on fluorescent probe for selective and sensitive detection of hydrogen sulfide. *Analytica Chimica Acta* **2015,** *879*, 104-110.

[913] Vengaian, K. M.; Britto, C. D.; Sekar, K.; Sivaraman, G.; Singaravadivel, S., Phenothiazine-diaminomalenonitrile based Colorimetric and Fluorescence "Turn-off-on" Sensing of Hg^{2+} and S^{2-}. *Sensors and Actuators B-Chemical* **2016,** *235*, 232-240.

[914] Wang, L.; Tian, Y.; He, X.; Zhao, B.; Ma, W.; Yang, J.; Song, B., A new "on-off-on" fluorescent sensor for cascade recognition of Hg^{2+} and S^{2-} ion in aqueous medium. *Journal of Photochemistry and Photobiology A: Chemistry* **2018,** *358*, 300-306.

[915] Bu, F.; Zhao, B.; Kan, W.; Ding, L.; Liu, T.; Wang, L.; Song, B.; Wang, W.; Deng, Q., An ESIPT characteristic "turn-on" fluorescence sensor for Hg^{2+} with large Stokes shift and sequential "turn-off" detection of S^{2-} as well as the application in living cells. *Journal of Photochemistry and Photobiology A: Chemistry* **2020,** *387*, 112165.

[916] Kargar, M.; Darabi, H. R.; Sharifi, A.; Mostashari, A., A new chromogenic and fluorescent chemosensor based on a naphthol–bisthiazolopyridine hybrid: a fast response and selective detection of multiple targets, silver, cyanide, sulfide, and hydrogen sulfide ions and gaseous H_2S. *Analyst* **2020,** *145* (6), 2319-2330.

[917] Liu, Y.; Wang, H.; Zhang, R.; Mao, C.; Mu, W.; Jiang, L.; Ma, Q., A novel "on-off-on" fluorescent sensor based on TSPP-Ag^{+} for S^{2-} detection in real samples. *Journal of Porphyrins and Phthalocyanines* **2022,** *26* (10), 656-663.

[918] Mahapatra, A. K.; Manna, S. K.; Maiti, K.; Maji, R.; Das Mukhopadhyay, C.; Sarkar, D.; Mondal, T. K., Imino-phenolic-azodye appended rhodamine as a primary fluorescence "off-on" chemosensor for tin (Sn^{4+}) in solution and in RAW cells and the recognition of sulphide by AR-Sn. *Rsc Advances* **2014,** *4* (69), 36615-36622.

[919] Petruci, J. F. d. S.; Cardoso, A. A., Sensitive luminescent paper-based sensor for the determination of gaseous hydrogen sulfide. *Analytical Methods* **2015,** *7* (6), 2687-2692.

[920] Masood, M. A.; Chen, Y.; Yao, S.; Li, S.; He, W.; Guo, Z., A new palladium complex as a dual fluorometric and colorimetric probe for rapid determination of sulfide anion. *Journal of Photochemistry and Photobiology A: Chemistry* **2021,** *404*, 112885.

[921] Yu, M.; Du, W.; Zhou, W.; Li, H.; Liu, C.; Wei, L.; Li, Z.; Zhang, H., A 1,8-naphthalimide-based chemosensor with an off-on fluorescence and lifetime imaging response for intracellular Cr^{3+} and further for S^{2-}. *Dyes and Pigments* **2016,** *126*, 279-285.

[922] Pluth, M. D.; Tonzetich, Z. J., Hydrosulfide complexes of the transition elements: diverse roles in bioinorganic, cluster, coordination, and organometallic chemistry. *Chemical Society Reviews* **2020,** *49* (12), 4070-4134.

[923] Galardon, E.; Tomas, A.; Roussel, P.; Artaud, I., New fluorescent zinc complexes: towards specific sensors for hydrogen sulfide in solution. *Dalton Transactions* **2009,** (42), 9126-9130.

[924] Hartle, M. D.; Sommer, S. K.; Dietrich, S. R.; Pluth, M. D., Chemically Reversible Reactions of Hydrogen Sulfide with Metal Phthalocyanines. *Inorganic Chemistry* **2014,** *53* (15), 7800-7802.

[925] Hartle, M. D.; Delgado, M.; Gilbertson, J. D.; Pluth, M. D., Stabilization of a Zn(II) hydrosulfido complex utilizing a hydrogen-bond accepting ligand. *Chemical Communications* **2016,** *52* (49), 7680-7682.

[926] Strianese, M.; Lamberti, M.; Pellecchia, C., Chemically reversible binding of H_2S to a zinc porphyrin complex: towards implementation of a reversible sensor via a "coordinative-based approach". *Dalton Transactions* **2017,** *46* (6), 1872-1877.

[927] Strianese, M.; Lamberti, M.; Pellecchia, C., Interaction of monohydrogensulfide with a family of fluorescent pyridoxal-based Zn(II) receptors. *Dalton Transactions* **2018,** *47* (48), 17392-17400.

[928] Strianese, M.; Guarnieri, D.; Lamberti, M.; Landi, A.; Peluso, A.; Pellecchia, C., Fluorescent salen-type Zn(II) Complexes As Probes for Detecting Hydrogen Sulfide and Its Anion: Bioimaging Applications. *Inorganic Chemistry* **2020,** *59* (21), 15977-15986.

[929] Strianese, M.; Vykhovanets, V.; Blal, N.; Guarnieri, D.; Landi, A.; Lamberti, M.; Peluso, A.; Pellecchia, C., Paper-Strip-Based Sensors for H_2S Detection: A Proof-of-Principle Study. *Sensors* **2022,** *22* (9), 3173.

[930] Strianese, M.; Ferrara, G.; Vykhovanets, V.; Blal, N.; Guarnieri, D.; Landi, A.; Lamberti, M.; Peluso, A.; Pellecchia, C., Sol-Gel Dipping Devices for H_2S Visualization. *Sensors* **2023,** *23* (4), 2023.

[931] Strianese, M.; D'Auria, G. J.; Lamberti, M.; Landi, A.; Peluso, A.; Varriale, A.; D'Auria, S.; Pellecchia, C., Salen, salan and salalen zinc(II) complexes in the interaction with HS^-: time-resolved fluorescence applications. *Dalton Transactions* **2023,** *52* (5), 1357-1365.

[932] Strianese, M.; Brenna, S.; Attilio Ardizzoia, G.; Guarnieri, D.; Lamberti, M.; D'Auria, I.; Pellecchia, C., Imidazo-pyridine-based zinc(II) complexes as fluorescent hydrogen sulfide probes. *Dalton Transactions* **2021,** *50* (46), 17075-17085.

[933] Strianese, M.; Milione, S.; Bertolasi, V.; Pellecchia, C.; Grassi, A., Heteroscorpionate-Based Co^{2+}, Zn^{2+}, and Cu^{2+} Complexes: Coordination Behavior, Aerobic Oxidation, and Hydrogen Sulfide Detection. *Inorganic Chemistry* **2011,** *50* (3), 900-910.

[934] Bartelmess, J.; Valderrey, V.; Rurack, K., Development of a “Turn-on” Fluorescent Probe-Based Sensing System for Hydrogen Sulfide in Liquid and Gas Phase. *Frontiers in Chemistry* **2019,** *7*.

[935] Mirra, S.; Milione, S.; Strianese, M.; Pellecchia, C., A Copper Porphyrin for Sensing H_2S in Aqueous Solution via a "Coordinative-Based" Approach. *European Journal of Inorganic Chemistry* **2015,** (13), 2272-2276.

[936] Hartle, M. D.; Tillotson, M. R.; Prell, J. S.; Pluth, M. D., Spectroscopic investigation of the reaction of metallo-protoporphyrins with hydrogen sulfide. *Journal of Inorganic Biochemistry* **2017,** *173*, 152-157.

[937] Kraus, D. W.; Wittenberg, J. B., Hemoglobins of the Lucina pectinata/bacteria symbiosis. I. Molecular properties, kinetics and equilibria of reactions with ligands. *Journal of Biological Chemistry* **1990,** *265* (27), 16043-16053.

[938] Rizzi, M.; Wittenberg, J. B.; Coda, A.; Fasano, M.; Ascenzi, P.; Bolognesi, M., Structure of the Sulfide-reactive Hemoglobin from the Clam Lucina pectinata: Crystallographic Analysis at 1.5 Å Resolution. *Journal of Molecular Biology* **1994,** *244* (1), 86-99.

[939] Ramos-Alvarez, C.; Yoo, B.-K.; Pietri, R.; Lamarre, I.; Martin, J.-L.; Lopez-Garriga, J.; Negrerie, M., Reactivity and Dynamics of H_2S, NO, and O_2 Interacting with Hemoglobins from Lucina pectinata. *Biochemistry* **2013,** *52* (40), 7007-7021.

[940] Strianese, M.; De Martino, F.; Pellecchia, C.; Ruggiero, G.; D'Auria, S., Myoglobin as a New Fluorescence Probe to Sense H_2S. *Protein and Peptide Letters* **2011,** *18* (3), 282-286.

[941] Dulac, M.; Melet, A.; Galardon, E., Reversible Detection and Quantification of Hydrogen Sulfide by Fluorescence Using the Hemoglobin I from Lucina pectinata. *Acs Sensors* **2018,** *3* (10), 2138-2144.

[942] Strianese, M.; Palm, G. J.; Milione, S.; Kühl, O.; Hinrichs, W.; Pellecchia, C., A FRET Enzyme-Based Probe for Monitoring Hydrogen Sulfide. *Inorganic Chemistry* **2012,** *51* (21), 11220-11222.

[943] Strianese, M.; Palm, G. J.; Kohlhause, D.; Ndamba, L. A.; Tabares, L. C.; Pellecchia, C., Azurin and HS^-: Towards Implementation of a Sensor for HS^- Detection. *European Journal of Inorganic Chemistry* **2019,** (6), 885-891.

[944] Wintner, E. A.; Deckwerth, T. L.; Langston, W.; Bengtsson, A.; Leviten, D.; Hill, P.; Insko, M. A.; Dumpit, R.; VandenEkart, E.; Toombs, C. F.; Szabo, C., A monobromobimane-based assay to measure the pharmacokinetic profile of reactive sulphide species in blood. *British Journal of Pharmacology* **2010,** *160* (4), 941-957.

[945] Shen, X.; Pattillo, C. B.; Pardue, S.; Bir, S. C.; Wang, R.; Kevil, C. G., Measurement of plasma hydrogen sulfide in vivo and in vitro. *Free Radical Biology and Medicine* **2011,** *50* (9), 1021-1031.

[946] Shen, X.; Peter, E. A.; Bir, S.; Wang, R.; Kevil, C. G., Analytical measurement of discrete hydrogen sulfide pools in biological specimens. *Free Radical Biology and Medicine* **2012,** *52* (11), 2276-2283.

[947] Ditrói, T.; Nagy, A.; Martinelli, D.; Rosta, A.; Kožich, V.; Nagy, P., Comprehensive analysis of how experimental parameters affect H_2S measurements by the monobromobimane method. *Free Radical Biology and Medicine* **2019,** *136*, 146-158.

[948] Bogdándi, V.; Ida, T.; Sutton, T. R.; Bianco, C.; Ditrói, T.; Koster, G.; Henthorn, H. A.; Minnion, M.; Toscano, J. P.; van der Vliet, A.; Pluth, M. D.; Feelisch, M.; Fukuto, J. M.; Akaike, T.; Nagy, P., Speciation of reactive sulfur species and their reactions with alkylating agents: do we have any clue about what is present inside the cell? *British Journal of Pharmacology* **2019,** *176* (4), 646-670.

[949] Benchoam, D.; Semelak, J. A.; Cuevasanta, E.; Mastrogiovanni, M.; Grassano, J. S.; Ferrer-Sueta, G.; Zeida, A.; Trujillo, M.; Möller, M. N.; Estrin, D. A.; Alvarez, B., Acidity and nucleophilic reactivity of glutathione persulfide. *J Biol Chem* **2020,** *295* (46), 15466-15481.

[950] Liu, C.; Chen, W.; Shi, W.; Peng, B.; Zhao, Y.; Ma, H.; Xian, M., Rational Design and Bioimaging Applications of Highly Selective Fluorescence Probes for Hydrogen Polysulfides. *Journal of the American Chemical Society* **2014,** *136* (20), 7257-7260.

[951] Zeng, L.; Chen, S.; Xia, T.; Hu, W.; Li, C.; Liu, Z., Two-Photon Fluorescent Probe for Detection of Exogenous and Endogenous Hydrogen Persulfide and Polysulfide in Living Organisms. *Analytical Chemistry* **2015,** *87* (5), 3004-3010.

[952] Yu, F.; Gao, M.; Li, M.; Chen, L., A dual response near-infrared fluorescent probe for hydrogen polysulfides and superoxide anion detection in cells and in vivo. *Biomaterials* **2015,** *63*, 93-101.

[953] Gao, M.; Yu, F.; Chen, H.; Chen, L., Near-Infrared Fluorescent Probe for Imaging Mitochondrial Hydrogen Polysulfides in Living Cells and in vivo. *Analytical Chemistry* **2015,** *87* (7), 3631-3638.

[954] Gao, M.; Wang, R.; Yu, F.; You, J.; Chen, L., A near-infrared fluorescent probe for the detection of hydrogen polysulfides biosynthetic pathways in living cells and in vivo. *Analyst* **2015,** *140* (11), 3766-3772.

[955] Wang, X.; Sun, Q.; Zhao, L.; Gong, S.; Xu, L., Visualization of hydrogen polysulfides in living cells and in vivo via a near-infrared fluorescent probe. *JBIC Journal of Biological Inorganic Chemistry* **2019,** *24* (7), 1077-1085.

[956] Zhang, C.; Sun, Q.; Zhao, L.; Gong, S.; Liu, Z., A BODIPY-based ratiometric probe for sensing and imaging hydrogen polysulfides in living cells. *Spectrochimica Acta Part A: Molecular and Biomolecular Spectroscopy* **2019,** *223*, 117295.

[957] Han, Q.; Mou, Z.; Wang, H.; Tang, X.; Dong, Z.; Wang, L.; Dong, X.; Liu, W., Highly Selective and Sensitive One- and Two-Photon Ratiometric Fluorescent Probe for Intracellular Hydrogen Polysulfide Sensing. *Analytical Chemistry* **2016,** *88* (14), 7206-7212.

[958] Zhou, L.; Yuan, G.; Hu, S., A 4-Hydroxy-1,8-Naphthalimide-Based Turn-on Two-Photon Fluorescent Probe for Hydrogen Polysulfide Sensing. *Journal of Applied Spectroscopy* **2020,** *86* (6), 1071-1076.

[959] Han, Q.; Ru, J.; Wang, X.; Dong, Z.; Wang, L.; Jiang, H.; Liu, W., Photostable Ratiometric Two-Photon Fluorescent Probe for Visualizing Hydrogen Polysulfide in Mitochondria and Its Application. *ACS Applied Bio Materials* **2019,** *2* (5), 1987-1997.

[960] Han, Q.; Yang, L.; Song, Y.; Ru, J.; Zhang, H.; Jiang, H.; Wang, X., A ratiometric fluorescent probe for monitoring the changes in the level of hydrogen polysulfides in mitochondria during stimulus-induced redox imbalance. *Dyes and Pigments* **2021,** *188*, 109190.

[961] Han, Q.; Liu, X.; Wang, X.; Yin, R.; Jiang, H.; Ru, J.; Liu, W., Rational design of a lysosomal-targeted ratiometric two-photon fluorescent probe for imaging hydrogen polysulfides in live cells. *Dyes and Pigments* **2020,** *173*, 107877.

[962] Tian, M.; Xu, J.; Ma, Q.; Li, L.; Yuan, H.; Sun, J.; Zhu, N.; Liu, S., A novel lysosome-located fluorescent probe for highly selective determination of hydrogen polysulfides based on a naphthalimide derivative. *Spectrochimica Acta Part A: Molecular and Biomolecular Spectroscopy* **2022,** *268*, 120708.

[963] Zhang, J.; Zhu, X.-Y.; Hu, X.-X.; Liu, H.-W.; Li, J.; Feng, L. L.; Yin, X.; Zhang, X.-B.; Tan, W., Ratiometric Two-Photon Fluorescent Probe for in Vivo Hydrogen Polysulfides Detection and Imaging during Lipopolysaccharide-Induced Acute Organs Injury. *Analytical Chemistry* **2016,** *88* (23), 11892-11899.

[964] Sun, J.; Bai, Y.; Ma, Q.; Zhang, H.; Wu, M.; Wang, C.; Tian, M., A FRET-based ratiometric fluorescent probe for highly selective detection of hydrogen polysulfides based on a coumarin-rhodol derivative. *Spectrochimica Acta Part A: Molecular and Biomolecular Spectroscopy* **2020,** *241*, 118650.

[965] Yang, L.; Yang, N.; Gu, P.; Wang, C.; Li, B.; Zhang, Y.; Ji, L.; He, G., A novel flavone-based ESIPT ratiometric fluorescent probe for selective sensing and imaging of hydrogen polysulfides. *Spectrochimica Acta Part A: Molecular and Biomolecular Spectroscopy* **2022,** *271*, 120962.

[966] Liu, T.; Peng, Q.; Wang, J.; Yu, C.; Huang, X.; Luo, Q.; Zeng, Y.; Hou, Y.; Zhang, Y.; Luo, A.; Zou, Z.; Chen, M.; Peng, Y., A FRET-based ratiometric fluorescent probe for

hydrogen polysulfide detection in living cells and zebrafish. *Spectrochimica Acta Part A: Molecular and Biomolecular Spectroscopy* **2022,** *267*, 120524.

[967] Liu, S.; Zhao, X.; Ma, Q.; Wang, G.; Hou, S.; Ma, Y.; Lian, Y., An ICT-FRET-based ratiometric fluorescent probe for hydrogen polysulfide based on a coumarin-naphthalimide derivative. *Spectrochimica Acta Part A: Molecular and Biomolecular Spectroscopy* **2023,** *302*, 123041.

[968] Shang, H.; Chen, H.; Tang, Y.; Guo, R.; Lin, W., Construction of a two-photon fluorescent turn-on probe for hydrogen persulfide and polysulfide and its bioimaging application in living mice. *Sensors and Actuators B: Chemical* **2016,** *230*, 773-778.

[969] Ren, Y.; Zhang, L.; Zhou, Z.; Luo, Y.; Wang, S.; Yuan, S.; Gu, Y.; Xu, Y.; Zha, X., A new lysosome-targetable fluorescent probe with a large Stokes shift for detection of endogenous hydrogen polysulfides in living cells. *Analytica Chimica Acta* **2019,** *1056*, 117-124.

[970] Hou, P.; Wang, J.; Fu, S.; Liu, L.; Chen, S., A new turn-on fluorescent probe with ultra-large fluorescence enhancement for detection of hydrogen polysulfides based on dual quenching strategy. *Spectrochimica Acta Part A: Molecular and Biomolecular Spectroscopy* **2019,** *213*, 342-346.

[971] Liu, J.; Yin, Z., A resorufin-based fluorescent probe for imaging polysulfides in living cells. *Analyst* **2019,** *144* (10), 3221-3225.

[972] Wang, C.; Xu, J.; Ma, Q.; Bai, Y.; Tian, M.; Sun, J.; Zhang, Z., A highly selective fluorescent probe for hydrogen polysulfides in living cells based on a naphthalene derivative. *Spectrochimica Acta Part A: Molecular and Biomolecular Spectroscopy* **2020,** *227*, 117579.

[973] Fang, Q.; Yue, X.; Han, S.; Wang, B.; Song, X., A rapid and sensitive fluorescent probe for detecting hydrogen polysulfides in living cells and zebra fish. *Spectrochimica Acta Part A: Molecular and Biomolecular Spectroscopy* **2020,** *224*, 117410.

[974] Huang, X.; Liu, H.; Liu, G.; Wang, R.; Fan, C.; Pu, S., A colorimetric and fluorescent probe for selective sensing and imaging of hydrogen polysulfides. *Journal of Photochemistry and Photobiology A: Chemistry* **2020,** *391*, 112373.

[975] Meng, J.; Liu, H.-C.; Guo, Y.-Y.; Wang, F.; Pi, D.-J.; Yu, Q.-Z., Discovery of a triphenylamine-benzofuran derivative as fluorescent probe for hydrogen polysulfide in tea samples. *Spectrochimica Acta Part A: Molecular and Biomolecular Spectroscopy* **2023,** *288*, 122191.

[976] Ma, J.; Fan, J.; Li, H.; Yao, Q.; Xu, F.; Wang, J.; Peng, X., A NIR fluorescent chemodosimeter for imaging endogenous hydrogen polysulfides via the CSE enzymatic pathway. *Journal of Materials Chemistry B* **2017,** *5* (14), 2574-2579.

[977] Zhang, X.; Zhang, L.; Gao, M.; Wang, Y.; Chen, L., A near-infrared fluorescent probe for observing thionitrous acid-mediated hydrogen polysulfides formation and fluctuation in cells and in vivo under hypoxia stress. *Journal of Hazardous Materials* **2020,** *396*, 122673.

[978] Liu, F.-L.; Yuchi, X.-X.; Zhang, M.-H.; Huang, J.; Hu, X.-W.; Man, R.-J., A fluorescent probe derived from Berberrubine for detecting hydrogen polysulfide in food samples. *Spectrochimica Acta Part A: Molecular and Biomolecular Spectroscopy* **2022,** *267*, 120491.

[979] Li, K.-B.; Chen, F.-Z.; Yin, Q.-H.; Zhang, S.; Shi, W.; Han, D.-M., A colorimetric and near-infrared fluorescent probe for hydrogen polysulfides and its application in living cells. *Sensors and Actuators B: Chemical* **2018,** *254*, 222-226.

[980] Zhao, L.; Sun, Q.; Sun, C.; Zhang, C.; Duan, W.; Gong, S.; Liu, Z., An isophorone-based far-red emitting ratiometric fluorescent probe for selective sensing and imaging of polysulfides. *Journal of Materials Chemistry B* **2018,** *6* (43), 7015-7020.

[981] Di, X.; Ge, C.; Liu, Y.; Shao, C.; Zhu, H.-L.; Liu, H.-K.; Qian, Y., Monitoring hydrogen polysulfide during ferroptosis with a two-photon fluorescent probe. *Talanta* **2021,** *232*, 122467.

[982] Zhang, F.; Han, J.; Wang, J.; Li, X.; Wang, Y.; Wang, B.; Song, X., A near-infrared fluorescent probe for hydrogen polysulfides detection with a large Stokes shift. *Spectrochimica Acta Part A: Molecular and Biomolecular Spectroscopy* **2020,** *242*, 118755.

[983] Xiang, C.; Li, C.; Xiang, J.; Luo, Y.; Peng, J.; Deng, G.; Wang, J.; Kolemen, S.; Li, H.; Zhang, P.; Gong, P.; Cai, L., An easily available lysosomal-targeted ratiometric fluorescent probe with aggregation induced emission characteristics for hydrogen polysulfide visualization in acute ulcerative colitis. *Materials Chemistry Frontiers* **2021,** *5* (20), 7638-7644.

[984] Li, K.-B.; Chen, F.-Z.; Zhang, S.; Shi, W.; Han, D.-M.; Cai, C.; Chen, C.-X., A nile red-based near-infrared fluorescent probe for endogenous hydrogen polysulfides in living cells. *Analytical Methods* **2017,** *9* (45), 6443-6447.

[985] Li, W.; Zhou, S.; Zhang, L.; Yang, Z.; Chen, H.; Chen, W.; Qin, J.; Shen, X.; Zhao, S., A red emitting fluorescent probe for sensitively monitoring hydrogen polysulfides in living cells and zebrafish. *Sensors and Actuators B: Chemical* **2019,** *284*, 30-35.

[986] Zhang, L.; Liu, H.; Wu, C.; Zheng, Y.; Kai, X.; Xue, Y., A near-infrared fluorescent probe that can image endogenous hydrogen polysulfides in vivo in tumour-bearing mice. *Organic & Biomolecular Chemistry* **2021,** *19* (4), 911-919.

[987] Zhao, H.; Qi, F.; Xiong, Y.; Lu, J., A chemiluminescent sensor for imaging endogenous hydrogen polysulfides in a living system. *Analyst* **2023,** *148* (14), 3347-3353.

[988] Chen, W.; Rosser, E. W.; Matsunaga, T.; Pacheco, A.; Akaike, T.; Xian, M., The Development of Fluorescent Probes for Visualizing Intracellular Hydrogen Polysulfides. *Angewandte Chemie International Edition* **2015,** *54* (47), 13961-13965.

[989] Chen, W.; Pacheco, A.; Takano, Y.; Day, J. J.; Hanaoka, K.; Xian, M., A Single Fluorescent Probe to Visualize Hydrogen Sulfide and Hydrogen Polysulfides with Different Fluorescence Signals. *Angewandte Chemie International Edition* **2016,** *55* (34), 9993-9996.

[990] Yang, F.; Gao, H.; Li, S.-S.; An, R.-B.; Sun, X.-Y.; Kang, B.; Xu, J.-J.; Chen, H.-Y., A fluorescent τ-probe: quantitative imaging of ultra-trace endogenous hydrogen polysulfide in cells and in vivo. *Chemical Science* **2018,** *9* (25), 5556-5563.

[991] Ma, Y.; Xu, Z.; Sun, Q.; Wang, L.; Liu, H.; Yu, F., A semi-naphthorhodafluor-based red-emitting fluorescent probe for tracking of hydrogen polysulfide in living cells and zebrafish. *Spectrochimica Acta Part A: Molecular and Biomolecular Spectroscopy* **2021,** *247*, 119105.

[992] Mi, L.; Lin, B.; Jin, J.; Zhang, H.; Chen, H.; Cheng, Z.; Wu, J.; Liu, H., Development of an activatable red emissive fluorescent probe for imaging hydrogen disulfide upregulation in living cells and zebrafish. *Analytica Chimica Acta* **2022,** *1226*, 340288.

[993] Fang, Y.; Chen, W.; Shi, W.; Li, H.; Xian, M.; Ma, H., A near-infrared fluorescence off–on probe for sensitive imaging of hydrogen polysulfides in living cells and mice in vivo. *Chemical Communications* **2017,** *53* (62), 8759-8762.

[994] A, A. H.; Sreedharan, S.; Ali, F.; Smythe, C. G.; Thomas, J. A.; Das, A., Polysulfide-triggered fluorescent indicator suitable for super-resolution microscopy and application in imaging. *Chemical Communications* **2018,** *54* (30), 3735-3738.

[995] Li, J.-B.; Wang, Q.; Liu, H.-W.; Yuan, L.; Zhang, X.-B., A bioluminescent probe for imaging endogenous hydrogen polysulfides in live cells and a murine model of bacterial infection. *Chemical Communications* **2019,** *55* (31), 4487-4490.

[996] Choi, H. J.; Lim, C. S.; Cho, M. K.; Kang, J. S.; Park, S. J.; Park, S. M.; Kim, H. M., A two-photon ratiometric probe for hydrogen polysulfide (H_2S_n): Increase in mitochondrial H_2S_n production in a Parkinson's disease model. *Sensors and Actuators B: Chemical* **2019,** *283*, 810-819.

[997] Liang, L.; Li, W.; Zheng, J.; Li, R.; Chen, H.; Yuan, Z., A new lysosome-targetable fluorescent probe for detection of endogenous hydrogen polysulfides in living cells and inflamed mouse model. *Biomaterials Science* **2020,** *8* (1), 224-231.

[998] Meng, W.; Shi, W.; Chen, Y.; Zhang, H.; Zhao, J.; Li, Z.; Xiao, K., A red emitting fluorescent probe for imaging mitochondrial hydrogen polysulfide in living cells and tissues. *Sensors and Actuators B: Chemical* **2019,** *281*, 871-877.

[999] He, Z.; Qiu, Z.; Liao, L.; Zhang, C.; Hu, S.; Zhao, S., Design and synthesis of photoacoustic probe for in situ imaging of hydrogen polysulfides in organs in vivo. *Sensors and Actuators B: Chemical* **2023,** *381*, 133423.

[1000] Kawagoe, R.; Takashima, I.; Uchinomiya, S.; Ojida, A., Reversible ratiometric detection of highly reactive hydropersulfides using a FRET-based dual emission fluorescent probe. *Chemical Science* **2017,** *8* (2), 1134-1140.

[1001] Umezawa, K.; Kamiya, M.; Urano, Y., A Reversible Fluorescent Probe for Real-Time Live-Cell Imaging and Quantification of Endogenous Hydropolysulfides. *Angewandte Chemie International Edition* **2018,** *57* (30), 9346-9350.

[1002] Hou, Y.; Yang, X.-F.; Zhong, Y.; Li, Z., Development of fluorescent probes for hydrogen polysulfides by using cinnamate ester as the recognition unit. *Sensors and Actuators B: Chemical* **2016,** *232*, 531-537.

[1003] Guo, J.; Yang, S.; Guo, C.; Zeng, Q.; Qing, Z.; Cao, Z.; Li, J.; Yang, R., Molecular Engineering of α-Substituted Acrylate Ester Template for Efficient Fluorescence Probe of Hydrogen Polysulfides. *Analytical Chemistry* **2018,** *90* (1), 881-887.

[1004] Meng, W.; Chen, Y.; Feng, Y.; Zhang, H.; Xu, Q.; Sun, M.; Shi, W.; Cen, J.; Zhao, J.; Xiao, K., An off–on fluorescent probe for the detection of mitochondria-specific protein persulfidation. *Organic & Biomolecular Chemistry* **2018,** *16* (34), 6350-6357.

[1005] Fu, L.; Chen, C.; Chen, W.; Huang, J.; Xiao, J.; Yang, L.; Sheng, J.; Song, X., The unique substitution-cyclization reaction cascade inspired highly selective H_2S_n probe development. *Sensors and Actuators B: Chemical* **2020,** *304*, 127382.

[1006] Chen, W.; Yue, X.; Zhang, H.; Li, W.; Zhang, L.; Xiao, Q.; Huang, C.; Sheng, J.; Song, X., Simultaneous Detection of Glutathione and Hydrogen Polysulfides from Different Emission Channels. *Analytical Chemistry* **2017,** *89* (23), 12984-12991.

[1007] Niu, P.; Rong, Y.; Wang, Y.; Ni, H.; Zhu, M.; Chen, W.; Liu, X.; Wei, L.; Song, X., A bifunctional fluorescent probe for simultaneous detection of GSH and H_2S_n ($n > 1$) from different channels with long-wavelength emission. *Spectrochimica Acta Part A: Molecular and Biomolecular Spectroscopy* **2021,** *257*, 119789.

[1008] Rong, Y.; Niu, P.; Liu, X.; Chen, W.; Wei, L.; Song, X., Double-channel based fluorescent probe for differentiating GSH and H_2S_n ($n>1$) via a single-wavelength excitation with long-wavelength emission. *Sensors and Actuators B: Chemical* **2021,** *344*, 130224.

[1009] Chen, W.; Yue, X.; Sheng, J.; Li, W.; Zhang, L.; Su, W.; Huang, C.; Song, X., Rational development of a highly selective ratiometric fluorescent probe for hydrogen polysulfides. *Sensors and Actuators B: Chemical* **2018,** *258*, 125-132.

[1010] Han, L.; Shi, R.; Xin, C.; Ci, Q.; Ge, J.; Liu, J.; Wu, Q.; Zhang, C.; Li, L.; Huang, W., Mitochondrial Specific H_2S_n Fluorogenic Probe for Live Cell Imaging by Rational Utilization of a Dual-Functional-Photocage Group. *ACS Sensors* **2018,** *3* (9), 1622-1626.

[1011] Tsukamoto, K.; Ohsawa, H.; Nishiyama, R.; Maeda, H., 3′-O-(2-Nitrobenzenesulfonyl)fluorescein as a Fluorescent Probe for Hydrogen Polysulfides by Straightforward One-Step Deprotection. *Analysis & Sensing* **2022,** *3* (3), e202200084.

[1012] Feng, Q.; Song, Y.; Ma, Y.; Deng, Y.; Xu, P.; Sheng, K.; Zhang, Y.; Li, J.; Wu, S., Molecular engineering of benzenesulfonyl analogs for visual hydrogen polysulfide fluorescent probes based on Nile red skeleton. *Spectrochimica Acta Part A: Molecular and Biomolecular Spectroscopy* **2023,** *296*, 122658.

[1013] Xie, P.; Zhu, Y.; Wang, Y.; Gao, G.; Jiang, S.; Guo, F., A fluorescent probe for discrimination of cysteine/homocysteine, glutathione and hydrogen polysulfides. *Research on Chemical Intermediates* **2021,** *47* (3), 1123-1138.

[1014] Chen, W.; Rosser, E. W.; Zhang, D.; Shi, W.; Li, Y.; Dong, W.-J.; Ma, H.; Hu, D.; Xian, M., A Specific Nucleophilic Ring-Opening Reaction of Aziridines as a Unique Platform for the Construction of Hydrogen Polysulfides Sensors. *Organic Letters* **2015,** *17* (11), 2776-2779.

[1015] Chen, W.; Liu, C.; Peng, B.; Zhao, Y.; Pacheco, A.; Xian, M., New fluorescent probes for sulfane sulfurs and the application in bioimaging. *Chemical Science* **2013,** *4* (7), 2892-2896.

[1016] Sakaguchi, M.; Marutani, E.; Shin, H.-s.; Chen, W.; Hanaoka, K.; Xian, M.; Ichinose, F., Sodium Thiosulfate Attenuates Acute Lung Injury in Mice. *Anesthesiology* **2014,** *121* (6), 1248-1257.

[1017] Shieh, M.; Ni, X.; Xu, S.; Lindahl, S. P.; Yang, M.; Matsunaga, T.; Flaumenhaft, R.; Akaike, T.; Xian, M., Shining a light on SSP4: A comprehensive analysis and biological applications for the detection of sulfane sulfurs. *Redox Biology* **2022,** *56*, 102433.

[1018] Han, X.; Song, X.; Li, B.; Yu, F.; Chen, L., A near-infrared fluorescent probe for sensitive detection and imaging of sulfane sulfur in living cells and in vivo. *Biomaterials Science* **2018,** *6* (3), 672-682.

[1019] Gao, M.; Wang, R.; Yu, F.; You, J.; Chen, L., Imaging and evaluation of sulfane sulfur in acute brain ischemia using a mitochondria-targeted near-infrared fluorescent probe. *Journal of Materials Chemistry B* **2018,** *6* (17), 2608-2619.

[1020] Jiang, G.; Li, M.; Wen, Y.; Zeng, W.; Zhao, Q.; Chen, C.; Yuan, H.; Liu, C.; Liu, C., Visualization of Sulfane Sulfur in Plants with a Near-Infrared Fluorescent Probe. *ACS Sensors* **2019,** *4* (2), 434-440.

[1021] Neill, D. L.; Chang, Y.-C.; Chen, W.; Li, L.; Xian, M., A smartphone based device for the detection of sulfane sulfurs in biological systems. *Sensors and Actuators B: Chemical* **2019,** *292*, 263-269.

[1022] Takano, Y.; Hanaoka, K.; Shimamoto, K.; Miyamoto, R.; Komatsu, T.; Ueno, T.; Terai, T.; Kimura, H.; Nagano, T.; Urano, Y., Development of a reversible fluorescent probe for reactive sulfur species, sulfane sulfur, and its biological application. *Chemical Communications* **2017,** *53* (6), 1064-1067.

[1023] Gao, M.; Wang, R.; Yu, F.; Li, B.; Chen, L., Imaging of intracellular sulfane sulfur expression changes under hypoxic stress via a selenium-containing near-infrared fluorescent probe. *Journal of Materials Chemistry B* **2018,** *6* (41), 6637-6645.

[1024] Gao, M.; Wang, R.; Yu, F.; Chen, L., Evaluation of sulfane sulfur bioeffects via a mitochondria-targeting selenium-containing near-infrared fluorescent probe. *Biomaterials* **2018,** *160*, 1-14.

[1025] Han, X.; Yu, F.; Song, X.; Chen, L., Quantification of cysteine hydropersulfide with a ratiometric near-infrared fluorescent probe based on selenium–sulfur exchange reaction. *Chemical Science* **2016,** *7* (8), 5098-5107.

[1026] Wang, Y.; Zhang, L.; Zhang, S.; Liu, Z.; Chen, L., High Spatiotemporal Resolution Observation of Glutathione Hydropersulfides in Living Cells and Tissue via a Two-Photon Ratiometric Fluorescent Probe. *Analytical Chemistry* **2019,** *91* (12), 7812-7818.

[1027] Huang, Y.; Yu, F.; Wang, J.; Chen, L., Near-Infrared Fluorescence Probe for in Situ Detection of Superoxide Anion and Hydrogen Polysulfides in Mitochondrial Oxidative Stress. *Analytical Chemistry* **2016,** *88* (7), 4122-4129.

[1028] Gao, M.; Zhang, X.; Wang, Y.; Liu, Q.; Yu, F.; Huang, Y.; Ding, C.; Chen, L., Sequential Detection of Superoxide Anion and Hydrogen Polysulfides under Hypoxic Stress via a Spectral-Response-Separated Fluorescent Probe Functioned with a Nitrobenzene Derivative. *Analytical Chemistry* **2019,** *91* (12), 7774-7781.

[1029] Gong, X.; Yang, X.-F.; Zhong, Y.; Chen, H.; Li, Z., A flavylium-based turn-on fluorescent probe for imaging hydrogen polysulfides in living cells. *RSC Advances* **2016,** *6* (91), 88519-88525.

[1030] Zhou, H.; Tang, J.; Sun, L.; Zhang, J.; Chen, B.; Kan, J.; Zhang, W.; Zhang, J.; Zhou, J., H_2S_2-triggered off-on fluorescent indicator with endoplasmic reticulum targeting for imaging in cells and zebrafishes. *Sensors and Actuators B: Chemical* **2019,** *278*, 64-72.

[1031] Chung, J.; Li, H.; Lim, C. S.; Kim, H. M.; Yoon, J., Two-photon imaging of hydrogen polysulfides in living cells and hippocampal tissues. *Sensors and Actuators B: Chemical* **2020,** *322*, 128564.

[1032] Qiu, T.; Wei, H.; Cheng, D.; Zhang, L.; Jiang, C.; Luo, S.; Yuan, L.; Zeng, Z., Towards perylenequinonoid: Effective application to reversible fluorescent probe for monitoring hydrogen persulfide in solvents and living cells. *Talanta* **2017,** *164*, 529-533.

[1033] Hartle, M. D.; Hansen, R. J.; Tresca, B. W.; Prakel, S. S.; Zakharov, L. N.; Haley, M. M.; Pluth, M. D.; Johnson, D. W., A Synthetic Supramolecular Receptor for the Hydrosulfide Anion. *Angewandte Chemie International Edition* **2016,** *55* (38), 11480-11484.

[1034] Vázquez, J.; Sindelar, V., Supramolecular binding and release of sulfide and hydrosulfide anions in water. *Chemical Communications* **2018,** *54* (46), 5859-5862.

[1035] Kumar, P.; Kumar, V.; Pandey, S.; Gupta, R., Detection of sulfide ion and gaseous H_2S using a series of pyridine-2,6-dicarboxamide based scaffolds. *Dalton Transactions* **2018,** *47* (28), 9536-9545.

[1036] Fargher, H. A.; Lau, N.; Richardson, H. C.; Cheong, P. H.-Y.; Haley, M. M.; Pluth, M. D.; Johnson, D. W., Tuning Supramolecular Selectivity for Hydrosulfide: Linear Free Energy Relationships Reveal Preferential C–H Hydrogen Bond Interactions. *Journal of the American Chemical Society* **2020,** *142* (18), 8243-8251.

[1037] Mitchell, E. J.; Beecroft, A. J.; Martin, J.; Thompson, S.; Marques, I.; Félix, V.; Beer, P. D., Hydrosulfide (HS^-) Recognition and Sensing in Water by Halogen Bonding Hosts. *Angewandte Chemie International Edition* **2021,** *60* (45), 24048-24053.

[1038] Meyer, A. J.; Dick, T. P., Fluorescent Protein-Based Redox Probes. *Antioxidants & Redox Signaling* **2010,** *13* (5), 621-650.

[1039] Lukyanov, K. A.; Belousov, V. V., Genetically encoded fluorescent redox sensors. *Biochimica Et Biophysica Acta-General Subjects* **2014,** *1840* (2), 745-756.

[1040] Schwarzländer, M.; Dick, T. P.; Meyer, A. J.; Morgan, B., Dissecting Redox Biology Using Fluorescent Protein Sensors. *Antioxidants & Redox Signaling* **2016,** *24* (13), 680-712.

[1041] Potter, M. N.; Green, J. R.; Mutus, B., Fluorescein isothiocyanate, a platform for the selective and sensitive detection of S-Nitrosothiols and hydrogen sulfide. *Talanta* **2022,** *237*, 122981.

[1042] Chen, W.; Matsunaga, T.; Neill, D. L.; Yang, C.-t.; Akaike, T.; Xian, M., Rational Design of a Dual-Reactivity-Based Fluorescent Probe for Visualizing Intracellular HSNO. *Angewandte Chemie International Edition* **2019,** *58* (45), 16067-16070.

[1043] Cerda, M. M.; Fehr, J. M.; Sherbow, T. J.; Pluth, M. D., Progress toward colorimetric and fluorescent detection of carbonyl sulfide. *Chemical Communications* **2020,** *56* (67), 9644-9647.

[1044] Chen, S.; Chen, Z.-j.; Ren, W.; Ai, H.-w., Reaction-Based Genetically Encoded Fluorescent Hydrogen Sulfide Sensors. *Journal of the American Chemical Society* **2012,** *134* (23), 9589-9592.

[1045] Chen, Z.-j.; Ai, H.-w., A Highly Responsive and Selective Fluorescent Probe for Imaging Physiological Hydrogen Sulfide. *Biochemistry* **2014,** *53* (37), 5966-5974.

[1046] Youssef, S.; Zhang, S.; Ai, H.-w., A Genetically Encoded, Ratiometric Fluorescent Biosensor for Hydrogen Sulfide. *ACS Sensors* **2019,** *4* (6), 1626-1632.

[1047] Montoya, L. A.; Pluth, M. D., Organelle-Targeted H_2S Probes Enable Visualization of the Subcellular Distribution of H_2S Donors. *Analytical Chemistry* **2016,** *88* (11), 5769-5774.

[1048] Chen, J.; Zhao, M.; Jiang, X.; Sizovs, A.; Wang, M. C.; Provost, C. R.; Huang, J.; Wang, J., Genetically anchored fluorescent probes for subcellular specific imaging of hydrogen sulfide. *Analyst* **2016,** *141* (4), 1209-1213.

[1049] Le Trionnaire, S.; Perry, A.; Szczesny, B.; Szabo, C.; Winyard, P. G.; Whatmore, J. L.; Wood, M. E.; Whiteman, M., The synthesis and functional evaluation of a mitochondria-targeted hydrogen sulfide donor, (10-oxo-10-(4-(3-thioxo-3H-1,2-dithiol-5-yl)phenoxy)decyl)triphenylphosphonium bromide (AP39). *MedChemComm* **2014,** *5* (6), 728-736.

[1050] Williams, A. T. R.; Winfield, S. A.; Miller, J. N., Relative fluorescence quantum yields using a computer-controlled luminescence spectrometer. *Analyst* **1983,** *108* (1290), 1067-1071.

[1051] Wang, R., The Gasotransmitter Role of Hydrogen Sulfide. *Antioxidants & Redox Signaling* **2003,** *5* (4), 493-501.

[1052] Mancardi, D.; Penna, C.; Merlino, A.; Del Soldato, P.; Wink, D. A.; Pagliaro, P., Physiological and pharmacological features of the novel gasotransmitter: Hydrogen sulfide. *Biochimica et Biophysica Acta (BBA) - Bioenergetics* **2009,** *1787* (7), 864-872.

[1053] Jha, S.; Calvert, J. W.; Duranski, M. R.; Ramachandran, A.; Lefer, D. J., Hydrogen sulfide attenuates hepatic ischemia-reperfusion injury: role of antioxidant and antiapoptotic signaling. *American Journal of Physiology-Heart and Circulatory Physiology* **2008,** *295* (2), H801-H806.

[1054] Cao, X.; Ding, L.; Xie, Z.-z.; Yang, Y.; Whiteman, M.; Moore, P. K.; Bian, J.-S., A Review of Hydrogen Sulfide Synthesis, Metabolism, and Measurement: Is Modulation of

Hydrogen Sulfide a Novel Therapeutic for Cancer? *Antioxidants & Redox Signaling* **2019,** *31* (1), 1-38.

[1055] Fu, M.; Zhang, W.; Wu, L.; Yang, G.; Li, H.; Wang, R., Hydrogen sulfide (H_2S) metabolism in mitochondria and its regulatory role in energy production. *Proceedings of the National Academy of Sciences* **2012,** *109* (8), 2943-2948.

[1056] Wei, H.; Zhang, R.; Jin, H.; Liu, D.; Tang, X.; Tang, C.; Du, J., Hydrogen Sulfide Attenuates Hyperhomocysteinemia-Induced Cardiomyocytic Endoplasmic Reticulum Stress in Rats. *Antioxidants & Redox Signaling* **2010,** *12* (9), 1079-1091.

[1057] Taniguchi, S.; Kang, L.; Kimura, T.; Niki, I., Hydrogen sulphide protects mouse pancreatic β-cells from cell death induced by oxidative stress, but not by endoplasmic reticulum stress. *British Journal of Pharmacology* **2011,** *162* (5), 1171-1178.

[1058] Jiang, B.; Tang, G.; Cao, K.; Wu, L.; Wang, R., Molecular Mechanism for H_2S-Induced Activation of KATP Channels. *Antioxidants & Redox Signaling* **2010,** *12* (10), 1167-1178.

[1059] Dongó, E.; Beliczai-Marosi, G.; Dybvig, A. S.; Kiss, L., The mechanism of action and role of hydrogen sulfide in the control of vascular tone. *Nitric Oxide* **2018,** *81,* 75-87.

[1060] Song, Z. J.; Ng, M. Y.; Lee, Z.-W.; Dai, W.; Hagen, T.; Moore, P. K.; Huang, D.; Deng, L.-W.; Tan, C.-H., Hydrogen sulfide donors in research and drug development. *MedChemComm* **2014,** *5* (5), 557-570.

[1061] Levinn, C. M.; Cerda, M. M.; Pluth, M. D., Activatable Small-Molecule Hydrogen Sulfide Donors. *Antioxidants & Redox Signaling* **2020,** *32* (2), 96-109.

[1062] Powell, C. R.; Dillon, K. M.; Matson, J. B., A review of hydrogen sulfide (H_2S) donors: Chemistry and potential therapeutic applications. *Biochemical Pharmacology* **2018,** *149,* 110-123.

[1063] DeLeon, E. R.; Stoy, G. F.; Olson, K. R., Passive loss of hydrogen sulfide in biological experiments. *Analytical Biochemistry* **2012,** *421* (1), 203-207.

[1064] Fosnacht, K. G.; Pluth, M. D., Activity-Based Fluorescent Probes for Hydrogen Sulfide and Related Reactive Sulfur Species. *Chemical Reviews* **2024**.

[1065] Li, L.; Lin, Z.; Cheng, Y.; Tang, Y.; Zhang, Z., A cysteine-triggered fluorogenic donor base on native chemical ligation for tracking H_2S delivery in vivo. *Analyst* **2021,** *146* (24), 7374-7378.

[1066] Chen, Y.; Zhao, R.; Tang, C.; Zhang, C.; Xu, W.; Wu, L.; Wang, Y.; Ye, D.; Liang, Y., Design and Development of a Bioorthogonal, Visualizable and Mitochondria-Targeted Hydrogen Sulfide (H_2S) Delivery System. *Angewandte Chemie International Edition* **2022,** *61* (6), e202112734.

[1067] Li, L.; Zhang, Z., A fluorogenic H_2S donor activated by reactive oxygen species for real-time monitoring in cells and in vivo. *Spectrochimica Acta Part A: Molecular and Biomolecular Spectroscopy* **2022,** *264*, 120243.

[1068] Zhao, X.; Ning, L.; Zhou, X.; Song, Z.; Zhang, J.; Guan, F.; Yang, X.-F., An Activatable Near-Infrared Fluorescence Hydrogen Sulfide (H_2S) Donor for Imaging H_2S Release and Inhibiting Inflammation in Cells. *Analytical Chemistry* **2021,** *93* (11), 4894-4901.

[1069] Hua, W.; Zhao, J.; Gou, S., A naphthalimide derivative can release COS and form H_2S in a light-controlled manner and protect cells against ROS with real-time monitoring ability. *Analyst* **2020,** *145* (11), 3878-3884.

[1070] Zhang, N.; Hu, P.; Wang, Y.; Tang, Q.; Zheng, Q.; Wang, Z.; He, Y., A Reactive Oxygen Species (ROS) Activated Hydrogen Sulfide (H_2S) Donor with Self-Reporting Fluorescence. *ACS Sensors* **2020,** *5* (2), 319-326.

[1071] Hu, Y.; Li, X.; Fang, Y.; Shi, W.; Li, X.; Chen, W.; Xian, M.; Ma, H., Reactive oxygen species-triggered off-on fluorescence donor for imaging hydrogen sulfide delivery in living cells. *Chemical Science* **2019,** *10* (33), 7690-7694.

[1072] Liu, J.; Zhao, M.; Zhao, F.; Song, X.; Ye, Y., $ONOO^-$-triggered fluorescence H_2S donor for mitigating drug-induced liver injury. *Sensors and Actuators B: Chemical* **2023,** *378*, 133131.

[1073] Sharma, A. K.; Nair, M.; Chauhan, P.; Gupta, K.; Saini, D. K.; Chakrapani, H., Visible-Light-Triggered Uncaging of Carbonyl Sulfide for Hydrogen Sulfide (H_2S) Release. *Organic Letters* **2017,** *19* (18), 4822-4825.

[1074] Yao, M.; Lu, Y.; Shi, L.; Huang, Y.; Zhang, Q.; Tan, J.; Hu, P.; Zhang, J.; Luo, G.; Zhang, N., A ROS-responsive, self-immolative and self-reporting hydrogen sulfide donor with multiple biological activities for the treatment of myocardial infarction. *Bioactive Materials* **2022,** *9*, 168-182.

[1075] Zhao, X.; Ding, M.; Ning, L.; Yuan, F.; Li, J.; Guo, Y.; Mu, Y.; Zhang, J., Biothiol-triggered H_2S release from a near-infrared fluorescent H_2S donor promotes cutaneous wound healing. *Acta Materia Medica* **2022,** *1* (4), 476-485.

[1076] Yuan, F.; He, X.; Lu, Y.; Ning, L.; Zhao, X.; Zhang, S.; Guan, F.; Guo, Y.; Zhang, J., Photoactivated Hydrogen Sulfide Donor with a Near-Infrared Fluorescence Report System for Accelerated Chronic Wound Healing. *Analytical Chemistry* **2023,** *95* (17), 6931-6939.

[1077] Wang, N.; Fang, Y.; Wang, X.; Bai, J.; Hua, H.; Li, D., A photoactivated H_2S donor based on a coumarin structure with real-time monitoring capability. *Chemical Communications* **2023,** *59* (58), 8949-8952.

[1078] Venkatesh, Y.; Das, J.; Chaudhuri, A.; Karmakar, A.; Maiti, T. K.; Singh, N. D. P., Light triggered uncaging of hydrogen sulfide (H_2S) with real-time monitoring. *Chemical Communications* **2018,** *54* (25), 3106-3109.

[1079] Mahato, S. K.; Bhattacherjee, D.; Barman, P.; Bhabak, K. P., Thioredoxin reductase-triggered fluorogenic donor of hydrogen sulfide: a model study with a symmetrical organopolysulfide probe with turn-on near-infrared fluorescent emission. *Journal of Materials Chemistry B* **2022,** *10* (13), 2183-2193.

[1080] Mahato, S. K.; Bhattacherjee, D.; Bhabak, K. P., The biothiol-triggered organotrisulfide-based self-immolative fluorogenic donors of hydrogen sulfide enable lysosomal trafficking. *Chemical Communications* **2020,** *56* (56), 7769-7772.

[1081] Zhao, Y.; Cerda, Matthew M.; Pluth, M. D., Fluorogenic hydrogen sulfide (H_2S) donors based on sulfenyl thiocarbonates enable H_2S tracking and quantification. *Chemical Science* **2019,** *10* (6), 1873-1878.

[1082] Dickinson, B. C.; Huynh, C.; Chang, C. J., A Palette of Fluorescent Probes with Varying Emission Colors for Imaging Hydrogen Peroxide Signaling in Living Cells. *Journal of the American Chemical Society* **2010,** *132* (16), 5906-5915.

[1083] Hornum, M.; Mulberg, M. W.; Szomek, M.; Reinholdt, P.; Brewer, J. R.; Wüstner, D.; Kongsted, J.; Nielsen, P., Substituted 9-Diethylaminobenzo[a]phenoxazin-5-ones (Nile Red Analogues): Synthesis and Photophysical Properties. *The Journal of Organic Chemistry* **2021,** *86* (2), 1471-1488.

[1084] Yuan, L.; Lin, W.; Zhao, S.; Gao, W.; Chen, B.; He, L.; Zhu, S., A Unique Approach to Development of Near-Infrared Fluorescent Sensors for in Vivo Imaging. *Journal of the American Chemical Society* **2012,** *134* (32), 13510-13523.

[1085] Greenspan, P.; Fowler, S. D., Spectrofluorometric studies of the lipid probe, nile red. *Journal of Lipid Research* **1985,** *26* (7), 781-789.

[1086] Greenspan, P.; Mayer, E. P.; Fowler, S. D., Nile red: a selective fluorescent stain for intracellular lipid droplets. *Journal of Cell Biology* **1985,** *100* (3), 965-973.

[1087] Abdel-Mottaleb, M. S. A.; El-Sayed, B. A.; Abo-Aly, M. M.; El-Kady, M. Y., Fluorescence-properties and excited state interactions of 7-hydroxy-4-methylcoumarin laser dye. *Journal of Photochemistry and Photobiology A: Chemistry* **1989,** *46* (3), 379-390.

[1088] Bueno, C.; Villegas, M. L.; Bertolotti, S. G.; Previtali, C. M.; Neumann, M. G.; Encinas, M. V., The Excited-State Interaction of Resazurin and Resorufin with Aminesin Aqueous Solutions. Photophysics and Photochemical Reaction¶. *Photochemistry and Photobiology* **2002,** *76* (4), 385-390.

[1089] Chauhan, P.; Bora, P.; Ravikumar, G.; Jos, S.; Chakrapani, H., Esterase Activated Carbonyl Sulfide/Hydrogen Sulfide (H_2S) Donors. *Organic Letters* **2017,** *19* (1), 62-65.

[1090] Bailey, J. L.; Cole, R. D., Studies on the Reaction of Sulfite with Proteins. *Journal of Biological Chemistry* **1959,** *234* (7), 1733-1739.

[1091] Fosnacht, K. G.; Cerda, M. M.; Mullen, E. J.; Pigg, H. C.; Pluth, M. D., Esterase-Activated Perthiocarbonate Persulfide Donors Provide Insights into Persulfide Persistence and Stability. *ACS Chemical Biology* **2022,** *17* (2), 331-339.

[1092] Kolluru, G. K.; Shen, X.; Bir, S. C.; Kevil, C. G., Hydrogen sulfide chemical biology: pathophysiological roles and detection. *Nitric Oxide* **2013,** *35*, 5-20.

[1093] Gemici, B.; Wallace, J. L., Anti-inflammatory and cytoprotective properties of hydrogen sulfide. *Methods Enzymol* **2015,** *555*, 169-93.

[1094] Zhao, W.; Wang, R., H(2)S-induced vasorelaxation and underlying cellular and molecular mechanisms. *Am J Physiol Heart Circ Physiol* **2002,** *283* (2), H474-80.

[1095] Elrod, J. W.; Calvert, J. W.; Morrison, J.; Doeller, J. E.; Kraus, D. W.; Tao, L.; Jiao, X.; Scalia, R.; Kiss, L.; Szabo, C.; Kimura, H.; Chow, C. W.; Lefer, D. J., Hydrogen sulfide attenuates myocardial ischemia-reperfusion injury by preservation of mitochondrial function. *Proc Natl Acad Sci U S A* **2007,** *104* (39), 15560-5.

[1096] Alvarez, L.; Bianco, C. L.; Toscano, J. P.; Lin, J.; Akaike, T.; Fukuto, J. M., Chemical Biology of Hydropersulfides and Related Species: Possible Roles in Cellular Protection and Redox Signaling. *Antioxid Redox Signal* **2017,** *27* (10), 622-633.

[1097] Paul, B. D.; Snyder, S. H., H_2S: A Novel Gasotransmitter that Signals by Sulfhydration. *Trends in Biochemical Sciences* **2015,** *40* (11), 687-700.

[1098] Mustafa, A. K.; Gadalla, M. M.; Sen, N.; Kim, S.; Mu, W.; Gazi, S. K.; Barrow, R. K.; Yang, G.; Wang, R.; Snyder, S. H., H2S signals through protein S-sulfhydration. *Sci Signal* **2009,** *2* (96), ra72.

[1099] Francoleon, N. E.; Carrington, S. J.; Fukuto, J. M., The reaction of H(2)S with oxidized thiols: generation of persulfides and implications to H(2)S biology. *Arch Biochem Biophys* **2011,** *516* (2), 146-53.

[1100] Greiner, R.; Pálinkás, Z.; Bäsell, K.; Becher, D.; Antelmann, H.; Nagy, P.; Dick, T. P., Polysulfides link H2S to protein thiol oxidation. *Antioxid Redox Signal* **2013,** *19* (15), 1749-65.

[1101] Benchoam, D.; Cuevasanta, E.; Möller, M. N.; Alvarez, B., Hydrogen Sulfide and Persulfides Oxidation by Biologically Relevant Oxidizing Species. *Antioxidants (Basel)* **2019,** *8* (2).

[1102] Benchoam, D.; Cuevasanta, E.; Möller, M. N.; Alvarez, B., Persulfides, at the crossroads between hydrogen sulfide and thiols. *Essays Biochem* **2020,** *64* (1), 155-168.

[1103] Cuevasanta, E.; Lange, M.; Bonanata, J.; Coitiño, E. L.; Ferrer-Sueta, G.; Filipovic, M. R.; Alvarez, B., Reaction of Hydrogen Sulfide with Disulfide and Sulfenic Acid to Form the Strongly Nucleophilic Persulfide. *J Biol Chem* **2015,** *290* (45), 26866-26880.

[1104] Ida, T.; Sawa, T.; Ihara, H.; Tsuchiya, Y.; Watanabe, Y.; Kumagai, Y.; Suematsu, M.; Motohashi, H.; Fujii, S.; Matsunaga, T.; Yamamoto, M.; Ono, K.; Devarie-Baez, N. O.; Xian, M.; Fukuto, J. M.; Akaike, T., Reactive cysteine persulfides and S-polythiolation regulate oxidative stress and redox signaling. *Proc Natl Acad Sci U S A* **2014,** *111* (21), 7606-11.

[1105] Dóka, É.; Ida, T.; Dagnell, M.; Abiko, Y.; Luong, N. C.; Balog, N.; Takata, T.; Espinosa, B.; Nishimura, A.; Cheng, Q.; Funato, Y.; Miki, H.; Fukuto, J. M.; Prigge, J. R.; Schmidt, E. E.; Arnér, E. S. J.; Kumagai, Y.; Akaike, T.; Nagy, P., Control of protein function through oxidation and reduction of persulfidated states. *Sci Adv* **2020,** *6* (1), eaax8358.

[1106] Millikin, R.; Bianco, C. L.; White, C.; Saund, S. S.; Henriquez, S.; Sosa, V.; Akaike, T.; Kumagai, Y.; Soeda, S.; Toscano, J. P.; Lin, J.; Fukuto, J. M., The chemical biology of protein hydropersulfides: Studies of a possible protective function of biological hydropersulfide generation. *Free Radic Biol Med* **2016,** *97*, 136-147.

[1107] Yang, C. T.; Devarie-Baez, N. O.; Hamsath, A.; Fu, X. D.; Xian, M., S-Persulfidation: Chemistry, Chemical Biology, and Significance in Health and Disease. *Antioxid Redox Signal* **2020,** *33* (15), 1092-1114.

[1108] Vandiver, M. S.; Paul, B. D.; Xu, R.; Karuppagounder, S.; Rao, F.; Snowman, A. M.; Ko, H. S.; Lee, Y. I.; Dawson, V. L.; Dawson, T. M.; Sen, N.; Snyder, S. H., Sulfhydration mediates neuroprotective actions of parkin. *Nat Commun* **2013,** *4*, 1626.

[1109] Kasamatsu, S., Persulfide-Dependent Regulation of Electrophilic Redox Signaling in Neural Cells. *Antioxid Redox Signal* **2020,** *33* (18), 1320-1331.

[1110] Cao, X.; Cao, L.; Ding, L.; Bian, J. S., A New Hope for a Devastating Disease: Hydrogen Sulfide in Parkinson's Disease. *Mol Neurobiol* **2018,** *55* (5), 3789-3799.

[1111] Kimura, Y.; Koike, S.; Shibuya, N.; Lefer, D.; Ogasawara, Y.; Kimura, H., 3-Mercaptopyruvate sulfurtransferase produces potential redox regulators cysteine- and glutathione-persulfide (Cys-SSH and GSSH) together with signaling molecules H(2)S(2), H(2)S(3) and H(2)S. *Sci Rep* **2017,** *7* (1), 10459.

[1112] Yadav, P. K.; Martinov, M.; Vitvitsky, V.; Seravalli, J.; Wedmann, R.; Filipovic, M. R.; Banerjee, R., Biosynthesis and Reactivity of Cysteine Persulfides in Signaling. *Journal of the American Chemical Society* **2016,** *138* (1), 289-299.

[1113] Libiad, M.; Sriraman, A.; Banerjee, R., Polymorphic Variants of Human Rhodanese Exhibit Differences in Thermal Stability and Sulfur Transfer Kinetics. *J Biol Chem* **2015,** *290* (39), 23579-88.

[1114] Wedmann, R.; Onderka, C.; Wei, S.; Szijártó, I. A.; Miljkovic, J. L.; Mitrovic, A.; Lange, M.; Savitsky, S.; Yadav, P. K.; Torregrossa, R.; Harrer, E. G.; Harrer, T.; Ishii, I.; Gollasch, M.; Wood, M. E.; Galardon, E.; Xian, M.; Whiteman, M.; Banerjee, R.; Filipovic, M. R., Improved tag-switch method reveals that thioredoxin acts as depersulfidase and controls the intracellular levels of protein persulfidation. *Chem Sci* **2016,** *7* (5), 3414-3426.

[1115] Cuevasanta, E.; Möller, M. N.; Alvarez, B., Biological chemistry of hydrogen sulfide and persulfides. *Archives of Biochemistry and Biophysics* **2017,** *617*, 9-25.

[1116] Park, C.-M.; Weerasinghe, L.; Day, J. J.; Fukuto, J. M.; Xian, M., Persulfides: current knowledge and challenges in chemistry and chemical biology. *Molecular BioSystems* **2015,** *11* (7), 1775-1785.

[1117] Fukuto, J. M.; Hobbs, A. J., A comparison of the chemical biology of hydropersulfides (RSSH) with other protective biological antioxidants and nucleophiles. *Nitric Oxide* **2021,** *107*, 46-57.

[1118] Bailey, T. S.; Pluth, M. D., Reactions of isolated persulfides provide insights into the interplay between H2S and persulfide reactivity. *Free Radic Biol Med* **2015,** *89*, 662-7.

[1119] Cerda, M. M.; Hammers, M. D.; Earp, M. S.; Zakharov, L. N.; Pluth, M. D., Applications of Synthetic Organic Tetrasulfides as H(2)S Donors. *Organic letters* **2017,** *19* (9), 2314-2317.

[1120] Bolton, S. G.; Cerda, M. M.; Gilbert, A. K.; Pluth, M. D., Effects of sulfane sulfur content in benzyl polysulfides on thiol-triggered H(2)S release and cell proliferation. *Free Radic Biol Med* **2019,** *131*, 393-398.

[1121] Hankins, R. A.; Suarez, S. I.; Kalk, M. A.; Green, N. M.; Harty, M. N.; Lukesh, J. C., 3rd, An Innovative Hydrogen Peroxide-Sensing Scaffold and Insight Towards its Potential as an ROS-Activated Persulfide Donor. *Angew Chem Int Ed Engl* **2020,** *59* (49), 22238-22245.

[1122] Wang, Y.; Dillon, K. M.; Li, Z.; Winckler, E. W.; Matson, J. B., Alleviating Cellular Oxidative Stress through Treatment with Superoxide-Triggered Persulfide Prodrugs. *Angew Chem Int Ed Engl* **2020,** *59* (38), 16698-16704.

[1123] Yu, B.; Zheng, Y.; Yuan, Z.; Li, S.; Zhu, H.; De La Cruz, L. K.; Zhang, J.; Ji, K.; Wang, S.; Wang, B., Toward Direct Protein S-Persulfidation: A Prodrug Approach That Directly Delivers Hydrogen Persulfide. *J Am Chem Soc* **2018,** *140* (1), 30-33.

[1124] Zheng, Y.; Yu, B.; Li, Z.; Yuan, Z.; Organ, C. L.; Trivedi, R. K.; Wang, S.; Lefer, D. J.; Wang, B., An Esterase-Sensitive Prodrug Approach for Controllable Delivery of Persulfide Species. *Angew Chem Int Ed Engl* **2017,** *56* (39), 11749-11753.

[1125] Yuan, Z.; Zheng, Y.; Yu, B.; Wang, S.; Yang, X.; Wang, B., Esterase-Sensitive Glutathione Persulfide Donor. *Org Lett* **2018,** *20* (20), 6364-6367.

[1126] Dillon, K. M.; Carrazzone, R. J.; Wang, Y.; Powell, C. R.; Matson, J. B., Polymeric persulfide prodrugs: Mitigating oxidative stress through controlled delivery of reactive sulfur species. *ACS Macro Lett* **2020,** *9* (4), 606-612.

[1127] Chaudhuri, A.; Venkatesh, Y.; Das, J.; Gangopadhyay, M.; Maiti, T. K.; Singh, N. D. P., One- and Two-Photon-Activated Cysteine Persulfide Donors for Biological Targeting. *J Org Chem* **2019,** *84* (18), 11441-11449.

[1128] Harpp, D. N.; Granata, A., Organic sulfur chemistry. XXI. Trisulfide formation by alkoxide decomposition of sulfenylthiocarbonates. *Tetrahedron Letters* **1976,** *17* (35), 3001-3004.

[1129] Harpp, D. N.; Granata, A., Cyclic trisulfides by alkoxide decomposition of bis(sulfenyl) thiocarbonates. *Journal of Organic Chemistry* **1979,** *44*, 4144-4148.

[1130] Everett, S. A.; Folkes, L. K.; Wardman, P.; Asmus, K. D., Free-Radical Repair by a Novel Perthiol: Reversible Hydrogen Transfer and Perthiyl Radical Formation. *Free Radical Research* **1994,** *20* (6), 387-400.

[1131] Khodade, V. S.; Aggarwal, S. C.; Pharoah, B. M.; Paolocci, N.; Toscano, J. P., Alkylsulfenyl thiocarbonates: precursors to hydropersulfides potently attenuate oxidative stress. *Chemical Science* **2021,** *12* (23), 8252-8259.

[1132] Sawahata, T.; Neal, R. A., Use of 1-fluoro-2,4-dinitrobenzene as a probe for the presence of hydrodisulfide groups in proteins. *Analytical Biochemistry* **1982,** *126* (2), 360-364.

[1133] Heymann, E.; Junge, W., Characterization of the Isoenzymes of Pig-Liver Esterase 1. Chemical Studies. *European Journal of Biochemistry* **1979,** *95* (3), 509-518.

[1134] Provencher, L.; Jones, J. B., A Concluding Specification of the Dimensions of the Active Site Model of Pig Liver Esterase. *The Journal of Organic Chemistry* **1994,** *59* (10), 2729-2732.

[1135] Giles, G. I.; Jacob, C., Reactive Sulfur Species: An Emerging Concept in Oxidative Stress. *Biological Chemistry* **2002,** *383* (3-4), 375-388.

[1136] Gruhlke, M. C. H.; Slusarenko, A. J., The biology of reactive sulfur species (RSS). *Plant Physiology and Biochemistry* **2012,** *59*, 98-107.

[1137] Mishanina, T. V.; Libiad, M.; Banerjee, R., Biogenesis of reactive sulfur species for signaling by hydrogen sulfide oxidation pathways. *Nature Chemical Biology* **2015,** *11* (7), 457-464.

[1138] Rohwerder, T.; Sand, W., The sulfane sulfur of persulfides is the actual substrate of the sulfur-oxidizing enzymes from Acidithiobacillus and Acidiphilium spp. *Microbiology* **2003,** *149* (7), 1699-1710.

[1139] Griffiths, K.; Ida, T.; Morita, M.; Lamb, R. J.; Lee, J. J.; Frenneaux, M. P.; Fukuto, J. M.; Akaike, T.; Feelisch, M.; Madhani, M., Cysteine hydropersulfide reduces lipid peroxidation and protects against myocardial ischaemia-reperfusion injury - Are endogenous persulfides mediators of ischaemic preconditioning? *Redox Biology* **2023,** *60*, 102605.

[1140] Akaike, T.; Ida, T.; Wei, F.-Y.; Nishida, M.; Kumagai, Y.; Alam, M. M.; Ihara, H.; Sawa, T.; Matsunaga, T.; Kasamatsu, S.; Nishimura, A.; Morita, M.; Tomizawa, K.; Nishimura, A.; Watanabe, S.; Inaba, K.; Shima, H.; Tanuma, N.; Jung, M.; Fujii, S.; Watanabe, Y.; Ohmuraya, M.; Nagy, P.; Feelisch, M.; Fukuto, J. M.; Motohashi, H., Cysteinyl-tRNA synthetase governs cysteine polysulfidation and mitochondrial bioenergetics. *Nature Communications* **2017,** *8* (1), 1177.

[1141] Bianco, C. L.; Akaike, T.; Ida, T.; Nagy, P.; Bogdandi, V.; Toscano, J. P.; Kumagai, Y.; Henderson, C. F.; Goddu, R. N.; Lin, J.; Fukuto, J. M., The reaction of hydrogen sulfide with disulfides: formation of a stable trisulfide and implications for biological systems. *British Journal of Pharmacology* **2019,** *176* (4), 671-683.

[1142] Kasamatsu, S.; Nishimura, A.; Morita, M.; Matsunaga, T.; Abdul Hamid, H.; Akaike, T., Redox Signaling Regulated by Cysteine Persulfide and Protein Polysulfidation. *Molecules* **2016,** *21* (12), 1721.

[1143] Parent, A.; Elduque, X.; Cornu, D.; Belot, L.; Le Caer, J.-P.; Grandas, A.; Toledano, M. B.; D'Autréaux, B., Mammalian frataxin directly enhances sulfur transfer of NFS1 persulfide to both ISCU and free thiols. *Nature Communications* **2015,** *6* (1), 5686.

[1144] Bridwell-Rabb, J.; Fox, N. G.; Tsai, C.-L.; Winn, A. M.; Barondeau, D. P., Human Frataxin Activates Fe–S Cluster Biosynthesis by Facilitating Sulfur Transfer Chemistry. *Biochemistry* **2014,** *53* (30), 4904-4913.

[1145] Dóka, É.; Pader, I.; Bíró, A.; Johansson, K.; Cheng, Q.; Ballagó, K.; Prigge, J. R.; Pastor-Flores, D.; Dick, T. P.; Schmidt, E. E.; Arnér, E. S. J.; Nagy, P., A novel persulfide detection method reveals protein persulfide- and polysulfide-reducing functions of thioredoxin and glutathione systems. *Science Advances* **2016,** *2* (1), e1500968.

[1146] Giovinazzo, D.; Bursac, B.; Sbodio, J. I.; Nalluru, S.; Vignane, T.; Snowman, A. M.; Albacarys, L. M.; Sedlak, T. W.; Torregrossa, R.; Whiteman, M.; Filipovic, M. R.; Snyder, S. H.; Paul, B. D., Hydrogen sulfide is neuroprotective in Alzheimer's disease by

sulfhydrating GSK3β and inhibiting Tau hyperphosphorylation. *Proceedings of the National Academy of Sciences* **2021,** *118* (4), e2017225118.

[1147] Portillo-Ledesma, S.; Sardi, F.; Manta, B.; Tourn, M. V.; Clippe, A.; Knoops, B.; Alvarez, B.; Coitiño, E. L.; Ferrer-Sueta, G., Deconstructing the Catalytic Efficiency of Peroxiredoxin-5 Peroxidatic Cysteine. *Biochemistry* **2014,** *53* (38), 6113-6125.

[1148] Kawamura, S.; Otsuji, Y.; Nakabayashi, T.; Kitao, T.; Tsurugi, J., Aralkyl Hydrodisulfides. IV. The Reaction of Benzyl Hydrodisulfide with Several Nucleophiles. *The Journal of Organic Chemistry* **1965,** *30* (8), 2711-2714.

[1149] Tsurugi, J.; Nakabayashi, T.; Ishihara, T., Aralkyl Hydrodisulfides.1 III. The Reaction with Tertiary Phosphines. *The Journal of Organic Chemistry* **1965,** *30* (8), 2707-2710.

[1150] Tsurugi, J.; Abe, Y.; Nakabayashi, T.; Kawamura, S.; Kitao, T.; Niwa, M., Aralkyl hydrodisulfides. XI. Reaction with amines. *The Journal of Organic Chemistry* **1970,** *35* (10), 3263-3266.

[1151] Pan, J.; Carroll, K. S., Persulfide Reactivity in the Detection of Protein S-Sulfhydration. *ACS Chemical Biology* **2013,** *8* (6), 1110-1116.

[1152] Bailey, T. S.; Zakharov, L. N.; Pluth, M. D., Understanding Hydrogen Sulfide Storage: Probing Conditions for Sulfide Release from Hydrodisulfides. *Journal of the American Chemical Society* **2014,** *136* (30), 10573-10576.

[1153] Böhme, H.; Zinner, G., Über Darstellung und Eigenschaften von Alkyl-hydro-polysulfiden. *Justus Liebigs Annalen der Chemie* **1954,** *585* (1), 142-149.

[1154] Tsurugi, J.; Abe, Y.; Kawamura, S., Synthesis of 2-Substituted Ethyl Hydrodisulfides. *Bulletin of the Chemical Society of Japan* **2006,** *43* (6), 1890-1892.

[1155] Chatterji, T.; Keerthi, K.; Gates, K. S., Generation of reactive oxygen species by a persulfide (BnSSH). *Bioorganic & Medicinal Chemistry Letters* **2005,** *15* (17), 3921-3924.

[1156] Heimer, N. E.; Field, L.; Neal, R. A., Biologically oriented organic sulfur chemistry. 21. Hydrodisulfide of a penicillamine derivative and related compounds. *The Journal of Organic Chemistry* **1981,** *46* (7), 1374-1377.

[1157] Tsurugi, J.; Kawamura, S.; Horii, T., Aryl hydrodisulfides. *The Journal of Organic Chemistry* **1971,** *36* (24), 3677-3680.

[1158] Vasas, A.; Dóka, É.; Fábián, I.; Nagy, P., Kinetic and thermodynamic studies on the disulfide-bond reducing potential of hydrogen sulfide. *Nitric Oxide* **2015,** *46*, 93-101.

[1159] Zhang, D.; Macinkovic, I.; Devarie-Baez, N. O.; Pan, J.; Park, C.-M.; Carroll, K. S.; Filipovic, M. R.; Xian, M., Detection of Protein S-Sulfhydration by a Tag-Switch Technique. *Angewandte Chemie International Edition* **2014,** *53* (2), 575-581.

[1160] Dillon, K. M.; Matson, J. B., A Review of Chemical Tools for Studying Small Molecule Persulfides: Detection and Delivery. *ACS Chemical Biology* **2021,** *16* (7), 1128-1141.

[1161] Powell, C. R.; Dillon, K. M.; Wang, Y.; Carrazzone, R. J.; Matson, J. B., A Persulfide Donor Responsive to Reactive Oxygen Species: Insights into Reactivity and Therapeutic Potential. *Angewandte Chemie International Edition* **2018,** *57* (21), 6324-6328.

[1162] Artaud, I.; Galardon, E., A Persulfide Analogue of the Nitrosothiol SNAP: Formation, Characterization and Reactivity. *ChemBioChem* **2014,** *15* (16), 2361-2364.

[1163] Kawamura, S.; Nakabayashi, T.; Kitao, T.; Tsurugi, J., Aralkyl Hydrodisulfides. VI. The Reaction of Benzhydryl Hydrosulfide with Several Neucleophiles. *The Journal of Organic Chemistry* **1966,** *31* (6), 1985-1987.

[1164] Sharma, J.; Champagne, P. A., Benchmark of density functional theory methods for the study of organic polysulfides. *Journal of Computational Chemistry* **2022,** *43* (32), 2131-2138.

[1165] Sharma, J.; Champagne, P. A., Mechanisms of the Reaction of Elemental Sulfur and Polysulfides with Cyanide and Phosphines. *Chemistry – A European Journal* **2023,** *29* (32), e202203906.

[1166] Ritchie, C. D.; Sager, W. F., An Examination of Structure-Reactivity Relationships. In *Progress in Physical Organic Chemistry*, 1964; pp 323-400.

[1167] Saund, S. S.; Sosa, V.; Henriquez, S.; Nguyen, Q. N. N.; Bianco, C. L.; Soeda, S.; Millikin, R.; White, C.; Le, H.; Ono, K.; Tantillo, D. J.; Kumagai, Y.; Akaike, T.; Lin, J.; Fukuto, J. M., The chemical biology of hydropersulfides (RSSH): Chemical stability, reactivity and redox roles. *Archives of Biochemistry and Biophysics* **2015,** *588*, 15-24.

[1168] Taft, R. W., Jr., Linear Free Energy Relationships from Rates of Esterification and Hydrolysis of Aliphatic and Ortho-substituted Benzoate Esters. *Journal of the American Chemical Society* **1952,** *74* (11), 2729-2732.

[1169] Benavides, G. A.; Squadrito, G. L.; Mills, R. W.; Patel, H. D.; Isbell, T. S.; Patel, R. P.; Darley-Usmar, V. M.; Doeller, J. E.; Kraus, D. W., Hydrogen sulfide mediates the vasoactivity of garlic. *Proceedings of the National Academy of Sciences* **2007,** *104* (46), 17977-17982.

[1170] Amagase, H., Clarifying the Real Bioactive Constituents of Garlic. *The Journal of Nutrition* **2006,** *136* (3), 716S-725S.

[1171] Liang, D.; Wu, H.; Wong, M. W.; Huang, D., Diallyl Trisulfide Is a Fast H_2S Donor, but Diallyl Disulfide Is a Slow One: The Reaction Pathways and Intermediates of Glutathione with Polysulfides. *Organic Letters* **2015,** *17* (17), 4196-4199.

[1172] Cai, Y.-R.; Hu, C.-H., Computational Study of H_2S Release in Reactions of Diallyl Polysulfides with Thiols. *The Journal of Physical Chemistry B* **2017,** *121* (26), 6359-6366.

[1173] Huang, G.-T.; Yu, J.-S. K., Enzyme Catalysis that Paves the Way for S-Sulfhydration via Sulfur Atom Transfer. *The Journal of Physical Chemistry B* **2016,** *120* (20), 4608-4615.

[1174] Landry, A. P.; Moon, S.; Kim, H.; Yadav, P. K.; Guha, A.; Cho, U.-S.; Banerjee, R., A Catalytic Trisulfide in Human Sulfide Quinone Oxidoreductase Catalyzes Coenzyme A Persulfide Synthesis and Inhibits Butyrate Oxidation. *Cell Chemical Biology* **2019,** *26* (11), 1515-1525.e4.

[1175] Cuevasanta, E.; Reyes, A. M.; Zeida, A.; Mastrogiovanni, M.; De Armas, M. I.; Radi, R.; Alvarez, B.; Trujillo, M., Kinetics of formation and reactivity of the persulfide in the one-cysteine peroxiredoxin from Mycobacterium tuberculosis. *Journal of Biological Chemistry* **2019,** *294* (37), 13593-13605.

[1176] Pedre, B.; Dick, T. P., 3-Mercaptopyruvate sulfurtransferase: an enzyme at the crossroads of sulfane sulfur trafficking. *Biological Chemistry* **2021,** *402* (3), 223-237.

[1177] Zhao, Y.; Bhushan, S.; Yang, C.; Otsuka, H.; Stein, J. D.; Pacheco, A.; Peng, B.; Devarie-Baez, N. O.; Aguilar, H. C.; Lefer, D. J.; Xian, M., Controllable Hydrogen Sulfide Donors and Their Activity against Myocardial Ischemia-Reperfusion Injury. *ACS Chemical Biology* **2013,** *8* (6), 1283-1290.

[1178] Kasamatsu, S.; Ida, T.; Koga, T.; Asada, K.; Motohashi, H.; Ihara, H.; Akaike, T., High-Precision Sulfur Metabolomics Innovated by a New Specific Probe for Trapping Reactive Sulfur Species. *Antioxidants & Redox Signaling* **2021,** *34* (18), 1407-1419.

[1179] Zhang, L.; Zhang, X.; Wu, Y.-D.; Xie, Y.; Fukuto, J. M.; Schaefer, H. F., The reaction of alkyl hydropersulfides (RSSH, R = CH3 and ^{t}Bu) with H_2S in the gas phase and in aqueous solution. *Physical Chemistry Chemical Physics* **2019,** *21* (2), 537-545.

[1180] Frisch, M. J.; Trucks, G. W.; Schlegel, H. B.; Scuseria, G. E.; Robb, M. A.; Cheeseman, J. R.; Scalmani, G.; Barone, V.; Petersson, G. A.; Nakatsuji, H.; Li, X.; Caricato, M.; Marenich, A. V.; Bloino, J.; Janesko, B. G.; Gomperts, R.; Mennucci, B.; Hratchian, H. P.; Ortiz, J. V.; Izmaylov, A. F.; Sonnenberg, J. L.; Williams-Young, D.; Ding, F.; Lipparini, F.; Egidi, F.; Goings, J.; Peng, B.; Petrone, A.; Henderson, T.; Ranasinghe, D.; Zakrzewski, V. G.; Gao, J.; Rega, N.; Zheng, G.; Liang, W.; Hada, M.; Ehara, M.; Toyota, K.; Fukuda, R.; Hasegawa, J.; Ishida, M.; Nakajima, T.; Honda, Y.; Kitao, O.; Nakai, H.; Vreven, T.; Throssell, K.; J. A. Montgomery, J.; Peralta, J. E.; Ogliaro, F.; Bearpark, M. J.; Heyd, J. J.; Brothers, E. N.; Kudin, K. N.; Staroverov, V. N.; Keith, T. A.; Kobayashi, R.; Normand, J.; Raghavachari, K.; Rendell, A. P.; Burant, J. C.; Iyengar, S. S.; Tomasi, J.; Cossi, M.;

Millam, J. M.; Klene, M.; Adamo, C.; Cammi, R.; Ochterski, J. W.; Martin, R. L.; Morokuma, K.; Farkas, O.; Foresman, J. B.; D. J. Fox *Gaussian 16,* Gaussian, Inc.: Wallingford, CT, 2019.

[1181] Chai, J.-D.; Head-Gordon, M., Long-range corrected hybrid density functionals with damped atom–atom dispersion corrections. *Physical Chemistry Chemical Physics* **2008,** *10* (44), 6615-6620.

[1182] Dunning, T. H., Jr.; Peterson, K. A.; Wilson, A. K., Gaussian basis sets for use in correlated molecular calculations. X. The atoms aluminum through argon revisited. *The Journal of Chemical Physics* **2001,** *114* (21), 9244-9253.

[1183] Marenich, A. V.; Cramer, C. J.; Truhlar, D. G., Universal Solvation Model Based on Solute Electron Density and on a Continuum Model of the Solvent Defined by the Bulk Dielectric Constant and Atomic Surface Tensions. *The Journal of Physical Chemistry B* **2009,** *113* (18), 6378-6396.

[1184] Bootsma, A. N.; Wheeler, S., Popular Integration Grids Can Result in Large Errors in DFT-Computed Free Energies. *ChemRxiv* **2019**, 10.26434/chemrxiv.8864204.v5.

[1185] Luchini, G.; V., A.-R. J.; Guan, Y.; Funes-Ardoiz, I.; Paton, R. S. *GoodVibes*, 2019.

[1186] Grimme, S., Supramolecular Binding Thermodynamics by Dispersion-Corrected Density Functional Theory. *Chemistry – A European Journal* **2012,** *18* (32), 9955-9964.

[1187] Legault, C. *CYLview*, Université de Sherbrooke: 2009.

[1188] Tocco, G.; Eloh, K.; Laus, A.; Sasanelli, N.; Caboni, P., Electron-Deficient Alkynes as Powerful Tools against Root-Knot Nematode Melodogyne incognita: Nematicidal Activity and Investigation on the Mode of Action. *Journal of Agricultural and Food Chemistry* **2020,** *68* (40), 11088-11095.